CONF-700101(Vol.1)

XA04N0736 - 0869

Symposium on

ENGINEERING WITH NUCLEAR EXPLOSIVES

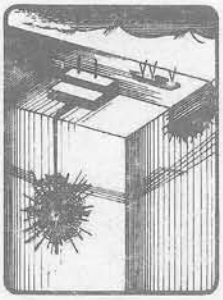

JANUARY 14-16, 1970
LAS VEGAS, NEVADA

INIS-XA-N--228

SPONSORED BY
THE AMERICAN
NUCLEAR SOCIETY

IN COOPERATION
WITH
THE UNITED STATES
ATOMIC ENERGY
COMMISSION

ORGANIZING COMMITTEE:

P. Kruger, General Chairman
Stanford University

J. Knox, Program Chairman
Lawrence Radiation Laboratory

H. Coffer, Local Chairman
CER Geonuclear

W. Talley, Finance Chairman
University of California, Davis

J. Philip, Publication Chairman
USAEC, San Francisco

F. Chilton, Publicity Chairman
Stanford Research Institute

PROCEEDINGS

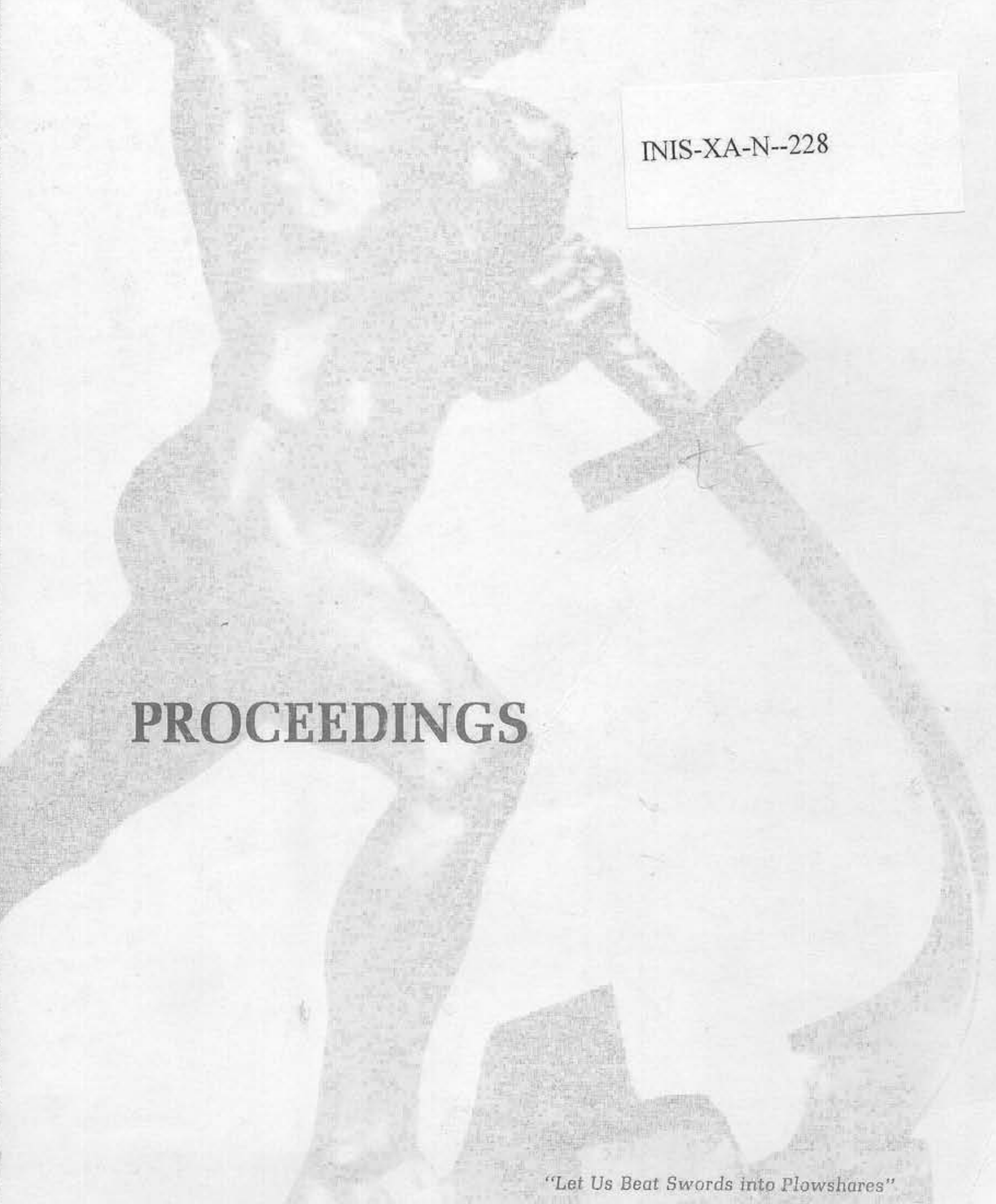

"Let Us Beat Swords into Plowshares"

Evgeniy Vuchetich
Gift to United Nations.
December 1959

LEGAL NOTICE

This report was prepared as an account of Government sponsored work. Neither the United States, nor the Commission, nor any person acting on behalf of the Commission:

A. Makes any warranty or representation, expressed or implied, with respect to the accuracy, completeness, or usefulness of the information contained in this report, or that the use of any information, apparatus, method, or process disclosed in this report may not infringe privately owned rights; or

B. Assumes any liabilities with respect to the use of, or for damages resulting from the use of any information, apparatus, method, or process disclosed in this report.

As used in the above, "person acting on behalf of the Commission" includes any employee or contractor of the Commission, or employee of such contractor, to the extent that such employee or contractor of the Commission, or employee of such contractor prepares, disseminates, or provides access to, any information pursuant to his employment or contract with the Commission, or his employment with such contractor.

This report has been reproduced directly from the best available copy.

Printed in USA. This report consists of 2 volumes. Price $6.00 for the 2 volume set. Available from the Clearinghouse for Federal Scientific and Technical Information, National Bureau of Standards, U. S. Department of Commerce, Springfield, Virginia 22151.

USAEC Division of Technical Information Extension, Oak Ridge, Tennessee

CONF-700101(Vol.1)
NUCLEAR EXPLOSIONS–PEACEFUL APPLICATIONS (TID-4500)

Symposium On

ENGINEERING WITH NUCLEAR EXPLOSIVES

January 14–16, 1970
Las Vegas, Nevada

PROCEEDINGS

Issuance Date: May 1970

Sponsored By

The American Nuclear Society

In Cooperation with

United States Atomic Energy Commission

FOREWORD

The Plowshare program is in good company these days—practically all the scientific and technological projects are getting polemical lumps. Dr. Alvin M. Weinberg of the Oak Ridge National Laboratory places the critics in four principal categories: (1) the scientific muckrakers, (2) those who see a waning in the relevance of science and technology to public interest, (3) those who decry the side effects of technology, and (4) the scientific abolitionists—the nihilists of the seventies. Plowshare has a fifth group of detractors—those who emotionally link Plowshare to nuclear weapons and wish that both would go away.

These critics seem to have forgotten a major word and a concept—moderation.

When Judge Alfred A. Arraj handed down his decision in the Denver U. S. District Court on the Rulison case, he wrote the following in discussing radiation standards:

> The field of radiation protection is constantly changing with the appearance of new scientific knowledge on the biological effects of ionizing radiation. Careful decisions must be made in the context of contemporaneous knowledge. Such decisions cannot be indefinitely postponed if the potentials of atomic energy are to be fully realized. All that is required to establish reasonableness of the decision setting a standard under the statutory directive to protect the public health and safety is that it be made carefully in light of the best of available scientific knowledge. Absolute certainty is neither required nor possible.

That the Plowshare program has friends is obvious from the quality and quantity of the erudite papers in this volume. With time and education it may be possible to return moderation and reasonableness to the affairs of man. In such a climate, Plowshare would flourish.

Chet Holifield

PREFACE

This symposium on "Engineering with Nuclear Explosives" reports to the Plowshare community, both national and international, the progress achieved since April 1964, the date of the Third Plowshare Symposium. In structuring the technical presentations, contributions of broadest interest were placed at the beginning, thus forming a common base of current information and applied science understanding developed in support of Plowshare technology. Sessions of speciality or pertaining to specific areas of application and engineering follow logically in the program. The Plenary Session reviewed the current status of the Plowshare Program from the technical, government, and industrial points of view. The 112 papers presented at 15 technical sessions covered all technical aspects of the Plowshare Program. The conference summary reviewed principal themes, areas of significant advance, and subjects requiring further attention that emerged during the technical conference. This proceedings is the record of the symposium.

The Program Committee wishes to commend all the authors and speakers for their most responsive cooperation in meeting deadlines associated with publication; without this cooperation the proceedings of this conference could not have been printed so promptly. The committee acknowledges with gratitude the editorial assistance of Mrs. Irene Keller, Division of Technical Information Extension, USAEC, Oak Ridge, in the efficient publication of these proceedings.

Joseph B. Knox
Program Chairman

TECHNICAL GROUP FOR NUCLEAR EXPLOSION ENGINEERING

The American Nuclear Society, in recognition of the growing importance of the Plowshare Program as a means of using nuclear energy for peaceful purposes, established in 1968 a Technical Group for Nuclear Explosion Engineering. The Technical Group formulated a policy to provide a forum for open discussion, dissemination, and publication of information on the scientific and technical aspects of the scientific, civil, and industrial applications of nuclear explosions.

A Special Session on Nuclear Excavation was held in September 1968 to summarize that area of technology. The proceedings of that session are available from the American Nuclear Society. Since 1964, the date of the Third Plowshare Symposium, there has been significant progress in all aspects of the phenomenological understanding, predictive capability of effects, effects involving radioactivity, and nuclear operations of Plowshare technology. The Organizing Committee trusts that their commitment to timely dissemination of information has been reasonably met with the Symposium, the opportunity for discussions, and the record provided by these Proceedings.

The vital statistics of the symposium are as follows: registration, 620; peak attendance in technical sessions, 800; press representatives, 28; number of foreign countries represented, 16; number of universities represented, 24; U. S. industrial firms, 117; number of foreign industrial firms, 18; one international agency, the IAEA; and 5 foreign governmental agencies. These data are included here as a part of the record.

Organizing Committee

Paul Kruger
Stanford University

Wilson K. Talley
University of California, Davis

Frank Chilton
Stanford Research Institute

John F. Philip
U. S. Atomic Energy Commission

Henry F. Coffer
CER Geonuclear Corp.

Joseph B. Knox
University of California,
Lawrence Radiation Laboratory

CONTENTS

VOLUME 1

OIL AND GAS

RADIOACTIVITY II

VOLUME 2

MINERAL RECOVERY

NUCLEAR OPERATIONS

SEISMIC EFFECTS

WATER RESOURCES DEVELOPMENT

SCIENTIFIC APPLICATIONS

UNDERGROUND ENGINEERING APPLICATIONS

XA04N0737

IMPROVING THE QUALITY OF LIFE— CAN PLOWSHARE HELP?

Remarks by
Theos J. Thompson, Commissioner
U. S. Atomic Energy Commission
at the Symposium on
Engineering with Nuclear Explosives
Las Vegas, Nevada
January 14, 1970

It is an honor to have been asked to open this Symposium on ''Engineering with Nuclear Explosives'' sponsored by the American Nuclear Society in cooperation with the United States Atomic Energy Commission. In one sense, this meeting comes at an unfortunate time. There are budgetary problems within all the branches of the Federal Government. There are misunderstandings on the part of the public in regard to the positive benefits that can accrue to mankind through the use of nuclear energy and in regard to the precautions being taken to protect the public from any adverse effects. The Plowshare Program is but one of several of our major programs that have been centrally affected by these problems of public acceptance and fiscal support.

But in another sense this is perhaps the best time for such a meeting. At no time has there been such need for public understanding of the benefits of such a program. At no time has there been such a need for better ideas. New challenges have been raised. We must meet them.

Devotion to the idea of progress—that is social change and technological change leading to improvements in our quality of life—is one of the most fundamental precepts of the American philosophy of life. Not all change is progress, of course. That is why we try out new ideas, new technologies on a small scale. We test, we observe, we look for adverse side effects, we study interrelations and long term effects. We do not and should not proceed to large scale operations until we are convinced that any adverse effects are small and not of great consequence. When we proceed to larger steps we must still continue to monitor for adverse long term effects.

But, a danger that is perhaps greater than that of the threat to our environment caused by making changes is the largely unrecognized, but perhaps growing rejection of those American ideals that have made this relatively young country a leader in the world of today. Our history has been based on a belief in change—in encouraging new ways of doing things. We have believed that change leads to progress. Yet today our society appears to stand on the verge of rejecting change and progress in favor of stagnation and retreat. Many are ready to reject new technologies on the basis that the old ones have not been perfect.

Technological progress is blamed by a vocal segment of our population for most of the ills that we are heir to—in my opinion, such blame is not properly placed. Trying new and well thought out technological advances designed to improve the quality of our life is a necessity which will as a minimum allow us to handle our burgeoning population until we develop socially acceptable ways to limit it. To do otherwise, to reject technology while the twin dooms of overpopulation and famine move relentlessly forward ready to engulf us is most dangerous. Without the aid of an ever improving technology, our social problems will overtake us and doom us. We have no viable choice but to make progress in our application of technology to the welfare of mankind.

To this particular audience I need not defend technology, nor do I have to point out that if, for instance, we are to solve our pollution problems, we are going to have to rely on technology for the greatest fraction of the assistance we need. I do wish, however, to make this audience aware of the great emphasis that President Nixon and our Government is placing on the improvement of our environment and the improvements of the quality of life.

President Nixon on the first day of January 1970 — the first day in the decade of the seventies — signed the National Environmental Policy Act of 1969. That Act declares that it is the policy of the U. S. Government "to create and maintain conditions under which man and nature can exist in productive harmony." The Act creates a three man Council on Environmental Quality within the White House to recommend environmental policies to the President and it requires all Federal agencies to take into account the environmental impact of all actions they propose. Of course as you know, the AEC has been doing this since its establishment.

Senator Henry Jackson, Chairman of the Senate Interior Committee and a key member of the Joint Committee on Atomic Energy, was the principal author of this Bill. Congress, in passing this Act, and President Nixon, in signing this Act, are looking forward to a positive program for the improvement in the quality of our air, water, and landscape. I might note parenthetically here that the interest of the Joint Committee on Atomic Energy in environmental matters goes back a long time. In the 1950s, Mr. Chet Holifield, then a subcommittee chairman, now the Chairman of the full Committee, conducted hearings on the biological and environmental effects of nuclear war. Those hearing reports are still being used as basic references.

It is symbolic, I believe, that the President chose the National Environmental Policy Act to be the first act of this new decade. There is no question but that many of us, our generation and the generation which is following us, are concerned about the problems of our environment and are eager to do something about it.

I firmly believe that technology can contribute greatly in our efforts to improve our environment. Few people realize it but the quality of the air in Pittsburgh and the air in London has, through changes in the kind of fuel used, been improved. Both of those cities have cleaner air today than they did a few years ago. I, and many of you here, know that the use of nuclear fuel for our central power stations can further reduce the amount of pollutants that are put into the atmosphere by fossil fuels. Technology can help to give us a better environment. There are many ways that I believe Plowshare can help in our fight to improve the quality of our environment. I want to mention a few of those ways in these opening remarks, but more importantly I would like to inspire all who are here to think constructively of more ways to utilize Plowshare so as "to create and maintain conditions under which man and nature can exist in productive harmony."

Plowshare, as we all know, is a research and development program of the Atomic Energy Commission. It has not yet achieved its goal of becoming a viable commercial enterprise, but it has achieved some important research advances. Let me start by mentioning one of those important achievements. More than five years ago, and before it was fashionable to talk knowingly of ecological system studies, the Atomic Energy Commission, under its Plowshare program, was funding a broad and deep ecology study. I refer to the study on the "Environment of the Cape Thompson Region, Alaska." By the way, I have no connection with the naming of that Cape. The Thompsons just have a way of popping up in the oddest kinds of environment.

The Cape Thompson study was in connection with the Commission's investigation of a possible site for a harbor for northern Alaska that might be excavated by nuclear means. That project, called Chariot, was probably a few years before its time. Today we know about the vast oil resources of the Northern Slope and we know of the need for a harbor up there to be used by tankers plying the Northwest Passage. The creation of harbors in Alaska, or in Australia, or in Asia, or at the tip of South America is in my opinion not a defilement of the environment or of nature, but an example of a "condition under which man and nature can exist in productive harmony" and, as the President stated, creating such conditions is to be our national policy. In the past, man has created few harbors because he has not had the technological means to do so. I believe that the Plowshare program, if permitted to continue experiments both to produce nuclear explosives with minimal amounts of fission output and to carry out cratering experiments with emplacement techniques which reduce to lower and lower levels the radioactive releases, will in time demonstrate the ease with which man can create a harbor. In time perhaps even barren wastes can be made to flower by creating inland "harbors" in deserts into which rivers may be guided or inland lakes with seawater flowing into them.

We must note that in the name of protecting the environment many are suggesting that even minimal amounts of radioactivity, amounts below the normal levels that have always existed for mankind, should not be even temporarily introduced into the environment. These people don't even pause to ask themselves about the positive benefits of these new possibilities—they simply reject them on the basis of very low observable effects whose extreme extrapolation might be detrimental. It is as though we decided not to get out of bed anymore because we might slip on the way to the bathroom. It is a sign of age—of giving up, of growing old, of decaying. If we take this attitude, we must take it about all interactions of man and his environment and we will soon conclude that we can no longer create conditions under which man and nature can exist in productive harmony. In fact, in the ultimate application of this philosophy, we should each of us stop breathing. There would be no production, but stagnation, no harmony, but discord between man and nature.

Let me now briefly mention a few other contributions that Plowshare can make. There are few things uglier in my opinion than the open holes left by strip mining and the mountains of tailings that are piled up from many mines. One need only fly over great stretches of the mining areas of the United States to see this. An explosion deep underground of nuclear devices in ore bearing formations breaking up the rock and thus permitting the leaching of the ore and bringing to the surface the metals contained without the terrible defacement of the landscape is one of the things I have in mind. I also believe that we can add more and more natural resources to our reserves by this method including the addition of gas by explosive stimulation of tightly packed formations and of shale oil by retorting underground in cavities created by Plowshare explosions. The National Environmental Policy Act of 1969 calls for the "widest range of beneficial uses of the environment without degradation, risk to health or safety, or other undesirable and unintended consequences" and "achieve a balance between population and resource use which will permit high standards of living and a wide sharing of life's amenities." How else are we to get at the resources locked deep in the bowels of the earth?

The creation of underground storage areas for natural gas, petroleum, chemicals, radioactive wastes, industrial and municipal waste products would take these products out of the biosphere and eliminate the possibility of surface leakage due to acts of nature or man and would improve the aesthetics of the landscape by removing unsightly storage tanks and make available valuable surface space. This would indeed be a wide ranging beneficial use of the environment without degradation.

One of our fastest growing needs if we are to continue a high and improved standard of living is electricity. Aside from the fuel needs—and I think nuclear power, fission—and eventually fusion—will provide the majority of the fuel—we need cooling water. I believe a way exists for Plowshare to contribute here also. By the middle of the next century the surface water runoff may be inadequate for our power needs, let alone for our other necessary uses of water. One of the ways to better manage our water resources is to conserve some of the runoff which now is lost to the sea. We could do so by creating large underground storage areas for water or by breaking up rock between natural aquifers to allow the recharging of those aquifers which are now depleted.

Another possibility for Plowshare, but perhaps limited in scope because of the vast requirements for energy that we have is to tap the heat from naturally occurring "geothermal" areas for electrical power generation. In areas of Oregon, California, Nevada, Utah, Washington, Idaho and Montana, dry geothermal layers exist at depths of a mile or two underground and at temperatures of 300° to 500°C. By breaking up this rock in place it should be possible to pump down water and bring up steam to run turbines. As you know, New Zealand, Italy and Iceland do have wet geothermal formations which provide steam for electrical power generation.

All technology utilizes natural resources and interacts with the environment. Our goal in the 1970s must be to minimize man's insults to the environment. By going underground with mining applications, by providing for better utilization of our resources and conserving them, including the saving of runoff water, we can improve the quality of our environment. Plowshare can help us to accomplish these things and I am sure that you gentlemen will think of even more ways and better ways that Plowshare can contribute to a productive and enjoyable harmony between man and his environment and thus help achieve this and the other purposes mentioned in the National Environmental Policy Act of 1969. Some of these other purposes are best illustrated by what Plowshare can do and what it has already done. Plowshare can promote efforts which will reduce or eliminate damage to the environment and biosphere. Plowshare has already in its research such as the Cape Thompson ecological studies and the Gasbuggy experiment enriched our understanding of the ecological systems and natural resources important to the Nation. We can all agree here, I hope, that Plowshare has the capability to improve the quality of our environment, enrich our understanding of the ecology and natural resources and enhance our efforts to achieve a productive harmony between man and nature.

My remarks this morning are made at the opening of this conference. I would hope that when this symposium ends on the 16th all will be able to answer the question I have posed in my title, "Improving the Quality of Life—Can Plowshare Help?", in the affirmative.

XA04N0738

THE FUTURE OF PLOWSHARE*

John S. Kelly, Director
Division of Peaceful Nuclear Explosives
U. S. Atomic Energy Commission

Since the last general symposium on Plowshare in 1964, significant progress has been made 1) in improving our understanding of explosion phenomenology, 2) in developing suitable explosive designs, and 3) in applying the technology to specific applications in the industrial, public works and scientific areas. The papers to be presented at this symposium will discuss in depth the progress that has been made in each of these areas, and to some degree, what still remains to be accomplished, so I will not attempt to go into detail here. However, I would like to take a few minutes to summarize where the technology stands today, where we believe it is going, and most importantly, how we hope to get there.

In the excavation area, both Cabriolet and Schooner extended cratering experience in hard rock to higher yields. We also conducted Project Buggy, the first nuclear row-charge experiment. Buggy involved the simultaneous detonation of five 1.1 kiloton nuclear explosives, spaced 150 feet apart at a depth of 135 feet. The explosion created a smooth channel about 865 feet long, 254 feet wide and 70 feet deep. Two very significant contributions from Buggy were information on spacing between the explosives and on lip height. Buggy demonstrated that explosives can probably be spaced somewhat farther apart than previously thought without significantly affecting the smoothness of the channel. This could result in considerable savings in future row-charge excavations. We were also particularly pleased that, as predicted, the height of the lips at the end of the ditch was less than half the height of the lips on the sides--some 14 feet versus 41 feet. This is extremely important for the connecting of ditches. The data obtained from Buggy, Schooner and other experiments have been used to extend and refine our predictive capability.

---

*This paper was delivered by Richard Hamburger, Assistant Director for Technical Operations, Division of Peaceful Nuclear Explosions, U. S. Atomic Energy Commission.

Most dramatic has been the success in developing an explosive for excavation purposes. Based on our success to date, we can assume, due to 1) the amount of scavenging during the venting process, 2) the effect of special emplacement techniques and extensive neutron shielding, and 3) the use of low fission explosives, that the sum of fission products airborne in the radioactive cloud and in the fallout for each nuclear explosive detonated may be expected to be as low as the equivalent of 20 tons. Further, the tritium release may be less than 20 kilocuries per kiloton of total yield, and the sum of the activation products airborne in the radioactive cloud and in the fallout may be expected to be as low as the amounts shown in this chart.

REPRESENTATIVE SET OF INDUCED RADIOACTIVITIES
AT DETONATION TIME
(TOTAL IN CLOUD AND FALLOUT)

NUCLIDE PRODUCTION, KILOCURIE FOR YIELD OF

NUCLIDE	100 KT	1 MT	10 MT
Na^{24}	200	800	2000
P^{32}	0.1	0.4	0.8
Ca^{45}	0.01	0.03	0.06
Mn^{54}	0.1	0.3	0.7
Mn^{56}	600	2000	5000
Fe^{55}	0.04	0.15	0.3
Fe^{59}	0.04	0.15	0.3
W^{185}	6	10	14
W^{187}	300	500	700
Pb^{203}	1000	7000	20000
Other	15	20	40

NOTE: This is not a complete list, and the amounts given may be upper limits rather than best estimates.

In the area of completely contained explosions, analyses of Gnome, Handcar and relevant weapons test data have improved our understanding of such things as cavity and chimney formation, fracture characteristics and containment. Using this data, computer codes were successfully developed and are being improved to predict such effects.

Two application experiments have also been conducted jointly with industry--Project Gasbuggy, the first joint government-industry nuclear experiment to investigate nuclear stimulation of a low productivity gas reservoir, and Project Rulison, the second such venture. The technical results of these experiments will be given in subsequent papers. I am happy to be able to add, however, that the results to be presented on Gasbuggy now make it possible to say that it was completely successful in every respect, including stimulation.

Some progress has also been made in the scientific area in using nuclear explosions to create heavy isotopes. The most successful experiments to date have produced fermium-257, starting from uranium-238, a process requiring 19 successive captures and 8 or 9 subsequent beta decays. Eventually, we hope to produce long-lived isotopes of mendelevium, element 102, lawrencium, and even higher atomic numbers.

While the technology has moved forward since 1964, experiments are still needed to improve our understanding of basic phenomenology. We have to examine the effect of greater depths and different rocks on chimneying and cratering mechanisms; and the interaction of multiple explosions still remains to be investigated both in the contained and cratering area. The possibility of enhancing useful effects and minimizing or eliminating undesirable effects remains to be explored.

Explosive designs suitable for specific applications must be developed. I noted earlier the progress made on the excavation explosive. Similar efforts must be undertaken to design explosives suitable for other applications. In this respect both Gasbuggy and Rulison provided valuable insight into the type characteristics and design trade-offs most appropriate for the gas stimulation application, for example, weighing the costs of using more expensive fuel against savings resulting from reduced product contamination.

Fielding operations must also be streamlined. The single cable emplacement firing technique used by LASL in Rulison was a step in this direction. The radio firing approach being developed by LRL also promises to simplify fielding operations, eliminating the need for ground cable and providing for a more efficient use of equipment and personnel.

The progress made in the non-technical areas of the program has been as significant as the technical advances. In particular, I refer to the Gasbuggy and Rulison projects. As important as the technical objectives was the joint industry-government nature of these experiments. Gasbuggy and Rulison provided invaluable concrete experience in how such cooperative efforts can be realized. Many mistakes were made, as can be expected in any such first undertaking. We, however, have learned from these experiences. More importantly, Gasbuggy and Rulison demonstrated that government and industry can successfully work together to develop this technology.

Another significant development is the increasing interest in the international community--an interest, I might say, which is reflected in the participation in this symposium today. Probably the most graphic example of this interest is the inclusion of an article on peaceful nuclear explosions in the Nonproliferation Treaty, which is expected to come into effect early this year. Article V of that Treaty assures that the potential benefits of the peaceful applications of nuclear explosions will be made available to the non-nuclear weapon states party to the Treaty. It further stipulates that such benefits will be available on a non-discriminatory basis and that the charge for the explosive devices used will be as low as possible and exclude any charge for research and development.

Subsequent to the negotiation of the NPT, the Soviet Union acknowledged that they were pursuing a program in this area and expressed their intention to provide a peaceful nuclear explosion service in conformance with the Treaty. This announcement came in Vienna last April following the first technical talks on peaceful nuclear explosions held between the Soviet Union and the United States.

During the past year, partially as a result of the NPT, the IAEA has become more active in the field of peaceful nuclear explosions. Recently a report was prepared by the IAEA Board of Governors on the Agency's role in connection with nuclear explosions for peaceful purposes. The report concluded, among other things, that the "Agency should approach the subject on an evolutionary basis, devoting its energy initially to the exchange and dissemination of information." Implementing this policy, the Agency is currently planning a panel on the peaceful nuclear explosion technology to be held this coming March.

A third key development in the non-technical area has been the introduction of legislation, during the last two sessions of Congress, to extend AEC's authority to provide nuclear explosion services on a commercial basis. AEC's current authority is limited to projects that have a research, development or demonstration purpose. We contemplate that such a government-provided service would consist of the design and fabrication of the nuclear explosive, its transportation to the emplacement site, supervision of its emplacement in the prepared hole, and its arming and firing. The service would also include appropriate technical reviews, including those related to safety. The user would be responsible, subject to AEC review and approval, for all other aspects of the project, including detailed project definition, preparation of the emplacement site and hole, and operational and safety support.

One of the key factors in the success or failure of our efforts to bring the technology to commercial fruition has been and will continue to be our interaction with the users of the technology in industry, government, or the scientific community. From the beginning we have relied on a continuing dialogue with such groups for guidance and support. We believe that improving and extending this dialogue is essential for the further development of this technology. Accordingly, we have taken a number of steps both to improve communication with users of the technology and to develop more efficient methods of operations to meet the changing needs of the technology as it approaches practical use.

One of the basic steps we have taken has been to reorganize the AEC Plowshare staff both in the field and at Headquarters. Program management responsibility, including that for coordination and cooperation with industry, the public, and other interested agencies and organizations, has been centralized in the Division of Peaceful Nuclear Explosives. In addition, the Nevada Operations Office has established the Office of Peaceful Nuclear Explosives to serve as a central point for working with industry in the design of field operations for joint projects. We believe this reorganization will enable the government to deal more efficiently with our partners in developing this technology.

We also recognize that, if the government's role in providing the technology is to be kept to the minimum, suitable criteria and standards for operations must be developed and published. Government interfaces with the users must be clearly delineated and overall management and operations must be simplified. Effort is underway to accomplish this.

We are also developing a number of planning guides to help industry understand what the government requirement will be for joint projects. Guides on management procedures and safety planning are currently being prepared. In addition, guides will be developed on:

a. Nuclear operations procedures
b. Engineering, construction & support consideration
c. Public acceptance
d. Security and classification considerations
e. Site acceptability considerations

The development of suitable radiation standards for products recovered with the aid of nuclear explosions is another area we are actively pursuing. The Oak Ridge National Laboratory is currently investigating possible exposure pathways to the public from such products and the amount of radiation exposure which might result. We believe such information will permit the progressive and timely development of regulations which are related to the specific condition prevailing at the various stages of development.

We also recognize that there is a very real requirement for seeing that the technical data in the program is made available to the users as expeditiously and as fully as possible. Accordingly, efforts are underway to improve and facilitate the dispersion of technical data generated under the Plowshare program. Open files on projects Gasbuggy and Rulison have already been established at the USBM Office of Mineral Resource at Denver, Colorado; the USBM Bartlevsille Petroleum Research Center at Bartlesville, Oklahoma; and at the University of Nevada, Las Vegas, Nevada. This practice will be followed for subsequent experiments.

In addition, a considerable amount of other data has been identified of interest to the program and action is being taken to make more of this data available to industry. Classification is, of course, part of this question. However, almost all of the data on the explosion effects is unclassified. In addition, on a case by case basis, we have declassified diameters, yields and other characteristics of the nuclear explosives themselves, for example, data on the radioactivity in natural gas. Some data, however, because of security reasons, still remains classified. We are in the process of reviewing this data, and hope eventually to declassify all data not related to the internal design, operation and manufacture of the explosive. Specifically, we hope to declassify all pertinent data on explosive characteristics, such as yield, diameter size, weight, costs and external explosion effects such as debris, neutron flux, etc. Our objective is to declassify all pertinent data and make it available as expeditiously as possible so that industry and others will have everything required to assess the technical and economic factors of any particular project and to evaluate independently the public health and safety considerations.

In addition to the dissemination of technical data, steps have also been taken to make all pertinent cost data available. This past December a paper was presented at the AIF Annual Conference on the Costs of Plowshare Projects, and a report on the hardcore costs of projects Gasbuggy and Schooner was also published. We view these reports as part of a continuing effort to be updated as projects are conducted.

As I indicated above, our relationship with the user, whether it be industry, government, or the scientist, is basic to the successful development of the Plowshare technology. If we are to meet your needs, we must continue to work with you and exchange ideas.

Accordingly, it is in this vein that I would like to offer for your consideration a somewhat different approach to the development of various applications. Specifically, I would like to invite the users or potential users to join with us in developing programs of such breadth and length as to see an application through to the complete evaluation of its potential. In this I believe we need to design multi-year programs to solve the technical, administrative, and sometimes legal problems that exist as barriers to such development. Such programs, I believe, should scope out the developmental functions and costs associated with a particular application. They should consider such things as the sequence and nature of developmental experiments; appropriate related explosive development and testing; the creation or adaption of the necessary conventional production and distribution plants and equipment; and the definition of codes and standards for product use. These total development costs could then be weighed against the potential benefits to be obtained from the use of a developed technology, for instance, the potential increase in natural gas supply and consequent benefits that would be passed on to the consumer. Such an application approach has the added advantage that each project would be viewed in light of its contribution to the development of the total application and not as an individual technical achievement.

In a sense, this is the approach we have been following informally. It certainly is consistent with our current project-oriented effort. However, we believe that such an application-oriented approach as described above would permit both the user and the government to delineate more clearly the potential returns from their investment in the technology. The need for more precise cost-benefit analysis is becoming crucial as government funds for research and development become more scarce and the intensity of the competition for these funds increases. I believe Plowshare can meet both the cost-benefit and the environment tests and prove its worth. I further believe realistic, achievable, and challenging goals will help us in this endeavor.

Accordingly, in closing, I urge you to join in establishing meaningful goals for Plowshare. Now is the time for defining our aims--for determining where and how we are going to go.

We <u>can</u> have natural gas from nuclearly stimulated wells flowing into pipelines by 1975!

We <u>can</u> recover oil from oil shale and copper from low-grade deposits in this decade!

The development of definitive programs to achieve these goals--and achieving them--will require the best efforts of all of us here. I urge all of you to accept this exciting challenge--to give your best efforts to making Plowshare a reality in this decade.

XA04N0739

AN INDUSTRIAL VIEW OF THE PLOWSHARE PROGRAM

By
Sam Smith
Director, Exploration
El Paso Natural Gas Company
January 14, 1970

I was asked to present industry's evaluation of the Plowshare program. However, since I have not polled my colleagues on the various issues, my statements can reflect only my opinions. These viewpoints have evolved from extensive interaction since 1963 with government and industry participants in the Plowshare program.

During the first decade of the Atomic Energy Commission's Plowshare program, the scientific feasibility of industrial applications of underground nuclear explosive technology was established by the Rainier, Gnome, Hardhat, Shoal, Salmon and Handcar experiments.

A new era for examination of the technical and economic feasibility of industrial applications of nuclear explosives began with the Gasbuggy detonation in 1967. This era must be accompanied by close coordination between government and industry which was not required when government alone was establishing scientific feasibility. My talk on "industry's view of underground nuclear engineering" will be concentrated on problems which must be resolved to make the transition from scientific feasibility to technical and economic feasibility.

The distinctions between "contained" and "cratering" applications go far beyond the differences in technology. Cratering objectives have been defined, funded by the government, pursued with a readiness date in mind, and supported by a national policy. Thus far, underground nuclear engineering has enjoyed few of these benefits.

Industry's objective in underground nuclear engineering is to establish a viable enterprise which will benefit the public. While individual company approaches to research and development may vary, their basic needs do not. In the field of underground nuclear engineering, each company requires adequate information to plan effectively and execute responsibilities efficiently.

Industry spokesmen have analyzed and expounded on their needs at hearings, conventions, symposia and industrial meetings. They have done this so often and so well that they have achieved virtually unanimous agreement on the following needs:

1. Establishment of well-defined government organization and policy relating to responsibility and authority so as to eliminate uncertainties as to where responsibility and authority lie.
2. Provision for government budgetary support necessary to sustain the required level of technical and scientific effort on the part of the government.
3. Agreement upon procedures for site evaluation, project definition and project execution.
4. Establishment of safety criteria and procedures.
5. Establishment of a program to develop optimum nuclear explosives designed for individual underground nuclear engineering applications.

6. Development of data on which meaningful standards for product marketability can be based.
7. Improvement in government-industry communication in the technical, scientific and administrative areas.
8. Declassification and dissemination of appropriate reports, data, theories, procedures and techniques developed by the laboratories and other technical contractors to the Atomic Energy Commission.

In recognition of these needs there have been a number of constructive responses from the Atomic Energy Commission. As examples, information is being made more readily available through the establishment of project open files and publication of pertinent reports such as the Nevada Operations Office's NVO-40, entitled "Technical Discussions of Offsite Safety Programs for Underground Nuclear Detonations." Certain organizational and procedural changes, such as the establishment of the Office of Peaceful Nuclear Explosives at the Nevada Operations Office, have been undertaken enabling the government to be more responsive to industry's participation in the Plowshare program. The entry of Los Alamos Scientific Laboratory into Plowshare program work should provide a broader and more flexible base of technical and scientific support. The joint study efforts of El Paso Natural Gas Company and Oak Ridge National Laboratory relating to postshot radioactivity in Gasbuggy gas should provide helpful information in development of product quality standards. Establishment of the Facer group, also known as the

Plowshare Operational Procedures Committee, is evidence of the government's desire to understand industry's capabilities, as well as its practices. These actions do not deal with nor can they solve all the scientific and operational problems of industry and government, but they are tangible demonstrations of progress.

It is at the policy level that governmental response to industry's needs is disappointing. The Bureau of the Budget apparently believes that industry should fund a minimum of 80% of the cost of all research and development experiments. And yet, it is uncertain when government funding will be made available for device design research.

If government's responses at the policy level are evaluated in terms of our nation's need for greatly increased natural gas reserves and the proposed Hosmer legislation, then these responses must be considered inadequate. When government research on underground nuclear engineering is compared to other areas of government energy research and cratering technology, the inequity is apparent.

What appears to be needed is the formulation of a national policy which recognizes the contribution that can be made by underground nuclear engineering in the development of natural resources. This policy support should be sufficient to sustain this research and development program while government and industry resolve their technical and practical problems. Directly or indirectly, this young government-industry Plowshare relationship has encountered virtually every variety of political, budgetary, environmental, legal and public relations problem.

The following are examples of proposed changes which I feel may be detrimental: The Department of the Interior proposed at the Hosmer Bill hearings in May of last year that it acquire a share of the authority exercised by the Atomic Energy Commission. During the week of October 27, 1969, Representative Jonathan Bingham (D.-N.Y.) proposed legislation granting authority to the U. S. Public Health Service for licensing procedures. In addition, this legislation would grant authority to the Federal Power Commission to veto certain Atomic Energy Commission proposals based on judgments relating to the economic and technical feasibility of the projects.

Earlier in October, legislation was also introduced by Senator Mike Gravel (D.-Alas.) and co-sponsored by Senator Edmund A. Muskie (D.-Me.) to establish a 15-member commission to examine the potential environmental effects of Plowshare applications. Therefore, at a time when industry feels there is a great need for government to simplify its operational structure and minimize the points of necessary contact, these may become more numerous and cumbersome.

In view of the potential which appears to lie in the use of nuclear explosives to stimulate natural gas reservoirs, industry is perplexed by the low level of federal funding for underground nuclear engineering. Virtually every authority on the nation's energy supply and requirements is concerned about the future adequacy of gas supply. In its September 1969 report, the Future Requirements Committee, a study group representing the gas industry, in cooperation with the Denver Research

Institute of the University of Denver, estimated that from 1968 to 1990 the United States will require 761 trillion cubic feet of natural gas.[1] This is about 2.6 times the nation's current proven reserves.[2] Recently the Chairman of the Federal Power Commission acknowledged the need for price incentives to promote increased domestic drilling.[3] However, even assuming the FPC found a usable formula tomorrow, the lag between exploration and development of a producing field involves an average time period of about seven years. Moreover, it is reasonable to assume that the recent reduction in the depletion allowance on oil and gas production and the proposed liberalizing of oil import controls will tend to reduce the present low levels of spending for domestic exploration. It had been hoped that nuclear stimulation of natural gas reservoirs and, possibly, in situ oil shale retorting, would help alleviate the gas supply problem. Without question, a higher level of government funding to help develop these technologies could hasten the day when nuclear stimulation might become an important factor in gas supply. To date, there have been only two government-industry projects and these were natural gas reservoir

---

[1] Future Natural Gas Requirements of the United States, Volume 3, September, 1969, prepared by the Future Requirements Committee under the auspices of the Gas Industry Committee.

[2] Reserves of Crude Oil, Natural Gas Liquids and Natural Gas in the United States and Canada as of December 3, 1968, Volume 23, May, 1969, published jointly by the American Gas Association, Inc., American Petroleum Institute and Canadian Petroleum Association.

[3] Speech by Chairman of the Federal Power Commission, John N. Nassikas, before American Gas Association Financial Forum, Scotsdale, Arizona, October 17, 1969.

stimulation experiments. Government and industry presently have three more such applications under study as well as one underground gas storage project, one copper leaching project and one oil shale retorting project. All of these are underground nuclear engineering applications.

In addition to prospective energy fuel shortages, the nation's consumption of minerals will increase greatly by the turn of the century. For example, demand for iron is expected to increase nearly 175%; lead more than 200%; zinc nearly 375%; copper more than 200%; and coal more than 250%.[4] Estimated worldwide percentage increases in fuel[5] and mineral[6] consumption are at least as high, and in most cases, much higher than projections for the United States. Underground nuclear engineering is theoretically capable of helping satisfy such future resource needs. Our international proclamations in support of the Non-Proliferation Treaty leave little doubt that much is expected of Plowshare technology and that this technology will be made available to non-nuclear nations.

Industry is traditionally optimistic, whether it be in the face of adversity or upon embarking on a new venture. In attempting to develop underground nuclear engineering, industry faces both tests at the same time. Underground nuclear engineering is not proven although the need

---

[4] "Mineral Resources in our Environment" by Orlo Childs, given at 13th National Conference of the U. S. National Commission for UNESCO in San Francisco, California, November 23, 1969.

[5] "Forecast for the Seventies," Oil and Gas Journal, November 10, 1969, pp. 162-164.

[6] "Mineral Resources in our Environment" by Orlo Childs.

for it has been established. The development of this technology is complex, yet industry's personnel are handicapped by inadequate information and limited communication with the laboratories' personnel. Efforts to develop accurate economic studies are difficult because device characteristics and cost remain speculative. Consequently, industry is frustrated by lack of greater government action.

There is one further imposing obstacle -- namely, public acceptance. In the Plowshare context, public acceptance requires the satisfactory resolution of related legal, public relations and environmental considerations.

We have unquestionably entered the age of environmental concern. This concern is not new but the intensity and quality of the concern is new. Environmental concern has a long history. There are references to pollution in the Bible and documented pollution problems during the time of the Roman Empire. In the 13th century, an edict was issued against the burning of coal in London because it was contributing to air pollution. In retrospect, it is probably fortunate that this edict was rescinded before the forests of Europe were stripped. Even then the problem of man's energy needs and his environment was complex and required the weighing of alternatives.

We frequently forget that nature is capable of damage to the environment far beyond the capacity of man. Earthquakes, floods, tornadoes, volcanic eruptions, blizzards and droughts have occurred throughout man's history. The point is that both man and nature are potentially destructive. However, many times only the dedicated application of technology has been or is capable of repairing damage to the environment.

Unquestionably, the environment has suffered from the actions of man. Some of this damage has been unavoidable, some the result of ignorance, and unfortunately, some has resulted from lack of responsibility. Fortunately, the prospect of further damage to the environment resulting from irresponsible action is diminishing. However, we must consciously recognize that the expanding population and improved standard of living will require continued modification of our environment.

There are strong indications that the "environmental crisis" may become the major national issue. The reason is that the quality of environment is a matter of universal concern. There have been too many problems, whether real or imagined, created by pesticides, herbicides, fungicides, food additives and air and water pollution to permit relaxation of concern. It is in this context that industry and government are trying to refine underground nuclear explosive technology and seek its public acceptance.

This will be an uphill struggle because there has been and will continue to be opposition even to contained underground explosions. At the present time there is a difference of opinion within the scientific community concerning the adequacy of radiation exposure standards. It is essential that this problem be resolved because in most cases industry's objective will be the production and utilization of natural gas, oil, copper or other products. These products must be marketable to justify industry's, or for that matter, government's continued participation in the development of the Plowshare program. Product quality acceptance by the public is possible if the radiation standards continue to be supported by research and if divergent opinions are spanned by effective communication. This is a plea for perspective which recognizes that, in the long run, man and his environment must both be served or neither will be. Technology, in itself, will not be feared if recognized as the tool and not the master, and profitable operations will become less suspect if they are viewed as a test of efficiency.

It is usually a mistake to try to solve all problems related to a complex technology at once, and this principle certainly applies to underground nuclear engineering. There must, however, be an awareness by industry and government of the problems of the Plowshare program and a joint commitment to solve those problems.

To return to an idea expressed earlier, the best assurance of success would be the establishment of a national objective that recognizes the contribution that can be made by underground nuclear engineering in the recovery of natural resources for present and future generations. Certainly, more rapid progress in the use of this technology will result if government and industry can cooperatively utilize their respective technical and financial resources.

A national objective would also provide a better atmosphere in which diverse groups could contribute more effectively to a solution. Today's situation almost defies solution because of the many factions with differing interests. To be constructive and in the public interest, the act of opposition should carry with it an affirmative obligation and willingness to help develop mutually acceptable alternatives.

Though we live in a world largely of our own making, in many respects our alternatives are limited. The rapidly increasing population is consuming great quantities of the earth's natural resources. The use of underground nuclear engineering can be helpful in making available natural resources while, at the same time, we work to preserve and enhance the quality of our environment. The means of accomplishing these objectives are limited. Government and industry jointly must dedicate their talents and resources toward satisfying natural resource requirements, for to paraphrase Longfellow, "All our strength is in our union." This "union" of government and industry in developing underground nuclear engineering for the common good can occur only when the needs of both partners have been satisfied.

XA04N0740

NUCLEAR EXPLOSIVE DEVELOPMENT

B. Clark Groseclose
Lawrence Radiation Laboratory, University of California
Livermore, California 94550

Introduction

The nuclear explosive itself is the point about which the Plowshare program revolves. The energy potential of a thermal neutron fissionable material such as Pu^{239} or U^{235} of $\sim$17 kt/kg or of Li^6D of $\sim$60 kt/kg is indeed impressive. Such large energy densities allow many applications for nuclear explosives that are unthinkable for conventional high explosives.

This country has been involved in the design of nuclear explosives for almost thirty years. A question often asked is, "Why do we still need design effort on nuclear explosives? Hasn't all the possible design work been done?". In a partial reply, let me give an analogy. Why work on nuclear reactors? They were successful even before the first explosive worked. Why should new accelerators be designed? They have worked for many decades.

The obvious answer to these questions is that new data, new theories, new insights into the problems and thus new possibilities are found and new requirements are continually being formulated. The development of larger and faster computers has allowed an enormous increase in the design calculations for nuclear explosives. Approximations in the physics involved in the calculations must be made in order to obtain solutions in a finite time, but these approximations can be made more accurately as the computing capability increases. Additional calculational capability also allows the designer to examine his design under a variety of possible conditions and configurations. The net effect is a much more sophisticated design. New developments in the area of materials and material properties open doors that have hitherto been closed. We have seen an increasing emphasis on the interaction of the explosive with its environment. Very specific applications require tailored features such as low fission yield, low fusion yield, low residual radioactivity in particular species, small diameter, low weight, low cost, etc.

The Plowshare program in particular imposes stringent requirements on the design of the nuclear explosive since the explosive is to be used in a peaceful environment with the safety of life and property as foremost requirements of the project. In addition, a Plowshare program must eventually compete economically with programs based on conventional sources of energy.

Characteristics of Nuclear Explosives

In the design of a nuclear explosive, two general forms of energy release are available. These are the fission of a heavy nucleus or the fusion of light nuclei. The source of the energy release is clearly demonstrated by a plot of the average binding energy per nucleon as a function of mass number. Both fission and fusion reactions move the resulting mass numbers toward the maximum value of average binding energy per nucleon. Of course, the binding energy is not the only consideration in these reactions. Detailed examination of nuclear properties shows the best isotopes for fission considering reaction cross section, material availability and material properties are U^{235} and Pu^{239}, while the best candidates for fusion are the two heavier isotopes of hydrogen, i.e. deuterium and tritium. Tritium can be produced during the explosion by a neutron reaction with Li^6 so Li^6D can be a fuel for nuclear explosives. The physical characteristics of an explosive (such as size, weight, residual radioactivity, interaction with the environment, neutrons emitted, etc.) depend in great measure on the source of the energy.

Tradeoffs are possible in the design area, and explosives can be tailored to some extent for specific applications. Each desired characteristic can usually be traded-off with other characteristics. For example, the diameter of the explosive can be reduced, but at the cost of increased usage of the fuel materials — which means increased dollar cost. The weight can be decreased with an increase in cost. The residual radioactivity can be reduced with an increase in cost and/or diameter. Because these trade-offs are possible, it is necessary to view the entire operation in which the explosive is involved and minimize the total cost — not just reduce costs in one particular area. For example, it doesn't make sense to drill a smaller diameter hole for a savings of $100,000 in drilling costs if the smaller explosive will cost $200,000 more. It also may not make sense to use a smaller diameter explosive if the clean-up of the additional post-explosion radioactivity costs more than drilling a larger diameter hole. An over-all systems approach is needed in order to present the most economical approach to Plowshare applications.

Because we cannot share all the details of our trade-off information with industrial concerns, it is doubly important that they supply the design laboratories with the results of their analyses. If we have good information on their costs (for example, drilling costs) and their assessment of the problems associated with radioactivity, then we as explosive designers are better able to make rational decisions as to the particular design characteristics to emphasize at this point in time. Since we cannot develop a new Plowshare explosive for each experiment, we must make reasonable compromise decisions and proceed with them. It is desirable that some methods of communication on a classified basis be found.

Plowshare Applications

Plowshare applications fall into three general categories; excavation, underground engineering, and purely scientific. In figure 1 I've noted some characteristics of the ideal Plowshare explosive. These are not quite the ideal characteristics since the ideal explosive leaves no residual radioactivity, is infinitesimally small and light, costs nothing, and has a yield which is continuously selectable from zero on up — before, during and after the detonation. Ignoring these characteristics of the ideal "ideal Plowshare explosive", let me call your attention to the real, ideal explosive.

For excavation, the explosive should leave minimal radioactivity in the crater and fallout areas. This leads to the requirement of minimum fission yield and maximum fusion yield since the fission products contribute very heavily to residual radioactivity. Diameter and weight are not particularly serious problems. It is important that few neutrons be allowed to enter the soil since soil activation could produce a significant part of the total radioactivity.

REQUIREMENTS ON PLOWSHARE EXPLOSIVES

EXCAVATION
- Minimal Post-Explosion Radioactivity
  - Low Fission
  - Minimum Number of Neutrons to Soil
- Reasonable Cost
- Reliable

UNDERGROUND ENGINEERING (Hydrocarbon Stimulation)
- Minimal Post-Explosion Gaseous Radioactivity
  - All Fission
  - Minimum Number of Neutrons to Soil
- Minimum Diameter Consistent With Cost
- Environmentally Hard
- Reliable

SCIENTIFIC (Heavy Element Production)
- Large Neutron Fluence

Figure 1

For underground engineering, fission products (except for Kr^{85}) do not generally appear to be troublesome, but tritium from either the explosive or neutron reactions with trace lithium in the soil is quite a problem where hydrocarbons are involved. Calculations show that approximately 3% of all neutrons which escape into the soil will produce tritium in typical shales. In addition, tritium might be produced in second order reactions if boron is used as a shielding material. Thus for hydrocarbon applications a fission explosive should be used, but with no neutrons allowed to leak to the soil. Diameter might be a serious problem, but device, emplacement, and product utilization costs as a function of diameter must be considered together. The environment seen by this explosive can become quite harsh as evidenced by the current estimate of hydrostatic pressure up to 20,000 psi and temperature up to 450^0F at maximum depth. To protect against these conditions requires part of the available diameter, and thus the environment is a serious constraint on the device design.

The scientific applications thus far pursued by Plowshare relate primarily to attempts to produce very heavy elements by multiple neutron captures in heavy nuclei. These require an explosive which will produce a very large, low energy neutron flux. Another application has been an experiment to measure neutron cross section using the nuclear explosive as the source of neutrons. Device diameter, weight, and cost are secondary concerns for such applications.

Current Status and Future

The current status of specific explosives for these purposes may be described as follows.

A. Excavation

The majority of our design effort for the past few years has been devoted to an explosive for excavation purposes. Several tests at the Nevada Test Site have shown the device to be very reliable. Currently we are redesigning several parts of the device to further reduce the residual radioactivity. If the tests of these changes are successfully executed as scheduled, by the summer of 1970 we will have a design which we are confident can provide any yield desired for excavation purposes. Both residual explosive and soil-induced radioactivity would be at very low levels compared with those expected from a fission explosive. For example, we would be able to provide a 1-Mt crater which would permit, according to the dose criterion of 5r per year or 3r per 3 months, permanent living on the crater lip soon after detonation. This explosive would weigh approximately 15 tons and would measure about 50" in diameter.

B. Underground Engineering

Even though there are several areas of interest in underground engineering, I've directed my remarks to explosives for use in hydrocarbon applications. To this time, the AEC has not developed an explosive tailored to the needs of this program. Explosives have been provided for the Gasbuggy and Rulison events, but these have been spillover from the weapons program. They have left much more tritium than would be left by a specially designed device.

In order for our current design calculations to be most productive, we have made decisions as to the explosive characteristics to emphasize at this time. It appears to us that tritium is of prime importance. Reduced diameter is important, but is probably not worth the price of greatly increased post-explosion tritium. Also, multiple explosions in one hole can reduce the importance of diameter. Thus we have reached a compromise design goal of very low tritium in an explosive of reasonable diameter.

It now appears that we can provide within a year an explosive of less than 12" diameter at a yield of 50 kt and with a very low level of post-explosion tritium. This device would be able to withstand the environment of deep gas stimulation. With additional time for device development and at additional dollar cost per device, an explosive with essentially the same post-explosion tritium and environmental hardness but with a smaller diameter could be developed if necessary. Again the question of diameter should be decided on the basis of over-all system studies. I must emphasize that these statements of what we can do are based on our technical capability and not on our budgetary condition.

Ternery fission in which a triton will be released occurs with a frequency of 1 in 10^4 and thus sets a lower limit on post-explosion tritium of about 0.1 mg/kt. It is probably impossible to keep all neutrons from the soil since delayed neutrons from the fission fragments are emitted with half-lives of up to 56 seconds. If about one-half of these delayed neutrons were captured in soil, they could contribute an additional 0.1 mg/kt of tritium. Thus a reasonable lower limit on tritium is $\sim$0.2 mg/kt or 10 mg from a 50-kt fission explosion. This limit could be approached only with a fission explosive with essentially no prompt neutrons reaching the soil or producing tritium in shielding materials.

C. Scientific

Previously reported experiments conducted by both the Lawrence Radiation Laboratory and the Los Alamos Scientific Laboratory have achieved an effective neutron fluence of approximately 13 gm-moles of neutrons per square centimeter. An experiment conducted by LRL this past summer, the Hutch event, appears to have achieved a fluence about a factor of three higher. Since this entire scientific area will be discussed in detail in another session, I'll forego additional discussion at this time.

Summary

In summary, nuclear explosives have been and can be designed especially for Plowshare applications.

A. Up to this time, excavation has received the major emphasis, and the excavation explosive will be in an excellent position for actual utilization if our presently scheduled experiments for this year are successfully carried out.

B. An explosive especially designed for hydrocarbon stimulation has not been tested, but the current paper studies show that some designs are very promising. A tested design leaving a very small amount of post-explosion tritium could be available within a year of commencing hardware effort.

C. A device to provide a very high neutron flux has been successfully tested, and the continuation of device design effort in this area depends on the scientific value of the information obtainable from such experiments.

Explosive design and development for Plowshare applications has always been an interesting problem. With technical requirements being more and more determined by a striving for the infinitesimal, the future for the explosives designer shows promise of being even more challenging.

A continuing program of device development is needed to assure the optimum explosive for each application at each point in time.

XA04N0741

UNDERGROUND NUCLEAR EXPLOSIONS*

Gary H. Higgins

Lawrence Radiation Laboratory, University of California
Livermore, California 94550

ABSTRACT

In the Third Plowshare Symposium, held in 1964, data from a number of nuclear explosions were presented. At that time the basic elements of the nuclear explosion appeared to be well understood and relationships for predicting the gross nuclear effects were presented. Since that time, additional work has been done and many of the concepts have been extended. For example, nuclear explosions have been conducted at greater depths and with much greater yields. The physical and chemical properties of the material in which the explosions occur have been more accurately measured and related to explosion effects. Interpretation of the new information seems to indicate that the earlier relationships are valid over the ranges of energy and depths for which data is available but that effects relating to cavity and chimney sizes or fracturing had been overestimated at great depths of burst and higher yields.

INTRODUCTION

This paper reviews the state of understanding of nuclear explosion effects that might be applied to industrial or civil engineering works. The word we have used to describe all of these effects is "phenomenology." Figures 1a and 1b describe the effects of nuclear explosions that are included in the definition of this term.

DISCUSSION

Explosion effects relevant to the Plowshare Program, now almost 13 yr old, have been reviewed several times. The Third Plowshare Symposium in 1964 did not have a summary paper on explosion phenomenology, but among the thirty-odd papers included in the Proceedings[1] four established the state of the art as it existed at that time. Boardman, Rabb, and McArthur described their impressions of the importance of geologic factors in determining cavity radii, chimney heights, extent of fracturing, permeability of the wall rock, and so forth. They derived their conclusions in the form of empirical scaling laws based on observations of a number of nuclear explosions performed for weapons testing and Plowshare purposes.

---

*Work performed under the auspices of the U.S. Atomic Energy Commission.

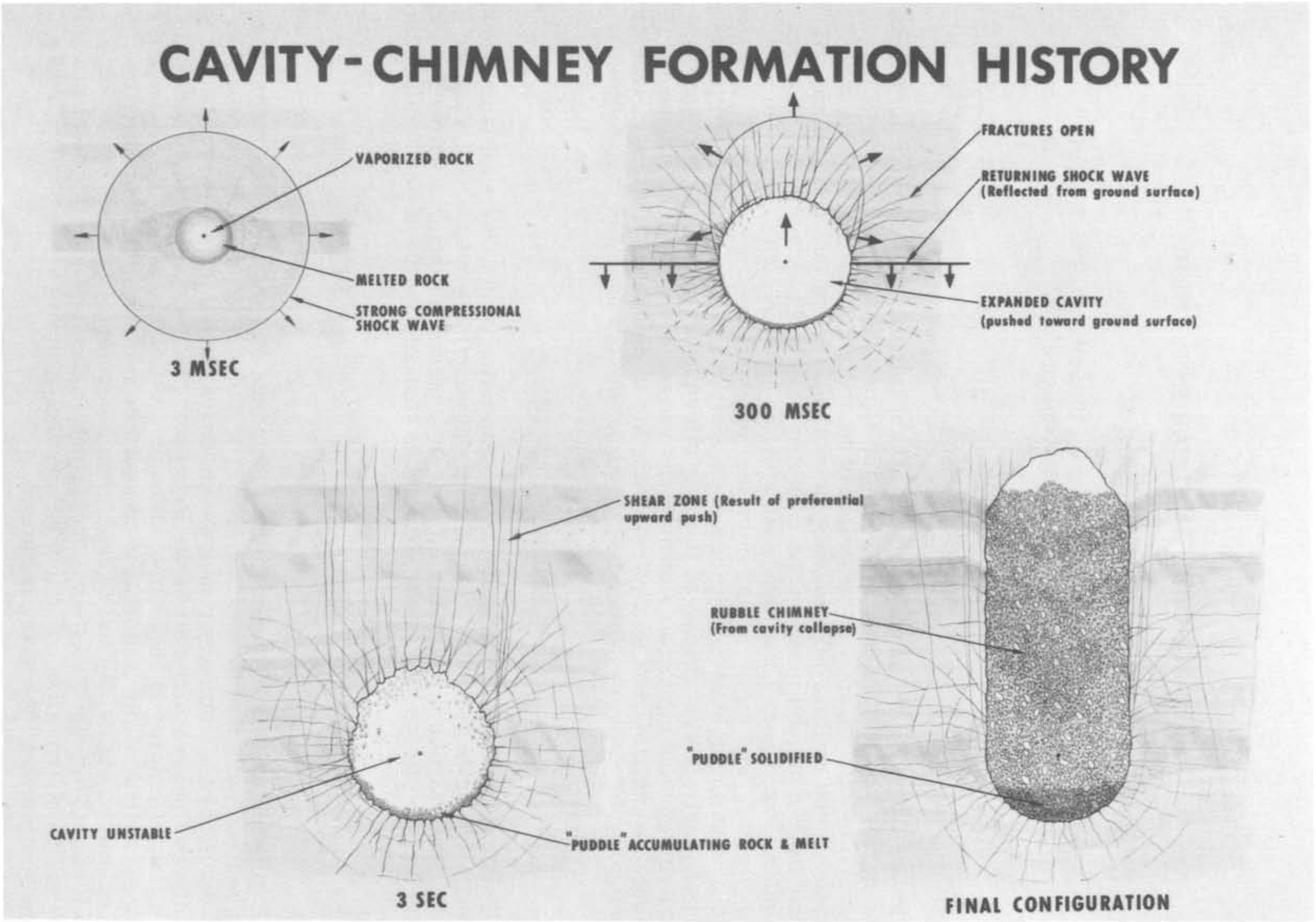
CAVITY-CHIMNEY FORMATION HISTORY
VAPORIZED ROCK
MELTED ROCK
STRONG COMPRESSIONAL SHOCK WAVE
3 MSEC
FRACTURES OPEN
RETURNING SHOCK WAVE (Reflected from ground surface)
EXPANDED CAVITY (pushed toward ground surface)
300 MSEC
SHEAR ZONE (Result of preferential upward push)
RUBBLE CHIMNEY (From cavity collapse)
"PUDDLE" SOLIDIFIED
CAVITY UNSTABLE
"PUDDLE" ACCUMULATING ROCK & MELT
3 SEC
FINAL CONFIGURATION

Fig. 1a. Cavity and chimney formation history.

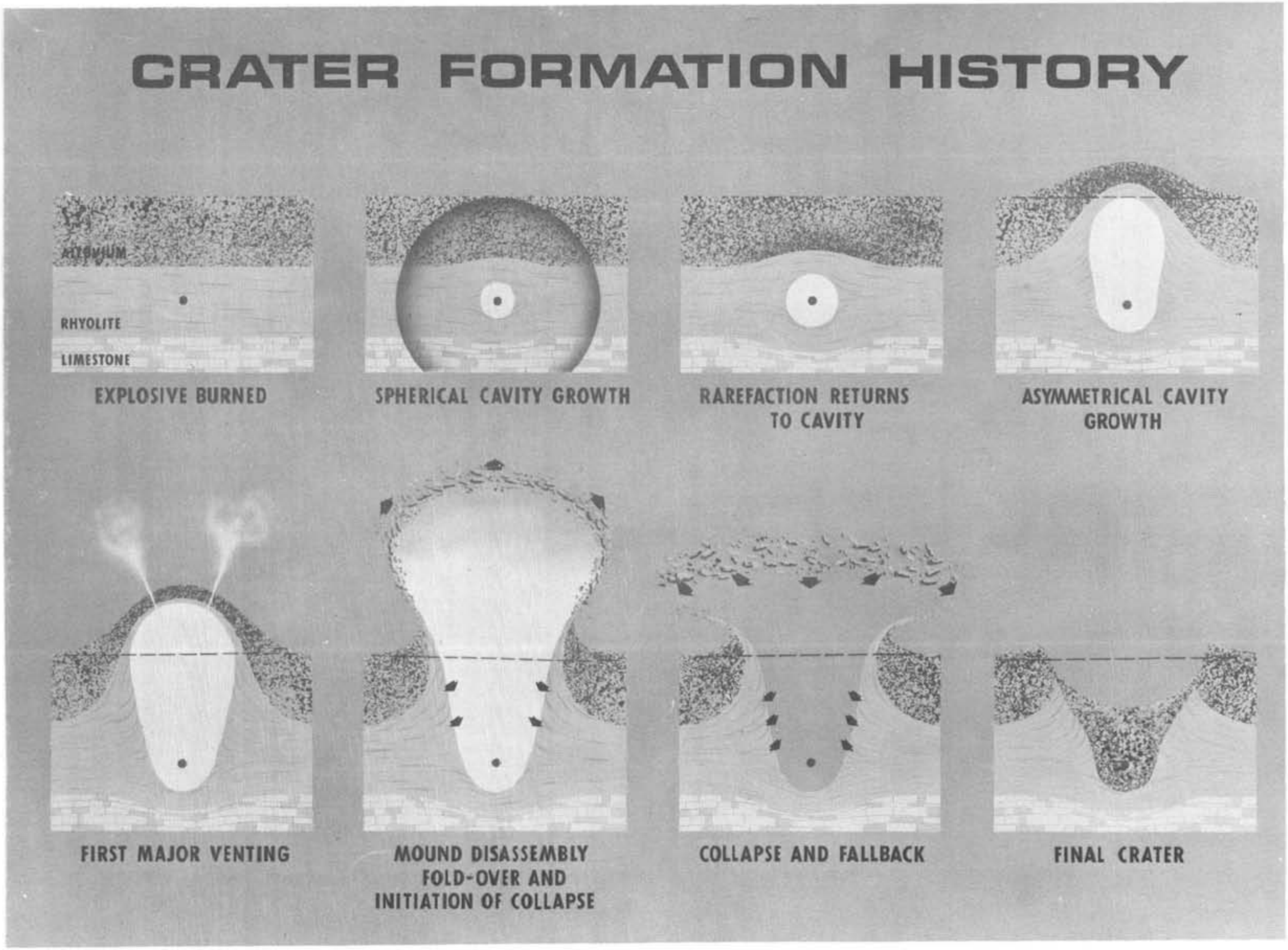

Fig. 1b. Crater formation history.

T. R. Butkovich, in his paper, described the first successful SOC code calculations of explosion effects in which measurable properties of the rock and the conditions of the explosion (such as yield, depth of burst, and so forth) were related through integration of a differenced form of the equations of motion. He calculated the cavity size and the stress amplitude vs distance. He did not attempt a discussion of fracturing, chimney height, or permeability.

Milo Nordyke summarized the state of the art in nuclear and chemical cratering. He presented empirical scaling laws that could be used for predicting crater dimensions from explosive yields and depth of bursts. Separate curves were presented for each material. He also discussed the equivalence of rows of single explosives with continuous line charges for producing trenches and summarized an empirically based scaling theory used by the Soviets for HE cratering calculations.

Knox and Terhune described an attempt to calculate crater dimensions using, for the early part of the calculation, the same method described by Butkovich for deeply buried explosions. After the very early spherical process was complete and as the crater was formed, the material to be excavated was treated as an incompressible fluid with friction. Calibrating friction from one explosion, they were able to reproduce the results of another in the same material but unable to correctly describe craters in a different material.

Since the Third Plowshare Symposium there have been several other papers that have attempted to summarize nuclear explosion phenomenology.[2-5] Reviewing all these documents allows some general conclusions to be drawn. The focus of efforts to understand phenomenology applicable to the Plowshare Program has been understanding those effects that have some applications. In other words, the research conducted in the program has been aimed at applications rather than at purely academic understanding. Efforts to quantitatively explain the cavity size, fracture radius, chimney height, chimney permeability, and permeability of the fractured region for contained explosions and the cratering dimensions, air blast, and radioactivity in dust from cratering explosions have evolved in directions dictated by needs for gas stimulation, ore leaching, harbor construction, canal building, and so forth.

In January 1961 a working symposium was held at the University of Nevada in Reno. At that time nuclear explosion effects applicable to the mining industry were described to the mining faculty and the Bureau of Mines. All of the data—the hard facts—were based on explosions in volcanic tuff, a rock of little practical interest to the mining industry. Their obvious question was, "But what happens in granite?" The 1964 paper of Boardman, Rabb, and McArthur[1] was the answer. Five widely different geologic materials were described. When the Interoceanic Canal was evaluated using nuclear explosives as a hypothetical excavation technique (in 1959), engineers engaged in the study were presented cratering data and speculations based on experience in Nevada Test Site alluvial material. Their obvious question was, "How do craters form in columnar basalt?" Papers in the afternoon session today provide some of the answers.[6]

Thus we see a continual development in which research is used to provide the basis for an engineering assessment of applications. In this dialectic, the research discipline groups evolve theories. Field experiments are conducted, measurements made, the data are analyzed, the theory is modified, and new experiments are designed. Finally, there will be a satisfactory conformity between theory and experiment. This circle of evolution is demonstrated in Fig. 2. Members of the Soviet Academy of Sciences have proceeded in developing their assessment of the Plowshare Program and nuclear explosive phenomenology in much the same way.[7] Their conclusion is:

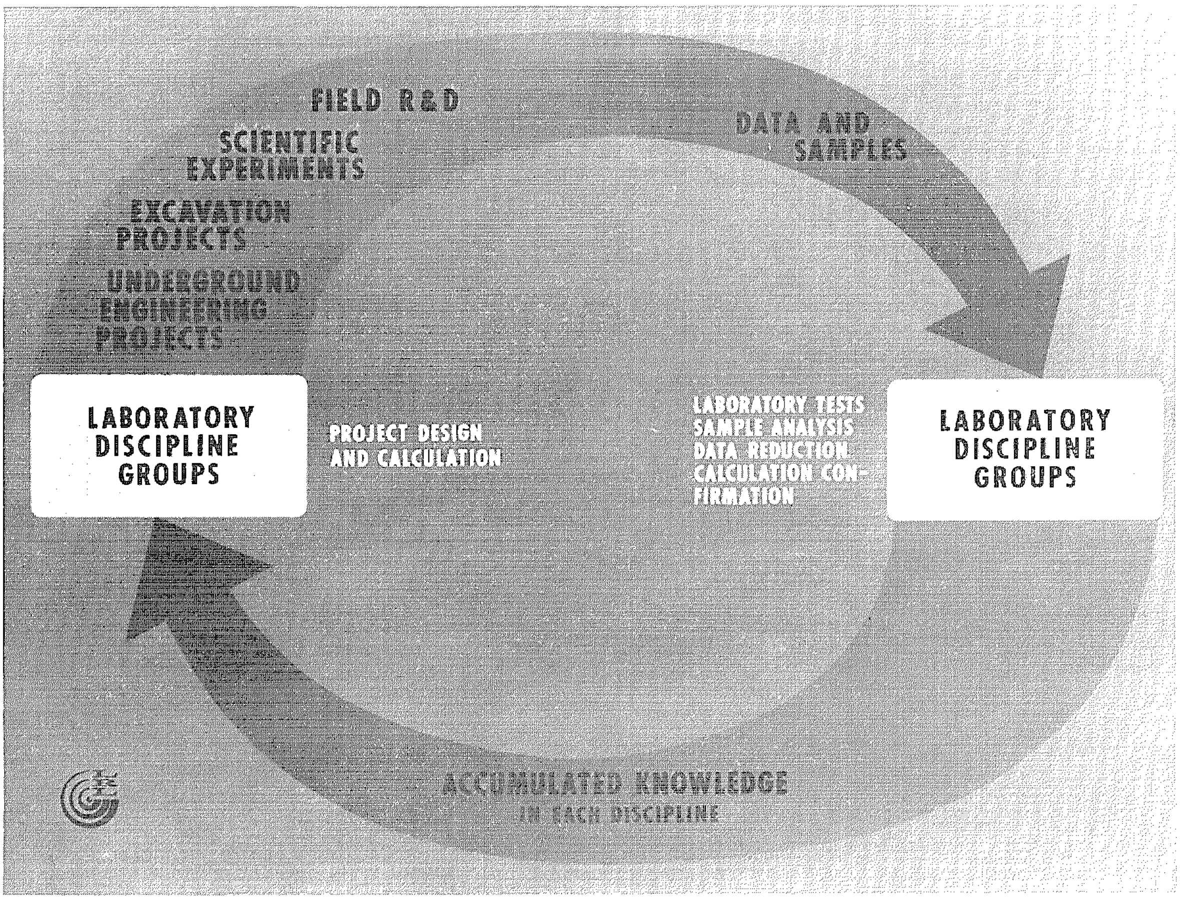

Fig. 2. Circle of evolution of theory and experiment.

> "An underground nuclear explosion is a complex phenomenon, and its description by stages seems to be a waste of time since we shall encounter countless unsolved problems in the process, which will in no way clarify the possibilities of a practical use of the explosion.
>
> "If, however, we decide to analyze the concrete purpose of an explosion, the necessary detailed description of the phenomenon and an adequate evaluation of the desired effects may be obtained with ease even at the present level of knowledge.
>
> "Keeping in mind the pertinent applications possible at the present time, we attempted to isolate the basic parameters of the explosion effect and analyze prognostication methods. We also investigated certain unsolved problems important for practical applications.
>
> "The experience necessary for a more accurate definition of the prognostication of the mechanical effect may be accumulated during the conduct of both types of explosions, industrial as well as investigative."

In the succeeding section evolution of two of the phenomena related to explosions will be examined as examples of changes in understanding.

Following the first series of underground nuclear explosions in volcanic tuff, Johnson and Violet[8] in 1958 published a summary of the phenomenology as it was understood from postshot explorations and calculations. Figure 3 is a reproduction of their understanding of the formation of the chimney. They

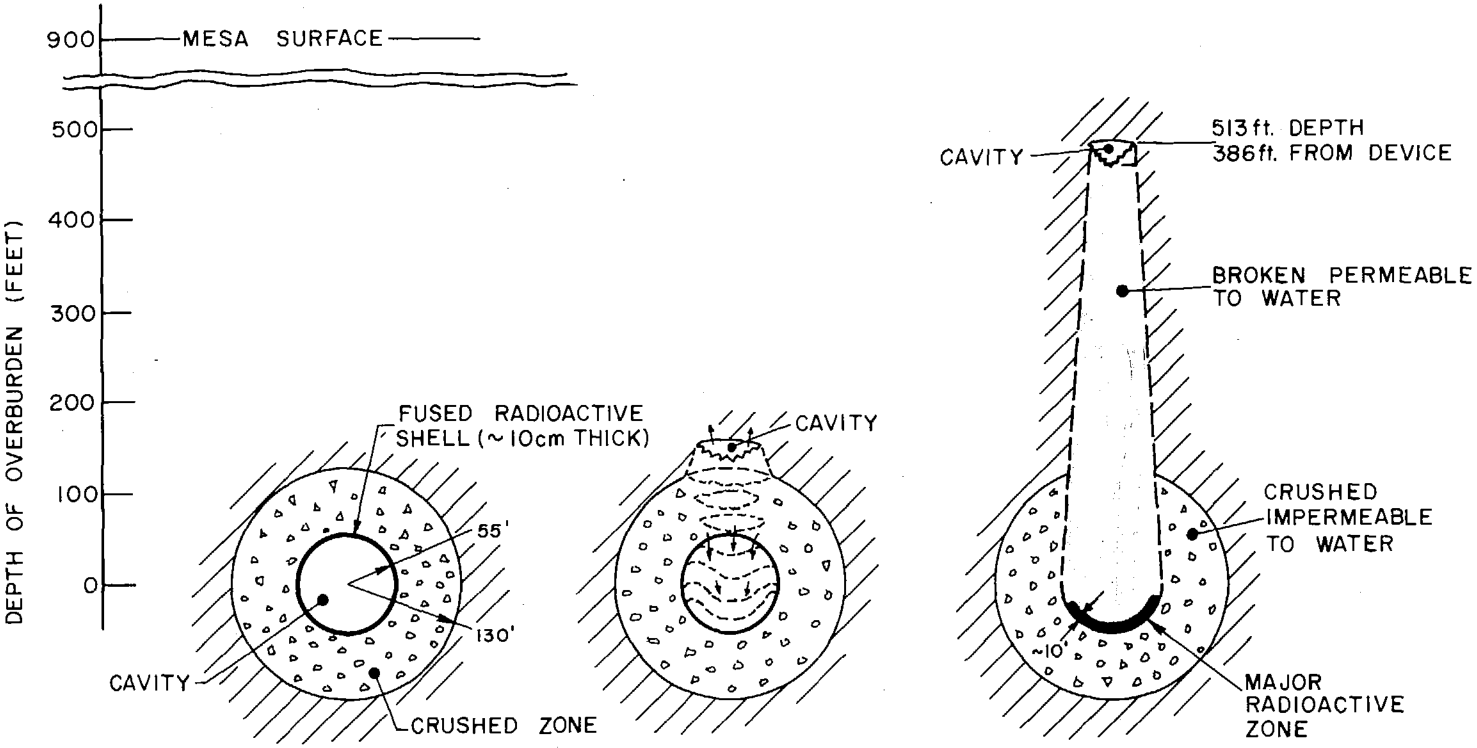

-A-
Cavity before collapse

-B-
Intermediate collapse

-C-
Final collapse

Fig. 3. Strongly affected zones surrounding detonation point (reconstruction).

show an initial cavity surrounded by a crushed region that was, in their view, compacted and impermeable to the migration of fluids. As the cavity in the center of this region collapsed, it formed a broken, permeable chimney that progressed upward roughly 4-1/2 times the radius of the initial cavity.

By late 1964, after experiments in salt and granite had been performed, Boardman, Rabb and McArthur[9] had evolved a somewhat more sophisticated view based on analyses of applications of nuclear explosives to mining. Their concern was almost exclusively with the chimney, which they thought was the most useful aspect of the explosive for mining. They observed empirically that the chimney height in these materials was related to the cavity radius and that the height of broken material was between 4 and 6 times the radius of the cavity. Further, they observed that the cavity radius could be predicted from an empirical equation relating the explosive energy W, the depth-of-burst h, and the material density with the relationship

$$R_c = C \frac{W^{1/3}}{(\rho h)^{1/4}} .$$

The experimental determinations of the constant C varied from 260 to 350, depending on the material. While they discussed the vertical extent of fractures and related it empirically to the cavity radius, their picture of the Rainier Event (shown in Fig. 4) makes no indication of a concern for the fractured radius in other directions or the crushed region described earlier by Johnson and Violet.[8]

As interest in the stimulation of petroleum production grew in the Plowshare Program, more emphasis and interest was focused on the fractured region. Starting with the observations of Rawson[10] of fractures from the Gnome results, Coffer et al.[1] concluded that the fractures that extend beyond the chimney could have a significant effect on gas production in addition to the gas that would be produced by the well bore represented by the nuclear chimney. Subsequently, Cherry, Larson, and Rapp,[11] after several years of research and the development of a model for brittle failure, were able to compute the distance to which fractures would extend. They then observed an amazing coincidence between the limit of fracturing and the height of the chimney, and with this observation they were able, for the first time, to suggest a reason for the anomalously small chimney (only three times the cavity radius) observed in dolomite. Figure 5 is the view of the chimney region that has resulted from all of these conclusions. Note the presence of a spherical fractured region extending in all directions from the explosion point and a chimney resulting from migration of the cavity upward just through the fractured zone.

Later, in the sessions titled "Underground Nuclear Effects I and II," the calculational and experimental methods that allow analysis such as shown in Fig. 5 will be discussed in great detail.

Taking nuclear excavation as a completely different example, the development of the understanding of crater dimensions as a function of explosive yield and depth of burst can be followed. In 1961, Milo Nordyke[12] presented a brief history, analysis, and theory of cratering. He concluded from the analysis of a large number of events in desert alluvium that crater dimensions could be defined by scaling the 3.4 root of the energy and that a curve, as shown in Fig. 6, could be used to derive a radius and depth, given an explosive yield and depth of burst. In addition, he suggested that the calculational method later developed and presented by Knox and Terhune[1] might be used to compute crater dimensions from more basic input parameters. In his paper in 1964, after the presence of subsidence craters was noted in desert alluvium, Nordyke modified the curves to include the effect of material compaction. Figure 7 is his presentation of the radius as a function of depth-of-burst scaling curve

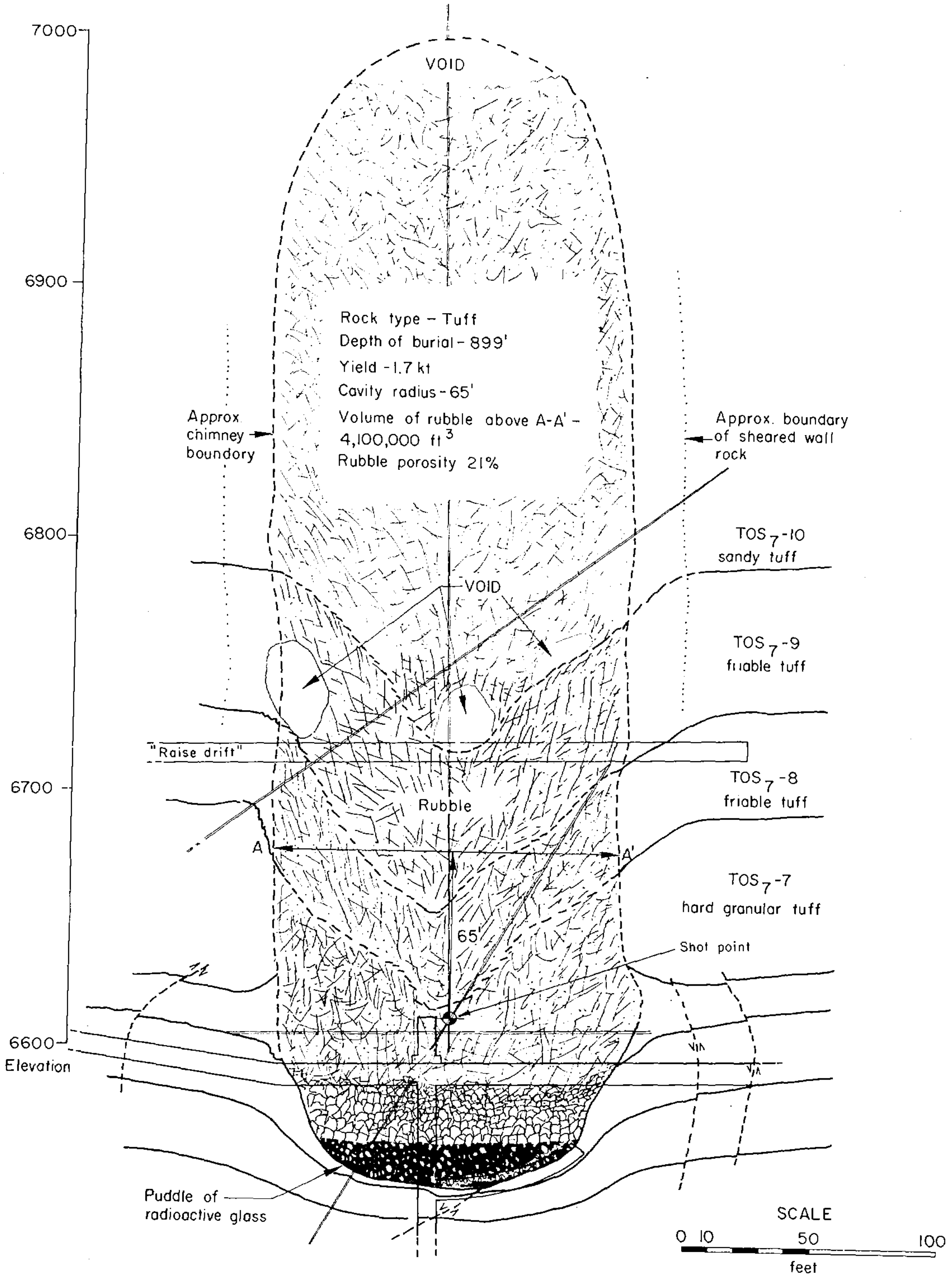

Fig. 4. Rainier schematic cross section.

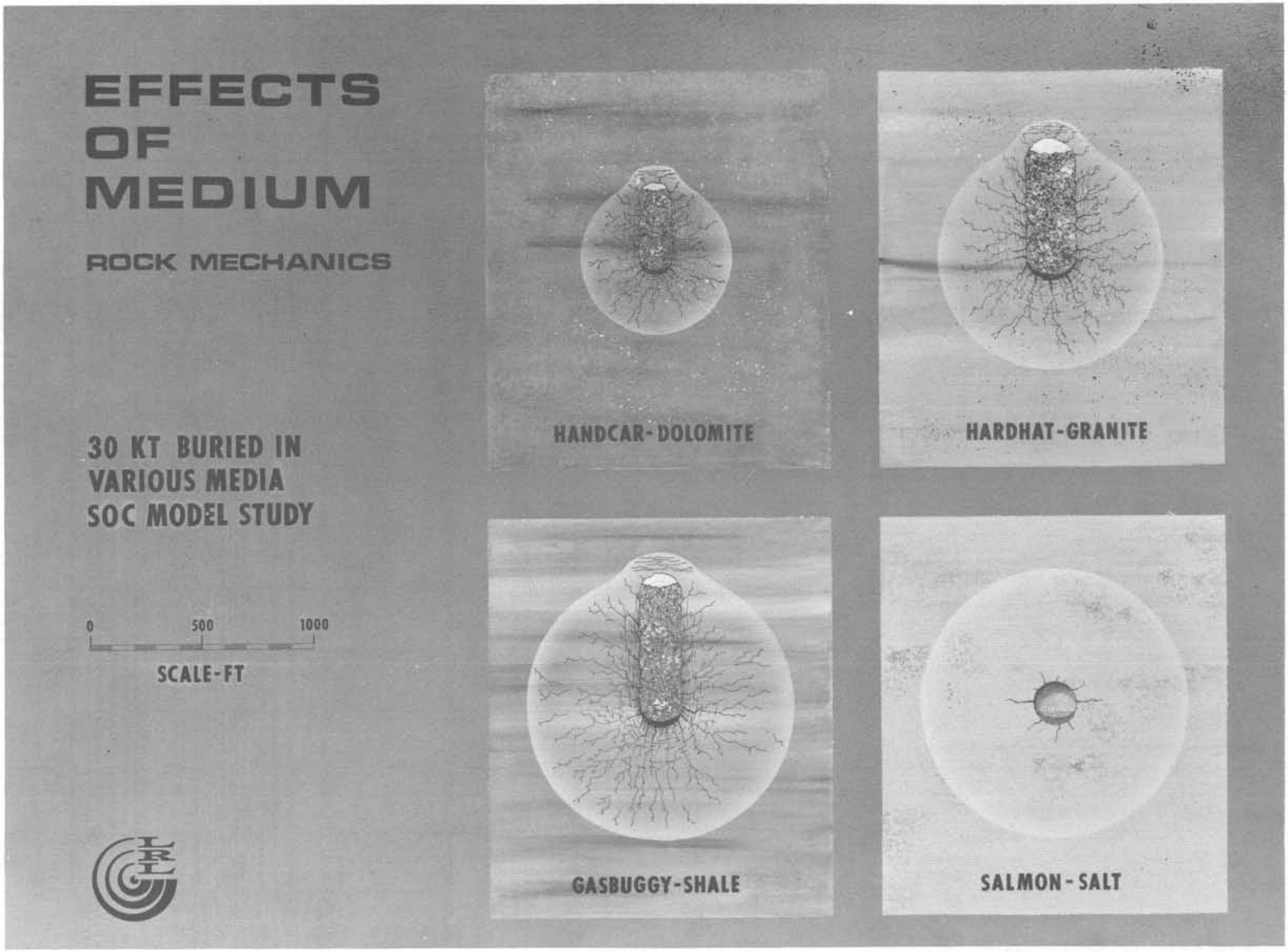

EFFECTS
OF
MEDIUM

ROCK MECHANICS

30 KT BURIED IN
VARIOUS MEDIA
SOC MODEL STUDY

Fig. 5. Effects of the medium on a 30 kt shot.

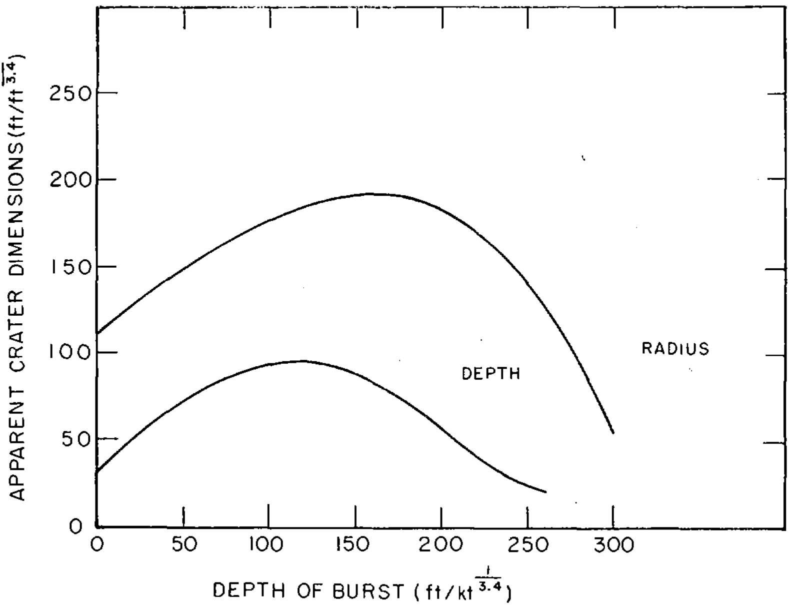

Fig. 6. Correlation of apparent crater dimensions with depth of burst for NTS alluvium. Curves were fitted to the data by least squares. Data are from HE craters.

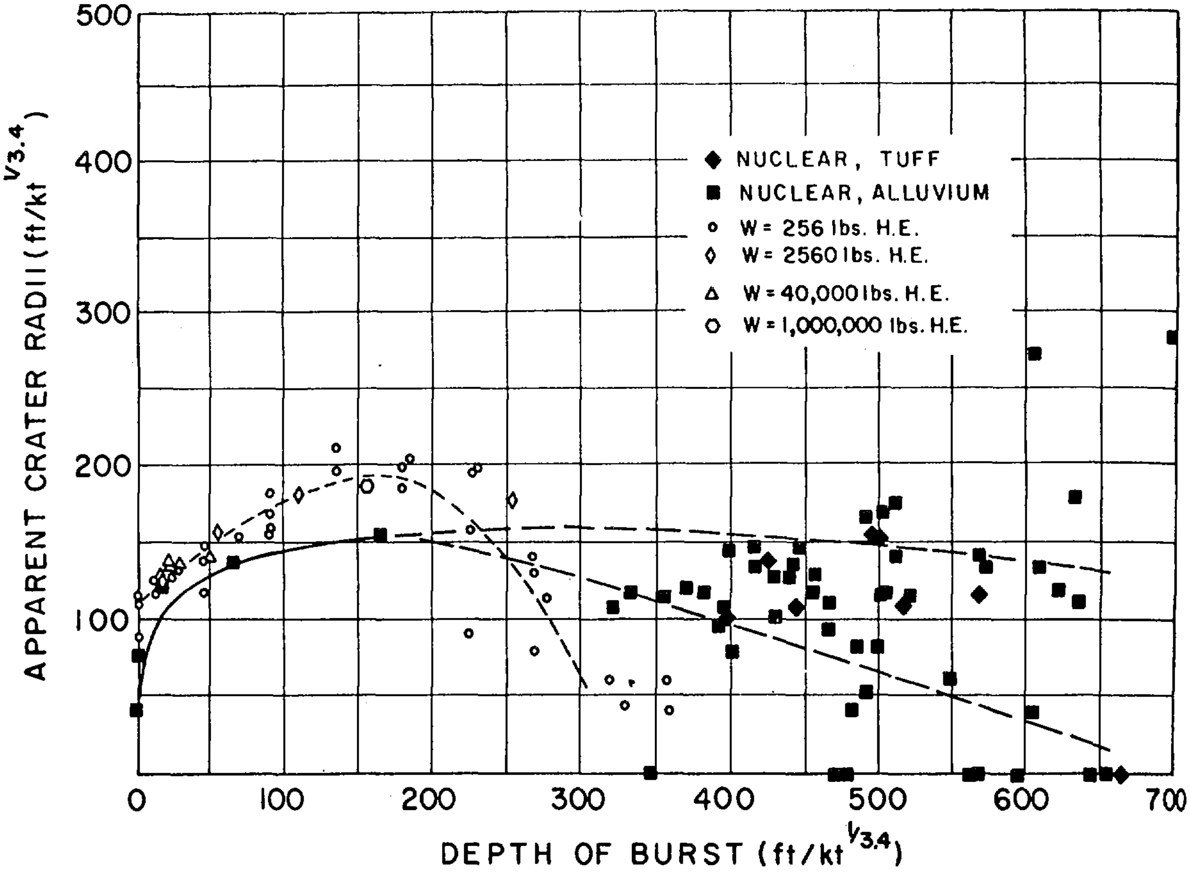

Fig. 7. Correlation of HE and nuclear explosive apparent crater radius with depth of burst for NTS desert alluvium.[1]

still using the 3.4 root of yield. Figure 8 is his presentation of the data as it then existed, applied to basalt. After an additional nuclear experiment in basalt, in which no crater was produced by a nuclear explosion buried at a scaled depth of 183 $ft^{1/3.4}$, Johnson and Higgins analyzed the same data as shown in Fig. 9.

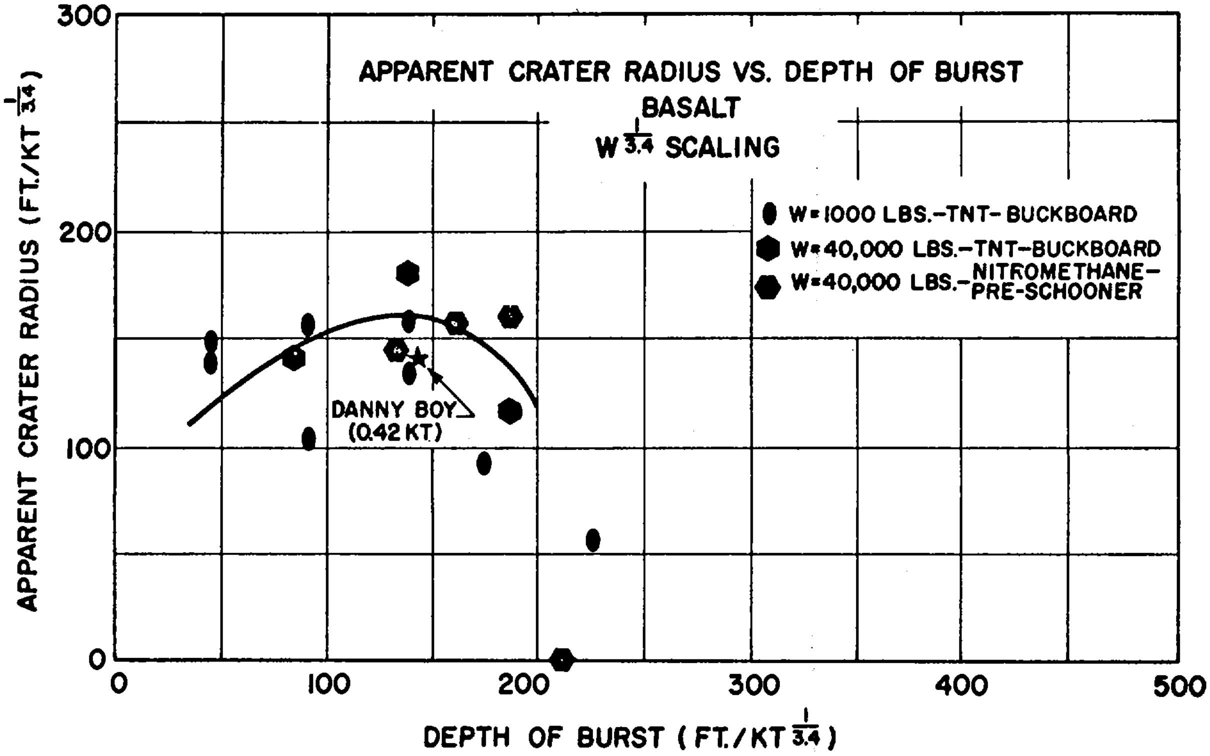

Fig. 8. Correlation of HE and nuclear explosive apparent crater radius with depth of burst for basalt.[1]

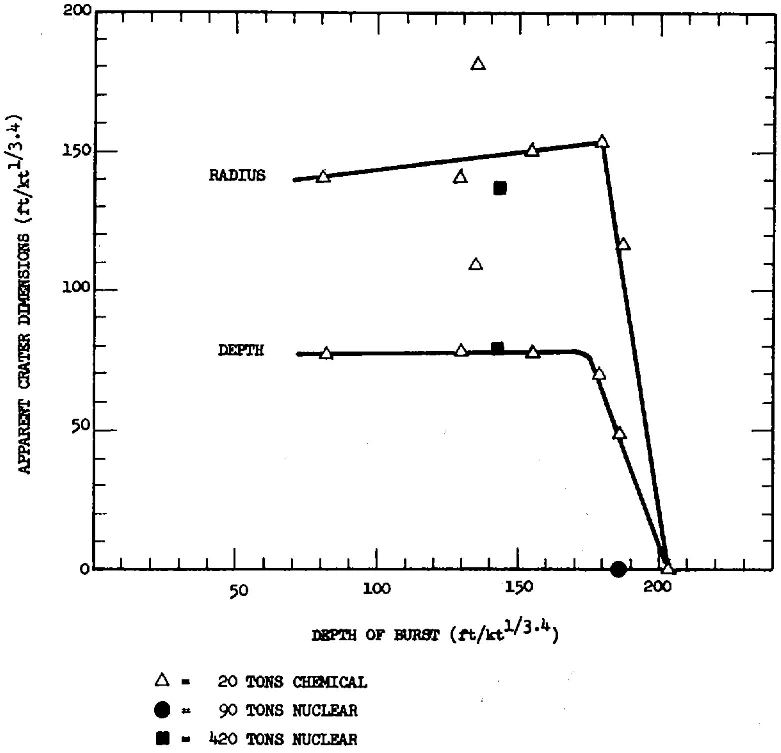

Fig. 9. Fig. 8 reworked using newer data.[13]

The dilemma presented by the failure of the Sulky Event to crater stimulated research efforts in understanding cratering on a more fundamental basis. The development of the understanding of fracturing and materials properties discussed earlier was, at about this time, extended to the two-dimensional problem of cratering using the TENSOR calculation. This evolved through several field experiments and continuing laboratory research until the cratering curves shown in Fig. 10 were calculated. The afternoon session "Excavation I" contains a more detailed discussion of these results.

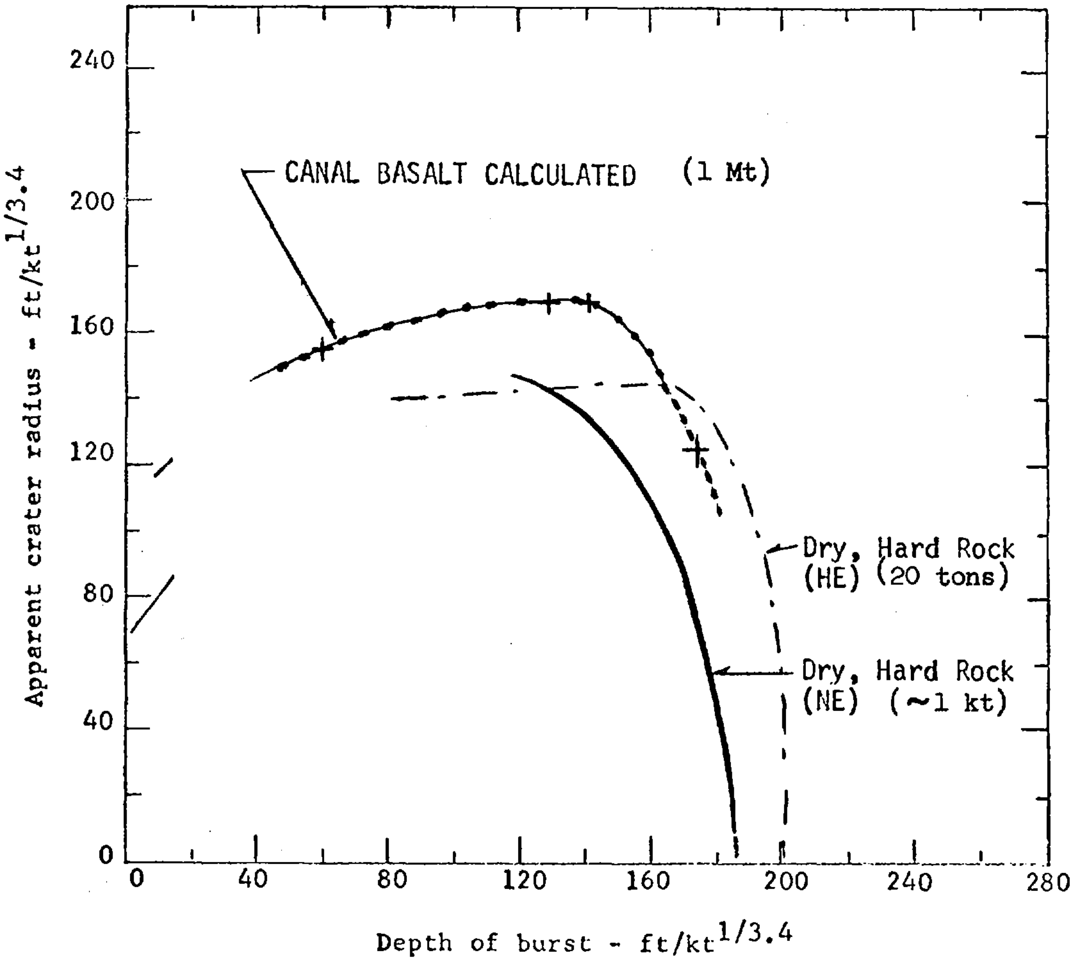

Fig. 10. Further refinement of the correlation of apparent crater radius with depth of burst.

CONCLUSIONS

Examination of past research developments permits one to speculate about the next steps that are likely to be taken in understanding nuclear explosion phenomenology. It is apparent that the application of nuclear explosives to oil shale retorting, minerals recovery, and gas stimulation all depend rather critically on the permeability of the chimney and the fractured region. Although it is now possible to calculate the extent of the fractured region, there is no satisfactory way now available to assess its permeability. There are experimental observations in which no apparent change in permeability follows fracturing. There are other cases in which the permeability seems to vary nonlinearly from a high value near the boundary of the chimney to the value of the preshocked rock at approximately the limit of fracturing. Other possibilities can be imagined, and considerable field and research work will be necessary to determine the parameters that govern permeability.

Practical application of nuclear explosives to gas stimulation depends on detonations at considerable depths of burial—10,000 to 20,000 ft. The current understanding of the effect of confining pressure on materials suggests that many materials will not fracture from explosions at these great depths but the explosions will cause only in spherical cavities surrounded by plastically deformed rather than fractured rocks.

It is also known that pore pressure in rock mitigates the effect of increased confining pressure, causing fractures to occur at a greater than expected depth. No tested method for including the effect of fluid in pores is yet available in the material models used for calculating induced fracturing. Understanding this has particular significance both in understanding the extent of fracturing at great depth applied to gas stimulation and, perhaps, in an increased understanding of the causes of deep-focus earthquakes.

The application of nuclear explosions to construction of harbors and canals is limited by safety considerations of the effects produced by ground shock or air blast. Each of these, in turn, is related to the amount of explosive energy required to create a given excavation. The gas that does the work of excavation in a nuclear explosion is created by shock vaporization. The larger the amount of gas for a given explosive energy, the more work can be accomplished with the same yield. The details of the vaporization process of rock after it has been subjected to high pressure are presently unknown. Limited experience suggests that considerably more gas is produced than is presently assumed. If so, estimates of crater dimensions at larger explosive energies may be underestimated, and unnecessarily conservative safety restrictions may be imposed. These are but a few ideas; as new applications are examined in greater detail, other research questions will undoubtedly arise.

REFERENCES

1. Engineering with Nuclear Explosives (Proceedings of the Third Plowshare Symposium), U.S. Atomic Energy Commission Division of Technical Information Extension, Oak Ridge, Tenn., Rept. TID-7695 (1964).

2. G. W. Johnson and G. H. Higgins, Rev. Geophys. 3, 365 (1965).

3. P. Kruger, Nuclear Civil Engineering, Stanford University, Calif., Department of Civil Engineering Technical Rept. No. 70 (1966).

4. E. Teller, W. K. Talley, G. H. Higgins, and G. W. Johnson, The Constructive Uses of Nuclear Explosives (McGraw-Hill Book Company, New York, 1968).

5. J. S. Kahn and L. S. Germain, Phenomenology and Containment of Underground Nuclear Explosions, Lawrence Radiation Laboratory, Livermore, Rept. UCRL-50482 (1968).

6. This Symposium, papers 1, 3, 4, and 5 of "Excavation I" session.

7. Mechanical Effect of Underground Nuclear Explosions—Moscow, U.S.S.R., 1969, Report of the Institute of Terrestrial Physics of the U.S.S.R. Academy of Sciences.

8. G. W. Johnson and C. E. Violet, Phenomenology of Contained Underground Nuclear Explosions, Lawrence Radiation Laboratory, Livermore, Rept. UCRL-5124 Rev. 1 (1958).

9. C. Boardman, D. Rabb, and R. McArthur, Characteristic Effects of Contained Nuclear Explosions for Evaluation of Mining Applications, Lawrence Radiation Laboratory, Livermore, Rept. UCRL-7350 (1963).

10. D. E. Rawson, Trans. Am. Geophys. Union 44, 149 (1963).

11. J. T. Cherry, D. B. Larson, and E. G. Rapp, Computer Calculations of the Gasbuggy Event, Lawrence Radiation Laboratory, Livermore, Rept. UCRL-50419 (1968).

12. M. D. Nordyke, Principles of Nuclear Excavation, Lawrence Radiation Laboratory, Livermore, Rept. UCRL-6578 Rev. II (1961).

13. G. W. Johnson and G. H. Higgins, J. Brit. Nucl. Energy Soc. 5, 60 (1966).

XA04N0742

ENGINEERING EFFECTS OF UNDERGROUND NUCLEAR EXPLOSIONS

Charles R. Boardman
CER Geonuclear Corporation
Las Vegas, Nevada

ABSTRACT

Useful effects of contained underground nuclear explosions are discussed in light of today's most promising potential applications. Relevant data obtained through exploration of explosion environments of nine U.S. tests in competent rock are summarized and presented as a practical basis for estimating magnitudes of effects.

Effects discussed include chimney configuration, permeability, and volume as well as rubble particle size distributions and extents of permeability change in the chimney wall rock. Explosion mediums include shale, granite, dolomite, and salt.

INTRODUCTION

Currently recognized engineering effects of underground nuclear explosions are simply broken and displaced rock. Data presented at the Third Plowshare Symposium indicated that the magnitudes of these effects were predictable within reasonable limits for both contained and cratering explosions at relatively shallow depth (< 2,000') in alluvium, volcanic rock, granite, and salt. Since 1964, further testing experience has been gained in these mediums as well as in dolomite, shale, and a sandstone/shale sequence.

The cratering data obtained during this period have been summarized and presented at the November 1968 ANS International Meeting in Washington, D. C. (Nuclear Applications and Technology, Vol. 7/ No. 3, Sept. 1969). This paper, therefore, summarizes United States contained explosion data since 1964. Also, because most Plowshare projects under consideration are planned for relatively competent rock, the data from tests in alluvium and volcanic tuff (both relatively incompetent) are excluded.

The parameters of primary interest related to the breakage and displacement of rock resulting from a nuclear explosion include the following:

1. Chimney configuration
2. Chimney void volume
3. Chimney permeability
4. Rubble volume
5. Rubble particle size
6. Permeability of the rock outside the chimney

The magnitudes of these parameters are discussed as functions of explosive yield, depth of burst, and rock type.

CHIMNEY CONFIGURATION

Since 1964 the U.S. has conducted seven contained explosions in relatively dense, competent rock. Basic data from these explosions and subsequent explorations are presented in Table 1 along with Shoal and Hardhat (granite) data which have been revised slightly since the 1964 symposium. Also included are the data from the two coupled contained explosions in salt, Gnome and Salmon.

Cavity radii presented in this table are defined as the radius of the sphered volume of chimney void, determined by analysis of air or gas pressure-time curves. These values correspond quite closely to radii determined by analysis of radiation and temperature logs of post-shot exploratory holes.

As indicated in the table, exploratory data are available for eleven explosions. The chimneys produced by two of these explosions, Dolomite I and II, extended into relatively weak, highly porous tuff and alluvium and, as a consequence, intersected the Earth's surface. Therefore, the only data presented for these two chimneys are those taken from that portion of the chimney in dolomite.

TABLE 1 Basic Data From Eleven U.S. Contained Nuclear Explosions

Medium	Project Name	Date	Depth of Burst ft	Explosive Energy W, kt	Cavity Radius R_c, ft	Chimney Height Above Shot Point ft	$R_c/W^{1/3}$ ft/kt$^{1/3}$
Granite	Piledriver	6/02/66	1,520	61 ± 10[a]	146[b]	910[b]	37.2
	Shoal	10/26/63	1,208	13.1 ± 1.2[a]	88[c]	356[c]	37.3
	Hardhat	2/15/62	939	4.9 ± 1.5[a]	64[d]	281[e]	37.7
Shale/ Sandstone	Gasbuggy	12/10/67	4,240	26	85[f]	333[g]	28.6
	Rulison	9/10/69	8,430	40	*	*	
Dolomite	Handcar	11/05/64	1,320	12 ± 1[h]	68[i]	223[i]	29.6
	I						30.0
	II						29.5
Andesite	Longshot	10/29/65	2,300	80	*	*	
Salt	Gnome	12/10/61	1,184	3.4 ± 0.5[h]	61[j]	90[k]	40.5
	Salmon	10/22/64	2,716	5.3 ± 0.5[h]	54[l]	54[m]	31.0

---

* Not yet determined

a. LASL Radiochemistry Dept.
b. Boardman, Oct. 1967
c. Boardman, Sept. 1966
d. Boardman, June 1965
e. McArthur, Feb. 1963
f. Ward and Lemon, Sept. 1968
g. Rawson, et al, Sept. 1968
h. LRL Radiochemistry Dept.
i. Boardman, Dec., 1966
j. Tracy, 1961
k. Rawson, et al, 1964
l. Boardman and Booty, Apr. 1965
m. Rawson, et al, July 1966

Chimneys in competent rock other than salt are found to approximate upright cylinders with generally rounded tops and bottoms. The chimney radius is somewhat greater (10-20%) than that of the final cavity prior to collapse and the height above shot point varies between 3.3 and 6.2 times the cavity radius. The chimney height/cavity radius relationship is presented graphically in Figure 1. Two chimney radii have been determined directly by underground excavation (Piledriver and Hardhat), and one (Handcar) by optical survey. These measured values are presented in Table 2.

The observed symmetry of the Hardhat chimney with respect to the shot point is excellent; the measured radius being essentially the same on one side as on the other. Since only one point was determined for Piledriver, its degree of symmetry is unknown. The Handcar chimney, on the other hand, is asymmetric, at least near the apex. Here the chimney axis is displaced approximately 23 feet from a vertical projection of the shot point; the direction of displacement being approximately the same as the dip of the dolomite beds. It is possible, therefore, that separations along the inclined bedding planes may have contributed to the asymmetry.

In order to properly design nuclear explosion projects, a means of estimating chimney height and radius is essential. The basic parameters needed are the initial cavity radius and the bulking characteristics of the rock. The extent to which calculated explosion-produced fracturing takes place is also useful for explosions which produce a sufficiently small void span to permit a stable arch to be formed (Cherry, May 1968).

The empirical basis for calculating cavity radii in relatively dense competent rock covers the range of yields desired for currently planned projects and will soon cover the range of desired depths. Fortunately, extrapolations from results in alluvium and tuff are no longer necessary.

The granite and dolomite data provide a conservative basis for estimating cavity radii for relatively shallow contained Plowshare explosions (< 2000'). The simple cube root energy scaling equation appears adequate at these shallow depths.

$$R_c = CW^{1/3} \qquad (1)$$

where R_c = Cavity radius, ft
C = 37.4 for dense silicate rocks (2.5-2.7 g/cc)
29.7 for dense dolomite and limestone (2.7-2.8 g/cc)
W = Explosive energy, kilotons

Deeper explosions are expected to produce proportionally smaller cavities because of the greater lithostatic load against which the cavity must expand. This is illustrated by the curves in Figure 2. This plot indicates that the Gasbuggy (shale) explosion at 4,240 ft produced a much smaller cavity than would be expected from an explosion of comparable yield in granite at considerably shallower depths (1000 to 1500 ft).

The relative effect of the lithostatic load is masked by differences in the expansion properties of vaporized granite and shale as well as differences in

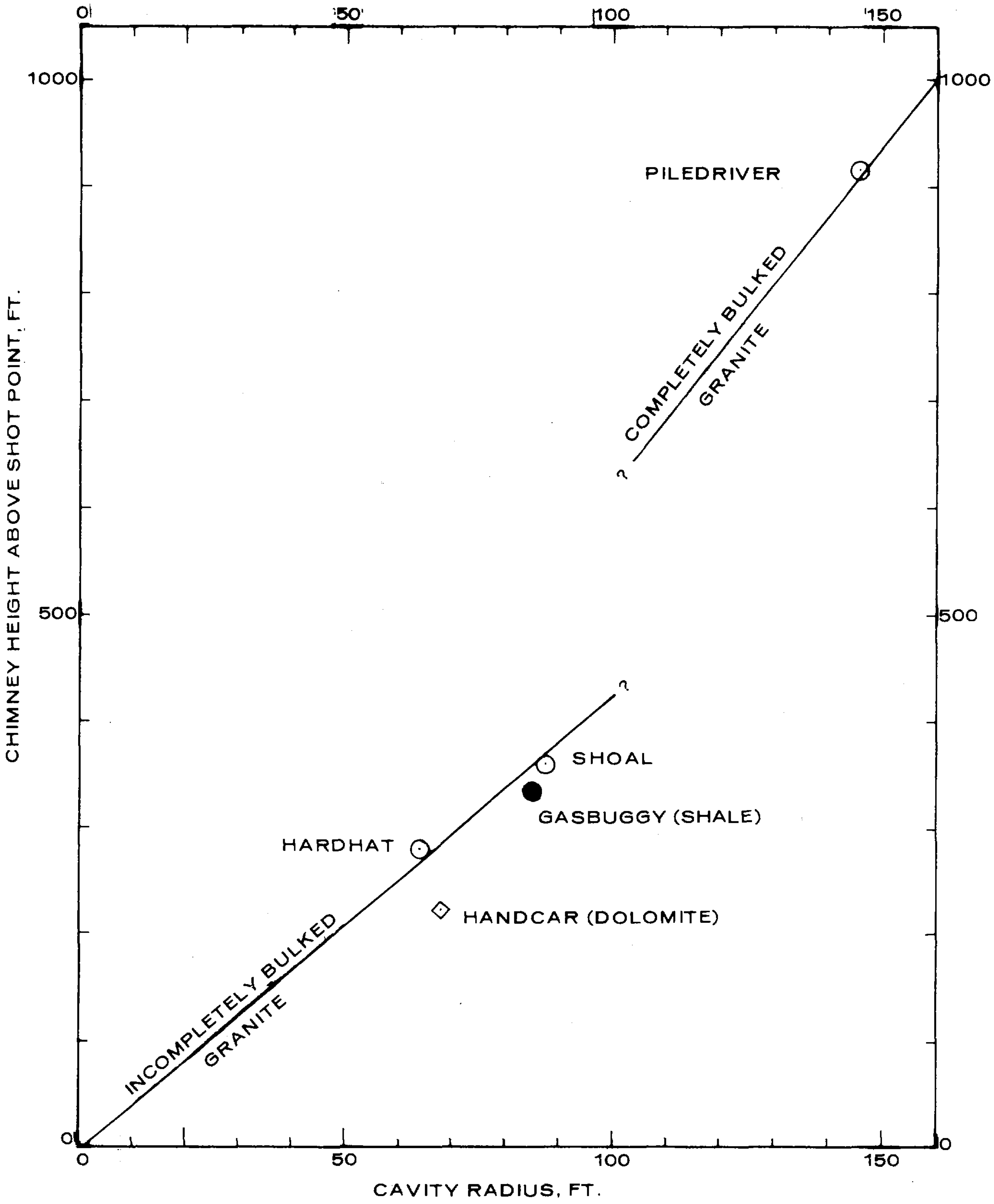

Figure 1

Chimney Height as a Function of Cavity Radius

TABLE 2 Maximum Observed Chimney Radii

Explosion	Vert. Distance of Measurement Point Above Shot Point Level, ft.	Cavity Radius, R_c, ft.	Maximum Observed Chimney Radius, R_{ch}, ft.	R_{ch}/R_c
Hardhat	90	64	69[a]	1.08
Piledriver	100	146	160[b]	1.10
Handcar	185	68	82[c]	1.20

---

[a] McArthur, Feb. 1963

[b] Rabb, Oct. 1968

[c] Boardman, Dec. 1966

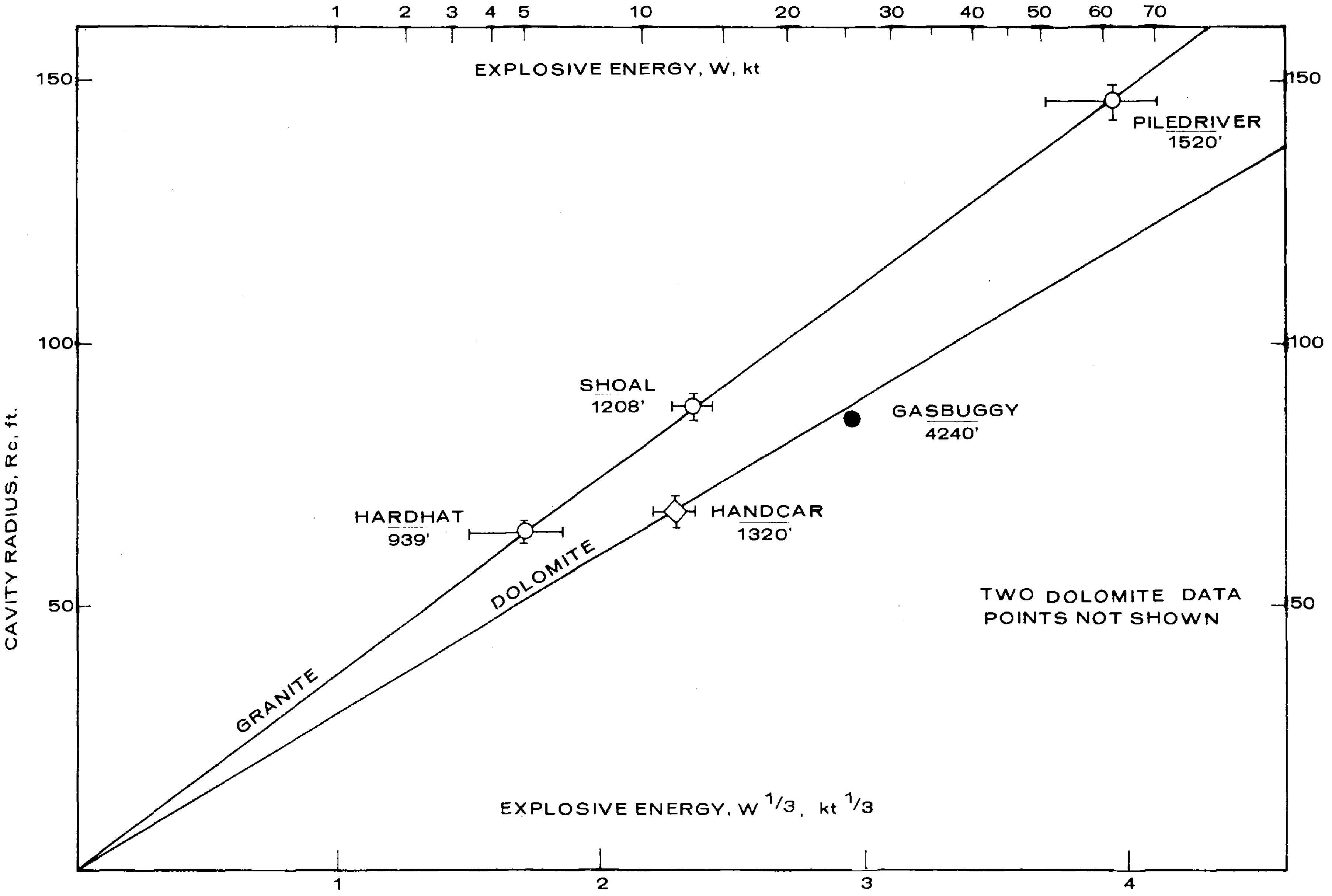

Figure 2 Cavity Radius as a Function of Explosive Energy

the permanent compaction of the rock during cavity expansion. The expansion properties of vaporized granite and largely silicate shale with a low water content should not be significantly different. (Higgins and Butkovich - Feb., 1967)

The in-situ bulk compactibilities of these two rocks on the other hand are not well known. Loading and unloading tests on small consolidated specimens (Stephens, et al, March, 1969) indicate that the Lewis shale from Gasbuggy is considerably more compactible than the granodiorite from Hardhat. While extrapolation of such responses of laboratory specimens to those of jointed, faulted, and/or bedded rock masses is risky, it is probably safe to assume that, at a minimum, Lewis shale would undergo at least as much compaction as granite. Based on this assumption, conservative engineering approximations of silicate rock cavity radii at intermediate depths can be made by interpolation between the shale (Gasbuggy) and granite (Piledriver, Shoal, Hardhat) values.

A scaling equation such as that of Higgins and Butkovich (Feb., 1967) is useful in such an interpolation. This equation is:

$$R_c = C \frac{W^{1/3}}{(\rho h)^{\alpha}} \qquad (2)$$

where R_c = Cavity radius, ft.
W = Explosive yield, kt
ρ = Overburden density, g/cc
h = Depth of burst, ft.
α = .324 for dense silicate rock (2.5-2.7 g/cc)
C = 580 for shale
509 for granite

At shallow depths (< 2,000'), however, the existing data do not fit this equation as well as equation (1). For a given rock type, the values of C shown in Table 1 do not vary significantly (within ± 2-3%) while the empirical constants calculated using the Higgins/Butkovich equation for both dolomite and granite data vary within about ± 20%. Three possible explanations of this rather wide variation are that at shallow depths:

1. The bulk compactibility of the rock exerts such a large influence on cavity size that the overburden effect is dwarfed.

2. The seismic wave reflected from the surface may assist in additional cavity growth by relieving some of the stress against which the cavity gases are expanding, and/or

3. The approximation of lithostatic pressure may not be valid due to tectonic stresses.

Having obtained an approximation of the cavity radius, the chimney radius and height can be estimated by the relationships:

$$R_{ch} = 1.1\, R_c \qquad (3)$$

where: R_{ch} and R_c are chimney and cavity radii in consistent units

and $H_{ch} = KR_c$ (4)

where H_{ch} = Chimney height above the shot point, ft.

R_c = as previously defined

$K = 4.4 \pm^{1.8}_{1.1}$, based on existing data

Exploration by drilling into the shot point region indicates that the zone of rock just outside the cavity is highly porous, brittle, and consequently weak (Boardman, Oct., 1966). It is expected that the failure of the rock in this zone upon collapse of the cavity is primarily responsible for the observed differences in R_c and R_{ch}.

The rather large variation in observed chimney heights can be attributed to a combination of differences in bulking characteristics and capability of the rock to support a stable arch. Of the five chimneys for which the chimney heights have been determined, three were found to have fairly large apical voids; Handcar, Shoal and Hardhat. The Gasbuggy and Piledriver chimneys apparently bulked completely full. LRL downhole photographs of the Handcar and Piledriver chimney apices are presented in Figure 3 and 4, respectively.

It is possible that the diameter of the Piledriver chimney (~320 ft) was too large for an arch to form. The next largest granite chimney diameter, that of Shoal (~195 ft), was sufficiently small to permit formation of a 36 ft high void (Boardman, Sept., 1967). Hardhat (diameter 138 ft) also had an apical void with height of 34 ft (McArthur, Feb., 1963). The percent voids in the rubble of the granite chimneys have been estimated as follows:

Piledriver, 18% Shoal, 23% Hardhat, 20%

Because of this rather close agreement, had the Shoal and Hardhat apical voids collapsed, the chimney height scaling constants, K would have varied within a more limited range; probably about 5.7 ± 10%.

The percent voids in the Gasbuggy chimney rubble is estimated to be ~25% while that of Handcar is only 13%. Had the Handcar chimney bulked full with rubble it is estimated that its K value would have been about 6; close to that of Piledriver. Based on these considerations, a practical upper limit for the chimney height scaling factor K would seem to be ~6 - 7.

CHIMNEY VOID VOLUME

The current basis for estimating the amount of chimney storage volume in relatively dense, competent rock is provided by the results of low pressure air injection tests on four chimneys -- Hardhat, Shoal, Piledriver, and Handcar, and high pressure gas flow testing on the Gasbuggy chimney. The measured void volumes are presented in Table 3 and plotted as a function of explosive energy in Figure 5.

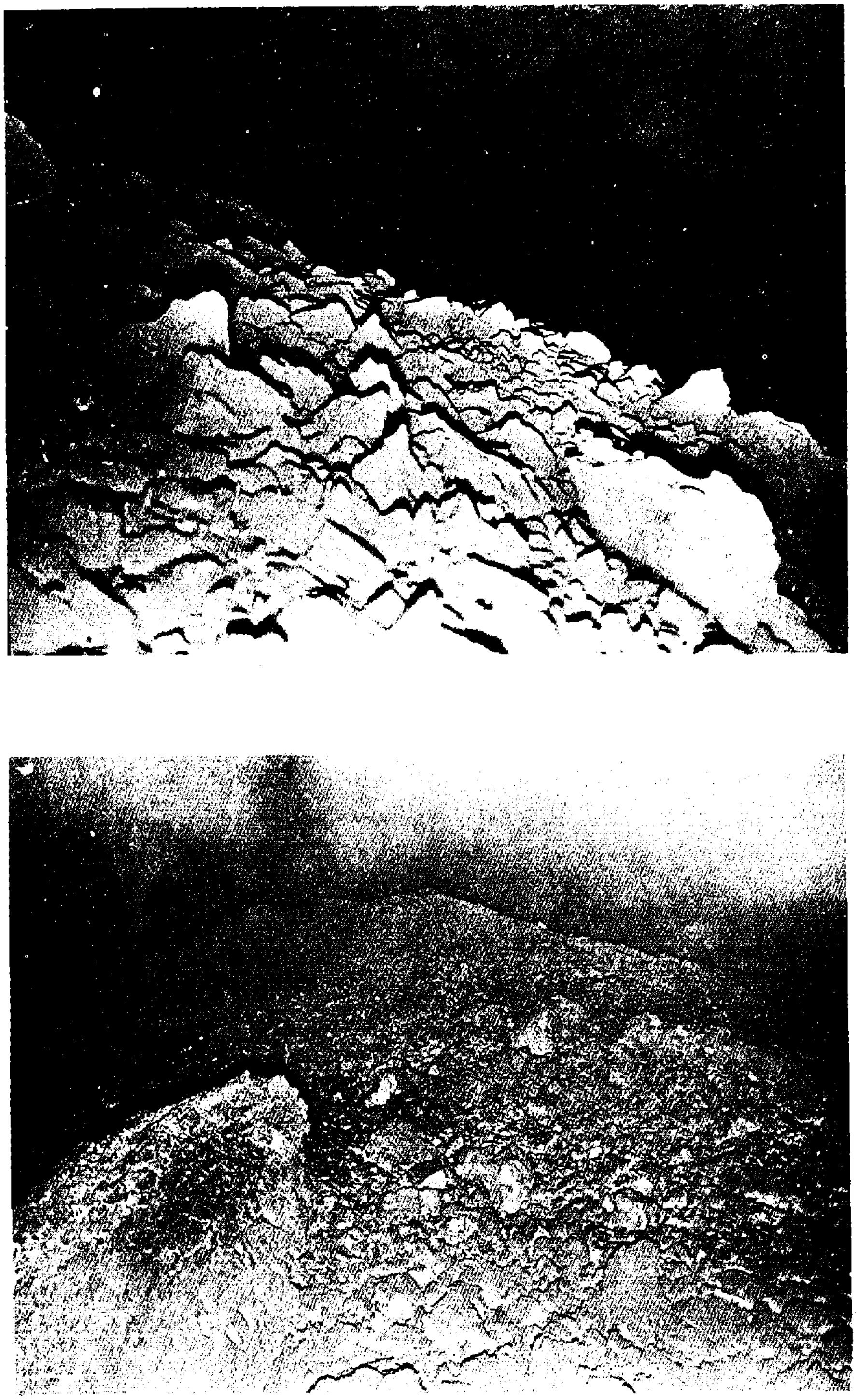

Figure 3

LRL Downhole Photographs of Handcar Chimney Apex
(Boardman - December 1966)

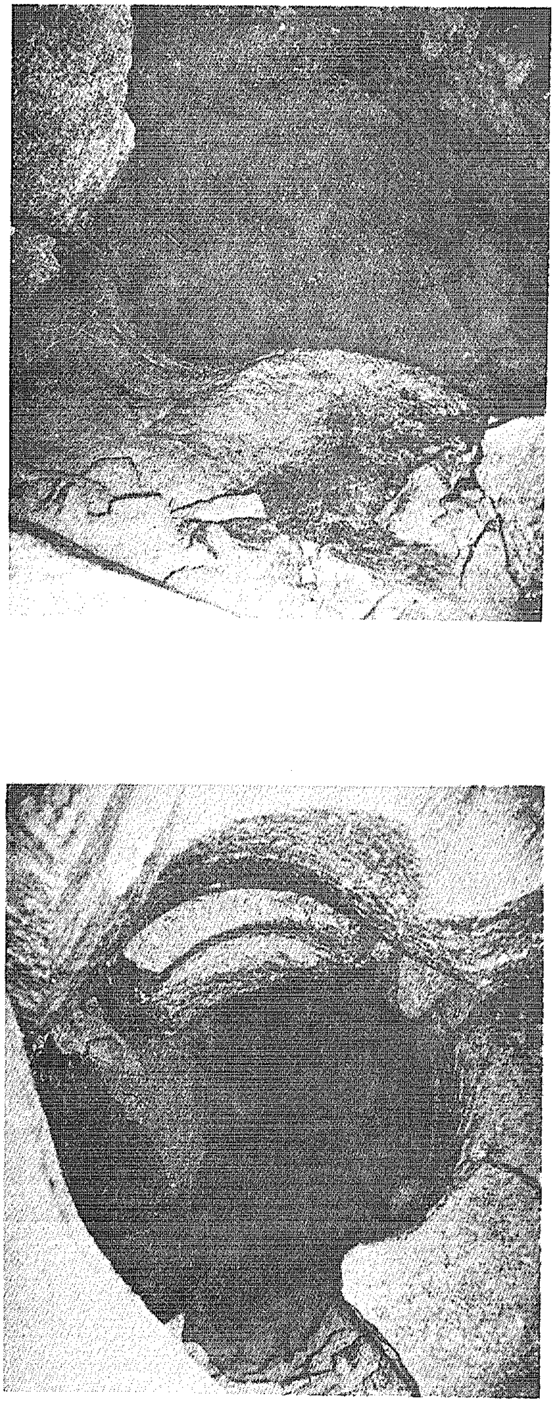

Figure 4

LRL Downhole Photographs of the Piledriver Chimney Apex
(Hole diameter is ~ 10 inches) (Boardman - October 1967)

TABLE 3 Measured Chimney Void Volumes in Dense, Competent Rock

Rock Type	Project	Explosive Energy, W, kt	Chimney Void Volume, V_c, Million ft.	V_c/W $10^6 ft^3/kt$
Granite	Hardhat	4.9±1.5	1.09±.1	.227
	Shoal	13.1±1.2	2.85±.3	.217
	Piledriver	61±10	13.0 ±1.3	.213
Dolomite	Handcar	12±1	1.31±.13	.108
Shale	Gasbuggy	26	2.6	.100
	Rulison	40		

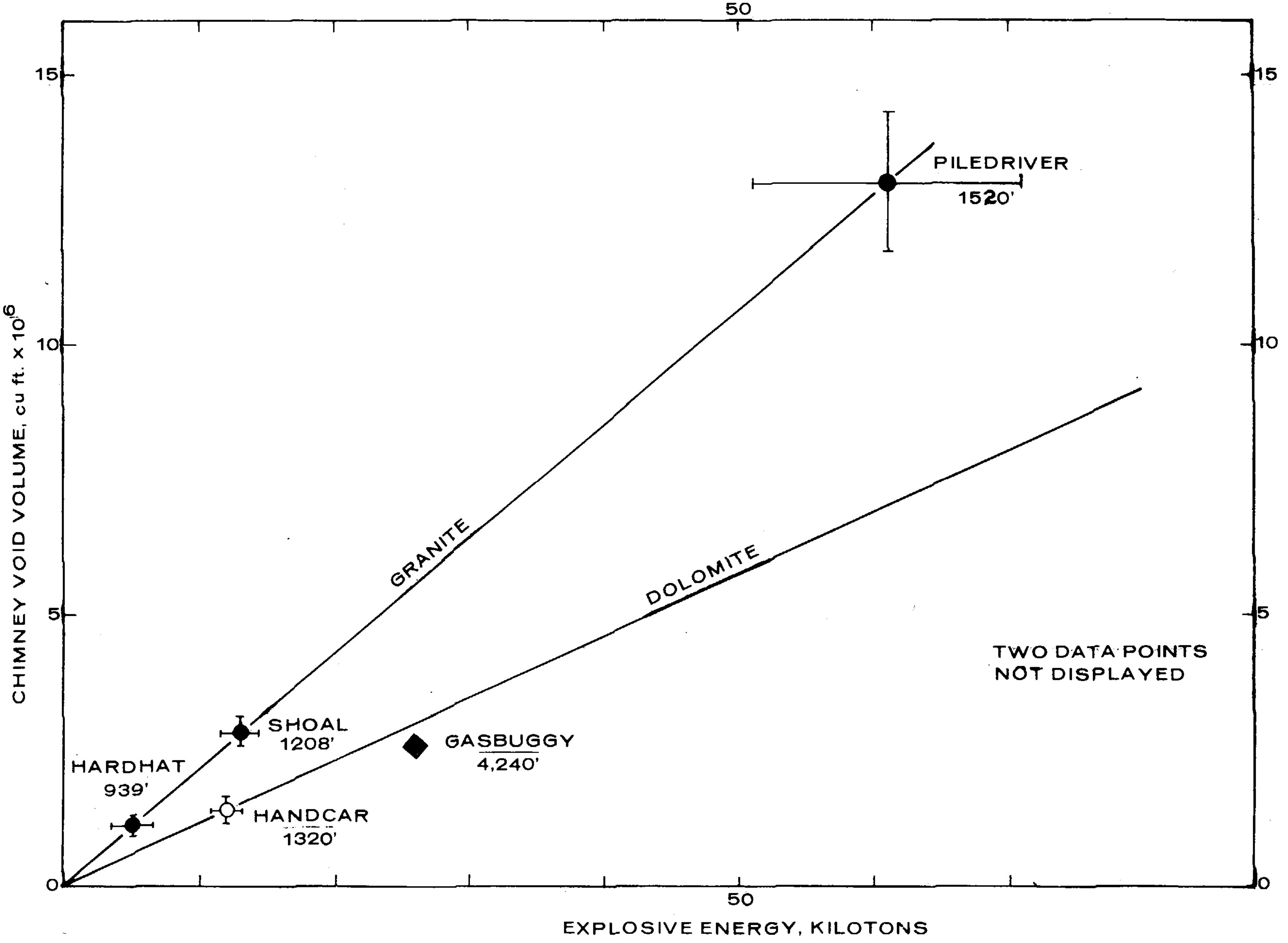

Figure 5 Chimney Void Volume as a Function of Explosive Energy

The chimney void volumes determined by these tests are believed to approximate the volumes of the cavities just prior to collapse. In fact, the radii of the sphered void volumes of the Hardhat, Handcar, and Shoal chimneys are essentially the same (within 1 - 2%) as the radii determined by analysis of gamma ray and temperature logs. Logs have not been obtained from the base of the Piledriver and Gasbuggy chimneys. The chimney radius has been determined for Piledriver, however, as indicated previously. By applying the Hardhat R_{ch}/R_c ratio to Piledriver, a cavity radius of 148 feet is obtained. This value compares favorably with the Piledriver radius of sphered chimney void volume of 146 feet.

These data indicate that for explosions at 1000 - 2000 feet depths, about 200, 000 and 100, 000 ft^3 chimney void space are expected to be produced per kiloton explosive energy in granite and dolomite, respectively. At depths around 4, 000 ft about 100, 000 ft^3/kt are expected in shale. Volumes for intermediate depths can be scaled using the appropriate equations for cavity radii already presented.

CHIMNEY PERMEABILITY

While no direct measurement has been made, analyses of data from pressurization tests indicates that the permeability of dolomite and granite chimneys is very large.

All four chimneys, (Hardhat, Shoal, Piledriver, and Handcar) when pressurized with air, responded essentially like a leaky tank. The pressure rose rapidly during air injection and declined slowly afterward.

Each chimney was pressurized at least four times with measured air masses. The observed pressure increases, when corrected for leakage to the chimney walls and treated with Boyle's Law and Newton's Law of Conservation of Mass, indicated the chimney void volumes discussed in the previous section.

Similar tests on the Salmon (5. 3 kt in salt) cavity yielded similar results. This cavity contained essentially no rubble and its permeability is estimated to be on the order of trillions of darcies. It is recognized, of course, that the flow path through the granite and dolomite chimneys cannot be as simply approximated as that of the Salmon cavity. However, the fact that these chimneys do respond to a pressure pulse in essentially the same manner as an open cavity indicates that for all practical purposes their resistance to fluid flow is inconsequential.

Rodean (1965), in a study of the rubble particle statistics of the Hardhat chimney calculated a representative granite rubble column permeability of about $4x10^5$ darcies based on considerations of particle size distribution and rubble porosity. Very large permeabilities can also be expected from chimneys in shale and sandstone as indicated by the Gasbuggy chimney's response during gas withdrawal tests. It, too, behaved much like a large tank.

RUBBLE VOLUME

As indicated previously, chimney heights, and consequently rubble volumes, are a function of the rock's bulking characteristics, as well as its capability of supporting a stable arch.

Depending upon the relative effect of these two characteristics, the volume of rubble can vary by a wide margin - as much as 50% or more, in light of Handcar results. For applications, the success of which depends to a great extent upon the volume of rubble produced, this variation is of much concern.

While there appear to be no obvious solutions to the problem of inefficient bulking, it is probable that means of inducing additional collapse can be developed for resistant arches. An attempt to induce further collapse of the Handcar arch demonstrated that it was rather stable and that considerably more explosive than the 180# detonated would be required to accomplish more than spall a few feet of rock from the roof (Boardman et al, Dec., 1966).

The estimated volumes and tonnages of rubble produced by U.S. tests in competent rock are presented in Table 4. Except for Handcar, these estimates were obtained by assuming: 1. The chimney radius above shot point level to be 1.1 R_c. 2. The chimney apex and base to be hemispherical with radii of 1.1 R_c and R_c, respectively, and 3. The chimney void volume to be equal to the original cavity volume. Handcar rubble volume was estimated on a similar basis except that the volumes of the apical void and rubble mound were estimated from optical survey data which were not obtained for the other chimneys.

Based on these estimates, for relatively shallow contained explosions in granitic rock (1,500 ft ±) about 60 - 85,000 tons of rubble per kt can be expected. If the Shoal and Hardhat apical voids were to be collapsed the lower limit of this range would be ~70,000 tons. Since the Handcar apical void volume is estimated to be greater than 50% of the total Handcar chimney void volume it is expected that with collapse of this apical void the rubble volume would be at least doubled.

RUBBLE PARTICLE SIZE

Rubble particle size studies have been conducted for Piledriver (Rabb, 1968), Hardhat (Rodean, 1965) and Handcar (Boardman, et al, Dec., 1966). The summarized results of these studies are presented in Figure 6.

The Hardhat and Piledriver data were obtained by analysis of photographs of the face of drifts at successive stages of advance into the chimney located 90 feet and 100 feet above shot point, respectively. The Handcar data were taken from downhole photographs such as the one presented in Figure 7.

As indicated by Figure 6, the samplings are roughly similar in that at least 85% by weight of the rock fragments were less than 4 feet in diameter. This similarity is remarkable considering the differences in rock properties and relative position in the chimney of the sampling locations.

The weight-median particle diameters of the three samples are

TABLE 4 Estimated Rubble Tonnages Produced by Contained Explosions in Competent Rock

Project Name	Estimated Rubble Volume ft^3	Estimated Mean Density of Rubble Blocks, g/cc	Estimated Rubble Tonnage	Tons/kt
Piledriver	64,000,000	2.65	5,200,000	85,000
Shoal	10,200,000	2.65	840,000	64,000
Hardhat	3,400,000	2.65	280,000	57,000
Handcar	3,100,000	2.7	260,000	22,000
Gasbuggy	7,100,000	2.5	500,000	22,000

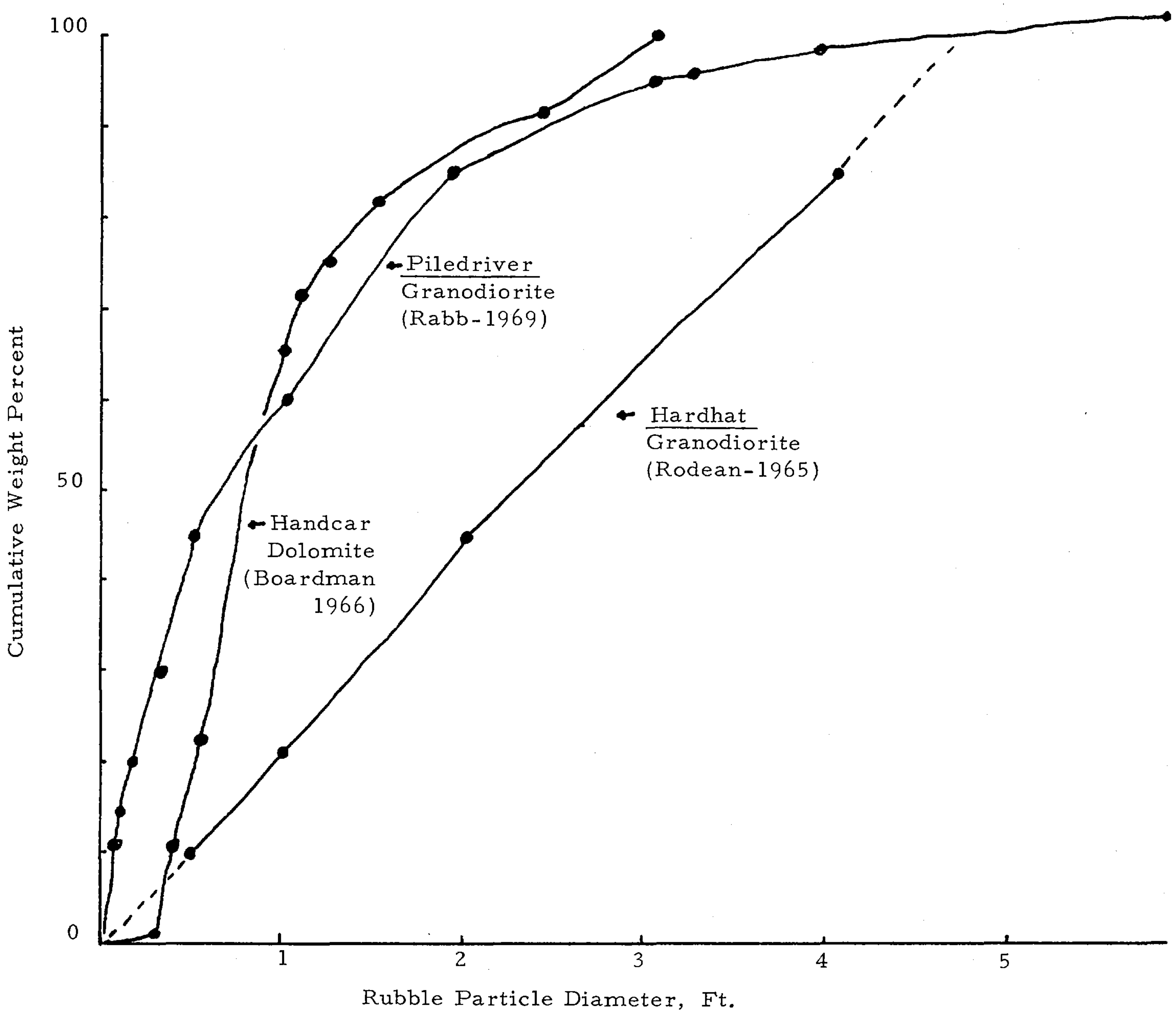

Figure 6

Comparison of Rubble Particle Size Distributions - Hardhat, Handcar, Piledriver

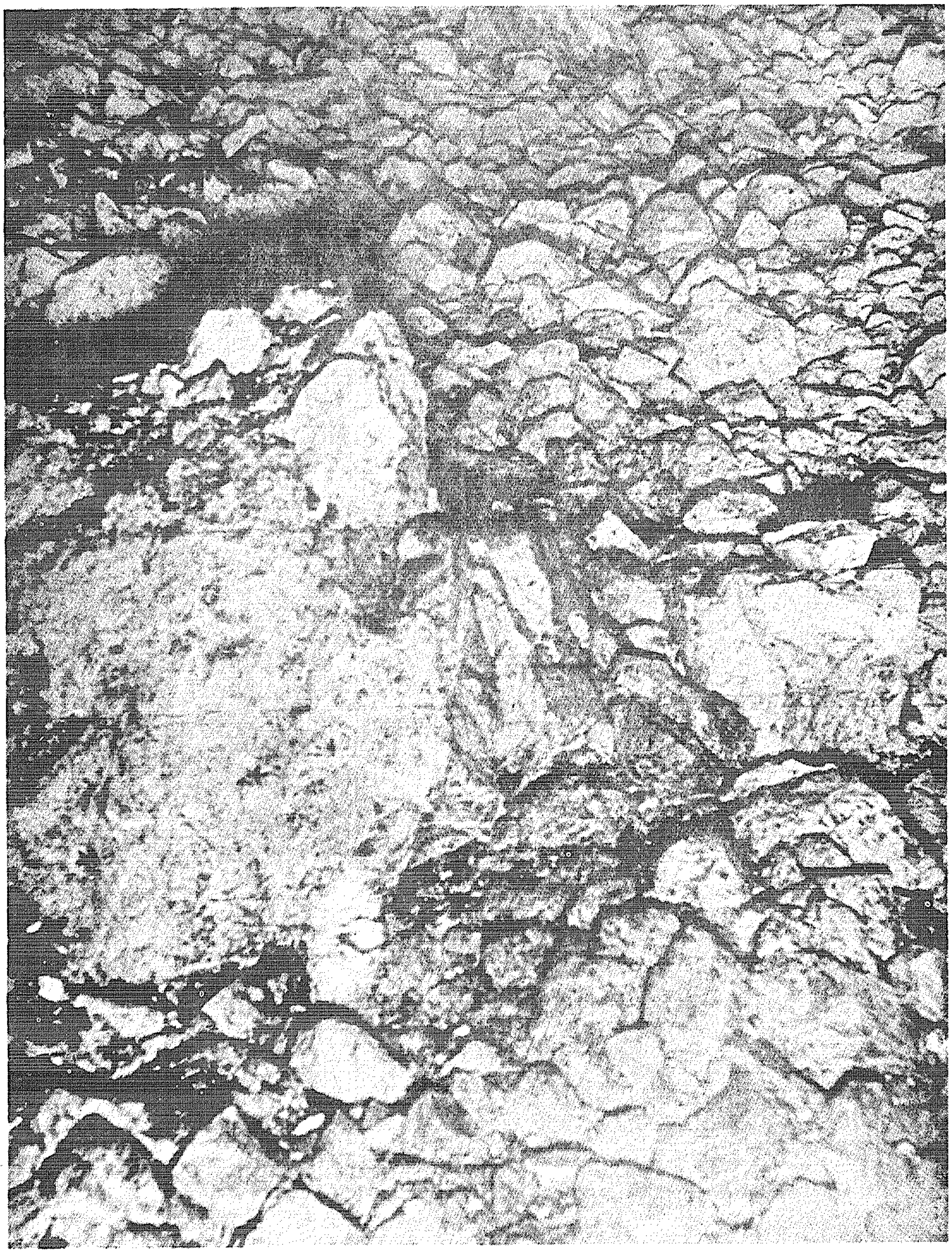

Figure 7

LRL Downhole Photograph of Handcar Rubble at Base of Apical Void (Boardman - December 1966) (Diameter of large block in foreground is 3 to 4 feet) approximately 2 feet for Hardhat and approximately .7 feet for Piledriver and Handcar.

The 1964 analysis of particle size data from tuff chimneys seemed to indicate a relationship between chimney diameter and particle size distribution; i.e., larger blocks associated with larger chimney diameters (Boardman, et al, 1964). It is apparent from a comparison of the Piledriver and Hardhat data that such a relationship apparently does not exist for granitic rock. Since the Piledriver samples had been subjected to the pressure exerted by an 800 ft column of rubble, as opposed to a column less than 200 feet high for Hardhat, the observed difference would be expected. Possibly the tuff blocks deformed more plastically under similar conditions, thus enabling relatively larger particles to survive.

PERMEABILITY OF FRACTURED ROCK OUTSIDE CHIMNEY

The permeability of rock surrounding a nuclear chimney is altered as a result of the mass displacement which accompanies cavity growth and the subsequent collapse of rock overlying the cavity. The overall fracture permeability of the rock mass as well as the permeability of the rock matrix are altered.

Indications of the extent to which permeability changes may have occurred have been obtained by monitoring drilling fluid circulation losses, in-situ measurements, and laboratory measurements on core samples. Also, fractures have been documented from exposures on walls of underground workings and in cores.

Data related to permeability changes (primarily drilling fluid loss and fracture observations) were presented at the Third Plowshare Symposium for tuff (Rainier), salt (Gnome), and granodiorite (Hardhat). These data appeared to indicate "fracture extents" of 1.5 R_c below, 2-3 R_c alongside and 6-8 R_c vertically above shotpoint, where R_c is the cavity radius. Additional measurements have subsequently been obtained for Shoal, Piledriver, Hardhat, Handcar, and Gasbuggy.

Available results of fracture permeability observations in the region above the chimney are presented in Table 5. These observations are in excellent agreement with the 1964 data. The media in which these explosions occurred were faulted and jointed and consequently were assumed to have considerable natural fracture permeability. Except for Handcar, no pre-shot in-situ measurements were made. Therefore, the estimated extents of increased permeability in the table are based upon observed increases over levels encountered at shallower depths in the exploratory holes (excluding shallow spalled zone permeabilities). The magnitude of the increase was on the order of a factor of 3 for Piledriver and Handcar; i.e., from several hundred millidarcies to around one darcy. The Hardhat and Shoal magnitudes are not known.

When available, the Gasbuggy and Rulison results should be much more definitive since the pre-shot permeabilities of these mediums were considerably lower. Possible indications of "fracturing", a casing constriction and

TABLE 5 Estimated Extents of Increased Permeability E_k Vertically Above Shot Point Level

Rock Type	Project	Estimated Extent of Increased Permeability E_k, feet	E_k/R_c	Measurement Technique
Granitic	Hardhat	484[a]	7.6	Drilling fluid circulation losses
	Shoal	608[b]	6.9	Drilling fluid circulation losses
	Piledriver	1030 ± 36[c]	7.1 ± .2	Air pressurization tests
Dolomite	Handcar	425 ± 105[d]	6.2 ± 1.5	Air pressurization tests

a. McArthur, 1963
b. Atkinson, 1964
c. Boardman, Oct., 1967
d. Boardman, Dec., 1966

casing offset, were observed in holes near Gasbuggy as far as 613 ft and 390 ft vertically above shot point level, respectively (Martin, Feb., 1969). These distances correspond to 7.2 R_c and 5.2 R_c and compare favorably with the data in Table 5.

Fracture permeability of rock alongside a chimney has been measured and reported for one explosion - Hardhat. Air pressurization tests were conducted on horizontal and vertical holes drilled into the walls of an exploratory drift located ~90 ft above shot point level. Results of these tests are shown in Figure 8 (Boardman and Skrove, 1966). These data indicate a considerably higher fracture permeability on the average near the chimney; possibly several orders of magnitude higher than pre-shot (exclusive of fault zones) out to at least 2.6 R_c from the vertical axis of the chimney (3.3 R_c radial from shot point). Lower levels of change may have also extended as far as 6 R_c or more from the chimney's vertical axis. These furtherout measurements were made in a drift which existed pre-shot and consequently, the contribution to the observed permeabilities of shock wave interaction with the drift walls is not known.

Atkinson (1964) determined that rock located 445 feet or 5 R_c laterally from the vertical axis of the Shoal chimney moved into an open hole. Operational difficulties precluded obtaining definitive information on permeability change, however. It is also suspected that spall at the free face of the hole influenced the rock movement.

No post-shot in-situ permeability measurements have been reported to date for the region below shot point.

Matrix permeability measurements have been reported for Hardhat (Short, 1964). The permeability of granodiorite core samples from post-shot exploratory holes near the chimney had apparently undergone permeability increases out to approximately 115 feet or 1.8 R_c from shot point. Maximum measured matrix permeability of wall rock samples was 44 microdarcies in the interval located between 1.3 R_c and 1.8 R_c from shot point. The maximum measured permeability of pre-shot samples and of samples further than 1.8 R_c from the shot point was approximately 12 microdarcies. Immediately below the base of the chimney (1.0 R_c - 1.2 R_c) is a zone of crushed rock which yielded core permeabilities of ~15 millidarcies (Mehta, et al, 1964).

CONCLUDING REMARKS

The foregoing data, along with those presented at the 1964 symposium, currently serve as the empirical basis for engineering design of U.S. contained Plowshare explosions. The results of the Rulison project, when available will greatly expand this empirical base, providing data applicable not only to gas production stimulation, but also to all currently conceived applications.

Other projects are necessary, of course, to achieve the degree of sophisticated knowledge required for further development of the technology. Gross estimates of fracture extents must be replaced with refined estimates of the extents of enhanced permeability and the degree of enhancement, not only for the exploitation of hydrocarbon deposits, but also for deposits of oil

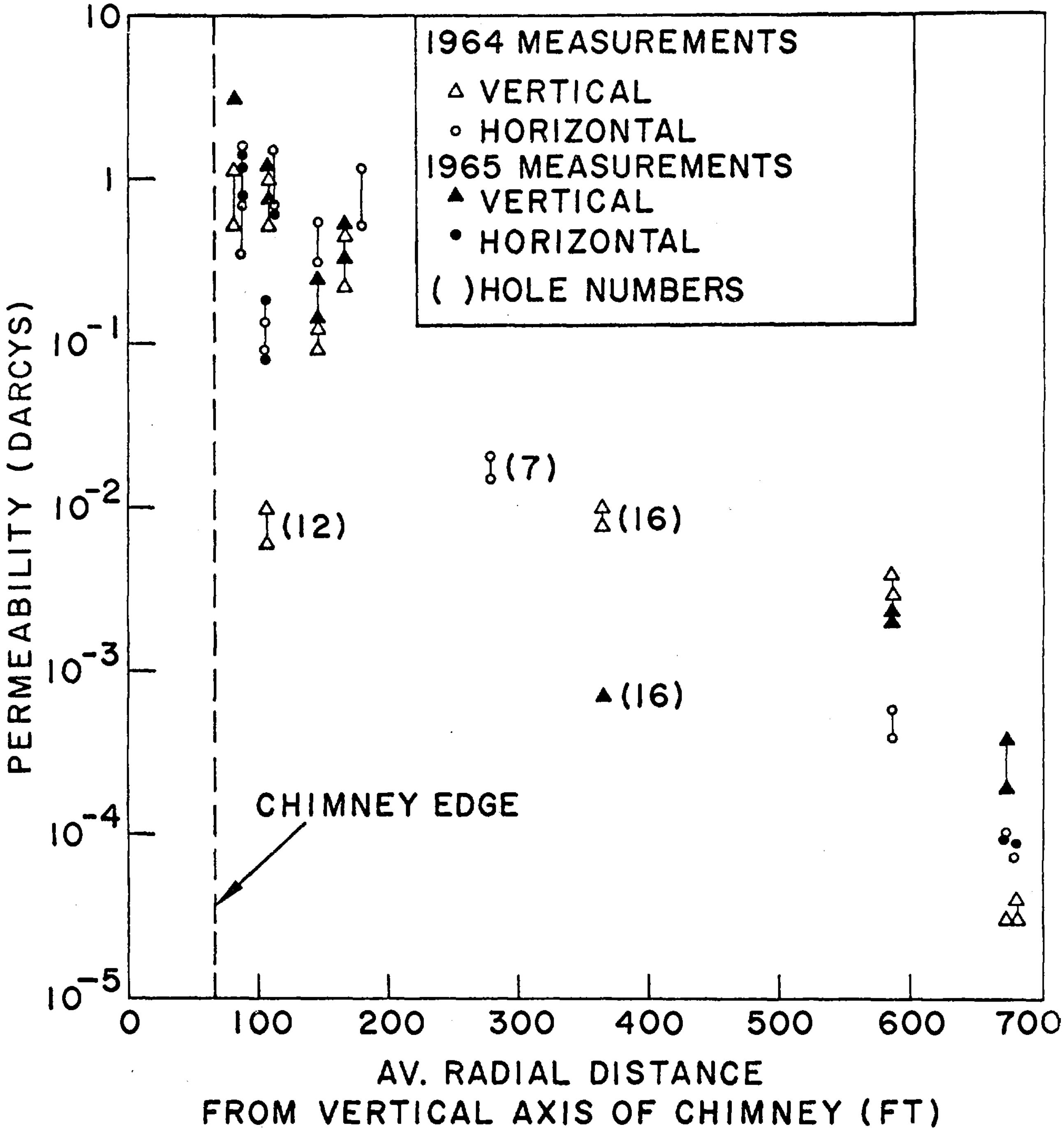

Figure 8

In Situ Permeability of Hardhat Chimney Wall Rock as a Function of Radial Distance from Vertical Axis of Chimney shale and metallic ores. The applicability of the granite and dolomite particle size data to these latter deposits must also be experimentally determined, if not directly, by actual in-situ leaching or retorting.

Finally, once we have mastered the engineering effects of single explosions, the full scale development of our resources will no doubt require our taking advantage of the interaction of simultaneous or near simultaneous explosions as well as the interaction of explosions with adjacent chimneys. Significant engineering effects are expected based upon the observed disturbances of the Logan (5.4 kt) chimney in volcanic tuff by the Blanca (22 kt) explosion during the late 1950's (W. D. Richards, 1961).

REFERENCES

Atkinson, C. H., Subsurface Fracturing from Shoal Nuclear Detonation, PNE 3001, June 1964.

Boardman, C. R., Results of an Exploration into the Top of the Piledriver Chimney, UCRL-50385, UCLRL, Oct. 1967.

Boardman, C. R., A Measurement of the Volume of Void in the Shoal Chimney, UCRL-50150, UCLRL, Sept. 1967.

Boardman, C. R., A Measurement of the Void Volume and Fracture Permeability Resulting from the Hardhat Event, UCID-4893, Rev. 1, UCLRL, June 1965.

Boardman, C. R. Macrodeformation Resulting From the Handcar Event, UCRL-50149, UCLRL, Dec. 1966.

Boardman, C. R. and W. Booty, A Measurement of the Voume of Void Created by the Salmon Event, UCID 4991, UCLRL, Apr. 1965.

Boardman, C. R., Some Characteristics of the Hardhat Chimney and Surrounding Wall Rock, UCRL 50177, UCLRL, Oct. 1966.

Boardman, C. R., David D. Rabb, and R. D. McArthur, Responses of Four Rock Mediums to Contained Nuclear Explosions, JGR, Vol. 69, No. 16, Aug. 1964.

Boardman, C. R. and J. Skrove, Distribution in Fracture Permeability of a Granitic Rock Mass Following a Contained Nuclear Explosion, Journal of Petroleum Tech., May 1966.

Cherry, J. T., D. B. Larson, E. G. Rapp, Computer Calculations of the Gasbuggy Event, UCRL 50419, UCLRL, May 1968.

Higgins, G. H. and T. R. Butkovich, Effect of Water Content, Yield, Medium and Depth of Burst on Cavity Radii, UCRL 50203, UCLRL, Feb. 1967.

Martin, William B., Preliminary Observations of Post-shot Geologic Effects of the Gasbuggy Nuclear Stimulation, Northeast San Juan Basin, N. M. Regional Meeting of the Rocky Mountain Section of the AAPG, Albuquerque, Feb. 24, 1969.

McArthur, R. D., Geologic and Engineering Effects, The Hardhat Event, GNI-63, UCLRL, Feb. 1963.

Mehta, M. V. S. Gupta, and W. M. Somerton, Changes in Physical Properties of Rocks in the Vicinity of an Underground Nuclear Explosion, UCRL 13105, UCLRL, Feb. 1964.

REFERENCES

Rabb, D. D., Size Distribution Study of Piledriver Particles, UCRL-50489, UCLRL, Oct. 1968.

Rawson, D. E., P. Randolph, C. Boardman and V. Wheeler, Post Explosion Environment Resulting from the Salmon Event, JGR Vol. 71, No. 14, July 15, 1966.

Rawson, D. E., C. R. Boardman, and W. Chazan, The Environment Created by a Nuclear Explosion in Salt, PNE 107F, 1964.

Rawson, D. E., Korver, J.A., Pritchard, R. L. and Martin, W., Postshot Geologic Investigations - Proj. Gasbuggy, UCRL-71354,SPE, Sept. 29, 1968.

Richards, W. D., Private communication, 1961.

Rodean, H. C., The Particle Statistics of Rubble Produced by Underground Nuclear Explosions, Geophysics Vol. 30, No. 4, Aug. 1965.

Short, N.M., Effects of Shock Pressures From a Nuclear Explosion on Mechanical and Optical Properties of Granodiorite, UCRL 7944, UCLRL, Sept. 1964.

Stephens, D. R., E. M. Lilley, H. Louis, Pressure-Volume Equation of State of Consolidated and Fractured Rocks to 40 Kbar, UCRL 71238, UCLRL, Mar. 1969.

Tracy, James, Private communication, 1961.

Ward, Don C. and R. F. Lemon, Status of Reservoir Evaluation Project Gasbuggy, SPE, Sept. 29, 1968.

XA04N0743

EMPLACEMENT ENGINEERING[*]

Ernest E. Hill
Lawrence Radiation Laboratory, University of California
Livermore, California 94550

Emplacement Engineering can be defined as that portion of a nuclear explosive project that is concerned with the emplacement of the explosive. This definition would then include virtually everything except the design and fabrication of the explosive and the post-shot-effects program. For future commerical application, the post-shot-effects program will essentially disappear.

This emplacement portion of a nuclear explosive project constitutes a large fraction of the total project cost, but it has largely been overshadowed by the explosive and explosive-effects portions. As we move into commercial applications, Emplacement Engineering must receive more attention from both industry and government.

To place emplacement costs in their proper relationship with total projects costs, we have performed a study of commerical underground nuclear explosive applications such as gas stimulation. Although there are many intangibles in such a study, we have been able to at least obtain some feel for the relative fractional costs of the non-explosive costs compared with the explosive costs. This study involved estimating the cost elements for applications using a single explosive at 5,000 ft, 10,000 ft, and 15,000 ft. For each depth, the cost estimates were made for a range of emplacement hole and explosive diameters.

Results of these estimates for explosive-related costs, hole-related costs, and total costs are shown for the three depths considered on Figs. 1, 2 and 3. Note that the explosive package outside diameter is assumed as 2 inches less than the hole (or casing) inside diameter for all cases.

For the 5,000-ft application the explosive-related costs dominate, and of particular importance is the indicated diameter for minimum total cost which occurs at approximately a 17.5-in. hole (15.5-in. explosive).

The hole-related costs are in the same range as the explosive-related costs for the 10,000-ft application. For this case, the minimum total cost occurs at approximately a 14-in. hole (12-in. explosive).

The 15,000-ft application presents quite a different picture. Here the hole-related costs run two to three times the explosive-related costs, but the diameter of minimum total cost has only decreased to a 12.5-in. hole (10.5-in. explosive).

When the total cost curves are compared (Fig. 4), the point of minimum total cost provides a curve that appears to be asymptotic to a hole diameter of approximately 12 in. (10-in. explosive). It is also obvious that for the deeper

---

[*] Work performed under the auspices of the U. S. Atomic Energy Commission.

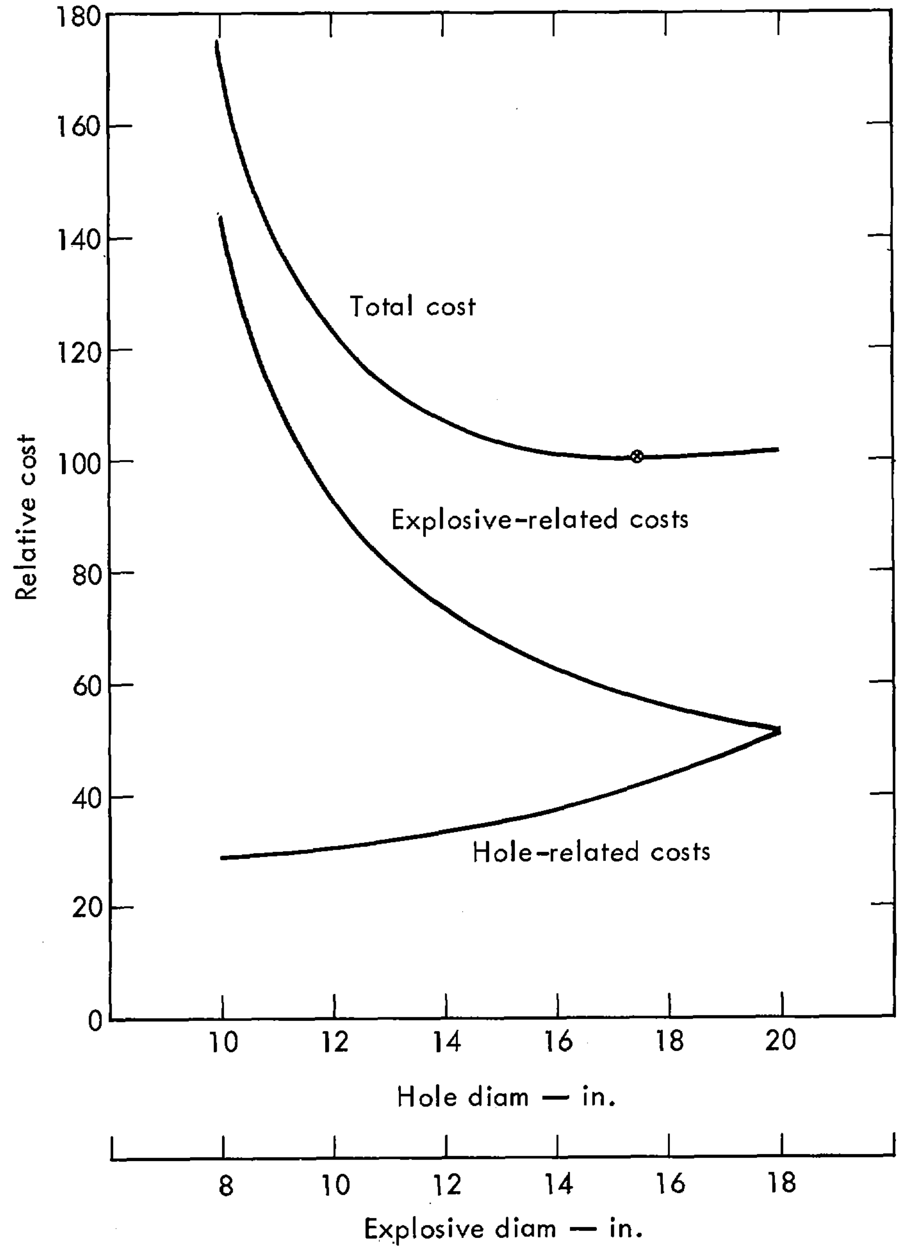

Fig. 1. Estimates for explosive-related, hole-related and total costs at 5,000-ft depth of hole.

applications, the strong dependence on hole-related costs results in an almost linear dependence of total cost to hole depth.

It is also of interest to compare (Fig. 5) the fraction of hole-related costs to the total cost for the depths and diameter of interest. It is demonstrated here that for applications at depths exceeding approximately 7,500 ft, the hole-related costs constitute over 50% of the total cost.

The foregoing is intended only to demonstrate that the costs of Emplacement Engineering constitutes a major portion of the costs of a nuclear explosive operation. Conventional petroleum recovery operations would normally involve drilling costs and if the exploratory hole is successful, then completion costs to convert the exploratory hole to a producing well. A nuclear stimulation application involves drilling an emplacement hole, emplacing the

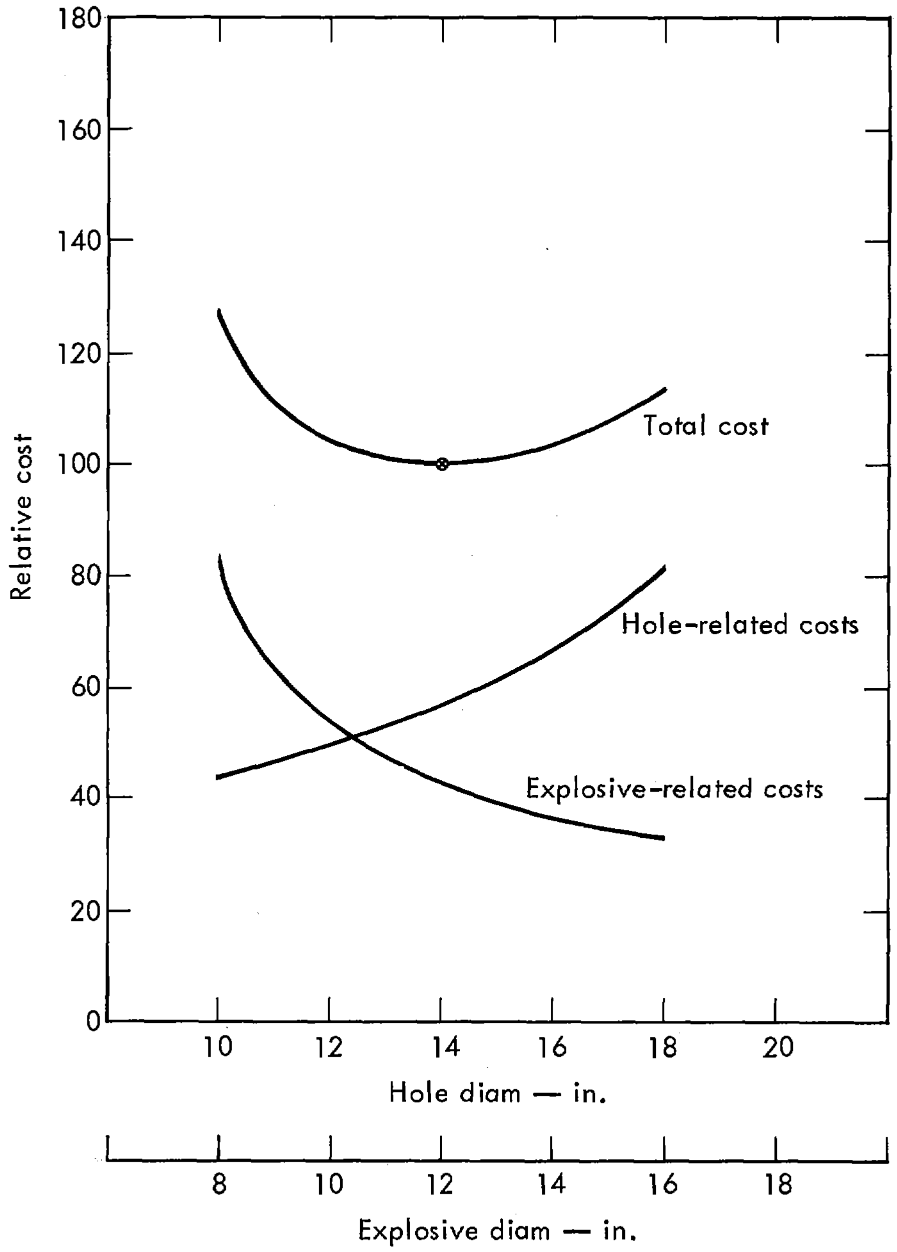

Fig. 2. Estimates for explosive-related, hole-related and total costs at 10,000-ft depth of hole.

explosive, detonation, drill-back, and finally completion of the producing well. The last two operations, drill-back and completion, are essentially the same as the conventional operation. The first three operations plus the explosive cost constitute the additional cost that must be economically justified by increased recovery of product due to nuclear stimulation. Emplacement Engineering can then also be defined as the engineering program to reduce emplacement (hole-related) costs to a minimum for a given application.

There are, of course, many areas of interest that could be productive in this development program. To name a few:

1. Development of the capability to drill intermediate-diameter holes to depths of 15,000 ft or more. By intermediate is meant inside hole diameters

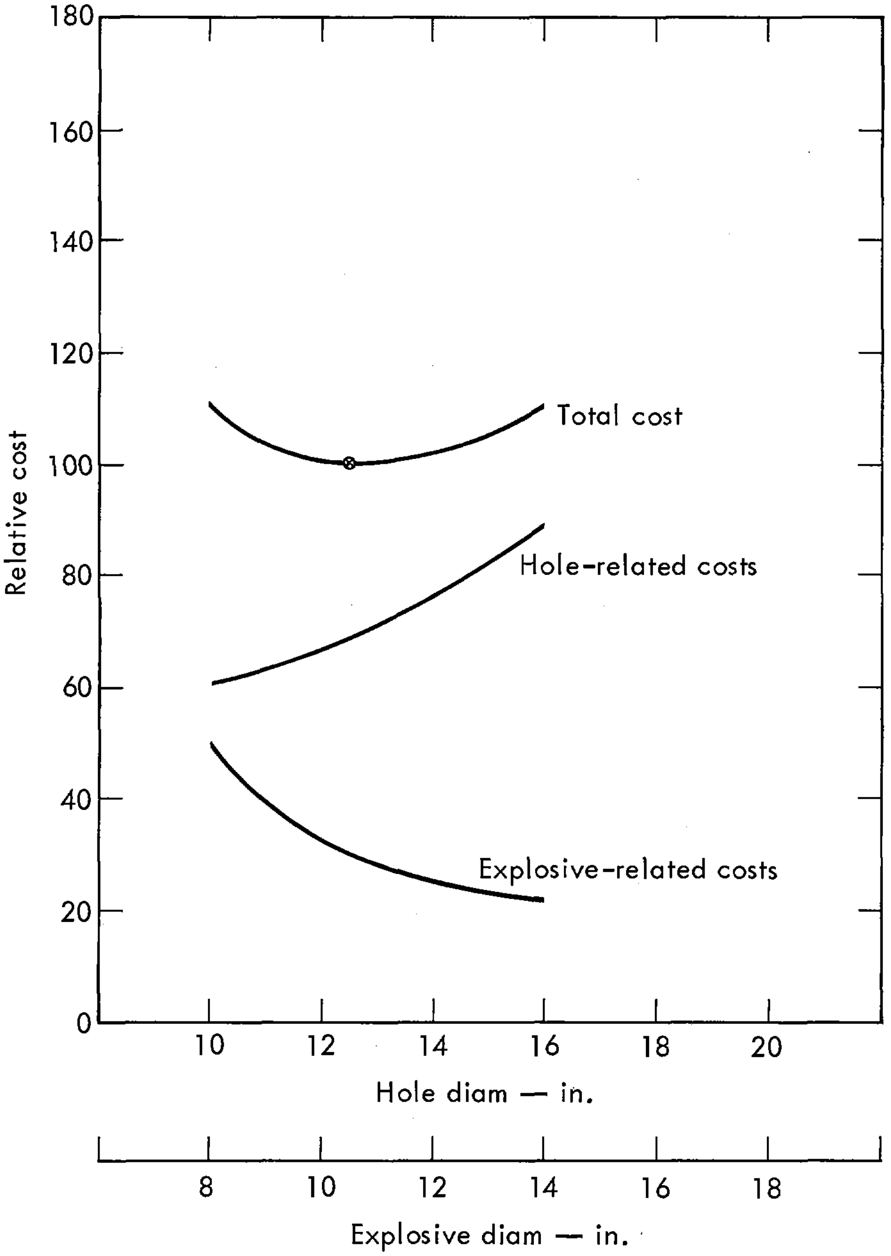

Fig. 3. Estimates for explosive-related, hole-related and total costs at 15,000-ft depth of hole.

of approximately 12 in. to the bottom of the hole. Obviously included in the capability of drilling such holes is the requirements of minimum cost.

2. Development of low-cost techniques for the emplacement of the explosive package. This would include development of support cables and communication cables, or a combination of both that would withstand the temperatures and pressures expected.

3. Development of stemming techniques to utilize low-cost materials, preferably those that are available at the site. Included in this area would be methods to automate material handling during stemming.

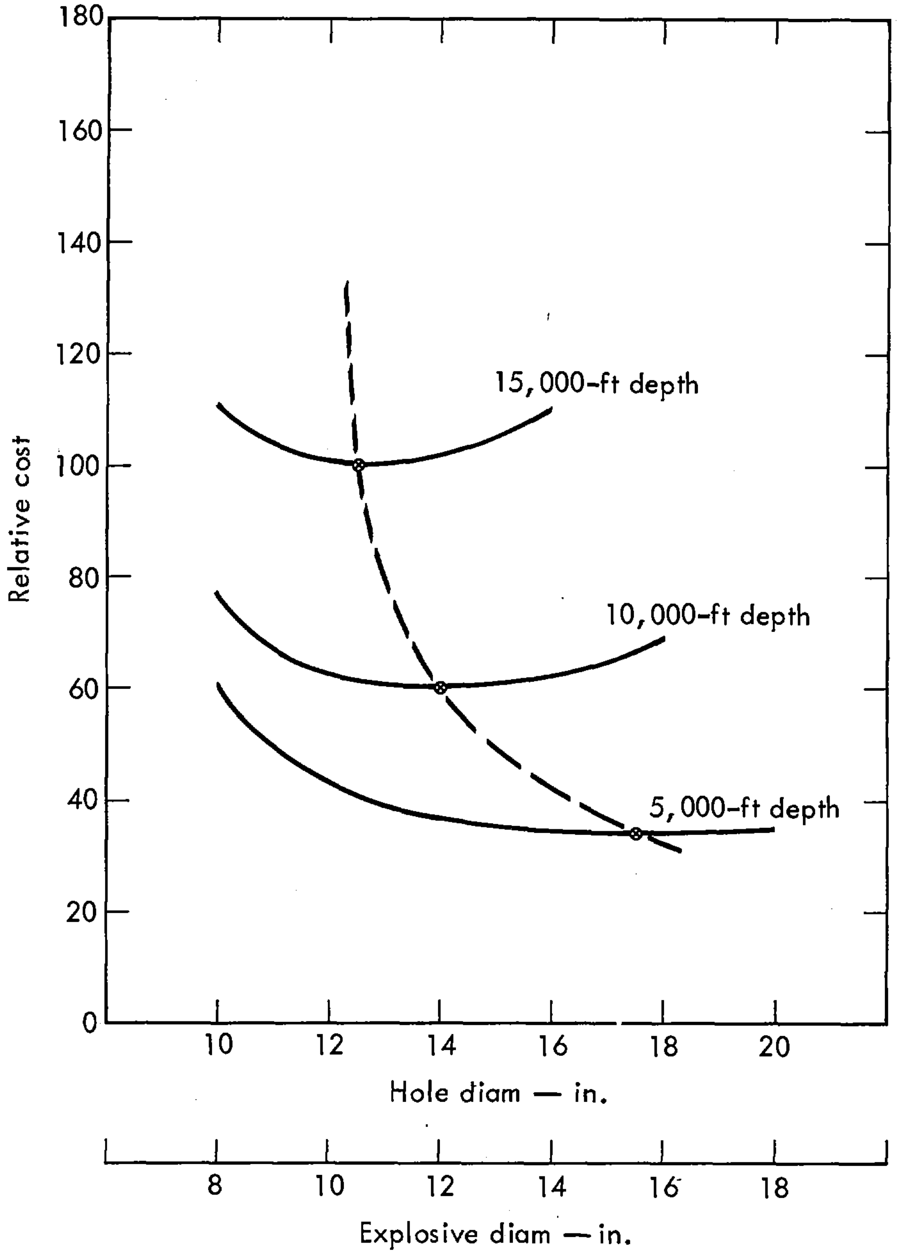

Fig. 4. Comparison of total cost curves at 5,000-, 10,000- and 15,000-ft depths of hole.

4. Development of stemming techniques that would facilitate reentry and thereby eliminate the additional cost of drill-back. This is particularly vital for deep applications where the cost of drilling the equivalent of two holes would, in most cases, make the application uneconomical.

5. Development of simplified detonation systems to provide low operational costs combined with high reliability and safety.

6. Development of environmental control systems for the nuclear explosive. Expected design parameters might be as high as 450°F and 20,000 psi, with the explosive system maintained at 150°F and 1 atmosphere.

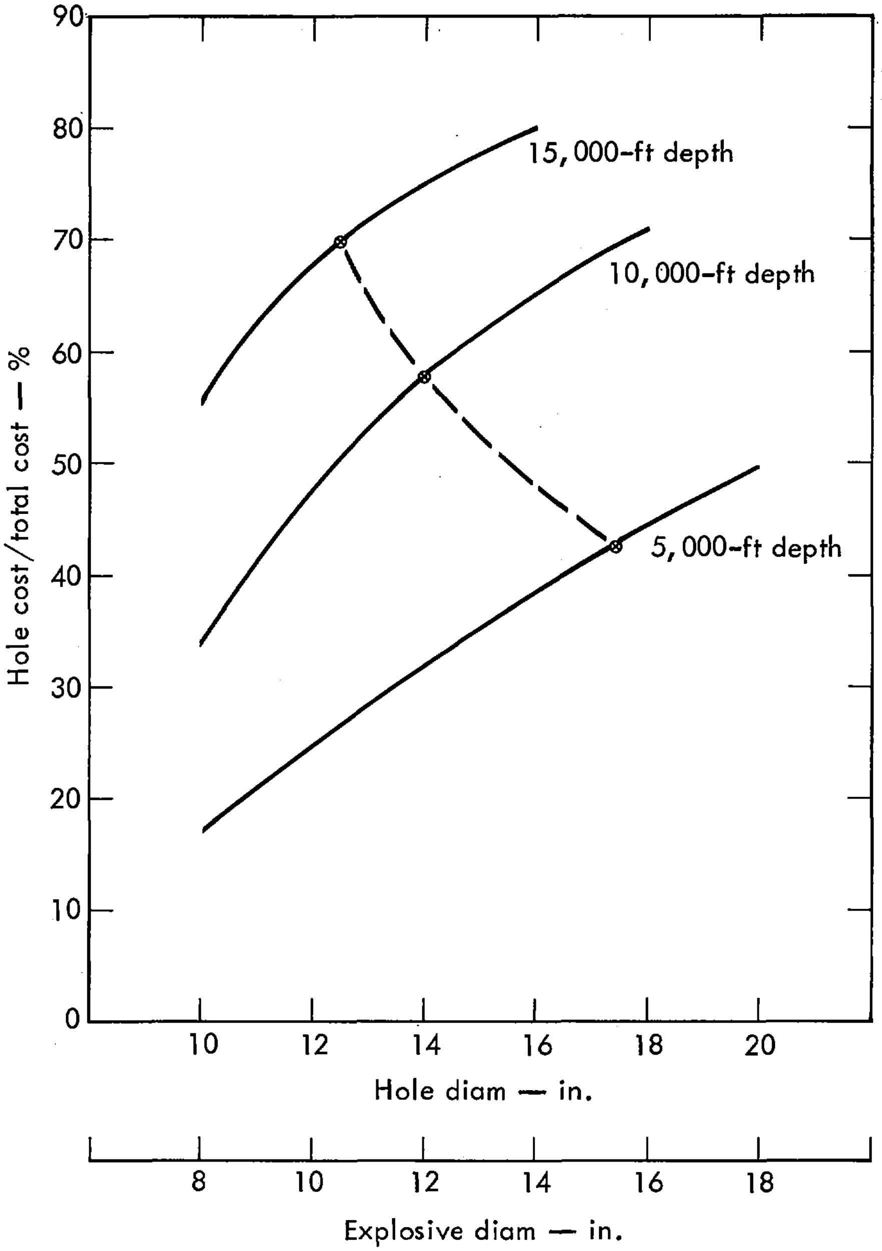

Fig. 5. Comparison of fraction of hole-related costs and total cost for 5,000-, 10,000- and 15,000-ft depths of hole.

The above six areas for development are abviously not all-inclusive, but they do represent a major portion of the presently indicated requirements. Of these, the first is obviously one in which industry must provide the majority of development effort. The next three (2, 3, and 4) represent areas that should be a joint effort between industry and government (AEC, AEC contractors, and other government agencies) with industry taking the dominant role. The last two (5 and 6) areas also represent joint effort between industry and government, but in these instances, the government should take the dominant role.

Concurrent with the above efforts, the AEC Laboratories should develop a small-diameter, low-cost nuclear explosive for Plowshare underground engineering applications. It is hoped that we have demonstrated here the vital necessity to also reduce the explosive emplacement and fielding costs. The results of both efforts could move nuclear explosive engineering into an era of commerically attractive enterprises.

XA04N0744

SUMMARY OF GEONUCLEAR EFFECTS

Donald E. Rawson

Explosives Engineering Services
Gulf General Atomic Incorporated

I. INTRODUCTION

Geonuclear effects are considered here to include all of the interactions between underground nuclear explosions and the surrounding earth material. They constitute a large spectrum of effects that starts with the complex chemistry of the explosion "fireball" and continues in space until the teleseismic signals in the earth have attenuated and in time until the radioactive products have decayed. This paper does not treat the total spectrum but is restricted to those effects which are of direct use to possible nonexcavation engineering projects and the major side effects that could detract from the use of nuclear explosions for such projects. Emphasis is given to possible methods of enhancing the desired geonuclear effects and minimizing the deleterious ones.

Those who have directly participated in developing nuclear explosive technology cannot help but be impressed by the terrific potential for useful work associated with this energy source. Those who have viewed this developing technology from the periphery (the potential industrial market, the concerned public, and specialists in many allied fields) are certainly interested in the potential benefits but cannot help but be impressed by the attendant risks.

Figure 1 illustrates schematically some of the useful geonuclear effects balanced against the associated side effects. More experience and increased knowledge of these effects will affect both project costs and public opinion. These factors will determine how the balance will tilt in relation to specific nuclear explosion engineering projects.

II. GEONUCLEAR EFFECTS

Since this is a very general discussion of geonuclear effects associated with potential engineering applications, oversimplifications and generalities are made which reflect the author's judgments. Exact treatment of the "pros and cons" of geonuclear effects should be restricted to specific applications and specific sites.

2.1. Useful Geonuclear Effects

A considerable amount of theoretical and experimental data and experience exists in this area. Development and engineering can help translate this knowledge into an applied technology. The author believes that this goal will be advanced with increased emphasis on developing methods to enhance the useful effects and control and/or minimize the adverse side effects.

2.1.1. Void Volume

Void volume generated by varying nuclear explosive yields at different depths and in different rock materials can generally be predicted to within about 50% of subsequent measurement if the major element rock chemistry, bulk density, porosity, and percent water saturation are known. With more refined equation-of-state data and strength properties of rock, or previous experience in very similar material, predictions of void volume are within 20% of measured values.

Storage applications are probably most dependent upon knowledge of the void volume produced. Depths for such applications are in the region from 3000 to 5000 ft for natural gas storage (to take advantage of the nonideal compressibility of methane).

There appears to be significant potential for enhancing the cavity volume at a given explosive yield by boosting the working gas (rock vaporized by the explosion) with water added at the time of explosive emplacement. The cavity volume variation as a function of water content can be estimated as follows:(1)

$$V = \frac{RT\,Wm_v}{P\bar{M}}$$

where V = cavity volume in ft^3,

R = gas constant, 2.9×10^{-3} atm-ft^3/mole-$^\circ$K,

T = vaporization temperature of SiO_2 at P in $^\circ$K,

P = overburden pressure in atm,

W = yield in kt,

$\bar{M}$ = average molecular weight of SiO_2/H_2O gas at T and P in g,

m_v = mass of vaporized rock, 90×10^6 g/kt.

Solution of this equation for Gasbuggy at a 4240-ft depth, a 297-atm overburden pressure, 26 kt, and varying water content of the vaporized rock is summarized as follows:

5% water by wt . . . 2.1×10^6 ft^3 cavity volume
11% water by wt . . . . 2.5×10^6 ft^3 cavity volume
50% water by wt . . . 4.5×10^6 ft^3 cavity volume

The example illustrates the magnitude of potential void volume enhancement with water. Surrounding the explosive with water can also virtually eliminate neutron activation that would otherwise occur from interactions with rock. Production of tritium from deuterium in water is about a factor of 10^{-6} below tritium production from lithium in rock.(2)

The engineering methods of producing the space to emplace large quantities of water around the explosive have not been demonstrated. This space may be produced by a combination of underreaming of the emplacement hole, hole expansion and breakage with chemical explosives, and special drilling techniques to remove rubble from the expanded hole. The emplacement concept is illustrated in Fig. 2.

2.1.2. Fragmented Rock

Fragmented rock is defined as that material which has been broken and bulked as a consequence of an explosion. This would be the chimney rubble for deeply contained explosions. The accuracy with which tons of rock broken from single, deeply contained charges can be predicted is roughly proportional to the accuracy of predicting chimney height (assuming the cavity radius can be anticipated with a small error). Without previous experience in a very similar geologic setting or other experimental work, it is possible that predictions could be off by a factor of two or more.

Some qualitative statements can be made about chimney development:

1. Rock that is characterized by high density, low porosity, high strength, and brittle failure will tend to bulk significantly upon breakage and chimney development. This will result in a chimney height equal to or less than the radius of fracturing by the explosion.

2. Rock that responds plastically will not chimney appreciably (for example, salt). However, if the material has a low arch strength, it will form a tall chimney without a large amount of bulking and will chimney higher than a radius fractured by the explosion.

3. Other factors being equal, the chimney height will be less with deep scaled depths of burial for the charges.

4. Other factors being equal, taller chimneys will develop with large yields (greater than 100 kt) because few materials in nature can support the size of the undercutting arch. Also, as the cavity size gets larger, more compaction and less bulking occur with the fragmented chimney material.

There is a need to compile mining experience in a variety of rock materials and different structural geologic settings because such empirical data are very relevant to judging and predicting chimney height. Methods of both enhancing chimney height (for some stimulation applications) and inhibiting chimney development (where overlying aquifers exist) should be developed.

Termination of the upward development of a "nuclear" chimney might be accomplished by using chemical explosives and blasting agents to "pre-split"

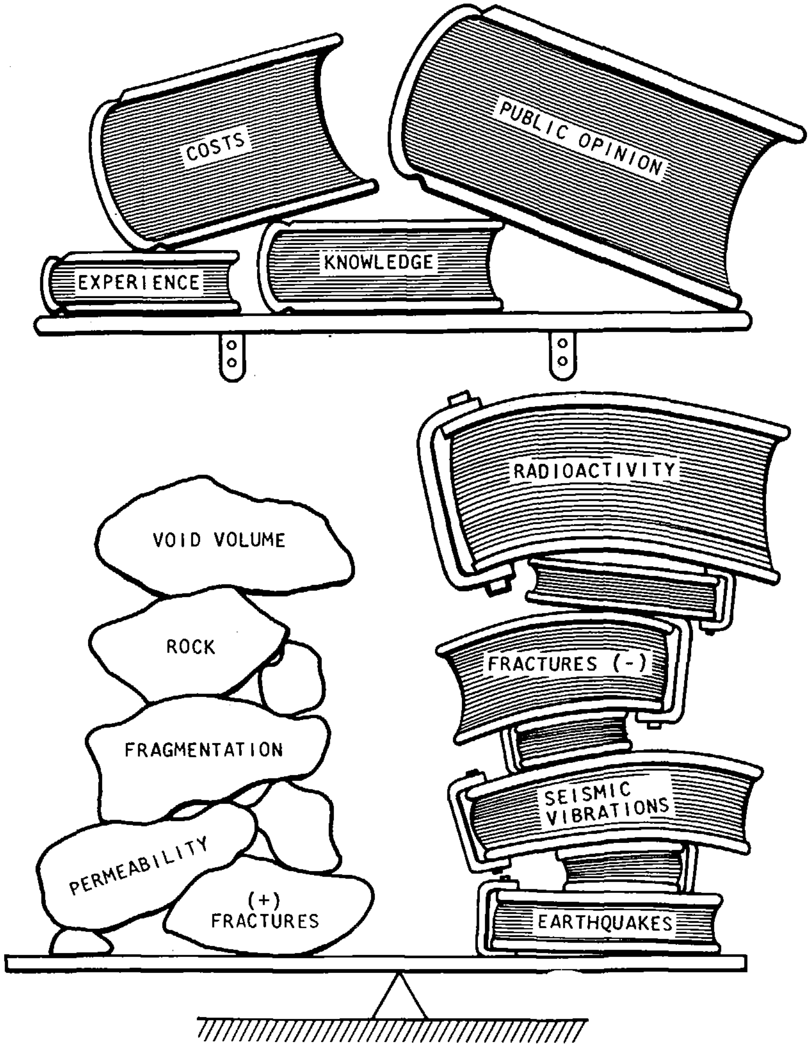

Fig. 1 — Major geonuclear effects of nonexcavation explosions: the "pros and cons".

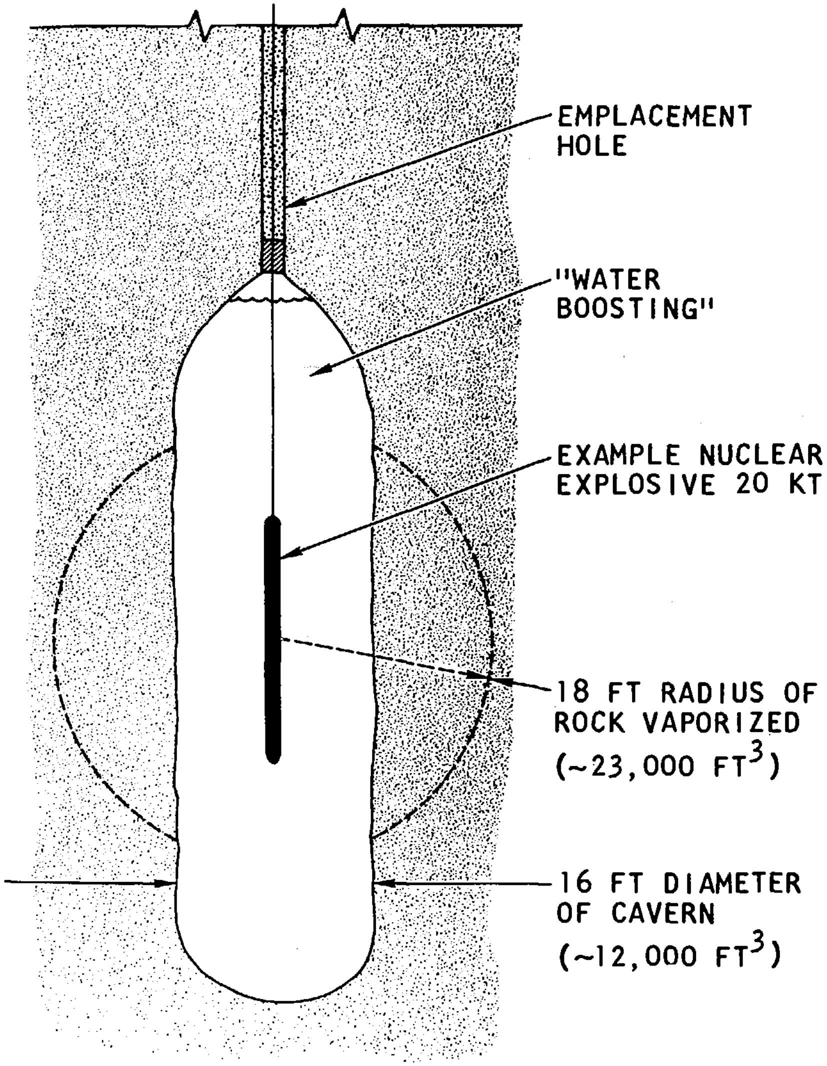
EMPLACEMENT HOLE
"WATER BOOSTING"
EXAMPLE NUCLEAR EXPLOSIVE 20 KT
18 FT RADIUS OF ROCK VAPORIZED (~23,000 FT^3)
16 FT DIAMETER OF CAVERN (~12,000 FT^3)

Fig. 2 — Emplacement of a nuclear explosive in an enlarged cavern containing water: "water boosting".

a region where one wants the chimney to stop. This concept is illustrated schematically in Fig. 3. The pre-splitting operation provides a zone of rock with no tensile strength and is expected to terminate the propagation of rock failure induced by the subsequent shot in a manner analogous to conventional pre-split mining methods. The engineering methods for creating space for the large charges of chemical explosives and blasting agents are the same as those described earlier for emplacing water around the nuclear explosive. First the "burn hole" would be produced and then the emplacement space for subsequent surrounding charges. These charges would be detonated using short time delays for optimum breakage.

Figure 4 illustrates a method of enhancing a nuclear explosion chimney with chemical explosives or blasting agents by using delay charges of explosives to propagate normal chimney development. This technique would initiate early chimney development, cause additional rock breakage, and force some compaction of the chimney rubble. The early chimney development would also tend to quench Br^{85} and Se^{85}, which are precursors of Kr^{85}, and thus holds the possibility of reducing concentrations of that gaseous fission product in the chimney gas.(3)

Virtually all of the present nuclear explosive experience related to fragmenting rock is associated with single explosion charges. There are virtually no nuclear explosion effects data, even for single charges in the scale depth range of 200 to 325 $W^{1/3}$ (W = the charge weight in kt). This is a very important region if it is desired to produce maximal amounts of fragmented rock for a given explosive yield and leave the rock broken in place. However, considerable data for both multiple explosive charges and experience in this intermediate scaled depth of burial range have been generated from conventional large-scale quarry blasting.

Figure 5 illustrates a typical quarry shot array with the depth of burial and charge spacing related by the $W^{1/3}$ scaling relation. The row of charges effectively kicks out the toe of the quarry by developing a shear plane to the bench, undercutting the overlying material and also heaving it. As a result, the jointing and other natural weakness in the rock fail, which causes fragmentation to a size roughly defined by the natural distribution of these weaknesses. Quarrying experience illustrates the necessity to consider interacting effects of the distribution and orientation of natural weakness in the rock, the extent of new fractures from the explosion, the depth and magnitude of spall, surface topography, reinforcement of shock waves, and also the coalescence of cavity gas between charges. Understanding the relationship of these factors is important for optimizing the useful work done and evaluating the hazards of vented radioactivity and seismic vibrations from multiple charges.

2.1.3. Permeable Fractures

The value of fractures beyond the fragmented chimney rubble depends in large part upon the useful permeability of those fractures and their frequency and distribution. This is especially true for applications of nuclear explosions involving fluids such as oil and gas reservoir stimulation, in-situ ore leaching, and in-situ oil shale retorting. As yet, there is no theoretical basis for predicting induced fracture permeability, and the experimental data are scarce and limited to a few geologic settings. It is commonly assumed that if rock is

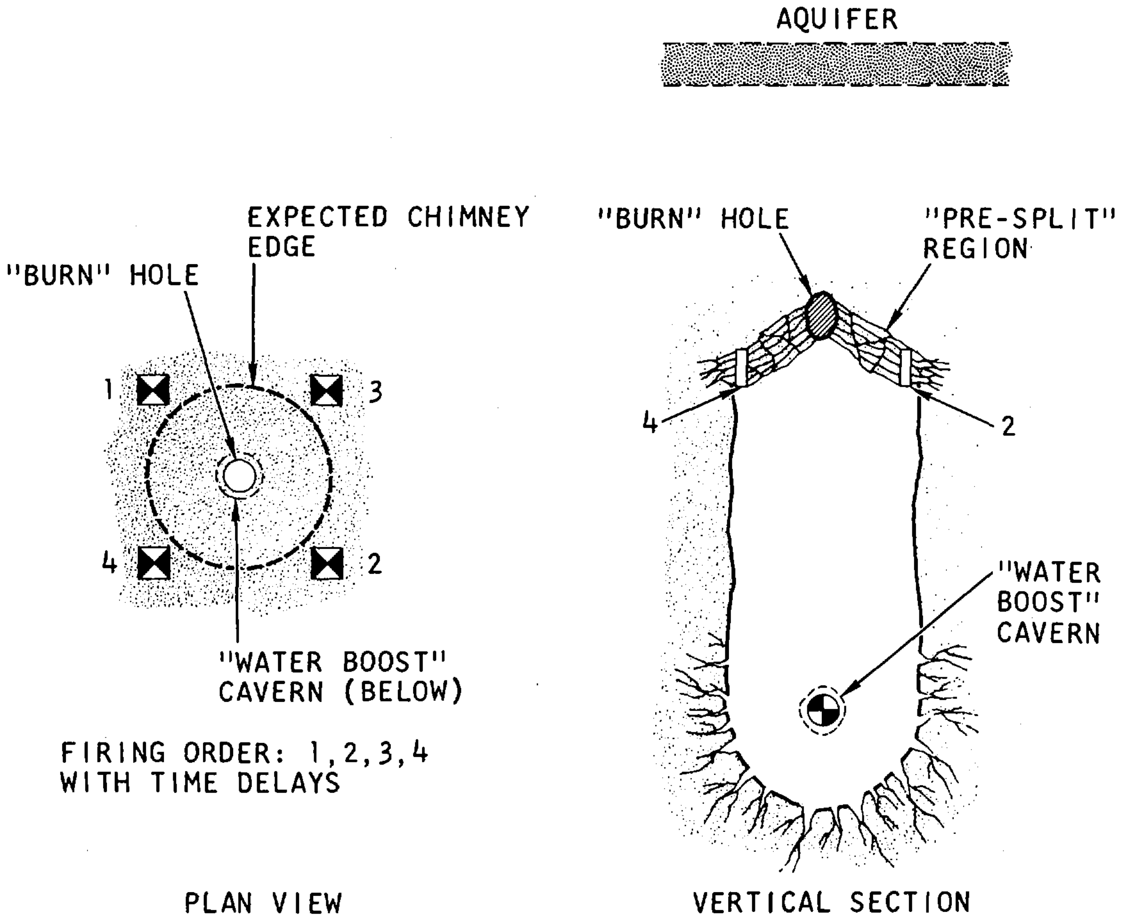

Fig. 3 — Concept for terminating chimney development.

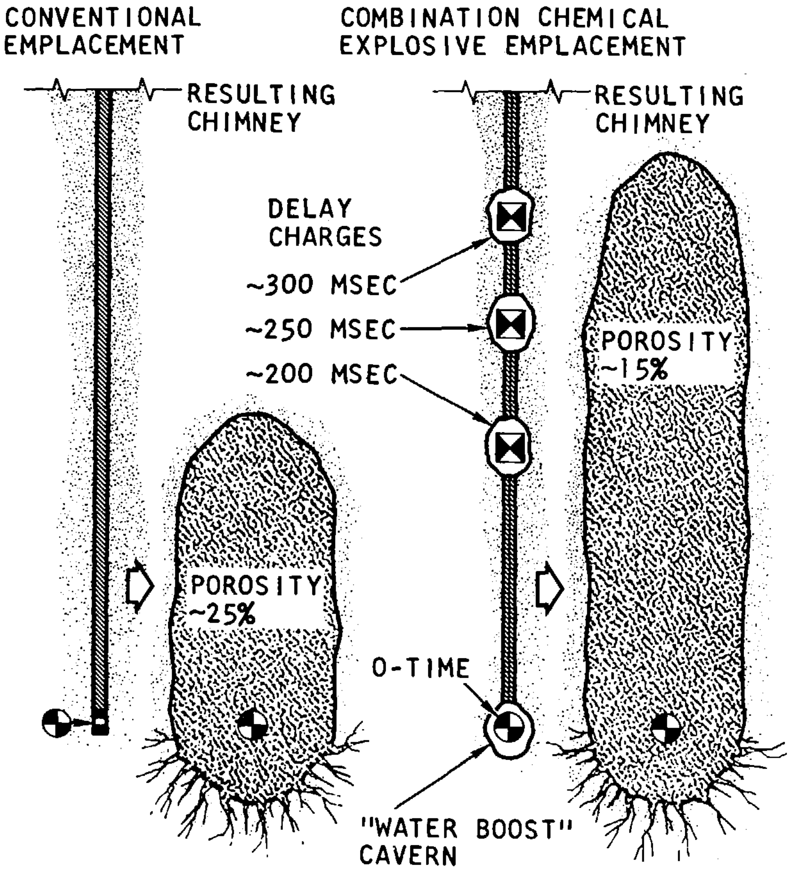

Fig. 4 — Concept for enhancing chimney development.

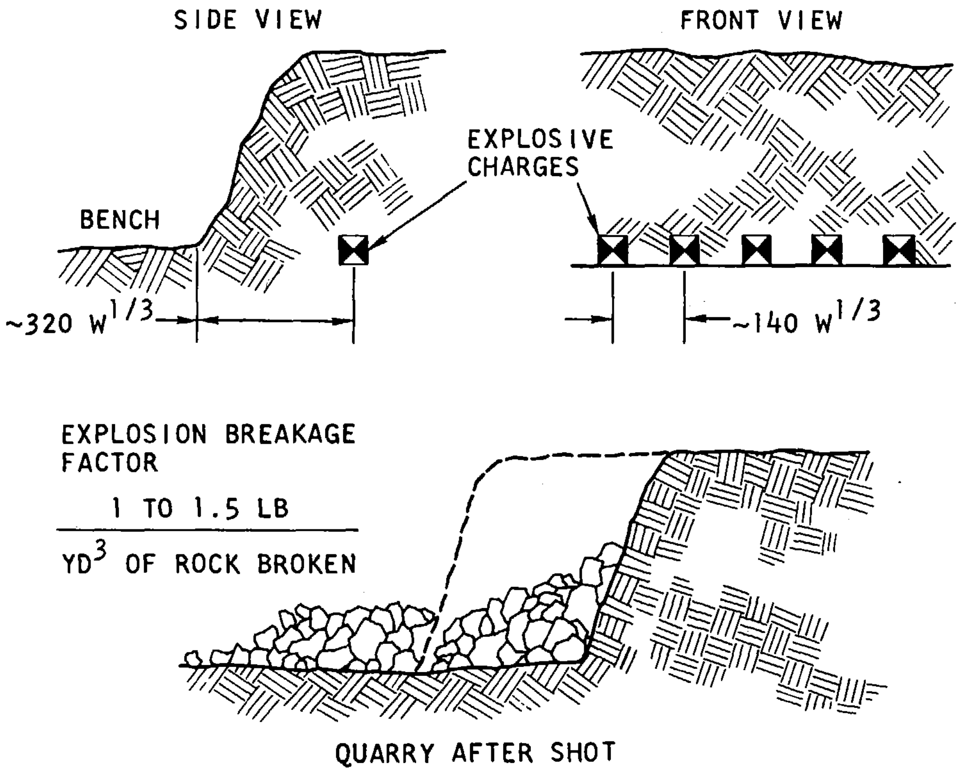

Fig. 5 — Typical quarry, illustrating the cube-root scaling of charge locations.

fractured, it will leak appreciable quantities of radioactivity or, from an optimistic view, the fracturing will allow significant increased flow of natural gas. These are both probably true if the rock undergoes brittle failure and significant differential motion, such as occurs when there is breakage to a free face.

For such applications as rock breakage for in-situ ore leaching or oil shale retorting, it is very desirable and probably an economic necessity to develop intensive permeable fracturing between chimneys. In each chimney, porosity and permeability are going to waste, some of which should be translated into the fractured zones between chimneys. If nuclear explosives were packaged to survive shock loadings up to about 1 kbar, then shooting an array pattern with time delays between detonation of the charges would be possible. Thus, a second charge could break toward the cavity produced by the first charge. This concept is illustrated in Fig. 6. It would be most desirable to build the delay into the explosive package so that there would be no dependence upon external wire leads that could be broken. If the explosive canister cannot provide the required insensitivity to shock, protection could be accomplished in enlarged emplacement holes filled with the appropriate shock-absorbing material.

For applications such as gas reservoir stimulation, the spacing of charges is probably much larger than for the leaching and retorting cases, and thus it is more difficult to enhance fracture permeability. Since most nuclear explosion projects for gas stimulation are intended for low-permeability reservoirs, and the gas in place is in the pore spaces in the rock rather than existing fracture porosity, it is important to establish if there is a threshold permeability below which stimulation by fracturing is of little value. This question should be answered prior to undertaking a full-scale nuclear explosion project.

Another significant question concerns the ability of fractures produced at great depth (4,000 to 20,000 ft) to stay open and keep the useful permeability that is produced by the nuclear explosion. Figure 7 illustrates a method by which fracture permeability as a function of time might be determined before conducting nuclear explosion stimulation tests at a given site. In this method, the vertical hole is drilled below the proposed shot depth for the nuclear charge. The hole is underreamed over a short vertical section, loaded with a few tens of tons of chemical explosive or blasting agent, shot, and cleaned out by the appropriate drilling technique. This creates a void for a subsequent explosive charge to break to. A permeable plug is then set above the void at a point where a whipstock is set. Next, a sidetrack hole is drilled and underreamed at the same level as before, but approximately 20 to 50 ft away. Chemical explosives and blasting agents are then loaded and shot in the hole, breaking and fracturing to the first cavity. Gas can then be circulated under controlled conditions through the fractures to determine the effective permeability produced and monitor changes as a function of time.

2.2. Hazardous Geonuclear Effects

The two major concerns associated with nonexcavation applications of nuclear explosives are, of course, the disposition of the various radioactive species and the severity of seismic vibrations.

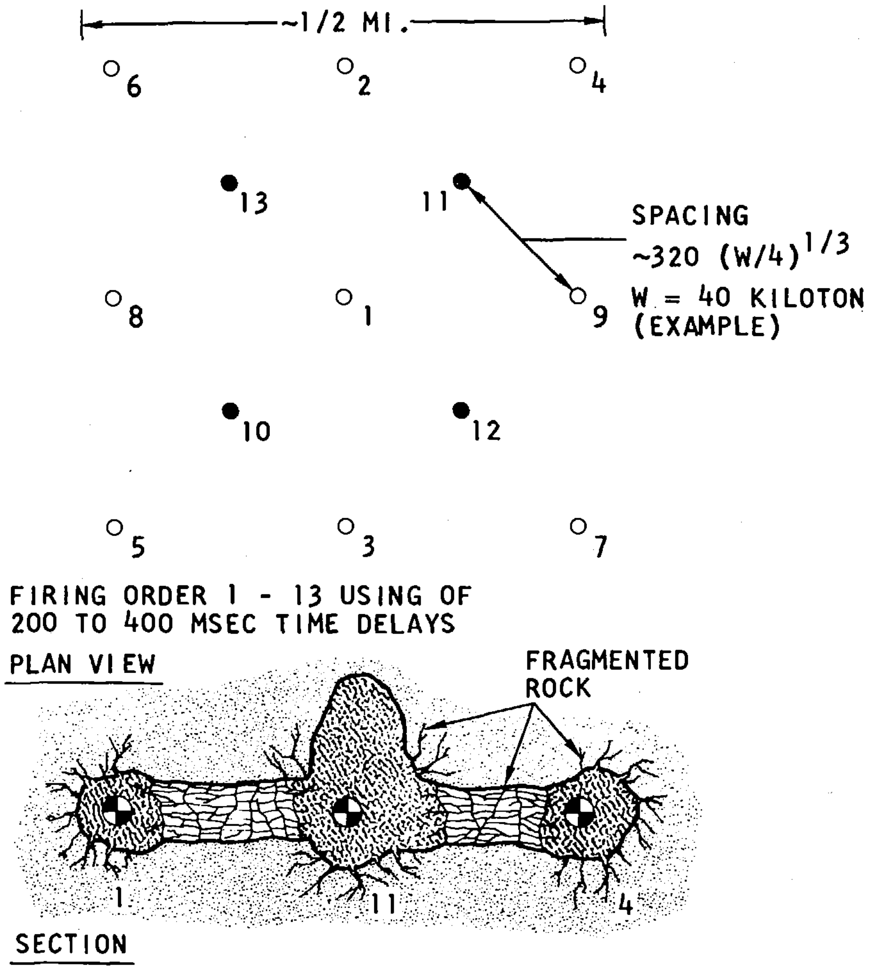

Fig. 6 — Concept for delay firing of nuclear explosives in an array to optimize permeable fracturing.

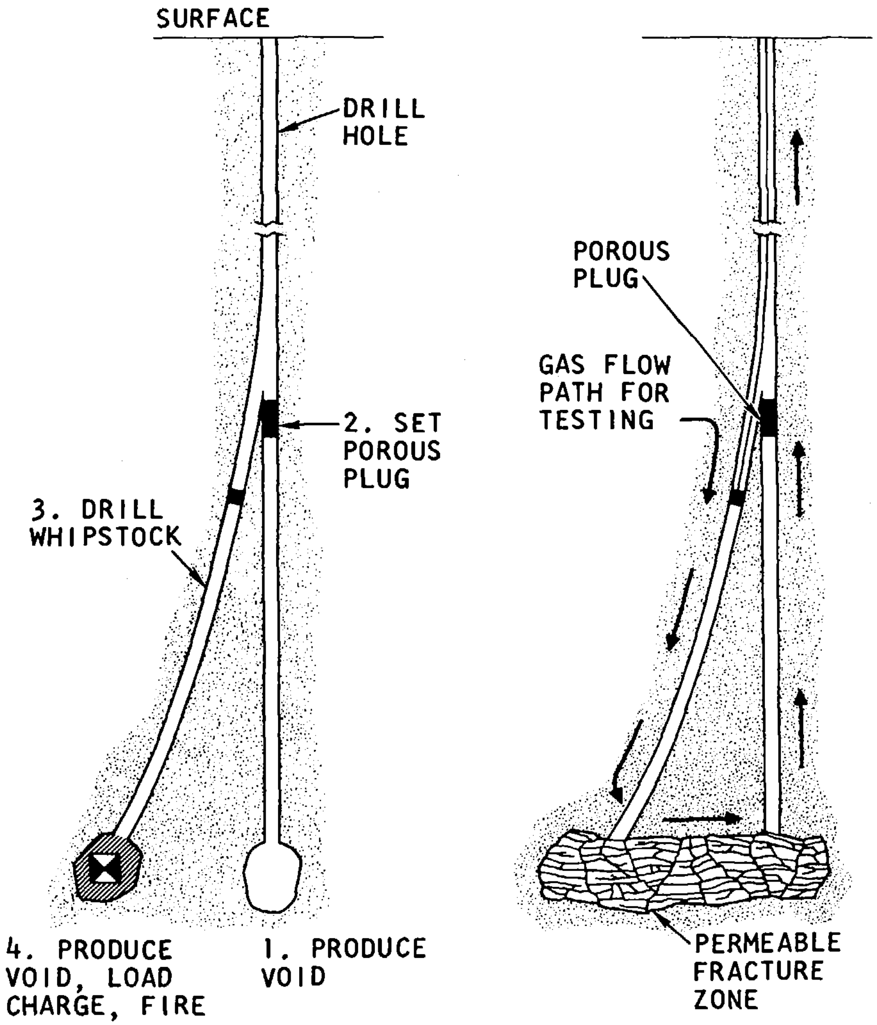

Fig. 7 — Concept for testing persistence of fracture permeability as a function of time.

Some reduction of the potential hazards is a natural by-product of some of the enhancement concepts previously described. Water added to the explosive emplacement greatly reduces induced tritium production and other neutron activation products that would normally be produced from the rock. The possibility exists for isolating some fraction of gaseous or volatile radioactive species from the chimney gas by initiating early chimney collapse. The use of tens to hundreds of tons of chemical explosives and blasting agents to help produce an underground void for some of the enhancement concepts also allows a seismic calibration of a new site prior to the actual nuclear explosion.

The concept of pre-splitting to terminate chimney growth may help reduce development of permeable paths to overlying aquifers or leakage to the atmosphere. At shallow scaled depths of burial and in applications involving multiple firing of nuclear explosive charges, the risk of leaking or venting radioactivity to the atmosphere is increased, and a theoretical and experimental base for prediction is not yet well defined. In the long run, it appears that more potential exists for reducing the radioactive hazards than the seismic hazards. However, the radioactivity is of more concern as another pollutant to the biosphere.

2.2.1. Radioactivity

The first place to try to modify and control those radioactive species that are hazardous if introduced into the biosphere is at the source. Some flexibility exists in the design and packaging of nuclear explosive systems, in the selection of the best explosive system for a particular application and geologic setting, and in the method of explosive emplacement. Advances in all of these areas are of the utmost importance if there is to be an applied nuclear explosion technology.(4)

In addition to adding water around the explosive, the same space can be considered for other additives that would modify the "fireball" chemistry. For thermonuclear explosives that produce large quantities of tritium (T), it is desirable to make the "fireball" oxidizing so that all hydrogen and thus tritium ends up with water as HTO. Although this does not eliminate tritium contamination of hydrocarbons introduced into the chimney, it changes the contaminating processes from direct gas mixing to slower chemical exchange processes. With tritium preferentially residing with water, the more water it mixes with, the smaller will be the amount of it that can exist as water vapor to exchange directly with added hydrocarbon gases.

A good oxidizing agent would thus be one that can be added to water and is cheap. An excellent candidate is ammonium nitrate (NH_4NO_3). It can be mixed with water and, if desired, cross-linking agents can be added to form a gel. This slurry could be added to the emplacement hole right after the storage volume is cleaned out. The nuclear explosive could be introduced at a later time. As the ammonium nitrate slurry is somewhat acid, the explosive should be protected from corrosion. Carbon-14 and tritium are activation products of NH_4NO_3, so the first foot or so around the explosive should be shielded by just water.

Ammonium nitrate is itself a blasting agent, and the nuclear explosive would act as a fantastic primer, causing the reaction $2NH_4NO_3 \rightarrow 2N_2 + 4H_2O + O_2$.

This reaction plus the additional water yields a large quantity of working gas, replacing much of the rock vapor produced in the "unboosted" case. The added nitrogen and oxygen gas represents an improvement over plain "water boosting." Since these additives reduce the amount of rock vapor present in the working gas and since water is a rather efficient heat exchanger, the cavity gas temperature should drop more rapidly upon chimney collapse. This drop could be speeded up by using delay charges to force collapse and increase chimney height as discussed earlier. This technique holds promise for trapping the radioactive tin and antimony in the glass that solidifies from the silicate rock melt, thus keeping I^{131}, the daughter product, more restricted to the glass.

Modification of the geometry of the emplacement hole around the nuclear explosive also holds considerable promise for isolating an appreciable fraction of the radioactivity from either the chimney or overlying aquifers. Declassification efforts are reputedly under way, and further open research in this area should prove of real value in the effort to control the distribution of radioactive debris.(5)

2.2.2. Seismic Vibrations

One of the most fundamental problems that arises from seismic vibrations produced by explosions is determining where the beginning of real seismic damage to structures occurs. It is somewhere above the point of human perception of the vibrations; and for practical considerations above normal excitation from walking in the building, slamming doors, and road traffic. This problem has faced the conventional blasting industries for years, and a number of classic investigations have provided the foundation for present guidelines to blasting practice. One criterion that seems to be generally confirmed by blasting experience is energy ratio, ER:(6, 7)

$$ER = \frac{a^2}{f^2}$$

where a is acceleration in ft/sec^2 and f is frequency in cycles per second.

Figure 8 illustrates the general blasting guidelines, relating ER to amplitude and frequency.(6) The region below an ER of 3 is generally considered safe and free from plaster cracking where construction quality is good and the structures are not abnormally prestressed by such processes as settlement. An ER of 1 is generally thought to contain a safety factor but is well above vibration levels that are easily perceptible.

Figure 9 compares the spectral response of a hypothetical building in Hattiesburg to the 5-kt Salmon event with the corresponding response of another hypothetical structure in Las Vegas to ground motion produced by the 1.2-Mt* Boxcar event.(8) According to Nadolski, the pseudo-absolute acceleration (PSAA) is approximately twice the actual ground acceleration measured.(9) The corresponding ER is about 0.07 in Hattiesburg and 0.002 in Las Vegas for the same frequency of 3 to 4 cycles per second (see Fig. 9).

---

[*] Announced United States Nuclear Tests, USAEC, Nevada Operations Office, July 1, 1969.

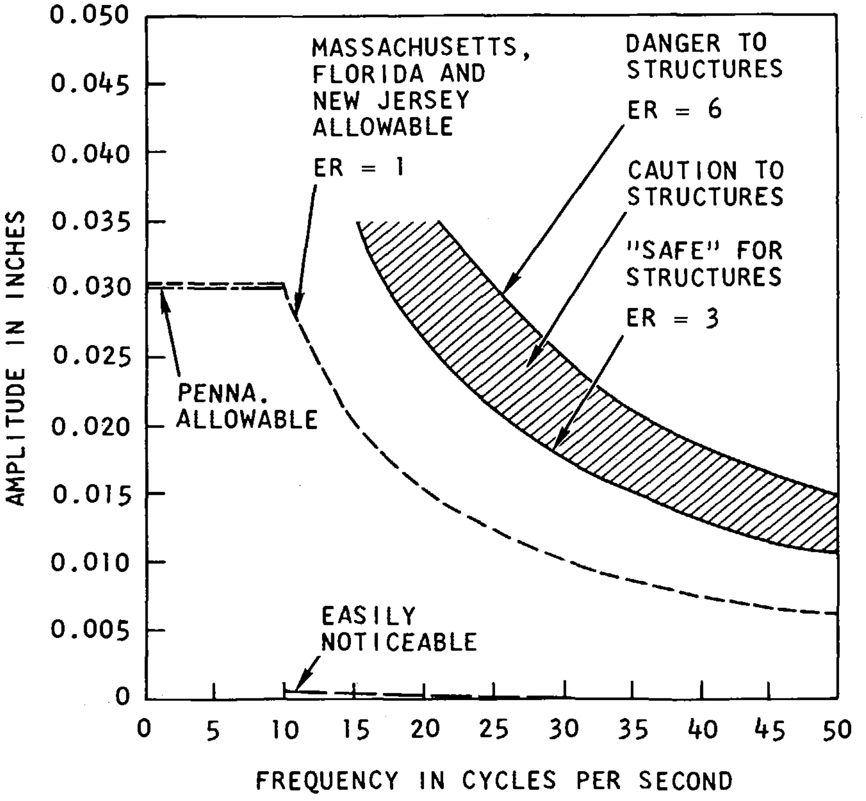

Fig. 8 — Energy ratios related to frequency, amplitude, and damage to structures.

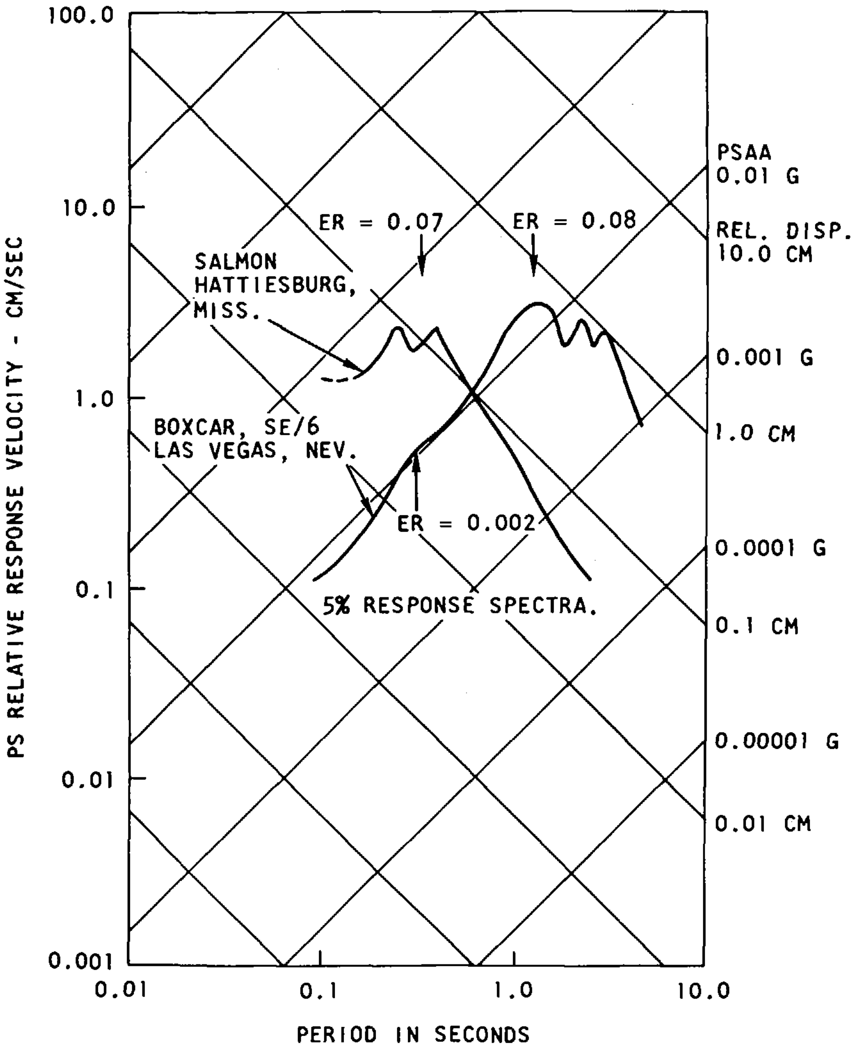

Fig. 9 — Comparison of response spectra and energy ratios for two nuclear explosions (four-way log plot).

The point of this discussion is to emphasize that the blasting industry has been applying acceleration and frequency criteria as indicators of potential damage. However, the important question is: What criterion does predict real damage to structures? Assuming that a building responds as a simple or even a very complex oscillator to the measured ground motion probably does not provide a proper model if the apparent damage observed on buildings is characteristic of foundation settlement.

Nuclear explosions, because of their size, can involve large populations that feel the seismic vibrations. One area where chemical explosions excite reactions in large populations is Dade County, Florida (the vicinity of Miami). In that area, near-swamp conditions exist and the porous Miami oolite formation is widespread within a few feet of the surface. Because of the population growth and the demand for aggregate and fill, there are many quarries and other blasting activities that can be felt in nearby residences and buildings. Vibrations from chemical explosions in the oolite material are naturally filtered to low frequencies (approximately 4 cps) over short distances. Damage complaints are commonly received from blasting down to an ER of 0.02 and even as low as an ER of 0.005. This extreme corresponds to an explosion in that area of 60 lb at a distance of 1.25 miles.(10) The state recognizes the blasting allowable up to an ER of 1, but the practice of granting blasting permits within the county commonly holds the ER to very low values--equal to or less than those measured in Hattiesburg from the Salmon event. This enforcement policy is judged to be an attempt to reduce damage complaints to near zero. Documentation before and after blasts in a sampling of nearby structures is routine, and over the years considerable information has been accumulated. Mr. Robert Banning is one person who performs this service in the Dade County area, and he has not observed damage caused by blasting below an ER of 1.(10)

It is extremely important, therefore, that such concepts as PSAA not be adopted as criteria for estimating seismic damage until considerable preshot and postshot documentation of actual minor architectural damage is developed. A PSAA of 10 to 15 cm/sec^2 may be a good estimate of the vibration energy sufficient to agitate a population so they will examine their structures and complain of cracks observed. The Florida experience is consistent with this PSAA value, and a similar ER value is on the order of 0.01. Ordinary ditch blasting in the vicinity of Niagara Falls precipitated 3000 damage claims.(11) It would be worthwhile to examine that experience in detail to see what evidence and documentation exist that are related to the causing of real damage.

There is still a great deal to be learned about how chemical explosions, nuclear explosions, and earthquakes can cause damage to a variety of structures in different geologic settings. This information is needed for improving building codes and building practice, refining blasting limits, and providing a greater degree of safety to the public. Good public relations and competent engineering seismology are required so that both nuclear explosion projects and projects conducted with chemical explosions are not unduly hampered.

III. CONCLUSION

Presently, the benefits and risks associated with the effects of nonexcavation nuclear explosions are not well established as a foundation for an applied technology. Suggestions have been made of possible ways to enhance the useful effects and minimize the hazards. Cross-fertilization of nuclear and chemical explosion technology will make a significant contribution to these goals and to the commercialization of nonexcavation explosive engineering techniques.

REFERENCES

1. Boardman, C. R., and J. Toman, "Use of Nuclear Explosive Devices for Development of Underground Storage Caverns," USAEC Report UCRL-14746, Lawrence Radiation Laboratory, Livermore, April 20, 1966.

2. Selph, W. E., Gulf General Atomic Incorporated, unpublished data.

3. Smith, C. F., Lawrence Radiation Laboratory, Livermore, private communication.

4. Gofman, J. W., and Arthur R. Tamplin, "Federal Radiation Council Guidelines for Radiation Exposure of the Population-at-Large--Protection or Disaster?," testimony presented before the Subcommittee on Air and Water Pollution, Committee on Public Works, United States Senate, 91st Congress, November 18, 1969.

5. Curtis, Harold, U. S. Atomic Energy Commission, Dept. of Peaceful Nuclear Explosives, private communication.

6. Leet, L. Don, Vibrations from Blasting Rock, Harvard University Press, Cambridge, Massachusetts, 1960.

7. Crandell, F. J., "Ground Vibration Due to Blasting and Its Effect Upon Structures," J. Boston Soc. Civ. Eng., 36, No. 2, 222-245 (April 1949).

8. Blume, J. A., "Ground Motion Effect," in "Proceedings for the Symposium on Public Health Aspects of Peaceful Uses of Nuclear Explosives, Las Vegas, Nevada, April 1969," Southwestern Radiological Health Laboratory Report SWRHL-82, 1969.

9. Nadolski, M. E., "Architectural Damage to Residential Structures from Seismic Disturbances," USAEC Report UCRL-71015, Lawrence Radiation Laboratory, Livermore, 1968.

10. Banning, Robert, private communication.

11. Hammon, S., and N. Hammon, "Panic and/or Inexperience in the Handling of Mass Claims Resulting from Explosions. Remarks on the paper 'Survey of Complaints of Seismic Related Damage to Surface Structures Following the Salmon Underground Nuclear Detonation,' by Dean V. Power," Bull. Seismol. Soc. Amer., 58, No. 3, 1169-1172 (1968).

XA04N0745

LOADING-UNLOADING PRESSURE-VOLUME CURVES FOR ROCKS*

D. R. Stephens and E. M. Lilley
Lawrence Radiation Laboratory, University of California
Livermore, California 94550

ABSTRACT

The stress-strain codes (SOC and TENSOR) used to calculate phenomenology of nuclear explosion for the Plowshare Program require inter alia the pressure-volume relationships of the earth media. In this paper we describe a rapid and accurate method to obtain pressure-volume data to 40 kb at 25°C for rocks. These experimental results may also be related to the in situ elastic properties of the rock and to other laboratory measurement of properties, such as ultrasonic experiments with pressure and Hugoniot determinations.

Qualitative features of the pressure-volume curves can be related to the initial porosity of the rock. A porous rock is usually quite compressible at low pressures. If the porosity is in the form of narrow cracks, the cracks are closed at a pressure of about 3 to 6 kb, after which the rock is much less compressible. If the porosity is in the form of spherical pores, it is not necessarily removed even at pressures of 40 kb, depending on the strength of the rock, and the compressibility is higher at all pressures than for a similar rock containing no porosity.

Data for water-saturated samples show the phase transformation due to free water at about 10 and 22 kb. However, the presence of "nonliquid" water, which is loosely contained within the lattice of clay or zeolitic minerals or adsorbed on particle surfaces, is also observed.

INTRODUCTION

One of the most important requirements of the Plowshare Program is preshot prediction of the physical effects of a nuclear explosion in a given media. This includes pressure, velocity, and acceleration profiles, crater geometry and ejecta patterns for a cratering experiment, and chimney geometry and extent of fracturing in an underground experiment. Although much useful information may be gained from empirical, scaled data, an accurate prediction can only be made from a first-principle calculation using the actual physical properties of the medium. Cherry[1,2] has described a number of these calculations. Since the properties of the rock in the explosion environment may vary widely from one area to another, equation-of-state data must be obtained for each rock type. One of the important sections of an equation of state is the pressure-volume (PV) behavior of materials.

---

*Work performed under the auspices of the U. S. Atomic Energy Commission.

Schock[3] and Heard[4] describe other portions of the equation of state. "Equation of state" as used at LRL implies data on the inelastic behavior of the material as well as its elastic properties.

In this paper we describe a method both rapid and accurate to 5% to obtain pressure-volume data to 40 kb;* we also present some considerations and limits on the type of data to be expected, results of several materials studied, and a comparison of experimental results with elastic theory models. We obtain isothermal data by this method. The PV data required in the calculations are the Hugoniot for initial pressurization followed by isentropic unloading. These PV paths are readily calculated from the isotherms.

EXPERIMENTAL

Two types of equipment are used for these bulk PV measurements. One is a piston-cylinder die employing a solid pressure-transmitting medium (PTM) end-loaded in a double-acting hydraulic press, which is capable of maximum pressures of 40 kb. The other is also a piston cylinder die, but employs a liquid PTM to obtain data at pressures of 5 kb or less. The solid PTM system is insensitive to data below 5 kb, since the PTM does not approximate a fluid at lower pressures.

The die and sample assembly for the 40-kb system are shown in Fig. 1.

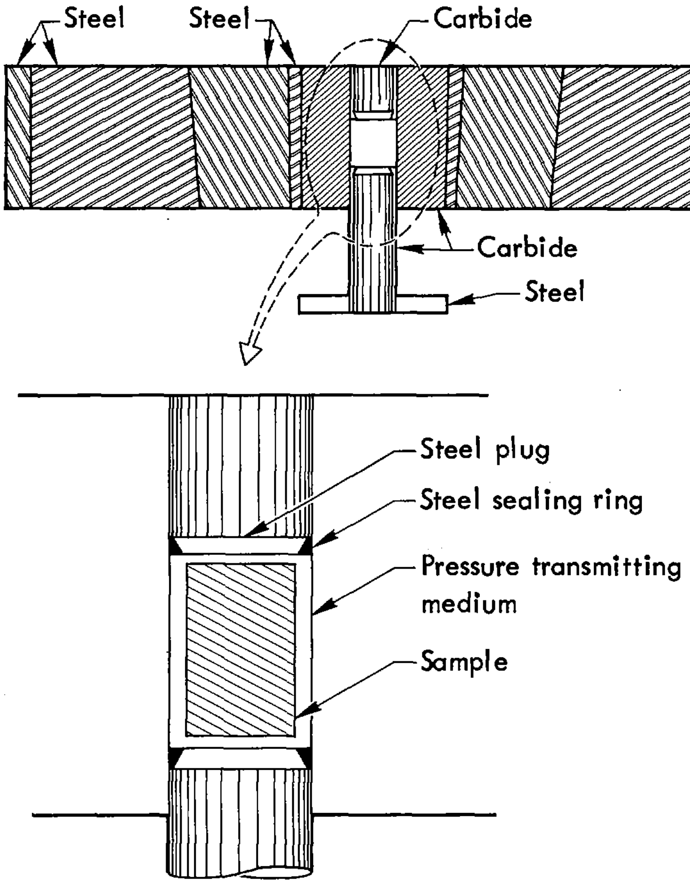

Fig. 1. 40-kb die and sample assembly.

---

*1 kb = 10^9 dynes/cm^2 = 987 atm.

The pistons are packed with steel sealing rings and plugs to prevent extrusion of the PTM. We use either tin or lead as the PTM. Both metals have a low shear strength and are quite ductile; thus the principal stresses, especially above a few kb, approximate hydrostatic conditions.

One ram of the press end-loads the top and bottom of the tungsten carbide core, while the other ram presses on the tungsten carbide piston. This end-loading serves to add support to the core and prevent transverse fracture.

In the piston-displacement method, corrections are necessary to obtain the true volume change. These include the contraction of the pistons, expansion of the bore of the die, and other pressure effects. Therefore, we use gold as a standard and measure its compression to correct for these distortions.

We have used PV data for gold both from Bridgman's work[5] and that of Daniels and Smith.[6] Although the two sets of data differ somewhat, the compressibility of gold is sufficiently small that the differences are not important in our work.

Displacement is measured by a rectilinear potentiometer and applied force by a load cell. In previous work[7-9] these two signals were displayed on a xy recorder while pressures were increased and decreased manually. We now use a completely computer-controlled system, described in detail by Grens.[10] Briefly, a PDP-9 computer is programmed to perform loading and unloading cycles (up to 10) upon the sample, with a slow and constant loading and unloading rate of about 1 kb/min, and to read and store the displacement versus force data.

With this method, calculations are quite simple. After a sample has been pressed to the maximum pressure of 30 to 40 kb, a hysteresis loop of piston displacement versus pressure is obtained for each run, which establishes the friction as described by Bridgman.[11] The true displacement, and therefore the compression, is then obtained. The friction is taken as essentially one-half the difference in pressure of the ascending and descending loops, neglecting the first part of the descending loop.

Blank runs are made with gold before and after sample runs. The gold volumes are made equal to the samples; the amounts of other materials, such as steel rings and plugs and the pressure transmitting medium, remain constant from run to run. With the known volume of gold as a function of pressure, the volume of the sample is also known. These calculations are also carried out with the aid of the PDP-9 computer.

Two dies are used; one has a 0.5-in. bore and takes a sample 0.460 in. in diameter by 1 in. long, and the other has a 1-in. bore and takes a sample 0.88-in. in diameter by 1 in. long. The larger size is preferred for very heterogeneous materials.

The 5-kb liquid system is shown schematically in Fig. 2. Octoil-S is the pressure-transmitting fluid in this system. The diameter of the bore of the die is 1-1/4 in., permitting 1-in.-diam samples. The samples are either copper-jacketed or coated with epoxy to prevent access of the PTM to the sample. Control and calculation with this system are similar to the 40-kb system; blank runs are made as already described.

We use the 5-kb liquid system for very compressible rocks only. Errors in volume are larger in this system than in the solid device, as the Octoil PTM is much more compressible than tin or lead. For the solid system, the errors are ±0.2% in initial density or ±5% in change in volume or pressure. Errors in

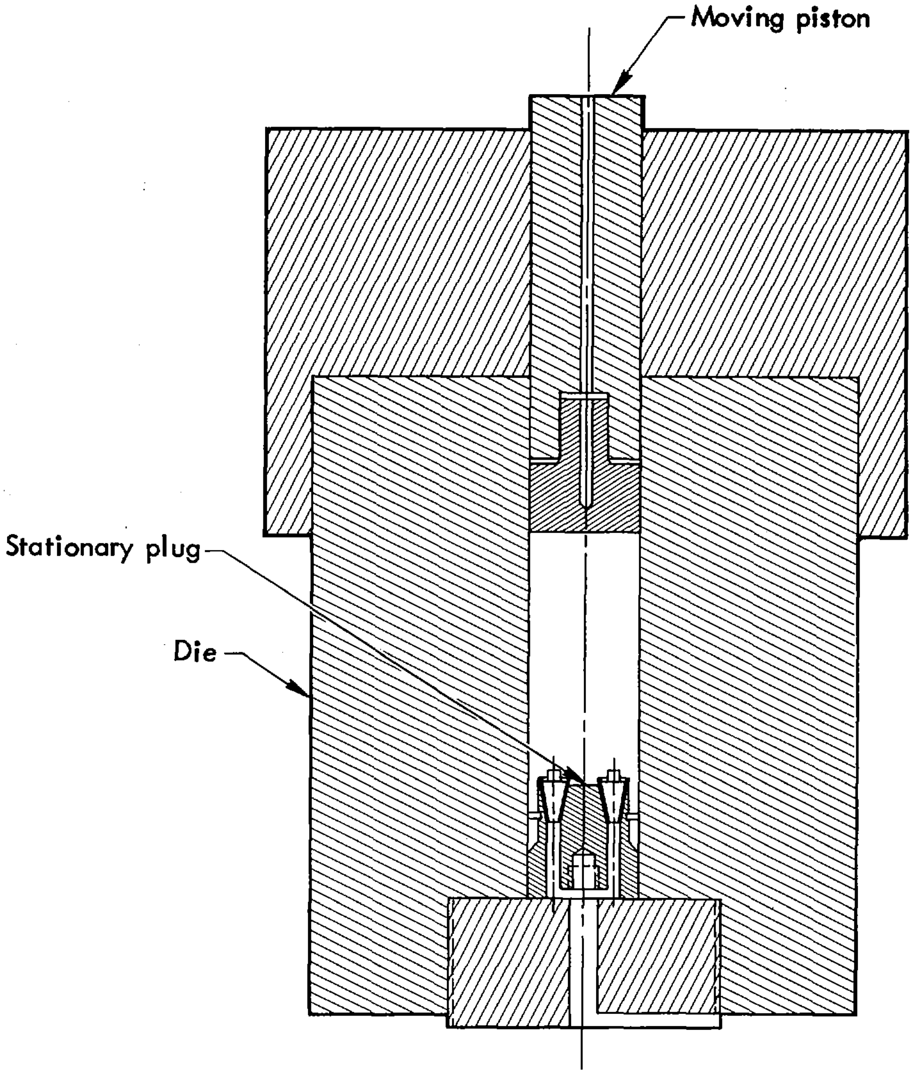

Fig. 2. Liquid PV cell.

the liquid system are not as well established. Errors in pressure are no more than ±1%, but errors in volume for incompressible rocks are as much as 10%. For compressible rock the errors are approximately 5%. A somewhat smaller version of the liquid cell is described by Keller.[12]

In some cases, it is desirable to obtain data with fractured specimens, as PV curves may change when rocks are fractured by shock loading. In addition, since rock near a detonation may undergo several cycles of stress application and release, it is also necessary to obtain sequential loading-unloading PV curves for the same materials. This would not be necessary for samples without porosity. However, most rocks of interest are very porous and the loading-unloading paths are different even when loaded to only 1 kb.

We use two methods of fracturing samples. One is to drop a weight on the sample from a known height; second is to detonate a small charge of high explosive near the sample. The two methods produce deformed rock with fracture patterns which roughly approximate those observed in rock recovered from the vicinity of nuclear explosions.[13] This is reasonable, since both methods produce a rather intense stress wave which propagates through and fractures the rock at a high strain rate. The actual stress histories of the two methods are complex; however, the peak stresses in the high-explosive method are at least an order of magnitude higher than in the dropping-weight test.

PRESSURE-VOLUME CONSIDERATIONS

In principle, it is possible to calculate the pressure-volume relationship for any rock if the rock contains no porosity and the volume fractions and compressibilities of the minerals are known. Compressibilities as a function of pressure for many minerals have been given (for example, in Birch's compilation[14]) and the compressibility of the aggregate may then be determined from the Reuss and Voigt limits.

Hill[15] showed that these methods yield upper and lower bounds for the average compressibility β,

$$\beta_V < \beta < \beta_R ,$$

where β_V is the Voigt compressibility, β_R is the Reuss compressibility, and

$$\beta = -\frac{1}{V_0}\left(\frac{\partial V}{\partial P}\right)_T$$

In the Reuss averaging method, stress is assumed to be uniform throughout the aggregate, and

$$\beta_R = \sum_i X_i\beta_i , \tag{1}$$

where X_i = volume fraction of component i.
The difficulty with this model is that, under pressure, the distorted grains can fit together only with some peripheral fracture and/or intracrystalline flow.

In the Voigt model, strain is assumed to be uniform throughout the aggregate and

$$\frac{1}{\beta_V} = \sum_i \frac{X_i}{\beta_i} . \tag{2}$$

The difficulty with this model is that the forces between grains are not in equilibrium.

The two methods yield values which usually agree within a few percent. Brace[16] has described the method in detail and has applied it to several dense rocks. We have also used the method to describe the compression of a granodiorite and a dolomite.[8]

However, most rocks are porous and require consideration of porosity effects on compressibility. Walsh[17] has shown that the compressibility of porous solids can be calculated if the porosity consists of a low concentration of either spheres or narrow cracks and, in the latter case, the geometry of the cracks are known.

The effect of spherical pores on compressibility is[17]

$$\beta_{eff} = \beta_i (1 + a\eta_P) \tag{3}$$

where β_{eff} is the actual compressibility of porous rock, β_i is the intrinsic compressibility of material of theoretical density, η_P is the porosity due to spherical pores and <u>a</u> is defined below:

$$a = \left(\frac{3}{2}\right)\left(\frac{1 - \nu}{1 - 2\nu}\right)\left(\frac{1}{1 - \eta_P}\right)$$

where ν is Poisson's ratio.

For low porosity and a Poisson's ratio between 0.2 and 0.33, a varies between 2 and 3.

The effect of narrow fractures on compressibility is[17]

$$\beta_{\text{eff}} = \beta_i \left(1 + a\overline{C}^3\right) \tag{4}$$

where a is a constant and $\overline{C}^3$ is (average fracture length) cubed per unit volume.

Walsh[17] showed by evaluating the constant in Eq. (4) that the effects upon compressibility of fractures and spherical pores at equal concentrations are equivalent, if the diameter of the spherical pores is about two-thirds the average fracture length. Thus, for equal total porosity at any given state, fractures have a much greater effect on compressibility than do spherical pores.

Walsh[17] also showed that P_c, the pressure to elastically close an elliptical crack, is approximately

$$P_c = E\alpha \tag{5}$$

where E is Young's modulus and α is the ratio of minor axes to major axes of the elliptical crack. As discussed by Walsh[17] and shown experimentally by Brace[16] and the authors,[8,9] fracture porosity disappears at moderate pressure. For many rocks, E is approximately 500 to 1000 kb and crack porosity disappears at a few kb; hence, α is of the order of 10^{-3} to 10^{-2}.

Of necessity, the preceding considerations are somewhat idealized. At least some of the porosity in rocks does not take the form of either spherical pores or narrow fractures of given length. In addition, the theory described assumes that the rock in the vicinity of the pore or fracture is elastic and isotropic. Obviously, at sufficiently high pressures, component minerals near an opening may undergo brittle failure or intragranular flow. It can be shown[9] that the locus of failure of an empty spherical pore in an elastic, isotropic, infinite medium is the point at which the shear strength of the medium is equal to three-fourths the mean pressure. Experience with most dry silicate rocks shows that, at 5 to 10 kb, the shear strengths are in the range 6 to 10 kb and increase with pressure.[18] Spherical pores in such rocks probably will not fail at 10 kb. It is assumed, of course, that the rocks satisfy the criteria of the model (elastic, isotropic, empty pores, etc.). It is reasonable to expect the shear strength to increase with pressure and, in fact, this is indicated in experiments by Riecker[19] and by Giardini[20] to pressures of 80 kb. Therefore, spherical pores may survive in strong rocks at our maximum pressure of 40 kb. However, spherical pores in many weak sedimentary materials, such as calcite and clay shales, should be closed at considerably less than 40 kb.

Thus, it appears that spherical pores may persist to 40 kb in moderately strong rocks. Pores of other geometry may fail at lower pressures. Even at failure, porosity may not completely disappear; for if the rock is brittle, material will spall into the cavity and some porosity will remain.

RESULTS AND DISCUSSION

Our experimental data will now be described and compared to the theoretical and empirical considerations just discussed.

Loading data for Stirling quartzite are shown in Fig. 3 and in Table I. The rock is from hole UeNb, an exploratory hole near the proposed Sturtevant cratering experiment. The material is described by Schock.[3] Note that both samples, from 500- and 900-ft depths (Schock Type B and Type C & D, respectively), are more compressible than quartz. This may be due in part to impurities in the quartzite; however, a more important reason is the porosity in each sample; at least 0.5% in the 500-ft sample and 1.6% in the 900-ft sample. These porosities are based on the initial specific volume and the specific volume after pressurizing to 40 kb and unloading. It is a lower limit, since

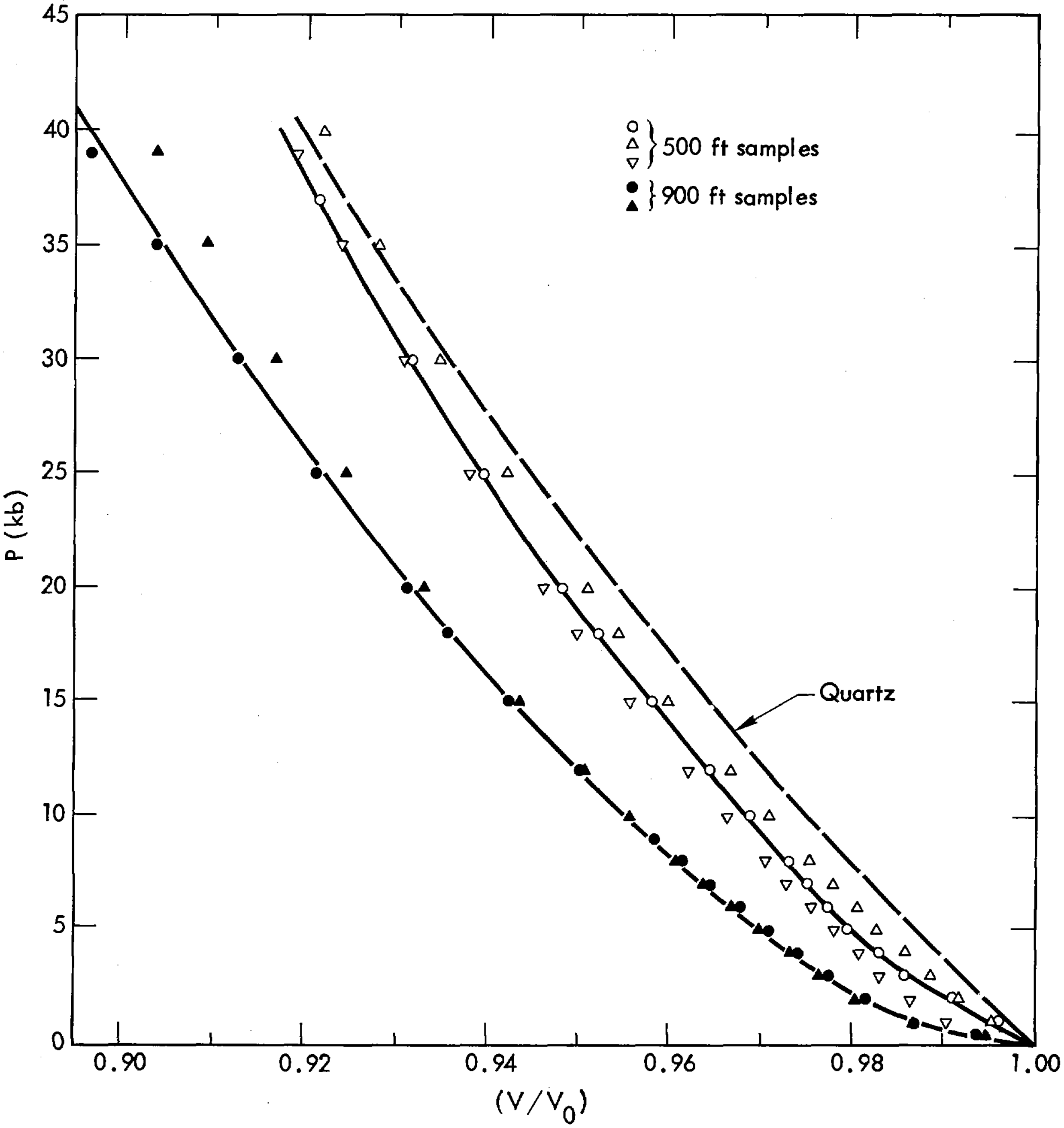

Fig. 3. Loading PV data for Stirling quartzite, hole UeNb. Data for quartz shown for comparison.

Table I. Loading-unloading PV data for Stirling quartzite, hole UeNb, 1.5% H_2O.

500-ft samples			900-ft samples		
ρ_0 = 2.650 g/cm^3			ρ_0 = 2.516 g/cm^3		
K_0 = 220 kb			K_0 = 76 kb		
P	V/V_0		P	V/V_0	
(kb)	loading	unloading	(kb)	loading	unloading
0	1.0000	0.9947	0	1.0000	0.9837
1	0.9954	.9912	1	0.9868	.9795
2	.9909	.9882	2	.9812	.9755
3	.9867	.9852	3	.9769	.9716
4	.9831	.9824	4	.9735	.9682
5	.9800	.9798	5	.9701	.9648
6	.9776	.9775	6	.9670	.9620
7	.9752	.9752	7	.9640	.9593
8	.9730	.9730	8	.9610	.9565
10	.9685	.9685	10	.9552	.9515
12	.9642	.9642	12	.9501	.9467
15	.9578	.9578	15	.9429	.9400
18	.9519	.9519	18	.9361	.9339
20	.9480	.9480	20	.9319	.9300
25	.9393	.9393	25	.9221	.9211
30	.9315	.9315	30	.9130	.9126
35	.9240	.9240	35	.9045	.9045
40	0.9170	0.9170	40	0.8964	0.8964

some porosity probably remains after such a pressure excursion. Compressibilities of the quartzites as a function of pressure on loading and unloading are shown in Fig. 4, along with the compressibility of quartz according to Anderson et al.[21] The plots show that the compressibilities above 5 kb for the 500-ft samples were identical above 5 kb and in reasonable agreement with the quartz data. One can then infer that the porosity in the 500-ft sample was eliminated by pressures of 5 kb and that, according to Eq. (5), the porosity was in the form of narrow cracks of aspect ratio 5×10^{-3} or smaller. Data for the 900-ft samples imply that the compressibility for loading and unloading were different up to 35 kb. Thus, the porosity in these samples may have been elliptical with a much higher aspect ratio.

The results imply that at low pressures, on release some of the porosity recovers. A large increase in compressibility above that for quartz appears to begin for the 900-ft specimens at about 11 kb and for the 500-ft samples at about 4 kb. Using the single crystal quartz data as a model, we can compute that the 500-ft samples contained 0.7% porosity initially and 0.2% upon unloading; for the 900-ft samples, 2.4% initial porosity and 0.8% upon unloading.

Loading PV data for five Green River oil shales are shown in Fig. 5. These samples were studied for preliminary calculation of the Bronco experiment, which is planned as an oil shale stimulation experiment in the Plowshare underground engineering program. Samples marked (A) are from the USBM Anvil Points Mine, Rifle, Colorado, while samples marked (B) are from Colorado Core Hole No. 3, Rio Blanco County. The material is usually a carbonate rock (marlstone) containing kerogen, a hydrocarbon having a high molecular weight. A typical analysis for the kerogen-free rock is shown in Table II. Since the carbonate rock is much denser than the kerogen (ρ = 2.7 as compared to 1.0) a low sample density usually denotes a high kerogen

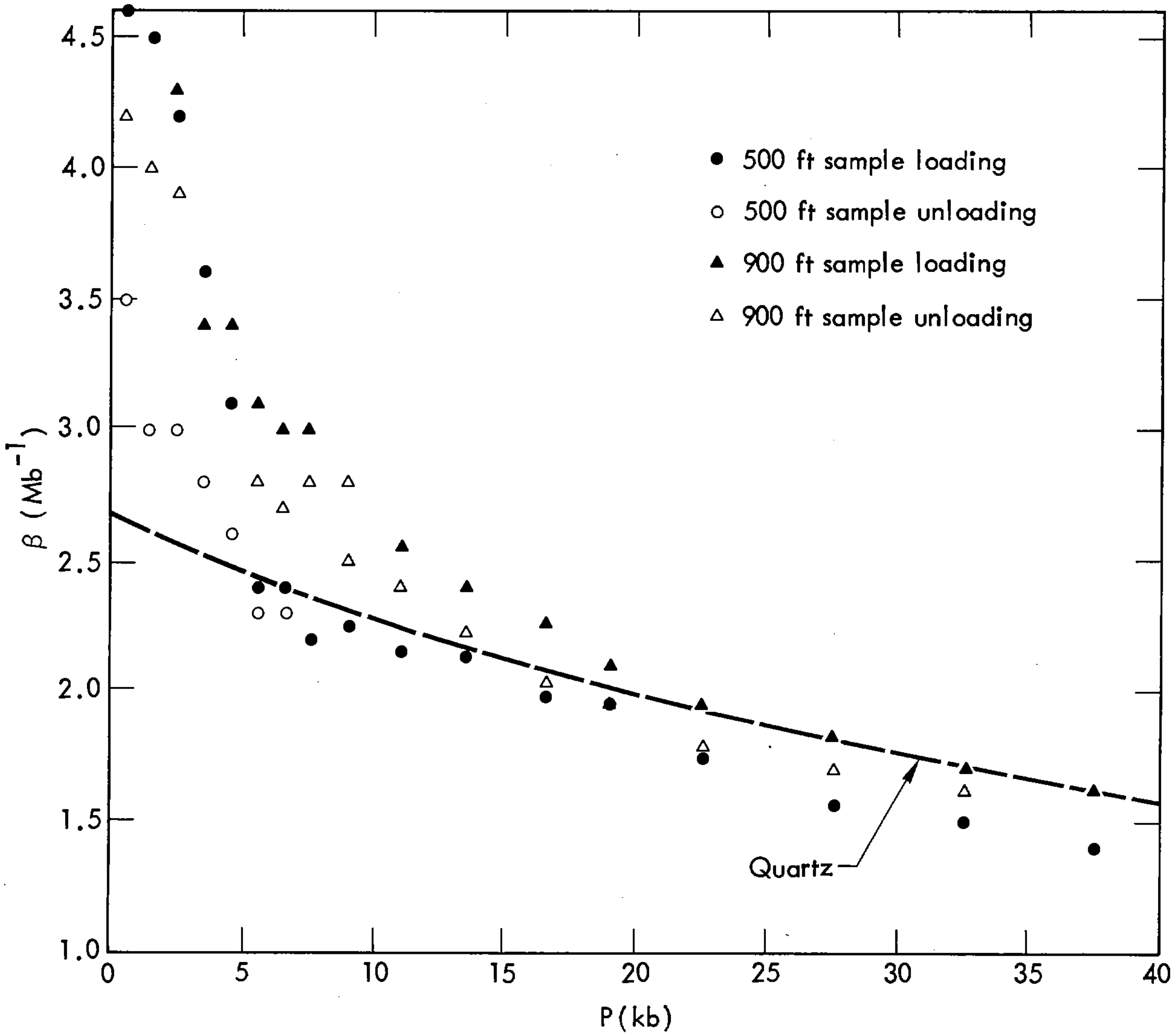

Fig. 4. Compressibilities (β) versus pressure for Stirling quartzite. Data for quartz shown for comparison.

content. Since the kerogen is more compressible than the rock, one then expects the lower density samples to be more compressible than higher density specimens. However, this is not the case unless the samples are divided into two groups, those with about 0.7% initial porosity and those with about 4% porosity. Then, a low initial density correlates with compressibility.

Table II. Typical analysis for Green River oil shales, oil excluded.

Mineral	Volume %
Dolomite	48
Feldspar	21
Quartz	13
Illite	13
Analycite	4
Pyrite	1

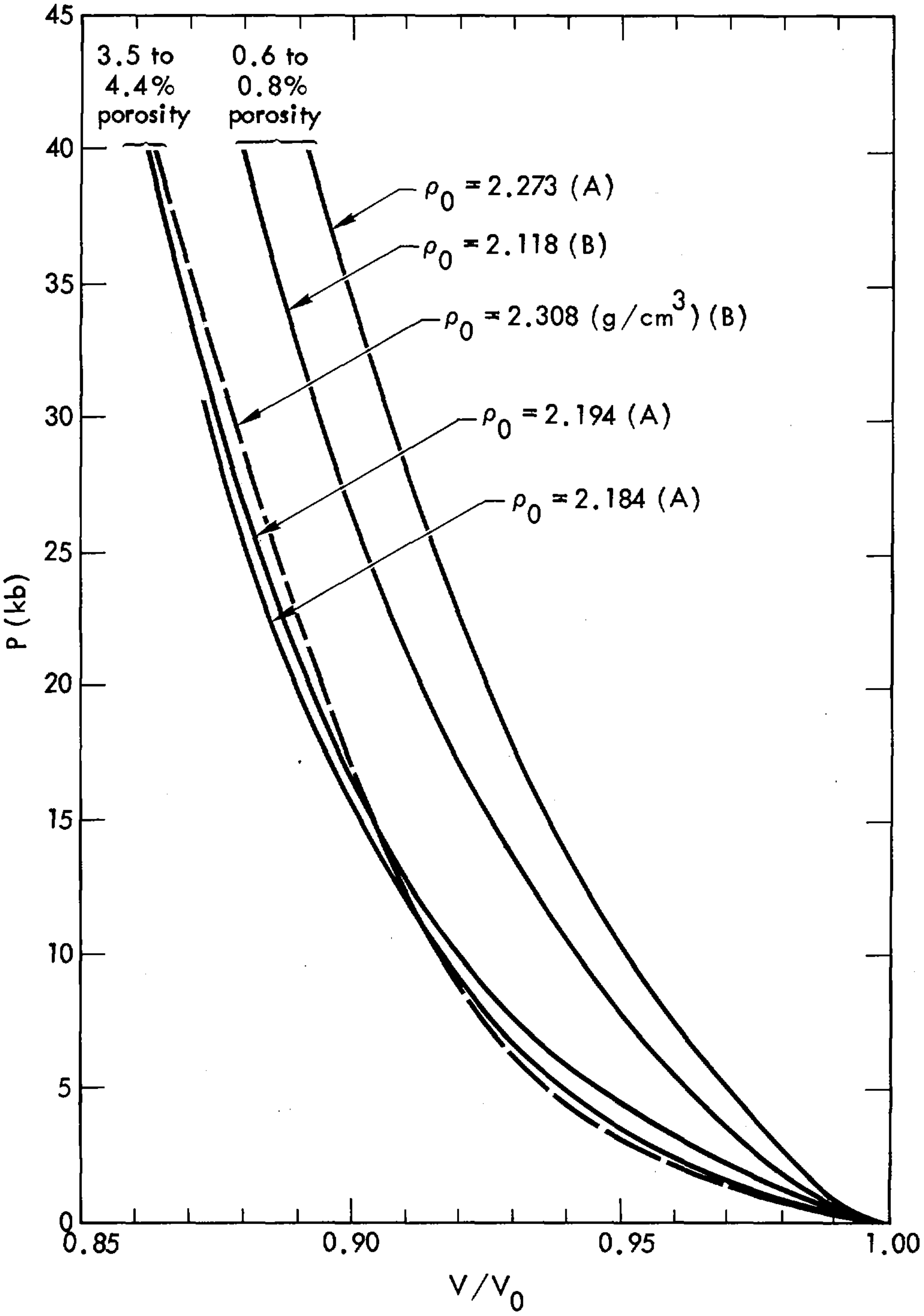

Fig. 5. Pressure versus relative volume for Green River oil shales, loading data.
A Anvil Points Mine samples
B CCH3 samples
Initial densities and porosities are indicated.

It is usual practice to infer oil content of an oil shale from a plot of oil content with density. The preceding shows that this is a dangerous practice, at least for small samples, as the density is also a function of gas-filled porosity.

Complete loading-unloading data for these shales are shown in Tables III-VII.

Table III. Loading-unloading PV curves for Green River oil shale, Anvil Points Mine samples. $\rho_0 = 2.184\ g/cm^3$; minimum gas-filled porosity: 3.7%. Bulk modulus at 0.2 kb: K = 62 kb.

P (kb)	Loading v (cm^3/g)	 $\frac{V}{V_0}$	Unloading v (cm^3/g) From 0.6 kb	 From 1.2 kb	 From 3.7 kb	 From 31 kb
0	0.4578	1.0000	0.4545	0.4545	0.4482	0.4409
0.2	.4553	0.9945				—
0.4	.4537	.9910				—
0.6	.4523	.9880				—
1.0	.4493	.9814				.4355
1.2	.4478	.9782				—
2.0	.4417	.9648				.4321
3.0	.4368	.9541				.4295
3.7	.4338	.9476				—
5.0	.4298	.9388				—
7.0	.4250	.9284				.4208
10.0	.4194	.9161				.4165
15.0	.4127	.9015				.4115
20.0	.4075	.8901				.4075
25.0	.4033	.8809				.4033
30.0	.3997	.8731				.3997
31.0	0.3991	0.8718				0.3991

Table IV. Loading-unloading PV curves for Green River oil shale, Anvil Points Mine. $\rho_0 = 2.194\ g/cm^3$. Minimum gas-filled porosity: 3.5%. K = 65 kb.

P (kb)	Loading $\frac{V}{V_0}$	 v (cm^3/g)	Unloading v (cm^3/g) From 0.7 kb	 From 1.3 kb	 From 7.5 kb	 From 40 kb
0	1.0000	0.4558	0.4532	0.4521	0.4454	0.4399
0.25	0.9965	.4542				—
0.5	.9930	.4526				—
0.7	.9899	.4512				—
1.0	.9840	.4485				.4365
1.3	.9794	.4464				2 kb — .4324
3.0	.9634	.4391				.4292
5.0	.9478	.4320				.4247
7.5	.9307	.4242				7 kb — .4210
10.0	.9190	.4189				.4168
15.0	.9035	.4118				.4110
20.0	.8923	.4067				.4060
25.0	.8828	.4024				.4022
30.0	.8752	.3989				.3989
35.0	.8679	.3956				.3956
40.0	0.8627	0.3932				0.3932

Table V. Loading-unloading PV curves for Green River oil shale, CCH-3, 2808 ft. ρ_0 = 2.308 g/cm^3. Minimum gas-filled porosity: 4.4%. K_0 = 39 kb.

	Loading		Unloading v (cm^3/g)					
P (kb)	v (cm^3/g)	$\frac{V}{V_0}$	From 0.25 kb	From 0.7 kb	From 1.5 kb	From 4 kb	From 9 kb	From 40 kb
0	0.4332	1.0000	0.4307	0.4283	0.4257	0.4201	0.4167	0.4130
0.5	.4276	0.9871						—
1	.4229	.9762						.4104
2	.4163	.9610						.4082
3	.4120	.9511						.4062
4	.4082	.9423						.4044
5	.4054	.9358						.4027
7	.4014	.9266						.3999
10	.3969	.9162						.3962
15	.3916	.9040						.3910
20	.3875	.8945						.3868
25	.3839	.8862						.3831
30	.3805	.8783						.3799
35	.3772	.8707						.3770
40	0.3740	0.8633						0.3740

Table VI. Loading-unloading PV curves for Green River oil shale, CCH3, 2310 ft level. ρ_0 = 2.118 g/cm^3. Minimum gas filled porosity: 0.6%. Bulk modulus at 0.2 kb. K = 62 kb.

	Loading		Unloading v (cm^3/g)					
P (kb)	v (cm^3/g)	$\frac{V}{V_0}$	From 0.25 kb	From 0.7 kb	From 1.5 kb	From 4 kb	From 9 kb	From 40 kb
0	0.4722	1.0000	0.4720	0.4717	0.4709	0.4699	0.4690	0.4695
0.2	.4704	0.9962						—
0.5	.4682	.9915						—
1	.4658	.9864						.4640
2	.4622	.9788						.4602
3	.4595	.9731						.4568
4	.4568	.9674						.4539
5	.4544	.9623						.4515
7	.4501	.9532						.4477
10	.4446	.9416						.4425
15	.4372	.9259						.4360
20	.4311	.9130						.4304
25	.4263	.9028						.4256
30	.4220	.8937						.4217
35	.4186	.8865						.4184
40	0.4157	0.8803						0.4157

Table VII. Loading-unloading PV curves for Green River oil shale, Anvil Points Mine. $\rho_0 = 2.273$ g/cm^3. Minimum gas-filled porosity: 0.8%. Bulk modulus at 0.2 kb: K = 87 kb.

	Loading		Unloading v (cm^3/g)			
P (kb)	v (cm^3/g)	$\frac{V}{V_0}$	From 0.25 kb	From 0.7 to 1.3 kb	From 7.5 kb	From 40 kb
0	0.4400	1.0000	0.4386	0.4375	0.4375	0.4365
0.1	.4381	0.9957				
0.25	.4371	.9934				
0.5	.4361	.9911				
0.7	.4355	.9898				
1	.4347	.9880				.4325
2	.4328	.9836				.4294
3	.4314	.9805				.4273
5	.4273	.9711				.4231
7.5	.4229	.9611				.4093
10	.4182	.9505				.4163
15	.4121	.9366				.4113
20	.4076	.9264				.4072
25	.4035	.9170				.4033
30	.3986	.9059				.3986
35	.3956	.8991				.3956
40	0.3925	0.8920				0.3925

Tuff samples from the cratering experiment Schooner exhibited two typical types of phenomena; the effects of water and of large amounts of gas-filled porosity.

Rock from shot depth to the surface at the Schooner site at the Nevada Test Site was composed of tuff. Four layers were recognized for calculations of the experiment and so four rock types were chosen to represent these layers. The layers and samples selected are shown in Table VIII. An attempt was made to adjust the water content of the samples to be equal to experimentally measured water contents of the <u>in-situ</u> rock.[22]

Table VIII. Layering at the Schooner site and samples selected.

Layer	Depth (ft)	Logged density range	Mean	Sample depth selected (ft)	Density	Water content wt %	Minimum gas-filled porosity
1	0-120	2.22-2.39	2.30	41	2.356	0.3	3.4
2	120-235	1.24-1.88	~1.55	154	1.766	8.4	25.0
3	235-370	1.42-1.82	1.60	304	1.604	27.6	12.0
4	370-475	2.15-2.25	2.20	398	2.306	0.3	5.3

Rock at the Schooner site has been described in detail by Ramspott.[23] Our samples may be described as follows: 41-ft depth, densely welded ash-flow tuff, Trail Member of Thirsty Canyon Tuff; 154-ft depth, partially welded ash-flow tuff, Spearhead Member of Thirsty Canyon Tuff; 304-ft depth, reworked tuff, Rocket Wash Member of Thirsty Canyon Tuff; 398-ft depth, densely welded ash-flow tuff, Grouse Canyon member of Belted Range tuff.

The dense tuffs from 41 and 398 ft are typical of hard rock. Data are given in Tables IX and X and in Fig. 6. They are mineralogically different, as the two PV curves cross at about 11 kb.

Table IX. Loading-unloading PV curves for consolidated Schooner tuff, hole Ue20u No. 3, 41-ft level.

Loading		Unloading					
P (kb)	v (cm^3/g)	From 0.15 kb	From 0.5 kb	From 1.25 kb	From 2.5 kb	From 5 kb	From 27 kb
0	0.4245	0.4207	0.4163	0.4158	0.4158	0.4143	0.4102
0.2	.4232						—
0.5	.4211						.4090
1	.4180						.4076
2	.4149						.4054
3	.4130						.4035
5	.4081						.4000
7	.4040						.3972
10	.3994						.3934
15	.3929						.3884
20	.3867						.3843
25	.3810						.3810
27	0.3785						0.3785

Table X. Loading-unloading PV curves for consolidated Schooner tuff, hole Ue20u No. 3, 398-ft level.

Loading		Unloading v (cm^3/g)						
P (kb)	v (cm^3/g)	From 0.15 kb	From 0.5 kb	From 1.25 kb	From 2.5 kb	From 5 kb	From 27 kb	From 40 kb
0	0.4336	0.4335	0.4325	0.4298	0.4275	0.4271	0.4185	0.4107
0.2	.4325						—	—
0.5	.4308						.4153	.4081
1	.4280						.4132	.4058
2	.4226						.4102	.4022
3	.4180						.4076	.3993
5	.4116						.4032	.3950
7	.4061						.3993	.3915
10	.4000						.3935	.3871
15	.3908						.3876	.3813
20	.3834						.3825	.3766
25	.3770						.3770	.3727
27	.3745						0.3745	.3711
30	.3712							.3690
35	.3665							.3653
40	0.3617							0.3617

The tuff from 304 ft was saturated with water, since field measurements indicated a perched water table at that depth. Data are shown in Fig. 7 and in Table XI. The volume discontinuities at constant pressure in the figure are due to phase transformations in the water. Water freezes at 9.7 kb, and at 21.3 kb transforms from a pseudo-orthorhombic to the bcc structure.[24,25] These transitions in the tuff are very sharp and reversible; the pressures are close to that of pure water (9.7 and 22.7 kb for the tuff). However, the volume

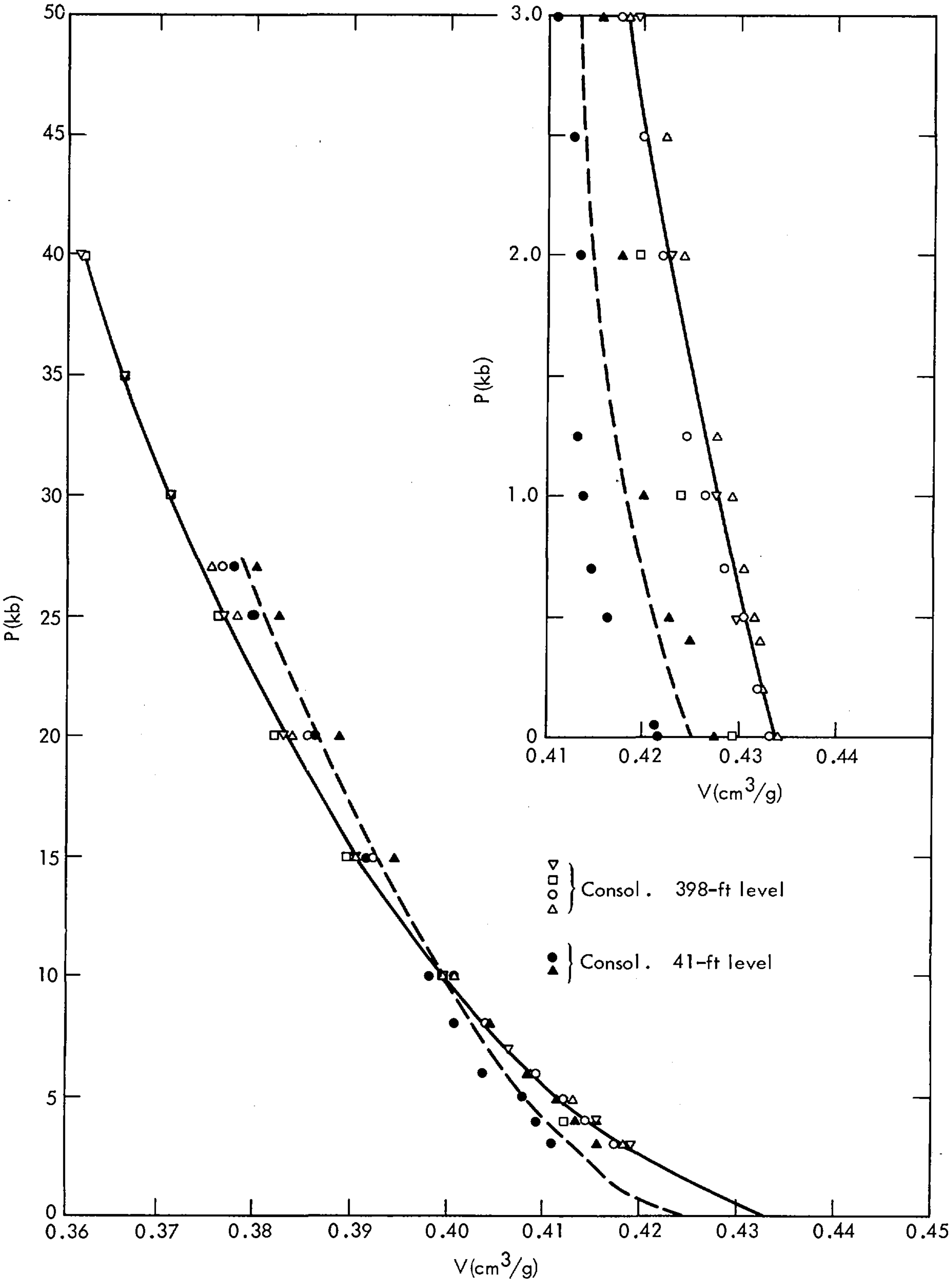

Fig. 6. Loading PV curves for Schooner tuff, hole Ue20u No. 3.

changes should have been larger than observed for an inert mixture of rock and water. We believe that much of the water in this rock is not "free"; it is in a loosely bound state. Water can be adsorbed on or bound within the zeolites which are abundant in this rock. Water loosely combined with a rock in this way is described as "nonliquid water" by clay mineralogists.[26]

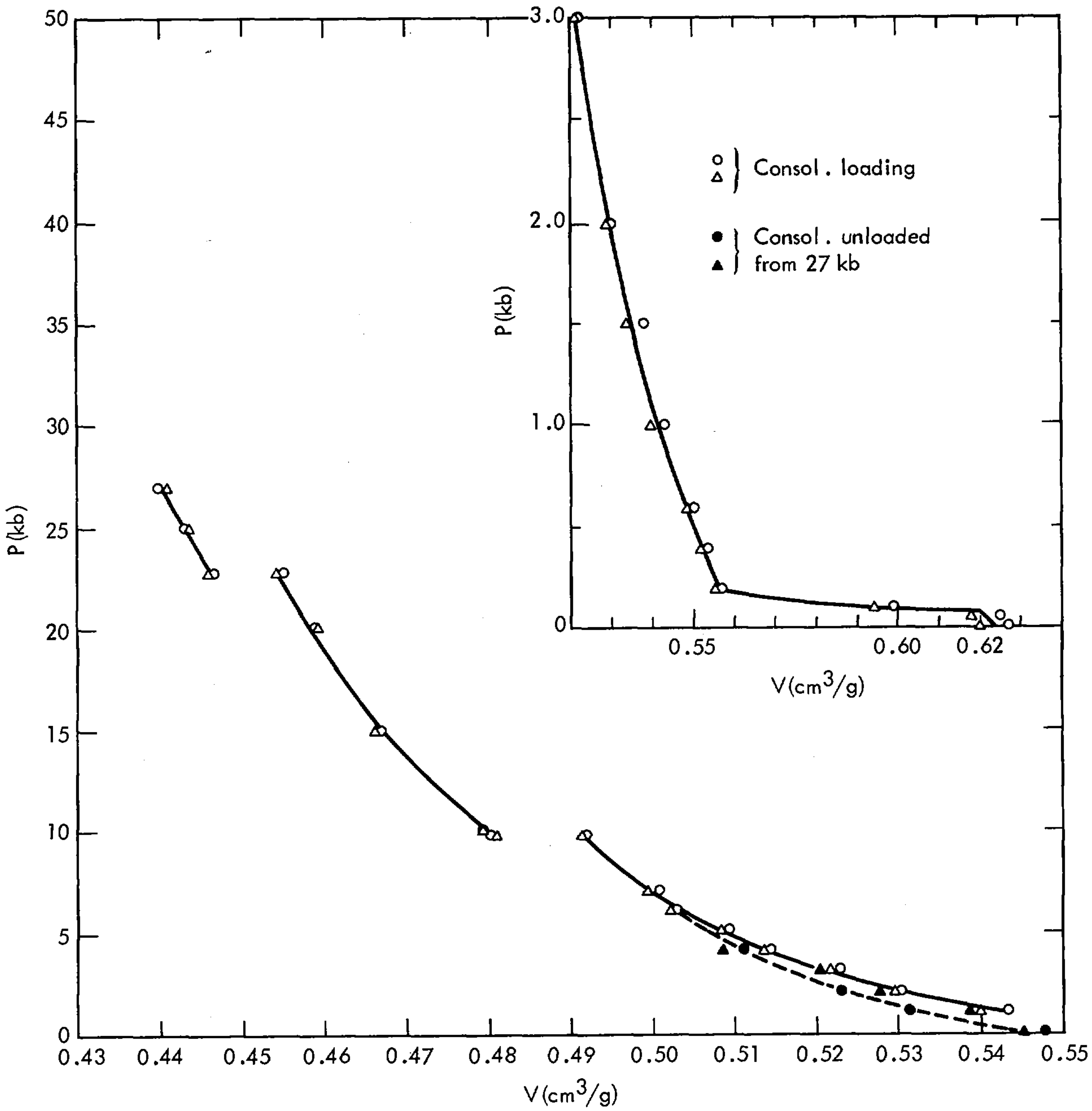

Fig. 7. PV curves for Schooner tuff, hole Ue20u No. 3, 304-ft level.

As described earlier,[9] our PV measurements offer a qualitative way to estimate the amounts of nonliquid water. The amount of free water in the rock can be calculated from the volume changes due to the water transitions in the sample compared to the volume changes found for pure water.[24] Presumably, the "nonliquid" water would not undergo the phase transition of pure water, since, being in a different chemical state, its thermodynamics would also be different. From the total water liberated from this rock at 100°C (27.6%) and the amount of free water indicated from the phase transformation (14%), we estimate that ~13.6% or about half of the water in this tuff is nonliquid in nature.

The data for this tuff indicate the presence of about 12% gas-filled porosity which was permanently removed by pressures of 6 kb or more. The presence of large amounts of gas-filled porosity in a supposedly water-saturated

Table XI. Loading-unloading PV curves for consolidated Schooner tuff, hole Ue20u No. 3, 304-ft level.

Loading		Unloading v (cm^3/g)					
P (kb)	v (cm^3/g)	From 0.2 kb	From 0.6 kb	From 1.5 kb	From 3 kb	From 6 kb	From 27 kb
0	0.6235	0.5630	0.5530	0.5520	0.5497	0.5487	0.5465
0.05	.6314						—
0.2	.5567						—
0.5	.5503						.5390
1	.5419						.5334
2	.5300						.5246
3	.5220						.5172
5	.5080						.5070
7	.4997						.4997
9.7	.4918						.4918
9.7	.4806						.4806
10	.4798						.4798
15	.4672						.4672
20	.4585						.4585
22.7	.4541						.4541
22.7	.4464						.4464
25	.4432						.4432
27	0.4404						0.4404

rock is unexpected. Some of the rock seems to contain non-interconnecting pore space. Some voids may not communicate to the rock surface; they may be surrounded by impermeable rock. The presence of juvenile gas may also preclude the presence of water.

The low-pressure portion of the PV data is typical of weak and compressible rock.[9] The PV curve from zero to 50 bars indicates a reasonable value for the bulk modulus (15 kb) followed by a very compressible region from 50 bars to 200 bars where porosity is rapidly removed. Above this pressure, the PV curve approaches normal behavior. One can see that the compressibility is constant to 50 bars, and then is quite low in the compaction interval.

The rock from 154 ft liberated 8.4% water when heated to 100°C. The data, shown in Fig. 8, show that it is also a weak and compressible rock. The PV curve from 1 bar to 100 bars indicates a bulk modulus of 28 kb, followed by a region where the rock begins to fracture, and the compressibility is quite high to 2 kb. The PV curve above this pressure is normal. The phase transformations due to water can be detected, but they are faint and hysteretic, as can be seen from Table XII. About half of the water seems to be "nonliquid." Some hysteresis of the transitions may be expected, since the small amount of free water below 10 kb can migrate to the region of lowest mean stress in the rock. The rock strength also promotes some hysteresis. As water transforms it decreases in volume, while the matrix surrounding the water tends to resist the deformation necessary to assume the new pore shape.

The PV data described are useless for calculations of any nuclear experiment if they are taken on samples which are not representative of the medium. Careful analysis of the geology of the nuclear site always proceeds selection of samples for equation-of-state studies. First, the results of the in-situ logging program are examined. These consist of geology, density and acoustic velocity logs. In addition, laboratory examinations of core samples provide information on mineralogy, acoustic velocity, water content, bulk density and grain

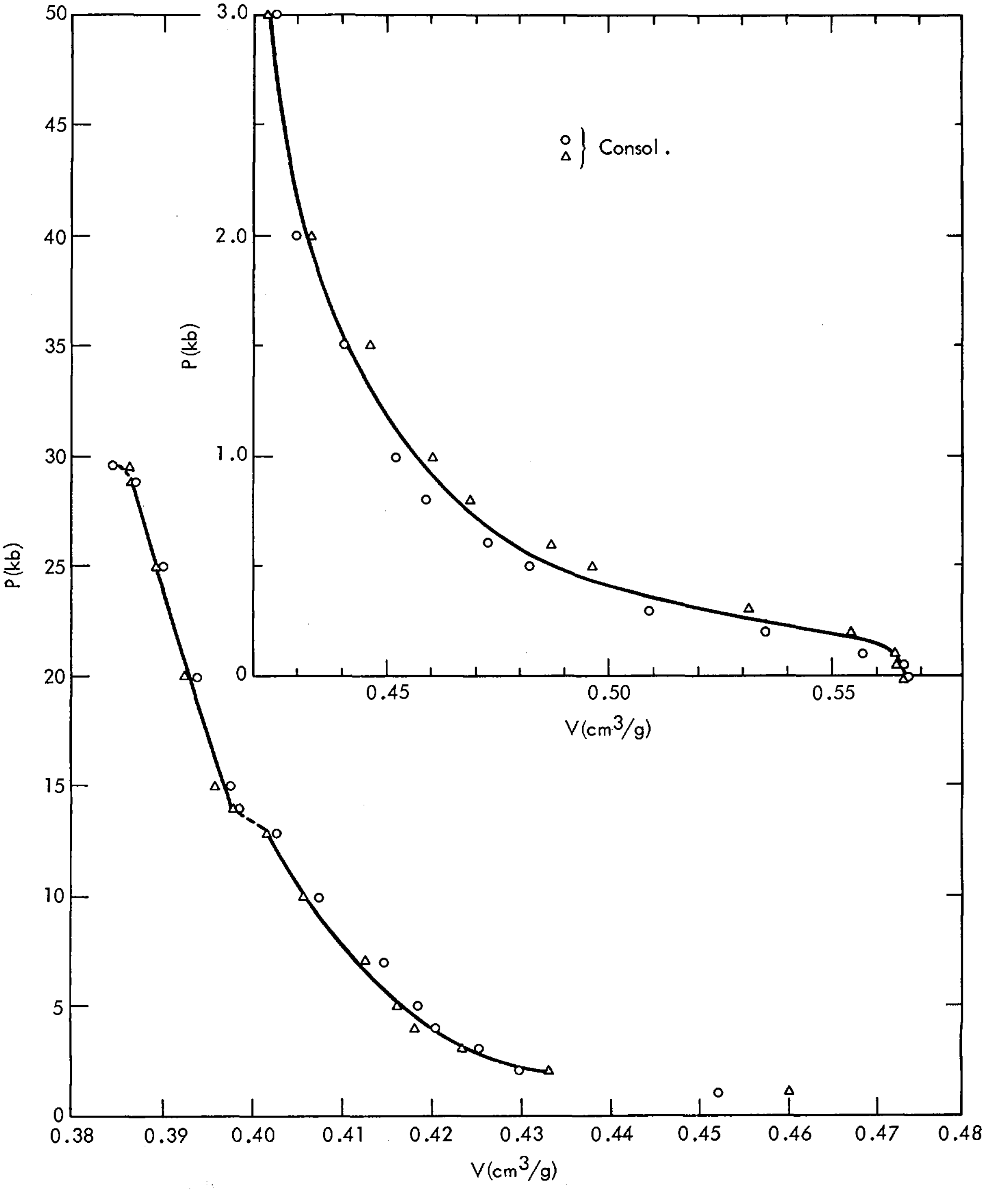

Fig. 8. Loading PV curves for Schooner tuff, hole Ue20u No. 3, 154-ft level.

density. A careful study of the total information with the event geologist and members of the calculational and equation-of-state groups then allow us to choose rock cores which seem most representative of the most frequently encountered rock types at the site.

After data are taken, we can check some of our data against the previously described data. We will illustrate this with the selection of samples for the Schooner event.

Table XII. Loading-unloading PV curves for consolidated Schooner tuff, hole Ue20u No. 3, 154-ft level.

Loading		Unloading v (cm^3/g)					
P (kb)	v (cm^3/g)	From 0.2 kb	From 0.6 kb	From 1.5 kb	From 3.5 kb	From 7 kb	From 30 kb
0	0.5663	0.5488	0.4800	0.4488	0.4353	0.4289	0.4233
0.05	.5653						—
0.1	.5643						—
0.3	.5200						—
0.5	.4880						.4217
1	.4567						.4202
2	.4323						.4176
3	.4240						.4152
4	.4198						.4131
5	.4165						.4112
7	.4120						.4079
9.5	—						.4042
10	.4062						—
11.9	—						.3978
12.8	.4020						—
14	.3977						—
15	.3970						.3954
20	.3929						.3917
25	.3892						.3889
28.8	.3866						—
29.6	0.3850						0.3850

As mentioned previously, four rock layers were chosen for calculations with the properties described in Table VIII.

An inspection of the density log indicates that layer 3 is composed of more or less the same material; the density varies in a random way in the interval. However, in layer 2 (120-235 ft) there seems to be three discrete layers of density 1.55, 1.88 and 1.25. Unfortunately, little core was recovered from this interval so we were unable to study any of the extremes in rock type indicated by the log. Our sample density for this layer seems to be too high. However, no other available cores were as close to the assumed mean density as the one used. The other three samples seemed to adequately represent the layers of interest. Note, however, that all of our samples are of a higher density than the log. This is generally true of logged densities versus laboratory values.

Therefore, our samples, except for the 154-ft sample, agreed with the density log criteria. We then compare our experimental compressibility to one calculated from the logged acoustic velocities. The onset of shear waves could not be reliably determined from the log; however, the compressional velocities could readily be detected. Both velocities are needed for calculation of compressibility (see Ref. 3). To permit calculating the compressibility from the logged data, we assumed values for Poisson's ratio. Poisson's ratio for porous tuffs are reported to be of the order of 0.11.[14] Poisson's ratio for the dense tuff was arbitrarily assumed to be 0.25. Results are shown in Table XIII. Again, except for the 154-ft sample, the experimental and calculated numbers are in reasonable agreement.

Table XIII. Elastic values for Schooner tuff.

Sample depth (ft)	Experimental bulk modulus (kb)	Calculated bulk modulus (kb)	Logged value for V_p (ft/sec)	Poisson's ratio (assumed)
41	63	63.5	7215	0.25
154	28	10.1	3850	0.11
304	15	17.9	5376	0.11
398	79	72.7	7800	0.25

In conclusion, we can state that samples for PV studies can be selected that are representative of geological formations and that the data thus obtained can be used for meaningful calculations of the effects of nuclear explosions in rock.

The qualitative nature of the PV data can be explained from experimental data on minerals and consideration of the effects of porosity and water content. A quantitative prediction of the PV curves of most rocks is usually not possible, however, due to effects of water, unknown pore geometry and in many cases, unknown mineralogy. Therefore, experimental PV measurements are almost always necessary.

ACKNOWLDGMENT

We wish to thank H. C. Heard and R. N. Schock for valuable discussions, and for reading the manuscript.

REFERENCES

1. J. T. Cherry, ANS Topical Meeting, Jan. 14-16, 1970, Las Vegas, Nevada.
2. J. T. Cherry, Intern J. Rock Mech. Min. Sci. 4, 1 (1967).
3. R. N. Schock, ANS Topical Meeting, Jan. 14-16, 1970, Las Vegas, Nevada.
4. H. C. Heard, ANS Topical Meeting, Jan. 14-16, 1970, Las Vegas, Nevada.
5. P. W. Bridgman, Collected Experimental Papers. Paper No. 168, Vol. 6, 189-234, 1964.
6. W. B. Daniels and C. S. Smith, Phys. Rev. 111, 713 (1958).
7. D. R. Stephens, J. Geophys. Res. 69, 2967 (1964).
8. D. R. Stephens and E. M. Lilley, "Static PV Curves of Cracked and Consolidated Earth Materials to 40 Kilobars," UCRL-14711, Lawrence Radiation Laboratory, Livermore, 1966; Proc. Conf. Shock Metamorphism of Natural Materials, B. M. French and N. M. Short, eds. (Mono Press, Baltimore, 1968).
9. D. R. Stephens, E. M. Lilley and H. Louis, Intern J. Rock Mech. Min. Sci. (in press).
10. J. Z. Grens, to be published.
11. P. W. Bridgman, Collected Experimental Papers, Paper No. 134, Vol. 6, 21-50, 1964.
12. H. B. Keller, "A Hydrostatic Pressure Cell for Pressure-Volume Measurements to 5 Kilobars," UCRL-50611, Lawrence Radiation Laboratory, Livermore, 1969.
13. I. Y. Borg, private communication.
14. F. P. Birch, "Compressibility, Elastic Constants," Sect. 7, Handbook of Physical Constants, S. P. Clark, Jr., ed., Geol. Soc. Am. Memoir 97, 1966.
15. R. Hill, Proc. Phys. Soc., London, A65, 349 (1952).
16. W. F. Brace, J. Geophys. Res. 70, 391 (1965).
17. J. G. Walsh, J. Geophys. Res. 70, 381 (1965).

18. J. Handin, "Strength and Ductility," Sect. 11 in Handbook of Physical Constants, S. P. Clark, Jr., ed., Geol. Soc. Am. Memoir 97, 1966.
19. R. E. Riecker, "Shear Deformation of Nevada Test Site Rocks, Samples to 60 kb and 1000°C," Air Force Weapons Lab., Kirtland AFB, New Mexico, Second Quarterly Report, 1966.
20. A. A. Giardini, Trans. Am. Geophys. Union, 50, 673 (1969).
21. O. L. Anderson, E. Schreiber and R. C. Liebermann, Rev. Geophys. 6, 491 (1968).
22. A. E. Lewis and L. D. Ramspott, Trans. Am. Geophys. Union 50, 155 (1969). Abstract.
23. L. D. Ramspott, to be published.
24. P. W. Bridgman, Collected Experimental Papers, Paper No. 138, Vol. 6, 399-424, 1964.
25. S. Block, C. E. Weir and G. J. Piermarini, Science 148, 947 (1965).
26. R. E. Grim, Clay Mineralogy (McGraw-Hill, New York, 1953).

XA04N0746

DYNAMIC ELASTIC MODULI OF ROCKS UNDER PRESSURE[*]

R. N. Schock

Lawrence Radiation Laboratory, University of California
Livermore, California 94550

ABSTRACT

Elastic moduli are determined as a function of confining pressure to 10 kb on rocks in which Plowshare shots are to be fired. Numerical simulation codes require accurate information on the mechanical response of the rock medium to various stress levels in order to predict cavity dimensions. The theoretical treatment of small strains in an elastic medium relates the propagation velocity of compressional and shear waves to the elastic moduli. Velocity measurements can provide, as unique code input data, the rigidity modulus, Poisson's ratio and the shear wave velocity, as well as providing checks on independent determinations of the other moduli. Velocities are determined using pulsed electro-mechanical transducers and measuring the time-of-flight in the rock specimen. A resonant frequency of 1 MHz is used to insure that the wavelength exceeds the average grain dimension and is subject to bulk rock properties. Data obtained on a variety of rock types are presented and analyzed. These data are discussed in terms of their relationship to moduli measured by static methods as well as the effect of anisotropy, porosity, and fractures. In general, fractured rocks with incipient cracks show large increases in velocity and moduli in the first 1 to 2 kb of compression as a result of the closing of these voids. After this, the velocities increase much more slowly. Dynamic moduli for these rocks are often 10% higher than corresponding static moduli at low pressure, but this difference decreases as the voids are closed until the moduli agree within experimental error. The discrepancy at low pressure is a result of the elastic energy in the wave pulse being propagated around cracks, with little effect on propagation velocity averaged over the entire specimen.

INTRODUCTION

Perhaps the most fundamental key to the successful use of explosives in programs ultimately designed to produce economic benefits is the accurate a priori prediction of the effects produced by such explosives. These effects include parameters such as cavity dimensions, fracturing perimeter and others, all of which are highly dependent on the properties of the material or materials which are to be subjected to the explosive process. What is needed is a complete equation of state of the media over the appropriate pressure-temperature region. Part of this characterization involves the response to elastic and/or inelastic deformation at stress levels considerably above ambient. This paper deals with the study of the elastic deformation of rocks

---

[*] Work performed under the auspices of the U. S. Atomic Energy Commission.

at pressures to 10 kb.* The method employed involves the passage of longitudinal and transverse acoustic waves. The laboratory techniques will be described and examples of data given for several contrasting rock types.

PROCEDURE

1. Theoretical

The fundamental assumption of elasticity theory is that linear stress is proportional to linear strain,

$$\sigma_{ij} = C_{ijkl}\epsilon_{kl}$$

where σ is stress, ϵ is strain, C is the elastic constant, and i, j, k, l are indices on a Cartesian coordinate system. Considering the processes as isothermal and reversible and reducing redundancies, the number of independent elastic constants is found to be 21.[1] Further restriction to material with orthorhombic or higher symmetry reduces the elastic constants to a symmetrical matrix with a maximum of nine independent components. In such a medium, the principle stresses are

$$\sigma_1 = C_{11}\epsilon_1 + C_{12}\epsilon_2 + C_{13}\epsilon_3 \tag{1}$$

$$\sigma_2 = C_{12}\epsilon_1 + C_{22}\epsilon_2 + C_{23}\epsilon_3 \tag{2}$$

$$\sigma_3 = C_{13}\epsilon_1 + C_{23}\epsilon_2 + C_{33}\epsilon_3 \tag{3}$$

$$\sigma_4 = C_{44}\epsilon_4 \tag{4}$$

$$\sigma_5 = C_{55}\epsilon_5 \tag{5}$$

$$\sigma_6 = C_{66}\epsilon_6 , \tag{6}$$

using the simplified suffix notation 12 → 6, 13 → 5, 23 → 4, etc. If the material is considered to be isotropic (principal axes of stress and strain are identical) the matrix further reduces such that

$$C_{11} = C_{22} = C_{33}$$

$$C_{44} = C_{55} = C_{66} = 1/2(C_{11} - C_{12})$$

$$C_{12} = C_{13} = C_{23} .$$

The propagation of a wave involving only longitudinal stresses involves a wave equation whose solution[2] is

$$V_P = (C_{11}/\rho)^{1/2} , \tag{7}$$

where V_P is the velocity of the compressional wave and ρ is density. In the case of transverse stresses, the velocity of the shear wave is

$$V_S = (C_{44}/\rho)^{1/2} . \tag{8}$$

---

*1 bar = 10^6 dyne cm^{-2} = 0.987 atm = 14.5 psi.

The rigidity modulus μ is σ_4/ϵ_4 with other stresses zero, and is therefore C_{44}. If $\sigma_2 = \sigma_3 = 0$, σ_1/ϵ_1, from Eqs. (1)-(3), is

$$E = \frac{C_{44}(3C_{12} - 2C_{44})}{C_{12} + C_{44}} , \tag{9}$$

the definition of Young's modulus. Poisson's ratio ν is ϵ_3/ϵ_1 for the same conditions, and

$$\nu = E/(2\mu) - 1 . \tag{10}$$

The bulk modulus (reciprocal of the volume compressibility) $K = -P/\Delta$, with $-P = \sigma_1 = \sigma_2 = \sigma_3$ and $\Delta = \epsilon_1 + \epsilon_2 + \epsilon_3$, where P = pressure. Therefore,

$$K = 1/3\ C_{11} + 2/3\ C_{12} . \tag{11}$$

Equations (11), (8) and (7) combine to give the familiar

$$V_P = [(K + 4/3\ (\mu))/\rho]^{1/2} .$$

Bedded sedimentary rocks are generally quite symmetrical about the plane of bedding. In addition, their properties within any one bed are essentially isotropic, resulting in a principal axis of symmetry normal to the bedding plane. The elastic constant matrix (1)-(6) for transversely isotropic media is thus reduced by

$$C_{11} = C_{22}$$

$$C_{44} = C_{55}$$

$$C_{13} = C_{23}$$

$$C_{66} = 1/2\ (C_{11} - C_{12})$$

where the principal symmetry axis is labeled 3. C_{11}, C_{33}, C_{44}, and C_{66} may be determined from V_{P11}, V_{P33}, V_{S13}, and V_{S12} respectively, through

$$C = V^2\rho.$$

A determination of V_P at 45° to the principal axis yields the fifth independent constant,

$$C_{13} = \left\{[2\rho V^2_{45^\circ} - 1/2(C_{11} + C_{33} + 2C_{44})]^2 - [1/2(C_{11} - C_{33})]^2\right\}^{1/2} - C_{44}$$

One is now in a position to determine the anisotropic variation in elastic moduli for such a media. In this case,

$$E_1 = \frac{M}{C_{11}C_{33} - C_{13}^2}$$

$$E_3 = \frac{M}{C_{11}^2 - C_{12}^2}$$

where M is the elastic constant matrix for normal components. For Poisson's ratio,

$$\nu_{12} = \frac{C_{12}C_{33} - C_{13}^2}{C_{11}C_{33} - C_{13}^2}$$

$$\nu_{13} = \frac{C_{13}(C_{11} - C_{12})}{C_{11}C_{33} - C_{13}^2}$$

$$\nu_{31} = \frac{C_{13}}{C_{11} + C_{12}}$$

and for compressibility,

$$\beta_1 = (C_{33} - C_{13})/D$$

$$\beta_3 = (C_{11} + C_{12} - 2C_{13})/D$$

$$\beta_{vol} = (C_{11} + C_{12} + 2C_{33} - 4C_{13})/D$$

where $D = (C_{11} + C_{12})C_{33} - 2C_{13}^2$. Equivalent expressions are given by Nye.[1]

In all cases, a correction for the change in sample length and density with pressure is applied by continuously integrating the computed bulk modulus over the pressure range according to the analytical procedure developed by Cook.[3]

Thus, determinations of V_P and V_S are sufficient to completely characterize the response to elastic deformations of an elastic solid. Since the wave travels through the material at some finite frequency, elastic moduli determined in this manner are referred to as dynamic moduli, as opposed to moduli directly determined by static methods. Birch[4] has raised the question of whether the moduli that determine the wave velocities are compatible with statically determined moduli. Ide[5] has shown from resonance work on cylinders that both E and ν determined dynamically may differ markedly from those determined statically in non-compacted rocks. To complicate matters, many rocks show non-linear stress-strain curves at low stress levels.[6] In a study of this problem, Simmons and Brace[7] compared bulk moduli determined by static methods with those calculated from velocity data. Their results show that moduli determined by acoustic methods are within a few percent of those measured directly at pressures above 2 to 3 kb. Below this pressure the variance is generally at least 10%, the dynamic moduli being higher. Simmons and Brace ascribe this difference to the presence of cracks which affect the static moduli but do not affect the propagation of an acoustic wave. These are cracks which close with the application of a few kilobars of pressure. Walsh[8] has derived a theoretical relationship between the dimensions of an elliptical crack and the pressure at which it closes,

$$P_c = E\alpha \, , \tag{12}$$

where α is the minor/major axis ratio.

Birch[4] gives an excellent review of the existing measurements of compressional velocity and the frequencies at which they were measured. There appears to be no frequency dependence between 100 Hz and 10 MHz for fairly uniform dense rocks. In the case of extreme anisotropy and/or large defect concentration, nothing is known of the frequency dependence of the moduli. For shear waves, Peselnick and Outerbridge[9] found no significant dependence of velocity over the range 4-10^7 Hz in Solenhofen limestone, a very fine-grained, compact rock.

2. Experimental

Numerous papers have dealt with the various laboratory techniques used to measure the compressional and shear velocity of rocks as a function of pressure. These are summarized and combined with existing data in the work of Birch[4,10] and Simmons.[11,12] Because of the strong attenuation in most rocks, the method most suitable is that of simple transmission. In this study, measurements are made at room temperature on cylindrical specimens with approximate dimensions 19 × 27 mm.

Plane waves are generated and received by piezoelectric transducer discs of polycrystalline $Pb(Zr,Ti)O_3$, whose fundamental vibration frequency is between 1 and 5 MHz. The shear expanding ceramic discs are not mode-pure, and as a result some compressional energy is produced. In most cases, the amplitudes of the arriving compressional and shear wave are different enough to allow an unambiguous determination of the shear-wave arrival. The frequency range is chosen so that the wave length is longer than the average grain dimension, and the wave propagation will be dependent on bulk rock properties. The specimen assembly is shown in Fig. 1. The transducers are coupled to the specimen with a viscous polystyrene resin. A thin copper strip serves as an electrical ground, and the whole assembly is cast in a polyurethane resin. This resin is excellent for transmitting pressure while rendering the sample impervious to the pressure fluid. The sample assembly is then placed in a piston-cylinder pressure vessel utilizing a hydrocarbon pressure fluid.

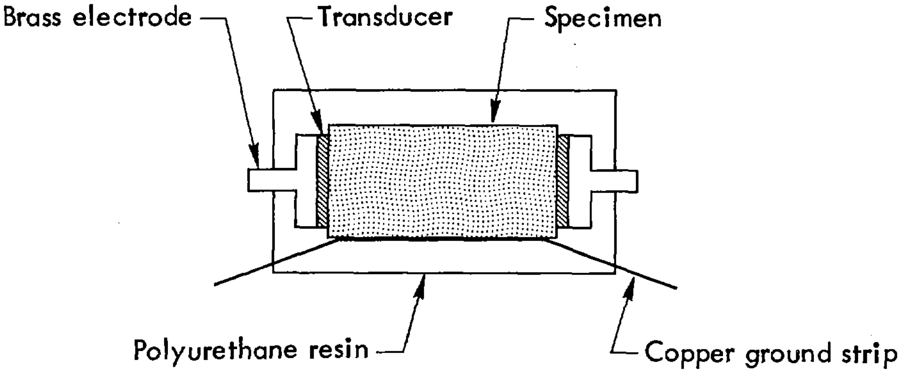

Fig. 1. Schematic representation of the specimen, transducers and surrounding resin.

The associated electronic equipment is shown in Fig. 2. A negative pulse (pulse 1) is used to simultaneously trigger a pulsed oscillator, the sweep of a dual-beam oscilloscope, and a second pulse generator (pulse 2). The signal from the pulsed oscillator is then sent to the transducer at one end of the specimen and to one input of an oscilloscope fast-rise preamplifier. The received signal from the sample is amplified and filtered before being sent to the other input of the preamplifier. The observed signals are then horizontally amplified and swept across the oscilloscope screen. The received signal is aligned with the negative output from the second pulse generator by adjusting

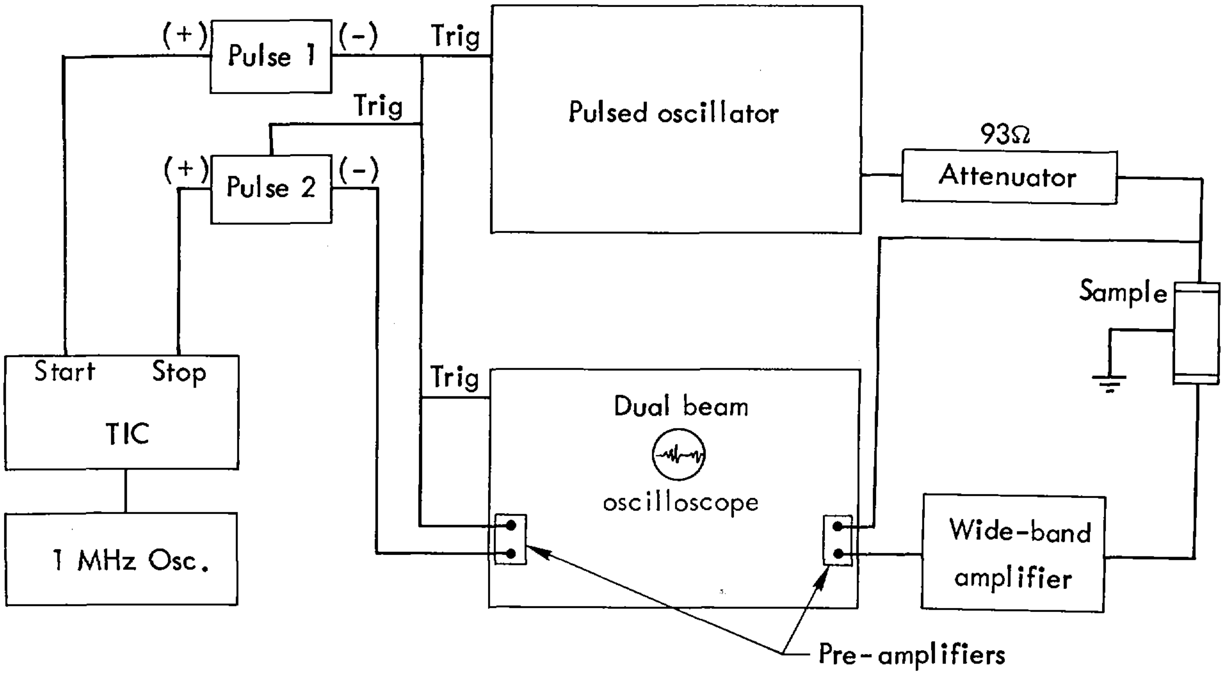

Fig. 2. Block diagram of the travel-time measuring system.

its internal delay circuit. Both pulse generators have their positive outputs connected to the start and stop inputs of a time-interval counter where the delay-time in the sample and attendant leads is displayed. A correction for the delay in cable leads and phase shifts in electronics is obtained by measuring the delay through four different lengths of polycrystalline Al_2O_3 and extrapolating back to zero length.

The accuracy of the travel-time measurements is affected by several factors. Among these are, the accuracy of the time-interval counting system, and the precision of measuring the arrival of the initial energy from the sample. A complete discussion is given by Birch[4,10] and Simmons.[11,12] Velocities determined are generally accurate to about 1%, which leads to accuracies of approximately 2, 6, 10 and 8% in rigidity, bulk, and Young's moduli and Poisson's ratio, respectively.

RESULTS

Data for several contrasting rock types are given in this section to illustrate (1) the type and features of the data obtained, and (2) the variation in elastic properties with stress that one may expect in rocks. Two rock types are treated as isotropic, one as anisotropic, and one as both. These rocks as to type, locality and initial density are:

Westerly granite, Westerly, R. I., $\rho_0 = 2.630$ g cm^{-3}, homogeneous, medium-fine-grained, low-porosity, granite.

Dome Mt. andesite, Chukar Mesa, Nev., $\rho_0 = 2.640$ g cm^{-3}, homogenous, very-fine-grained extrusive rock with a porosity, consisting of small vesicles and minute fractures, of approximately 7%. This rock was the medium for the Buggy row-cratering experiment.

Stirling quartzite, Emigrant Valley, Nev., from the site of the forthcoming Sturtevant cratering experiment.

Type A, $\rho_0 = 2.580$ g cm^{-3},
gray, medium-grained, silica-cemented
sedimentary quartzite, with relatively few impurities.

Type B, $\rho_0 = 2.495$ g cm^{-3},
red, fine-grained, slightly ferrouginous quartzite.

Type C, $\rho_0 = 2.630$ g cm^{-3},
red, very-fine-grained ferrouginous and/or arkosic
siltstone.

Type D, $\rho_0 = 2.620$ g cm^{-3},
same as above.

Green River Shale, CCH3, 2310-ft level, Rifle, Colorado,
$\rho_0 = 2.075$ g cm^{-3},
silty kerogenous marlstone, described as "poor" in its kerogen content and having 0.6% porosity.

Compressional and shear-wave velocities in Westerly granite obtained on increasing pressure are shown in Fig. 3. Data similar to these are typical of most dense, unaltered, crystalline igneous rocks. The relatively large

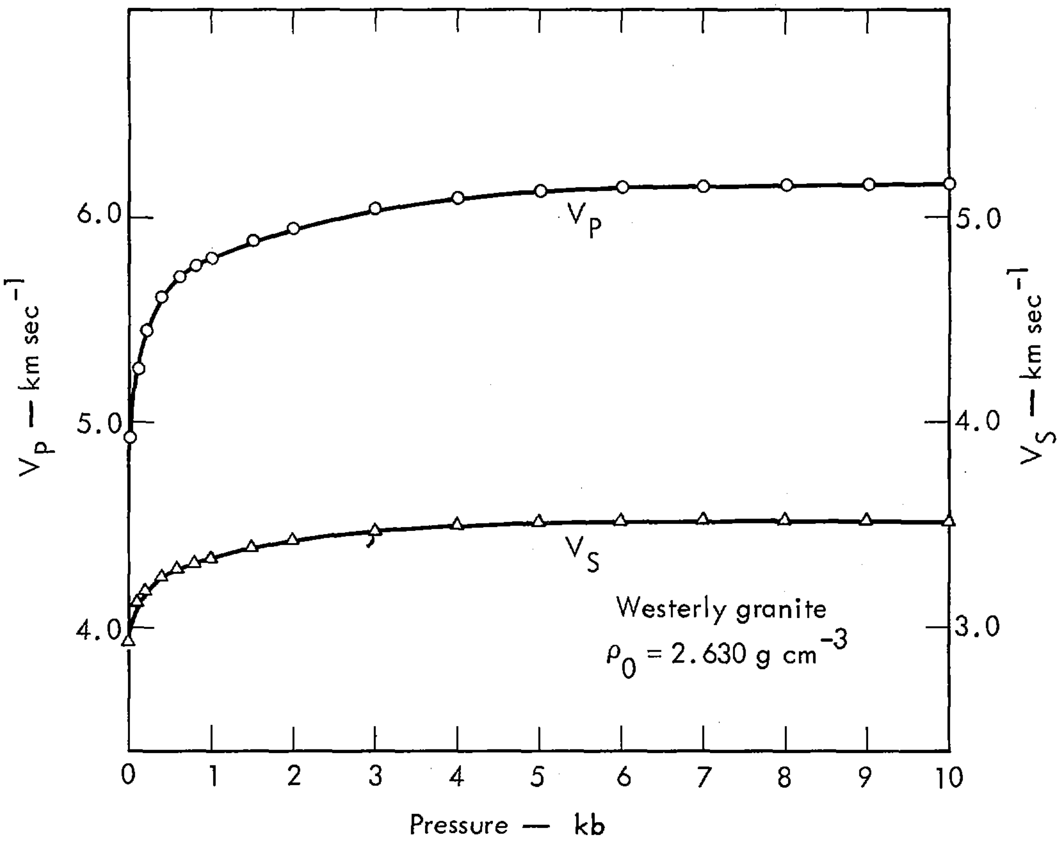

Fig. 3. Compressional wave-velocity (V_P) and shear wave-velocity (V_S) in Westerly granite with pressure.

increase in velocity in the first several hundred bars of compression seems to represent the closing of cracks or fractures, resulting in increased wave transmission. The low levels of stress required by Walsh's[8] model indicates rather long narrow fractures with α in Eq. (12) being of the order of 10^{-3}. The variation in computed moduli (Fig. 4) is, of course, sympathetic with the velocity variation. Above 1-2 kb the rock shows continued increase in velocity and moduli, but at a decreasing rate as stiffer pores and cracks are closed. At pressures above 6 kb, the moduli have pressure coefficients which are lower than those for even the stiffest minerals present in granite (dK/dP approx 6 for quartz). Eventually, as pores and cracks are squeezed shut, the rock moduli at elevated pressures should resemble those for an average of its constituent minerals. Pressure coefficients which are apparently lower than for individual minerals may be explained by either (1) propagation of pre-existing cracks, including those just closed, or (2) the onset of fracturing unrelated to any previous cracks. In either case, propagation velocities are hindered in their normal increase and the rock does not stiffen with increasing pressure as these cracks are created. At pressures higher than 10 kb, the velocities will again begin to rise with pressure, as they must when cracks are not a factor.

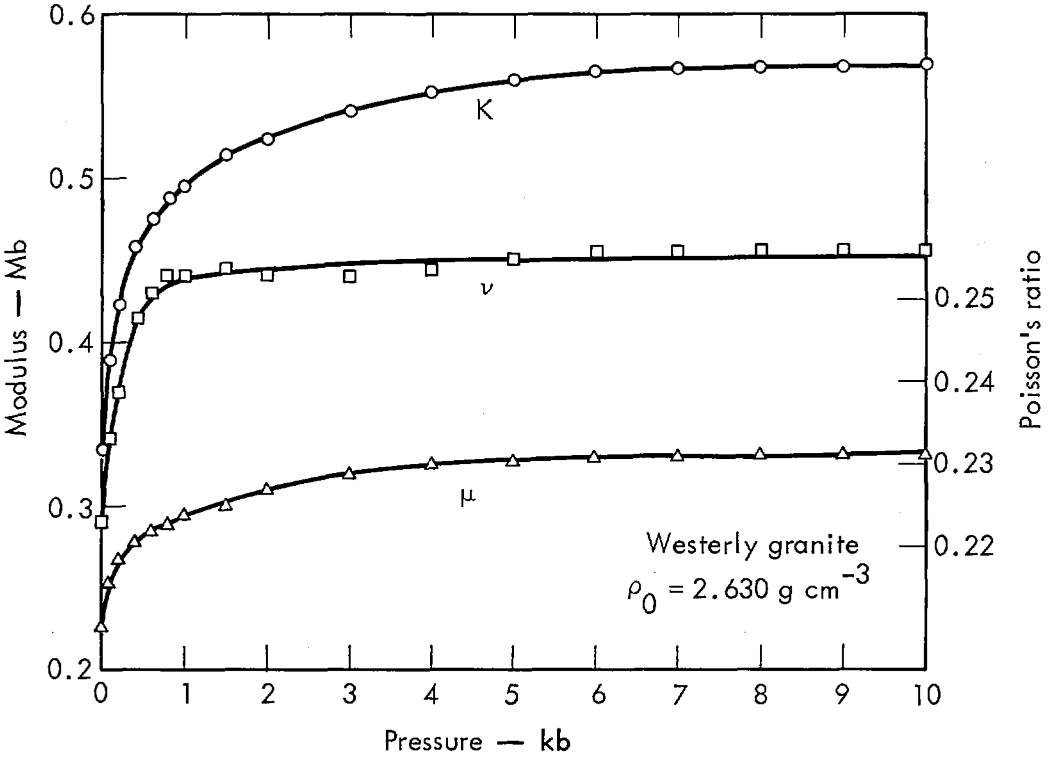

Fig. 4. Bulk modulus (K), rigidity modulus (μ), and Poisson's ratio (ν) for Westerly granite with pressure.

Figures 5 and 6 show the velocity and moduli data, respectively, to 10 kb in Dome Mt. andesite. The less-rapid increase in velocity than with granite seems to be indicative of an average distribution of stronger cracks. Above 3 kb these cracks seem to have closed, and the pressure coefficients resemble those in granite at this stress level. However, at about 7 kb the pressure

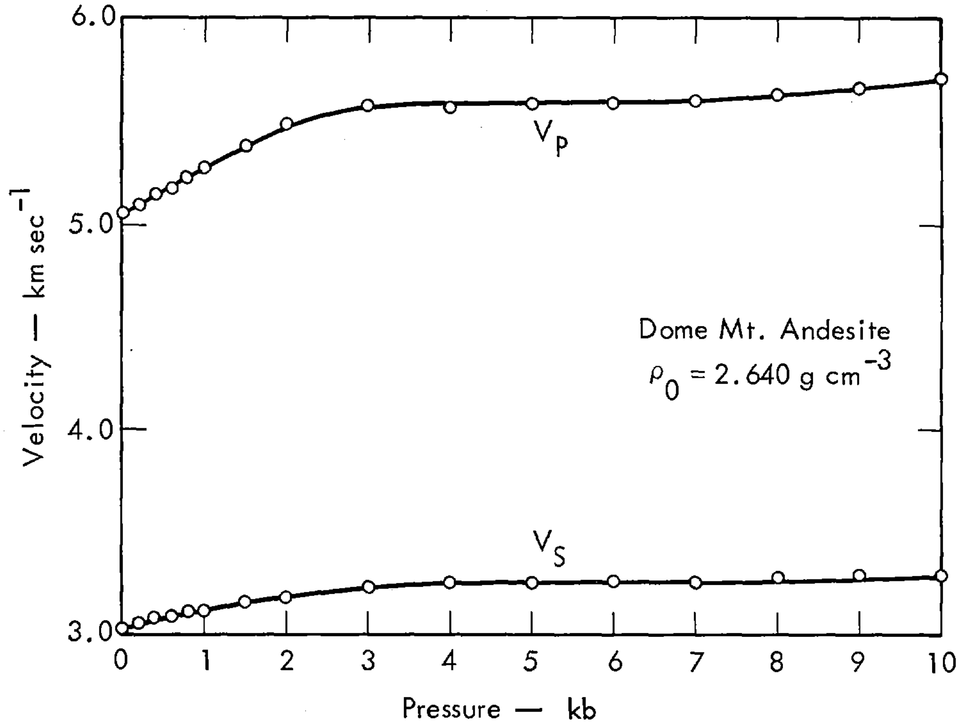

Fig. 5. V_P and V_S in Dome Mt. andesite with pressure.

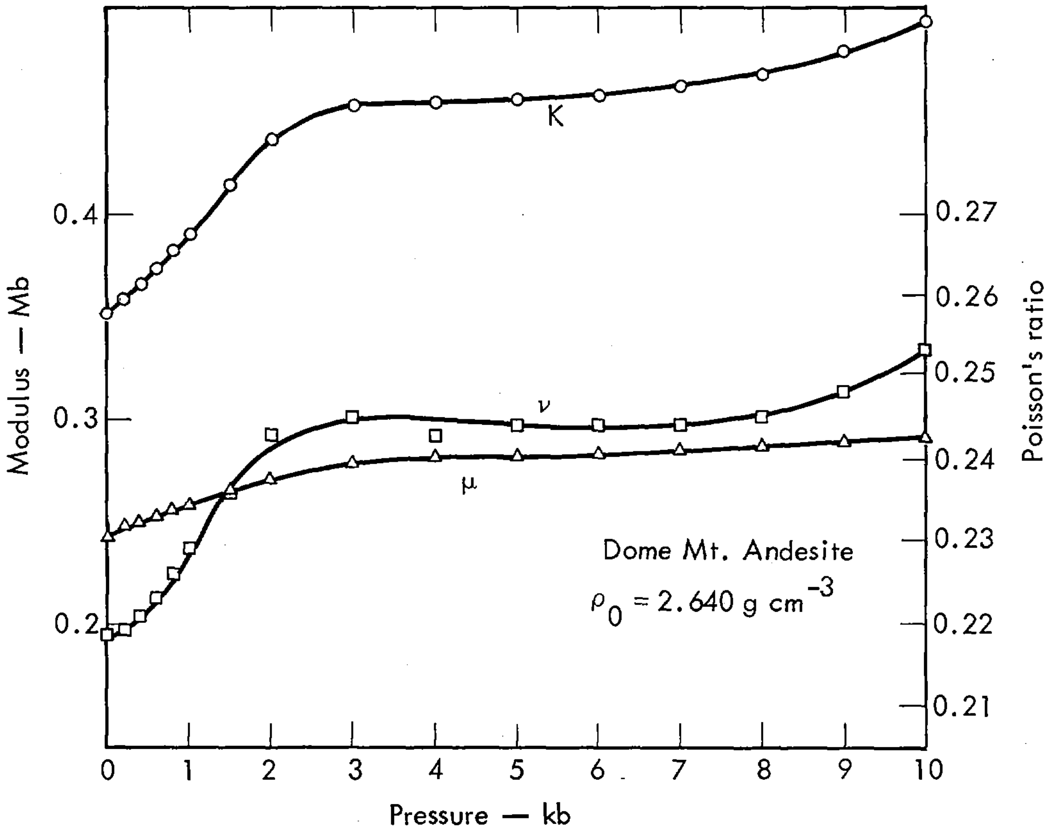

Fig. 6. K, μ, and ν for Dome Mt. andesite with pressure.

dependence increases markedly. Although no definitive interpretation can be made, it is suggested that this may represent the beginning of the breakdown of stronger pores or cracks. According to the Walsh model, these are much more open with respect to their width/length ratio and, due to the different stress levels necessary to close these openings, indicate that a completely different type pore is responsible. Some of the porosity in this rock is known to exist as small vesicles which are nearly spherical, and which Stephens[13] has shown are still closing at 40 kb.

Figure 7 illustrates the moduli obtained for three different types of Stirling quartzite. Worthy of immediate note is the $\mu/K > 1$ relationship under ambient conditions. This results in a low Poisson's ratio, typical of sedimentary quartzites. The ratio μ/K becomes less than 1 at 0.5 kb in Type C quartzite, at 1.5 kb in Type B, and not at all to 10 kb in Type A. These observations are a reflection of the inherent nature of sedimentary quartzites where the petrofabric may be described as strong interlocking grains with a significant percentage of void space. With the application of stress, some of the grains experience large stress concentrations at their edge and some of the void space is broken down, the amount depending on the strength of the matrix. Since the grains interlock to a high degree, the shear modulus variation with stress is primarily a result of increased friction between grains.

The pressure dependence of the bulk modulus and the absolute value of the shear modulus may be directly correlated with the mineralogic composition of the individual types. The highest bulk and shear moduli under ambient conditions are found for Type A. This is a manifestation of the larger grain size and mineralogic purity of the rock type. The shear modulus in this case is controlled only by interlocking quartz grains, and is therefore quite high. The bulk modulus starts out fairly high, but does not increase rapidly with the initial increase in pressure, as is true of most rocks. This is because quartz* grains are holding void space open and are collapsing with increasing pressure at a nearly constant rate. The bulk modulus does not increase rapidly, and Poisson's ratio stays low (0.09-0.08) to at least 10 kb. On the other hand, the very-fine-grained Type C contains significant amounts of ferrouginous and/or argillaceous material which is interspersed with the quartz matrix to (1) decrease the shear modulus, and (2) allow a large percentage of the void space to collapse in the first 1 kb of confining stress. Poisson's ratio thus rises from 0.10 at atmospheric pressure through 0.125 ($K = \mu$) at 0.4 kb, to a value greater than 0.22 above 2 kb. The bulk modulus in this case rapidly approaches the bulk modulus of quartz. In Type B the percentage of material other than quartz is again greater than for Type A, but is much less than Type C. As might be predicted, the bulk modulus, and consequently Poisson's ratio, increases more slowly with confining stress than for Type C.

Stirling quartzite is not truly isotropic, and the moduli presented above by assuming isotropy are only approximations to the actual moduli. The validity of these approximations is related directly to the degree of anisotropy of the rock. Type D Stirling quartzite was therefore treated as an anisotropic rock and five independent velocities measured according to the procedure outlined above. The results are shown in Figs. 8-11. Predictably, the rock is more compressible across the bedding plane than along it (Fig. 11), although this difference is essentially non-existent above 3 kb. The stiffness in both directions (Fig. 9) initially increases with increasing confining stress. However, above 1 kb, E_1 decreases with increasing pressure. This may be related to quartz grains breaking down with increasing pressure, in the manner

---

*Yield strength 15-30 kb at 0-10 kb confining stress.

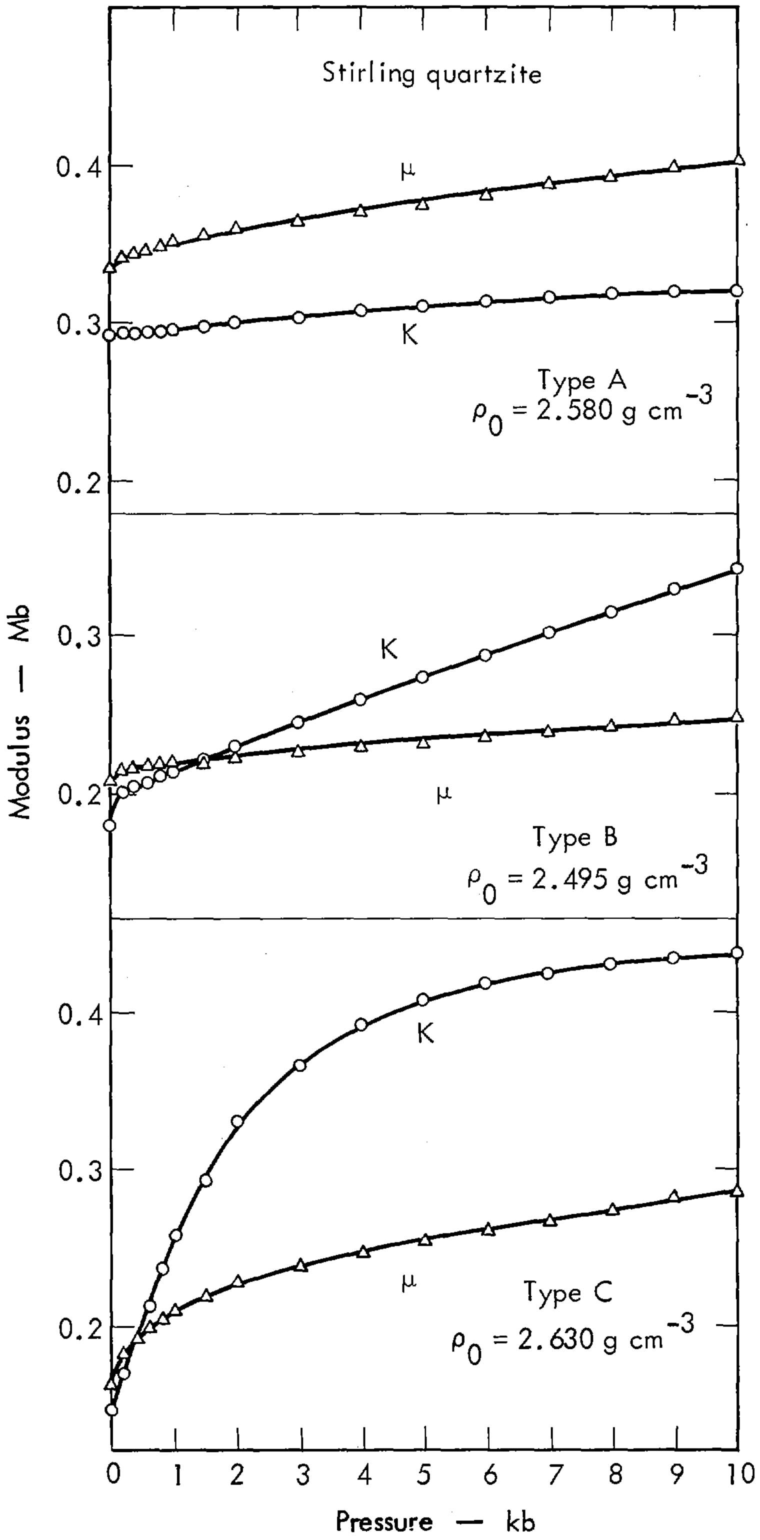

Fig. 7. K and μ for Types A, B, and C Stirling quartzite with pressure.

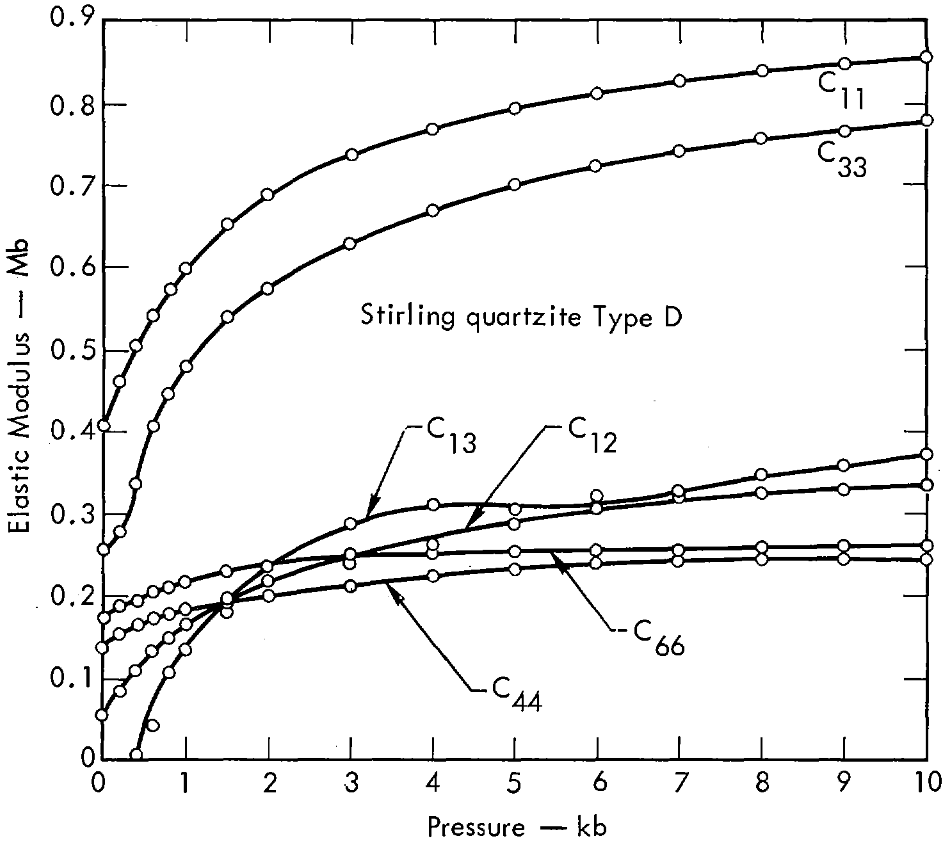

Fig. 8. The six elastic constants for Type D Stirling quartzite with pressure.

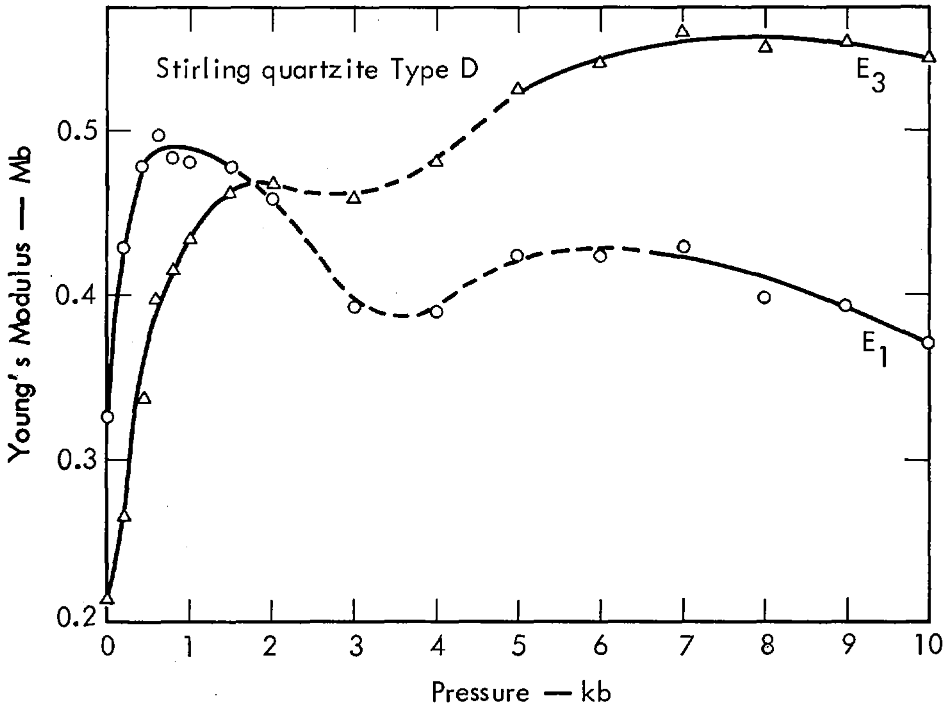

Fig. 9. Directional Young's moduli (E_1 and E_3) for Type D Stirling quartzite with pressure.

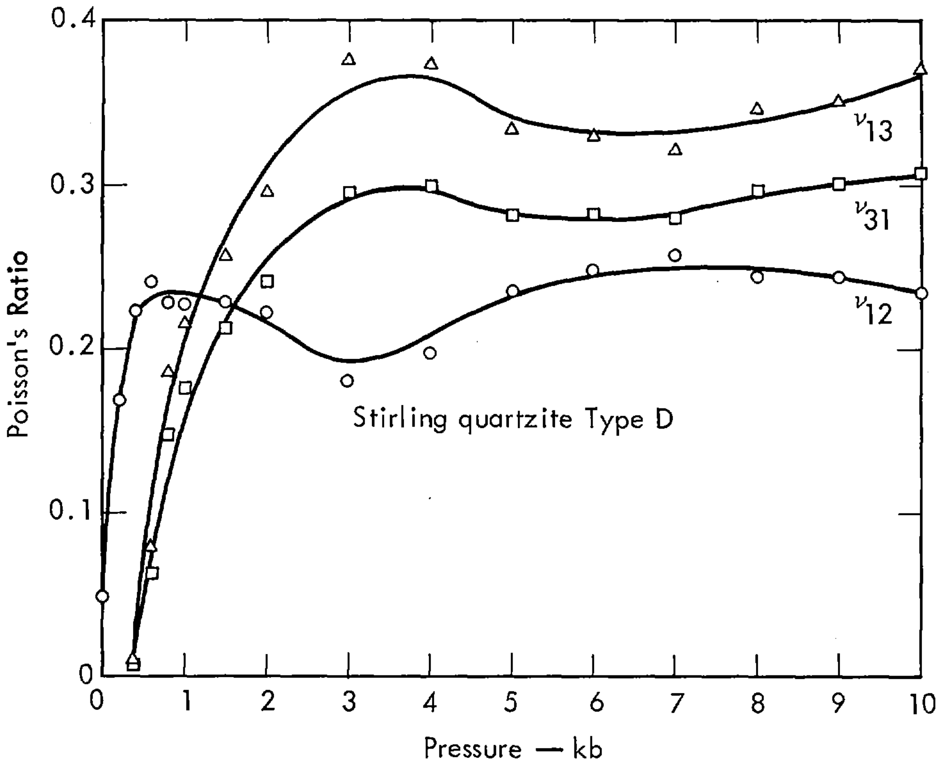

Fig. 10. Directional Poisson's ratios (ν_{12}, ν_{13}, ν_{31}) for Type D Stirling quartzite with pressure.

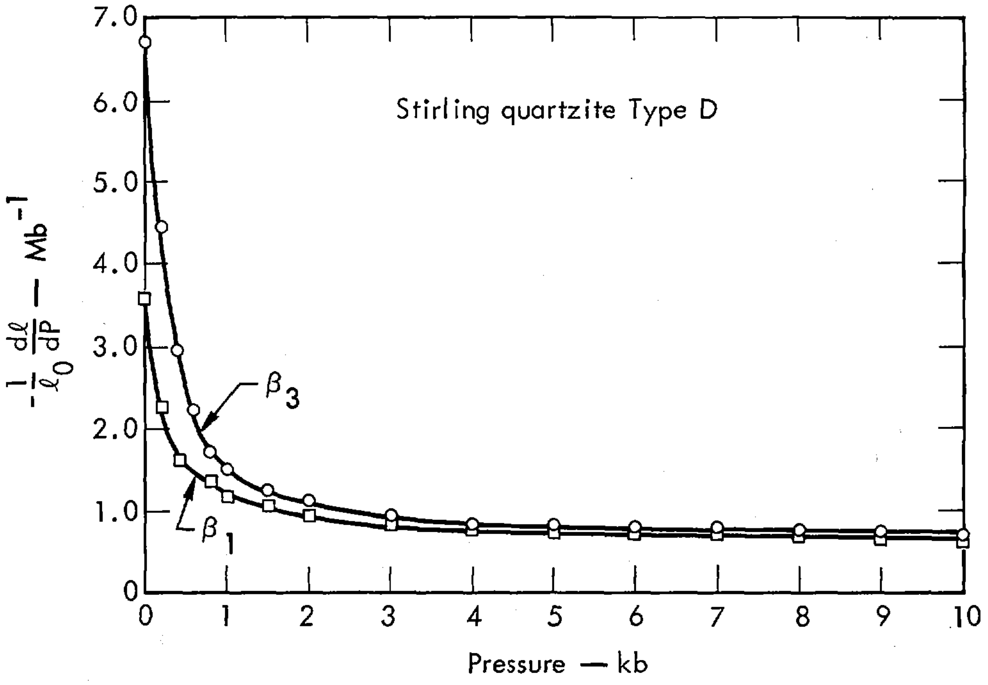

Fig. 11. Directional compressibilities (β_1 and β_3) for Type D Stirling quartzite with pressure.

shown above for Type A, after the initial non-quartz material has compacted. The non-quartz material is significant as an interbed material, affecting strength across the beds more than in them. While the beds become relatively weak to linear stress with increasing confining stress, they become strong to radial stress (Fig. 10). This is again presumably related to the interlocking detrital, quartz grains resulting in little radial strain when the material is in shear with both components in the bedding plane. The strength data in Fig. 9 show a weakness at 2-3 kb that may or may not be real. The initial negative ν_{13} and ν_{31} values result from the initially low C_{11} values, which strongly affect C_{12} and C_{13} and are an unlikely result complicated by the presence of cracks which decrease the apparent stiffness to linear compression across the bedding plane. This conclusion was arrived at by considering many measurements under ambient conditions on different specimens of the same rock-type where negative Poisson's ratios were found in some samples and not in others.

Green River shale was also treated as anisotropic (Figs. 12-15). Unlike most rocks, the compressibilities decrease gradually with pressure and the pressure coefficients remain high even at 10 kb (Fig. 15). This suggests that large linear fractures do not play a significant role in the elastic deformation of laboratory-sized samples. The anisotropy in compressibility is still pronounced at 10 kb. An indication of the degree of anisotropy is shown in Fig. 14. The high Poisson's ratio within the plane of bedding may be related to the kerogen content and its behavior as a weak viscous fluid.

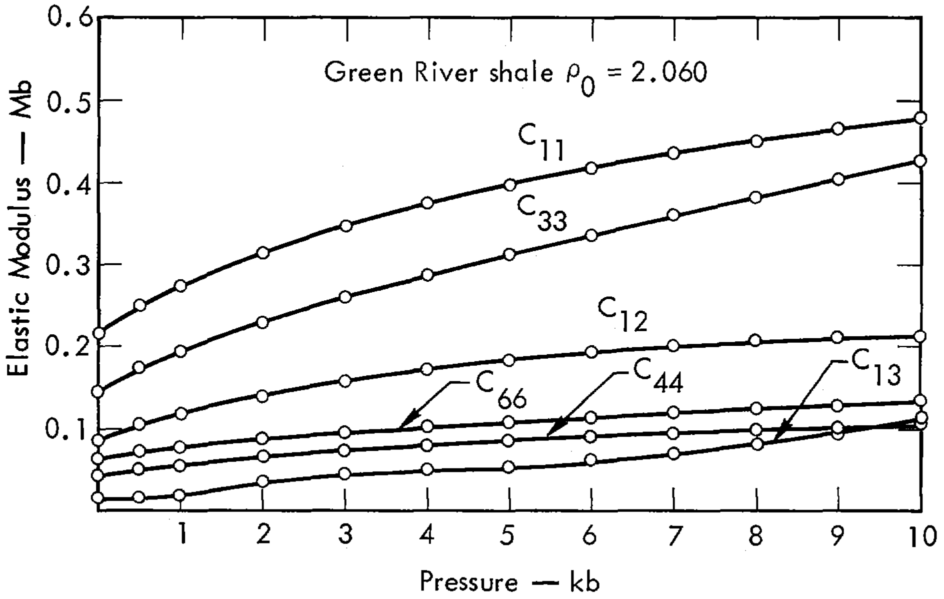

Fig. 12. The six elastic constants for Green River shale with pressure.

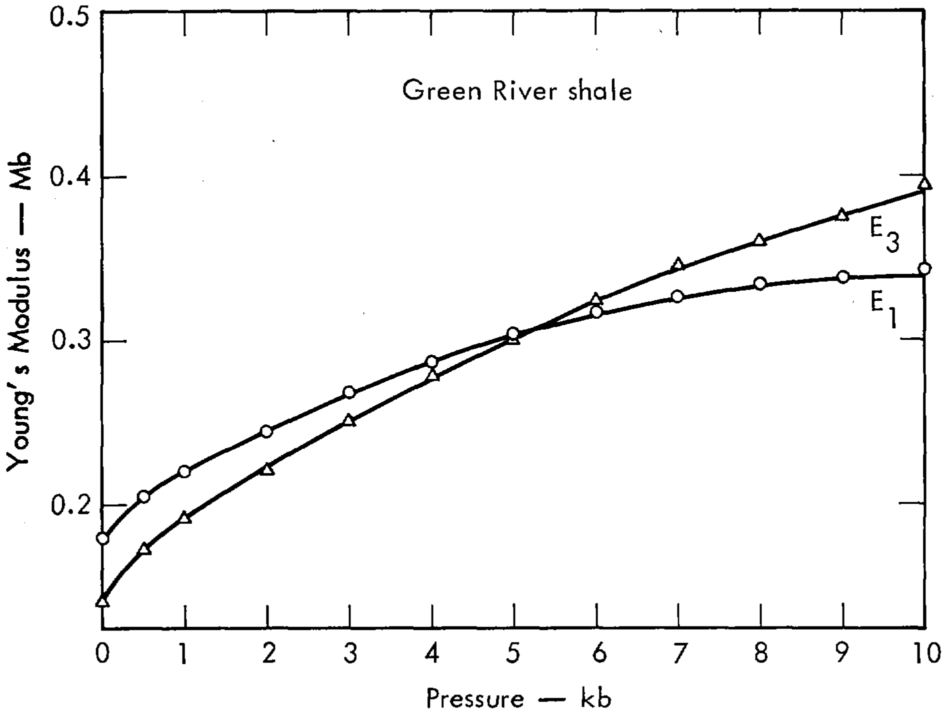

Fig. 13. E_1 and E_3 for Green River shale with pressure.

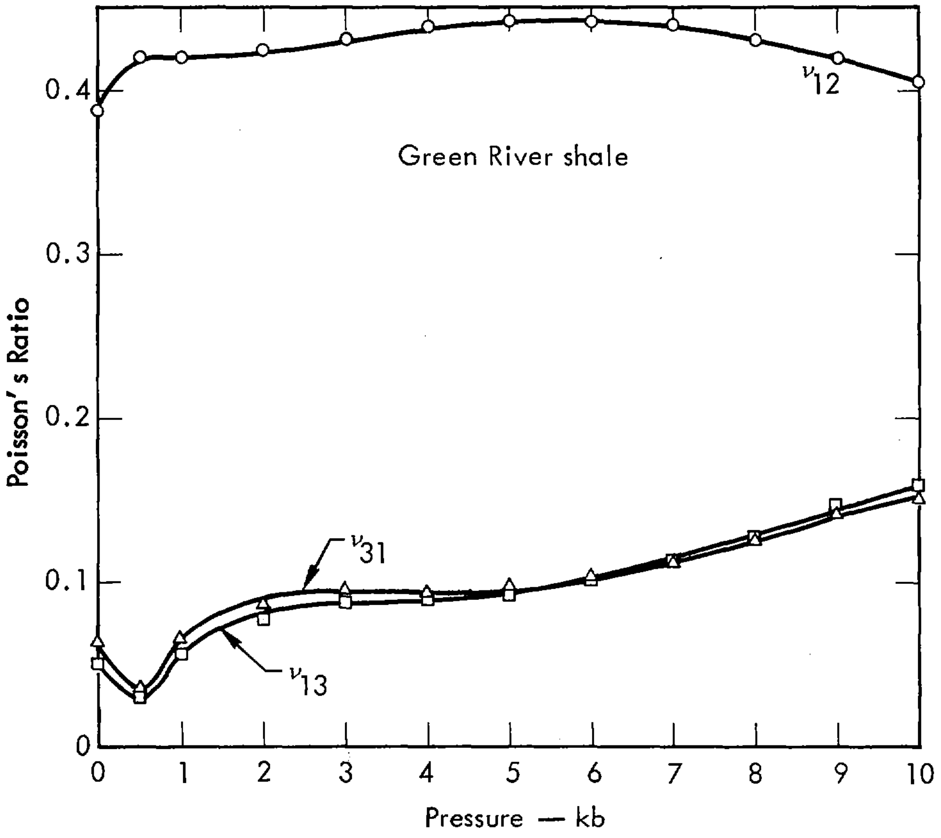

Fig. 14. ν_{12}, ν_{13}, and ν_{31} for Green River shale with pressure.

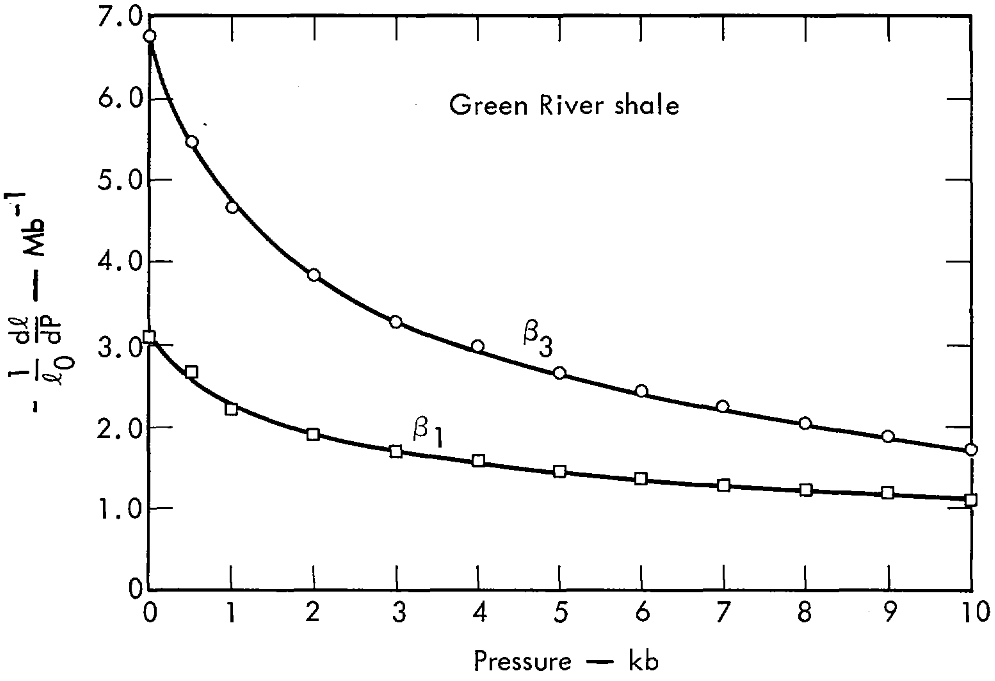

Fig. 15. β_1 and β_3 for Green River shale with pressure.

CONCLUSIONS

Measurements of transmission velocities on rocks, made in the laboratory under simulated natural stress conditions, are used to compute elastic moduli and their pressure derivatives. The velocities and elastic moduli are found not to vary with pressure in a simple manner, but rather to exhibit a behavior that, other than showing a general increase with stress, is unpredictable. This behavior may vary not only from rock type to rock type, but also within a specific type. Physical anisotropy, such as bedding, is found to introduce significant departures from the average in directional moduli. In general, the elastic moduli and their behavior with stress and direction reflect the chemical and physical nature of a particular rock type.

ACKNOWLEDGMENTS

H. Louis was responsible in large part for obtaining travel-time data on the rocks discussed. Discussions and comparison of data with D. R. Stephens and H. C. Heard contributed measureably to an understanding of the results.

REFERENCES

1. J. F. Nye, *Physical Properties of Crystals*; (Oxford Univ. Press, London) 1957, pp. 133-137.
2. A. E. H. Love, *A Treatise on the Mathematical Theory of Elasticity* (Cambridge Univ. Press, London, 1927), Chapt. 13.
3. R. K. Cook, J. Acoust. Soc. Am. **29**, 445 (1957).
4. F. J. Birch, J. Geophys. Res. **66**, 2199 (1961).
5. J. M. Ide, Proc. Natl. Acad. Sci. U. S. **22**, 482 (1933).
6. W. F. Brace, in *State of Stress in the Earth's Crust*; W. R. Judd, ed., (American Elsevier, New York, 1964).
7. J. Simmons and W. F. Brace, J. Geophys. Res. **70**, 5649 (1965).
8. J. B. Walsh, J. Geophys. Res. **70**, 381 (1965).
9. L. Peselnick and W. F. Outerbridge, J. Geophys. Res. **66**, 581 (1961).
10. F. J. Birch, J. Geophys. Res. **65**, 1083 (1960).
11. J. Simmons, J. Geophys. Res. **69**, 1123 (1964).
12. J. Simmons, Proc. IEEE **53**, 1337 (1965).
13. D. R. Stephens and E. M. Lilley, in *Shock Metamorphism of Natural Materials*, B. M. French and N. M. Short, eds. (Mono Book Corp., Baltimore, 1968).

XA04N0747

THE INFLUENCE OF ENVIRONMENT ON THE INELASTIC BEHAVIOR OF ROCKS[*]

Hugh C. Heard

Lawrence Radiation Laboratory, University of California
Livermore, California 94550

ABSTRACT

The mechanical response of earth materials are demonstrably dependent upon the environment during deformation as well as the physical properties of the rock masses themselves. Among the most important of these environmental parameters are mean pressure, pore fluid pressure, temperature, strain rate, and the relative magnitude of the intermediate principal stress (σ_2) compared to the maximum (σ_1) and minimum (σ_3) stresses. Important inherent properties of rocks include anisotropy, homogeneity, porosity, permeability, grain size, and mineral composition.

Calculation of the response of rocks to a nearby nuclear detonation requires knowledge of the deviatoric stress-strain behavior as well as the resulting mechanisms of deformation: fracture or flow. For calculations beginning at times of the order of 10^{-3} sec after detonation, that is, when peak pressures are $\sim 10^6$ bars and lasting to $\sim 10^2$ sec when cavity pressures have decayed to $\sim 10^2$ bars, broad limitations may be imposed on the possible deformation environment. Here, mean pressures range from 10^6 to 10^2 bars, pore pressures from 10^6 to 1 bar, temperatures from 1500° to 50°C, and strain rates from 10^6 to 10^{-3} per sec; σ_2 may range in value from that of σ_3 on loading to that of σ_1 on unloading. Using present technology, it is virtually impossible to measure the mechanical behavior of rock materials under controlled conditions over much of the above range. This behavior must be largely inferred from data gathered at less extreme conditions.

Quantative data illustrating the effect of the deformation environment upon the strength and brittle-ductile behavior are presented for a suite of rocks of interest to the Plowshare program; among these are limestone, quartzite, granite, sandstone and "oil-shale." More limited results are also presented illustrating the effect of planar anisotropies as well as of grain size upon mechanical properties. The available data then may be used to infer the mechanical response of rocks at the more extreme conditions near a nuclear detonation.

INTRODUCTION

It has long been recognized that the mechanical behavior of rock materials, both elastic as well as inelastic, may be much enhanced or degraded by altering the conditions or environment under which the loading occurs. In the previous

---

[*] Work was done under the auspices of the U. S. Atomic Energy Commission.

two papers, D. Stephens and R. Schock describe the change in compressibility, Young's modulus, shear modulus, and Poisson's ratio with mean pressure. In this contribution, I concentrate on the inelastic behavior of rocks as determined from the differential stress-strain curve resulting from a standard triaxial test. Macroscopic fracture or flow of a material may be inferred from the shape of such a curve; and, in addition, the strength (or more specifically the yield point, ultimate strength, and rupture strength) may be read directly from it. In addition to mean pressure mentioned above, the following are among the main environmental parameters influencing the behavior of rock materials: pore fluid pressure; state of stress, or relative value of the intermediate principal stress; temperature; and strain rate. Many of these parameters have already been explored singly for a large number of rocks of variable anisotropy, homogeneity, porosity, permeability, grain size, and mineral composition. Only a few rocks have been studied in which the relative effect of all five environmental parameters have been evaluated; thus these existing data then allow a semiquantative estimate of selected rock behavior at the expected conditions existing in the immediate vicinity of an underground nuclear detonation. These estimates may then serve as input for the computer code calculations. For unevaluated rock types, much may be inferred from the existing information.

The total stress field imposed upon a small volume element of porous and permeable rock may be thought of as the sum of an applied deviatoric stress, plus a mean pressure, plus an interstitial fluid pressure. The deviatoric portion is completely specified by nine components: six shear and three normal. If the volume element under consideration is in rotational equilibrium, by suitably choosing our coordinate axes we may resolve these nine into the three principal component stresses S_1, S_2, and S_3. Since neither the mean pressure, P_m, nor the pore pressure,* P_p, contain shear components, the fluid pressure may be subtracted from the mean pressure to give the effective mean pressure, P_m eff, and this in turn may be added to S_1, S_2, and S_3 to give the three principal effective stresses σ_1, σ_2, and σ_3. The maximum principal stress is then σ_1, the intermediate is σ_2, and σ_3 is the minimum, with compression taken as positive. Thus we may write the stress tensor acting on this small volume element as

$$\begin{bmatrix} S_1 + P_m - P_p & 0 & 0 \\ 0 & S_2 + P_m - P_p & 0 \\ 0 & 0 & S_3 + P_m - P_p \end{bmatrix} = \begin{bmatrix} \sigma_1 & 0 & 0 \\ 0 & \sigma_2 & 0 \\ 0 & 0 & \sigma_3 \end{bmatrix} \quad (1)$$

EFFECTS OF THE ENVIRONMENTAL PARAMETERS

An increase in the hydrostatic or confining pressure, P_c, surrounding a test sample, regardless of the type of test (i. e., compression, torsion, extension, bending, etc.), may significantly increase the strength of the sample as well as alter the shape of the resulting differential stress-strain curve. This behavior is well documented for virtually every common type of rock for many kinds of tests.[1-6] Figure 1 shows the first quantative example of this effect for marble and sandstone.[1] Here the differential stress, $\sigma_1 - \sigma_3$, is plotted versus axial strain for compression of cylindrical samples tested over a range of confining pressures (noted for each curve, in bars). Any increase

---

*Assuming a low viscosity fluid in only very slow motion through the rock pores.

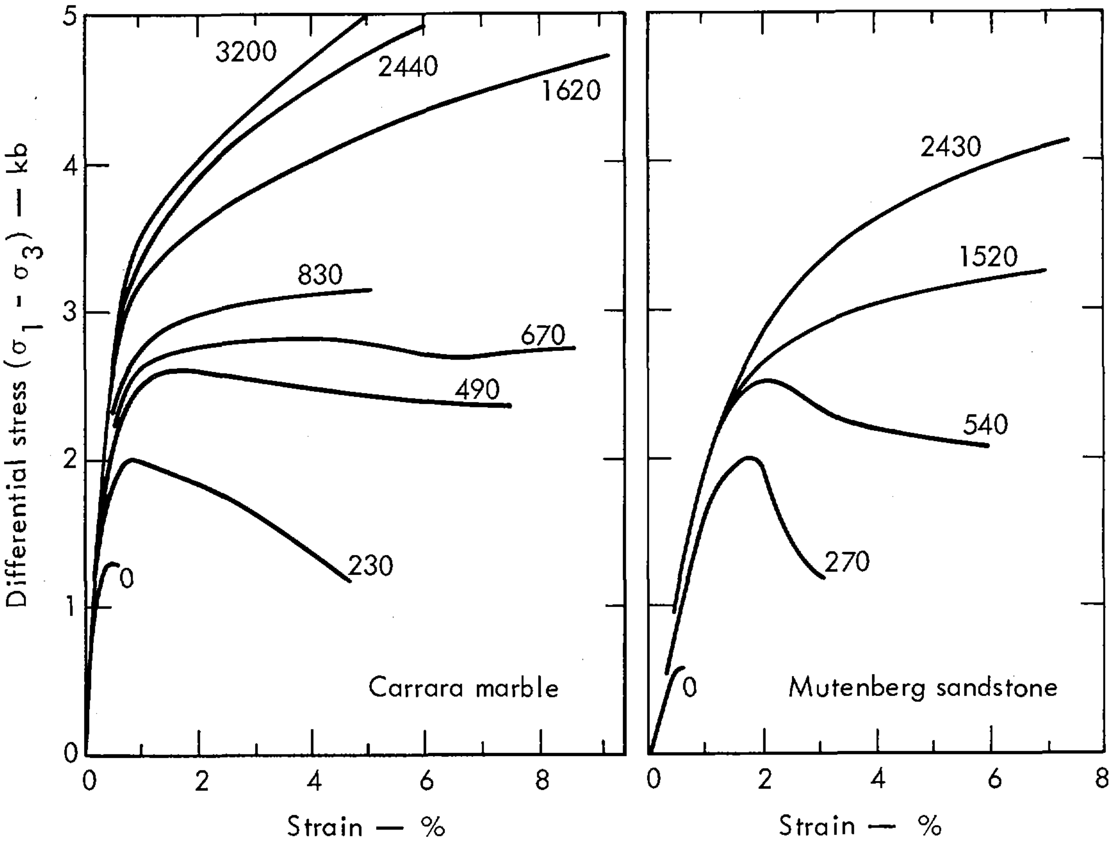

Fig. 1. Stress-strain curves for dry Carrara marble and Mutenberg sandstone compressed at different confining pressures (shown in bars for each curve) at room temperature (Ref. 1).

in strength is reflected in equation (1) both as a change in S_1, S_2, and S_3 and an increase in P_m; the increase of hydrostatic pressure occurs only in P_m. The increase in differential stress commonly ranges from zero up to about six times the confining pressure increment, depending on the internal friction of the rock and the test type.[2] Note also in Fig. 1 that the ductility or permanent strain before onset of macroscopic fracture (which may be correlated to a marked change of slope of the stress-strain curve) is also significantly increased by the addition of confining pressure.

In a porous and permeable rock, an increase of pore fluid pressure (or a decrease in the effective mean pressure) is known to lower the failure strength and ductility, thus promoting fracture at the expense of distributed flow.[7-9] Figure 2 illustrates such behavior in a sandstone.[7] It should be noted here that the mechanical properties are identical at similar effective mean pressures. If, however, the rock is partially impermeable to the fluid, the fluid pressure is not uniform throughout the test sample or if it is not maintained constant during the test, then the strength and ductility may be very much different.[3,7,8] Figure 3 emphasizes this point for a dolomite rock.[7]

The mechanical behavior of a rock is also quite sensitive to the type of imposed stress field, that is, the relative value of σ_2 compared to σ_1 and σ_3 may affect both the strength and ductility.[1,10,4,11]

In examining results from triaxial compression, extension, and torsion tests, it should be remembered that σ_2 ranges from equality with σ_3 in

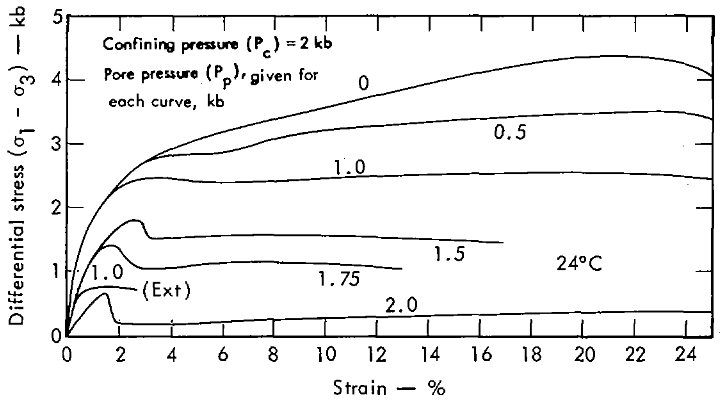

Fig. 2a. Stress-strain curves for Berea sandstone deformed at different pore water pressures. All tests at 2 kb confining pressure and 24°C; all in compression except curve marked Ext (Ref. 7).

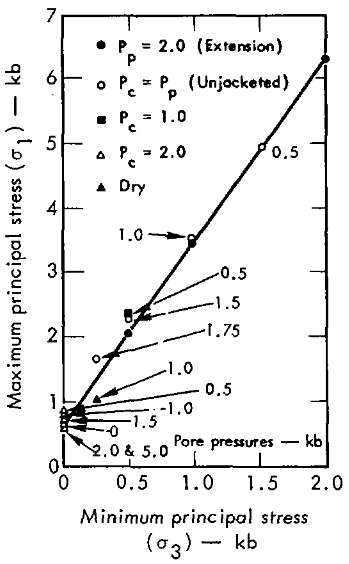

Fig. 2b. Maximum principal stress versus minimum principal stress at the ultimate strength of Berea sandstone at 24°C (Ref. 7).

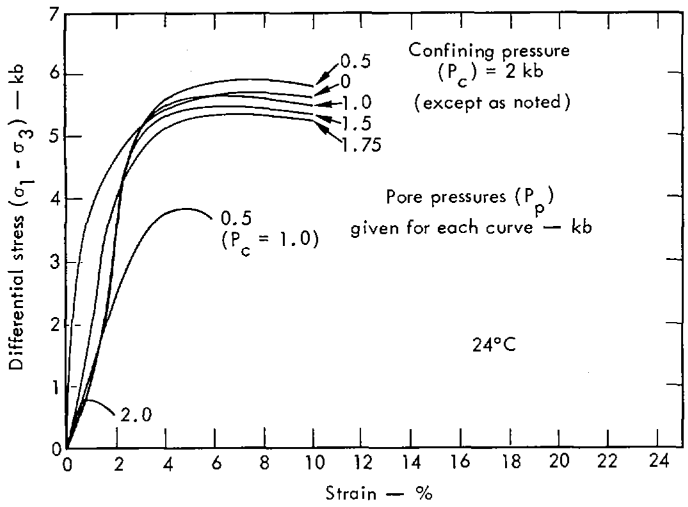

Fig. 3a. Stress-strain curves for Hasmark dolomite compressed at 24°C and at different pore water pressures. All at 2 kb confining pressure except curve marked P_c = 1.0 (Ref. 7).

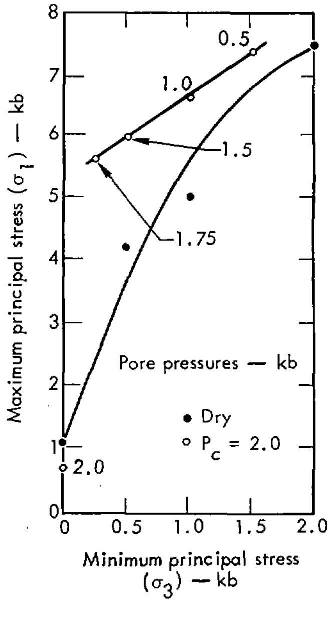

Fig. 3b. Maximum principal stress versus minimum principal stress at the ultimate compressive strength of Hasmark dolomite at 24°C (Ref. 7).

in compression to equality with σ_1 in extension; in torsion, σ_2 equals neither and is midway in value between σ_1 and σ_3. Figure 4 shows failure envelopes as deduced from stress-strain data for these very different stress states on a limestone.[3,4] The largest discrepancies occur at low mean pressures, where internal friction is most important. At high pressure, they begin to converge with a much decreased slope and thus are beginning to approximate a von Mises solid. Relative ductility is also strongly influenced by the stress state, as will be documented below.

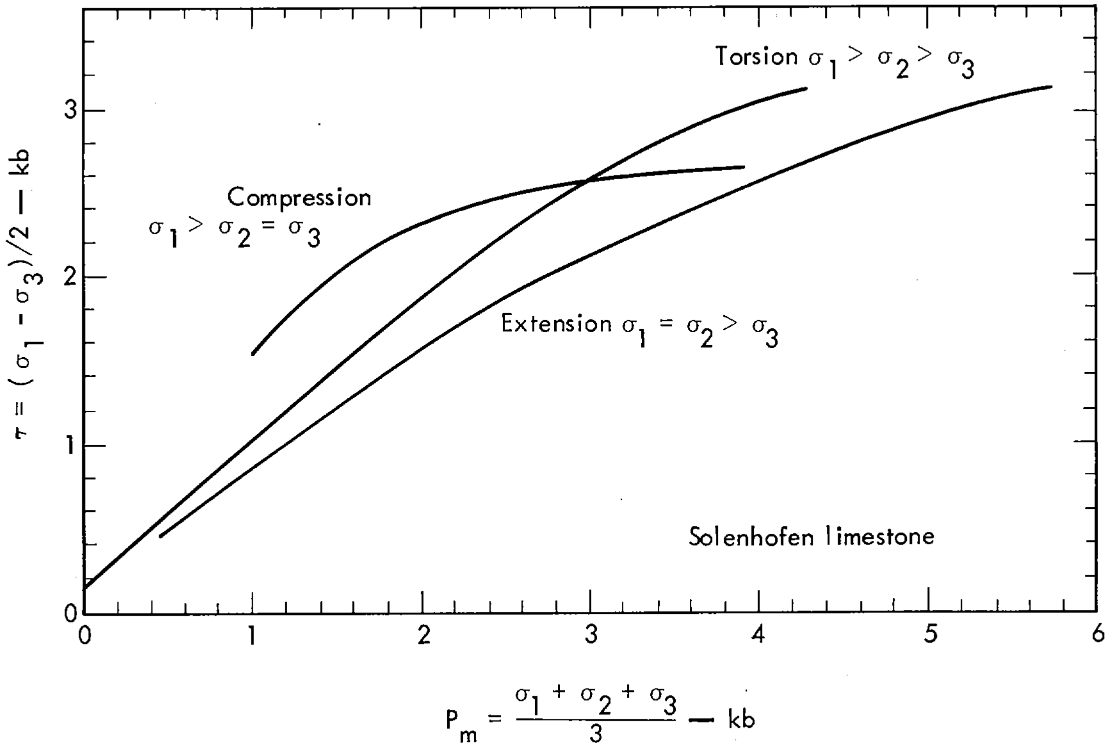

Fig. 4. Shear stress versus mean pressure for triaxial compression, torsion, and extension of Solenhofen limestone tested at 25°C, dry, and at a strain rate of 10^{-4}/sec. Data from Block 3,5 (Refs. 3,4).

Test temperature is also important in altering the mechanical response of the rock. Moderate increases in the test temperature lower the stress-strain curve and increase the ductility.[3,12-16] Brittle behavior at lower temperatures is replaced by uniform flow at the higher temperatures. Occasional deviations from this general behavior pattern do exist for a few rocks in restricted temperature ranges, but these may be explained by secondary effects such as phase changes in the component minerals or work hardening due to an increase in ductility. Figure 5 illustrates the effect of temperature for a granite and a basalt tested in compression.[12] Most common rocks show roughly a two- to threefold decrease in strength for a 500°C temperature rise above ambient. Enhancement of ductility may be much greater in certain rocks for similar increases in temperature.

Changes in the rate of application of load upon mechanical properties of rock has only recently been extensively explored. An increase in strain rate is observed to raise the stress-strain curve as well as to decrease the ductility.[9,14-18] This behavior may be seen in Fig. 6 for a quartzite tested in compression. In rocks tested at conditions where ductilities are not large, a decade increase in strain rate may increase the differential stress by roughly 5%.[9,17] However, if the deformation environment favors high ductilities, similar increases in strain rate may produce strength enhancements ranging up

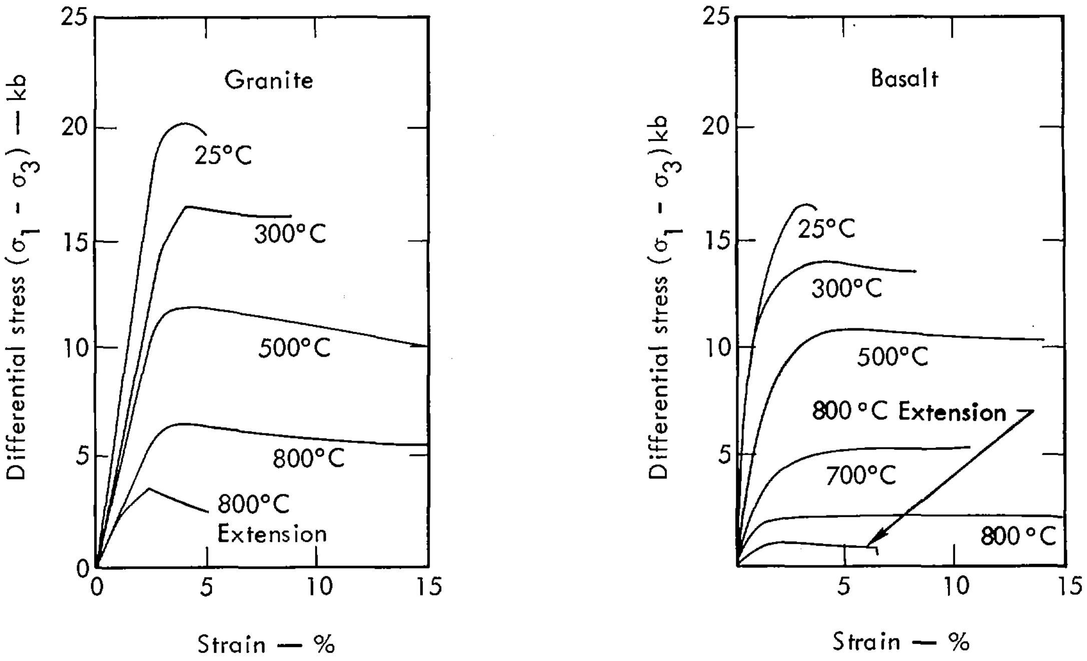

Fig. 5. Stress-strain curves for Westerly granite and basalt tested at 5 kb containing pressure, dry, and at a strain rate near 10^{-4}/sec. All data in compression except where noted (Ref. 12).

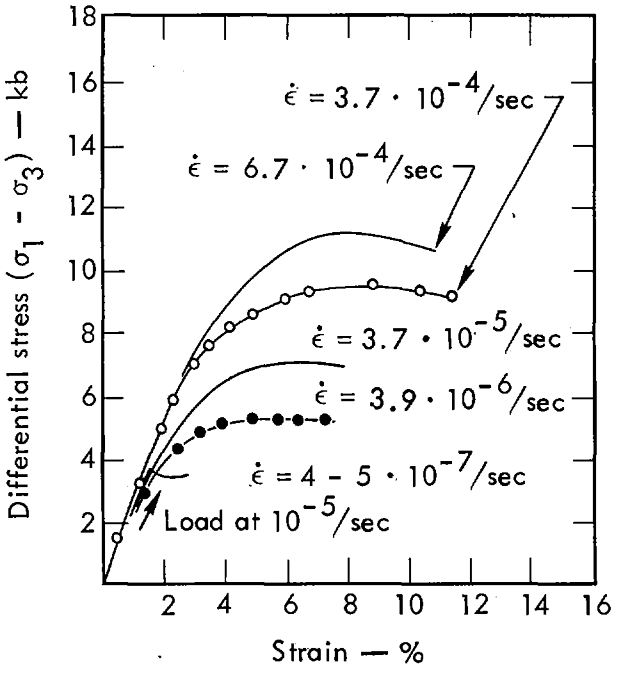

Fig. 6. Stress-strain curves for Simpson orthoquartzite tested at 8 kb confining pressure, dry. All tests were at 900°C in compression and over a wide spectrum of strain rates. Lowest curve loaded to yield point at 10^{-5}/sec strain rate, deformation continued then at lower quoted rate (Ref. 15).

to 20%.[14,15,18] Very large (orders of magnitude) degradations in ductility may accompany such increases in strain rate.[4]

RELATIVE DUCTILITY AND FRACTURE ORIENTATION

When the mechanical responses of a rock from triaxial tests are compared over a wide range of environmental conditions, it is convenient to classify the behavior as brittle, transitional, or ductile, depending both upon an arbitrary amount of permanent strain before onset of macroscopic fracture and upon the shape of the stress-strain curve. One definition suggests that, for permanent strains of less than 1% after the yield point, the rock be classified as brittle; for 3 to 5%, transitional; and, for any strain greater than 5%, ductile.[3] When a rock material does fail in a brittle fashion, two different species of planar fractures are recognized: shear and extensile, with each possessing a unique orientation to the stress field regardless of the type of test. Extensile fractures are normal to σ_3; any movement is essentially parallel to σ_3. Shear fractures, on the other hand, occur at low angles (usually 10 to 30 deg) to σ_1 and contain σ_2 in their plane. All movements are predominantly parallel to the more or less planar surface. In Fig. 7, which schematically illustrates the spectrum of macroscopic deformational behavior for the compression, torsion, and extension cases, brittle fracture occurs at the left. When the surrounding environment is suitably altered, fracture is progressively suppressed until only macroscopic ductile flow is present (right).[19,4] At intermediate ductilities (transitional behavior), cohesion is retained across the shear fracture and they are better termed faults, in exactly the same sense as that used by the field geologist; some ductile flow occurs. Brittle fracture may be inhibited and ductile flow enhanced (shift from left to right in Fig. 7) by increasing the mean pressure, or temperature; an increase in pore fluid pressure, σ_2, or strain rate has just the opposite effect. The strength of a rock material, as schematically shown in the stress-strain curves, may be raised by an increase in mean pressure or strain rate. Increasing pore fluid pressure or temperature tends to lower the strength. By increasing σ_2, strengths may be either raised or lowered, depending upon relative ductilities.

One useful method of comparing the relative ductilities between rock types or within a given rock as its environment of deformation becomes modified is to compare the relative transitions from brittle fracture to ductile flow as defined above. The effect of several of the environmental parameters upon this transition has been studied in only a very few rocks. Figure 8 compares the relative effects of mean pressure, stress state, temperature and strain rate in limestone.[3,4,16] The effect of the pore fluid pressure has been evaluated[3] but for clarity is not plotted here. For this rock, all parameters are important in affecting the mean pressure for transition. The relative magnitude of each depends on the increments compared; in general, these changes are nonlinear.

ESTIMATION OF THE ENVIRONMENT NEAR A NUCLEAR DETONATION

Before we can infer the mechanical behavior of rock materials in the vicinity of a nuclear detonation, we must estimate the transient environment resulting from the interaction of the event itself with the emplacement medium. Existing physical measurements taken from many such detonations, along with machine calculations based upon simple models,[20,21] yield ranges of mean pressures, pore fluid pressures, stress states, temperatures, and strain rates, depending both on the time and the radial distance.

Typically, the deposition of energy at detonation time is produced in a period of the order of 10^{-7} sec.[22] This energy instantly vaporizes all material in the immediate vicinity of the device. The resulting rapid loading from

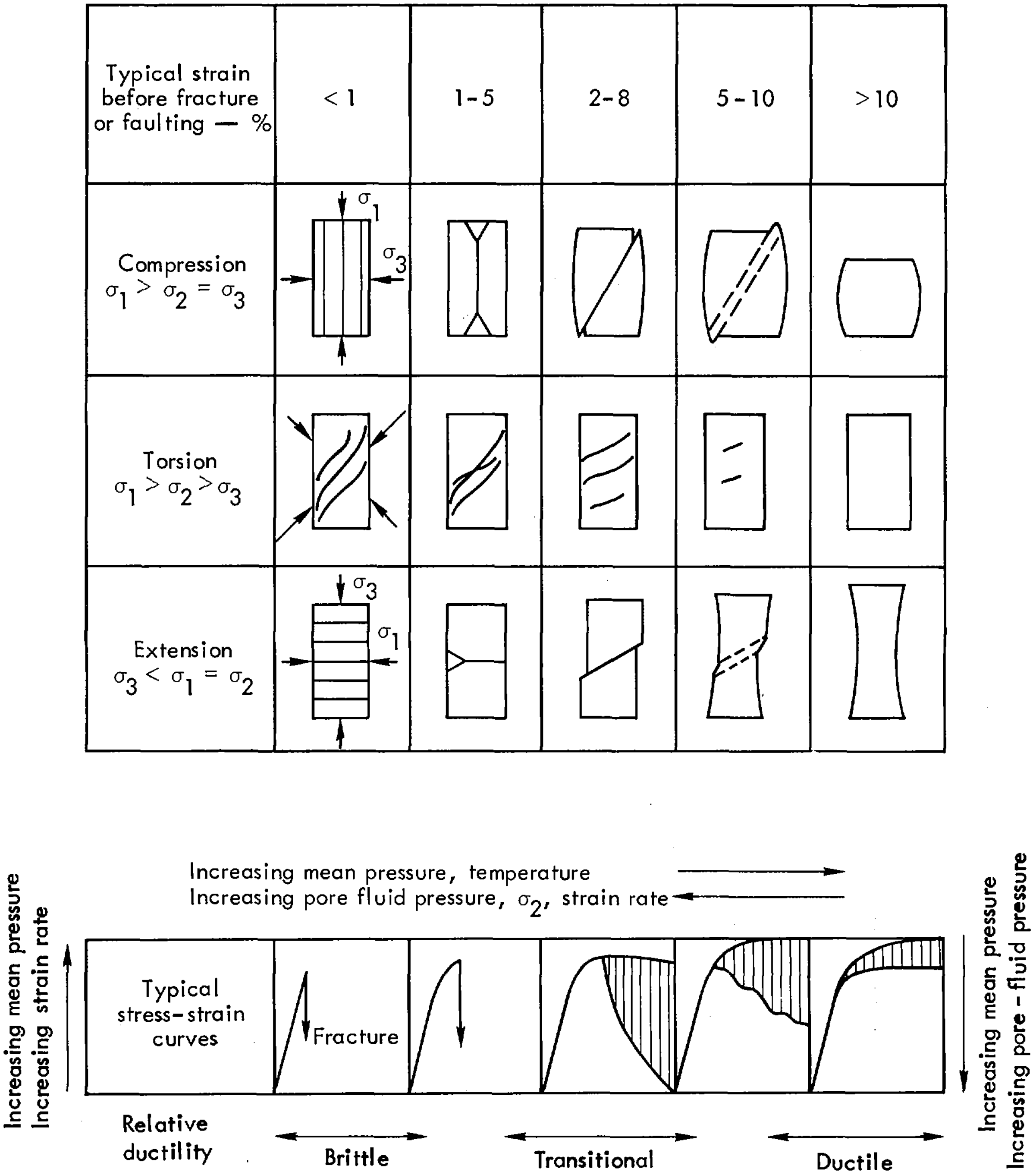
Typical strain before fracture or faulting — %
< 1
1-5
2-8
5-10
>10
σ_1
σ_3
Compression
$\sigma_1 > \sigma_2 = \sigma_3$
Torsion
$\sigma_1 > \sigma_2 > \sigma_3$
σ_3
σ_1
Extension
$\sigma_3 < \sigma_1 = \sigma_2$
Increasing mean pressure, temperature
Increasing pore fluid pressure, σ_2, strain rate
Increasing mean pressure
Increasing strain rate
Typical stress-strain curves
Fracture
Increasing mean pressure
Increasing pore - fluid pressure
Relative ductility
Brittle
Transitional
Ductile

Fig. 7. Schematic of mechanical behavior of rock materials illustrating stress-strain and fracture, flow characteristics for compressive, torsional, and extensile loading. The stress-strain curve for brittle behavior is predictable; for transitional or ductile flow it may occur anywhere within the shaded region. Increasing mean or pore fluid pressure, σ_2 temperature, and strain rate shift the ductility response horizontally (top). A change in mean or pore fluid pressure, temperature, and strain rate will increase or decrease strength as shown on right or left sides. σ_2 may increase or decrease strength (derived from Refs. 19,4).

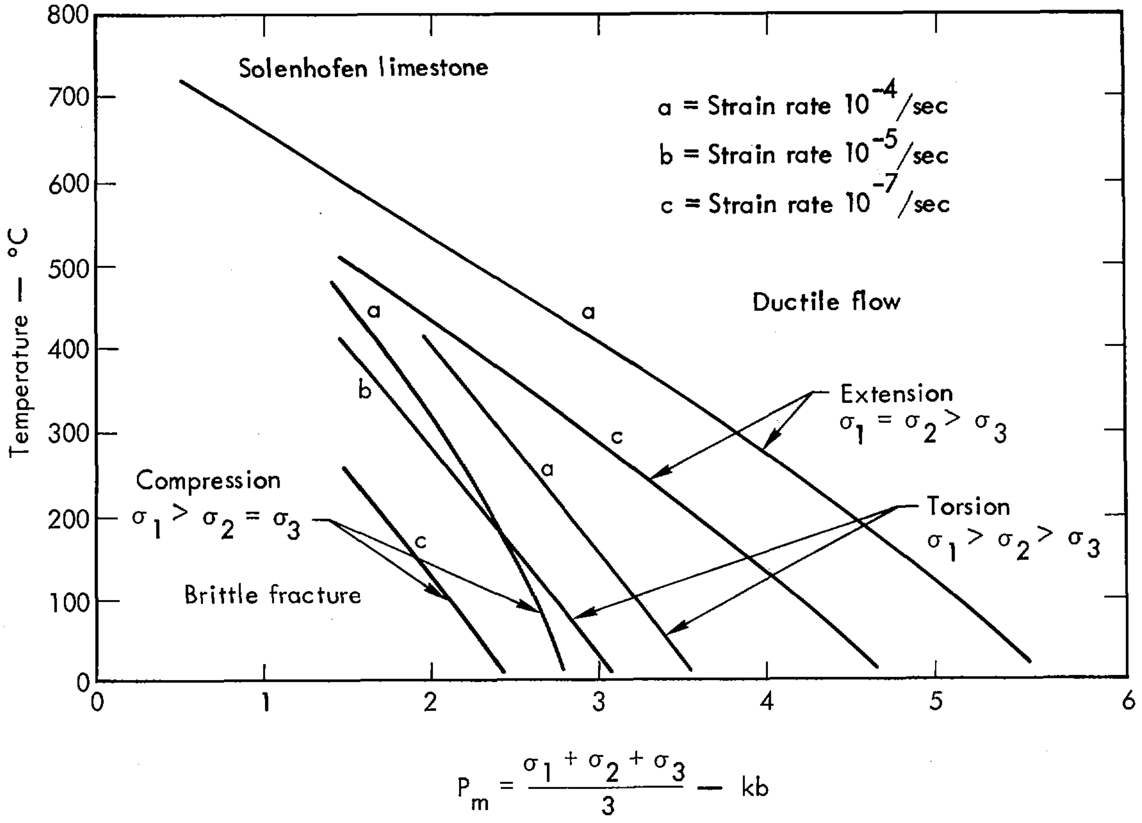

Fig. 8. Brittle-ductile transition for Solenhofen limestone (dry). Brittle behavior occurs to the left of each boundary; ductile flow predominates to right of each curve. Note relative effect of mean stress, stress state (σ_2) temperature, and strain rate on transition (Refs. 3,4,16).

detonations in the low-intermediate to high yield range (20 to 1000 kt) generates shock pressures in the megabar range that then move out radially and decay to values of the order of 10^2 bars after periods of several hundred seconds. As the deviatoric stresses associated with this compressional shock wave are greater (at least at short distances) than the yield point of the surrounding material, the rocks undergo irreversible flow, fracture, or only elastic deformation, depending on the peak cavity pressure, the radial distance, and the inherent rock properties. At discontinuities in the medium (i. e., density, elastic and inelastic behavior, etc.) the wave may be reflected or refracted into compressional and/or shear waves with different properties; and, in certain geometries, these waves may mutually interfere. Viewed simply, the initial compressive wave exerts a loading much like a triaxial compression test ($\sigma_1 > \sigma_2 = \sigma_3$) and the reflected tensile wave would be akin to triaxial extension ($\sigma_1 = \sigma_2 > \sigma_3$). In both cases, the fractures are oriented as schematically shown in Fig. 7. In other cases with mutually interfering waves, the loading may be somewhere intermediate between the above, and the fracture pattern would be much more complicated. During the period of this shock loading, the cavity growth first accelerates, then, as the gases cool, decelerates. Order-of-magnitude calculations in which typical elastic moduli, velocities, and peak pressures[20,22] are used show that strain rates very near the detonation point may be as great as 10^5 to 10^6 per sec. At distances near 1 km, these may decrease to ~10^{-3} per sec. The deposition of dilatational and distortional strain energy in the rock at the margin of the cavity is large enough to induce melting. These temperatures, ~1000° to 2000°C, fall off extremely rapidly with distance until values at 100 m are only tens to a few degrees above ambient. The pore fluid pressures in an initially dry, porous rock would not be expected to change during the history of the explosion except perhaps very near the cavity, where the high temperatures would generate fluids from melting or decomposition of mineral phases present (i.e., "clays," carbonates). In the case of an initially water-saturated, moderately porous rock, pore pressures can be expected to equal the shock pressures out to distances of several kilometers. However, in low-porosity, saturated materials, the pore pressures may initially equal the shock pressure; but, as the rock fractures, the pressure is relieved locally, and thus its behavior may be intermediate between the previous two cases.

The computer-based predictions of rock mass movements leading to cavity radii, crater geometries, fracture radii, or surface ground motions require knowledge of the inelastic rock behavior (as well as the elastic constants) in the above environmental range. Using present techniques, it is virtually impossible to evaluate some of these properties under controlled conditions over much of the above range. For example, it would be difficult to accomplish a controlled triaxial compression test at a strain rate of 10^4 per sec at a mean pressure of 100 kb. Most mechanical property tests (inelastic) serving as input to these codes are carried out at strain rates of 10^{-3} to 10^{-5} per sec, usually in compression. Tests are most frequently made at room temperature; dry and confining pressures rarely exceed 5 to 10 kb. The problem is, then, to evaluate mechanical effects over as wide a range in environmental parameters as is feasible in the laboratory, to get the best possible basis for extrapolation to those conditions that cannot be conveniently controlled.

ESTIMATION OF ROCK BEHAVIOR NEAR A NUCLEAR DETONATION

The main characteristics of a series of stress-strain curves (ultimate strength, stress after fracture, and relative ductility) taken over a range of pressure may be conveniently plotted as shear stress, τ, $\frac{\sigma_1 - \sigma_3}{2}$ versus P_m in a failure envelope. Figure 9 illustrates failure envelopes for both dry and water-saturated, 500- to 501-ft, Stirling quartzite[23,24] samples tested at a strain rate of 10^{-4} per sec. For the dry rock, both the loci of points indicating initial fracture and the strength after first fracture are shown. In the wet rock these are identical. This figure illustrates the magnitude of the effect that pore fluid pressure (for saturation when P_p = confining pressure) may have on mechanical behavior. When these curves are extrapolated to much higher mean pressures, the slope of each can be expected to decrease and eventually approach zero. As the water in the wet rock undergoes a liquid-solid transformation near 10-kb mean pressure, the envelope can be expected to show a discontinuity having an initial increase in strength followed by a monatonically decreasing slope. Any further solid-solid phase transitions may either raise or lower the wet or dry envelopes, depending on the strength of the high-pressure phase. The dry quartzite is brittle to the highest mean pressures tested; in contrast, the wet material is macroscopically ductile at all pressures greater than about 1 kb. The effect of σ_2 on strength and ductility can be expected to be qualitatively similar to that illustrated for limestone in Fig. 4. Mechanical properties would be essentially independent of temperature over nearly the entire affected zone; only in very close proximity to the explosion itself will the temperature be high enough to markedly affect the strength and ductility.[12,15] An increase in strain rate will be likely to raise either envelope approximately 3% to 10% per tenfold increase in rate.[15,16]

Figure 10 summarizes the failure envelopes for five different ashfall and lithic tuffs (density ~ 1.9) from NTS tested in compression, in both the dry and the saturated condition, and at the usual rate. In view of the heterogeneity of the material, it is surprising that the envelopes agree so well. At low mean pressures, the porous dry tuff is very compressible[23] and thus, when a small

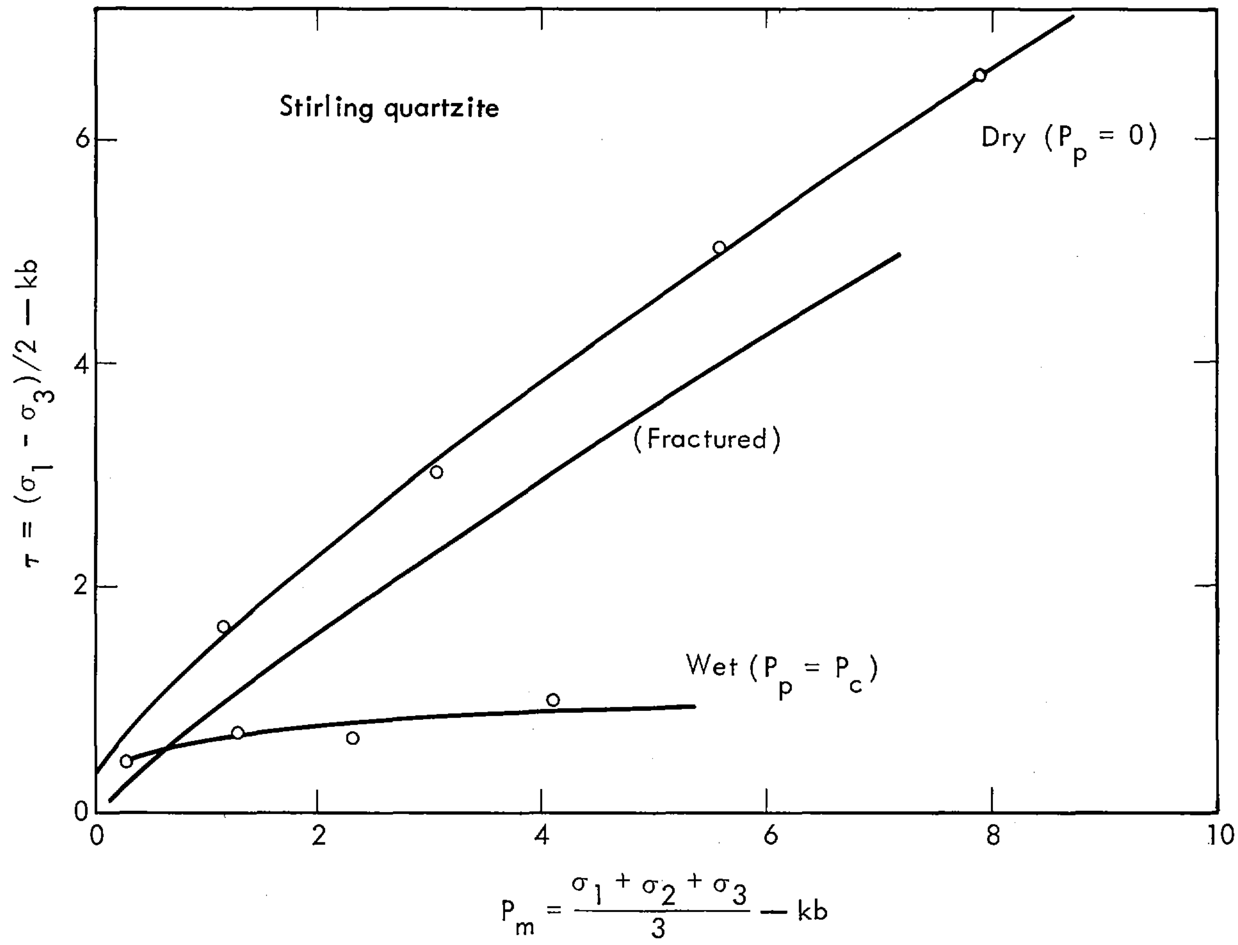

Fig. 9. Failure envelopes for dry and fluid saturated Stirling quartzite (500-501 ft) tested in compression at a strain rate of 10^{-4}/sec, 25°C. Top envelopes are for dry tests (pore pressure, $P_p = 0$). In bottom envelope, P_p = confining pressure, P_c. Curve 6 labeled "fractured" demonstrates strength of the dry rock after initial rupture.

deviatoric stress is superimposed, only macroscopic ductility is observed. This behavior is believed to account for the initial low slope of the envelopes as well as inflections in some curves caused by accelerating pore collapse at higher mean pressures. The water-saturated material is ductile at all mean pressures and has a miniscule strength. Effects of σ_2, temperature, and strain rate on mechanical properties would be expected to be similar to those discussed above for the Stirling rock.

Figure 11 illustrates the dry and water-saturated failure envelopes for Hardhat grandiorite in compression at a strain rate of 10^{-4} per sec at 25°C. This rock is somewhat similar in behavior to the quartzite shown in Fig. 9, except that the water-saturated Hardhat granodiorite is brittle. It has been shown that saturated silicate aggregates of low permeability (such as the Hardhat granodiorite) that also possess low porosity (>1%) expand slightly as the fracture stress is approached. This positive increase in crack volume locally lowers the pore fluid pressure and, at high strain rates, the fluid pressure in larger, preexistent fractures cannot maintain equilibrium throughout the sample. This low local pore pressure is then reflected by an anomalously large increase in strength (with strain rate) until the "wet" strength becomes identical with that of the dry material. This "dilatency hardening"[17] is expected to grossly affect strength when viewed on a small

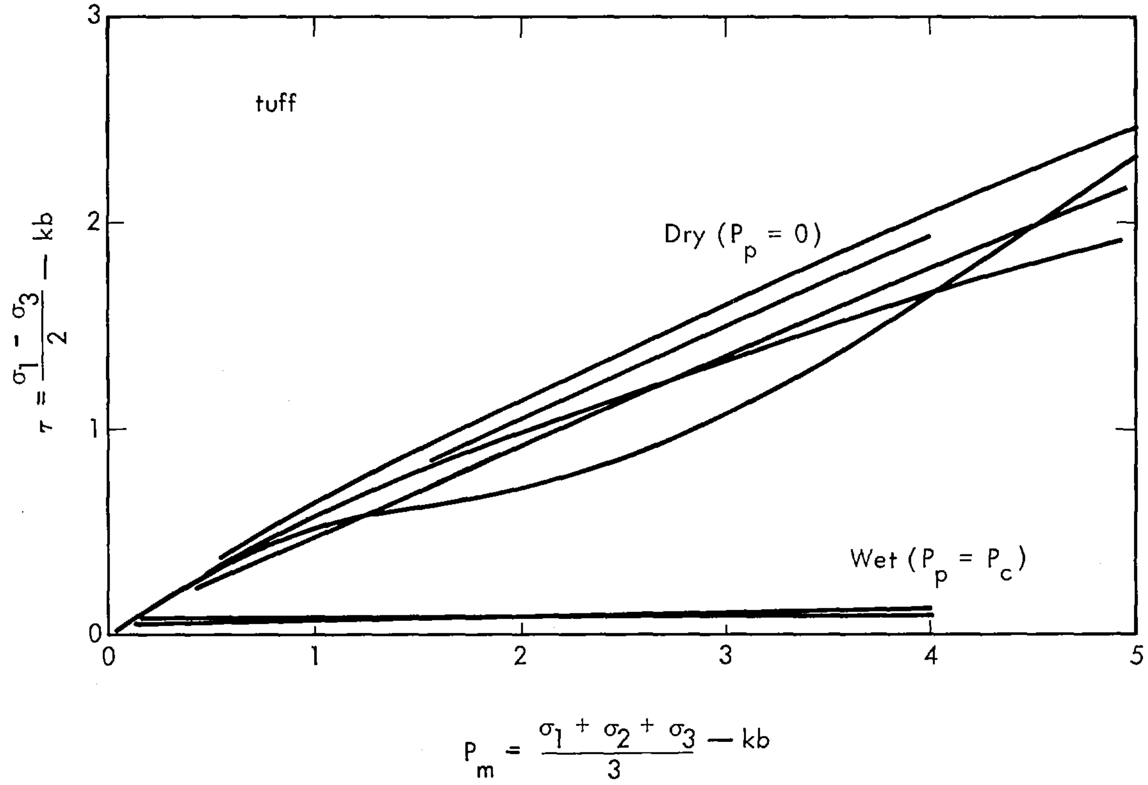

Fig. 10. Failure envelopes for five lithic and ashfall tuffs from NTS. Compression, 25°C, strain rate = 10^{-4}/sec. Top curves for the case P_p = 0; bottom shows range of strengths for these materials when wet (P_p = P_c).

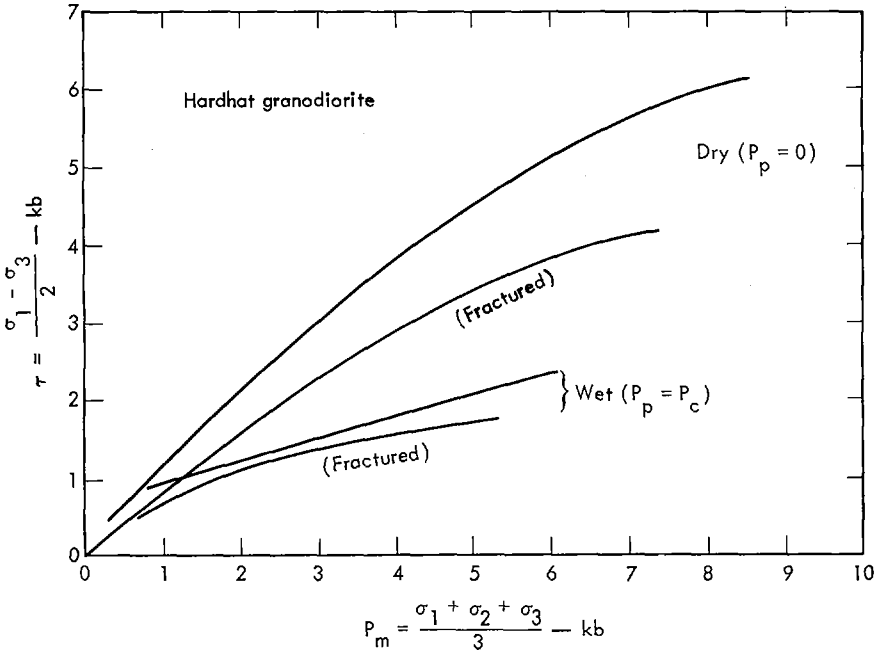

Fig. 11. Failure envelopes for Hardhat granodiorite tested in compression, 25°C, at a strain rate of 10^{-4}/sec. "Fractured" curves show strength of dry (P_p = 0) and wet (P_p = P_c) rock after first fracture.

scale; but if the overall large rock mass contains a pervasive water-filled joint system with appreciable volume, then the overall mechanical properties can be expected to approximate that illustrated for the wet granodiorite with the usual correction in strength with strain rate (5 to 10% per decade).[16,17]

Mechanical properties in the two principal directions of Green River shale ("oil shale") are summarized in Fig. 12. These data are for dry compression at 10^{-4} per sec strain rate for two different density materials, 2.28 and 2.19 g per cm^3, corresponding to Fisher assays of 18 and 26 gal per ton of oil, respectively. Both materials were taken near samples already discussed earlier by Stephens[23] and Schock.[24] The higher density, low-assay material is approximately 50% stronger when compared to the richer marlstone. The brittle-ductile transitions for either parallel or perpendicular loading directions in the low-assay marl also occur at much higher mean pressures compared to the richer material. Anisotropies in the material (layering) seem to have only a secondary effect on strength for both rocks. Minimum strengths are to be expected near 30 deg to the bedding for both rocks;[6] here, each material may be lowered by 10 to 20%, based on the perpendicular envelope. No data are available evaluating the effect of strain rate on strength or ductility. However, strengths should increase with strain rate in a qualitatively similar fashion as noted above for the other materials.

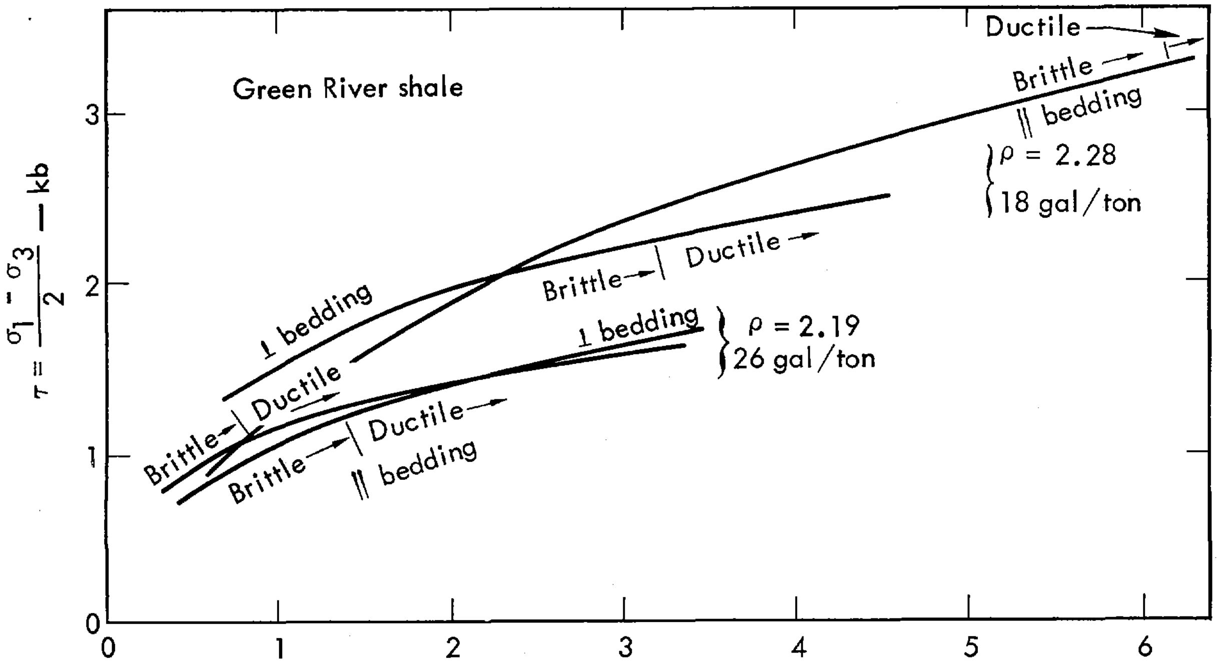

Fig. 12. Failure envelopes for two principal directions in two kerogeneous marlstones ("oil shale") with 2.19 and 2.28 g/cc density, respectively. Tests carried out in compression, dry, at a strain rate of 10^{-4}/sec. For clarity, envelopes showing strength after fracture are not shown.

REFERENCES

1. Th. von Kármán, "Festigkeitsversuche unter allseitigem Druck," *Zeits. Ver. deutsch. Ingenieure 55,* 1749-1757 (1911).
2. J. Handin and R. V. Hager, Jr., "Experimental Deformation of Sedimentary Rocks under Confining Pressure: Tests at Room Temperature on Dry Samples," *Amer. Assoc. Petroleum Geol. Bull. 41,* 1-50 (1957).
3. H. C. Heard, "Transition from Brittle Fracture to Ductile Flow in Solenhofen Limestone as a Function of Temperature, Confining Pressure, and Interstitial Fluid Pressure," in *Rock Deformation, Geol. Soc. Amer. Memoir 79,* (1960), pp. 193-226.
4. J. Handin, H. C. Heard and J. N. Magouirk, "Effects of the Intermediate Principal Stress on the Failure of Limestone, Dolomite and Glass at Different Temperatures and Strain Rates," *Jour. Geop. Res. 72,* 611-640 (1967).
5. F. A. Donath, "Experimental Study of Shear Failure in Anisotropic Rocks," *Geol. Soc. American Bull. 72,* 985-990 (1961).
6. R. McLamore and K. F. Gray, "The Mechanical Behavior of Anisotropic Sedimentary Rocks," in *Trans. ASME Paper No. 66-Pet-2* (New Orleans, 1966), pp. 1-12.
7. J. Handin, R. V. Hager, Jr., M. Friedman and J. Feather, "Experimental Deformation of Sedimentary Rocks under Confining Pressure: Pore Pressure Tests," *Amer. Assoc. Geol. Bull. 47,* 717-755 (1963).
8. L. H. Robinson, "Effects of Pore and Confining Pressures on Failure Characteristics of Sedimentary Rocks," *Colorado Sch. Mines Quart. 54,* 177-199 (1959).
9. S. Serdengecti and G. D. Boozer, "The Effects of Strain Rate and Temperature on the Behavior of Rocks Subjected to Triaxial Compression," in *4th Symposium on Rock Mechanics* (Penn. State Univ., 1961), pp. 83-97.
10. R. Böker, "Die Mechanik der bleibenden Formänderungen in kristallinisch aufgebauten Körpern," *Ver. deutsch. Ingenieure Mitt. Forschungsarbeiten 175,* 1-51 (1915).
11. M. S. Paterson, "Triaxial Testing of Materials at Pressures up to 10,000 Kg/sq. cm. (150,000 lb/sq. in.)," *Jour. Instit. Engineers, Australia,* 23-29 (1964).
12. D. T. Griggs, F. J. Turner and H. C. Heard, "Deformation of Rocks at 500°-800°C," in *Rock Deformation,* Geol. Soc. Amer. Memoir 79 (1960), pp. 30-104.
13. J. Handin and R. V. Hager, Jr., "Experimental Deformation of Sedimentary Rocks under Confining Pressure: Tests at High Temperature," *Amer. Assoc. Petroleum Geol. Bull. 42,* 2892-2934 (1958).
14. H. C. Heard, "Effect of Large Changes of Strain Rate in the Experimental Deformation of Yule Marble," *Jour. Geol. 71,* 162-195 (1963).
15. H. C. Heard and N. L. Carter, "Experimentally Induced 'Natural' Intragranular Flow in Quartz and Quartz Aggregates," *Am. Jour. Sci. 266,* 1-42 (1968).
16. H. C. Heard, *The Effect of Large Changes in Strain Rate in the Experimental Deformation in Rocks. Ph. D. Diss., University of California, Los Angeles (1962).*
17. W. F. Brace and R. J. Martin III, "A Test of the Law of Effective Stress for Crystalline Rocks of Low Porosity," *Int. Jour. Rock Mech. Min. Sci. 5,* 415-426 (1968).
18. H. C. Heard and N. L. Carter, "Temperature and Rate Dependent Deformation in Halite," *Am. Jour. Sci.* (in press) (1970).
19. D. T. Griggs and J. Handin, "Observations on Fracture and a Hypothesis of Earthquakes," in *Rock Deformation,* Geol. Soc. Amer. Memoir 79 (1960), pp. 347-364.

20. J. T. Cherry, "Computer Calculations of Explosion Produced Craters," *Int. Jour. Rock Mech. Min. Sci. 4*, 1-22 (1967).
21. M. L. Wilkins, *Calculation of Elastic-Plastic Flow*, Lawrence Radiation Laboratory, Livermore, Rept. UCRL-7322, Rev. 1 (1969).
22. L. S. Germain and J. S. Kahn, *Phenomenology and Containment of Underground Nuclear Explosions*, Lawrence Radiation Laboratory, Livermore, Rept. UCRL-50482 (1968).
23. D. R. Stephens, *Loading-Unloading Pressure-Volume Curves for Rocks*, to be presented at ANS Topical Meeting, Las Vegas, January 14-17, 1970.
24. R. N. Schock, paper to be presented at ANS Topical Meeting, Las Vegas, January 14-17, 1970.

XA04N0748

NUMERICAL SIMULATION OF STRESS WAVE PROPAGATION FROM UNDERGROUND NUCLEAR EXPLOSIONS*

J. T. Cherry and F. L. Petersen
Lawrence Radiation Laboratory, University of California
Livermore, California 94550

ABSTRACT

This paper presents a numerical model of stress wave propagation (SOC) which uses material properties data from a preshot testing program to predict the stress-induced effects on the rock mass involved in a Plowshare application. SOC calculates stress and particle velocity history, cavity radius, extent of brittle failure, and the rock's efficiency for transmitting stress. The calculations are based on an equation of state for the rock, which is developed from preshot field and laboratory measurements of the rock properties.

The field measurements, made by hole logging, determine in situ values of the rock's density, water content, and propagation velocity for elastic waves. These logs also are useful in judging the layering of the rock and in choosing which core samples to test in the laboratory. The laboratory analysis of rock cores includes determination of hydrostatic compressibility to 40 kb, triaxial strength data, tensile strength, Hugoniot elastic limit, and, for the rock near the point of detonation, high-pressure Hugoniot data.

Equation-of-state data are presented for rock from three sites subjected to high explosive or underground nuclear shots, including the Hardhat and Gasbuggy sites. SOC calculations of the effects of these two shots on the surrounding rock are compared with the observed effects. In both cases SOC predicts the size of the cavity quite closely. Results of the Gasbuggy calculations indicate that useful predictions of cavity size and chimney height can be made when an adequate preshot testing program is run to determine the rock's equation of state. Seismic coupling is very sensitive to the low-pressure part of the equation of state, and its successful prediction depends on agreement between the logging data and the static compressibility data. In general, it appears that enough progress has been made in calculating stress wave propagation to begin looking at derived numbers, such as number of cracks per zone, for some insight into the effects on permeability. A listing of the SOC code is appended.

1. INTRODUCTION

The important engineering effects associated with an underground (noncratering) Plowshare application are the increase in permeability of the reservoir rock, the height of the chimney, and the amount of seismic energy generated by the nuclear explosion. A fundamental goal of the Plowshare

---

*Work performed under the auspices of the U. S. Atomic Energy Commission.

program is to predict these effects when an explosive of known yield is detonated at a given depth in a given medium.

This paper presents results from a numerical technique called SOC which calculates the propagating stress field in the medium surrounding an explosive source and the resultant effects on the medium. We attempt to relate directly predicted changes in the medium, namely fracturing and cavity size, to permeability change and chimney height. Seismic coupling is obtained from the calculated displacement history of a particle in the elastic region.

Part 2 of the paper describes a general numerical approach to stress wave propagation. Part 3 discusses the material properties needed to relate stress to deformation in an equation of state. These properties are obtained by preshot field and laboratory measurements. Part 4 compares SOC numerical solutions with experimental observations for sites where nuclear or high explosive shots were made. The SOC calculations are based on material properties obtained from laboratory tests on selected rock samples. A listing of the SOC code is given in the Appendix.

2. THE NUMERICAL MODEL

A wave is a time-dependent process that transfers energy from point to point in a medium. A wave propagates through a medium because of a feedback loop that exists between the various physical properties of the medium that are changed by the energy deposition.

The cycle followed in calculating stress wave propagation is presented in Fig. 1. We start at the top of the loop, with the applied stress field. The equation of motion provides a functional relation between the stress field and the resulting acceleration of each point in the medium. Accelerations, when

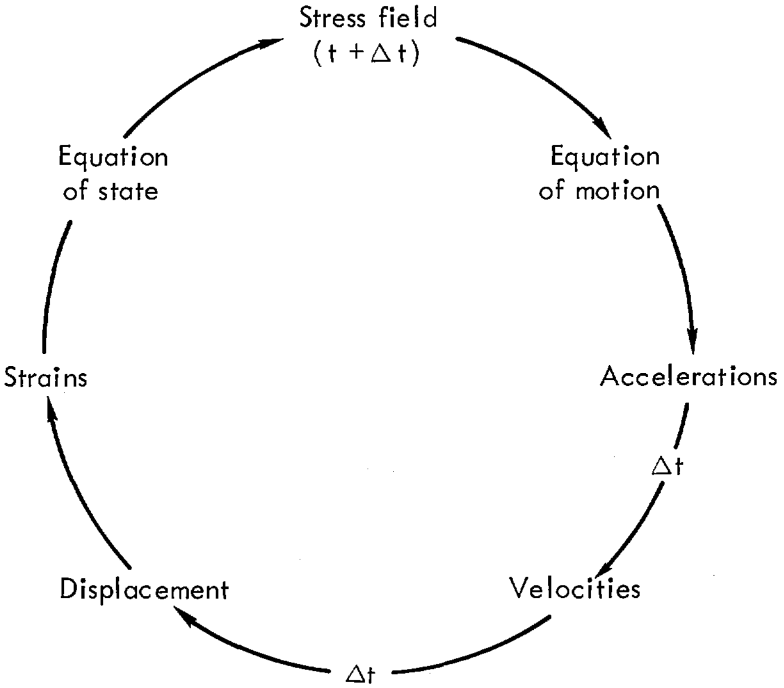

Fig. 1. Cycle of interactions treated in calculating stress wave propagation.

allowed to act over a small time increment Δt, produce new velocities; velocities produce displacements, displacements produce strains, and strains produce a new stress field. Time is incremented by Δt and the cycle is repeated. The analysis of this loop is provided by a computer program, SOC, which solves the equations of continuum mechanics for spherical symmetry by finite difference methods.

2.1 Equation of Motion

The fundamental equations of continuum mechanics (conservation of mass, linear momentum, and angular momentum) combine to produce the following equation of motion for spherical symmetry, taken from Keller[1]:

$$\rho \dot{u} = -\left(\frac{\partial P}{\partial R} + \frac{4}{3}\frac{\partial K}{\partial R} + 4\frac{K}{R} + g\right), \qquad (1)$$

where ρ is the density, $\dot{u}$ is the particle acceleration, g is a body force used to include gravity effects, and the stress tensor in the spherically symmetric coordinate system is written as the sum of an isotropic tensor and a deviatoric tensor,

$$\begin{bmatrix} T_{RR} & 0 & 0 \\ 0 & T_{\theta\theta} & 0 \\ 0 & 0 & T_{\phi\phi}=T_{\theta\theta} \end{bmatrix} = \begin{bmatrix} -P & 0 & 0 \\ 0 & -P & 0 \\ 0 & 0 & -P \end{bmatrix} + \begin{bmatrix} -\frac{4}{3}K & 0 & 0 \\ 0 & \frac{2}{3}K & 0 \\ 0 & 0 & \frac{2}{3}K \end{bmatrix}. \qquad (2)$$

We see from equation (2) that

$$P = -\frac{1}{3}\left(T_{RR} + 2T_{\theta\theta}\right),$$
$$K = \frac{T_{\theta\theta} - T_{RR}}{2}. \qquad (3)$$

Equation (1) is differenced by establishing a Lagrangian coordinate system (j) in the material. These coordinates move with the material and assume discrete values: 0, 1, 2, . . . , j - 1, j, j + 1, ... This coordinate system divides the material into volume elements or zones, with the mass in each zone remaining constant. At zero time each Lagrangian coordinate (j) has a unique Eulerian coordinate R_j^0; after n cycles, corresponding to a time t^n, the Eulerian coordinate is R_j^n.

Equation (1) is transformed into the Lagrangian (j) coordinate system. Each stress component (Σ) in this equation is a scalar function of position (R) and time (t). If the Eulerian coordinate (R) is considered to be a function of j and t then we can write

$$\frac{\partial \Sigma}{\partial j} = \frac{\partial \Sigma}{\partial R}\frac{\partial R}{\partial j}. \qquad (4)$$

Equation (4) is easily solved for $\partial\Sigma/\partial R$.

The time derivative of velocity simplifies considerably in the Lagrangian system since j is independent of time. In the Eulerian system we have

$$\dot{u} = \frac{\partial u}{\partial t} + \frac{dR}{dt}\frac{\partial u}{\partial R}, \qquad (5)$$

while in the Lagrangian system we have simply

$$\dot{u} = \frac{\partial u_j}{\partial t}. \tag{6}$$

Using equations (4) and (6), we obtain the following first-order difference approximation to the equation of motion (superscripts denote cycle, subscripts denote Lagrangian coordinate, and $R_j^n - R_{j+1}^n > 0$):

$$u_j^{n+\frac{1}{2}} = u_j^{n-\frac{1}{2}} - \Delta t^n \left(\frac{\Delta P/\Delta j}{\rho(\Delta R/\Delta j)} + \frac{4}{3} \frac{\Delta K/\Delta j}{\rho(\Delta R/\Delta j)} + B + g \right), \tag{7}$$

where

$$\frac{\Delta P}{\Delta j} = P_{j-\frac{1}{2}}^n + Q_{j-\frac{1}{2}}^{n-\frac{1}{2}} - P_{j+\frac{1}{2}}^n - Q_{j+\frac{1}{2}}^{n-\frac{1}{2}},$$

$$\frac{\Delta K}{\Delta j} = K_{j-\frac{1}{2}}^n + QK_{j-\frac{1}{2}}^{n-\frac{1}{2}} - K_{j+\frac{1}{2}}^n - QK_{j+\frac{1}{2}}^{n-\frac{1}{2}},$$

$$2\rho \frac{\Delta R}{\Delta j} = \frac{M_{j-\frac{1}{2}}}{V_{j-\frac{1}{2}}^n} \left(R_{j-1}^n - R_j^n \right) + \frac{M_{j+\frac{1}{2}}}{V_{j+\frac{1}{2}}^n} \left(R_j^n - R_{j+1}^n \right),$$

$$\frac{B}{8} = \frac{K_{j+\frac{1}{2}}^n + QK_{j+\frac{1}{2}}^{n-\frac{1}{2}}}{R_j^n + R_{j+1}^n} \left(\frac{V_{j+\frac{1}{2}}^n}{M_{j+\frac{1}{2}}} \right) (1 - \xi) + \frac{K_{j-\frac{1}{2}}^n + QK_{j-\frac{1}{2}}^{n-\frac{1}{2}}}{R_{j-1}^n + R_j^n} \left(\frac{V_{j-\frac{1}{2}}^n}{M_{j-\frac{1}{2}}} \right) \xi,$$

$$\xi = \frac{R_j^n - R_{j+1}^n}{R_{j-1}^n - R_{j+1}^n}.$$

The following quantities are calculated at the beginning of the problem in the generator (see Appendix 2) and are saved.

$$V_{j+\frac{1}{2}}^0 = \left(R_j^0 \right)^3 - \left(R_{j+1}^0 \right)^3, \tag{8}$$

$$DV_{j+\frac{1}{2}}^0 = \left(mu_{j+\frac{1}{2}}^0 \right) \left(V_{j+\frac{1}{2}}^0 \right), \tag{9}$$

$$V_{j+\frac{1}{2}}^0 = DV_{j+\frac{1}{2}}^0 + V_{j+\frac{1}{2}}^0, \tag{10}$$

$$M_{j+\frac{1}{2}} = \rho_{j+\frac{1}{2}}^I V_{j+\frac{1}{2}}^0, \tag{11}$$

where $\rho_{j+\frac{1}{2}}^I$ is the input material density and $mu_{j+\frac{1}{2}}^0$ is the volume compression due to the overburden pressure.

Equation (7) provides a functional relation between the existing stress gradients (which are obtained from the values of stress in each zone and the positions of these zones at time t^n) and the acceleration of each meshpoint. This acceleration when allowed to act over a small time increment Δt^n changes the velocity of each meshpoint (j) to $u_j^{n+\frac{1}{2}}$.

2.2 Strain Calculation

After the motion of the material under the influence of the existing stress field has been calculated from equation (7), we must now find how this motion alters the stress field.

If we assume that the medium is isotropic, then the stress-strain relation (Hooke's law) has the following form for spherical symmetry:

$$\dot{T}_{RR} = \lambda\frac{\dot{V}}{V} + 2\mu\frac{\partial u}{\partial R}, \tag{12}$$

$$\dot{T}_{\theta\theta} = \dot{T}_{\phi\phi} = \lambda\frac{\dot{V}}{V} + 2\mu\frac{u}{R}, \tag{13}$$

where λ and μ are the Lamé constants and V is the volume.

From the conservation of mass we have

$$\frac{\dot{V}}{V} = \frac{\partial u}{\partial R} + 2\frac{u}{R}. \tag{14}$$

The dot represents a time derivative along a particle path. This will allow us to write the stress-strain relation in incremental form where strain changes will be referred to the current configuration of the element.

We use equation (3) to find $\dot{P}$ and $\dot{K}$:

$$\dot{P} = -k\frac{\dot{V}}{V}\left(\text{where } k = \lambda + \frac{2}{3}\mu \text{ is the bulk modulus}\right), \tag{15}$$

$$\dot{K} = \mu\left(\frac{u}{R} - \frac{\partial u}{\partial R}\right). \tag{16}$$

The total volumetric strain is defined as

$$mu = \frac{V^0 - V}{V}, \tag{17}$$

and equation (15) is replaced by

$$P = f(mu, e), \tag{18}$$

where e is the specific internal energy. The determination of f(mu, e) represents a major part of the equation-of-state work, and will be discussed in the equation-of-state section of the paper.

The strain components given by equations (16) and (17) are calculated in the code using time-centered coordinates at $n + \frac{1}{2}$ as follows (all subscripts at $j + \frac{1}{2}$ are deleted):

$$R_j \equiv R_j^{n+\frac{1}{2}} = R_j^n + \frac{1}{2}\Delta t^{n+\frac{1}{2}} u^{n+\frac{1}{2}},$$

$$\Delta R_j^{n+1} = \Delta R_j^n + \Delta t^{n+\frac{1}{2}} u_j^{n+\frac{1}{2}},$$

$$R_j^{n+1} = R_j^0 + \Delta R_j^{n+1},$$

$$\Delta V^{n+\frac{1}{2}} = \Delta t^{n+\frac{1}{2}} \left\{ 3 \left[\left(R_{j+1}\right)^2 u_{j+1}^{n+\frac{1}{2}} - \left(R_j\right)^2 u_j^{n+\frac{1}{2}} \right] + \left(\frac{\Delta t^{n+\frac{1}{2}}}{2} \right)^2 \left[\left(u_{j+1}^{n+\frac{1}{2}} \right)^3 - \left(u_j^{n+\frac{1}{2}} \right)^3 \right] \right\}$$

$$= V^n - V^{n+1} ,$$

$$DV^{n+1} = DV^n + \Delta V^{n+\frac{1}{2}} = \left(R_j^0\right)^3 - \left(R_{j+1}^0\right)^3 - V^{n+1} ,$$

$$V^{n+1} = V^0 - DV^{n+1} - DV^0 ,$$

$$V^{n+\frac{1}{2}} = V^{n+1} + \frac{1}{2} \Delta V^{n+\frac{1}{2}} ,$$

$$mu^{n+1} = \frac{DV^{n+1} + DV^0}{V^{n+1}} = \frac{V^0 - V^{n+1}}{V^{n+1}} , \tag{19}$$

$$\left(\frac{\Delta K}{\mu} \right)^{n+\frac{1}{2}} = - \frac{1}{2} \left(\frac{\Delta V^{n+\frac{1}{2}}}{V^{n+\frac{1}{2}}} + 3 \, \frac{\left(u_j^{n+\frac{1}{2}} - u_{j+1}^{n+\frac{1}{2}} \right) \Delta t^{n+\frac{1}{2}}}{R_j - R_{j+1}} \right) . \tag{20}$$

The last two equations above represent the strain terms that are used in the code to calculate P^{n+1} and K^{n+1} respectively.

2.3 Calculation of Mean Stress (P)

In the code the calculation of mean stress depends on the state of the material. During shock loading, equation (18) becomes

$$P_H^{n+1} = f_H(mu^{n+1}) , \tag{21}$$

where f_H is determined from hydrostatic compressibility and Hugoniot measurements on core samples.

The calculation during release depends on the maximum internal energy that has been deposited in the zone. If $e_{j+\frac{1}{2}}^{max} > e_v^I$ then P^{n+1} is calculated using a set of gas tables developed by Butkovich[2] in which P is listed as a function of energy with density as the parameter. The quantity e_v^I is the vaporization energy which is related to the difference between the shock-deposited internal energy and the area under the Hugoniot (the shaded area in Fig. 2). The vaporization energy is obtained from the equation in Fig. 2, where P_v is the pressure value for which the shaded area is just equal to the vaporization "waste heat" for the material (2800 cal/g for SiO_2 in this case).

If $e_f^I \leq e^{max} < e_v^I$ where e_f^I is the melt energy, then the pressure on release is calculated by

$$P^{n+1} = P_H^{n+1} + \Gamma\left(e^n - e_H\right),$$

where

P_H^{n+1} is the Hugoniot pressure,

e^n is the internal energy at t^n,

$$e_H = \frac{1}{2} P_H^{n+1} \frac{mu^{n+1}}{1 + mu^{n+1}},$$

$$\Gamma = \Gamma^I \left[\frac{e^{max} - e_f^I}{e_v^I - e_f^I}\right].$$

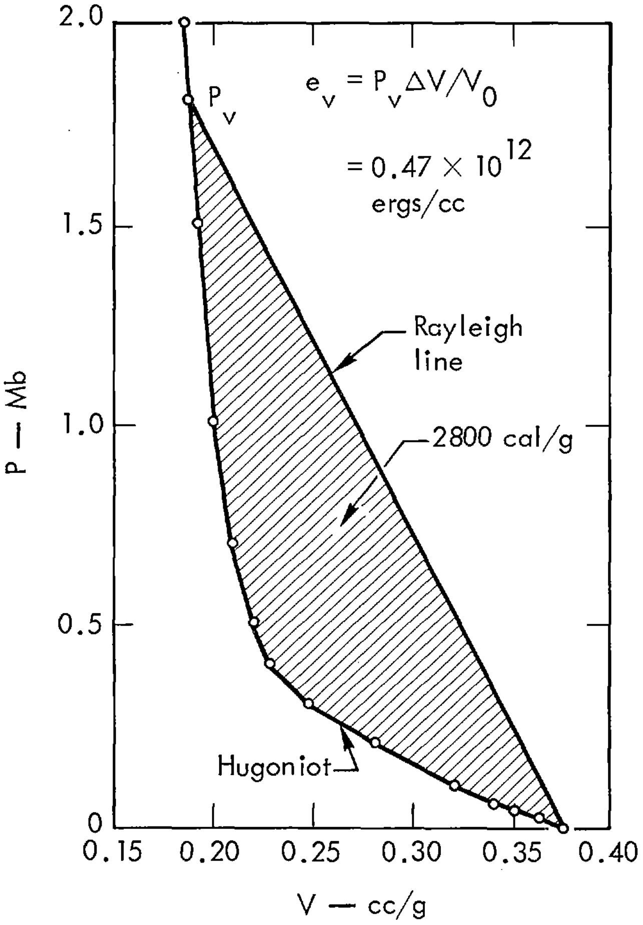

Fig. 2. Calculation of vaporization energy.

The quantity Γ^I is an input quantity specified in the equation of state. In order to assure a reasonable continuity of release paths for e^{max} near e_v^I, the gas tables are merged into the Hugoniot using equation (22). We have found that values of Γ^I between 0.85 and 1 produce an acceptable transition between the Hugoniot and the well-defined part of the gas tables. The melt energy e_f^I is determined the same way as e_v^I (see Fig. 2), except that the "waste heat" value for melting (shaded area between the curves) is less, being 600 cal/g for SiO_2.

If the hydrostatic compressibility data indicate that the material locks in the P-V plane on release (Fig. 3), then the code will accept one input release path in the equation of state. This release path is usually the experimentally determined hydrostatic unloading path from 40 kb (the pressure limit of our apparatus).

The point in the P-mu plane where the experimental loading and unloading hydrostats merge, $mu_{\frac{1}{2}}^I$, is input in the equation of state. If $mu_{j+\frac{1}{2}}^{max} \geq mu_{\frac{1}{2}}^I$ then the release path follows the input unloading curve. If

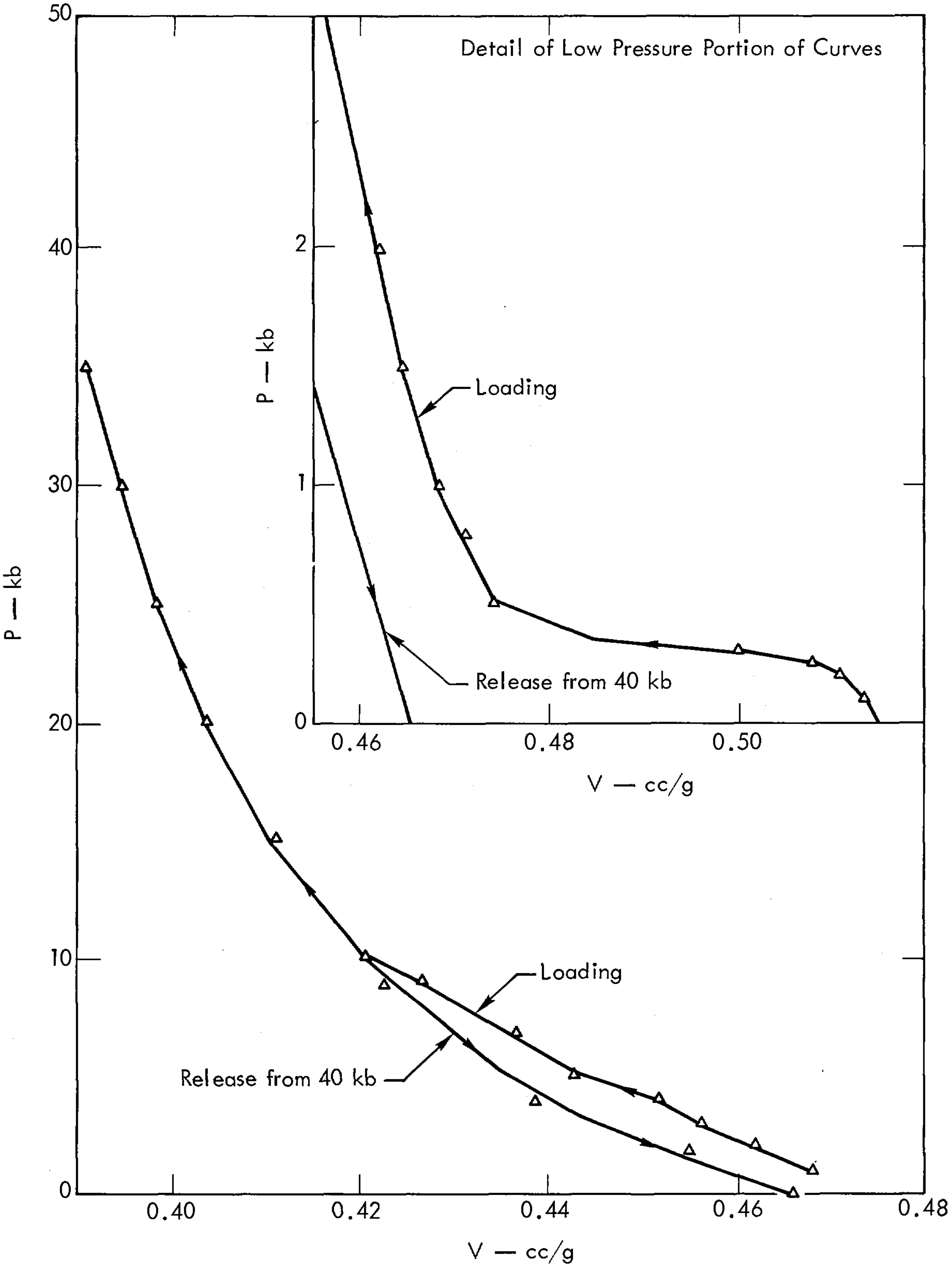

Fig. 3. Compressibility of DF-5A grout.

$mu^{max}_{j+\frac{1}{2}} < mu^{I}_{2}$ then the release path is determined such that

$$\left(\frac{dP}{dmu}\right)^{n+\frac{1}{2}}_{j+\frac{1}{2}} = \left(\frac{dP}{dmu}\right)_L + \frac{mu^{max}_{j+\frac{1}{2}}}{mu^{I}_{2}}\left[\left(\frac{dP}{dmu}\right)_u - \left(\frac{dP}{dmu}\right)_L\right], \tag{23}$$

where $(dP/dmu)_L$ and $(dP/dmu)_u$ are the slopes of the loading and unloading hydrostats for $P^{n}_{j+\frac{1}{2}}$. The pressure on release becomes

$$P^{n+1} = P^n + \left(\frac{dP}{dmu}\right)^{n+\frac{1}{2}} \frac{V^0 \Delta V^{n+\frac{1}{2}}}{V^{n+1}(V^{n+1} + \Delta V^{n+\frac{1}{2}})}. \tag{24}$$

2.4 Calculation of Deviatoric Stress (K)

Equation (20) represents the initial attempt by the code to calculate K^{n+1}:

$$\tilde{K}^{n+1} = K^n + \mu^I \left(\frac{\Delta K}{\mu}\right)^{n+\frac{1}{2}}. \tag{25}$$

The quantity μ^I is the rigidity modulus from the equation of state. At the present time the code accepts either a constant rigidity modulus or a constant Poisson's ratio.

Adjustment of the $\tilde{K}^{n+1}$ calculated in equation (25) is permitted if the zone is undergoing plastic flow or brittle failure. The code uses two strength tables, one for the consolidated and one for the cracked state, a strain rate value K^I_2, and a brittle-ductile transition point P^I_1 in the failure routines. The strength tables will be discussed in the equation-of-state section.

If $P^{n+1} + \frac{1}{3}\tilde{K}^{n+1} \geq P^I_1$ and if $|\tilde{K}^{n+1}| > \left(K^I_2\right)(a)$ then plastic flow develops and

$$\begin{aligned} K^{n+1} &= \left(K^I_2\right)(a)\ \text{sign}\ (\tilde{K}^{n+1})\ \text{for}\ e^n \leq e^I_f \\ &= 0\ \text{for}\ e^n > e^I_f, \end{aligned} \tag{26}$$

where

$$a = \frac{e^I_f - e^n}{e^I_f}.$$

The plastic strain $(\Delta\epsilon_p)$ associated with the adjustment (flow rule) in equation (26) is

$$\Delta\epsilon_p = \frac{|\tilde{K}^{n+1}| - \left(K^I_2\right)(a)}{\mu}. \tag{27}$$

If $P^{n+1} + \frac{1}{3}\tilde{K}^{n+1} < P^I_1$ and if $|\tilde{K}^{n+1}|$ is greater than the value of K allowed by the appropriate strength table, then a crack is allowed to propagate through the zone with a velocity C_V given by Bieniawski[3] as

$$C_v = 1.14 \sqrt{\frac{\mu}{\rho^I\left(3 + \frac{\mu}{k}\right)}} \ . \tag{28}$$

A crack length C_L and a crack ratio C_R are calculated:

$$\begin{aligned} C_L^{n+1} &= C_1^n + C_v \Delta t^{n+\frac{1}{2}} , \\ C_R &= \frac{C_L^{n+1}}{4\left(R_j^{n+1} - R_{j+1}^{n+1}\right)} \le 1 \ . \end{aligned} \tag{29}$$

A limiting value of K is calculated,

$$K_{Lim} = |\tilde{K}^{n+1}| \left[1 - \frac{C_v C_R}{4\left(R_j^{n+1} - R_{j+1}^{n+1}\right)} \Delta t^{n+\frac{1}{2}}\right] \le K_2^I . \tag{30}$$

Equation (26) is used to calculate K^{n+1} with K_2^I replaced by K_{Lim}.

The form of equation (30) represents a compromise between a dislocation theory formulation and a Maxwell solid formulation in which the viscosity η is replaced by

$$\eta = \frac{4\mu \Delta R}{C_v C_R} \ . \tag{31}$$

The relaxation of the deviatoric components of stress during brittle failure has been observed experimentally by Byerlee[4] under quasi-static loading. Ahrens and Duvall[5] have measured the attenuation of the elastic precursor in three quartz rocks in one-dimensional plane geometry and found that on the "elastic" Hugoniot

$$F = -\frac{dK_{Lim}}{dt} \approx 40 \frac{kb}{\mu sec} \tag{32}$$

with a relaxation time of 0.7 μsec. Equation (30) gives

$$-\frac{dK_{Lim}}{dt} = \frac{|\tilde{K}^{n+1}|}{0.7} \tag{33}$$

assuming $C_R = 1$ and $4\Delta R/C_V = 0.7$ μsec. Since the difference between the precursor radial stress and the isothermal hydrostat is about 40 kb for the rocks Ahrens and Duvall considered, then

$$\tilde{K}^{n+1} \approx \left(\frac{3}{4}\right) (40) \text{ kb.}$$

Using this value of $\tilde{K}^{n+1}$ in equation (33) gives 43 kb/μsec for F.

Equation (3) is used to describe the relaxation of the stress deviator during brittle failure. No attempt is made to distinguish between "tensile" or "shear" failure in the crack routine itself.

The internal energy and stability calculations are the standard formulations of Cherry[6] for an adiabatic Lagrangian code using artificial viscosity.

The total energy in the problem (internal, kinetic, and gravitational) is determined at specified times and compared with the input energy. Agreements within 1% or less are considered normal. The listing of the code is given in Appendix 1.

3. DETERMINING AN EQUATION OF STATE FOR THE ROCK AT A PARTICULAR SITE

The equation of state for the rock at a particular site is developed from field logging and from laboratory tests on selected rock samples. Ideally these programs should include the following:

3.1 Logging Program

(1) Density log
(2) Elastic velocity log
    (a) Compressional velocity
    (b) Shear velocity

Hopefully, these logs will permit a judgment concerning both the layering of the medium and the choice of core for laboratory testing.

3.2 Core Tests

(1) Hydrostatic compressibility up to 40 kb
    (a) Loading
    (b) Unloading
(2) Triaxial tests at various confining pressures and saturation levels.
    (a) Consolidated
    (b) Cracked
(3) Tensile strength
(4) Hugoniot elastic limit
(5) High pressure Hugoniot data (loading and release) for the rock near the point of detonation.

The core tests that are now relatively standard are those involving hydrostatic compressibility, triaxial strength, and, to some extent, the shock Hugoniot. Experimental techniques that measure Hugoniot release are still in the developmental stage.

3.3 Hydrostatic Compressibility and Hugoniot Data

Figure 3 shows the measured loading and unloading hydrostatic isotherms for a "locking" solid (DF-5A grout).* This locking feature is typical of most of the dry porous rock encountered at the Nevada Test Site (NTS) and is responsible for the severe seismic decoupling characteristic of the site.

Figure 4 shows the static isotherm along with Hugoniot data for Hardhat granite. The 10-kb offset between the Hugoniot elastic limit (HEL) and the hydrostat is maintained for the

$$P_H^{n+1} = f_H(mu^{n+1})$$

code input (equation(21)).

The Rayleigh line drawn through the HEL intersects the Hugoniot at 320 kb. The slope of the Rayleigh line in the P-V plane is proportional to the

---

*See Sec. 4.1, "Model Studies."

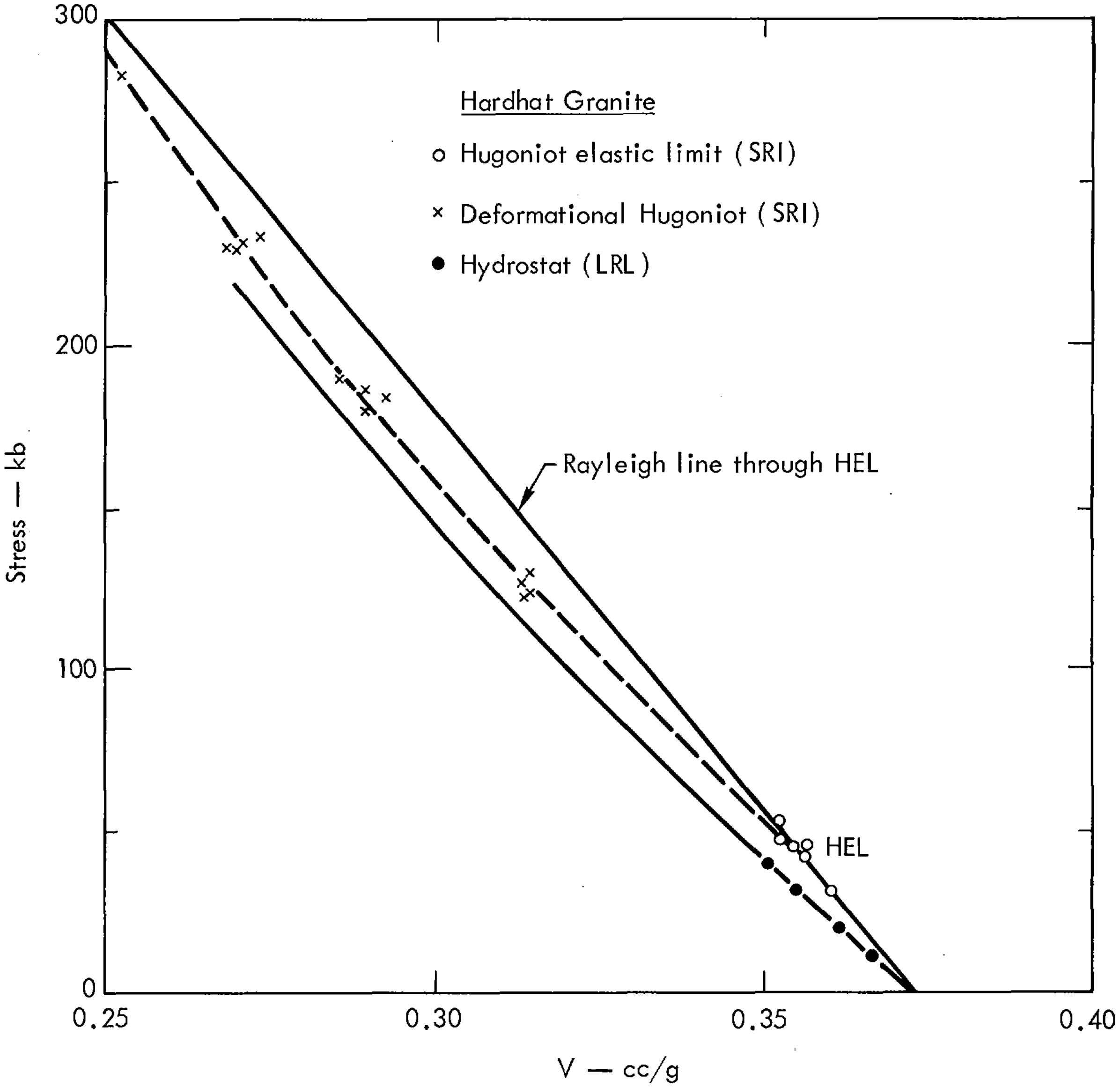

Fig. 4. Hugoniot and compressibility data for Hardhat granite.

square of the shock velocity (u_s):

$$\frac{P - P_0}{V_0 - V} = \left(\rho_0 u_s\right)^2 . \qquad (34)$$

For shock states below 320 kb the first arrival corresponds to the Rayleigh line through the HEL (5.9 m/msec) with an amplitude of 45 kb.

3.4 Strength Data

An attempt has been made to develop a failure criterion, in terms of stress invariants, capable of describing the onset of failure in brittle materials. The important stress invariants used are mean stress (P), the second deviatoric invariant (I_{2D}), and the third deviatoric invariant (I_{3D}).

In terms of principal stresses T_{11}, T_{22}, T_{33} (positive for tension), we have

$$P = -\frac{T_{11} + T_{22} + T_{33}}{3},$$

$$I_{2D} = \frac{1}{6}\left(T_{11} - T_{22}\right)^2 + \left(T_{11} - T_{33}\right)^2 + \left(T_{22} - T_{33}\right)^2 \tag{35}$$

$$= \frac{1}{2}\left(T_1^2 + T_2^2 + T_3^2\right),$$

where $T_1 = P + T_{11}$, $T_2 = P + T_{22}$, and $T_3 = P + T_{33}$ are the stress deviators,

$$I_{3D} = T_1 T_2 T_3 .$$

We assume that strength can be expressed in terms of I_{2D}:

$$Y \equiv \left(3I_{2D}\right)^{\frac{1}{2}} .$$

The results of various destructive tests (compression, extension, and hollow torsion) on glass, dolomite, granite, and limestone have been presented by Handin et al.[7] and Mogi.[8] They demonstrated that I_{2D} plotted versus P did not give a consistent failure surface when the test type changed.

Mogi also found that the compression and extension test data are consistent if P is replaced by $\overline{P}$, where

$$\overline{P} = -\frac{T_{11} + T_{33} + bT_{22}}{2}, \tag{36}$$

T_{22} is the intermediate principal stress, and $0 \leq b \leq 0.1$ depending on the rock type. This suggests that if I_{3D} is combined with P such that

$$\overline{P} = P - a\left(\frac{I_{3D}}{2}\right)^{1/3}, \tag{37}$$

then Mogi's formulation is obtained for $b = 0$ if $a = 0.5$.

Figures 5-16 show Y vs P and vs $\overline{P}$, where $\overline{P}$ is given by equation (37) with $a = 0.5$ and $Y = \left(3I_{2D}\right)^{\frac{1}{2}}$. Each point on a given plot is determined by evaluating the appropriate invariants from the existing stress field at failure. Replacing P by $\overline{P}$ not only improves the consistency of the various tests but well defines the brittle-ductile transition for limestone. It would be easy to improve the consistency even more by allowing "a" to vary with the rock type. However, in our applications the variability of the core obtained from a particular site is more than sufficient to mask changes in "a" with rock type, even if a large variety of strength tests were available.

Equations (2), (35), and (37) give the following relations between Y, $\overline{P}$, and K:

$$\begin{aligned} Y &= 2|K| = |T_{\theta\theta} - T_{RR}| , \\ \overline{P} &= P + \frac{K}{3} = -\frac{T_{RR} + T_{\theta\theta}}{2} . \end{aligned} \tag{38}$$

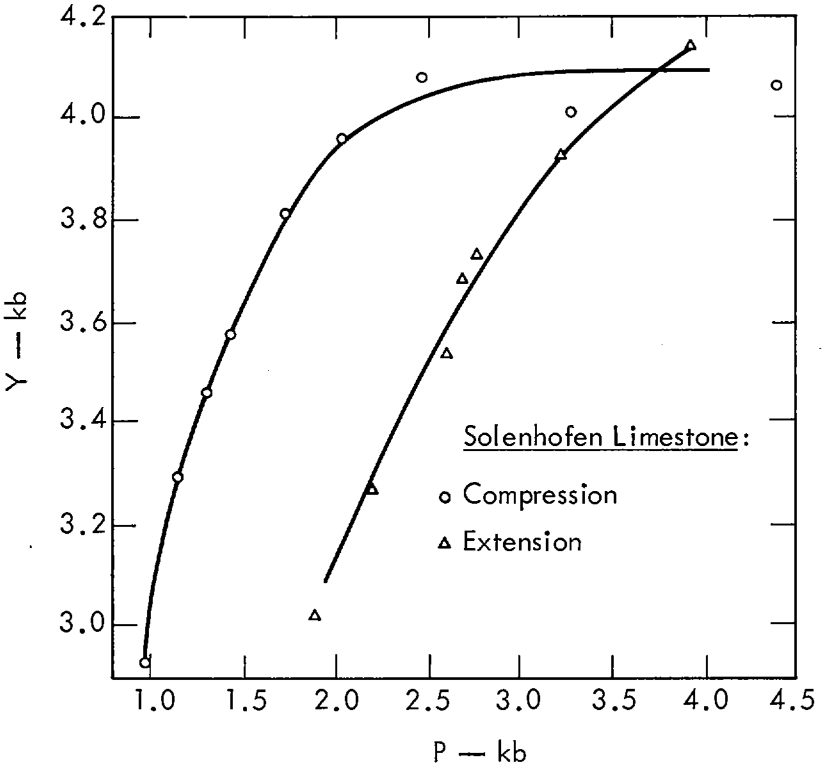

Fig. 5. Yield strength (Y) vs P for Solenhofen limestone (data of Mogi[8]).

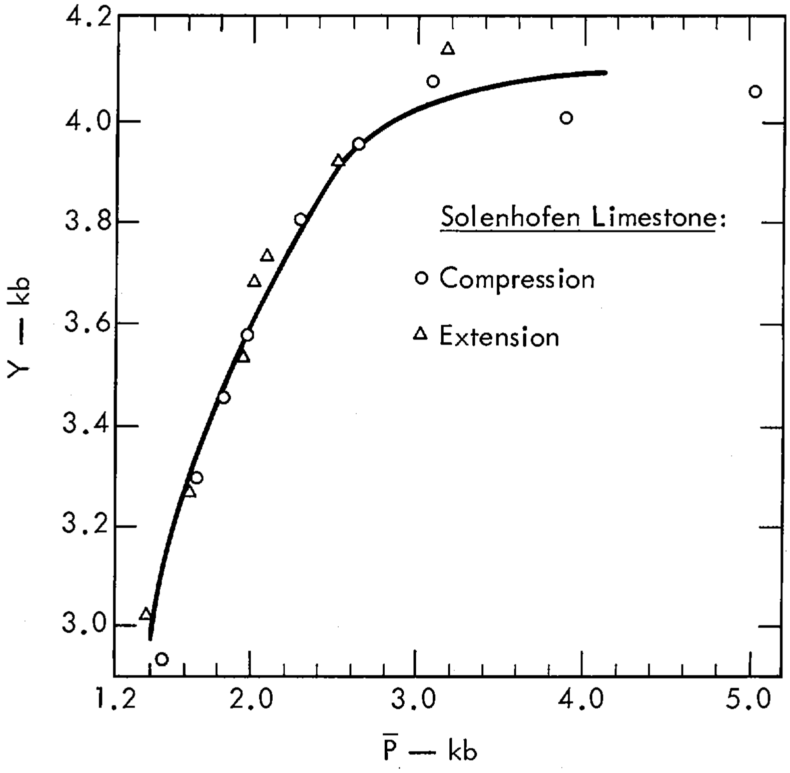

Fig. 6. Y vs $\overline{P}$ for Solenhofen limestone (data of Mogi[8]).

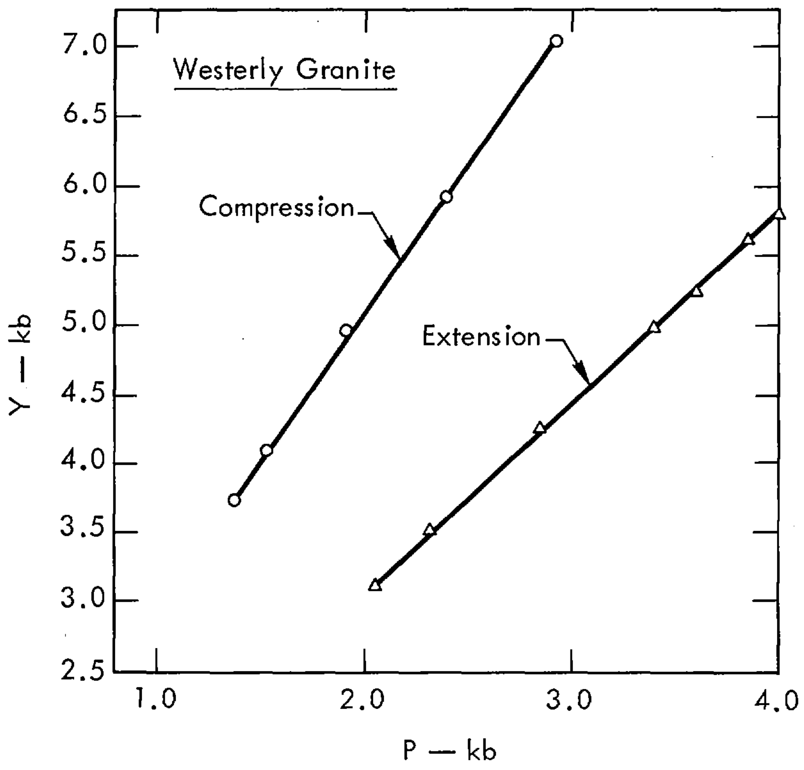

Fig. 7. Y vs P for Westerly granite (data of Mogi[8]).

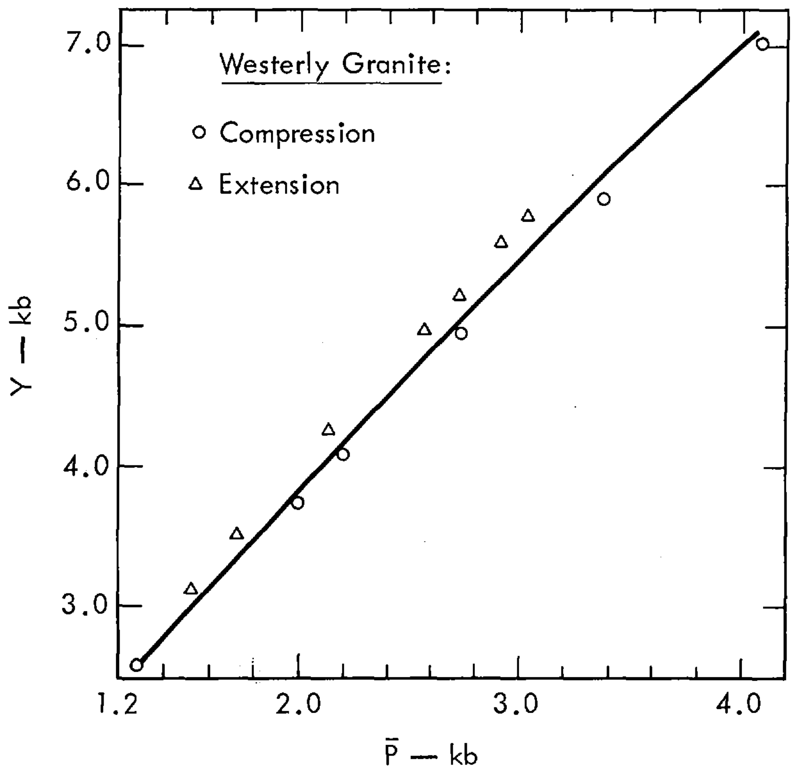

Fig. 8. Y vs $\overline{P}$ for Westerly granite (data of Mogi[8]).

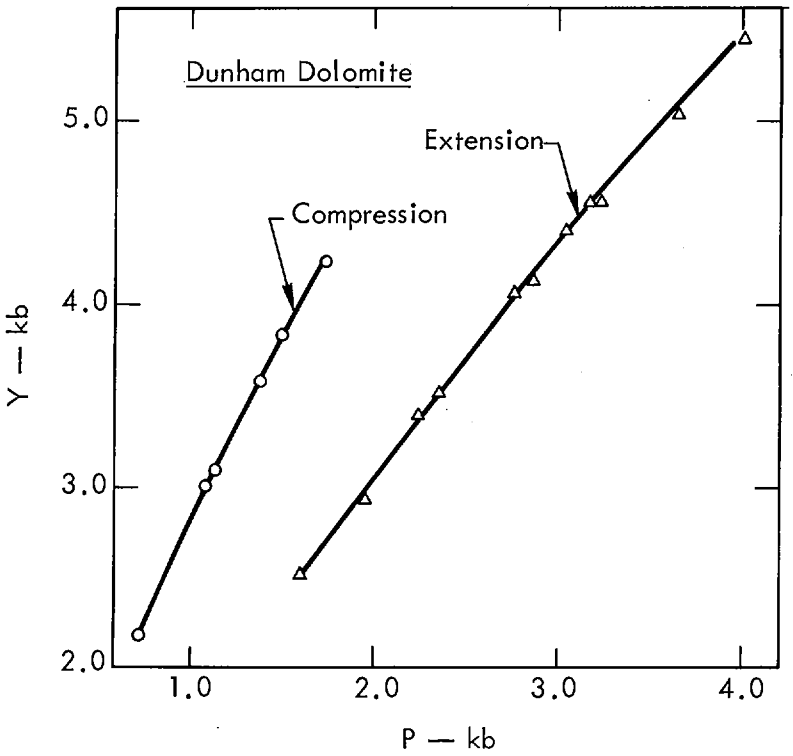

Fig. 9. Y vs P for Dunham dolomite (data of Mogi[8]).

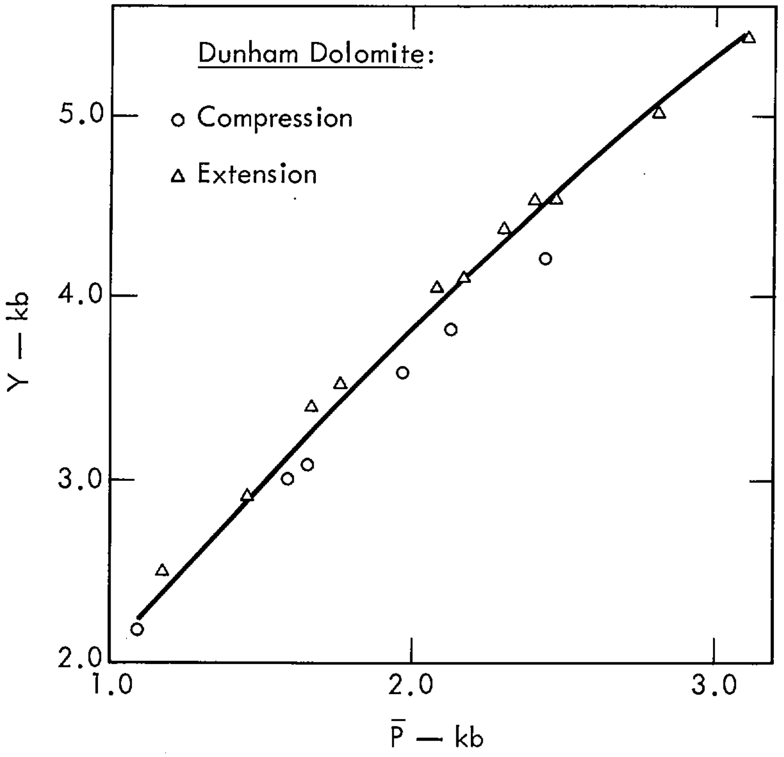

Fig. 10. Y vs $\overline{P}$ for Dunham dolomite (data of Mogi[8]).

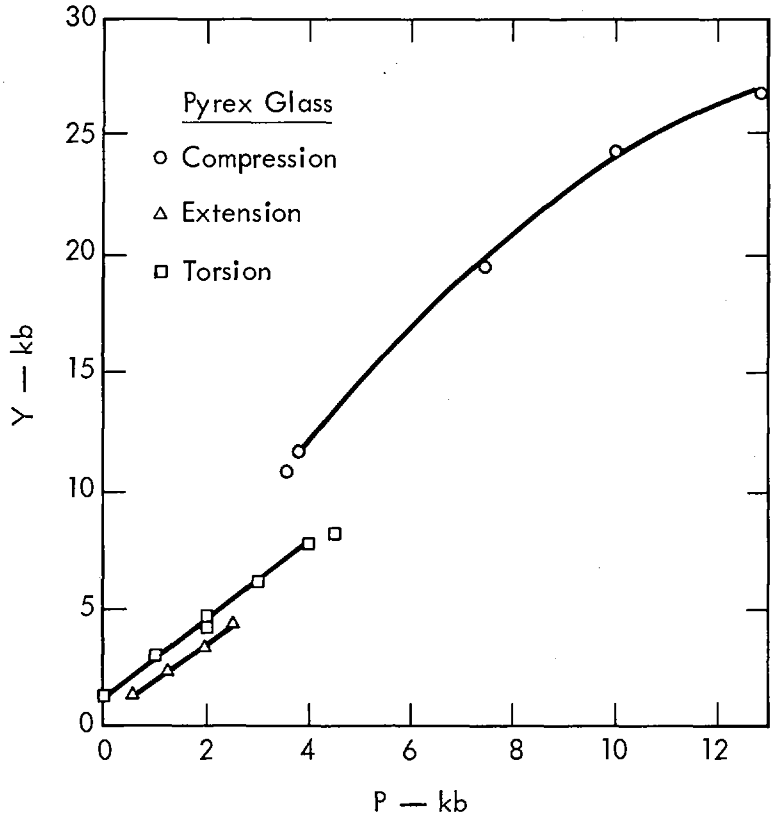

Fig. 11. Y vs P for Pyrex glass (data of Handin et al.[7]).

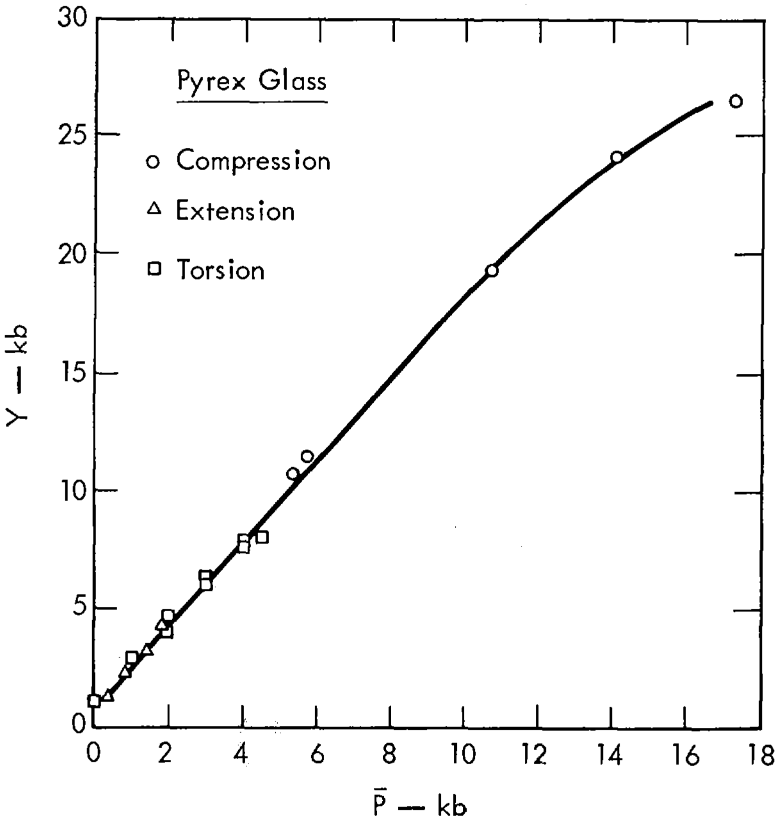

Fig. 12. Y vs $\overline{P}$ for Pyrex glass (data of Handin et al.[7]).

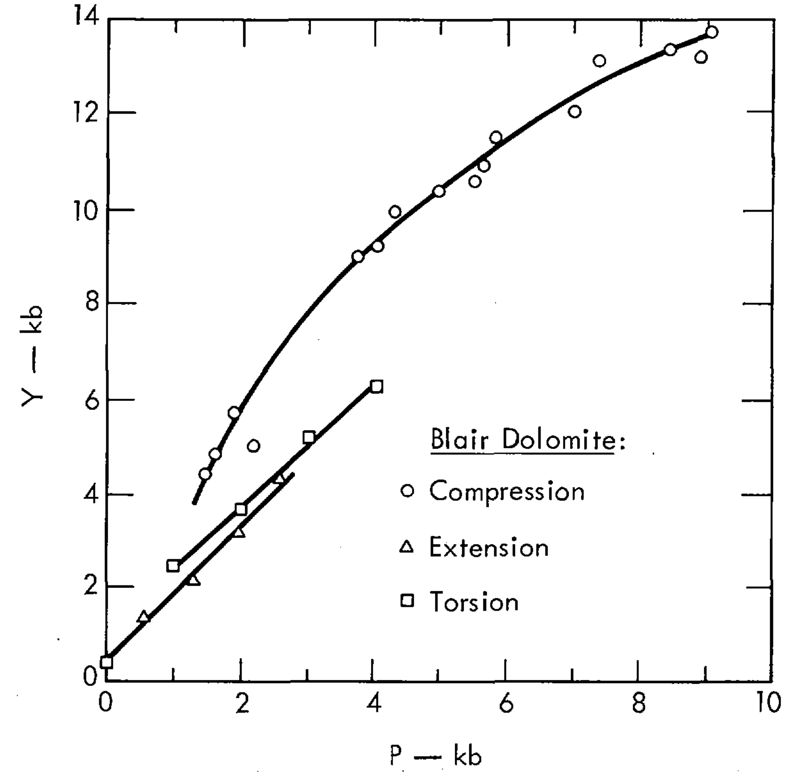

Fig. 13. Y vs P for Blair dolomite (data of Handin et al.[7]).

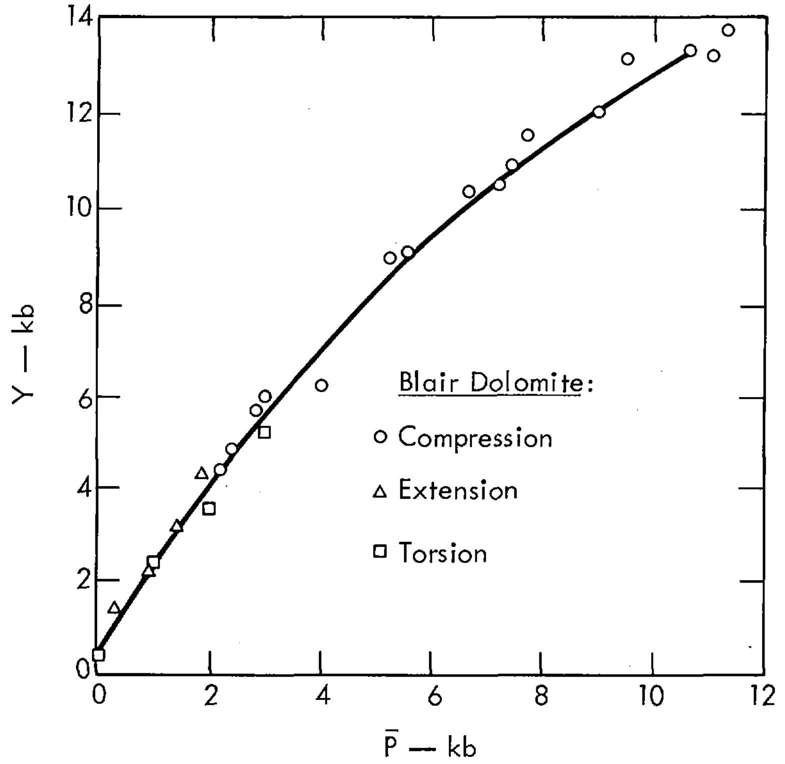

Fig. 14. Y vs $\overline{P}$ for Blair dolomite (data of Handin et al.[7]).

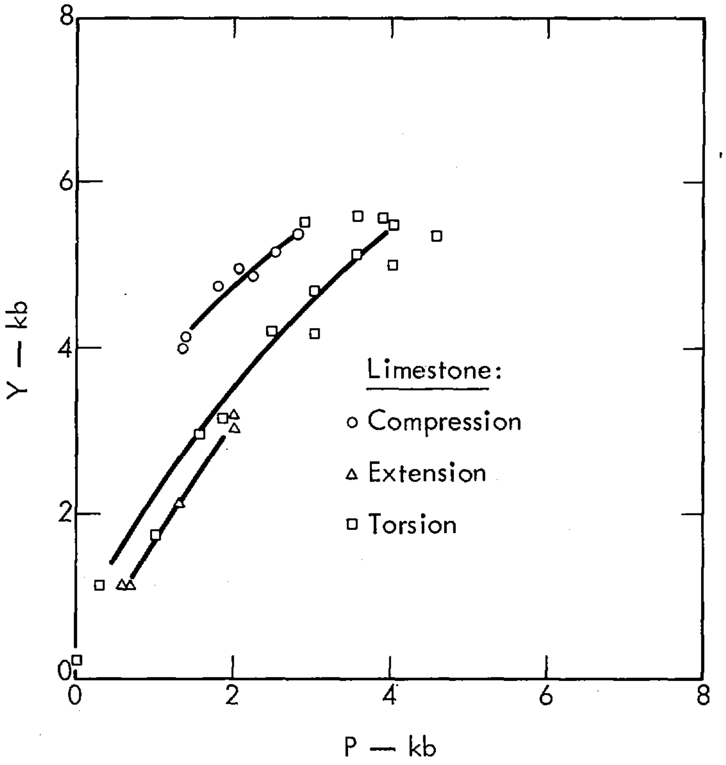

Fig. 15. Y vs P for limestone (data of Handin et al.[7]).

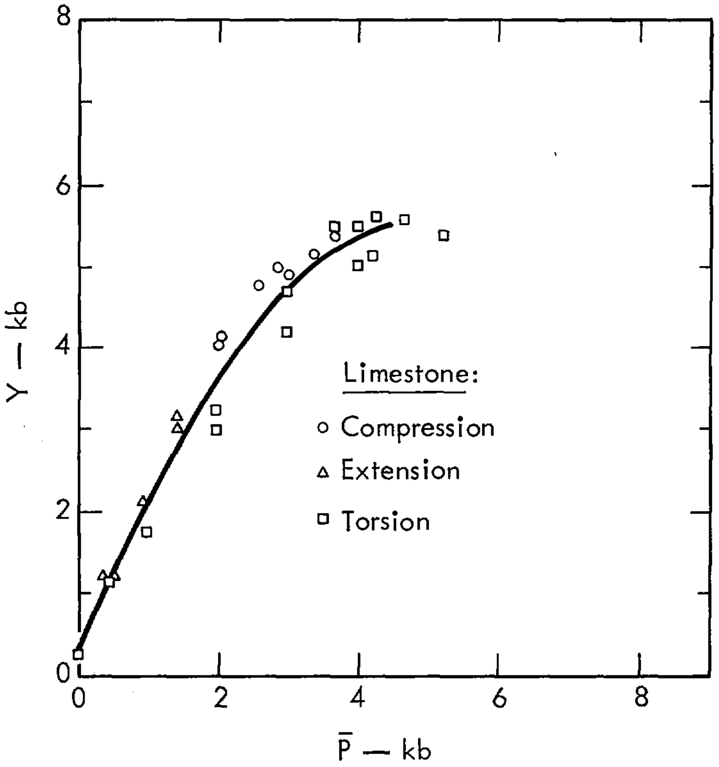

Fig. 16. Y vs $\overline{P}$ for limestone (data of Handin et al.[7]).

The failure criterion in the code is a table of Y/2 vs $\overline{P}$. The table is determined from triaxial compression test data, the tensile strength, and the Hugoniot elastic limit, where Y/2 and $\overline{P}$ are evaluated for each test.

4. COMPARISON OF CALCULATIONS AND EXPERIMENTAL RESULTS

4.1 Model Studies

Model studies were done in which a charge of high explosive and a number of pressure transducers at various distances from the charge were imbedded in a large block of grout which was allowed to set and harden. When the charge was detonated in the hardened grout, the resultant stress history was determined from the pressure transducer data.

The grout was a special mix called DF-5A, developed by the U. S. Army Corps of Engineers. It was poured into an approximately cubical form 60 cm on a side, with the top side given a slight cylindrical curvature to facilitate study of its free surface behavior by shadowgraph photography. A 4-cm-diam spherical charge of LX-04 high explosive was placed 14 cm below this free surface. Ten pressure transducers sensitive to radial stress were placed at distances between 4.5 and 14 cm from the charge. The transducers were all at least 10 cm below the free surface, and most of them were below the level of the charge. For the experiment, the entire form was buried in sand or gravel with only the free surface protruding.

The explosive was detonated and the free surface velocity was measured with a streaking camera in "shadowgraph" configuration. The cylindrical free surface simplified this measurement. Pressure transducers were 1.25-cm-diam, 0.5-mm-thick Z-cut tourmaline disks (Hearst et al.[9]). A characteristic of the DF-5A grout is the presence of voids due to air in the mix, a desirable feature both for transducer bonding and for producing the "locking solid" behavior characteristic of porous rocks.

The purpose of the experiment was to compare the experimental results with the code solutions. These calculations were performed using the material properties furnished from laboratory tests on grout samples. Figure 3 shows the loading and unloading hydrostats measured for the grout. Figure 17 shows the strength data obtained from triaxial compression tests. We regard the wet strength as the equilibrium strength and attempt to compensate for the difference between the wet and dry materials by including a strain rate term (K_2^I, equation (31)) of 4 kb in the equation of state. A Poisson's ratio of about 0.2 was obtained from ultrasonic measurements on grout cylinders. The equation of state of LX-04 has been published by Wilkins.[10]

Figures 18, 19, and 20 compare calculated and measured radial stress histories at 6.5, 7.5, and 9 cm. At 7.5 and 9 cm the calculated peak radial stress is high and the shock arrives too fast. Figure 21 compares calculated and measured peak radial stress versus radial distance. Again the high calculated value is apparent. The calculated free surface (spall) velocity was 60 m/sec compared to an observed value of 53 m/sec, rather encouraging agreement considering this measurement is the easiest to obtain and probably the most reliable part of the experimental effort.

In view of the complexity of the grout equation of state, the agreement between calculation and experiment is considered to be good, at least encouraging enough to warrant improvement in the stress-history measurement techniques (too many gauge failures now occur) and to ask for a detailed study of the variability of the grout material properties.

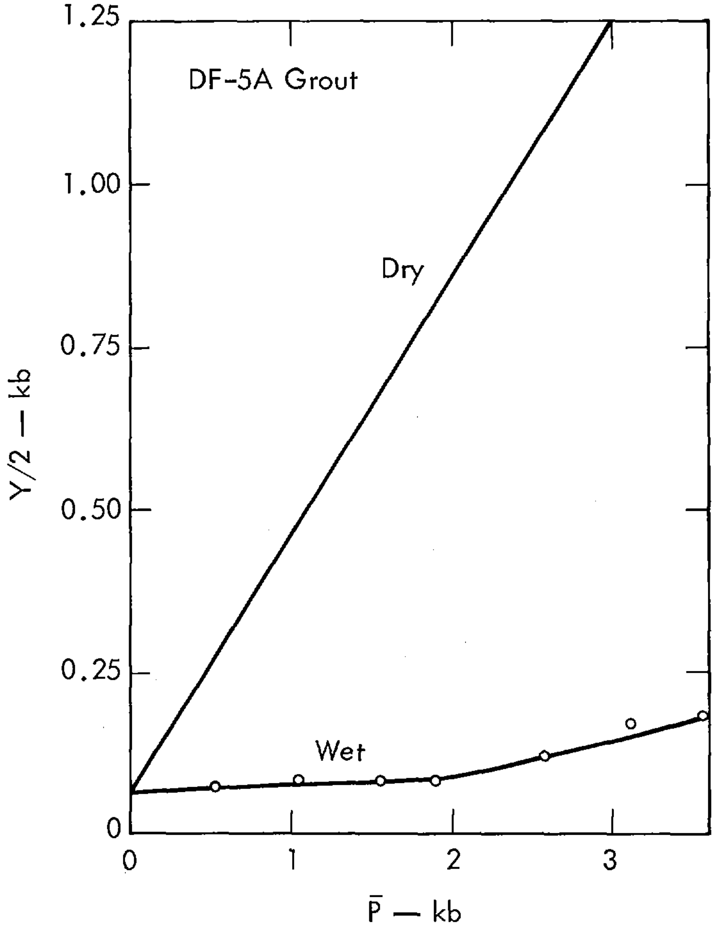

Fig. 17. Strength of DF-5A grout.

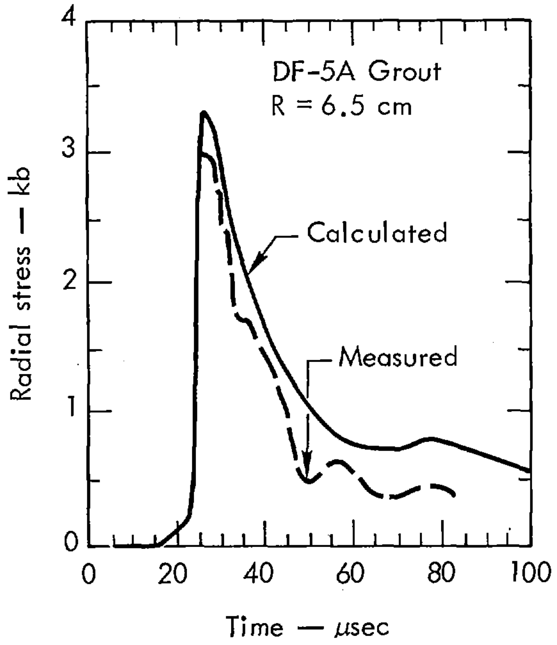

Fig. 18. Stress history in DF-5A grout 6.5 cm from high explosive detonation.

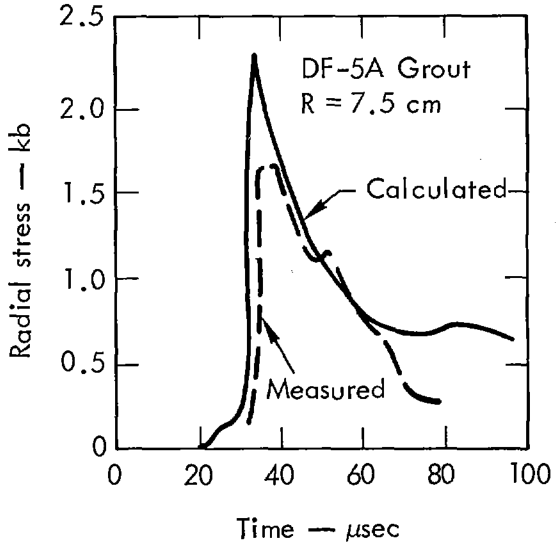

Fig. 19. Stress history in DF-5A grout 7.5 cm from high explosive detonation.

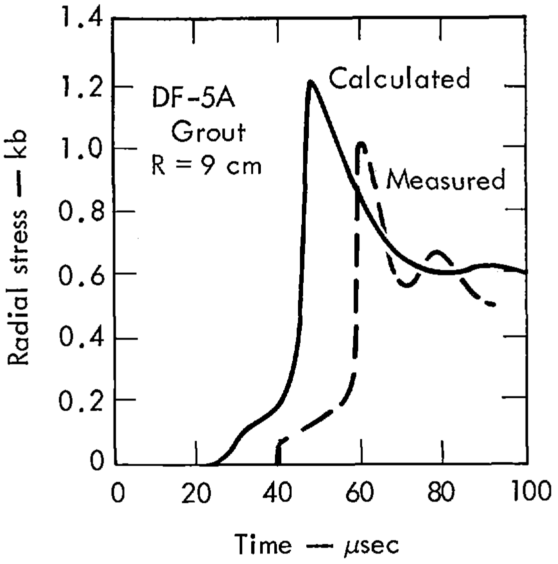

Fig. 20. Stress history in DF-5A grout 9 cm from high explosive detonation.

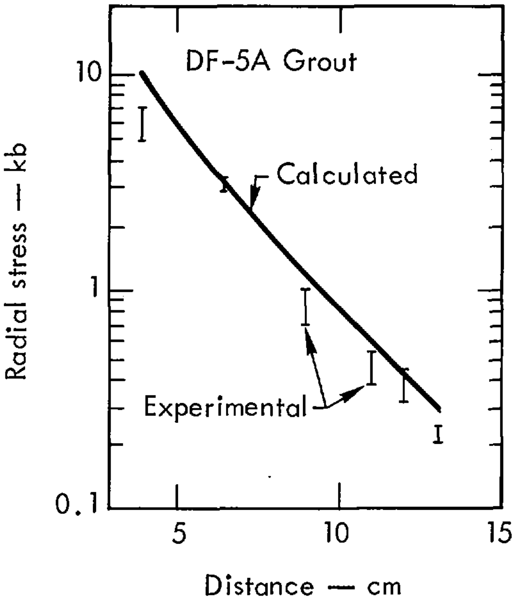

Fig. 21. Peak radial stress in DF-5A grout vs distance from high explosive detonation.

4.2 Hardhat Granite

The Hardhat Event was a 5-kt contained nuclear explosion at a depth of 290 m in granite at NTS. Figure 4 shows the static isotherm along with Hugoniot data obtained from granite cores taken at the Hardhat site. The 10-kb offset between the HEL and the static isotherm is maintained for the code input. Figure 22 gives the granite strength (Y/2 vs $\overline{P}$) for various states of the test sample. The strength data that give best agreement between calculation and observation are the wet, precracked values. In order to make these strength data consistent with the HEL data of Fig. 4, a strain rate term $\left(K_2{}^{I}\right.$, equation (30)$\left.\right)$ of 7.5 kb was included in the equation of state. This value corresponds to the 10-kb offset between the static isotherm and the HEL. A Poisson's ratio of about 0.28 was obtained from ultrasonic laboratory measurements.

The calculation was begun by uniformly distributing 5 kt of internal energy in a sphere of radius 3.15 m at normal density (2.67 g/cc) and using the appropriate gas tables for this region (SiO_2 + 1% H_2O, Butkovich^2). Code calculations show that the mass of rock vaporized is proportional to the yield, and for silicate rocks approximately 70×10^6 g/kt is vaporized. The value 3.15 m corresponds to the radius of vaporization for the 5-kt source.

Figure 23 shows calculated and observed peak radial stress versus scaled radius. Figures 24, 25, 26, and 27 show calculated radial stress versus distance at 4, 16, 24, and 40 msec. A striking feature of this sequence is the emergence of the precursor (P) and the decay of the main shock.

Figures 28 and 29 show calculated and measured radial stress versus time at 62 and 120 m. The experimental stress-history data do not exhibit the strong precursor obtained from the calculations. This may be due, in part, to the weak grouting material used for an impedance match between the transducer and the granite formation.

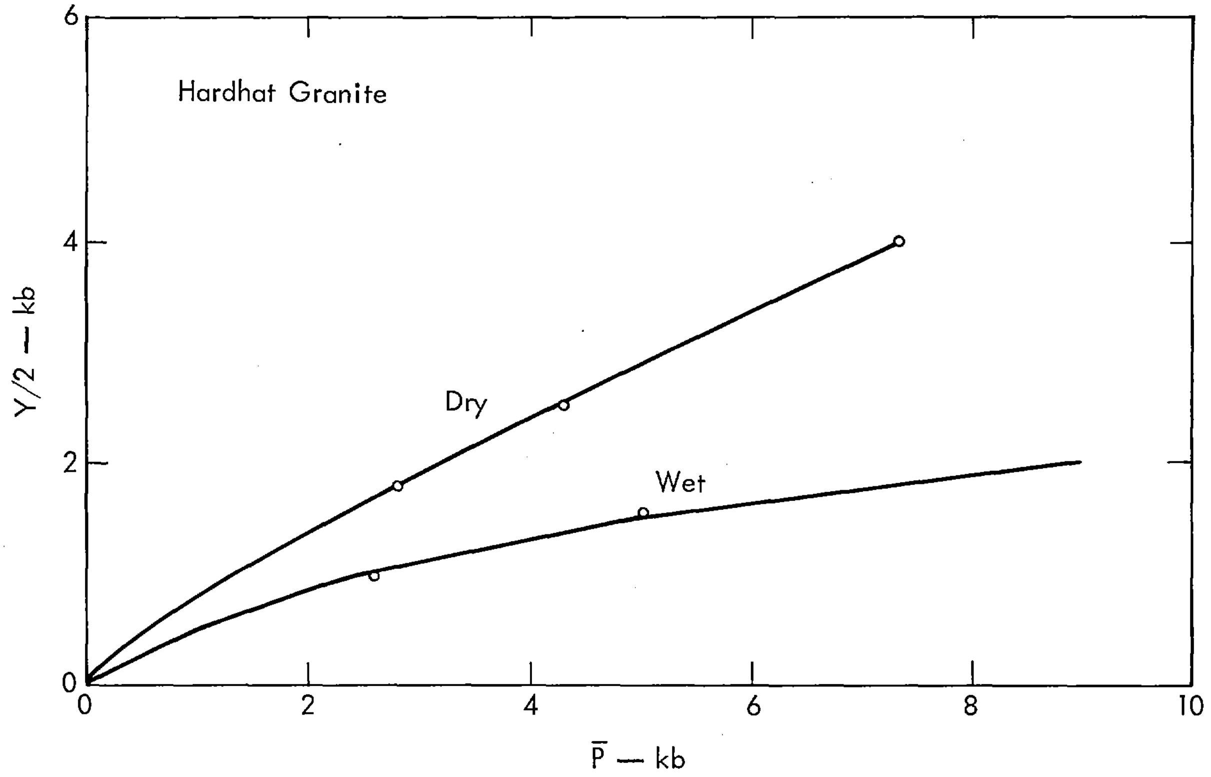

Fig. 22. Strength of Hardhat granite.

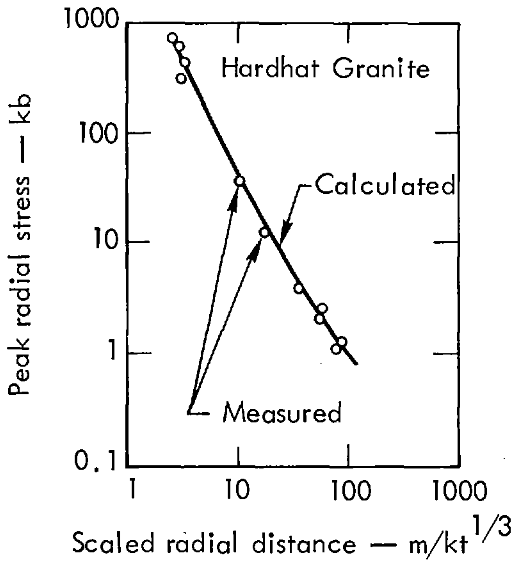

Fig. 23. Calculated and observed peak radial stress in Hardhat granite as a function of scaled distance from a nuclear shot.

The calculation gives a final cavity radius (corresponding to the initial gas-rock interface at 3.15-m radius) of 20.4 m. The measured Hardhat cavity radius is 19 m. Figure 30 gives the calculated and observed reduced

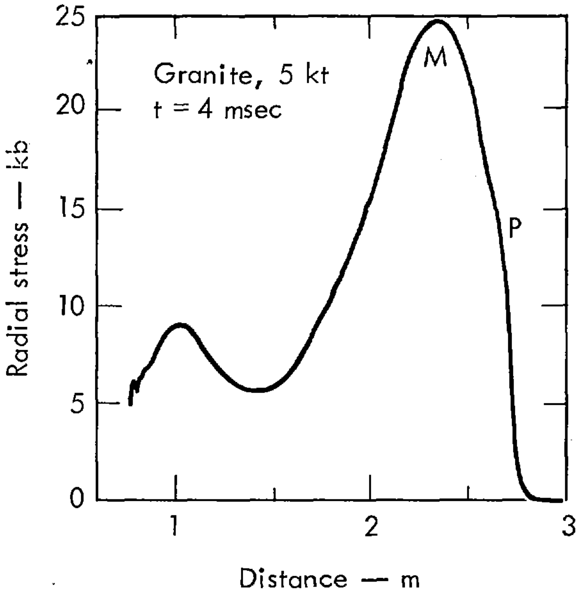

Fig. 24. Calculated radial stress vs distance, 4 msec after a 5-kt shot in Hardhat granite.

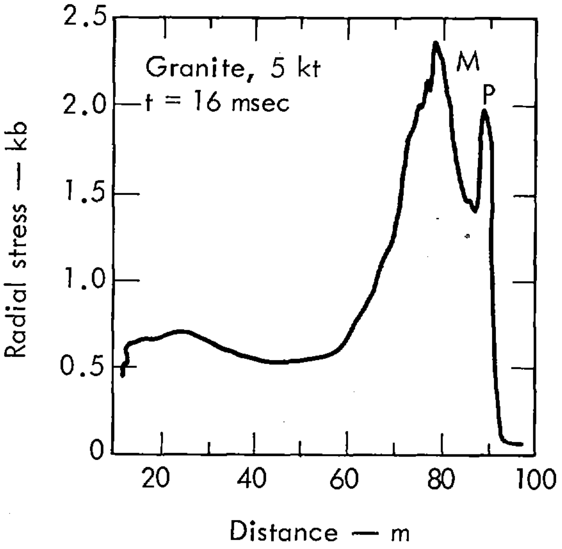

Fig. 25. Calculated radial stress vs distance, 16 msec after a 5-kt shot in Hardhat granite.

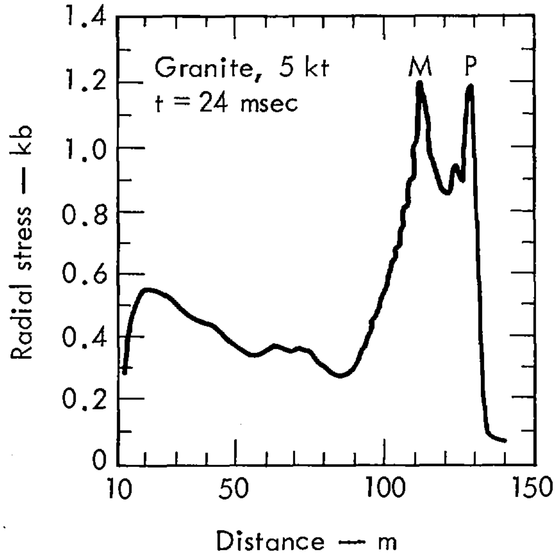

Fig. 26. Calculated radial stress vs distance, 24 msec after a 5-kt shot in Hardhat granite.

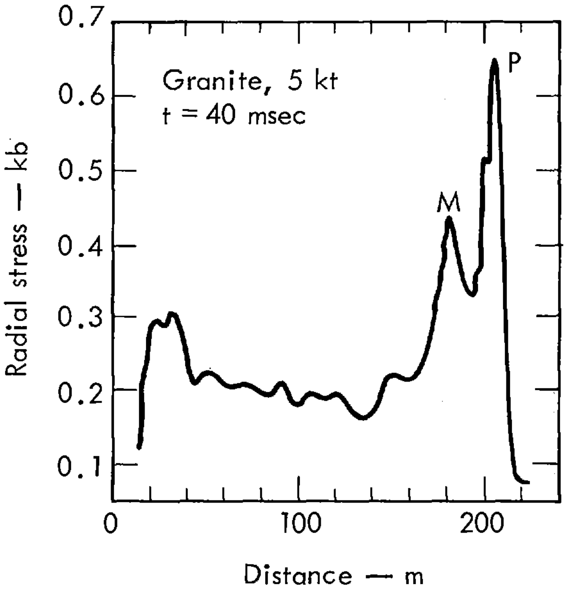

Fig. 27. Calculated radial stress vs distance, 40 msec after a 5-kt shot in Hardhat granite.

displacement potential (RDP) obtained from displacement versus time for a particle in the "elastic" region.

The RDP is a measure of the seismic efficiency of the medium. For a spherical outgoing elastic wave whose displacement is S_R we can write

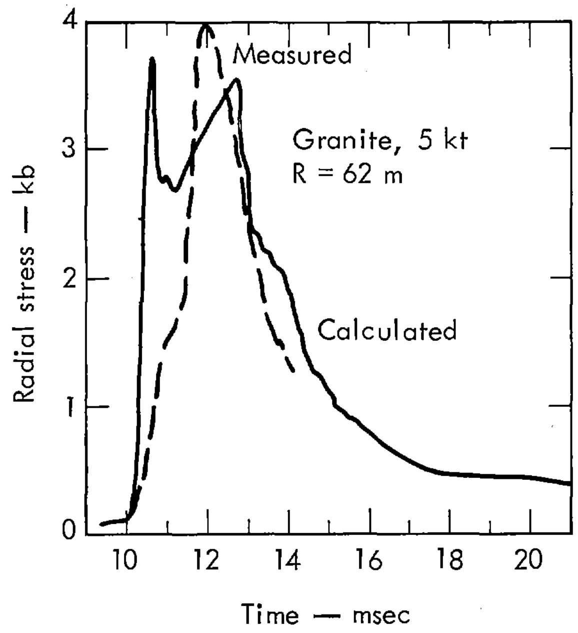

Fig. 28. Calculated and measured stress history in Hardhat granite, 62 m from a 5-kt shot.

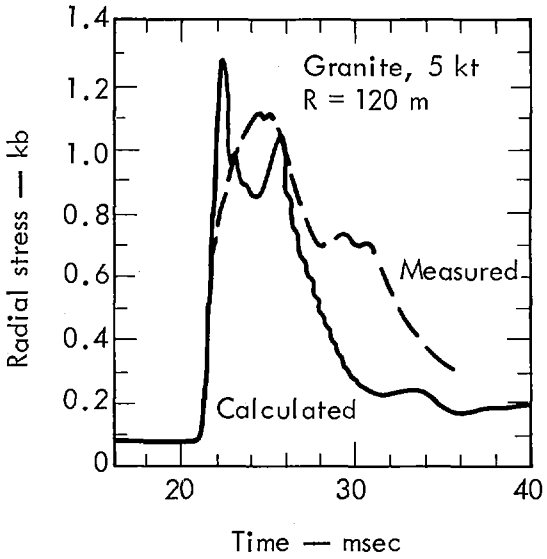

Fig. 29. Calculated and measured stress history in Hardhat granite, 120 m from a 5-kt shot.

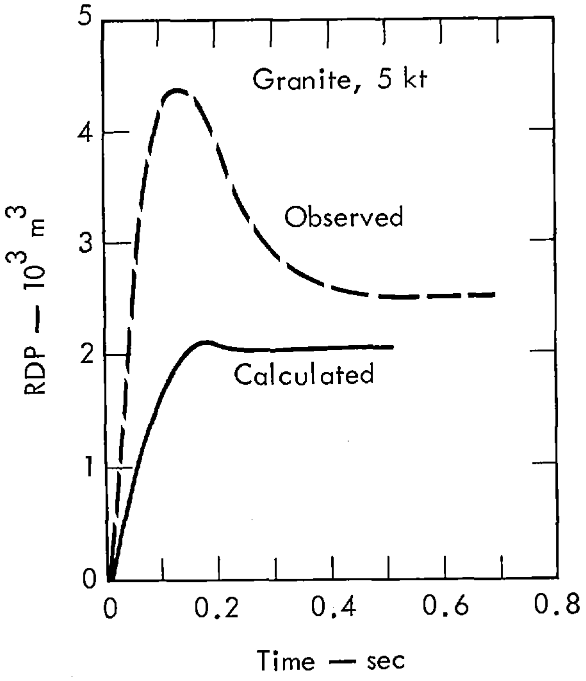

Fig. 30. Calculated and observed reduced displacement potential (RDP) for a 5-kt shot in Hardhat granite.

$$S_R = \frac{\partial}{\partial R}\left[\frac{f(t - R/V_P)}{R}\right] ; \qquad (39)$$

we define the RDP as:

$$\text{RDP} = f(t - R/V_P),$$

where

$$V_P = \sqrt{\frac{k + \frac{4}{3}\mu}{\rho}} .$$

The RDP, obtained by integrating equation (39), gives the source function that determines the displacement of a particle at any point in the elastic region. The source function should scale from one shot to another by multiplying the RDP by the ratio of the yields involved.

The calculated and observed steady-state values of RDP agree. The early time disagreement could be due to the surface reflection returning to the instrument 60 msec from the onset of the direct wave (Werth and Herbst [11]). No calculation incorporating reasonable changes in the equation of state has been able to produce the observed overshoot in RDP.

Figure 31 shows the number of times a zone has cracked versus distance for the Hardhat calculation. This number is saved by the code for each

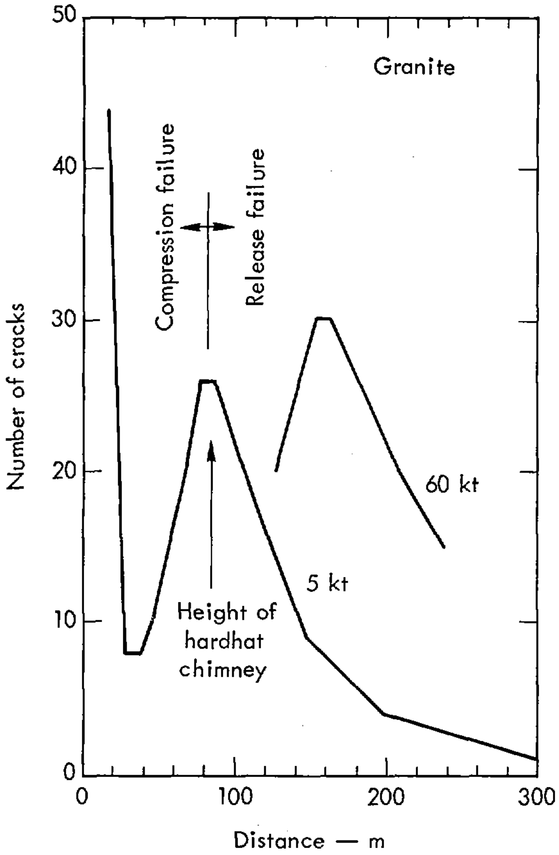

Fig. 31. Calculated number of cracks produced in Hardhat granite vs distance from the shot.

zone and increased by 1 each time the material strength is exceeded. The number can only be increased after the deviatoric component of stress (K) relaxes to half the value allowed by the strength table and after C_R (equation (29)) equals 1. At this point the relaxation of K (equation (30)) ceases and equation (25) is used to obtain K^{n+1} ($K^{n+1} = \tilde{K}^{n+1}$). This scheme for exiting from the crack routine emphasizes release failure (where $\tilde{K}^{n+1}$ calculated from equation (25) is less than K^n) over compression failure. This number has its largest value (44) at the cavity boundary due to the divergence there as the cavity expands, falls to a minimum value of 8 between 30 and 40 m where compression failure is the controlling mechanism, and then increases to a maximum of 26 between 80 and 90 m. This maximum is due to zone failure changing from compression (failure at the shock front) to release (failure behind the shock front) at $R \approx 90$ m. It is interesting that the observed height of the Hardhat chimney falls within this maximum.

Additional calculations for larger yields show that the maximum not only increases but the shape broadens as indicated by the 60-kt plot given in Fig. 31. This suggests that as the yield increases the bulking of the rock, as it collapses into the cavity, should eventually become the controlling factor in determining chimney height.

The crack number, assuming it is calculated correctly, should be related to permeability changes in the medium. Apparently permeability is both difficult and expensive to measure. However, Fig. 31 suggests that permeability should reach a minimum between 30 and 40 m from the cavity for 5 kt. This zone of low permeability might serve a useful purpose in some applications by helping to limit the spread of gas-borne radioactivity from the cavity; however, unless it is removed by chimney collapse, it might severely limit the effectiveness of reservoir stimulation.

4.3 Gasbuggy

Gasbuggy was an experiment in nuclear stimulation of a gas-bearing formation in Rio Arriba County, New Mexico, sponsored jointly by the U. S. Atomic Energy Commission, the El Paso Natural Gas Company, and the U. S. Bureau of Mines. A 25-kt nuclear explosive was detonated 1280 m underground, in the Lewis shale formation 12 m below the gas-bearing Pictured Cliffs sandstone. The objective was to evaluate the effectiveness of the nuclear explosion in increasing the permeability of the Pictured Cliffs formation and thus improving the recovery of gas from it.

The best experimental measurements, in terms of stress wave propagation, were obtained by Sandia Laboratories (Perret[12]) in a deep borehole

457 m from the emplacement hole. This part of the experiment was funded by the Advanced Research Projects Agency (ARPA).

Logging data near the emplacement hole and in the ARPA instrument hole indicate that the compressional velocity in the Lewis shale ranges from 4.75 to 3.87 m/msec and the density varies from 2.4 to 2.6 g/cc. Figure 32 shows the loading and unloading static compressibility data for the Lewis shale. The loading data give a bulk modulus of about 160 kb (curve A) and an initial density of 2.61 g/cc. Using a Poisson's ratio of 0.3 (obtained from the shear velocity log) we obtain a compressional velocity of about 3 m/msec, a value that is not consistent with the logging data.

In order to obtain a reasonable value for the compressional velocity we have found it necessary to ignore all the loading compressibility data below 3 kb on the basis that these data are probably influenced heavily by both the release of overburden pressure (0.3 kb) on the core and the coring technique itself. The loading compressibility curve B shown in Fig. 32 was accordingly assumed for the Lewis shale. This curve, having a bulk modulus of 215 kb, gives a compressional velocity of 3.5 m/msec, in fair agreement with the logging data.

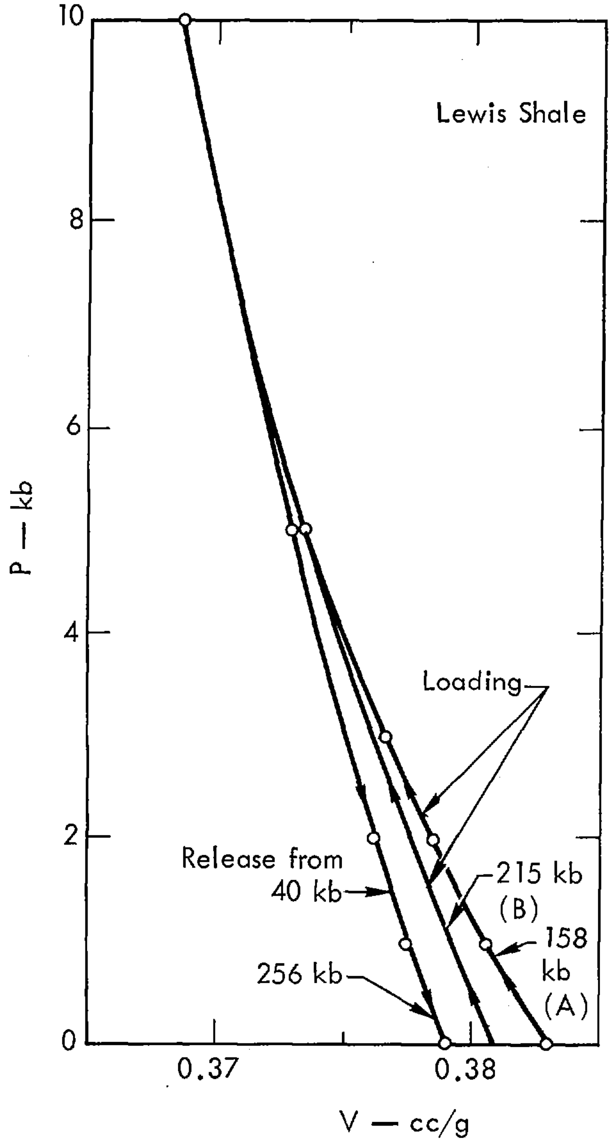

Fig. 32. Compressibility of Lewis shale, the formation in which the Gasbuggy explosive was located.

This change in compressibility curves severely affects the seismic coupling. The effect is due entirely to the attenuation of the stress wave by the pressure release calculation (equation (24)) in the code. As indicated in Fig. 32, the measured static release path from 40 kb has a slope of 256 kb, corresponding to a rarefaction speed of about 3.7 m/msec. These rarefactions overtake the slower moving (3.0 m/msec) compression front and continuously decrease its stress and particle velocity.

Figure 33 shows measured and calculated displacement versus time at 467 m from the 25-kt source. The difference between the two calculations is obtained by changing the compressibility curve from A to B as discussed above (Fig. 32). The sensitivity of this part of the calculation to changes in the "locking" portion of the equation of state seems dramatic until one considers the magnitude of the changes that are being made in the only material attenuation mechanism operative in the code (rarefaction velocity compared to shock velocity).

Figure 34 gives the measured and calculated RDP corresponding to the displacement of Fig. 33. We see

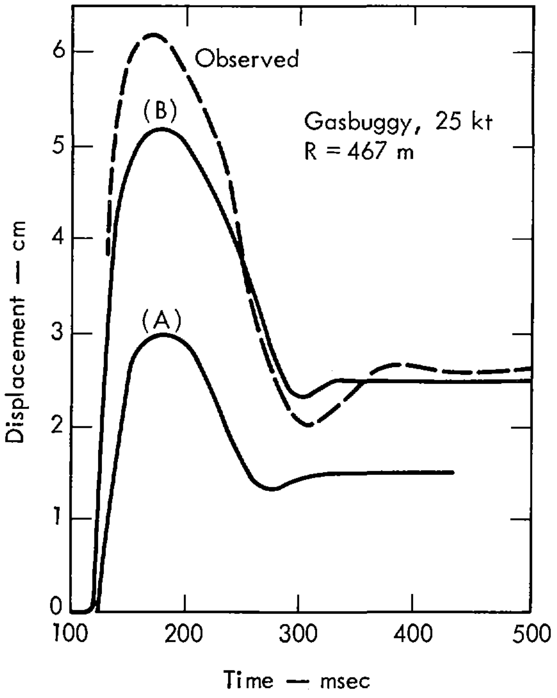

Fig. 33. Calculated and observed displacement history in Lewis shale 467 m from the 25-kt Gasbuggy shot.

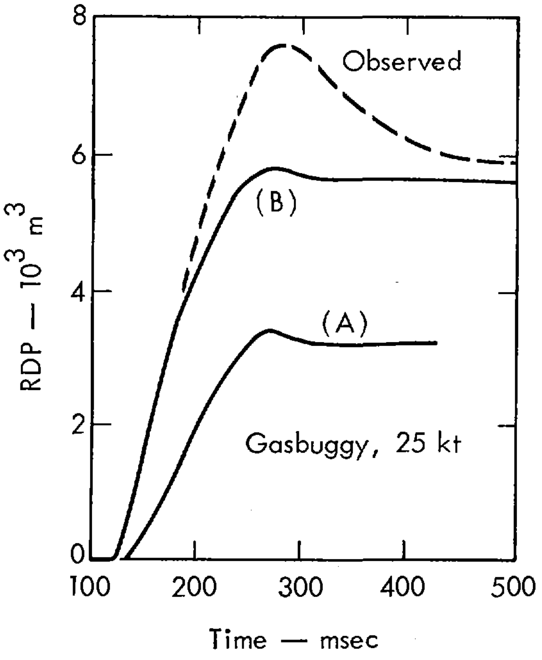

Fig. 34. Calculated and observed reduced displacement potential (RDP) for Gasbuggy shot.

that with compressibility curve B twice as much energy is coupled into the elastic region as with curve A. These calculations indicate that a detailed equation-of-state effort is required before a seismic coupling calculation can be attempted. Even then, since the low pressure part of the equation of state seems to control the coupling, we may not be able to predict this parameter with confidence. The key issue would seem to be obtaining agreement between the sonic logs and the static compressibility data. The Gasbuggy experiment represented the first time such severe disagreement existed between the field and laboratory data.

Calculations indicating severity of fracture (similar to those for Hardhat, Fig. 31) have been performed for the Gasbuggy environment. Figure 35 shows the geological layering for the site. Figure 36 shows the compressibility curves for the Lewis shale, the Pictured Cliffs sandstone, and the Fruitland coal. Figure 37 shows the strength curves used in the calculations.

Figure 38 shows calculations of number of cracks per zone vs distance from the shot point for paths vertically upward through the various layers (layered calculation) and also for paths outward into the sandstone (Pictured Cliffs calculation). As noted preshot, the coal seam located between 100 and 112 m above the shot point reduces the fracturing at this distance, which corresponds to the measured height of the Gasbuggy chimney. This highly compressible coal seam also sends a rarefaction into the Pictured Cliffs formation, and the fracture number is increased accordingly. The observed postshot casing failures and gas entries are also consistent with the calculated data of Fig. 38.

The calculated cavity radius was 26.3 m for the layered calculation and 25.8 m for the Pictured Cliffs calculation. These values compare closely with the 25.4-m value inferred from flow tests.

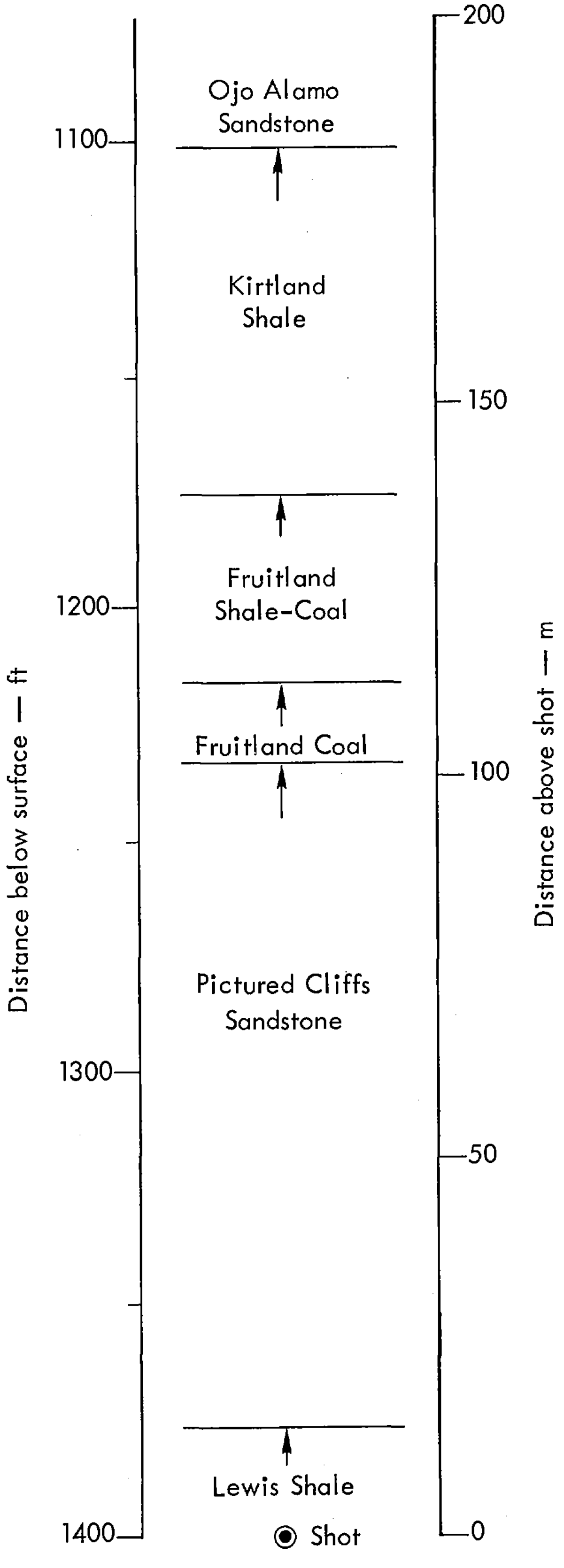

Fig. 35. Geological layering at Gasbuggy site.

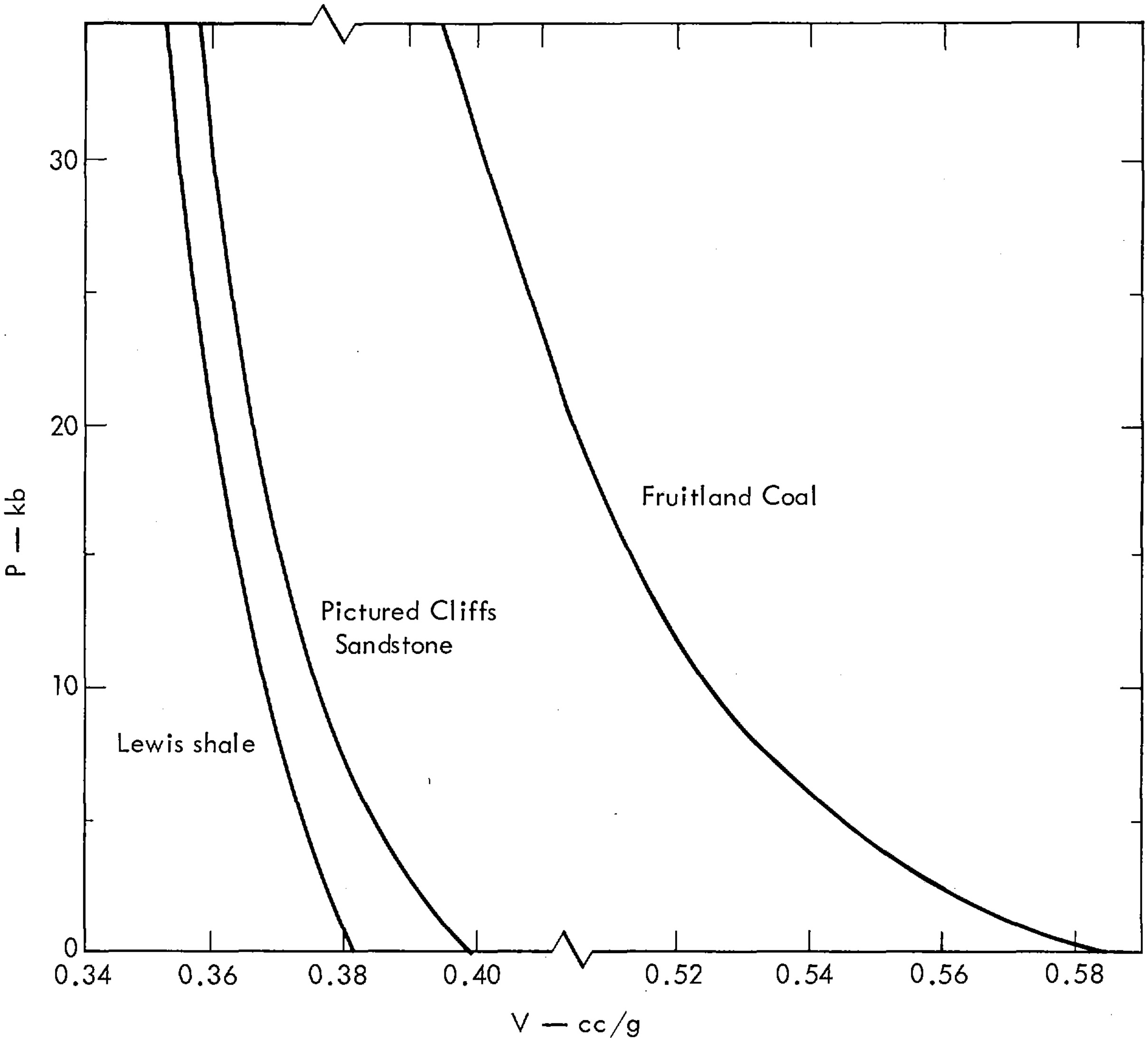

Fig. 36. Compressibility of Gasbuggy rocks.

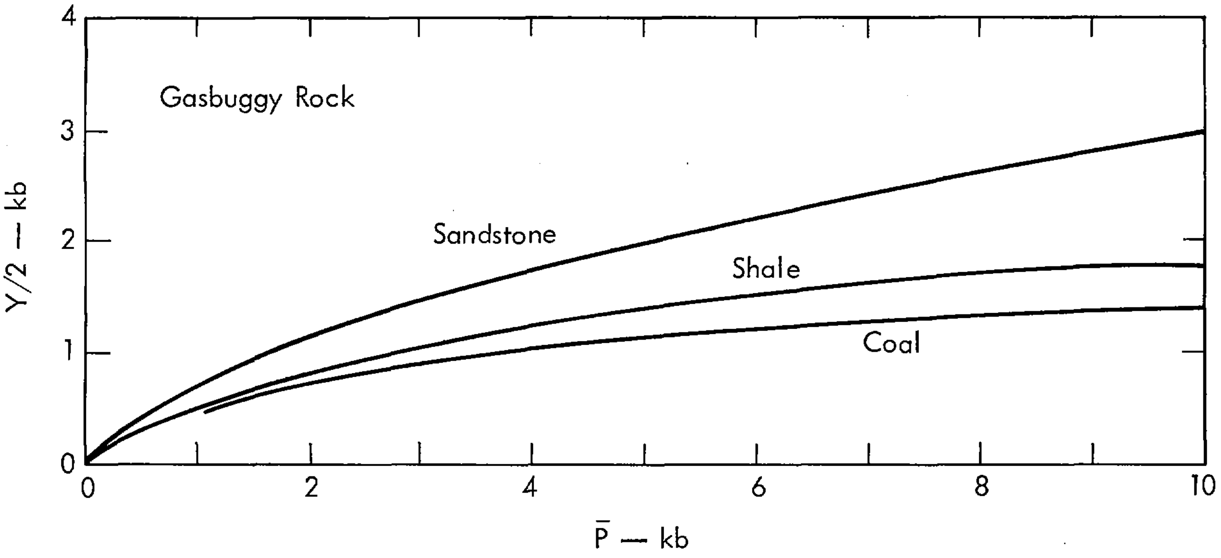

Fig. 37. Strength of Gasbuggy rocks.

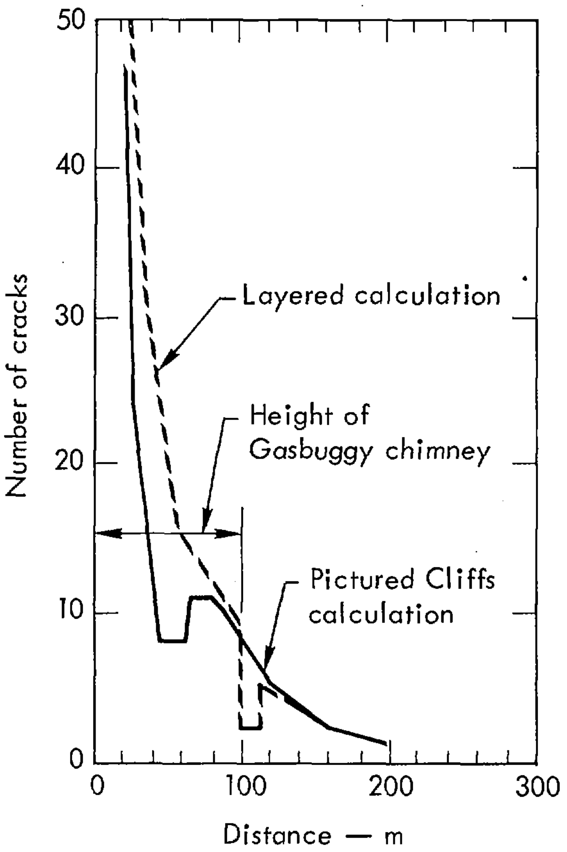

Fig. 38. Calculated number of cracks vs distance from the Gasbuggy shot, for paths upward through the various layers and outward through the Pictured Cliffs sandstone.

5. CONCLUSIONS

A numerical model of stress wave propagation has been presented. We have included a listing of the SOC code (see Appendix) and have given a discussion of the material properties required to obtain a prediction of the stress-induced effects on the rock mass involved in an application. These effects include chimney height, seismic coupling, and permeability change. The seismic coupling parameter was shown to be primarily dependent on the low pressure part (<3 kb) of the equation of state. For high yields the controlling factor for chimney height should be cavity volume.

Future effort is required in the areas of Hugoniot release (especially for a fluid-saturated environment), laboratory strength measurements, and failure criteria. A significant improvement in the equation of state would result if the *in situ* rigidity modulus could be measured directly.

The preshot calculations for the Gasbuggy experiment indicate that useful predictions of cavity radius and chimney height can be made when an adequate effort is made to obtain equation-of-state data for the rock involved.

In general the code seems to be doing well enough in predicting stress wave propagation that we can begin looking at derived numbers — such as number of cracks per zone — for some insight into predicting stress-induced changes in permeability.

6. REFERENCES

1. J. B. Keller, "Geometrical Acoustics, I. The Theory of Weak Shock Waves," *J. Appl. Phys.* *25*, 938 (1954).
2. T. R. Butkovich, *The Gas Equation of State of Natural Materials*, Lawrence Radiation Laboratory, Livermore, Rept. UCRL-14729 (1966).
3. Z. T. Bieniawaski,"Fracture Dynamics of Rocks," *Intern. J. Fracture Mech.* *4*, 415 (1968).
4. J. D. Byerlee, "Frictional Characteristics of Granite Under High Confining Pressures," *J. Geophys. Res.* *72*, 3639 (1967).
5. T. J. Ahrens and G. E. Duvall, "Stress Relaxation Behind Elastic Shock Waves in Rocks," *J. Geophys. Res.* *71*, 4349 (1966).
6. J. T. Cherry, "Computer Calculations of Explosion Produced Craters," *Intern. J. Rock Mech. and Mining Sci.* *4*, 1 (1967).
7. J. Handin, H. C. Heard, and J. N. Magouirk, "Effects of the Intermediate Principal Stress on the Failure of Limestone, Dolomite, and

Glass at Different Temperatures and Strain Rates," *J. Geophys. Res.* *72*, 611 (1967).

8. K. Mogi, "Effect of the Intermediate Principal Stress on Rock Failure," *J. Geophys. Res.* *72*, 5117 (1967).
9. J. R. Hearst, G. B. Irani, and L. B. Geesaman, "Piezoelectric Response of Z-Cut Tourmaline to Shocks up to 21 Kilobars," *J. Appl. Phys.* *36*, 3440 (1965).
10. M. Wilkins, B. Squier, and B. Halperin, *The Equation of State of PBX 9404 and LX 04-01*, Lawrence Radiation Laboratory, Livermore, Rept. UCRL-7797 (1964).
11. G. C. Werth and R. F. Herbst, *Comparison of Amplitudes of Seismic Waves from Nuclear Explosions in Four Media*, Lawrence Radiation Laboratory, Livermore, Rept. UCRL-6962 (1962).
12. W. R. Perret, *Gasbuggy Seismic Source and Surface Motion*, Sandia Laboratories, Albuquerque, Rept. PNE-1002 (1969).

APPENDIX 1. SOC LISTING

```
*       LIST 8
*       CARDS COLUMN
*       FORTRAN               NORM
C       VERSION CURRENT OCTOBER 1969
        CLICHE COMMON
COMMON WHICH CAN VARY WITH TIME
        COMMON NC, JN, LN, TT, IR, LX, ENI, RN(1202), DRMX(1202), VMX(1202
       1), PX(1202), GMX(1202), SIGR(1202), SIGT(1202), XMU(1202), AM(1202
       2), C1(1202), DR(1202), DV(1202), DVO(1202), EO(1202), ISV(1202),
       3 P(1202), Q(1202), GK(1202), TK(1202), VN(1202), VO(1202), AMU(120
       42), E(1202), I(1202), R(1202), V(1202), TC(12), TIC(12), RPL(25),
       5 DT, DTH, DTN, DTPR, EPP, ETOT, FDT, HDT1, IL, IPI, IPO, ITCX,
       6 IRANK, NCD, PJM, PTS, GXT, RJH, STR, SXN, TPR, HDTH, TTS
COMMON WHICH REMAINS THE SAME FOR DURATION OF PROBLEM
        COMMON DPLOT, IEPLOT, IRPLOT, IHEAD(8), GR, DXT, PLOD(100), GAS(27
       128), PT(400), FMU(400), DPM(400), PTC(200), FMC(200), DPC(200),
       2 FK(200), FP(200), DFK(200), CK(200), CP(200), CKP(200), AK(10),
       3 VI(10), RM(10), AMZ(10), AM1(10), AM2(10), GXK(10), RZO(10), P1(1
       40), P2(10), GSL(10), GCT(10), SE(10), EF(10), FV(10), GSI(10),
       5 IT(10), ITT(10), IP(10), RB(11), RHO(11), GK(10), CF, CCN, HCCN,
       6 IRZ, REZF, IWRT(4), PPR(61), TP(61), IVR, IALF
COMMON WHICH IS USED FOR GENERAL CALCULATION BUT NOT SAVED
        COMMON ABF(4004), ABA(4004), ABB(4004), BF(200), EN(11), OCH(11),
       1 FMC(11), EDP(6), EDT(6), EDTL(6), ING(25), FNG(25), ION(4), PRI,
       2 IC(2), MO(2), ID(8), A, ABS, AMC, AME, AMP1, B, BARK, C, CKL, CRC
       3, CTC, CZO, CAVR, CRTI, CVFL, CVRC, D, DP, DU, DEC, DR1, DR2, DRH,
       4 DRS, DTV, DV1, DVK, EW, EOV, EKL, ETA, ETW, EJTH, EROU, FA, FST,
       5 FSTM, FSTR, G1, G2, GAM, GLN, GM1, GMU, IBX, III, IIJ, IPR, IPDT,
       6 ITER, ITOT, ITIME, ITOTL, ITSTP, J, K, L, LL, LP, M, N, NN, NP,
       7 NCYC, OFF, PCT, PL3, PL4, PQ1, PQ2, PBAR, QO, QS, QKS, QSAV, R21,
       8 R22, RDR, RH1, RH2, ROR, RZ1, RADT, RH21, RH22, RMV1, RMV2, SK,
       9 SLC, SLE, SLP, SMU, SDSP, SLP1, STAB, TV, TAR, TBR, TER, TK1
        COMMON TK2, TG1, TQ2, TRR, TERK, VCC, VDV, VM1, VM2, VN1, VNH,
       1 VOL1, VOL2, WT, YN1, RIX(10), GW, F, S, AD, AF, DA, DB, DC, DD,
       2 KIM, ZETA, LIL
        EQUIVALENCE (YN1, RIX(1))
        EQUIVALENCE (ION(4),PRI)
        EQUIVALENCE (ING,FNG)
        END CLICHE
        USE COMMON
C       READ 6B AND WRITE 6A
        CALL REGST
        N=.LOC.ABF(1)
        J=.LOC.ZETA
        N=J-N
        DO 1 LIL=1,N
        ABF(LIL)=0.
      1 CONTINUE
        CALL REWIND (16)
        CALL CLOCK (MO(1), MO(2))
        CRTI=1.
        NCYC=J=5
        L=16
      2 BUFFER IN (16,1) (DPLOT,IALF)
      3 IF (UNIT,16,M) 3, ,219,219
        CALL REDEOF (16)
        J=
      4 BUFFER IN (16,1) (NC,TTS)
      5 IF (UNIT,16,M) 5, ,220,220
        BACKSPACE FILE 16
       CALL BSPACE (16)
       CALL FSPACE (16)
       READ INPUT TAPE 2, 950, (ID(J), J=1,8)
       READ INPUT TAPE 2, 951, GW, ITIME, A, STR
       STP=100.*STR
       CALL ASSIGN (7,0,10HSOCPLOTBUF,40200)
C      SET UP RUNNING TIME
       IF (ITIME) ,7,7
       IF (IBANK) 6, ,6
       IBANK=-ITIME
     6 ITIME=IBANK
     7 IBX=1
       TTS=MAX1F(GW*1000.,TTS)
CHECK  FOR RIGHT TAPE
       DO 8 J=1,8
       IF (IHEAD(J)-ID(J)) ,8,
       WRITE OUTPUT TAPE 3, 954, (IHEAD(J), J=1,8)
       CALL ERROR (0.)
     8 CONTINUE
       K=6
       IF (A) , ,9
       CALL WRSO
       GO TO 10
     9 CALL REDEOF (6)
       CALL BSPACE (6)
    10 CALL WRST
       CALL WRTEOF (6)
       CALL BSPACE (6)
       CALL BANDP (ION(1), ION(3))
       B=ION(2)
       B=B/PRI
       A=B-40.
       ION(1)=A
       IF (ITIME) , ,11
       ITIME=ION(1)
       GO TO 12
    11 ITIME=XMINOF(ION(1), ITIME)
    12 ITOTL=B
       IF (NC) 13, ,13
CYCLE  1 CONSTANTS INITIALIZED
       CALL BANDP (ION(1), ION(3))
       A=ION(2)
       A=A/PRI
       ITOT=A
       ITOT=ITOTL-ITOT
       GO TO 15
CHECK  CLOCK FOR TIME STOP - INCREMENT COUNTER
C      EVERY 20 CYCLES GOES TO 10 INSTEAD OF 11
    13 ITSTP=0
       CALL BANDP (ION(1), ION(3))
       A=ION(2)
       A=A/PRI
       ITOT=A
       ITOT=ITOTL-ITOT
    14 ITSTP=ITSTP+1
CALCULATE DELTA T
       A=1.1*DTH
       B=(SQRTI(SXN))/3.
       B=MIN1F(B,A)
       DT=.5*(B+DTH)
```

```
      DTH=B
CHECK FOR PRESSURE PROFILE
   15 IF (IPO-2) 20,16,
C     OUTER PRESSURE PROFILE
      L=1
      GO TO 17
C     INNER PRESSURE PROFILE
   16 L=LX
   17 TK(L)=0.
   18 A=DIMF(TP(IPI+1),TT)
      IF (A) 19, ,19
      IPI=IPI+1
      IF (TP(IPI+1)) , ,18
      IPO=1
      GO TO 20
   19 A=TT-TP(IPI)
      B=TP(IPI+1)-TP(IPI)
      P(L)=PPR(IPI)+(PPR(IPI+1)-PPR(IPI))*A/B
      EPP=EPP+(PJM*HDT1+P(L)*DTN)*V(L-1)*CCN*(3.*RJH*RJH+FDT*V(L-1)*V(L-
     11))
      ETOT=EPP+ENI
CYCLE CONSTANT INITIALIZATION
   20 PCT=BARK=0.
      TT=TT+DTH
      HDT1=.5*DT
      HDTH=.5*DTH
      DTN=DTH-HDT1
      FDT=HDTH*HDTH
      L=IR
      SXN=DXT
      QXT=ABSF(QXT)
      VCC=1.0E-3*QXT/SQRTF(AK(L)*RHO(L+1))
      VCC=MIN1F(VCC,1.0E-8)
      QXT=1.
      PQ1=P(JN)+Q(JN)
      TQ1=TK(JN)+QK(JN)
      IF (I(JN)) ,21,
      DR1=DR(JN-1)-DR(JN)+RN(JN-1)-RN(JN)
      R21=DR(JN-1)+DR(JN)+RN(JN-1)+RN(JN)
      VOL1=VN(JN)-DVO(JN)
      VM1=(VOL1-DV(JN))/AM(JN)
      TK1=TQ1*VM1/R21
      RMV1=DR1/VM1
      RH1=R(JN-1)+V(JN-1)*HDTH
      RH21=RH1*RH1*V(JN-1)
CALCULATION OF J-LINES BEGINS HERE
   21 DO 144 J=JN,LN
      GAM=0.
      III=(I(J)-1)/100+1
      EO(J)=E(J)
      VO(J)=V(J)
CALCULATE EQUATIONS OF MOTION
      IF (R(J)) 218,27,
      PQ2=P(J+1)+Q(J+1)
      TQ2=TK(J+1)+QK(J+1)
      IF (I(J+1)) ,28,
      DR2=DR(J)-DR(J+1)+RN(J)-RN(J+1)
      R22=DR(J)+DR(J+1)+RN(J)+RN(J+1)
      VOL2=VN(J+1)-DVO(J+1)
      VM2=(VOL2-DV(J+1))/AM(J+1)
      TK2=TQ2*VM2/R22
      RMV2=DR2/VM2
      IF (I(J)) ,29,
      ROR=(TK2*DR1+TK1*DR2)/(DR1+DR2)
      RDR=.5*(RMV1+RMV2)
   22 A=(PQ1-PQ2)/RDR
      IF (V(J)) ,23,
      VCC=1.E-20
   23 DV1=DT*(1.333333333*(TQ1-TQ2)/RDR+A+8.*ROR+GR)
      V(J)=V(J)-DV1
      IF (ABSF(V(J))-VCC) 30,30,
   24 C=DTH*V(J)
      RH2=R(J)+.5*C
      RH22=RH2*RH2*V(J)
      DR(J)=DR(J)+C
      R(J)=RN(J)+DR(J)
      DRS=R(J-1)-R(J)
      IF (I(J)) ,113,
   25 C=(V(J)-V(J-1))*(V(J)*(V(J-1)+V(J))+V(J-1)*V(J-1))
      C=DTH*(3.*(RH22-RH21)+FDT*C)
      DV(J)=DV(J)+C
      VN1=VOL1-DV(J)
      VNH=VN1+.5*C
      D=(DV(J)+DVO(J))/VN1
      AMP1=D+1.
      EDV=C/VN(J)
      DVK=C/VNH
      ETA=VN(J)/VNH
      VDV=VN(J)*C/(VN1*(VN1+C))
      DU=V(J-1)-V(J)
      DRH=RH1-RH2
      IF (DU) ,26,26
      ERDU=ETA*DU*RHO(L+1)
      QSAV=ERDU*DU
   26 TER=3.*DTH*DU/DRH
      TERK=DVK+TER
      IF (III-3) 31,31,
      IF (I(J)-400) 116,125,125
 CALCULATE BOUNDARY CONDITIONS
   27 RH2=RH22=0.
      GO TO 25
   28 RDR=.5*RMV1
      ROR=TK1
      GO TO 22
   29 RDR=.5*RMV2
      ROR=TK2
      GO TO 22
 CALCULATIONS MADE WHEN LITTLE OR NO ACTIVITY EXISTS
   30 V(J)=0.
      IF (V(J-1)) 24, ,24
      RH2=R(J)
      RH22=0.
      IF (III-3) 113,113,
      IF (III-4) ,24,
      C=DR1*(R(J-1)*R2)+R(J)*R(J))
      PCT=C*P(J)+PCT
      GO TO 113
 CALCULATE SLOPE AND PRESSURE FOR I LESS THAN 300
   31 N=IT(L)+1
      NP=IP(L)+1
      PL =SLP=SMU=0.
      IF (XMU(J)-2.*GCT(L)*AM2(L)) ,47,47
      IF (XMU(J)) 56, ,
      IF (D-XMU(J)) 32, ,
      XMU(J)=D
      GO TO 42
   32 IF (XMU(J)-AM1(L)) 42,42,
      IF (III-2) 34, ,
      IF (P(J)) , ,34
      IF (XMU(J)-AM2(L)) 33, ,
      XMU(J)=.98*AM2(L)
   33 XMU(J)=-XMU(J)
      GO TO 56
   34 IF (XMU(J)-AM2(L)) ,48,48
      IF (D-.95*XMU(J)) ,42,42
C - SPECIAL UNLOADING SCHEME - A -
      IF (D-AM1(L)) , ,35
      SLP=AK(L)
      GO TO 41
   35 DO 36 K=NP,NP+38
      IF (P(J)-PT(K)) 37,37,
      IF (FMU(K+1)-FMU(K)) 37,37,
   36 CONTINUE
      K=NP+38
   37 SLE=DPM(K)
      DO 38 K=N,N+18
      IF (P(J)-PTC(K)) 39,39,
      IF (FMC(K+1)-FMC(K)) , ,38
      SLC=SLE
      GO TO 40
   38 CONTINUE
      K=N+18
   39 SLC=DPC(K)
   40 SLP1=SLE+XMU(J)*(SLC-SLE)/AM2(L)
      SLP=SLP1-AM1(L)*(SLP1-AK(L))/D
   41 PL3=P(J)+SLP*VDV
      GO TO 65
CALCULATE ELASTIC P-MU TABLE - B -
   42 ABS=D
      CALL PSUB
      GO TO 65
      ENTRY PSUB
      DO 44 K=NP,NP+38
      IF (ABS-FMU(K)) ,45,43
      PL3=PT(K-1)+(ABS-FMU(K-1))*DPM(K)
      GO TO 46
   43 IF (FMU(K+1)-FMU(K)) 45,45,
   44 CONTINUE
      K=NP+38
   45 PL3=PT(K)+(ABS-FMU(K))*DPM(K)
   46 SLP=DPM(K)
      RETURN PSUB
CALCULATE CRUSHED P-MU TABLE
   47 XMU(J)=MAX1F(D,XMU(J))
   48 SLP=AK(L)*.01
      ABS=D
      DO 51 K=N-1,N+18
      IF (D-FMC(K)) 49, ,50
      PL3=PTC(K)
      SLP=DPC(K)
      GO TO 52
   49 IF (K-N) 52, ,
      PL3=PTC(K-1)+(D-FMC(K-1))*DPC(K)
      SLP=DPC(K)
      GO TO 52
   50 IF (FMC(K+1)-FMC(K)) , ,51
      CALL PSUB
      GO TO 52
   51 CONTINUE
      CALL PSUB
   52 IF (D-.985*XMU(J)) ,65,65
      ABS=XMU(J)
      PL4=PL3
      SLP1=SLP
      CALL PSUB
      GAM=.5*PL3*XMU(J)/(1.+XMU(J))
      GAM=GXK(L)*(GAM-EF(L))/(EV(L)-EF(L))
      IF (GAM) , ,53
      PL3=PL4
      SLP=SLP1
      GO TO 65
   53 GAM=MIN1F(GAM,GXK(L))
      ABS=D
      IF (D) , ,54
      PL4=GSL(L)*D
      PL3=SLP=0.
      SLP1=GSL(L)
      GO TO 55
   54 CALL PSUB
   55 DP=GAM*(E(J)-.5*PL3*D/AMP1)
      PL4=PL4+DP
      SLP=SLP1+.5*GAM*((PL4+P(J))/ETA-(.5*(D+AMU(J))*SLP+PL3/ETA))/ETA
      PL3=PL4
      IF (SLP) ,65,65
      SLP=.01*AK(L)
      GO TO 65
CALCULATE S.L.S.
   56 IF (D-AMZ(L)) , ,57
      PL3=0.
      SLP=AK(L)
      GO TO 65
   57 DO 58 K=N,N+18
      IF (P(J)-PTC(K)) 62, ,
      IF (FMC(K+1)-FMC(K)) 59,59,
   58 CONTINUE
   59 DO 60 K=NP,NP+38
      IF (P(J)-PT(K)) 61, ,
      IF (FMU(K+1)-FMU(K)) 61,61,
   60 CONTINUE
      K=NP+38
   61 ABS=FMU(K-1)+(P(J)-PT(K-1))/DPM(K)
      SLP=DPM(K)
      GO TO 63
   62 ABS=FMC(K-1)+(P(J)-PTC(K-1))/DPC(K)
      SLP=DPC(K)
   63 IF (D-ABS) ,64,64
      IF (ABS-AMZ(L)) ,64,
      SLP=(D-AMZ(L))*SLP/(ABS-AMZ(L))
   64 PL3=P(J)+SLP*VDV
      IF (PL3) ,65,65
      PL3=0.
C - EXIT -
   65 IF (E(J)-EF(L)) ,66,66
      IF (GAM) 67,67,
      C1(J)=ISV(J)=0.
   66 SK=SMU=0.
      GO TO 103
   67 WT=(EF(L)-ABSF(E(J)))/EF(L)
      IF (PL3+TK(J)/3.-P1(L)) ,68,68
      IF (PL3) 69,69,
      IF (III-2) 70,79,79
   68 C1(J)=ISV(J)=0.
      IF (III-2) 70, ,
      I(J)=I(J)-200
      III=1
      GO TO 70
   69 IF (III-2) 70, ,
      ISV(J)=-XABSF(ISV(J))
      PL3=SK=QKS=SMU=C1(J)=0.
      QS=QSAV
      SLP=AK(L)
      SDSP=SQRTI(AK(L)/RHO(L+1))
      GO TO 104
CALCULATIONS FOR I(J) LESS THAN 100
   70 IF (RM(L)) , ,71
      AME=SLP*SE(L)*WT
      GO TO 72
   71 AME=RM(L)*WT
   72 SMU=AME
      IF (AME/SLP-1.501) 73,73,
      I(J)=I(J)+500
      WRITE OUTPUT TAPE 3, 975, AME, SLP, D, PL3, 1
      CALL ERROR (1.)
   73 SK=TK(J)-.5*AME*TERK
      ABS=PL3+SK/3.
      DO 76 K=N,N+18
      IF (ABS-EP(K)) ,74,75
      EKL=EK(K-1)+(ABS-EP(K-1))*DEK(K)
      GO TO 77
   74 EKL=EK(K)+(ABS-EP(K))*DEK(K)
      GO TO 77
   75 IF (EP(K+1)) 76, ,76
      IF (EP(K)) ,74,74
   76 CONTINUE
      K=N+18
      EKL=EK(K)+(ABS-EP(K))*DEK(K)
   77 EKL=EKL*WT
      EKL=MAX1F(0.,EKL)
      IF (PL3+SK/3.-P1(L)) 78, ,
      EKL=P2(L)*WT
      IF (SK-EKL) 103,103,
      SK=SIGNF(EKL,SK)
      GO TO 103
   78 IF (ABSF(SK)-EKL) 103, ,
      I(J)=I(J)+200
      III=3
      C1(J)=0.
      ISV(J)=1
CALCULATIONS FOR I(J) GREATER THAN 100
   79 IF (RM(L)) , ,80
```

```
       AMC=SLP*SE(L)*WT
       GO TO 81
    80 AMC=RM(L)*WT
    81 GW=(D-AMZ(L))/(PZO(L)-AMZ(L))
       GW=MIN1F(1.,GW)
       IF (GW) , ,82
       C1(J)=SK=SMU=0.
       ISV(J)=-XABSF(ISV(J))
       GO TO 103
    82 AMC=SMU=GW*AMC
       IF (AMC/SLP-1.501) 83,83,
       I(J)=I(J)+500
       WRITE OUTPUT TAPE 3, 976, AME, SLP, D, PL3
       CALL ERROR (1.)
    83 ABS=PL3+TK(J)/3.
       DO 86 K=N,N+18
       IF (ABS-CP(K)) ,84,85
       CKL=CK(K-1)+(ABS-CP(K-1))*CKP(K)
       GO TO 87
    84 CKL=CK(K)+(ABS-CP(K))*CKP(K)
       GO TO 87
    85 IF (CP(K+1)) 86, ,86
       IF (CP(K)) ,84,84
    86 CONTINUE
       K=N+18
       CKL=CK(K)+(ABS-CP(K))*CKP(K)
    87 CKL=CKL*WT*GW
       CKL=MAX1F(0.,CKL)
       IF (ISV(J)) , ,89
       SK=TK(J)-.5*AMC*TERK
       IF (ABSF(SK)-CKL) 103, ,
       C1(J)=0.
       ISV(J)=XABSF(ISV(J))+1
 CRACK EQUATIONS
    89 IF (ISV(J)-1) , ,91
       IF (RM(L)) , ,90
       AME=SLP*SE(L)*WT
       IF (AME/SLP-1.501) 92,92,
       I(J)=I(J)+500
       WRITE OUTPUT TAPE 3, 975, AME, SLP, D, PL3, 2
       CALL ERROR (1.)
    90 AME=RM(L)*WT
       GO TO 92
    91 AME=AMC
    92 CZO=.1*DRS
       CTC=CZO+C1(J)
       CTC=MIN1F(CTC,DRS)
       AME=AMC+(1.-CTC/DRS)*(AME-AMC)
       CVEL=1.14*SQRTI(AME/(RHO(L+1)*(3.+AME/SLP)))
       PL4=CKL
       C1(J)=C1(J)+CVEL*DTH
       CRC=.25*C1(J)/DRS
       IF (CRC-1.) 94, ,
       CRC=1.
       IF (ABSF(TK(J))-.5*CKL) 93,93,
       C1(J)=C1(J)-CVEL*DTH
       GO TO 94
    93 ISV(J)=-XABSF(ISV(J))
       C1(J)=0.
    94 SK=TK(J)-.5*AME*TERK
```

```
      GW=P2(L)*WT
      CKL=ABSF(SK)*(1.-CVEL*CRC*DTH/DRS*.25)*WT
      IF (XABSF(ISV(J))-2) 95,95,
      CKL=MIN1F(CKL,PL4)
      GO TO 96
   95 CKL=MIN1F(CKL,GW)
   96 CKL=MAX1F(0.,CKL)
      IF (ABSF(SK)-CKL) 102,102,
      SK=SIGNF(CKL,SK)
  102 SMU=AME
CALCULATE Q
  103 SDSP=SQRTI((SLP+1.33333333*SMU)/RHO(L+1))
      IF (DU) ,104,104
      QS=QSAV-VI(L)*SDSP*ERDU
      QKS=-.5*VI(L)*SMU/SLP*RHO(L+1)*ETA*SDSP*DRH/DTH*TERK
      QKS=MIN1F(QKS,.5*WT*P2(L))
CALCULATE ENERGY
  104 IF (QS-GK(L)) ,105,105
      QS=0.
  105 PBAR=(PL3+QS)*DTN+PG1*HDT1
      IF (I(J)-390) , ,106
      BARK=(SK+QKS)*DTN+TG1*HDT1
  106 DEC=(PBAR*EDV-.6666666666*BARK*(EDV+TER/ETA))/DTH
      E(J)=E(J)+DEC
      IF (I(J)-390) , ,111
      IF (RHO(L+1)*AMP1-10.) , ,107
      IF (D-.985*XMU(J)) ,111,111
      IF (E(J)-EV(L)) 111, ,
  107 IF (III-2) ,108,109
      I(J)=I(J)+400
      GO TO 110
  108 I(J)=I(J)+300
      GO TO 110
  109 I(J)=I(J)+200
  110 III=5
CALCULATE STABILITY
  111 DU=MIN1F(0.,DU)
      FA=4.*DU
      TV=2.*VI(L)
      STAB=(DRS*DRS)/(FA*FA+(TV*TV+1.)*SDSP*SDSP)
      AMU(J)=D
      P(J)=PL3
      TK(J)=SK
      QK(J)=QKS
      Q(J)=QS
      IF (STAB) 112,112,
      IF (SXN-STAB) 112,112,
      SXN=STAB
      RADT=R(J)
  112 IF (I(J)-390) 113,113,
      PCT=(VOL1-DV(J))*P(J)+PCT
CLEAR OUT AND SHIFT FOR NEXT J-LINE
  113 D=AMP1=PL3=SK=QS=QKS=BARK=QSAV=DRS=0.
      IF (QXT) 115, ,
      IF (QXT-Q(J)) , ,114
      QXT=Q(J)
      GO TO 115
  114 IF (Q(J+1)) 115,115,
      IF (J-JN-10) 115,115,
      QXT=-QXT
  115 DR1=DR2
      R21=R22
      VOL1=VOL2
      VM1=VM2
      TQ1=TQ2
      TK1=TK2
      RMV1=RMV2
      PQ1=PQ2
      RH1=RH2
      RH21=RH22
 CHECK FOR REGION BOUNDARY
      IF (RN(J)-RB(L+1)) , ,144
      LL=L
      L=L+1
      GO TO 144
 CALCULATE H.E.
  116 IF (C1(J)) , ,119
      DTV=TT*RM(L)-RN(J)+RN(LX-2)
      IF (DTV) 114, ,
      DTV=.4*DTV/(RN(J-1)-RN(J))
      IF (DTV-1.) 117, ,
      DTV=1.
      C1(J)=1.
  117 QO=AMZ(L)+1.
      SLP=QO*D/(AMP1*AMZ(L))
      IF (D) 119, ,
      IF (SLP-1.) 118,118,
      C1(J)=1.
  118 PL3=SLP*DTV*RHO(L+1)*RM(L)*RM(L)*AMZ(L)/QO
      SLP=PZO(L)/AMZ(L)
      GO TO 124
  119 N=IP(L)+1
      DO 122 K=N,N+18
      IF (D-FMU(K)) ,120,121
      PL3=PT(K-1)+(D-FMU(K-1))*DPM(K)
      GO TO 123
  120 PL3=PT(K)
      GO TO 123
  121 IF (PT(K+1)) ,120,
  122 CONTINUE
      K=N+38
      PL3=PT(K)
  123 SLP=DPM(K)
  124 SDSP=SQRTI(SLP/RHO(L+1))
      IF (DU) ,105,105
      QS=QSAV-VI(L)*SDSP*ERDU
      GO TO 104
 CALCULATE GAS
  125 N=ITT(L)
      IF (GSI(L)-100.) ,138,
 CALCULATE LONG GAS TABLE
      IF (DU) ,126,126
      SLP=P(J)/(E(J)*AMP1)*(E(J)+PQ1/AMP1)
      QS=QSAV-VI(L)*SQRTI(SLP/RHO(L+1))*DU*ETA*RHO(L+1)
  126 ETW=E(J)+(P(J)+QS)*EDV
      EW=ETW/RHO(L+1)
      GMU=AMP1*RHO(L+1)
      GLN=LOGF(GMU)
      DO 134 K=N,N+9
      IF (GAS(K)-GMU) 133, ,
  127 M=(K-N+1)*64+20+N
      DO 131 NN=N+20,N+83
      IF (GAS(NN)-EW) 130,130,
      IF (NN-N-20) , ,129
  128 G2=GAS(M)
      G1=GAS(M-64)
      GO TO 132
  129 G2=EW-GAS(NN-1)
      G1=GAS(M-65)+G2*GAS(M+576)
      G2=GAS(M-1)+G2*GAS(M+640)
      GO TO 132
  130 IF (GAS(NN+1)) ,128,
      M=M+1
  131 CONTINUE
      GM1=.667
      GO TO 137
  132 IF (K-N) 136, ,136
      GM1=G2
      GO TO 137
  133 IF (GAS(K+1)-GAS(K)) 126,126,
  134 CONTINUE
  135 N=K
      GO TO 127
  136 GM1=G1+(G2-G1)*(GLN-GAS(K+9))/(GAS(K+10)-GAS(K+9))
  137 PL3=GM1*EW*GMU
      EJTW=(.5*(P(J)+PL3)+QS)*EDV+E(J)
      PL3=GM1*AMP1*EJTW
      SLP=GM1*(EJTW+(PL3+QS)/ETA)
      SMU=0.
      GO TO 103
CALCULATE SHORT P-V GAS TABLES
  138 DO 141 K=N+1,N+69
      IF (D-GAS(K+70)) 140, ,139
      PL3=GAS(K)
      K=K+1
      GO TO 143
  139 PL3=GAS(K-1)+(D-GAS(K+69))*GAS(K+140)
      GO TO 143
  140 IF (GAS(K+1)) ,142,
  141 CONTINUE
      K=N+68
  142 PL3=GAS(K)+(D-GAS(K+70))*GAS(K+140)
  143 SDSP=SQRTI(GAS(K+140)/RHO(L+1))
      SLP=GAS(K+140)
      SMU=0.
      IF (DU) ,105,105
      QS=QSAV-VI(L)*SDSP*ERDU
      GO TO 104
  144 CONTINUE
CYCLE END - DO REZONING, PLOTTING AND EDITING
      III=IIJ=2
      IF (NC) , ,149
CYCLE 1 CALCULATIONS
      DO 145 J=JN,LN
      IF (V(J)) 146, ,146
  145 CONTINUE
  146 A=J-5
      A=MAX1F(1.,A)
      JN=A
      DO 147 N=1,L
      IF (RN(JN)-RB(N+1)) ,148,148
  147 CONTINUE
  148 IR=N
      NC=III=1
      GO TO 169
  149 NC=NC+1
      IF (JN-1) 153,153,
      IF (V(JN+4)) 150, ,150
      IF (V(JN+3)) ,153,
  150 JN=JN-1
      DO 151 N=1,10
      IF (RN(JN)-RB(N+1)) ,152,152
  151 CONTINUE
  152 IR=N
  153 IF (IRZ) ,164,
 CALCULATE DEZONE
      IF (NC-200) 164,164,
      RZ1=REZF*(R(JN)-R(JN+1))
      DO 163 J=JN,LN
      IF (R(J)) 164,164,
      IF (IVR-1) ,154,
      IF (I(J-1)) 155, ,155
  154 IF (1.5*RN(J)-R(J)) , ,163
  155 A=R(J-1)-R(J)
      IF (A-RZ1) , ,163
      IF (A/R(J)-.04) , ,163
      IF (R(J)-R(J+1)-R(J-2)+R(J-1)) , ,156
      IF (I(J+1)-400) , ,156
      IF (R(J+1)) ,156,
      K=J+1
      GO TO 157
  156 K=J
  157 IF (XMU(K)) 158, ,
      IF (XMU(K-1)),159,159
      XMU(K)=XMU(K-1)
      GO TO 159
  158 IF (XMU(K-1)) 159, ,
      XMU(K-1)=XMU(K)
 CHECK REGION BOUNDS - DEZONING CAN OCCUR
  159 DO 160 N=1,10
      IF (RN(K-1)-RB(N)) ,163,161
  160 CONTINUE
  161 IF (I(K-1)) ,163,
 C - WEIGHTING OF VARIABLES
      LX=LX-1
      LN=LN-1
      A=VN(K)+VN(K-1)
      B=VN(K)-DV(K)-DVO(K)
      C=VN(K-1)-DV(K-1)-DVO(K-1)
      GW=B+C
      E(K)=(E(K)*VN(K)+E(K-1)*VN(K-1))/A
      EO(K)=(EO(K)*VN(K)+EO(K-1)*VN(K-1))/A
      TK(K)=(TK(K)*B+TK(K-1)*C)/GW
      P(K)=(P(K)*B+P(K-1)*C)/GW
      XMU(K)=(XMU(K)*B+XMU(K-1)*C)/GW
      DVO(K)=DVO(K)+DVO(K-1)
      DV(K)=DV(K)+DV(K-1)
      AMU(K)=(DV(K)+DVO(K))/GW
      VN(K)=A
      AM(K)=AM(K)+AM(K-1)
      C1(K)=0.
      ISV(K)=-XABSF(ISV(K))
C - DEZONE
      DO 162 N=K,LN+2
      R(N-1)=R(N)
      DR(N-1)=DR(N)
      V(N-1)=V(N)
      AMU(N-1)=AMU(N)
      P(N-1)=P(N)
      TK(N-1)=TK(N)
      QK(N-1)=QK(N)
      Q(N-1)=Q(N)
      E(N-1)=E(N)
      I(N-1)=I(N)
      RN(N-1)=RN(N)
      XMU(N-1)=XMU(N)
      C1(N-1)=C1(N)
      ISV(N-1)=ISV(N)
      AM(N-1)=AM(N)
      VN(N-1)=VN(N)
      DRMX(N-1)=DRMX(N)
      VMX(N-1)=VMX(N)
      SIGR(N-1)=SIGR(N)
      SIGT(N-1)=SIGT(N)
      QMX(N-1)=QMX(N)
      PX(N-1)=PX(N)
      DV(N-1)=DV(N)
      DVO(N-1)=DVO(N)
      EO(N-1)=EO(N)
      VO(N-1)=VO(N)
  162 CONTINUE
      GO TO 164
  163 CONTINUE
CHECK FOR STOP TIME, EDIT OR PLOT TIME
  164 IF (ITIME) 165,165,
      IF (ITIME-ITOT) 166, ,
  165 IF (TTS-TT) 166, ,
      IF (STR) 167,167,
      IF (RN(JN)-STR) , ,167
  166 III=IIJ=1
      IBANK=0
      OFF=1.
      GO TO 172
  167 IF (TPR-TT) , ,168
      TPR=TPR+DTPR
      III=1
  168 IF (TC(ITCX+2)-TT) , ,169
      IF (TIC(ITCX+2))169,169,
      DTPR=TIC(ITCX+2)
      TPR=DTPR+TC(ITCX+2)
      ITCX=ITCX+1
  169 IF (DPLOT) 170,170,
      IF (TT-PTS) 170, ,
      IIJ=1
CHECK SENSE SWITCH 1
  170 IF (SENSE SWITCH 1) ,171
      III=IIJ=1
      OFF=-1.
  171 IF (III-1) ,172,
      IF (IIJ-1) 188, ,188
  172 DO 173 J=JN,LN
      IF (I(J)-390) 173,173,
      CAVR=R(J-1)
      GO TO 174
  173 CONTINUE
      CAVR=0.
      GO TO 175
  174 CVRC=PCT/(CAVR*CAVR*CAVR)
  175 IF (III-1) 180, ,180
C - EDIT
      IF (NCYC) ,176,
      WRITE OUTPUT TAPE 3, 956, (IHEAD(N), N=1,7), (IWRT(N), N=1,4),
     1 MO(1), MO(2)
      NCYC=0
      GO TO 177
  176 WRITE OUTPUT TAPE 3, 957, (IHEAD(N), N=1,8), (IWRT(N), N=1,4)
  177 WRITE OUTPUT TAPE 3, 958, NC, DT, DTH, TT, RADT
      DO 178 J=JN-1,LN
      I(J)=XSIGNF(I(J),ISV(J))
  178 CONTINUE
      WRITE OUTPUT TAPE 3, 959, ((J-1), DR(J), R(J), V(J), AMU(J), P(J),
     1 Q(J), TK(J), QK(J), E(J), I(J), J=JN,LN+1)
      DO 179 J=JN-1,LN
      I(J)=XABSF(I(J))
  179 CONTINUE
CALCULATE ENERGY EDIT OR PLOT
  180 DO 181 J=1,51
      EN(J)=BF(J)=0.
  181 CONTINUE
      K=1
      M=I(2)
      FST=VN(1)*EO(1)
      DO 182 J=1,LN
      FSTR=VN(J+1)*EO(J+1)
      FSTM=AM(J)+AM(J+1)
      A=FSTM*V(J)*VO(J)
      B=FST+FSTR
      FST=FSTR
      GW=DR(J)*GR*FSTM
      EN(K)=EN(K)+A
      OCH(K)=OCH(K)+B
      BF(K)=BF(K)+GW
      M=M/100+1
      EDP(M)=EDP(M)+A
      EDT(M)=EDT(M)+B
      BF(M+11)=BF(M+11)+GW
      M=I(J+1)
      IF (RN(J)-RB(K+1)) , ,182
      EN(K)=EN(K)*CF
      OCH(K)=HCCN*OCH(K)
      BF(K)=HCCN*BF(K)
      ENC(K)=EN(K)+OCH(K)+BF(K)
      K=K+1
  182 CONTINUE
      DO 183 N=1,K-1
      EN(K)=EN(K)+EN(N)
      OCH(K)=OCH(K)+OCH(N)
      BF(K)=BF(K)+BF(N)
  183 CONTINUE
      ENC(K)=EN(K)+OCH(K)+BF(K)
      DO 184 M=1,5
      EDP(M)=EDP(M)*CF
      EDT(M)=EDT(M)*HCCN
      BF(M+11)=BF(M+11)*HCCN
      EDP(6)=EDP(6)+EDP(M)
      EDT(6)=EDT(6)+EDT(M)
      BF(17)=BF(17)+BF(M+11)
      EDTL(M)=EDP(M)+EDT(M)+BF(M+11)
  184 CONTINUE
      EDTL(6)=EDP(6)+EDT(6)+BF(17)
      IF (III-1) 188, ,188
      WRITE OUTPUT TAPE 3, 952
      WRITE OUTPUT TAPE 3, 960, (EN(L), OCH(L), BF(L), ENC(L), L=1,K)
      WRITE OUTPUT TAPE 3, 953
      WRITE OUTPUT TAPE 3, 960, (EDP(L), EDT(L), BF(L+11),EDTL(L),L=1,6)
      IF (ETOT) 185, ,185
      ETOT=ENI=EDTL(6)
  185 WRITE OUTPUT TAPE 3, 961, ETOT
      IF (CAVR) , ,186
      WRITE OUTPUT TAPE 3, 962
      GO TO 187
  186 WRITE OUTPUT TAPE 3, 963, CVRC
  187 A=ETOT-EDTL(6)
      IF (A) ,188,
 CHECK ENERGY
      IF (ABSF(A/ETCT)-.5) 188,188,
      OFF=1.
      ITJ=1
      WRITE OUTPUT TAPE 3, 964
 C - DO R PLOT IF TIME
  188 IF (IL-25) , ,190
      IF (TT-RPL(IL)) 190, ,
      IF (CRTI-1.) 189, ,
      CALL CRTID (2HAV,1,0)
      CALL FRAME
      CRTI=0.
  189 CALL RPLOT
      IL=IL+1
 COMPUTE MAX. VALUES FOR PLOT
  190 IF (IRPLOT) 192,192,
      DO 191 J=JN,LN
      DRMX(J)=MAX1F(DRMX(J),DR(J))
      VMX(J)=MAX1F(VMX(J),V(J))
      QMX(J)=MAX1F(GMX(J),Q(J))
      PX(J)=MAX1F(PX(J),P(J))
      A=P(J)-.6666666666*TK(J)
      8=P(J)+1.333333333*TK(J)
      SIGR(J)=MAX1F(SIGR(J),B)
      SIGT(J)=MAX1F(SIGT(J),A)
  191 CONTINUE
  192 RJH=R(LX-1)-V(LX-1)*HDTH
      PJM=P(LX)
 CHECK FOR TERMINATING
      L=1
      IF (OFF) 214, ,213
 CALCULATE DUMP TIME ON 6A (TAPE OR DISK)
      IF (NC-NCD) 193, ,
      K=6
      CALL WRST
      CALL WRTEOF (6)
      CALL BSPACE (6)
      NCD=NCD+1000
  193 IF (ITOT-IPDT-900) 195, ,
      IPDT=ITOT
      IF (DPLOT) 194,194,
      ABF(IBX)=-1000.
      CALL PLTOUT
  194 K=16
      CALL WRST
      BACKSPACE FILE 16
      CALL BSPACE (16)
CHECK FOR PLOT DATA
  195 IF (IIJ-1) 212, ,212
      PTS=PTS+DPLOT
      DO 196 J=JN,LN
      IF (Q(J)) 196,196,
      IF (Q(J)-Q(J-1)) ,196,196
      C=RN(J-1)
      GO TO 197
  196 CONTINUE
      C=0.
  197 N=III=1
      M=0
      DO 203 J=JN,LN
  198 IF (N-25) , ,204
      IF (RN(J)-PLOD(N)) ,200,203
      IF (RN(J-1)-PLOD(N)) 201,199,
      IF (RN(J)+RN(J-1)-2.*PLOD(N)) ,200,200
  199 ING(N)=J-1
      GO TO 202
  200 ING(N)=J
      GO TO 202
  201 ING(N)=0
      N=N+1
      GO TO 198
  202 M=M+1
      N=N+1
  203 CONTINUE
  204 IF (IBX-3815) 208,208,
      K=7*(M+2+IEPLOT)
      IF (IBX-4004+K) 208, ,
C - PLOT BUFFER FULL - WRITE ON 6B
      ABF(IBX)=-1000.
      IF (IPB-10) ,207,207
      BUFFER OUT (7,1) (ABF,ABF(4004))
  205 IF (UNIT,7,K) 205,206, ,
      WRITE OUTPUT TAPE 3, 977
  206 IPB=IPB+1
      IBX=1
      GO TO 208
  207 CALL PLTOUT
      IPB=0
      K=16
      CALL WRST
      BACKSPACE FILE 16
      CALL BSPACE (16)
      CALL FSPACE (16)
      IBX=1
C - STORE PLOT DATA IN BUFFER
  208 ABF(IBX)=-1.
```

```
      ARF(IRX+1)=TT
      ARF(IBX+2)=CAVR
      ARF(IRX+3)=CVRC
      ARF(IBX+4)=C
      ARF(IRX+5)=M
      IRX=IRX+7
      DO 209 N=1,25
      IF (ING(N)) 209,209,
      J=ING(N)
      ARF(IRX-1)=PLOD(N)
      ARF(IRX)=DR(J)
      ARF(IRX+1)=V(J)
      A=TSV(J)
      ARF(IBX+2)=SIGNF(C1(J),A)
      ARF(IBX+3)=AMU(J)
      ARF(IBX+4)=P(J)
      ARF(IBX+5)=TK(J)
      IRX=IRX+7
  209 CONTINUE
      IF (IEPLOT) 211,211,
      ARF(IBX-1)=-100.
      ARF(IBX)=ETOT
      DO 210 N=1,6
      ARF(IBX+1)=EDTL(N)
      IRX=IBX+1
  210 CONTINUE
      IRX=IBX+1
      GO TO 212
  211 ARF(IBX-1)=-10.
  212 IF (ITSTP-20) 14,13,13
  213 L=2
CALCULATE BALANCE OF REAL TIME IN ACCOUNT (NEG. RUNNING TIME) AND RESET
  214 IF (IBANK) 215,215,
      IBANK=IBANK-ITOT
  215 III=2
C - EMPTY PLOT BUFFER ONTO 6B BEFORE TERMINATION.
      IF (DPLOT) 216,216,
      CALL PLTOUT
C - WRITE FINAL DUMP ON 6B
  216 K=16
      CALL WRST
      K=6
      CALL PLOTE
      CALL WRST
      CALL WRTEOF (6)
      CALL UNLOAD (6)
      CALL CLOCK (IC(1),IC(2))
      WRITE OUTPUT TAPE 3, 966, ITOT, IC(1),IC(2)
      WRITE OUTPUT TAPE 3, 967
      CALL OOND3A(3)
      CALL OOND3A(61)
      IF (L-1) ,217,
      READ INPUT TAPE 2, 971, L
      IF (L-8) 217, ,217
C - CALL PLOT
      CALL CHAIN (5,5)
C - UNLOAD TAPES - CALL EXIT - NO PLOT
  217 CALL UNLOAD (16)
      CALL EXIT
CREATE EXIT IF RADIUS NEGATIVE
```

```
  218 WRITE OUTPUT TAPE 3, 968, J-1
      CALL ERROR (1.)
C - TAPE READ ROUTINES
  219 CALL TSTR
      GO TO (221,2,2,2), IJ
  220 CALL TSTR
      GO TO (221,4,4,4), IJ
  221 WRITE OUTPUT TAPE 3, 972
      PRINT 972
      CALL OOND3A(3)
      CALL OOND3A(61)
      CALL EXIT
C     MAIN CODE TAPE SUBROUTINES
      ENTRY TSTO
      CALL BSPACE (K)
      DO 900 M=1,(5-N)
      CALL WRBLNK (K)
  900 CONTINUE
      N=N-1
      RETURN TSTO
      ENTRY WRSO
      N=5
  901 BUFFER OUT (K,1) (DPLOT,IALF)
  902 IF (UNIT,K,M) 902,904, ,
      CALL TSTO
      IF (N-1) 901, ,901
      WRITE OUTPUT TAPE 3, 908, K
      IF (K-6) 903, ,903
      RETURN WRSO
  903 CALL OOND3A(3)
      CALL COND3A(61)
      CALL EXIT
  904 CALL WRTEOF (K)
      RETURN WRSO
      ENTRY WRST
      N=5
  905 BUFFER OUT (K,1) (NC,TTS)
  906 IF (UNIT,K,M) 906,907, ,
      N=N-1
      IF (N-1) 905, ,905
  907 RETURN WRST
      ENTRY TSTR
      CALL BSPACE (L)
      J=J-1
      RETURN TSTR
C     FORMAT STATEMENTS
  908 FORMAT ( 7H1 TAPE ,I3,38H IS BAD, PLEASE REPLACE IT AND RESTART)
  950 FORMAT (8A10)
  951 FORMAT (E7.0,I7,2E7.0)
  952 FORMAT (///35H ENERGY TOTALS PER ORIGINAL REGIONS)
  953 FORMAT (///33H ENERGY TOTALS PER MATERIAL STATE)
  954 FORMAT (60H TAPE 6B AND CARD I.D. ARE NOT THE SAME, PROBLEM TERMIN
     1IATED///22H  TAPE IS FOR PROBLEM ,8A10)
  956 FORMAT (1H1/8H SOC II ,7A10,4A10//, 9H STARTED ,1A8, 4H ON ,1A8/)
  957 FORMAT (1H1/8A10,4A10)
  958 FORMAT (///43H N CYCLE    DELTA T(N)  DELTA T(N+.5)  TIME//1X,I6,
     11X,3E14.5//42H  DELTA T CONTROLLED BY ZONE WITH RADIUS =,E14.5)
  959 FORMAT (///120H   J    DELTA R      RADIUS       VELOCITY    MU
     1      PRESSURE     SHCCK        K R-THETA   K SHOCK      ENERGY      ST
     2ATE//(1X,I4,9E12.5,I7))
```

```
960 FORMAT (//69H   KINETIC ENERGY     INTERNAL ENERGY   GRAVITY
   1     TOTAL ENERGY//(4E18.10))
961 FORMAT (///17H ENERGY INPUT IS ,E18.10)
962 FORMAT (///35H THIS IS A PRESSURE PROFILE PROBLEM)
963 FORMAT (///36H VOLUME WEIGHTED CAVITY PRESSURE IS ,F12.5)
964 FORMAT (18H  BAD ENERGY CHECK/)
966 FORMAT (26H PROBLEM TERMINATED AFTER ,I6,8H SECONDS///13H THE TIME
   1 IS ,1A8,13H THE MACHINE ,1A8)
967 FORMAT (1H1)
968 FORMAT (1H1///19H NEGATIVE R AT J = ,I4,14H CHECK PROBLEM)
971 FORMAT (I1)
972 FORMAT  (65H 3 BAD READS OF 68, CHECK TAPE AND UNIT, THEN RESTART
   1THIS JOB    )
973 FORMAT (60H  ERROR IN THIS PROBLEM.  DO NOT TRY TO CONTINUE OR RES
   1TART.)
974 FORMAT (1H1///47H SLOPE LESS THAN OR EQUAL TO ZERO.  CHECK INPUT//
   1//117H CYCLE DELTA T(N)  DELTA T(N+.5)  J   STATE   P(N+1)
   2SLOPE         MU(N+1)       P(N)          MU(N)          MU MAX//1X,I6,
   32F12.5,2I6,5E13.5,E12.5)
975 FORMAT (1H1///30H MU-E/SLOPE GREATER THAN 1.501///60H       MU-E
   1      SLOPE         MU N+1          PRESSURE    LOC.//4F14.5,I1)
976 FORMAT (1H1///30H MU-C/SLOPE GREATER THAN 1.501///60H       MU-C
   1      SLOPE         MU N+1          PRESSURE          //4F14.5)
977 FORMAT (45H  BAD DISK WRITE, MAY BE SOME BAD PLOT POINTS)
    END
```

```
*       LIST 8
*       CARDS COLUMN
*       FORTRAN                 RPLOT
        SUBROUTINE RPLOT
        USE COMMON
        A=R(JN)
        DO 1 J=JN,LN
        IF (I(J)-390) 1, ,
        B=R(J-1)
        LP=J-1
        GO TO 2
      1 CONTINUE
        B=R(LN)
        LP=LN
      2 YN1=GW=V(J)
        F=S=P(JN)
        AD=AF=TK(JN)
        DA=DB=EO(JN)=P(JN)+1.3333333*TK(JN)
        DC=DD=VO(JN)=P(JN)-.66666667*TK(JN)
        DO 3 J=JN+1,LP
        YN1=MAX1F(YN1,V(J))
        GW=MIN1F(GW,V(J))
        F=MAX1F(F,P(J))
        S=MIN1F(S,P(J))
        AD=MAX1F(AD,TK(J))
        AF=MIN1F(AF,TK(J))
        VO(J)=P(J)-.66666667*TK(J)
        EO(J)=P(J)+1.3333333*TK(J)
        DA=MAX1F(DA,EO(J))
        DB=MIN1F(DB,EO(J))
        DC=MAX1F(DC,VO(J))
        DD=MIN1F(DD,VO(J))
      3 CONTINUE
        K=LP-JN+1
        DO 12 J=1,10,2
        IF (RIX(J)-RIX(J+1)) 12,12,
        CALL SETCH (10.,2.,0,0,0,0)
        GO TO (4,5,6,8,9), J/2+1
      4 WRITE OUTPUT TAPE 100, 450, (IHEAD(N), N=1,8), TT
        L= JN+12020
        GO TO 7
      5 WRITE OUTPUT TAPE 100, 451, (IHEAD(N), N=1,8), TT
        L= JN
        GO TO 7
      6 WRITE OUTPUT TAPE 100, 452, (IHEAD(N), N=1,8), TT
        L=JN+3606
      7 CALL MAPG(B, A, RIX(J+1), RIX(J))
        CALL TRACE (R(JN), P(L), K)
        GO TO 11
      8 WRITE OUTPUT TAPE 100, 453, (IHEAD(N), N=1,8), TT
        L=JN
        GO TO 10
      9 WRITE OUTPUT TAPE 100, 454, (IHEAD(N), N=1,8), TT
        L=JN+8414
     10 CALL MAPG (B, A, RIX(J+1), RIX(J))
        CALL TRACE (R(JN), EO(L), K)
     11 CALL FRAME
     12 CONTINUE
        RETURN
    450 FORMAT (8A10/30H VELOCITY VERSUS RADIUS AT T = ,E12.5)
```

```
451 FORMAT (8A10/30H PRESSURE VERSUS RADIUS AT T = ,E12.5)
452 FORMAT (8A10/31H K-R THETA VERSUS RADIUS AT T = ,E12.5)
453 FORMAT (8A10/30H RADIAL STRESS VERSUS R AT T = ,E12.5)
454 FORMAT (8A10/34H TANGENTIAL STRESS VERSUS R AT T = ,E12.5)
    END
```

```
*       LIST8
*       CARDS COLUMN
*       FORTRAN              PLTO
        SUBROUTINE PLTOUT
        USE COMMON
        CALL REWIND (7)
        BUFFER IN (7,1) (ABA(1),ABA(4004))
        M=4005
        J=1
        DO 7 N=1,IPB
      1 IF (UNIT,7,K) 1,2,,
        WRITE OUTPUT TAPE 3, 901
      2 IF (N-IPB) ,3,3
        BUFFER IN (7,1) (ABA(M),ABA(M+4003))
      3 BUFFER OUT (16,1) (ABA(J),ABA(J+4003))
      4 IF (UNIT,16,K) 4,5,,
        WRITE OUTPUT TAPE 3, 900
      5 IF (N-IPB) ,8,8
        IF (M-1) , ,6
        M=4005
        J=1
        GO TO 7
      6 M=1
        J=4005
      7 CONTINUE
      8 CALL REWIND (7)
        BUFFER OUT (16,1) (ABF(1), ABF(4004))
      9 IF (UNIT,16,K) 9,10,,
        WRITE OUTPUT TAPE 3, 900
     10 CALL WRTEOF (16)
        RETURN
    900 FORMAT (51H BAD TAPE READ/WRITE, PLOT MAY HAVE SOME BAD POINTS)
    901 FORMAT (51H BAD DISK READ/WRITE, PLOT MAY HAVE SOME BAD POINTS)
        END
```

```
*       CARDS COLUMN
*       LIST 8
*       FORTRAN
        SUBROUTINE BANDP (IBA,ITL)
        USE COMMON
C
C       CALL BANDP(A,B)
C       STORES ASCII USER NUMBER IN A(1)
C       STORES NUMBER OF SECONDS IN BANK ACCOUNT IN A(2)  INTEGER
C       STORES TL IN B(1) INTEGER SECONDS
C       STORES PRIORITY IN B(2)  FLOATING PT
C
        COMMON /GOBCOM/ GCOM
        ADDRESS ZETA
        DIMENSION IBA(2), ITL(2)
        ZETA=0
        KIM = (24018.SHL.48).UN.((.LOC.ERROR) .SHL.30) .UN.(.LOC.IBA(1))
        GCOM=(10048.SHL.18).UN.(.LOC.KIM)
        GO TO ZETA
 ERROR  GO TO OK
        GO TO ERROR
  OK    IBA(2) =IBA(2) / 1000000
        KIM =(24038.SHL.48).UN.((.LOC.ERR) .SHL.30 ) .UN.(.LOC.ITL(1))
        GCOM=(10048.SHL.18).UN.(.LOC.KIM)
        GO TO ZETA
  ERR    GO TO THRU
        GO TO ERR
  THRU  ITL(1)= ITL(1) / 1000000
        RETURN
        END
```

```
*       LIST 8
*       CARDS COLUMN
*       FORTRAN               ERROR
        SUBROUTINE ERROR (ERR)
        USE COMMON
        CALL UNLOAD (16)
        CALL UNLOAD (6)
        IF (CRTI) 1, ,1
        CALL PLOTE
      1 IF (ERR) 3,3,
        WRITE OUTPUT TAPE 3, 100, NC, DT, DTH, TT, RADT
        DO 2 J=JN,LN
        I(J)=XSIGNF(I(J),ISV(J))
      2 CONTINUE
        WRITE OUTPUT TAPE 3, 101, (J-1, DR(J), R(J), V(J), AMU(J), P(J),
       1 Q(J), TK(J), QK(J), E(J), I(J), J=JN,LN+1)
      3 CALL COND3A (3)
        CALL COND3A (61)
        CALL EXIT
    100 FORMAT (18H1    ERROR PRINTOUT///43H N CYCLE     DELTA T(N)  DELTA T
       1(N+.5)  TIME///X,I6,1X,3E14.5//42H  DELTA T CONTROLLED BY ZONE WIT
       2H RADIUS =,E14.5)
    101 FORMAT (///120H  J    DELTA R       RADIUS       VELOCITY          MU
       1      PRESSURE     SHOCK         K R-THETA    K SHOCK       ENERGY      ST
       2ATE//(1X,I4,9E12.5,I7))
        END
```

APPENDIX 2. GENERATOR

```
*       LIST 8
*       CARDS COLUMN
*       FORTRAN              GEN
        CLICHE GENCOM
        COMMON NC(2), JN, LN, TT, IR, LX, ENI, RN(1202), HH(8414), IH(8414
      1),   AM(1202), C1(1202), DR(1202), DV(1202), DVO(2404), ISV(1202),
      2 P(1202), Q(1202), GK(1202), TK(1202), VN(1202), VO(1202), AMU(120
      32), E(1202), I(1202), R(1202), V(1202), TC(12), TIC(12), RPL(25),
      4 DT, DTH, DTN, DTPR, FPP, ETOT, FDT, HDT1, IL, IPI, IPO, ITCX,
      5 TRANK, NCD, PJM, PTS, GXT, RJH, STR, SXN, TPR, HDTH, TTS
COMMON CONSTANT FOR RUN
        COMMON DP, IE, IX, IDX(8), GR, DXT, PL(100), GAS(2728), PT(400),
      1 PM(400), PD(400), CP(200), CM(200), CD(200), PK(200), PR(200),
      2 DK(200), SS(200), SP(200), SD(200), AK(10), VI(10), RM(10), AMZ(1
      30), AM1(10), AM2(10), XK(10), PZO(10), P1(10), P2(10), SKQ(10),
      4 B(10), SE(10), EF(10), EV(10), SI(10), IT(10), ITT(10), IP(10),
      5 RB(11), RHO(11), GK(10), CF, CCN, HCCN, IRZ, REZF, IW(4), PPR(61)
      6, TP(61), IVR, IALF
COMMON USED IN GENERATION ONLY
        COMMON ITL(10), IAM(100), DNC, GI(11), EN(11), IZ(11), IES(11),
      1 FNC(11), GL(11), J, K, L, M, N, JJ, INN, ICLK, MACH, A, D, F, G,
      2 IKT(80), IM, IC(9), H(16), HP(40), HM(40), HD(40), HC(20), HCM(20
      3), HCD(20), HE(20), HK(20), HDD(20), HGAM(20), HPRE(20), HDP(20),
      4 HG(10), HGL(10), HGE(64), HGG(640), HGD(640), HGDE(64), ZP(400),
      5 ZM(200),KX, II, NN, NO, MP, IN, AST, JL, LLP, AAA, YY1, YY2, ZZ1,
      6 ZZ2, KL, ZZ, YY, LLG, BA, X, KG, DX, KE, NNN, IS, IV
        EQUIVALENCE (HH,IH)
        EQUIVALENCE (IC(1), IM)
        EQUIVALENCE (NC(2), JN)
        ENDCLICHE
        USE GENCOM
        CALL REGST
        CALL CRTID (2HAV,1)
        CALL FRAME
        N=.LOC.NC
        J=.LOC.KE
        NNN=J-N
        DO 1 IS=1,NNN
        NC(IS)=0
      1 CONTINUE
        CALL CLOCK (ICLK, MACH)
        IVR=IPO=IPI=LN=LX=INN=1
        READ INPUT TAPE 2, 900, (IDX(N), N=1,8), DP, DTPR, F, J, IX, IE,
       1 K, IRZ, L
        READ INPUT TAPE 2, 901, RB(1), TTS, DX, IR, M, A, IV, REZF
        IF (REZF) , ,2
        REZF=.2
      2 IF (IR-J) , ,3
        II=J
        GO TO 4
      3 II=IR
      4 READ INPUT TAPE 2, 902, (RB(N    GK(N), EN(N), IZ(N), IES(N), TC(N)
       1, TIC(N), N=2,II+1)
        IALF=3
        IPO=K+IPO
        RB(1)=RB(1)*100.
        DO 5 N=2,II+1
        RB(N)=RB(N)*100.
        TC(N)=TC(N)*1000.
        TIC(N)=TIC(N)*1000.
```

```
    5 CONTINUE
      DP=DP*1000.
      DTPR=DTPR*1000.
      F=F*1000.
      TTS=TTS*1000.
      DX=DX*1000.
      CCN=4.18879
      HCCN=.5*CCN
      CF=.25*CCN
      QXT=1.
      DTH=1.E-3
      DT=HDT1=.5E-3
      HDTH=FDT=DTN=0.
      DXT=DX*DX*9.
      IF (DP) ,7,
      DO 6 K=1,25,5
      READ INPUT TAPE 2, 903, (C1(N), N=K,K+4)
      IF (C1(K+4)) 7,7,
    6 CONTINUE
    7 IF (F) 11, ,12
      DO 8 K=1,25,5
      READ INPUT TAPE 2, 903,(RPL(N), N=K,K+4)
      IF (RPL(K+4)) 9,9,
    8 CONTINUE
    9 DO 10 K=1,25
      RPL(K)=RPL(K)*1000.
   10 CONTINUE
      GO TO 14
   11 F=TTS/25.
   12 RPL(1)=F
      DO 13 K=2,25
      RPL(K)=RPL(K-1)+F
   13 CONTINUE
   14 CALL ZONER
      K=0
      DO 21 N=1,IR
      R(K+1)=RN(K+1)=RB(N)
      IF (IZ(N+1)) ,15,15
      LN=LN-IZ(N+1)
      GO TO 16
   15 LN=LN+IZ(N+1)
   16 ENC(N+1)=EN(N+1)*4.186E7/(CCN*(RB(N)**IALF-RB(N+1)**IALF))
      DO 20 K=K+1,LN-1
      IF (GL(N+1)) , ,17
      F=RN(K)*RN(K)*RN(K)
      F=F-GI(N+1)
      IF (F-.1) 18,18,
      F=F**.33333333
      RN(K+1)=R(K+1)=F
      GO TO 18
   17 RN(K+1)=R(K+1)=(RN(K)-GI(N+1))
      GI(N+1)=GI(N+1)/GL(N+1)
   18 I(K+1)=IES(N+1)
      E(K+1)=ENC(N+1)
      IF (L) 19, ,19
      AMU(K+1)=GK(N+1)
      GO TO 20
   19 V(K+1)=GK(N+1)
   20 CONTINUE
      K=K-1
   21 CONTINUE
      R(K+1)=RN(K+1)=RB(N)
      IF (DP) ,42,
      NN=IR+1
      K=1
   22 IF (C1(K)) 23,23,
      C1(K)=C1(K)*100.
      K=K+1
      IF (K-25) 22,22,35
   23 IF (IES(NN)-400) 24, ,
      NN=IR
   24 JJ=27-K-NN
      F=RN(1)
      IF (JJ) 25,25,
      G=JJ
      F=(RB(1)-RB(NN))/G
   25 G=PL(1)=RB(NN)
      JJ=26-K
      DO 34 N=1,JJ
      DO 28 II=1,K
      IF (C1(II)) , ,26
      C1(II)=G
      K=K+1
      GO TO 29
   26 IF (G-C1(II)) ,32,28
      NO=K=K+1
   27 C1(NO)=C1(NO-1)
      NO=NO-1
      IF (NO-II) , ,27
      C1(II)=G
      GO TO 29
   28 CONTINUE
   29 IF (K-25) , ,35
      IF (G-RB(NN)) 30, ,30
      NN=NN-1
      G=PL(1)
   30 IF (G+F-RB(NN)) ,32,31
      G=G+F
      GO TO 34
   31 PL(1)=G
      G=RB(NN)
      GO TO 34
   32 F=RN(1)
      NO=27-K-NN+1
      IF (NO) 33,33,
      G=NO
      F=(RB(1)-RB(NN))/G
   33 G=PL(1)=RB(NN)+F
      NN=NN-1
   34 CONTINUE
   35 JJ=25
      NN=1
      IF (C1(JJ)) , ,36
      C1(JJ)=C1(JJ-1)
      C1(JJ-1)=.5*(C1(JJ)-C1(JJ-2))+C1(JJ-2)
   36 DO 39 N=1,LN
      IF (C1(JJ)-RN(N)) 39,37,
      IF (2.*C1(JJ)-RN(N)-RN(N-1)) 37,37,
      PL(NN)=RN(N-1)
      GO TO 38
```

```
37    PL(NN)=RN(N)
38    NN=NN+1
      JJ=JJ-1
      IF (JJ) 40,40,
39    CONTINUE
40    DO 41 JJ=1,25
      C1(JJ)=0.
41    CONTINUE
      F=TTS/DP
      IF (F-9600.) 42,42,
      DP=TTS/9600.
42    LX=LX+LN
      NO=M
      INN=1
      DO 50 N=1,NO
      CALL MATRD
      IF (H(16)-100.) ,43,
      CALL GASRD
      GO TO 48
43    DO 45 K=1,70,3
      READ INPUT TAPE 2, 906, (HG(JJ), HG(JJ+70), JJ=K,K+2)
      DO 44 JJ=K,K+2
      IF (JJ-1) 44,44,
      IF (HG(JJ+70)-HG(JJ+69)) , ,44
      IF (HG(JJ+70)) ,46,
      WRITE OUTPUT TAPE 3, 955, IM
      DNC=1.
      GO TO 48
44    CONTINUE
45    CONTINUE
46    DO 47 K=1,JJ
      IF (HG(K+70)) ,47,
      HG(K+70)=1./(HG(K+70)*H)-1.
      IF (K-1) 47,47,
      F=HG(K+70)-HG(K+69)
      IF (F) ,48,
      HG(K+140)=(HG(K)-HG(K-1))/F
47    CONTINUE
48    DO 49 K=1,1690
      IH(INN)=IC(K)
      INN=INN+1
49    CONTINUE
50    CONTINUE
      II=JJ=NN=MP=1
      DO 66 K=1,IR
      N=IES(K+1)
51    IF (N-100) 52,52,
      N=N-100
      GO TO 51
52    IF (IAM(N)) 64, ,64
      IAM(N)=K
      DO 53 IN=1,M*1690,1690
      IF (IH(IN)-N) ,54,
53    CONTINUE
      WRITE OUTPUT TAPE 3, 957, N
      DNC=1.
      GO TO 66
54    DO 55 NO=1,1690
      IC(NO)=IH(IN)
      IN=IN+1
```

```
 55 CONTINUE
    IN=1
    DO 56 NO=K,K+169,10
    AK(NO)=H(IN)
    IN=IN+1
 56 CONTINUE
    RHO(K+1)=AK(K)
    IF (IES(K+1)-400) , ,57
    IF (IES(K+1)-389) 57,57,
    ENC(K+1)=EF(K)*AK(K)*4.186E-2
 57 IN=1
    DO 58 NO=MP,MP+39
    PT(NO)=HP(IN)
    PM(NO)=HM(IN)
    PD(NO)=HD(IN)
    IN=IN+1
 58 CONTINUE
    IN=1
    DO 59 NO=NN,NN+19
    CP(NO)=HC(IN)
    CM(NO)=HCM(IN)
    CD(NO)=HCD(IN)
    PK(NO)=HE(IN)
    PR(NO)=HK(IN)
    DK(NO)=HDD(IN)
    SS(NO)=HGAM(IN)
    SP(NO)=HPRE(IN)
    SD(NO)=HDP(IN)
    IN=IN+1
 59 CONTINUE
    NO=IN=1
    IF (HG(NO)-HG(NO+1)) ,61,
    DO 60 INN=JJ,JJ+1363
    GAS(INN)=HG(NO)
    NO=NO+1
 60 CONTINUE
    ITT(K)=JJ
    JJ=JJ+1364
    GO TO 62
 61 ITT(K)=0
 62 DO 63 INN=II,II+7
    IKT(INN)=IC(IN+1)
    IN=IN+1
 63 CONTINUE
    IP(K)=MP
    IT(K)=NN
    ITL(K)=II
    MP=MP+40
    NN=NN+20
    II=II+8
    GO TO 66
 64 IN=IAM(N)
    IP(K)=IP(IN)
    IT(K)=IT(IN)
    ITL(K)=ITL(IN)
    ITT(K)=ITT(IN)
    INN=K
    DO 65 NO=IN,IN+169,10
    AK(INN)=AK(NO)
    INN=INN+10
```

```
65 CONTINUE
   RHO(K+1)=AK(K)
   IF (IES(K+1)-400) , ,66
   IF (IES(K+1)-389) 66,66,
   ENC(K+1)=EF(K)*AK(K)*4.186E-2
66 CONTINUE
   N=2
   DO 68 IN=1,LN
   IF (ENC(N)) 67,67,
   E(IN)=ENC(N)
67 IF (RN(IN)-RB(N)) 68, ,68
   N=N+1
68 CONTINUE
   IF (IPO-1) ,72,
   DO 70 N=1,60,4
   READ INPUT TAPE 2, 907, (HH(K), K=1,8)
   K=1
   DO 69 IN=N,N+3
   TP(IN)=HH(K)*1000.
   PPR(IN)=HH(K+1)
   K=K+2
69 CONTINUE
   IF (TP(IN-1)) ,71,
70 CONTINUE
71 IF (TP) ,72,
   TT=TP
72 WRITE OUTPUT TAPE 3, 958, ICLK, MACH
   IF (IRZ) ,73,
   IW(1)=(10HSPHERE     )
   GO TO 74
73 IW(1)=(10HSPHERE NOT)
74 IW(2)=(10H REZONED  )
   IF (IV) ,75,
   IW(3)=(10H HORIZONTA)
   IW(4)=(10HL         )
   GO TO 76
75 IW(3)=(10H VERTICAL )
   IW(4)=(10H          )
76 DO 77 N=2,IR
   IF (IES(N)-389) 77,77,
   IF (IES(N)-400) , ,77
   EN(N)=ENC(N)*(RB(N-1)**IALF-RB(N)**IALF)*CCN/4.186E7
77 CONTINUE
   WRITE OUTPUT TAPE 3, 959, (IDX(N), N=1,8), (IW(N), N=1,4)
   WRITE OUTPUT TAPE 3, 963, (RB(1), TTS, DX, A, REZF)
   IF (L) ,78,
   WRITE OUTPUT TAPE 3, 964
   V(1)=0
   GO TO 79
78 WRITE OUTPUT TAPE 3, 965
   AMU(1)=0
79 WRITE OUTPUT TAPE 3, 966, (RB(N), RHO(N), GK(N), EN(N), ENC(N),
  1 IZ(N), IES(N), GL(N), N=2,IR+1)
   IF (DP) ,80,
   WRITE OUTPUT TAPE 3, 967, DP, (PL(N), N=1,25)
80 WRITE OUTPUT TAPE 3, 995, (RPL(K), K=1,25)
   IL=1
   IF (IX) ,81,
   WRITE OUTPUT TAPE 3, 968
81 IF (IE) ,82,
      WRITE OUTPUT TAPE 3, 969
   82 WRITE OUTPUT TAPE 3, 970, DTPR
      IF (J) 83,83,
      WRITE OUTPUT TAPE 3, 971, (TC(N), TTC(N), N=2,J+1)
   83 DO 164 N=1,100
      AST=0.
      IF (IAM(N)) ,164,
      II=IAM(N)
      K=ITL(II)
      J=JL=IP(II)
      L=IT(II)
      D=AK(II)
      IF (D) , ,84
      DNC=1.
      WRITE OUTPUT TAPE 3, 996, N
   84 IF (PT(J)) , ,85
      J=J+1
      GO TO 84
   85 AK(II)=PD(J)
      DO 88 J=JL,JL+39
      IF (PM(J)) 86, ,86
      IF (J-JL) ,86,
      IF (PM(J-1)) 86, ,
      ZP(J)=0.
      J=J-1
      GO TO 89
   86 F=PM(J)+1.
      IF (F) 87, ,87
      ZP(J)=0.
      GO TO 88
   87 ZP(J)=1./(D*F)
   88 CONTINUE
   89 IF (N-89) 94,94,
      CALL SETCH (10.,2.,0,0,0,0)
      WRITE OUTPUT TAPE 100, 949, (IDX(LLP), LLP=1,8), N
      LLP=J-JL
      CALL MAPGLL (ZP(J), ZP(JL+1), PT(JL+1), PT(J))
      CALL TRACE (ZP(JL+1), PT(JL+1), LLP)
      CALL FRAME
      WRITE OUTPUT TAPE 3, 972, (IKT(J), J=K,K+7), N, D, RM(II), AMZ(II)
     1, PZO(II), EF(II)
      WRITE OUTPUT TAPE 3, 975
      IF (ZP(JL)) 90, ,90
      WRITE OUTPUT TAPE 3, 976, PT(JL), PM(JL), PD(JL)
      GO TO 91
   90 WRITE OUTPUT TAPE 3, 977, PT(JL), ZP(JL), PM(JL),PD(JL)
   91 DO 93 J=JL+1,JL+39
      IF (PD(J)-PD(J-1)) ,92,92
      IF (PD(J)) ,92,
      WRITE OUTPUT TAPE 3, 800, PT(J), ZP(J), PM(J), PD(J)
      AST=1.
      GO TO 93
   92 WRITE OUTPUT TAPE 3, 977, PT(J), ZP(J), PM(J), PD(J)
   93 CONTINUE
      GO TO 138
   94 WRITE OUTPUT TAPE 3, 973, (IKT(J), J=K,K+7), N, D, (AK(J), J=II,
     1 II+149,10)
      IF (PT(JL)-PT(JL+1)) 95, ,
      WRITE OUTPUT TAPE 3, 974
      GO TO 138
```

```
 95 DO 97 J=JL,JL+39
    IF (ZP(J+1)) , ,97
 96 CALL SETCH (10.,2.,0,0,0,0)
    WRITE OUTPUT TAPE 100, 961, (IDX(LLP), LLP=1,8), N
    CALL MAPG (ZP(J), ZP(JL), PT(JL), PT(J))
    LLP=J-JL+1
    CALL TRACE (ZP(JL), PT(JL), LLP)
    CALL FRAME
    GO TO 98
 97 CONTINUE
    J=JL+39
    GO TO 96
 98 IF (CP(L)-CP(L+1)) ,118,118
    DO 99 J=L,L+19
    IF (CP(J)-CP(J+1)) ,100,100
 99 CONTINUE
100 IF (CM(J)-AM2(II)) ,104,104
    WRITE OUTPUT TAPE 3,  951, AM2(II), N, CM(J)
    AM2(II)=CM(J)
    DO 103 LLP=1,IR
    AAA=IES(LLP)
101 IF (AAA-100) 102, ,
    AAA=AAA-100
    GO TO 101
102 IF (AAA-N) 103, ,103
    AM2(LLP)=AM2(II)
103 CONTINUE
104 DO 107 LLP=L,L+39
    IF (PM(LLP)-CM(J)) 107,106,
105 J=J-1
    IF (J-L) , ,104
    WRITE OUTPUT TAPE 3, 950
    DNC=1.
    GO TO 108
106 IF (PT(LLP)-CP(J)) 105,108,105
107 CONTINUE
108 DO 111 J=L,L+19
    IF (CM(J)) 109, ,109
    IF (L-J) ,109,
    IF (CM(J-1)) 109, ,
    ZM(J)=0.
    GO TO 111
109 F=CM(J)+1.
    IF (F) 110, ,110
    ZM(J)=0.
    GO TO 111
110 ZM(J)=1./(D*F)
111 CONTINUE
    CALL SETCH (10.,2.,0,0,0,0)
    WRITE OUTPUT TAPE 100, 952, (IDX(LLP), LLP=1,8), N
    LLP=J
112 IF (PT(LLP)-.04) ,113,113
    LLP=LLP+1
    IF (PT(LLP)) 112, ,112
    LLP=LLP-1
113 MP=LLP
    LLP=L
114 IF (CP(LLP)-.04) , ,115
    LLP=LLP+1
    IF (CP(LLP)) 114, ,114
```

```
      LLP=LLP-1
  115 YY1=MIN1F(ZP(MP), ZM(LLP))
      YY2=MAX1F(ZP(JL), ZM(L))
      ZZ1=MIN1F(PT(JL), CP(L))
      ZZ2=MAX1F(PT(MP), CP(LLP))
      LLP=LLP-L+1
      MP=MP-JL+1
      CALL MAPG (YY1, YY2, ZZ1, ZZ2)
      CALL TRACE (ZP(JL), PT(JL), MP)
      CALL TRACEC (1HC,ZM(L),CP(L),LLP)
      CALL FRAME
      DO 117 J=L,L+19
      IF (ZM(J+1)) , ,117
  116 LLP=J-L+1
      CALL SETCH (10.,2.,0,0,0,0)
      WRITE OUTPUT TAPE 100, 962, (IDX(LLP), LLP=1,8), N
      LLP=J-L+1
      CALL MAPG (ZM(J),ZM(L),CP(L),CP(J))
      CALL TRACE (ZM(L), CP(L), LLP)
      CALL FRAME
      GO TO 125
  117 CONTINUE
      J=L+19
      GO TO 116
  118 CALL FRAME
      IF (PZO(II)) 119, ,119
      DNC=1.
      WRITE OUTPUT TAPE 3, 994, N
  119 IF (EF(II)) 120, ,120
      DNC=1.
      WRITE OUTPUT TAPE 3, 997, N
  120 WRITE OUTPUT TAPE 3, 978
      IF (ZP(JL)) 121, ,121
      WRITE OUTPUT TAPE 3, 976, PT(JL), PM(JL), PD(JL)
      GO TO 122
  121 WRITE OUTPUT TAPE 3, 977, PT(JL), ZP(JL), PM(JL), PD(JL)
  122 DO 124 J=JL+1,JL+39
      IF (PD(J)-PD(J-1)) ,123,123
      IF (PD(J)) ,123,
      WRITE OUTPUT TAPE 3, 800, PT(J), ZP(J), PM(J), PD(J)
      AST=1.
      GO TO 124
  123 WRITE OUTPUT TAPE 3, 977, PT(J), ZP(J), PM(J), PD(J)
  124 CONTINUE
      GO TO 138
  125 IF (PZO(II)) 126, ,126
      DNC=1.
      WRITE OUTPUT TAPE 3, 994, N
  126 IF (EF(II)) 127, ,127
      DNC=1.
      WRITE OUTPUT TAPE 3, 997, N
  127 WRITE OUTPUT TAPE 3, 998
      KL=L
      DO 135 J=JL,JL+19
      IF (J-JL) , ,130
      IF (ZP(J)) 128, ,128
      IF (ZM(KL)) 129, ,129
      WRITE OUTPUT TAPE 3, 981, PT(J), PM(J),PD(J), CP(KL), CM(KL), CD(K
     1L)
      GO TO 135
```

```
128 IF (ZM(KL)) 130, ,130
    WRITE OUTPUT TAPE 3, 999, PT(J), ZP(J), PM(J), PD(J), CP(KL),CM(KL
   1), CD(KL)
    GO TO 135
129 WRITE OUTPUT TAPE 3, 954, PT(J), PM(J), PD(J), CP(KL), ZM(KL),
   1CM(KL), CD(KL)
    GO TO 135
130 IF (PD(J)-PD(J-1)) ,132,132
    IF (PD(J)) ,132,
    IF (CD(KL)-CD(KL-1)) ,131,131
    IF (CD(KL)) ,131,
    WRITE OUTPUT TAPE 3, 801, PT(J), ZP(J), PM(J), PD(J), CP(KL), ZM(
   1 KL), CM(KL), CD(KL)
    AST=1.
    GO TO 134
131 WRITE OUTPUT TAPE 3, 802, PT(J), ZP(J), PM(J), PD(J), CP(KL),
   1 ZM(KL), CM(KL), CD(KL)
    AST=1.
    GO TO 134
132 IF (CD(KL)-CD(KL-1)) ,133,133
    IF (CD(KL)) ,133,
    WRITE OUTPUT TAPE 3, 803, PT(J), ZP(J), PM(J), PD(J), CP(KL),
   1 ZM(KL), CM(KL), CD(KL)
    AST=1.
    GO TO 134
133 WRITE OUTPUT TAPE 3, 993, PT(J), ZP(J), PM(J), PD(J), CP(KL),
   1 ZM(KL), CM(KL), CD(KL)
134 KL=KL+1
135 CONTINUE
    DO 137 J=JL+20,JL+39
    IF (PD(J)-PD(J-1)) ,136,136
    IF (PD(J)) ,136,
    WRITE OUTPUT TAPE 3, 800, PT(J), ZP(J), PM(J), PD(J)
    AST=1.
    GO TO 137
136 WRITE OUTPUT TAPE 3, 977, PT(J), ZP(J), PM(J), PD(J)
137 CONTINUE
138 IF (AST-1.) 139, ,
    WRITE OUTPUT TAPE 3, 804
139 WRITE OUTPUT TAPE 3, 1000
    IF (PR(L)-PR(L+1)) ,145,145
    WRITE OUTPUT TAPE 3, 980
    DK(L)=0.
    WRITE OUTPUT TAPE 3, 982, (PK(J), PR(J), DK(J), J=L,L+19)
    YY=ZZ=PK(L)
    DO 143 J=L+1,L+19
    YY=MIN1F(YY,PK(J))
    ZZ=MAX1F(ZZ,PK(J))
    IF (PR(J)) 143, ,143
    IF (PR(J+1)) 143, ,143
    J=J-1
140 IF (YY-ZZ) ,146,
    CALL SETCH (10.,2.,0,0,0,0)
    WRITE OUTPUT TAPE 100, 953, (IDX(LLP), LLP=1,8), N
    LLP=J-L+1
    YY1=PR(L)
    IF (PK(L)-PK(L+1)) 141, ,141
    YY1=PR(L+1)-(PR(L+1)-PR(L))/100.
141 ZZ1=PR(J)
    IF (PK(J-1)-PK(J)) 142, ,142
```

```
      ZZ1=PR(J-1)+(PR(J)-PR(J-1))/100.
  142 CALL MAPG (YY1, ZZ1, YY, ZZ)
      CALL TRACE (PR(L), PK(L), LLP)
      GO TO 144
  143 CONTINUE
      J=L+19
      GO TO 140
  144 K=K+1
      GO TO 146
  145 WRITE OUTPUT TAPE 3, 983
  146 IF (SP(L)-SP(L+1)) 147, ,
      CALL FRAME
      GO TO 151
  147 IF (K) 148, ,148
      WRITE OUTPUT TAPE 3, 1000
  148 WRITE OUTPUT TAPE 3, 984, (SS(J), SP(J), SD(J), J=L,L+19)
      IF (YY-ZZ) ,147,
      DO 150 J=L+1,L+19
      IF (SP(J)) 150, ,150
      IF (SP(J+1)) 150, ,150
      J=J-1
  149 LLP=J-L+1
      CALL TRACEC (1HC,SP(L),SS(L),LLP)
      CALL FRAME
      GO TO 151
  150 CONTINUE
      J=L+19
      GO TO 149
  151 L=ITT(II)
      IF (L) 157,157,
      IF (SI(II)-100.) 158, ,158
      WRITE OUTPUT TAPE 3, 985, D
      DO 154 J=L,L+69
      IF (GAS(J+70)) 152, ,152
      IF (GAS(J+71)) 152, ,152
      HG(J)=GAS(J)=GAS(J+140)=0.
      GO TO 154
  152 F=GAS(J+70)+1.
      IF (F) 153, ,153
      HG(J)=0.
      WRITE OUTPUT TAPE 3, 976, GAS(J), GAS(J+70), GAS(J+140)
      GO TO 154
  153 HG(J)=1./(D*F)
      WRITE OUTPUT TAPE 3, 977, GAS(J), HG(J), GAS(J+70), GAS(J+140)
  154 CONTINUE
      DO 156 J=L,L+69
      IF (GAS(J+1)) , ,156
  155 CALL SETCH (10.,2.,0,0,0,0)
      WRITE OUTPUT TAPE 100, 956, (IDX(LLP), LLP=1,8), N
      LLP=J-L+1
      CALL MAPGLL (GAS(J),GAS(L),HG(L),HG(J))
      CALL TRACE (GAS(L), HG(L), LLP)
      CALL FRAME
      GO TO 164
  156 CONTINUE
      J=L+69
      GO TO 155
  157 WRITE OUTPUT TAPE 3, 986
      GO TO 164
  158 WRITE OUTPUT TAPE 3, 987, N
```

```
      WRITE OUTPUT TAPE 3, 988, (GAS(J), J=L,L+9), (GAS(J), J=L+10,L+19)
      WRITE OUTPUT TAPE 3, 989, (GAS(J),GAS(J+64),GAS(J+128),GAS(J+192),
     1GAS(J+256),GAS(J+320),GAS(J+384),GAS(J+448),GAS(J+512),GAS(J+576),
     2GAS(J+640), J=L+20,L+83)
      F=GAS(L+84)
      DO 159 J=L+85,L+639
      IF (GAS(J)) 159,159,
      F=MIN1F(F,GAS(J))
  159 CONTINUE
      CALL MAPGSL (F,5.,GAS(L+20),10000.)
      J=0
      DO 160 LLP=L+20,L+83
      IF (GAS(LLP)) 161,161,
      J=J+1
  160 CONTINUE
      J=64
  161 DO 162 LLP=L,L+9
      IF (GAS(LLP)) 163,163,
      LLG=(LLP-L+1)*64+20+L
      CALL TRACE (GAS(LLG), GAS(L+20), J)
  162 CONTINUE
  163 CALL SETCH (10.,2.,0,0,0,0)
      WRITE OUTPUT TAPE 100, 960, (IDX(J), J=1,8), N
      CALL FRAME
  164 CONTINUE
      CALL PLOTE
      IF (IPO-2) 167,165,
      IF (IPO-3) , ,167
      WRITE OUTPUT TAPE 3, 990
      GO TO 166
  165 WRITE OUTPUT TAPE 3, 991
  166 WRITE OUTPUT TAPE 3, 992, (TP(N), PPR(N), N=1,60)
  167 DO 172 N=1,IR
      L=LLP=IP(N)+1
  168 IF (PT(L)) , ,169
      L=L+1
      GO TO 168
  169 AK(N)=PD(L)
      DO 170 L=LLP,LLP+38
      IF (PM(L)-AM1(N)) 170, ,
      GL(N)=PD(L)
      GO TO 171
  170 CONTINUE
      GL(N)=PD(L)
  171 GK(N)=0.
      IF (IES(N+1)-389) , ,172
      SF(N)=1.5*(1.-2.*SF(N))/(1.+SE(N))
  172 CONTINUE
      CALL INIT
C     FORMAT STATEMENTS RELATING TO READING TAPE 2
  800 FORMAT (2X, 4E14.5,1H*)
  801 FORMAT (2X, 2(4E14.5, 1H*))
  802 FORMAT (2X, 4E14.5,1H*, 4F14.5)
  803 FORMAT (2X, 4E14.5, 1X, 4F14.5,1H*)
  804 FORMAT (57H * - DENOTES PHASE CHANGE IN LOADING AND UNLOADING CURV
     1ES)
  900 FORMAT (8A10/3E9.0,I2,2(2X,I1),1X,I1,6X,I1,11X,I1)
  901 FORMAT (3E9.0,I2,2X,I2,3X,F7.0,I1,6X,E6.0)
  902 FORMAT (2E9.0,E8.0,I5,I3,2X,2E7.0)
  903 FORMAT (5E10.0)
```

```
 906 FORMAT (6E12.5)
 907 FORMAT (8E7.0)
C       FORMAT STATEMENTS RELATING TO OUTPUT ON TAPE 3
 949 FORMAT (28X,8A10,/35X,37H H.E.  P VERSUS V         FOR MATERIAL ,I3)
 950 FORMAT (///68H THE LOADING AND UNLOADING TABLES DO NOT MERGE. CORR
    1ECT AND RESTART.)
 951 FORMAT (////13H  THE MU-2 = ,E12.5,14H FOR MATERIAL ,I2,29H BUT TH
    1E LAST TABLE ENTRY IS ,E12.5,24H THE CODE HAS CHANGED IT)
 952 FORMAT (28X,8A10,/35X,49HP VERSUS V LOADING AND UNLOADING    FOR M
    1ATERIAL ,I2)
 953 FORMAT (28X,8A10,/35X,49HK VERSUS P CONSOLIDATED AND CRUSHED FOR M
    1ATERIAL ,I2)
 954 FORMAT (2X,E14.5,14H     INFINITE  ,6E14.5)
 955 FORMAT (32H P-V GAS TABLE OUT OF ORDER FOR ,I3)
 956 FORMAT (28X,8A10,/35X,29H P VERSUS V GAS FOR MATERIAL ,I2)
 957 FORMAT (22H NO DATA FOR MATERIAL , I3,32H CAN BE LOCATED.  INPUT E
    1RROR    )
 958 FORMAT (34H1      SOC GENERATOR        STARTED , 1A8, 4H ON , 1A8//)
 959 FORMAT (8A10,4A10)
 960 FORMAT (28X,8A10,/35X,45H E IN 10**12 ERGS/GM VS GAMMA-1 FOR MATER
    1IAL ,I2)
 961 FORMAT (28X,8A10,/35X,37HP VERSUS V LOADING         FOR MATERIAL ,I2)
 962 FORMAT (28X,8A10,/35X,37HP VERSUS V UNLOADING       FOR MATERIAL ,I2)
 963 FORMAT (//90H     OUTER RADIUS     STOP TIME       DT MAX       OVERBU
    1RDEN  REZONE FACTOR                       //4X,4(E12.5,2X),E12.5)
 964 FORMAT(//105H     INNER RADII      RHO ZERO      VELOCITY     ENERGY (
    1KT)     ENERGY (DEN)    N    EOS       RADIUS FACTOR      )
 965 FORMAT(//105H     INNER RADII      RHO ZERO     MU ZERO       ENERGY (
    1KT)     ENERGY (DEN)    N    EOS       RADIUS FACTOR      )
 966 FORMAT (1X,5E14.5,I6,I5,E18.5)
 967 FORMAT (///35H PLOT AGAINST TIME AT INTERVALS OF ,E12.5,24H FOR TH
    1E FOLLOWING RADII//(5E14.5))
 968 FORMAT (///17H PLOT PEAK VALUES)
 969 FORMAT (///17H PLOT EDIT VALUES)
 970 FORMAT (//23H INITIAL DELTA PRINT = ,E12.5////)
 971 FORMAT (46H      CHANGE TIME   NEW POINT AND EDIT INTERVAL/(E16.5,
    1E25.5))
 972 FORMAT (1H1/8A10//10H MATERIAL ,I3//82H         RHO ZERO       D
    1        MU (C.J.)      P (C.J.)        E (ZERO)             /(2X,5E14.5
    2))
 973 FORMAT (1H1/8A10//10H MATERIAL ,I3//114H        RHO ZERO       K
    1   VISCOSITY        R M            MU - 0       MU - 1        MU - 2
    2   GAMMA                  /2X,8E13.5/114H      P - 0         P - 1
    3   P - 2         GAMMA SLOPE GAMMA CONST.  SIGMA            EF
    4   EV                 /2X,8E13.5)
 974 FORMAT (///33H NO P-MU TABLES FOR THIS MATERIAL)
 975 FORMAT (//20H          H. E. CURVE //58H            P              V
    1          MU              DP/DMU)
 976 FORMAT (2X,E14.5,14H     INFINITE  ,2E14.5)
 977 FORMAT (2X, 4E14.5)
 978 FORMAT (//20H        LOADING CURVE//58H             P              V
    1          MU              DP/DMU)
 979 FORMAT (///30H UNLOADING TABLE FOR MATERIAL ,I3/57H          P
    1       V                 MU              DP/DMU)
 980 FORMAT (//24H  CONSOLIDATED K-P TABLE//42H          K
    1P             DK/DP/)
 981 FORMAT (2X,E14.5,14H     INFINITE  ,3E14.5,14H     INFINITE  ,2E14.5
    1)
 982 FORMAT (2X, 3E14.5)
 983 FORMAT (/36H NO K PSI=1 TABLES FOR THIS MATERIAL)
 984 FORMAT (///19H  CRUSHED K-P TABLE//39H       K             P
    1      DK/DP//(2X,3E14.5))
 985 FORMAT (74H1       P           V              MU         DP/DMU
    1 MU FOR DENSITY OF ,E14.5//)
 986 FORMAT (///32H NO GAS TABLES FOR THIS MATERIAL)
 987 FORMAT (28H1   GAS TABLES FOR MATERIAL , I3/)
 988 FORMAT (/118H            RHO 1      RHO 2      RHO 3      RHO 4
    1    RHO 5     RHO 6      RHO 7      RHO 8      RHO 9      RHO 10/
    210X,10E11.4/118H           LOG RHO    LOG RHO    LOG RHO    LOG R
    3HO    LOG RHO   LOG RHO    LOG RHO    LOG RHO    LOG RHO    LOG R
    4HO/10X,10E11.4)
 989 FORMAT (/118H  ENERGY   GAMMA-1    GAMMA-1    GAMMA-1    GAMMA-1
    1   GAMMA-1    GAMMA-1   GAMMA-1    GAMMA-1    GAMMA-1    GAMMA-1/
    2(F10.3,10E11.4))
 990 FORMAT (24H1 OUTER PRESSURE PROFILE//)
 991 FORMAT (24H1 INNER PRESSURE PROFILE//)
 992 FORMAT (24H        TIME          P/(2E14.5))
 993 FORMAT (2X, 4E14.5, 1X, 4E14.5)
 994 FORMAT(/26H  P-ZERO IS 0 FOR MATERIAL, I2,20H CORRECT AND RESTART)
 995 FORMAT(/54H  INTERVALS AT WHICH PLOTS VERSUS RADIUS WILL BE TAKEN/
    1 //(5E14.5))
 996 FORMAT (/42H  RHO IS LESS THAN OR = TO 0 FOR MATERIAL ,I2,24H
    1CORRECT AND RESTART)
 997 FORMAT(/25H  EF IS ZERO FOR MATERIAL, I2, 20H CORRECT AND RESTART)
 998 FORMAT (///93H                LOADING CURVE
    1                         UNLOADING CURVE//109H       P
    2   V            MU         DP/DMU          P            V
    3     MU          DP/DMU)
 999 FORMAT (2X,5E14.5,14H    INFINITE  ,2E14.5)
1000 FORMAT (1H1)
     END
```

```
*       LIST 8
*       CARDS COLUMN
*       FORTRAN                 INIT
        SUBROUTINE INIT
        USE GENCOM
        L=J=2
        IF (IV) 3, ,3
        GR=.98E-9
        IF (I(2)-300) , ,5
        P(1)=0.
        P(2)=P(1)+.5*GR*RHO(2)*(R(1)-R(2))
        J=3
      1 IF (I(J)-300) , ,5
        P(J)=RHO(L)*(RN(J-2)-RN(J-1))
        IF (RN(J)-RB(L)) , ,2
        L=L+1
      2 P(J)=P(J-1)+.5*GR*(P(J)+RHO(L)*(RN(J-1)-RN(J)))
        J=J+1
        IF (J-LN) 1,1,5
      3 IF (A) ,6,
        J=1
        A=1.E-6*A
      4 IF (I(J)-300) , ,5
        P(J)=A
        J=J+1
        IF (I(J)) ,5,
        IF (J-LN) 4,4,
      5 J=L=2
      6 IF (I(J)-389) , ,10
        N=IP(L-1)+1
        DO 8 K=N,N+39
        IF (P(J)-PT(K)) , ,7
        AMU(J)=PM(K)+(P(J)-PT(K))/PD(K)
        GO TO 28
      7 IF (PT(K+1)-PT(K)) 9,9,
      8 CONTINUE
        K=N+39
      9 AMU(J)=PM(K)+(P(J)-PT(K))/PD(K)
        GO TO 28
     10 IF (I(J)-400) , ,11
        AMU(LX-1)=AMZ(L-1)
        GO TO 30
     11 IF (E(J)) ,28,
        N=ITT(L-1)
        IF (SI(L-1)-100.) 16, ,16
        DO 15 K=N,N+69
        IF (AMU(J)-GAS(K+70)) 14, ,12
        P(J)=GAS(K)
        GO TO 28
     12 IF (K-N)  ,13,
        K=K-1
     13 P(J)=GAS(K)+(AMU(J)-GAS(K+70))*GAS(K+141)
        GO TO 28
     14 IF (GAS(K+1)) , ,15
        P(J)=GAS(K)+(AMU(J)-GAS(K+70))*GAS(K+140)
        GO TO 28
     15 CONTINUE
        GO TO 28
     16 A=E(J)/RHO(L)
        BA=(AMU(J)+1.)*RHO(L)
      X=LOGF(BA)
      DO 24 K=N,N+9
      IF (GAS(K)-BA) 23, ,
   17 NN=(K-N+1)*64+20+N
      DO 21 II=N+20,N+83
      IF (GAS(II)-A) 20,18,
      IF (II-N-20) , ,19
   18 A=GAS(NN)
      BA=GAS(NN-64)
      GO TO 22
   19 A=A-GAS(II-1)
      BA=GAS(NN-65)+A*GAS(NN+576)
      A=GAS(NN-1)+A*GAS(NN+640)
      GO TO 22
   20 IF (GAS(II+1)) 18,18,
      NN=NN+1
   21 CONTINUE
      X=.67
      GO TO 27
   22 IF (K-N) 26, ,26
      X=A
      GO TO 27
   23 IF (GAS(K+1)-GAS(K)) 25,25,
   24 CONTINUE
      K=N+9
   25 N=K
      GO TO 17
   26 X=BA+(A-BA)*(X-GAS(K+9))/(GAS(K+10)-GAS(K+9))
   27 P(J)=X*E(J)*(AMU(J)+1.)
   28 IF (RN(J)-RB(L)) , ,29
      L=L+1
   29 J=J+1
      IF (J-LN) 6,6,
   30 DO 31 J=2,LN
      A=RN(J-1)+RN(J)
      DV(J)=(RN(J-1)-RN(J))*(A*A-RN(J-1)*RN(J))
      DVO(J)=AMU(J)*DV(J)
      VN(J)=DVO(J)+DV(J)
      DV(J)=0.
      IF (I(J)-100) 31,31,
      ISV(J)=-1
      DR(J)=0.
   31 CONTINUE
      N=2
      AM=AM(LX)=0.
      DO 32 J=2,LN
      AM(J)=RHO(N)*VN(J)
      IF (RB(N)-RN(J)) 32, ,32
      N=N+1
   32 CONTINUE
      WRITE OUTPUT TAPE 3, 993, (IDX(N), N=1,8), (IW(N), N=1,4), ((J-1),
     1 RN(J), AM(J), VN(J), DVO(J), AMU(J), P(J), E(J), I(J), J=1,LX)
      JN=IR=1
      TPR=DTPR
      DO 33 J=1,8414
      HH(J)=0.
   33 CONTINUE
      J=K=1
      DO 35 N=1,LN
      IF (RN(N)-PL(J)) 34, ,34
      PL(J+25)=AK(K)
      PL(J+50)=SE(K)*AK(K)
      PL(J+75)=RHO(K+1)
      J=J+1
      IF (J-25) , ,36
   34 IF (RN(N)-RB(K+1)) 35, ,35
      K=K+1
   35 CONTINUE
      RJH=R(LX-1)
      PJM=P(LX)
   36 CALL REWIND (16)
      N=5
   37 BUFFER OUT (16,1) (DP,IALF)
   38 IF (UNIT,16,K) 38,40, ,
      CALL TCSTO
      GO TO (39,37,37,37), N
   39 WRITE OUTPUT TAPE 3, 994
      PRINT 994
      CALL UNLOAD (16)
      CALL CLOCK (K,L)
      WRITE OUTPUT TAPE 3, 995, K, L
      CALL OOND3A(61)
      CALL OOND3A(3)
      CALL EXIT
   40 CALL WRTEOF (16)
      N=5
   41 BUFFER OUT (16,1) (DNC,TTS)
   42 IF (UNIT,16,K) 42,43, ,
      CALL TCSTO
      GO TO (39,41,41,41), N
   43 IF (DNC-1.) ,44,
      WRITE OUTPUT TAPE 3, 999
      PRINT 999
      GO TO 45
   44 WRITE OUTPUT TAPE 3, 997
      PRINT 997
   45 CALL UNLOAD (16)
      CALL OOND3A(3)
      CALL OOND3A(61)
      CALL EXIT
      ENTRY TCSTO
      CALL BSPACE (16)
      DO 46 K=1,6-N
      CALL WRBLNK (16)
   46 CONTINUE
      N=N-1
      RETURN TCSTO
  908 FORMAT (I1)
  993 FORMAT (24H1     OVERBURDEN PRINTOUT///,8A10,4A10///110H     J     R-ZE
     1RO          MASS              VOLUME           DELTA V           MU
     2PRESSURE        ENERGY            STATE/(1X,I4,7E14.7,I7))
  994 FORMAT (38H 6B IS NOT GOOD, REPLACE IT AND HIT GO)
  995 FORMAT (15H TAPE 6B BAD AT,1A8,4H ON ,1A6)
  996 FORMAT (20H TAPE 6B REPLACED AT,1A8,4H ON ,1A6)
  997 FORMAT (50H1 ERROR IN GENERATOR INPUT, CORRECT AND REGENERATE)
  999 FORMAT (20H GENERATION COMPLETE)
 1000 FORMAT (1H1)
      END
*     LIST 8
*     CARDS COLUMN
*        FORTRAN             MATRD
         SUBROUTINE MATRD
         USE GENCOM
         READ INPUT TAPE 2, 904, (IC(K), K=2,9), IM, (H(K), K=1,7)
         READ INPUT TAPE 2, 905, (H(K), K=8,16)
         DO 1 K=1,40,4
         READ INPUT TAPE 2, 906, (HP(IN), HM(IN), IN=K,K+3)
         IF (HP(K+3)) , ,1
         IF (HP(K+2)) 1,2,2
       1 CONTINUE
       2 DO 8 IN=1,40
         IF (IN-1) 4, ,4
         HD(IN)=0.
         IF (HM(IN+1)-HM(IN)) ,8,8
         DO 3 K=1,40
         IF (HM(K)) ,8,
         HM(K)=1./(HM(K)*H)-1.
         IF (ABSF(HM(K))-1.E-5) , ,3
         HM(K)=0.
       3 CONTINUE
         GO TO 8
       4 F=HM(IN)-HM(IN-1)
         IF (F) ,5,7
         IF (HP(IN)) ,5,
         WRITE OUTPUT TAPE 3, 951, IM
         DNC=1.
       5 DO 6 K=IN,40
         HP(K)=HM(K)=HD(K)=0.
       6 CONTINUE
         GO TO 9
       7 HD(IN)=(HP(IN)-HP(IN-1))/F
       8 CONTINUE
       9 DO 10 K=1,20,4
         READ INPUT TAPE 2, 906, (HC(IN), HCM(IN), IN=K,K+3)
         IF (HC(K+3)) 11,11,
      10 CONTINUE
      11 IF (HCM(1)-HCM(2)) 13, ,13
         DO 12 K=1,60
         HC(K)=0.
      12 CONTINUE
         GO TO 20
      13 DO 19 K=1,20
         IF (K-1) 15, ,15
         HCD(K)=0.
         IF (HCM(K+1)-HCM(K)) ,19,19
         DO 14 IN=1,20
         IF (HCM(IN)) ,19,
         HCM(IN)=1./(HCM(IN)*H)-1.
         IF (ABSF(HCM(IN))-1.E-5) , ,14
         HCM(IN)=0.
      14 CONTINUE
         GO TO 19
      15 F=HCM(K)-HCM(K-1)
         IF (F) ,16,18
         IF (HC(K)) ,16,
         WRITE OUTPUT TAPE 3, 952, IM
         DNC=1.
      16 DO 17 IN=K,20
         HC(IN)=HCM(IN)=HCD(IN)=0.
      17 CONTINUE
      GO TO 20
   18 HCD(K)=(HC(K)-HC(K-1))/F
   19 CONTINUE
   20 DO 25 K=1,20,4
      READ INPUT TAPE 2, 906, (HE(IN), HK(IN), IN=K,K+3)
      DO 24 IN=K,K+3
      IF (IN-1) ,24,
      HDD(IN)=0.
      F=HK(IN)-HK(IN-1)
      IF (F) ,21,23
      IF (HK(IN)) ,21,
      WRITE OUTPUT TAPE 3, 953, IM
      DNC=1.
   21 DO 22 K=IN,20
      HE(K)=HK(K)=HDD(K)=0.
   22 CONTINUE
      GO TO 26
   23 HDD(IN)=(HE(IN)-HE(IN-1))/F
   24 CONTINUE
   25 CONTINUE
   26 DO 31 K=1,20,4
      READ INPUT TAPE 2, 906, (HGAM(IN), HPRE(IN), IN=K,K+3)
      DO 30 IN=K,K+3
      IF (IN-1) ,30,
      HDP(IN)=0.
      F=HPRE(IN)-HPRE(IN-1)
      IF (F) ,27,29
      IF (HPRE(IN)) ,27,
      WRITE OUTPUT TAPE 3, 954, IM
      DNC=1.
   27 DO 28 K=IN,20
      HPRE(K)=HGAM(K)=HDP(K)=0.
   28 CONTINUE
      GO TO 32
   29 HDP(IN)=(HGAM(IN)-HGAM(IN-1))/F
   30 CONTINUE
   31 CONTINUE
   32 RETURN
  904 FORMAT (8A10/I2,2E8.0,2E7.0,3E8.0)
  905 FORMAT (9E7.0)
  906 FORMAT (8E7.0)
  951 FORMAT (///40H THERE IS A MU OUT OF ORDER IN MATERIAL ,I3,14H LOAD
     1ING CURVE)
  952 FORMAT (///40H THERE IS A MU OUT OF ORDER IN MATERIAL ,I3,16H UNLO
     1ADING CURVE)
  953 FORMAT (///71H A PRESSURE IS OUT OF ORDER IN THE CONSOLIDATED K-P
     1 TABLE FOR MATERIAL ,I3)
  954 FORMAT (///65H A PRESSURE IS OUT OF ORDER IN THE CRUSHED K-P TABLE
     1 FOR MATERIAL ,I3)
      END
*     LIST 8
*     CARDS COLUMN
*     FORTRAN             ZONER
      SUBROUTINE ZONER
      USE GENCOM
      K=IR+1
      DO 1 IN=1,11
      GT(IN)=0.
      GL(IN)=1.
    1 CONTINUE
```

```
      IZ(1)=IES(1)=0
      DO 14 INN=1,IR+1
      IF (IZ(K)) 3,2,
      F=IZ(K)
      GI(K)=(RB(K-1)-RB(K))/F
      GL(K)=1.
      IF (IZ(K-1)) ,13,13
      K=K-1
      GL(K)=1.001
      CALL FINDR
      GO TO 13
    2 IF (GI(K+1)) 20,20,
      G=RB(K-1)-RB(K)
      F=G/GI(K+1)
      IZ(K)=F
      F=IZ(K)
      GI(K)=G/F
      GL(K)=1.
      GO TO 13
    3 NO=K-1
      IF (IZ(K)+1) 7, ,20
      IF (NO-1) 20,5,
      DO 4 IN=1,K-1
      IF (IZ(NO)) ,5,6
      NO=NO-1
    4 CONTINUE
      GO TO 20
    5 F=LOGF(1.+.05*(RB(NO)-RB(NO+1))/GI(NO+2))
      F=F/LOGF(1.05)+1.
      IZ(NO+1)=-F
      GL(K)=1.05
      CALL FINDR
      GO TO 13
    6 F=IZ(NO)
      GI(NO)=GI(NO+1)=((RB(NO-1)-RB(NO))/F)
      GL(NO)=1.
    7 DO 12 IN=NO+1,K
      IF (IZ(IN)) 8, ,20
      G=RB(IN-1)-RB(IN)
      F=G/GI(IN)
      IZ(IN)=F
      F=IZ(IN)
      GI(IN)=GI(IN+1)=G/F
      GL(IN)=1.
      GO TO 12
    8 GL(K)=1.001
      IF (IES(IN)-400) , ,11
      IF (I7(IN)+1) 10, ,20
      F=RB(IN-1)-RB(IN)+GI(IN+1)
      IF (GI(IN+1)) , ,9
      F=LOGF(GI(IN-1)/(1.05*GI(IN-1)-.05*(F+GI(IN-1))))/LOGF(1.05)+1.
      IZ(IN)=-F
      GL(IN)=1.05
      CALL FINDR
      GO TO 12
    9 GL(IN)=(F-GI(IN+1))/(F-GI(IN-1))
      F=LOGF(GI(IN-1)/GI(IN+1))/LOGF(GL(IN))+1.
      IZ(IN)=-F
   10 CALL FINDR
      GO TO 12
   11 IF (IZ(IN)+1) 10, ,20
      X=(RB(IN-1)+GI(IN-1))**IALF
      F=RB(IN-1)**IALF
      X=F/(X-F)+1.
      IZ(IN)=-X
      X=-IZ(IN)
      GL(IN)=0.
      GI(IN)=F/X
   12 CONTINUE
      K=NO
   13 IF (K-1) 15, ,
      IF (GI(K)) 14,14,
      K=K-1
      GO TO 13
   14 CONTINUE
   15 NO=0
      DO 19 K=2,10
      IF (RB(K-1)) 19,19,
      NO=XABSF(IZ(K))+NO
      IF (IZ(K)-1) 19, ,19
      IF (IES(K)-IES(K-1)) ,16,
      IF (IES(K)-IES(K+1)) 19, ,19
      IZ(K+1)=IZ(K+1)-1
      NO=NO-1
      RB(K+1)=RB(K)
      GI(K+1)=GI(K)
      IN=K
      GO TO 17
   16 IZ(K)=IZ(K-1)-1
      GL(K)=GL(K-1)
      GI(K)=GI(K-1)
      IN=K-1
   17 DO 18 JJ=IN,IR+1
      RB(JJ)=RB(JJ+1)
      RHO(JJ)=RHO(JJ+1)
      EN(JJ)=EN(JJ+1)
      IZ(JJ)=IZ(JJ+1)
      IES(JJ)=IES(JJ+1)
      GK(JJ)=GK(JJ+1)
      GI(JJ)=GI(JJ+1)
      GL(JJ)=GL(JJ+1)
   18 CONTINUE
      IR=IR-1
      IF (K-IR-1) 19, ,
      IF (NO-1200) , ,21
      RETURN
   19 CONTINUE
      IF (NO-1200) , ,21
      RETURN
   20 DNC=1.
      WRITE OUTPUT TAPE 3, 951
      RETURN
   21 DNC=1.
      WRITE OUTPUT TAPE 3, 952, NO
      RETURN
  951 FORMAT (33H ZONING ERROR - NO SPECIFIED SIZE)
  952 FORMAT (I5,53H ZONES CALCULATED, MAX. NO. IS 1200, FIX AND RESUBMI
     1T)
      END
*     LIST 8
*       FORTRAN              FINDR
        SUBROUTINE FINDR
        USE GENCOM
        IF (IES(K)-400) , ,1
        F=RB(K-1)-RB(K)+GI(K+1)
        G=GI(K+1)
        GO TO 2
      1 F=RB(K-2)-RB(K)
        GI(K)=GI(K-1)=G=RB(K-2)-RB(K-1)
      2 JJ=-IZ(K)+1
        IVR=2
        DV(2)=JJ
        DV(3)=LOGF(F/G)
        DV(4)=GL(K)
        DV(5)=G/F
        DO 3 JJ=1,1000
        GL(K)=EXPF((DV(3)+LOGF(DV(4)-1.+DV(5)))/DV(2))
        IF (ABSF(GL(K)-DV(4))-1.E-7) 4,4,
        DV(4)=GL(K)
      3 CONTINUE
        IZ(K)=-IZ(K)
        GL(K)=1.
        F=IZ(K)
        GI(K)=(RB(K-1)-RB(K))/F
        RETURN
      4 IF (IES(K)-400) 5, ,
        GL(K)=1./GL(K)
        RETURN
      5 IF (GL(K)-1.1) 6,6,
        WRITE OUTPUT TAPE 3, 950, GL(K)
        DNC=1.
      6 GI(K)=((RB(K-1)-RB(K)+GI(K+1))*(GL(K)-1.)+GI(K+1))/GL(K)
        RETURN
    950 FORMAT (92H   THE R CALCULATED IS GREATER THAN 1.1, EXECUTION OF T
       1HIS PROBLEM DELETED, CHECK INPUT - R=,E12.5)
        END
```

```
*       CARDS COLUMN
*       FORTRAN            GASRD
        SUBROUTINE GASRD
        USE GENCOM
        READ INPUT TAPE 2, 907, (HG(K), K=1,10)
        IF (HG(1)) 16,16,
        DO 3 K=1,63,8
        READ INPUT TAPE 2, 906, (HGE(IN), IN=K,K+7)
        DO 1 IN=K,K+7
        HGDE(IN)=HGE(IN)-HGE(IN-1)
      1 CONTINUE
        IF (HGE(K+7)) , ,3
        DO 2 IN=K+8,64
        HGE(IN)=HGDE(IN)=0.
      2 CONTINUE
        GO TO 4
      3 CONTINUE
      4 KG=1
        DO 8 K=1,10
        IF (HG(K)) 9,9,
        HGL(K)=LOGF(HG(K))
        KE=1
        DO 6 IN=KG,KG+62,8
        READ INPUT TAPE 2, 906, (HGG(NO), NO=IN,IN+7)
        IF (HGE(KE+7)) , ,6
        DO 5 NO=IN+8,KG+63
        HGG(NO)=HGD(NO)=0.
      5 CONTINUE
        GO TO 7
      6 KE=KE+8
      7 KG=KG+64
      8 CONTINUE
      9 KG=K
        IF (H(16)) ,13,13
        NO=1
        DO 12 K=1,KG-1
        NNN=1
        DO 10 IN=NO,NO+63
        HGG(IN)=HGG(IN)/(HG(K)*HGE(NNN))
        NNN=NNN+1
        IF (HGE(NNN)) 11,11,
     10 CONTINUE
     11 NO=NO+64
     12 CONTINUE
     13 DO 15 K=2,64
        IF (HGE(K)) 18,18,
        DO 14 IN=K,64*(KG-1),64
        HGD(IN)=(HGG(IN)-HGG(IN-1))/HGDE(K)
     14 CONTINUE
     15 CONTINUE
        RETURN
     16 DO 17 K=1,1364
        HG(K)=0.
     17 CONTINUE
     18 RETURN
    906 FORMAT (8E7.0)
    907 FORMAT (10E7.0)
        END
*       LIST 8
*       CARDS COLUMN
```

XA04N0749

Theoretical model of the early phases of an underground explosion

I. G. Cameron and G. C. Scorgie
(Atomic Weapons Research Establishment, Aldermaston, Berkshire, England)

1. Introduction

In the early phases of the intense underground explosions contemplated in peaceful applications the rock near the explosive exhibits fluid behaviour; at great distances its behaviour can usefully be investigated in terms of linear elasticity; and at intermediate distances we think of a solid exhibiting various inelastic effects including cracking and tensile fracture. The present paper outlines a mathematical model that attempts to include in some degree the main features of this range of behaviour. A more detailed treatment than is given here, and its relationship to the work of others, is given in a paper by the authors [1].

A computer program ATHENE has been written based on this model and its use is illustrated by examining some aspects of two types of explosions. One is a chemical explosion which eventually formed a crater and the other a nuclear explosion which remained wholly contained.

2. Conservation equations

The equations expressing conservation of mass, momentum and energy can be written respectively as

$$\frac{dV}{dt} = V\varphi, \qquad \text{..... (2.1)}$$

$$\frac{du_r}{dt} = V\,(T'_{rs,s} - p_{,r}) \qquad \text{..... (2.2)}$$

$$\frac{dE}{dt} + p\,\frac{dV}{dt} = V\,T'_{rs}\,\varepsilon'_{rs} \qquad \text{..... (2.3)}$$

Fixed rectangular cartesian co-ordinates are x_r, with r running from 1 to 3, a comma denoting partial differentiation with respect to a co-ordinate, and repeated suffixes implying summation. V is the specific volume, φ is the divergence of the velocity u_r, T_{rs} is the stress tensor and T'_{rs} its deviator, p is the mean pressure, E is the specific internal energy, ε_{rs} is the strain rate tensor (i.e. the symmetric part of the velocity gradient) and ε'_{rs} is its deviator. Time differentiation following the motion of a particle is denoted by d/dt. The energy equation has already been specialised to the case of no energy transfer by radiation or conduction of heat.

In the general case these equations provide five of the total of eleven needed to determine the eleven quantities comprising V, P, E, and the elements of u_r and T'_{rs}. The remaining six equations must come from the constitutive relations appropriate to the particular material.

3. Constitutive relations for inviscid fluid

For the inviscid fluid we have immediately the five equations expressed by

$$T'_{rs} = 0 \; . \qquad \text{..... (3.1)}$$

The sixth relation is an equation of state

$$E = E\,(p,V)\;, \qquad \text{..... (3.2)}$$

expressing the internal energy as a known function of the pressure and specific volume. Of course, if the equation of state is adequately expressed by a relation between p and V alone, the energy equation (2.3) becomes superfluous.

4. Constitutive relations for elastic solid

An essential feature of the mathematical model is its description of the elastic solid in terms of strain rate rather than strain. It is this feature that enables both solid and fluid behaviours to be readily comprehended in one model. It might seem that all we need do is to take the time-derivatives of both sides of the equation expressing Hooke's law for stress and strain which can be written

$$T_{rs} = \lambda\theta\delta_{rs} + 2\mu e_{rs}\;, \qquad \text{..... (4.1)}$$

where λ and μ are the Lamé parameters, e_{rs} is the strain tensor and θ is its divergence (the dilatation). However a little care is needed if we are to arrive at an equation that makes physical sense. The point is now well understood, and we write

$$\frac{\delta T_{rs}}{\delta t} = \lambda\varphi\delta_{rs} + 2\mu\varepsilon_{rs}\;, \qquad \text{..... (4.2)}$$

with

$$\frac{\delta T_{rs}}{\delta t} = \frac{dT_{rs}}{dt} - \omega_{rq}\,T_{qs} - \omega_{sq}\,T_{qr}\;, \qquad \text{..... (4.3)}$$

where ω_{rs} is the skew symmetric part of the velocity gradient. The stress-rate defined by (4.3) is that measured in a frame rotating at the local angular velocity of the material. Clearly it is such a quantity as this, intrinsic to the material and independent of the fixed laboratory frame, that we must expect to relate to the strain rate ε_{rs} experienced by the material.

Equation (4.2) provides six constitutive relations for the elastic solid. In some instances these equations may be more usefully handled in two groups by introducing the deviators T'_{rs} and ε'_{rs}. In this way equation (4.2) is replaced by

$$\frac{\delta T'_{rs}}{\delta t} = 2\mu\varepsilon'_{rs}\;, \qquad \text{..... (4.4)}$$

and

$$\frac{dp}{dt} = -\,\kappa\varphi\;, \qquad \text{..... (4.5)}$$

where the bulk modulus is $\kappa = \lambda + 2\mu/3$. For a material of this sort, with constant bulk modulus, the energy equation (2.3) is superfluous; the ten variables comprising V, U_r, T_{rs} can be found by solving the ten equations comprised in (2.1), (2.2), (4.4) and (4.5).

Although the constitutive relation (4.5) is adequate for many purposes, cases arise in which it has to be replaced by an equation of state of the type of (3.2). In such cases we must again introduce the energy equation (2.3).

5. Constitutive relations for inelastic solid

5.1 The basic equation (4.2) for the elastic solid can be inverted to give

$$\varepsilon_{rs} = \frac{1}{2\mu} \left(\frac{\delta T_{rs}}{\delta t} + \frac{\lambda}{\kappa} \frac{dp}{dt} \delta_{rs} \right) . \qquad \ldots\ldots (5.1)$$

Various types of inelastic behaviour can be represented by augmenting this equation to obtain

$$\varepsilon_{rs} = \frac{1}{2\mu} \left(\frac{\delta T_{rs}}{\delta t} + \frac{\lambda}{\kappa} \frac{dp}{dt} \right) + h_{rs} , \qquad \ldots\ldots (5.2)$$

where h_{rs} is chosen to suit the particular inelastic effect in question. Six additional relations are needed to determine the symmetric tensor h_{rs}.

Some generalities may be noted before taking up particular inelastic effects. We may invert equation (5.2) to give

$$\frac{\delta T_{rs}}{\delta t} = \lambda\varphi\delta_{rs} + 2\mu\varepsilon_{rs} - (\lambda h\delta_{rs} + 2\mu h_{rs}) , \qquad \ldots\ldots (5.3)$$

where $h = h_{rr}$.

Again it is sometimes convenient to introduce the deviator h'_{rs} of the inelastic strain rate, replacing equation (5.2) by the pair

$$\varepsilon'_{rs} = \frac{1}{2\mu} \frac{\delta T'_{rs}}{\delta t} + h'_{rs} , \qquad \ldots\ldots (5.4)$$

$$\varphi = - \frac{1}{\kappa} \frac{dp}{dt} + h . \qquad \ldots\ldots (5.5)$$

5.2 Elastic-plastic solid

Applying these ideas to the elastic-plastic solid, we identify h_{rs} with the plastic strain rate. For many solids the physical facts are expressed by the six equations

$$h'_{rs} = \frac{1}{m} T'_{rs} \qquad \ldots\ldots (5.6)$$

$$h = 0 \qquad \ldots\ldots (5.7)$$

where m is a positive scalar invariant of h_{rs}. Because of the introduction of m we need one more equation, and this is provided by the plastic yield criterion. For example, the criterion of von Mises can be written

$$T'_{rs} T'_{rs} \leqslant \frac{2}{3} Y^2 , \qquad \ldots\ldots (5.8)$$

where Y is the yield strength under uniaxial stress. Thus in (5.6) we can replace m by $(2Y^2/3h'_{pq} h'_{pq})^{\frac{1}{2}}$.

5.3 Fracture of elastic solid

An extreme case of inelastic behaviour arises when a solid undergoes tensile fracture. Because we are using essentially a continuum model it is clear that not all aspects of the real fracturing material can be exactly represented. For example, the increase in gross specific volume, resulting from the void volume, is spread through the continuous material of the mathematical model. Consequently we have to distinguish between V_m, the true specific volume of the actual material (excluding void volume), and V, the bulk specific volume (including void volume). V_m satisfies the equation

$$\frac{1}{V_m}\frac{dV_m}{dt} = -\frac{1}{\kappa}\frac{dp}{dt} , \qquad \text{..... (5.10)}$$

where κ is the bulk modulus of the unfractured material. Combining this with equation (1.1) and (5.5) gives

$$\frac{V}{V_m} = \exp\left\{ \int_o^t h dt \right\} , \qquad \text{..... (5.11)}$$

where time zero is the measured from onset of fracture. This equation gives a physical meaning to the quantity h.

To describe the onset of fracture we put

$$h_{rs} = h n_r n_s , \qquad \text{..... (5.12)}$$

where n_r is unit normal to the fracture plane. Thus equation (5.3) becomes

$$\frac{\delta T_{rs}}{\delta t} = \lambda\varphi\delta_{rs} + 2\mu\varepsilon_{rs} - h\ (\lambda\delta_{rs} + 2\mu n_r n_s) . \qquad \text{..... (5.13)}$$

Regarding the act of fracture as described by an impulsive h, and letting H denote the time integral over the brief interval in which fracture occurs, we find that the stress increment produced by fracture is

$$\Delta T_{rs} = -H\ (\lambda\delta_{rs} + 2\mu n_r n_s) . \qquad \text{..... (5.14)}$$

Just prior to fracture the plane normal to n_r was a plane of principal stress F (the tensile strength of the material); hence

$$n_s\ \Delta T_{rs} = -F\ n_r ,$$

giving

$$H = \frac{F}{\lambda + 2\mu} \qquad \text{..... (5.15)}$$

Hence

$$\frac{V}{V_m} = \exp\left\{ \frac{F}{\lambda + 2\mu} \right\} . \qquad \text{..... (5.16)}$$

Following the creation of a crack we assume that the plane of fracture is translated with the material and shares its rotation. A more general form of h_{rs} is taken than (5.12) such that the plane of fracture remains a principal stress plane and that the stress across this plane remains zero. The form of (5.12) cannot be retained subsequent to the creation of a crack as this would imply that n_r is a principal direction of the strain rate tensor for which there is no à priori reason.

6. Remarks on the computer program

The main features of the model outlined above have been programmed for the computation of axially symmetric motions. The co-ordinates are Lagrangian, thereby dispensing with the need to handle explicitly the equation expressing conservation of mass. Much of the computational technique derives directly from earlier programs written for fluid motion. For example, shocks are catered for by including in the momentum and energy equations artificial viscosity terms which obviate the need to consider the shock front as a discontinuity in the flow field. The viscous term q which is added to the pressure p is taken in the form

$$q = -\frac{b^2 A}{V_o V^2} \left| \frac{\partial V}{\partial t} \right| \frac{\partial V}{\partial t} , \qquad \ldots\ldots (6.1)$$

where A is the area of a finite difference mesh, V_o is the original specific volume of the material, and b is a parameter that is adjusted to give the best compromise between high damping of computational oscillations and minimum smearing of shocks.

The finite difference equations are written in cylindrical co-ordinates, distance R being measured from the symmetry axis, and distance Z being measured along it. Thus the volume element is formed by rotating a mesh in the (R,Z)-plane about the symmetry axis.

A computational cycle for the solid phase takes the following course. At the beginning of the cycle the specific volume and the velocity and stress fields are known. Hence the components of the strain rate tensor are found, together with the increment in the stress deviator from equation (4.4). The new stress deviator, calculated for the end of the time step, is substituted in the yield criterion (5.8). If the criterion is violated the elements of the stress deviator are reduced by a common factor so chosen that the reduced deviator satisfies the yield criterion. (A more detailed discussion than can be given here establishes the range of validity of this process.) The new value of pressure is now calculated using either equation (4.5) or an equation of state (3.2), depending on which is most appropriate to the physical conditions of the problem. If equation (3.2) is selected, it has to be solved in conjunction with the energy equation (1.3). Next, the new values of the stress tensor are used to calculate the new values of the velocity from the momentum equation (1.2). The new specific volume is, of course, readily found because the co-ordinate system is Lagrangian; otherwise we should have to use equation (1.1) explicitly. Thus, finally, we have calculated all the quantities needed for the beginning of the next time step.

Calculations, in general, are divided into two phases, a spherically symmetric phase and an axially symmetric phase. In the initial stages of an explosion the pressures and accelerations are much greater than the lithostatic pressure and gravity which may be neglected. Subsequently, of course, the lithostatic pressure may become important, or the initial shock wave may be reflected at the free surface of the ground, both conditions giving rise to a two-dimensional axially symmetric calculation. In the case of an explosion which eventually forms a crater it is convenient to change from a one to a two dimensional calculation when the initial shock is about halfway towards the free surface.

Figure 1 shows a typical mesh at the start of the axially symmetric phase though to avoid confusion only about half the number of meshes in each direction has been shown. Our interest does not extend to large distances at which small strain sets in and we impose the lithostatic pressure as a boundary condition at some radial distance. A non-uniform mesh is used, the resolution decreasing with distance from the point of the explosion.

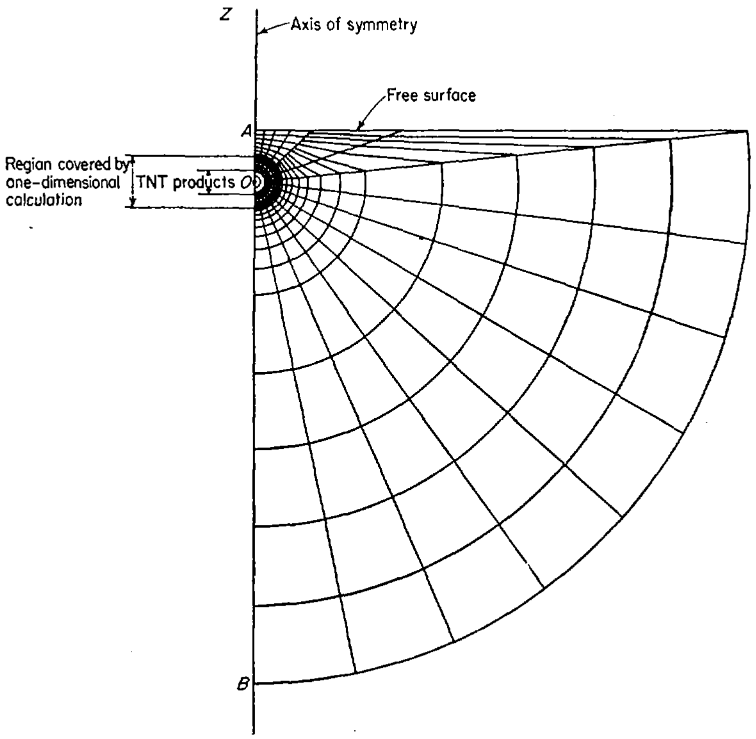

Figure 1. Typical mesh at the start of an axisymmetric calculation

7. Numerical examples

To illustrate the use of the program we consider some aspects of two different types of explosion, the one a cratering shot and the other a wholly contained one. For the former we examine the way in which the strength of the rock affects the gross aspects of the ground motion and compare the free surface position for one of the calculations with the observations at several times prior to venting. For rock that is sufficiently weak, provided that the charge is large enough it is to be expected that violent motion will penetrate to the surface of the ground and the surface disturbance may be so severe that the cavity containing the gaseous explosion products breaks through to the surface. As the strength of the rock is increased, other things remaining equal, the surface disturbance diminishes until, for sufficiently strong rock, the explosion products never succeed in breaking through to the surface.

These features are illustrated by some calculations based on Scooter, a 500 ton TNT explosion at a depth of 38 m in alluvium. Figure 2 shows the calculated early motion of the ground surface and the wall of the cavity containing the explosion products for each of three assumptions concerning the strength of the rock. In case (i) the rock is assumed to remain solid at all times, its yielding strength being 50 bars. In case (ii) the rock is assumed solid with a yield strength of 50 bars, as before, until a time (taken as 14 ms) when the interaction of stress waves in the overburden fractures it so severely that it behaves substantially like a fluid, i.e. its yield strength falls to zero. Case (iii) is like case (ii) but the transition to fluid like behaviour is delayed until 90 ms.

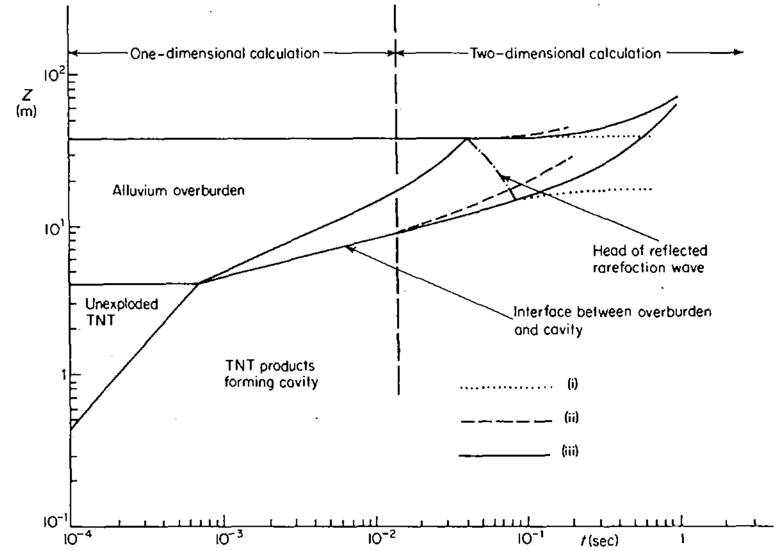

Figure 2. Radius-time curve for Scooter, an explosion of 500 tons of H.E. (ii) $Y = 0$ $t > 0.014$ secs (i) $Y = 0.05$ Kb $t > 0.014$ secs (iii) $Y = 0.05$ Kb $0.014 < t < 0.09$ sec, $Y = 0$ $t > 0.09$ sec.

It is seen that, for the solid rock of case (i), the motion of the ground surface is slight and the expansion of the gas cavity is falling off markedly at the termination of the calculation. Transition to fluid like behaviour at 90 ms, case (iii), results in appreciable motion of the ground surface, and the gas cavity is still expanding quite strongly at the termination of the calculation. Transition to fluid like-behaviour at the earlier time of 14 ms, enhances both the ground motion and the expansion of the gas cavity.

Figure 3 shows four two-dimensional pictures of the cavity and free surface as calculated by ATHENE for the most realistic example, case (iii), together with the observed height of the free surface as shown by the arrows. For time 0.8 sec the figure also shows the observed shape of the free surface. Comparing the theoretical and experimental results it can be seen that ATHENE overestimates the height of the free surface. It must, however, be remembered that this is only an illustrative calculation with several deficiencies. For this particular calculation only a very simple model of tensile fracture was included, namely assuming that the rock behaves like a fluid after 14 m secs. Again only a single p-V relation for consolidated alluvium has been used which does not describe the alluvium in sufficient detail under all conditions. True allowance should be made for different loading and unloading curves in addition to distinguishing between consolidated and crushed alluvium.

As a second example, to show the various types of rock behaviour that ATHENE can represent, an exploratory one dimensional calculation has been done based on Hardhat in which a 5 kt nuclear device was exploded at a depth of 286 m in granite. Shear failure was assumed to have occurred if

$$T'_{rs} T'_{rs} = {}^{2}/_{3} G^{2} ,$$

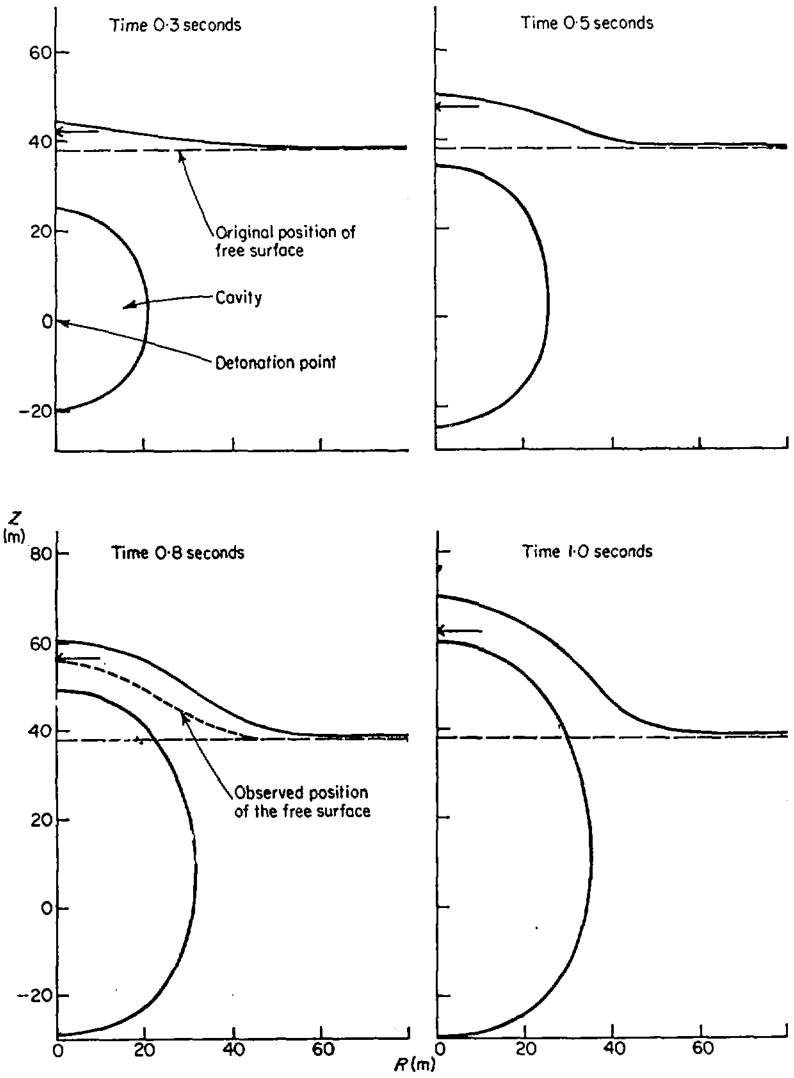

Figure 3. Shapes of the cavity and free surface for Scooter as calculated by ATHENE. Arrows indicate the observed maximum height of the free surface.

G being a parameter of the rock. This relation is similar to the yield condition and in many cases G is identified with Y the yield strength in tension. Cracks were allowed to open if a principal stress exceeded the rock's tensile strength and close if the void volume, $(V - V_m)$, went negative.

Figure 4 shows the radius-time plot of the early stages of the explosion. It can be seen that at 40 m secs there are several regions; going from the inside to the outside we have (i) a region formed by the vapourized device and rock immediately surrounding the device, (ii) a region of molten rock, (iii) a region in which the rock has undergone shear failure, i.e. the rock has been crushed (iv) a region in which the rock has first cracked in the radial direction and then failed in shear, (v) a region in which there are just radial cracks and (vi) a region which has deformed elastically. At 40 m secs the radial crack region is still expanding though the boundaries between regions inside this are stationary.

These calculations are qualitatively consistant with observation in that there do exist molten regions, regions of varying degrees of crushed rock and

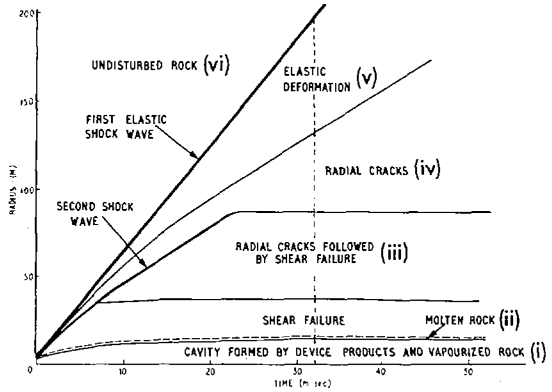

Figure 4. Calculation by ATHENE of the first 40 m secs of Hardhat, a 5 Kt contained nuclear explosion in granite.

a large region with radial cracks. Being a one-dimensional calculation it cannot simulate the chimney effect but the liquid/crushed rock boundary of 15 m and boundary between regions (iii) and (iv) of 90 m are consistant with the observed cavity radius of 19.2 metres and chimney height (measured from the detonation point) of 86 metres.

8. Conclusion

By adopting a flow or incremental model of solid behaviour we have seen that it is possible to extend the well known computational techniques of fluid dynamics to include many aspects of solid behaviour, both elastic and inelastic. The two exploratory numerical examples show qualitative agreement with observation though for good quantitive agreement a more detailed description of the rock is probably required.

Reference

1. Cameron I.G. and Scorgie G.C., J. Inst. Maths and Applics 4 (1968) 194-222.

XA04N0750

Computation of Fluid Flow in Distending Tunnels with Mass, Momentum and Energy Exchange with the Walls

J. R. Maw (AWRE, Aldermaston, UK)

1. Introduction

When calculating the effects of an underground explosion it may be useful to be able to calculate the flow of the very hot gaseous products along pipes or tunnels.

For example it might be possible to treat a fault in the surrounding rock as an idealised pipe forced open by the high pressure generated by the explosion.

Another possibility might be the use of a specially constructed tunnel to channel the energy released in some preferred direction.

In such cases the gas flow is complicated by several phenomena. The cross section of the pipe may vary with axial distance and also distend with time. Heat will be lost to the walls of the pipe which may be ablated leading to entrainment of wall material into the gas flow. In addition wall friction will tend to retard the flow.

This paper describes a simple computer program, HAT, which was written to calculate such flows.

The flow is assumed to be quasi-one-dimensional in that flow quantities such as pressure density and axial velocity do not vary across the pipe. However the radius of the pipe may vary both with axial distance and with time. Sources or sinks of mass, momentum and energy are included in the governing equations which allow simulation of the phenomena described above.

The governing equations are derived in Eulerian form and approximated using an extension of the finite difference scheme of Lax [1]. A brief outline of the computational procedure is given.

To demonstrate the capabilities and assess the accuracy of the program two simple problems are calculated using HAT

(i) The motion of a shock along a converging pipe.

(ii) The effect of mass addition through the walls on the motion of a shock along a uniform pipe.

In both cases results obtained using HAT are compared with theoretical analyses of the motion.

2. Derivation of the Conservation Equations

Consider the mass, axial momentum and total energy balance in an elemental disc bounded by the walls of the pipe and two fixed cross sections distance δx apart (see figure 1). Ignore body forces such as gravity.

As mentioned in the introduction assume that the flow properties are uniform across the pipe and that velocity components other than the axial component are negligible. The mass, axial momentum and total energy of the fluid in the disc are then

$$\pi R^2\ \rho\ \delta x\ ,\ \pi R^2\ \rho u\ \delta x\ ,\ \pi R^2\ \rho(e + \frac{1}{2}u^2)\delta x$$

respectively, where $R(x,t)$ is the radius of the pipe and ρ, u, e are respectively the density, axial velocity and specific internal energy of the fluid.

The rate of change of mass in the disc must be balanced by the net rate of inflow of mass into the disc

$$\frac{\partial}{\partial t}(\pi R^2\ \rho\ \delta x) = -\frac{\partial}{\partial x}(\pi R^2\ \rho u)\delta x + 2\pi R\ m\ \delta x \qquad \text{.... (1)}$$

where $-\frac{\partial}{\partial x}(\pi R^2\ \rho u)\ \delta x$ is the net rate of inflow of mass into the disc through the plane faces and $2\pi R\ m\ \delta x$ is the rate of inflow through the curved surface, m being the rate of inflow per unit curved surface area.

The equation of conservation of mass may thus be written as

$$\frac{\partial}{\partial t}(R^2\ \rho) + \frac{\partial}{\partial x}(R^2\ \rho u) = 2R\ m \qquad \text{.... (2)}$$

Using similar arguments the equation of conservation of momentum is found to be

$$\frac{\partial}{\partial t}(R^2\ \rho u) + \frac{\partial}{\partial x}(R^2\ \rho u^2) + \frac{\partial}{\partial x}(R^2\ p) = 2R\tau \qquad \text{.... (3)}$$

where p is the fluid pressure and τ represents the contribution per unit curved surface area to the rate of change of momentum. τ may include the axial momentum of material entering the pipe, frictional drag and the effect of pressure forces on the walls of the pipe.

Finally the equation of conservation of energy is

$$\frac{\partial}{\partial t}\left[R^2\ \rho(e + \frac{1}{2}u^2)\right] + \frac{\partial}{\partial x}\left[R^2\ \rho u(e + {}^{P}/_{\rho} + \frac{1}{2}u^2)\right] = 2\ R\ H \qquad \text{.... (4)}$$

where H is the contribution per unit curved surface area to the rate of change of total energy. H may include the energy of material entering the pipe, the rate of working of frictional forces and the rate of working of forces acting on the pipe walls if the walls are expanding.

Equations (2), (3) and (4) form the basis of the program. In addition an equation of state linking p, ρ and e and supplementary equations for determining R, m, τ and H are required.

3. The Finite Difference Equations

Before expressing (2), (3) and (4) in finite difference form it is convenient to introduce the following variables

$$\begin{aligned} Q &= R^2\ \rho & E &= R^2\ \rho(e + \frac{1}{2}u^2) \\ K &= R^2\ \rho u & P &= R^2\ p \end{aligned} \qquad \text{.... (5)}$$

Equations (2), (3) and (4) may then be written as

$$\frac{\partial Q}{\partial t} + \frac{\partial K}{\partial x} = 2\ R\ m \qquad \text{.... (6)}$$

$$\frac{\partial K}{\partial t} + \frac{\partial}{\partial x}\left(\frac{K^2}{Q} + P\right) = 2\ R\ \tau \qquad \text{.... (7)}$$

$$\frac{\partial E}{\partial t} + \frac{\partial}{\partial x}\left[\frac{K}{Q}(E + P)\right] = 2\,R\,H \qquad \ldots.\ (8)$$

The equation of state is written in the form

$$P = R^2 f\left(\frac{Q}{R^2}, \frac{E}{Q} - \frac{1}{2}\frac{K^2}{Q}\right) \qquad \ldots.\ (9)$$

where $p = f(\rho, e)$.

For example the perfect gas equation of state

$$p = (\gamma - 1)\rho e \qquad \ldots.\ (9a)$$

becomes

$$P = (\gamma - 1)\left(E - \frac{1}{2}K^2/_Q\right) \qquad \ldots.\ (9b)$$

γ being the ratio of specific heats.

The difference scheme used is an extension of the explicit, first order, centred space difference scheme of Lax [3].

The time and space derivatives are replaced by finite differences as follows

$$\frac{\partial \phi}{\partial t} \sim \frac{\phi_k^{n+1} - \frac{1}{2}\left(\phi_{k-1}^n + \phi_{k+1}^n\right)}{\Delta t_n} \qquad \ldots.\ (10a)$$

$$\frac{\partial \phi}{\partial x} \sim \frac{\phi_{k+1}^n - \phi_{k-1}^n}{2\Delta x} \qquad \ldots.\ (10b)$$

where $\phi_k^n = \phi(k\Delta x, t_n)$

and $t_{n+1} = t_n + \Delta t_n$

The terms on the right hand sides of (6), (7) and (8) are represented as follows:

$$2R\psi = \frac{1}{2}\left(R_{k+1}^n + R_{k-1}^n\right)\left(\psi_{k+1}^n + \psi_{k-1}^n\right) \qquad \ldots.\ (10c)$$

Explicit equations for Q, K and E at time t_{n+1} in terms of the variables at time t_n may then be written down.

$$Q_k^{n+1} = \frac{1}{2}\left(Q_{k-1}^n + Q_{k+1}^n\right) - \frac{\Delta t_n}{2\Delta x}\left(K_{k+1}^n - K_{k-1}^n\right)$$
$$+ \frac{1}{2}\left(R_{k+1}^n + R_{k-1}^n\right)\left(m_{k+1}^n + m_{k-1}^n\right) \qquad \ldots.\ (11)$$

$$K_k^{n+1} = \frac{1}{2} \left(K_{k-1}^n + K_{k+1}^n \right) - \frac{\Delta t_n}{2\Delta x} \left(\frac{(K_{k+1}^n)^2}{Q_{k+1}^n} + P_{k+1}^n \right.$$

$$\left. - \frac{(K_{k-1}^n)^2}{Q_{k-1}^n} - P_{k-1}^n \right) + \frac{1}{2} \left(R_{k+1}^n + R_{k-1}^n \right) \left(\tau_{k+1}^n + \tau_{k-1}^n \right) \qquad \text{.... (12)}$$

$$E_k^{n+1} = \frac{1}{2} \left(E_{k-1}^n + E_{k+1}^n \right) - \frac{\Delta t_n}{2\Delta x} \left(\frac{K_{k+1}^n}{Q_{k+1}^n} \left(E_{k+1}^n + P_{k+1}^n \right) \right.$$

$$\left. - \frac{K_{k-1}^n}{Q_{k-1}^n} \left(E_{k-1}^n + P_{k-1}^n \right) \right) + \frac{1}{2} \left(R_{k+1}^n + R_{k-1}^n \right) \left(H_{k+1}^n + H_{k-1}^n \right)$$

.... (13)

These equations together with the equation of state and the supplementary equations for R, m, τ and H are then used to advance the solution in time.

The calculation proceeds as follows:

(i) Given the solution at time $t = t_n$ (11), (12) and (13) give values of Q, K and E at time t_{n+1}.

(ii) The value of R at t_{n+1} is obtained from an auxiliary routine.

(iii) The equation of state gives the value of P at t_{n+1}.

(iv) If required for output purposes the values of the actual physical variables ρ, p, u and e at t_{n+1} are computed from the computational variables Q, K, E and P.

(v) New values of m, τ and H are computed from auxiliary routines.

(vi) Since the variables are now all known at t_{n+1} the calculation is repeated.

Lax gives a necessary condition for the stability of his difference scheme

$$\frac{\Delta t}{\Delta x} < \frac{1}{|u| + c} \qquad \text{.... (14)}$$

where c is the sound speed.

Provided that the fundamental wave equation nature of the equations is not affected it may be expected that this condition will still hold when source terms are present.

The Lax difference scheme introduces diffusion terms into the finite difference approximation. As a consequence discontinuities in the flow can be treated automatically since they are spread over several meshes. The diffusion coefficient is, however, proportional to ${(\Delta x)^2}/{\Delta t}$ so that very small time steps would result in a large diffusion coefficient and hence not very sharp discontinuities. In order to keep discontinuities as sharp as possible the time step should be as large as possible consistent with the stability condition (14).

Accordingly at each step in the calculation Δt is calculated by

$$\Delta t = \frac{\Delta x}{\max(|u| + c)} \qquad \text{.... (15)}$$

where $\max(|u| + c)$ is the maximum value of $|u| + c$ over the flow field.

4. The Motion of a Strong Shock along a Converging Pipe

4.1 Theory

Chisnell [2] has shown that for a perfect gas the speed of propagation U of a strong shock along a pipe with non-uniform cross section is given by

$$\frac{U}{U_o} = \left(\frac{R}{R_o}\right)^{-\kappa} \qquad \text{.... (16)}$$

where R is the radius of the pipe at the shock, the suffix 0 denotes some reference value and κ is a constant which depends on the specific heat ratio γ of the gas, ($\kappa = 0.394$ for $\gamma = 1.4$).

From (16) the distance X travelled by the shock can be obtained. Suppose that the radius of the pipe is given by

$$R = R_o\, g(x) \qquad \text{.... (17)}$$

where $g(0) = 1$

and that U_o is the shock speed where the radius is R_o.

Then $$\frac{dX}{dt} = U = U_o[g(X)]^{-\kappa} \qquad \text{.... (18)}$$

and hence $$\int_o^X [g(s)]^{-\kappa} ds = \int_o^t U_o\, dt. \qquad \text{.... (19)}$$

assuming that $X = 0$ when $t = 0$.

Equation (19) gives X implicitly as a function of t.

4.2 Comparison of the results of HAT calculations with the theory

The program HAT was used to calculate the flow resulting from the initial conditions shown in figure 2. At the left hand end of the pipe the values of u, p and ρ were maintained at their initial values. The initial conditions were chosen to give a shock travelling with speed 6 along the uniform section of the pipe.

Figure 3 compares the distance travelled by the shock as given by HAT with the theoretical value as obtained for this situation from equation (19). The agreement is seen to be very good.

Figure 1

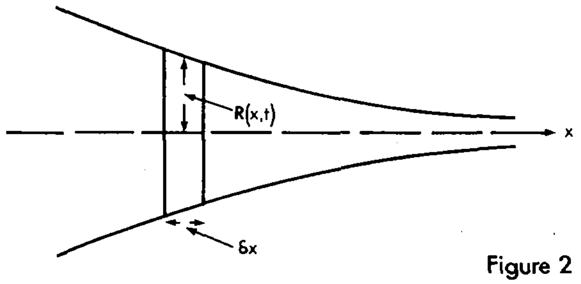

Figure 2

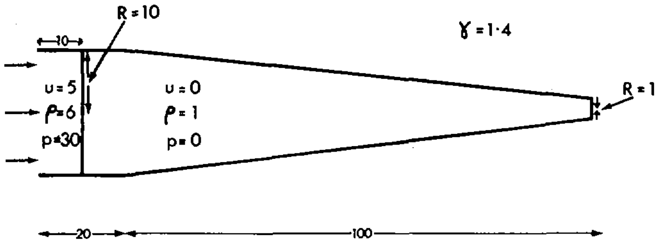

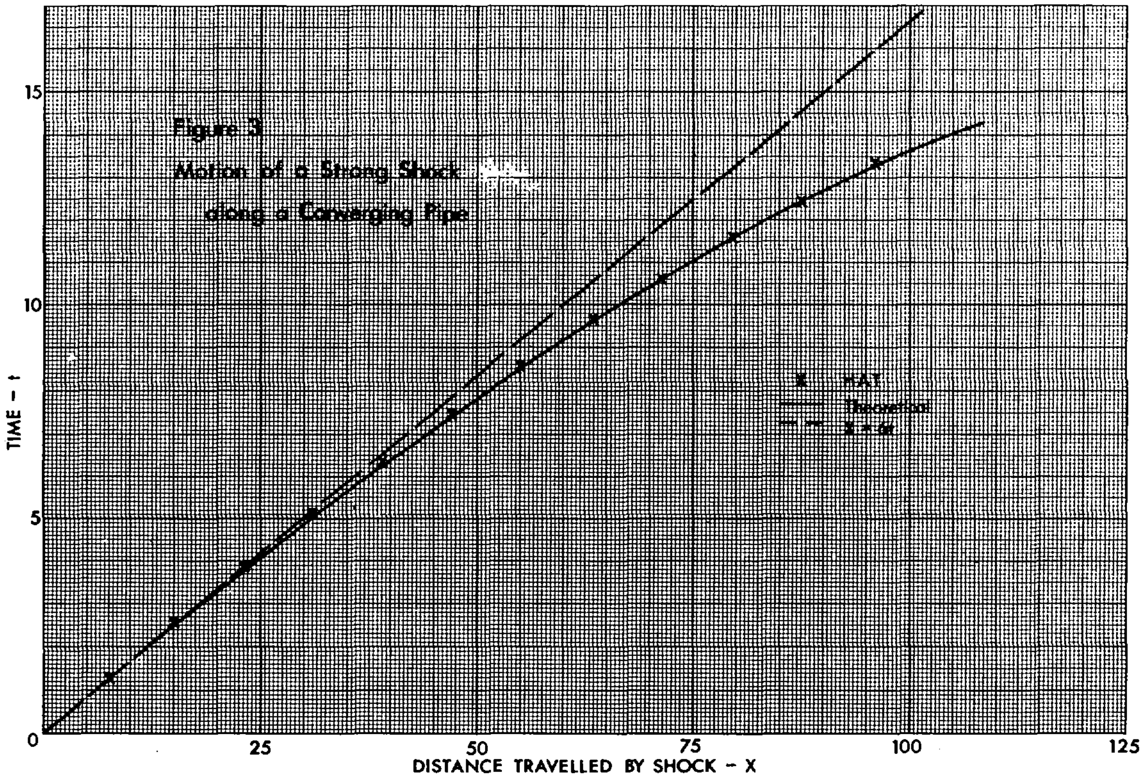

Figure 3
Motion of a Strong Shock
along a Converging Pipe

To see whether the same agreement could be obtained when the pipe converged more quickly a second calculation was carried out using the same initial conditions for u, p and ρ but in a pipe whose radius varied linearly from 10 down to 1 over a distance of 10 units. In this case there was again no significant difference between the computed and theoretical results.

In this latter case the agreement is probably only academic since the radius of the pipe varies so rapidly that the flow is no longer even approximately one-dimensional.

5. The Attenuation of a Strong Shock due to Mass Addition through the walls of the pipe

5.1 Theory

Consider the problem of a strong shock moving along a pipe of uniform radius with mass entering the flow through the pipe walls. Suppose that at any point mass is entering at a rate $\alpha\ \rho\ u$ per unit area of the walls where α is a constant and ρ and u are the density and velocity of the fluid at that point. Physically α is the ratio of the mass flow per unit area of the pipe walls to the axial mass flow per unit cross sectional area of the pipe. Suppose further that the added mass has no momentum or energy.

The conservation equations (2), (3) and (4) are for this situation

$$\frac{\partial}{\partial t}(R^2\rho) + \frac{\partial}{\partial x}(R^2\rho u) = 2R\,\alpha\,\rho u \qquad \text{.... (20)}$$

$$\frac{\partial}{\partial t}(R^2\rho u) + \frac{\partial}{\partial x}(R^2\rho u^2) + \frac{\partial}{\partial x}(R^2 p) = 0 \qquad \text{.... (21)}$$

$$\frac{\partial}{\partial t}\left[R^2\rho(e + \frac{1}{2}u^2)\right] + \frac{\partial}{\partial x}\left[R^2\rho u(e + {}^{p}/_{\rho} + \frac{1}{2}u^2)\right] = 0 \qquad \text{.... (22)}$$

Assuming a perfect gas equation of state and remembering that R is constant these equations may be used to give a characteristic relation

$$\frac{\partial p}{\partial t} + (u + a)\frac{\partial p}{\partial x} + \rho a\left(\frac{\partial u}{\partial t} + (u + a)\frac{\partial u}{\partial x}\right) = \frac{2\alpha}{R}\rho u^2\left(\frac{\gamma - 1}{2}u - a\right) \qquad \text{.... (23)}$$

where

$$a^2 = \frac{\gamma p}{\rho}$$

(23) implies that

$$\frac{dp}{dt} + \rho a\frac{du}{dt} = \frac{2\alpha}{R}\rho u^2\left(\frac{\gamma - 1}{2}u - a\right) \qquad \text{.... (24)}$$

along the characteristic $\frac{dx}{dt} = u + a$.

Whitham [3] showed that in many cases it was possible to determine the motion of a shock by applying the characteristic relation to the flow immediately behind the shock.

Now for a strong shock the conditions immediately behind the shock are given by

$$p = \frac{2}{\gamma + 1} \rho_o U^2$$

$$u = \frac{2}{\gamma + 1} U \qquad \text{.... (25)}$$

$$\rho = \frac{\gamma + 1}{\gamma - 1} \rho_o$$

$$a = \frac{\sqrt{2\gamma(\gamma-1)}}{\gamma + 1} U$$

where U is the shock speed and ρ_o is the fluid density ahead of the shock.

Substituting (25) in (24) gives after some simplification

$$\left(2 + \sqrt{\frac{2\gamma}{\gamma - 1}} \right) \frac{dU}{dt} = \frac{2\alpha}{R} \frac{2}{\gamma + 1} \left(1 - \sqrt{\frac{2\gamma}{\gamma - 1}} \right) U^2 \qquad \text{.... (26)}$$

or

$$\frac{dU}{dt} = \frac{2\alpha}{R} F(\gamma) U^2 \qquad \text{.... (27)}$$

where

$$F(\gamma) = \frac{2}{\gamma + 1} \frac{1 - \sqrt{\frac{2\gamma}{\gamma - 1}}}{2 + \sqrt{\frac{2\gamma}{\gamma - 1}}} \qquad \text{.... (28)}$$

$$= - 0.295 \qquad \text{for } \gamma = 1.4$$

Putting

$$\beta = - \frac{2\alpha}{R} F(\gamma)$$

gives

$$\frac{dU}{dt} = - \beta U^2 \qquad \text{.... (29)}$$

which can be integrated to give

$$\frac{U}{U_o} = \frac{1}{1 + \beta U_o t} \qquad \text{.... (30)}$$

where $U = U_o$ when $t = 0$.

It then follows that the distance X travelled by the shock is

$$X = \frac{1}{\beta} \log(1 + \beta U_o t) \qquad \text{.... (31)}$$

5.2 Comparison of the results of HAT calculations with the theory

A HAT calculation was done starting from the initial conditions shown in figure 4 with mass addition at a rate $\alpha \rho u$ per unit wall area with in this case $\alpha = 0.1$. For a uniform flow this rate of mass addition would double the mass in the pipe in 10 units of time. Figure 5 compares the position of the shock as given by HAT with the theoretical position as given by equation (31), the agreement being very good.

Figure 5 also shows the results of a second calculation using the same initial conditions but with $\alpha = 1.0$ that is ten times the rate of mass addition.

Figure 4

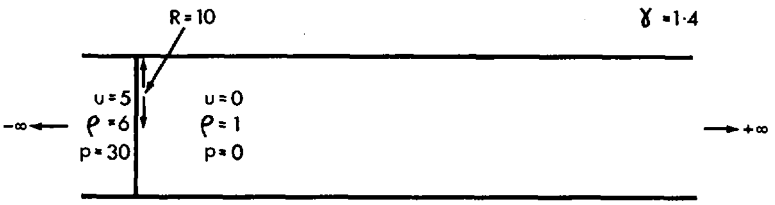

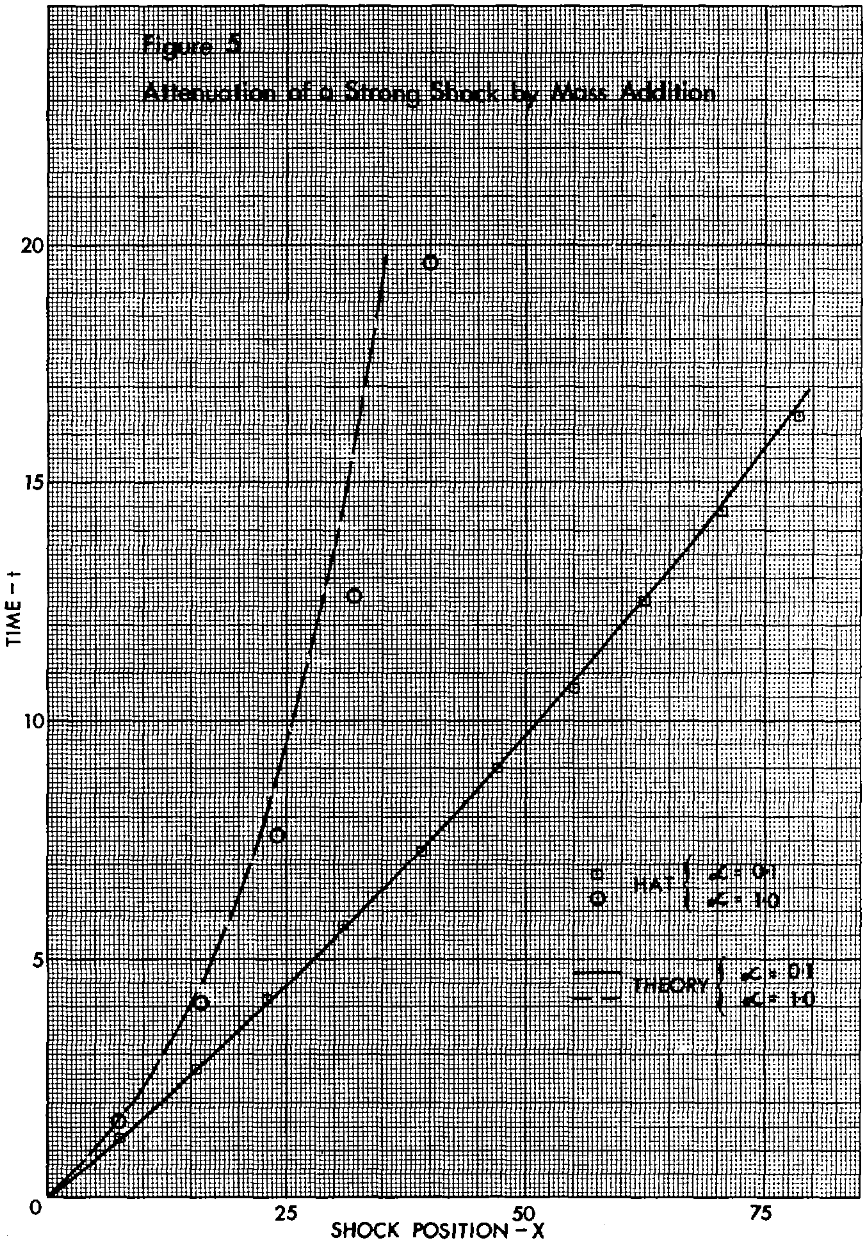
Figure 5

Attenuation of a Strong Shock by Mass Addition

The mesh size used was the same as in the first calculation ($\Delta x = 0.25$). The agreement is not nearly as good but it was found that by taking a smaller mesh size the agreement could be improved.

The lack of agreement when the rate of mass addition is large appears to be connected with the mass added to the flow in one time step. The ratio of the mass added in a time step to the mass already present in the pipe is

$$\lambda = \frac{2R\ \alpha\ \rho u\ \Delta t}{R^2\ \rho} = \frac{2\alpha}{R}\ u\ \Delta t$$

Now $$u\ \Delta t \simeq \Delta x$$

so that $$\lambda \simeq \frac{2\alpha}{R}\ \Delta x$$

with $\alpha = 0.1$ $R = 10$ and $\Delta x = 0.25$ $\lambda \simeq 0.005$.

It would appear therefore that in order to obtain accurate solutions it is necessary to restrict the mass added in a time step to of order 0.5% of the mass already present in the pipe.

References

1 P. D. Lax. Weak Solutions of Nonlinear Hyperbolic Equations and Their Numerical Computation. Commims. Pure Appl. Math 7 pp 159-192 (1954).

2 R. F. Chisnell. The motion of a shock wave in a channel, with applications to cylindrical and spherical shock waves. J.F.M. 2 pp 286-298 (1957).

3 G. B. Witham. On the propagation of shock wave, through regions of non-uniform area or flow. J.F.M. 4 pp 337-360 (1958).

XA04N0751

The French experimentation at the underground nuclear testing site in the Sahara desert

André GAUVENET

Commissariat à l'Energie Atomique - France -

The present paper will be essentially an introduction to the technical exposes which will be delivered during the Las Vegas Meeting.

My presentation is divided in two parts. In the first part, I intend to summarize very briefly the experience that has been gained from the underground nuclear shots which took place in the Sahara desert from 1961 to 1966.

In the second part, I shall give you an idea of the studies at present carried on in France in the domain of peaceful applications of nuclear explosions.

1. - Underground tests in the Sahara desert

1.1. - General considerations

Between 1961 and 1966, 13 nuclear shots have been fired in a granitic massif of the Hoggar (in the Southern part of the Sahara). All these tests have been executed in the same experimental conditions. The massif, called the Taourirt Tan Affella, is a dome of ellipsoidal shape having a size of 8 Km on 5,6 Km. The height above the sea level is 2000 m ; the summit of the mountain dominates the surrounding plateau by 1000 m. The rock is an alcaline granite exhibiting a network of big fractures which cut the massif in sections.

An interesting characteristic of the testing site is the great homogeneity of the medium as regards the mechanical properties as well as the chemical composition.

This homogeneity together with the constancy of the experimental conditions give an interesting set of easily comparable results in a rather limited domain.

The phenomenology of underground explosions was studied theorically as early as 1960 to foresee and to explain the various observable effects. This was compulsory since no shot was known at this time to have been fired in a granitic rock. Fears had been raised about the efficiency of the explosions containment. Our specialists were also concerned about difficulties in after-shot drilling due to the high temperature foreseen in the central core, resulting from the very low water content in the rock.

As concerns the containment of the explosions, the problems of the shape of the end galleries (snail shapes) and of the stemming devices have been rapidly settled.

Safety questions resulting of the high temperatures in the cavities have been solved by using servocontrolled drilling mechanisms.

1.2. - Measurement of the various effects of the explosions

Each of these tests has given us the opportunity of making numerous measurements, first of all in order to confirm and to improve containment techniques.

Near ground zero, times of the arrival of the shock wave, pressures, speeds, accelerations and displacements have been the subject of systematic studies (cf Mr. Delort's Paper).

A computation numerical code has been established, in good agreement with the experimental results. This part of our activities is nevertheless not included in the reports given at this conference.

Other parameters have been measured after the shot, either in the drilling holes or in the extracted samples. Most of the dynamical effects measured at the time of the explosion give results very close to the similar data observed at the occasion of the American tests in granite (Hardhat, Shoal, Pile driver).

On the contrary results of the drilling operations effected after the shots give evidence of considerable differences between French and American shots in apparently similar environment.

The most important divergences concern the dimensions of the cavities and of the chimneys resulting from the explosions. For the same yield, the volume of cavities and chimneys observed in the Sahara are about 5 times smaller than similar volumes in the U.S. experiments. Mr. Derlich will discuss this problem in his paper.

The quantity of melted rock is nevertheless the same in both cases as it could be expected a priori. Therefore the final disposition of lava in the cavities is not the same in both types of experiments. These particularities will be discussed in various reports.

We hope that the discussion of such results could be much rewarding as regards the knowledge concerning the effects of underground explosions.

At a greater distance of ground zero, between 15 and 50 Km, seismic measurements have been effected at the earth surface and at a depth of several tens of meters.

The seismic network being always in the same position, whatever the shot, the effects of explosions of very different yields have been measured and compared for quasi-constant distances. This has permitted us to obtain laws for the ground motion : Mr. Ferrieux will give them in his report.

Gaseous samples have been systematically analysed by chemical and radiochemical methods. These analyses have shown that, in such a granitic environment, the chemical composition of these gases was always the same. Computations have permitted to check the chemical equilibria which are of course dependent on temperature.

Underground Shots in the SAHARA

Detonations	Yield(1)	Date	Time U. T.	Longitude E	Latitude N
			h m s ms	' "	' "
Agate	f	7.11.61	11.29.59.931	5.03.07,6	24.03.25,5
Beryl	m	1.5.62	10. 0. 0. 458	5.02.30,8	24.03.46,8
Emeraude	f	18.3.63	10.02. 0. 351	5.03.07,9	24.02.28,9
Amethyste	f	30.3.63	9.59. 0. 328	5.03.25,2	24.02.36,0
Rubis	m	20.10.63	13. 0. 0. 011	5.02.19,0	24.02.07,8
Opale	f	14.2.64	11. 0. 0. 347	5.03.08,6	24.03.13,1
Topaze	f	15.6.64	13.40. 0. 367	5.02.04,4	24.03.59,8
Turquoise	f	28.11.64	10.30. 0. 035	5.02.30,1	24.02.30,7
Saphir	m	27.2.65	11.30. 0. 039	5.01.52,3	24.03.31,4
Jade	f	30.5.65	11. 0. 0. 037	5.03.03,1	24.03.18,0
Corindon	f	1.10.65	10. 0. 0. 043	5.02.02,6	24.03.53,7
Tourmaline	f	1.12.65	10.30. 0. 088	5.02.48,9	24.02.37,4
Grenat	f	16.2.66	11. 0. 0. 035	5.02.28,4	24.02.39,0

(1) "f" means "faible" (weak) for a yield smaller than nominal (20 kt) "m" means "moyen" (middle) for a yield greater than nominal

The computation code, developed at this occasion may present some interest in the frame of certain industrial applications, such as oil shales, oil stimulation and so on (cf Mr. Picq's report).

In other respects, Mr. Delort's paper on nuclear stimulation of hydrocarbons gives the results of a computation using a bidimensional code on the fluid flow in fractured zones.

A schematic representation of the fractured zones has been used, following measurements obtained in the Hoggar drillings. We have also used on the spot measurements of the dimensions of the different zones (cavity, chimney, crusted zone, fractured zone, zone with residual strains). An example of the computation of the fluid flow will be given in a fictitious situation.

The last report, somewhat more remote from industrial applications, is concerned with the effect on the rock constituents of cumulative effects of heat and shock wave resulting from the explosions. This is the result of practical observations in the drilling and in the extracted samples (cf Mr. Faure's paper).

These few subjects have been selected for presentation at the Las Vegas meeting. We have concentrated almost exclusively on experimental results obtained at the time of the Hoggar shots, whose aim was not to explore the peaceful applications of nuclear explosions ; they made it possible nevertheless to acquire a significative experience in this domain. Other subjects have been published in the written form. Up to now the Commissariat à l'Energie Atomique has issued about 20 reports, all of them easily available.

I should like to add that we carried out one nuclear cratering experiment, all other tests having been fired in the atmosphere or at the water surface. We tried besides to use for pure scientific purposes one of our tests, for measurement of neutron reactions cross sections. This last attempt showed us the difficulties created by the association of a scientific project with an experiment specifically aimed at another purpose. In this field as well as in other domains it can be difficult to associate various and sometimes contradictory activities around a single experiment.

2. - Present and Future of peaceful applications of nuclear explosions at the " Commissariat à l'Energie Atomique " (C E A)

Since the end of the French underground tests (1966), available results have been collected, systematized and compared to U.S. data. This was possible thanks to the remarkable American literature which has been published on the subject.

Thoughts have been expressed inside our organization about possible industrial applications of nuclear explosions.

In 1969, the " C E A " took a step further in creating a specialized project called the Apex Project (Apex for " Applications des Explosions "). The project is under the supervision of a steering Comittee under the direct authority of the High Commissioner ; it is coordinated by a general secretary and includes study groups, in charge of every basic technique which could be useful in our domain, namely :

- study of specific nuclear devices.
- radiological and seismological safety.

- phenomenological studies.
- general applications.

Other groups study some precise applications ; these are for the present time paper studies carried on with the collaboration of specialists of various French organizations.

It is too early to discuss any detailed programme since our propositions are now at the " brainstorming " stage. They have of course to be selected, approved and of course financed by our authorities.

Taking account of the preliminary studies, as well as of our practical possibilities, we think that the first tests which would be made for specific applications will relate to the hydrocarbons field. I take this expression in a rather broad meaning, including oil and gas stimulation, oil storage and even production of chemicals. Choices will be decided later on, but we do not contemplate for the near future any cratering tests for civil engineering purposes unless specific questions were asked for, the corresponding applications being evidently excluded on the French territory, at least in the next few years.

3. - Conclusion

We have the feeling that these techniques are promising, technically and in certain cases economically. We are nevertheless strongly aware of the various difficulties we will have to surmount in the future.

We think it possible to establish a precise programme in not too distant a future. We hope to be able to discuss it at the occasion of the next Plowshare meeting ; whatever the future of these techniques, we believe that time is needed for their developing from the experimental stage to an industrially and economically proved technique. Stress will have to be put during this transition period on technical problems as well as on public education which is according to our point of view a very important requirement.

XA04N0752

SUMMARY OF NUCLEAR-EXCAVATION APPLICATIONS*

John Toman
Lawrence Radiation Laboratory, University of California
Livermore, California 94550

ABSTRACT

Although many nuclear-excavation applications have been proposed, few have been seriously considered and none have been brought to fruition. This paper summarizes and discusses specific examples of a canal, a harbor, a highway cut and a nuclear quarry, all of which have been studied in some detail. It is believed that useful demonstration projects—such as a deep-water harbor and a nuclear quarry—can be safely accomplished with existing technology. Current assessments of the feasibility of constructing a sea-level canal in either Panama or Colombia appear to be favorable from a technical viewpoint. The concept of close spacing in row-charge designs has made it possible to greatly reduce the estimated required salvo yields for both proposed canals. Salvo yields have been reduced from 35 Mt to 13 Mt in Colombia and 11 Mt in Panama. As a result, the seismic motions predicted for large cities in these countries are similar to motions produced in populated areas in the United States by nuclear tests and earthquakes in which no real damage to residential or high-rise structures was noted.

INTRODUCTION

Ever since the Plowshare program was formally established in 1957, many potential applications for nuclear excavation have been proposed and reported.[1,2] Although none of these proposed applications have been brought to fruition, a number of them appear to be economical as well as feasible from a technical and public-safety standpoint. Continued progress has been made in improving excavation techniques, in developing improved explosives, and in predicting effects, including seismic motions, radioactivity, and air blasts. This paper reviews and summarizes major excavation applications that have previously been reported in detail and analyzes them with respect to current technical knowledge. The general applications discussed are canals, harbors, highway cuts, and nuclear quarries.

TRANSISTHMIAN SEA-LEVEL CANAL

The most detailed and costly investigations and studies so far conducted by the AEC, its contractors, and the Corps of Engineers have been for the most ambitious project yet contemplated—a transisthmian sea-level canal. A recent evaluation of this project by the Lawrence Radiation Laboratory, Livermore, has led to a significant reduction in the individual and salvo yields deemed necessary in earlier studies.[3] These reduced yield requirements resulted from information gained in recent cratering experiments, from the adoption of a family of explosive yields with smaller

---

[*] Work performed under the auspices of the U. S. Atomic Energy Commission.

incremental steps, and from taking advantage of the enhancement of single-charge dimensions that is inherent in multiple row charges. As a result, the largest single salvo yield of 35 Mt has been reduced to 13 Mt for Route 25 in Colombia and 11 Mt for Route 17 in Panama. The significance of this reduction is that the seismic motions predicted for large cities in these countries are now similar to motions produced in populated areas in the United States by tests at the Nevada Test Site and by earthquakes for which no real damage to residential or high-rise structures has been noted. Of equal importance from a feasibility standpoint is the fact that the largest single-charge yield is now 3 Mt. If the experimental program progresses as scheduled, then within a year this yield will be less than a factor of 5 higher than existing cratering experience, and the uncertainties in the scaling dimensions over this range amount to only 10%.

A. The Close-Spacing Concept

The single most important factor in reducing individual and salvo yields is the enhancement of row-crater dimensions over that of single-crater dimensions. The amount of enhancement or increase above the maximum single-crater dimensions at a specified yield is related to the spacing between the explosives and to the depth of burst. Enhancements of 25 to 40% are readily achievable in row-crater dimensions, yet single-charge yields would have to be increased by a factor of 2 to 3 to produce similar single-crater dimensions. In essence, the apparent yield of the explosives in a row charge increases as the charges are brought closer together due to interaction between the charges.

The amount of enhancement achievable appears to be controlled mostly by economics. The cost of nuclear excavation is virtually a linear function of the number of explosives used rather than the yields of the explosives. For example, the projected charge is about $500,000 for a 200-kt explosive and only $600,000 for a 2000-kt explosive. The need for one additional explosive and its accompanying emplacement hole at $200,000 to $500,000 quickly eliminates the justification for a close-spacing concept except in large projects like a sea-level canal, where the nuclear-excavation cost is minor in comparison to the total project cost, or in projects where a substantial reduction in seismic motion is the overriding factor.

When the spacing between the explosives in a row charge with a fixed number of explosives is gradually reduced, the row crater becomes shorter and shorter and more and more elliptical until a single-charge-like crater is formed whose dimensions are proportional to the sum of the yields of the individual explosives. In the existing canal studies, a minimum ratio of 2 between the crater length and the crater width has been selected. This is achieved with five explosives, assuming enhancements of 25 to 30%.

Although a sufficient number of chemical-explosive row charges have been fired to support the concept of enhancement through close spacing, an insufficient number of chemical-explosive rows and no nuclear-explosive rows have been detonated to definitely establish the spacings and depths of burst required for specific enhancements.

Estimates of the required spacings and depths of burst are given by two different analytic procedures. The first procedure, which is described in Appendix A, assumes that the velocity fields of adjacent charges add vectorally and that the resulting velocity field or mound velocity is comparable to that of a single higher yield explosive at the same actual depth of burst. This general approach was used successfully in designing the nuclear row experiment, Buggy I.[4] The second procedure assumes that regardless of the spacing, there is a constant enhancement of the volume of material excavated by each row charge over that excavated by an optimum single charge. For a specified enhancement of the linear dimensions of a row, this procedure selects a spacing that provides the predetermined apparent crater volume for each row charge.[5]

As a first approximation in the second procedure, the depth of burst for a row of explosives is based on the apparent yields of the explosives. A 30% enhancement of row-crater dimensions would therefore require the explosives in the row to be buried 30% deeper than is optimum for the actual explosive yields. If the burial depths are not increased in this way, the increase in explosive energy per unit length (i.e., the apparent increase in the individual explosive yields) results in the apparent depth of burst for the row being shallower than optimum. Consequently, the enhancement of the row-crater dimensions is reduced and the crater depths tend to expose the shot points, as was evidenced in the Pre-Gondola III row-charge experiment.[6] In this experiment, the crater half-width was enhanced by 23% over the apparent radius of a single crater (R_a) and the crater depth was enhanced by 38% when the depth of burst was increased to about 10% deeper than optimum. The crater depth virtually exposed the shot points. In a follow-on experiment performed by the Nuclear Cratering Group at LRL, the crater half-width was enhanced by 36% and the apparent depth by 38% when the depth of burst was 29% deeper than optimum.[7] These latter enhancements were produced at a larger spacing (0.7 $R_{a_{max}}$) than that used in Pre-Gondola III (0.6 $R_{a_{max}}$).

Figure 1 illustrates the concept of close spacing with a typical cratering curve. Points A, B, and C represent the scaled dimensions of three rows of charges at the same depth of burst but with three different spacings. In row A, the spacing between the explosives is too large and there is no increase in dimensions over those of the optimum single-charge crater. The apparent yields of the row explosives are still larger than the actual yields, for the dimensions are larger than those of a single explosive at the same depth of burst. The apparent yield of the explosives in row A is given by

$$W_{ap} = \left(\frac{OA}{OA'}\right)^{3.4} W ,$$

where W_{ap} is the apparent yield, W is the actual yield, and OA and OA' are distances taken from Fig. 1.

In row B, the spacing and depth of burst are optimum. The increase in dimensions over those of the optimum single-charge crater is proportional to the apparent yield of the row explosives, or (OB/OB') = (DB/DA). The apparent yield of the explosives in row B is given by

$$W_{ap} = \left(\frac{OB}{OB'}\right)^{3.4} W .$$

In row C, the spacing between the explosives is too close for this depth of burst. The dimensions are much larger than those of the optimum single-charge crater, but the enhanced dimensions are not proportional to the apparent yield of the explosives. The apparent yield of the explosives in row C is given by

$$W_{ap} = \left(\frac{OC}{OC'}\right)^{3.4} W.$$

The expected dimensions at the optimum depth of burst for the spacing in row C are shown as point C". The apparent yield of the row explosives is unchanged since point C" is plotted in such a way that (OC/OC') = (OC"/OB').

The increase in the dimensions of row C'' over those of the optimum single-charge crater is now proportional to the apparent yield of the row explosives.

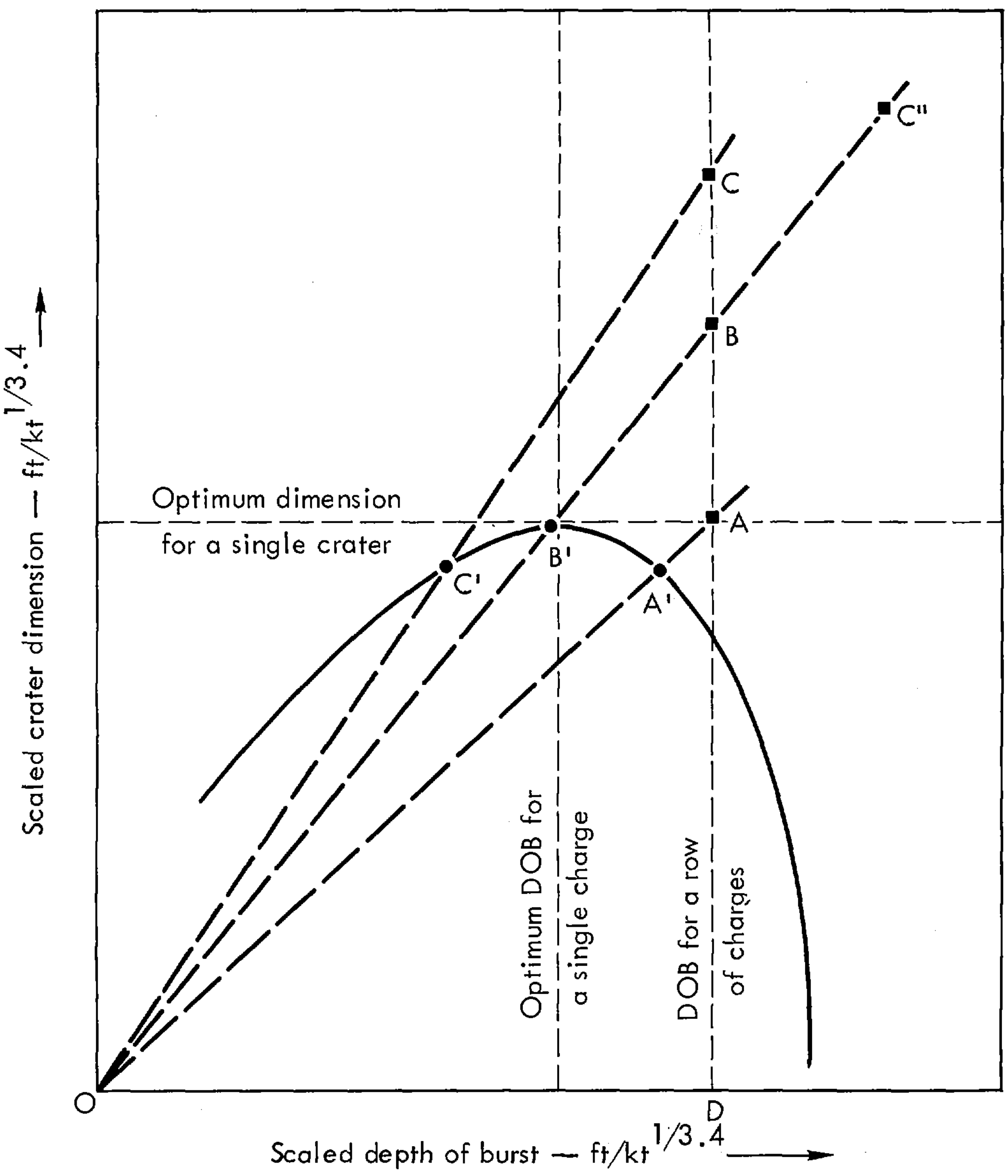

C''
C
B
A
Optimum dimension for a single crater
B'
C'
A'
Optimum DOB for a single charge
DOB for a row of charges
Scaled crater dimension — ft/kt$^{1/3.4}$
O
D
Scaled depth of burst — ft/kt$^{1/3.4}$

Fig. 1. Illustration of the close-spacing concept. The solid line is a typical single-charge cratering curve.

B. Consequences of Close Spacing in Interoceanic-Canal Studies

The impact of various degrees of row-charge enhancement is shown in Fig. 2. This graph shows the required yield of a single charge in a row of charges to produce a 1000-ft by 60-ft "navigation prism" at sea level for various heights of cut. Also shown is a similar curve used in the 1964 interoceanic-canal study in which no enhancement was assumed.[8]

The 1964 study assumed scaled dimensions of 140 ft/kt$^{1/3.4}$ for the crater radius and 80 ft/kt$^{1/3.4}$ for the crater depth.[8] These are the scaled Danny Boy[9] dimensions—the only data for nuclear detonations in hard, dry rock available at this time. A parabolic cross section for the crater was used in the 1964 study rather than the hyperbolic cross section used in a study just completed. The difference in crater shape has a large effect on

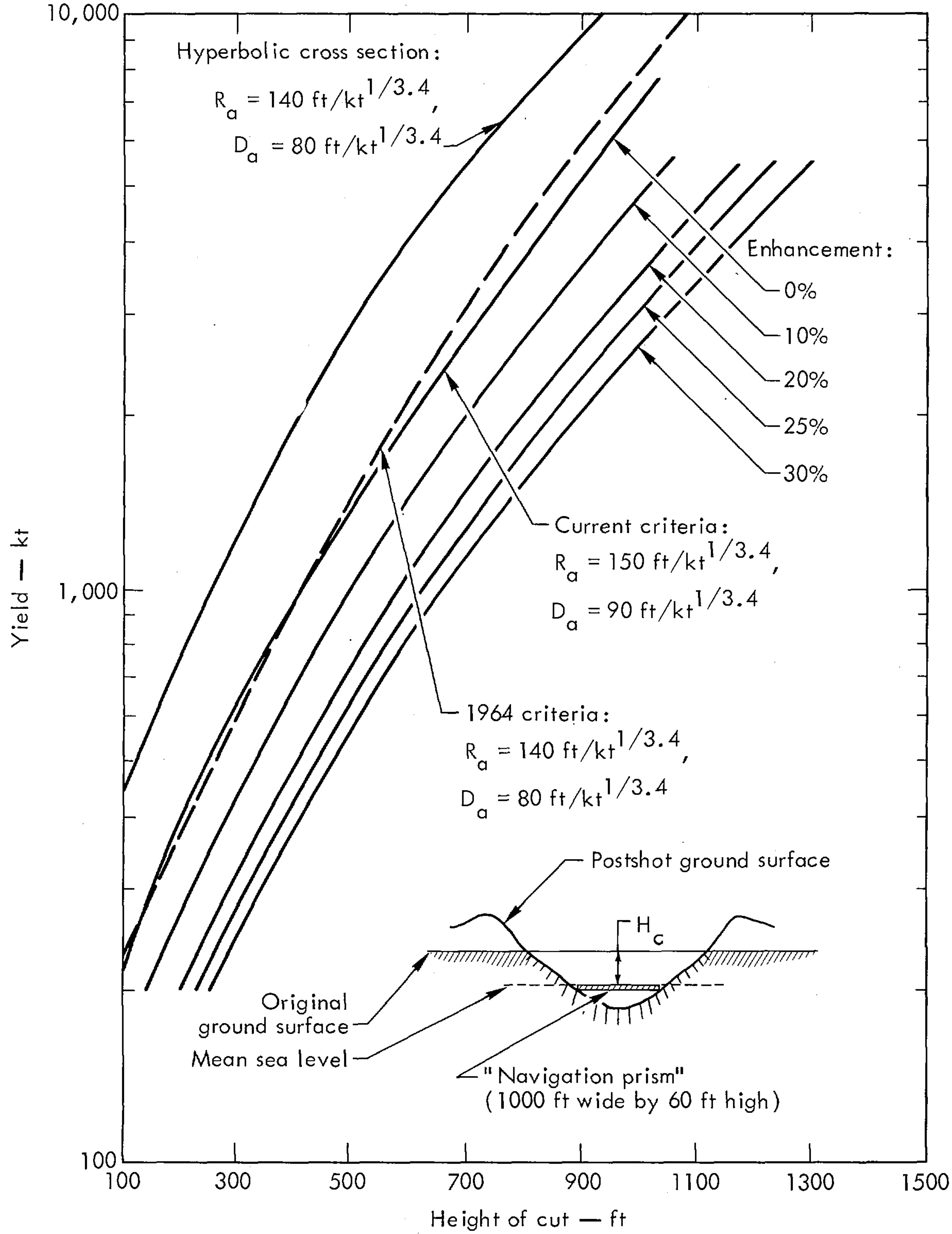

Fig. 2. Required yield of a single charge in a row of charges versus height of cut for a 1000-ft by 60-ft "navigation prism" at mean sea level (H_c = height of cut, R_a = apparent-crater radius, and D_a = apparent-crater depth).

yield requirements. The top curve in Fig. 2 shows what the yield requirements would have been in the 1964 study if a hyperbolic cross section had been used. The recent Cabriolet and Schooner experiments at a somewhat shallower depth of burst than Danny Boy lead to the conclusion that scaled single-charge dimensions of 150 $ft/kt^{1/3.4}$ and 90 $ft/kt^{1/3.4}$ for the crater radius and depth are more appropriate.

In the current study, a yield of 5.5 Mt per explosive would be required for a height of cut of 900 ft if there were no enhancement of row-crater dimensions. At 25% enhancement, the yield drops to 2.5 Mt per explosive, with a minimum of five explosives per salvo needed to satisfy the criteria that the length of the row of craters be at least twice the width. In the 1964 study, the single-explosive yield was set at 10 Mt, although the height-of-cut curve indicates that a 6.0-Mt explosive would have been sufficient. The reason for this is that the next higher yield had to be used in the family of explosive yields available at that time: 0.1, 0.2, 0.5, 1.0, 2.0, 5.0, and 10 Mt. A large fraction of the total yield required by the 1964 study stemmed from the large gaps in available explosive yields. Now, however, the current excavation-explosive design permits yield steps of 0.1, 0.2, 0.3, 0.5, 0.7, 1.0, 1.5, 2.0, 2.5, and 3.0 Mt. This family of yields has been incorporated in the current study. No need is seen for a single-explosive yield of more than 3.0 Mt,for this will cut through elevations of more than 1000 ft if the single-charge dimensions are appropriately enhanced.

Table I and II provide a comparison of the 1964 and current studies of Route 17A in Panama and Route 25E in Colombia. The 1964 study has been modified so that the lengths of nuclear excavation proposed in that study are comparable to the lengths proposed in the current study. Most of Route 25E and all of Route 17A were considered suitable for nuclear excavation in 1964, so the number of explosives and the total yield reported in the 1964 study are much larger than the totals shown in Tables I and II.

Table I. Comparison of 1964 study (modified for length) and current study of Route 17A in Panama.[a]

1964 study			Current study		
Salvo No.	Number of explosives	Salvo yield (Mt)	Salvo No.	Number of explosives	Salvo yield (Mt)
1	18	9.0	1	16	5.0
2	31	9.2	2	16	4.5
3	10	5.0	3	5	5.5
4	14	10.0	4	13	4.3
5	10	9.5	5	12	5.2
6	9	11.0	6	15	5.0
7	10	12.0	7	8	4.9
8	4	3.5	8	9	4.9
9	9	10.0	9	9	5.1
10	30	10.2	10	8	5.6
			11	5	5.2
			12	8	5.0
			13	7	5.8
			14	7	7.1
			15	5	11.0
			16	7	4.9
			17	7	6.5
			18	7	4.9
			19	14	2.8
Total	145	120.9		178	103.2

[a] Requirements for the main navigation channel only. Additional explosives and salvos are provided for river diversions.

Table II. Comparison of 1964 study (modified for length) and current study of Route 25E in Colombia.[a]

1964 study			Current study		
Salvo No.	Number of explosives	Salvo yield (Mt)	Salvo No.	Number of explosives	Salvo yield (Mt)
1	19	12.6	1	10	5.3
2	6	13.0	2	12	5.2
3	4	35.0	3	7	5.3
4	4	30.0	4	5	5.6
5	4	11.0	5	5	13.0
6	10	9.5	6	5	9.5
7	6	9.0	7	7	5.4
8	7	10.0	8	7	6.4
9	4	10.0	9	9	4.7
10	4	10.0	10	5	3.9
11	4	17.0	11	5	5.9
12	4	14.0	12	5	5.4
13	4	11.0	13	5	6.5
14	4	14.0	14	5	9.0
15	9	10.0	15	6	5.4
16	17	10.0	16	8	4.0
17	10	5.0	17	9	5.1
Total	120	231.1		115	105.6

[a] Requirements for the main navigation channel only. Additional explosives and salvos are provided for river diversions.

For Route 17A (Table I), the most significant change is the reduction of the 35-Mt salvo yield in the 1964 study to a maximum of 11 Mt in the current study. The remaining salvo yields could have been reduced to about 5 Mt by reducing the number of explosives in each salvo and increasing the number of salvos. For Route 25E (Table II), there is a tremendous improvement over the 1964 plan. The total yield has been reduced by more than a factor of 2 while retaining about the same number of explosives. In contrast to Route 17A, only a few salvos could have been reduced to 5 Mt on Route 25E because the average elevation of the nuclear portion of Route 25E is much higher than that of Route 17A. The need for additional explosives in the close-spacing concept is somewhat compensated for in the current study by the use of spacings 15% larger than those assumed in the 1964 study in salvos for which the yield is not critical.

An important factor that has not been included in the current study and that could lead to still further reductions in yield is the difference in cratering characteristics between the kinds of rock found along the canal routes and the dry, hard rock at the Nevada Test Site on which both studies are based. The canal rocks are saturated with water, making them weaker, and the increased water vapor leads to a stronger gas-acceleration phase in the cratering process. The scaled crater dimensions for saturated rocks are therefore expected to be larger than those for dry rocks. Cratering calculations employing LRL's TENSOR code and an equation of state derived from rock samples along both routes indicate that crater dimensions at the megaton level may be 10 to 15% larger than those assumed in the current study.[10] A 10% increase in crater dimensions would reduce yield requirements by about one-third.

1. Seismic Motion

At the time of the 1964 study, ground-motion data were quite limited, for the largest single contained explosion up to that time was about 200 kt and no damage from nuclear detonations had occurred. Subsequent information obtained from explosions at the megaton level and from low-yield detonations away from NTS and close to populated areas pointed out the need to reduce the salvo yields presented in the 1964 study. A significant finding was that complaints were received for minor architectural damage, such as hairline cracks in masonry structures, at very low levels of ground motion. Although such damage is a nuisance and does not affect the structural integrity of a building, the payment for such damage could be an important economic factor in nuclear excavation.

Figure 3 summarizes experience to date on complaints of architectural damage versus pseudo absolute acceleration. Pseudo absolute acceleration is the calculated response of a structure (treated as a single-degree-of-freedom system) to the actual ground acceleration. Although Fig. 3 shows that complaints have been received for motions as low as 3 cm/sec^2, damage complaints have generally not been recognized as valid below about 40 cm/sec^2.

Table III compares the pseudo absolute accelerations expected for the closest large cities to Routes 17A and 25E at several yields. These values are shown for comparative purposes only since recent improvements in predictive techniques indicate that these accelerations will actually be lower than indicated.

Table III. Seismic motions expected in the closest large cities to the proposed canal routes.[a]

City	Distance from closest detonation (km)	Yield (Mt)	Expected pseudo absolute acceleration[b] (cm/sec^2)
Route 17A			
Panama City, Panama	180	35	63
		11	30
		5	18
Route 25E			
Medellin, Colombia	230	35	53
		13	27
		5	15

[a] Taken from Ref. 12.

[b] These values are applicable only to buildings that are less than five stories high.

Much higher levels of motion will be experienced closer to the nuclear detonations. In the current study it is assumed that all nonproject personnel will be evacuated from areas in which the ground acceleration is expected to be 0.3 g or higher. Between 0.3 and 0.1 g, special precautions will be needed to avoid possible injury. A possible precaution would be to have people stand outdoors away from buildings so that loose objects will not fall on them.

High-rise structures respond differently to ground motions than low structures do. A plot similar to Fig. 3 is not available for high-rise

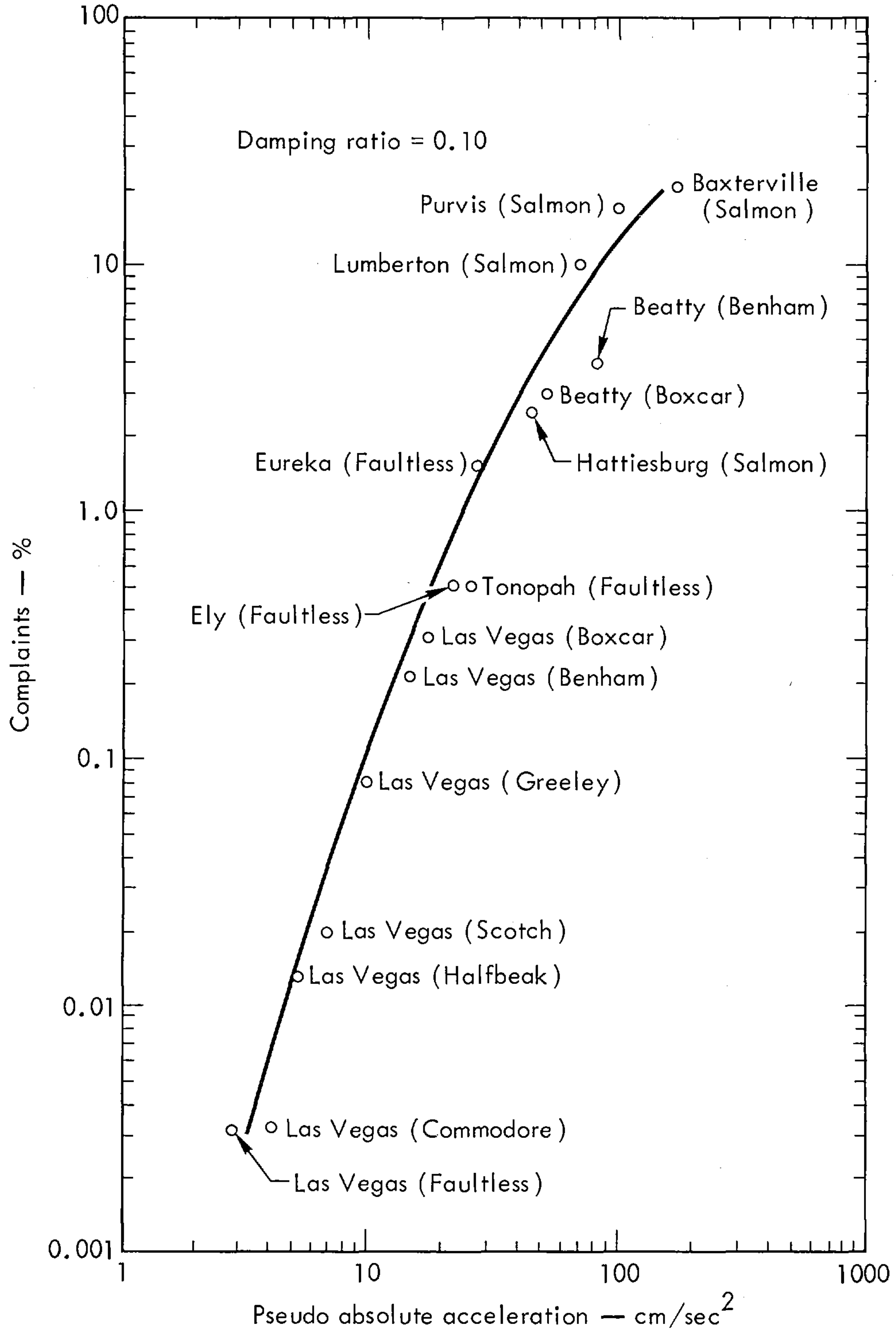

Fig. 3. Relationship between pseudo absolute acceleration and complaints of architectural damage for eight nuclear events: Salmon (Mississippi), Faultless (central Nevada), Commodore (Yucca Flat), and Boxcar, Benham, Greeley, Halfbeak, and Scotch (Pahute Mesa). Values for the ordinate are derived by dividing the total number of complaints from a given town by the total number of structures in that town and then multiplying by 100. Taken from Ref. 11.

structures because no damage to such buildings has occurred as a result of nuclear testing. The largest motions to which high-rise buildings in Las Vegas have been subjected so far resulted from a 1.2-Mt detonation (Boxcar). At a period of 1 sec (the natural response of tall buildings is between 1.0 and 5.0 sec), the pseudo relative velocity of the upper stories was about 3 cm/sec, which corresponds to a pseudo acceleration of about 20 cm/sec^2.

Additional information on high-rise structures is available from earthquakes. The Tehachapi/Bakersfield earthquake of 1952 generated motions in Los Angeles that were equivalent to those from a 20- to 30-Mt nuclear explosion at the same distance of 160 km. No structural damage to high-rise structures occurred, although many of them had been constructed prior to the establishment of rigorous building codes.[3] Pseudo response motions corresponding to velocities of about 20 cm/sec and accelerations of 50 to 100 cm/sec^2 were measured for periods between 1.0 and 2.0 sec. Figure 4 compares the velocity response of tall buildings to various seismic shocks and shows the calculated response spectrum for 5- and 10-Mt explosions at 180 km.

Techniques for predicting the response of high-rise structures to seismic motions have been developed and will continue to be improved and refined as more experimental data at high yields become available. The spectral-matrix method can provide a time history of the response of a real high-rise structure to any specified seismic wave train.[13] The accuracy of these code calculations is dependent on the data available for the design and construction of the real building and on the accuracy of the predicted ground-motion history.

A difficulty that is encountered in predicting the response of a limited number of high-rise structures in Central and South America to high-yield canal detonations is that building-design data may not be available. Even when such data exists and indicates a structurally sound design, there is no assurance that the actual construction methods employed have followed the design criteria. For this reason, the detonation plans and schedules proposed for Routes 17A and 25E contain provisions for increasing salvo yields from approximately 1.0 to 3.0 Mt to 9.0 Mt. Detailed calculations, analyses, and inspection will be needed to identify individual structures that may be sensitive to the low predicted levels of ground motion. To preclude the possibility of personal injury, such buildings could be evacuated at shot time, or they could be purchased and razed. It is believed that the purchase of a limited number of buildings would not alter the economic feasibility of constructing a sea-level canal with nuclear explosives.

2. Air Blast

Although air-blast effects must be considered in any feasibility study, their impact is mainly one of operational restraint along with the associated cost of limiting detonations to only those days that have the desired meteorology. Atmospheric focusing of the acoustic wave generated by a cratering explosion could result in overpressures sufficient to break windows at ranges of several hundred kilometers. These acoustic-wave reflections are controlled by the temperatures and winds aloft.

Data collected during the site investigations for Routes 17A and 25E indicate that there is a sufficient number of days each year in which no air-blast effects would occur.[3] The proposed operational procedures would require only three or four such days during the year. The explosive packages and firing systems are capable of standing by on a ready basis for as long as six months if necessary. Four or five salvos could be detonated on any acceptable firing day at intervals of about one hour or less. Except on

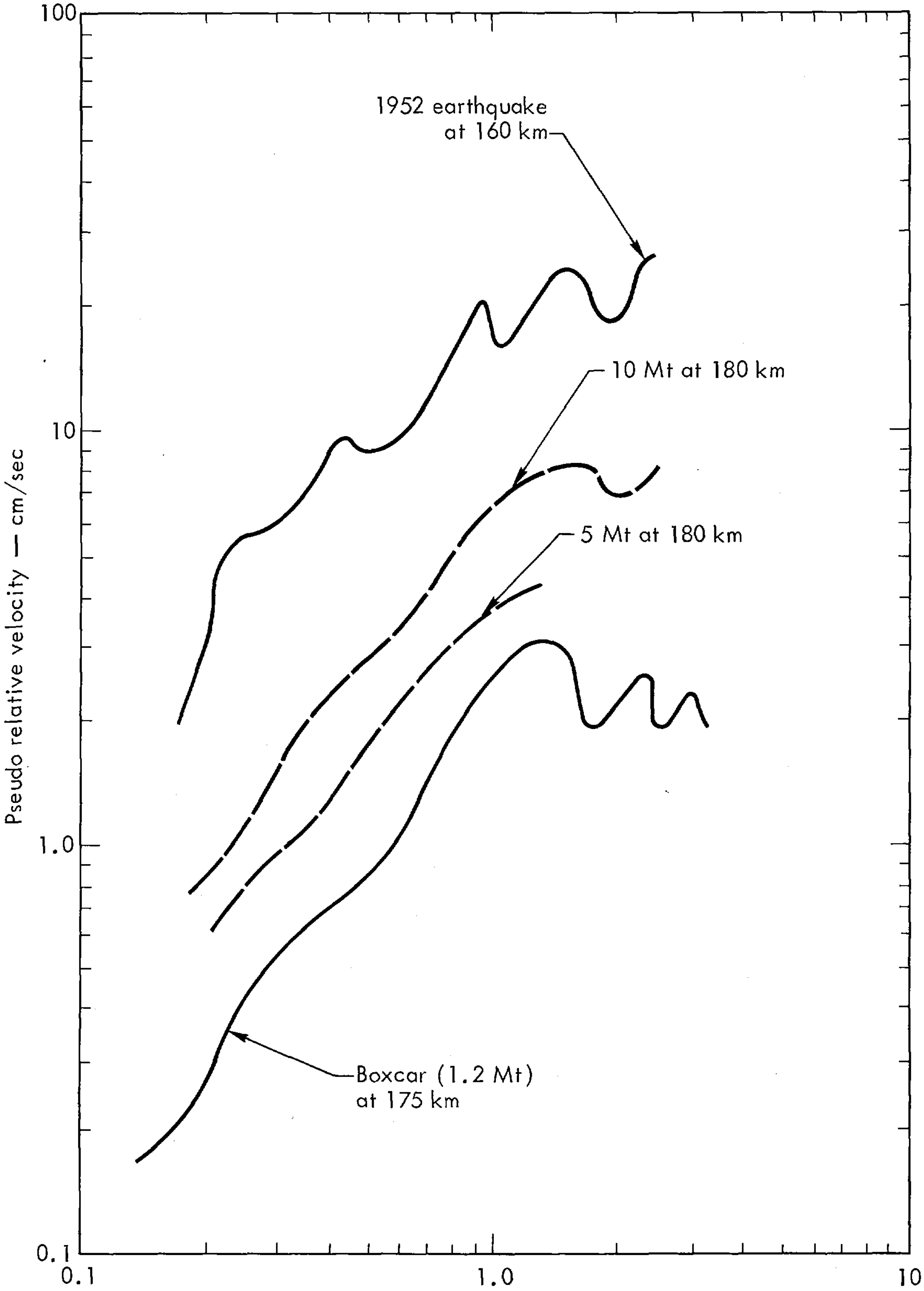

Fig. 4. Velocity response of high-rise structures to seismic shocks. The two dashed curves are calculated. Taken from Ref. 3.

the actual detonation day, construction operations such as emplacement-hole drilling and emplacement of explosives would continue in a normal fashion during the waiting period.

Direct air blasts at close ranges are not particularly affected by meteorological conditions. They can be controlled only by assuring that the evacuation area is sufficiently large to preclude personal injury from breaking glass.

3. Radioactivity

LRL is continuing to improve the design of a nuclear excavation explosive so that less fission- and neutron-induced radioactivity is produced. However, no matter how much the explosive design is improved, radioactivity will still be produced and precautionary measures will still need to be taken. The main result of improving an explosive design over that assumed in the current study would be to reduce the size of the evacuation area needed to contain the local fallout to within safe levels. The infinite-dose contour of 0.34 R, which is based on the explosive design used in the current study, is almost contained within the evacuation areas required for seismic safety (0.3 g) around Routes 17A and 25E. People residing outside the 0.34-R contour would receive an external exposure of less than 340 mR in a lifetime, or a small fraction of the total exposure of about 10,000 mR in a lifetime due to natural background radiation. Internal exposures derived from radioactivity concentrated in food chains do not appear to be significant outside the 0.34-R contour.[14] Provisions are made for continuously monitoring foodstuffs to ensure that human exposure is well below recommended guidelines. In a practical sense, the evacuation area will be significantly larger than the 0.34-R contour. For control purposes, the area will be extended to include natural barriers such as rivers or mountain ridges.

HARBOR CONSTRUCTION

The use of nuclear explosives to construct deep-water harbors is probably the most straightforward application of nuclear excavation at this time since the degree of accuracy required in the crater dimensions is not expected to be critical. The ground surface will generally be at about sea level, and salvo yields can be kept quite low. Because of the low elevations, row-charge enhancement is not a factor in harbor design, and in fact is undesirable. The spacing between explosives should be as wide as possible in order to optimize the harbor area and minimize the harbor depths created by each explosive. Explosives with a spacing of $1.5R_a$ would provide about 50% more surface area per explosive than explosives in a close-spaced row would (assuming 25% enhancement of crater width at a spacing of $0.8R_a$). This is illustrated by the comparison between close and wide spacing shown in Fig. 5. Figure 6 shows an idealized situation for a nuclear-excavated harbor. Even with wide spacing between 200-kt explosives, the estimated harbor depth may still be deeper than required or desired.

If a harbor is to be constructed where the ground surface is below mean low tide, several unknowns are encountered. The first unknown deals with the water waves generated by the detonation and whether hazardous conditions will be created for some distance along the shoreline. The second unknown deals with the formation of crater lips and whether they will survive the returning water waves. The third unknown concerns the nature of the fallback material and whether significant changes in the crater shape should be expected if the fallback material is entrained in sufficient water to liquefy or "quicken" it upon deposition.

It is believed that the generation of water waves can be quantitatively determined analytically, and LRL is currently studying this problem. It is unlikely that the generation of water waves will seriously affect this proposed application, although it must be considered in any safety analysis.

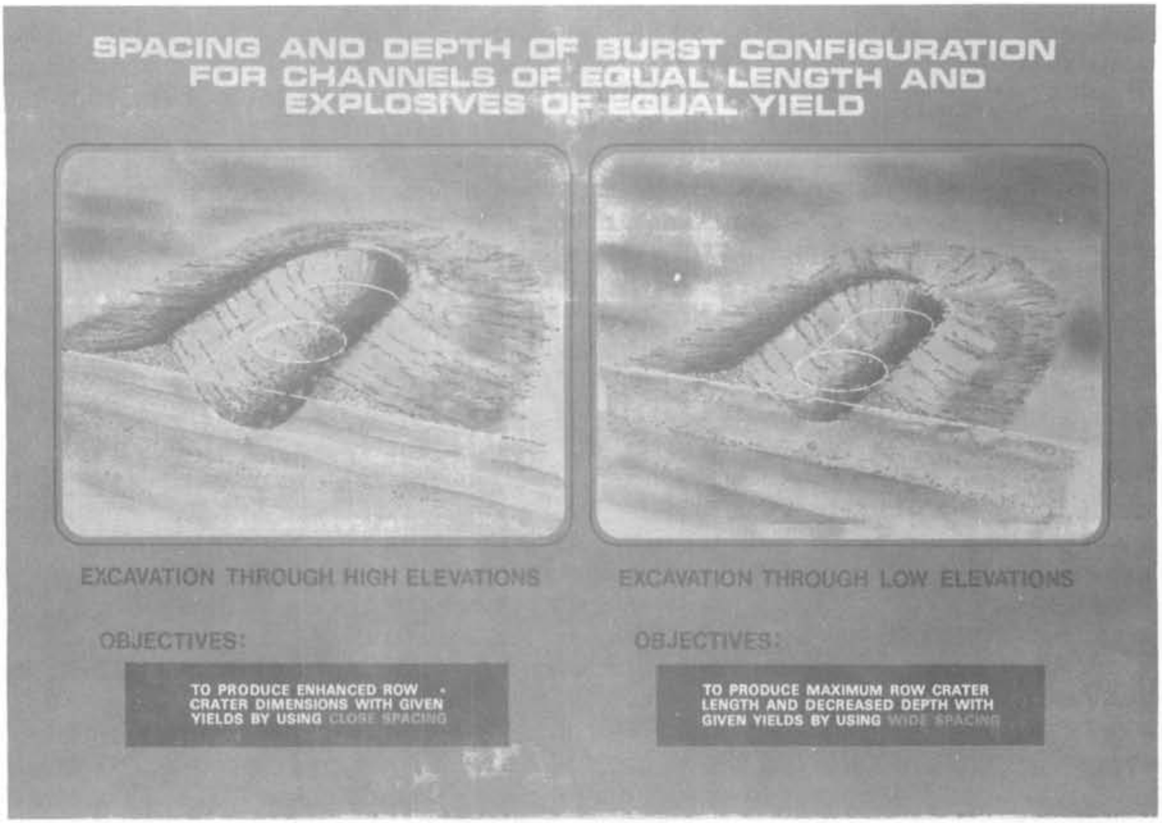
SPACING AND DEPTH OF BURST CONFIGURATION FOR CHANNELS OF EQUAL LENGTH AND EXPLOSIVES OF EQUAL YIELD
EXCAVATION THROUGH HIGH ELEVATIONS
EXCAVATION THROUGH LOW ELEVATIONS
OBJECTIVES:
TO PRODUCE ENHANCED ROW CRATER DIMENSIONS WITH GIVEN YIELDS BY USING CLOSE SPACING
OBJECTIVES:
TO PRODUCE MAXIMUM ROW CRATER LENGTH AND DECREASED DEPTH WITH GIVEN YIELDS BY USING WIDE SPACING

Fig. 5. Illustration of row-charge excavation—close versus wide spacing between explosives.

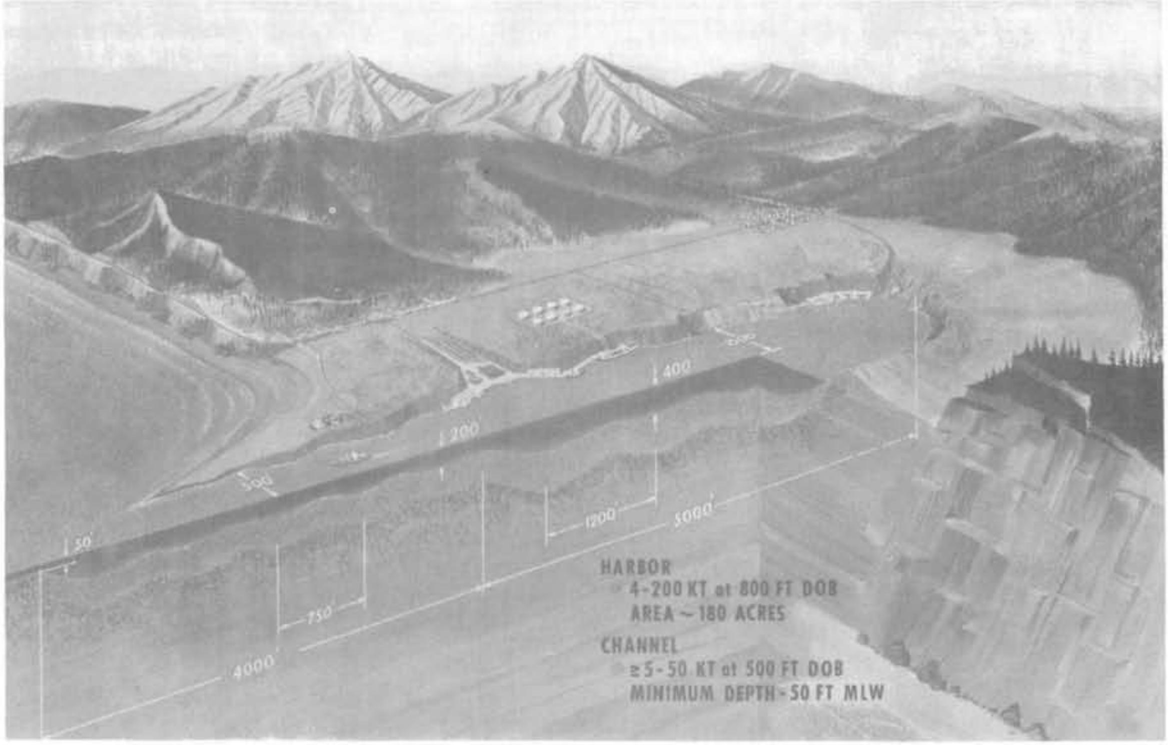

Fig. 6. Idealized plan for excavating a harbor with nuclear explosives.

The questions of lip formation and crater shape are much more difficult to resolve analytically, and experiments are needed. Some preliminary information is available from the calibration charges fired as a prelude to Project Tugboat, a chemical-explosive experiment designed to produce a shallow harbor for small boats at Kawaihae, Hawaii.[15] Five cratering charges produced no lips at all and very broad, shallow craters.[16] If crater lips were initially formed, they and most of the ejecta material were subsequently washed back into the craters by the returning water waves. The cratered material consisted of a low-strength, high-porosity coral, and the apparent crater was probably due entirely to compaction. With mean low tide as the reference plane, the water overburden probably ranged between 12 and 20% of the total depth of burst.

If crater lips are essential as a breakwater for a nuclear-excavated harbor, it is clear that the geology of the site is a critical factor. The upthrust portion of a crater lip in hard, competent rock is most likely to survive the turbulence of returning water waves. Where less competent rock exists, the yield requirements for a harbor may be dictated by the height required for the upthrust lip. In the Danny Boy experiment (0.42 kt at a depth of burst of 110 ft), about 14.5 ft of the average lip height of 24 ft was the result of upthrust.[17] For 100 kt in similar relatively incompactible rock, the upthrust portion of the lip height would be expected to be about 75 ft, assuming that lip heights can be scaled according to $W^{1/3.4}$, where W is the explosive yield. The lack of nuclear-cratering experiments in rock formations having the same equation of state precludes a definitive empirical relationship. In compactible rock (low strength and high porosity), permanent displacement of the ground surface is greatly reduced since the initial cavity that forms during the detonation continues to expand mainly by compaction of the surrounding medium rather than by displacement.

Geology similar to that encountered in the Schooner experiment[18] (31 kt at a depth of burst of 355 ft) might possibly be suitable, but the yield requirements would be dictated by the upthrust required. The Schooner lip height averaged only 44 ft, of which probably only about 25 to 30 ft was upthrust. Since the yield of Schooner is a factor of about 75 larger than Danny Boy, these dimensions are small in comparison to the 14.5 ft of upthrust measured in Danny Boy. Some of this difference can be attributed to the difference between the scaled depths of burst (deeper cratering charges produce greater upthrust), but geology is the major factor. The Danny Boy basalt is a dense, competent rock from the detonation point to the ground surface. For Schooner, the rock from the ground surface to a depth of 120 ft is a dense, competent welded tuff. From 120 to 337 ft (near the detonation point), the rock is very weak, highly porous, and has a density between 1.25 and 1.5 g/cc. A single-charge yield of about 1.0 Mt would be required to produce an upthrust height of about 75 ft in Schooner-like rock as compared to the 100 kt required for dense rock.

The change in crater shape that results when the fallback material acts like a fluid upon deposition can be quite easily estimated from existing data. Crater widths would not be affected, but crater depths would be significantly reduced. The resulting crater shape would be more ideal for a harbor than the expected hyperbolic cross section. As an example, a cross section of the Schooner crater is compared in Fig. 7 with the shape that would have resulted if all the fallback material had been in a fluid state. The size and shape of the true crater, then, determines the resulting apparent crater. The volume of the fallback material is determined from the difference between the volume of the true crater and that of the apparent crater. The volume and approximate shape of the true crater are estimated from TENSOR calculations for the Schooner experiment.[18] The volume of the apparent crater has been measured by aerial survey. If ejecta material were to be

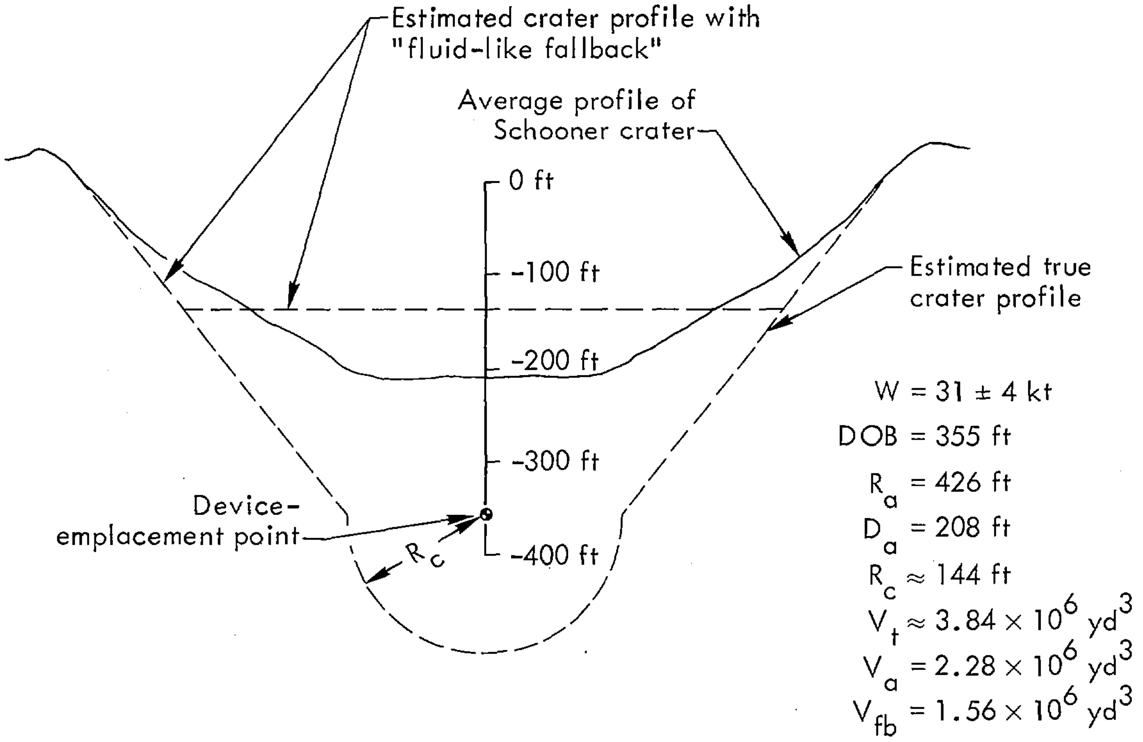
Estimated crater profile with "fluid-like fallback"
Average profile of Schooner crater
0 ft
-100 ft
-200 ft
-300 ft
-400 ft
Estimated true crater profile
Device-emplacement point
R_c
$W = 31 \pm 4$ kt
DOB = 355 ft
$R_a = 426$ ft
$D_a = 208$ ft
$R_c \approx 144$ ft
$V_t \approx 3.84 \times 10^6$ yd^3
$V_a = 2.28 \times 10^6$ yd^3
$V_{fb} = 1.56 \times 10^6$ yd^3

Fig. 7. Estimated changes in the shape of the Schooner crater that would have occurred if the fallback had had fluid properties (W = yield, DOB = depth of burst, R_a = apparent-crater radius, D_a = apparent-crater depth, R_c = cavity radius, V_t = true-crater volume, V_a = apparent-crater volume, and V_{fb} = fallback volume).

washed back into the crater, the depth would become even shallower. It is unlikely that analytical techniques for determining the volume of "washback" material can be developed because of the large number of variables and unknowns involved. A demonstration at full yield would be required.

A. Cape Keraudren Harbor

A proposed harbor-excavation project at Cape Keraudren, Australia, was studied in some detail in 1968.[19] The specific site and plan were developed in response to a request from a major shipping firm. An agreement could not be reached with potential buyers on the cost of the ore that was to be shipped out of Cape Keraudren, so the shipping firm was forced to withdraw its proposal. The Australian Atomic Energy Commission has shown considerable interest in harbor excavation and is continuing to study alternative locations. Exploitation of the vast ore deposits in northwestern Australia requires deep-water harbors from which the ore can be shipped to countries like Japan.

The sea bottom along the coast of northwestern Australia generally slopes downward at a rate of less than 10 ft/mile. At Cape Keraudren, vessels with a 60-ft draft can approach only to within 4 miles of the shoreline at high tide, which has a range of 25 ft.

The harbor plan provided for the simultaneous detonation of five 200-kt explosives spaced 1100 ft apart and buried at about 750 ft. The harbor thus produced was to be about 6000 ft long, 1600 ft wide, and 200 to 400 ft deep. The total lip heights were estimated to be 200 to 300 ft on the sides and 30 to 60 ft on the ends. An artist's conception of the harbor is shown in Fig. 8. The harbor was designed to handle ore carriers of 100,000 to 147,000 tons deadweight and the following approximate dimensions: length, 1000 ft; beam, 135 ft; and draft, 60 ft. Two alternatives were considered—one that would tie the end of the row crater to the shoreline, and one that would place the row crater about 7500 ft off-shore to reduce the amount of conventional dredging required to provide access to the open sea. A causeway was to tie the off-shore harbor to the shoreline.

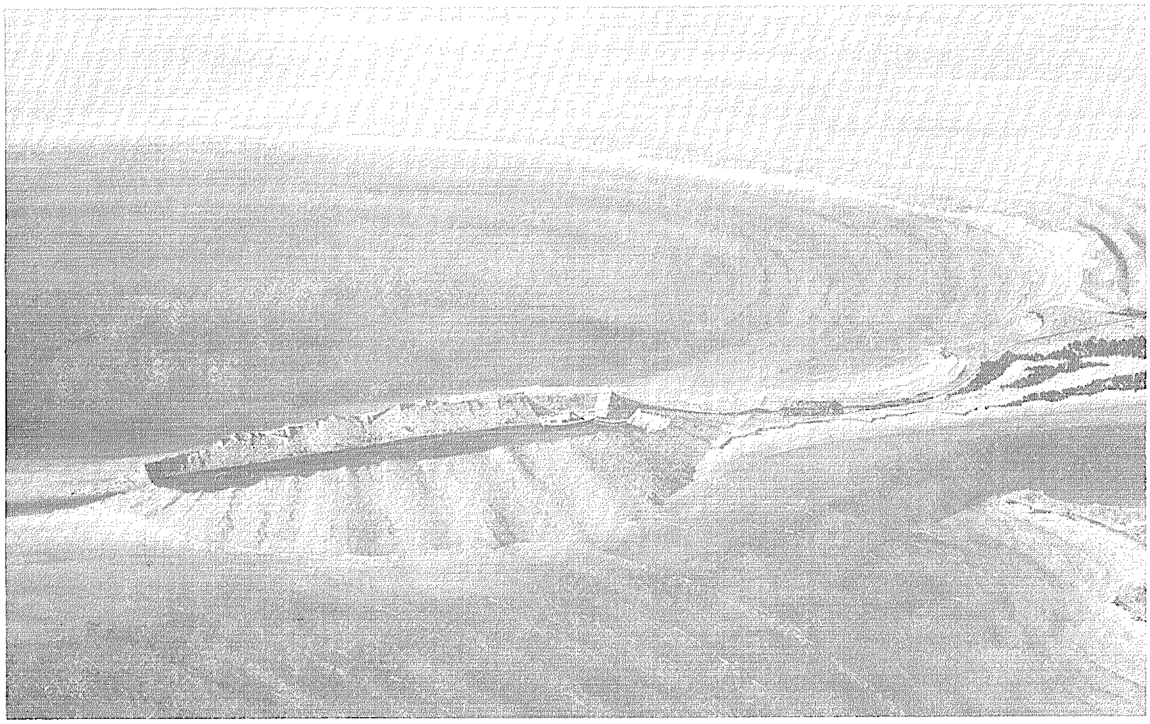

Fig. 8. Plan for excavating a harbor at Cape Keraudren, Australia.

For the off-shore harbor, the sea bottom is about 20 to 24 ft below mean low tide. Little information is available concerning the geology of this site, and that only to a depth of 100 ft. Up to 13 ft of silty sand on the ocean bottom is underlain by a layer of hard-to-soft limestone with a known thickness of 18 to 32 ft. The limestone increases in thickness toward the shore and emerges as 20- to 25-ft-high cliffs at Cape Keraudren. The limestone is underlain by an unknown thickness of interbedded quartz sand, clay, and sandstone. Additional geologic investigations would be required to establish the suitability of this site.

A preliminary safety analysis based on a limited amount of site data revealed no major deterrent to pursuing further detailed investigations and analyses.

It would appear that construction of a relatively-low-cost harbor (less than $20 million) would be a reasonable first step in demonstrating the usefulness of nuclear excavation as an engineering tool. The tremendous amount of information that would be obtained is directly applicable to much larger projects such as an interoceanic canal, and would provide a real basis for comparing conventional versus nuclear excavation.

HIGHWAY CUTS

A number of potential projects involve cutting passes through mountain ranges for highways and railroads to reduce distances and grades. In most cases, such massive cuts would not even be considered with conventional excavation because of the high cost and the long period of construction time required. Conventional excavation becomes more competitive as the height of cut is reduced, and in general, nuclear excavation would not be considered for cuts of less than 100 ft.

Of all the excavation applications proposed, a highway cut requires the highest degree of accuracy in the prediction of crater dimensions, for either over- or under-excavation requires correction by conventional methods. The elevation of the bottom of the row crater and the uniformity of that elevation are the features that must be predicted accurately. Crater depths, however, are the most difficult parameter to predict at optimum and deeper-than-optimum depths of burst where a significant amount of fallback material is involved. At such depths of burst, the depth of the apparent crater is sensitive not only to the size of the true crater and the volume of the fallback material, but also to the bulking factor of the fallback material and to the fallback's angle of repose with dynamic placement. A bulking factor is the ratio of the in-situ rock density to the bulk density of the fallback or ejecta. Cratering calculations with the TENSOR code can be used to determine the size of the true crater and the volume of the fallback material,[20] but there is no similar analytical technique that can start with an in-situ rock formation, predict the particle-size distribution resulting from the cratering process, and determine the changes in crater shape caused by the dynamic compaction that derives from the kinetic energy of the fallback material.

The bulking factors of the fallback material in the nuclear cratering experiments conducted to date can be estimated quite easily, but the degree of accuracy is unknown. The verification of bulking factors and representative particle-size distributions requires extensive and expensive postshot investigations. However, Table IV summarizes the dimensions and volumes of three nuclear cratering experiments (Danny Boy, Cabriolet, and Schooner) and shows a calculated value for the bulking factor. Although the estimated bulking factor is smallest for the highest explosive yield, the differences in the characteristics of the three kinds of rock involved may be the most important factor. Information from contained experiments indicates a trend toward lower bulking factors at higher yields.

Figure 9 uses the Danny Boy crater to show the estimated effect on crater shape and depth of changes in the bulking factor. At 80 and 70% of the original bulking factor of the fallback material, the crater depths would increase by about 8 and 16% respectively. Hence, uncertainties in crater depths are reduced in excavations that take place in materials and at yields that produce low bulking factors.

Crater depths would be most predictable at relatively shallow depths of burst in which the shot points are exposed. However, the amount of radioactivity released would be considerably greater than that at optimum depths of burst and would be about a factor of 2 greater than that assumed per explosive in the canal safety analysis. The basic mechanisms that control the release of radioactivity in cratering events are still not well known, but studies are continuing.

Table IV. Summary of nuclear-crater dimensions and estimated bulking factors.

Event	Kind of rock	Yield (kt)	Depth of burst (ft)	R_c[a] (ft)	R_a[b] (ft)	D_a[c] (ft)	V_t[d] (10^4 yd^3)	V_c[e] (10^4 yd^3)	V_a[f] (10^4 yd^3)	V_ℓ[g] (10^4 yd^3)	V_{up}[h] (10^4 yd^3)	V_{fb}[i] (10^4 yd^3)	V_e[j] (10^4 yd^3)	Bulking factor[k]
Danny Boy	Basalt	0.42	110	37	107	62	7.7	0.78	3.6	8.0	2.4	4.1	5.6	1.33
Cabriolet	Trachyte	2.3	170	75	181	117	37	6.5	18	24.2	6.5	19	17.7	1.09
Schooner	Tuff	31	355	144	426	208	384	47	228	275	47	156	228	1.06

[a] R_c = cavity radius; value for Danny Boy measured,[21] values for Cabriolet and Schooner taken from TENSOR calculations.[18,22]

[b] R_a = apparent-crater radius; all values measured.[23]

[c] D_a = apparent-crater depth; all values measured.[23]

[d] V_t = true-crater value; all values calculated by $V_t = (\pi/3)\mathrm{DOB}\left(R_a^2 + R_c^2 + R_aR_c\right) + (2/3)\pi R_c^3$.

[e] V_c = volume of initial cavity around detonation point; all values calculated by $V_c = (4/3)\pi R_c^3$.

[f] V_a = apparent-crater volume; all values measured.[23]

[g] V_ℓ = apparent-lip volume; all values measured.[23]

[h] V_{up} = true-lip volume (upthrust); value for Danny Boy measured,[24] values for Cabriolet and Schooner arbitrarily assumed to be equal to V_c

[i] V_{fb} = fallback volume; all values calculated by $V_{fb} = V_t - V_a$.

[j] V_e = ejecta volume; all values calculated by $V_e = V_{al} - V_{tl}$.

[k] All values calculated by $BF = (V_e + V_{fb})/[V_t - (V_c/2)]$. Measured bulking factors in the Danny Boy lip in two trenches were 1.44 and 1.19.[17] A measured bulking factor in the Cabriolet lip ranged from 1.11 to 1.16.[25]

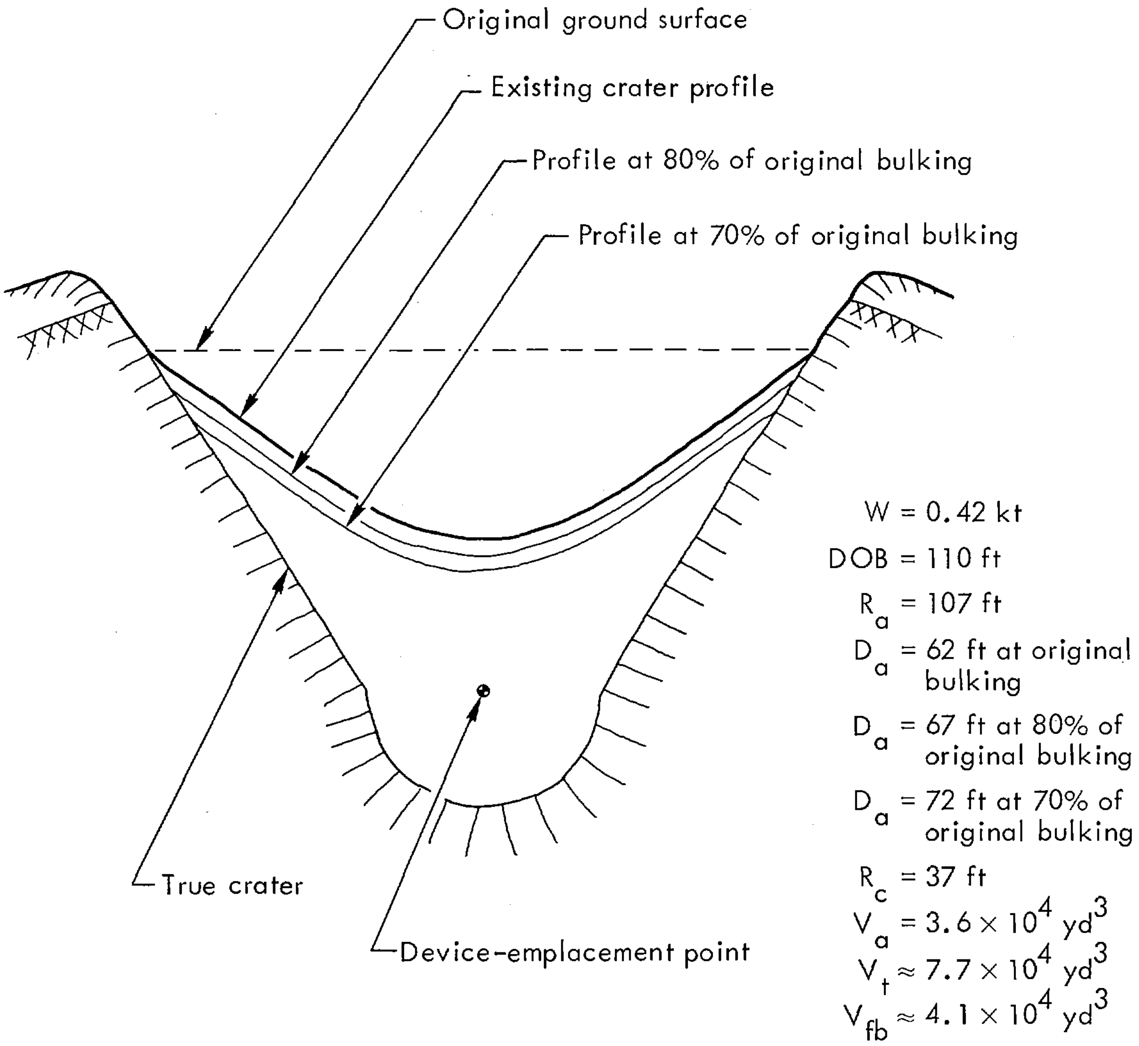
Original ground surface
Existing crater profile
Profile at 80% of original bulking
Profile at 70% of original bulking
True crater
Device-emplacement point
W = 0.42 kt
DOB = 110 ft
R_a = 107 ft
D_a = 62 ft at original bulking
D_a = 67 ft at 80% of original bulking
D_a = 72 ft at 70% of original bulking
R_c = 37 ft
$V_a = 3.6 \times 10^4$ yd^3
$V_t \approx 7.7 \times 10^4$ yd^3
$V_{fb} \approx 4.1 \times 10^4$ yd^3

Fig. 9. Estimated changes in the shape of the Danny Boy crater that would have occurred at different bulking factors of the fallback material (W = yield, DOB = depth of burst, R_a = apparent-crater radius, D_a = apparent-crater depth, R_c = cavity radius, V_t = true-crater volume, V_a = apparent-crater volume, and V_{fb} = fallback volume).

Highway cuts that must be made with more than one salvo because of yield limitations imposed by the projected seismic motion pose another problem. The connection of row charges results in the preferential ejection of some material into the previously excavated row. The amount of the material and its distribution within the adjoining crater is difficult to predict. Some experimental data are available for row-charge connections with chemical explosives at the 1- to 30-ton level, but these data cannot be directly applied to nuclear explosives at the 100-kt level. A mathematical model for this directed-explosion effect would require a three-dimensional code that does not exist and that may be impractical to develop. Simplifications may be possible to allow calculation with the two-dimensional TENSOR code, but verification will need to be obtained experimentally. The problem of row-charge connections is not as critical in a sea-level canal because it appears that there is sufficient volume below the navigation prism to accept the ejecta.

A. Project Carryall

Project Carryall is the name given to a proposed nuclear cut in the Bristol Mountains near Amboy in southern California. The cut was to be used for an interstate highway and a railroad. A feasibility study by the California State Division of Highways, the Atchison, Topeka, and Santa Fe Railway Company, the Lawrence Radiation Laboratory, and the U.S. Atomic Energy Commission was completed in 1964. The study concluded that the

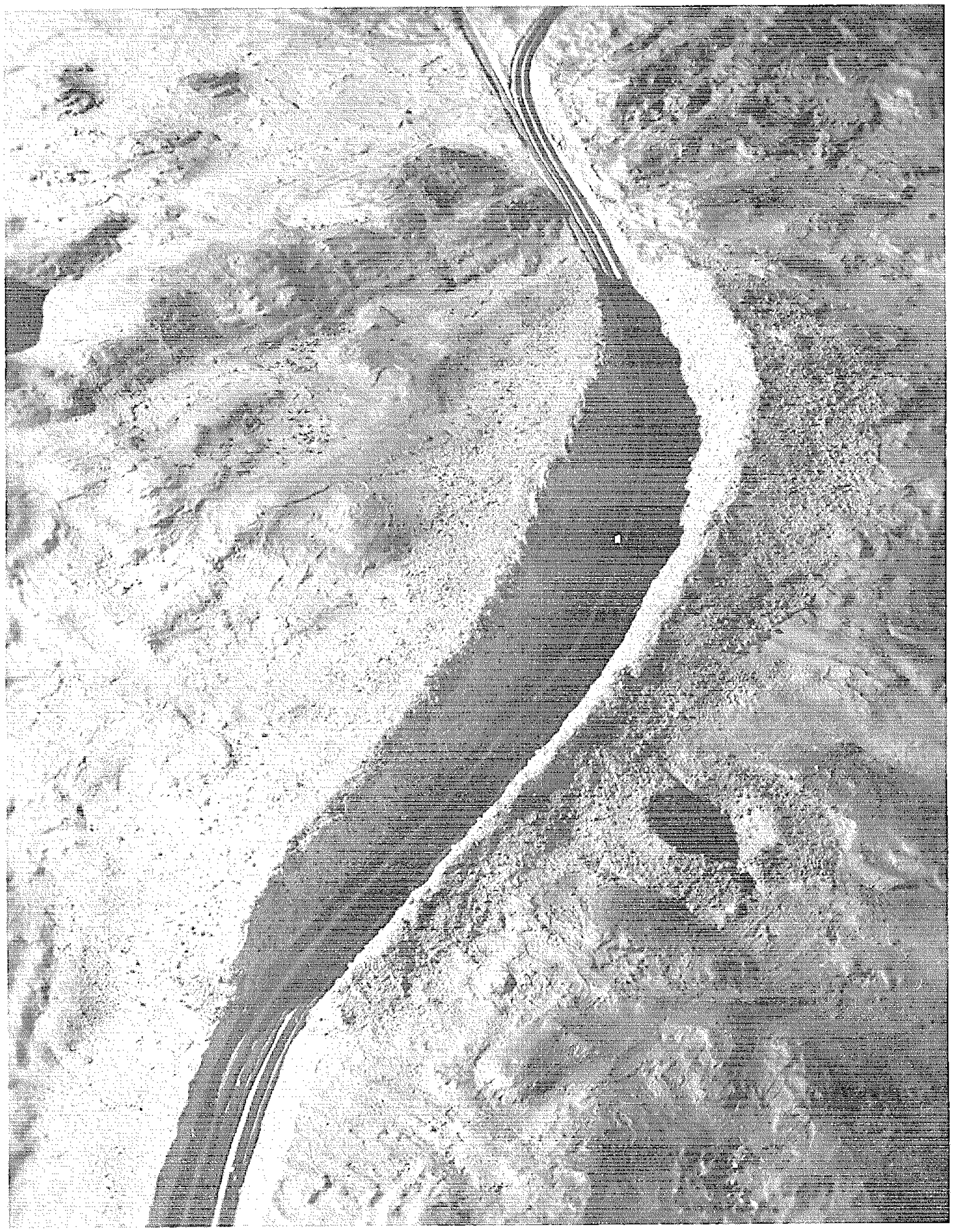

Fig. 10. Model of the proposed Carryall project.

project appeared to be technically feasible providing that nuclear row-cratering experiments were first conducted at NTS.[26] The study also concluded that the nuclear solution was $8,000,000 cheaper than the conventional solution, not counting the cost of the nuclear explosives. This project did not proceed beyond the feasibility study primarily because the time required to execute the requisite experiments at NTS was not compatible with the deadline for completing the interstate highway system.

Figure 10 shows a model of the proposed project. A conventional cut through this portion of the Bristol Mountains was deemed to be economically impractical. The proposed realignment, however, would have shortened the railway by 15 miles and saved 50 min of freight-train time.

The nuclear cut was to be about 2 miles long and was estimated to require a total yield of 1.83 Mt from 23 explosives. The largest single-explosive yield was 200 kt. The height of cut varied from 100 to 340 ft. As can be seen in Fig. 10, the excavation was slightly curved to avoid higher cut elevations. The only advantage to incorporating the close-spacing concept in the Carryall plan would be to allow the alignment to be straightened by going through higher elevations with no increase in explosive yields. With 25% enhancement of single-crater dimensions, 100 kt would be sufficient for a height of cut of 435 ft and 200 kt would be sufficient for 535 ft.

An interesting feature of the Carryall project was the use of a single 100-kt crater to solve a drainage problem. The volume of this crater would hold the maximum possible flood of 850 acre-ft expected in the nearby Orange Blossom Wash. This water would otherwise flow into the cut. The water trapped in such a crater would be dissipated by evaporation and some seepage. The conventional solution would have required the construction of threebridges, a channel, a dike, and riprap for slope protection.

NUCLEAR QUARRIES

A retarc (rubble mound) generated by a nuclear explosive at a depth much deeper than optimum for cratering in hard rock is potentially one of the most useful nuclear-excavation applications suitable for employment within the continental United States. In addition to producing large volumes of broken rock economically when placed close to the area of utilization,[27] the retarc can also be used as a dam. The major advantages of the retarc in comparison to craters include a much smaller release of radioactivity and the fact that relatively small yields produce a sufficient amount of broken rock to construct very large structures such as rock-fill dams.

The Sulky experiment (0.085 kt at a depth of burst of 90 ft; see Figs. 11 and 12) is the model on which potential nuclear-quarry applications are based. A practical concept of a nuclear quarry is shown in Fig. 13. Here, the detonation takes place on a hillside so that the rock within the true crater is more readily accessible to loading equipment.

Knowledge of the fragment-size distribution is an important consideration for most nuclear-quarry applications. The distribution of preshot fractures, including the development of joint sets, is probably the most important single factor determining the final size distribution of explosion-broken rock.[17,27] No data are available for the fragment-size distribution resulting from a nuclear explosion in a massive rock formation where the existing fractures and joint sets are widely spaced. The economics of a nuclear quarry could be altered if a significant amount of secondary blasting is required to reduce large blocks to manageable and useful dimensions.

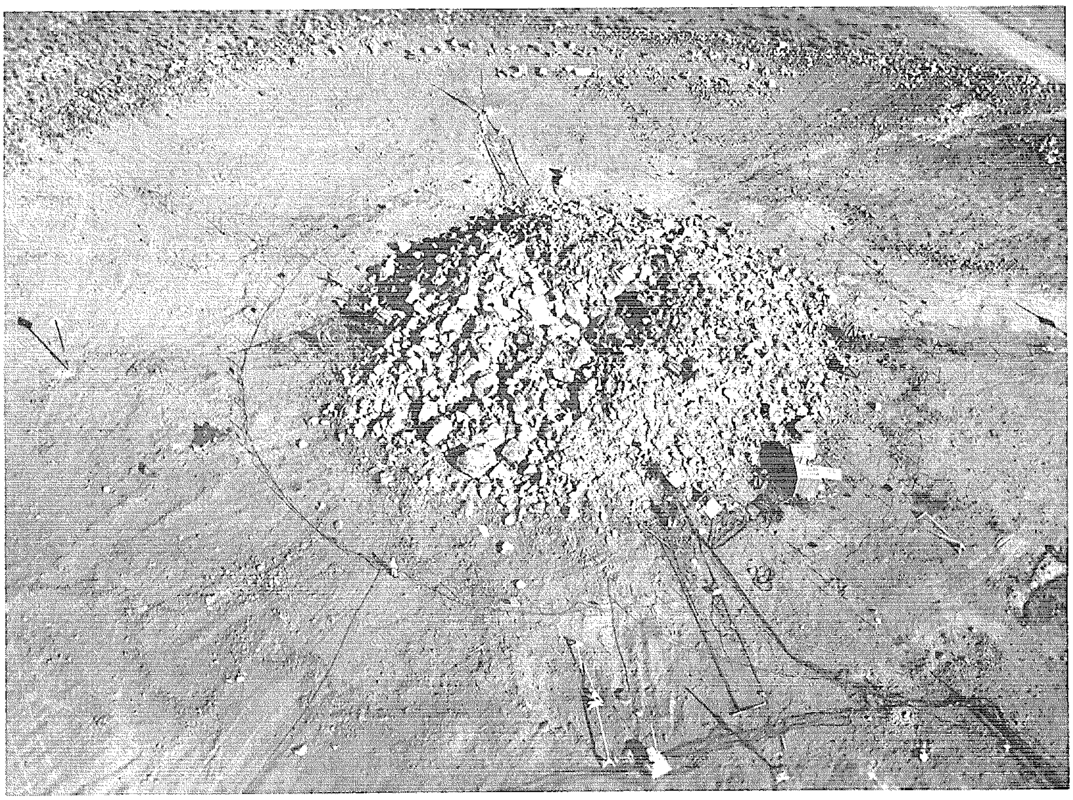

Fig. 11. Aerial view of the Sulky retarc.

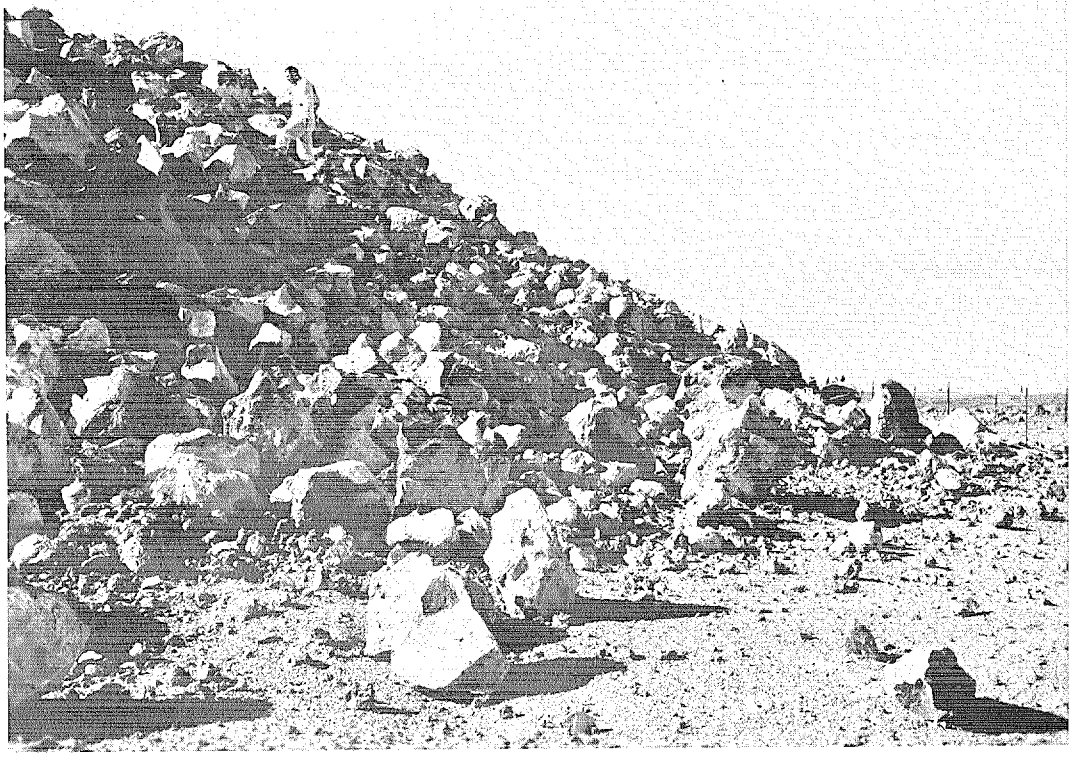

Fig. 12. Edge of the rubble mound formed by the Sulky experiment.

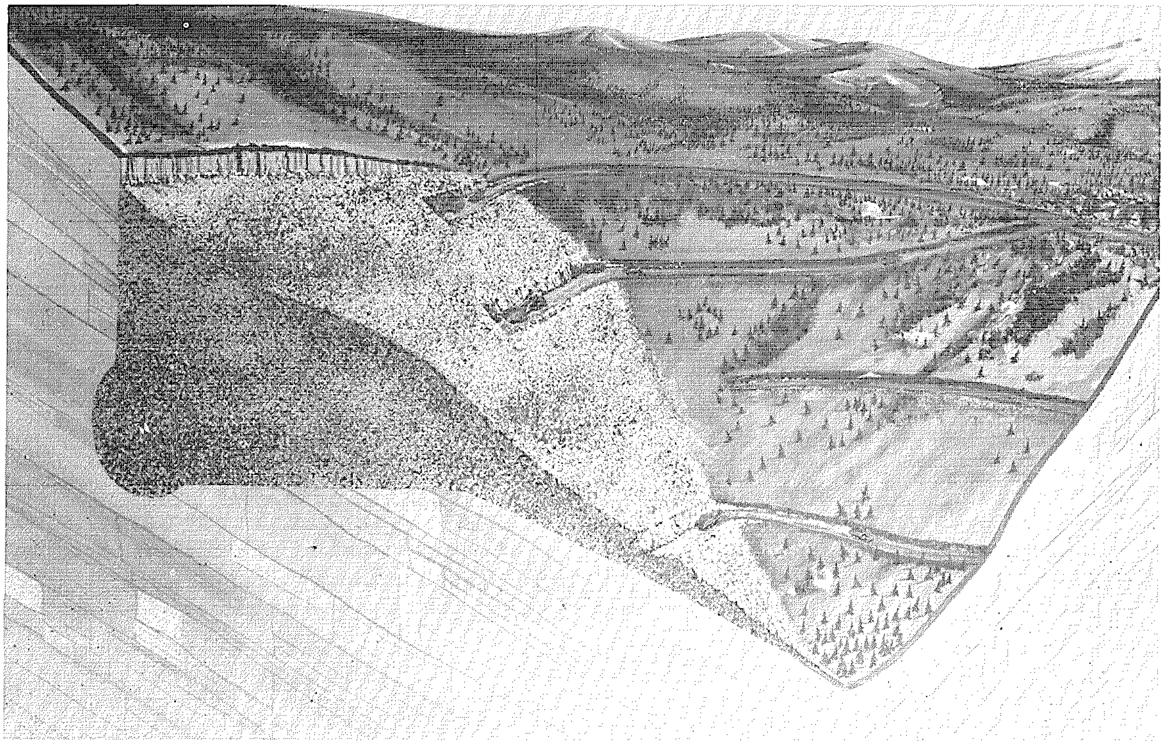

Fig. 13. Illustration of the nuclear-quarry concept.

The size of the evacuation area for a nuclear-quarry detonation is determined primarily by seismic considerations. Only a small amount of radioactivity would be vented to the atmosphere, and most of that is gaseous and does not result in fallout. The radioactivity produced is mixed and diluted into the large volume of broken rock at low levels. With a thermonuclear explosive, the isotope of primary concern is tritium in the form of THO. The rock aggregate can be washed prior to use and the wash water controlled and disposed of in a safe manner. Depending on the site and its geohydrologic characteristics, precautions may be necessary to preclude uncontrolled leaching of the tritium or other radionuclides from the retarc rubble.

A. Project Travois

Project Travois is a joint experiment of the AEC and the Corps of Engineers to demonstrate the nuclear-quarry application. Studies conducted by the Corps of Engineers produced three possibilities involving the production of quarry rock for rock-fill dams. The Twin Springs Dam Project near Boise, Idaho, was ultimately selected as the most promising site for an experiment. Preliminary site investigations conducted by the Corps of Engineers indicate that the rock there is suitable for a nuclear quarry, and a savings of about $1,000,000 is estimated in comparison with the conventional solution.[28] This savings does not include the expanded operational, safety, and technical programs that would be conducted during the experimental stage of any proposed application. No effort has been expended on Project Travois for more than a year, and there is no schedule for resuming this effort because priorities for government funds have been revised in favor of other projects within the state.

In the Travois experiment, it is expected that the detonation of a 40-kt explosive placed 685 ft from the nearest free surface in terrain with a 30-deg slope would produce in excess of 7,000,000 yd^3 of quarry rock.

This is more rock than is needed to construct the Twin Springs dam, which has a crest length of 1390 ft and a maximum height of 470 ft. The haul distance from the quarry to the damsite is about 1.5 miles.

It is believed that nuclear quarries can be constructed safely within the continental United States and should be considered for all construction projects that require large volumes of broken rock. A comparison of nuclear effects between nuclear quarries and other excavation applications has been reported by Knox.[2] Data from Project Travois would provide the basis for a realistic evaluation of nuclear-quarry applications as well as contribute to a useful end product. The experiment would primarily provide the information needed to determine both the minimum radiological safety controls for this application and the most efficient techniques for recovering the quarry rock.

Information from Project Travois would also be directly applicable to the concept of using nuclear retarcs for in-situ leaching of ore deposits that are near the ground surface. Figure 14 illustrates this concept with a series of retarcs detonated simultaneously to enhance the volume of rock fractured. The solution-mining system that would be employed and the technical and practical questions that need to be resolved by experiment are similar to those discussed in the Project Sloop feasibility study.[29]

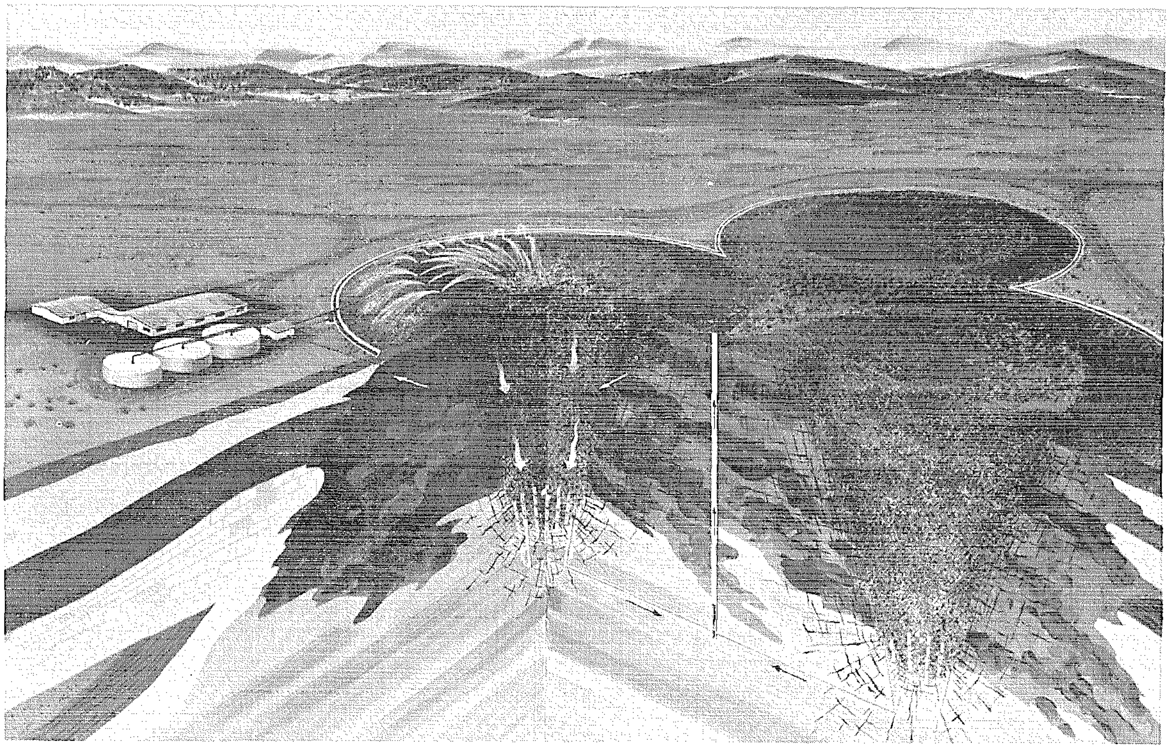

Fig. 14. Artist's concept of the use of retarcs for in-situ leaching of ore deposits.

OTHER APPLICATIONS

A number of additional concepts employing nuclear-excavation techniques have been proposed and reported, but no sense of urgency has developed to propel these concepts into a project status. Examples include the removal of overburden from ore bodies; reservoirs for flood control, irrigation, and groundwater recharge; crater-lip dams; and directed explosions for ejecta and bulk dams. In some applications, the technology has

Table V. Suggestions for possible nuclear excavations.[a]

Canals (navigation)

Interoceanic Canal — Panama, Colombia
Isthmus of Kra — Malaysia
Simpson Strait — Canada
Seoul (to Yellow Sea) — South Korea
Alternate Suez Canal — United Arab Republic
Luzon Island — Philippine Islands
Parana River — Argentina
Madeira River — Brazil
Mackenzie River Delta — Canada

Canals (diversion)

Mediterranian Sea to Chotts Depression — Tunisia, Algeria
Mediterranean Sea to Qattara Depression — United Arab Republic
Jonglei Canal — Sudan
Tempisque Valley — Costa Rica
Lake Titicaca — Bolivia
Ganges to Hooghly Rivers — India
Andes Mountains (east slope to west slope) — South America
Trinity, Mad, and Eel Rivers — California

Railroad or Highway Cuts

Boca Pass — California
Bristol Mountains — California
Buenaventura to Bogota — California
Chile to Argentina (three routes)

Water Resources (reservoirs, aqueducts)

Feather River — California
Ord River — Australia
Beni River — Bolivia
Paraquay River — Argentina and Paraquay
Mekong River — Southeast Asia
Swamp drainage — South Korea
Ambuklao Reservoir (silting basin) – Philippine Islands

Dams (landslides, construction of spillway sites, production of aggregates)

Rio Bio-Bio (several sites) — Chile
Nari and Hab Rivers — Pakistan
Rampart Dam — Alaska
Camelback Dam — Arizona
Cochiti Dam — New Mexico
Tarbela Dam — Pakistan

Harbors

Shemya Island — Alaska
Nome — Alaska
Arica — Chile
Salaverry — Peru
Cape Keraudren — Australia

[a] Taken from Ref. 33.

not been sufficiently advanced to permit qualified judgments to be made on the suitability of using nuclear explosives. This is particularly true in the general area of water-resources development, where additional studies are needed to define the problem of surface- and groundwater contamination in flooded craters and retarcs.

The Soviet Union has used directed-explosion techniques for many years in the construction of earth- and rock-fill dams.[30-32] Unfortunately, these construction projects are not reported in detail. It is known that relatively small charges of chemical explosives were used in comparison with the nuclear yields that are felt to be necessary for nuclear excavation to be economically attractive. The analytical procedures used to design projects with directed chemical explosives should be applicable to nuclear explosives when the differences in the energy source are properly considered. Because of the present rate at which nuclear-excavation experiments are being performed (seven experiments since 1962), and because of the need to obtain more critical information on the effects of higher yields, material properties, and row-charge interactions, it will be many years before the techniques of directed explosions are developed to the point where large projects can be undertaken with confidence.

The greatest potential for nuclear excavation lies in underdeveloped nations. Nuclear excavation can be used to accelerate the growth and prosperity of these nations because projects not previously considered economically or technically feasible now appear to be possible. Typical projects would include the removal of natural barriers that have limited transportation or have prevented the diversion of rivers to provide the water needed for development. Water-resources projects such as dams and reservoirs would help conserve the available supply of water and prevent damage from flooding. Another possibility is a canal to connect the Qatarra Depression in the United Arab Republic with the Mediterranean Sea to provide hydroelectric power. Table V, which is a partial list of the possible nuclear-excavation applications that have been suggested, is included only to show the world-wide distribution of such projects. Many of these suggestions may not be feasible for nuclear excavation, or they may be better solved conventionally.

The impetus to proceed with such projects may come from the Non-Proliferation Treaty in which the United States and the Soviet Union have assured nonnuclear signatories of the treaty that they will not lose the potential benefits of peaceful applications if they renounce the acquisition of nuclear explosives. The United States has further announced that it will continue its research and development in the Plowshare program in order to make the benefits of such explosions available to nonnuclear signatories without delay.

CONCLUSIONS

There are useful demonstration projects that it is believed can be accomplished safely with existing technology. Examples are a deep-water harbor and a nuclear quarry. Data from such projects as these will greatly increase our knowledge of cratering and associated phenomena in a different environment from that at the Nevada Test Site. Current assessments of the feasibility of constructing a sea-level canal with nuclear explosives in Panama and Colombia are favorable from a technical viewpoint. Although additional experiments and studies will be required before this ambitious project is executed, the knowledge gained will probably eliminate some of the conservatism in the current analysis as well as provide the most economic and efficient design. The concept of close spacing in row-charge designs has made it possible to greatly reduce required salvo yields so that the seismic motions predicted for large cities near such detonations are now similar to the motions produced in populated areas by nuclear tests and earthquakes in which no real damage to residential or high-rise structures has been noted.

Nuclear excavation promises to accelerate the growth and prosperity of many nations for the benefit of all. It is an effective tool that can be developed to conserve man's most precious resource—water.

APPENDIX A: VECTOR ADDITION OF VELOCITY PROFILES

The required spacing between the explosives in a row can be estimated by adding the vertical velocity profiles of adjacent charges. The vertical mound velocities obtained in this manner should be an upper limit, for it is assumed that the peak pressures and the resulting particle velocities arrive at all points of interaction at the same time. The velocity profile used is the one that results at the ground surface primarily from spall; it does not include gas acceleration.

Figure A-1 shows the vertical velocity profile from the Sulky experiment[34] normalized to the peak velocity at surface ground zero (V_{SGZ}). Horizontal distances along the surface are shown as a fraction of the depth of burst (DOB).

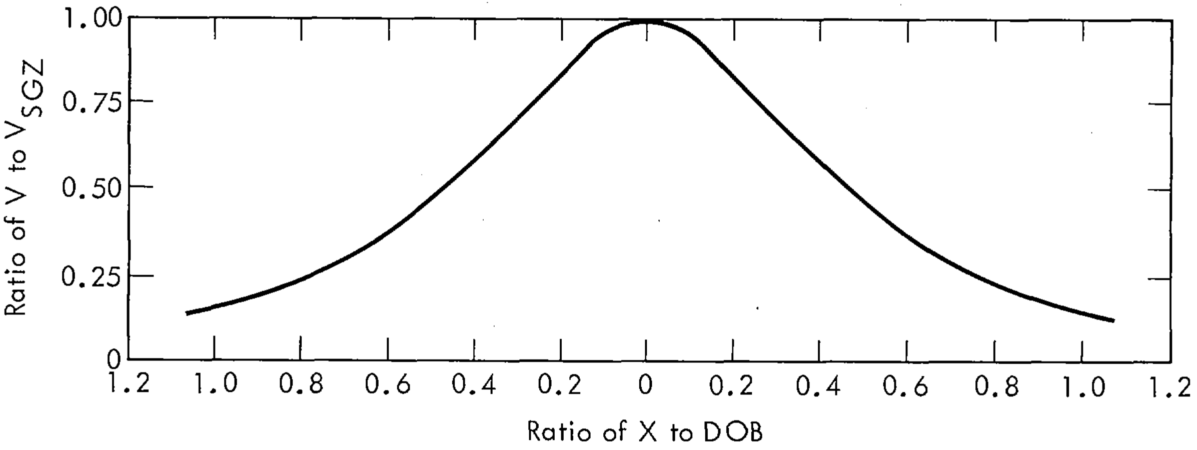

Fig. A-1. Vertical velocity profile from the Sulky experiment normalized to the peak velocity at surface ground zero (V = vertical velocity, V_{SGZ} = peak velocity at surface ground zero, X = distance along ground surface, and DOB = depth of burst).

Figure A-2 shows the resulting vector addition when the spacing (S) between explosives is 0.75DOB, or S/DOB = 0.75. The resulting average vertical velocity(V_R) along a row axis is shown to be 1.56 times the V_{SGZ} of a single charge, or V_R/V_{SGZ} = 1.56. If the DOB is chosen to be 160 ft for the 1-kt explosive, then V_R is determined to be equivalent to the peak vertical spall velocity (V_{SGZ}) of a single 2.5-kt explosive buried at 160 ft. The apparent yield (W_{ap}) of the explosives in a row is defined here as the yield of a single explosive at the same depth of burst as the row explosives that would be required to produce the peak velocity obtained by vector addition. If the row dimensions are proportional to W_{ap} as shown by points B and C'' in Fig. 1, the dimensions of the row crater will be 30% larger than that of a 1-kt cratering explosion at an optimum depth of burst.

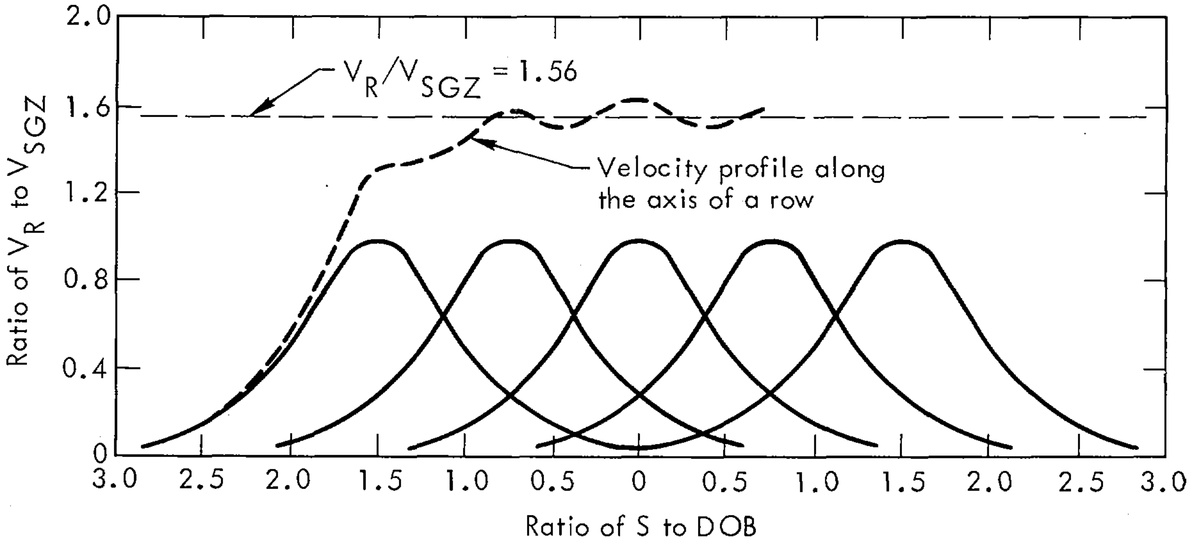

Fig. A-2. Vector addition of single-charge velocity profiles for nuclear explosions in dry, hard rock at S = 0.75DOB (V_R = average vertical velocity along row axis, V_{SGZ} = peak vertical spall velocity, S = spacing, and DOB = depth of burst).

Figure A-3 is a plot of V_R/V_{SGZ} versus S/DOB as determined from Fig. A-2. The resulting relationship for nuclear explosives in dry, hard rock is

$$V_R/V_{SGZ} = 1.2(S/DOB)^{-0.95} \ . \tag{A-1}$$

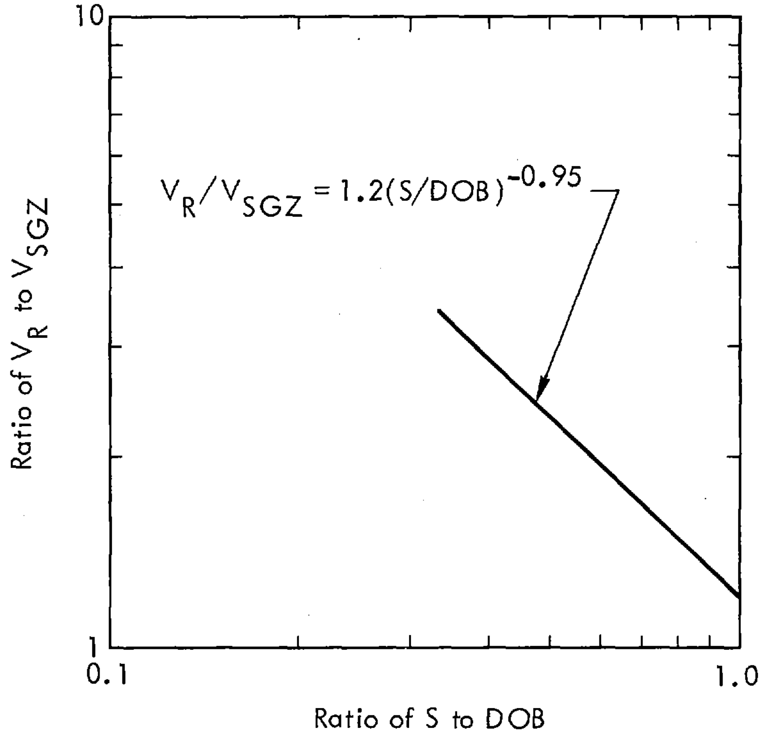

Fig. A-3. Plot of V_R/V_{SGZ} versus S/DOB for nuclear explosions in dry, hard rock (V_R = average vertical velocity along row axis, V_{SGZ} = peak vertical spall velocity, S = spacing, and DOB = depth of burst).

The next step is to determine the relationship between V_R (obtained by vector addition) and W_{ap} for dry, hard rock. This is accomplished by using the data shown in Fig. A-4, which is a plot of V_{SGZ} versus DOB for both nuclear and chemical cratering experiments. Only data from Danny Boy and Sulky are used to determine the relationship shown for nuclear explosives in Eq. A-2 because Buggy, Cabriolet, and Schooner occurred in layered rock formations having different properties.[23] For nuclear explosives, then,

$$V_{SGZ} = 2.98 \times 10^5 (DOB)^{-1.54} \ . \tag{A-2}$$

From Eq. (A-2), it can be shown that

$$V_R/V_{SGZ} = \left(\frac{W_{ap}^{1/3}}{W^{1/3}}\right)^{1.54} = \left(\frac{W_{ap}}{W}\right)^{0.51} , \tag{A-3}$$

where W is the actual yield of the row explosives. Figure A-5 is a plot of S/DOB versus W_{ap}/W as derived from Eqs. (A-1) and (A-3). The relationship is

$$S/DOB = 1.2\left[\frac{W_{ap}}{W}\right]^{-0.53} \ . \tag{A-4}$$

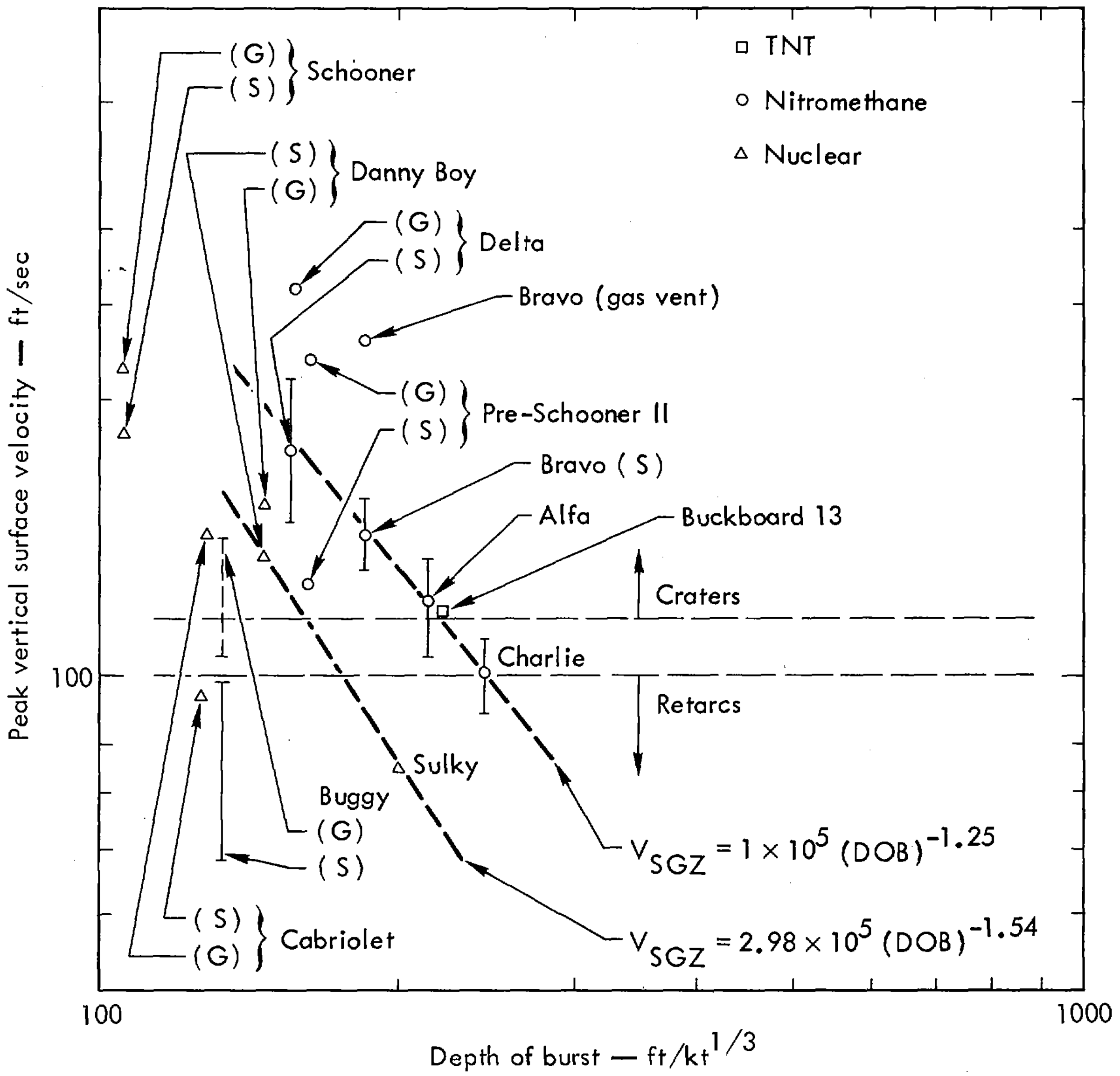

Fig. A-4. Plot of peak vertical surface velocity versus depth of burst for nuclear and chemical cratering experiments in dry, hard rock (V_{SGZ} = peak vertical spall velocity, G = acceleration due to gas, and S = acceleration due to spall).

To complete the nuclear close-spacing concept, Fig. A-6 is a plot showing the required DOB versus S/DOB for 1 kt. This was determined by selecting a peak spall velocity for the single-charge crater at the optimum point on the cratering curve. A value of 190 ft/sec was chosen for dry, hard rock. Then, for any S/DOB, a DOB is determined from Eqs. (A-1) and (A-2) such that $V_R \approx 190$ ft/sec. The resulting equations are

$$\mathrm{DOB} = \left[\frac{3.58 \times 10^5}{V_R}\right]^{0.65} (\mathrm{S/DOB})^{-0.62} \qquad \text{(A-5)}$$

and, for $V_R = 190$ ft/sec,

$$\mathrm{DOB} \approx 135(\mathrm{S/DOB})^{-0.62} . \qquad \text{(A-6)}$$

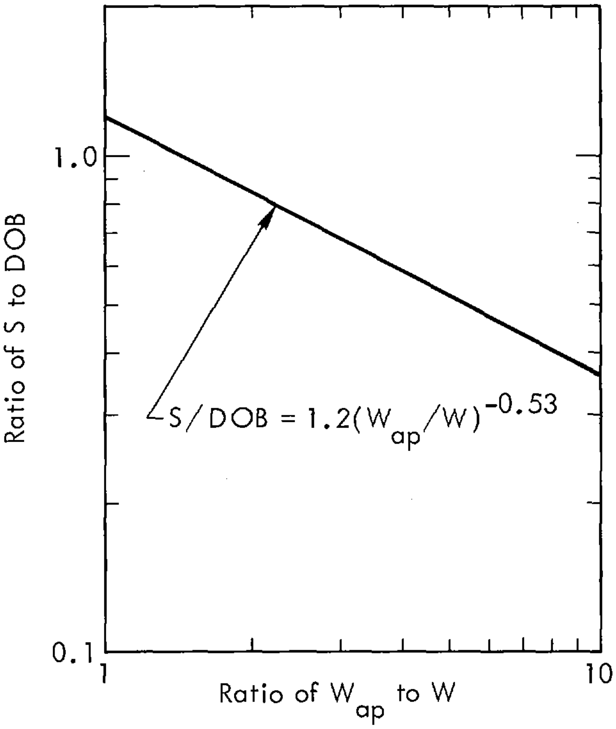

Fig. A-5. Plot of S/DOB versus W_{ap}/W for a 1-kt nuclear explosion in dry, hard rock (S = spacing, DOB = depth of burst, W_{ap} = apparent yield, and W = actual yield).

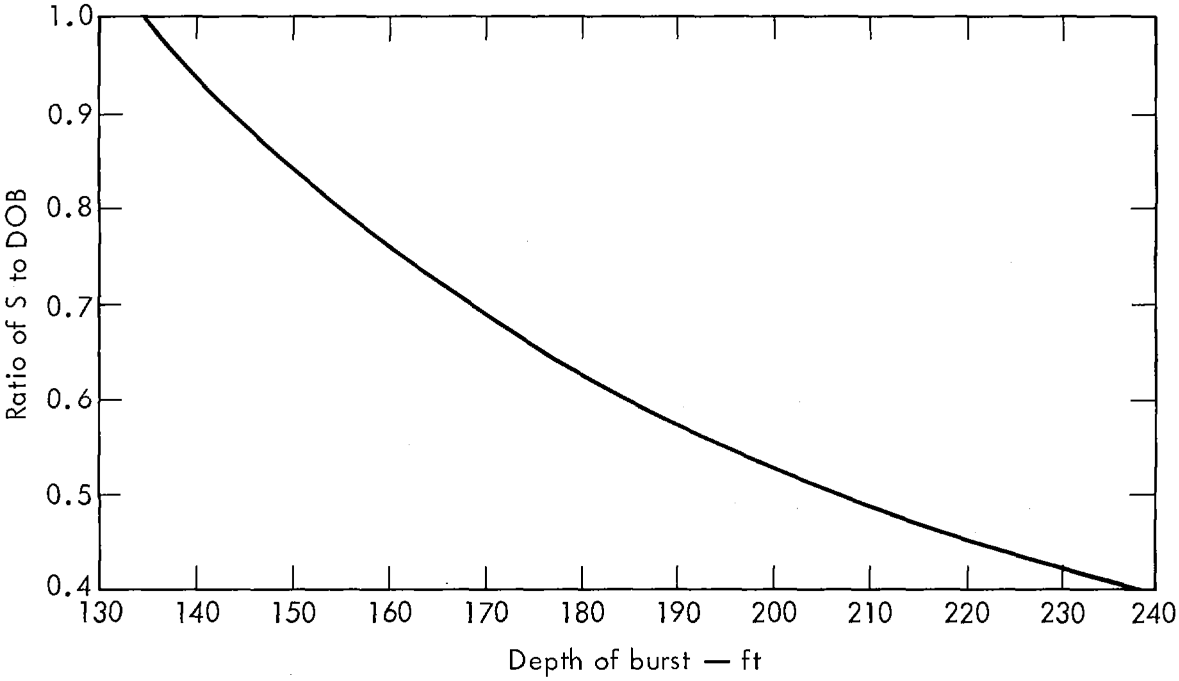

Fig. A-6. Plot of S/DOB versus DOB for a 1-kt nuclear explosion in dry, hard rock (S = spacing and DOB = depth of burst).

Finally, Fig. A-7 shows row-charge enhancement as a function of S, where S is defined as a fraction of the optimum crater radius (R_a) for 1 kt. The R_a for a 1-kt explosive in dry, hard rock is assumed to be 150 ft. For the current interoceanic-canal study, enhancements of 1.25 and 1.3 are assumed for spacings of 0.8 and 0.75R_a in comparison to the values of 1.32 and 1.45 obtained with the procedures presented here.

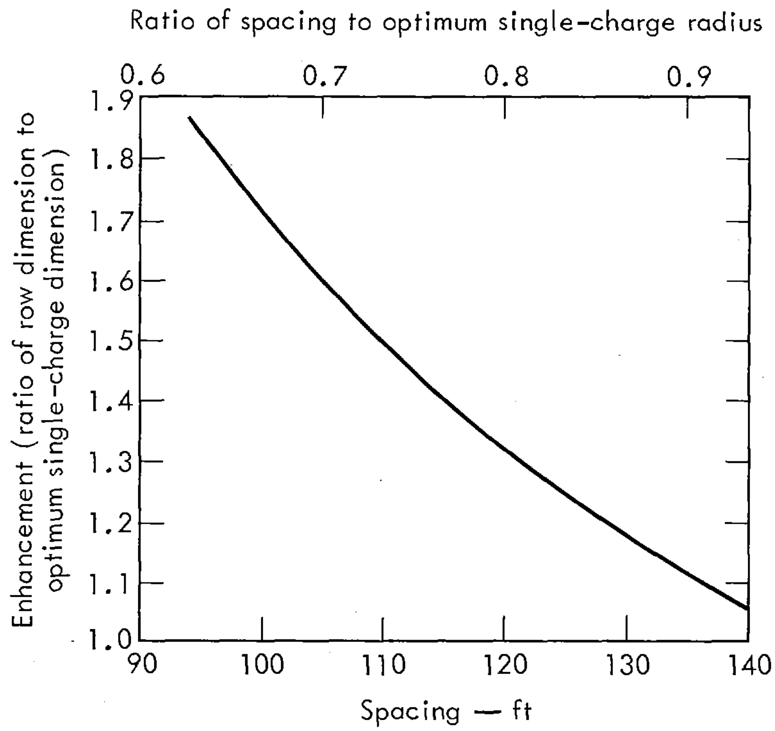

Fig. A-7. Row-crater enhancement versus spacing and S/R_a for a 1-kt nuclear explosion in dry, hard rock (S = spacing and R_a = optimum single-charge radius).

The U.S. Army Engineer Nuclear Cratering Group conducted a series of row excavations in September and October 1969 that were designed to investigate close-spacing concepts. Six rows containing from five to nine 1-ton charges of chemical explosive (nitromethane) were detonated in Bear Paw shale at Ft. Peck, Montana.[35] The preliminary results[7] are shown in Fig. A-8, in which they are compared to curves derived for chemical explosives in Bear Paw shale and nuclear explosives in dry, hard rock. The upper and lower predicted curves for shale result from the differences in the vertical surface-velocity profiles between shallow and deep charges (see next paragraph). In the nuclear case in dry, hard rock, the velocity profiles for Danny Boy and Sulky appear to be quite similar.

The upper shale curve in Fig. A-8 is based on the velocity profile of a single 1-ton charge (SC-2) that was somewhat shallower than optimum, the lower curve on that of a 1-ton charge (SC-3) much deeper than optimum.[36] The resulting relationships are

$$V_R/V_{SGZ} = 1.75(S/DOB)^{-0.89} \text{ for SC-2} \qquad (A\text{-}7)$$

and

$$V_R/V_{SGZ} = 1.52(S/DOB)^{-0.89} \text{ for SC-3.} \qquad (A\text{-}8)$$

The peak spall velocities versus depth of burst for chemical explosives in shale are identical to those for chemical explosives in dry, hard rock as shown in Fig. A-4. That is,

$$V_{SGZ} = 1 \times 10^5 DOB^{-1.25} . \qquad (A\text{-}9)$$

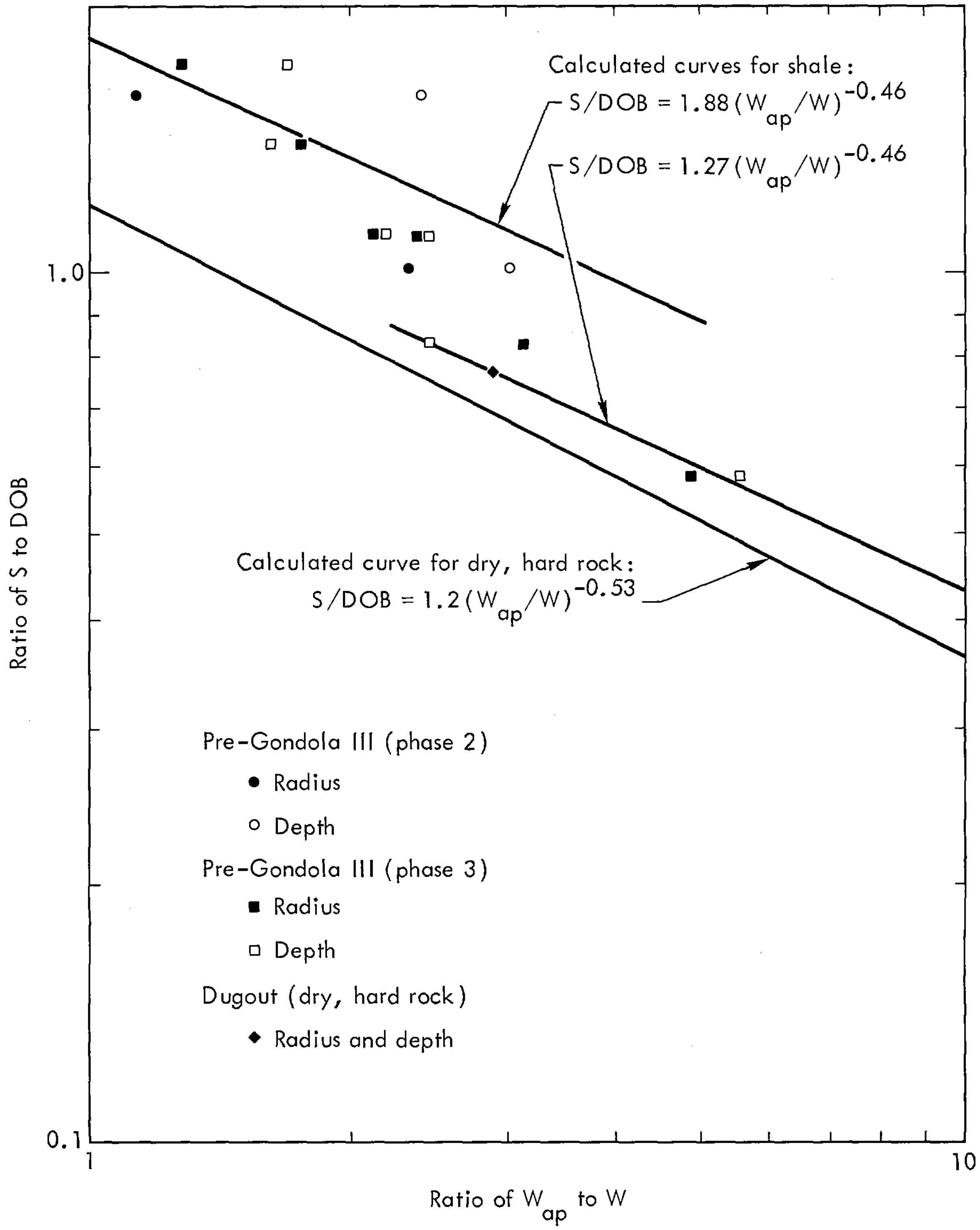

Fig. A-8. Close-spacing concept — experimental data versus calculated curves. Dugout was a nuclear experiment, the others were chemical. (S = spacing, DOB = depth of burst, W_{ap} = apparent yield, and W = actual yield).

The relationships between S/DOB and W_{ap}/W as derived from Eqs.(A-7), (A-8), and (A-9) are

$$S/DOB = 1.88\left(\frac{W_{ap}}{W}\right)^{-0.46} \quad \text{with the SC-2 profile} \qquad (A-10)$$

and

$$S/DOB = 1.27\left(\frac{W_{ap}}{W}\right)^{-0.46} \quad \text{with the SC-3 profile .} \qquad (A-11)$$

The agreement between calculated and experimental values is remarkably good in view of the number of variables and unknowns involved in row-charge experiments and the assumptions used in the vector addition of surface velocities. Only two row-charge experiments have been conducted in dry, hard rock—Dugout[37] and Buggy.[4] The spacing between the nuclear explosives in the Buggy experiment (S/DOB = 1.1) was too large for any noticeable enhancement to occur, but this cannot be stated positively because no single-charge craters exist at the Buggy site for comparison. Significant enhancement did occur in the Dugout experiment, which consisted of five 20-ton charges of nitromethane spaced 45 ft apart and buried 59 ft deep (S/DOB = 0.76). The row dimensions were 36 to 37% larger than the optimum single crater, which leads to an apparent yield of 2.8 times the actual yield. Dugout is plotted in Fig. A-8 above the nuclear curve but on the shale curve. The velocity profile applicable to Dugout is similar to that used for the lower shale curve, and the relationship of V_{SGZ} to DOB as shown in Fig. A-4 is also identical for nitromethane in both shale and dry, hard rock. A curve derived for chemical explosives in dry, hard rock would therefore be identical to the lower shale curve.

Additional field experiments are needed to further refine the close-spacing concept. Invaluable information has been gained from chemical experiments, but a nuclear row with relatively high yields is needed to provide the data necessary to refine the detonation design for a sea-level canal.

REFERENCES

1. E. Teller, W. K. Talley, and G. H. Higgins, Constructive Uses of Nuclear Explosives (McGraw-Hill Book Company, Inc., New York, 1968).
2. J. B. Knox, "Nuclear Excavation: Theory and Applications," Nucl. Appl. Technol. 7, 189 (1969).
3. G. C. Werth, A. Holzer, R. W. Terhune, H. A. Tewes, J. Toman, and W. R. Woodruff, Interim Canal Assessment of June 1969, report UCRL-50689, Lawrence Radiation Laboratory, Livermore (1969).
4. J. Toman, "Project Buggy: A Nuclear Row Excavation Experiment," Nucl. Appl. Technol. 7, 243 (1969).
5. B. B. Redpath, "A Concept of Row Crater Enhancement," this Proceedings.
6. J. E. Lattery, G. Steinhardt, B. Anderson, J. Reed, J. B. Andrews, G. Smith, W. Mickey, and R. Ballard, Project Pre-Gondola III, Phase II: Connecting Row-Charge Experiment, Summary Report, report PNE-1117, Nuclear Cratering Group, Livermore (to be published).
7. Private communication from B. B. Redpath, Nuclear Cratering Group, Livermore.
8. Isthmian Canal Studies, 1964, reports PNE-1999 through -2006, U.S. Atomic Energy Commission, U.S. Army Engineers, and Panama Canal Company (1964).
9. M. D. Nordyke and W. Wray, "Cratering and Radioactivity Results from a Nuclear Cratering Detonation in Basalt," J. Geophys. Res. 69, 675 (1964).
10. R. W. Terhune, T. F. Stubbs, and J. T. Cherry, "Nuclear Cratering on a Digital Computer," this Proceedings.
11. M. E. Nadolski, "Architectural Damage to Residential Structures from Seismic Disturbances," Bull. Seism. Soc. Am. 59, 487 (1969).

12. *Interoceanic Canal Ground Motion Report*, report NVO-1163-125, Environmental Research Corporation, Alexandria (1967).
13. J. A. Blume, "Ground Motion Effects," *Proceedings, Symposium on Public Health Aspects of Peaceful Uses of Nuclear Explosives* (U.S. Public Health Service, Washington, D.C., 1969).
14. Private communication from Y. C. Ng, Lawrence Radiation Laboratory, Livermore.
15. *Technical Concept for Project Tugboat: Explosive Excavation of Kawaihae Light Draft Harbor*, unnumbered report, Nuclear Cratering Group, Livermore (1969).
16. W. E. Vandenberg and W. C. Day, "Excavation Research with Chemical Explosives," this *Proceedings*.
17. R. C. Nugent and D. C. Banks, *Project Danny Boy: Engineering-Geologic Investigations*, report PNE-5005, U. S. Army Engineer Waterways Experiment Station, Vicksburg (1966).
18. H. A. Tewes, "Results of the Schooner Excavation Experiment," this *Proceedings*.
19. Private communication from M. D. Nordyke, Lawrence Radiation Laboratory, Livermore.
20. J. T. Cherry, "Computer Calculations of Explosion-Produced Craters," *Intern. J. Rock Mech. Min. Sci.* 4, 1 (1967).
21. N. M. Short, *Project Danny Boy: The Definition of True Crater Dimensions by Postshot Drilling*, report WT-1834, Lawrence Radiation Laboratory, Livermore (1964).
22. H. A. Tewes, "Results of the Cabriolet Excavation Experiment," *Nucl. Appl. Technol.* 7, 232 (1969).
23. J. Toman, "Summary of Results of Cratering Experiments," *Proceedings, Symposium on Public Health Aspects of Peaceful Uses of Nuclear Explosives* (U.S. Public Health Service, Washington, D.C., 1969).
24. J. F. Leisek, *Postshot Geologic Investigations of the Danny Boy Nuclear Cratering Experiment in Basalt*, report UCRL-7803, Lawrence Radiation Laboratory, Livermore (1964).
25. Private communication from A. D. Frandsen, Nuclear Cratering Group, Livermore.
26. H. C. Prentice, "Application of Nuclear Explosives for a Mountain Pass Highway and Railroad," *Proceedings, Third Plowshare Symposium* (U.S. Atomic Energy Commission, Oak Ridge, 1964).
27. S. M. Hansen and J. Toman, *Aggregate Production with Nuclear Explosives*, report UCRL-12180, Rev. 2, Lawrence Radiation Laboratory, Livermore (1965).
28. *Nuclear Quarrying Feasibility Study, Twin Springs Dam and Reservoir, Boise River, Idaho*, unnumbered report, U.S. Army Engineer District, Walla Walla (1966).
29. *Sloop*, report PNE-1300, Kennecott Copper Corporation, U.S. Atomic Energy Commission, U.S. Bureau of Mines, and Lawrence Radiation Laboratory, Livermore (1967).
30. L. J. Circeo Jr., *Engineering Properties and Applications of Nuclear Excavations*, report UCRL-7657, Lawrence Radiation Laboratory, Livermore (1964).
31. "Russians Fire Off an Instant Rockfill Dam," *Eng. News-Record*, May 30, 1968, p. 24.
32. S. White, "Building a Dam with a Bang," *New Scientist*, November 14, 1968.
33. L. J. Vortman, *Nuclear Excavation*, report SC-DC-69-1716, Sandia Laboratories, Albuquerque (1969).
34. R. Brower and D. Wilson, *Project Sulky: Scientific Photography*, report PNE-710F, EG&G, Inc., Las Vegas (1966).
35. *Technical Concept for Project Pre-Gondola III, Phase III: Connection of Pre-Gondola II Crater to Ft. Peck Reservoir and Row Crater Connection Experiment*, unnumbered report, Nuclear Cratering Group, Livermore (1969).

36. W. G. Christopher and J. E. Lattery, *Project Pre-Gondola I, Crater Studies: Surface Motion*, report PNE-1107, Part II, Nuclear Cratering Group, Livermore (1969).

37. M. D. Nordyke, *Project Dugout: Technical Director's Summary Report*, report PNE-600F, Lawrence Radiation Laboratory, Livermore (1965).

XA04N0753

Status of the Interoceanic Canal Study

Brigadier General R. H. Groves, USA
Corps of Engineers
Engineering Agent for the Atlantic-Pacific
Interoceanic Canal Study Commission

You have asked me to report on the current status of work being done by the Atlantic-Pacific Interoceanic Sea-Level Canal Study Commission, of which I am the Engineering Agent. Our studies are not as yet completed, although there is no reason at this time to doubt that the 1 December 1970 deadline for the Commission's final report will be met. Since it has not been published, I am unable to pass on to you any of its conclusions; they simply do not exist today. And it would be improper for me to reveal the substance of the Commission's deliberations to date or to speculate upon what their outcome may be. But many elements of the work being conducted under my supervision - The Engineering Feasibility Study - are already in the public domain. It is to them that my remarks here are addressed.

Of the six basic routes we have considered in our studies (FIGURE 1) for possible sea-level canal alinements, four could involve nuclear excavating techniques. The so-called nuclear alternatives are Route 8 along the Nicaragua-Costa Rica border, Route 17 across the Darien Isthmus of Panama, Route 23 crossing the Panama-Colombia border and Route 25 across the western tip of Colombia. The conventionally excavated routes are Route 10 west of the Panama Canal Zone and Route 14 along the alinement of the present canal. The engineering studies examine from a technical standpoint the feasibility of constructing these routes and estimate their costs. To accomplish this we have made conceptual designs for canals capable of transitting at least 40,000 vessels annually (and possibly several times that many) and of accommodating ships of up to 250,000 dwt in size. Thus, in terms of basic requirements, all alternatives - conventional and nuclear - have been made comparable.

Beginning with the northernmost route, let us now consider the four nuclear alternatives. Route 8 (FIGURE 2) is 137 miles in length. Its maximum elevations are slightly less than 800 feet in the Continental Divide and about 400 feet through the so-called Eastern Divide. The rock to be excavated is primarily volcanic tuff.

It is readily apparent that this route is not competitive with other nuclear alternatives because of its location in a relatively well developed, built-up region. Its construction would require the evacuation of more than one-quarter million people from the exclusion area for the duration of nuclear operations and for about a year thereafter. This would almost certainly be politically unacceptable. There would be an additional requirement on shot days for the temporary evacuation of an estimated 30,000 people from high rise buildings in Managua and San Jose to avoid casualties from possible structural collapse caused by ground shock. The magnitude of these problems can be expressed to some degree in terms of the estimated cost of their resolution. In this case, they constitute a major part - \$1.7 billion - of the Route 8 construction costs which we estimate to be \$3.5 billion.

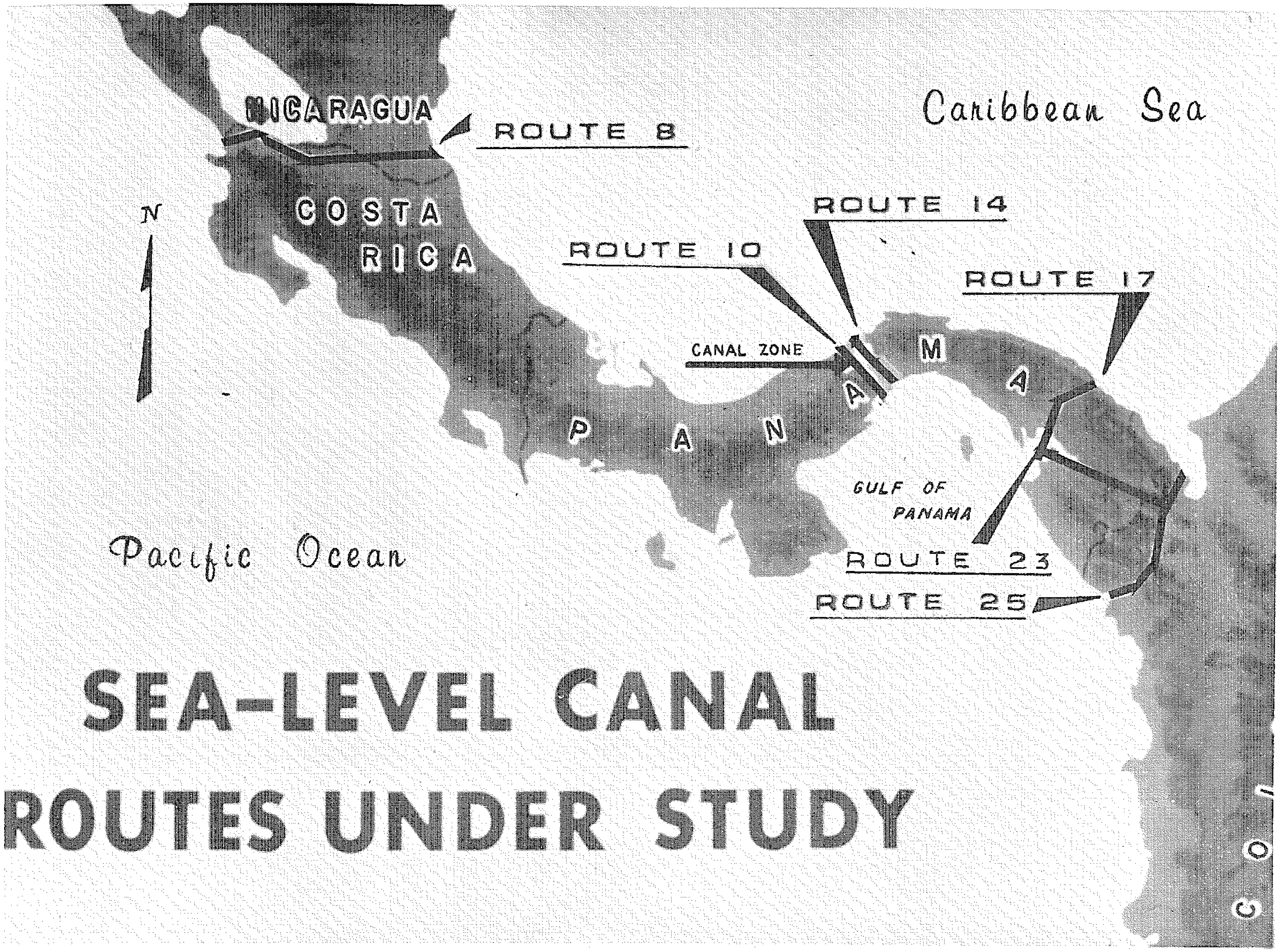

Figure 1. Routes selected for investigation by the Atlantic-Pacific Interoceanic Canal Study Commission. Route number system was established by an earlier study.

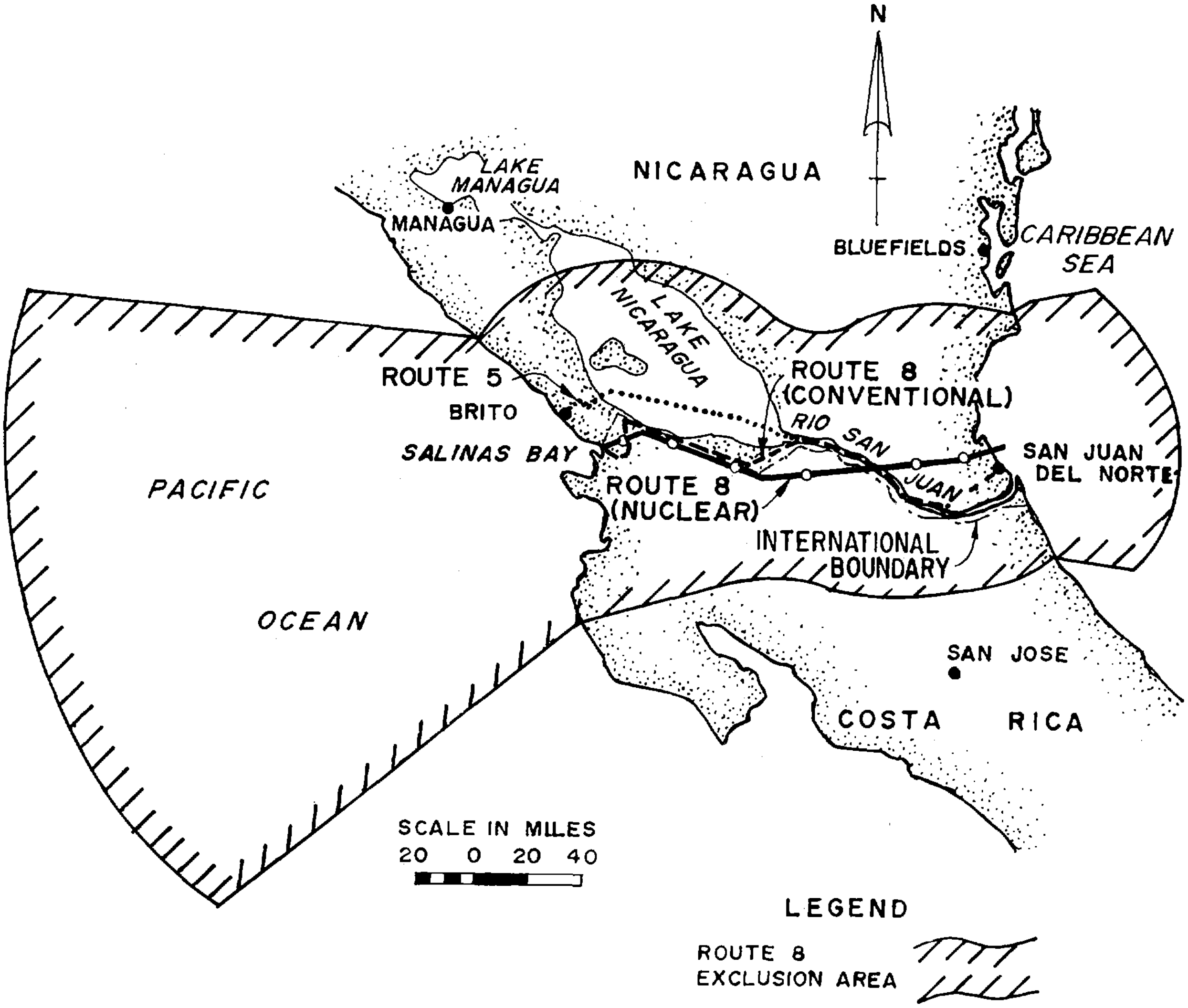

ROUTE 8

Figure 2. Alinement of Route 8, showing tentative nuclear exclusion area.

At the start of our studies in 1964, Route 17 (FIGURE 3) was thought to be the only alternative that could be built for less than one billion dollars. Since then our exploratory drilling in the Chucunaque Valley has identified an extensive formation of clay shales. Called Sabana Shale, this is a very poor construction material. From what we have learned about it, we would expect it to be unstable unless the bank slopes of any cuts we might make through it were extremely flat, possibly approaching slopes as flat as 1 on 14 in the higher elevations.

Our present conceptual design of this 49 mile-long canal calls for nuclear excavation through the Pacific Hills and through the Continental Divide on the Atlantic side. The reach through the Pacific Hills is about ten miles long, averaging about 250 feet in elevation, and cuts through a maximum elevation of nearly 800 feet. The Divide cut is nearly 20 miles long, averaging 400 feet in elevation, reaching a maximum of 980 feet. Rock in the Divide is mainly pyroclastic and volcanic basalts, while the Pacific Hills are formed mostly of sedimentary rock of volcanic, pyroclastic or tuffaceous origin.

On the assumption that nuclear excavation is found to be engineeringly feasible, the nuclear design calls for 250 devices in 27 separate detonations of from one to eleven megatons. The largest single charge would be three megatons. Some 40,000 people now live in the exclusion area. Although relatively speaking, the economic burden imposed by moving them is not large - about $140 million - the social and political consequences of this project for Panama might make it unacceptable.

In the final analysis, however, the economic feasibility of Route 17 hinges on the method employed to cut through the Chucunaque Valley. We have investigated many ways to use nuclear explosives for this, including overexcavation, slope flattening by hydraulicking and subsidence cratering. The most promising results have been obtained from arrays of explosives; however, we have not yet achieved the stable bank slope conditions that we must have. At the present time, we believe that the flattest slopes we could produce by nuclear means would be on the order of 1 on 8, and even that capability has not yet been demonstrated. Consequently, our estimates currently show the Chucunaque reaches to be constructed by conventional means at a cost of $1.8 billion of the total $2.9 billion estimated for this alternative.

Recently the Colombian Government requested informally that we evaluate Route 23 (FIGURE 4) which might offer certain political advantages over other routes. Unfortunately, by then we had withdrawn our personnel and equipment from the field; consequently, we have had to base our estimates for that route upon the limited data which have been accumulated by others.

At 470 feet, its Divide elevation is among the lowest of the routes under consideration. Much of its 140-mile length is scarcely above sea level and could be excavated by hydraulic dredges, but the Divide cut would pass through elevations greater than 100 feet for about 25 miles and should be considered for nuclear excavation. Our very superficial knowledge of its geology indicates that the Divide consists largely of tuffs, limestones and interbedded sands and shales. Assuming that they are competent and that we could employ nuclear techniques, we would estimate the construction costs of this route to be approximately $3.0 billion. We should note, however, the possibility that the Sabana Shale formation found on Route 17 extends into this area, making nuclear excavation of this entire reach unlikely.

The Divide cut of Route 25 (FIGURE 5) at the Pacific end of this alternative, would pass through 20 miles of uplifted volcanic rock and overlying sediments, with an average elevation of 500 feet and a 930 foot maximum. Almost all of the remaining 80 miles of this alinement lie in the Atrato River's estuary and,

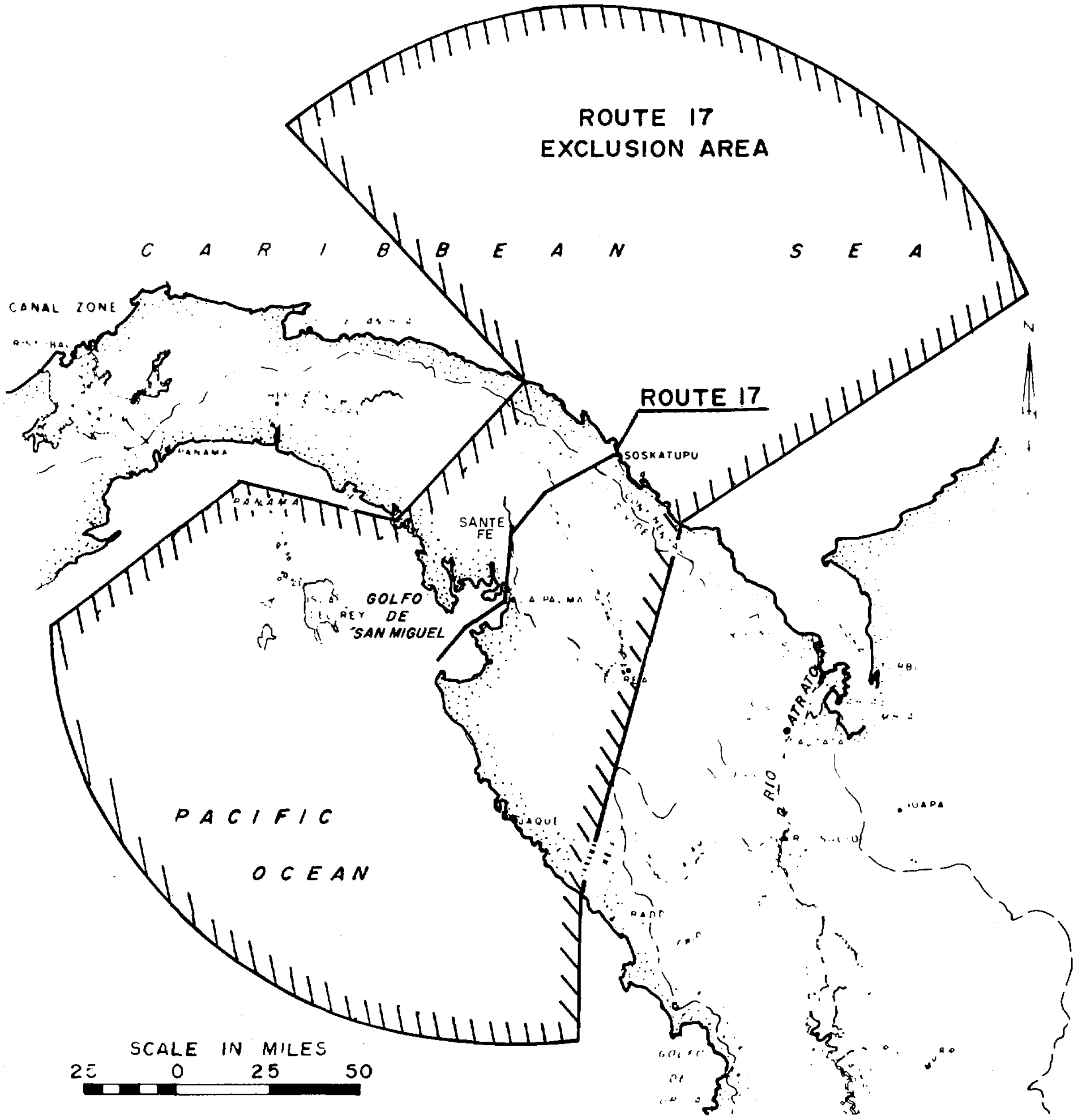

ROUTE 17

Figure 3. Alinement of Route 17, showing tentative nuclear exclusion area.

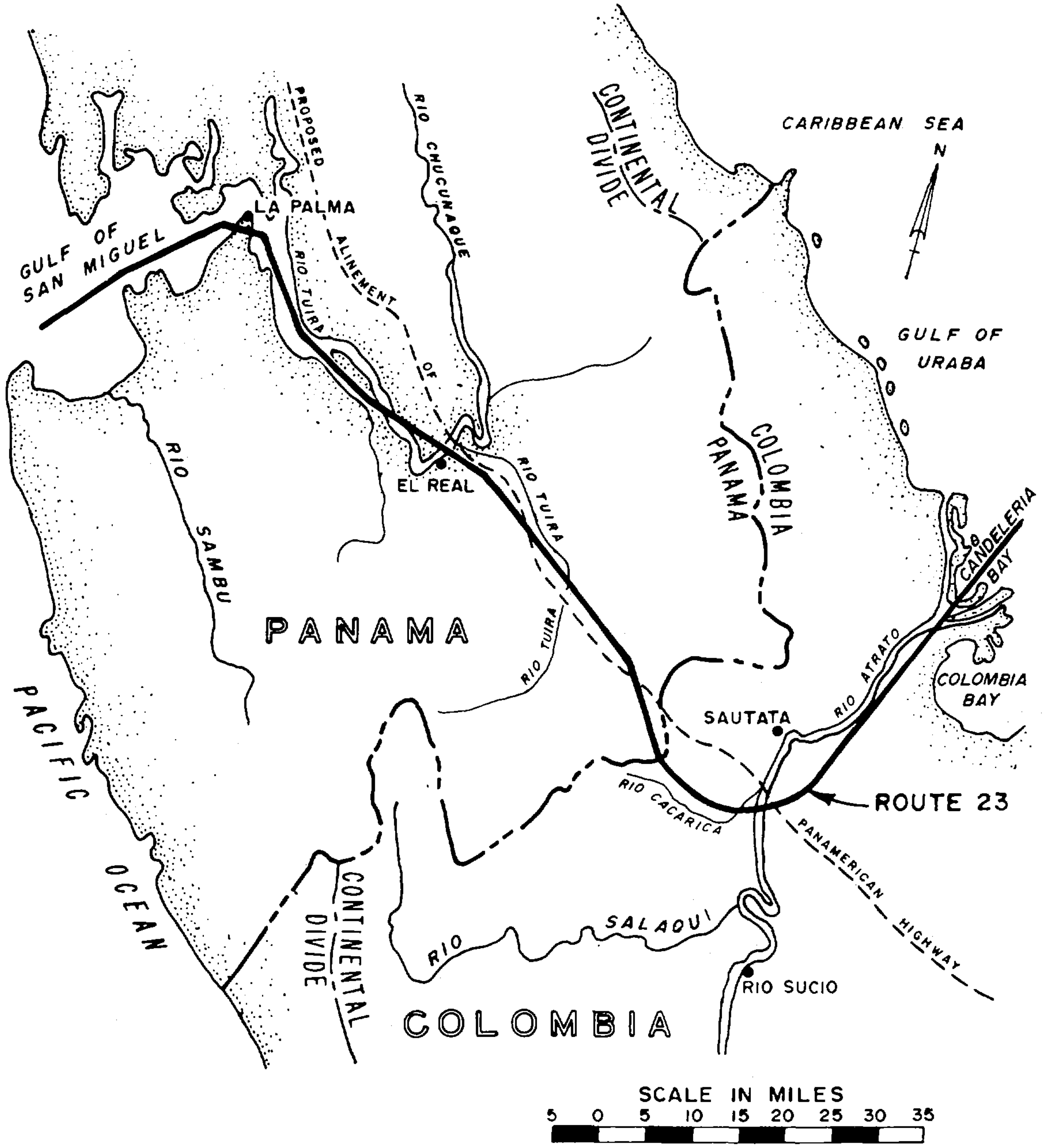

ROUTE 23

Figure 4. Tentative alinement of Route 23.

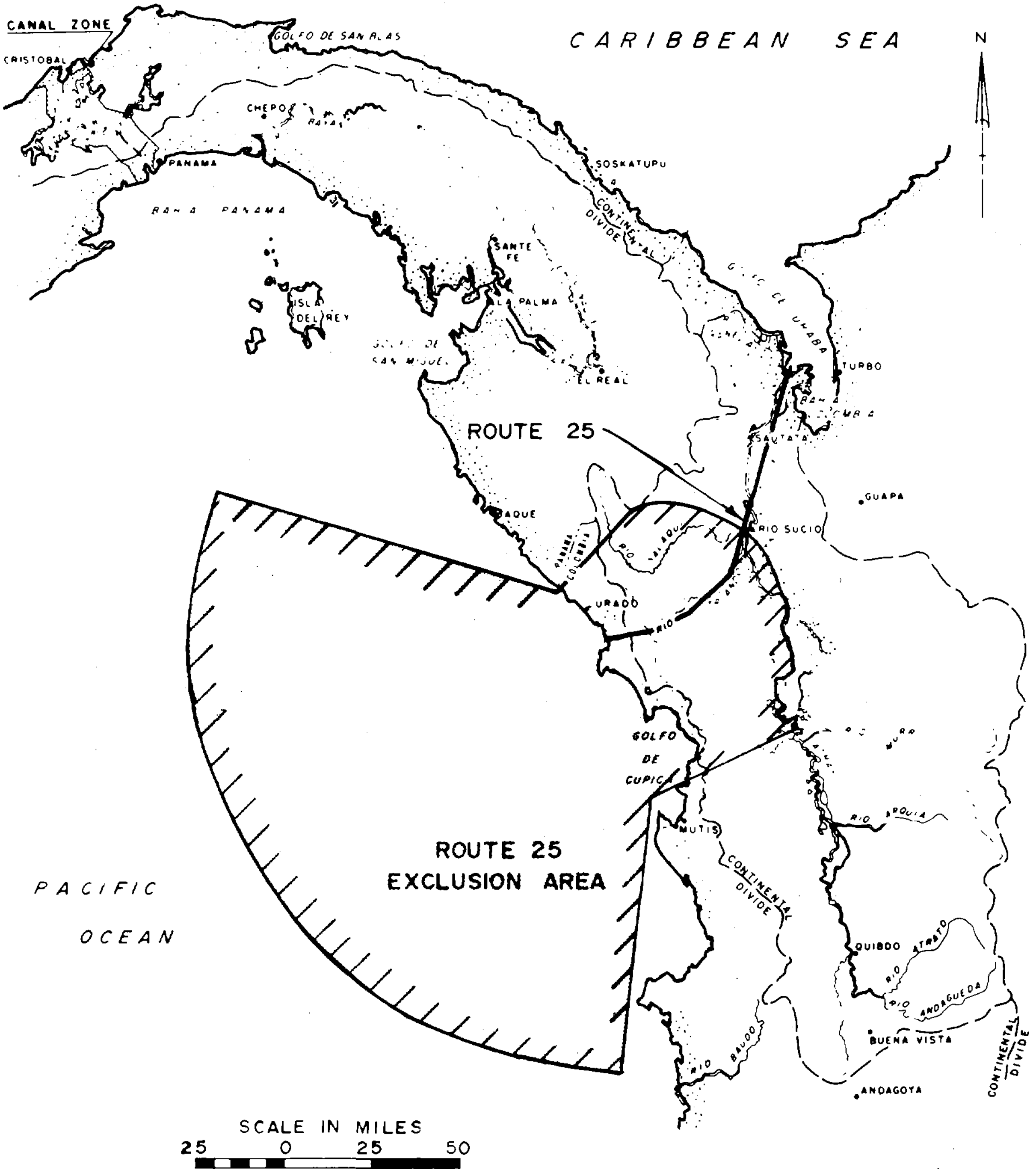

ROUTE 25

Figure 5. Alinement of Route 25, showing tentative nuclear exclusion area.

while they would be excavated conventionally, almost all of this work could be done by relatively cheap hydraulic dredging. Consequently, in terms of excavation costs only, Route 25 appears to be the least expensive alternative, nuclear or conventional, by a considerable margin, at our current estimate of $1.9 billion provided, again, that nuclear excavation is found engineeringly feasible.

This sum is based on a design calling for 150 nuclear explosives ranging in yield between 0.1 and 3.0 megatons. They would be fired in 21 separate detonations ranging from 0.9 to 13 megatons. The total yield would be 120 megatons.

Again, we run into fallout problems. The estimated long term land exclusion area covers more than 3,000 square miles and is presently inhabited by as many as 20,000 people. Serious seismic effects are not likely to be felt outside of this area.

Time does not permit me to discuss the wholly conventional routes. Suffice it to say that our investigations have convinced us that both are engineeringly feasible. We estimate their construction costs to be $2.7 billion for Route 10 and $2.8 billion for Route 14. From this (FIGURE 6) we might conclude that the Route 25 nuclear solution is by far the most economical; it has nearly a billion-dollar advantage over the cheapest conventional solution. But I cannot at this point in time recommend nuclear construction to the Commission. I am unable to do so because we do not yet know enough about nuclear excavation.

A stated purpose of the Commission's study has been to determine "the best means of constructing a sea-level canal connecting the Atlantic and Pacific Oceans, whether by conventional or nuclear excavation, and the estimated cost thereof." Implicit in this purpose, and prerequisite to its accomplishment, are the development and verification of necessary nuclear excavation technology.

By now it should be apparent to you that the Plowshare testing program designed to support the Commission's study will not be completed before our investigations are terminated. Our inability to conduct the tests needed to prove out nuclear excavation theory leaves large gaps in our knowledge, making it impossible for us to state unequivocally that nuclear excavating techniques are feasible. Nor do we have any valid basis for comparing construction costs of routes relying in whole or in part upon these nuclear techniques with other routes in which only proven conventional construction methods would be employed.

But we do have good reasons for believing that nuclear excavation might offer the best method for constructing a canal under certain conditions. In the course of our work on this study the potential advantages of nuclear excavation have become increasingly clear - as have its limitations. The advantages which it promises are probably most easily described in economic terms, as shown in these current best estimates of the costs of excavating large volumes of hard rock by three different means - conventional dry excavation, nuclear explosives and chemical explosives (FIGURE 7).

Our understanding of these methods is not equally well developed; hence, our cost estimates are not uniformly accurate, but they are certainly good enough to arouse our interest in nuclear excavation for large volumes. Note the economies of scale which appear to be available from nuclear excavating techniques. Note, too, where we hope to arrive with chemical explosives in the very near future. We would expect to employ whichever of these methods is least costly for the volume to be excavated (FIGURE 8), all other considerations being equal. On this basis, it would seem likely that nuclear excavating techniques will be widely used in the future if only we can equalize all of these other considerations. This makes it imperative that the work undertaken to support the canal studies be pushed through to completion.

NUCLEAR EXCAVATED SEA-LEVEL CANAL CONSTRUCTION COSTS

(millions of dollars)

ROUTE	CONVENTIONAL EXCAVATION	NUCLEAR EXCAVATION	ASSOCIATED NUCLEAR COSTS	SUPPORTING CONSTRUCTION	TOTAL CONSTRUCTION
8	100	900	1,700	800	3,500
17	1,800	300	200	600	2,900
23					3,000*
25	800	300	100	700	1,900
Comparative Costs - Conventional Canal Construction					
10	2,200	—	—	500	2,700
14	2,300	—	—	500	2,800

Based on a capability to handle at least 40,000 transits annually of ships up to 250,000 dwt. These costs are based on present construction cost estimates.

* Preliminary estimate

Figure 6. Current estimated costs for routes proposed for nuclear excavation. All except Route 8 would have a significant portion excavated by conventional means.

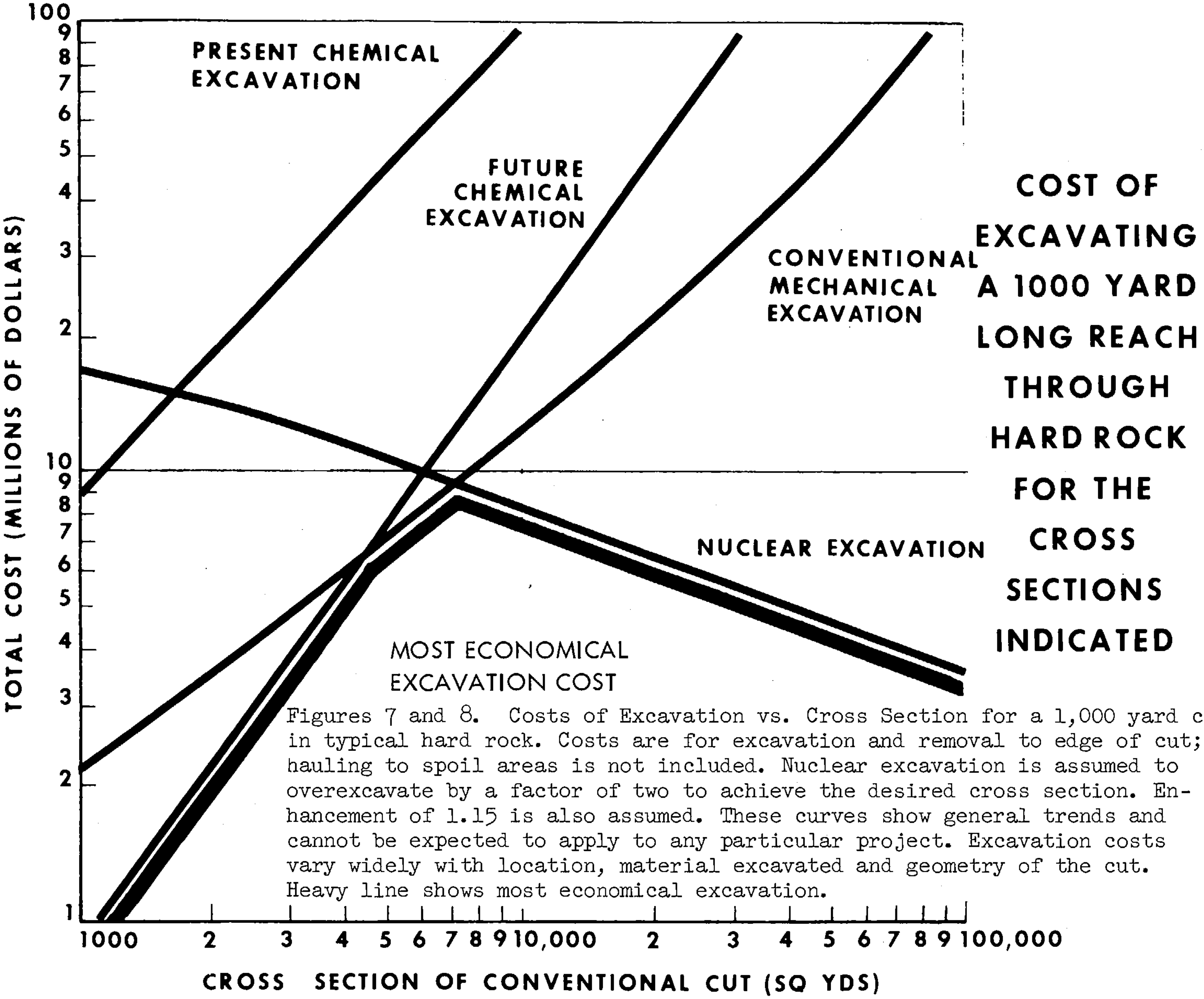

Figures 7 and 8. Costs of Excavation vs. Cross Section for a 1,000 yard cut in typical hard rock. Costs are for excavation and removal to edge of cut; hauling to spoil areas is not included. Nuclear excavation is assumed to overexcavate by a factor of two to achieve the desired cross section. Enhancement of 1.15 is also assumed. These curves show general trends and cannot be expected to apply to any particular project. Excavation costs vary widely with location, material excavated and geometry of the cut. Heavy line shows most economical excavation.

I would hope that those who move on toward our goal of a proven, useful nuclear excavation technology, will take full advantage of the knowledge and experience we have gained while studying these isthmian canals. Much of what we have done could be instructive to those who must carry on our work. To that end let me attempt a brief critique of our efforts to date as I view them. In so doing I do not intend to imply criticism of any individual or agency participating in this study. Speaking with benefit of hindsight, I have nothing but admiration and respect for those who have contributed to the present state of our knowledge of this very difficult subject. But, also with the benefit of hindsight, I believe we can discern where we must apply greater efforts in the future if we are ever to see civil engineering projects constructed by nuclear means.

My critique will be in three parts - our accomplishments, our unresolved problems, and what we might do differently in the future. Taking them in that order, by way of accomplishment we can point with pride to:

-- Having developed a much clearer and more accurate picture of the probable cost and effort required to construct a sea-level canal with nuclear explosives;

-- To having stimulated the theoretical determination and experimental verification of nuclear cratering effects of yields up to 35 kilotons, and for crater predictions into the megaton range for single and row charges in varying media and terrain;

-- To having shown by large scale chemical explosive tests, the feasibility of connecting row craters to form a continuous channel; and

-- To having prepared detailed nuclear operations plans which could serve as a guide for any future nuclear excavation project.

In these and in many other facets of our work we have made real contributions to man's knowledge. We must not permit them to be forgotten; we must continue to build upon them and to expend our knowledge.

Those items which might be listed among the group headed "Unresolved Problems" all stem from the lag in the testing program associated with Plowshare. Tests have not yet been conducted in the megaton yields and hence we do not have assurance that our present cratering scaling relationships will apply in that range. The practicability of nuclear excavation in rock of high water content has not been demonstrated. We have not yet developed and demonstrated our ability to design and execute row charge excavations at high yields and in varying terrain, to connect row craters smoothly, and to perform nuclear excavation in relatively weak materials, producing structurally stable craters. The tests that were planned in order to achieve these goals must be made. Although they will involve additional effort and expenditures, the savings that could ensue are far greater by comparison. I, for one, am convinced that our country cannot afford to overlook the overwhelming advantages promised by the use of nuclear energy for the execution of large civil works projects.

Finally, let us turn to the matter of what we might do in the future in addition to presently planned programs.

Until now we have made an intensive effort to maximize efficiency and economy by increasing explosive yields. There are strong inducements to do this, as we have seen in the way that the direct nuclear excavation costs fall off dramatically with increasing yields. But as we go to higher yields, we reap consequences which work against the ultimate employment of nuclear explosives, especially in close proximity to inhabited areas.

Consider this in light of the Corps of Engineers current assessment of what lies ahead of us in the field of water resources development. Although we anticipate some major projects, such as interbasin water supply transfers, it is becoming increasingly clear to us that most of our work in the future will be to provide services to an urbanized society. We expect that demands for water related public works will grow, but as we meet them we will place our principal emphasis on the use and management of resources for human ends and services rendered, rather than on the number or size of projects built. This is the policy we are pursuing in the Corps today. I believe its basic principles are equally applicable to our work in developing nuclear excavation technology.

I believe the time has come when we must intensify our efforts on the low yield explosives. Already, the Corps has underway a program to develop, test and employ chemical explosives in the sub-kiloton and low kiloton ranges for excavation. As we look ahead to the projects which the Corps or other agencies like us might build in the future, we cannot visualize many where explosives could be employed with yields greater than 50 kilotons; on the other hand, there are very many, indeed, where small yields could be employed, if available. So, where does that leave us today? Consider the unit cost curves for yields in the 20 to 50 kiloton range (FIGURE 9) and you will find that they are very close to the margin. If we throw into the equation such intangibles as preserving the ecological status quo, we probably do not have at this time a competitive alternative to conventional excavating techniques. The lesson here is clear; we must work harder to develop better small yield nuclear explosives.

And, they must be clean explosives. As we use smaller yields to make deep cuts, we will have to work in stages. If such work is to be economically feasible, we must be able to re-enter the site quickly and get back to work. At the present time this is not possible. The fact that the total radioactivity produced and released per unit of energy decreases as yield increases may lead us to make explosives radiologically cleaner by making them larger, reinforcing our tendency to rely on larger yields. But it is also a fact that the total amount of radioactive materials produced and released increases as yields increase. As we move up the scale to larger yields, we soon come up against more stringent restrictions, such as the Limited Test Ban Treaty of 1963, which prohibits us from carrying out any nuclear explosion which causes radioactive debris to be present outside our territorial limits, and which, as President Kennedy said, "speaks for itself, there are no hidden meanings." And finally, do not forget that on every side voices are being raised to preserve and protect our environment. We should have no illusions about this movement; either we are going to have to revise some of our present beliefs about efficiency and economy to accommodate it, or we will become completely bogged down in fruitless argument. So, again the lesson to be learned from the canal studies is clear - we must reorient our future efforts so as to develop smaller, even cleaner nuclear excavating explosives which are efficient, economical and capable of being used in proximity to people.

How, then, shall we assess our work in the Engineering Feasibility Study?

Summing up our present situation, I would say that we have not yet attained the objectives of our study, as they pertain to nuclear excavation, nor are we likely to do so in the time remaining to us. We have not yet established the feasibility of constructing by nuclear means a sea-level interoceanic canal; we are unable to state unequivocally that were this technique feasible, it would be the best.

We know now that a conventionally constructed canal is technically feasible and we know its approximate cost. We are confident from a purely engineering

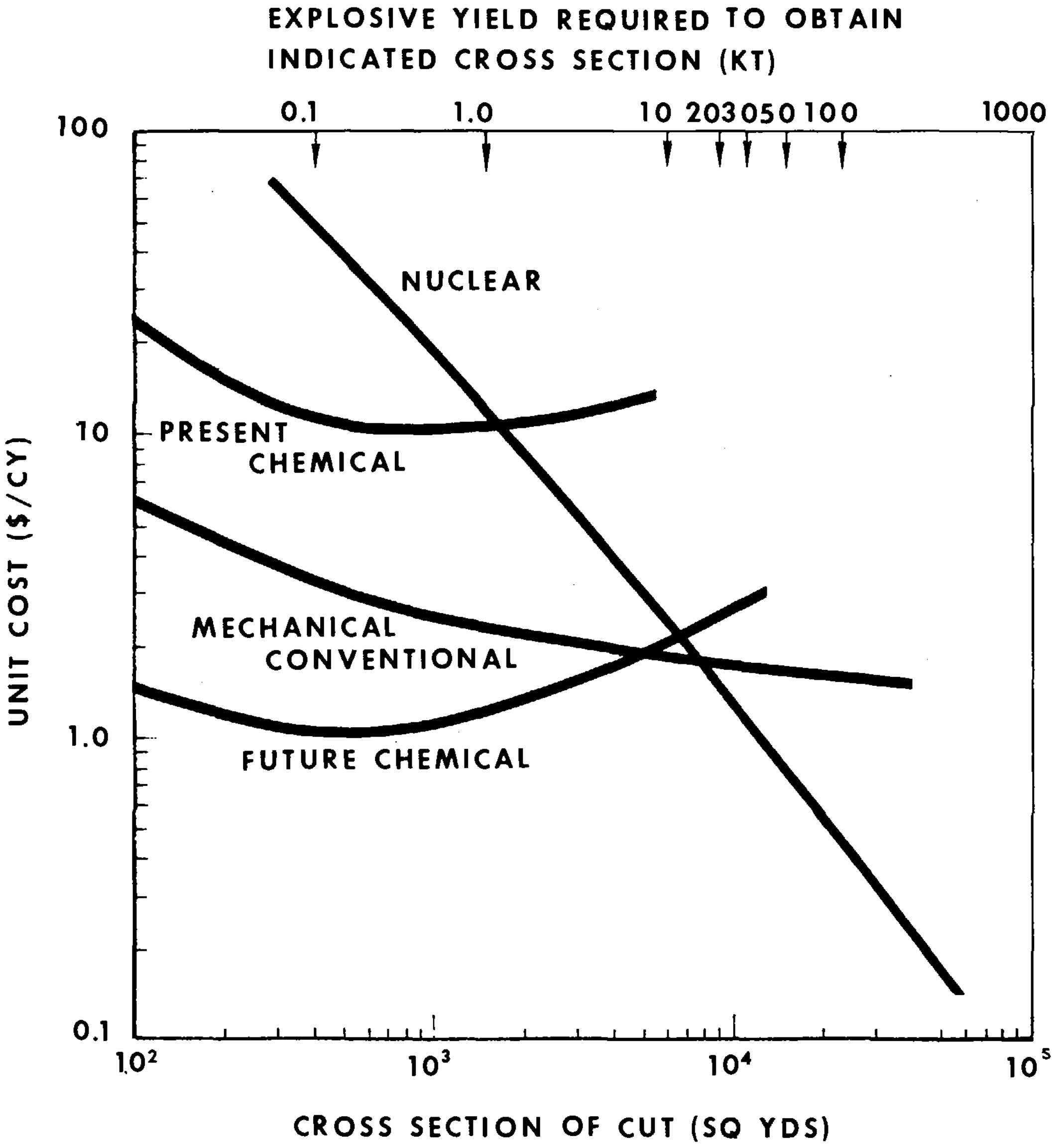

HARD ROCK EXCAVATION COSTS

Figure 9. Unit cost of excavation in hard rock. Assumptions are as for Figure 7.

standpoint that it could be built, if desired.

But we recognize that the question of its technical feasibility, even though answered favorably, will not in itself govern the decision on a new canal. Many other factors - diplomatic, military, political, sociological, economic and ecological, to name but a few - must also be considered and any one of them can influence the course of action which is finally adopted.

While a conventionally-constructed canal is feasible today, we cannot be sure that it would be the best solution to the canal problem until such time as we know more about nuclear excavation technology than we now know. I would expect that the necessary knowledge can be acquired before construction of a new canal begins, if only the Plowshare investigations now planned are executed.

Yet, no matter when the final decision is reached concerning the sea-level canal or what it may be, I am convinced that the case for developing nuclear excavation technology is fully capable of standing on its own merits. In its techniques are such vast potentials for applications to public works that its technology must be fully developed, regardless of how the canal question is settled. And if, by developing it, the well-being of our fellow Americans is enhanced, all the time and effort that have gone into the Engineering Feasibility Study will have been worthwhile.

XA04N0754

THE NONPROLIFERATION TREATY AND PEACEFUL USES OF NUCLEAR EXPLOSIVES

Thomas Ehrlich

School of Law
Stanford University

I.

In the past, nuclear arms control and peaceful uses of nuclear explosives were seen by many proponents of each as competing--if not opposing--interests. At one extreme, some viewed peaceful uses as an annoying irritant on the way to general and complete disarmament.[1] At the other extreme, some considered arms-control arrangements--particularly those limiting nuclear testing--as bothersome barriers to realizing the full benefits of peaceful nuclear explosions.[2] Most people found themselves somewhere between those extremes. But most also felt a continuing tension between essentially opposing forces.

In my judgment, this polarity has been significantly altered by the 1968 Treaty on the Nonproliferation of Nuclear Weapons.[3] I believe that the future use of nuclear explosives for peaceful purposes will depend in large measure on the international arrangements worked out under the treaty. I also believe that the success of the treaty in checking proliferation of nuclear weapons is contingent, in substantial part, on those peaceful-uses arrangements. In the areas covered by the treaty, therefore, I view active development of peaceful uses for nuclear explosives as complementing rather than conflicting with nuclear arms control.

The treaty is primarily a security agreement. It is aimed at reducing the risk of nuclear war by establishing permanency in the current separation of nuclear-weapon and non-nuclear-weapon nations. By its terms, each nuclear-weapon state agrees not to transfer nuclear weapons or other nuclear explosive devices to any recipient, and each non-nuclear-weapon state agrees not to receive such weapons or devices. The non-nuclear-weapon parties are also obligated to negotiate safeguards agreements with the International Atomic Energy Agency covering peaceful-uses activities. And all signatories agree not to transfer fissionable material to those parties unless they are subject to such agreements.[4]

These provisions are all part of a scheme to limit the likelihood that the existing nuclear oligopoly will be broken. All impose positive obligations on the non-nuclear-weapon states without corresponding obligations on the nuclear powers. The treaty also includes, however, two important commitments by those powers. First, they are bound under Article VI to "pursue negotiations in good faith on effective measures relating to cessation of the nuclear arms race at an early date." Second, the nuclear-weapon states promise in Article V to ensure that the "potential benefits of any peaceful applications of nuclear explosions will be made available" to non-nuclear-weapon nations.

II.

Among the five nuclear powers, the United States, the Soviet Union, and the United Kingdom have now ratified the treaty. France has declared that it will not sign, but that it welcomes the agreement and will abide by its terms. Communist China has also refused to join, but it has given no indication to date that it will encourage nuclear proliferation.

The United States and the Soviet Union were the principal negotiators of the treaty; they were also its prime sponsors. But they delayed ratifying the agreement until December 1969. As now appears, the delay was due to the Soviet Union's refusal to ratify until the West German Government had signed; the desire to preclude German acquisition of nuclear weapons was a principal motivation in Soviet support for the treaty. The United States, in turn, withheld its ratification until Soviet approval was assured. As of December 1, 1969, 94 nations had signed the agreement; 26 of them had ratified it.[5]

It is by no means certain that the treaty will ever enter into force. That requires the ratification of 17 additional nations. It is more questionable whether the treaty, if it does become operative, will succeed in checking the proliferation of nuclear-weapon states. That requires the adherence of most of the near-nuclear-weapon--or "threshold"--nations.

At least seven nations apparently have the capacity to produce nuclear weapons and the necessary delivery systems within five to ten years after a national decision to do so; more than a dozen others are not far behind.[6] Four of the threshold states--India, Israel, Japan, and West Germany--believe they have serious security problems for which nuclear weapons are a plausible solution. Only one of the four, West Germany, has signed the agreement, and Mr. Brandt's Government has indicated that it will not ratify until adequate safeguards arrangements are negotiated.[7]

The near-nuclear-weapon states are crucial to the success of the treaty; particularly the four just named. For each one that delays, others may hesitate as well. Pakistan probably will not ratify unless India is a party; some African nations may abstain unless South Africa joins; Arab states will presumably refuse without Israel. Brazil is holding back; will other South American nations sign without her? Timing will be critical in each threshold nation's process of deciding on ratification. And in several cases, time appears to be running out.

What pressures may induce at least most of the near-nuclear-weapon states to conclude that their national interests can be best served by joining the agreement? The United States and the Soviet Union did sponsor a resolution in the United Nations Security Council that sought to give some assurance to non-nuclear-weapon states against nuclear attack.[8] But much more will depend on the success of the nuclear-weapon states in fulfilling their two critical obligations under the treaty.

III.

The initial draft of the treaty by the Soviet Union and the United States contained no concrete commitment by nuclear powers to work toward limiting their own nuclear arms. But at a Conference of the Non-Nuclear-Weapon States organized under United Nations auspices in 1968,[9] many of those states insisted that such commitments be included in the treaty and that those commitments be honored if the agreement is to succeed. The terms of Article VI were accordingly added to require good-faith negotiations on limiting the arms race.

The strategic arms limitation talks (SALT) between the United States and the Soviet Union are scheduled to begin next April. It is not now possible to predict whether they will lead to agreement on significant arms-control measures, particularly on the crucial questions of deploying MIRV and ABM systems. It it possible to predict, however, that unless those talks do produce major steps toward Soviet and American arms limitations, the treaty will fail to halt the spread of nuclear weapons. Why should non-nuclear-weapon states bind themselves to abstinence unless nuclear-weapon countries restrict their superior military power? The prime argument in favor of the treaty is an abstract and global one: The proliferation of nuclear powers would create a dangerous world. But within any particular nation the main arguments against signing are usually quite specific and national, and the dangers they postulate are difficult to disprove.[10]

Even if the SALT talks do lead to significant bilateral arms-control measures, near-nuclear-weapon states such as Sweden demand that the nuclear nations go further. The Nonproliferation Treaty imposes an international regime of controls on the non-nuclear-weapon nations. Several threshold nations are emphatic that the superpowers must accept a similar regime covering nuclear explosions in all environments.[11] As part of that arrangement, an international mechanism would pass on all proposals for peaceful-uses explosions, whether by nuclear-weapon or by non-nuclear-weapon countries.

Under the 1963 Limited Test Ban Treaty, the nuclear powers are free to conduct underground nuclear explosions that contain resulting radioactive debris within national borders.[12] Some non-nuclear-weapon states have argued that only a comprehensive ban would remove the discriminatory features of the current international regime that allows nuclear-weapon states direct access to important economic and technological benefits that non-nuclear-weapon states can obtain, if at all, only indirectly.[13] This position has particular significance for projects that raise at least a substantial possibility of spreading radioactive debris beyond national borders. The Indian Government and other key threshold states have proposed that any international agreement to authorize such projects should not be through amendment of the Limited Test Ban Treaty, but in the context of a comprehensive ban and a separately negotiated agreement establishing an international regime to regulate all nuclear explosions.[14]

IV.

In the eyes of many non-nuclear-weapon states a comprehensive ban is thus a link between arms control and peaceful uses--two major aspects of the quid pro quo demanded by those states in exchange for adherence to the Nonproliferation Treaty. Along with arms-control measures, they are insistent that the nuclear powers must carry out their obligation to share the peaceful benefits of nuclear explosives.

The representative of Afghanistan to the Conference of Non-Nuclear States argued, for example, that "the fate of the treaty . . . depends not only on the adoption of specific disarmament measures by the nuclear-weapon Powers, but also on the speed with which they fulfill their obligation under the treaty to contribute to the further development of the peaceful uses of nuclear energy."[15] The non-nuclear-weapon states did not present a united front on the scope of the obligation, any more than on other questions, for their interests differed, particularly in relation to their level of industrialization. Near-nuclear-weapon countries such as Canada were concerned primarily lest they be precluded from competition in the non-military nuclear field. Developing nations concentrated on exacting maximum benefits for their own economic growth.[16] The representative of Peru, for example, claimed that "the main use of nuclear energy should be to accelerate the development of countries and regions faced with problems that cannot be solved by conventional methods. Injustices of any kind which divide the countries of the international community should be eliminated."[17] But all non-nuclear-weapon states seem agreed that the commitment of the nuclear parties to assist other signatories in exploiting the peaceful benefits of nuclear explosives offers an important opportunity both for a rapid expansion of peaceful-uses development and for a major contribution to the success of the Nonproliferation Treaty. What is that commitment and how is it to be met?

Article V of the Treaty provides that:

> Each of the Parties . . . undertakes to pursue measures to insure that . . . under appropriate international observation and through appropriate international procedures, potential benefits from any peaceful applications of nuclear explosions will be made available to non-nuclear-weapon States Party to the Treaty on a non-discriminatory basis and that the charge . . . will be as low as possible . . . .

The original United States-Soviet draft of the agreement included only a general reference to peaceful uses in the preamble.[18] The two superpowers favored a separate agreement on the subject. India and Brazil on the other hand, opposed any prohibition against the possession and use of nuclear explosive devices for peaceful purposes. They wanted an exemption for peaceful-uses explosions along the lines of the agreement establishing a Latin American Nuclear-Free Zone.[19] Other non-nuclear nations, although recognizing that the similarity of weapon and non-weapon nuclear technology requires a total ban, insisted on specific treaty language to ensure that they would participate in the benefits of peaceful uses.

In fact, the debate at the Conference of the Non-Nuclear-Weapon States made it clear that many countries have quite unrealistic expectations of those benefits for their own development. The very hesitancy of the United States and the Soviet Union in agreeing to Article V seems to have spurred on some non-nuclear-weapon countries in their vision of possible benefits. Brazil, for example, has suggested linking the Amazon and the Rio de la Plata by nuclear explosion.[20] Bolivia has proposed exploitation of its mineral resources.[21] The threshold nations have been more cautious; their projects may include the Australian harbor proposal and oil and gas development in Canada. Other proposals, particularly from least-developed nations, seem to bear little resemblance to reality.[22] My point, however, is not to weigh the relative merits of alternative proposals, but rather to emphasize the intensity of feeling, particularly among developing countries, that the nuclear powers must provide substantial peaceful-uses assistance. In considering these pressures, the United States may have to reconcile potential conflicts between the commercial interests of American private firms in the nuclear field and American foreign-policy interests in carrying out Article V obligations.[23]

Article V provides that the benefits from peaceful applications shall be offered "pursuant to a special international agreement or agreements, through an appropriate international body with adequate representation of the non-nuclear-weapon States." Bilateral agreements are also suggested as an alternative vehicle for transferring peaceful-uses benefits, although several nations opposed this reference on the ground that multilateral control is essential to preclude discrimination. Bilateral accords will certainly be needed concerning each specific project, but all seem to agree now that international machinery is needed to carry out the mandate of Article V.

Whatever arrangements are made under Article V, each nuclear-weapon power will insist that any nuclear device it provides for a peaceful-uses explosion must remain in its control at all times. This position seems required under Article I, which forbids any transfer of "control" over a nuclear explosive device to "any recipient whatsoever." But any provision of nuclear explosions for peaceful purposes by a nuclear-weapon state to a non-nuclear-weapon nation must be "under appropriate international observation and through appropriate international procedures." Such services are to be provided "pursuant to a special international agreement or agreements." Article V provides that negotiations on this matter are to begin as soon as possible after the treaty enters into force. It seems likely, however, that a number of key nations will not ratify the treaty--and thus limit their bargaining power--unless they are assured of a satisfactory outcome to the negotiations. The Eighteen Nation Disarmament Conference will probably provide a principal forum, though a good deal of private consultation will also be needed.

The treaty provides no detailed guidance for working out arrangements to ensure that nuclear-weapon states carry out their basic obligation under Article V to share the benefits of peaceful nuclear explosions, and do so on a non-discriminatory basis and at the lowest possible cost. It would undermine the treaty purposes if each nuclear-weapon state were to decide on a wholly unilateral basis the extent to which it would contribute. At the same time, it seems equally improper to conclude that a non-nuclear-weapon state has a legal claim against the United States, for example, for any and all information, material, or other assistance desired. As a practical matter, the problem may be more apparent than real, for the nuclear-weapon states must realize that their willingness to meet their commitments under Article V is an important element in the success of the treaty as a whole.

It is entirely possible, however, that neither superpower will be willing to assist South Africa, for example, in the development of its mineral resources. Is refusal on foreign-policy grounds precluded by the requirement that peaceful-uses services be offered on a "non-discriminatory" basis? United States representatives have stated that they anticipate no shortage of nuclear explosive devices for peaceful purposes.[24] They have also committed the United States to arrangements under Article V that will "make clear that, once the participating nuclear Powers are prepared to undertake practical applications of peaceful nuclear explosives, they will not withhold nuclear detonation services to others because of extraneous considerations."[25] But what about a Cuban request to develop a new harbor with nuclear explosives? The Senate Foreign Relations Committee, in its favorable report on the treaty, stated that it "specifically rejects any suggestion that Article V constitutes an across-the-board pledge by the United States to support foreign . . . projects."[26] In the eyes of many nations, however, that is precisely the pledge made by the United States.

In all events, what if the United States and the Soviet Union are both willing to conduct a peaceful nuclear explosion in a particular country? Canada, among others, has urged that "the international body" designated under Article V not be placed in the position of having to designate a particular supplier in response to a request for peaceful nuclear explosion services, but that the decision should instead be left to the requesting state.[27] Sweden, on the other hand, has suggested that nuclear-explosive devices "might be committed to a formal 'pool' for allocation, by this body, to interested customers."[28]

V.

From the outset of the treaty negotiations, the United States and the Soviet Union have urged that the I.A.E.A. assume the duties of the "international body" referred to in Article V.[29] Their arguments are based mainly on the technical competence of the Agency and the broad terms of its enabling Statute. The Agency is granted authority by that Statute to "encourage and assist research on, and development and practical application of, atomic energy for peaceful purposes throughout the world . . . ."[30] It is also authorized to serve as an intermediary for the supply of services for peaceful nuclear explosions.

The great majority of nations support the view that the I.A.E.A. should be designated as the "international body" under Article V. The United Nations Secretary General and the Agency's Board of Governors both concur in this view.[31] But a number of non-nuclear-weapon states, particularly among the developing countries, claim that the I.A.E.A. Board is dominated by nuclear-weapon powers and their allies, and call for a major restructuring of the Board to give them a stronger voice in the Agency's governance.[32] It now appears probable that the Board will be reorganized to provide increased representation for non-nuclear-weapon nations. Some of those nations, however, have called for either a special body within the Agency or a wholly separate entity. Their demands are apparently the reason why the Agency is not referred to specifically in Article V as it is in Article III concerning safeguards arrangements. And those demands also help to explain the requirement in Article V that the "international body" must have "adequate representation of non-nuclear-weapon States." In all events, those states are united in the view that in the 1970's the nuclear-weapon powers have a primary obligation to develop their peaceful-uses technology so that they will be able to provide assistance when requested, and that in the interim the necessary international machinery must be perfected.[33]

It may well be that different institutions will be assigned different responsibilities. Consider the range of those responsibilities. There should be a clearinghouse for projects proposed by the non-nuclear-weapon states for submission to nations able to supply the necessary services. It is conceivable that this clearinghouse will also conduct feasibility studies of the proposals. The I.A.E.A. seems well-suited to undertake these functions because of its extensive experience in related fields. The Agency has in the past conducted extensive studies of economic, technical, and safety aspects of reactor proposals and has assisted in a study of health and safety aspects of using nuclear explosives in Panama.

Article V also calls for "appropriate international observation." This responsibility appears similarly suitable to the I.A.E.A. A number of difficult issues remain to be resolved, however, in working out the observation issues in the new agreement called for under Article V. Most important, what steps will be taken to assure that a nuclear device remains under the control of a nuclear-weapon state supplying explosion services and that the project is solely for peaceful purposes?

Questions may also arise whether particular nuclear explosion services are offered at the lowest possible cost, excluding any charge for research and development. I suspect that the "international agreement" referred to in Article V will also assign these functions to the I.A.E.A., but it is possible that a new body, or at least a new mechanism within the Agency, will be established. Currently, the Agency Board is ill-equipped to act as a dispute-settlement institution, particularly outside the areas of its current duties in fostering peaceful nuclear research and power projects, and safeguards for those activities. An ad hoc or permanent dispute-settlement institution of the type developed under other international agreements may offer a promising alternative.[34]

Perhaps the most likely area for employing an international institution apart from the I.A.E.A. is consistency with the Limited Test Ban Treaty. One interpretation of the 1963 treaty is that no nation may conduct any nuclear explosion on the territory of another nation since such an explosion would be "outside the territorial limits of the State under whose jurisdiction or control such explosion is conducted."[35] Under that view--when coupled with the requirement that nuclear explosive devices remain in the custody of nuclear-weapon states--those states would be precluded from carrying out their obligations under Article V of the Nonproliferation Treaty. Such a restricted interpretation seems inconsistent with the intent of the framers of both agreements. Even if the interpretation is generally rejected, however, there must be some mechanism for resolving alleged conflicts between the two treaties.

Suppose, for example, that under Article V Iran calls on the United States (or the Soviet Union) to explode a particular nuclear device in Iran for purposes of oil development, and the United States (or the Soviet Union) refuses on the basis that the explosion would violate its obligations under the 1963 treaty. It seems likely that non-nuclear-weapon states will insist on some dispute-settlement mechanism for such controversies to preclude the possibility of unilateral decision by a nuclear-weapon power. It also seems probable that the mechanism will be demanded before agreement to any peaceful-uses explosions--such as for a trans-isthmian canal[36]--that "cause radioactive debris to be present" beyond national borders. Even if a comprehensive test ban is concluded, the same basic issues will arise.

What kind of institution would be suitable for making decisions under the Limited Test Ban Treaty--or a comprehensive ban--concerning the risks involved in particular projects? A number of nations such as Mexico have stated that these matters must be resolved under United Nations jurisdiction, although in close-cooperation with the "international body" established under Article V.[37] Much may depend on the standards to be applied. If health hazards are viewed as the primary concern, then the World Health Organization--a United Nations subsidiary organ--is a possible candidate. In any case, some new fact-finding and adjudicatory entity may be needed to apply negotiated standards to particular cases.

The United States and the Soviet Union could well benefit from having these issues resolved on a multilateral basis. Such an arrangement would avoid each of the superpowers imposing its own standards in the face of political pressures from non-nuclear-weapon states desiring assistance, and it might also reduce public fears of the risks involved in peaceful nuclear explosions.[38] There are also advantages in allocating these functions to an institution that is not on the front lines of international political controversy, and in having the decisions, insofar as possible, viewed as technical ones. But this may require a fair degree of precision as to the applicable standards, and past efforts to reach agreement within the international scientific community on the health dangers from radioactive fallout have not been particularly successful.

A number of substantive and procedural questions will remain concerning consistency with the Limited Test Ban Treaty, apart from issues of standards. Whatever the mechanism chosen, what will be the scope of its jurisdiction, and will that jurisdiction be compulsory? Will the institution's decisions be binding or advisory, and will it be permanent or an ad hoc board be established for each decision? Will the institution review all proposals for peaceful-uses explosions made by non-nuclear-weapon states, or only those rejected by a nuclear power on the basis that the explosions might violate the 1963 agreement? Will non-nuclear-weapon states be able to seek advance clearance from the institution--a kind of international declaratory judgment--concerning particular proposals? Will third states that object to a peaceful-uses project be authorized to seek a ruling precluding that project--a kind of international injunction procedure? Whatever the standards chosen, will they be waivable and under what circumstances? These are the kinds of questions that may arise in the course of trying to establish the necessary arrangements to deal with this one aspect of the problem.

Until this point, we have been considering the extent of the nuclear-weapons states' obligation to provide peaceful-uses services to non-nuclear-weapon nations that are parties to the treaty. Do the nuclear powers also have an obligation not to provide such services to countries that do not ratify? Article V imposes no such requirement explicitly, though a number of nations would apparently support such a provision in the new agreement to be concluded under Article V.[39] Pakistan went further, and in a proposal obviously aimed at India, called on nuclear-weapon states to deny all nuclear assistance to states that did not ratify the treaty or negotiate a safeguards agreement with the I.A.E.A.[40] It seems in the long-term interests of the nuclear-weapon states to insist that nations desiring the peaceful benefits of nuclear explosives must be parties to the Nonproliferation Treaty. For some countries, this may be a substantial inducement; there seems every reason to make the most of it.

One final point. The Nonproliferation Treaty provides no explicit enforcement mechanism to handle violations of its terms. Instead, it adopts the same scheme developed in the Limited Test Ban Treaty: A party may withdraw "if it decides that extraordinary events, related to the subject matter of this Treaty, have jeopardized the supreme interests of its country." The 1968 agreement does go beyond the 1963 treaty by requiring not only three-months advance notice of withdrawal to other parties, but also notice to the United Nations Security Council and, more important, a statement of the reasons for withdrawal. This provision, makes it likely that, apart from withdrawal, enforcement of the Non-proliferation Treaty will be limited to adverse publicity by the I.A.E.A. and whatever other international arrangements are devised, with ultimate appeal to the Security Council. On issues arising under the treaty, the Council may avoid much of the cold-war standoff that has paralyzed it so often in the past. Hopefully, both the United States and the Soviet Union will view their interests in halting nuclear proliferation as out-weighing any short-term political gain from involving treaty controversies in cold-war politics.

At the same time, the Nonproliferation Treaty will not stand or fall on the issue of enforcement. The key will be the extent to which non-nuclear-weapon states find it in their interests to adopt the treaty strictures. In part, the resolution of this question by particular nations--and the threshold states are the most important--will turn on matters wholly outside the control of the nuclear-weapon countries. In part it will turn on the progress made by those countries toward limiting their own nuclear arms. But a key element in the decision of many non-nuclear-weapon states is whether they conclude that substantial benefits from peaceful nuclear explosives are available to them if they join the agreement.

For perhaps the first time, those states have some substantial leverage in nuclear affairs. They are no longer content with peaceful coexistence by the superpowers. They demand that American and Soviet resources now allocated to nuclear arms be used to help meet their development needs. Far from being mutually exclusive, therefore, arms control and peaceful uses reinforce each other in this area, and they must develop in conjunction. The United States can take advantage of the opportunity by a major expansion of its Plowshare Program, directed particularly to helping other nations.

FOOTNOTES

1. For an example of concern about the impact of peaceful-uses programs on arms-control arrangements, see the testimony of Dr. H.D. Smyth in Hearings on Frontiers in Atomic Energy Research Before the Subcommittee on Research and Development of the Joint Committee on Atomic Energy, 86th Cong., 2d Sess. 11 (1960).

2. This sentiment is harder to document, but it has sometimes emerged in my discussions with individuals active in the Plowshare Program.

3. For the text of the treaty and a full analysis of its legal implications, see Willrich, Non-Proliferation Treaty: Framework for Nuclear Arms Control (1969). For a briefer treatment, see Firmage, The Treaty on the Non-Proliferation of Nuclear Weapons, 63 A.J.I.L. 711 (1969). See also Note, The Nonproliferation Treaty and Peaceful Applications of Nuclear Explosions, 20 Stan. L. Rev. 1030 (1969); Koop, Plowshare and the Nonproliferation Treaty, 12 Orbis 793 (1968). For a step-by-step account of the treaty negotiations from a United States perspective, and the texts of many relevant documents, see U.S. Arms Control and Disarmament Agency, International Negotiations on the Treaty of the Nonproliferation of Nuclear Weapons (1969).

4. Like numerous international agreements, the treaty raises almost as many questions as it resolves--perhaps more. A range of issues concerning safeguards arrangements with I.A.E.A., and the role of EURATOM in such arrangements, remain to be settled. See Scheinman, Nuclear Safeguards, the Peaceful Atom, and the IAEA, International Conciliation, March 1969, No. 572. A cluster of problems also relate to peaceful-uses research, and particularly to fission-free explosive research. See Van Cleave, "The Non-proliferation Treaty and Fission-Free Explosive Research," 11 Orbis 1055 (1968). Here, however, my focus is on the actual use of nuclear explosives for peaceful purposes and the international arrangements concerning such uses that are called for under the treaty. Even in that area, it is not possible here to do more than suggest some of the principal questions involved.

5. Information supplied by the Assistant Legal Adviser for Treaty Affairs, U.S. Dept. of State.

6. See Hearings on the Nonproliferation Treaty Before the Senate Comm. on Foreign Relations, 90 Cong., 2d Sess. 31 (1968) (statement by the Atomic Energy Commission).

7. See German Embassy Press Release, "Government of the Federal Republic of Germany Signs Non-Proliferation Treaty," Nov. 28, 1969.

8. UNSC Res. 255 (1968). The resolution, U.N. Security Council Res. 255 (1968), is reprinted in U.S. Arms Control and Disarmament Agency, International Negotiations on the Treaty on the Nonproliferation of Nuclear Weapons 155 (1969).

9. For the Final Document of the Conference, see U.N. Doc. A/CONF. 35/10 (1968). The Conference proceedings are summarized in Gellner, The Conference of Nuclear Weapons States, 1968; A Survey of Views and Proposals," in Hearings on the Nonproliferation Treaty Before the Senate Comm. on Foreign Relations, 91st Cong., 2d Sess. pt 2, at 450 (1969).

10. This argument is forcefully developed in Young, The Control of

Proliferation: The 1968 Treaty in Hindsight and Forecast (Adelphi Papers No. 56, April 1969).

11. See., e.g., U.N. Doc. A/CONF. 35/C.2/SR.10, at 110 (1968).

12. Treaty Banning Nuclear Weapon Tests in the Atmosphere, in Outer Space, and Under Water, Aug. 5, 1963, art. I, [1963] 2 U.S.T. 1313, T.I.A.S. No. 5433.

13. This pressure by the non-nuclear-weapon states is not an isolated phenomenon. Many are increasingly resentful at what they describe as the combined efforts of the United States and the Soviet Union to maintain monopoly positions, particularly in nuclear arms. The recent United Nations General Assembly rejection of the seabed agreement negotiated by the two superpowers is another example. See N.Y. Times, Dec. 16, 1969, p. 8, col. 8. See generally id., Dec. 1, 1969, p. 6, col. 1.

14. See U.N. Doc. A/CONF. 35/C.2/SR.12, at 129 (1968). The relationship between a comprehensive ban and peaceful uses of nuclear explosives, in the eyes of many countries, can be seen in Resolution L adopted by the Conference of Non-Nuclear Weapon States. U.N. Doc. A/CONF. 35/10, at 18-19 (1968).

15. U.N. Doc. A/CONF. 35/C.2/SR.9, at 97 (1968).

16. For a study of the differing positions held by non-nuclear-weapon states and of related issues raised in this paper, see Scheinman, Nuclear Safeguards, the Peaceful Atom, and the IAEA, International Conciliation, March 1969, No. 572.

17. U.N. Doc. A/CONF. 35/C.2/SR.12, at 131 (1968). A representative of the U.A.R. put the point more sharply. Developing nations, he said, want to avoid being "turned into a nuclear market comparable to the old semi-colonial markets, in the sense that those countries would supply nuclear raw materials to the advanced States, from which they would acquire finished industrial products . . . ." U.N. Doc. A/CONF. 35/C.2/SR.7, at 66 (1968).

18. See U.S. Dept. of State, [1967] Documents on Disarmament 338-41. The first agreed United States-Soviet Union draft was submitted on August 24, 1967. For a history of the subsequent revisions, see Arms Control and Disarmament Agency, International Negotiations on the Treaty on the Nonproliferation of Nuclear Weapons (1969).

19. For the text of the Treaty for the Prohibition of Nuclear Weapons in Latin America (Treaty of Tlatelolco), see U.N. Doc. A/C.1/946 (1967). The United States and the United Kingdom both signed Protocol II to the Treaty, thereby undertaking not to use or threaten to use nuclear weapons against the parties.

20. See Koop, Plowshare and the Nonproliferation Treaty, 12 Orbis 793, 809 (1968).

21. See U.N. Doc. A/CONF. 35/C.2/SR.9, at 98 (1968).

22. For a discussion of the potential benefits of peaceful nuclear technology for developing countries, see U.N. Doc. A/7568 (1968).

23. See Young, The Control of Proliferation: The 1968 Treaty in Hindsight

and Forecast 15 (Adelphi Papers No. 56, April 1969).

24. See U.N. Doc. A/7678, at 39 (1968).

25. U.S. Dept. of State, [1967] Documents on Disarmament 173.

26. S. Exec. Rep. No. 9, 90th Cong., 2d Sess. 14 (1968).

27. See U.N. Doc. A/7678, at 13 (1969).

28. See U.S. Dept. of State, [1967] Documents on Disarmament 248, 250.

29. For a summary of national and other views on the "international body," see U.N. Doc. A/7678 (1969).

30. Statute of the International Atomic Energy Agency, Oct. 26, 1956, art. III.A.1. [1957] 1 U. S.T. 1093, T.I.A.S. 3873.

31. See U.N. Doc. A/7678, at 6, 41-48 (1969).

32. See, e.g., U.N. Doc. A/CONF. 35/C.2/SR.5, at 39 (1968) (remarks of the Representative of Ghana).

33. See, e.g., U.N. Doc. A/CONF. 35/C.2/SR.9, at 100 (Remarks of the Representative of Pakistan).

34. The mechanisms established for the International Consortium for Satellite Communications and the International Coffee Agreement are two examples. See Chayes, Ehrlich, and Lowenfeld, International Legal Process, Vol. 1, Problems VIII and IX (1968).

35. Treaty Banning Nuclear Weapon Tests in the Atmosphere, in Outer Space, and Under Water, Aug. 5, 1963, art. I, [1963] 2 U.S.T. 1313, T.I.A.S. No. 5433. For an analysis of aspects of the Limited Test Ban Treaty relevant to this discussion, see Ehrlich, The 1963 Limited Test Ban Treaty and Civil Nuclear Engineering, in Proceedings, Symposium on Education for the Peaceful Uses of Nuclear Explosives (University of Arizona, 1969).

36. See Hearings on the Nuclear Test Ban Treaty Before the Senate Comm. on Foreign Relations, 88th Cong., 1st Sess. 210 (1963).

37. See U.N. Doc. A/7678, at 28 (1969).

38. See Willrich, Non-Proliferation Treaty: Framework for Nuclear Arms Control 145-46 (1969).

39. Mexico suggested that the benefits of peaceful nuclear explosives be accorded to all states that "have renounced nuclear weapons" by an "international contractual instrument." See U.N. Doc. A/7678, at 26-27 (1969). This proposal would cover a party to the Treaty for the Prohibition of Nuclear Weapons in Latin America even if it did not join the Nonproliferation Treaty.

40. See Scheinman, Nuclear Safeguards, the Peaceful Atom, and the IAEA, International Conciliation, March 1969, No. 572, at 53 (1969).

XA04N0755

RESULTS OF THE SCHOONER EXCAVATION EXPERIMENT*

Howard A. Tewes
Lawrence Radiation Laboratory, University of California
Livermore, California 94550

ABSTRACT

Project Schooner, a nuclear detonation in interlayered hard and soft, partially saturated volcanic rock, was executed as a part of the Plowshare Program for development of nuclear excavation techniques. The primary objectives of this experiment were: (a) to obtain experimental data on crater development and size in a new medium to further verify existing rock mechanics computer codes and calculational techniques; and (b) to determine the fractional release of radioactivity from a nuclear detonation in wet rock.

As was noted in the case of the Sedan experiment, appreciable (though relatively small) amounts of radioactivity were released to the environment from this detonation in hard, partially saturated rock. Although the thermonuclear explosive used in this experiment gave a yield of approximately 31 kilotons, only the equivalent of the fission products from about 370 tons of fission were distributed in both fallout and cloud. Data which have been reduced to date indicate that this released radioactivity underwent only a moderate amount of chemical fractionation, being much more similar in this respect to Sedan than to Danny Boy.

EXPERIMENTAL PROCEDURE

The Schooner thermonuclear explosive, with a nominal yield of 31 ± 4 kt, was detonated at 0800 PST on December 8, 1968, at a depth of 108 m. The experiment was carried out at the Nevada Test Site at the northern edge of the Pahute Mesa area, shown in Fig. 1. The region surrounding the mesa is mountainous and extremely rugged, but the topography at the site is relatively level with less than 10 m of relief within a 350-m radius. The surface rock exposed in the vicinity of the site is a dense, strong, dry volcanic rock (welded tuff) extending over several square miles and estimated to be 30 to 50 m thick. This rock is underlain by other tuffaceous members of varying density and porosity, as can be seen in Fig. 2, which shows the lithology of the site. All the tuff between the bottom of the Trail Ridge Member and the top of the Grouse Canyon Member (from 37 to 102 m) is low-density, high-porosity, weak rock. The Grouse Canyon Member (in which the nuclear explosive was detonated) is a dense, strong, welded tuff, similar to the surface rock.

Figure 3 is a summary of the porosity of the Schooner site rock obtained from samples recovered from the emplacement hole, as well as from one exploratory hole. Figure 4 shows the results of free-water determinations made on the same samples used for estimating medium porosity. It should be noted that the water content of the Grouse Canyon Member (around the Schooner

---

*Work performed under the auspices of the U.S. Atomic Energy Commission.

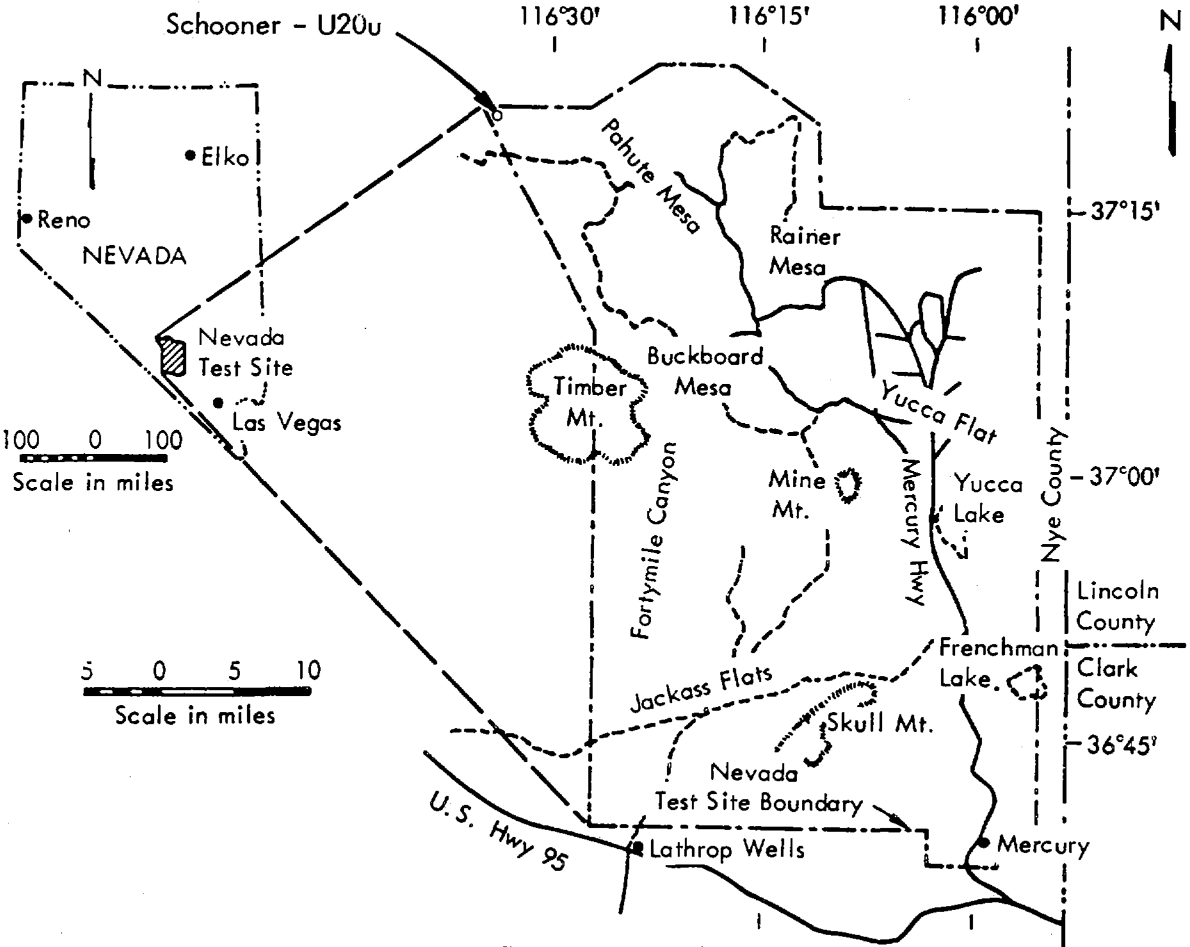

Fig. 1. Location of the Schooner nuclear-crater experiment.

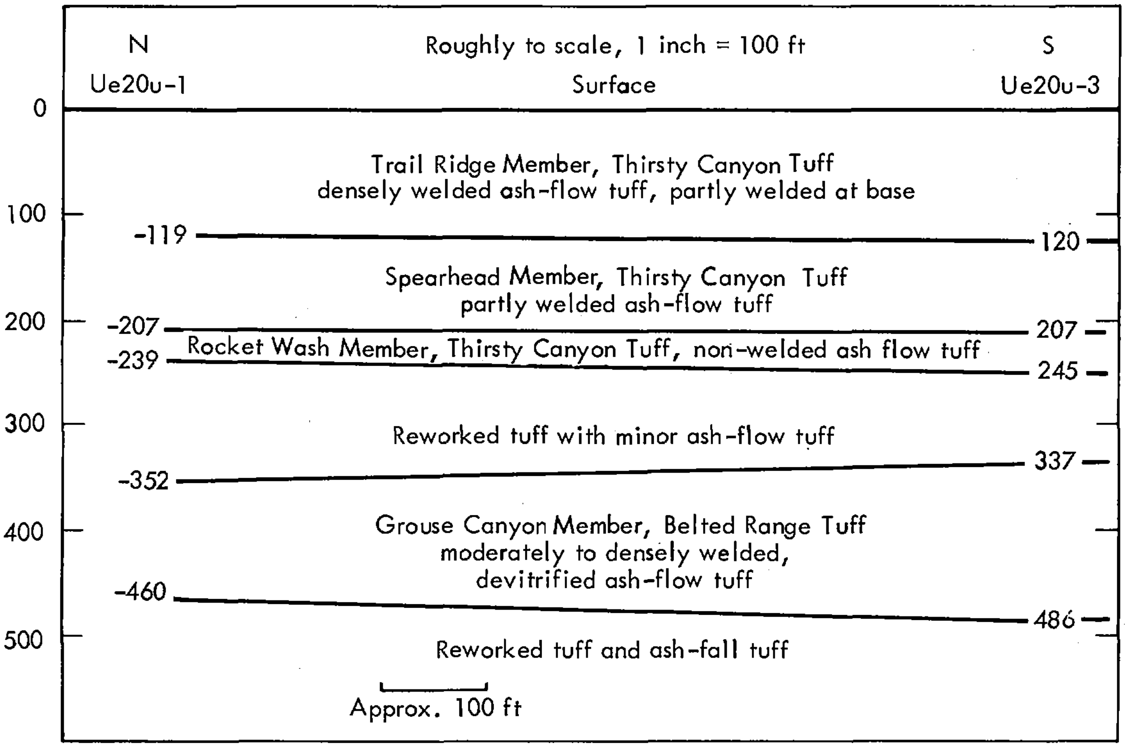
N
Ue20u-1
Roughly to scale, 1 inch = 100 ft
Surface
S
Ue20u-3
0
Trail Ridge Member, Thirsty Canyon Tuff
densely welded ash-flow tuff, partly welded at base
100
-119
120
Spearhead Member, Thirsty Canyon Tuff
partly welded ash-flow tuff
200
-207
207
Rocket Wash Member, Thirsty Canyon Tuff, non-welded ash flow tuff
-239
245
300
Reworked tuff with minor ash-flow tuff
337
-352
400
Grouse Canyon Member, Belted Range Tuff
moderately to densely welded,
devitrified ash-flow tuff
-460
486
500
Reworked tuff and ash-fall tuff
Approx. 100 ft

Fig. 2. Stratigraphic section of Ue20u-1 and Ue20u-3.

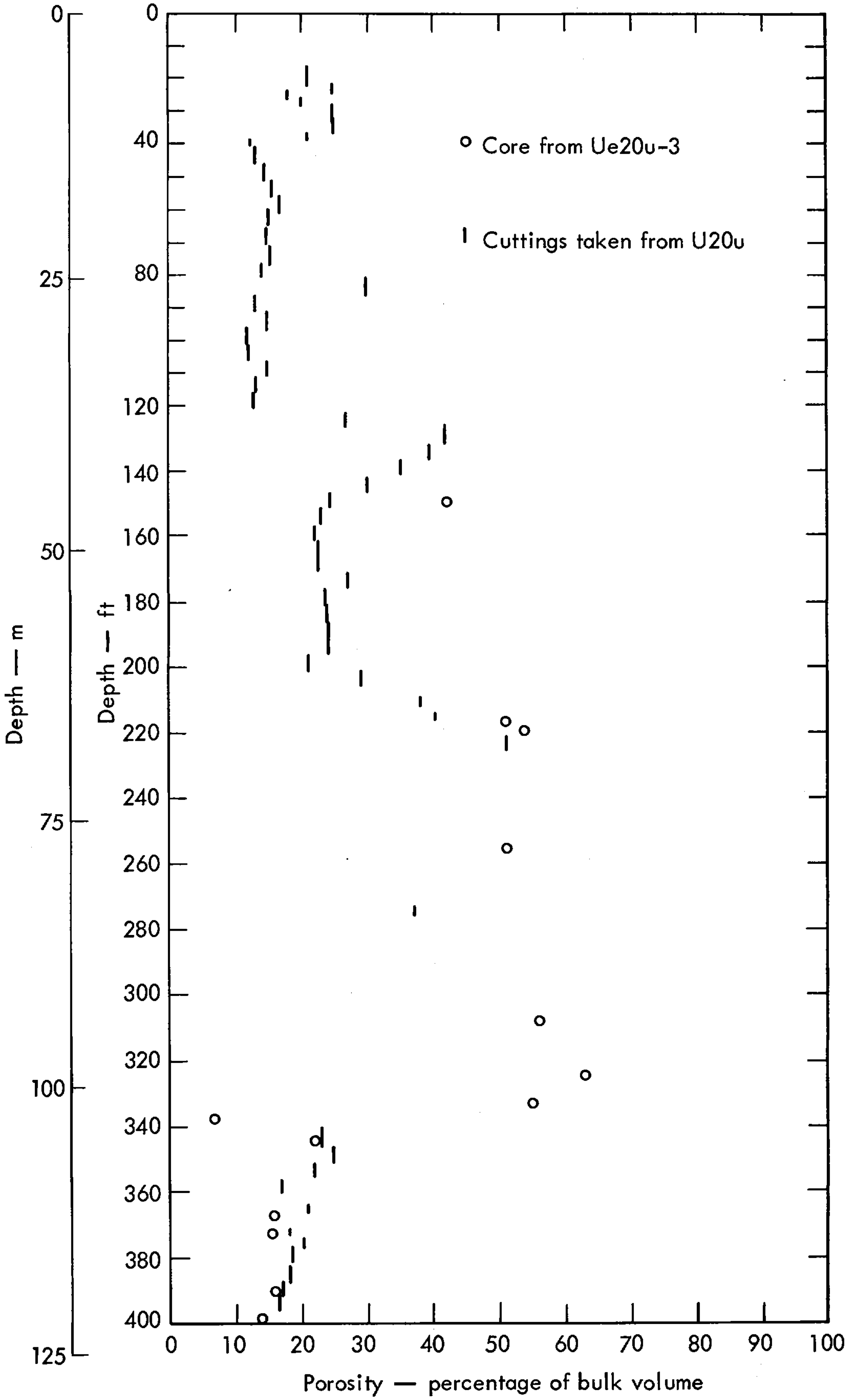

Fig. 3. Porosity of rock at the Schooner site.

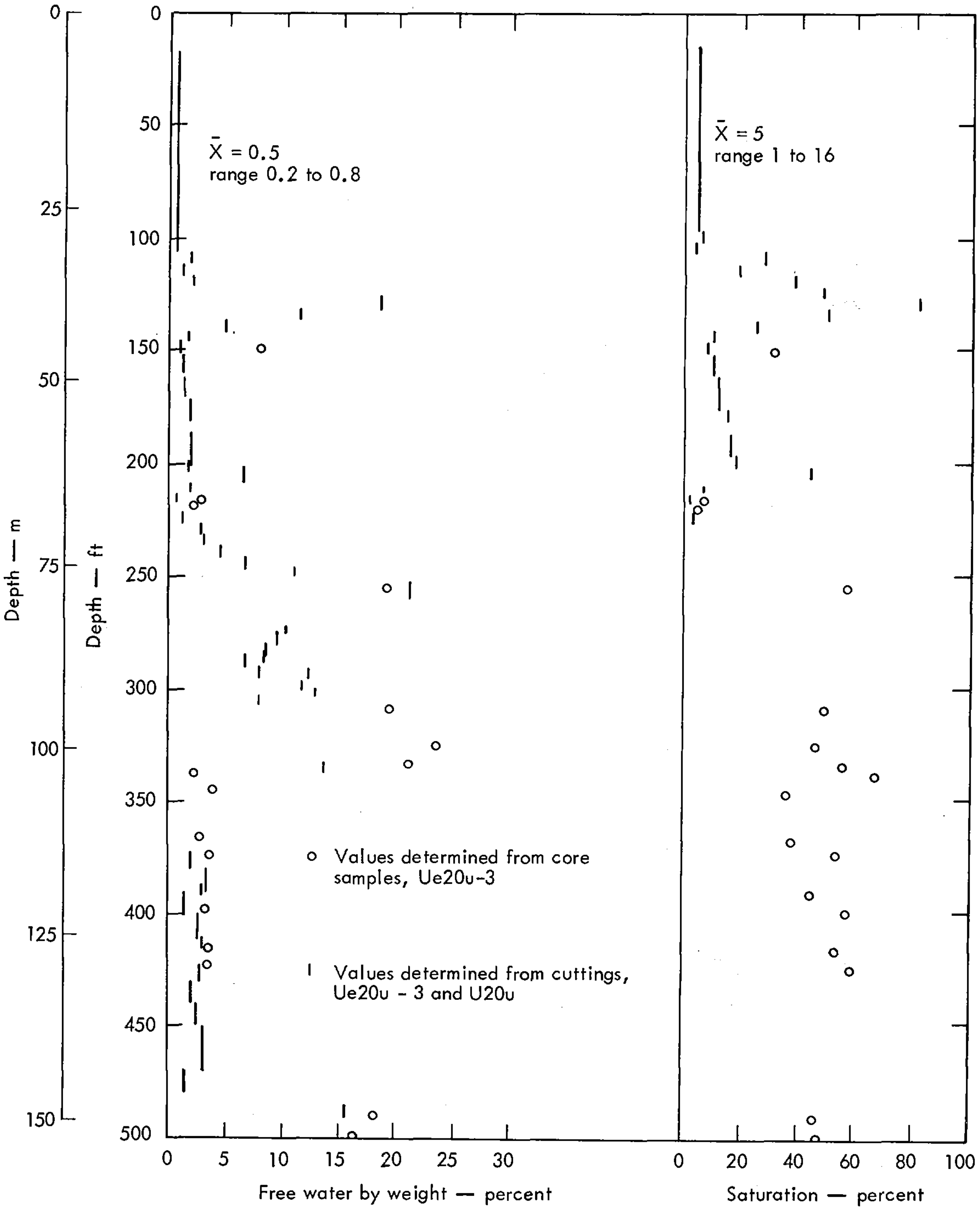

Fig. 4. Water content of rock samplings from Ue20u-3 and U20u.

detonation point) is about 3% while in the reworked tuff layer above a depth of 102 m (only about 6 m above the detonation point) the water content averages 20-25%.

Figure 5 is a summary of densities obtained from in-situ density logs, core and cutting samples from the emplacement hole, and from an exploratory hole. Figure 6 shows the seismic-velocity data obtained from a downhole-velocity survey taken in the exploratory hole (located about 20 m from the emplacement hole). The welded tuff-ash flow tuff interfaces can be clearly seen in the presentations of both the density and velocity as a function of depth.

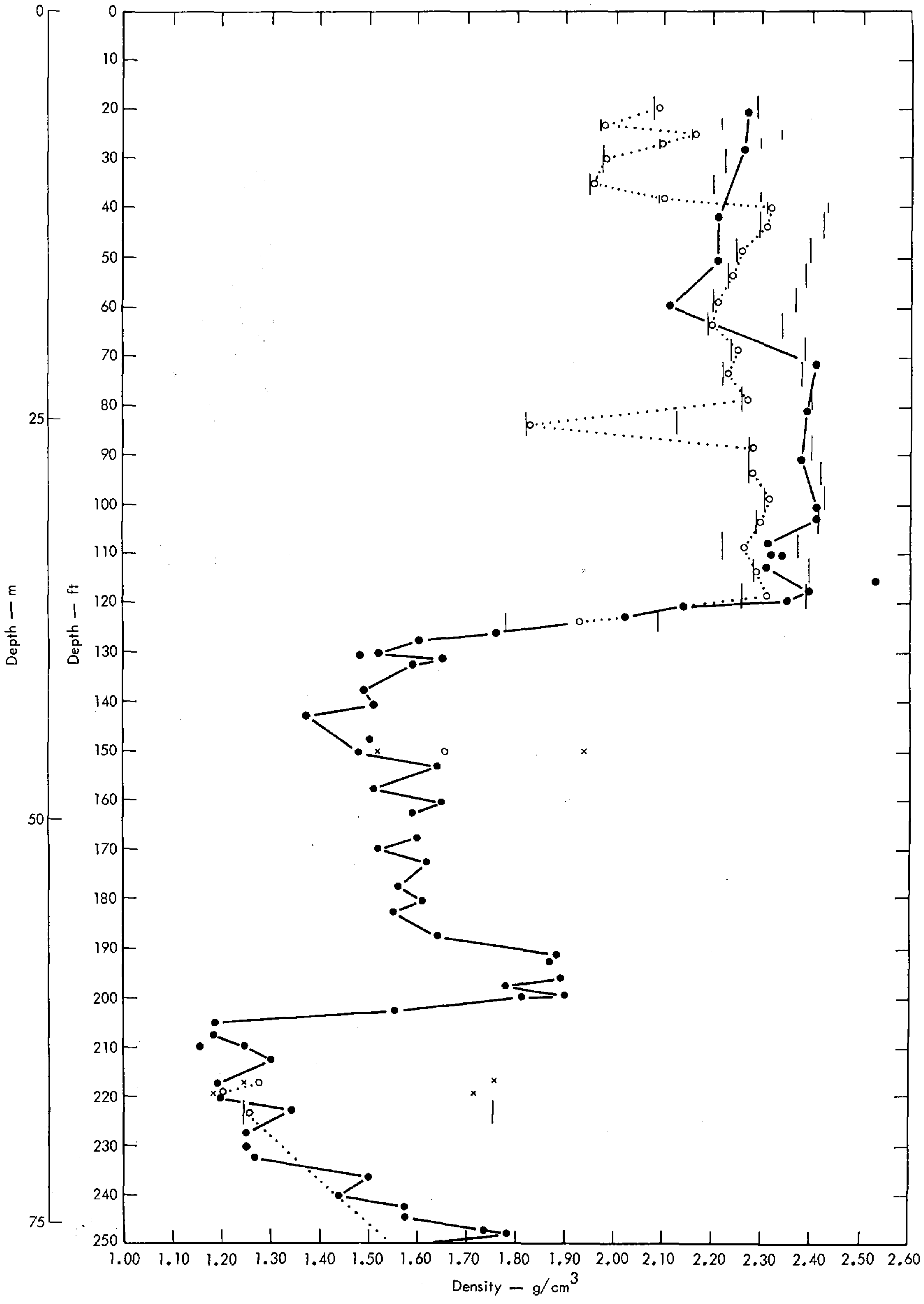

Fig. 5. Density plot of Ue20u-3.

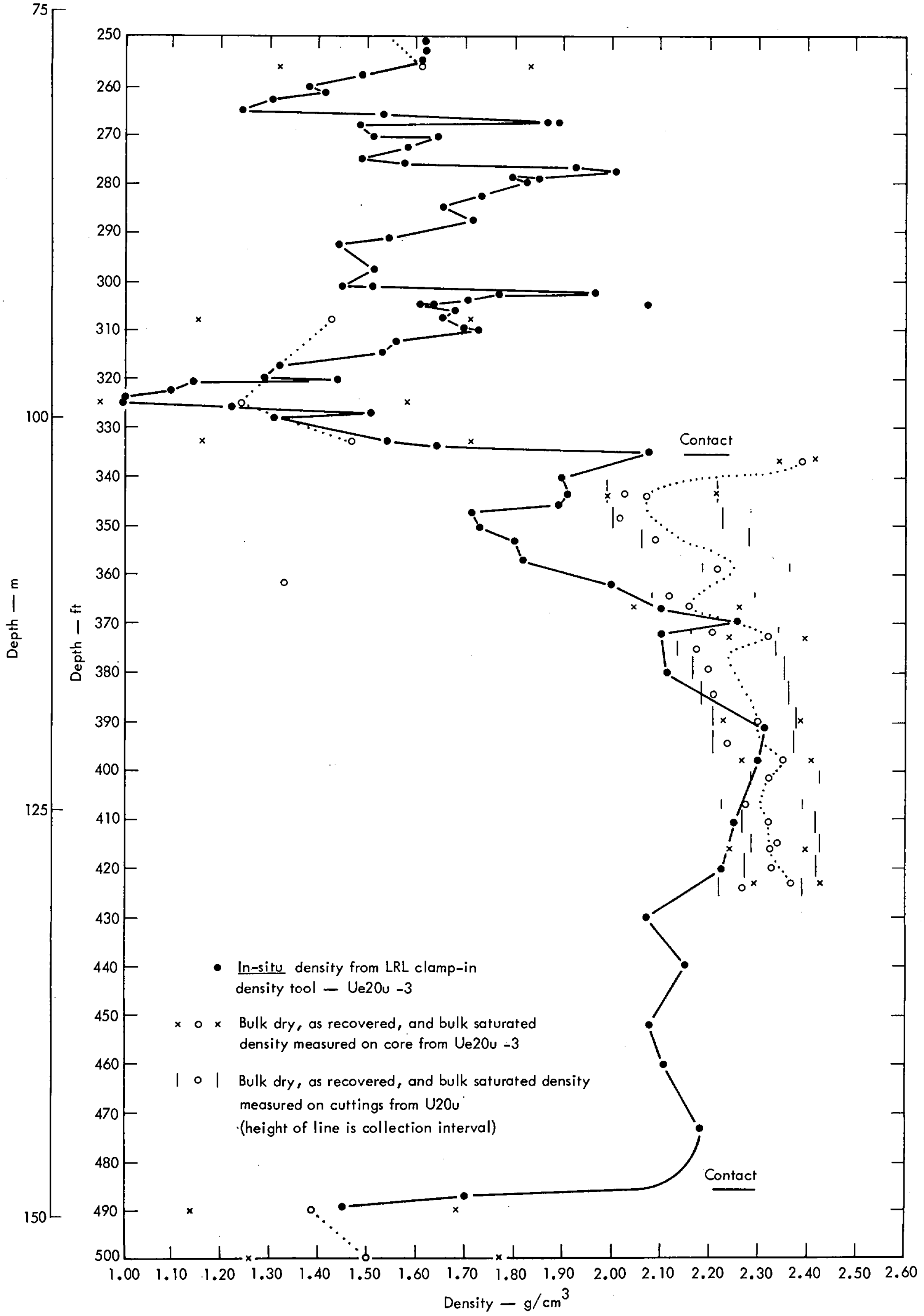

Fig. 5. (Continued).

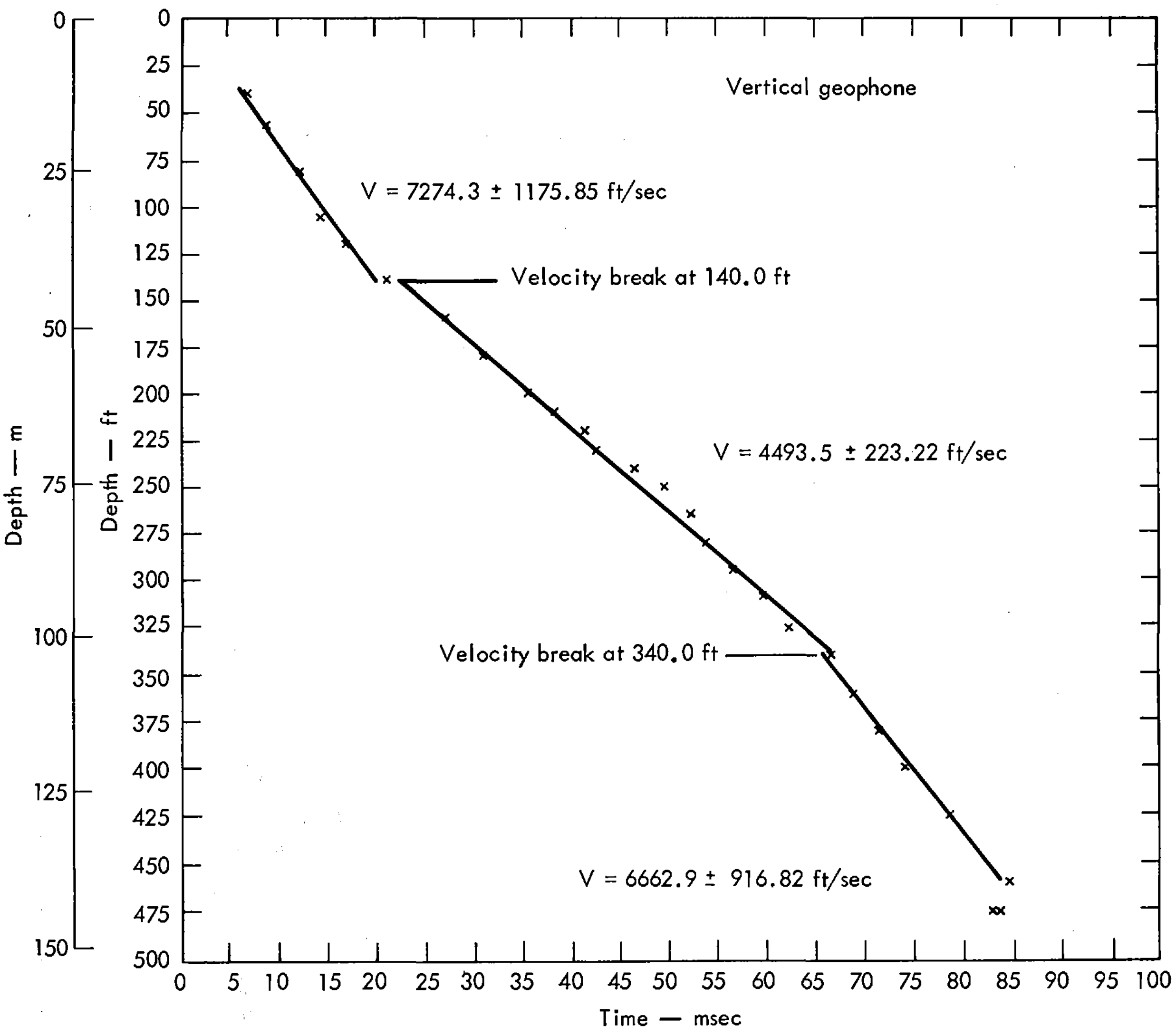

Fig. 6. Downhole velocity plot for Ue20u-3.

Figure 7a gives a summary[1] of the geologic data shown in the preceding five figures: Figure 7b indicates how the data were averaged and used as input to the cratering computations.

RESULTS

Detonation Description

Upon detonation, the ground surface appeared to mound (Fig. 8) in a normal manner, until escape of high-temperature gases occurred near the center of the mound at about 1.75 sec (Figs. 9 and 10). At this time, the dome was ~ 90 m above ground-surface elevation. Upon general mound disassembly material was ejected on ballistic trajectories with maximum altitudes as high as 900 m above the original surface and with impact points as far as 1800 m from ground zero (for missiles of appreciable size and weight). Figure 11 shows the early stages of mound development.

Crater Dimensions

Average dimensions of the Schooner crater are as follows:

Dimension	Measurement
Apparent average crater radius, R_a	129.9 m
Apparent average crater depth, D_a	63.4 m
Lip-crest radius, $R_{a\ell}$	147.2 m
Lip-crest height, $H_{a\ell}$	13.4 m
Radius of ejecta boundary, R_{eb}	538.9 m
Apparent crater volume, V_a	1,745,000 m^3
Apparent lip volume, $V_{a\ell}$	2,099,000 m^3

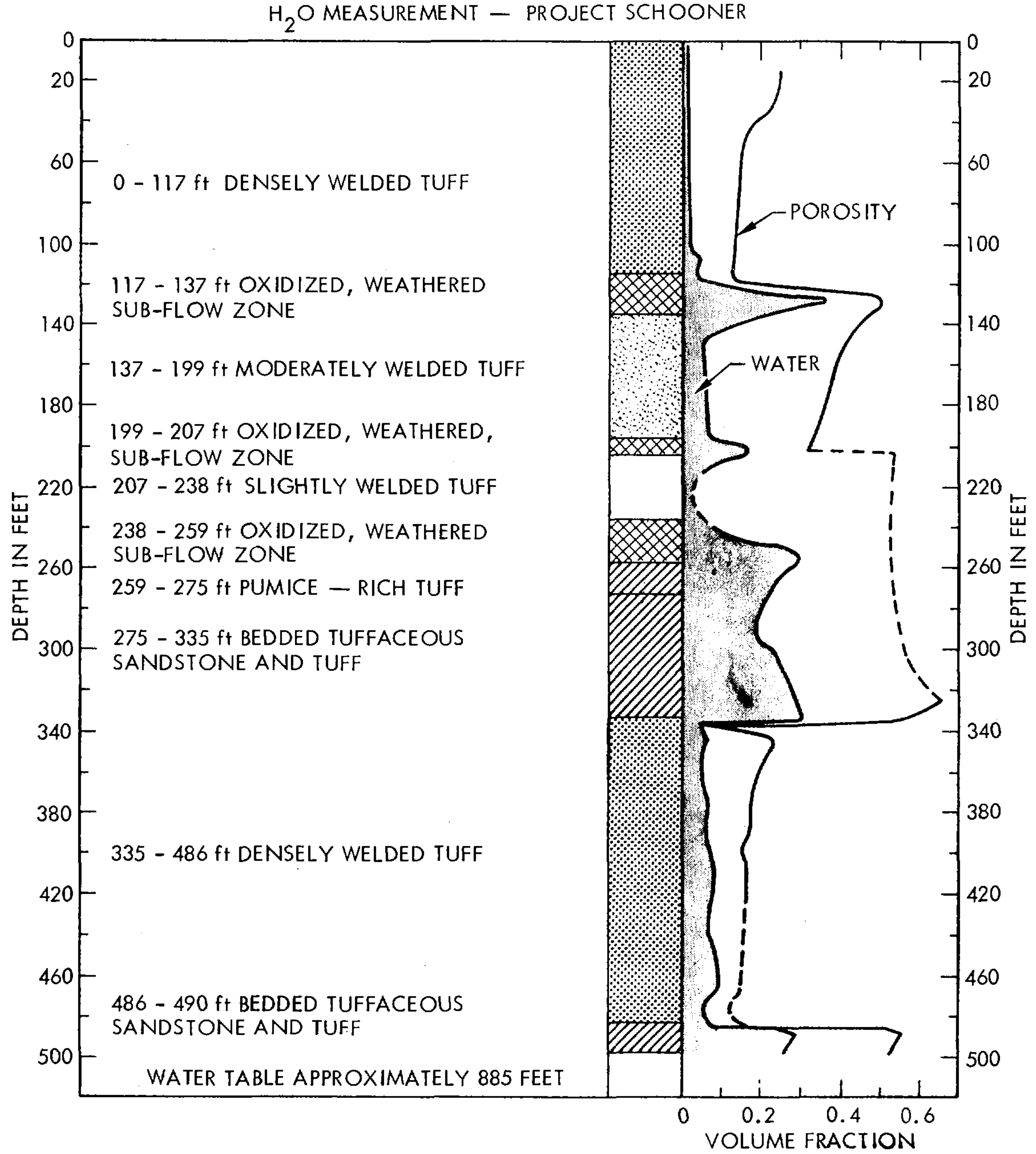

Fig. 7a. Summary of geological data for the Schooner site.

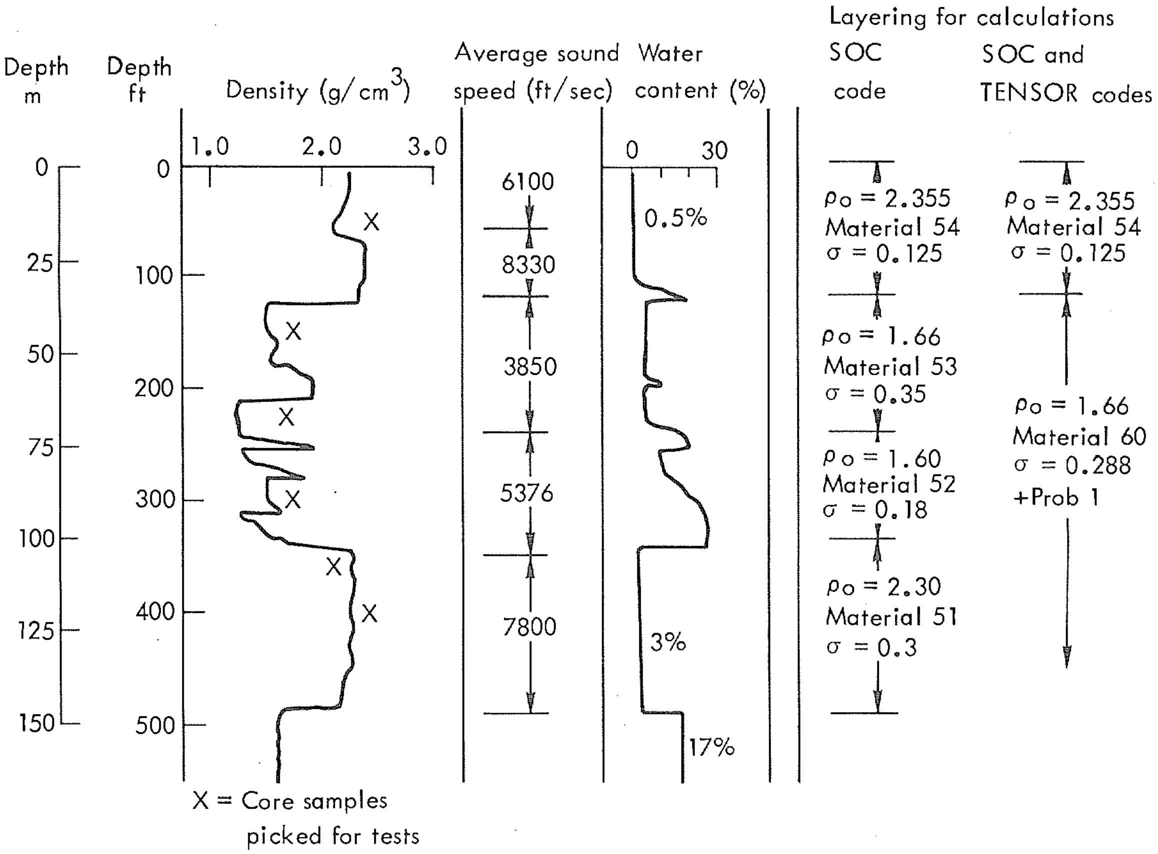

Fig. 7b. In situ measurements and layering for hole U20u.

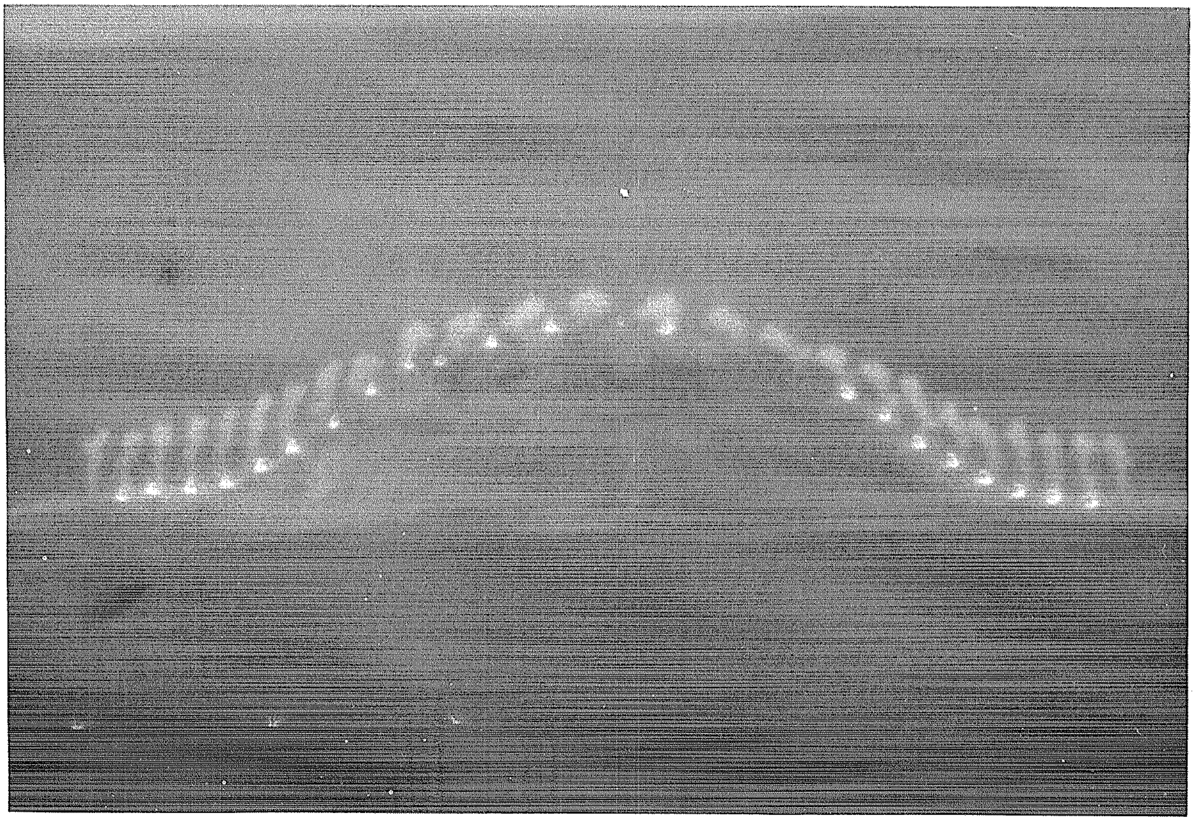

Fig. 8. Schooner mound prior to cavity rupture.

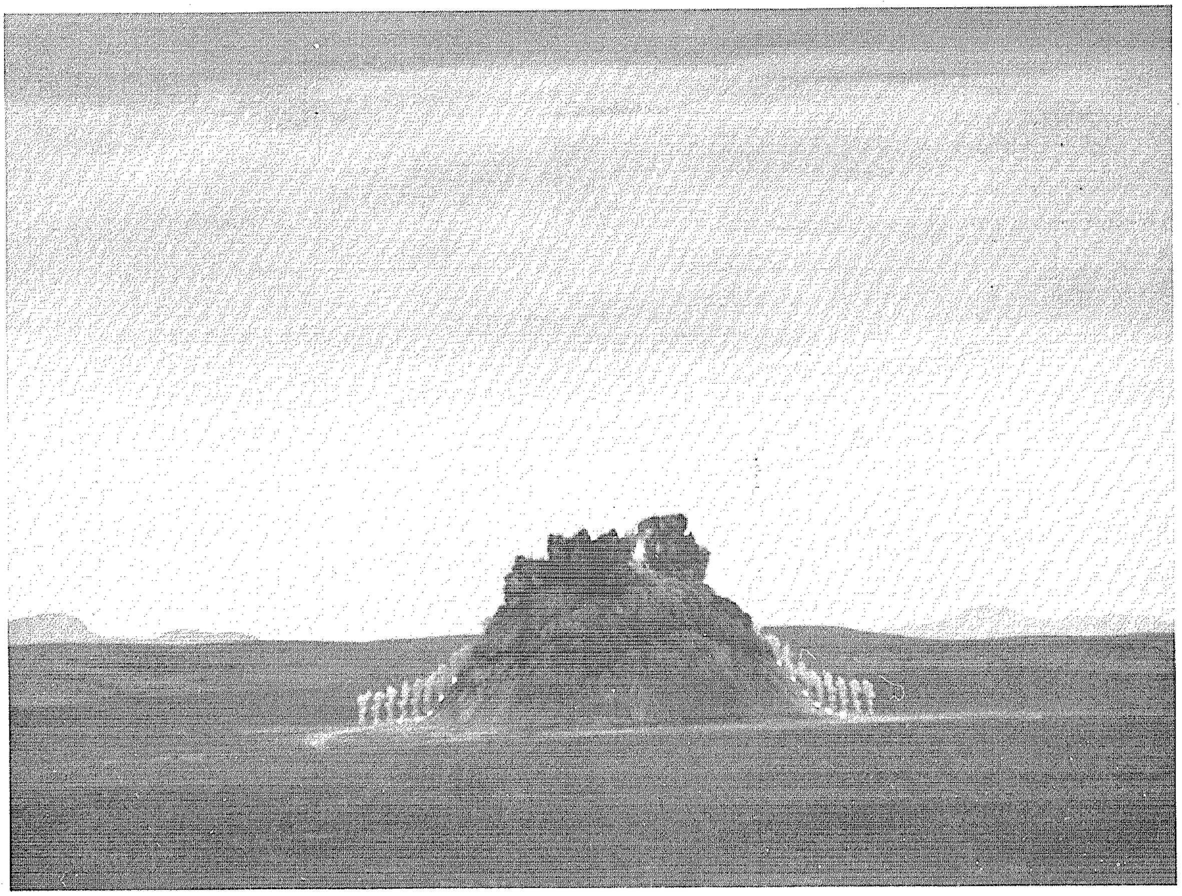

Fig. 9. Schooner mound rupture at 1.75 sec.

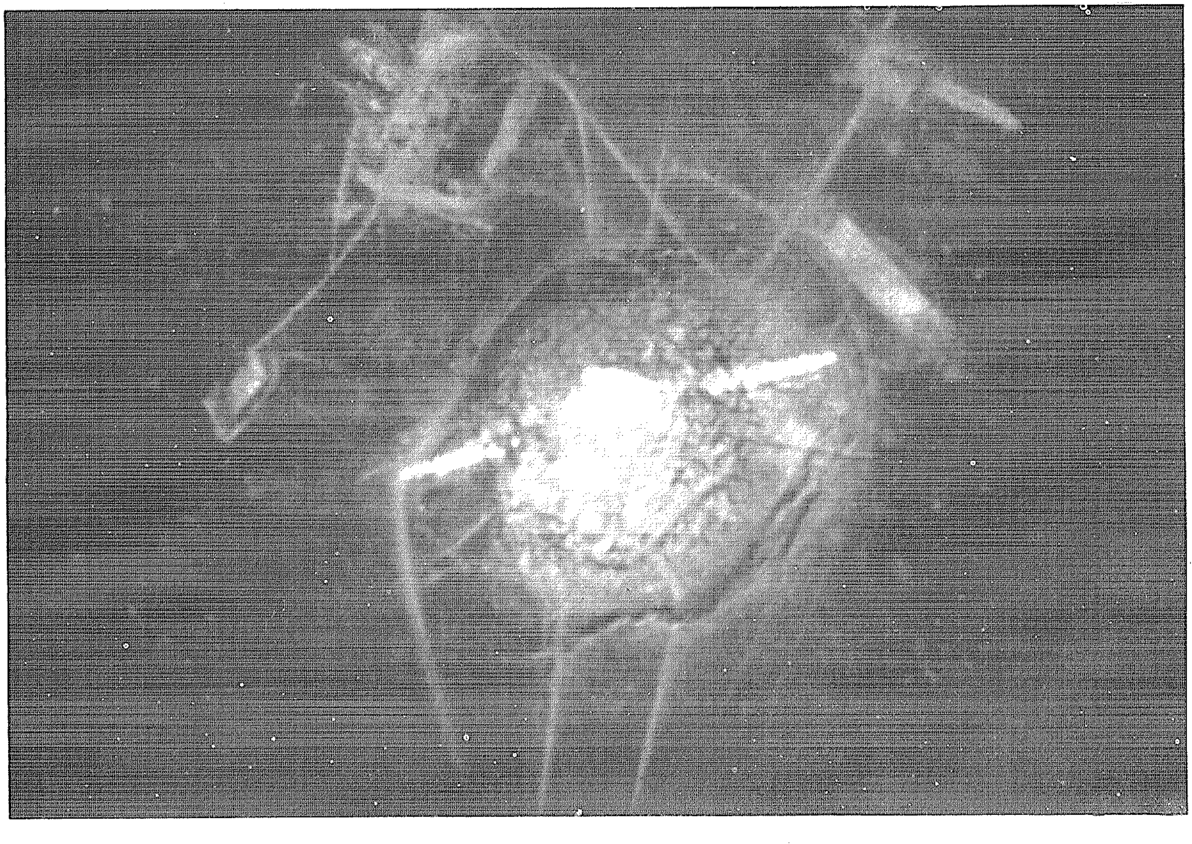

Fig. 10. Schooner mound rupture at 1.75 sec (vertical view).

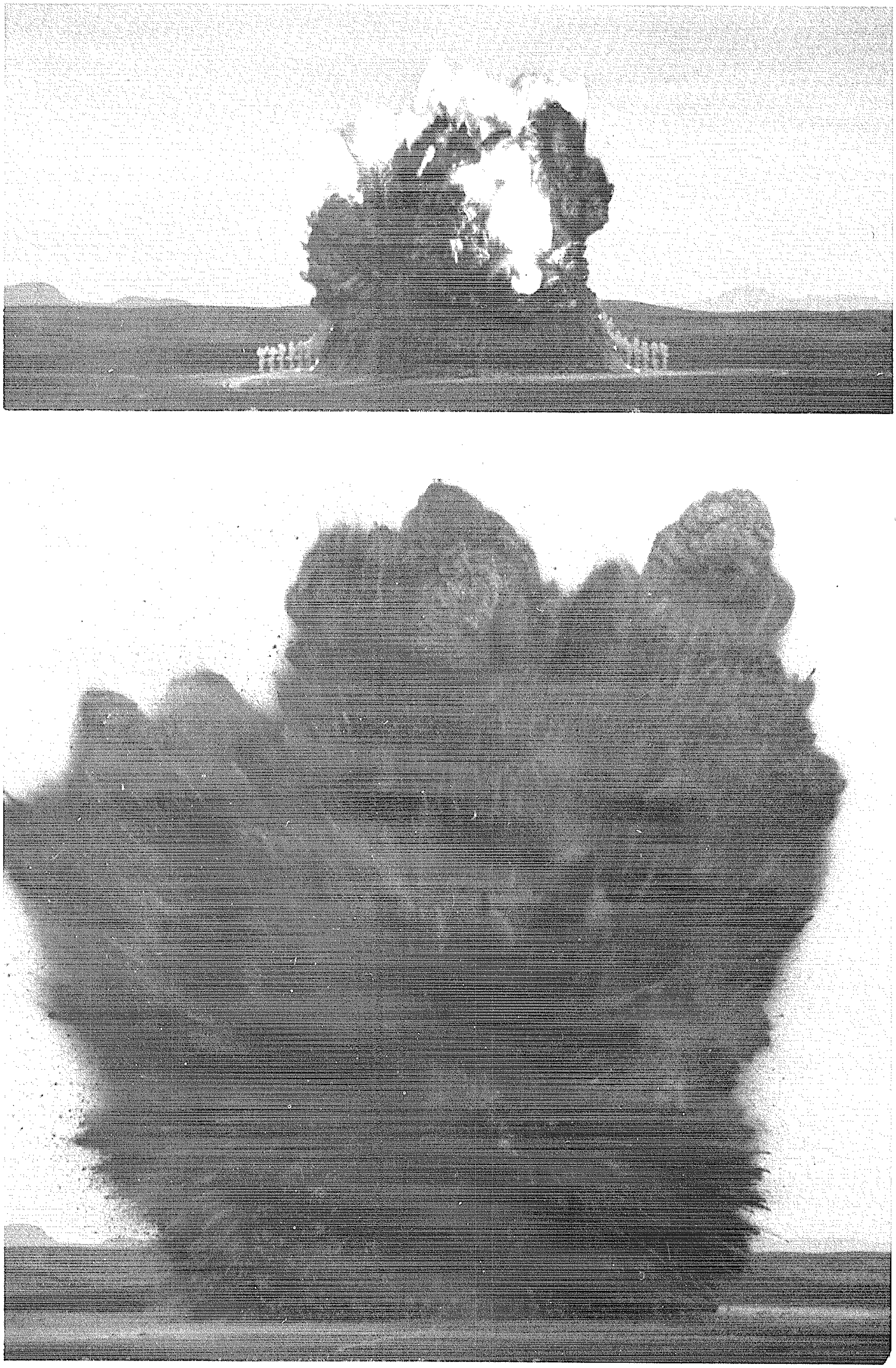

Fig. 11a and b. Two views of Schooner mound development.

Topography of the crater is shown in Fig. 12. The isopach contour profiles of the crater along orthogonal axes are given in Fig. 13. Figure 14 indicates the application of the above dimensions, and Fig. 15 is an aerial view of the crater.

It may be seen from an inspection of both Figs. 13 and 15 that this crater is somewhat atypical when compared with those resulting from previous nuclear detonations. Especially in the western quadrant of the crater, the presence of the strong, hard 30-m-thick surface layer of welded tuff resulted in a slope of approximately 75°, much steeper than the normally observed ~35-40°.

Surface Motion

The velocity of mound rise as a function of time has been found to be an extremely useful parameter in cratering physics studies. Not only does it provide critical data for verifying computerized cratering calculations, but it also has been employed in the formulation of a semi-empirical approach which

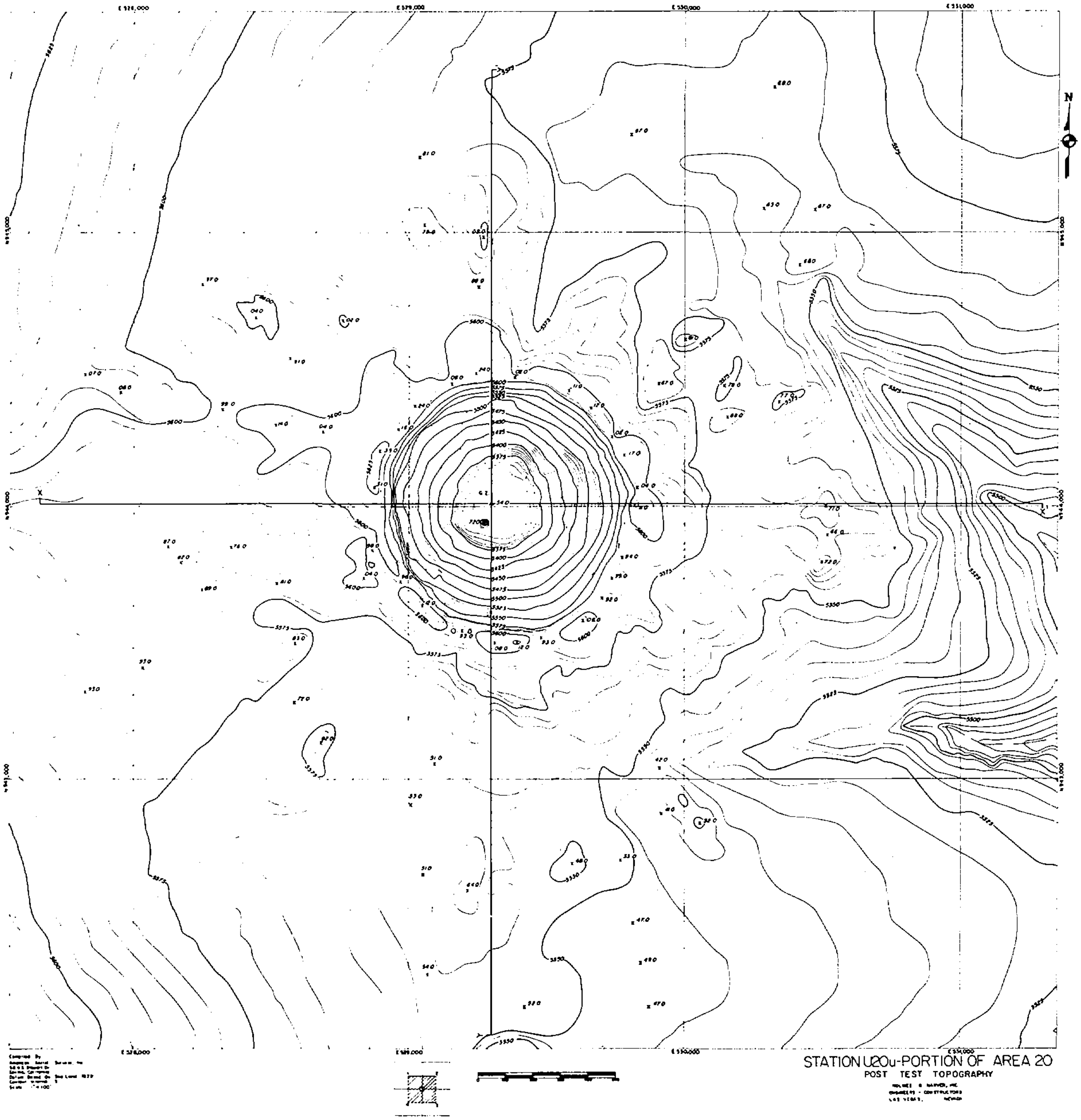

Fig. 12a. Project Schooner postshot topography.

enables an appropriate scaled depth of burst to be selected for a nuclear cratering detonation.

Two experimental techniques were employed in the Schooner Event to determine mound velocities: (1) Flares were emplaced 40 ft apart on a line crossing surface ground zero. The motion of these flares was recorded photographically subsequent to the detonation, and the resulting record of flare location as a function of time was analyzed to determine mound velocity. (2) Accelerometers were located at a number of the flare stations; data from these instruments were displayed on oscilloscopes, photographed, and the resulting record was analyzed to determine both accelerations and velocities. Data from the two techniques were found to be in good agreement.

Figures 16 and 17 represent plots of the Schooner surface motion over a period of time prior to mound disassembly. At times of the order of 200 msec, peak vertical velocities of about 50-55 m/sec due to surface spall were observed in the vicinity of surface ground zero. In the time period

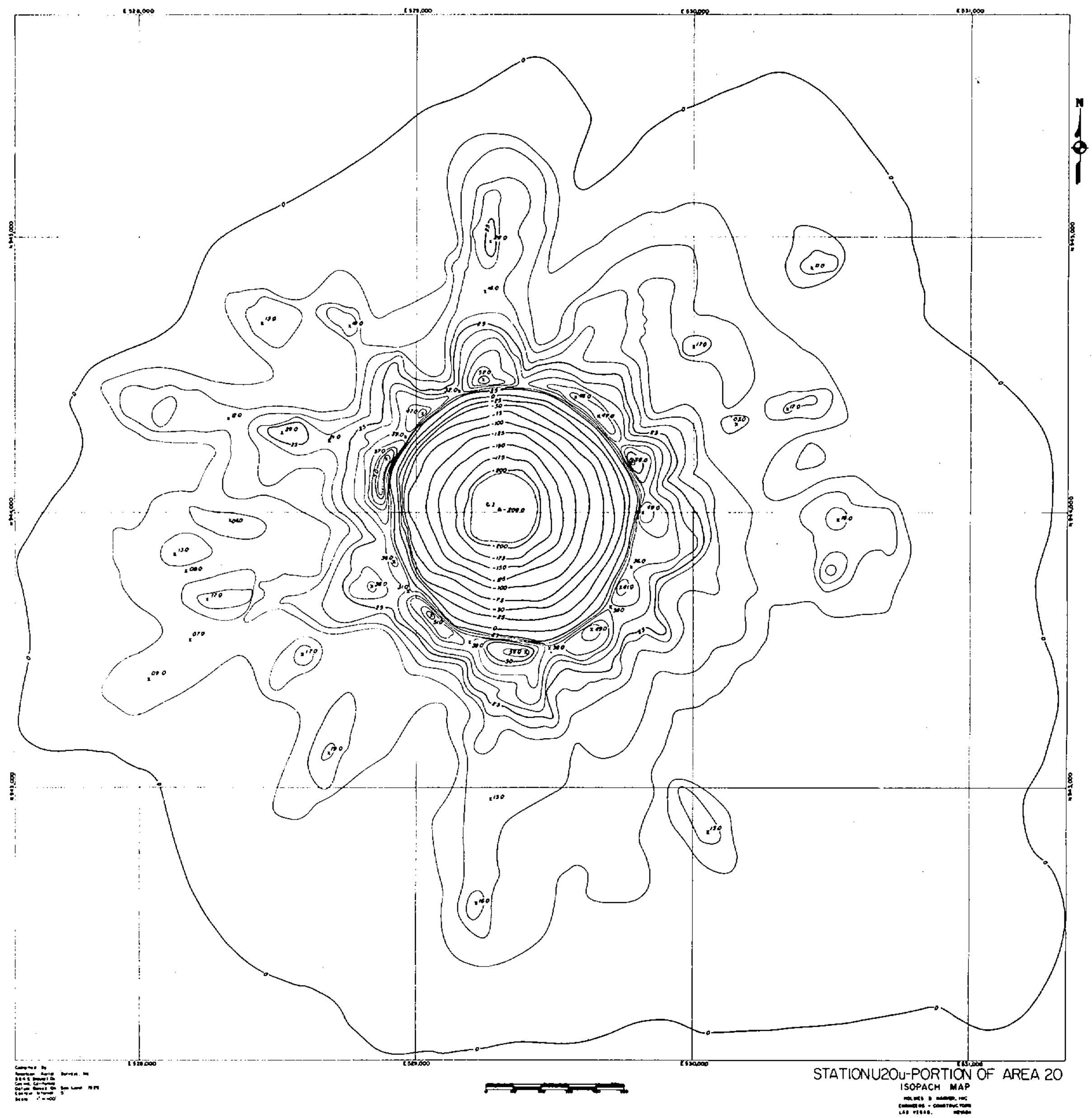

Fig. 12b. Project Schooner isopach map.

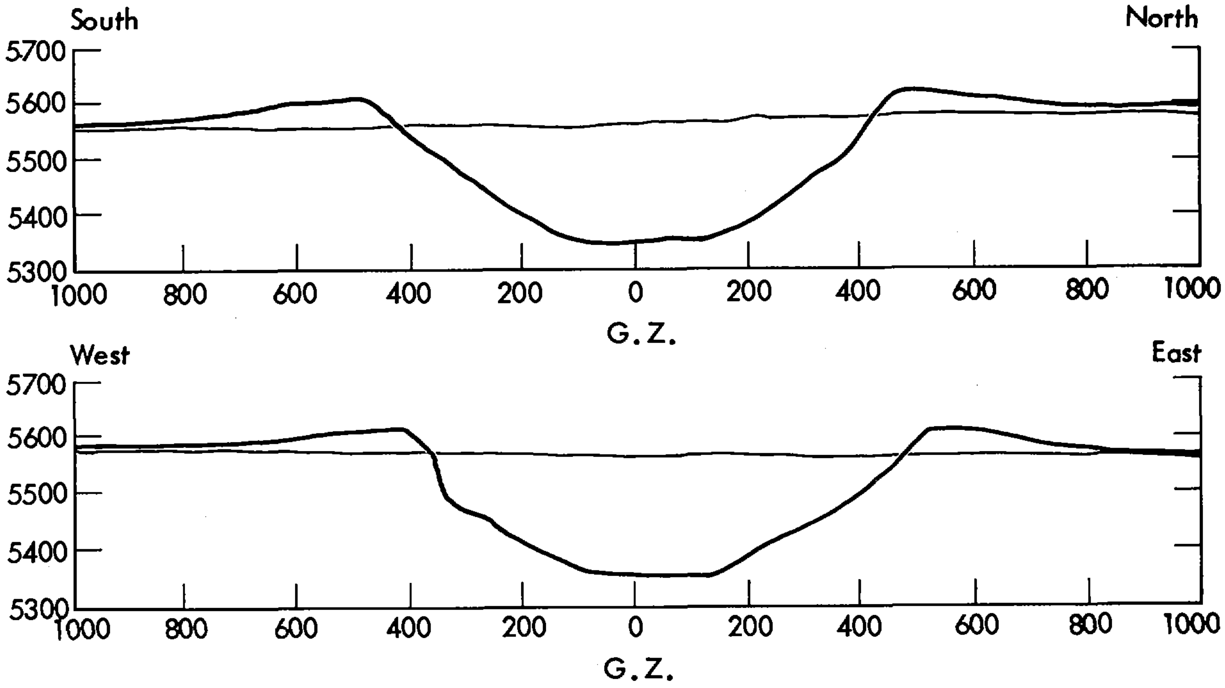

Fig. 13. Schooner crater orthogonal profiles.

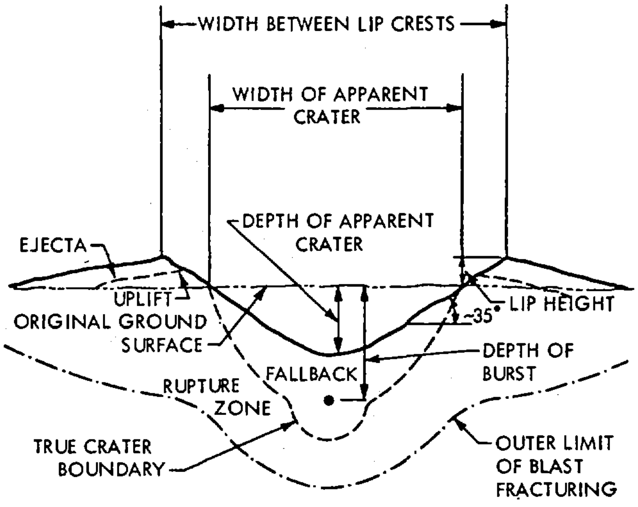

Fig. 14. Idealized cross section of a single-charge nuclear crater in basalt.

between 300 and 600 msec, the surface velocity remained relatively constant; however, after 600 msec, another distinct acceleration of the material became apparent. This phase of the mound growth is attributed to the continuing expansion of the vaporized material around the detonation site which, at this relatively late time has recompacted the debris above the shot point and then imparts additional energy to the rising mass. As can be seen from the record shown in Fig. 17, the flare target 24 m to the west of ground zero attained a maximum velocity of 65 m/sec before its motion could no longer be measured.

The surface velocities measured on Schooner are compared with those observed from other nuclear cratering detonations in dry or partially satu-

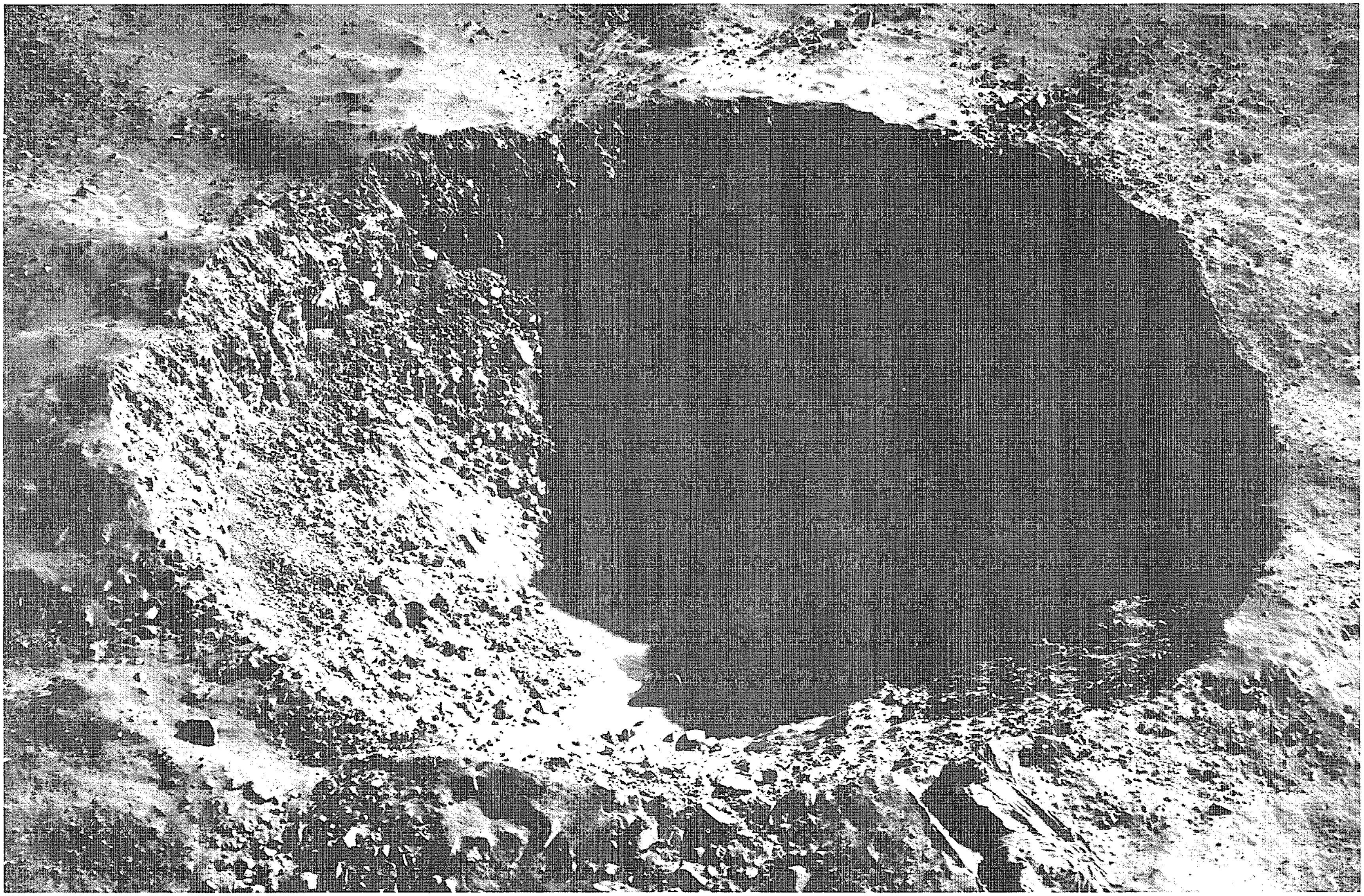

Fig. 15. Schooner crater.

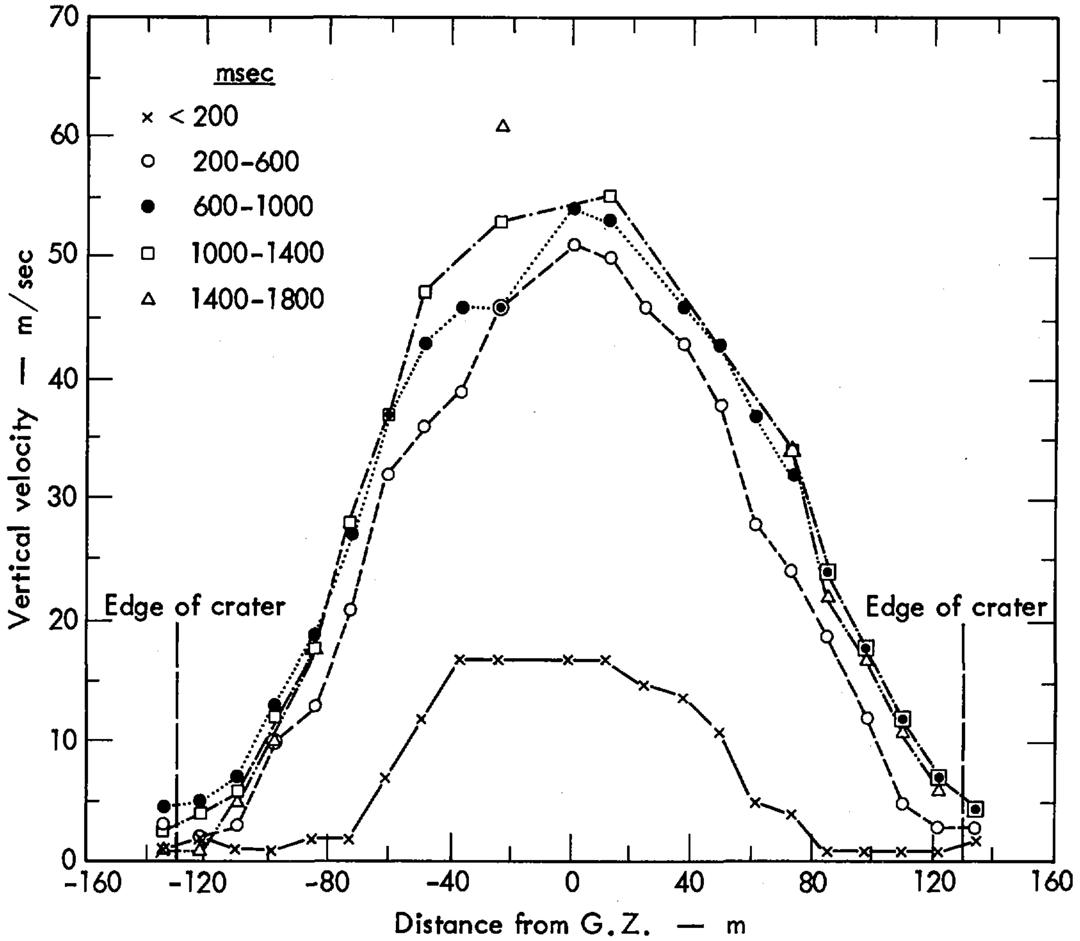

Fig. 16. Schooner surface motion.

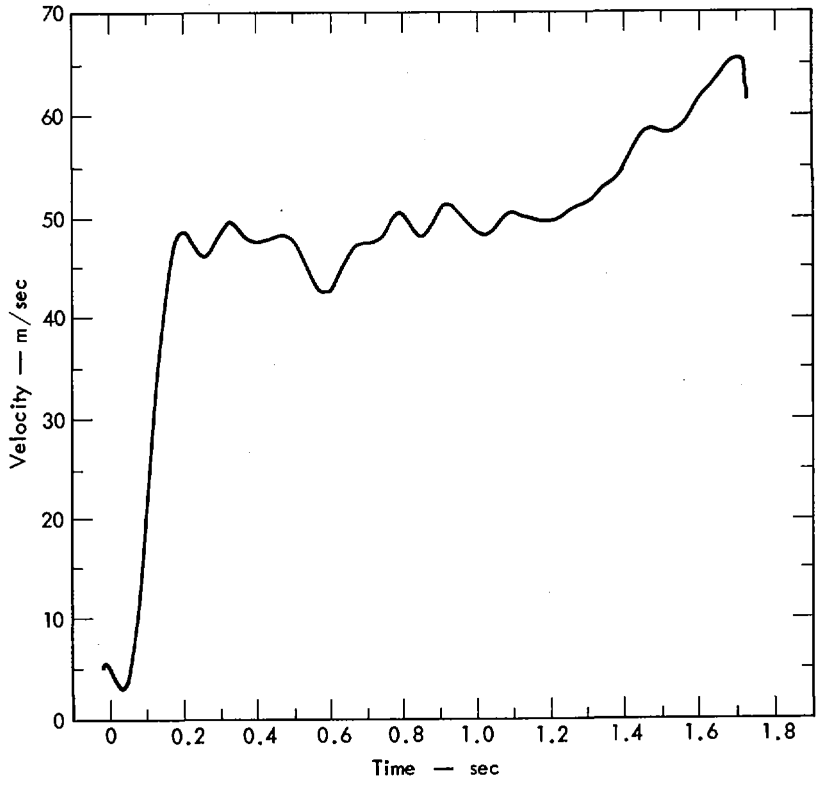

Fig. 17. Schooner vertical velocity (Target 10).

rated rock, shown in Fig. 18. It can be seen that the spall velocity lies on the line delineated by the Danny Boy and Sulky Events. It is of interest to note that, although the data shown in Fig. 18 were obtained from detonations in rock, the Sedan[2] mound spall velocity* lies very close to the line drawn to typify such nuclear cratering detonations.

On the basis of this mound velocity scaling analysis, it would appear that the Schooner detonation could have yielded a crater even if it had been emplaced at a significantly greater depth, perhaps as much as 135 m. Such an analysis should be approached with caution, however, for current experience does not allow a definitive evaluation to be made on the possible effects of such variables as geologic layering, moisture content of the environment, or fracture density of the rock.

COMPARISON OF SCALED CRATER DIMENSIONS AND CODE PREDICTIONS

Cratering experience to date in all media for both nuclear and chemical explosives is summarized in the cratering curves shown in Figs. 19 and 20. Previous studies reported by Nordyke[3] and Toman[4] have indicated that crater dimensions (radius and depth) scale as $W^{1/3.4}$ for the yield ranges within existing experience. From Fig. 19, it can be seen that the Schooner scaled crater radius is about what would be expected, considering the Danny Boy

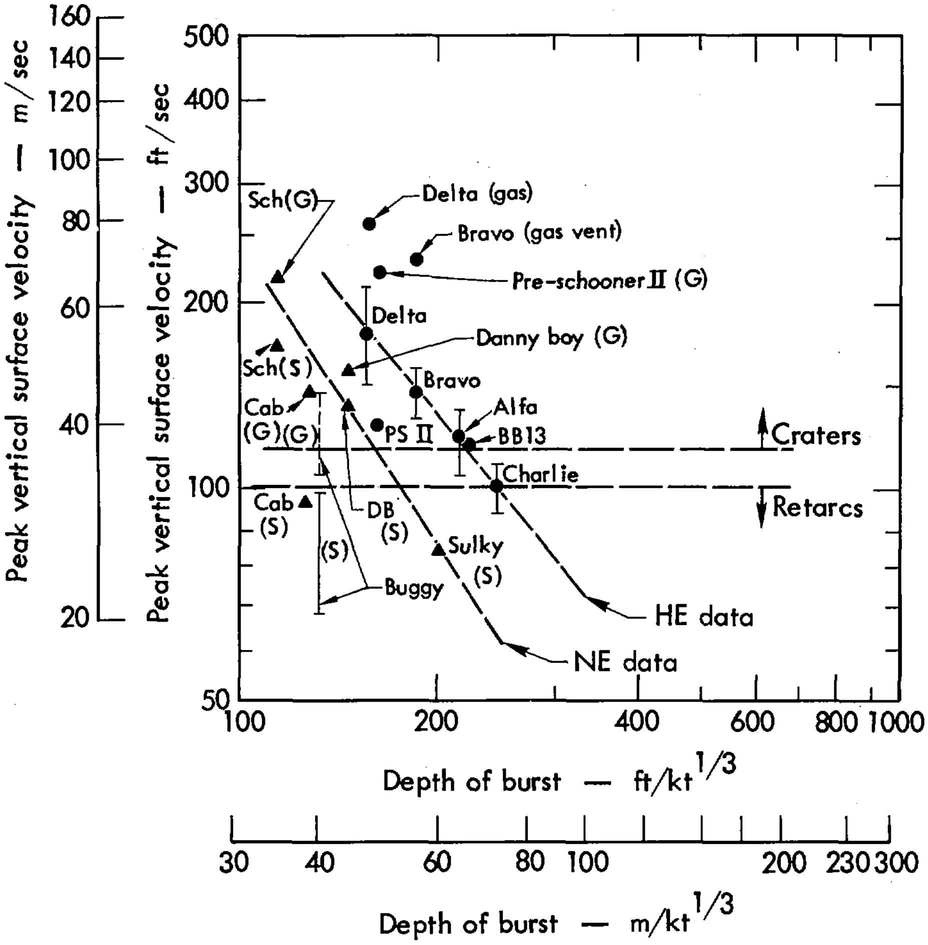

Fig. 18. Hard rock surface motion.

---

*Sedan, with a nominal yield of 100 kt, was fired at a depth of 193 m and gave a maximum spall velocity of 35 m/sec.

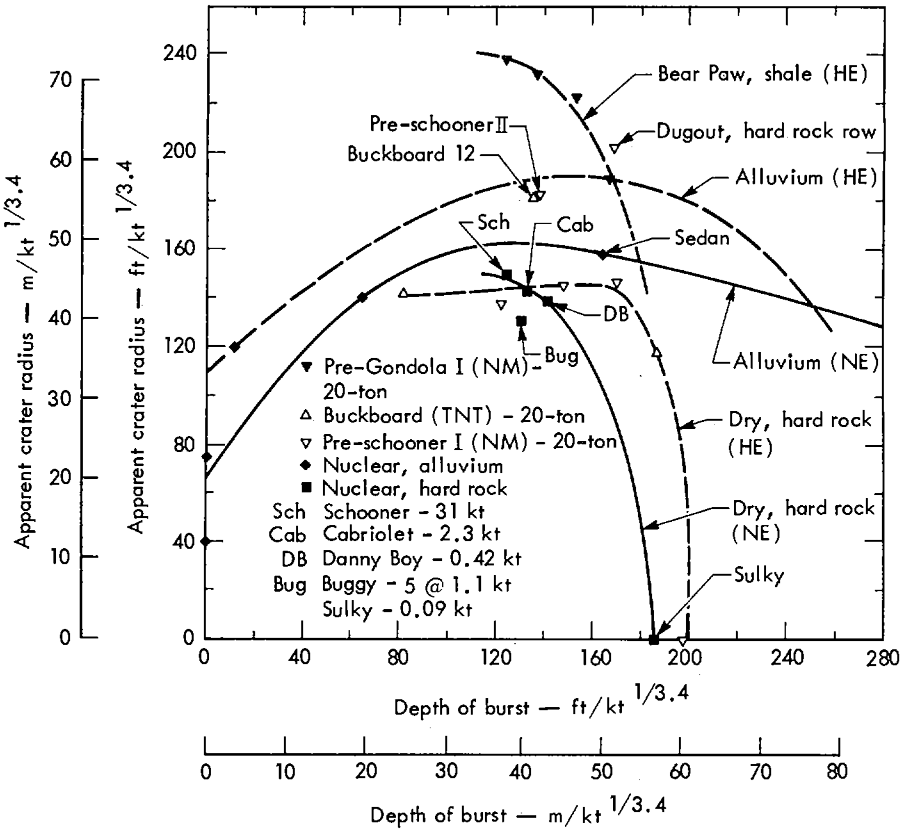

Fig. 19. Cratering data, scaled apparent crater radius versus scaled depth of burst.

and Cabriolet experience. (The Buggy crater may well be relatively small due to the complex geologic layering[5] which prevailed in the detonation site.)

Figure 20 indicates that both Schooner and Buggy gave scaled crater depths somewhat less than would be predicted by the curves shown in the figure. Again, the probable reason for the shallowness of the Buggy crater is the geologic variability of the emplacement medium; however, in the case of Schooner, it should be recalled that the scaled mound velocity curve (Fig. 18) suggested that this detonation was carried out at somewhat less than the "optimum" cratering depth. However, due to the layered geologic structure at the detonation site, emplacement of the explosive at the normal "optimum" cratering depth could have jeopardized the formation of a normal crater.

Figure 21 is a comparison between the observed Schooner crater (average dimensions) and that predicted using the SOC-TENSOR Codes.[6] It may be seen that while the computed crater radius is significantly smaller than that of the actual crater (by about 12-20%), the estimated depth agrees well with that observed.

However, it is of interest to note that the predicted peak surface spall velocity (34 m/sec) is almost 40% less than the 55 m/sec actually observed. Should the spall velocity have been as calculated, it can be seen from Fig. 18 that the Schooner velocity would have been only slightly higher than those observed on the Cabriolet and Buggy experiments, and hence, would have represented a case where crater formation was only marginal if spall were to be the only mechanism by which the overburden would be accelerated.

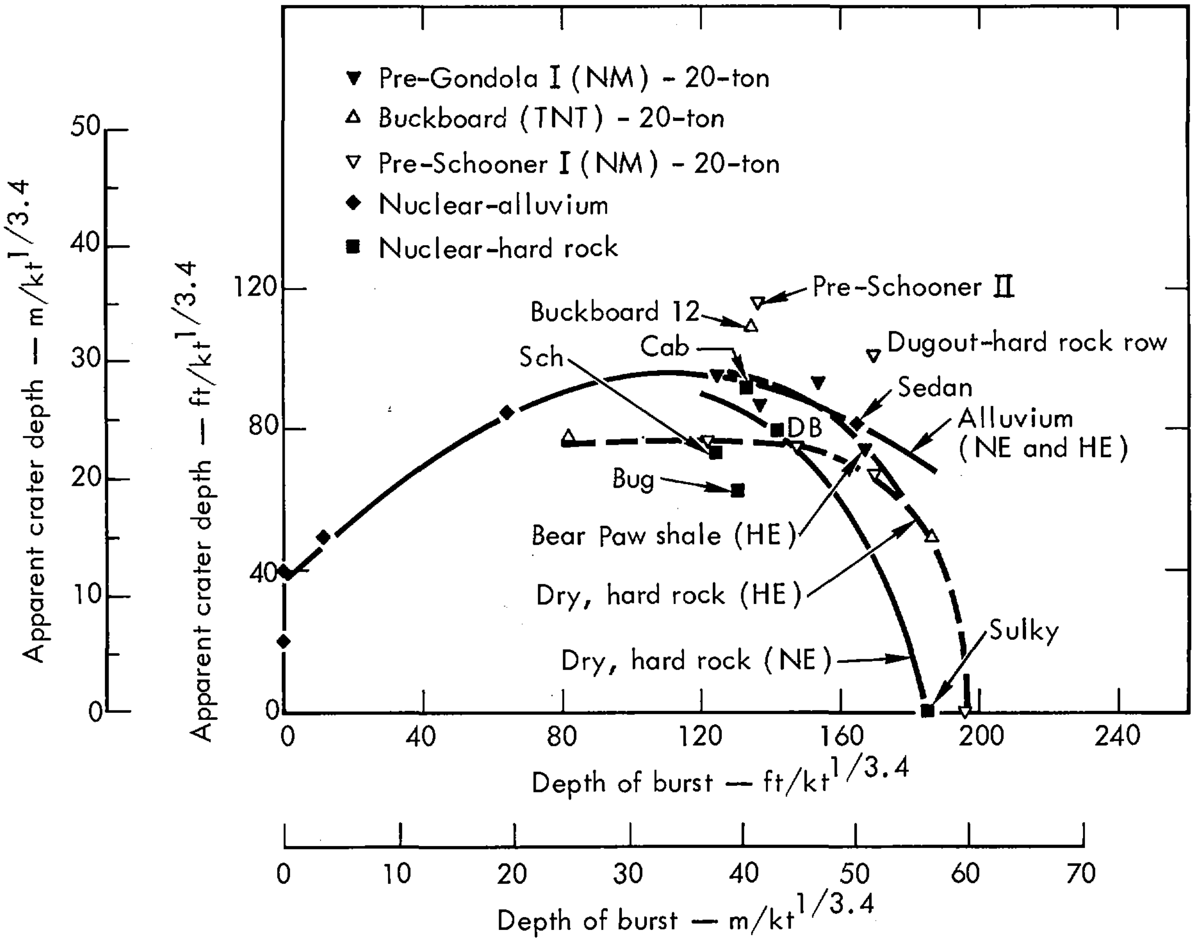

Fig. 20. Cratering data, scaled apparent crater depth versus scaled depth of burst.

More recent (postshot) calculations have been performed with the SOC-TENSOR codes in which the effect of the water in the Schooner environment has been weighted more heavily; the results of these computations agree more closely with the observed values for the crater dimensions and spall velocity. It should be noted that in all Schooner calculations, it was assumed that about 10% by weight of the cavity vapor consisted of water, since this is approximately the amount which should be present when the involvement of both the ash fall tuff and the welded tuff is considered.

It is felt that the present computational approach to cratering prediction, as modified by the Schooner experience, will allow the adequate prediction of events carried out in partially or completely saturated rock.

Radioactivity Studies

One of the primary objectives of the Schooner experiment was the study of the release and distribution of radioactivity resulting from this detonation in partially saturated rock. An extensive sampling program, both for the collection of fallout and cloud samples, was fielded. Data obtained are still in the process of being correlated and interpreted; however, some preliminary results can be reported at this time.

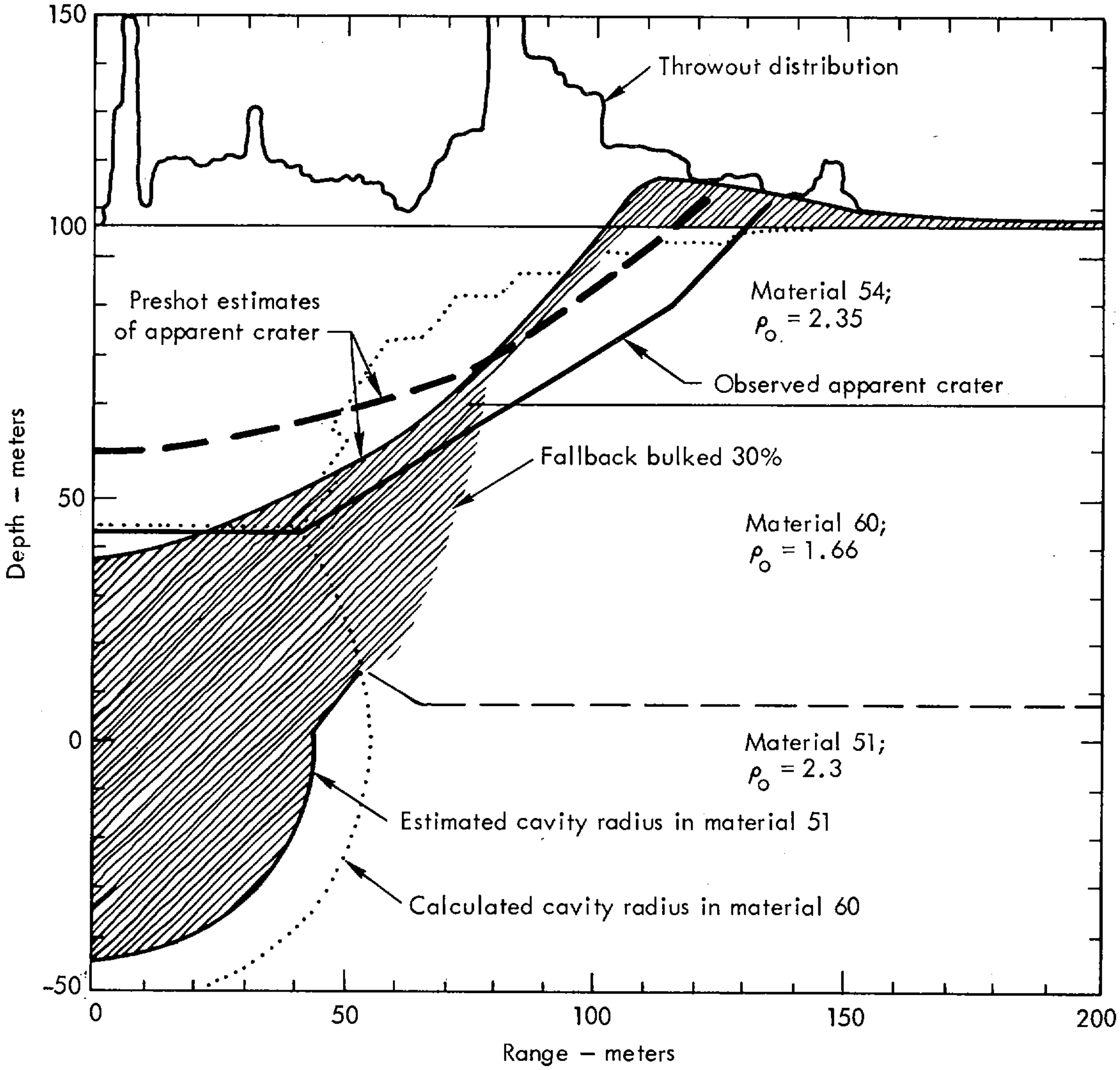

Fig. 21. Estimated and observed profiles of Schooner crater.

Cloud Size

The Schooner cloud at time of stabilization (4 min after detonation) represented a typical main cloud-base surge configuration, although the relative sizes of these two cloud components were notably different from those observed on the Sedan Event:

	Schooner	Sedan
Main Cloud		
Cloud diameter (m)	2420	2300
Cloud height (m above terrain)	3990	3600
Cloud volume (m^3)	1.5×10^{10}	1.0×10^{10}
Base Surge		
Cloud diameter (m)	4220	6800
Cloud height (m above terrain)	670	1200
Cloud volume (m^3)	9×10^9	4.3×10^{10}

At the time of the Schooner detonation, ground-level winds were southerly at about 5-10 knots, while the winds aloft were from the west-southwest at an average speed of 30 knots. These meteorological conditions are reflected in the observed fallout pattern as shown in Fig. 22, where the predominant contribution of the main cloud fallout is apparent.

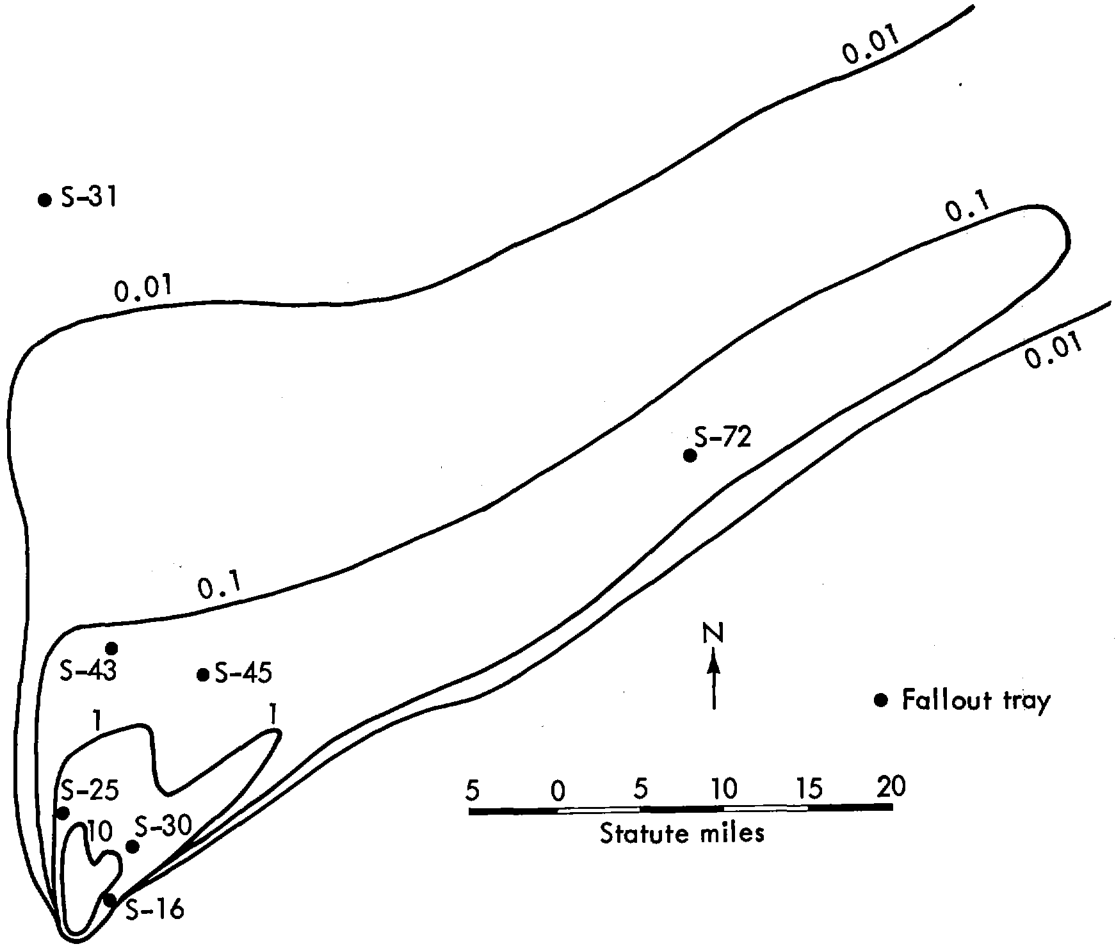

Fig. 22. Schooner fallout field (R/hr at H+1 hr).

RELEASED RADIOACTIVITY RESULTS

Fallout

As has been done for past events, the amount of radioactivity released as "close-in" fallout was defined as that which fell outside the limit of direct throwout. The pattern shown in Fig. 22 was integrated in the usual way; the areal distribution of the radioactivity in the observed pattern was integrated over the range from 0.36 to 604 square miles, and then extrapolated to an "infinite" area. Using an intensity of 3380 R/hr (at H+1 hr) as the exposure rate resulting from the fission products from 1 kt of fission being uniformly distributed over a 1-square-mile plane surface and a "terrain shielding factor" of 0.75, the observed fallout integral of 850 $(R/hr)_{H+1\ hr} \times mi^2$ can be seen to be equivalent to the radiation from the fission products resulting from ~ 340 tons of fission. Figure 23 gives the observed values for the gamma exposure rate (corrected to H+1 hr) along the "hot line" of the fallout field; as would be expected, this "hot line" represented a trace of the path of the Schooner main cloud. Also shown in Fig. 23 are the gamma exposure rates calculated using the KFOC computer program[7] (using as input the observed detonation time meteorology and measured total amount of radioactivity deposited in the fallout pattern). It can be seen that the calculated values agree with observed exposure rates within a factor of 3 at all distances, which, considering effects of terrain and other random variables, is considered to be adequate confirmation of the fallout model.

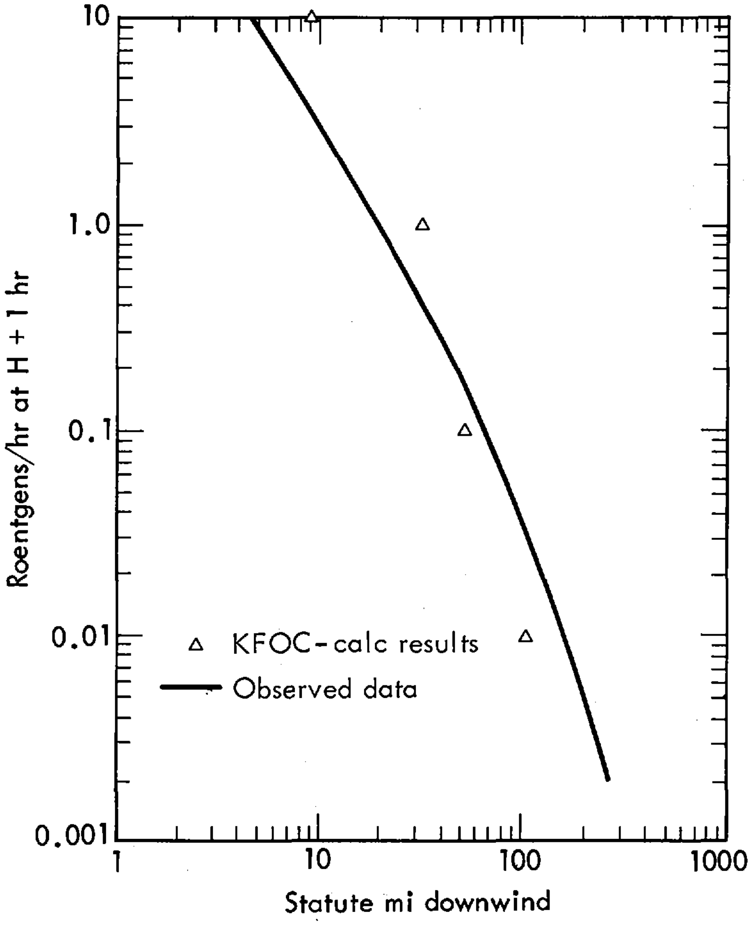

Fig. 23. Schooner main cloud hot line (H+1 hr) exposure rate.

Radiochemical results obtained from a number of fallout collectors are shown in Table I. The approximate locations of the six "close-in" trays are shown in Fig. 22; the other two collectors were too far from ground zero to be shown in the reference figure. It can be seen from the data given in Table I that there was a moderate amount of chemical fractionation within the fallout pattern, ranging from factors of 40 for some radionuclides to factors of only about 5 for the tungsten isotopes. Since the major contributor to the H+1-hr gamma exposure rate among the listed radioisotopes is obviously W^{187}, and since the correlation between radionuclide deposition and gross gamma field readings has not been found to be much better than about a factor of 2, the data given in Table I do not appear to be inconsistent. Obviously, there is some relative fractionation between the more "volatile" elements (such as tungsten) and those which display refractory behavior (such as manganese or yttrium).

Table I. Results of radiochemical analyses of samples from fallout trays and vaseline-coated tarpaulins, expressed as pCi/m^2 at zero time, divided by the gross gamma radiation field reading in R/hr (corrected to H+1 hr). Multiplying each number in a particular column by the factor shown at the head of the column will give the value of $(\mathrm{pCi/m^2})_0$, divided by the gamma field reading.

				Fission Products										Activation Products												
				$\frac{(\mathrm{pCi/m^2})_0}{(\mathrm{R/hr})_{\mathrm{H+1hr}}}$																						
Station	Azimuth	Distance from G.Z. (km)	$(\mathrm{R/h})_{\mathrm{H+1hr}}$	Sr^{89} (10^5)	Sr^{90} (10^2)	Zr^{95} (10^5)	Mo^{99} (10^5)	Ru^{103} (10^5)	Te^{132} (10^5)	I^{131} (10^5)	Cs^{137} (10^2)	Ba^{140} (10^5)	Ce^{141} (10^5)	Cr^{51} (10^5)	Mn^{54} (10^5)	Co^{57} (10^5)	Co^{58} (10^5)	Y^{88} (10^5)	Tm^{168} (10^5)	Ta^{182} (10^5)	Ta^{183} (10^5)	W^{181} (10^8)	W^{185} (10^8)	W^{187} (10^9)	Pb^{203} (10^5)
(Main cloud)																										
S-16	050°	3	1.3	—	—	13	420	14	92	36	—	41	19	—	38	17	95	25	9.4	17	270	3.8	11	18	330
S-30	040°	10	3	—	—	—	350	—	130	48	—	52	11	—	—	—	—	27	—	—	—	—	—	24	—
S-45	030°	27	0.37	—	—	1.3	48	5.9	59	22	—	8.8	3.4	—	4.8	2.1	14	2.6	1.0	2.2	33	2.4	7.4	10	—
S-72	055°	74	0.3	—	—	3.9	150	25	300	100	—	35	9.8	—	1.2	12	32	7.3	2.8	5.4	—	7.8	22	37	490
FFOCC-S-91	063°	270	0.009	1.2	8	0.8	—	7	—	30	4	1.2	2	7	2	0.8	6	1.3	0.4	1.0	—	2.2	6	—	—
FFOCC-S-53	059°	423	0.002	0.3	34	1.8	—	12	—	40	16	13	20	11	4	1.7	11	2.5	1.1	—	—	3.2	10	—	—
(Base surge)																										
S-25	000°	10	3	—	—	0.58	21	4.0	50	17	—	6.5	1.8	—	1.7	0.86	5.2	0.87	0.36	0.83	14	1.6	4.7	7.1	86
S-43	010°	27	0.17	—	—	0.74	28	4.3	58	17	—	6.4	2.1	—	2.3	1.4	6.6	1.3	—	1.2	17	1.8	5.3	8.5	—
Average				$2.3 \times 10^{12}\ \frac{\mathrm{fissions/m^2}}{(\mathrm{R/hr})_{\mathrm{H+1hr}}}$										—	3.9	3.5	17	4.9	1.8	2.9	38	2.9	8.5	15	240

When the geometric averages of the values given in Table I are taken (with the "far-out" collections given somewhat less statistical weight than the other data), the results shown in the bottom line are obtained; all fission product data have been averaged to obtain an estimate of the fissions/m^2 per $(\mathrm{R/hr})_{\mathrm{H+1\ hr}}$. When the average results are multiplied by the previously noted fallout integral, 850 $(\mathrm{R/hr})_{\mathrm{H+1\ hr}} \times \mathrm{mi}^2$, the total amounts of the various radionuclides in the Schooner fallout pattern are obtained; these are given in Table II. For purposes of comparison, results are also given in terms of equivalent tons of fission yield (expressed as dose rates at H+1 hr). It can be seen that the Schooner fallout field contained only about 2.5% as much fission debris as was observed for Sedan.[8] Although the amounts of induced radioactivities in the fallout are quite similar, the total radioactivity in the Schooner pattern is less than 25% of that measured in the case of Sedan.

Cloud

A number of aircraft samples were taken from both the Schooner main cloud and base surge at 12.5 min after the detonation. Radiochemical analytical results obtained from these samples are given in Table III. It can be seen that the three regions of the main cloud represented by the samples were remarkably similar with regard to the radionuclide concentrations detected. The two base surge samples showed somewhat less correspondence to each other, with the first having only about 40% as much radioactivity per m^3 as did the second.

Schooner main cloud and base surge volumes measured at time of stabilization (H+4 min) have been noted previously; using photographically documented rates of cloud growth as well as dimensional data obtained in the course of aircraft sampling, it has been estimated[9] that at H+12.5 min, the main cloud volume was about 4×10^{10} m^3. Similarly, the base surge was almost a factor of 2 larger at H+12.5 min (1.5×10^{10} m^3) than at H+4 min. Applying these corrected cloud volumes and using the geometric average of the measured cloud concentrations given in Table III, approximate total cloud burdens have been calculated[10] and are shown in Table IV.

Additional data[11] reported on Schooner cloud concentrations, as determined for times later than H+12.5 min, indicate that the relative radionuclide compositions of both the main cloud and the base surge changed only slightly with time; this is in marked contrast to the observations made on the base surge cloud from the Danny Boy experiment.[12]

Table II. Total amounts of several radionuclides deposited in Schooner fallout; comparison with Sedan fallout.

	Schooner		Sedan
Nuclide	Total Ci in Fallout[a]	Equivalent tons of fission[b]	Equivalent tons of fission in fallout[b]
Total fission products	5.1×10^{21}[c]	35	1400
Na^{24}	—	—	3
Sc^{44m}	—	—	0.3
Mn^{54}	850	0.002	—
Mn^{56}	—	—	3
Co^{57}	770	0.0003	—
Co^{58}	3700	0.01	—
Y^{88}	1080	0.007	0.03
Tm^{168}	400	0.002	—
Ta^{182}	640	0.002	—
Ta^{183}	8300	0.01	—
W^{181}	640,000	0.1	—
W^{185}	1.9×10^6	—	—
W^{187}	3.3×10^7	55	50
Pb^{203}	53,000	0.05	—
Other	—	250[d]	—
	Total:	~340	~1460

[a] Corrected to t_0.

[b] Exposure rate at H+1 hr.

[c] Total fissions.

[d] Estimated, including mainly short-lived radionuclides such as Na^{24} and Mn^{56}.

Table III. Results of radiochemical analyses of samples taken from both the main cloud and the base surge cloud at 12.5 min after detonation. These results are expressed in pCi/m^3 at zero time. Multiplying each number in a particular column by the factor shown at the head of the column will give the value of $(pCi/m^3)_0$.

$(pCi/m^3)_0$.

	Fission Products								Activation Products									
Sample identification	Mo^{99} (10^5)	Ru^{103} (10^4)	Te^{132} (10^5)	I^{131} (10^4)	Cs^{137} (10^1)	Ba^{140} (10^4)	Ce^{141} (10^3)	Nd^{147} (10^3)	Na^{24} (10^6)	Mn^{54} (10^3)	Co^{57} (10^3)	Co^{58} (10^4)	Y^{88} (10^3)	Ta^{183} (10^4)	W^{181} (10^6)	W^{185} (10^7)	W^{187} (10^8)	Pb^{203} (10^5)
Schooner main cloud #1	1.25	3.06	3.15	10.3	8.7	4.24	7.51	4.60	1.68	9.63	3.93	2.57	5.09	5.44	8.33	2.42	4.35	4.86
Schooner main cloud #2	0.93	2.24	2.74	8.70	8.8	3.64	6.27	7.34	1.32	7.23	3.14	2.00	4.70	4.73	6.58	1.83	3.68	4.08
Schooner main cloud #3	1.33	2.49	2.95	9.53	8.4	4.25	9.41	7.35	1.92	10.6	5.03	3.08	6.29	7.07	9.37	2.80	3.76	5.22
Schooner base surge #1	0.15	0.34	0.42	1.33	7.7	1.06	1.10	0.58	0.19	0.99	0.62	0.32	0.50	0.77	1.38	0.45	0.66	0.68
Schooner base surge #2	0.35	0.85	1.05	3.29	9.1	1.99	2.38	1.42	0.55	2.56	2.04	0.91	1.23	1.99	3.61	1.02	1.69	1.82

Table IV. Total amounts of several radionuclides in the Schooner clouds at H+12.5 min.

Nuclide	Main cloud[a]		Base surge[b]	
	Total Ci[c]	Equiv. tons of fission[d]	Total Ci[c]	Equiv. tons of fission[d]
Total fission products	2.2×10^{21}[e]	15	2.8×10^{20}[e]	2
Na^{24}	64,000	0.6	5000	0.05
Mn^{54}	360	0.0009	24	0.00006
Co^{57}	160	0.00006	17	0.000006
Co^{58}	1000	0.003	81	0.0002
Y^{88}	210	0.0015	12	0.00008
Ta^{183}	2300	0.003	190	0.0002
W^{181}	3.2×10^{5}	0.05	3.3×10^{4}	0.005
W^{185}	9.2×10^{5}	—	1.0×10^{5}	—
W^{187}	1.6×10^{7}	25	1.6×10^{6}	3
Pb^{203}	19,000	0.02	1700	0.0015
Other[f]		~9		~0.6
Totals:		~50		~6

[a] The estimated cloud volume is ~4×10^{10} m^3.

[b] The estimated cloud volume is ~1.5×10^{10} m^3.

[c] Corrected to t_0.

[d] Exposure rate at H+1 hr.

[e] Total fissions.

[f] Estimated; mainly short-lived radionuclides, such as Mn^{56}.

It is of interest to compare relative Schooner main cloud radionuclide burdens as determined by different sampling methods. In addition to the H+12.5-min aircraft sampling of the cloud, a number of other penetrations were made at later times; the data from these samples and cloud radiation level determinations have been correlated, using the large cloud dispersion model, 2BPUFF.[11,13] Also, at about H+1 hr, some 150 small particulate samplers were dropped through the cloud to obtain an estimate of the aerosol "lumpiness" (see Fig. 24), as well as to ascertain the total radionuclide inventory.[14] Results obtained from these different approaches are:

Sampling method	W^{181} cloud burden (corrected to t_0)
Aircraft, H+12.5 min	3.2×10^{5} Ci
Correlated late-time aircraft data	1.5×10^{5} Ci
Drop packages, H+1 hr	$(2.5\text{-}10) \times 10^{5}$ Ci

The only one of those three methods that may be said to give a good estimate of the "non-falling" cloud burden is the second. The H+12.5-min samples apparently contain in about equal amounts both the "non-falling" material, as well as radioactivity which was deposited as local fallout (though

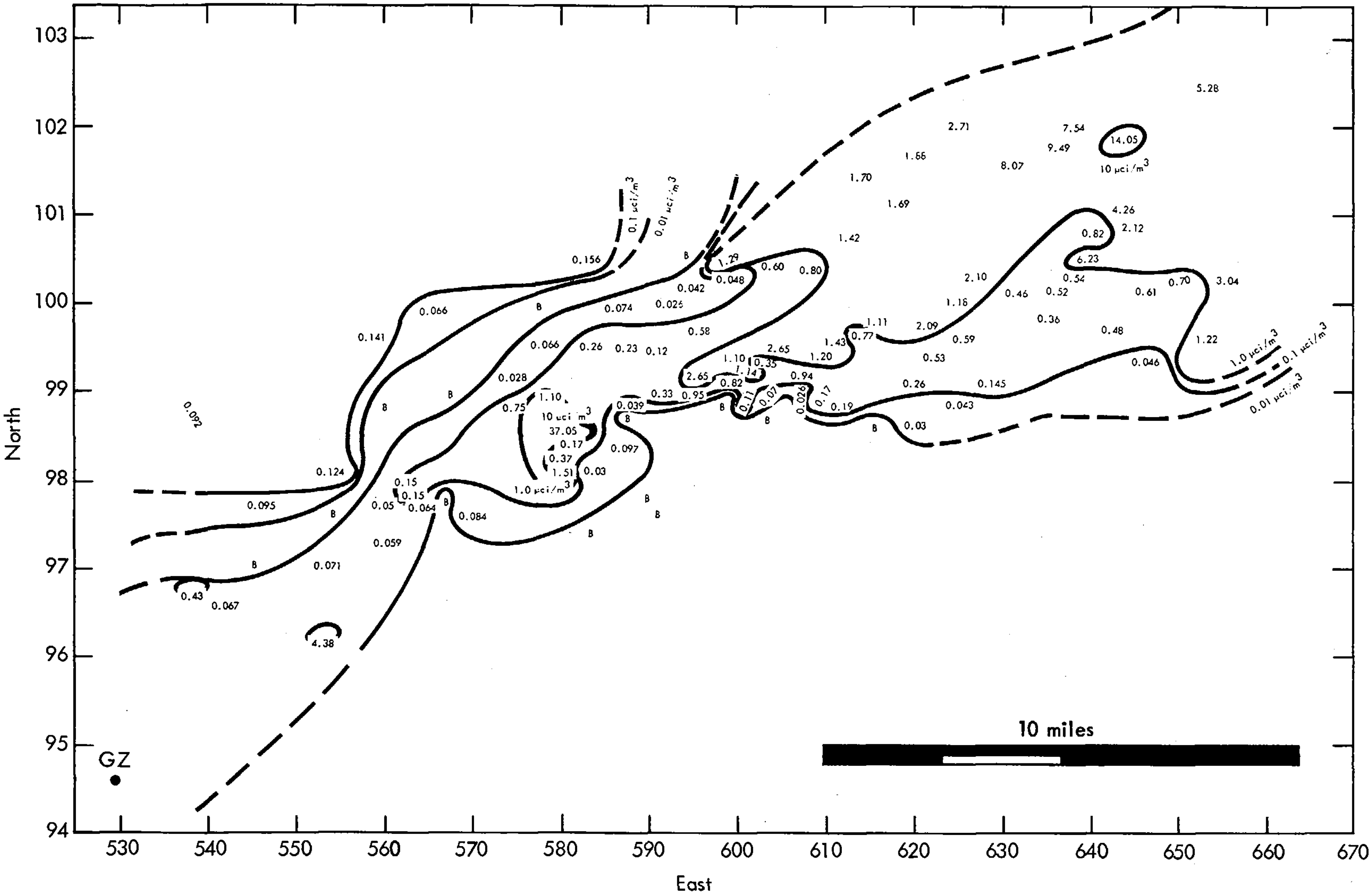

Fig. 24. The Schooner cloud contour based on measurements made at H+1 hr. The isopleths are based on the concentration of gross activity at H+50 hr integrated from 18,500 ft MSL to the terrain surface. The coordinates are based on the Central Nevada Grid Coordinate system and the unit is 10,000 ft. The dashed-line contours are based on extrapolated data. B = background reading.

perhaps at distances of 100 or more km from ground zero). The drop package samplers obviously collect a large amount of falling debris since they sample not only the visible cloud, but also all of the material beneath the cloud down to the surface of the ground.

Consequently, the main cloud radionuclide burdens summarized in Table IV should be divided by a factor of 2 to be representative of the "non-falling" cloud which contributes to long-range fallout.

Although the data relating to the base surge cloud burden are considerably less extensive than those obtained for the main cloud, the similar particle size distribution observed[14] in the H+12.5-min samples from both clouds would lead to the conclusion that about half of the radioactivity measured in base surge samples should be attributed to the "non-falling" debris.

On the basis of the foregoing discussion, the total released radioactivity from the Schooner Event may be summarized as:

	Equivalent tons of fission
Fallout	340
Main cloud	25
Base surge	3
Total:	~370

ADDITIONAL RESULTS

A number of other experimental programs were also conducted on the Schooner Event; some of the data from these programs have already been reported, but have not been discussed in this paper.

Extensive studies of the impact of the Schooner radioactive debris on the biosphere have been conducted by the Bio-Medical Division of the Lawrence Radiation Laboratory, and by the U. S. Public Health Service (Southwestern Radiological Health Laboratory), and preliminary reports[14,15] summarizing the results are available.

Air blast measurements were made (both at short and long range) by Sandia Laboratories (Albuquerque). Reports are not as yet published. A study of ejecta characteristics has been completed; a report on the data obtained is being published.[16]

ACKNOWLEDGMENTS

The author wishes to thank those scientists, both at LRL and elsewhere, whose data have been summarized in this report. In addition to those included in the references, the cooperation and help of a number of individuals were instrumental in the formulation of this paper; among these are:

J. B. Andrews, U. S. Army Corps of Engineers, Nuclear Cratering Group (long-range fallout collection);
T. A. Gibson, LRL (fallout field assessment);
J. R. Hearst, LRL (site geophysics);
W. R. Hurdlow, LRL (accelerometer program);
A. L. Prindle, LRL (radiochemical analysis);
L. D. Ramspott, LRL (site geology);
B. B. Redpath, U. S. Army Corps of Engineers, Nuclear Cratering Group (crater configuration);
R. F. Rohrer, LRL (surface motion analysis, cloud size assessment);

L. L. Schwartz, LRL (radiochemical analysis);
R. W. Terhune, LRL (cratering computations);

REFERENCES

1. A. E. Lewis and L. D. Ramspott, Trans. Am. Geophys. Union, 50, 155 (1969).
2. M. D. Nordyke and M. M. Williamson, "Project Sedan," PNE-242F, Lawrence Radiation Laboratory, Livermore, 1965.
3. M. D. Nordyke and W. Wray, "Cratering and Radioactivity Results from a Nuclear Cratering Detonation in Basalt," UCRL-6999, Rev. II, Lawrence Radiation Laboratory, Livermore, 1963.
4. J. Toman, "Summary of Results of Cratering Experiments," UCRL-71456, Lawrence Radiation Laboratory, Livermore, 1969.
5. J. Toman, Nucl. Appl. Tech. 7, 243 (1969).
6. J. T. Cherry, Intern. J. Rock Mech. Min. Sci. 4, 1 (1967).
7. J. B. Knox, "Prediction of Fallout from Subsurface Nuclear Detonations," 5th U. S. AEC Symp. Radioactive Fallout from Nuclear Weapons Tests, 1965, pp. 331-353.
8. J. A. Miskel, "Project Sedan: Radiochemical Studies," PNE-231, Lawrence Radiation Laboratory, Livermore, 1967.
9. J. J. Cohen, T. V. Crawford, and R. F. Rohrer, private communication.
10. R. W. Taylor, ed., "Plowshare Program Quarterly Report of the Chemistry Department, January through March 1969," UCRL-50015-69-1, Lawrence Radiation Laboratory, Livermore, 1969.
11. T. V. Crawford, "Diffusion and Deposition of the Schooner Clouds," to be published.
12. N. A. Bonner and J. A. Miskel, Science, 150, 489 (1965).
13. T. V. Crawford, "A Computer Program for Calculating the Atmospheric Dispersion of Large Clouds," UCRL-50179, Lawrence Radiation Laboratory, Livermore, 1966.
14. L. R. Anspaugh et al., "Bio-Medical Preliminary Report for Project Schooner," UCRL-50718, Lawrence Radiation Laboratory, Livermore, 1969.
15. "Preliminary Report of Off-Site Surveillance for Project Schooner," Southwestern Radiological Health Laboratory, Department of Health, Education, and Welfare, Public Health Service, Bureau of Radiological Health, January 1969.
16. R. W. Henny, "Schooner Ejecta Studies," to be published.

XA04N0756

NUCLEAR CRATERING ON A DIGITAL COMPUTER*

R. W. Terhune, T. F. Stubbs, and J. T. Cherry
Lawrence Radiation Laboratory, University of California
Livermore, California 94550

ABSTRACT

Computer programs based on the artificial viscosity method are applied to developing an understanding of the physics of cratering, with emphasis on cratering by nuclear explosives. Two established codes, SOC (spherical symmetry) and TENSOR (cylindrical symmetry), are used to illustrate the effects of variations in the material properties of various media on the cratering processes, namely shock, spall, and gas acceleration. Water content is found to be the most important material property, followed by strength, porosity, and compressibility.

Crater profile calculations are presented for Pre-Gondola Charley (20-ton nitromethane detonation in shale) and Sedan (100-kt nuclear detonation in alluvium). Calculations also are presented for three 1-Mt yields in saturated Divide basalt and 1-Mt yield in dry Buckboard basalt, to show crater geometry as a function of the burial depth for large explosive yields.

The calculations show, for megaton-level yields, that gas acceleration is the dominate mechanism in determining crater size and depends in turn on the water content in the medium.

INTRODUCTION

During the past decade, the concept of nuclear excavation has led to various engineering proposals, whose designs require a reliable procedure for determining the optimal explosive yields and depths of burial. The development of a reliable procedure requires, at least,

- An adequate understanding of the mechanisms of cratering with respect to variations in medium properties, yield, and depth of burial
- A means of correlating and extending the field experience.

Cratering with nuclear explosives is essentially a wave propagation phenomenon. Computer programs based on the artificial viscosity method of calculating shock wave propagation have had excellent success [Maechen and Sack (1963),[1] Cherry and Hurdlow (1966),[2] Wilkins (1969)[3]]. The first requirement for these calculations is a model of material behavior.

Cherry (1967)[4] developed a mathematical model for rock materials behavior and a corresponding measurement program, the results of which

---

*Work performed under the auspices of the U. S. Atomic Energy Commission.

were included in the codes SOC (spherical symmetry) and TENSOR (cylindrical symmetry). The key to his success in calculating Scooter (0.5 kt HE in alluvium) and Danny Boy (0.42 kt NE in basalt) was recognizing that separate descriptions were required of the material properties before and after failure. Since 1966, many equation-of-state measurements have been made on various types of rocks. The calculational model has been improved. This paper does not discuss in detail the calculation model (reports on the SOC and TENSOR codes are now being prepared) but does apply the codes to illustrate the "state of the art": that is, our present understanding of cratering phenomena.

MECHANICS OF CRATERING

In all wave propagation problems, the boundary conditions determine the nature of the solution. In cratering, the principal boundaries are (1) the cavity formed by the explosion and (2) the ground surface. Both of these boundaries are free. The stress wave interaction on these boundaries divides the process of crater formation into four observable, sequential phases: shock (compressive wave from cavity to ground surface), spall (rarefaction wave from ground surface to cavity), gas acceleration (recompaction wave toward ground surface), and ballistic trajectory (free fall).

Shock—The shock wave is a large stress discontinuity created when the restrained internal energy of a nuclear device is released. As the shock wave propagates in the medium, it compresses the rock, distributing internal and kinetic energy as it moves outward. The energy of the wave decays with distance from the source, and the state of rock changes in proportion to the energy deposited. Immediately around the source the rock is vaporized. This is followed by a region of melt. Crushed and fractured rock extends outward a considerable distance beyond the region of melt. The shock wave develops the conditions for formation of a large cavity around the source and imparts a momentum to the rock through which it travels.

Spall—A rarefaction wave is reflected when the shock wave reaches the free (ground) surface, relieving pressure in the rock as it travels back toward the cavity. Tension is developed in the rock, causing it to separate from the formation at a velocity characteristic of the momentum trapped in the rock. This increase in momentum establishes the conditions in the mound necessary for development of the gas acceleration phase. It also establishes the limits of the true crater above the shot point.

Gas Acceleration—Because rarefaction has relieved the pressures in the rock above the cavity (which still contains several hundred atmospheres of pressure), the resulting pressure differential accelerates the growth of the upper part of the cavity. Growth of the cavity may ultimately recompact the rarefied rock above it and additionally increase its momentum. The cavity expands rapidly toward the initial ground surface, forming the large observable mounds. Unrestrained spherical divergence of the mound leads to its disintegration, the horizontal component of velocity tending to drive the sides of the mound away from the crater area.

Ballistic Trajectory (Free Fall)—On general mound disintegration, the final cavity pressure (1 or 2 atm) is vented. The forces of gravitation and friction alone now affect each particle, which is on its own ballistic trajectory. The depth of the crater depends on the amount of fallback material and its bulking characteristics.

Figure 1 shows the effect of each mechanism on the particle velocity as a general function of time. The relative effect of each mechanism on the total mound velocity field depends on the material properties and defines

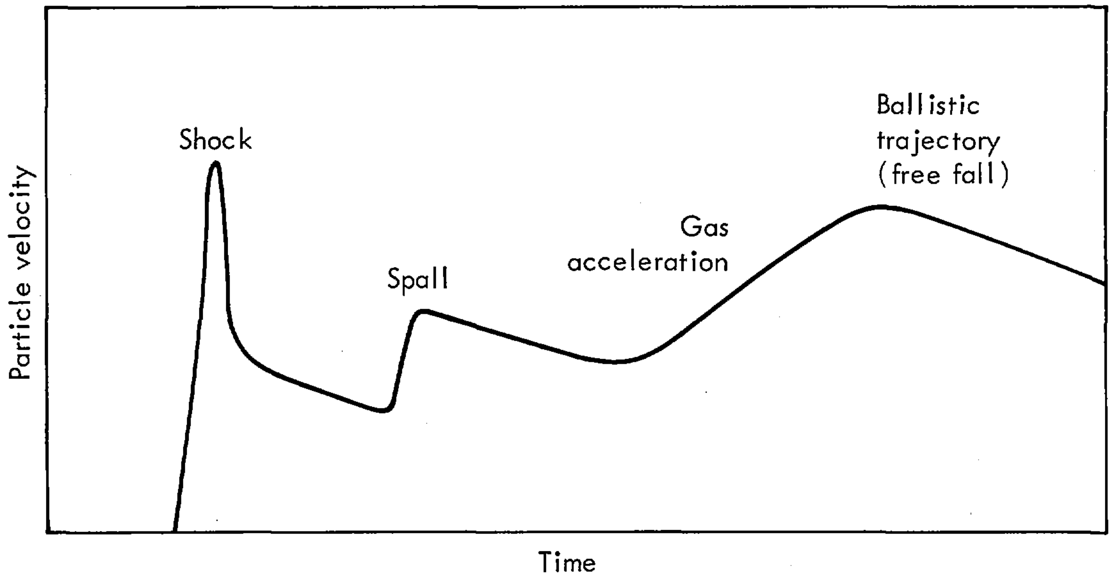

Fig. 1. Cratering mechanisms.

the cratering characteristics of a medium. The mound velocity field at the end of the gas acceleration phase determines the crater geometry.

THE CALCULATIONAL MODEL

For predicting crater geometry without merely scaling from past explosions, a numerical technique has been developed which integrates the conservation laws of mass momentum and energy on a digital computer. This numerical technique replaces the continuous spatial distribution of stress, density, velocity, etc., with a set defined at discreet positions (zones) in the medium.

At any given time the stress, density, coordinates, and particle velocity of each zone is known. The conservation of momentum equation in differenced form provides a functional relationship between the applied stress field and the resulting acceleration of each point in the grid. Accelerations produce new velocities when allowed to act over a small time increment, Δt; velocities produce displacements, displacements produce strains, and strains produce a new stress field. Time is incremented by Δt, and the cycle is repeated.

The calculations are simplified when a degree of symmetry is specified. The SOC code integrates the conservation equations written in spherical symmetry (there is only a radial direction of motion permitted), while the TENSOR code allows study of cylindrically symmetric problems (such as craters) where two spatial variables must be considered.

The manner in which the strain is related to stress is called the equation-of-state of the material. This equation-of-state must describe the various modes of material behavior (gas, fluid, solid) and allow for acceptable transitions among the modes. It must be determinable before the shot. Preshot logging and core tests have been used to satisfy this last requirement.

The preshot logging measurements are extremely important in determining the average properties of the entire rock structure and the layers of impedance mismatch. These logs also are needed for proper selection of the core samples and verification that the tests are representative of the site.

MATERIAL CHARACTERISTICS IMPORTANT IN CRATERING

The equation-of-state (EOS) defines the cratering efficiency of a medium; that is, the equation-of-state specifies the amount of internal energy of the explosive which will be converted into kinetic energy in the mound above the explosive by shock, spall, and gas acceleration.

We have found the following four equation-of-state parameters important in determining cratering efficiency:

- Compressibility
- Porosity (compactability)
- Water content
- Strength.

The first three relate to the hydrostatic loading and unloading characteristics of the medium. The fourth limits the permissible deviatoric stress in the rock.

Figure 2 compares the hydrostatic compressibility of the various types of rock listed in Table I. The difference between hydrostatic loading and unloading in these types of rock is a measure of their nonrecoverable porosity.

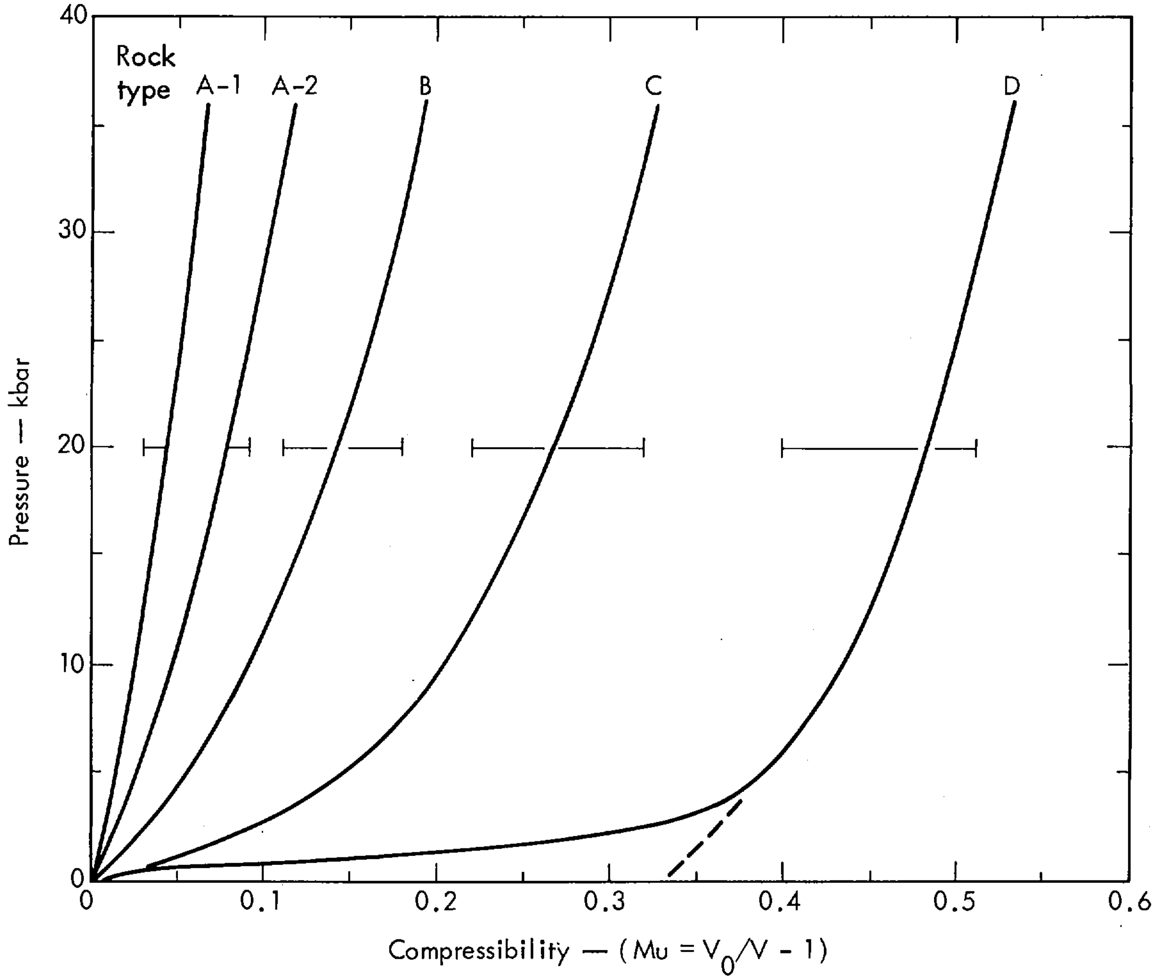

Fig. 2. Pressure-volume relationship for various rock types.

Table I. Significant parameters of various rock types.

Rock type	Rock and experiment	Density	Sound speed—ft/sec	Bulk modulus—kbar	Ref.
A-1	Canal basalt	2.65	18,000	388	7
	Cabriolet (deep layer)	2.53	13,012	394	5
	Hardhat	2.65	18,000	552-333	5
	Buggy basalt (type 1)	2.60	9,000	480	6
	Buckboard basalt (type 1)	2.6	7,200	236	5
	Pre-Schooner VIT (type 2)	2.3	8,000	256	5
A-2	Palanquin type 1	2.5	7,961	149	5
	Palanquin type 2	2.4	5,000	116	5
	Cabriolet type 2	2.3	5,000	97	5
	Faultless tuff	2.283	11,500	160	6
B	Bear Paw (Fort Peck) shale	2.2	6,000	50.5	6
	Buggy basalt (type 3)	2.38	5,000	77	6
	Greeley tuff	2.0	10,150	47.5	6
	Gas Bug sandstone	2.48	13,500	100	6
C	Cabriolet (type 3)	1.98	3,600	13.5	5
	Palanquin (type 3)	2.0	2,975	19.4	5
D	Buggy basalt (type 5)	1.94	3,600	18	6
	Alluvium	1.5	3,000	18	5
	Scroll	1.4	4,200	19-28	6

Table I gives the density, bulk modulus, and sound speed for the various rock types in their respective groupings.

Figure 3 shows the wide range of shear strengths versus pressure found among various rock samples in three general states: solid, fractured, and wet. Strength does not correlate as much with rock type (A-1, A-2, etc.) as it does with the state of the rock. The curves in this figure indicate a general trend in strength behavior; however, there are many exceptions to this idealized picture.[8]

The effect of material properties on the cratering mechanism can be illustrated readily by a parameter study on SOC.

Compressibility and Porosity

Figure 4 is a plot of the peak shock stress versus distance as calculated by SOC, illustrating the effect of compressibility on porosity on shock wave attenuation. It can be seen that peak pressures are attenuated more rapidly for the more compressible rock. If additionally the rock is compactible (porous), peak pressures are further attenuated. Figure 5 is the particle velocity corresponding with Fig. 4 at a specific time. (For the corresponding equation-of-state, see Fig. 2.) The peak particle velocity of the shock front is proportional to the shock stress and thus is controlled by the stress attenuation. It is interesting to note that the velocity field in the mound behind the shock varies slightly with compressibility and porosity.

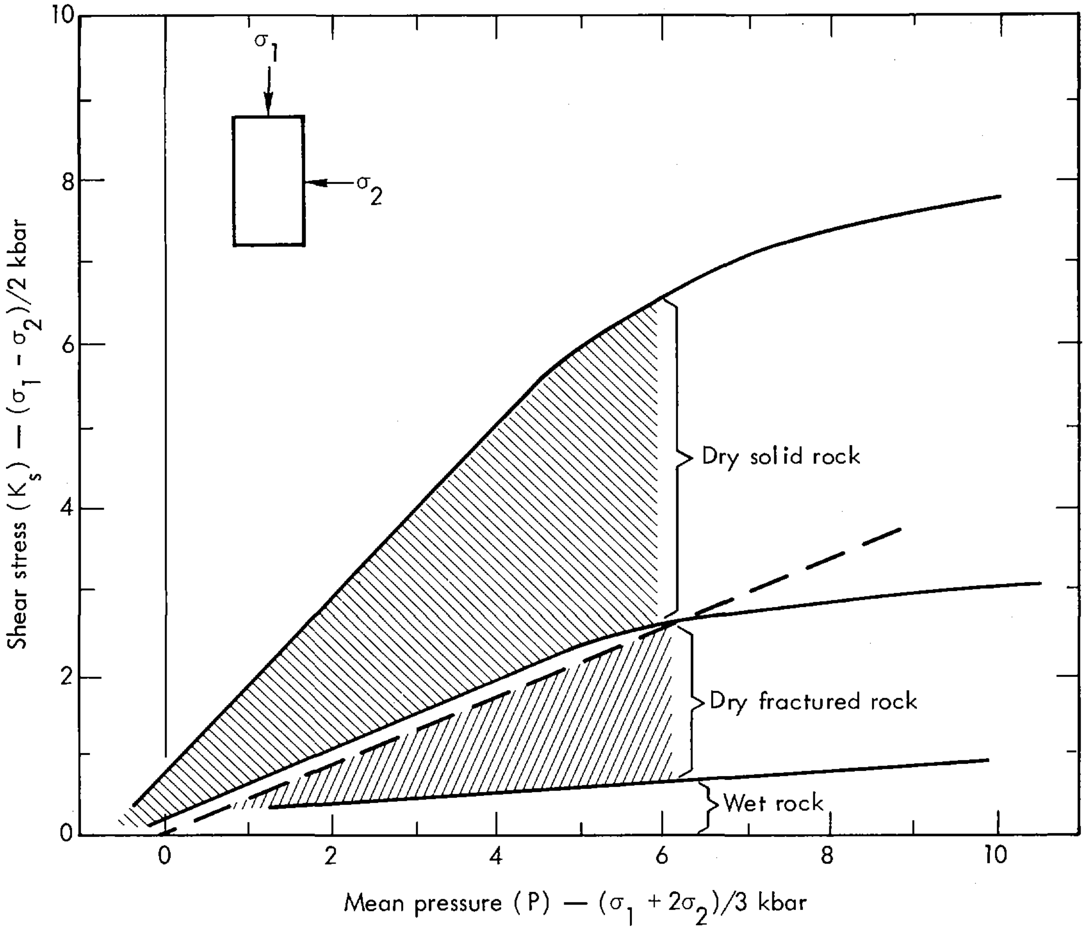

Fig. 3. Shear strength trends as a function of mean stress.

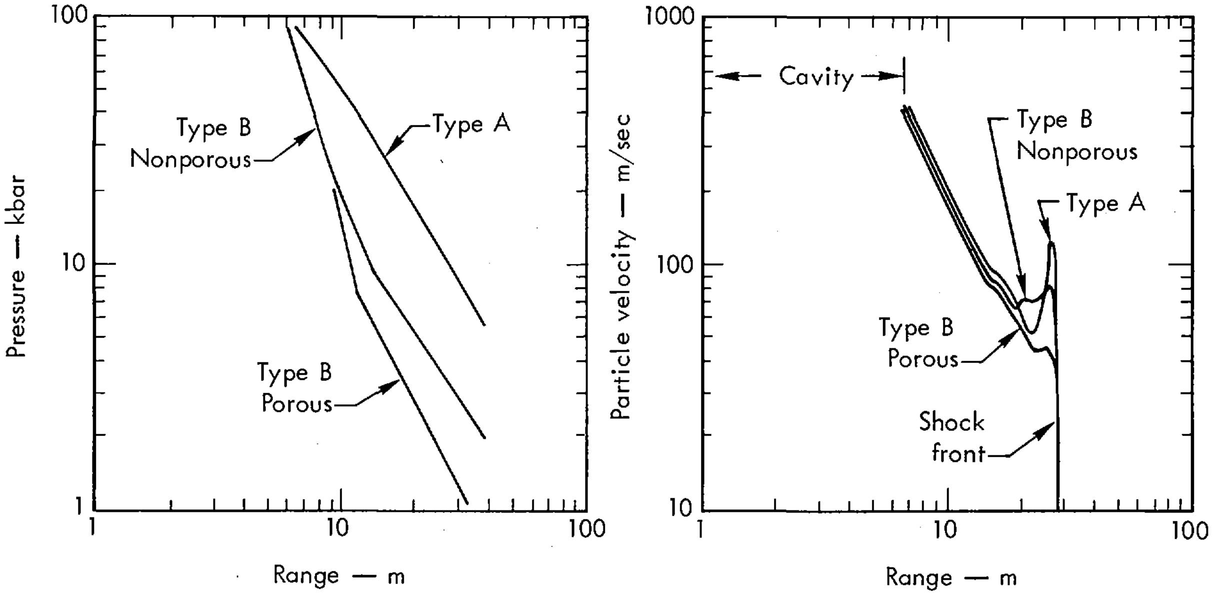

Fig. 4. Shock attenuation as a function of compressibility and porosity.

Fig. 5. Particle velocity as a function of compressibility and porosity.

Strength

The behavior of the shock wave due to shear stress variations is not a simple function of the shear strength but depends on the entire equation-of-state. Naturally, the higher the shear stresses allowed to develop, the more severe the attenuation.

An interesting parameter study is the effect of the fractured strength of the rock on the particle velocity of the entire mound. Figure 6 shows the decay of particle velocity behind the shock wave as the fractured strength is increased from 0-0.5 kbar to 5.0 kbar. The fractured rock strength is one of the primary equation-of-state parameters determining the cratering efficiency of the rock.

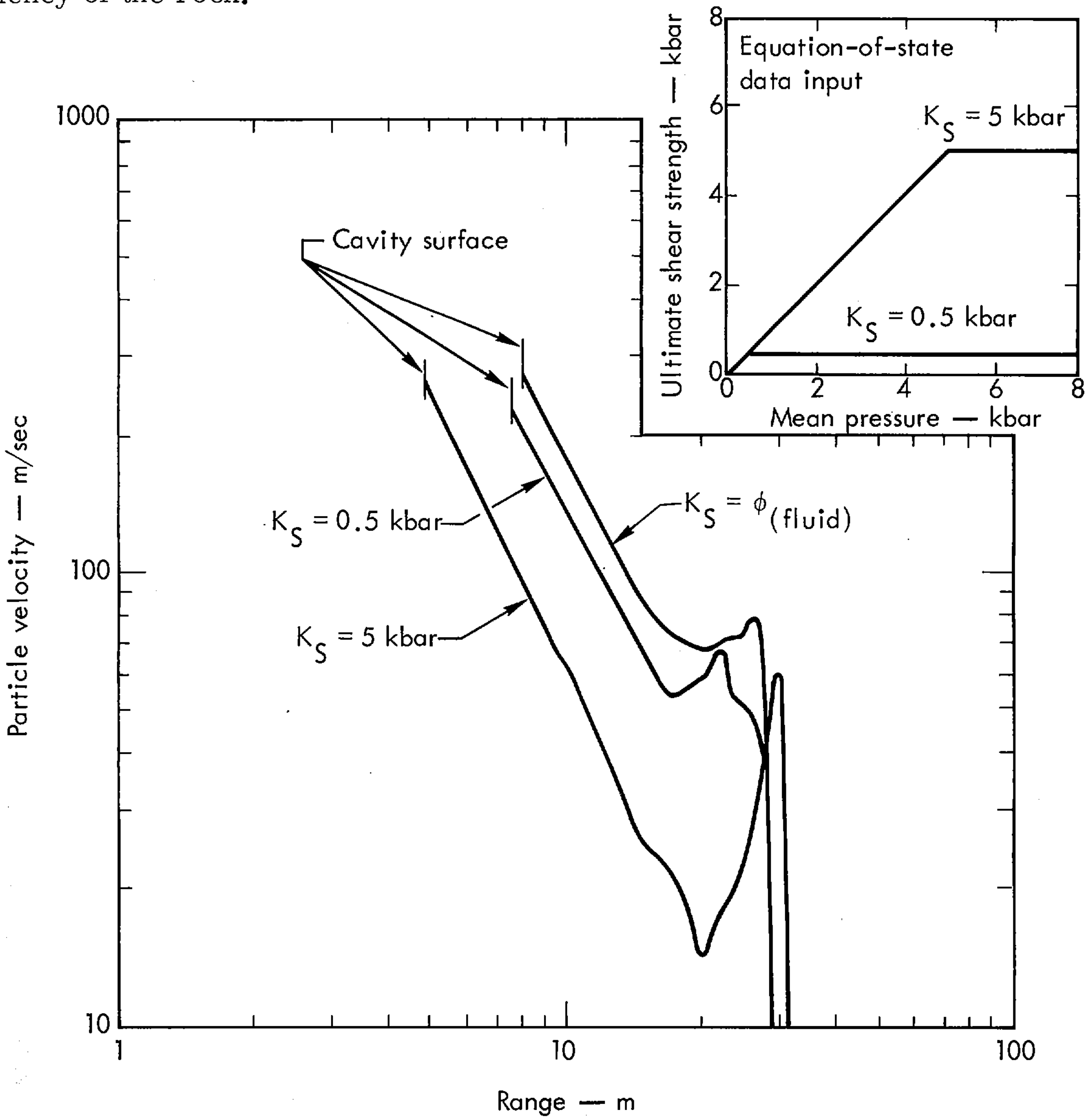

Fig. 6. Particle velocity as a function of shear strength.

A recent study in saturated quartz rock illustrates the sensitivity of the rock strength on the cratering efficiency, for burst depths greater than optimum. Strength data from the core tests indicates two distinct strength behavior characteristics,[9] as shown at the top of Fig. 7. To assess the effect of strength variations on the mound velocity field, two SOC calculations were made at 175 kt, using strength curves A and B. The yield was increased to 225 kt and a new calculation run with curve A. Figure 7 (lower) shows

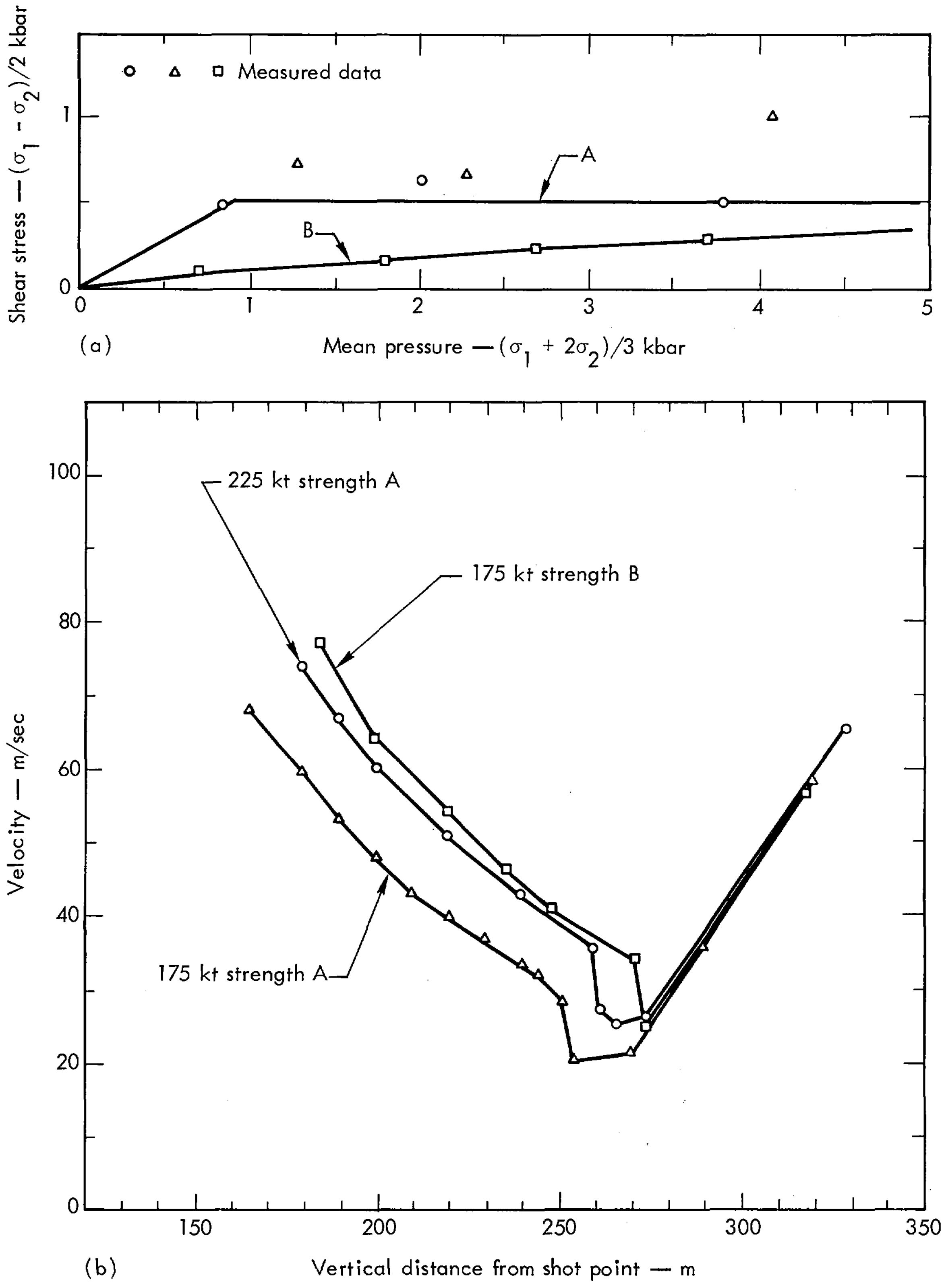

Fig. 7. Particle velocity as a function of shear strength and yield in saturated quartz.

that the reduction in strength results in the same mound velocity as a 25% increase in yield at the higher strength.

At optimum depth of burst or shallower depths, such a variation in strength is of little consequence in determining the crater radius; but for greater depths, strength variations play a dominate role in determining the crater size.

Water Content

Static tests have demonstrated that the presence of free water within a rock significantly reduces both its nonrecoverable porosity and the ultimate shear strength of the sample (Fig. 3). As indicated earlier, reducing either of these parameters leads to an increase in the cratering efficiency of the medium. Also, vaporization of free water in the rock by the shock wave, outside the initial radius of rock vaporization, creates a larger source region of which a significant fraction is noncondensable water vapor.

The effect of the larger source region, maintaining higher pressures than dry rock, is about a 10% increase in spall velocities. More significantly, this provides a strong, long lasting, gas acceleration phase.

Because there is a lack of experimental data on the release paths of a rock-water system, a simple approximation is made in the calculational model to simulate this effect.

Bjork et al.[10] developed an equation-of-state of water which gives the isentrope release paths from various shock states on the Hugoniot. The slopes of the isentrope, in general, vary from 1 to 2 in the log P-log V plane for pressures exceeding 150 kbar. The calculational model approximates this behavior for a rock water system using

$$P = P_H + \frac{\Gamma}{V}(E - E_H)$$

where

P is the pressure
E is the energy
V is the specific volume
Γ is the Grüneisen gamma

and subscript H refers to the Hugoniot values at a given specific volume. We further assume that

$\Gamma = 1$ $\quad P > 400$ kbar
$\phi < \Gamma < 1$ $\quad 400 \text{ kbar} > P > 100$ kbar
$\Gamma = \phi$ $\quad P < 100$ kbar.

Calculations using the Grüneisen gamma approximation behave in a manner similar to calculations with nitromethane. Nitromethane has a Chapman-Jouquet pressure of 143 kbar, and the cavity radius scales as 5.5 $\text{m/(kt)}^{1/3}$. For a nuclear shot in a dense medium, the radius at which the shock stress falls below 150 kbar scales as approximately 5.1 $\text{m/(kt)}^{1/3}$.

Cratering Efficiency

We have defined the cratering efficiency of the medium in terms of the kinetic energy developed in the mound by the explosive. The efficiency is determined in turn by the equation-of-state of the rock. To illustrate these relationships, mound velocity profiles were calculated on SOC for three media in which there is cratering experience. The first medium was

Bear Paw shale from the Fort Peck reservoir: saturated, nonporous, and extremely weak. The second was Sedan alluvium: very porous, moderately weak, and wet (10% water at the depth of the calculation). The third was NTS Buckboard basalt: dry, porous, and moderately strong.

Figure 8 shows the velocity profiles between cavity and free surface for the three media. These calculations were for a 1-kt nuclear yield at a depth of 40 m. The plots were taken at the moment the rarefaction wave arrives at the cavity, which varies because of differences in the compressional wave velocity for the medium. Figure 9 shows empirical, scaled

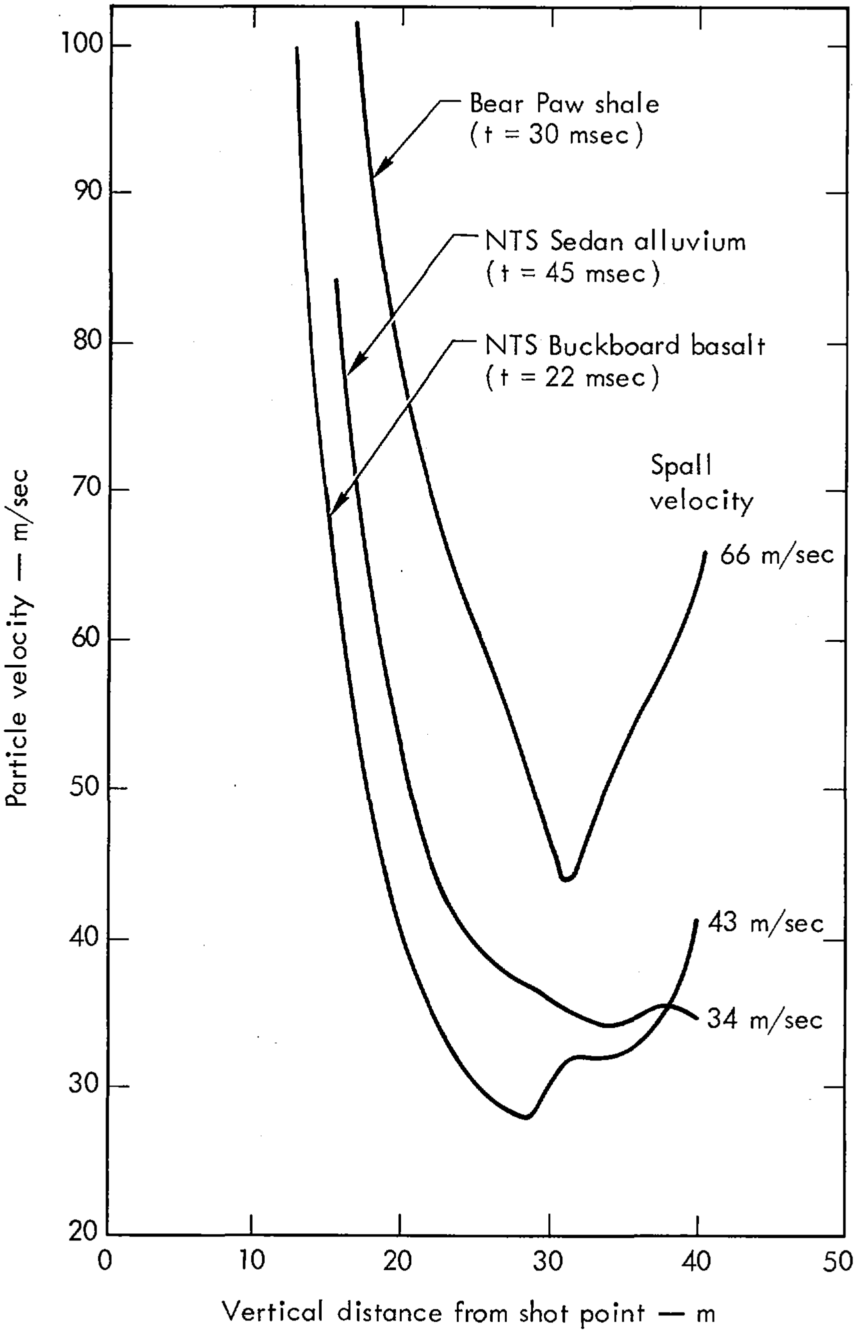

Fig. 8. Mound velocity field for three cratering media where t = time of arrival of rarefaction wave at cavity surface.

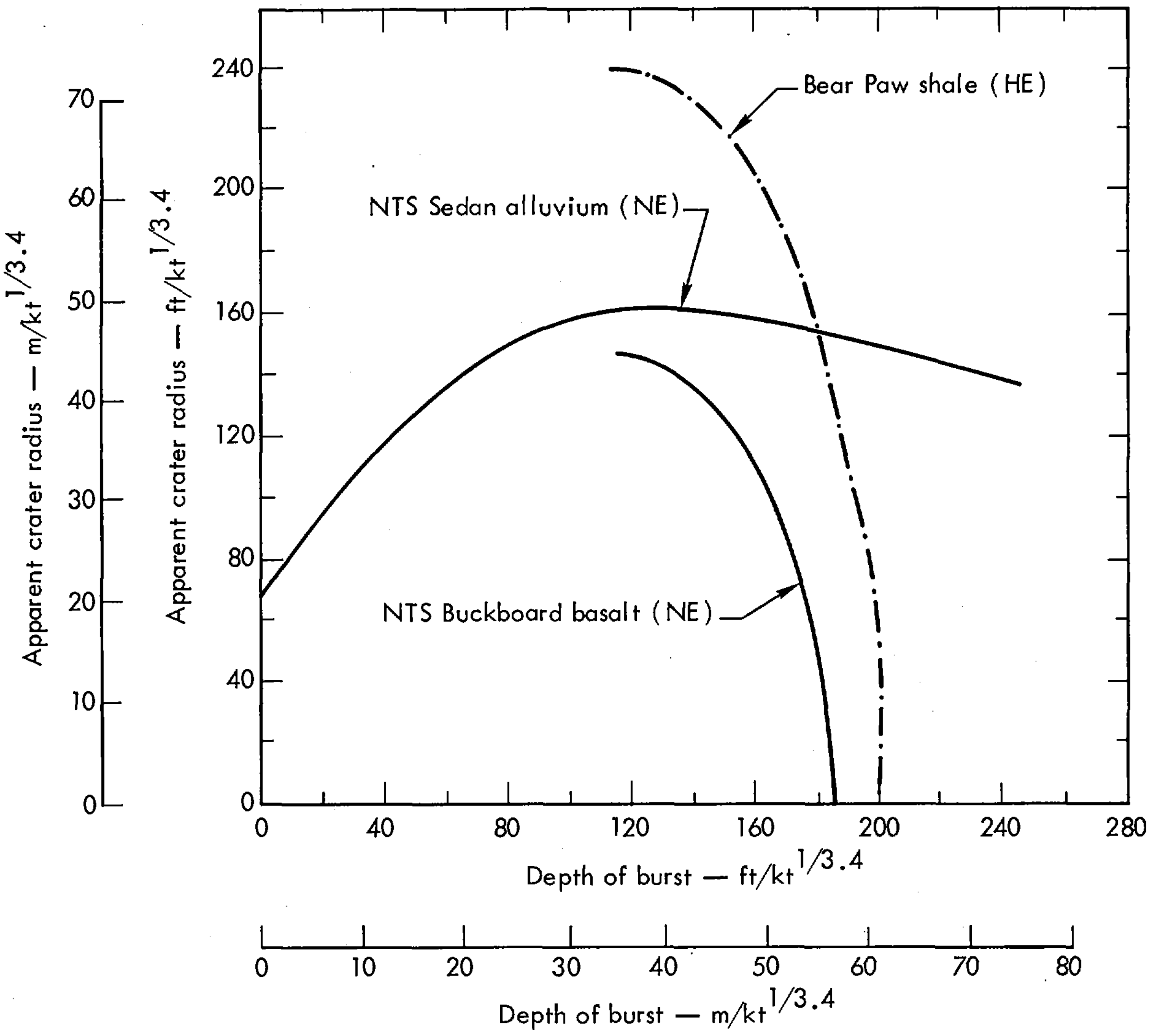

Fig. 9. Scaled crater radius curves.

cratering curves for the three media. Comparing the velocity curves with the cratering curves shows a definite correlation between the velocity field behind the spalled region and the crater radius.

In summary on this section: compressibility and porosity of the rock are the dominant factors in determining the energy delivered to a point in that medium. But the shear stress and length of time the stress operates primarily determine the velocity field behind the shock or the spalled region. The final velocity field through the mound then depends on the effectiveness of the gas acceleration phase.

If the material properties were listed in order of importance for determining the cratering efficiency of the medium, the list should be:

1. Water content
2. Shear strength
3. Porosity
4. Compressibility.

The water content is of primary importance because it decreases the rock compressibility and porosity and drastically reduces its shear strength. Water content also provides an additional energy source in expansion of the noncondensable water vapor. All of the above factors increase the velocity field of the mound and therefore the cratering efficiency of the medium.

CRATERING CALCULATIONS

Once the site, yield, and approximate depth of burial of a proposed cratering experiment are determined, the hole is drilled, and in situ velocity and density logs are run. From the density, compression, and shear velocity logs, core samples are selected for high pressure testing, mineralogy, porosity, and water content measurements. High pressure testing consists of (1) hydrostatic compressibility measurements, both loading and unloading, up to 40 kbar, (2) Hugoniot (150-700 kbar) data, and Hugoniot elastic limit if measurable, and (3) shear strength for confining pressures up to 10 kbar.

A best fit for Poisson's ratio is determined from the in situ logging data and the initial bulk modulus as determined from the hydrostatic compressibility measurements.

With the completion of the equation-of-state, a SOC calculation is made to determine the radius of vaporization, develop the gas tables for the vaporized rock, and check the EOS for errors. A TENSOR grid is established whereby the energy of the device is distributed uniformly throughout the cavity. The problem is monitored until the shock, spall and gas acceleration phases are completed and/or large pressure or velocity gradients are no longer present in the mound. At this time, a free fall throwout calculation is performed. The throwout calculation consists of removing from the grid and stacking on the ground surface those zones which are calculated to have sufficient velocity to clear the free surface. The ballistic trajectory of these zones determines their final position on the surface. Mass is conserved during the entire calculation.

The crater radius is determined by the location of the ejecta as calculated by the throwout code. Determination of the crater depth, however, is not direct calculation. The lower hemisphere of the cavity never reaches equilibrium in the TENSOR calculations. Also, overburden is neglected in the TENSOR code. The final position of the lower hemisphere of the cavity is determined by an averaging process involving spherical calculations with SOC (which considers overburden) and the existing velocity and pressure field around the cavity in TENSOR at the time of the throwout calculation.

In all calculations carried past 2 sec, the pressure gradient outside the lower cavity surface has reversed the velocity field of the material around the lower hemisphere.

This series of cratering calculations has resulted from a feasibility study on the proposal for a nuclear isthmus canal. The canal rock is saturated; unfortunately, cratering experiments in saturated media are limited to chemical explosives. The Pre-Gondola series (20 tons of nitromethane at various burst depths) provides a test of the codes in saturated media, with material properties at low pressures. Sedan, a 100-kt nuclear burst in alluvium with 10-20% water content, provides a test of the vaporized water expansion approximation.

Pre-Gondola Shale

The compressibility curve for Pre-Gondola shale is the type B curve in Fig. 2. The phase change of water reported by Stephens[6] at 10 kbar and 22 kbar has been smoothed out. The unconfined shear strength tests varied considerably but were consistent with 11 bars of residual strength after

2-3% strain. Figure 10 is a plot of the yield surface used in the calculation to represent this type of behavior (Bear Paw shale). Figure 11 compares

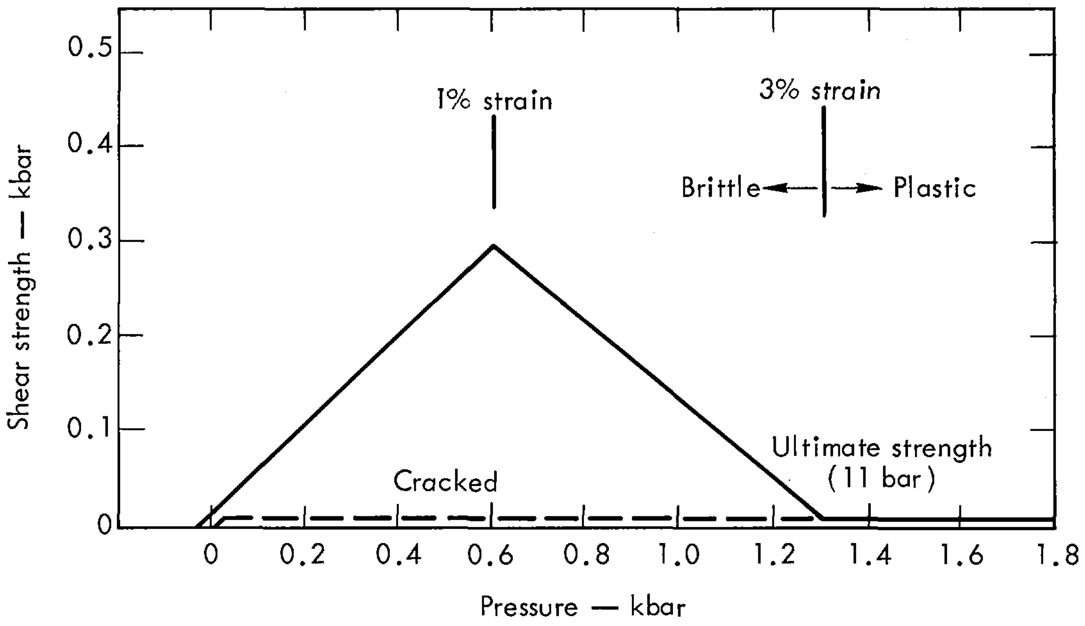

Fig. 10. Shear strength for Bear Paw shale at Fort Peck reservoir.

the measured radial stress at three gages with the SOC calculation for Pre-Gondola Bravo.[11] Figure 12 plots peak radial stress and velocity for Bear Paw shale, comparing measurements with the SOC calculation.

Figures 13 and 14 deal with Pre-Gondola Charley, one of a series of nitromethane cratering shots conducted by the U. S. Army Engineers Nuclear Cratering Group at LRL to determine the cratering curve for Bear Paw shale. Pre-Gondola Charley was a 20-ton burst at 42.5 ft. Figure 13 shows the peak velocity at various points on the mound surface as measured and calculated by TENSOR. Figure 14 is the resulting crater, with throwout calculation.

Agreement among the stress wave form and peak particle velocity measurements is excellent. The surface velocities calculated by TENSOR also agree well with the surface motion measurements at various distances from ground zero.

The throwout calculation at 107 msec yielded a slightly larger crater than measured, with very little fallback. This is not surprising in that the material in the mound around the cavity was compressed at 107 msec, and expansion of the rock to its original density or bulking was not taken into account.

Sedan

Sedan was a 100-kt nuclear cratering event buried at 635 ft in fairly competent alluvium. The water content at the Sedan site varies from about 10% in the first 30 m to about 20% at a depth of 300 m.[12]

Compressibility curve type D (Fig. 2) was used for the calculation. The ultimate shear strength had to be estimated (Fig. 15), as no experimental shear strength data exists. The material was assumed to behave ductilely above 0.4 kbar and a constant Poisson's ratio of 0.33 was used.

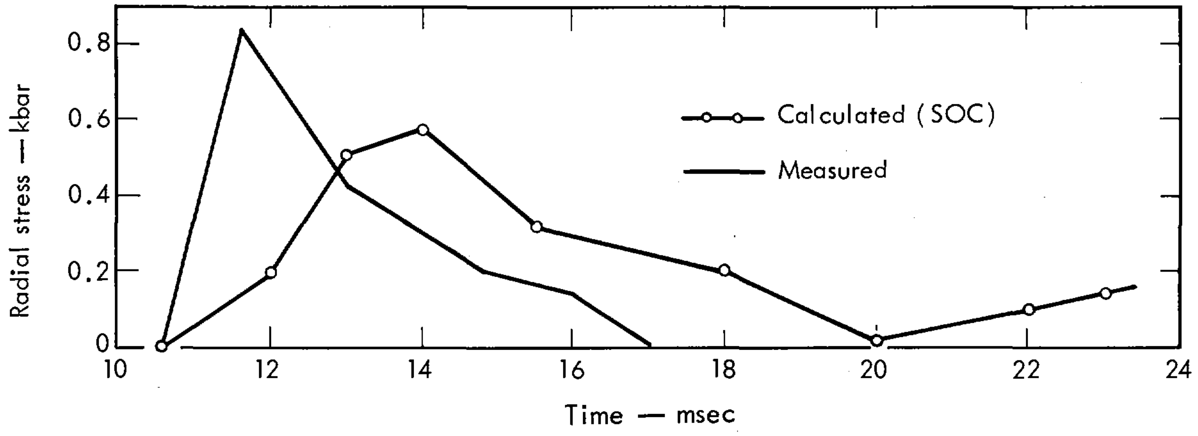

(a) Gage 2-o-2 (85-ft range)

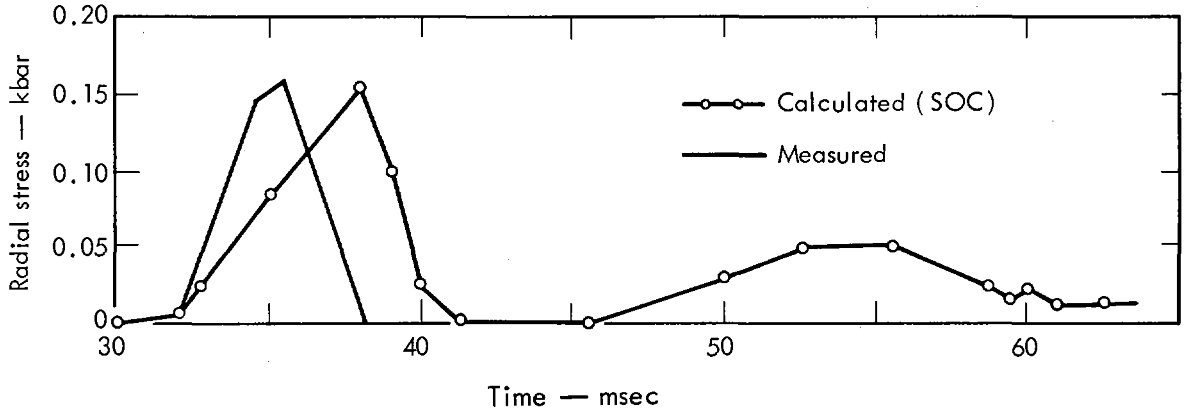

(b) Gage 22-o-9 (225-ft range)

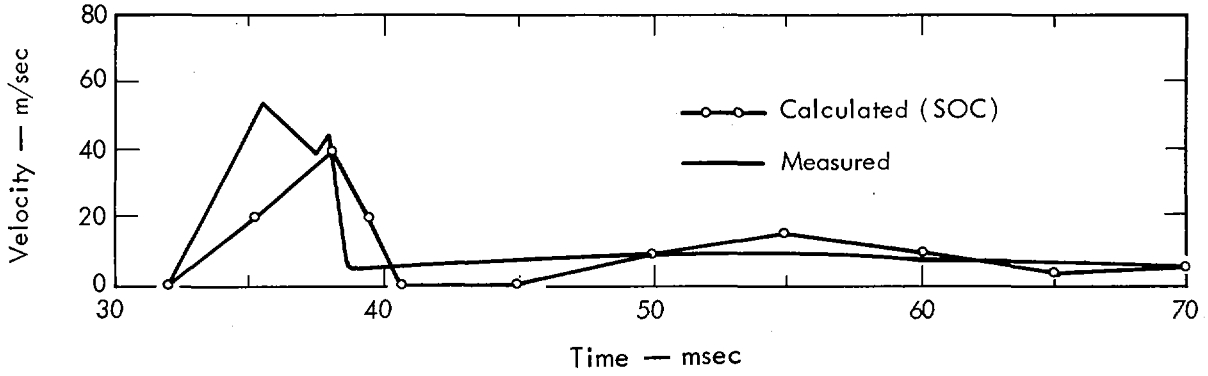

(c) Gage 23-u-5 (225-ft range)

Fig. 11. Measured and calculated stress history for Pre-Gondola Bravo.

The density varied at the site with depth from 1.6 g/cc to 1.8 g/cc, with corresponding sound velocities of 3000 ft/sec to 5000 ft/sec. For the calculation, a density of 1.7 g/cm^3 and compressional velocity of 4000 ft/sec were used.

Figure 16 compares the measured surface velocity for Sedan near ground zero with the velocity as calculated by TENSOR. The calculation of the spall velocity proved slightly high and the arrival of the recompaction front was later than calculated, but the calculation-measurement agreement of peak velocity at the end of the gas acceleration phase was excellent.

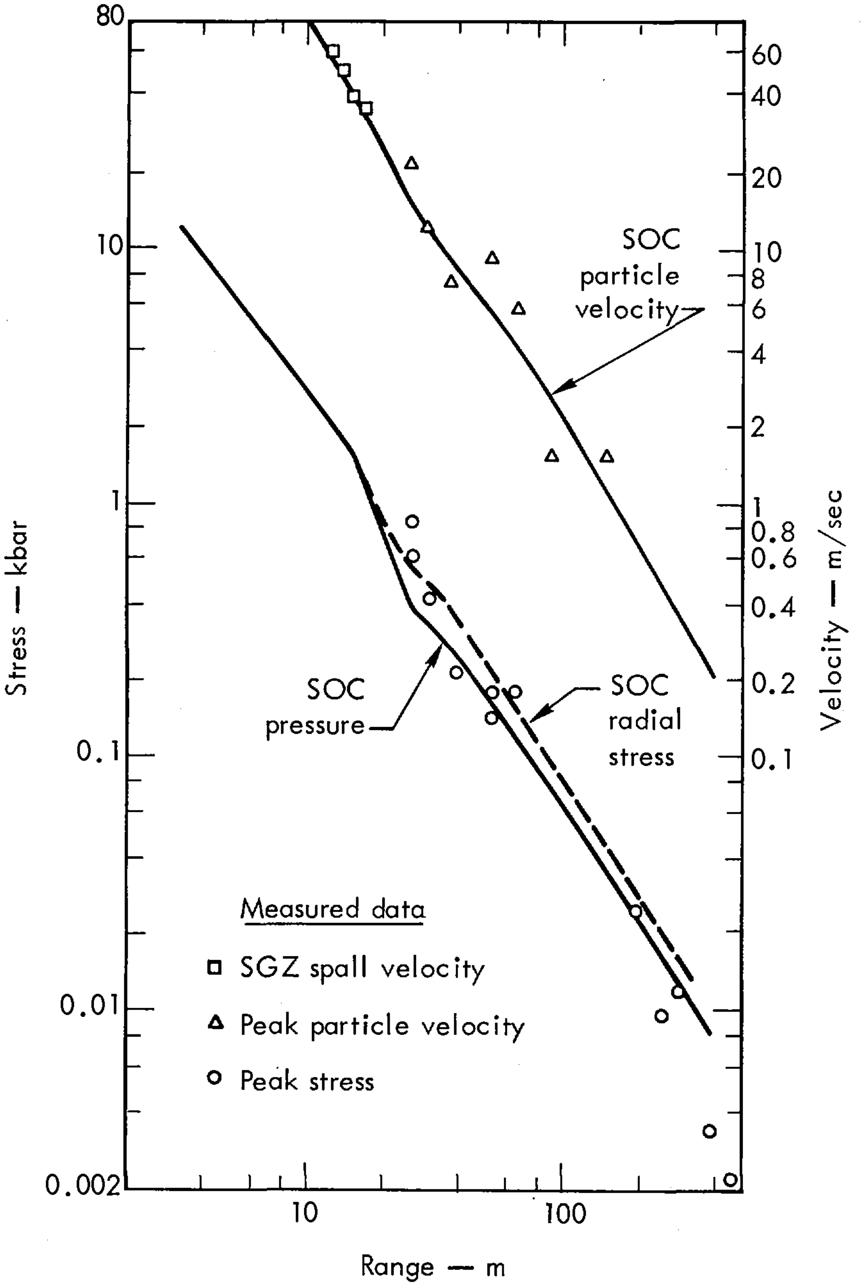

Fig. 12. Peak stress and particle velocity versus range, Pre-Gondola Bravo.

Figure 17 shows the Sedan crater profiled from the throwout calculation, which agrees well with the observed crater profile. Calculation of the cavity rebound agrees fairly well with the measured lower hemisphere of the cavity. Ejecta that did not clear the crater filled this volume for the correct depth.

The results of this calculation suggest that approximations made on the expansion behavior of water vapor are within reason and compatible with our experience and knowledge to date.

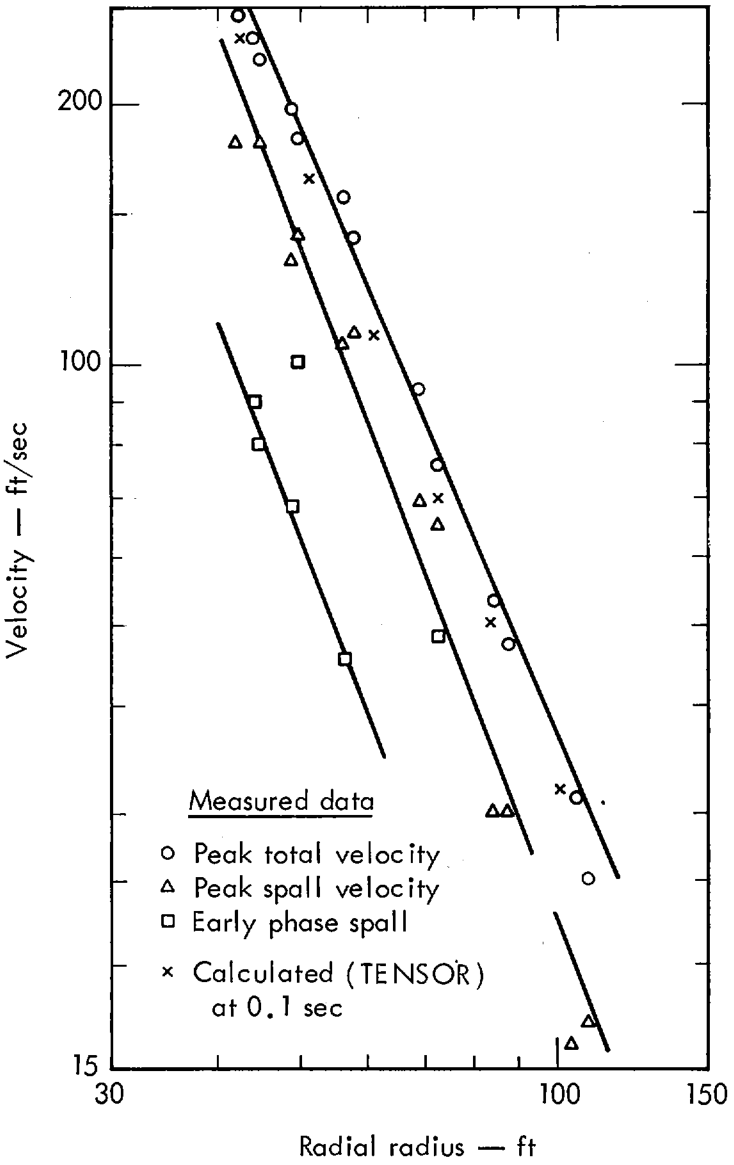

Fig. 13. Surface velocities versus radial range, Pre-Gondola Charley.

Buckboard Basalt

The Basalt type chosen for calculation was characteristic of the Danny Boy site on Buckboard Mesa NTS. The site is moderately fractured, with open fractures randomly oriented at a frequency of 5-10 ft. The density is 2.62 g/cm^3 with a compressional wave velocity of 7200 ft/sec. Figure 18 is the assumed strength curve, and Fig. 19 shows compressibility curve loading and unloading as measured by Stephens et al.[5] Strength measurements were not available. A constant Poisson's ratio of 0.33 was used.

Data on the Danny Boy Event (0.42 kt NE at a depth of 33 m), previously published by Cherry (1967),[4] were recalculated to check changes in the TENSOR code.

Figure 20 shows the crater as calculated, in excellent agreement with the experimental result.

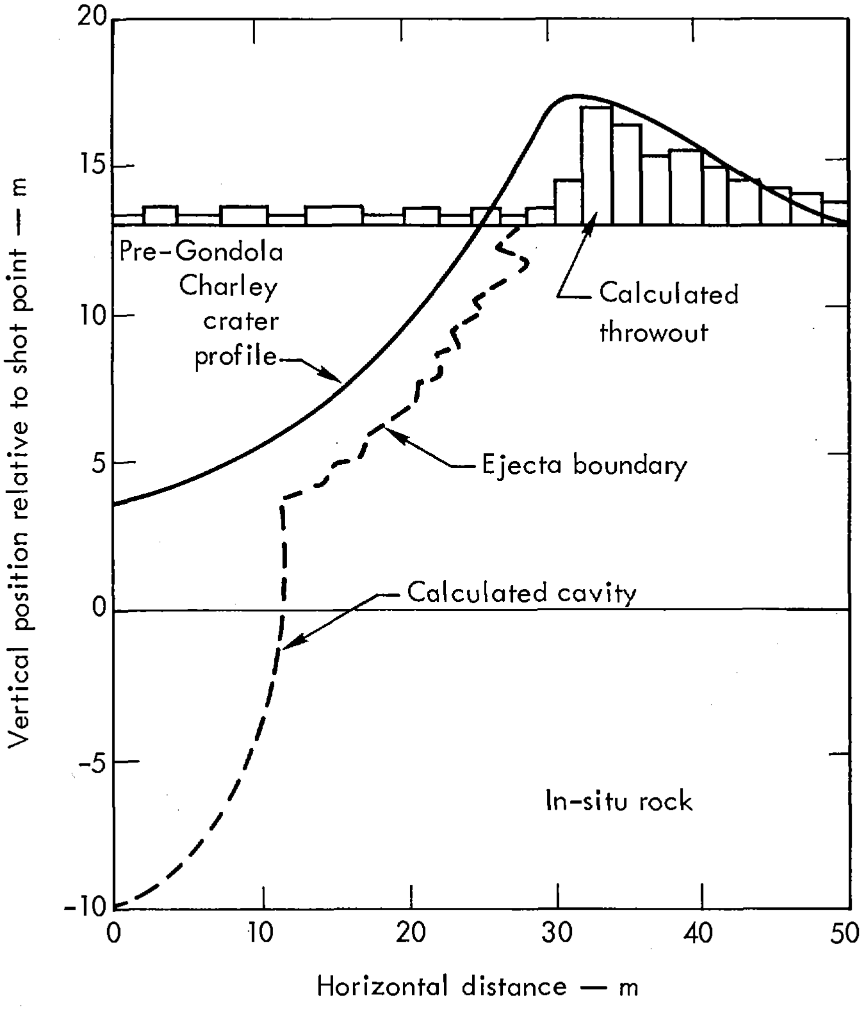

Fig. 14. Calculated crater profile for Pre-Gondola Charley.

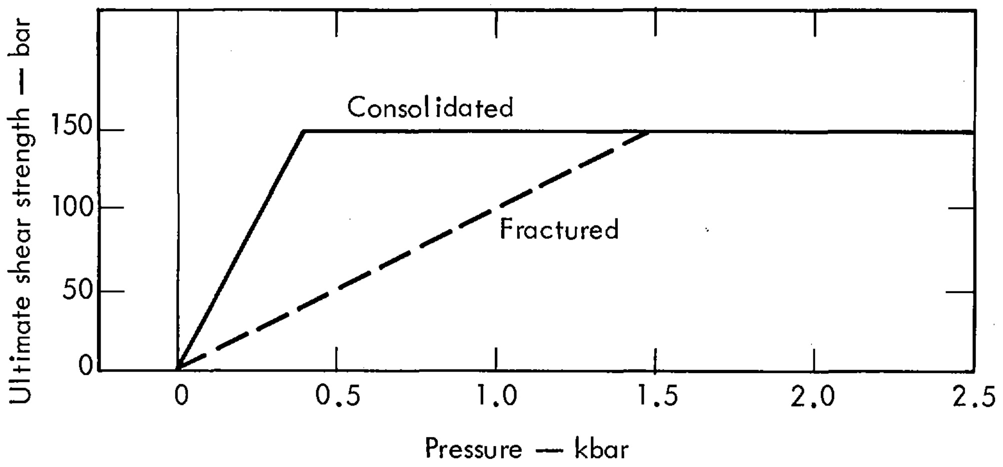

Fig. 15. Strength curve for Sedan crater calculation.

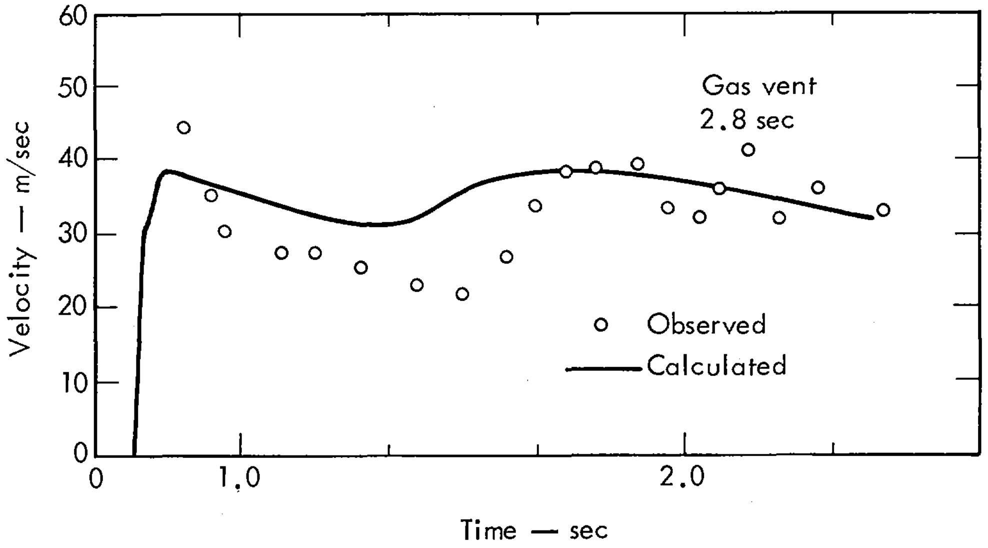

Fig. 16. Calculated and observed ground-zero surface velocity for Sedan.

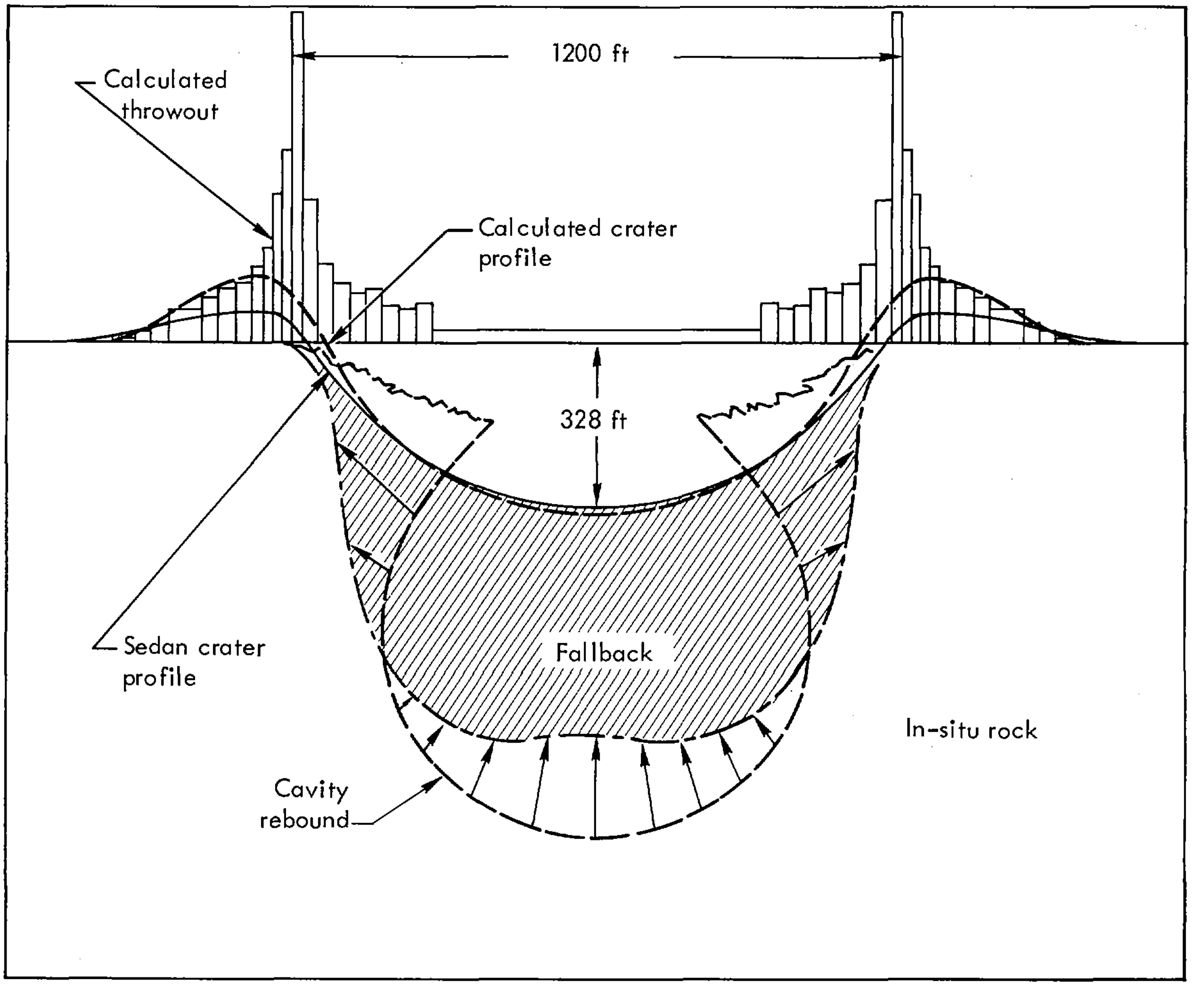

Fig. 17. Sedan crater profile at t = 2.4 sec.

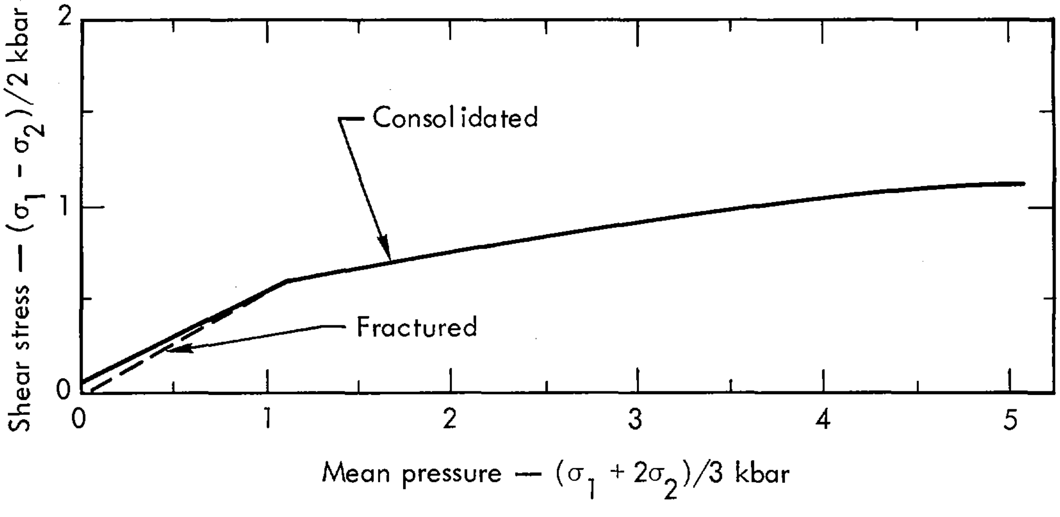

Fig. 18. Strength curve for Buckboard basalt.

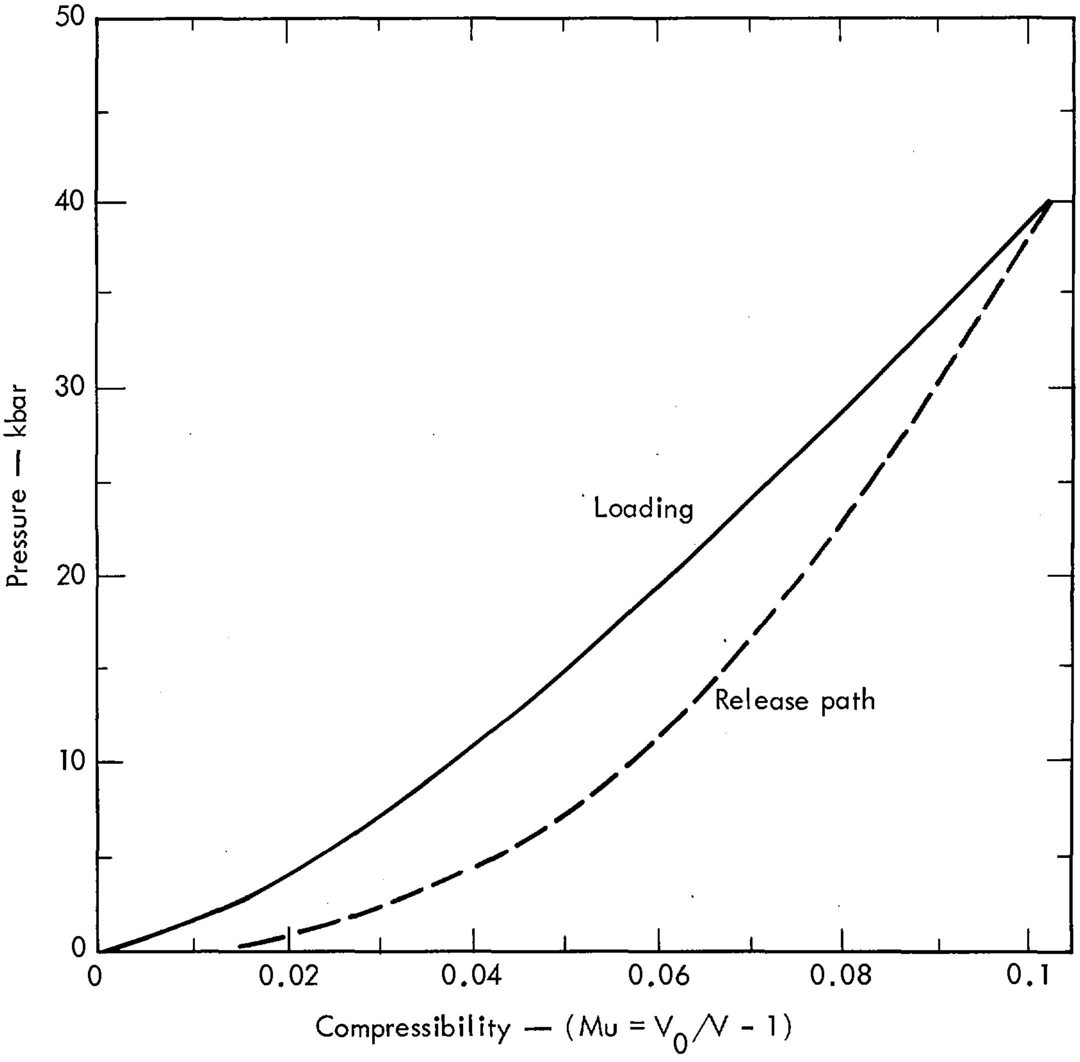

Fig. 19. Compressibility curves for Buckboard basalt.

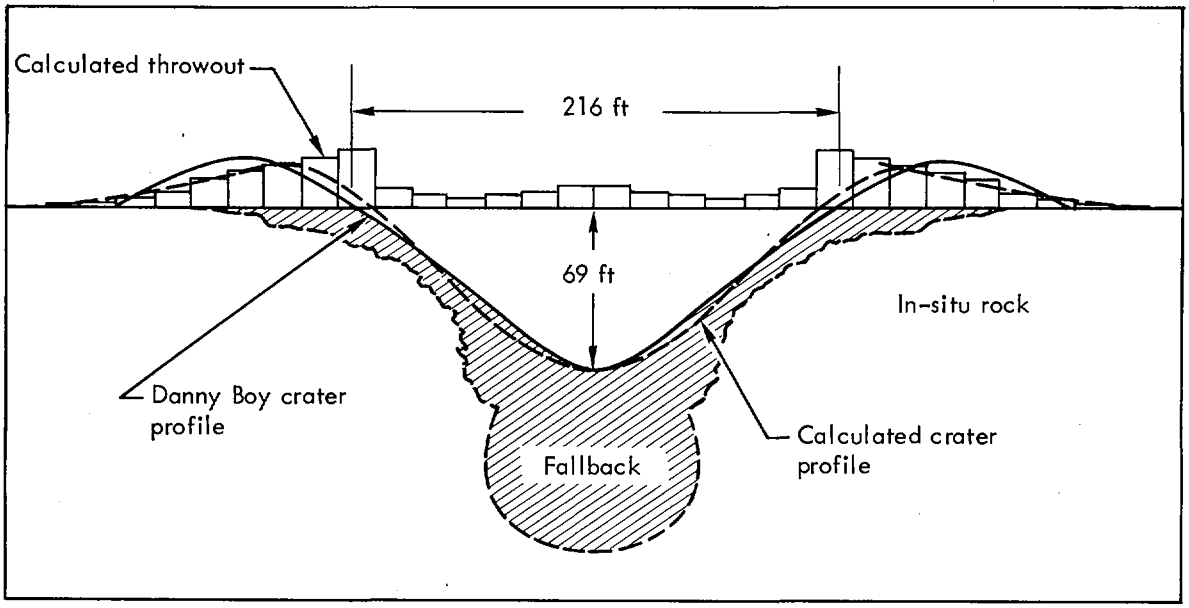

Fig. 20. Calculated crater profile for Danny Boy at t = 0.1 sec.

Next, a 1-Mt calculation at 328 m was performed to investigate the cratering efficiency of the basalt at high yields. The identical equation-of-state was used in the calculation as Danny Boy. Figure 21 shows the crater

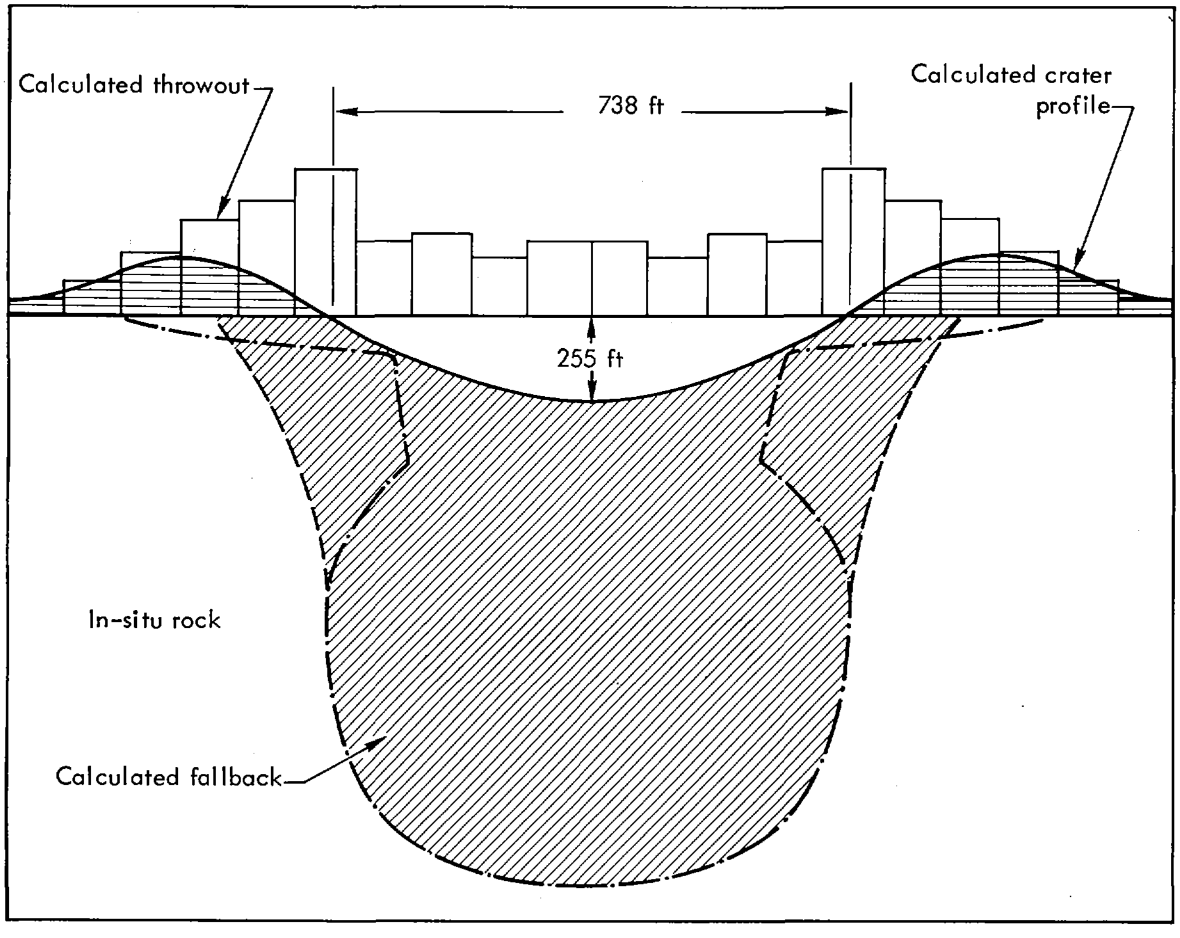

Fig. 21. Calculated crater profile for 1-Mt yield in Buckboard basalt, 328 m, at t = 1.5 sec.

profile as calculated. A large portion of the ejecta remained in the crater area with the resulting apparent crater due to compaction of the medium. A 10% bulking factor was used for the fallback. With 1/3.4 scaling, the megaton calculation was at the same-scale burst depth as Danny Boy. However, while Danny Boy was nearly optimum in crater size, the megaton burst barely produced a crater. In fact, the crater as shown in Fig. 21 appears deeper than that which would be actually realized; the calculation was terminated before the rebound of the lower hemisphere developed.

Canal Basalt

One of the major problems in designing an isthmus canal is the need to crater a sea-level channel through the Continental Divide. The following series of calculations provides the cratering characteristics of the Continental Divide for yields up to a megaton. The Continental Divide consists mainly of a dense, saturated basalt (Divide basalt) and a tuff agglomerate. Equation-of-state tests have indicated that the two rock types are so similar in their behavior that calculations are required only for the basalt.

The Canal basalt compressibility curve is type A-1, Fig. 2. The strength of the rock as function of pressure is shown in Fig. 22.[13] The brittle-ductile transition point is 0.5 kbar, and a Poisson's ratio of 0.3 was used in the calculations. The initial density was 2.65 g/cm^3.

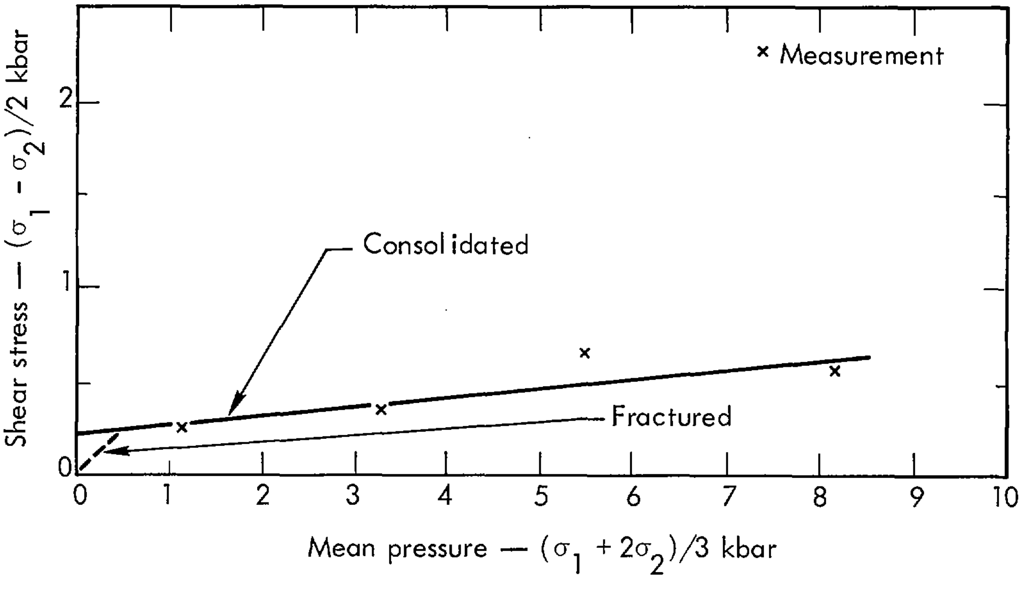

Fig. 22. Shear strength for Divide basalt.

To develop a correlation on the cratering efficiency of the Canal basalt, a calculation was made based on the Danny Boy yield and depth of burial (0.42 kt at 33 m). Figure 23 compares the calculated Canal basalt crater with the measured crater from Danny Boy. At this yield and depth of burst, the Canal basalt is about 25% more efficient as a cratering medium than Buckboard basalt. Spalling was the dominant cratering mechanism.

Figures 24 through 26 show 1-Mt crater calculations at burst depths of 139 m, 328 m, and 400 m, respectively, in Canal basalt.

At a depth of 139 m, a megaton crater is completely due to spalling. This problem was terminated at 200 msec, at which time the average mound velocity was 400 m/sec. The calculated crater may be slightly larger than that which would actually result, due to neglect of shear forces at the crater edges in the throwout calculation.

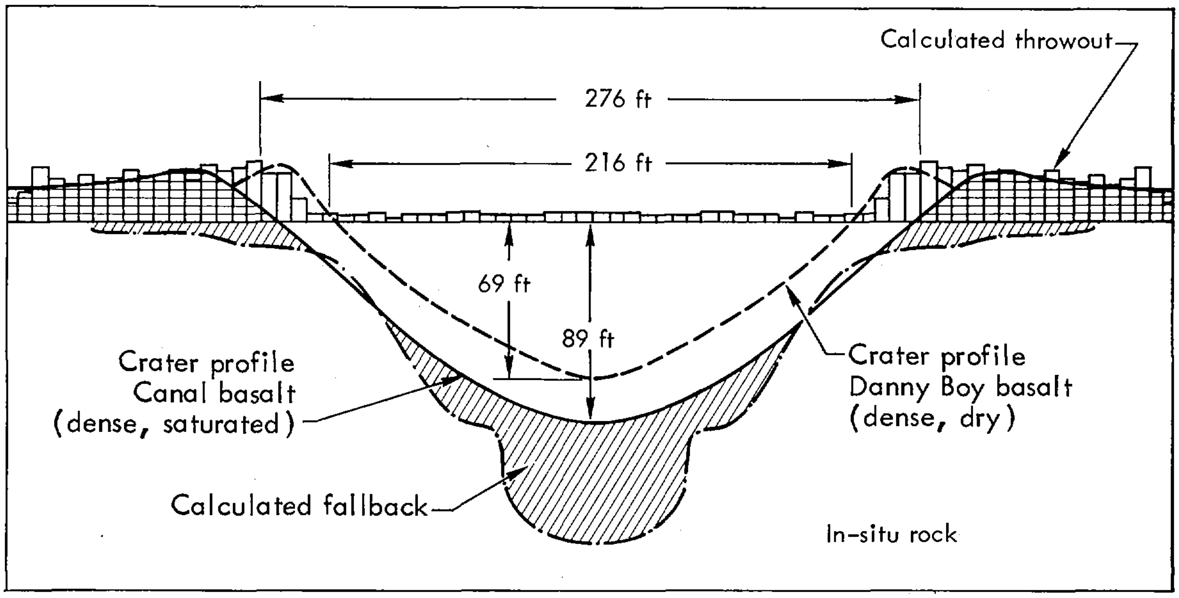

Fig. 23. Calculated crater profile for 0.42-kt yield in Divide basalt, 33 m, at t = 100 msec.

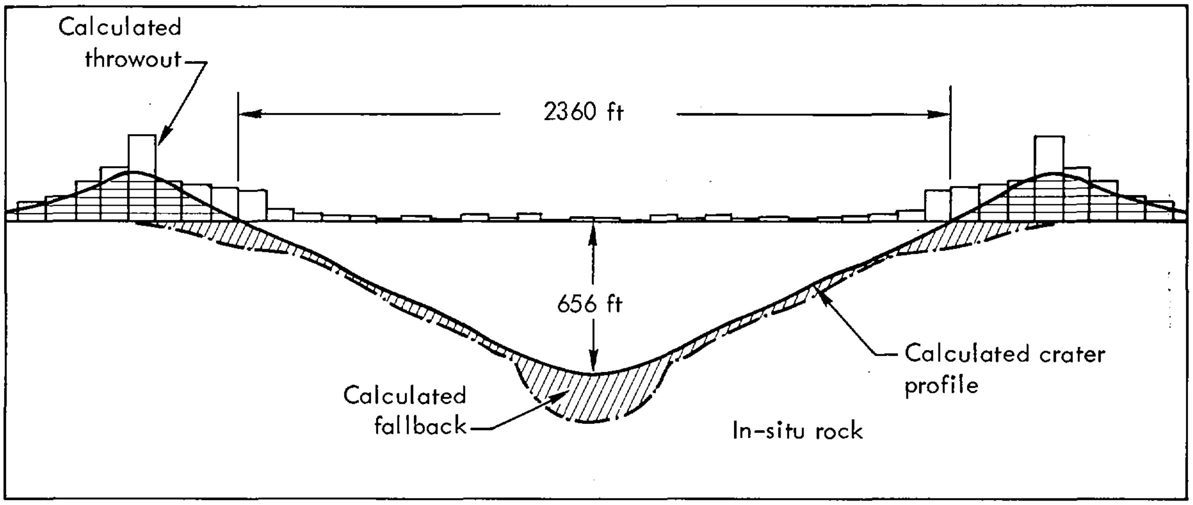

Fig. 24. Calculated crater profile for 1-Mt yield in Divide basalt, 139 m, at t = 200 msec.

At 328 m, a strong gas acceleration developed to enhance the dimensions of the crater. At 463 msec, when the existing velocity was primarly due to shock and spall, a throwout calculation gave an apparent crater radius of 260 m (855 ft) and depth of 170 m (560 ft). At 4.0 sec the gas acceleration phase was complete; the throwout calculation gave an apparent crater radius of 390 m (1280 ft) and depth of 228 m (748 ft).

At 400 m, gas acceleration was needed to form a crater. Even with gas acceleration, a considerable amount of the ejecta was calculated not to clear the cratering area.

SCALED CRATERING CURVES

Nordyke developed an empirical scaling law for apparent crater radius and depth versus depth of burst. The scaling law is length-divided by the yield in kilotons to the 1/3.4 power.

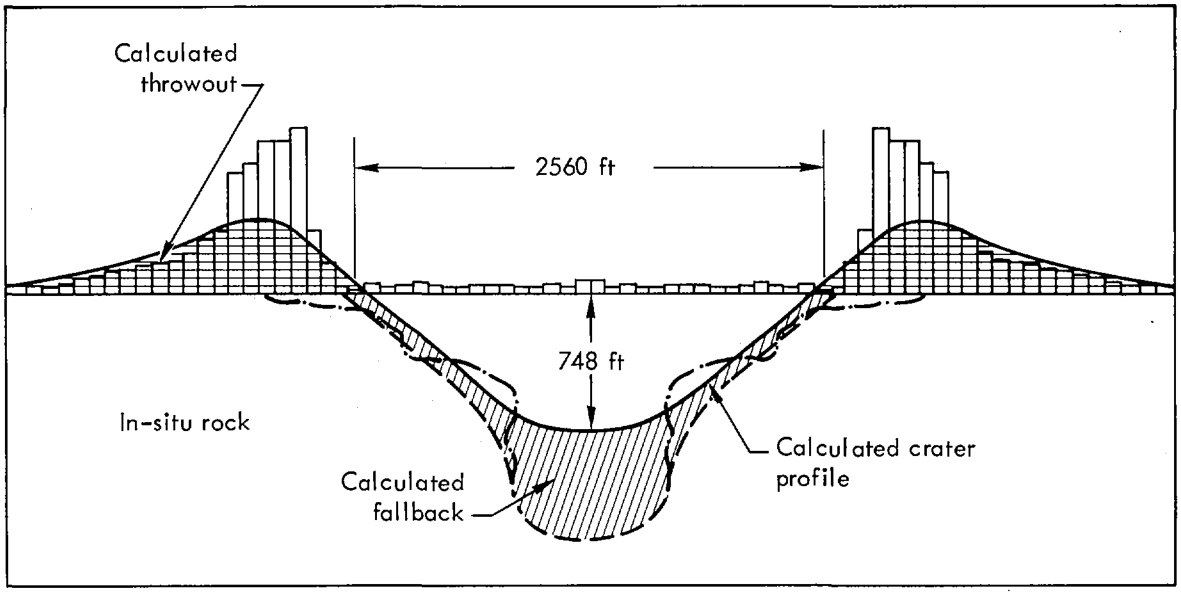

Fig. 25. Calculated crater profile for 1-Mt yield in Divide basalt, 328 m, at t = 3.0 sec.

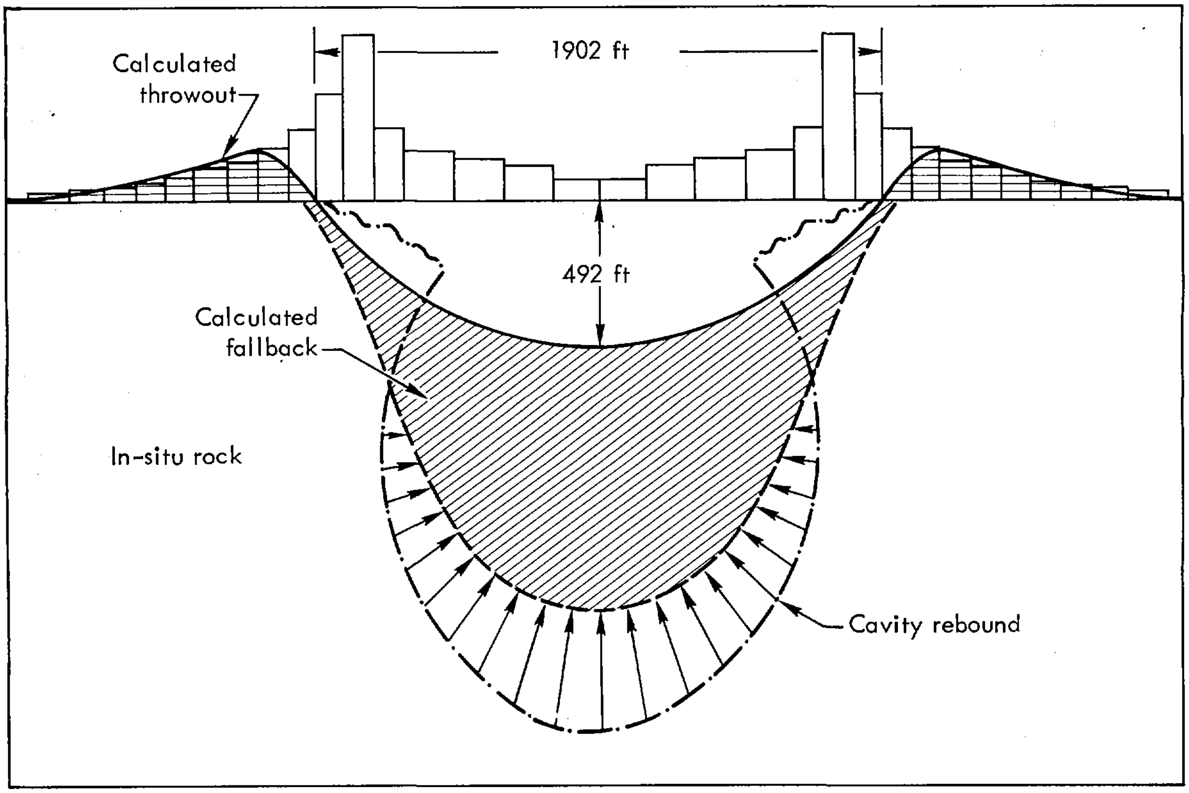

Fig. 26. Calculated crater profile for 1-Mt yield in Divide basalt, 400 m, at t = 4.0 sec.

Figures 27 and 28 show crater calculations with the scaled curves for crater radius and depth, respectively. Comparing the curve for Buckboard basalt at about 0.5 kt with the megaton calculation in Buckboard basalt shows considerable yield effect. The optimal depth of burial is much shallower

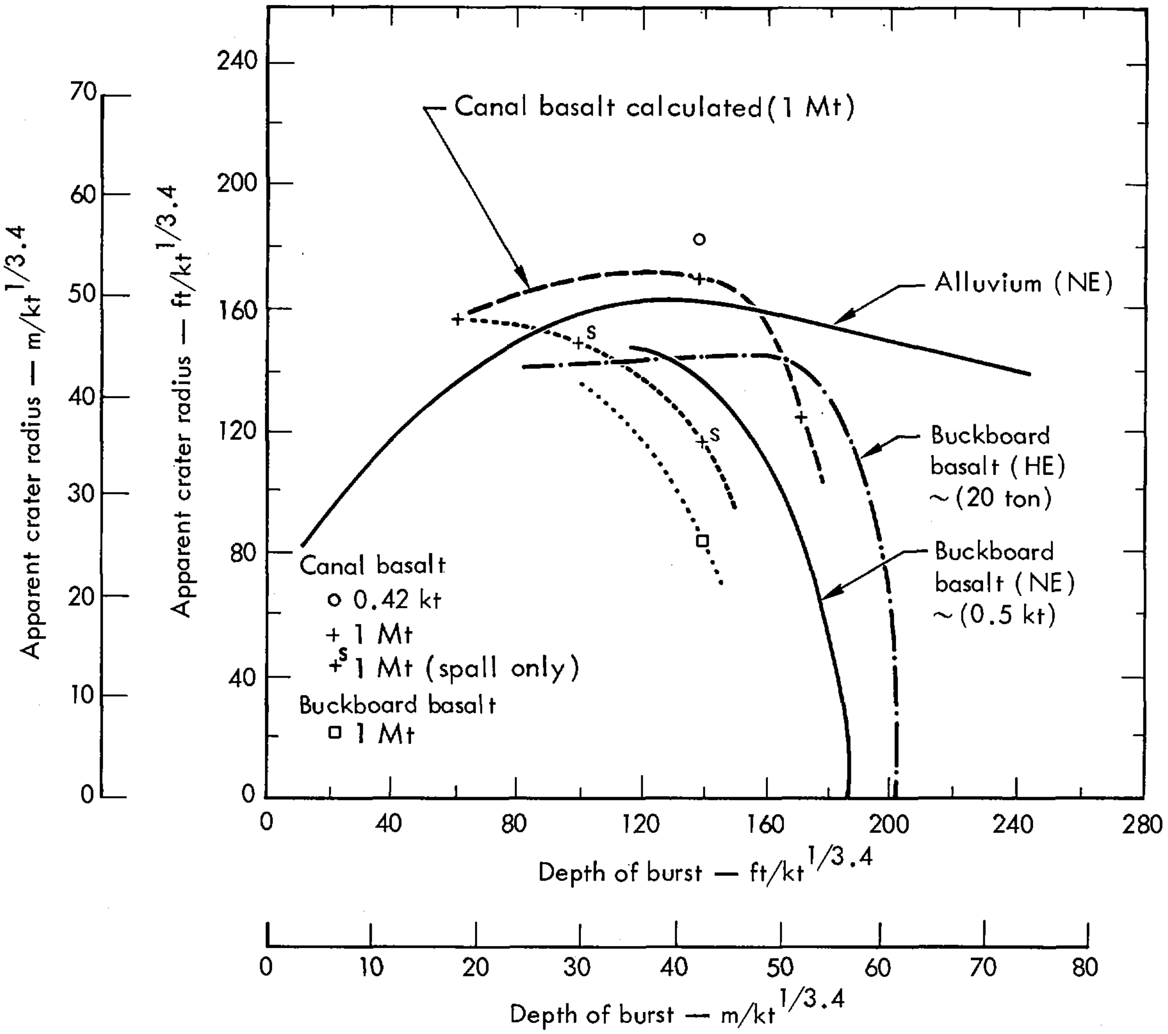

Fig. 27. Scaled crater radius curves.

(scalewise) for a megaton yield than for a yield on the order of 0.5 kt. The reason for this is that dry Buckboard basalt does not develop a strong gas acceleration phase due to lack of noncondensable products in the cavity gas. Thus gravity dominates in controlling the velocity field for much of the characteristic time-of-event, resulting in craters that scale more like yield to the 1/4 power.

The calculated cratering curve for Divide basalt differs in that, while the yield effect in crater size is small, the optimum burial depth for a 1-Mt yield is approximately the same as for a 0.5-kt yield. In this case, the saturated rock provides a strong gas acceleration phase.

The increase in crater size due to gas acceleration can be separated easily from spalling by performing a throwout calculation at the end of the spalling process. Plots of these calculations are shown in Fig. 27 by crosses with a superscript s. The optimum depth of burial (scalewise) is very shallow for spall craters, and this emphasizes the importance of the gas acceleration phase in cratering at the megaton level.

CONCLUSIONS

By the calculational approach, the importance and relationship of material parameters to cratering efficiency in various media have been

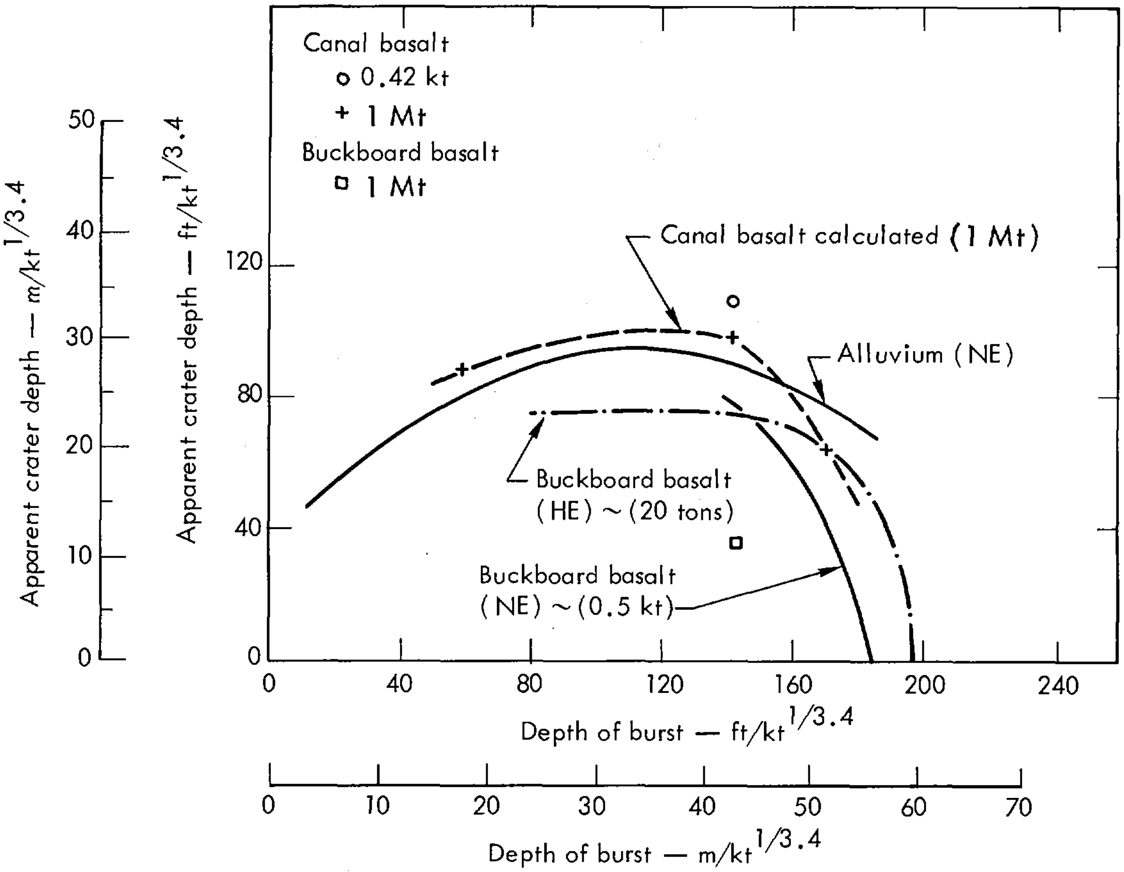

Fig. 28. Scaled crater depth curves.

illustrated. The water content of the medium has been emphasized because it enhances the medium as a stress transmitter, decreases the material strength such that high velocities are maintained, and provides noncondensable gas in the cavity for a strong gas acceleration phase.

Using a systematic method in the development of the equation-of-state, the codes have reproduced the dynamic measurements made on various field experiments. The resulting crater calculations are in good agreement.

A cratering curve for Divide basalt is presented, illustrating the need for a strong gas acceleration phase at the megaton-yield level.

Improvements in the equation-of-state are needed along with improvements in the codes. High pressure experimental data on the release paths of saturated rockare sorely needed. Constant improvements are being made on the calculational approach, in line with improved equation-of-state measurements. Hopefully, experimental data on the release paths of staturated rocks will soon be available. Also, plans are underway to include overburden in TENSOR by calculation of the initial stress field with the finite element method.

ACKNOWLEDGMENTS

The authors wish to thank Fran Peterson for her assistance in running the SOC code, John White for his help with the calculations, and Jim Shaw for his invaluable aid in running the TENSOR code.

REFERENCES

1. G. Maechen and S. Sack, "The Tensor Code," Lawrence Radiation Laboratory, Livermore, Rept. UCRL-7316 (1963).

2. J. T. Cherry and W. R. Hurdlow, "Numerical Simulation of Seismic Disturbances," Geophysics 31, 33-49 (1966).
3. M. L. Wilkins, "Calculation of Elastic Plastic Flow," Lawrence Radiation Laboratory, Livermore, Rept. UCRL-7322 (1969).
4. J. T. Cherry, "Computer Calculations of Explosion-Produced Craters," Int. J. Rock Mech. Min. Sci. 4, 1-22 (1967).
5. D. R. Stephens and E. M. Lilly, "Static PV Curves of Cracked and Consolidated Earth Materials to 40 Kilobars," Proceedings of Conference on Shock Metamorphism of Natural Materials, Greenbelt, Md., April 1966.
6. D. R. Stephens, E. M. Lilly, and H. Louis, "Pressure and Volume Equation of State of Consolidated and Fractured Rocks to 40 Kbars," Int. J. Rock Mech. Min. Sci. (to be published).
7. E. Chamberlain and G. Dante, "Solid Cell P-V Test Interoceanic Canal Studies Route 17," U. S. Army Terrestrial Science Center, Hanover, N. H.
8. H. C. Heard, "The Influence of Environment on the Inelastic Behavior of Rocks," ANS Symposium on Engineering with Nuclear Explosives, 1970.
9. H. C. Heard, private communication.
10. R. L. Bjork, K. N. Kreyehagen, and G. H. Wagner, private communication.
11. J. Day, D. Murrell, and W. Sherman, "Close In-Ground Motion, Earth Stress and Pore Pressure Measurement— Pre-Gondola I Series," PNE-1104, U. S. Army Nuclear Cratering Group, U. S. Army Corp of Engineers, 1967.
12. M. D. Nordyke and M. M. Williamson, "The Sedan Event," Lawrence Radiation Laboratory, Livermore, Rept. PNE-242F (1965).
13. W. S. Brown, J. J. Tanner, and K. L. DeVries, "The Effect of Presure on the Strength of Rock from Two Prospective Routes for an Interoceanic Canal," W. S. Brown Inc., Salt Lake City, Utah, 1969.

XA04N0757

EXCAVATION RESEARCH WITH CHEMICAL EXPLOSIVES

LTC William E. Vandenberg and Walter C. Day
U.S. Army Engineer Nuclear Cratering Group
Lawrence Radiation Laboratory
Livermore, California

INTRODUCTION

The U. S. Army Engineer Nuclear Cratering Group (NCG) is located at the Lawrence Radiation Laboratory in Livermore, California. NCG was established in 1962 and assigned responsibility for technical program direction of the Corps of Engineers Nuclear Excavation Research Program. The major part of the experimental program has been the execution of chemical explosive excavation experiments. In the past these experiments were preliminary to planned nuclear excavation experiments. The experience gained and technology developed in accomplishing these experiments has led to an expansion of NCG's research mission. The overall research and development mission now includes the development of chemical explosive excavation technology to enable the Corps of Engineers to more economically accomplish Civil Works Construction projects of intermediate size. The current and future chemical explosive excavation experiments conducted by NCG will be planned so as to provide data that can be used in the development of both chemical and nuclear excavation technology. In addition, whenever possible, the experiments will be conducted at the specific sites of authorized Civil Works Construction Projects and will be designed to provide a useful portion of the engineering structures planned in that project.

Currently, the emphasis in the chemical explosive excavation program is on the development of design techniques for producing specific crater geometries in a variety of media. Preliminary results of two such experiments are described in this paper; Project Pre-GONDOLA III, Phase III, Reservoir Connection Experiment; and a Safety Calibration Series for Project TUGBOAT, a small boat harbor excavation experiment.

IMPORTANCE OF CHEMICAL EXPLOSIVE EXPERIMENTS

The use of explosives for excavation involves more than merely producing craters or mounds of rock. One must be able to predict the geometry of the crater, or better still produce a desired geometry to fit a specific application. All of the foreseeable nuclear applications (1, 2) involve designs more complex than simple cratering under level terrain in a relatively dry medium. Specifically, aggregate production would be most ideally done under a topographic configuration that would maximize the volume of aggregate produced and make its recovery easiest. Ejecta dam construction would involve directed blasting techniques which would have to be uniquely tailored to the specific dam site. Canals and harbors will most often involve water saturated media or cratering under water. Canals and other cuts for land vehicle traffic will involve row cratering through varying terrain. All applications can involve unique geology, either layered and steeply dipping or in media for which no experience exists. Because it is infeasible to conduct enough nuclear experiments to develop the necessary engineering design techniques for each of the applications envisioned with the variety of geologic, hydrologic, and topographic features that can prevail, it will be necessary to derive this technology by a different route. One approach being taken to make the jump between a few cratering experiments and engineering design of complex applications uses computer calculations of the dynamic cratering process (Terhune, LRL). From an engineering standpoint, the ideal result of this program would be a set of design curves that would give the necessary emplacement information for each application and a set of physical site conditions prevailing. However, the current capability of the calculational technique is limited to two dimensions. Thus the set of curves, when they become available, will be limited to single-charge cratering in applications with an axis of symmetry. As indicated previously, these applications are the exception rather than the rule. In most real projects the use of this valuable calculational technique will still require an additional ingredient usually termed "engineering judgment". The use of engineering judgment implies experience of some related nature. It is this related experience that NCG is attempting to gain by using chemical explosives in relatively large concentrated charges in real construction projects.

Actually the chemical explosive excavation experiments contribute more than is implied by the previous statement. Though direct scaling from chemical explosive experience to nuclear explosive excavation cannot be done because of differences in the explosives' performance, (initial and subsequent pressures, temperatures and times) it is understanding how the cratered medium responds to a high shock loading and the nature of the gas cavity expansion that becomes important for predicting nuclear crater dimensions in the medium. If experimental cratering with chemical explosives in a medium can duplicate results of the calculational technique, based on a knowledge of the material properties, then it is more likely that nuclear cratering predictions for that medium made by the calculational technique will be valid.

It is within this framework of experience that adds to the empirical cratering application data and at the same time provides a laboratory for the computational technique that NCG's current chemical explosive test program is conceived.

THE RESERVOIR CONNECTION EXPERIMENT

The Reservoir Connection Experiment, executed in October 1969, was the last major experiment in the Pre-GONDOLA series of experiments. The Pre-GONDOLA experiments were designed to provide crater geometry data in a weak, saturated clay shale. The site selected for these experiments is located adjacent to the Fort Peck Reservoir, Fort Peck, Montana. A number of experiments have been conducted at the site during the past three years. These have included small-scale experiments in single, row, and array emplacement configurations. (3, 4). Yields have ranged from 64 to 2000 pounds per charge. All of these experiments were peripheral to the main row-charge experiment at the site which is shown in Figure 1 prior to the reservoir connection detonation. This photograph shows the 20-ton Pre-GONDOLA I single-charge craters, (5), the Pre-GONDOLA II row at the left center, (6), and the Pre-GONDOLA III, Phase II connecting row at the right center. (7). Project Pre-GONDOLA I, four 20-ton cratering detonations, executed in the fall of 1966, provided data on the variation of crater dimensions in clay shale with respect to depth of burst. The CHARLIE crater was partially filled in by the Pre-GONDOLA II five-charge row and is located at the extreme left of the long row crater. Pre-GONDOLA II, executed in June 1967, consisted of two 40-ton charges and three 20-ton charges spaced at approximately 80 feet and buried at 150 ft/kt$^{1/3.4}$ (48.8 to 59.9 ft). All five charges were detonated simultaneously to give the linear channel. During postshot engineering properties investigations, a wide trench was cut through the side lip and holes drilled into the rupture zone. The trench can be seen on the far side of the crater. Pre-GONDOLA III, Phase II provided the longest portion of the crater and consisted of seven charges, 30 tons each, all buried at the same elevation but with variable spacing between charges. Four of the charges were spaced at an average single-charge crater radius. The remaining three charges were spaced at 0.6 of the single-charge crater radius. Because the specific depth of burst (and consequently the crater radius-determined spacing) could not be established until some spacing was set, the design involved an iterative process starting with spacing based on the average depth of burst for the whole alinement and ending with spacing determined by actual depths of burst of adjacent charges. This charge configuration gave a very smooth, large crater which connected to the Pre-GONDOLA II crater. The Pre-GONDOLA III, Phase II row was executed during October 1968.

The last major experiment in the Pre-GONDOLA series was executed on 6 October 1969. This was Pre-GONDOLA III, Phase III, Reservoir Connection Experiment. In this experiment, five charges of varying yield and depth were placed (Figure 2) and simultaneously detonated to provide a connecting channel between the long crater shown in Figure 1 and the Fort Peck Reservoir. A varying terrain row cratering experiment of this scale had not been carried out previously. To complicate matters, a connection had to be made to the existing crater that would not leave a large amount of material blocking the channel. At the other end of the row, the objective was to connect directly to the reservoir with a minimum height end lip so that postshot excavation would not be necessary before water would fill the crater. The channel was designed to accommodate a navigation prism 67 ft. wide and 4 ft. deep at a water level of 2238 ft. The channel cross section was assumed to be hyperbolic with slope angles of 30°. No row crater enhancement was assumed in the design.

A preshot view of the crater showing construction activity is shown in Figure 3. Just after the detonation, Figure 4, water started to fill the crater. The water filling action, Figure 5, took about nine minutes. The final view, Figure 6, shows what the crater looked like when filled to the reservoir level. A composite of several sequential pictures taken of the detonation and resulting crater are shown in Figure 7. In one of these water can be seen spilling over the end lip into the crater. Crater profiles, center line and cross sections, are shown in Figure 8. The crater width at water level varies from a minimum of 100 feet to a maximum of 200 feet. The depth of water in the crater varies from a minimum of 13 feet to a maximum of 39 feet except at the entrance where the depth is approximately seven feet. The length of the water-filled portion of the crater is approximately 1370 feet. Although this work was totally experimental, it was very successful and graphically illustrates two proposed applications of large-scale explosive excavation, an inland harbor and a canal. In Figure 9 a tugboat is shown in the crater to provide some concept of scale.

KAWAIHAE SMALL BOAT HARBOR

Interest in the explosive excavation of harbors has generated the most current chemical explosive cratering project being conducted by NCG. This is Project TUGBOAT. (8). This explosive excavation experiment is designed to investigate the general concept of producing a harbor basin in shallow water in a near shore environment. The site for the experiment was picked to coincide with the site of a Congressionally authorized small boat harbor so that some benefit would be obtained from the expenditure of the R&D funds. This site is in Kawaihae Bay on the west side of the Island of Hawaii (Figure 10). The project is planned for execution in three phases. Phase I, executed 4 to 7 November 1969, was a cratering and safety calibration series of detonations. Phase II is planned as a row and an array detonation(s) of nominal 10-ton charges designed to excavate a berthing basin and entrance channel.

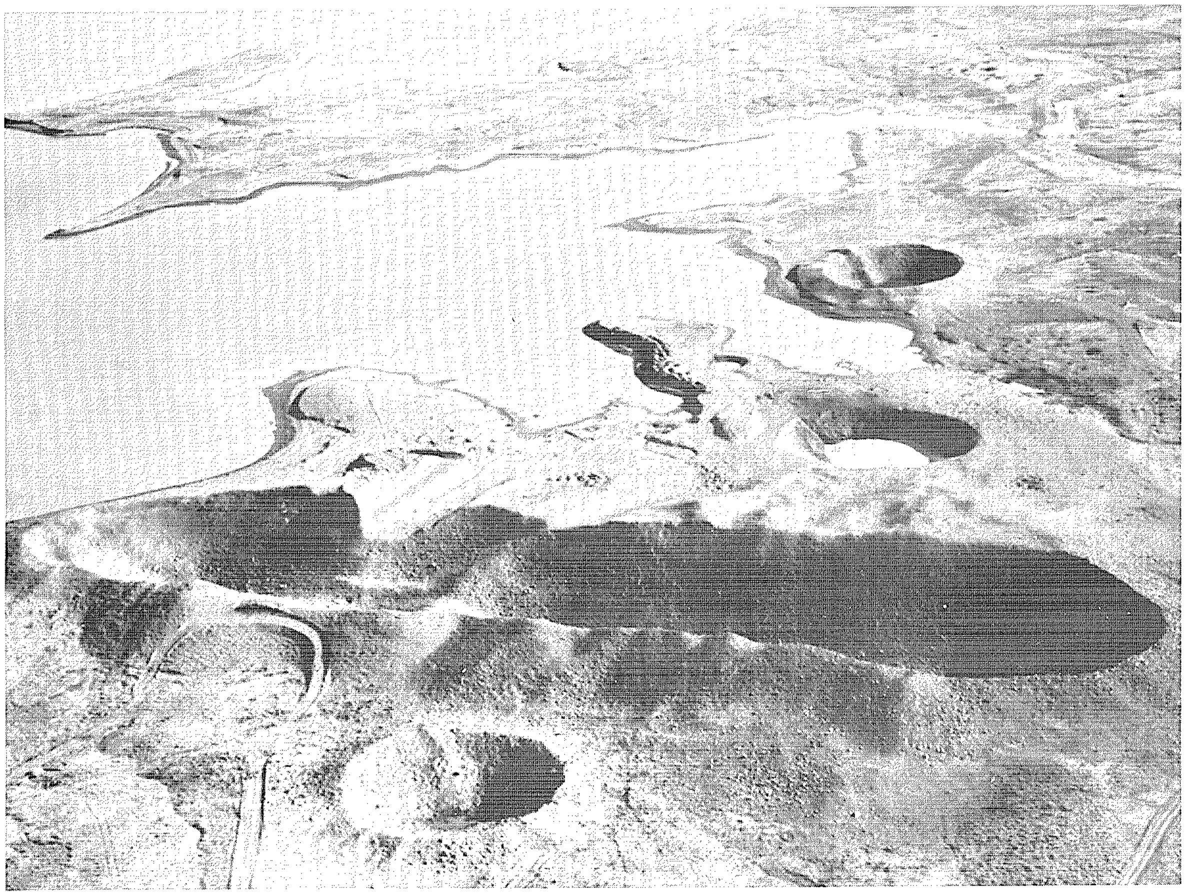

Figure 1. Pre-GONDOLA 20-ton single-charge craters and connecting row crater prior to execution of the reservoir connection experiment.

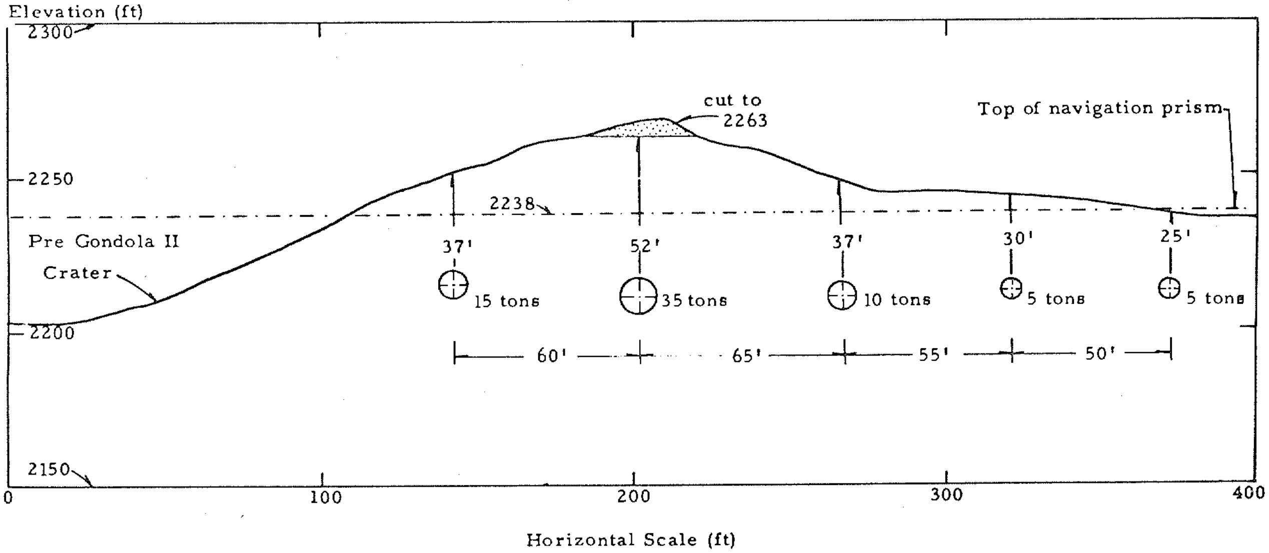

Figure 2. Centerline section drawing of the reservoir connection experiment, Pre-GONDOLA III, Phase III, showing charge depths, spacings and yields.

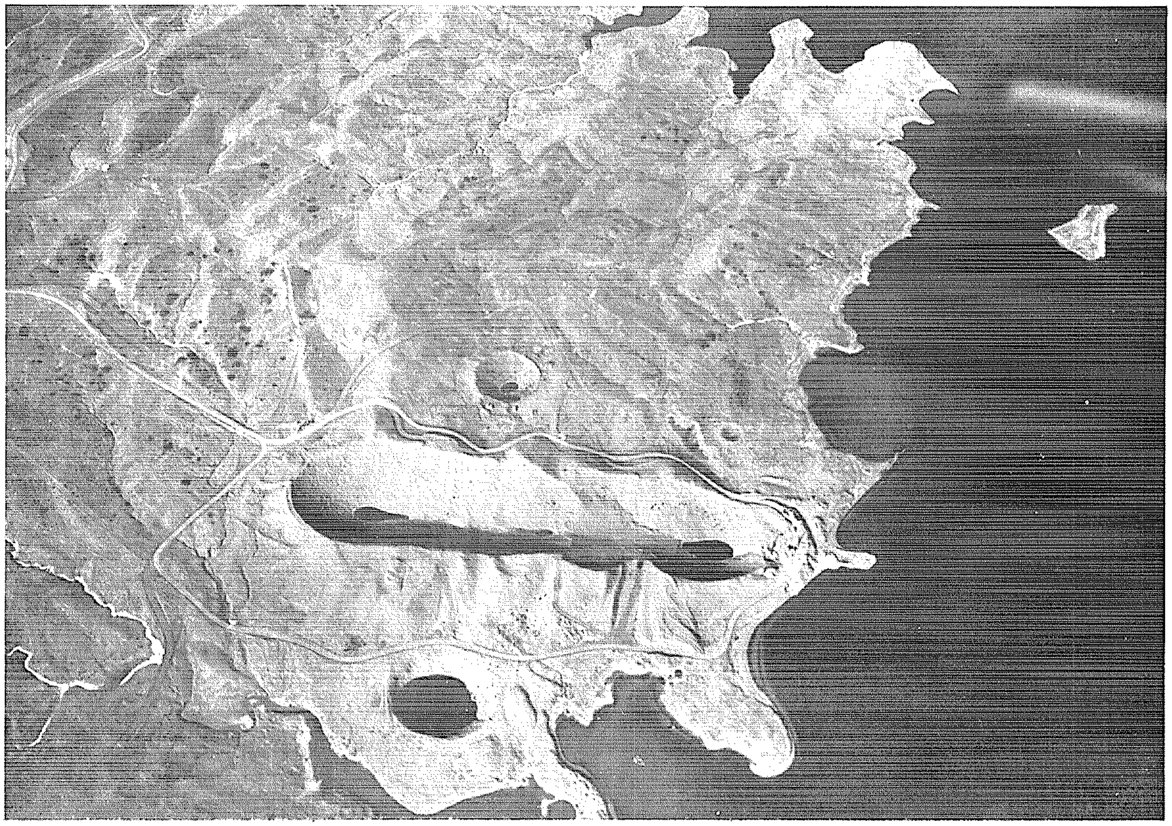

Figure 3. Preshot view of the Pre-GONDOLA III, Phase III, Reservoir connection experiment.

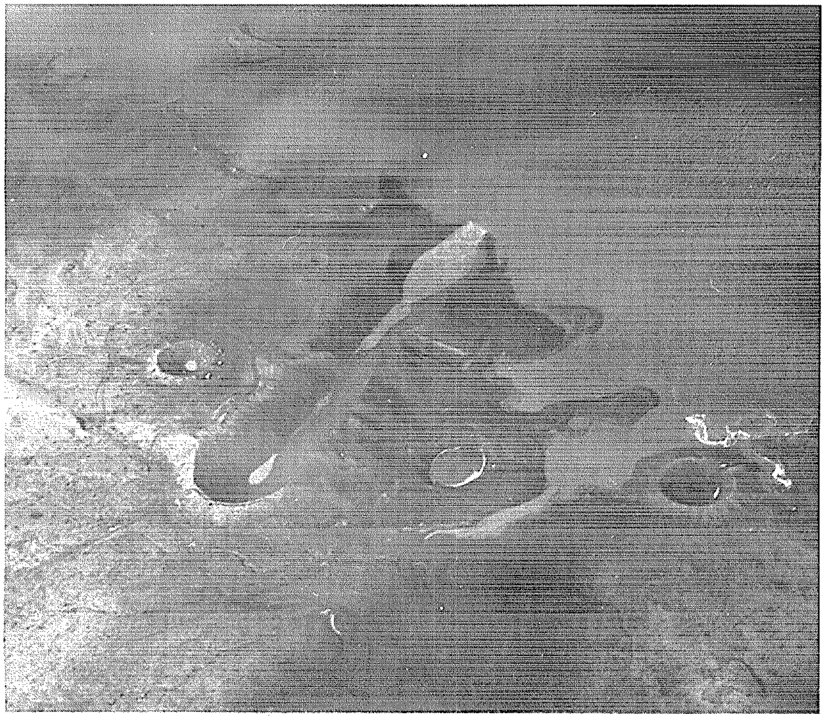

Figure 4. Connection experiment crater immediately following the detonation showing water starting to fill the crater.

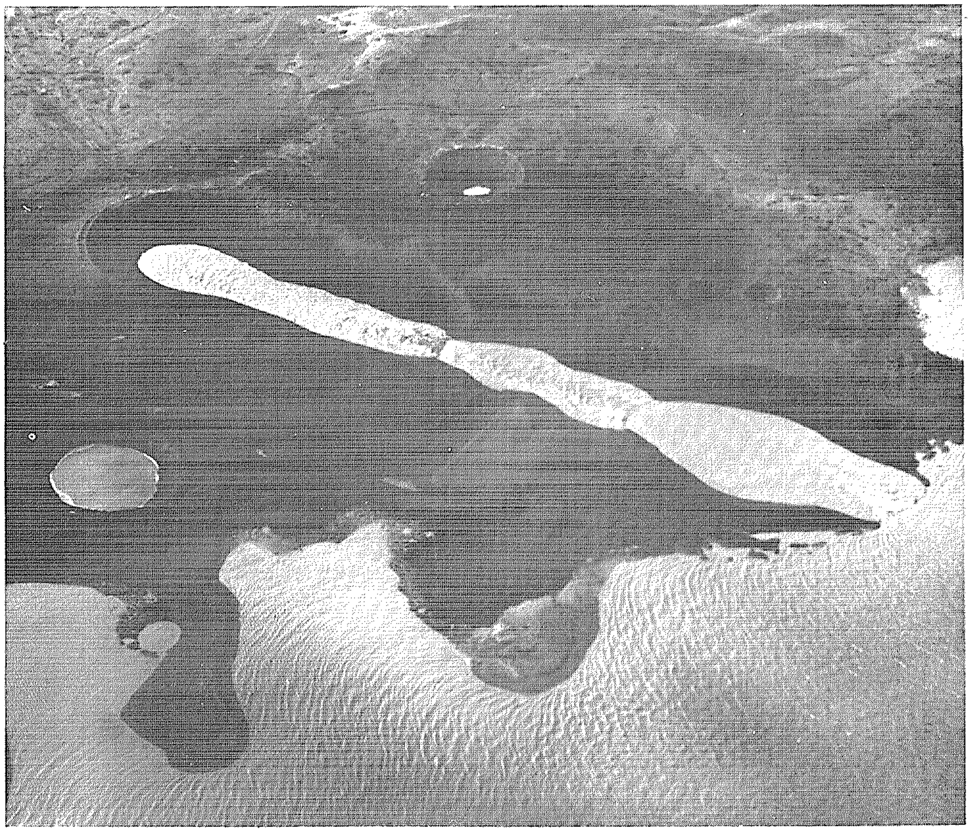

Figure 5. Reservoir connection experiment crater filling with water.

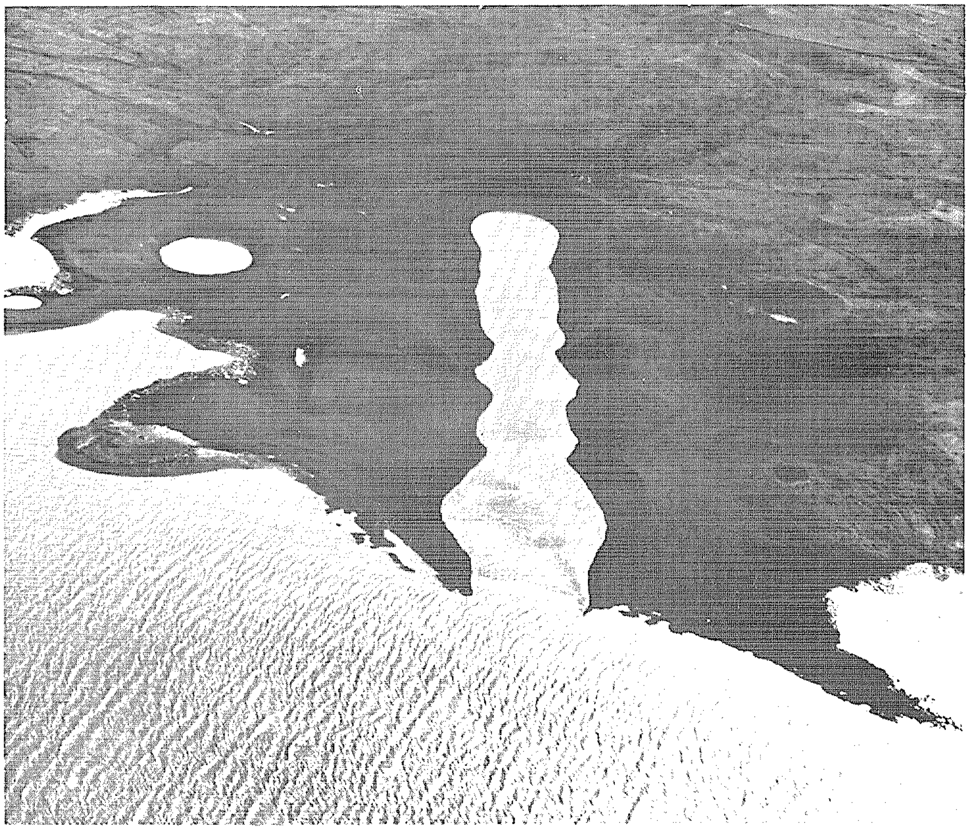

Figure 6. Reservoir connection experiment crater after water filling action was complete. Total filling time was about nine minutes.

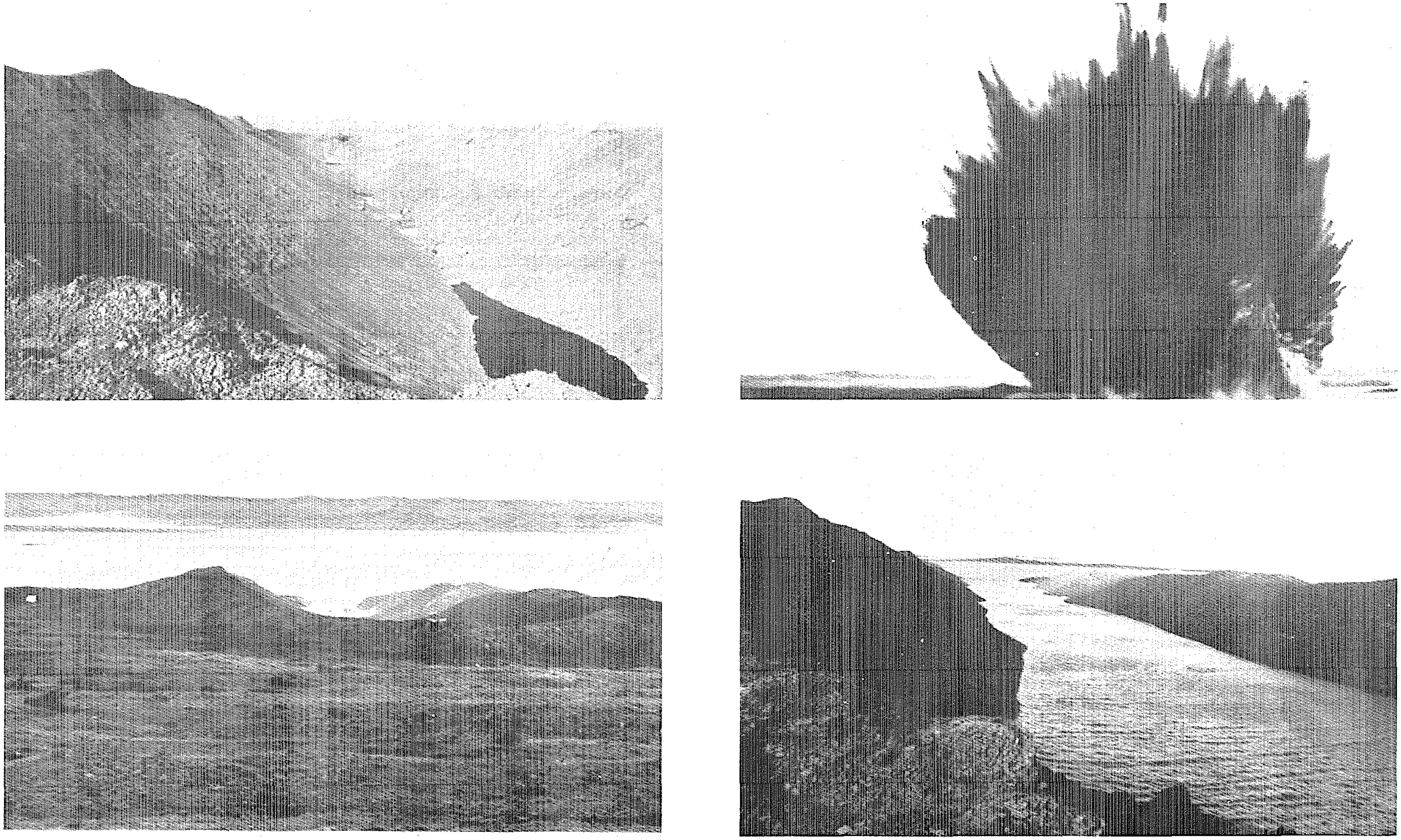

Figure 7. Sequential photos of the Reservoir connection experiment detonation and resulting crater.

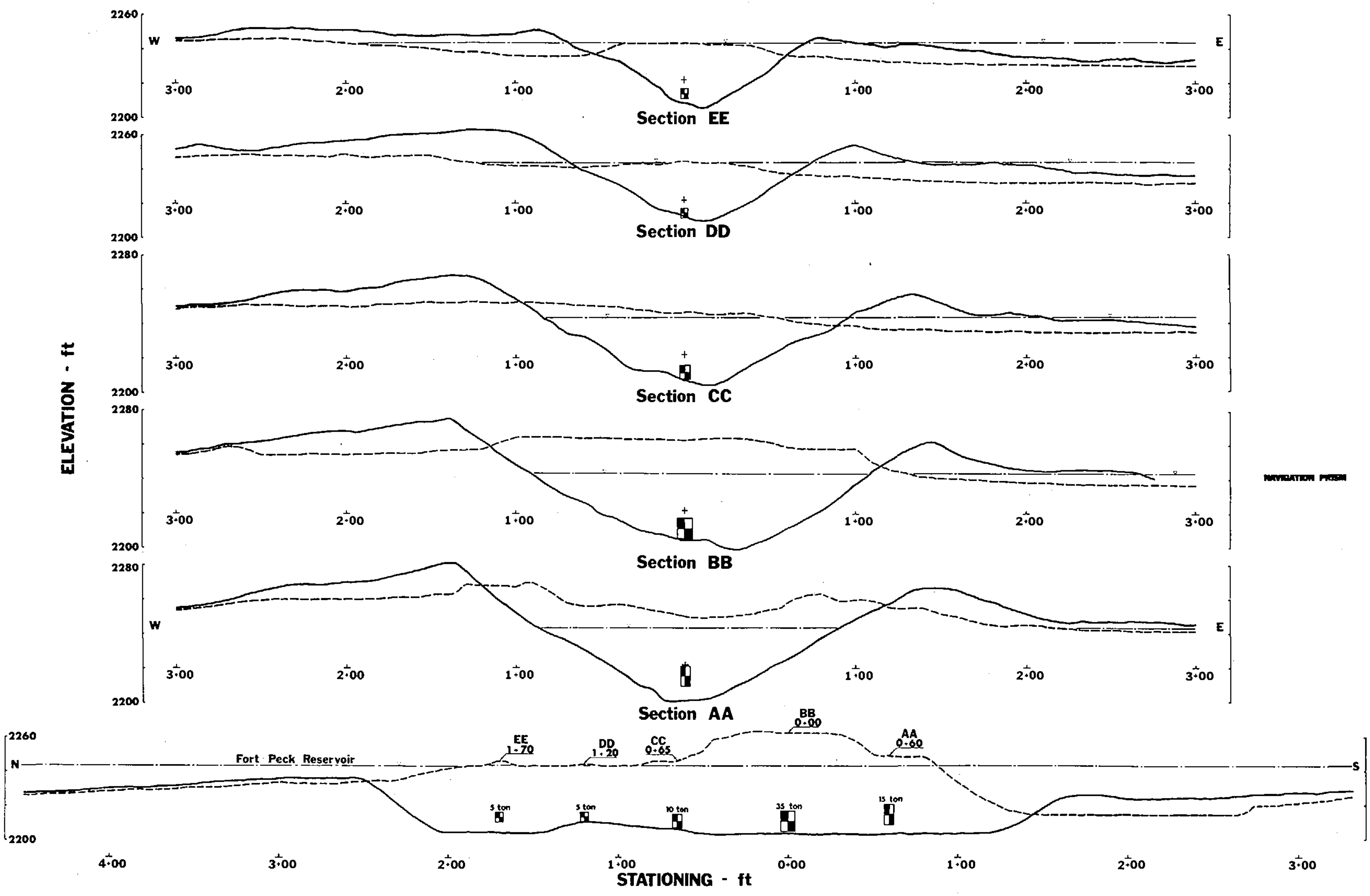

Figure 8. Centerline profile and cross sections, Reservoir connection experiment.

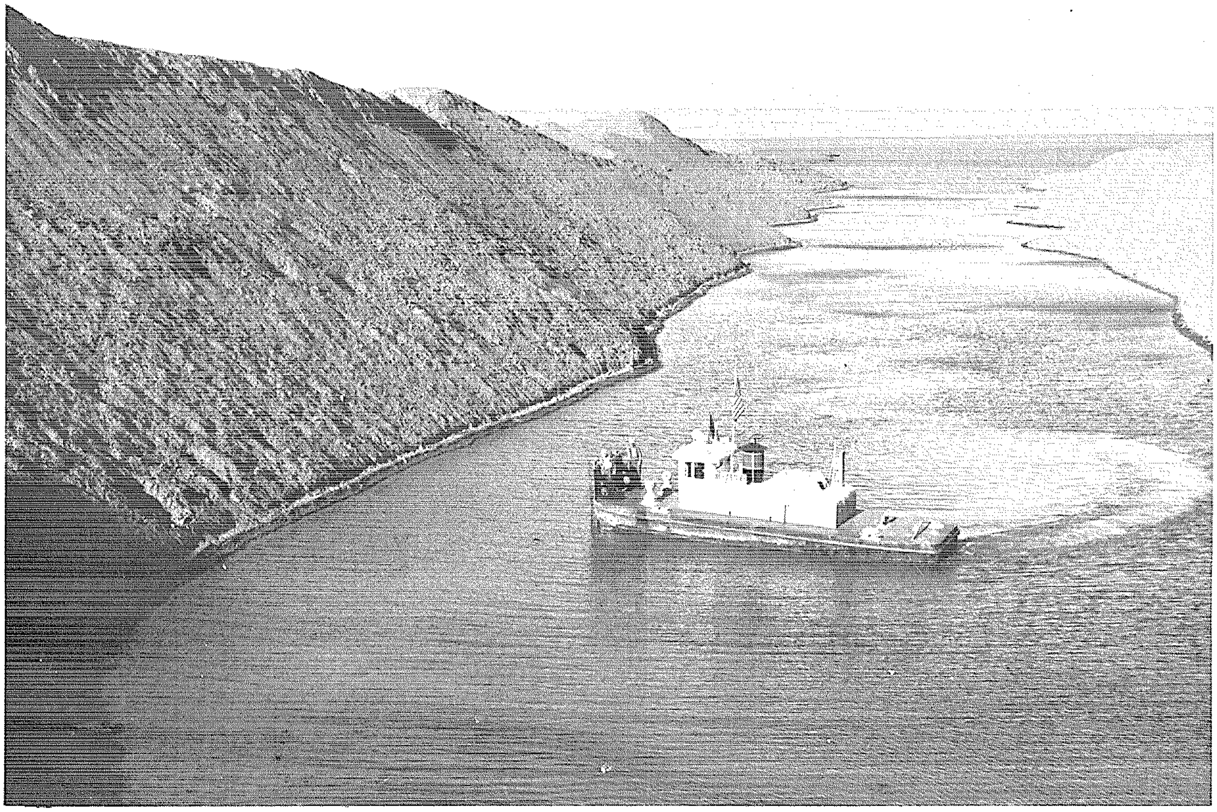

Figure 9. View of the Pre-GONDOLA crater with a tugboat in the channel.

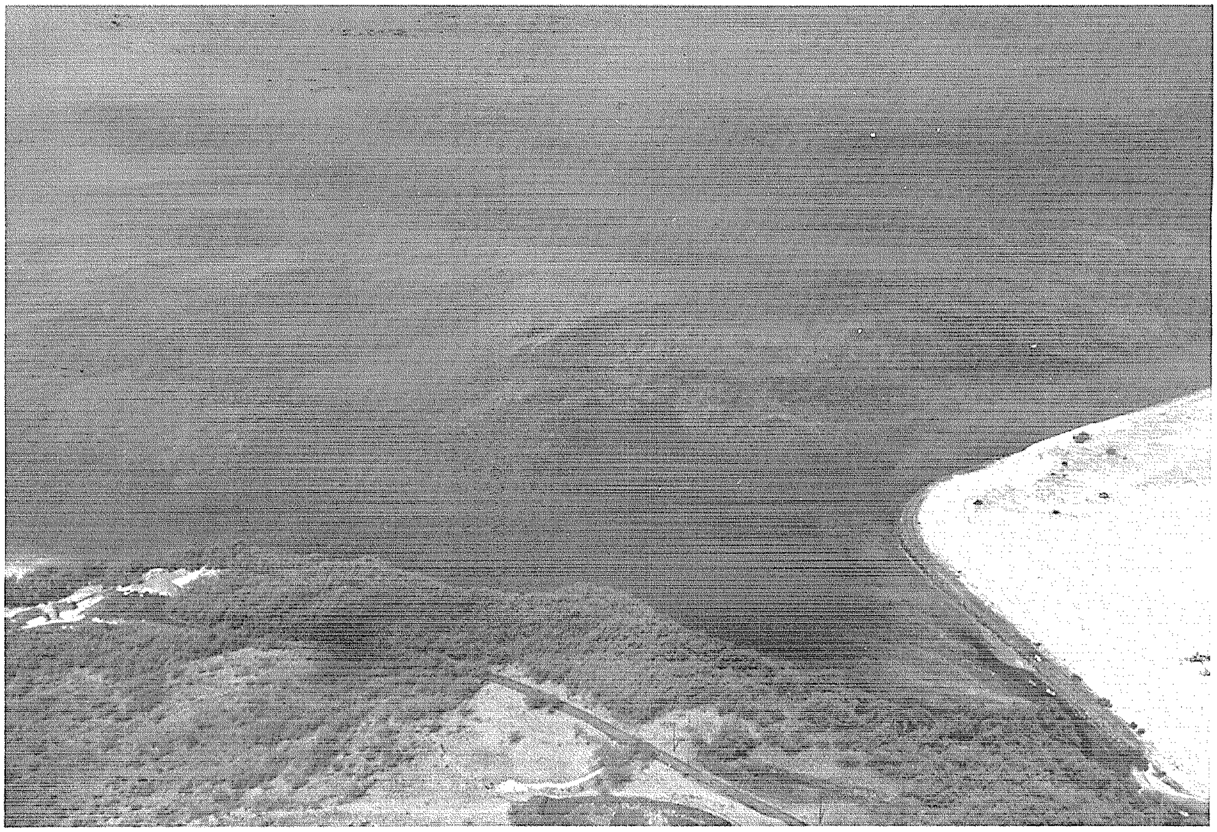

Figure 10. Project TUGBOAT site in Kawaihae Bay on the west side of the island of Hawaii.

Experience in cratering in a completely saturated medium overlain by water is almost nonexistent. Because of this, five detonations were included in the Phase I program, four each one-ton and one 10-ton. The one-ton charges were placed at depths ranging from 16 to 24 feet below mean lower low water level. The ten-ton charge was buried at 41 ft. below mean lower low water at what was predicted to be optimum for crater radius. This program was intended to provide crater dimension and safety data as a function of both depth of burst and yield.

The site medium is a coral limestone extending to 70 feet or more in depth and overlain by six to ten feet of water. The original concept for explosively excavating a harbor in this material assumed that the crater formation process would be similar to that experienced in previous dry land experiments and that a crater lip would form which could be used as the core for a breakwater. After laboratory testing data was obtained for the coral, it was evident that there might be some surprises. The porosity of the material ranged from 37 to 64 percent, and the compressive strength was variable and ranged from 760 to 1738 lbs/in^2. This data strongly indicated that the material would be compacted in the cratering process and very little ejecta would be available to form a lip that would extend above water. This indeed was the case for both the one-ton and ten-ton craters. Profiles of the craters are shown in Figures 11, 12 and 13. A profile of the ten-ton crater is shown in comparison to a dry land crater in Figure 14. As can be seen, there were no lips. The total apparent crater volume seems to result from crushing and compaction of the coral. The crater shape is more desirable for creating a harbor than that originally contemplated based on dry land experience in that it is very broad and of shallow depth.

Because the radii for these craters are so large and do not significantly change over the range of depths of burst in the 1-ton series, a cratering curve has not been plotted. The parameter chosen for row and array charge design is the radius over which a relatively flat bottom occurs. The project calls for a minimum channel depth of 12 ft. For the 10-ton Echo calibration detonation (Figure 13) the average radius over which a minimum 12 ft. depth occurs is estimated to be approximately 60 ft.

The design problem for the berthing basin is primarily one of assuring a relatively smooth bottomed crater with a minimum depth of 12 ft. NCG's test modeling facility at the Lawrence Radiation Laboratory has been modified to do one-pound tests in saturated sand and in saturated sand overlain by four inches of water. A few tests have been conducted in the test pit since the Project TUGBOAT, Phase I tests and interestingly enough the craters are similar in shape to those observed in saturated coral. Several array charge detonations have been done at very wide spacing. These tests show the best results when the spacing is approximately twice the radius of the flat bottomed portion of the single-charge craters.

The preliminary redesign of the harbor entrance channel and berthing basin is shown in Figure 15. The berthing basin design uses four 10-ton charges spaced 120 ft. apart in a square array. This four-charge-square array provides more berthing space than was provided by the original design which used 10 charges in two parallel rows of five each. Some overdepth was desirable in the outer portion of the entrance channel and therefore these charges were spaced a little closer at 100 ft. This design requires the use of eight ten-ton charges in the entrance channel.

With this redesign of the entrance channel and berthing basin the project can be accomplished with 60% of the total yield specified in the original design. The savings from the reduction in emplacement construction and amount of explosives needed is expected to cover the additional cost of building a

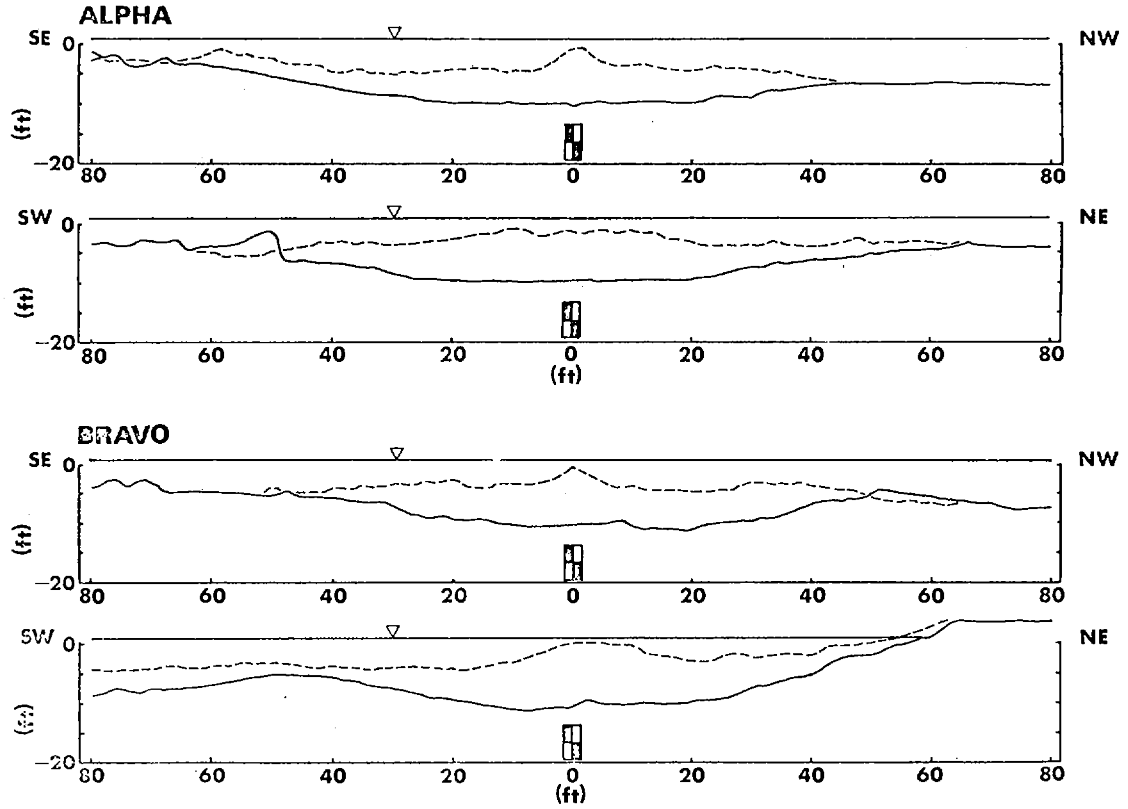
ALPHA

BRAVO

Figure 11. Project TUGBOAT, Phase I: ALPHA and BRAVO crater cross sections.

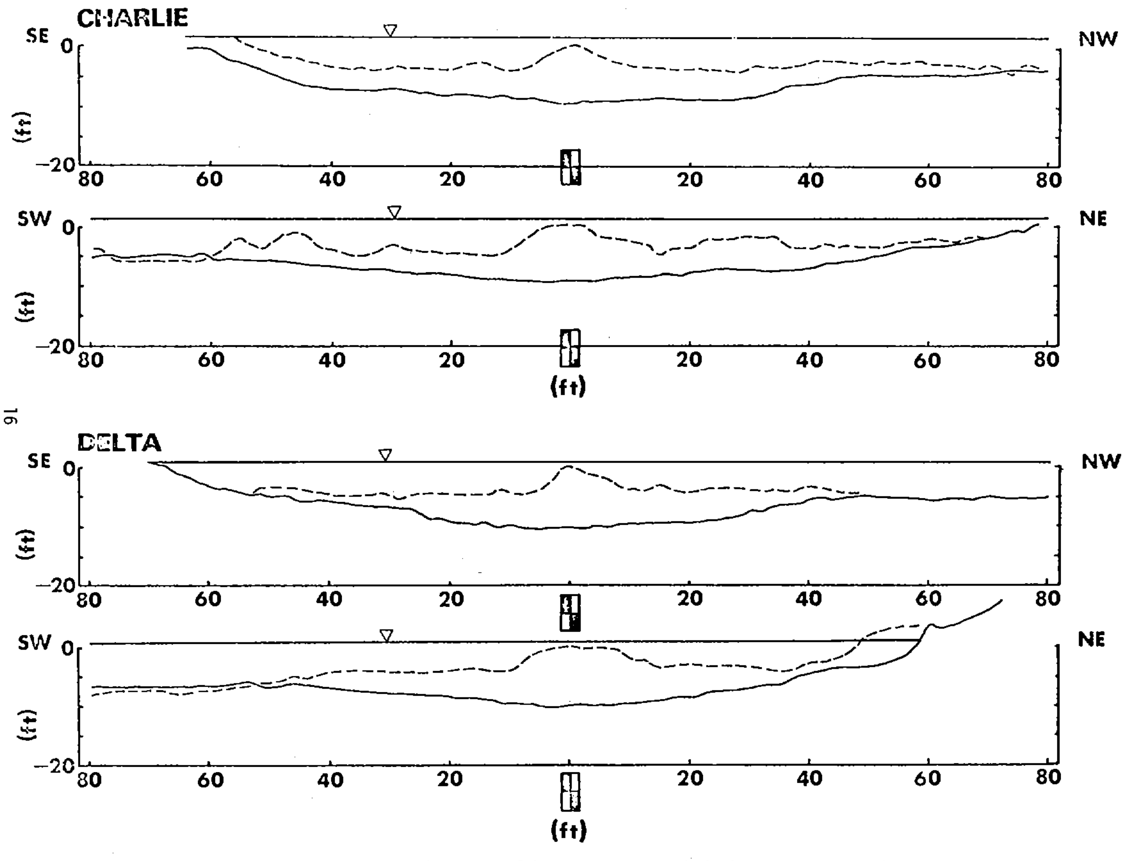
CHARLIE

DELTA

Figure 12. Project TUGBOAT, Phase I: CHARLIE and DELTA Craters.

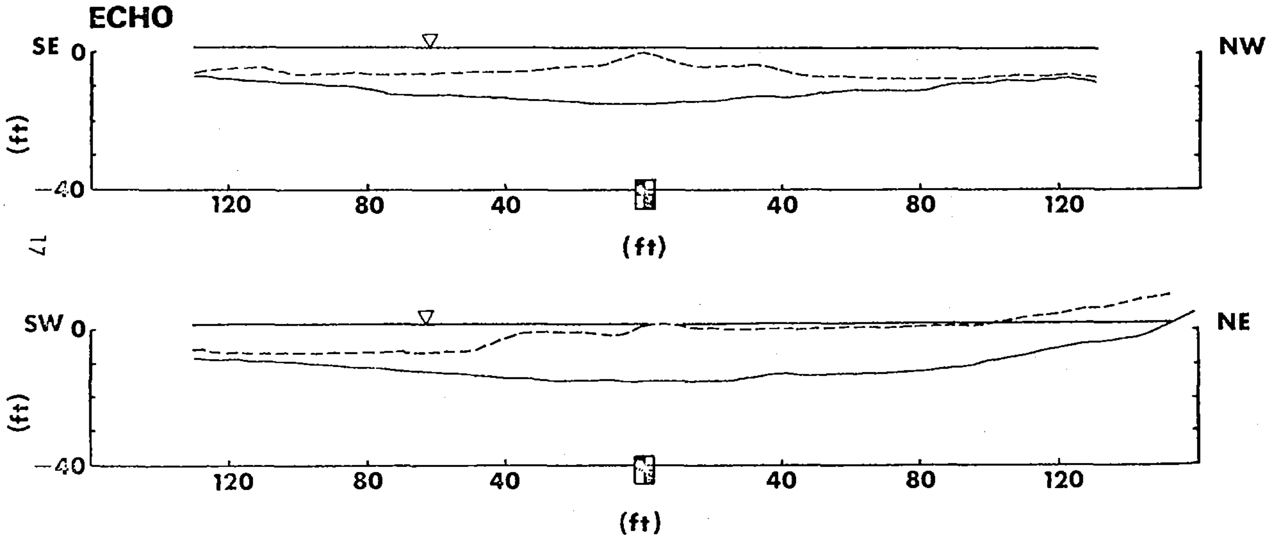

Figure 13. Project TUGBOAT, Phase I: ECHO crater cross section.

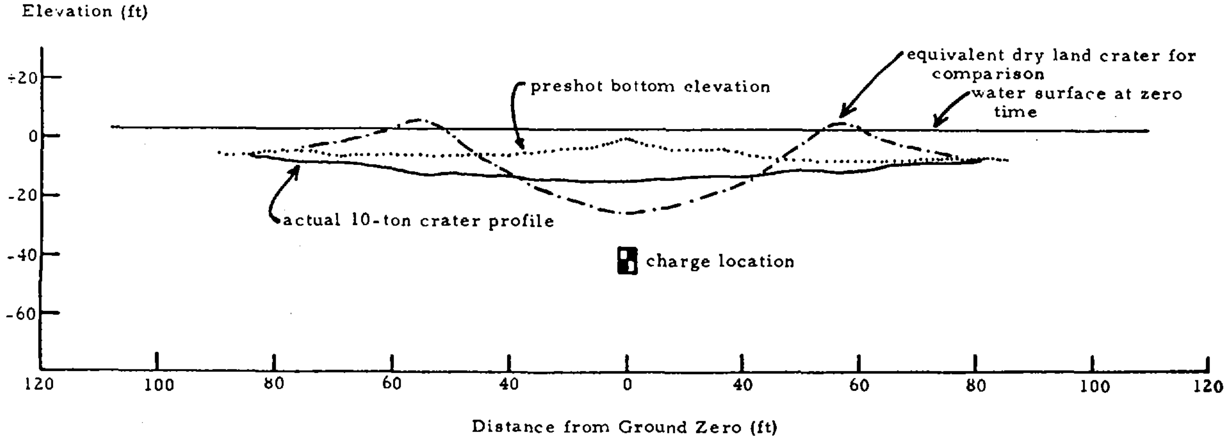

Figure 14. Profile of Project TUGBOAT, Phase I, 10-ton crater shown in comparison to an equivalent yield dry land crater.

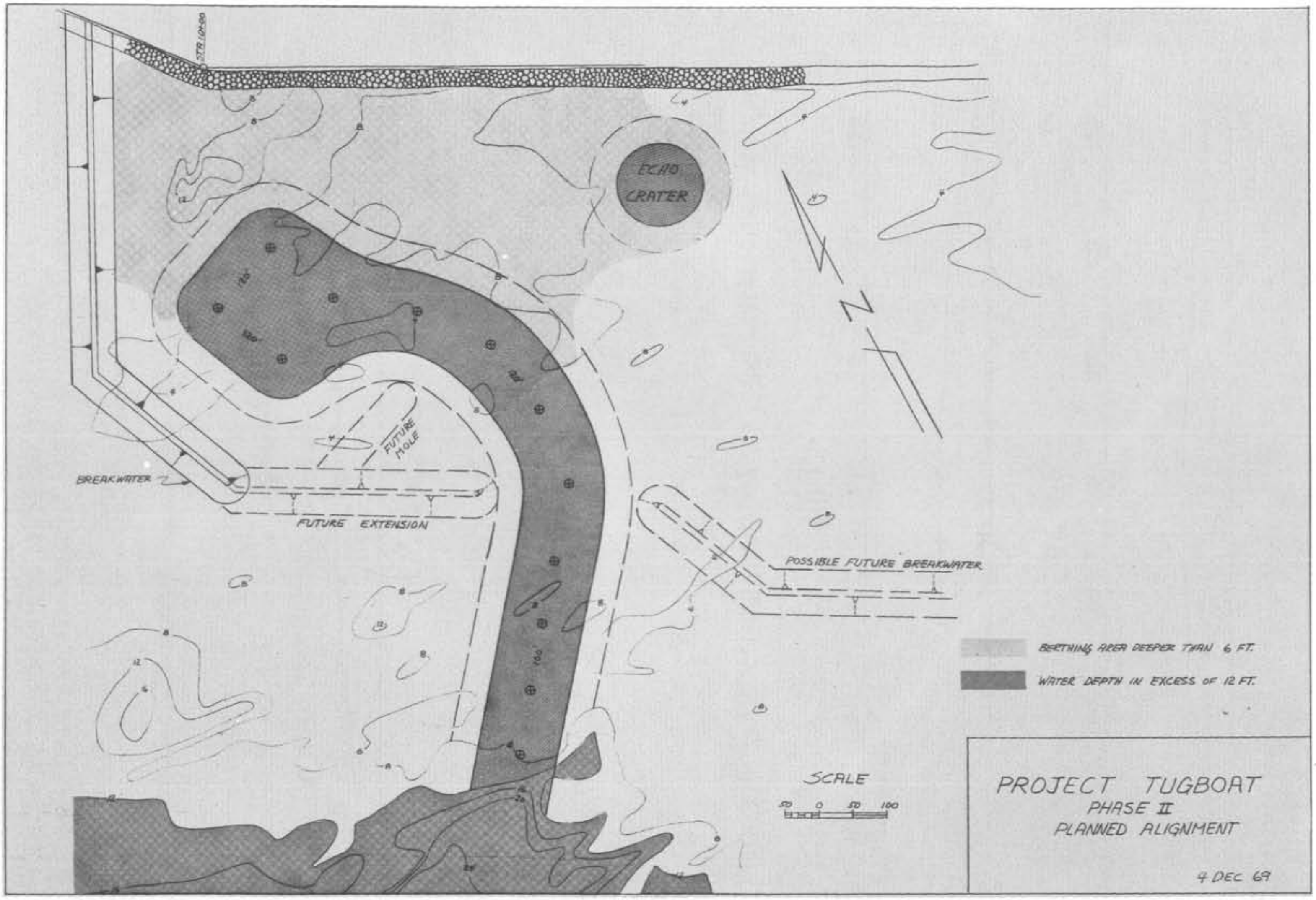

Figure 15. Project TUGBOAT revised design for Phase II, berthing basin and entrance channel excavation.

breakwater which will place a structural load on the near-crater area, something not yet attempted although necessary for many projected uses of explosive excavation, protect the cratered area for postshot material properties investigations and provide needed protection to the eventual harbor area.

FUTURE EXPERIMENTAL WORK

NCG plans to continue to conduct chemical explosive experiments in conjunction with Authorized Civil Works Projects to develop experience in all explosive excavation applications. As these experiments are conducted it is expected that the attendant publicity will generate wide interest and new projects, while at the same time making this new construction method acceptable as a routine alternative to be considered in the initial design phase of all large earthmoving projects.

The next major experiment under consideration involves the removal of a portion of Wayanda Ledge from the Sergius Narrows in Southeastern Alaska. Wayanda Ledge is an underwater rock mass which restricts navigation in a channel with existing very high tidal currents. The current general concept is to explosively remove a portion of the rock mass, depositing the broken rock in the deep portion of the channel. Site reconnaissance is under way at this writing. The material has been classed as a hard rock and will provide experience in excavation of a hard rock underwater. During a site calibration program at least one detonation will be planned to investigate the harbor concept originally planned for Project TUGBOAT; that is, a detonation in a competent medium in shallow water where the lip would provide protection for a harbor facility inside the crater.

NCG is also considering applying the experience in linear channel excavation to a river diversion and railroad relocation project in conjunction with the Trinidad Dam construction in southeastern Colorado. The required diversion channel is approximately 1700 ft. long. The depth of the cut required is approximately 38 ft. Several sidehill cuts are required for the railroad relocation. The medium at the site is classed as a low to moderate strength sandstone. This project will provide cratering calibration of a new medium (sandstone) and will provide practical experience in row excavation through slightly varying terrain and in connecting row design.

SUMMARY

As a result of the technology gained in NCG's experimental cratering work in the Plowshare Program, its mission has been expanded to include developing chemical explosive excavation technology. This mission is being accomplished by conducting chemical explosive experiments as part of Authorized Civil Works Construction Projects. Two recent experiments are contributing to this technology; Pre-GONDOLA III, Phase III, Reservoir Connection Experiment and a calibration series as part of Project TUGBOAT.

The Pre-GONDOLA tests, conducted over a period of four years, have produced data on excavation of weak saturated materials and on row crater formation characteristics and row crater connections. The most recent phase of the Pre-GONDOLA series was completed in October 1969, culminating in a reservoir-connection shot which created a linear channel connecting a previously excavated row crater to the Fort Peck reservoir. The channel connection resulted from detonation of five charges ranging in yield from five to thirty-five tons; the total charge was seventy tons.

Project TUGBOAT is designed to provide a portion of a planned small craft harbor in Kawaihae Bay, on the northwest coast of Hawaii. The project is being executed in three phases. Phase I was executed in November 1969; it consisted of five calibration shots in a coral medium overlain by several feet of water. The first four shots, at one-ton yield, produced craters very similar in shape and size to each other but very wide and shallow when compared to dry land experience. The craters had no lips. A single ten-ton detonation provided a scaling point for crater dimensions and for safety program measurements. The results of Phase I shots have been used to design the Phase II detonation of twelve ten-ton charges for entrance channel and berthing basin excavation, scheduled for April 1970. Because the craters were much larger than predicted, the project will be accomplished with about half the amount of explosives in the original design.

Future planned experiments include an underwater navigation hazard (rock) removal, river diversion channel excavation, and sidehill cuts for railroad relocation.

REFERENCES

1. Day, W. C.; "The Corps of Engineers Nuclear Construction Research Program", Nuclear Applications and Technology, Vol 7, pp. 253-268; September 1969.

2. Knox, J. B.; "Nuclear Excavation, Theory and Applications", Nuclear Applications and Technology, Vol 7, pp. 189-231; September 1969.

3. Kurtz, M. K. and Redpath, B. B.; "Project Pre-GONDOLA Seismic Site Calibration", PNE 1100; U. S. Army Engineer Nuclear Cratering Group, Lawrence Radiation Laboratory, Livermore, California; March 1968.

4. Cress, J. P., Lattery, J. E., Andrews, J. B., and Vortman, L. J.; "Project Pre-GONDOLA III, Phase I, Summary Report", PNE 1114; U. S. Army Engineer Nuclear Cratering Group, Lawrence Radiation Laboratory, Livermore, California; to be published.

5. Kurtz, M. K.; "Project Pre-GONDOLA I Technical Directors Summary Report", PNE 1102; U. S. Army Engineer Nuclear Cratering Group, Lawrence Radiation Laboratory, Livermore, California; May 1968.

6. Day, W. C., Kurtz, M. K., Steinhardt, G., Lattery, J., Frandsen, A. D., Redpath, B. B., and Cress, J.; "Project Pre-GONDOLA II Summary Report", PNE 1112; U. S. Army Engineer Nuclear Cratering Group, Lawrence Radiation Laboratory, Livermore, California; to be published.

7. Lattery, J. E., Steinhardt, G., Anderson, B., Reed, J., Andrews, J. B., Smith, G., Mickey, W., and Ballard, R.; "Project Pre-GONDOLA III, Phase II Summary Report", PNE 1117; U. S. Army Engineer Nuclear Cratering Group, Lawrence Radiation Laboratory, Livermore, California; to be published.

8. "Technical Concept for Project TUGBOAT; Explosive Excavation of Kawaihae Light Draft Harbor"; U. S. Army Engineer Nuclear Cratering Group, Lawrence Radiation Laboratory, Livermore, California; June 1969.

XA04N0758

RADIOACTIVITY FROM PLOWSHARE APPLICATIONS—SAFETY CONSIDERATIONS*

H. A. Tewes
Lawrence Radiation Laboratory, University of California
Livermore, California 94550

INTRODUCTION

When the Plowshare Program was first being seriously considered some 13 years ago, a number of applications immediately suggested themselves. However, it soon became obvious that most of these applications had the drawback of producing and distributing appreciable quantities of radioactivity to the environment. Thus, the Atomic Energy Commission, together with its contractors, formulated and put into effect a program aimed at dealing with this problem, both from the standpoint of reducing the amount of radioactivity released to the environment and understanding the impact of this radioactivity on the biosphere.

PLOWSHARE EXCAVATION PROGRAM

Comprehensive safety evaluations have been carried out in conjunction with that part of the Plowshare Program which involves the earth-moving uses of nuclear explosives. Since in these applications some radioactivity is released to the environment, it has been found necessary to formulate and seek to answer two key questions: (1) What is the distribution of the radioactivity resulting from these kinds of nuclear detonations? and (2) What is the impact of this radioactivity on man?

In the course of answering the first question, it is first necessary to understand the production of radioactivity from the nuclear explosives. During the past several years, a concerted program has been underway to design and test progressively "cleaner" nuclear excavation explosives. Not only is the amount of radioactivity produced per kiloton of yield being reduced, but a conscious effort is being made to select the materials used in explosive construction so that the radionuclides formed in the detonation will be those least objectionable from a radiobiological standpoint. Calculational techniques have been developed which enable an accurate estimate to be made of the total radionuclide inventory resulting from the detonation of a Plowshare explosive,[1,2] and which allow a reliable assessment to be made regarding the beneficial or detrimental effect of a proposed design change.

Once the total production of radioactivity by an excavation explosive, or the radioactivity "source term," can be reliably calculated, it is essential to gain an ability to predict the way in which this radioactivity is distributed once a detonation has taken place. This, then, involves a better understanding of the venting process during which the radioactivity is distributed into three environmental "compartments." One portion is injected into the atmosphere as

---

*Work performed under the auspices of the U. S. Atomic Energy Commission.

a long-range cloud; another portion remains as local fallout. Finally, an appreciable fraction remains in, or around, the crater as fallback and ejecta.

The existing predictive capability for ascertaining what fraction of the radioactivity produced goes into each of these three compartments is being steadily improved through more realistic modelling, and hopefully through computer simulation of the venting process.[3] While a satisfactory semi-empirical method[4] is currently being used in safety analyses for estimating the fractions of radioactivity which will appear in each of the three compartments, a more elegant theoretical approach is currently being formulated.

Once the fraction of radioactivity present in local fallout has been predicted, it is possible to calculate a fallout pattern which can be used for safety predictions. This is accomplished by using appropriate inputs for: climatology (turbulence and wind speed as a function of altitude); distribution of the radioactivity on debris of different particle size; and initial cloud configuration. The KFOC code[5] developed at the Lawrence Radiation Laboratory is currently being used for such calculations and has been found to be quite accurate in its predictions, as can be seen from a number of published results[5,6] which compare computational results with observations. With regard to the radioactivity present in the long-range cloud, Crawford[7-10] has developed a diffusion model which enables the cloud concentrations to be estimated as a function of time, and which also provides a capability for determining the deposition of material from the cloud over considerable distances from the detonation site. With regard to the radioactivity remaining in and around the crater, recent work by Koranda and his collaborators[11-13] has elucidated the distribution of this radioactivity within the ejecta material and the crater. Ancillary work[14,15] by other members of the Lawrence Radiation Laboratory Biomedical Division have enabled accurate assessments to be made regarding the availability of the radionuclides in this material to the biosphere. Thus, the current predictive capability for the distribution and biological uptake of the radioactivity from cratering experiments being conducted at the Atomic Energy Commission's Nevada Test Site are relatively good. However, a number of important unanswered questions remain with regard to radioactivity from Plowshare cratering applications, as differentiated from experiments.

One of the potential difficulties arises from the nature of the Nevada Test Site. It is representative of a desert environment, and, to date, no nuclear cratering experience has been gained by us in any other milieu. Thus it would be most desirable to obtain data from a detonation carried out in a saturated environment, similar to that which might be expected in a region where canals or harbors are to be constructed. The effect of a nuclear detonation in this new environment is as yet not known to us, and can only be inferred. The necessity for a nuclear detonation in a wet environment arises out of the need to determine possible hazards which may arise in an estuarian or marine environment subsequent to a large-scale nuclear application conducted in an area of this sort. Again, work has been done with regard to the availability to marine organisms of the radionuclides in debris from cratering experiments,[12,16] but it is not clear that such results would be directly applicable to the situation that might prevail following a detonation in an actual wet environment. It should be emphasized here that, while adequate information may not exist for the preparation of a safety analysis representing the "most probable" consequences of a nuclear cratering detonation, a conservative "worst case" safety study can be formulated. Such a "worst case" analysis will inevitably result in a large and costly safety program, geared to guard the public against hazards which may be quite unrealistic. Therefore, additional knowledge gained from experimental detonations in other than desert environments will allow the reduction of safety costs without increasing the risk to the public, and will make Plowshare canal and harbor projects more attractive economically.

While we have discussed gaps in knowledge relating to the effect of radioactivity in a marine environment, we should not neglect the areas of concern with regard to the terrestrial environment. Although the forage-to-cow-to-milk food chain pathway has been clearly elucidated for a number of radionuclides,[17] and while the soil-root pathway for the introduction of radionuclides to man has been considered extensively, there still exist a myriad of possible food chains through which radioactivity could be ingested by either large groups of the population, or possibly, by only a few people. Since the well-being of all is a primary concern of the Plowshare Program, continued support must be given to the assessment of radiological hazard by means of both probable and improbable paths of introduction, again with the objective of formulating minimum cost safety programs which are still in accord with the letter and spirit of FRC directives.

PLOWSHARE UNDERGROUND ENGINEERING PROGRAM

Up to this point we have considered a few of the aspects of the Plowshare excavation program which would seem at first glance to require the most intensive study with regard to the introduction of radioactivity into the environment. However, a number of questions also exist with regard to the radiological safety of underground engineering applications and experiments; exhaustive reviews of such questions have taken place in the course of both the Gasbuggy[18] and Rulison[19,20] Events. In these cases the key questions are: (1) What is a short-term radiological safety problem? and (2) What long-term problem exists relating to product contamination which may then result in radioactivity being introduced into the environment? The first question can be re-stated in the form: What chance is there that an appreciable fraction of the radioactivity resulting from an underground nuclear explosion may be injected rapidly into the environment through some sort of venting? Thus, this question is closely related to some of those which are raised with regard to an excavation experiment. However, by its very nature, an underground engineering explosive is considerably different from one used for excavation. In many cases, the types of radioactivity which are produced are significantly different because of the concern for product contamination. When gas or oil stimulation applications are being considered, there is a desire to minimize the amount of tritium available for incorporation into the organic product. For this reason, a thermonuclear explosive would be inappropriate, and a fission explosive must be employed. Consequently, should appreciable venting take place upon the detonation of an explosive of this sort, the contamination problem resulting to the immediate environs could be significant. Thus, we must be assured that the chance of appreciable venting from underground engineering applications is exceedingly small. Unfortunately, although a large number of tests have been carried out at the Nevada Test Site in a contained configuration, the results of a number of these are not truly applicable to proposed Plowshare applications. The basic reason for this lack of applicability is that comparing weapons development tests conducted in the interest of national defense with a Plowshare experiment can be like comparing apples and oranges. That is, it is possible that during a weapons test in an isolated area, a certain small risk of venting may be tolerated if assurances can be given that radiation levels offsite will not result in unacceptable exposures to people. Such a risk could not be justified in the case of a Plowshare experiment. Thus, Plowshare applications are envisaged as having adequate and tested stemming, and as being buried at extremely conservative depths; much deeper than those at which complete containment has been observed at the Nevada Test Site.

Consequently, the estimation of a "maximum credible vent" from a Plowshare underground engineering application is possibly as difficult as is the formulation of a maximum credible accident from a nuclear reactor. Here, we are obviously on the horns of a dilemma. While it is felt that the venting of appreciable quantities of radioactivity is very unlikely, yet an appropriate safety program must be employed so that if the "maximum credible vent" should occur, adequate safety precautions could be taken that would prevent the exposure of inhabitants in the area to unacceptable quantities of radioactivity. To date, a realistic safety model has not been used for underground engineering experiments. We have been using an extremely conservative model representing one of the worst ventings ever observed at the Nevada Test Site—where the scaled depth of burst was relatively shallow and the yield was relatively low. As more applicable experience is obtained with actual Plowshare underground engineering detonations, a more realistic approach will be possible while still insuring public safety.

Similar conservatism is used when reentry drilling is carried out subsequent to a detonation. The assumptions which are employed in the calculation of possible radiation exposures to persons in the vicinity of the detonation site include minimal atmospheric diffusion of the effluent, sudden and massive releases of contaminated gas, and complete mixing of all the radioactive inventory with the vented "vehicle" gases.

The other area of concern with regard to underground engineering safety is the product contamination of materials which are exposed to the radioactive environment produced by the detonated explosive. This is exemplified by the tritium which appears in natural gas from a well stimulated by a nuclear explosion. Although appropriate standards for tritium levels in natural gas have not as yet been formulated, it is obvious that the amount present should be reduced to the lowest possible level. The current approach to accomplishing this objective is three-pronged. First of all, explosives can be designed so as to minimize tritium production; secondly, controlled gas flaring can be continued until the concentration of radioactivity in product reaches acceptable levels; and finally, as will be reported later in this meeting, studies have been made on the possible decontamination of the products formed in these environments by chemical engineering methods.[21] While no actual data as yet exist with regard to the effectiveness of product decontamination, as the need for such a process becomes greater to insure economical utilization of Plowshare explosives, appropriate studies will undoubtedly be undertaken.

It should be obvious from the foregoing discussion that a primary concern of the Plowshare Program is to maintain the safety of the public, no matter what the application of the nuclear explosive may be. However, in order to adequately protect the public (of this country or of any country where the Plowshare Program may find an application) we must set appropriate standards for radioactivity present in the biosphere, or for radionuclide burdens within the human body. As you know, the International Commission on Radiological Protection,[22] and various other national[23,24] and international[25] bodies have formulated radiation exposure standards which are continually being carefully examined in the light of expanding knowledge. However, to date no data exist which unequivocally characterize the effects of low doses of radiation delivered at extremely slow rates to the human body. All standards to date have been evaluated by extrapolating data obtained from high doses of radiation delivered at relatively high rates to experimental animals and, in a few cases, from results of nuclear accidents to humans. Although these models are considered by some to be extremely conservative because of the nature of the extrapolation, other investigators feel that present radiation protection guidelines are too liberal and may need to be revised downward.[26]

Whether or not reductions in radiation exposure standards are appropriate is beyond the scope of this presentation. However, whatever radiation safety standards are set on the basis of experimental data and considered judgment of competent authorities, these standards are those which obviously will be applied to potential Plowshare projects. These standards must be met, whether it be by explosive design changes or by appropriate treatment of the products stimulated by nuclear explosions, in order for the Plowshare Program to become a viable force in future technology.

Finally, in order to accurately assess the desirability of the Plowshare Program, one must balance the advantages which accrue from the use of nuclear explosives for peaceful purposes against the possible detrimental effects of radiation.

Recent papers[27,28] have been written dealing with some possible methods of evaluating risk versus benefit; hopefully, these or some other approaches will allow an objective assessment to be made of the appropriateness of the various proposed uses of nuclear energy for peaceful purposes.

Although it is relatively easy to assign a monetary value to the benefit from a particular project, the risk has never been expressed in terms which permit a meaningful comparison to be made. Cohen's[27] approach considers that $250 worth of somatic and genetic damage results from the exposure of one person to one rem of radiation. Perhaps this approach is overly simplified, or can be attacked for other reasons; however, such an evaluation is badly needed—not only for the Plowshare Program, but for any operation which affects people and their environment. If a better criterion can be developed, it should by all means be developed with the greatest possible dispatch.

REFERENCES

1. H. A. Tewes, "Radioactivity Source Terms for Underground Engineering Applications," in Proc. Symp. Public Health Aspects of Peaceful Uses of Nuclear Explosives, SWRHL-82, Las Vegas, Nev., April 7-11, 1969, pp. 207-222.
2. R. M. Lessler, "Reduction of Radioactivity Produced by Nuclear Explosives," Proc. Fourth Plowshare Symp., Jan. 14-16, 1970, to be published.
3. J. B. Knox *et al.*, "Radioactivity Released from Underground Nuclear Detonations: Source Transport, Diffusion, and Deposition," Lawrence Radiation Laboratory, Livermore, UCRL-50230, 1967.
4. J. B. Knox, private communication.
5. J. B. Knox, "Prediction of Fallout from Subsurface Nuclear Detonations," 5th Atomic Energy Commission Symp. Radioactive Fallout from Nuclear Weapons Tests, 1965, pp. 331-353.
6. J. B. Knox, Nucl. Applications Tech. 7, 189 (1969).
7. T. V. Crawford, "A Computer Program for Calculating the Atmospheric Dispersion on Large Clouds," Lawrence Radiation Laboratory, Livermore, UCRL-50179, 1966.
8. T. V. Crawford, "Predicting and Sampling Nuclear Clouds from the Viewpoint of Diffusion Theory," Lawrence Radiation Laboratory, Livermore, UCRL-14983, 1966.
9. T. V. Crawford, "The Long-Range Diffusion of the Effluent Cloud from the Phoebus, 1B EP-IV Reactor Test of February 23, 1967," Lawrence Radiation Laboratory, Livermore, UCRL-50418, 1968.
10. T. V. Crawford, "Diffusion and Deposition of the Schooner Clouds," Proc. Fourth Plowshare Symp. Jan. 14-16, 1970, to be published.
11. J. J. Koranda, "Residual Tritium at Sedan Crater," Lawrence Radiation Laboratory, Livermore, UCRL-70292, 1967.
12. L. R. Anspaugh *et al.*, "Bio-Medical Division Preliminary Report for Project Schooner," Lawrence Radiation Laboratory, Livermore, UCRL-50718, 1969.

13. J. J. Koranda et al., "Postshot Distribution and Movement of Radionuclides in Nuclear Crater Ejects," Proc. Fourth Plowshare Symp., Jan. 14-16, 1970, to be published.
14. "Program Book for the Advisory Committee for Biology and Medicine of the U. S. Atomic Energy Commission," Lawrence Radiation Laboratory, Livermore, UCRL-14739, Part 2, 1966.
15. Y. C. Ng, "Estimation of the Internal Dose to Man from the Radionuclides Produced in a Surface Explosion of a Nuclear Device," Lawrence Radiation Laboratory, Livermore, UCRL-70894, 1968.
16. F. L. Harrison, "Radioactive Debris from Underground Nuclear Explosions: 1. Physical and Chemical Characteristics; 2. Biological Availability of the Radionuclides to Aquatic Animals," Lawrence Radiation Laboratory. Livermore, UCRL-50596, 1969.
17. "Prediction of the Maximum Dosage to Man from the Fallout of Nuclear Devices," Lawrence Radiation Laboratory, Livermore, UCRL-50163, 1968.
18. "Project Gasbuggy Planning and Program Directive," U. S. Atomic Energy Commission, Nevada Operations Office, August 1967.
19. "Project Rulison Feasibility Study," Austral Oil Company, Inc., and CER-Geonuclear Corporation,
20. "Project Rulison Definition Plan," CER-Geonuclear Corporation, March 26, 1969.
21. J. A. Wethington, "Possible Decontamination of Consumer Products from Gas Wells Stimulated by Nuclear Explosions," Proc. Fourth Plowshare Symp., Jan. 14-16, 1970, to be published.
22. Recommendations of the International Commission on Radiological Protection, ICRP Publ. 1-9 (Pergamon Press, London, 1959-1966).
23. Radiation Protection Guidance for Federal Agencies, Federal Radiation Council Rept. No. 1, Washington, 1960; Selected Radiation Protection Guides, Federal Radiation Council Rept. No. 2, Washington, 1961.
24. "Maximum Permissible Body Burden and Maximum Permissible Concentrations of Radionuclides in Air and Water for Occupational Exposure," Natl. Bur. Std. (U.S.) Handbook 69, 1959.
    "Somatic Radiation Dose for the General Population; Ad Hoc Committee Report of the National Committee on Radiation Protection and Measurements," Science 131, 482 (1960).
25. "Basic Safety Standards for Radiation Protection," International Atomic Energy Agency, Safety Series, Publ. 9, Vienna, 1962.
26. J. W. Gofman and A. R. Tamplin, "Low Dose Radiation, Chromosomes, and Cancer," 1969 IEEE Nucl. Sci. Symp., October 29, 1969.
27. J. J. Cohen, "The Plowshare Program: A New Challenge for the Health Physicist," 14th Annual Meeting of the Health Physics Society, Pittsburgh, Pa., June 1969.
28. C. Starr, "Social Benefit versus Technological Risk," Science 165, 1232 (1969).

XA04N0759

DIFFUSION AND DEPOSITION OF THE SCHOONER CLOUDS*

Todd V. Crawford
Lawrence Radiation Laboratory, University of California
Livermore, California 94550

ABSTRACT

Schooner was a 31-kt nuclear cratering experiment done as part of the U. S. Atomic Energy Commission's Plowshare Program.

Detonation was at 0800 PST on December 8, 1968 at the Nevada Test Site. The resulting cloud had ceased its dynamic growth by about H+4 min. Two distinct parts, a base surge and a main cloud, were evident. Thereafter, further cloud growth was by diffusion and fallout as the cloud moved downwind.

Aircraft sampling of the cloud at H+12.5 min revealed that the main cloud part contained about 10 times as much radioactivity as the base surge part. Later aircraft data, local fallout field measurements, and airborne particle size data indicate that the H+12.5-min cloud burdens, primarily the tungsten isotopes, were depleted by a factor of about 2, due to fallout, over the next few hours.

The remaining airborne cloud burdens for each cloud were used as input to diffusion calculations. Calculated main cloud center concentrations using observed cloud sizes, cloud burdens. and meteorology agree with measurements to better than a factor of 2 over $1\frac{1}{2}$ days. These postshot calculations and data are about a factor of 3 higher than calculations done preshot. Base surge calculations are consistent with available data to within about a factor of 4, but the data needed to perform as complete an analysis as was done for the main cloud do not exist.

Fallout, as distinguished from deposition of nonfalling debris, was important to a distance of about 500 km for the main cloud and to a distance of about 100 km for the base surge. At distances closer to ground zero, diffusion calculations under-predicted ground level concentration and deposition, but an isotopically scaled external gross gamma fallout calculation was within about a factor of 3 of the data.

At larger distances downwind for the base surge, ground level exposure rate calculations and deposition for a variety of nuclides agree to within about a factor of 3 of measurements.

INTRODUCTION

Schooner was a nuclear cratering experiment in a layered tuffaceous medium executed as part of the Plowshare Program for the development of

---

*Work performed under the auspices of the U. S. Atomic Energy Commission.

nuclear excavation. Schooner was detonated on December 8, 1968 at approximately 0800 PST at the Nevada Test Site. The yield was 31 ± 4 kt. The emplacement hole was at 116°33'57"W and 37°20'36"N. Surface ground zero (GZ) was 5562 ft above MSL.

The purpose of this paper is to describe the cloud which resulted from this detonation, the radioactive content of the two distinct parts of the cloud, their general paths, and to compare concentration measurements at cloud center and at ground level with calculations. In addition, deposition of a few nuclides will be examined out to several hundred kilometers.

INITIAL CONDITIONS

Following detonation of the Schooner device, the ground surface in the vicinity of GZ was observed to mound in the manner expected from previous cratering experiments. The first evidence of gas venting through the rising mound occurred at approximately 1.75 sec. At this time the mound had reached a height of about 270 ft above the original ground level. During the next minute or two, two distinct clouds were formed. The energy released by the venting of cavity gases to the atmosphere resulted in a main cloud which rose to a height of about 13,000 ft above ground surface. A base surge cloud was formed as the dust and dirt resulting from the excavation began to settle back to the ground surface. The top of the base surge cloud was about 2200 ft above the ground. Further vertical growth of the base surge cloud was limited by a temperature inversion whose base was about 2200 ft above the ground. Obviously, the energy content of the main cloud was sufficient to penetrate this temperature inversion. The dynamic growth, due to the energy released in the explosion, of both clouds had ceased by H+4 min.

The main cloud immediately started moving towards the ENE under the influence of winds which ranged from 14 knots at about 12,000 ft MSL to 33 knots at 16,000 ft MSL. The base surge cloud started moving towards the N under the influence of southerly winds of 5-10 knots. The H+4 min cloud sizes are summarized in Table I. In Table I the bottom of the main cloud is considered to be coincident with the top of the base surge.

Table I. Cloud dimensions at stabilization. Ground zero elevation = 1700 m.

	Main Cloud	Base Surge
Diameter (m)	2420	4220
Top above ground (m)	4000	670
Cloud center above ground (m)	2335	335

At H+12.5 min, a flight of five B-57 sampling aircraft penetrated the cloud. Three aircraft penetrated the main cloud and two aircraft penetrated the base surge. Exposure rate data were obtained on these penetrations. The filters exposed were returned to the Lawrence Radiation Laboratory where isotopic analysis was done for a variety of radionuclides. Knowing the total elapsed time in the cloud, as noted by the pilot when he penetrated and exited the visible cloud, and knowing the flow rate of air through the filter system, it is possible to calculate the air concentration of different radionuclides. Using visual and photographic measurements of cloud geometry it is possible to calculate the total cloud burden from the concentration data. These isotopic cloud burdens are presented in Table II.[1] Concentrations determined from aircraft samples within the same cloud varied from a few percent to about a factor of 2. To obtain a mean concentration for the whole cloud, a geometric average of all concentration measurements in that cloud was used. The cloud volume estimates were calculated from several sets of airborne photographs and from ground-mounted cameras. At H+12.5 min, volumes of 4×10^{10} m^3 for the main cloud and 1.5×10^{10} m^3 for the base surge were obtained. These are probably accurate to somewhat better than a factor of 2. Thus it is considered that the numbers in Table II represent the cloud burdens at H+12.5 min to an accuracy of about a factor of 2.

Table II. H+12.5-min cloud burdens.

Nuclide	Main Cloud Total Ci[a]	Base Surge Total Ci
Na^{24}	(6.4×10^4)[b]	(5.0×10^3)
Mn^{54}	(3.6×10^2)	(24)
Co^{57}	1.6×10^2	(17)
Co^{58}	(1.0×10^3)	(8.1×10^1)
As^{74}	(1.4×10^3)	1.4×10^2
Y^{88}	(2.1×10^2)	(12)
Mo^{99}	4.6×10^3	3.4×10^2
Ru^{103}	1.04×10^3	8.2×10^1
Te^{132}	1.16×10^4	9.8×10^2
I^{131}	3.8×10^3	3.2×10^2
Cs^{137}	3.46	1.3
Ba^{140}	1.6×10^3	2.2×10^2
Ce^{141}	3.0×10^2	24
Nd^{147}	2.5×10^2	14
Ta^{183}	(2.3×10^3)	1.9×10^2
W^{181}	3.2×10^5	3.3×10^4
W^{185}	9.2×10^5	1.0×10^5
W^{187}	1.56×10^7	1.6×10^6
Au^{196}	8.4×10^3	6.6×10^2
Pb^{203}	1.9×10^4	1.7×10^3
U^{237}	1.8×10^3	9.0×10^1

[a] Zero time Ci.

[b] Nuclide identified but analysis error is 10 to 20%.
Main cloud volume used = 4×10^{10} m^3.
Base surge cloud volume used = 1.5×10^{10} m^3.

As a separate check on the above methods of estimating cloud burdens, a parachute-borne air sampling program was conducted on Schooner.[2] The objective was to drop small parachute-borne samplers through the cloud from above. Each sampler would obtain a vertical integral of the cloud. Knowing the horizontal extent over which the parachute samples were dropped and the vertical path length, one could define a "box." If one had enough samples to get statistically representative concentration measurements throughout this "box," then it would be possible to calculate total airborne cloud burden without knowing the exact cloud geometry.

To accomplish the above objectives a total of 314 parachute-borne samplers were dropped from five C-130 aircraft. The drops occurred on two separate overflights at H+30 min and at H+1 hr; 260 of the samplers were successfully recovered and analyzed within a month after detonation.

The most complete set of data was obtained from the main cloud at H+1 hr, although the five aircraft did not fly over the leading edge of the cloud. Thus, the leading 15-20% of the cloud volume was missed in the sampling. However, taking the data obtained from the remainder of the cloud and extrapolating it forward to the leading edge results in a cloud burden between 2.5 $\times 10^5$ Ci and 1×10^6 Ci for W^{181} at H+1 hr for the main cloud. The H+12.5 min main cloud contained 3.2×10^5 Ci of W^{181} based on the B-57 sampling. Although this number should be depleted somewhat by fallout between H+12.5 min and H+1 hr, it falls within the range of values obtained with the parachute samplers. Considering the factor of 2 accuracy of the cloud volume estimates and the differences in sampling and counting systems, this is considered adequate agreement.

One of the main objectives of obtaining cloud burden information, such as that presented in Table II, is to provide a source term for cloud diffusion calculations. Diffusion calculations are used to predict the dilution of the clouds over a time period of a few days. A sampling time of H+12.5 min is early in the history of the cloud if one is concerned about the burden which is going to stay airborne for a long time. At H+12.5 min considerable material is still airborne which will appear in the local fallout pattern. In fact, if one examines the Schooner fallout field, one finds that about half the total activity which was deposited in local fallout fell at a distance further downwind than the cloud location at H+12.5 min. This implies that about half of the material which was airborne at the time of the above sampling appeared in the fallout pattern. In addition, a particle size study[3] of the material collected on the filters exposed in the cloud at H+12.5 min showed that about one-half of the total activity was associated with particles larger than 12 μ in diameter. Particles of this size and smaller have terminal velocities equivalent to large-scale vertical motions in the atmosphere and generally are not considered as falling. An independent comparison of main cloud concentration measurements at around H+3 to 4 hr and the concentrations which were measured at H+12.5 min also indicated a decrease of about a factor of 2 in burden, which is not explained by diffusion. Therefore, in the diffusion calculations which follow, the source terms used were one-half of those in Table II. This factor-of-2 fallout after H+12.5 min was assumed for both clouds, although data are only available to strongly defend it for the main cloud. The only data to defend this factor of 2 for the base surge is that the particle size distributions were about the same for both clouds.

Figure 1 shows the general path of both the base surge and the main cloud parts of the cloud. The calculations and measurements to follow will deal separately with the base surge and main cloud. However, Fig. 1 clearly implies that there was some debris spread between the paths of the two distinctive parts of the cloud.

MAIN CLOUD

The initial cloud size (Table I), one-half of the cloud burdens of Table II, and the along-track meteorology were used to develop input to diffusion calculations with the computer code 2BPUFF.[4] Meteorological input to the calculations were turbulence parameters based on an analysis of the winds, cloud altitude, and thermal structure of the atmosphere along the main cloud trajectory. Input data were prepared in much the same manner as has been done by this author in previous case studies.[5-7] This computer code was primarily developed to predict cloud center concentrations for times of a few days. Such a calculation for the Schooner main cloud is presented as Fig. 2.

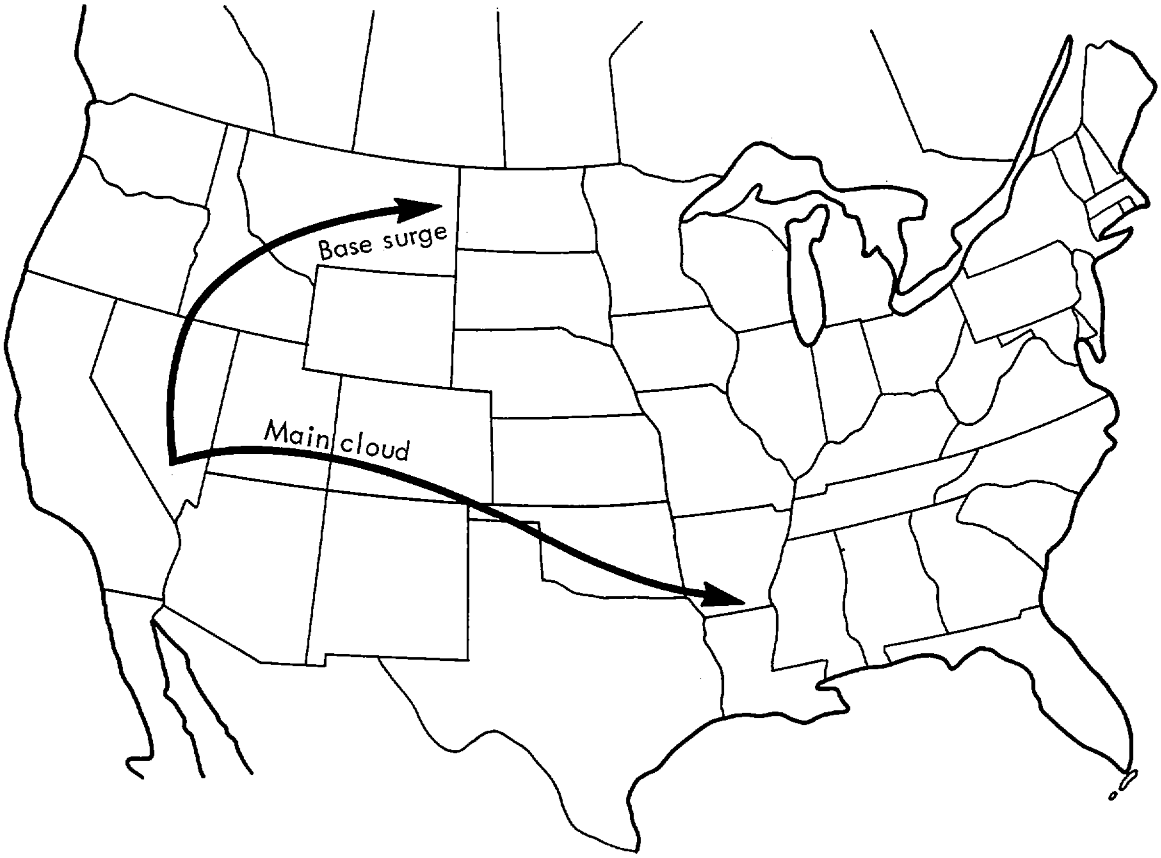

Fig. 1. General path of Schooner base surge and main clouds.

The calculated curves on Fig. 2 include radioactive decay and atmospheric dilution. Total radioactivity was obtained by adding all of the significant induced activities to the total fission products. Each was appropriately decayed with time. The diagnostic curve is a predicted cloud center concentration as a function of time, using the observed cloud sizes, cloud burdens, and along-track meteorology as discussed previously. The 120-km path average is also from the diagnostic calculation, but simulates the use of a sampling aircraft whose filter was first exposed at 60 km from the cloud center, and whose exposure was stopped at 60 km the other side of the cloud center. This is consistent with a sampling time of 20 min on an aircraft flying at 200 knots. At times of an hour or two, this is obviously too long an averaging path. The cloud is visible at these times. Over times of a few hours to 20 hr these types of filter exposure times are sometimes used and their effect, as seen on Fig. 2, can influence the type of data obtained.

The climatological curve on Fig. 2 is a calculation for the cloud center done months before the Schooner execution using preshot estimates of cloud burdens, cloud sizes, and climatology for the along-track meteorology. The open circles on this figure refer to exposure rate measurements. The pCi/m^3 concentration numbers on the left of Fig. 2 are converted to exposure rates on the right-hand side of Fig. 2 by using the assumption that one is in the middle of an infinite cloud of uniform concentration where the mean radionuclide gamma disintegration energy is 0.5 MeV. The solid dots are filter data. Only data which are considered to be reasonably representative of the Schooner main cloud are entered on Fig. 2. There are much more data which are not entered. The use of the word "representative" here refers to the location at which the sample was collected relative to the location of the main body of the debris. There is always the problem of being at the right place at the right time to get a "representative" sample. Now, obviously not all of

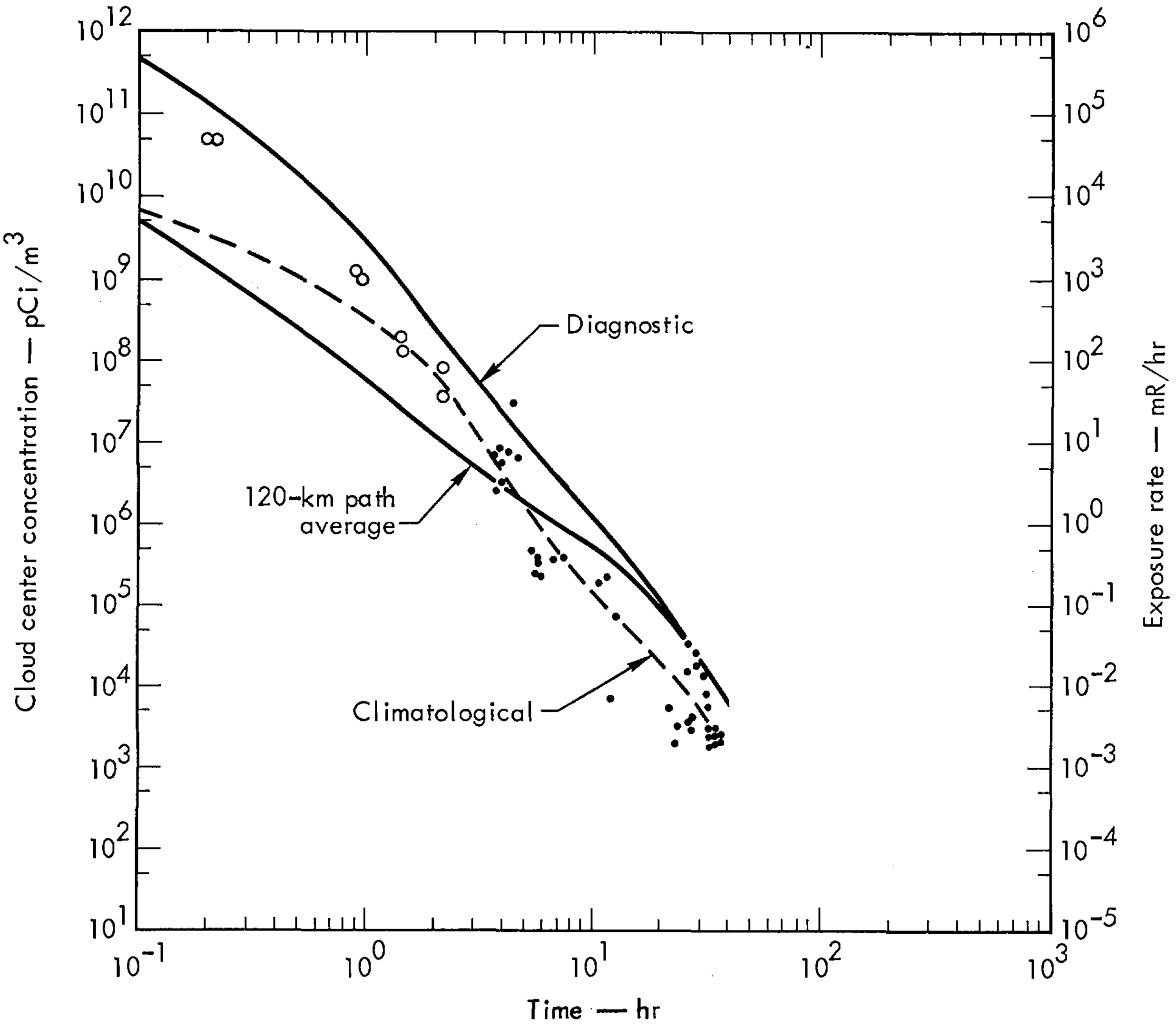

Fig. 2. Main cloud center total concentration as a function of time.

the data on Fig. 2 represents samples taken at the right place at the right time. However, there are enough data available to be reasonably sure that the high values at any one time are quite close to those which would be expected in the cloud center. As 2BPUFF calculations are for cloud center, one would expect the curves to be slightly above the uppermost data points. This seems to be the case for the diagnostic calculation. It should be emphasized here that the diagnostic calculations are not fitted to the late-time concentration data. They are done by using only the initial cloud burdens, cloud size, and along-track meteorology.

The difference between the climatological and the diagnostic calculations are one of initial cloud size, initial cloud burdens, and along-track meteorology. Even here we note that at times of 30 to 40 hr, the diagnostic calculation and the data are only about a factor of 3 above the climatological calculations.

Figure 3 presents the W^{187} calculations and data as a function of time for the Schooner main cloud. The nomenclature on this figure is the same as the previous one. There are fewer data points on Fig. 3 than on Fig. 2 because not all filters are analyzed isotopically. However, it is of interest to

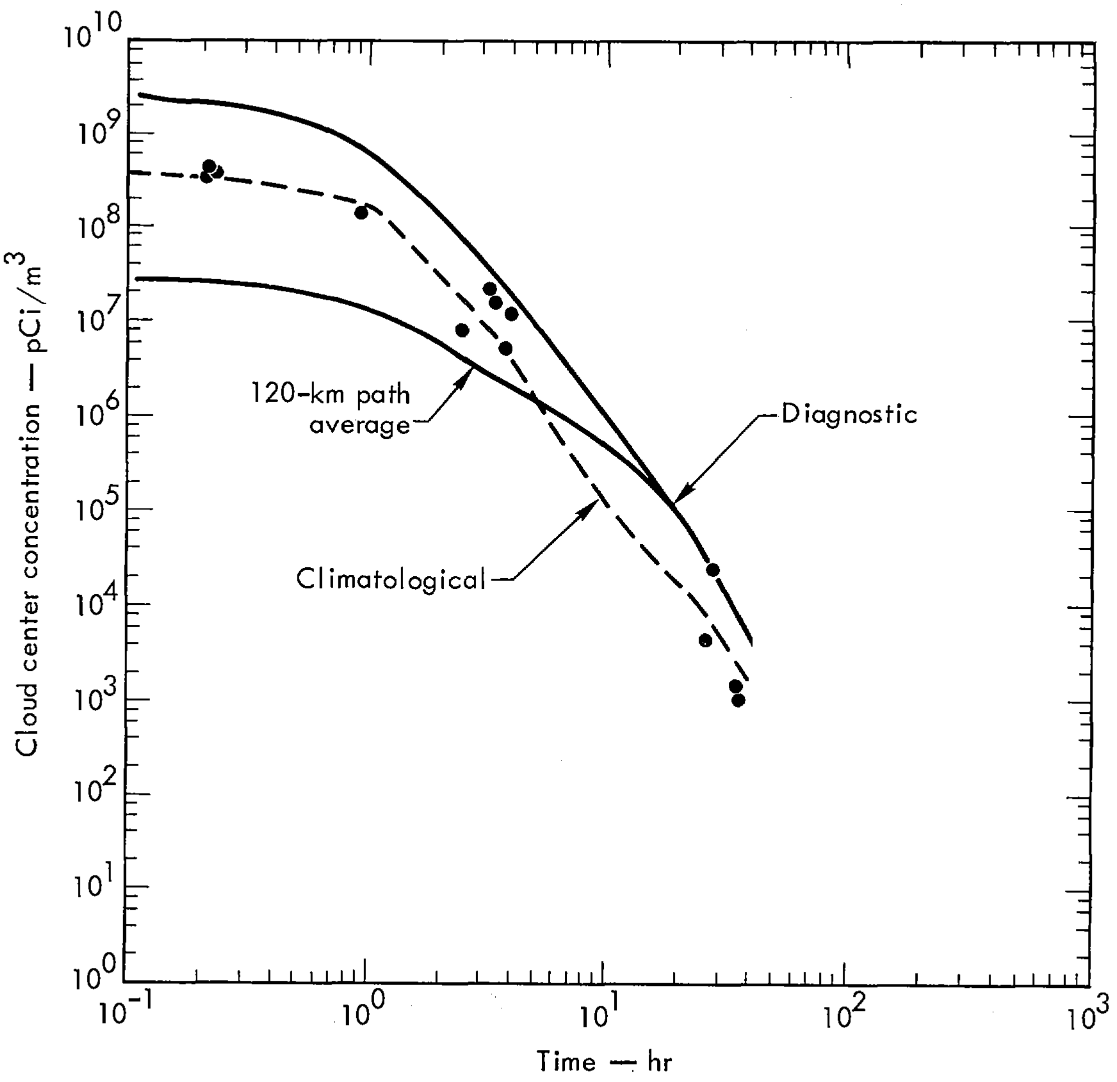

Fig. 3. Main cloud center W^{187} concentration as a function of time.

present these data, as the W^{187} isotope would be expected to dominate the total activity at times of about H+5 to about H+100 hr. This is illustrated by a comparison of Figs. 2 and 3. At lates times, W^{181} and W^{185} would become more important than W^{187} because of the 24-hr half-life of the latter nuclide. The W^{185} concentrations as a function of time are presented in Fig. 4 for the Schooner main cloud.

Now, on these three figures the diagnostic calculation was quite close to the peak values observed on Schooner at times of H+3 to H+40 hr. At earlier times, concentrations obtained with filters are somewhat lower than calculated cloud center concentration due to the filter being a line-average across a fairly small cloud. At late times, particularly after about 15 hr, the calculated concentration is relatively uniform across the cloud center. This is illustrated by the approach of the 120-km path average to the cloud center calculations at this time.

Ground-level concentrations are also calculated with 2BPUFF. Schooner provided the first opportunity to test these kinds of ground-level calculations

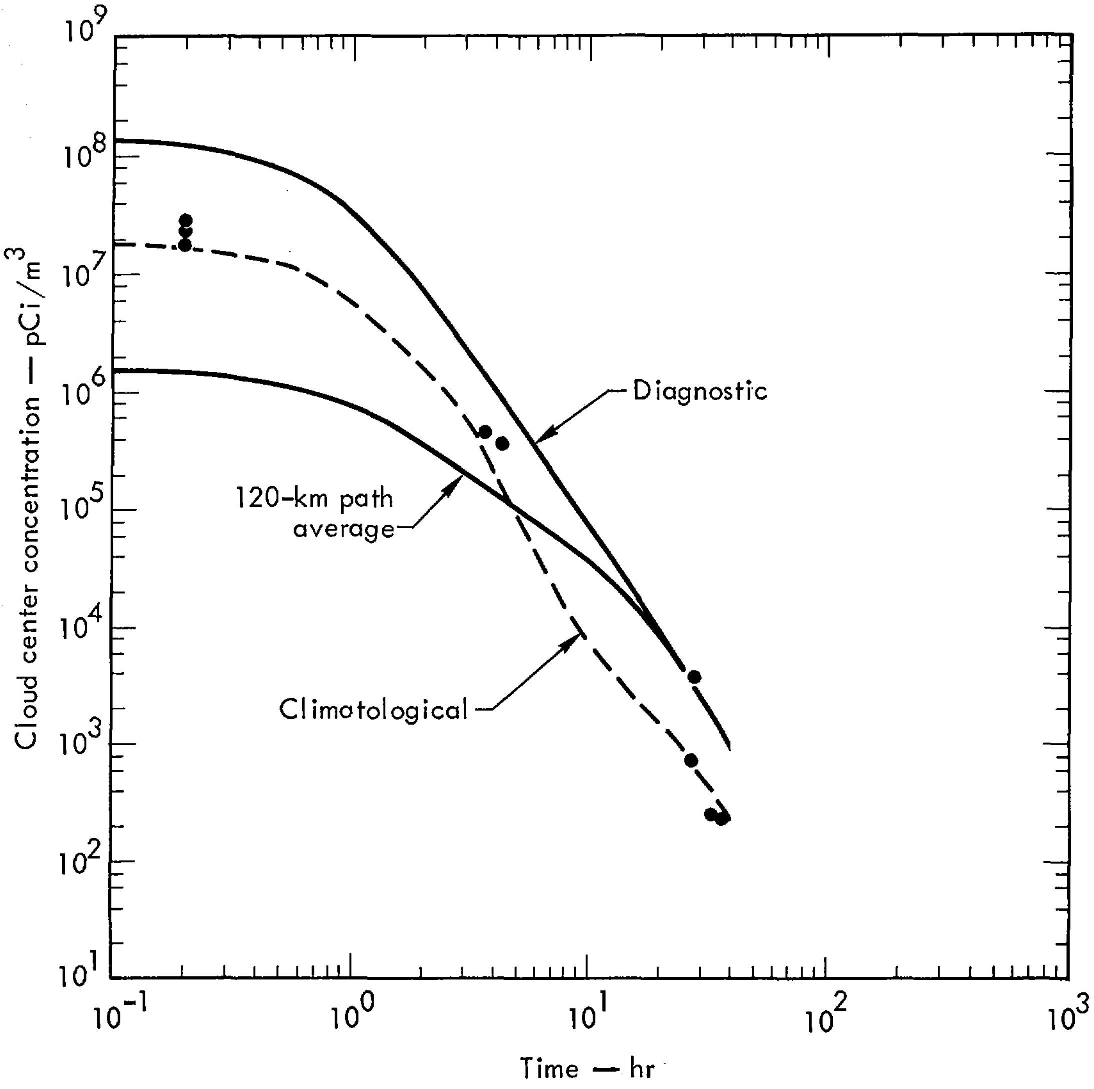

Fig. 4. Main cloud center W^{185} concentration as a function of time.

for a main cloud. Figure 5 presents such calculations. Initially, the ground-level concentrations are 2 to 3 orders of magnitude less than the main cloud center concentrations. The initial conditions of 2BPUFF are a Gaussian distribution through the cloud center. The total height of the cloud, the difference between main cloud top and base surge top in Table I, is set equal to four standard deviations. In Fig. 5, ground-level concentrations tend to increase with time due to diffusion downward from above, and in this particular problem, due to the ground surface rising up towards the cloud center as the cloud approaches the Rocky Mountains. However, it is obvious that this increase is more than offset by radioactive decay and horizontal diffusion. By 10 hr, the ground-level concentration is only an order of magnitude less than cloud center. This, it must be remembered, is at the crest of the Rocky Mountains in the calculation. As the main cloud continued on eastward, the terrain dropped away from the altitude of the cloud center. This causes, in the calculations, a very steep decrease in ground-level concentration with time.

The data points plotted on Fig. 5 are exposure rate measurements made by PHS[8] personnel. They fall above the calculated ground-level concentration, and in some cases just barely below the cloud center concentrations (compare Figs. 2 and 5). This is evidently due to the occurrence of fallout at these

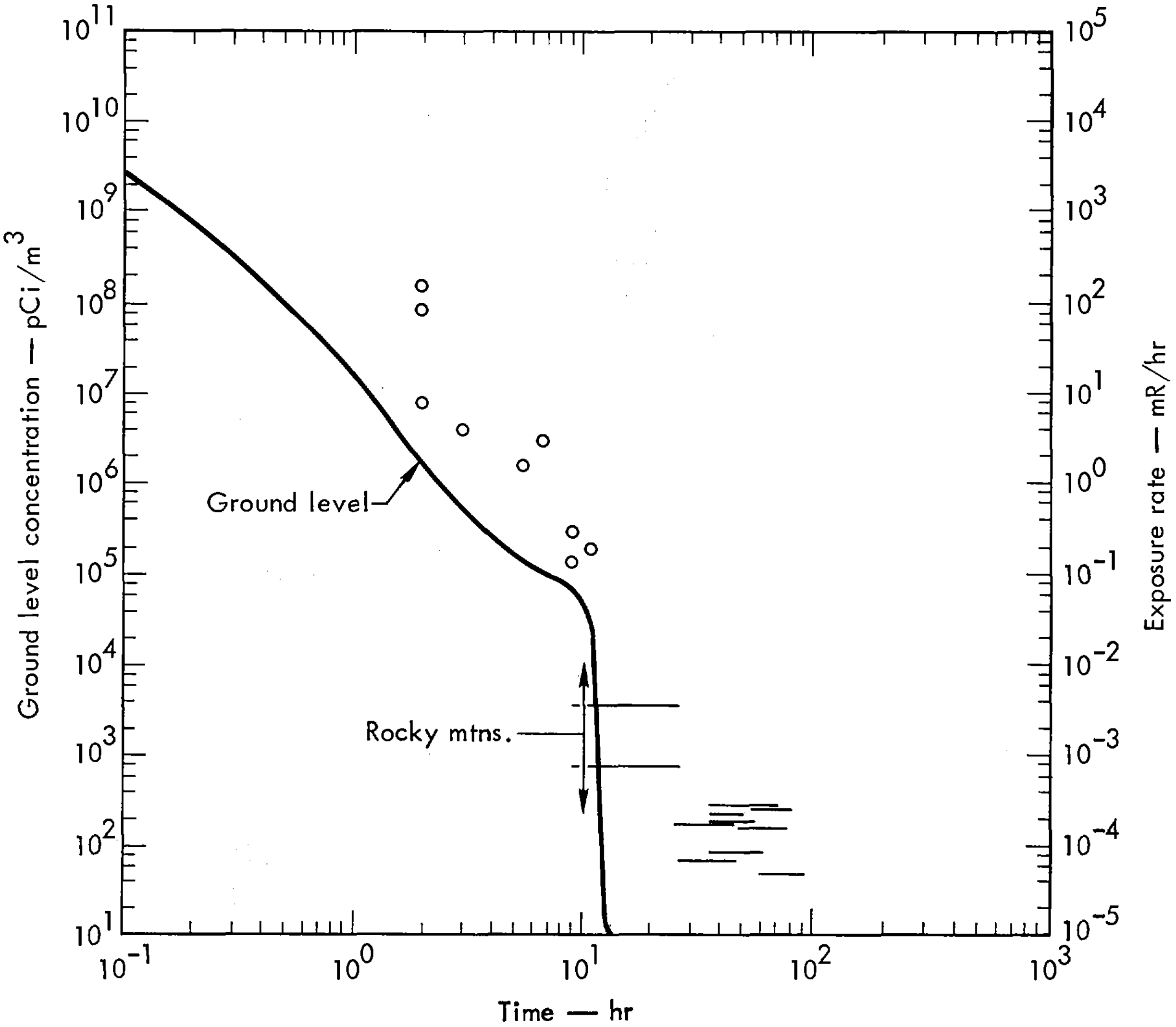

Fig. 5. Main cloud ground-level concentration as a function of time.

distances downwind. Fallout is not a part of the 2BPUFF diffusion calculation. Thus, any fallout occurring would tend to make the concentrations higher than predicted at the ground level. As the fallout contribution accumulated, the exposure rate increased.

For example, at Queen City Summit, which was 2 hr downwind and was the location that recorded 85-130 mR/hr peak exposure rates, a ground-level filter measurement was taken. A filter exposed from 0938 PST to 1713 PST contained about 300,000 pCi/m^3 of W^{187}. Examination of exposure rate measurements as a function of time at Queen City Summit suggests that a reasonable cloud passage time is about 4 hr. This implies an average concentration of W^{187} of about 600,000 pCi/m^3; at 2 hr this is about a factor of 3 below the curve on Fig. 5. For the purposes of the above discussion, it has been assumed that the W^{187} is the majority of the total activity. The importance of fallout at Queen City Summit is also illustrated by the fact that at the location which had a peak reading of 85 mR/hr at 0955 PST, the radiation level was only down to 60 mR/hr by 1700 PST and to 30 mR/hr by 1410 PST on the following day.

The importance of fallout decreased with time. This is illustrated at Garrison, Utah which had a peak exposure rate of 0.3 mR/hr at H+9 hr. The exposure rate measurements as a function of time imply that about 0.1 of the above 0.3 mR/hr was due to the cloud passage. The other 0.2 were due to the build-up of fallout. It should be noted on Fig. 5 that an exposure rate due to cloud passage of 0.1 mR/hr at H+9 hr is quite consistent with the calculation. The shape of the exposure rate data as a function of time at Garrison also suggests a cloud passage time of about 4 hr.

In addition, a filter was exposed at Garrison, Utah for 24 hr, from the morning of December 8 to the morning of December 9. This filter yielded 2800 pCi/m^3 decayed to end of time of collection. This value is indicated on Fig. 5 by the bar which runs from H+9 hr to about H+24 hr with a value of 2800 pCi/m^3. The bar is started at H+9 hr which is the time of cloud arrival. Now, if one corrects this filter data for a 4-hr passage time and for radioactive decay back to the time of cloud passage, one obtains a value close to 26,000 pCi/m^3 during cloud passage at Garrison, Utah. This is still somewhat below the calculation at this time, but is much closer to the exposure rate measurement at Garrison than is the filter concentration data to the exposure rate measurements at Queen City Summit.

The remainder of the bars on Fig. 5 refer to ground-level filter data. The length of the bar indicates the averaging time of the filter. The data refer to the peak filter for a variety of stations in the lee of the Rocky Mountains, generally under the path of the main cloud. However, it should be noted that the bulk of the peak readings at these stations occurred at times of 2 to 3 days. This is 1 to 2 days after the main cloud passed the area. This implies that some of the lower parts of the main cloud were trapped in the higher valleys of the Rockies and then slowly drifted down the eastern side of the Rockies at the speed of the surface winds. Thus, ground-level measurements of Schooner debris were obtained in the lee of the Rockies and the western edge of the Plain States. However, decay and atmospheric dilution reduced the levels to below background by the time the debris proceeded much further east. There were no significant ground-level values detected east of the Missouri River.

Dry deposition is calculated with the computer code 2BPUFF by multiplying an empirically determined deposition velocity (usually set equal to 1 cm/sec) times the calculated ground-level surface concentrations. This gives a flux of material towards the ground surface which is then integrated over the time of cloud passage. These calculations, along with the measurements of I^{131} deposition, are included in Fig. 6. Now, deposition calculations done in this manner are only applicable for distances downwind which are beyond the point of any significant fallout. In the case of the Schooner main cloud, calculations done in this manner are several orders of magnitude below the measurements at distances of about a hundred kilometers. The data indicated by x's on Fig. 6 come from fallout trays[1] and large plastic sheets[9] which were fielded and analyzed by LRL. The two dots are iodine in milk samples obtained by the PHS.[8] The fallout calculation was done postshot with the fallout code KFOC[10] using the observed winds, cloud heights, and amount of radioactivity which was deposited in the local fallout field. This calculation routinely yields a gross gamma exposure rate at H+1 hr as a function of distance from GZ. Measured isotopic fallout has been correlated to the H+1-hr exposure rates at the location of the fallout trays.[1] These data, for I^{131}, were used to convert the calculated H+1-hr exposure rate field to isotopic deposition.

The two different types of calculations on Fig. 6 converge at distances around 700-800 km. Past this distance, the calculated deposition drops markedly due to the cloud passing on eastward as the terrain drops away east of the Rockies. Except for one milk data point, all of the remainder of the data lie above the calculated deposition, but are consistent with the fallout calculation.

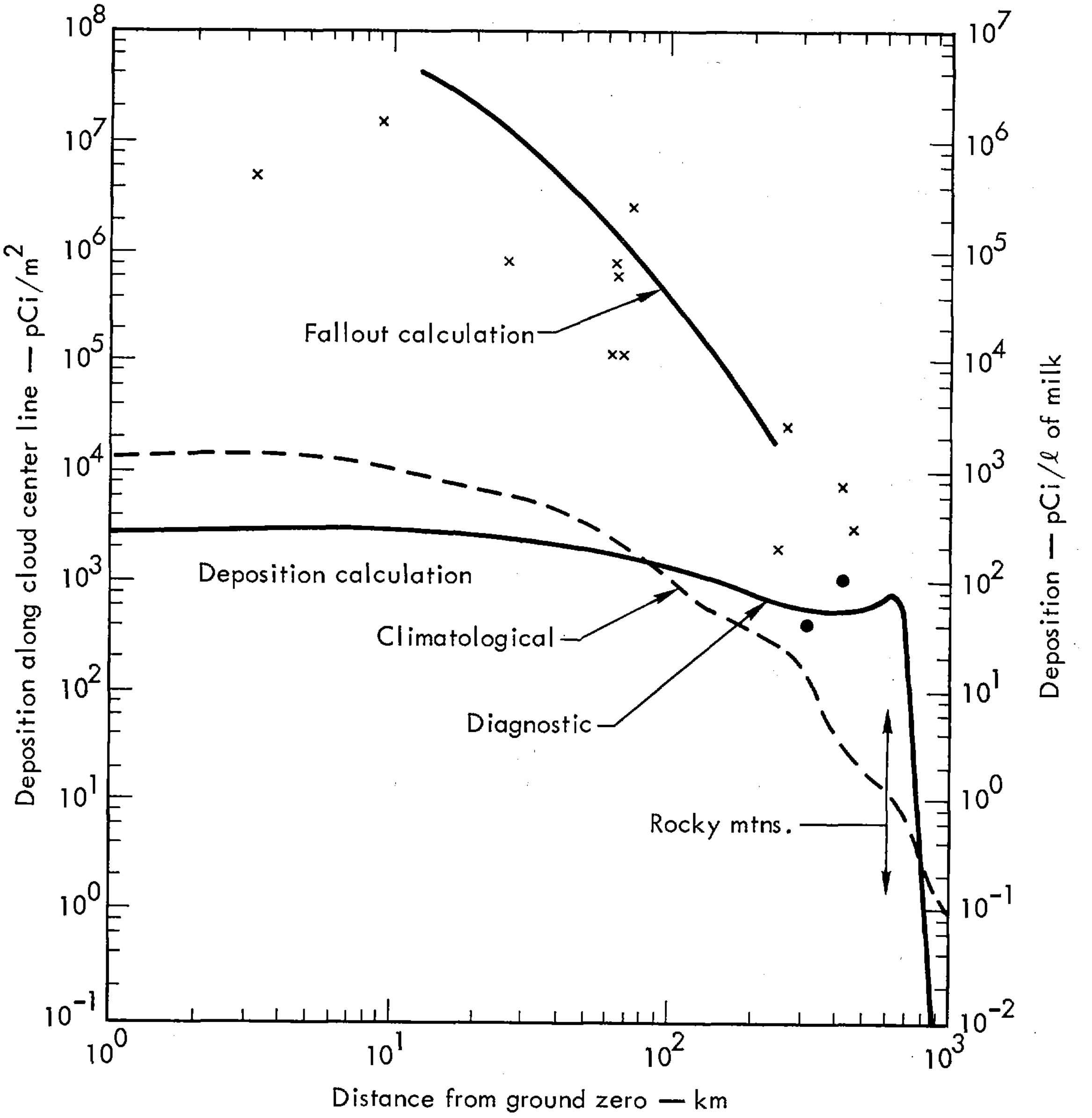

Fig. 6. Main cloud I^{131} deposition as a function of distance.

It should be noted that the distance of 450 km downwind represents a cloud travel time of about 7 hr. A 20-μ radius particle, with a density of 2.5, would take 8 to 9 hr to fall to the ground surface from the top of the main cloud on Schooner. Thus, it is readily apparent why fallout is still so important at distances of several hundred kilometers downwind for a main cloud. It also suggests the necessity of developing true isotopic fallout prediction methods. The method used to fit the fallout calculation in this paper assumes that one knows the relationship between isotopic deposition and the H+1-hr exposure rate. In Fig. 6, of course, it was possible to use measured Schooner values. But these values may well change from experiment to experiment.

Table III gives long-range deposition for several other nuclides of interest. Measurements, fallout calculations, and deposition calculations were done in the manner as discussed above for Fig. 6. Measured values relating pCi/m^3 to H+1 R/hr on Schooner only exist for Y^{88}, Mo^{99}, Te^{132},

Table III. Main cloud long-range deposition (pCi/m^2).

	64 to 68 km			243 to 270 km			423 to 480 km	
Nuclide	Meas.	Fallout Code	Deposition Code	Meas.	Fallout Code	Deposition Code	Meas.	Deposition Code
Mn^{54}	8(4)[a]			1(2)			8(2)	
	8(4)	6(5)	2(2)	2(3)	8(3)	6(1)	2(2)	5(1)
	2(5)							
Co^{58}	4(4)			5(2)			2(3)	
	4(4)	2(6)	5(2)	6(3)	3(4)	2(2)	6(2)	1(2)
	1(5)							
Y^{88}	6(4)			<8(1)			<5(2)	
	5(4)	2(5)	1(2)	1(3)	3(3)	3(1)	2(2)	3(1)
	1(5)							
Sr^{89}	—[b]			2(2)			6(1)	
	2(4)	7(4)	1(2)[c]	1(3)	1(3)	3(1)	3(2)	3(1)
	5(4)							
Sr^{90}	—			<3(0)			7(0)	
	1(2)	4(2)	6(-1)	8(0)	6(0)	2(-2)	5(0)	2(-2)
	3(2)							
I^{131}	≥8(5)			≥2(3)			>8(3)	
	≥6(5)	1(6)	2(3)	≥2(4)	2(4)	6(2)	>3(3)	5(2)
	—							
Cs^{137}	—			4(0)			3(0)	
	2(2)	1(3)	2(0)	4(0)	2(0)	5(-1)	2(0)	4(-1)
	7(2)							
Ba^{140}	3(5)			7(2)			3(3)	
	3(5)	7(5)	7(2)	1(3)	1(4)	2(2)	1(3)	2(2)
	—							
Ce^{141}	1(5)			2(2)			1(3)	
	8(4)	2(5)	1(2)	2(3)	3(3)	4(1)	2(2)	4(1)
	2(5)							
Ta^{182}	6(4)			—			—	
	5(4)	2(5)	—	9(2)	3(3)	—	—	—
	—							
W^{181}	7(7)			2(5)			6(5)	
	4(7)	1(8)	2(5)	2(6)	2(6)	5(4)	2(5)	4(4)
	1(8)							
W^{185}	—			5(5)			2(6)	
	1(8)	4(8)	5(5)	5(6)	5(6)	2(5)	7(5)	1(5)
	3(8)							

[a] 8(4) = 8×10^4.

[b] No measurements made of deposition or of initial cloud burden.

[c] Assumed same percent Sr as Cs in cloud.

I^{131}, Ba^{140}, Ce^{141}, and W^{187}. Production number ratios to Ba^{140} were used to estimate this relationship for the other nuclides in Table III. From H+12.5-min aircraft data, there are some indications that Mn^{54}, Co^{58}, and Ta^{182}

were more refractory than Ba^{140} and that Cs^{137}, W^{181}, and W^{185} were more volatile than Ba^{140}. Thus, the use of the Ba^{140} production number ratio might result in the fallout calculation in Tables III and IV being a factor of 3 to 5 too high for Mn^{54}, Co^{58}, and Ta^{182} and a factor of 2 to 3 too low for Sr^{89}, Sr^{90}, and Cs^{137}. The measured values of W^{187} pCi/m^2 to H+1 R/hr on Schooner were used, along with production ratios W^{181} and W^{185}, to estimate the W^{181} and W^{185} fallout. At distances of 27 km and greater, there appeared to be little fractionation with distance among the measured nuclides in the fallout data.

At distances of 64-68 km downwind, most nuclides measured seemed to be about a factor of 2 to 3 higher than the fallout calculation done in the above manner. A separate set of measurements with a fallout tray at 74 km gives deposition about twice the highest data in Table III. These later data are a much closer fit to the fallout calculation. The exception to this statement is Co^{58} which is about a factor of 20 higher than measured. Obviously the deposition calculation is several orders of magnitude below either the measurements or the fallout calculation.

The measurements and fallout calculations at the distance of 243-270 km were within about a factor of 3 of each other. For some nuclides the calculation is below the measurement, and it is visa-versa for other nuclides. The one exception here is the fallout calculation for Ba^{140} which is about an order of magnitude higher than measured. The deposition calculations are about 2 orders of magnitude below the fallout calculations and measurements. It was not possible to extrapolate the calculated fallout field to a distance of 423-480 km, although some fallout must still have been taking place. At these distances the deposition calculations are about an order of magnitude below measurements.

BASE SURGE

The base surge cloud moved slowly northward from GZ under the influence of light southerly winds. Much of this cloud was trapped in the north-south valleys in northern Nevada, and was not well-sampled by aircraft. It was still moving slowly northward through Northern Nevada valleys on D+1 day. With little aircraft data and without having completed a detailed meteorological analysis, the meteorological input to a diagnostic base surge calculation is not on as firm a footing as the previously presented main cloud calculation. However, using current best estimates for along-cloud track meteorology and the initial cloud sizes and base surge cloud burdens mentioned previously in this paper, a set of 2BPUFF calculations has been done for the base surge.

Figure 7 gives the calculated base surge cloud center concentrations and the available aircraft data. On this figure, data from all available aircraft samples and radiation readings which were taken anywhere near the base surge are included. The calculations on Fig. 7 are consistent with the observations but there is much less data than was obtained and presented in Fig. 2 for the main cloud.

Figure 8 gives the W^{187} measurements for the base surge cloud center. Note that the W^{187} measurements at almost 4 hr are about an order of magnitude below the diagnostic cloud center calculation, whereas on Fig. 7 the exposure rate measurement made at about the same time on the same aircraft was quite consistent with the diagnostic cloud center. This implies that the filter exposure included a significant amount of time away from the center of the cloud. Ground-level air concentration calculations are presented in Fig. 9 for the base surge, along with observations. In this case, the calculated

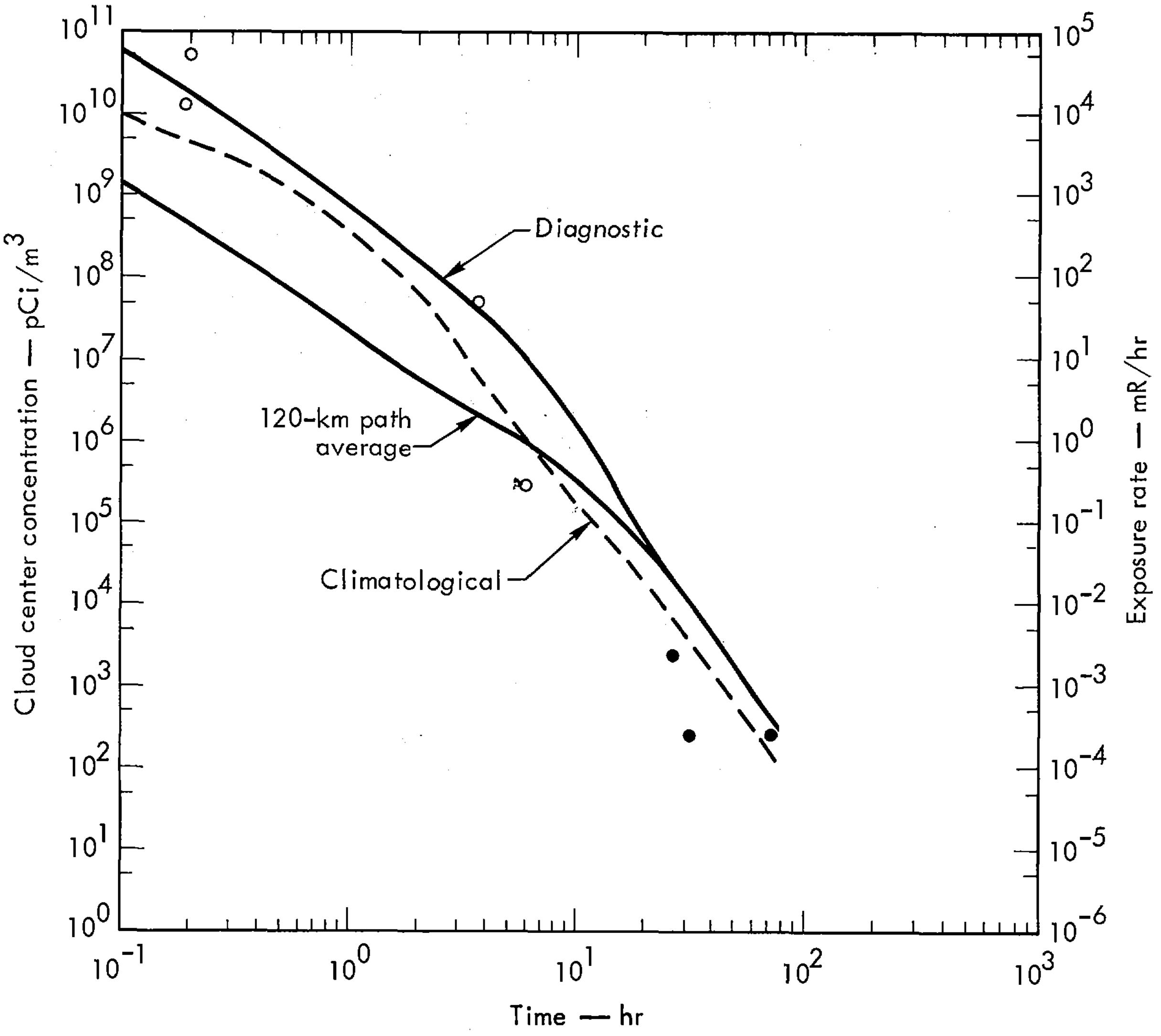

Fig. 7. Base surge cloud center total concentration as a function of time.

ground-level concentrations are very consistent with the exposure rate measurements made by the PHS.[8] In contrast to the main cloud, there is apparently little fallout taking place at times of 2 hr and later. In the case of the base surge, a 20-μ radius particle would have fallen from the top of the base surge to the ground level in a time period of about 3/4 hr. Thus, at times of 2 hr and later, fallout is not important for the base surge.

Ground-level filter data are shown by the bars on this figure, with the bar indicating the averaging time as well as the magnitude of concentration. The highest filter data presented on this figure is from Mountain Home, Idaho. The rest of the filters are from stations located in Idaho, Utah, Montana, Wyoming, and eastern Washington. In this case, the ground-level concentration calculation is quite consistent with the filter data. For this low-altitude base surge cloud, the time of arrival of the cloud at these locations is consistent with the times of maximum readings on the ground-level filter network. This is in marked contrast with the main cloud east of the Rockies.

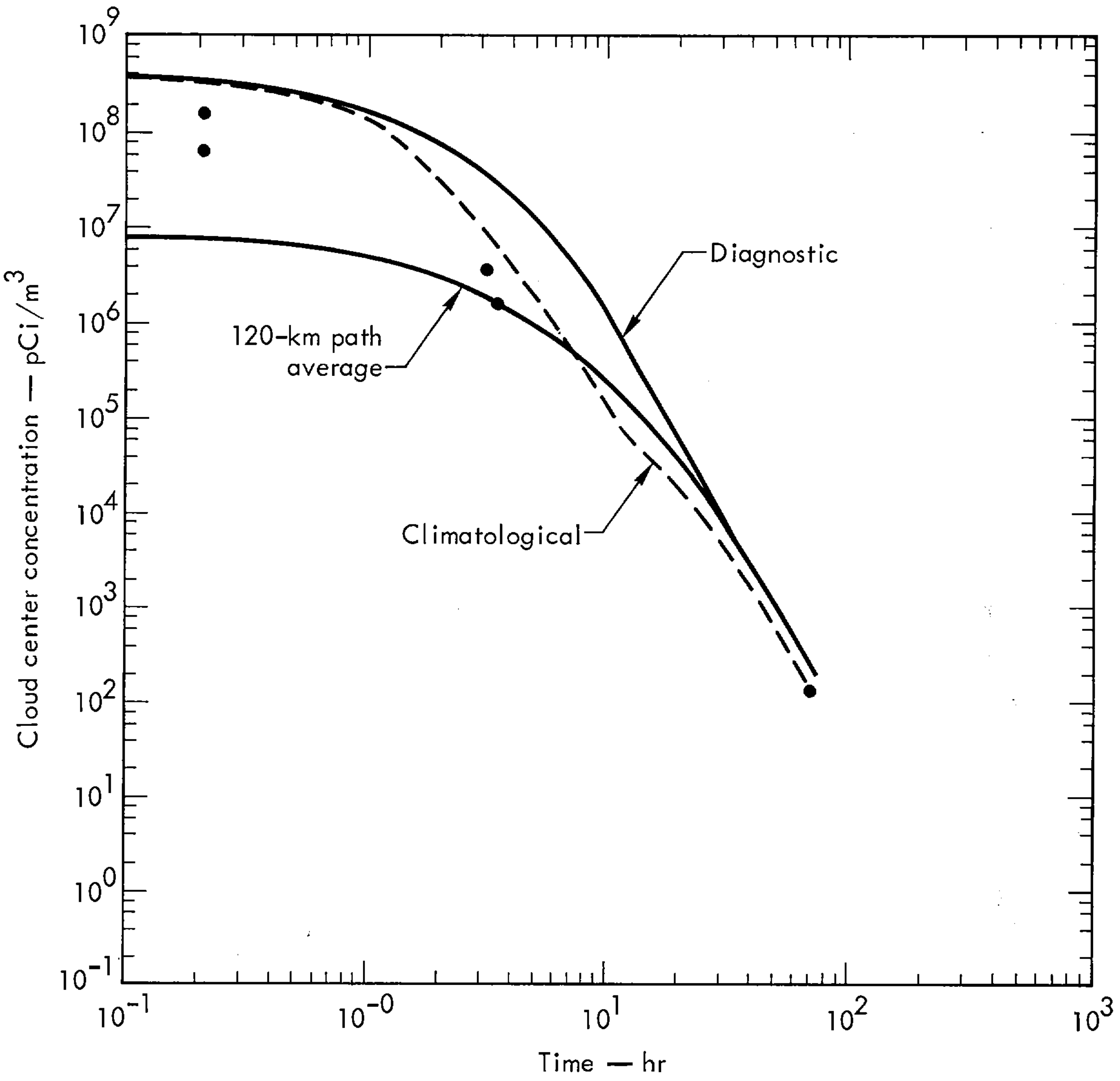

Fig. 8. Base surge cloud center W^{187} concentration as a function of time.

Base surge I^{131} deposition as a function of distance from GZ is given in Fig. 10. The fallout calculation and the deposition calculation converge at a distance of about 80-100 km. These two types of calculations are quite consistent with the data. The x's indicate the deposition data,[9] whereas the dots indicate milk concentration data.[8] The agreement between deposition calculations and measurements of I^{131} at distances of the order of 100 km and greater on Fig. 10 is quite consistent with similar studies done on the Plowshare cratering experiments Cabriolet and Buggy.[7] The difference between the climatological calculation and the diagnostic one is one of differences of initial cloud size, initial cloud burden, and along-track meteorology.

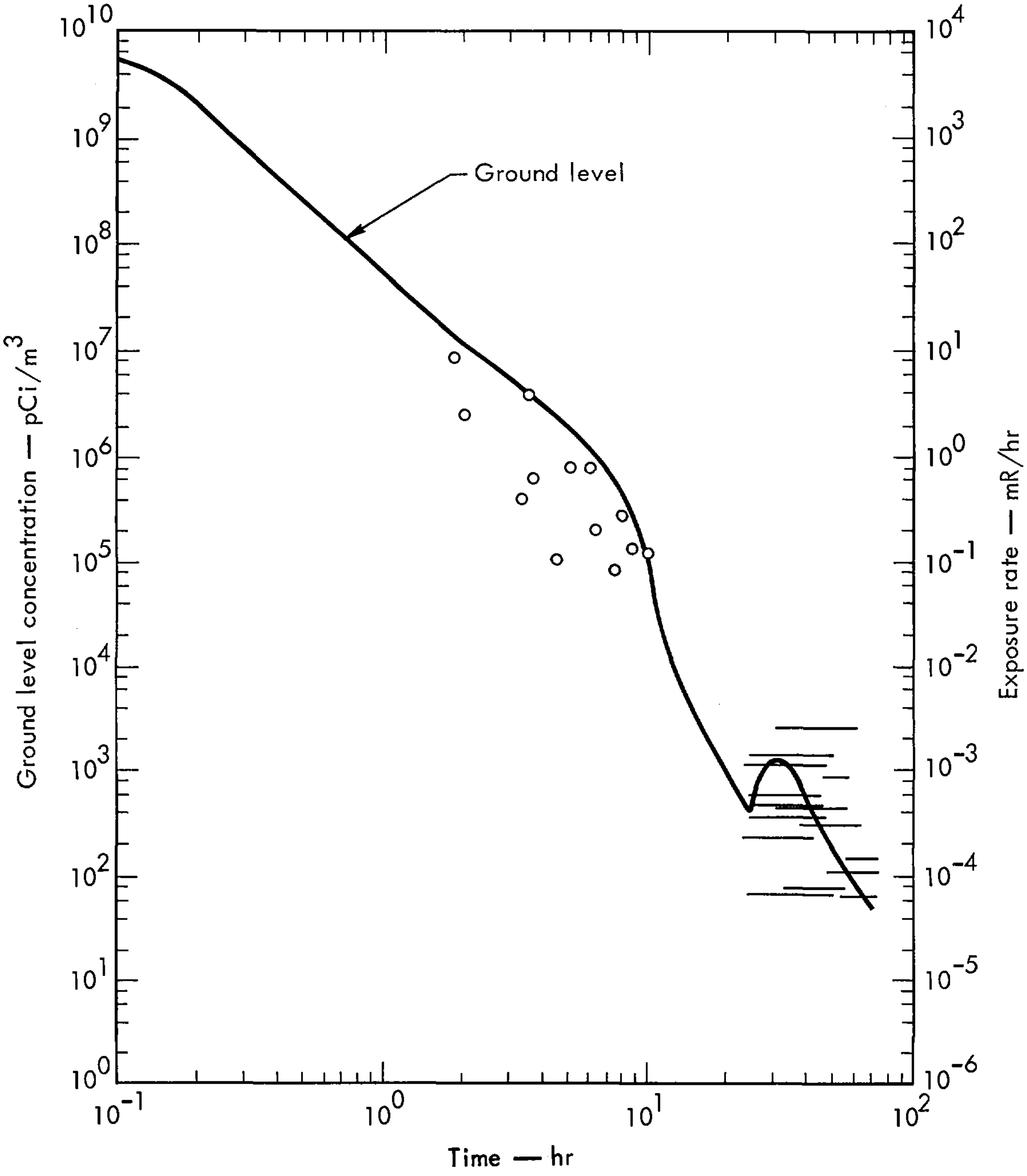

Fig. 9. Base surge ground-level total concentration as a function of time.

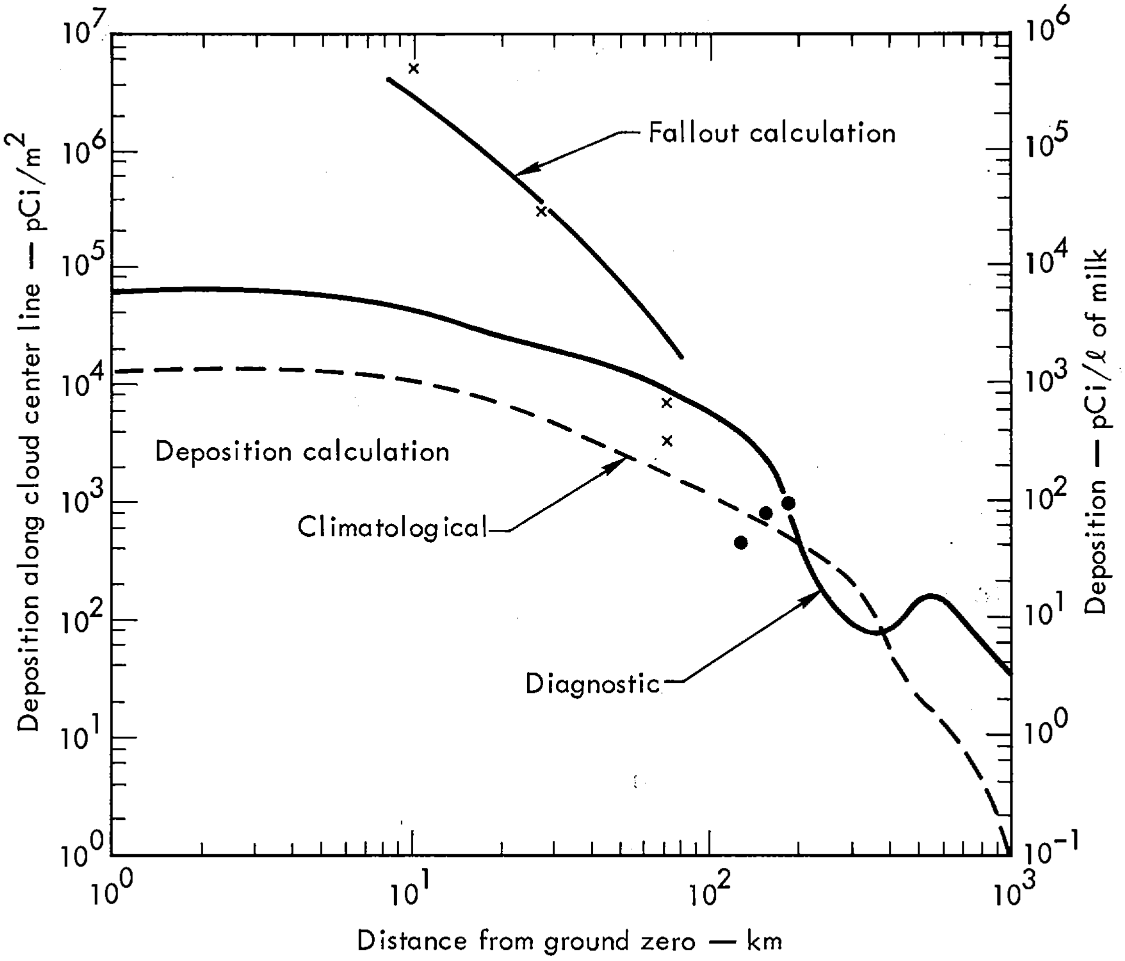

Fig. 10. Base surge I^{131} deposition as a function of distance.

Table IV is the long-range deposition from the base surge cloud for several nuclides besides I^{131}. At the distance of 70 km downwind, the fallout calculations are about a factor of 5 greater than deposition calculations and are somewhat higher than the measurement. There is more variability between the ratio of fallout calculation to measurement from nuclide to nuclide in this table than there was in Table III. Part of the reason may be due to less well-defined relations between pCi/m^3 and R/hr at H+1 on the base surge than on the main cloud, and also due to a less well-defined fallout calculation for the base surge than for the main cloud. At distances of 365 and 415 km downwind, the deposition calculations are within about a factor of 3 of the measurements.

Table IV. Base surge long-range deposition (pCi/m^2).

	70 to 71 km			365 km		415 km	
Nuclide	Meas.	Fallout Code	Deposition Code	Meas.	Deposition Code	Meas.	Deposition Code
Mn^{54}	4(2)[a]						
	2(2)	1(4)	6(2)	—	6(0)	—	6(0)
Co^{58}	1(3)						
	6(2)	4(4)	2(3)	—	2(1)	—	2(1)
Y^{88}	>2(2)						
	—[b]	4(3)	4(2)	—	4(0)	—	4(0)
Sr^{89}	>3(3)						
	—	1(3)	2(3)[c]	2(1)	2(1)	2(1)	2(1)
Sr^{90}	>6(0)						
	—	8(0)	1(1)[c]	<3(0)	1(-1)	3(0)	1(-1)
I^{131}	>7(3)						
	>3(3)	4(4)	8(3)	—	8(1)	—	8(1)
Cs^{137}	>3(1)						
	—	2(1)	3(1)	<1(0)	3(-1)	1(0)	3(-1)
Ba^{140}	>3(3)						
	>2(3)	1(4)	6(3)	—	6(1)	—	6(1)
Ce^{141}	>8(2)						
	>3(2)	4(4)	1(3)	—	1(1)	—	1(1)
Ta^{182}	—						
	—	4(3)	d	—	—	—	—
W^{181}	>9(5)						
	>3(5)	2(6)	9(5)	3(4)	9(3)	7(3)	9(3)
W^{185}	>3(6)						
	—	7(6)	3(6)	7(4)	3(4)	2(4)	3(4)

[a] 4(2) = 4 × 10^2.

[b] No measurement made.

[c] Assumed same percent Sr as Cs in cloud.

[d] No initial cloud burden with which to calculate deposition.

CONCLUSIONS

The Schooner detonation resulted in the formation of two clouds, a main cloud and a base surge cloud; adequate aircraft samples were obtained from this two-cloud system. These samples indicated about an order of magnitude more total radioactivity in the main cloud than in the base surge cloud. Cloud center concentration data and fallout data indicate cloud burdens at about H+12.5 min were depleted by about a factor of 2 over the next several hours due to local fallout.

Diagnostic cloud center concentration calculations done with the computer code 2BPUFF for the main cloud agree within a factor of 2 over times of a fraction of an hour to almost 40 hr. At times of 30-40 hr, the climatological calculations done preshot were about a factor of 3 lower than both the diagnostic calculations and the observations. Calculations done on the

Schooner base surge cloud are consistent with the available data within about a factor of 4. However, available data on the Schooner base surge is much less then on the Schooner main cloud. It should be noted that accuracies of a factor of 2 have been noted in the previous case studies of the Plowshare cratering experiments Cabriolet and Buggy[7] for diagnostic calculations with 2BPUFF.

Surface airborne concentrations and particulate "fallout" samples at distances out to several hundred kilometers under the Schooner main cloud include both deposition from the cloud and fallout. Fallout is not accounted for in current calculations made with 2BPUFF. Fallout causes the exposure rate measurements at times of 2-9 hr postshot to exceed those which were predicted at ground surface by 2BPUFF for the main cloud. This fallout also caused deposition amounts to be considerably higher than predicted by 2BPUFF at distances out to about 500 km. The use of fallout code calculations of the H+1-hr gross gamma external exposure rate and the correlations obtained with Schooner data between this exposure rate and isotopic deposition permitted the preparation of an isotopic fallout calculation. This approach was shown to have some merit for the Schooner main cloud, and the techniques should be exploited further.

The main cloud data also indicated ground surface concentrations appearing in the lee of the Rockies a day or two after cloud passage. This implies that part of the lower level of the main cloud was "scraped" off by the Rockies. This part of the main cloud was then carried by the surface winds towards the Plain States.

Ground surface concentrations and measurements agreed quite well under the base surge cloud out to about 2 days. At distances of beyond about 100 km deposition data also agree, within about a factor of 3, with the deposition calculations done with 2BPUFF.

REFERENCES

1. L. L. Schwartz, personal correspondence, March 1969.
2. J. C. Cohen, "Summary of Parachute-Borne Air Sampling Program on Schooner," Bio-Medical Division Preliminary Report for Project Schooner, Lawrence Radiation Laboratory, Livermore, Report UCRL-50718, 38-42, 1969.
3. R. E. Heft, personal correspondence, November 1969.
4. T. V. Crawford, "A Computer Program for Calculating the Atmospheric Dispersion of Large Clouds," Lawrence Radiation Laboratory, Livermore, Report UCRL-50179, 1966.
5. T. V. Crawford, "Long Range Diffusion of the NRX/EST EP-4A Effluent Cloud," Lawrence Radiation Laboratory, Livermore, Report UCRL-50299, 1967.
6. T. V. Crawford, "Long Range Diffusion of the Effluent Cloud From the Phoebus 1B EP-IV Reactor Tests of February 23, 1967," Lawrence Radiation Laboratory, Livermore, Report UCRL-50418, 1968.
7. T. V. Crawford, "Atmospheric Transport, Diffusion, and Deposition of Radioactivity," Proc. Symp. Public Health Aspects of Peaceful Uses of Nuclear Explosives, Las Vegas, Nevada, April 7-11, 1969.
8. Southwestern Radiological Health Laboratory, "Preliminary Report of Off-site Surveillance for Project Schooner," Dept. of Health, Education and Welfare, Public Health Service, Bureau of Radiological Health, January 1969.
9. A. L. Prindle, personal correspondence, November 1969.
10. J. B. Knox, "Prediction of Fallout From Subsurface Nuclear Detonation," Radioactive Fallout From Nuclear Weapons Tests, AEC Symposium Series 5, pp. 331-355, 1965.

XA04N0760

POSTSHOT DISTRIBUTION AND MOVEMENT OF RADIONUCLIDES IN NUCLEAR CRATER EJECTA*

John J. Koranda, John R. Martin, Robert Wikkerink
and Marshall Stuart
Bio-Medical Division
Lawrence Radiation Laboratory, University of California
Livermore, California 94550

ABSTRACT

The distribution and postshot movement of radionuclides in nuclear crater ejecta are discussed in this report. Continuing studies of tritium movement in ejecta at SEDAN crater demonstrate that variations in tritium concentration are correlated with seasonal rainfall and soil water movements. Losses of 27 mCi H^3/ft^2 are evident on SEDAN crater lip at the end of a three year period of measurements in which an unusually large flux of rain was received.

The distribution of gamma emitting radionuclides and tritium is described in the recently created SCHOONER crater ejecta field. The specific activity of radionuclides in the SCHOONER ejecta continuum is shown for ejecta collected from the crater lip to 17 miles from GZ. The movement of W^{181} and tritium into the sub-ejecta preshot soil is described at a site 3000 feet from GZ.

INTRODUCTION

During a nuclear cratering event, the movement of earth from the detonation site to the surrounding landscape takes place in a relatively short time. Within a few seconds, millions of tons of ejecta or excavated earth materials may be thrown out of the crater area onto the surrounding topography (throwout) or put into the air to travel varying distances as airborne debris (fallout). A large fraction of the total ejecta falls back into the crater (fallback).

During the cratering process, radioactivity is present in the contained incandescent plasma within the mound of earth lifted by the detonation. As the mound breaks up and venting occurs, radionuclides in gaseous and condensed chemical states are released into the immediate atmosphere. Radioactivity is also injected into or permeates the earth mass moved by the detonation. The distribution and fate of the radionuclides produced in the detonation in various kinds of nuclear crater ejecta is the subject of this report.

---

*Work performed under the auspices of the U.S. Atomic Energy Commission.

METHODS

Ejecta samples are collected from the crater areas by two methods, depending upon the nature of the ejecta. At SEDAN crater, where ejecta is sandy, sample holes are dug with posthole augers fitted with 4 to 6 foot extension handles. Ejecta samples to depths of 8 feet are routinely taken from sampling sites around SEDAN crater by these methods. In the second method used at craters in hard rock media, where the ejecta is mainly crushed rock, the samples are obtained with shovel and trowel from the vertical wall of a large trench or from a sample pit. Samples are poured into polypropylene sample jars approximately 250 ml in volume and the lids are taped to prevent water loss. These samples are placed in 1000 ml vacuum flasks in the laboratory after the sample jar opening has been covered with #1 Whatman filter paper. The filter paper prevents blow-out of ejecta particles during the vacuum distillation of the interstitial water in the ejecta sample. Extraction of the interstitial water (capillary and hygroscopic water) from the sample usually takes 24 hours at which time only an extremely small amount of hygroscopic water remains. Tritium concentrations are determined by analyzing the extracted water by liquid scintillation counting.

Gamma radioactivity is determined by taking a 5-10 gram aliquot of the same sample from which tritium had been extracted, and placing it in a standard 20 ml counting vial. W^{181} activity is determined with a 3 inch NaI well crystal and a 2 channel pulse height analyzer, which has been calibrated to count W^{181} disintegrations between 50 and 60 KeV in a single channel. Other gamma emitting radionuclides are determined with a 12 cc germanium diode and a 4096 channel pulse height analyzer. Spectra are accumulated on magnetic tape from a disc memory with a computer program developed by Dr. Robert Heft and William Phillips, Bio-Medical Division, Lawrence Radiation Laboratory.

The number of nuclear cratering events one might study to obtain information on the distribution of radionuclides in nuclear crater ejecta is limited. The SEDAN detonation[1] of July 1962 was the first large scale nuclear cratering experiment that permitted long-term studies of an ejecta field. Radioecological studies conducted by the Bio-Medical Division, Lawrence Radiation Laboratory, have been in progress at SEDAN crater since 1965.[2-5] The CABRIOLET and BUGGY events, conducted early in 1968, were small nuclear cratering shots in hard rock media on Pahute Mesa at the Nevada Test Site. The BUGGY event was a row-charge detonation employing five devices. The SCHOONER event of December 1968 was a larger example of nuclear cratering in hard rock and has provided an opportunity to study the distribution of radioactivity in nuclear crater ejecta where several factors varied significantly from the SEDAN detonation in Yucca Flat.

Few data are available on the distribution of radionuclides in nuclear crater ejecta. The distribution and mobility of radionuclides remaining in crater ejecta have considerable significance in any of the large scale engineering projects being considered by the Atomic Energy Commission. The feasibility of such projects may well hinge upon the postshot movement and environmental pathways of radionuclides in nuclear crater ejecta, both from airborne debris or as radionuclides transported from the nuclear crater site in water. We find that two ecological mechanisms are important in determining the feasibility of nuclear excavation projects - the movement and cycling of stable elements of radionuclides produced in an excavation event, and the pathways of water in natural environments. A portion of the current research in the Bio-Medical Division, Lawrence Radiation Laboratory, is directed toward these topics.[6]

RESULTS AND DISCUSSION

Sedan Studies

During the few seconds that the mound of earth is being lifted by the force of the detonation, gaseous radioactivity permeates the mound or lofted overburden, and many radionuclides have already condensed on the inside of the mound before significant venting occurs. These are typically found on the surface of the throwout or bulk ejecta. The bulk ejecta is the earth material that moved essentially en masse from the uplifted mound onto the surrounding land surface. The initial distribution of radioactivity in nuclear crater ejecta therefore is at least partially dependent upon the physical and chemical behavior of the isotope species in the incandescent plasma during the process of crater formation.

Another class of material produced in nuclear cratering experiments has been called missile ejecta.[7] This type of ejecta is composed of particles which are placed on high trajectories above the crater and which fall through the vented cloud onto the bulk ejecta at later times, and at farther distances from the crater. Missile ejecta may be deposited with base surge materials and exhibits a continuum relationship with the close-in fallout.

The distribution of radionuclides in the ejecta of SEDAN crater has been discussed by Koranda et al.,[3] Koranda et al.,[4] and Koranda and Martin.[5] Their findings indicate that those refractory radionuclides which are prominent in nuclear crater ejecta, are deposited in the highest concentration on the surface of the bulk ejecta around the crater.

Tritium distribution, however, has been considerably modified by postshot environmental effects. Figure 1 shows the distribution of tritium and gross gamma radioactivity in the SEDAN crater lip at four stations in May 1966. Gamma radioactivity drops rapidly with depth and at the depth where tritium maxima occur, it is only slightly above the background for preshot earth materials at the SEDAN site. No early tritium concentrations in SEDAN ejecta were made, therefore it is not possible to compare these data with early measurements. Based on experience and data obtained from other cratering experiments, tritium concentrations in SEDAN ejecta were very likely high in surface strata, decreasing with depth until contact with the buried preshot soil materials was reached. During the period after the detonation, the effects of seasonal rainfall and soil water movements have completely modified the initial distribution.

The mean annual rainfall received at the U.S. Weather Bureau Station near SEDAN crater is 3.1 inches. The portion of the annual rainfall that is effective in modifying tritium distribution in SEDAN ejecta is received in the winter. Usually the winter rainfall does not penetrate below 24 inches in northern Yucca Flat, but in recently disturbed materials one might expect greater penetration. An unusually high winter rainfall in 1965-66 at the Nevada Test Site produced dilution of soil water tritium concentrations at the 3 foot depth, as shown in Figure 2. In Figure 3, the distribution of rainfall for several years during the period of these measurements is shown.

Continuing measurements of tritium movement in sedan crater ejecta indicate that maximum tritium concentrations move in and out of the sampling zone (6-8 feet) accessible to us with hand tools. Data obtained from 3 stations on SEDAN crater lip are shown in Figures 4, 5, and 6. These data are expressed as disintegrations of tritium per gram of dry ejecta which eliminates the effect of variations in water content of the ejecta. The effects of a very large flux of winter rainfall received in January-February 1969 are evident in these data. Rainfall received in January 1969 immediately lowered concentrations in surface strata at the 1 foot depth, and by February dilution was evident in the deeper strata.

If the vertical distribution profile of tritium in the SEDAN ejecta is integrated and appropriate bulk density values are applied, the tritium data shown in Figures 4, 5, and 6 may be expressed in surface units of curies per square foot. Integrated surface tritium concentrations at 4 crater lip sites for a 3 year period are shown in Figure 7. The mean integrated surface concentration for the 4 crater lip sites in May 1966 was approximately 48 mCi/ft^2, and in August 1969, the mean concentration was approximately 21 mCi/ft^2. In the 3 year period, approximately 27 mCi/ft^2 were lost from the ejecta on SEDAN crater lip. This loss was mainly by evapotranspiration of soil water during the summer, but it is also apparent in the data shown in Figures 3, 4, and 5 that movement of soil water below the depth of sampling (8 feet) must occur. The heavy winter rainfall of 1969 caused considerable dilution in soil water tritium concentrations in the zone 1-6 feet and produced effects throughout the summer of 1969 as soil water was dissipated by evaporative and transpirational losses. Succulent plant cover in the form of dense growths of the summer annual, <u>Salsola kali</u> (Russian thistle), is present on SEDAN ejecta. Tissue-water concentrations in this plant species are essentially in equilibrium with the soil water tritium concentrations in the root zone.

It is apparent from these data that climatic, geologic, and biological parameters play an important role in the postshot distribution and movement of tritium in nuclear crater ejecta. The radionuclide present in SEDAN ejecta at this time in the highest concentration is tritium (greater than 20 mCi/ft^2).[6] Other radionuclides, even the more soluble ones such as Cs^{137}, which is not particularly prominent in nuclear crater ejecta, do not exhibit the degree of movement that tritium does in SEDAN ejecta. A very subtle level of Cs^{137} leaching[4] has been demonstrated in SEDAN ejecta, but most gamma-emitting radionuclides have remained in the surface strata of the ejecta where they were deposited.

<u>Schooner Studies</u>

In December 1968, the SCHOONER event produced a nuclear crater with an apparent average radius (R_a) of 129.9 meters and an apparent average depth (D_a) of 63.4 meters. The SCHOONER crater and its ejecta field are shown in Figure 8 which is a low level aerial photograph. Fine ejecta and some large missiles were deposited beyond 3000 feet from ground zero (GZ). The main purpose of the SCHOONER experiment was to examine cratering phenomena in a hard rock medium at intermediate explosive yields.

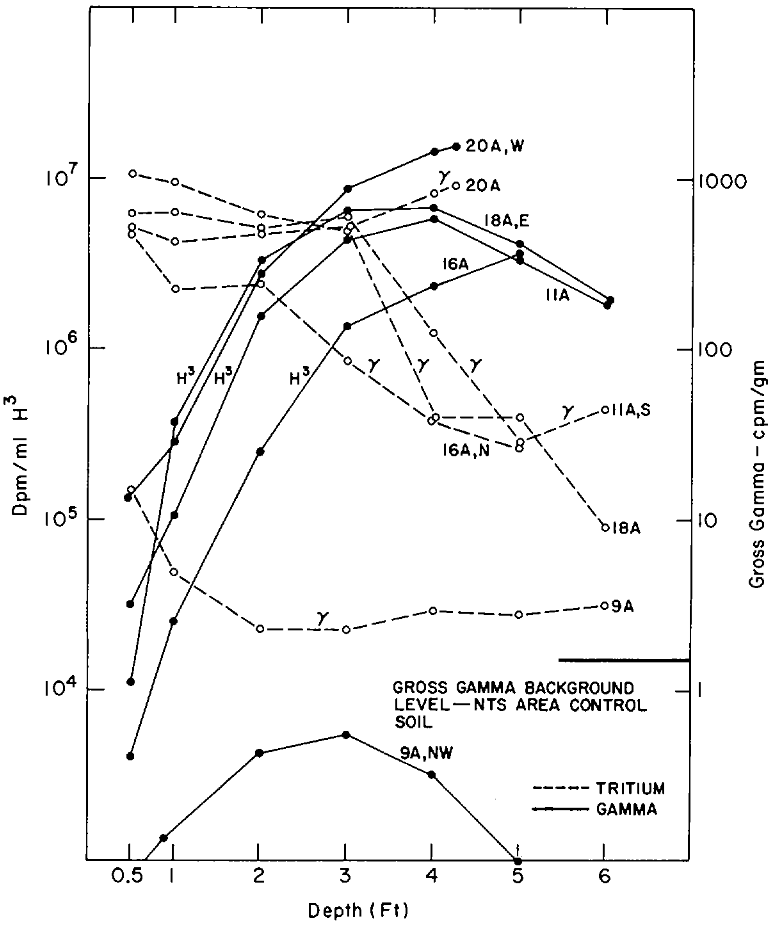

Figure 1

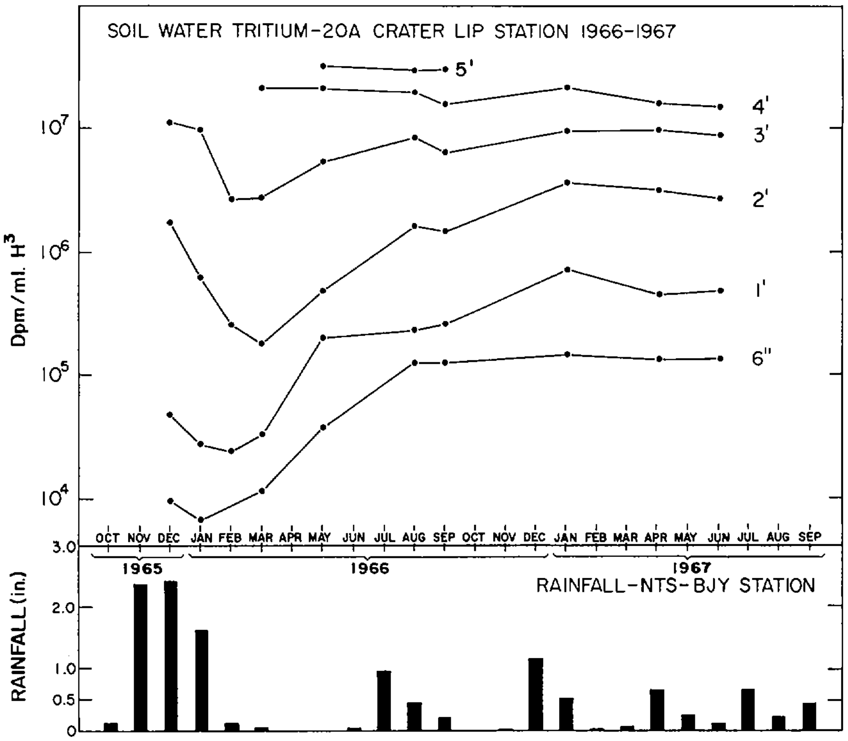

Figure 2

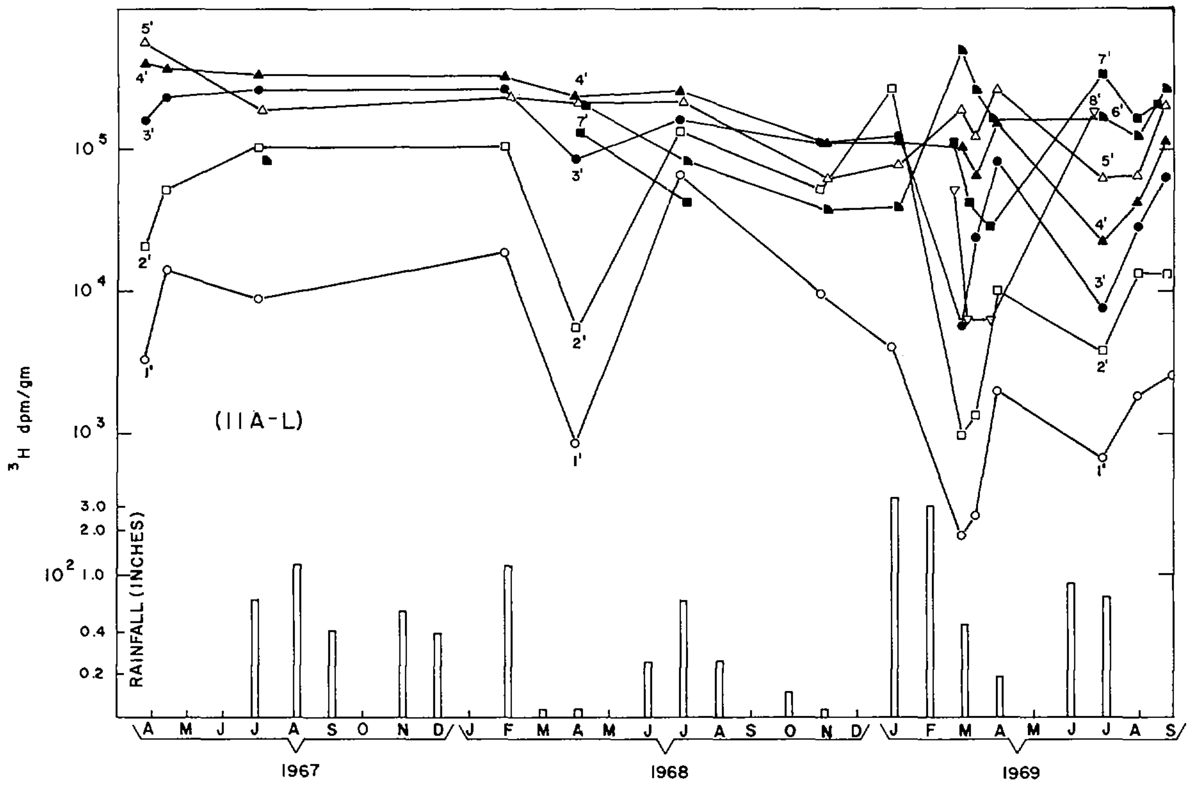

Figure 3

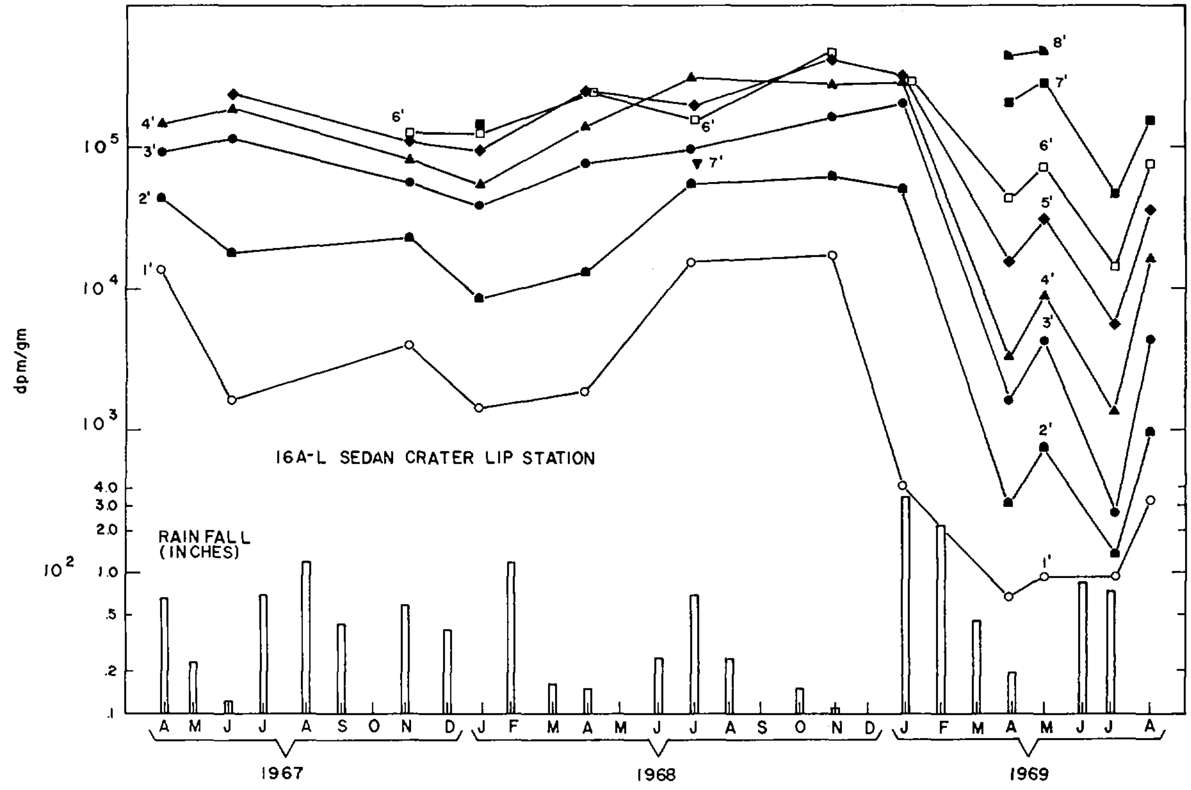

Figure 4

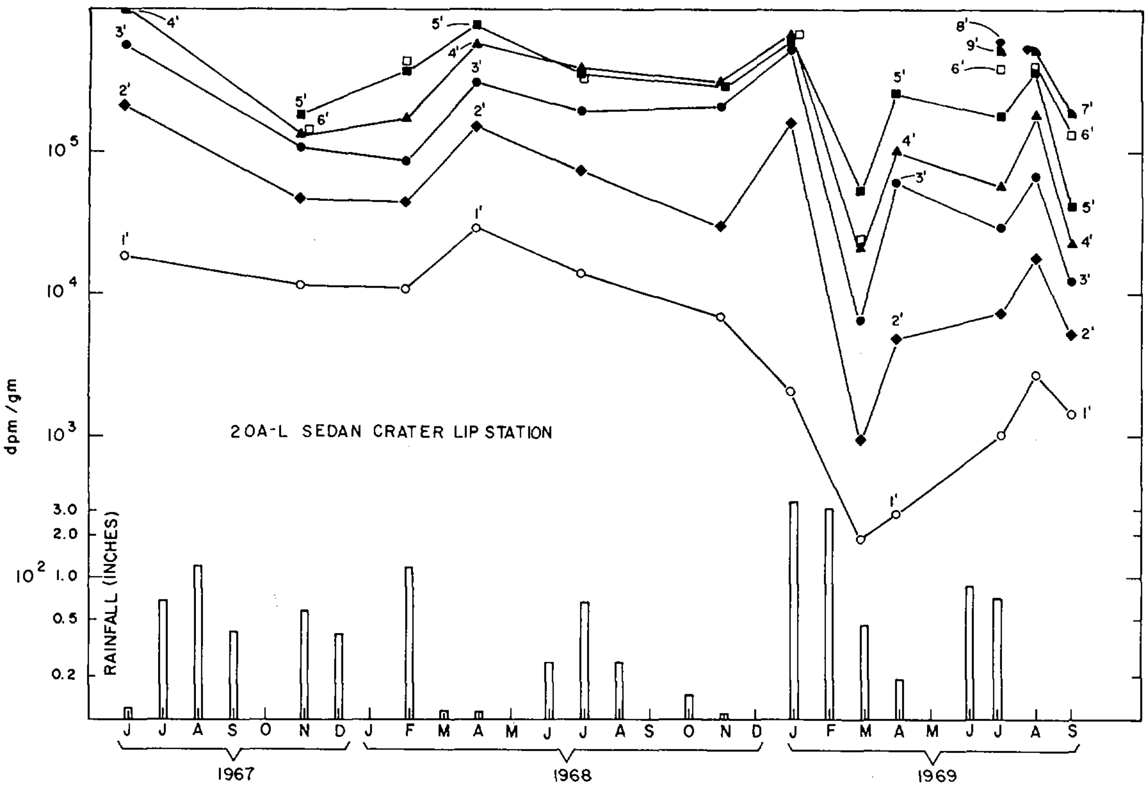

Figure 5

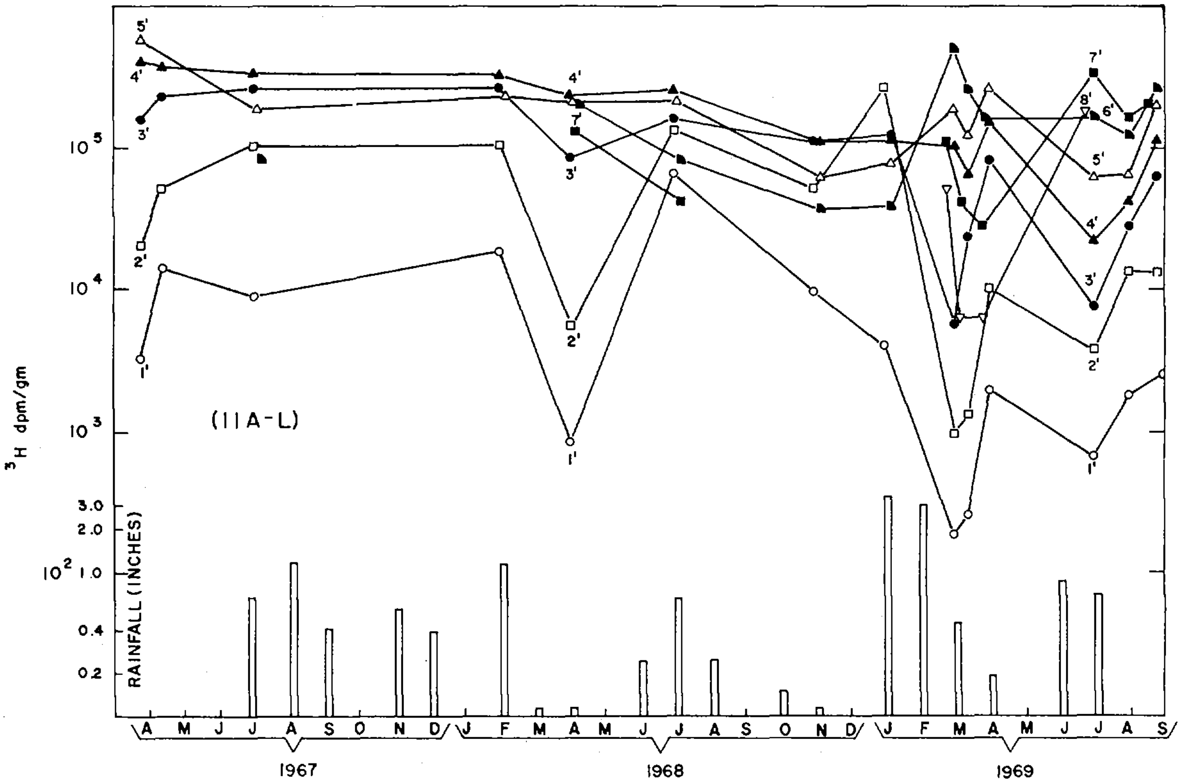

Figure 6

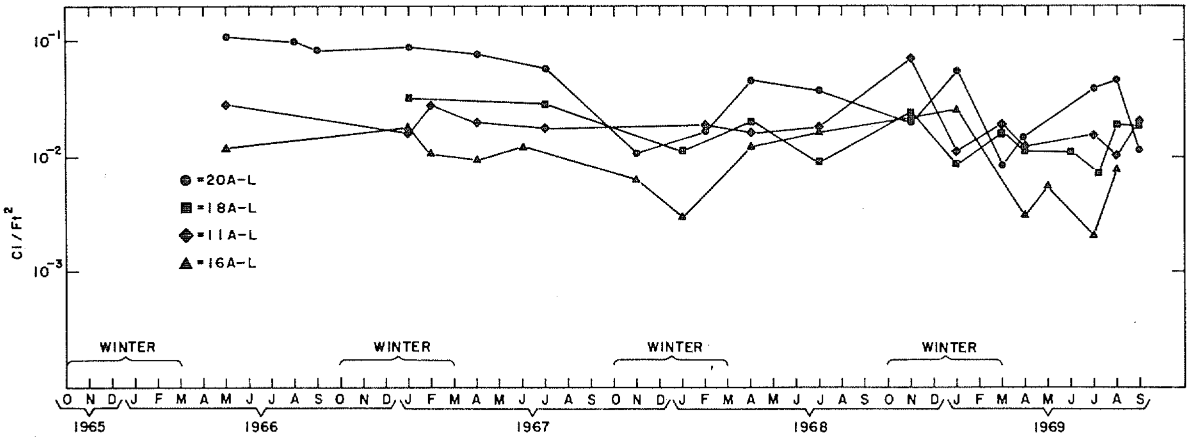

Figure 7

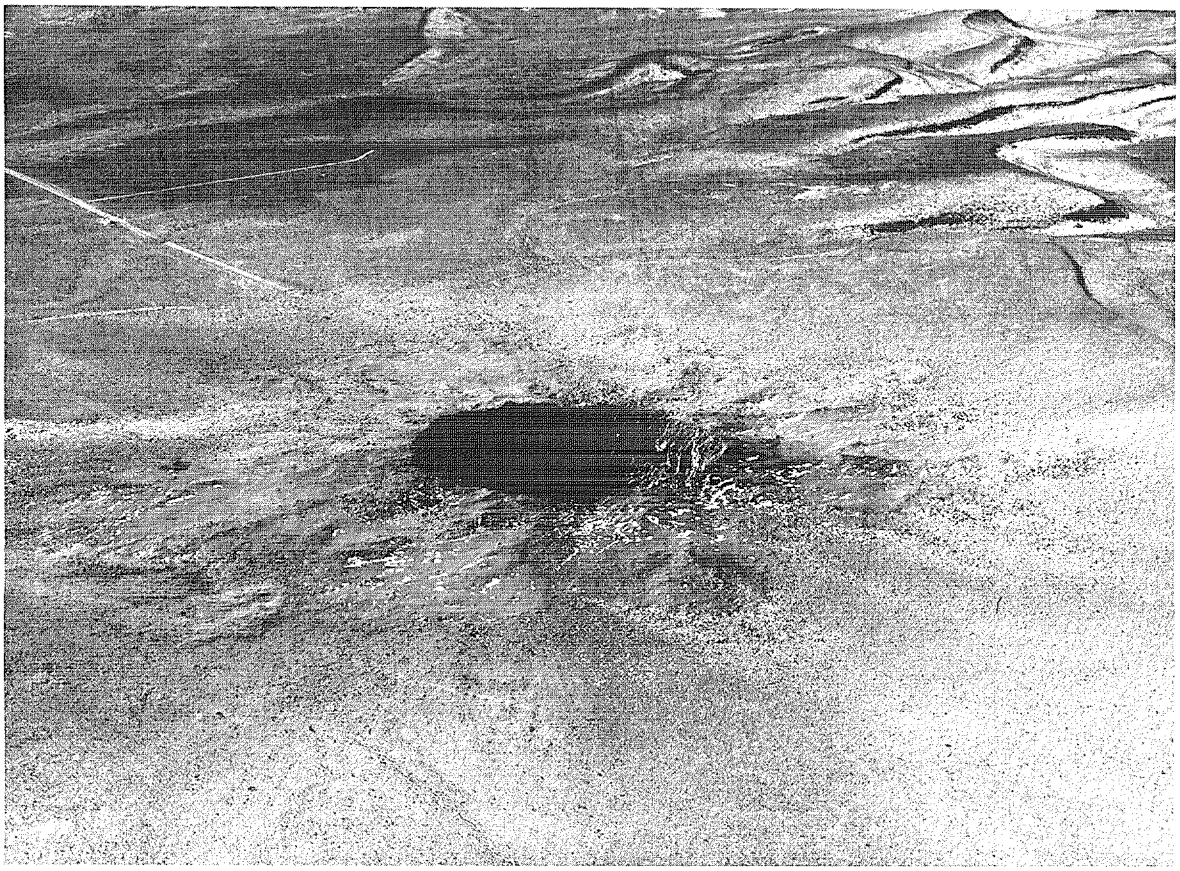

Figure 8

In January 1969, a series of ejecta samples were obtained at a distance of 3000 feet from GZ as sampling equipment was retrieved. An additional series of ejecta samples was obtained along a transect of the ejecta from the southeast edge of the throwout zone to approximately 800 feet from the crater lip. Concentrations of tritium and W^{181} in these samples have already been reported in preliminary report.[8]

In May and June 1969, it was possible to excavate a trench through the SCHOONER ejecta from 2000 feet from the crater to the crater lip on the southeast side of the crater. Figure 9 shows a phase of the excavation operation. Ejecta samples were collected from the wall of this trench at 1 foot depth intervals, and approximately every 50 feet along the trench. Surface ejecta and sub-ejecta samples at a depth of 1 foot were collected from 2500 feet from the crater to the edge of the throwout.

SCHOONER trench samples were processed in the manner described previously and tritium concentrations in the interstitial water, and gamma-emitting radionuclide concentrations per gram of dry ejecta were determined. A portion of the data obtained in the SCHOONER trench study will be presented here.

The concentrations of 6 radionuclides in vertical cross-sections of SCHOONER crater ejecta are shown in Figures 10 through 16. In the radionuclide profile of SCHOONER crater lip, shown in Figure 10, the distribution of radioactivity drops to a low concentration at a depth of 5-6 feet for all radionuclides. Concentrations at the maximum depth sampled (14 feet) are close to those found at the ejecta surface, while at 5-6 foot depth certain radionuclides were not detected. The deep region of radioactivity in the crater lip may be explained by the injection of radionuclides into the fractured, uplifted materials at the edge of the mound. This fractured, uplifted zone is later covered by bulk ejecta as the mound breaks up, and large masses of the mound at the contact of the uplifted zone may "hinge" and overturn onto the surface of the uplifted crater lip. High radioactivity is therefore found in the fractured, uplifted zone, and on the surface of the bulk ejecta. Certain radionuclides such as tritium and radioisotopes of tungsten permeate the mound and are found in relatively high concentrations throughout the bulk ejecta and the uplifted zone. Radionuclides that condense at high temperatures, and which begin to do so on the inside of the mound before it breaks up, are found mainly on the surface of the bulk ejecta, but also are apparently injected into the uplifted, fractured materials forming the crater lip.

If this is the mechanism that takes places radioactivity at depths of 14 feet in the crater lip, then at greater distances the increase in radioactivity in the deeper strata of the ejecta will not take place because the range of the injection phenomenon will not be very great. At 650-700 feet (Figures 12 and 13), only a small second peak of activity occurs. The stratum of lowered activity at 650-700 feet from the crater still occurs at a depth of 5 feet, however. There has not been enough rainfall to produce large scale leaching, especially of refractory radionuclides such as Nb^{95} and Y^{88}, and therefore these activity peaks are not zones of accumulation, but are depositional phenomena.

At 800 feet from the crater lip, the concentrations of five radionuclides decrease gradually with depth until the preshot soil surface is

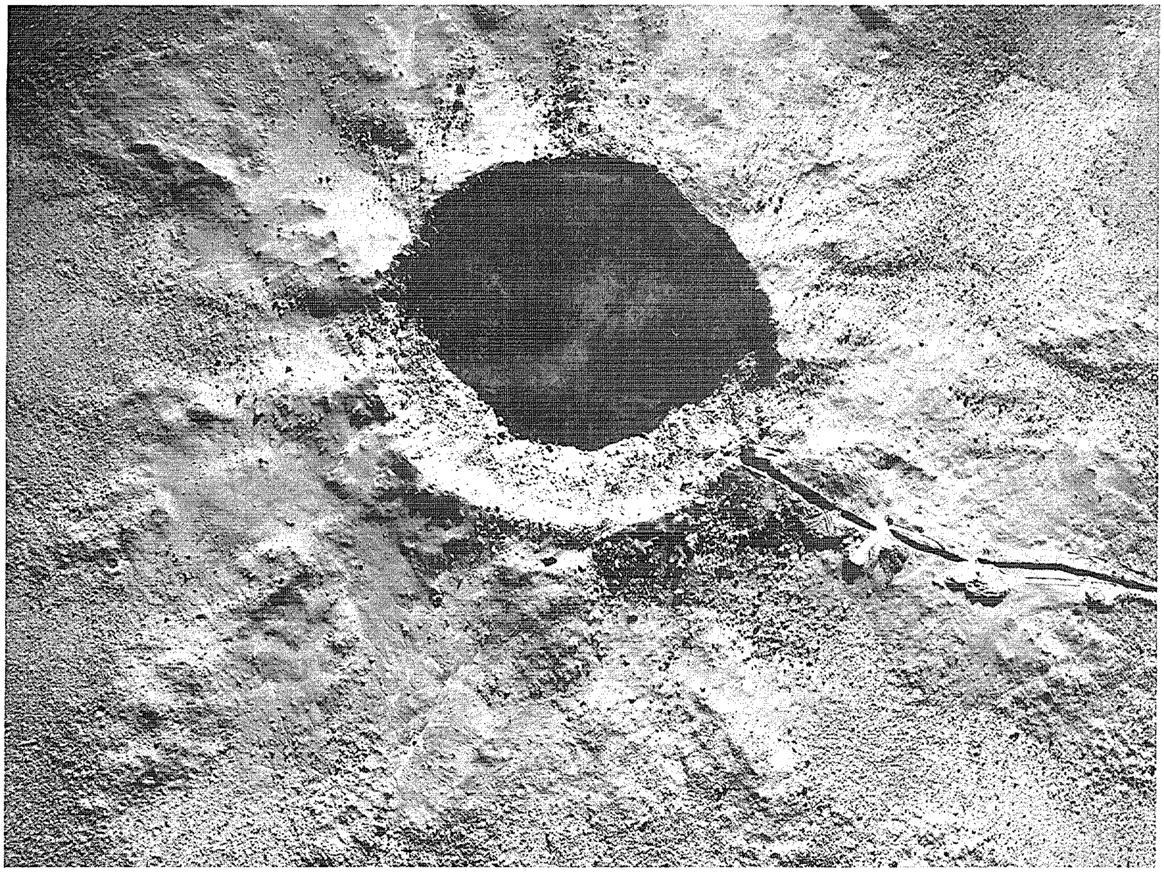

Figure 9

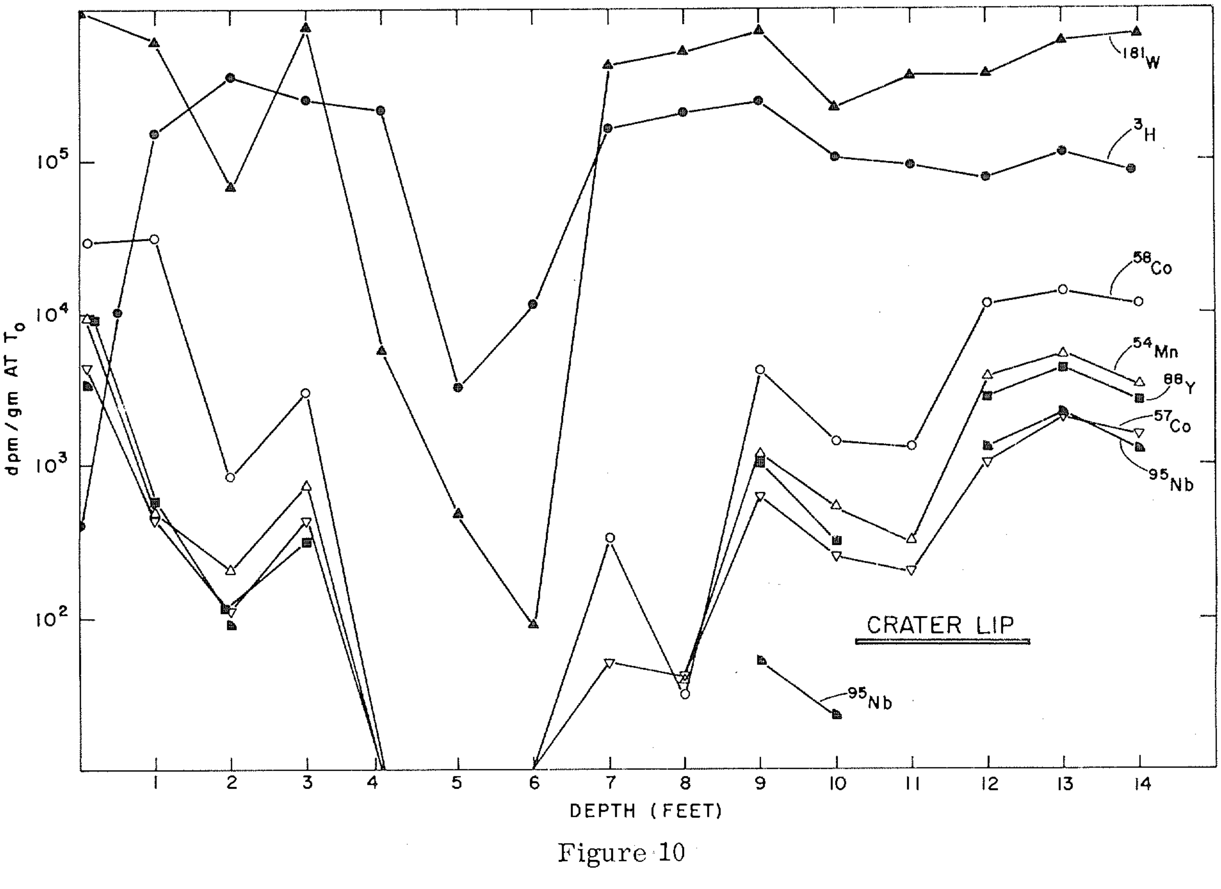

Figure 10

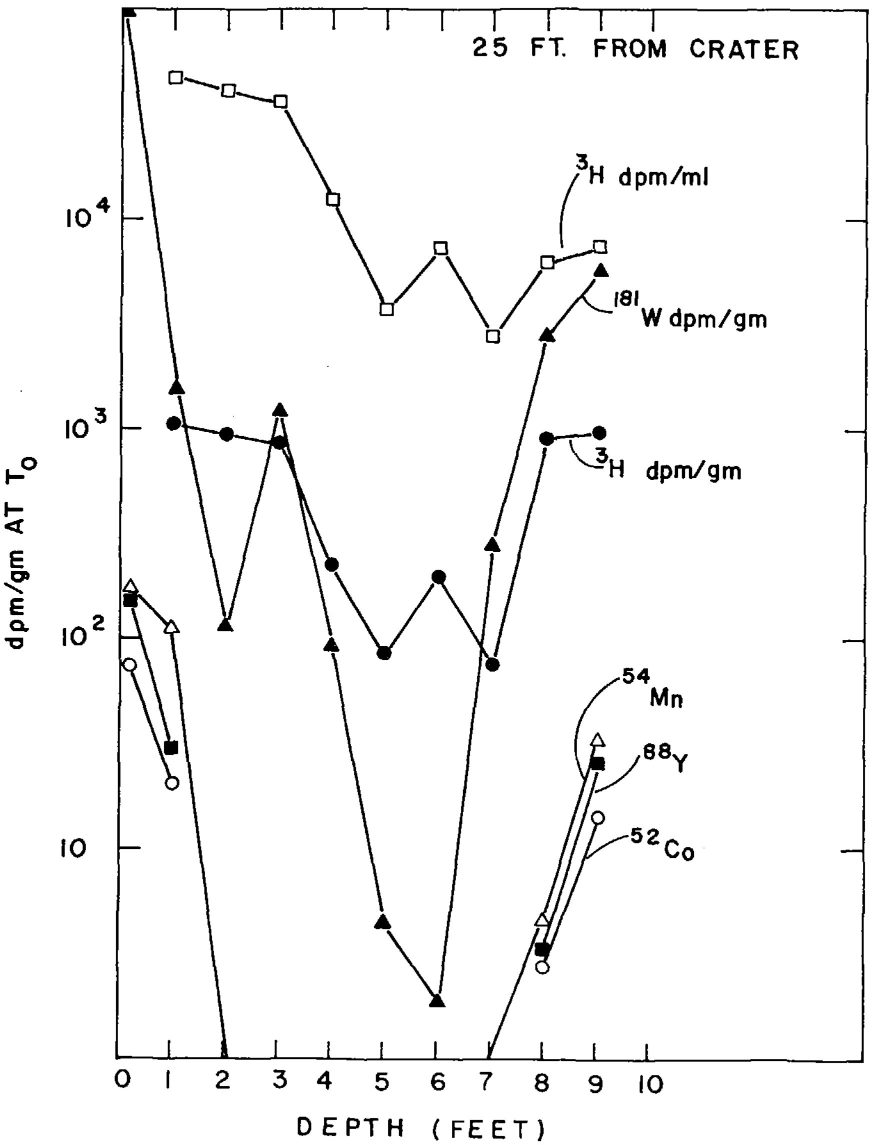

Figure 11

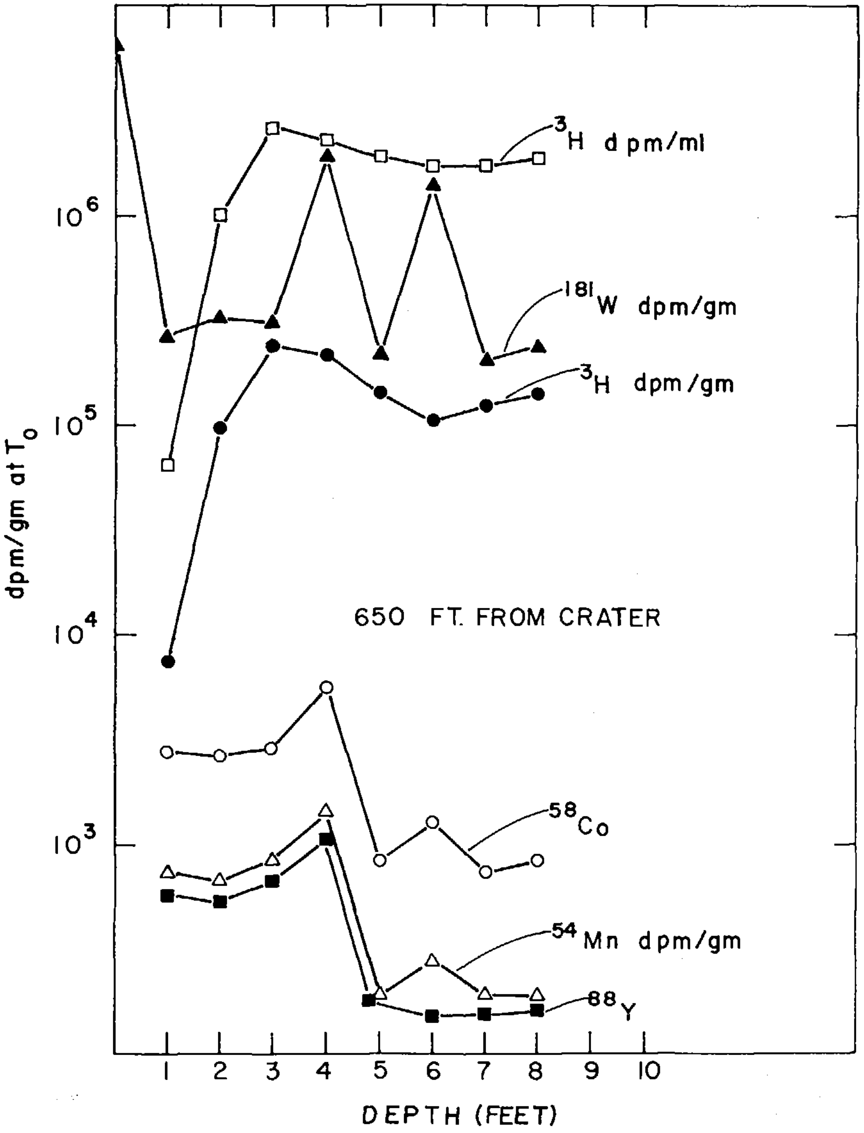

Figure 12

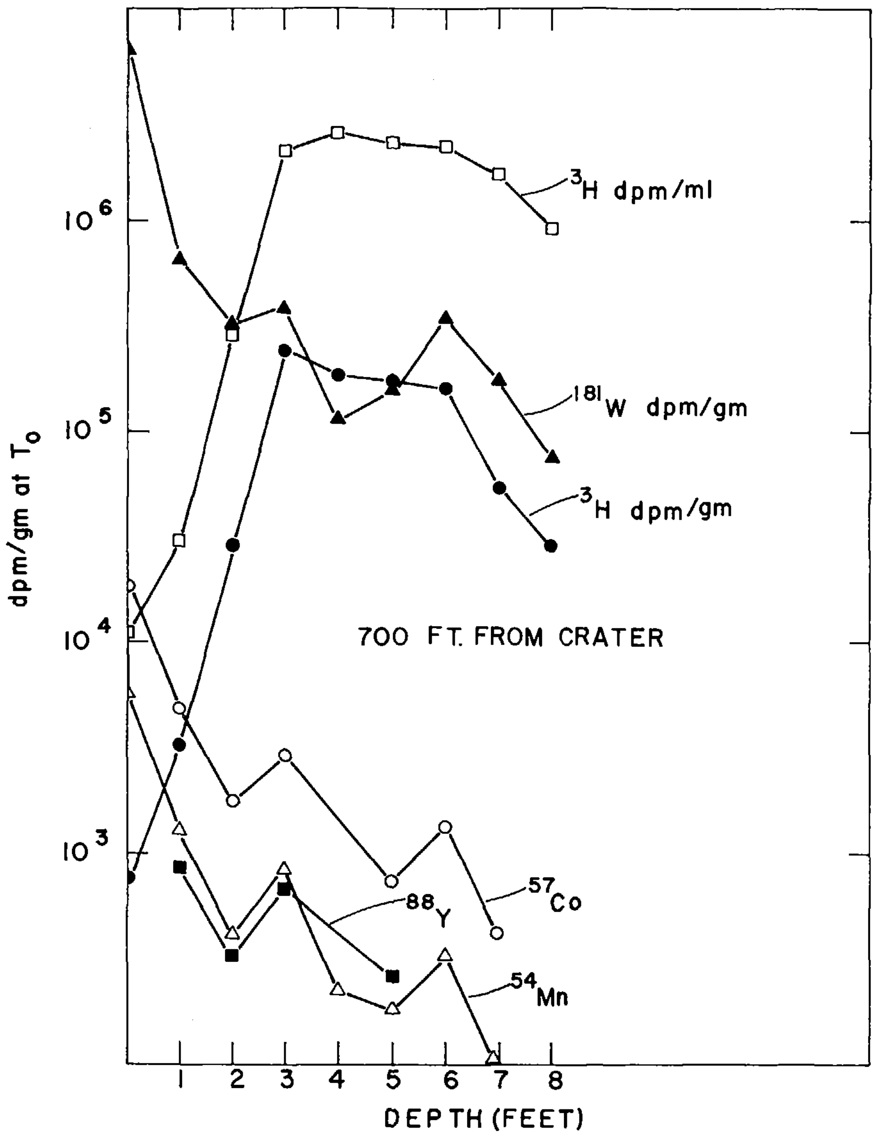

Figure 13

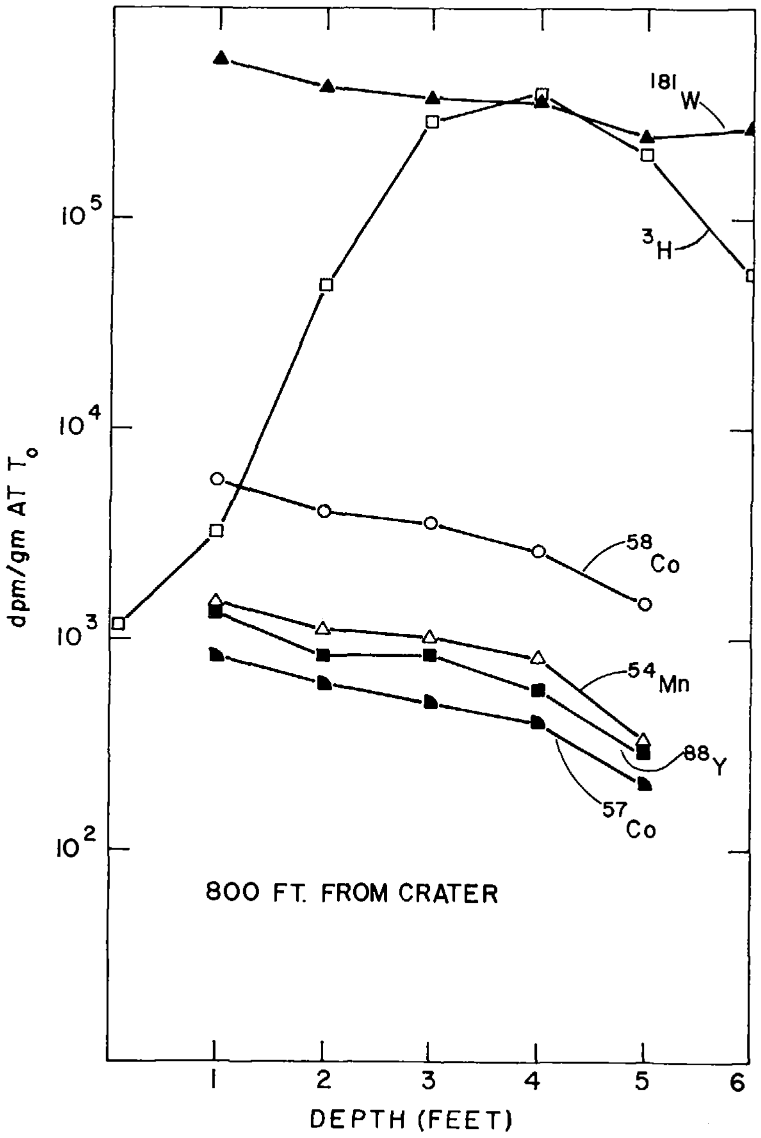

Figure 14

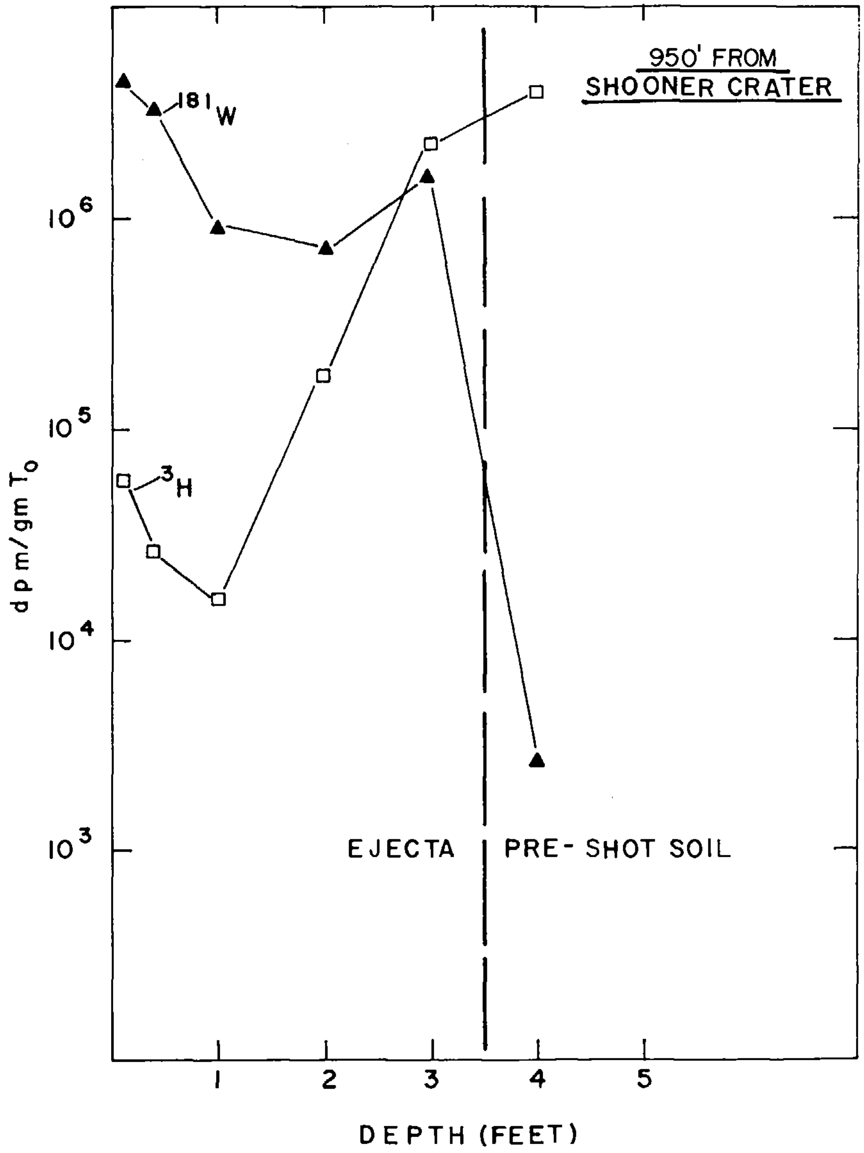

Figure 15

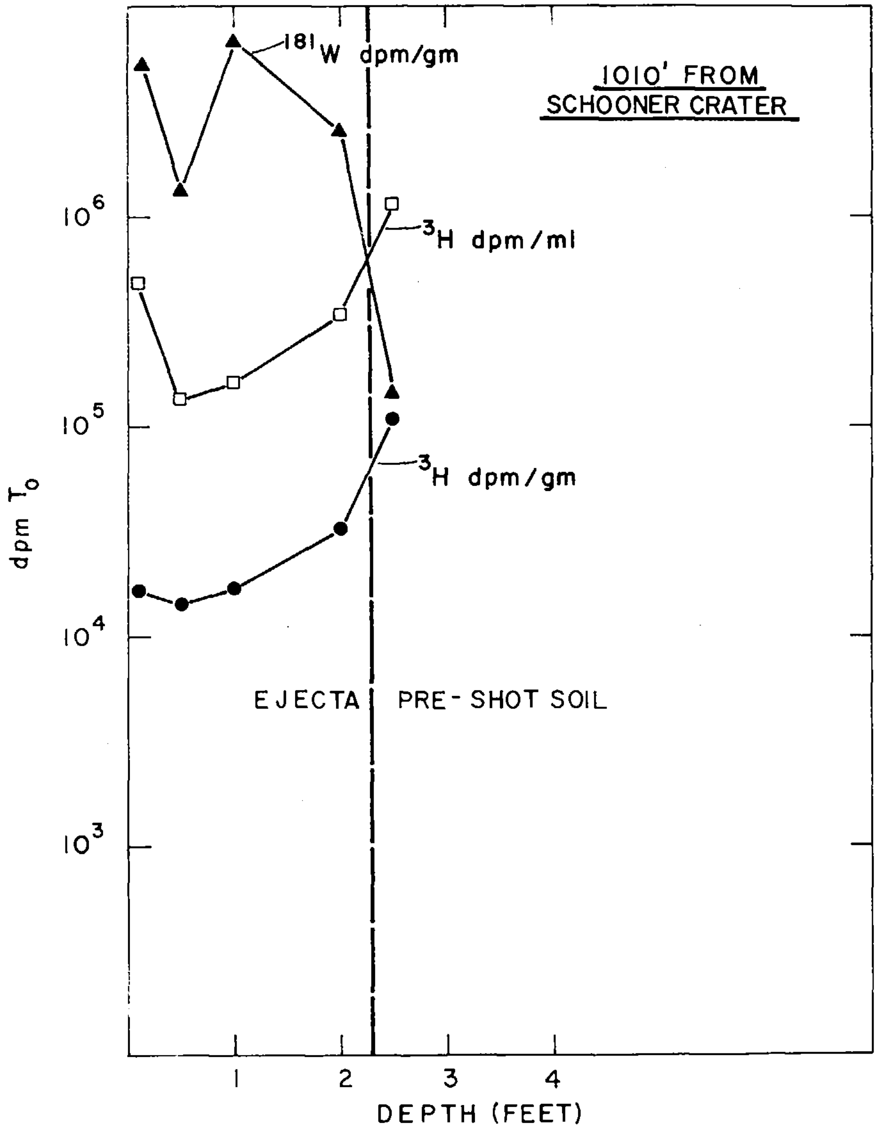

Figure 16

reached at 5 feet. Tritium distribution has been affected by winter and spring rainfall and the peak concentration is seen at 4 feet at the 800 foot station. Peak tritium concentrations are seen at 3 feet at 650 feet and 700 feet from the crater. The second tritium peak seen at depths of 9-14 feet in the crater lip profile is not believed to be caused by rainfall leaching and is a depositional feature.

At 950 feet from the crater, ejecta was approximately 38 inches deep. The distribution of W^{181} and H^3 at that site are shown in Figure 15. W^{181} activity drops rapidly when the parent material is reached whereas tritium activity reaches a maximum in the sub-ejecta preshot soil. This condition is repeated at 1010 feet from the crater, shown in Figure 16, where ejecta is approximately 28 inches deep, and maximum tritium activity in dpm/ml of soil water and dpm/gram of dry soil occur in the sub-ejecta soil.

The data obtained from the samples of ejecta taken from the zone of bulk ejecta transected by the SCHOONER trench indicate that radionuclide concentrations do not decrease continuously with depth, and that strata of high activity occur within the bulk ejecta. The excavation of CABRIOLET crater ejecta did not reveal a distribution of radioactivity as described here for the SCHOONER crater. The SCHOONER crater is the largest nuclear crater created in hard rock and it is possible that in higher yield detonations more uplift and fracture of the contiguous surface geology occurs, allowing radioactivity to be injected into this zone during or prior to venting. The complete analysis of SCHOONER trench data will reveal the extent of the deeper stratum of radioactivity and permit more conclusive statements concerning the distribution of radionuclides in SCHOONER ejecta.

From 1100 feet from the crater to the edge of visible ejecta, a thin covering of fine radioactive particles covers the preshot soil surface. This material is easily transported by the strong winds characteristic of the high desert climate, and at this time most of the ejecta deposited at 3000 feet from GZ has been moved by the wind. This area of shallow ejecta deposits was sampled in May and June 1969 when the trench was excavated. Data from 7 sampling sites in this area are shown in Table I. It is apparent that certain radionuclides have been leached from the surface layer of ejecta into the preshot soil profile. Tritium is the most mobile of the radionuclides in the ejecta and in most cases higher concentrations of tritium are found in the sub-ejecta preshot soil water. W^{181}, Co^{57}, and Mn^{54} also appear in the sub-ejecta soil, presumably having been leached by the same rainfall that translocated tritium from the ejecta into the preshot soil materials.

In January 1969, ejecta samples were obtained at a distance of 3000 feet from GZ as sampling equipment was retrieved. In Figure 17, data obtained at a site 3000 feet southeast of SCHOONER GZ during the first year postshot are shown. The sub-ejecta soil shows an accumulation of W^{181} where activity increased by approximately a factor of 4 during the 360 day period. Soil depths in this area are quite shallow and the parent material (bedrock) is usually encountered at depths less than 2 feet so that it will not be possible to follow the movement of W^{181} to any great depth in this soil system.

TABLE I

SPECIFIC ACTIVITY OF EJECTA COLLECTED AT THE EDGE OF SCHOONER CRATER EJECTA FIELD

	dpm/gram dry ejecta at T_0					
	H^{3}	Co^{57}	Mn^{54}	Nb^{95}	Y^{88}	W^{181}
1400 ft. surface	3.57×10^{2}	1.69×10^{3}	3.14×10^{3}	1.04×10^{3}	2.70×10^{3}	5.65×10^{6}
1400 ft, 1 foot	1.10×10^{3}	2.24	----*	----	----	1.16×10^{4}
1500 ft, surface	1.94×10^{2}	1.17×10^{4}	2.83×10^{4}	8.72×10^{3}	2.28×10^{4}	2.47×10^{6}
1500 ft, 1 foot	3.69×10^{2}	----	----	----	----	1.40×10^{5}
1600 ft, surface	1.39×10^{3}	2.95×10^{3}	5.73×10^{3}	2.63×10^{3}	4.82×10^{3}	1.10×10^{7}
1600 ft, 1 foot	3.65×10^{1}	----	----	----	----	1.92×10^{4}
2000 ft, surface	4.53×10^{1}	3.43×10^{3}	7.33×10^{3}	2.04×10^{3}	6.20×10^{3}	1.58×10^{6}
2000 ft, 1 foot	1.48×10^{3}	4.04	----	----	----	2.81×10^{5}
2100 ft, surface	1.64×10^{2}	1.40×10^{3}	2.53×10^{3}	9.26×10^{2}	2.08×10^{3}	1.20×10^{7}
2100 ft, .5 foot	51.9	----	----	----	----	1.01×10^{4}
2100 ft, 1 foot	79.8	----	----	----	----	1.49×10^{4}
2250 ft, surface	1.71×10^{2}	8.86×10^{2}	1.64×10^{3}	6.30×10^{2}	1.27×10^{3}	1.07×10^{7}
2250 ft, .5 foot	4.64×10^{2}	5.07	----	----	----	1.04×10^{7}
2250 ft, 1 foot	9.60×10^{2}	----	----	----	----	1.36×10^{4}
2350 ft, surface	2.50×10^{2}	1.24×10^{3}	2.21×10^{3}	9.70×10^{2}	1.65×10^{3}	1.31×10^{7}
2350 ft, .5 foot	3.17×10^{2}	16.3	31.0	----	----	4.57×10^{4}
2350 ft, 1 foot	7.80×10^{2}	----	----	----	----	7.36×10^{5}

*Not detected

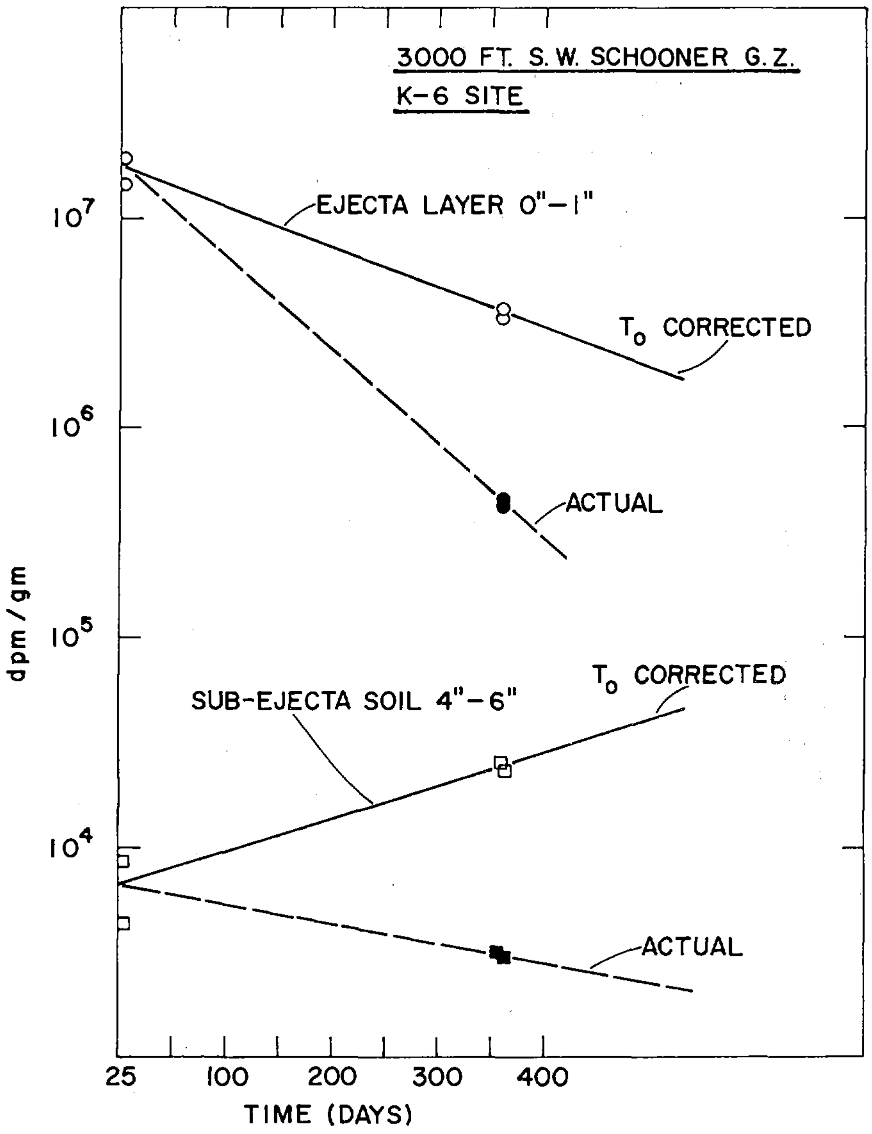
3000 FT. S.W. SCHOONER G.Z.
K-6 SITE
EJECTA LAYER 0"–1"
T_0 CORRECTED
ACTUAL
SUB-EJECTA SOIL 4"–6"
T_0 CORRECTED
ACTUAL
dpm / gm
10^7
10^6
10^5
10^4
25
100
200
300
400
TIME (DAYS)

Figure 17

The crater ejecta and close-in fallout represent a physical continuum of particles with a common source - the crater. The specific activity of ejecta from the surface of the crater lip, from the bulk ejecta area, from the base surge area, and from more distant fallout collection sites, is shown in Table II. Tritium concentrations decrease gradually with distance from the crater as the particles absorb more atmospheric water, and the tritium adsorbed on them becomes more diluted. Other radionuclides such as Co^{57}, may decrease slightly at 1-2 miles from GZ, but all radionuclides, except tritium, have essentially the same specific activity at 17 miles as they have at the crater lip. The specific activity of radionuclides in or on particles collected at 3000 feet, 4800 feet, 6000 feet, at 2 miles, and at 17 miles are shown in Tables III, IV, V, VI, VII, and VIII. These specific activity data when compared to those shown for bulk ejecta at the crater lip are seen to vary by less than a factor of 5 except for tritium. Tritium measurements on fallout particles made in the SCHOONER event could have been affected by losses before tray samplers were retrieved. Improved, self-closing trays will eliminate most of these losses in future experiments.

SUMMARY

Data obtained in long-term studies at SEDAN crater indicate that tritium is the most abundant radionuclide present in the ejecta at this time and that it exhibits complex movements which are correlated with seasonal soil water movement. Gamma radioactivity in SEDAN ejecta has not undergone any large translocations since shot-time.

The distribution of radionuclides in SCHOONER ejecta has been described in a series of cross-sections of the bulk ejecta of that crater. Two strata of high radioactivity were found in the crater lip, 1 at the surface and 1 at depths below 10 feet. Beyond 700 feet from the crater, radioactivity was found to decrease gradually with depth.

At the edge of the SCHOONER ejecta field, postshot movement of radionuclides was demonstrated by the presence of H^3 and W^{181}, and to a limited extent of Co^{57} and Mn^{54}, in the sub-ejecta preshot soil. The availability of these radionuclides in laboratory experiments with SCHOONER ejecta (Preliminary Report) corroborates the mobility of these isotope species.

The specific activity of radionuclides along the ejecta continuum namely, at the crater lip, in bulk ejecta, in the base surge area, and in fallout - has been compared. Except for some small variations along this particulate continuum, the specific activity of radionuclides on particles obtained at 17 miles, except for tritium, was very similar to that found on the crater lip.

TABLE II

SPECIFIC ACTIVITY OF RADIONUCLIDES IN SURFACE EJECTA AND FALLOUT FROM SCHOONER NUCLEAR CRATER

	Crater Lip	800 ft from Crater	4800 ft from GZ*	2 miles from GZ*	17 miles from GZ*
Co^{57}	4.31×10^{3}	2.30×10^{3}	6.59×10^{3}	7.33×10^{2}	4.13×10^{3}
Mn^{54}	9.62×10^{3}	6.20×10^{3}	1.09×10^{3}	6.50×10^{3}	8.33×10^{3}
Nb^{95}	3.37×10^{3}	2.10×10^{3}	5.38×10^{3}	3.53×10^{3}	3.51×10^{3}
Y^{88}	9.02×10^{3}	5.25×10^{3}	7.92×10^{2}	5.56×10^{3}	7.11×10^{3}
W^{181}	9.80×10^{6}	1.28×10^{7}	1.34×10^{7}	1.98×10^{7}	6.63×10^{6}
H^{3}	1.52×10^{5}	9.13×10^{4}	7.40×10^{3}	4.51×10^{3}	1.42×10^{3}

*Fallout tray samples.

TABLE III

SPECIFIC ACTIVITIES OF RADIONUCLIDES IN FALLOUT PARTICLES COLLECTED IN 2 × 2 FOOT TRAYS AT 3000 FEET FROM SCHOONER GZ

	SK-150A S-3 80° E.N.	SK-149C S-3 80° E.N.	SK-149B S-3 80° E.N.	SK-151A S-2A 30° E.N.	SK-152A S-2C 30° E.N.
			dpm/gram dry ejecta T_0		
Co^{57}	1.40×10^{3}	8.73×10^{2}	1.41×10^{3}	6.46×10^{2}	9.29×10^{2}
Ru^{103}	3.09×10^{3}	2.81×10^{3}	----	3.15×10^{3}	2.85×10^{3}
Mn^{54}	2.93×10^{3}	1.50×10^{3}	3.05×10^{3}	1.25×10^{3}	1.81×10^{3}
Nb^{95}	9.39×10^{2}	----	1.16×10^{3}	5.64×10^{2}	7.10×10^{2}
Co^{58}	9.13×10^{3}	5.10×10^{3}	9.15×10^{3}	3.82×10^{3}	5.78×10^{3}
Y^{88}	2.57×10^{3}	1.60×10^{3}	2.37×10^{3}	1.23×10^{3}	1.48×10^{3}
W^{181}	1.10×10^{7}	1.06×10^{7}	1.18×10^{7}	8.56×10^{6}	9.70×10^{6}
H^{3}	1.15×10^{5}	1.14×10^{5}	4.30×10^{5}	7.65×10^{4}	4.62×10^{4}
H^{3*}	1.22×10^{6}	8.15×10^{5}	1.46×10^{6}	4.04×10^{5}	2.52×10^{5}

*dpm per milliliter of adsorbed water extracted by vacuum distillation.

TABLE IV

SPECIFIC ACTIVITY OF RADIONUCLIDES IN FALLOUT PARTICLES COLLECTED IN 2 × 2 FOOT TRAYS AT 4800 FEET FROM SCHOONER GZ, 338° E. OF N.

	SK-146B	SK-146A	SK-148C	SK-147A	SK-145
	dpm/gram dry ejecta at T_0				
Co^{57}	7.01×10^2	6.33×10^2	6.16×10^2	6.56×10^2	5.92×10^2
Ru^{103}	2.87×10^3	2.49×10^3	2.09×10^3	2.35×10^3	2.65×10^3
Mn^{54}	1.29×10^3	1.23×10^3	9.87×10^2	9.77×10^2	9.84×10^2
Nb^{95}	6.26×10^2	4.86×10^2	----	5.01×10^2	5.39×10^2
Co^{58}	4.24×10^3	4.09×10^3	2.79×10^3	4.13×10^3	3.37×10^3
Y^{88}	9.60×10^2	8.53×10^2	4.54×10^2	8.85×10^2	8.08×10^2
W^{181}	1.27×10^7	1.74×10^7	1.27×10^7	1.27×10^7	1.16×10^7
H^3	7.34×10^3	3.34×10^3	7.87×10^3	6.80×10^3	6.68×10^3

TABLE V

SPECIFIC ACTIVITY OF RADIONUCLIDES IN FALLOUT PARTICLES COLLECTED IN 2 × 2 FOOT TRAYS AT 6000 FEET FROM SCHOONER GZ

	S-5-1 SK-144 32° E.N.	S-5-2 SK-142 32° E.N.	S-5-3 SK-143 32° E.N.
	dpm/gram dry weight at T_0		
Co^{57}	1.55×10^4	1.31×10^4	1.36×10^4
Ru^{103}	----	1.87×10^4	----
Mn^{54}	4.71×10^4	4.08×10^4	4.10×10^4
Nb^{95}	1.53×10^4	1.57×10^4	1.45×10^4
Co^{58}	1.27×10^5	9.94×10^4	1.08×10^5
Y^{88}	4.51×10^4	3.73×10^4	3.68×10^4
W^{181}	4.23×10^7	3.27×10^7	4.13×10^7
H^3	3.64×10^3	6.34×10^3	9.13×10^3

TABLE VI

SPECIFIC ACTIVITY OF RADIONUCLIDES IN FALLOUT PARTICLES COLLECTED IN 2 × 2 FOOT TRAYS AT 2 MILES FROM SCHOONER GZ

	S-12-1 SK-134 324° E.N.	S-12-2 SK-133 324° E.N.	S-13-1 SK-129 336° E.N.	S-13-2 SK-130 336° E.N.	S-16 SK-112A 53° E.N.
	dpm/gram dry weight at T_0				
Co^{57}	5.56×10^{2}	5.50×10^{2}	7.83×10^{2}	7.27×10^{2}	1.05×10^{4}
Ru^{103}	2.60×10^{3}	2.57×10^{3}	3.27×10^{3}	----	----
Mn^{54}	8.04×10^{2}	9.04×10^{2}	1.06×10^{3}	1.15×10^{3}	2.86×10^{4}
Nb^{95}	3.30×10^{2}	----	5.81×10^{2}	----	1.07×10^{4}
Co^{58}	3.09×10^{3}	3.31×10^{3}	4.10×10^{3}	3.64×10^{3}	8.15×10^{4}
Y^{88}	4.93×10^{2}	5.88×10^{2}	6.56×10^{2}	8.68×10^{2}	2.52×10^{4}
W^{181}	1.36×10^{7}	1.36×10^{7}	1.90×10^{7}	1.89×10^{7}	3.39×10^{7}
H^{3}	4.25×10^{3}	6.78×10^{3}	1.55×10^{3}	3.92×10^{3}	6.09×10^{3}

TABLE VII

SPECIFIC ACTIVITY OF RADIONUCLIDES IN FALLOUT PARTICLES COLLECTED IN 2 × 2 FOOT TRAYS AT 2 MILES FROM SCHOONER GZ

	S-14 SK-137 20° E.N.	S-14-1 SK-136 20° E.N.	S-14-2 SK-138 20° E.N.
	dpm/gram dry weight at T_0		
Co^{57}	6.05×10^{3}	7.92×10^{3}	8.17×10^{3}
Ru^{103}	----	----	----
Mn^{54}	1.64×10^{4}	2.24×10^{4}	2.29×10^{4}
Nb^{95}	5.58×10^{3}	7.70×10^{3}	7.25×10^{3}
Co^{58}	4.74×10^{4}	6.28×10^{4}	6.64×10^{4}
Ru^{106}	----	----	----
Y^{88}	1.29×10^{4}	2.18×10^{4}	1.97×10^{4}
W^{181}	2.73×10^{7}	3.26×10^{7}	3.49×10^{7}
H^{3}	7.18×10^{3}	7.39×10^{3}	4.40×10^{3}

TABLE VIII

SPECIFIC ACTIVITY OF RADIONUCLIDES IN FALLOUT PARTICLES COLLECTED IN 2 x 2 FOOT TRAYS AT 17 MILES FROM SCHOONER GZ

	S-43 SK-127 7° E.N.	S-44 SK-126 17° E.N.	S-45 SK-125 27° E.N.	S-46 SK-124 37° E.N.	S-47 SK-123 47° E.N.
	dpm/gram dry weight at T_0				
Co^{57}	1.27×10^3	8.59×10^2	1.17×10^4	2.44×10^3	4.48×10^3
Mn^{54}	1.87×10^3	1.57×10^3	2.30×10^4	5.57×10^3	9.76×10^3
Co^{58}	8.31×10^3	5.49×10^3	7.33×10^4	1.77×10^4	2.78×10^4
Y^{88}	1.82×10^3	1.26×10^3	1.91×10^4	4.69×10^3	8.69×10^3
W^{181}	3.73×10^6	6.19×10^5	6.66×10^6	1.36×10^6	2.08×10^7
H^3	1.63×10^4	3.63×10^3	1.58×10^4	4.23×10^3	3.14×10^4
Nb^{95}	----	8.56×10^2	7.76×10^3	1.97×10^3	4.47×10^3
Ru^{103}	----	----	----	2.88×10^3	----

REFERENCES

1. M. Nordyke and M.M. Williamson, "The Sedan Event," Lawrence Radiation Laboratory and U.S. Army Corps. of Engineers, Livermore, Rept. PNE-242F (1965).
2. J.J. Koranda, "Residual Tritium at Sedan Crater," 2nd Radioecology Symp., June, 1967, Ann Arbor, Mich. (1967).
3. J.J. Koranda, J.R. Martin, and R.W. Wikkerink, "Residual Tritium at Sedan Crater - Part II Soil and Ejecta Studies," Lawrence Radiation Laboratory, Livermore, Rept. UCRL-50360 (1967).
4. J.J. Koranda, J.R. Martin, and Robert W. Wikkerink, "Leaching of Radionuclides at Sedan Crater," 155th Natl. American Chemical Society Meeting, San Francisco, Calif., March 31-April 5, 1968.
5. J.J. Koranda and John R. Martin, "The Persistence of Radionuclides at Sites of Nuclear Detonations," Proc. Biomedical Symp., Biological Implications of the Nuclear Age, Lawrence Radiation Laboratory, Livermore, March 5-7, 1969.
6. B. Shore *et al.*, "The Fate and Importance of Radionuclides in Plowshare Events," U.S. Public Health Service Symp., Las Vegas, Nevada, April 7-11, 1969.
7. R.H. Carlson and W.A. Roberts, "Project Sedan: Mass Distribution and Throwout Studies," The Boeing Company, Seattle, Wash., PNE-217F (1963).
8. L.R. Anspaugh *et al.*, "Biomedical Division Preliminary Report for Project Schooner," Lawrence Radiation Laboratory, Livermore, Rept. UCRL-50718 (1969).

XA04N0761

RADIOECOLOGICAL STUDIES OF TRITIUM MOVEMENT IN A TROPICAL RAIN FOREST*

J.R. Martin, C.F. Jordan†, J.J. Koranda, and J.R. Kline†
Bio-Medical Division
Lawrence Radiation Laboratory, University of California
Livermore, California 94550

ABSTRACT

Several experiments on the movement of tritium in a tropical ecosystem have been conducted in the montane rainforest of Eastern Puerto Rico by the Bio-Medical Division of the Lawrence Radiation Laboratory, Livermore, in cooperation with the Puerto Rico Nuclear Center. Tritiated water was used as a tracer for water movement in: a) mature evergreen trees of the climax rainforest; b) soil and substory vegetation and c) rapidly growing successional species.

A feasibility study on the Atlantic Pacific Interoceanic Canal is currently being conducted. If thermonuclear explosives were used in constructing the canal, tritium would be deposited as tritiated water and distributed among the several biological compartments of the tropical ecosystem in that area. The main hydrogen compartments are water in the soil and in leaves, limbs and wood of forest trees. Organic tissue hydrogen comprises another compartment.

In the tree experiment, tritiated water was injected directly into several species of mature, broad leaved evergreen tropical trees. Transpiration and residence time for tritium was determined from analyses of leaves sampled during a several month period. Transpiration ranged from 4 ml/day/gm dry leaf for an understory <u>Dacryodes excelsa</u> to 10.0 and 13.8 ml/day/gm dry leaf for a mature <u>Sloanea berteriana</u> and <u>D. excelsa</u>, respectively. Mean residence time for the <u>S. berteriana</u> was 3.9 ± 0.2 days and the understory and mature <u>D. excelsa</u> values were 9.5 ± 0.4 and 11.0 ± 0.6 days, respectively.

In another experiment, tritiated water was sprinkled over a 3.68 m^2 plot and its movement down into the soil and up into the vegetation growing on the plot was traced. The pattern of water movement in the soil

---

* Work performed under the auspices of the U.S. Atomic Energy Commission.

† Formerly with the Puerto Rico Nuclear Center, presently with the Argonne National Laboratory.

was clearly demonstrated. The mean residence time for tritium in the soil and in trees was found to be 42 ± 2 days and 67 ± 9 days, respectively. The residence time for tritium in the trees in this experiment was considerably longer than for the single injected input pulse due to the continuous root uptake of tritium as the diffuse peak moved down into the soil past the root zone. Tritium was removed from the plot by transpiration and by interflow. Using transpiration rates from the previous experiment, rainfall records, tree density data and other measurements, average transpiration for the Puerto Rico rainforest was computed to be 3.64 kg/m^2/day. The effective capacity of the soil compartment was calculated to be 280 ± 12 kg/m^2.

In the final experiment, tritiated water was injected directly into several species of successional trees in a cleared plot. After several weeks, the trees were harvested and aliquots selected for bound tritium assay. The amount of tritium incorporated into the tissue was about 0.1 percent of the total amount applied to the tree.

Based on all experimental data, the distribution of tritium from a simulated rainout following a one megaton thermonuclear detonation is presented for a climax tropical rainforest and for successional vegetation. The fraction of input tritium remaining in each compartment as a function of time is tabulated. The residence time for each of the compartments determines the persistence of tritium deposited in a tropical ecosystem.

INTRODUCTION

Since thermonuclear explosives are being considered for a variety of peaceful applications, a study on tritium movement in the environment was initiated in order to determine the persistence and biological significance of this abundantly produced radioisotope in tropical regions. Several experiments on the movement of tritium in a tropical ecosystem have been conducted on the montane rainforest of Eastern Puerto Rico by the Bio-Medical Division of the Lawrence Radiation Laboratory, Livermore, California, in cooperation with the Puerto Rico Nuclear Center. Tritiated water was used as a tracer for water movement in: a) mature evergreen trees of the climax rainforest; b) soil and substory vegetation, and c) rapidly growing successional species.

If thermonuclear explosives were used in constructing a new Atlantic-Pacific Canal in Central America, tritium would be deposited as tritiated water and distributed among the several biological compartments of the tropical ecosystems of that area. The main hydrogen compartments are water in the soil and in forest trees. Organically bound hydrogen in plant tissues comprises another compartment. The flux of water through these compartments is a result of rainfall, soil water movement, plant uptake and transpiration. Previous studies of water and tritium movement in the tropical ecosystem have been based on ecological and hydrological estimates.

A model for the behavior of tritium based on the hydrogen budget of the rainforest was formulated by Odum and Bloom.[1] Charnell _et al._[2] cited the need for experimental data in their discussion on the hydrologic redistribution of radionuclides deposited in the environment following a nuclear excavation. They present a numerical model to estimate the rate of removal of radionuclides from fallout, ejecta and fallback.

Golley et al.[3] characterized the structure of tropical forests in Panama and Columbia. The tropical moist forest which makes up 75 percent of that area is similar in biomass and rainfall to the montane rainforest in Puerto Rico. McGinnis et al.[4] discuss the hydrologic budgets of the Panamanian tropical moist forest. They list the transfer functions and turnover (mean residence) times for eight water compartments of that ecosystem based on watershed hydrologic data.

The purpose of our experiments was to determine directly the pattern of movement and distribution of tritium in several compartments of the rainforest ecosystem by means of tritiated water tracers. Based on these experiments, the distribution of tritium from a simulated rainout following a hypothetical one megaton thermonuclear detonation can be defined for a climax tropical rainforest and for successional vegetation. The residence time for each of the compartments will determine the persistence and biological significance of tritium deposited in a tropical ecosystem.

EXPERIMENTS

The tree experiment (Experiment A) consisted of the injection of high specific activity tritiated water directly into three broad leaved evergreen tropical trees. One was a mature Dacryodes excelsa, one was a Sloanea berteriana, and one was an understory Dacryodes excelsa. A fifty foot tower erected adjacent to the trees provided access to the canopy top from which leaf samples were collected over a period of three months. Water was extracted from the leaf samples by freeze drying under vacuum. Assay for tritium in the leaf water was done by liquid scintillation counting. Dried tissue residues were also assayed for bound tritium.

In the plot experiment (Experiment B), 50 mCi of tritium in four liters of water was sprinkled uniformly over a 3.68 m^2 plot containing several substory tree species. Duplicate soil water collectors called Zero Tension Lysimeters (described by Jordan[5]), each with an effective collection area of 154 cm^2, were installed at each of four depths: just below the litter, and at 5", 10" and 15" below the soil surface. Leaf samples of four trees growing on the plot were picked and water extracted as in the tree experiment. Samples were collected daily during the first week and then at increasing intervals for nearly a year. Water vapor from the air was collected during the first week from sites above and around the plot by condensing it in cold traps.

The secondary successional experiment (Experiment C) was conducted in a portion of the rainforest which had been cleared several years earlier. Six successional trees ranging in height from 5 to 15 feet were injected with one millicurie of tritiated water. Leaf disc samples were taken daily to check the uptake of tritium. Two of the six trees were harvested within one week. The others were harvested one month after the tritium injection. Portions of the stem, roots and leaves were freeze dried and free water was vacuum extracted. Tritium assay was done on the free water and on dried tissue of these selected aliquots.

RESULTS AND DISCUSSION

Tree Experiment.

The results of the tree experiment indicate that tritium was incorporated into the tree water and moved with the transpiration stream. Figure 1 is a plot of tritium activity in leaves versus time (activity time curve) for the mature Dacryodes excelsa. The pattern of release represents an exponential removal of tritium from the tree. The mean residence time given in Table I is the fitted straight line portion of the curve beyond the peak. The data may indicate a species dependency as the Sloanea berteriana has a mean residence time of 3.9 ± 0.2 days while the understory and mature Dacryodes excelsa have mean residence times of 9.5 ± 0.4 and 11.0 ± 0.6 days, respectively.

Bergner,[6-11] in his theoretical analysis of tracer dynamics, has shown that the exchangeable mass in a biological system can be formally and exactly defined. Orr and Gillespie[12] recognized the wide applicability of this theoretical treatment in introducing their occupancy principle. The occupancy principle relates the integral of the activity time curve to the occupancy or mean residence time. The occupancy is defined as the total integral, with respect to time, of the tracer that is in the system. The occupancy principle states that the ratio of occupancy to capacity equals the reciprocal of the entry flow. In our analysis, the amount of tritium injected was equated to the product of entry flow or transpiration and the integral of the activity time curve. It is interesting to note that this independent engineering approach to the problem yielded the identical solution which was later recognized as being supported by Bergner's theoretical treatment of the biological system as explained by Orr and Gillespie.

Transpiration, F, (ml/day) for the trees can therefore be computed by dividing the amount of tritium injected, M, (dpm) by the integral, I, (dpm/ml/day) of the activity time curve.

$$F = M/I$$

As Orr and Gillespie show, this calculation does not depend on the manner of transport of the tracer through the biological system or on the usual assumption of instantaneous or complete mixing. The validity of the treatment depends only on the fact that the tracer enters into some relationship with any compartment of the system.

The regressions of Ogawa et al.[13] were used to estimate the dry biomass of the leaf compartment so that transpiration could be expressed as specific transpiration (ml/day/gm dry leaf). Transpiration, estimated leaf biomass and specific transpiration for the three trees, are given in Table I. Specific transpiration can be seen to increase with tree size. The shaded understory Dacryodes excelsa transpires 4.0 ml/day/gm dry leaf compared with 10.0 and 13.8 ml/day/gm dry leaf for the mature canopy trees Sloanea berteriana and Dacryodes excelsa.

No measurable tritium was found in the dried tissue of the leaf samples indicating that the incorporation of tritium in the bound hydrogen compartment was less than 0.1 percent. Kline et al.[14] discuss the tree experiment in greater detail. The value of the tree injection experiment lies in the use of the data to obtain a measure of transpiration in tropical trees which is used later in the analysis of water movement through the entire ecosystem.

Plot Experiment.

The movement of tritiated water down into the soil is illustrated in Figure 2 where the tritium activity of soil water is plotted as a function of depth for selected days following the surface application of tritium. The wave-like pattern is similar to that described by Zimmerman *et al.*[15] The rate of movement of the peak is slowed considerably after reaching the solum-sub-soil interface where the bulk density changes from 0.57 to 1.02 gm/cc.

A measure of the residence time for tritium in the soil was made by plotting the integral of each activity depth curve (corrected for the percent water) as a function of time. The curves were extrapolated beyond the depth of sampling so that virtually all of the tritium in the profile would be included in the integral. The plot is shown in Figure 3. The mean residence time was determined to 42 ± 2 days by a least squares fit of the data. If the integral is taken only over the sampling depth of surface to 15", the mean residence time is 37 ± 2 days. The intercept value in both cases gives an initial surface concentration of 13 ± 2 mCi/m^2 which agrees with the applied value of 13.6 mCi/m^2. Since the observed residence time in the soil based on the surface to 15" integral was very close to that determined for the total tritium profile integral, most of the loss mechanisms may be considered to be from the top 15" of soil in this ecosystem.

One loss mechanism is by transpiration. The leaf samples of the four tree species showed the same exponential removal of tritium by transpiration as in the tree experiment except that the average apparent residence time is much longer, 67 ± 9 days. A typical response curve is illustrated in Figure 4. The mean residence time is the straight line portion of the curve beyond the peak. The results are given in Table I.

The longer residence time of tritium in the trees of the plot experiment (67 days) compared with that observed in the tree experiment (4 to 11 days) is due to the coupling of the soil and tree water compartments. Rather than receiving a single injection in time as in the tree experiment, the trees in the plot experiment take up tritium over a period of time as the diffuse peak moves down past the root zone. The residence time in the soil will therefore control the residence time in the trees.

The longer apparent residence time in the trees (67 days) compared with the soil (42 days) of the plot may be explained by the unequal depth distribution of tritium shown in Figure 2. If deep tree roots take up a greater fraction of water than shallow roots, the early tree data will be relatively low with respect to the soil integral because a greater fraction of the transpiration will contain less tritium. At later times, as the tritium peak moves down past the deep roots, the transpiration will contain a greater fraction of higher specific activity tritiated water and the observed tree water will be relatively higher. The net effect would be a straight line with less slope and a longer residence time for the tree water.

Another possible explanation can be given if one considers that the soil compartment also loses tritium in lateral flow through the soil

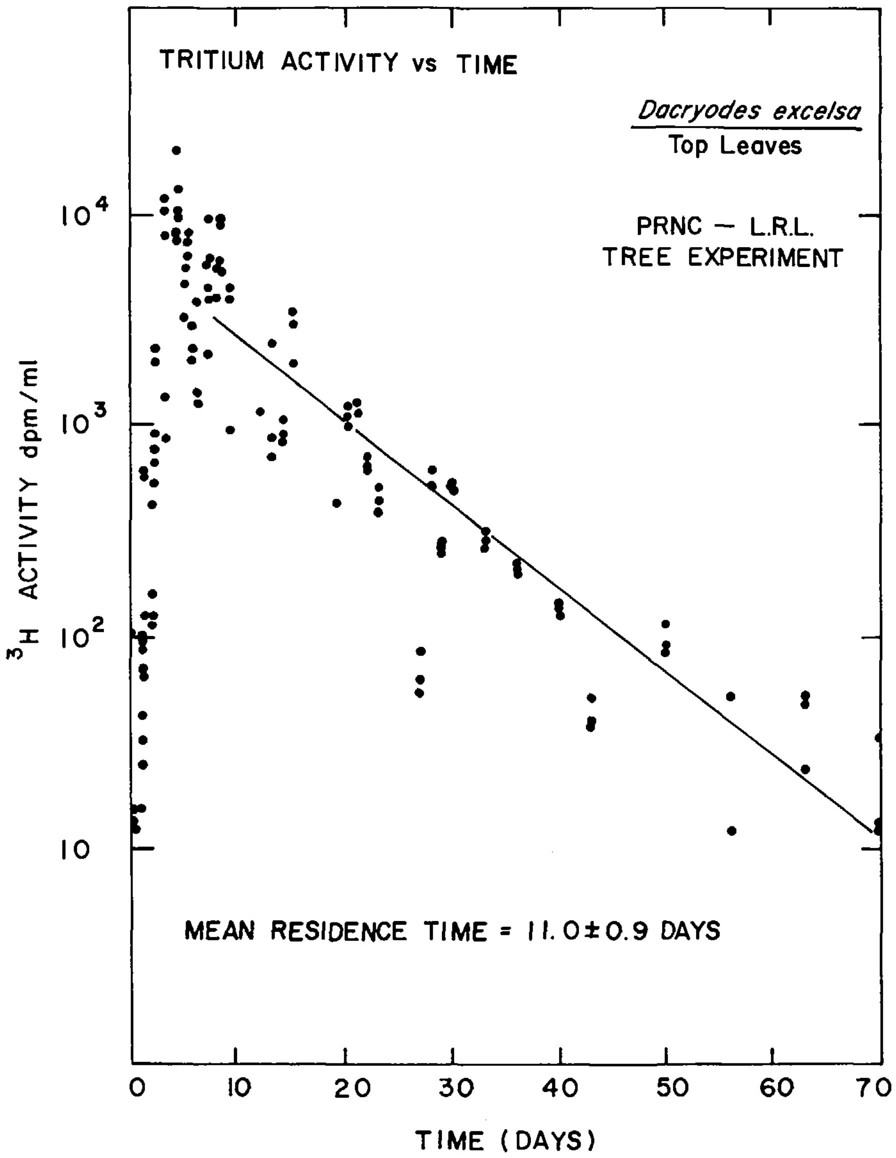

Figure 1

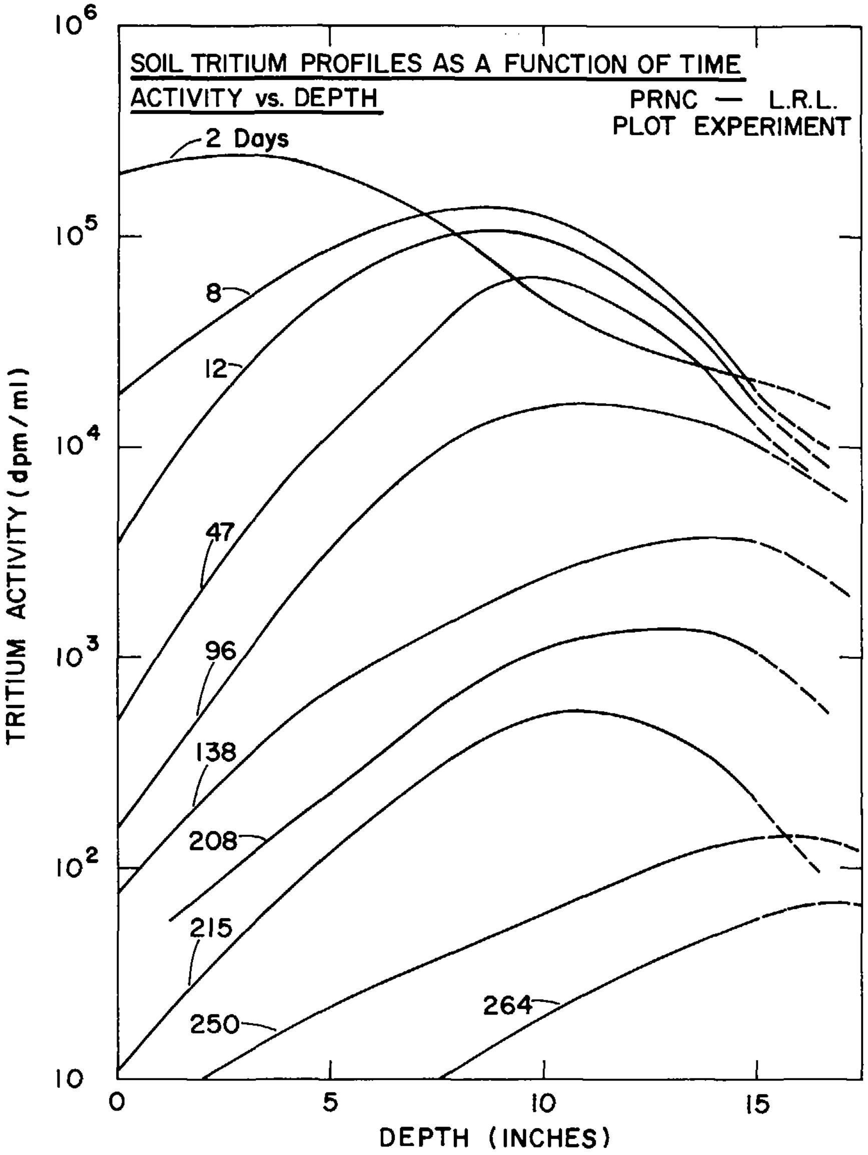

Figure 2

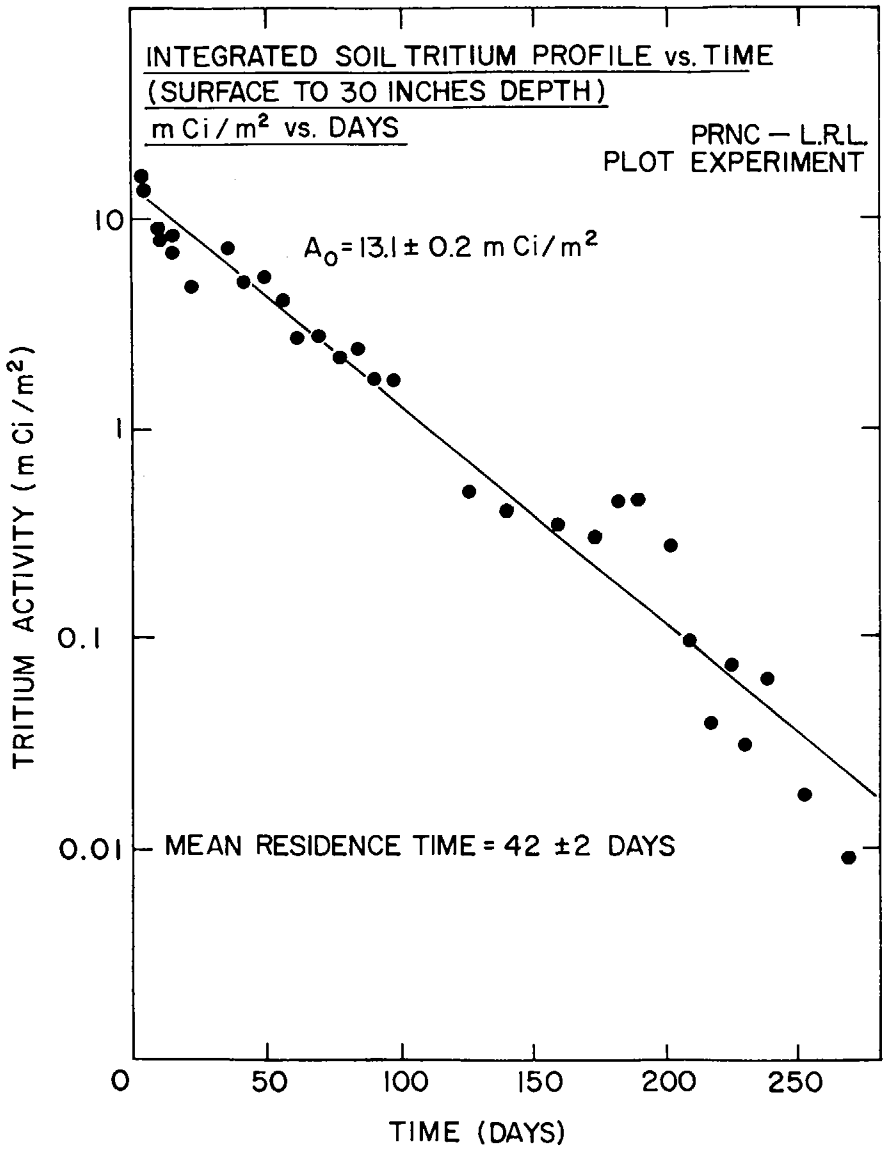

Figure 3

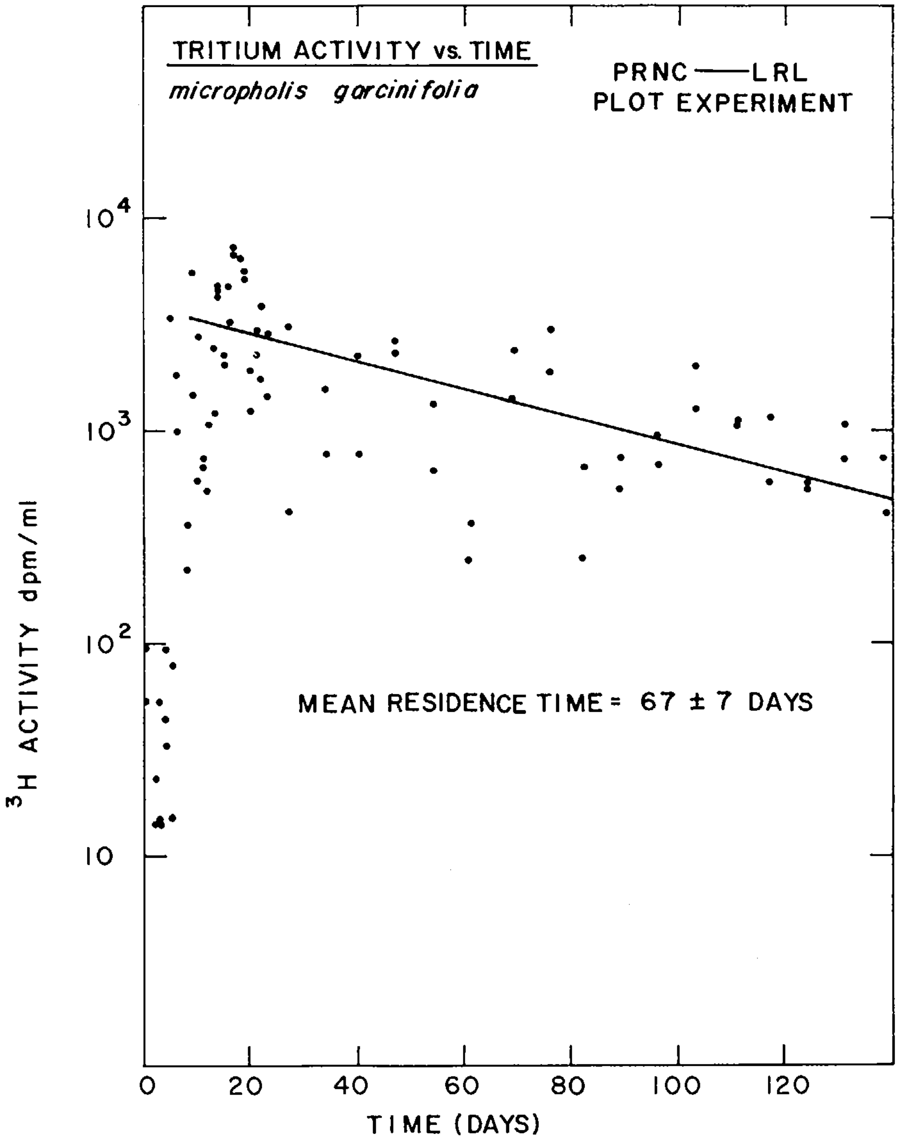

Figure 4

called subsurface runoff or interflow. The soil layer or solum of the rainforest is only 5 to 20 inches deep. Below the solum is a relatively impervious layer of higher bulk density sub-soil. The observed soil loss rate (λ_S) can be considered to be the sum of two loss rates, transpiration (λ_T) and interflow (λ_R).

$$\lambda_S = \lambda_T + \lambda_R$$

The loss rate, λ, is the reciprocal of the mean residence time (T) so that,

$$1/T_S = (1/T_T) + (1/T_R)$$

and
$$T_R = (T_T T_S)/(T_T - T_S)$$

The interflow soil residence time T_R for the 3.68 m^2 plot in this study is computed to be 111 ± 40 days in order to account for the difference between the tree residence time and the observed soil residence time. The relatively large uncertainty in T_R is due to the combination of uncertainties of T_S and T_T in the difference term ($T_T - T_S$). There would be no way to physically isolate the interflow and transpiration loss mechanisms. This analysis is given merely as a possible explanation for the difference in the observed residence times of tritium in the trees and soil.

The air moisture samples showed that the tritiated water vapor remained essentially at ground level. The samples at 100 cm above the plot were 100 times less than the level at 4 cm, and 5 to 10 times higher than the activity at 175 cm. Figure 5 shows the tritium activity at 4 cm and at 100 cm above the plot. The highest activity sampled at 4 cm above the center of the plot was 0.3 μCi/ml which corresponds to about 6×10^{-7} μCi/cc air.

In the discussion of the ecology of tritium movement in this plot experiment, Jordan et al.[16] show that the amount of tritium released to the air by evaporation from the soil surface was less than 0.1% of the total amount applied. Of this, 50% took place during the first half hour and 87% by the end of the first day after the application.

No measurable tritium was found in the dried leaf tissue of a large representative selection of samples.

Successional Experiment.

In contrast with the tissue sample analyses of the previous experiments, leaf, wood and root tissue of all the secondary successional species spiked with tritiated water showed measurable tritium concentrations. The amount of tritium incorporated into the tissue was about 0.1 percent of the total amount applied to the tree. The results are given in Table II. If trees of the mature forest incorporate tritium into the tissue at the same rate as the successional species, the tissue samples in the tree experiments would have been below the limit of detection of the bound tritium analysis. On the other hand, the large tritium activity to tree weight ratio of the successional experiment made the 0.1 percent value easily detectable.

The specific activity in new leaves and growing stem tips was 2 to 10 times higher than the old leaves or main portion of stems. In the Cecropia, for example, the new leaves were 4.8×10^3 dpm/gm compared

TABLE I

TRANSPIRATION AND MEAN RESIDENCE TIME FOR TRITIUM IN TROPICAL TREES

Tree Experiment Tree Species	Transpiration liters/day	Leaf Biomass* kg	Specific Transpiration ml/day/gm dry leaf	Mean Residence Time Days
Dacryodes excelsa (canopy)	372	27	13.8	11.0 ± 0.6
Dacryodes excelsa (understory)	1.8	0.44	4.0	9.5 ± 0.4
Sloanea berteriana (canopy)	140	14	10.0	3.9 ± 0.2
Plot Experiment				
Tree Species				Mean Residence Time Days
Palicourea riparia				59 ± 7
Manilkara bidentata				80 ± 7
Dacryodes excelsa				62 ± 5
Micropholis garcinifolia				67 ± 7
			Average	67 ± 9

*Leaf biomass estimated from regression of Ogawa *et al.*[13]

TABLE II

TRITIUM UPTAKE AND BOUND TRITIUM IN YOUNG SUCCESSIONAL TREES

Tree	Harvest Time $T-T_0$ Days	Leaves		Stem		Precent Tritium Uptake Into Tissue - %
		New dpm/gm	Old dpm/gm	Tip dpm/gm	Average dpm/gm	
Psychotria (O)	15			2.9×10^3	1.5×10^3	0.027
Psychotria (R)	55	1.4×10^3	5.0×10^2			0.014
Heliconia (Y)	49	9.0×10^4	1.1×10^4	2.0×10^4	3.0×10^3	0.16
Cecropia (P)	55	4.8×10^3	8.0×10^2	6.3×10^3	1.6×10^3	0.14

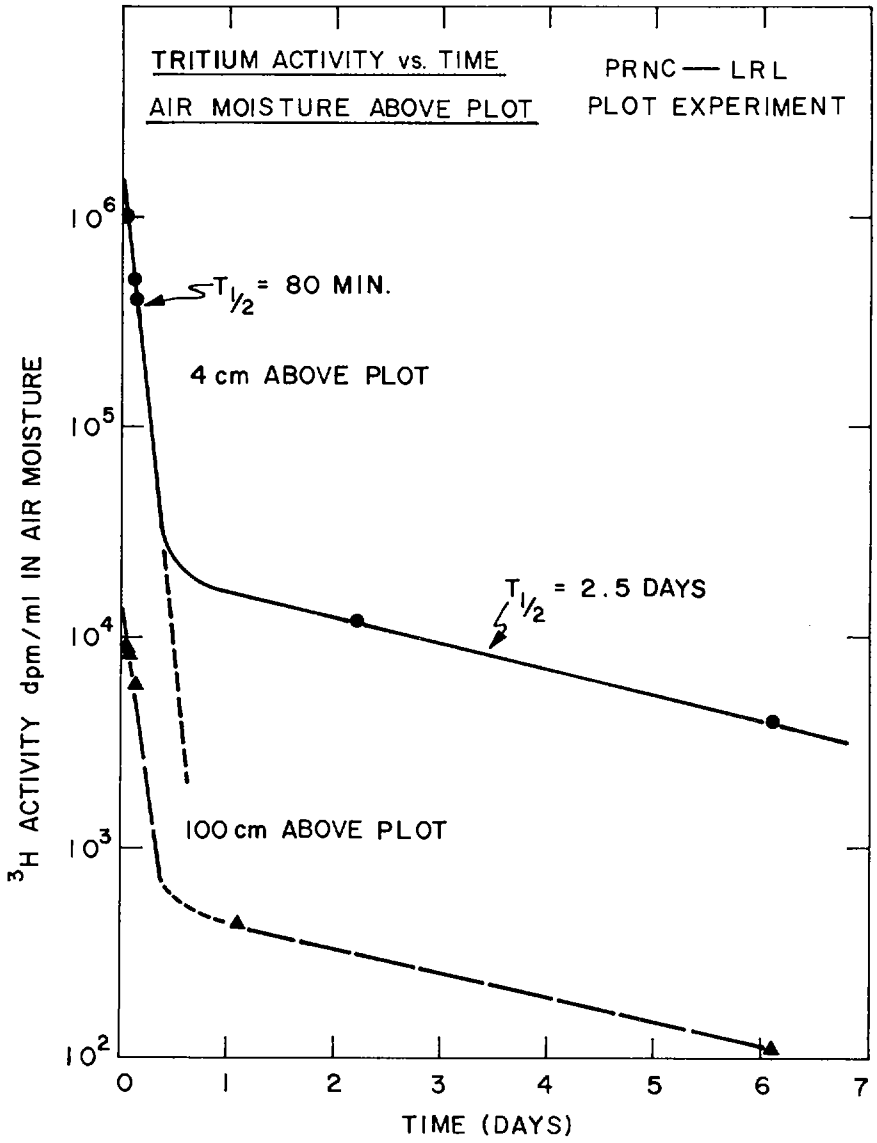
TRITIUM ACTIVITY vs. TIME
AIR MOISTURE ABOVE PLOT
PRNC — LRL
PLOT EXPERIMENT
$T_{1/2}$ = 80 MIN.
4 cm ABOVE PLOT
$T_{1/2}$ = 2.5 DAYS
100 cm ABOVE PLOT
^{3}H ACTIVITY dpm/ml IN AIR MOISTURE
10^6
10^5
10^4
10^3
10^2
0
1
2
3
4
5
6
7
TIME (DAYS)

Figure 5

with 800 dpm/gm for the old leaves. The tissue of the tip of the stem had 6.3×10^3 dpm/gm compared with an average value of 1.6×10^3 dpm/gm for the remainder of the stem. These data are also summarized in Table II.

ECOLOGICAL AND HYDROLOGICAL RELATIONSHIPS

The dry leaf biomass for the Puerto Rico rainforest was estimated to be 0.6 kg/m² by using the regressions of Ogawa et al.[13] on tree density data given in Table III.

Ogawa et al.[13] give the tree leaf biomass (W_L) in kg and stem biomass (W_S) as a function of height (H) in meters and diameter (D) in cm. of the trees in a tropical rainforest in Thailand.

$$W_L = W_S/(13.75 + 0.025\, W_S)$$

$$W_S = 0.0396\, (D^2 H)^{0.9326}$$

These regression equations were used to compute the leaf biomass of the individual trees (W_{LT}) for which transpiration (F_T) in liters/day was measured in Experiment A. Any systematic error introduced by the biomass estimate is cancelled because the same regression equations are used to determine the leaf biomass for a typical unit area of Puerto Rico rainforest in calculating its average transpiration (F_P).

$$F_P = W_{LP}(F_T/W_{LT})$$

The specific transpiration (F_T/W_{LT}) for the trees in Experiment A are given in Table I.

Average transpiration was computed by taking a weighted average of the substory and canopy tree specific transpiration rates determined in the tree experiment by assuming the transpiration rate to be a continuous function of tree size. Average transpiration for the rainforest was determined to be 3.64 kg/m²/day.

The annual water budget for the Puerto Rico rainforest was reported by Jordan.[17] Rainfall was measured as 281 cm which corresponds to 7.7 kg/m²/day. Throughfall represented 69% of the total and stemflow accounted for an additional 18%. The net input to the litter-soil layer is therefore 6.70 kg/m²/day. Of this, 3.64 kg/m²/day (54.5%) is transpired and 0.04 kg/m²/day (0.5%) evaporated directly leaving 3.02 kg/m²/day (45%) for interflow.

The water capacity in the surface to 10" deep layer is 128 kg/m². Below the 10" depth, the capacity is 23 kg/m²/inch of depth. By the occupancy principle of Orr and Gillespie,[12] the capacity is the product of occupancy or mean residence time, T, and the flow, F. The effective capacity of the soil compartment may then be calculated for the observed 42 ± 2 day occupancy of the coupled soil compartment where F = 6.66 kg/m²/day. The calculated effective capacity is 280 ± 12 kg/m² which corresponds to an effective depth of 16.6" or 42 cm. If transpiration were the only loss rate, the residence time for tritium in the soil would be

$$T = C/F = 280/3.64 = 77 \text{ days.}$$

TABLE III

TRANSPIRATION AND BIOMASS ESTIMATES FROM TREE DENSITY DATA

Tree Class			Density*	Dry Leaf Biomass	Transpiration†	Transpiration
	dia.*	ht. (est.**)	Trees/Hectare	(est.**)		
in.	cm	m		kgm/m^2	ml/day/gm leaf	kgm/day/m^2
4	10.2	8.3	355	0.0539	3.0	0.1617
6	15.2	11.1	425	0.1668	4.0	.6672
8	20.3	13.5	118	0.0864	5.0	.4320
10	25.4	15.4	81.4	0.0906	6.0	0.5436
12	30.4	17.0	33.3	0.0484	7.0	.3388
14	35.6	18.4	20.9	0.0385	8.0	.3080
16	40.6	19.6	22.2	0.0478	9.0	.4302
18	45.7	20.6	12.33	0.0294	10.0	.2940
20	50.8	21.6	4.93	0.0129	11.0	0.1419
22	55.9	22.3	3.70	0.0104	12.0	.1248
24	61.0	23.1	2.46	0.0073	13.0	.0949
26	66.0	23.8	2.46	0.0076	14.0	.1064
			Total	0.600 kgm/m^2		3.64 kgm/day/m^2

*Tree density for each diameter from Wadsworth.[20]

†Determined in tree experiment where T ranged from 4 for substory tree to 14 for largest canopy tree.

**Estimates derived from regressions of Ogawa et al.[13]

The importance of this will be seen in the discussion on the simulated tritium rainout in the following section.

TRITIUM RAINOUT SIMULATION

For a simulated rainout of tritium, we shall assume that a one megaton explosive gives a tritium cloud burden of 4×10^6 curies. Furthermore, if it is dispersed in a 100 square mile cloud, a rainout would deposit 15.4 mCi/m^2. In a tropical rainforest, the canopy leaves will intercept and evaporate about 13 percent of the incoming rain or 2 mCi/m^2. The net input to the soil litter layer would be 13.4 mCi/m^2 as stemflow and throughfall. This value is nearly identical to that applied in the systems experiment. These input values are approximations based on information available in the open literature. While they are believed to be reasonable, any arbitrary values could have been used because the mechanisms governing the movement of fallout tritium into the tropical ecosystem described in this report are independent of the initial values.

Although the tritium was applied to a small plot in the plot experiment, a rainout of tritium as simulated, would occur over a much wider area. Nevertheless, in this analysis the data from the plot experiment will be used to describe the movement of tritium following a rainout. Allowances for the effect of a large area deposition will be made where it is possible to do so.

Immediately after deposition, a small amount of tritium would be evaporated from the litter layer. The tritium concentration in air at the ground surface would be about 0.3 μCi/ml or 6×10^{-7} μCi/cc air. The air concentration would decrease rapidly as the tritium moved down into the soil. In the plot experiment, a two component exponential decrease of tritium in the air shown in Figure 5 was observed. The short component half-time was 80 minutes while the longer component showed a tritium removal half-time of 2.5 days.

The tritiated water vapor remained essentially at ground level and followed the natural air drainage down the side of the mountain. The activity at 100 cm above the plot was 100 times less than at the 4 cm level. Air sampling was discontinued after a week at which time the activity levels were at least two orders of magnitude lower than at the time of the application of tritium.

Since the rainout would occur over a large area of the rainforest, the removal of tritium from the air at a particular location would be longer because incoming air would contain tritium from above that site. Despite this, evaporation of tritium from the soil surface would decrease rapidly with time and the highest concentrations in air would remain close to the ground surface.

The pattern of movement of tritium in the soil will be that observed in Figure 2. Tritium will be removed from the soil at an exponential rate with a mean residence time of 42 ± 2 days.

If the interflow from the surrounding areas is such that tritium leaving a plot by interflow is balanced by tritium in interflow from above entering the plot, the residence time will be longer. In this case, transpiration will represent the only loss pathway and the residence time for the soil will be 77 days. Since the interflow velocity is low, the rainout area does not have to be very large in order for this equilibrium assumption to be valid with respect to a small plot within the rainout area.

Tritium in the vegetation in the area will increase to a peak in two to three weeks of about 2000 pCi/ml. It will then display an exponential removal of tritium with a mean residence time of 67 ± 9 days. If an equilibrium condition in the interflow exists, the residence time will be the same as for the soil, 77 days. The tissue bound compartment will have a tritium concentration of about 3 pCi/gm.

If the rainout were to occur on a cleared plot or in a food crop area, the growing vegetation could have a tritium concentration in the bound compartment of 6 to 30 pCi/gm. This does not imply any concentration factor but merely reflects the difference between photosynthetic binding of tritium and that which would become bound by exchange. The ratio of net production to plant size is higher in successional trees or growing plants than in mature forest trees.

The high flux of water in the rainforest results in a rapid turnover of water and short residence times compared with other areas. The rainforest vegetation tissue compartment can only incorporate whatever tritium is present during the time it is available. In a desert ecosystem, however, Koranda and Martin[18] have shown that the tissue bound tritium in annual herbaceous and woody perennial plants growing in a tritiated environment is in equilibrium with the relatively stable level of tritium in the water of such plants. In growth chamber studies, Chorney et al.[19] found that tissue bound tritium was essentially the same as that which occurred in tissue water during growth of an herbaceous plant. Because of the short residence time of tritium relative to the growth rate of tropical vegetation, no such equilibrium was observed in the tropical ecosystem.

Tritium in the bound state might be expected to have a longer residence time than the water passing through a plot. For example, bound tritium in leaves would have a mean residence time equal to the mean biological residence time of leaves on the tree. The residence time in the bound state was not determined directly. Since the water compartment has 2 to 4 times as much hydrogen as the tissue compartment of tropical vegetation, and the uptake of tritium from the water compartment into the bound state is a small fraction of the total amount available, the significant compartment would have to be the loose or free water of tropical vegetation.

Based on data obtained in the plot experiment, the distribution of tritium with time in a tropical ecosystem is shown in Table IV. Tritium remaining in the soil of the plot decreases at an exponential rate with a half-time of 29 days. By the end of six months, less than 2% of the original tritium remains in the soil.

Losses via interflow increase with time approaching a maximum value of 45.4% of the input of tritium. The trees take up tritium and reach a peak value at about 14 days after which the fraction of the input tritium remaining decreases at an exponential rate with a half-time of 47 days. During the first two weeks the amount of tritium transpired is small as the tritium rises up the tree stems. The greatest loss occurred during the third week when more than 8% of the original input of tritium was

TABLE IV

FRACTIONAL DISTRIBUTION WITH TIME OF TRITIUM INPUT TO TROPICAL RAIN FOREST SOIL

Time days	 months	Fraction in Soil Profile	Fraction in Trees	Fraction Transpired	Fraction Lost as Interflow
4		.9092	.0494	.0002	.0412
7		.8465	.0830	.0008	.0697
14		.7165	.1382	.0166	.1287
21		.6065	.1177	.0972	.1786
30		.4895	.1254	.1533	.2318
45		.3425	.1271	.2319	.2985
60	2	.2397	.1211	.2940	.3452
	3	.1173	.0984	.3836	.4007
	4	.0574	.0738	.4409	.4279
	5	.0280	.0524	.4783	.4413
	6	.0138	.0359	.5026	.4477
	7	.0067	.0241	.5182	.4510
	8	.0033	.0156	.5284	.4527
	9	.0016	.0104	.5347	.4533
	12	.0002	.0025	.5434	.4539
→ ∞		→ 0		→ .546	→ .454

transpired. The total transpiration loss increases with time approaching a maximum value of 54.6% of the input pulse.

CONCLUSIONS

Experiments were conducted to determine the pattern of movement and distribution of tritium in a tropical rainforest ecosystem.

An injection of tritiated water directly into understory and canopy evergreen tropical trees was used to determine the transpiration rate and residence time for water in the trees. Transpiration ranged from 2 to 370 liters/day. Mean residence times ranged from 4 to 11 days.

The distribution of tritium in the soil, air and trees was determined following an application of tritium to a 3.68 m^2 plot in the rainforest. The pulse of tritium showed an exponential decrease with time in the soil and in trees growing in the rainforest. The fraction of tritium remaining in the soil and trees as well as the fraction lost through transpiration and interflow are given as a function of time in Table IV. The mean residence time for tritium in the soil and in trees was found to be 42 ± 2 days and 67 ± 9 days, respectively. Using the transpiration rates from the previous experiment, rainfall records, tree density data and other measurements, average transpiration for the Puerto Rico rainforest was computed as 3.64 $kg/m^2/day$. The effective capacity of the soil compartment was calculated to be 280 kg/m^2.

Uptake of tritium into the tissue compartment of successional species was measured as 0.1% of the total amount of tritium applied to several emerging trees in a cleared plot in the rainforest. Because of the short residence time of tritium relative to the growth rate of tropical vegetation, tissue hydrogen does not equilibrate with tritiated water in the ecosystem.

The main hydrogen compartments of the tropical ecosystem are water in the soil and in trees of the forest. The persistence of fallout tritium is determined by the residence time of tritium in these compartments.

REFERENCES

1. H. T. Odum and S. G. Bloom, Hydrogen Budget and Compartments in the Rain Forest at El Verde, Puerto Rico, Pertinent to Consideration of Tritium Metabolism and Mathematical Formulation of the Hydrogen Budget Model, IOCS Memorandum BMI-2 (June 1, 1967).
2. R. L. Charnell, T. M. Zorich and D. E. Holly, Bio-Science 19, 799-803 (1969).
3. F. B. Golley, J. T. McGinnis, R. G. Clements, G. I. Child and M. J. Duever, Bio-Science 19, 693-696 (1969).
4. J. T. McGinnis, F. B. Golley, R. G. Clements, G. I. Child and M. J. Duever, Bio-Science 19, 697-700 (1969).
5. C. F. Jordan, Soil Science 105, 81-86 (1968).
6. P.-E. E. Bergner, J. Theoret. Biol. 1, 120 (1961).
7. P.-E. E. Bergner, J. Theoret. Biol. 1, 359 (1961).
8. P.-E. E. Bergner, Acta Radiol. 210, Suppl. 1 (1962).
9. P.-E. E. Bergner, J. Theoret. Biol. 6, 137 (1964).
10. P.-E. E. Bergner, In Dynamic Clinical Studies with Radioisotopes,

R.M. Kniseley and W.N. Tauxe, Eds. (AEC, Germantown, Md., (1964) pp. 13-15.
11. P.-E.E. Bergner, Science 150, 1048-1050 (1965).
12. J.S. Orr and F.C. Gillespie, Science 161, 138-139 (1968).
13. H. Ogawa, K. Yoda, K. Ogino and T. Kira, Nature and Life in Southeast Asia IV, 49 (1965).
14. J.R. Kline, J.R. Martin, C.F. Jordan and J.J. Koranda, Transpiration in Tropical Trees, submitted to Nature (1969).
15. U. Zimmerman, K.O. Munnich and W. Roether, Downward Movement of Soil Moisture Traced by Means of Hydrogen Isotopes, in Isotope Techniques in the Hydrologic Cycle, G.E. Stout, Ed., Geophysical Monograph Series No. 11, 28-36 (1967).
16. C.F. Jordan, J.J. Koranda, J.R. Kline and J.R. Martin, Tritium Movement in a Tropical Ecosystem, submitted to Bio-Science (1969).
17. C.F. Jordan, Water Budget of the Forest, in The Rain Forest Project Annual Report, Puerto Rico Nuclear Center Publ. #19, pp. 45-46 (June, 1968).
18. J.J. Koranda and J.R. Martin, The Persistence of Radionuclides at Nuclear Detonations, Proceedings of Bio-Medical Symposium Biological Implications of the Nuclear Age (March, 1969).
19. W. Chorney and N.J. Scully, Radiation Botany 5, 257-263 (1965).
20. F.W. Wadsworth, Director, Institute of Tropical Forestry, Rio Piedras, P.R., private communication.

XA04N0762

SUMMARY OF USSR REPORTS ON MECHANICAL AND RADIOACTIVITY EFFECTS OF UNDERGROUND NUCLEAR EXPLOSIONS

Paul Kruger
Civil Engineering Department
Stanford University
Stanford, California

Two reports have been issued by the USSR which examine the mechanical effects and radioactive contamination of the environment from underground nuclear explosions (1,2).

In reviewing the mechanical effects, the Institute of Terrestrial Physics of the USSR Academy of Sciences (1) emphasizes the advantages of nuclear explosives, namely the tremendous power and small dimensions, in the industrial and construction fields. The authors note that the mechanical effects are based not only upon the explosive yield but also upon the thermodynamic properties of the cavity gases during expansion. These properties may vary widely depending upon the rock material.

A list of the basic parameters affecting the mechanical effects of contained nuclear explosions includes: cavity volume, dimensions of the chimney, degree of rock fracturing, intensity of the compression wave as a function of distance from shot point, and seismic effects.

From investigations conducted during the past few years in the Institute of Terrestrial Physics, the authors are able to relate the maximum dimensions of the cavity to the strength and elasticity of the rock by the equation:

$$V = \frac{W}{\rho c^2} \, f\left(\frac{\sigma^*}{\rho c^2}\right) \tag{1}$$

where V = maximum cavity volume
W = explosion yield
ρ = rock density
c = longitudinal wave velocity
σ^* = radial stress at the edge of the elastic zone

The authors suggest, in discussing the maximum cavity size of contained nuclear explosions, that instead of assuming that the cavity expansion ceases when the cavity gas pressure equals the lithostatic pressure, accumulated data indicate that the cavity, upon reaching its maximum size, undergoes a certain compression. For example, evaluations made at the Institute of Terrestrial Physics indicate that the maximum cavity volume in the Salmon and Gnome events exceeded the final volume by 2 and 1.5 times, respectively.

With respect to chimney formation, several parameters are given which make delineation of explosion-produced effects difficult, e.g., irreversible deformation of rock blocks, heating of the medium, microfractures, elastic properties of the rock, and individual elongated cracks. These criteria for description of the effects have not yet been analyzed.

Evaluation is being made of the use of the compression wave history as a means of describing the extent of rock fractures since the latter can be measured reliably and since the fracture radius is much greater than the cavity radius. Measurements can be made of the maximum velocity of the medium displacement in the wave. It is assumed that the amplitude of the displacement velocity can be scaled for explosive yield and distance by the equation:

$$v_{max} = C\left(\frac{W^{1/3}}{R} \right)^{1.6} \tag{2}$$

where v = displacement velocity, μ/sec
W = explosion yield, kt TNT
R = displacement, μ
C = constant for the medium,
e.g., C=7 for granite, C=10 for rock salt

The seismic effect of the explosion is described in phases of source, propagation, and structures response. The source term is distinguished between contained and excavation explosions; considered a spherical compression wave for the former, and complex for the latter, in which the force of gravity plays an important role. The propagation through heterogeneous media under conditions of natural stratification is expected to be considerably different from propagation through an ideal elastic body.

Structures response is described by criteria established in the late 1930's in the Soviet Union. Experimental data for small explosions indicated that the maximum amplitude of surface displacement is the critical parameter which determines the danger zone for seismic effect. For small explosions, the threshold for damage to low rise buildings was determined to be approximately 10 cm/sec. This criterium is considered insufficient for large nuclear explosions because of the increased duration of the seismic signal. Further experiments are suggested to achieve a greater reliability for predicting seismic effects.

The mechanical effects of excavation by chemical explosives are described by the empirical equation:

$$W = k\,L^3 f\left(\frac{R}{L} \right) \tag{3}$$

where W = weight of the charge
L = line of least resistance
R = apparent radius of the crater
k = coefficient, involving the properties of the rock
and the efficiency of the explosives.

In comparing the effects of a nuclear explosion to the experiences gained with chemical explosives, it is noted that two characteristics are especially important, i.e., the greater initial energy density, making the thermodynamic properties of the rock more important, and the large scale of the explosions, making geometrical scaling laws unreliable. The gas acceleration phase of the nuclear explosion depends to a greater extent upon the presence of moisture and volatile products in the rock.

For excavation explosions, the list of basic parameters includes: dimensions of the crater, distribution of the ejecta, seismic effect, and foundation and slope stability. The properties of the medium with depth are also important in large-scale explosions; e.g., rock strength, scale of inhomogeneities, and fracture distribution. With these parameters generally unknown and the above characteristics of nuclear explosions, it is doubted that the scaling laws for excavation effects are adequate. Research is strongly recommended on modeling explosions. A special facility for simulating explosions accompanied by ejection in loose soils has been designed at the Institute of Terrestrial Physics. Results on the dependence of the crater radius upon the explosion energy have been satisfactorily obtained.

The phenomenology of radioactive contamination of the environment was described by Izrael, et.al. (2) for both contained and excavation explosions. They consider as the major restraint upon peaceful uses of nuclear explosions the radiation from the nuclear debris which contaminates the natural environment or the industrial products either removed from or stored in the explosion-produced cavities. They also consider it possible to avoid or reduce the radioactivity hazards for industrial use and to arrive at reasonable criteria and standards for radioactive debris beyond national borders.

The radioactivity history is influenced markedly by the hydrodynamic phase of the explosion. For example, the authors consider the temperature changes in the cavity during expansion. They noted that for media with 6.5 or less percent volatile materials, the cavity temperature at maximum cavity size will remain above the condensation temperature of the media. In excavations, where the gas phase imparts additional acceleration to the surface layers, the water content of the rock is an important parameter.

The description of the venting from an excavation nuclear explosion is illustrated with the geonuclear effects of the USSR test "1003". The data for this explosion and the dimensions of the crater configuration are summarized in Table 1. External observations of the shot noted the gas acceleration phase at 0.25 sec when the dome had a height of about 7 m and was rising with a velocity of 60-70 m/sec. Venting occurred at 0.4 sec when the dome had a height of 19 m and a peak velocity of 170 m/sec. The temperature of the luminous area reached 1900-2100°C at about one second.

The base surge spread in 35-40 sec with a diameter of 600 m, and the main cloud, 120 m diameter, rose to a height of 300 m, restricted by the presence of a temperature inversion.

It was noted that for deeply-buried explosions, venting can occur only through fissures and cracks in the geologic media. Since the flow rate of gases through such media is a relatively slow process, only the rare gas nuclides, primarily the krypton and xenon fission products, or very volatile elements, e.g. the halogens, can escape to the atmosphere. An expression is given for the time-integrated release of a particular nuclide, A_i:

$$A_i = 1.45 \times 10^{23} M_i W \frac{\lambda_i k}{k + \lambda_i} e^{-\lambda_i t_o} \qquad (4)$$

where

M_i = cumulative fission product yield of isotope i

W = fission yield, kt

λ_i = decay constant of isotope i

k = release rate from the cavity, the fractional volume removed per unit time

t_o = time since venting

Since the cavity gas temperature remains above the condensation temperature for a time long compared to the half lives of the rare gases, fractionation of fission products inside the cavity is not great. However, the initial distribution of the longer-lived daughter radionuclides, such as Sr^{89}, Sr^{90}, and Cs^{137}, having gaseous precusors depends upon the fracture and venting history. Fractionation of such nuclides can be great.

For scaled depths of burial less than 60-90 $m/kt^{1/3.4}$, venting and break through of the cavity gases is expected, accompanied by the formation of a base surge and a main cloud. The zones of radioactive contamination that must be considered include the base surge and main cloud in the atmosphere, the fallback and ejecta at the crater site, and the local and distant fallout tracks. The extent of the contamination of each of these zones is influenced by the total production of radioactivity, the vent fraction, and the degree of dilution in the atmosphere resulting frrm the prevailing meteorological conditions. The total amount of radioactivity includes both the fission products and the neutron-induced radioactivity.

The intensity (I, in Mev/sec) from the γ-ray emitting radionuclides produced in a 1 kt fission explosion as a function of time (t, in days) is shown as curve 1 in Figure 1. For industrial nuclear explosions in which the fission yield is a small part of the total explosive yield, the induced radioactivity plays an important role. Curve 2 in Figure 1 shows the corresponding data for the induced activity for equal integrated doses. The calculations of induced activity was based on thermal neutron irradiation of media with the chemical composition of clarkeite. For neutrons in the energy range of 10-100 eV, calculations show similar results for $t \leq 3.0$ days. The dashed curve in Figure 1 shows the greater induced activity for the period $10 \leq t \leq 300$ days expected for the higher-energy neutron activation. For the first 5 days, Na^{24} is the principle γ-ray emitting radionuclide. From 1 month to 1.5 years, Sc^{46} and Fe^{59} add significantly to the fission product gamma radiation; after 1 year, Co^{60} is important; and after 10 years, Eu^{152}.

The ratio of doses from induced activity, D_n, to fission product activity, D_o, can be estimated for contained nuclear explosions in which no significant fractionation occurs, from the ratios of the respective gamma radiation energies by

$$\frac{D_n}{D_o} = \frac{E_n}{E_o} = \frac{1.4 \times 10^{22}\ t_b^{0.2}}{W} \quad \Pi \sum_i \alpha_i \, E_{\gamma_i} \; e^{-\lambda_i t_b} \qquad (5)$$

where

W = fission yield, g fissioned material

Π = total neutron flux

α_i = the fraction of neutron producing the i^{th} isotope

E_{γ_i} = the γ-ray energy of isotope i

λ_i = the decay constant of isotope i

t_b = fallout time period along the track

For close-in fallout, where $t_b \cong$ 2-3 hours, the main dose from Na^{24} radiation, with $E_\gamma = 4.14$ Mev, leads to

$$\frac{D_n}{D_o} \cong 1.2 \times 10^{-23} \frac{\alpha \Pi}{q_g} \qquad (6)$$

For $\alpha = \alpha_{Na} = 0.09$, and $\Pi = 10^{24}$ neutrons, the two doses become equal for a yield, W = 1 kt or $q_g \cong 60$ g.

The two dose contributions can be combined into an "effective" fission yield without contribution from neutron activation which gives the same dose by

$$q_{eff} \cong q_g + 2.5 \times 10^{-24} t_b^{0.2} \Pi \sum_i \alpha_i E_{\gamma_i} e^{-\gamma_i t_b} \qquad (7)$$

This simplifies, for the close-in fallout track, to

$$q_{eff} \cong q_g + 10^{-24} \Pi \qquad (8)$$

The vent fraction is described as a function of yield and depth of burial by the scaled depth of burial parameter,

$$\bar{h} = \frac{h}{W^{1/3.4}} \text{ or } \frac{h}{W^{1/3}} \qquad (9)$$

Figure 2 shows the vent fraction, $\varphi(\bar{h})$, calculated for the USSR "1003" test and for 4 USA events. The vent fraction is also noted to be influenced in many cases by the properties and texture of the media and its water content. The authors note that the fraction of radioactive debris which remains in the radioactive cloud beyond the fallout track is only about 1 percent of the total radioactivity production and is likely to be constant for explosions within the range of scaled depths of burial of 35-55 $m/kt^{1/3.4}$.

The height of radioactive cloud (800m) for the Soviet "1003" experiment is compared to the USA Sedan (4200m) and Danny Boy (no main cloud) experiments. The characteristics of the"1003" cloud were determined by geophysical rocket probe sampling and by aircraft. The maximum radiation level in the cloud 107 minutes after the explosion was 0.82 r/hr. The cloud contained about 1.2 percent of the γ-ray emitting products of the explosion. Table 2 shows the ratio of dose from cloud radiation, D_c to radiation dose from deposited radioactivity, D_f as a function of distance from ground zero (G.Z.) in km.

Physical and chemical descriptions of the radioactive particles in the cloud are given. The particle shapes were generally irregular and of varying structure, including slag-like porous particles and "sugar-like" particles. The particle size distribution for samples collected between 0.3 to 4 hours generally followed a log normal distribution. About 90% of the radioactive particles had a diameter less than 0.5μ; the median diameter was about 2μ. The radioactivity content of the particles at 3 seconds was about 80% for particles with diameter greater than 10μ, while particles with diameter less than 0.5μ contained only 1%. Solubility tests with water and with 20% HCl a week after the explosion showed that 70 to 90% of the total activity of the sample was soluble. Nuclides such as I^{131}, Te^{132}, Ru^{103}, and Ce^{141} were about 70-80% soluble, while Ba^{140} was 90%.

The isotopic composition of debris in the base surge and the cloud were determined after sampling by rockets and aircraft and with radiochemical separations and γ-ray spectroscopy radiation measurements. Table 3 lists the enrichment factors of several fission products, relative to the number of Zr^{95} nuclei, for several characteristic samples. The data indicate that the dust column becomes impoverished with respect to volatile nuclides as well as those with volatile precusors after a few seconds. Cloud samples taken 70-80 km from G.Z. are enriched in these nuclides. The nuclides identified include Sr^{89}, Sr^{90} + Y^{90}, Sr^{91} + Y^{91}, Cs^{137}, Ba^{140} and smaller amounts of Ru^{103} and Ce^{141}. The isotopic composition of the dust column is similar to those of the fallback and ejecta samples.

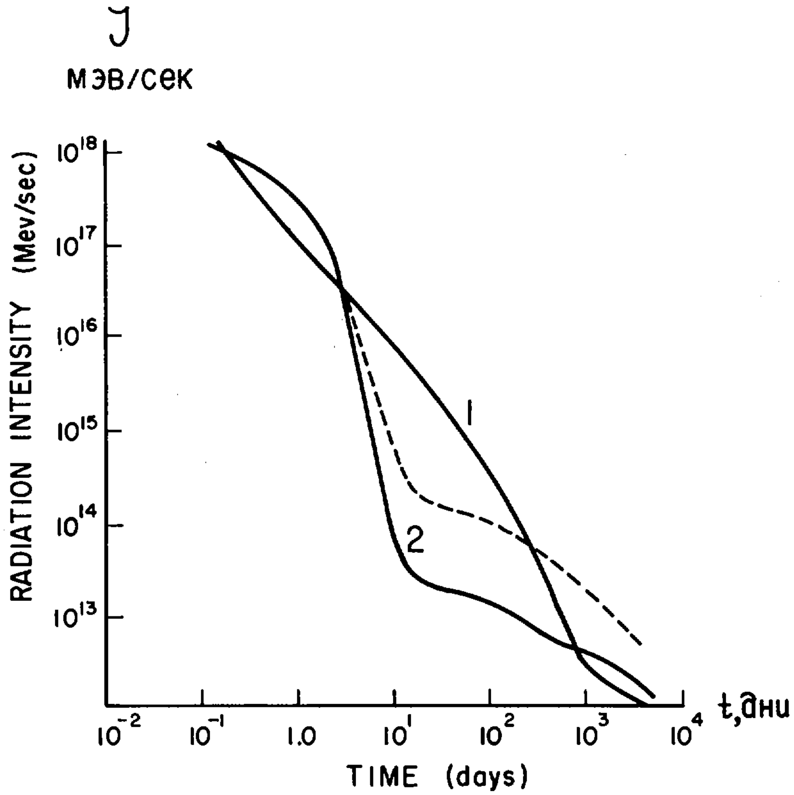

Figure 1. The γ-ray intensity of radionuclides from a 1 kt fission explosion as a function of time.

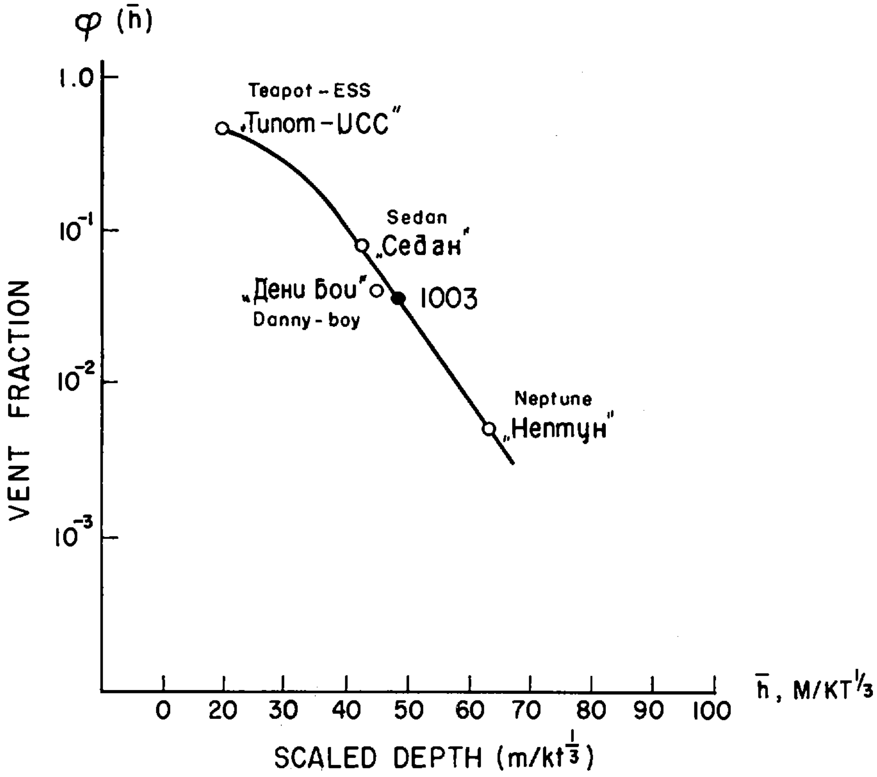

Figure 2. The vent fraction as a function of scaled depth of burial

TABLE 1

THE USSR "1003" NUCLEAR EXCAVATION

EXPLOSION DATA:

W = 1 KT ; All Fission

Z = 48 meters

Medium: Jointed Sandstone

ρ = 2.57-2.80 g/cm^3

Moisture = 0.8 wt %

RESULTS:

D_a = 31 m

R_a = 55 m

R_{al} = 65 m

R_{eb} = 150m

TABLE 2

RATIO OF CLOUD TO FALLOUT DOSES ALONG FALLOUT TRACK

	DISTANCE FROM GROUND ZERO (KM)				
	8	11	25	44	49
$\frac{D_c}{D_f}$	0.5	1.2	5.7	13.8	23.5

TABLE 3

ISOTOPIC COMPOSITION OF "1003" DEBRIS

Post-Explosion Sampling Time	Location	Zr^{95}	Zr^{97}	Ce^{144}	Mo^{99}	Ce^{141}	Ru^{103}	Ru^{106}	I^{131}	Ba^{140}	Y^{91}	Cs^{137}	Sr^{89}
3 sec	Dust Column above G.Z.	1.0	-	0.89	1.12	1.07	0.8	1.16	0.96	0.79	0.57	0.25	0.001
5 sec	Dust Column above G.Z.	1.0	1.12	0.75	1.12	0.63	1.28	0.0019	0.0094	0.37	0.31	0.1	0.0043
1.5 hrs	Main Cloud R = 70 km	1.0	1.08	0.89	1.1	4.9	3.35	0.63	0.175	37.4	26.2	34.8	93
2.4 hrs	Main Cloud R = 80 km	1.0	0.99	0.76	1.1	5.3	5.4	0.9	1.2	24.6	18.2	19	47.7
-	Crater Rubble	1.0	-	0.9	1.26	0.72	0.16	0.10	0.21	0.42	0.40	-	0.048
-	Lip Ejecta	1.0	-	0.94	-	1.6	0.34	0.51	0.42	0.83	0.95	0.226	0.176

An analysis is reported on the fractionation of radionuclides in the main cloud for nuclear excavations which had substantially different filtering properties during the mound disassembly. The "normal" excavations, "1003" and Danny-Boy are compared in Table 4 to Sulky, which created a rubble mound, and to Palanquin, which created a crater by gas-venting erosion.

The fallout pattern of the "1003" event was investigated for the distribution and time behavior of radiation levels, the partition of radioactivity between the off-site and on-site zones, and the depth profile of radioactivity in the ejecta zone. From aerial gammagraphs and with radiochemical analysis, γ-ray energy intensities were contoured at an elevation of one meter. The radiation levels in the fallout pattern were determined by integrating the radiation levels along the track's axis and transverse to its axis:

$$Q_{s\ell} = \int_R \int_\ell p(R,\ell) \; dR \; d\ell \tag{10}$$

where

$Q_{s\ell}$ = radiation level in the fallout pattern, (r/h) (km^2)

$p(R,\ell)$ = radiation intensity at (R,ℓ), at an altitude of 1 m, r/hr

R = distance along the track axis, km

ℓ = distance along the transverse axis, km.

This method differs somewhat from the U. S. method of integrating within the limits of the isolines. The total fallout was calculated on the basis that a radiation intensity of 1(r/hr)(km^2) corresponds to the energy release of 2.86 x 10^{15} Mev/sec. The deposition fraction is scaled to the total production of radiation produced in a 1 kt explosion.

Figure 3 shows the iso-intensity contours around the crater area, Figure 4 shows the fallout pattern along the cloud track, and Figures 5 and 6 show the distribution of radiation intensity at several times along the track's axis and along the transverse axis, respectively. It was noted that the mean velocity of the main cloud was about 40 km/hr, corresponding to the average wind speed in the 0-0.5 km layer. The radiation intensity was measured out to about 300 km, where, at H + 24 hours, the value at the surface was 5 μr/hr. The fraction of radioactivity deposited in the off-site fallout pattern was estimated to be 3.5% of the total amount produced. A comparison of the cloud velocity and fallout fraction for "1003" and several US excavation tests is given in Table 5. A comparison of the relative radiation intensities at H + 24 hours along the track's axis is shown in Figure 7. The curves are all adequately described by the inverse-square law. It is noted that the relative intensity is not affected significantly by the geometry of the source and the distribution of the radionuclides.

The depth profile of the lip was determined by radiochemical analysis of soil layers. Figure 8 illustrates the relation of activity with depth. The decrease is described by the empirical equation

$$A(z) = A_o \, e^{-0.066 \, z} \tag{11}$$

where

A_o = surface layer activity

z = depth, cm

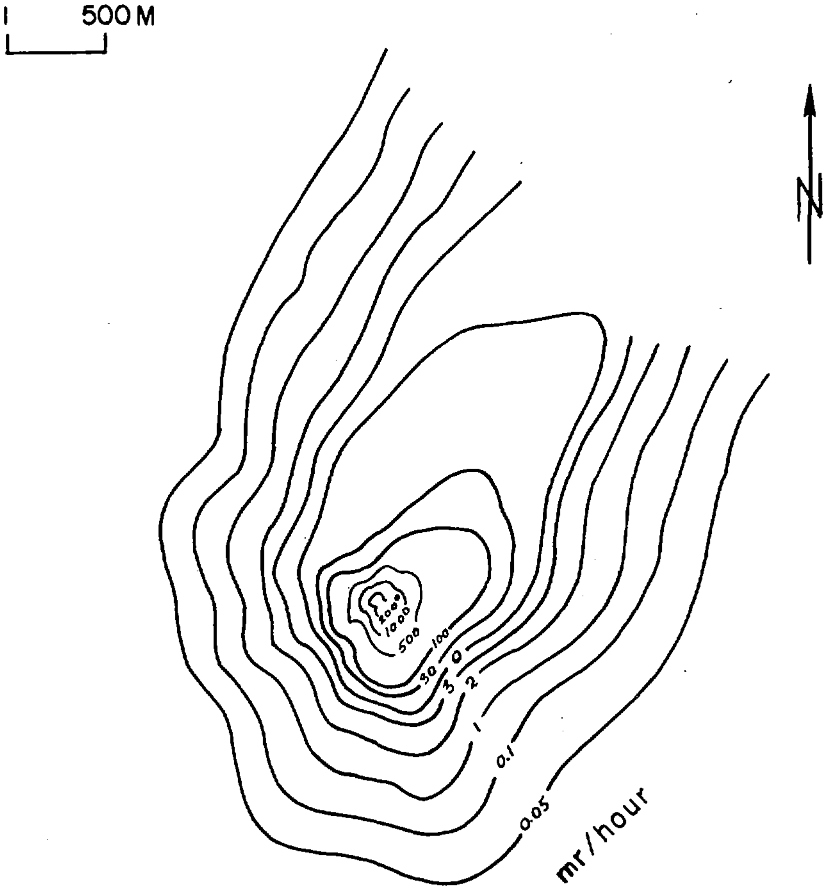

Figure 3. Gamma-ray intensity contours around the USSR "1003" nuclear excavation

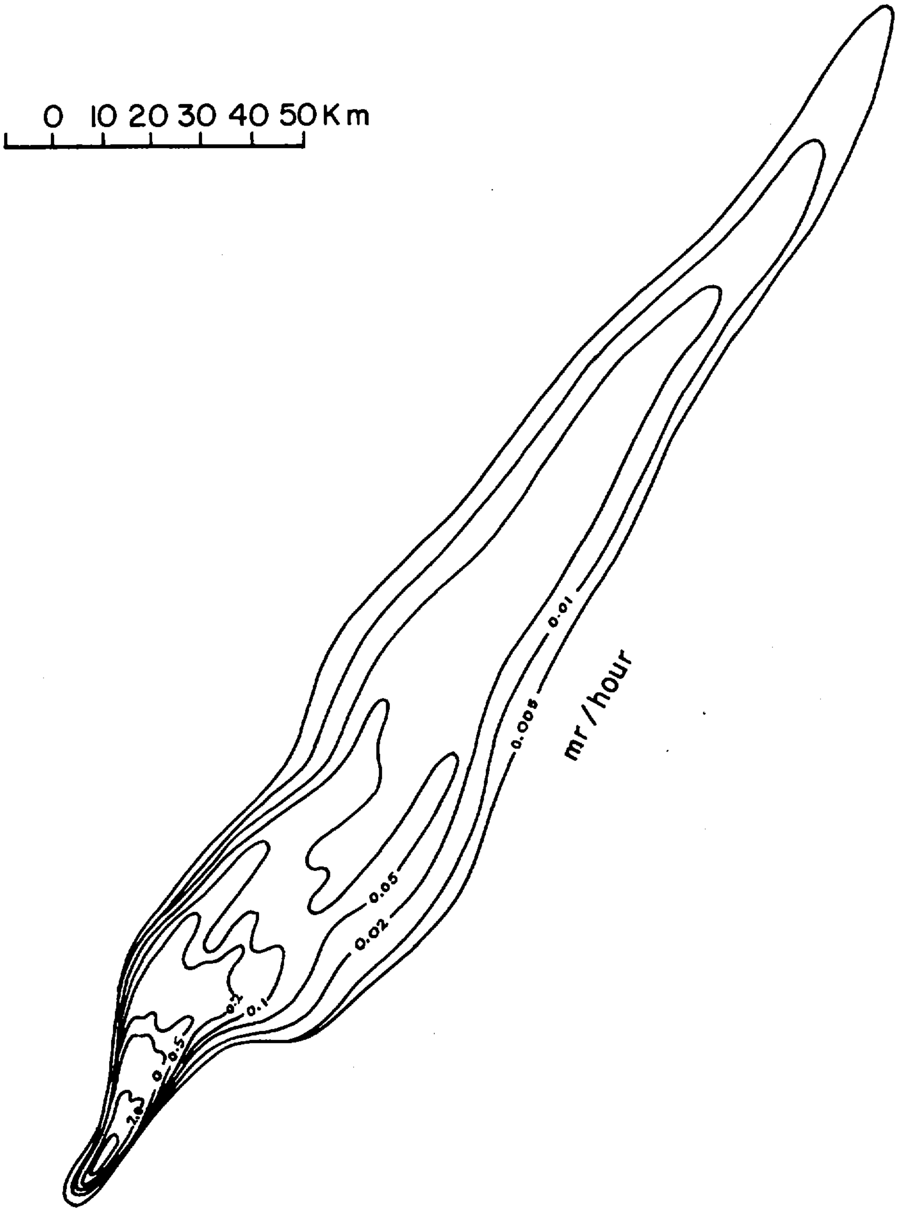

Figure 4. Fallout pattern along the "1003" cloud track.

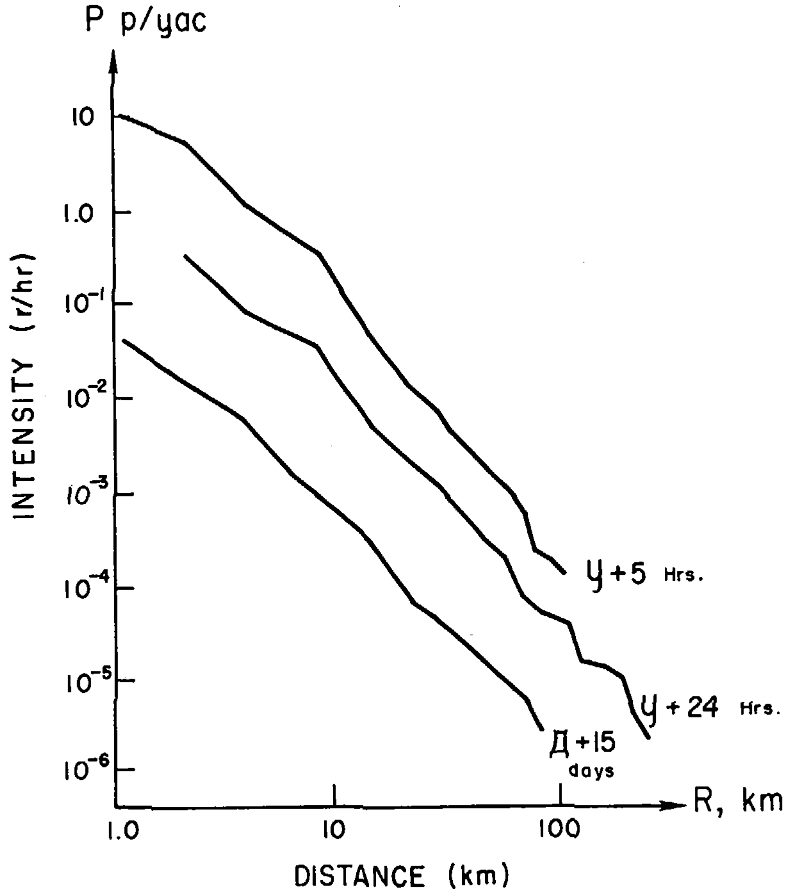

Figure 5. Radiation intensity along the "1003" track axis.

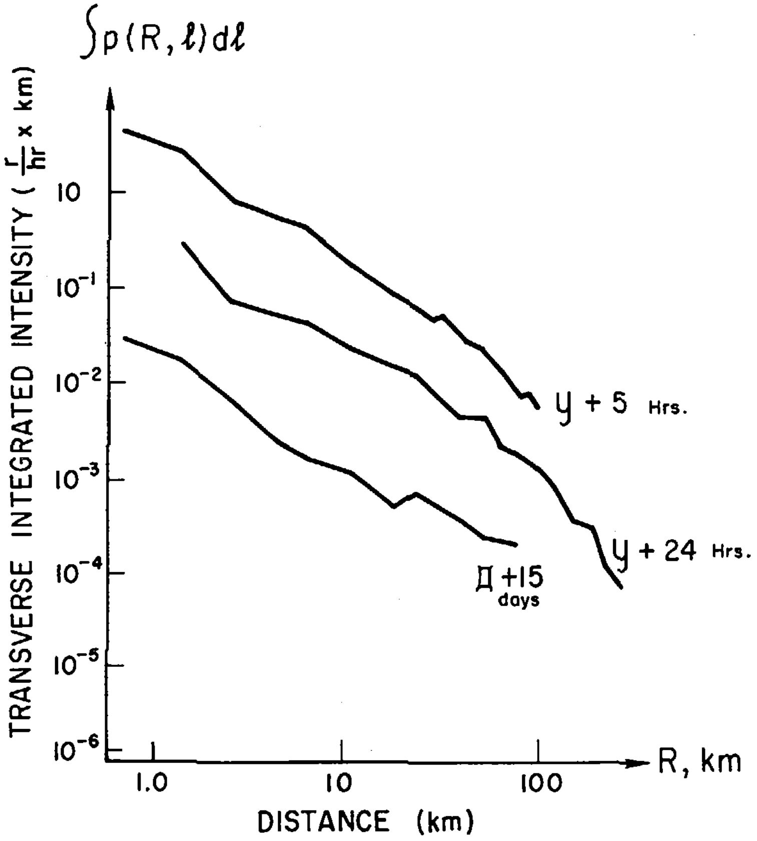

Figure 6. Radiation intensity along the "1003" transverse axis.

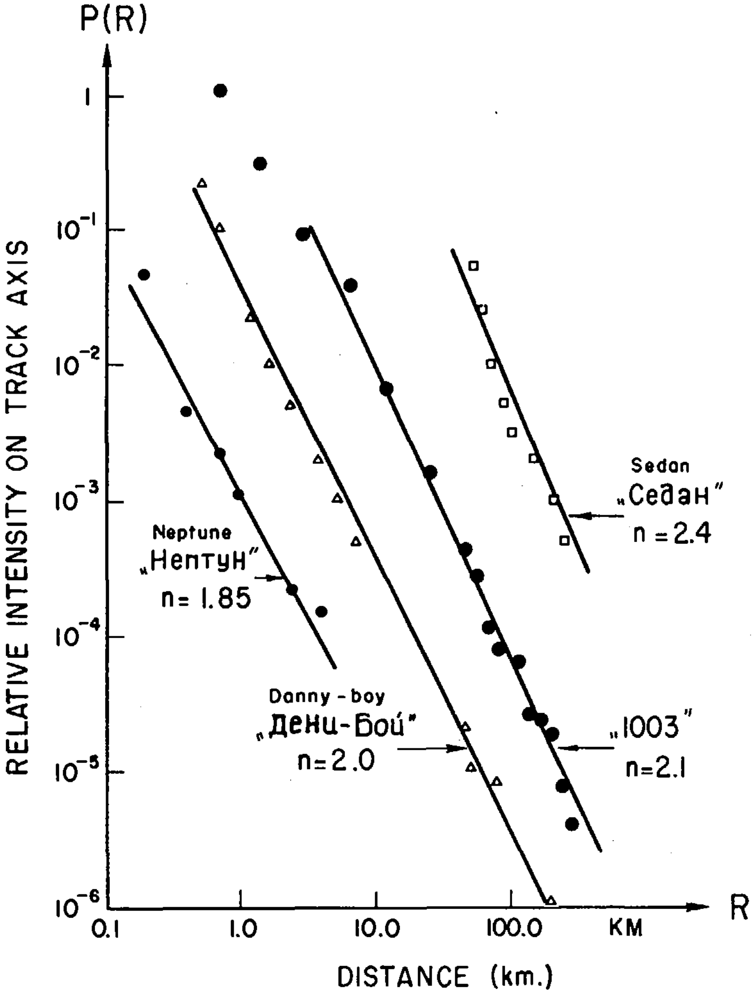

Figure 7. Comparison of radiation intensity along the track axis for several nuclear excavations.

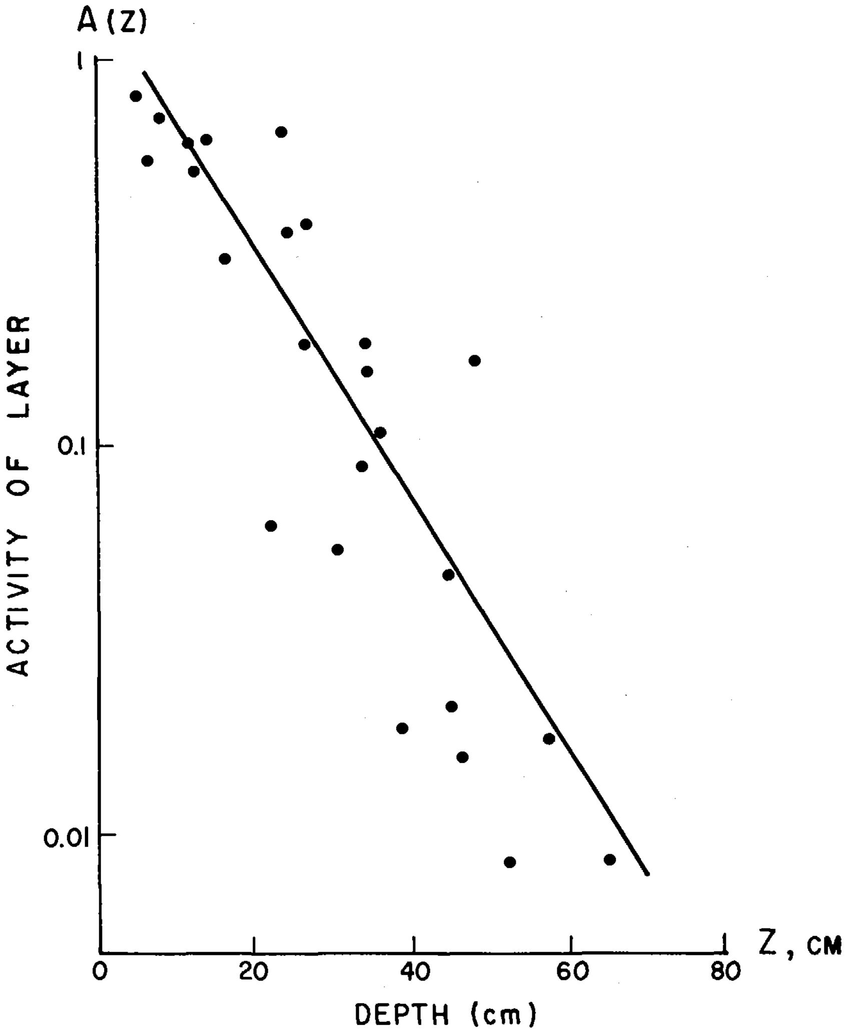

Figure 8. Radioactivity profile with depth in the "1003" crater lip.

It is noted that the activity at 1 meter was 1/100 of the surface activity and that 90% of the radioactivity is contained in the upper 52 cm. The total activity of the ejecta material was 10-15% produced. The isotopic composition is shown in Table 6. The depletion of the nuclides with gaseous precursers is also noted.

The volatile fission products in the cloud were followed by aircraft sampling using $AgNO_3$ and activated charcoal filters. The nuclides Xe^{133} and Xe^{135} were found, essentially unfractionated, during the period of 4 to 98 hours. Iodine isotopes were also detected, but the levels were reduced by factors of 10^3 to 10^4. The maximum radiation level of 2 mr/hr at 15 km from G.Z. occurred at H + 4 hours at an altitude of about 50 m. The flow rate of the radioactive gases at H + 74 hours was 1260 Ci/hr. The aerosol particles in the cloud were examined for their particle size distribution and their solubility.

The isotopic composition of the particles deposited on pans and soil out to 50 km were determined by radiochemical methods. The general observations included (1) deficiency in nuclides with gaseous precurors, (2) same composition as the ejecta, but with a slight enrichment of the volatile-precursor nuclides on the windward side of the crater, and (3) a decrease in apparent fractionation with distance along the track axis. The extent of isotopic fractionation was calculated in the same manner as for U. S. Tests. The isotopic fractionation coefficients for several nuclides are listed in Table 7.

The activity induced in the "1003" media is compared to that from a low-power USSR underground nuclear explosion in a salt bed. The production of radionuclides (relative to Zr^{95}) in samples from these two explosions is shown in Table 8. The difference in activation between salt and silicate rocks is readily apparent. At D + 200 days, the major activation products from "1003" were Mn^{54} (65%) and $Eu^{152,154}$ (23%), while those from "Camouflet" were Sb^{124} (90%) and Ta^{182} (8%).

The solubility of the fallout radioactivity was measured to estimate the hydrologic transport by overland flow, contamination of open reservoirs, infiltration into ground water, migration in soils, and biological availability. Leaching of the base surge and cloud fallout with distilled water indicated the solubility of the same nuclides as those on crater fallback and ejecta which are soluble. The relative content of the leach water was: $Sr^{89} \sim 70\text{-}90\%$, $Sr^{90} \sim 4\text{-}6\%$, $Ba^{140} \sim 0.5\text{-}2\%$, $Ru^{103,106} \sim 7\text{-}20\%$, and $Sb^{124} \sim 1.4\text{-}7\%$. The solubility coefficients of some of these nuclides, along the track axis, are illustrated in Figure 9.

The solubility data of these nuclides are related to their gaseous-precursor history; the most soluble nuclides being those adsorbed on particle surfaces after formation from their gaseous precursors. The solubility of nuclides without gaseous precusors was very low. The solubility coefficients are ordered, relative to 1.0 for Sr^{90}, as follows:

$$\begin{array}{ccccccccccccccc} Sr^{89} & > & Sr^{90} & > & Sb^{125} & > & Ba^{140} & > & Ru^{103,106} & > & Cs^{137} & > & Cs^{134} & > & (Mn^{54}Co^{60}Ce^{144}Y^{91}Zr^{95}) \\ 1.25 & & 1.0 & & 0.3 & & 0.24 & & 0.01 & & 0.04 & & 0.02 & & 0.01\text{-}0.001 \end{array}$$

The redistribution or subsequent transport of the radioactive debris has been examined for hydrologic transport, wind redistribution, and foliar deposition. During the year following the"1003" detonation, ground water flowed into the crater to a total volume of about 100 m^3. Radiochemical studies of the water in the crater were undertaken to examine the way the crater filled and the role played by groundwater in creating artificial reservoirs. The major nuclides observed were Sr^{89}, Sr^{90}, Ru^{103} and Ru^{106}. Also detected were Sb^{125} and Cs^{137}. From the data in Table 9, it was noted that the solubility properties were in agreement with expectations according to the position of the

TABLE 4

ISOTOPIC ENRICHMENT FACTORS IN THE "1003" MAIN CLOUD
(RELATIVE TO ZR-95)

NUCLIDE	PALANQUIN	DANNY-BOY	"1003"	SULKY
Sr^{89}, Cs^{137}	1-2	15-100	20-98	10^5
Ba^{140}	1.0	10	25-37	1.5×10^4
Ce^{141}	1.0	3.0	5.0	12

TABLE 5

COMPARISON OF USSR "1003" TO USA EXCAVATIONS

Event	W (kt)	h (m)	$\bar{h}$ ($m/kt^{1/3.4}$)	$\bar{h}$ ($m/kt^{1/3}$)	Dia. (m)	H (km)	V (km/hr)	Fraction of Radioactivity in Fallout (%)
"1003"	1.0	43	48	48	130	0.3	40	3.5
Sedan	100	194	50	42	370	4.5	22	~8.0
Danny Boy	0.42	33.5	43	45	65	0.3	24	4-7
Neptune	0.115	30.5		63	60	1.2	25	0.5
Teapot Ess	1.2	20.4		19	89	2.4		46

TABLE 6

ISOTOPIC COMPOSITION OF SURFACE EJECTA

Nuclide	Fraction (%)
Zr^{95}	14
Ru^{106}	14.2
Ru^{103}	13.6
Ce^{141}	15.1
Ce^{144}	15.0
Ba^{140}	11
Sr^{89}	6.0
Sr^{90}	9.4

TABLE 7

ISOTOPE FRACTIONATION COEFFICIENTS

Isotope	$(f_{i,95})_{ave}$	Range of Values
Sr^{89}	0.38	0.18-0.80
Sr^{90}	0.45	0.19-0.87
Ba^{140}	0.80	0.55-1.28
Ce^{141}	0.90	0.69-1.96
Ru^{103}	1.15	0.87-1.55

TABLE 8

RELATIVE PRODUCTION OF ACTIVATION PRODUCTS

		$N(Zr^{95})$	RATIO OF $N(i)$ TO $N(Zr^{95})$								
Event	Sample	(10^9 atoms/g)	Co^{60}	Mn^{54}	Zn^{65}	Ag^{110m}	Sb^{124}	Cs^{134}	Eu^{152}	Eu^{154}	Ta^{182}
"1003"	Ejecta	129	0.07	7×10^{-4}	-	-	-	0.01	-	-	-
"1003"	Ejecta	167	0.06	6×10^{-4}	-	-	-	0.01	-	-	-
"1003"	Crater Rubble	3408	0.13	0.01	0.001	-	-	0.02	0.03	0.02	0.004
Camouflet	Salt	233	0.06	0.06	-	0.08	0.97	-	Tr	Tr	0.16

TABLE 9

SOLUBILITY DISTRIBUTION IN USSR UNDERGROUND EXPLOSIONS

	IN WATER IN A NUCLEAR CRATER (% in)			IN WATER FROM A CAVITY IN SALT (% in)		
NUCLIDE	Colloids	Cations	Anions	Colloids	Cations	Anions
Sr^{90}	none	100	none	none	100	none
Cs^{137}	1.5	98.5	none	1.2	98.2	none
Ru^{106}	19.4	5.1	75.5	25.7	11.6	62.7
Sb^{125}	6.5	8.5	85	none	6.2	93.8

elements in the periodic table. The changes in concentration with time are illustrated in Figure 10.

Groundwater transport of the radionuclides was studied with a network of observation wells established at the "1003" site, at depths of 26 to 50 m, and located from 200 to 700 m from the emplacement hole. Systematic hydrogeological observations were begun two months after the detonation. The authors noted that the crater shape was preserved during the one year period and that the water levels in the wells were lowered by 0.7 to 1.3 m. They concluded that infiltration of groundwater into the crater occurred. Measurements in the observation wells confirmed the absence of radioactivity contamination in the wells even after several years following the explosion.

A series of laboratory measurements were made on the solubility of radionuclides on fallback and ejecta materials. Various solutions were used, such as distilled water at several pH, water with dissolved solids (Ca, Mg, Na, Cℓ) at a concentration of 1.3 g/ℓ, HCℓ solution, and water with EDTA complexing agent. The distribution coefficients for mass to volume ratios of 2 to 200 were determined for solution contact time of 10 days at room temperature. As an example, the results of the experiments with the water containing 1.3 g/ℓ of dissolved solids and crater rubble samples, conducted from D + 150 to D + 250 days, are shown in Figure 11. It was noted that for this time period, the soluble nuclides were Sr^{89,90}, Ru^{103,106}, and Sb^{125} with traces of Ce^{141,144} and Zr^{95}. Effects for specific radionuclides were noted in the experiments with varying volume to mass ratios, particle size distributions, and pH. Little effect was noted for changes in dissolved solids concentrations form 0.13 to 13 g/ℓ.

Transport by secondary dust redistribution was examined for varying wind conditions and for on-site operations by heavy earth-moving equipment and motor vehicles. Experiments were carried out during one summer at three selected sites around the crater, at which the dose rate, thickness, moisture content, particle size distribution, and surface wind speed were examined. Air contamination was noted to be influenced markedly by the moisture content and wind velocity. For example, at constant wind velocity, the concentration of radioactive material in the air increased by about a factor of 10 when the ground moisture decreased from 10.6 to 3%. For constant ground moisture of 3%, the concentration increased a factor of 5 when the wind velocity changed from 0.6 m/sec to 5 m/sec. Air contamination caused by motor vehicles was noted to be ten times, or more, greater than in the case of natural dust formation. The concentrations ranged from 0.5 to 500 x 10^{-12} Ci/ℓ. Foliar deposition was noted to be influenced by the extent of secondary wind redistribution. Differences in radionuclide composition of the foliar deposition and those at root level were noted.

A model for fallout prediction has been developed. The basic parameter in estimating the fallout pattern in the absence of wind shifts in the atmosphere is the settling velocity, v, of the radioactive particles. A simplification of the radioactive particle distribution in the base surge and main cloud is assumed such that at altitude H there is a point source of a polydispersed aerosol with distribution N(v), for which the observed fallout pattern can be calculated. The expression for the fallout pattern resulting from this distribution with a wind velocity V is

$$p(x,y) = \frac{QHV\ N(\frac{HV}{x})}{\sqrt{2\pi}\ \sigma_y(x)\ x^2}\ e^{-\frac{y^2}{2\sigma_y^{\,2}(x)}} \qquad (12)$$

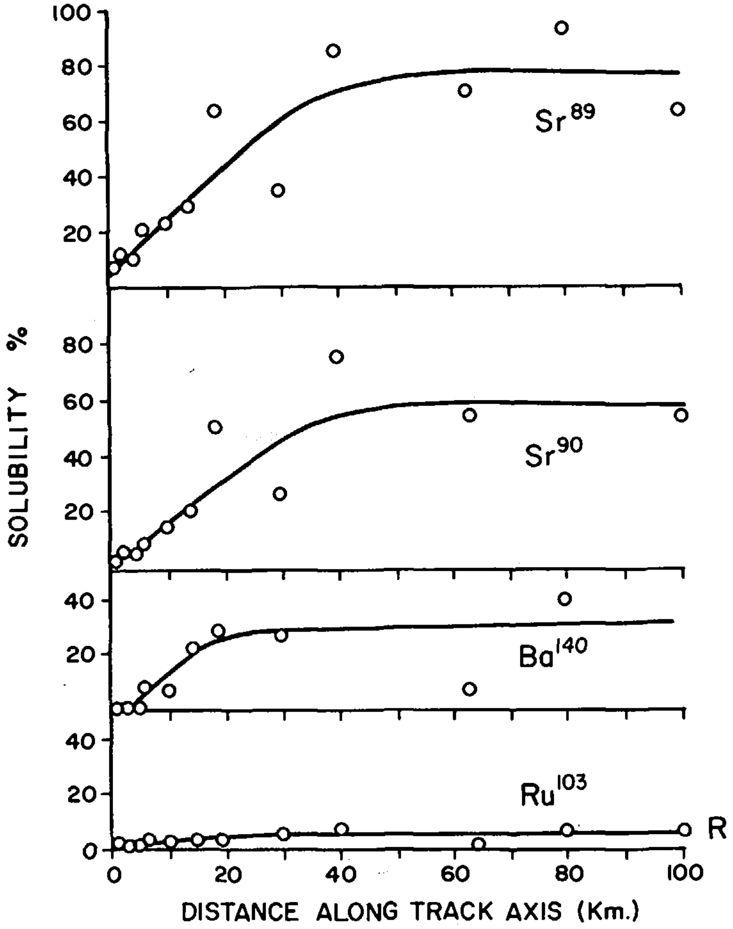

Figure 9. Solubility of radionuclides deposited along the track axis.

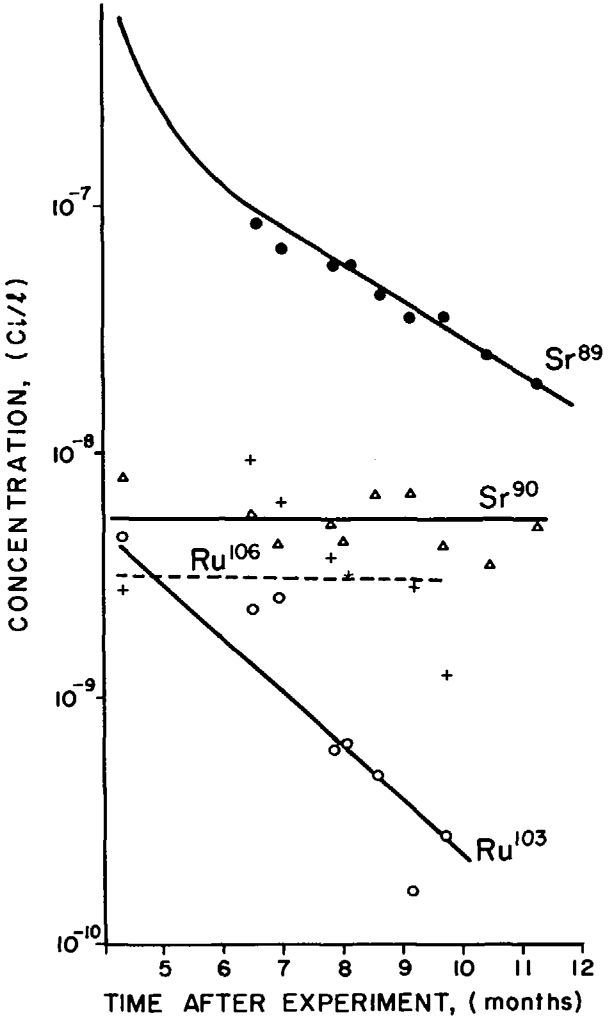

Figure 10. Radionuclide concentrations in crater water as a function of time.

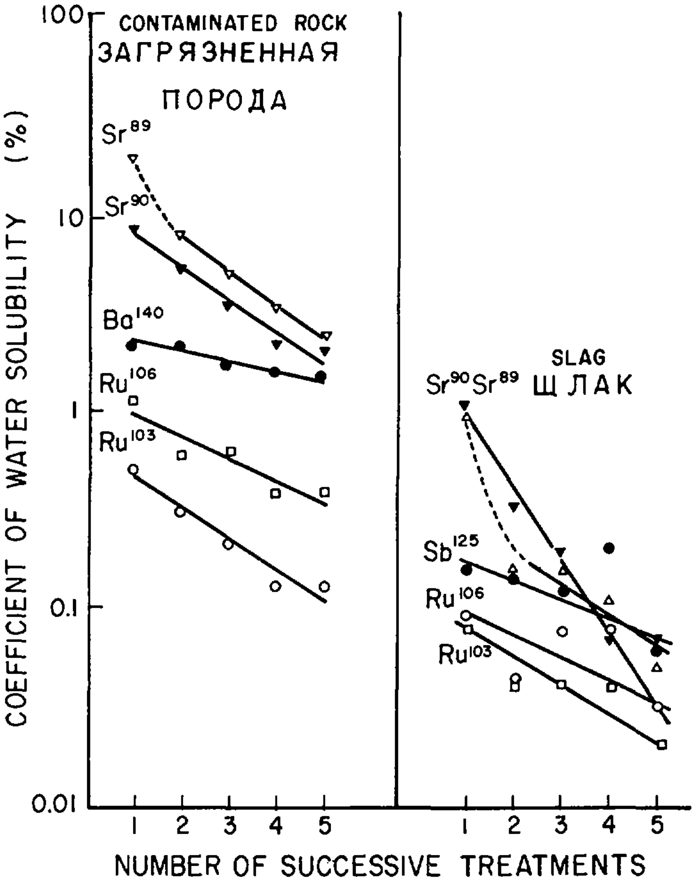

Figure 11. Radionuclide solubility as a function of successive exposures to water.

where

Q = total source strength, Ci

$\sigma_y^2(x)$ = the dispersion of the distribution $p(x,y)$ in the y direction, km

$N(\frac{HV}{x})$ = volume density of particles according to particle settling velocity, $v = \frac{HV}{x}$

The total radioactivity at $t = h + 1$ hours is related to the explosive yield W (in kt) by $A(h + 1) = 4.5 \times 10^8$ W and the dose rate can be related to the fallout pattern by

$$D(h = 1\ m) = k_1\ p(x,y)$$

where $k_1 \cong 10^{-5}$ r/hr/Ci/km^2.

Thus, equation (12) may be rewritten

$$p_t(x,y) = \frac{CW\mathrm{I}(\bar{h})HVF(v)}{\sqrt{2\pi}\ \sigma_y(x)x^2}\ e^{-\frac{y^2}{2\sigma_y^2(x)}} \tag{13}$$

where

$p_t(x,y)$ = γ-ray dose rate from the fallout pattern at an altitude h = 1 meter in r/hr at time t

C = constant, of appropriate units

W = explosive yield, kt

$\mathrm{I}(\bar{h})$ = fraction of the total radioactivity settling on the fallout pattern

x = distance from ground zero along the track axis, km.

The function $F(v)$ is related to the function $N(v)$ by the equation

$$F(v) = k_z\ N(v) \tag{14}$$

where $k_z \cong 4.5 \times 10^3$ r/hr/Ci/km^2, and is determined from the known experimental values in equation (13). The variance term is given by

$$\sigma_y(x) = \frac{\bar{p}}{\sqrt{2\pi}\ p(x,o)} \tag{15}$$

where

$p(x,0)$ = dose rate along the track axis

$\bar{p} = \int_{-\infty}^{\infty} p_1(x,y)\,dy$ = integral of the transverse distribution at distance x.

Figure 12 shows the relationship of $\sigma_y(x)$ with distance from G.Z. The data are described by the equation

$$\sigma_y(x) = \left[\sigma_o^2 + 0.01\ x^2\right]^{\frac{1}{2}} \tag{16}$$

where σ_o^2 is related to the horizontal dimension of the main cloud and defines the transverse distribution near ground zero. For distances where $\sigma_o^2 \ll 0.01x^2$; $\sigma = 0.1x$. Equation (13) can be rewritten:

$$\frac{0.1\sqrt{2\pi}\; p_t(x,o)\,(HV)^2}{kWI(h)} = v^3 F(v) \approx \varphi(v) \qquad (17)$$

in which the right side is a function only of v, the fall velocity of the particles. Experimental data for "1003", Sedan, Danny Boy, and Neptune are used to determine the function $\varphi(v)$. If $p_i(x,0)$ is used for each isotope, then the fallout intensity by isotope can be estimated by the appropriate function $\varphi_i(v)$. The data for "1003" indicate a general relation

$$\varphi(v) \cong v^n \qquad (18)$$

which can be used to estimate the dose rate along the track axis by the semi-empirical equation

$$p_t(x,o) = \frac{kWI(h)\,(HV)^n}{\sqrt{2\pi}\,(HV)^2 x^n} \qquad (19)$$

For $n = 2$, the H + 24 hour dose rate along the track axis is then

$$p_{24hr}(x,o) = \frac{25WI(h)}{x^2} \qquad (20)$$

Thus, equation (20) relates the extent of radioactivity contamination along the close-in fallout track axis to the explosive yield and the fractional deposition along the track. For the general time dependence of mixed radionuclides

$$A(t) = A(t{=}24hr)\,t^{-1.2} \qquad (21)$$

the general expression for the dose rate of fission products in the fallout pattern from an excavation nuclear explosion is given by

$$p_t(x,y) = \frac{1.15\times10^3 WI(h)\,t^{-1.2}}{x^2}\, e^{-y^2/0.02x^2} \qquad (22)$$

the infinite-time dose from $t = x/V$ is then

$$D(x,y) = \frac{5.75\times10^3 WI(h)\,V^{0.2}}{x^{2.2}}\, e^{-y^2/0.02x^2} \qquad (23)$$

A similar calculation is made for the fallout patterns resulting from the detonation of a row charge of nuclear explosives in which N explosives are emplaced in a line of length L. For the wind direction normal to the row, the doses D_N in the separate fallout tracks are given by

$$D_N(x,y) = ND_1(x,o)\sqrt{\frac{\pi}{2}}\;\frac{\sigma_y}{L}\left[\varphi\left(\frac{L-y}{\sigma_y}\right) + \varphi\left(\frac{y}{\sigma_y}\right)\right] \qquad (24)$$

where

$$\varphi(z) = \sqrt{\frac{2}{\pi}} \int_0^z e^{-t^2/2} dt \quad = \text{probability integral}$$

D_1 = dose from a single explosion

$\sigma_y^2 = (0.1x)^2$

For a given dose, the maximum dimension of the zone in direction x is reached when y = L/2, the center of the sector,

$$D_N(x,\frac{L}{2}) = ND_1(x,o) \sqrt{\frac{\pi}{2}}\, 2\, \frac{\sigma_y}{L}\, \varphi(\frac{L}{2\sigma_y}) \qquad (25)$$

For canal or other earth-moving projects in which the lengths of individual row-charge explosions will be of the order of tens of kilometers, the ratio $L/2\sigma$ will generally be less than unity. For this case, the expansion of the term $\varphi(z)$ is

$$\varphi(z) = \sqrt{\frac{2}{\pi}}\, z \left[1 - \frac{1}{6} z^2 + \dots \right] \qquad (26)$$

and

$$D_N(x,\frac{L}{2}) = ND_1(x,o) \left[1 - 0.167 (\frac{L}{2\sigma})^2 + \dots \right] \qquad (27)$$

Thus the maximum dimension of a fallout zone can be determined for a given total dose, e.g., 0.5r, by the equation

$$D_N(x,\frac{L}{2}) \cong ND_1(x,o) \qquad (28)$$

with maximum error $\leq$ 17% when $\frac{L}{2\sigma_y} < 1$.

A similar expression has been calculated for those excavations where an exclusion zone is required and population in that zone returns after some fixed period following the explosion. For a maximum infinite-time dose D^* which accumulates at a distance x^*, at another location $x < x^*$ at which the calculated dose accumulates from time t^* + exclusion time T following the detonation, it is shown that

$$x \cong x^* (\frac{t^*}{T})^{0.1} \qquad (29)$$

Equation (29) allows the calculation of the zone of temporary exacuation between the distances x and x^*

Further development is given to estimate the extent of long-range fallout to distances of the order of 10,000 km and to fallout levels which do not exceed the average values of background global fallout, 0.2-0.5 mCi/km^2-day. The fraction of total radioactivity from test "1003" in the long-range fallout was 0.65%. The dispersion of the long-range cloud is based on the semiempirical theory of turbulent diffusion for large-scale averaged meteorological conditions along the cloud trajectory. The source concentration C(x,y,z,t,h) is followed from the instantaneous point source concentration C(o,o,h,o,h) where h = height of the stabilized cloud, with the boundary condition

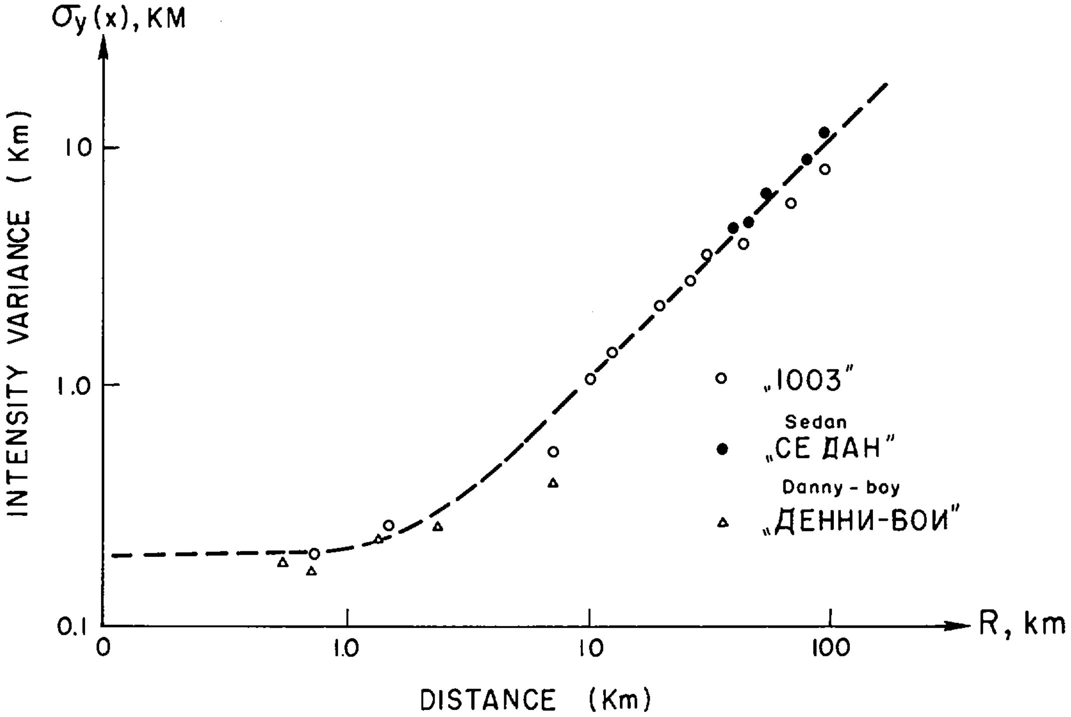

Figure 12. Comparison of the variance of the γ-ray intensity along the track axis of 3 excavation explosions.

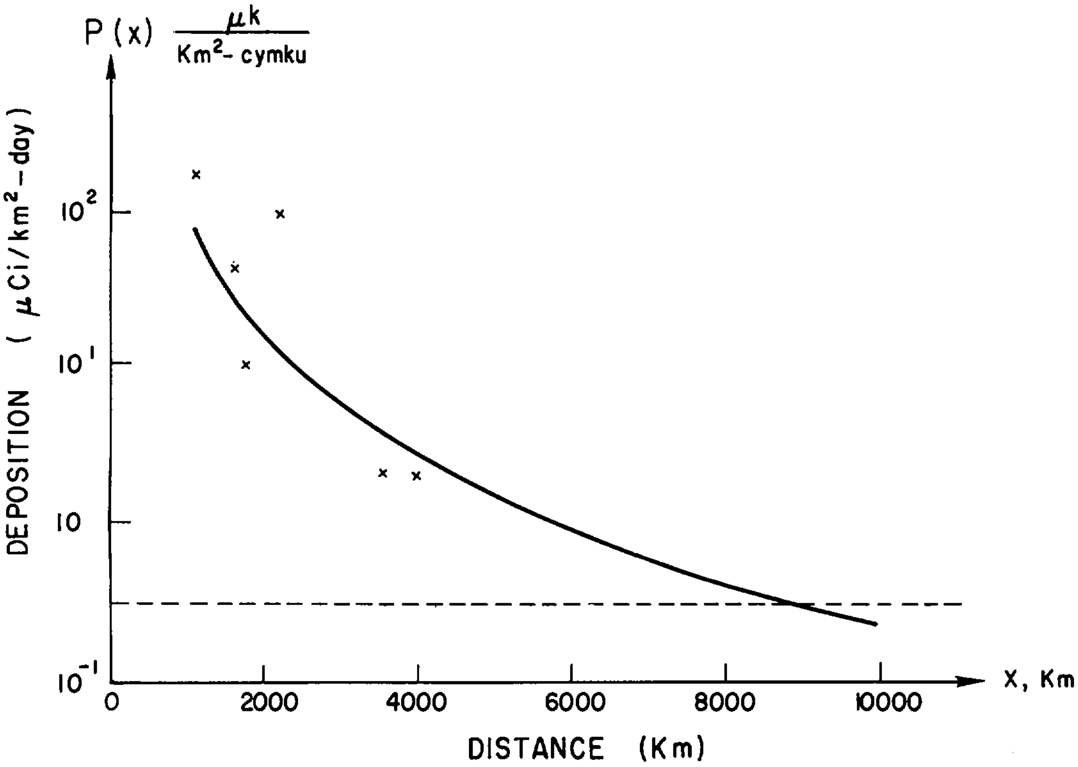

Figure 13. Fallout deposition rate as a function of distance along the track axis.

$$\left(k_z \frac{\partial C}{\partial z} - \beta C\right)_{z=z_o} = 0 \tag{30}$$

where

k_z = vertical diffusion coefficient

β = removal rate constant at the earth's surface (deposition velocity)

The expression for $C(x,y,z,t,h)$ is

$$C = \frac{Q(t)\, e^{-\frac{(x-Vt)^2}{2\sigma_x^2(t)} - \frac{y^2}{2\sigma_y^2(t)}}}{2\pi\, \sigma_x(t)\, \sigma_y(t)} \left[\frac{1}{2\sqrt{\pi k_z t}} \left\{ \exp\left(-\frac{(z-h)^2}{4k_z t}\right) + \exp\left(-\frac{(z+h)^2}{4k_z t}\right) \right\} - \frac{\beta}{k_z} \exp\left(\frac{\beta(z+h)}{k_z} + \frac{\beta^2 t}{k_z}\right) \mathrm{erfc}\left(\frac{\beta\sqrt{t}}{\sqrt{k_z}} + \frac{z+h}{2\sqrt{k_z t}}\right) \right] \tag{31}$$

where $Q(t)$ = total source in the distant fallout. It is assumed that for $t > 2$ days, the dispersion $\sigma(t)$ is given by

$$\sigma(t) \sim \sqrt{t} \tag{32}$$

and for literature values of $k_x = k_y = 10^9\ \mathrm{cm}^2/\mathrm{sec}$ and $k_z = 2 \times 10^5\ \mathrm{cm}^2/\mathrm{sec}$,

$$C(x,o,o,t,h) \cong \frac{2.4\times10^{-13}\ h\ Q(t)}{\beta t^{5/2}}\, e^{-\frac{h}{0.3\ t} - \frac{(x-Vt)^2}{1.4\times10^3\ t}} \tag{33}$$

where C is in $\mathrm{Ci/m^3}$. The fallout rate (in $\mathrm{Ci/km^2}$-hr) is then estimated from

$$\Pi = \beta C \tag{34}$$

Figure 13 shows the global fallout deposition rate for the test "1003" using a deposition velocity of $\beta \cong 3.6 \times 10^{-2}$ km/hr.

Acknowledgement

The assistance of the USAEC Division of Peaceful Nuclear Explosives in providing copies of the translations of the two USSR reports is gratefully acknowledged.

REFERENCES

(1) "Mechanical Effect of Underground Nuclear Explosions", Report of the Institute of Terrestrial Physics, USSR Academy of Sciences, Moscow, USSR, 1969.

(2) U. A. Izrael, V. N. Petrov, A. A. Pressman, F. A. Rovinsky, E. D. Stukin, and A. A. Ter-Saakov, "Radioactive Contamination of the Environment by Underground Nuclear Explosions, and Methods of Forecasting It", Moscow, USSR, 1969.

XA04N0763

UNDERGROUND NUCLEAR EFFECTS II

CAVITY PRESSURE HISTORY OF CONTAINED NUCLEAR EXPLOSIONS[*]

C. E. Chapin

Lawrence Radiation Laboratory, University of California
Livermore, California 94550

ABSTRACT

Knowledge of pressure in cavities created by contained nuclear explosions is useful for estimating the possibility of venting radioactive debris to the atmosphere. Measurements of cavity pressure, or temperature, would be helpful in evaluating the correctness of present code predictions of underground explosions. In instrumenting and interpreting such measurements it is necessary to have good theoretical estimates of cavity pressures. In this paper cavity pressure is estimated at the time when cavity growth is complete. Its subsequent decrease due to heat loss from the cavity to the surrounding media is also predicted.

The starting pressure (the pressure at the end of cavity growth) is obtained by adiabatic expansion to the final cavity size of the vaporized rock gas sphere created by the explosion. Estimates of cavity size can be obtained by stress propagation computer codes, such as SOC and TENSOR. However, such estimates require considerable time and effort. In this paper, cavity size is estimated using a scheme involving simple hand calculations. The prediction is complicated by uncertainties in the knowledge of silica water system chemistry and a lack of information concerning possible blowoff of wall material during cavity growth. If wall material blows off, it can significantly change the water content in the cavity, compared to the water content in the ambient media.

After cavity growth is complete, the pressure will change because of heat loss to the surrounding media. Heat transfer by convection, radiation and conduction is considered, and its effect on the pressure is calculated. Analysis of cavity heat transfer is made difficult by the complex nature of processes which occur at the wall where melting, vaporization and condensation of the gaseous rock can all occur. Furthermore, the melted wall material could be removed by flowing or dripping to the cavity floor. It could also be removed by expansion of the steam contained in the melt (blowoff) and by thermal stress fractures at the melt-solid interface.

There are three distinct heat transfer regimes, depending on the temperature of the cavity gas. When the cavity gas temperature is greater than the temperature at which wall material is removed by melting or blowoff, heat transfer occurs with mass removal. The water contained in the removed wall material is added to the cavity gas. As the cavity temperature decreases, due

---

[*] Work performed under the auspices of the U. S. Atomic Energy Commission.

to the heat loss, a temperature will be reached where the gaseous rock condenses. Thereafter, the gas is composed entirely of steam. Heat transfer during condensation is the second heat transfer regime. Following condensation the cavity gas will continue to cool, and material will continue to be removed from the walls as before. However, when the cavity cools sufficiently, the wall material becomes extremely viscous. Further heat transfer takes place by conduction into the walls. The heat transfer rate will be considerably reduced when this occurs since rock is a rather poor conductor of heat. Heat transfer by conduction is the third heat transfer regime.

A parametric study of pressure histories in contained underground nuclear explosions is made and the results of the calculations are compared with the limited experimental data available.

INTRODUCTION

Contained nuclear explosions produce a cavity of radioactive gas that can remain at great temperatures and pressures for many hours. To assure that the cavity gas will not escape from the cavity and contaminate the atmosphere, it is useful to have estimates of the expected cavity pressures and of how long they will be maintained. This is especially true for experiments which have large-diameter pipes connecting the cavity, perhaps through a series of valves, to the surface.

If a reliable measurement of cavity pressure following (or during) cavity growth could be made, it would be a useful check on our knowledge of the properties of the cavity gas and the accuracy of stress propagation codes like SOC and TENSOR. A study of cavity pressure history is an aid to devising such experiments.

In cratering experiments, the cavity gas expands to lower pressures and a larger size than it would if it was contained. Cavities in cratering shots also grow for a longer time than contained shots before the cavity gas finally breaks through the overlying mound. The time at which gases are vented to the atmosphere in a cratering experiment may be several seconds, in contrast to the few tenths of a second typical for full growth of the cavity in a contained explosion. During this longer expansion heat transfer, blow-off of wall material back into the cavity, and condensation of the rock gas could affect the air blast signal, gas acceleration of the mound, and the amount of radioactivity deposited in the immediate vicinity of the crater. These same processes might also occur in contained explosions and affect the cavity history. Consequently, study of the cavity pressure history in contained nuclear explosions may give useful information about processes of great interest in cratering experiments.

INITIAL CONDITIONS

A first step in analyzing cavity pressure history is to determine the starting conditions; that is, the pressure, temperature, etc. that exist when the cavity is just fully formed. In some cases this is impossible to do in any simple way. For example, wave reflections from the surface will affect cavity growth for those shots that are "close" to the surface, and it is desirable to bury the device as close as possible to the surface to minimize the cost of drilling the emplacement hole. This is especially true for large-yield (several hundred kiloton) shots. If accurate estimates of conditions in the cavity at the end of cavity growth are to be made in these situations, the only acceptable method is detailed computation of the stress-wave propagation using computers.

Rough estimates of cavity initial conditions can be made, however, by calculating the adiabatic expansion of the cavity gas from the initial sphere of vaporized rock created by the shock wave. Let P_V be the pressure in the vaporized sphere, V_V its volume, P_C the pressure in the cavity when cavity growth is complete and V_C the final volume of the cavity. For an adiabatic expansion of a perfect gas,

$$P_v V_v^{\gamma} = P_c V_c^{\gamma} . \tag{1}$$

The pressure in the vaporized sphere, P_V, is estimated by determining the amount of energy that can be deposited in the material by the shock wave which will just vaporize it. This energy is estimated to be about 2800 cal/g for silicate rocks. The amount of energy deposited in the material depends on the Hugoniot curve and the pressure-volume relationship the material follows after the passage of the shock wave. Butkovich[1] has determined vaporization pressure for different materials.

Higgins and Butkovich[2] estimated the volume of the vaporized sphere by using the relation

$$P_v V_v = (\bar{\gamma} - 1)W \tag{2}$$

where W is the energy released in the explosion. $\bar{\gamma}$ and γ were estimated from theoretical equation-of-state studies of the silica-water system made by Butkovich.[1] Assuming the final cavity pressure equal to the overburden pressure $P_0 = \rho g h$, Higgins and Butkovich combined the above formulas to obtain the following relation for cavity radius:

$$r_c = C \frac{W^{1/3}}{(\rho h)^{1/3\gamma}} \tag{3}$$

where C is the material-dependent constant,

$$C = \left[\frac{3(\bar{\gamma} - 1)P_v^{(1-\gamma)/\gamma}}{4\pi g^{1/\gamma}} \right]^{1/3} .$$

Higgins and Butkovich compared Eq. (3) with 45 nuclear detonations in tuff, alluvium, salt and granite and obtained a reasonable correlation, considering the inaccuracy of the data available for comparison.

The correlation is a little surprising since the adiabatic exponent is not constant as assumed by these authors. Figure 1 shows the values of $1/3\gamma$ required so that Eq. (1) can be true along an adiabatic path in two real materials. The adiabatic exponent is quite pressure-dependent, which is another way of saying that deviations from the perfect gas law are significant. Butkovich has also calculated cavity growth with the stress propagation code SOC in various media[3] and found that the cavity pressure after formation of the cavity is greater than the overburden pressure. He found it to be about 2.25 times as great for salt, 1.4 times as great for saturated tuff, and 2.0 times as great for granite.

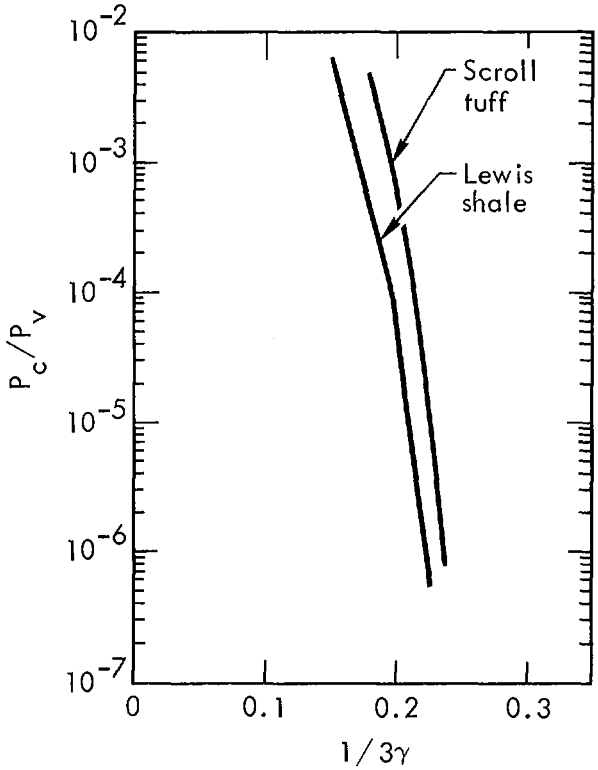

Fig. 1. Variation of the adiabatic exponent.

In view of these facts, I have used a slightly different method to estimate cavity pressure at the end of cavity growth than that used by Higgins and Butkovich. Computations by Butkovich[4] show that the mass of rock vaporized by the shock wave is about 70 metric tons per kiloton of yield for silicate rocks, and the density of the gas in the vaporized sphere is the same as its in-situ density. The volume V_V is calculated using these results instead of Eq. (2). The gas is expanded along an isentropic path using a real gas equation of state instead of the perfect gas assumption. The expansion is stopped at a pressure $P_c = KP_0$ where P_0 is the overburden pressure and K is a constant reflecting the material strength of the medium. At this pressure, the specific volume of the gas is known from the equation of state and the cavity size can be obtained since the mass of vaporized material is known.

The result of this calculation is shown in Figs. 2, 3 and 4 where $r_c/W^{1/3}$ is shown for various values of KP_0. A real gas Hugoniot curve was selected for the granite, tuff and aluvium materials in order to perform the calculation. Data from the same set of 46 nuclear detonations examined by Higgins and Butkovich are plotted on the curves using a value for K that gives the best fit to the curve. The unreasonable value K = 0.85 used for shots in tuff results because the

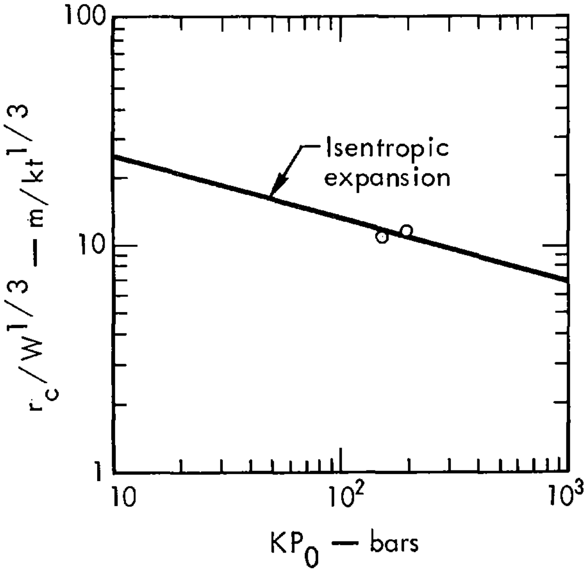

Fig. 2. Cavity radius of contained nuclear explosions in granite. Data points plotted with K = 2.0.

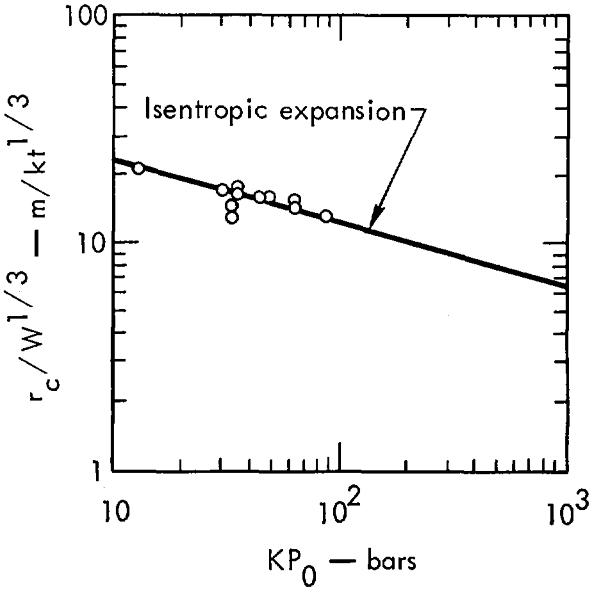

Fig. 3. Cavity radius of contained nuclear explosions in tuff. Data points plotted with K = 0.85.

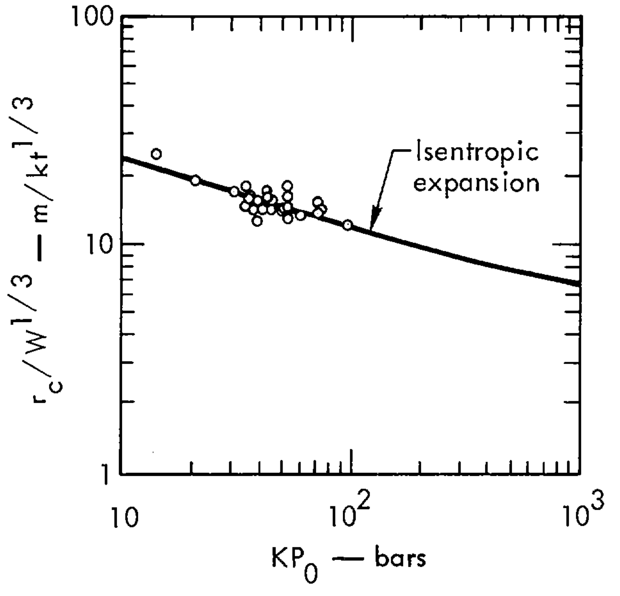

Fig. 4. Cavity radius of contained nuclear explosions in alluvium. Data point plotted with K = 1.25.

adiabatic selected was for Schooner tuff, and is probably not representative of the tuff the shots were actually fired in. The correlation is acceptable, however. The large scatter in the data for alluvium is because the data are inaccurate to begin with, and in addition no one adiabat is representative of the wide variety of materials that fall into the alluvium classification. In the calculations which follow, the cavity size used for granite and alluvium are those indicated respectively in Figs. 2 and 4.

BLOWOFF OF WALL MATERIAL

In the vicinity of the explosion center, the shock wave created by the explosion deposits enough energy in the material to completely vaporize it. Farther away, where the shock strength is attenuated, the shock wave will deposit enough energy to vaporize any water contained in the rock, but will be insufficient to vaporize the minerals that compose the rock. Consequently, the region surrounding the sphere of vaporized rock, the cavity wall, is a region of mixed phase. The gaseous component of the cavity walls can expand when the pressure in the cavity diminishes, blowing wall material back into the cavity. Figure 5 shows the isentropic expansion curves for shocked water at several shock pressures. The ordinate shows the ratio of

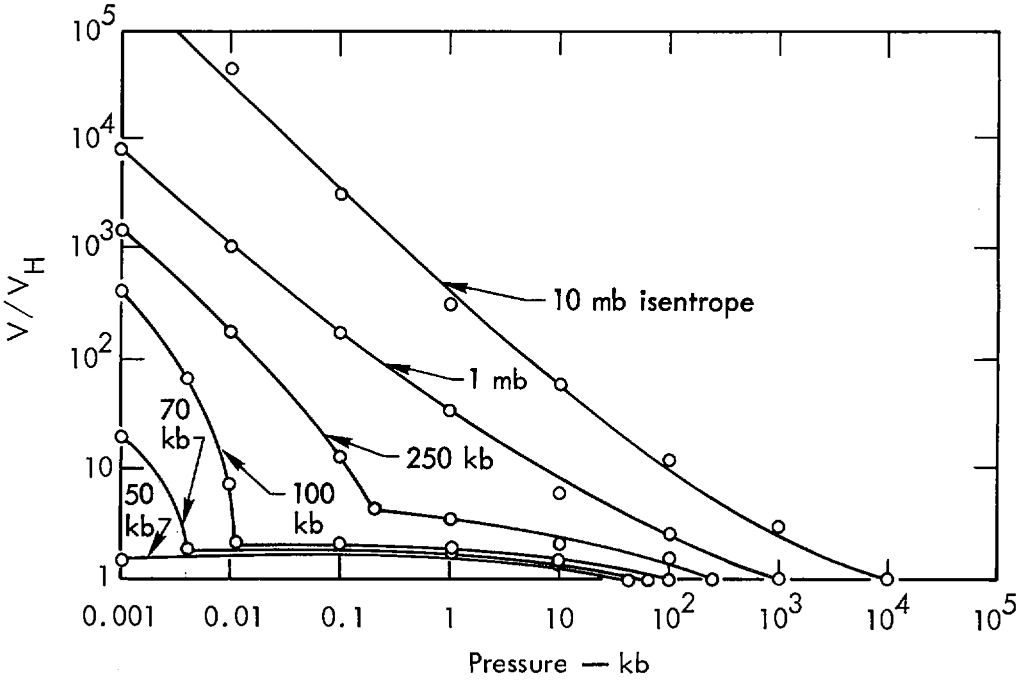

Fig. 5. Relative isentropic volume expansion of water from Hugoniot curve.

the adiabatically expanded volume to the shock volume. Water that is shocked to a pressure of 1 Mb will have expanded to about thirty times the volume it had when shocked if the pressure drops to 1 kb, and it will expand to about a thousand times that volume if the pressure drops to 10 bars. Shocked water therefore greatly expands after passage of the shock wave.

In a composite medium such as rock containing regions of water, it seems reasonable that a shock wave will shock the rock component differently than the water component. It is estimated, however, that the rock and water components reach pressure equilibrium within a time that is small compared to the time required for propagation of stress waves in the medium. The time required to reach thermal equilibrium is estimated to be about 1 second, a time that is long compared to the time required for cavity growth to be completed for all but very large yield explosions. Consequently, along the unloading path for the composite material, pressure equilibrium may be assumed between the water and rock components, but the water is assumed to follow an adiabatic expansion that may be different from the adiabatic expansion of the rock. Figure 6 shows some unloading paths calculated using this model for a rock containing 3% water. The curve labeled 1.79 Mb is the unloading path followed by the rock if it is shocked to a pressure of 1.79 Mb. For this material, 1.79 Mb is the greatest shock pressure that the material can sustain without being completely vaporized. Rock that unloads along this path is therefore material that is located at the interface between the vaporized gas sphere and the surrounding wall of melted rock, plus vaporized water. When the pressure in the material drops to 1 kb, the volume of the material is about 1.7 times greater than the volume it had before being shocked, and when the pressure reaches 100 bars, the material will have expanded to about 7.6 times its unshocked volume. This material could be expected, therefore, to expand back into the cavity as its pressure decreases during cavity growth.

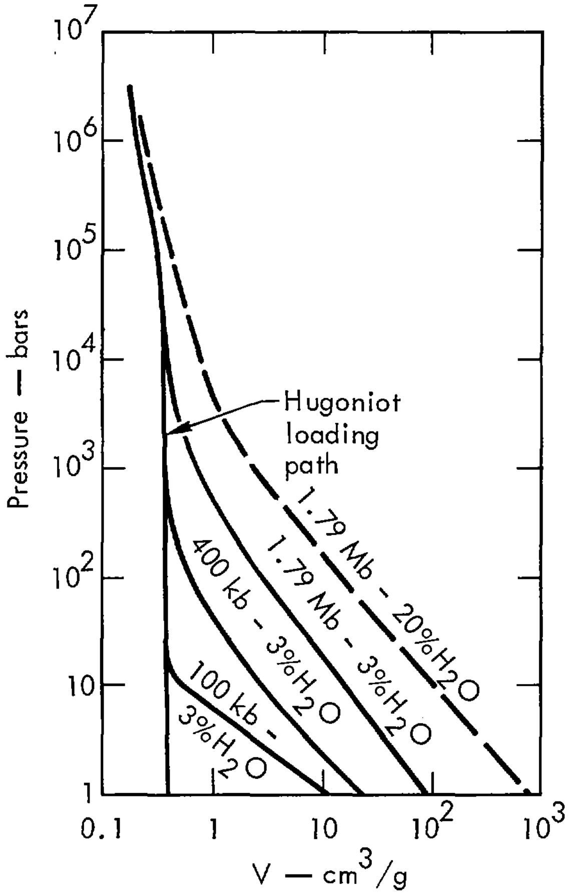

Fig. 6. Unloading paths for wet rock.

As shown in the figure, rock that is subjected to less shock pressure (and consequently is farther into the cavity walls from the vaporization-melt interface) also expands beyond its preshock volume, but the effect diminishes as the shock pressure decreases. Thus material farther into the cavity walls will expand less than material right at the interface.

Also shown is an estimate of the unloading path the material would follow if its water content were 20% rather than 3%. The presence of more water in the material enhances the expansion, as would be expected.

After the cavity is fully formed, thermal equilibrium between the rock and water contained in the rock can be expected to be reached in a time on the order of a second. I have performed calculations of the equilibrium composition of the silica water system using the HUG[5] computer code. From these computations, the ratio of gaseous volume to liquid volume at various temperatures and pressures can be obtained. These are shown in Figs. 7 and 8. The sharp rise in this ratio at the higher temperatures is where complete vaporization occurs. The gaseous volume is much greater than the liquid volume except for small concentrations of water at great pressures. If these results are accepted as a reasonable model of the behavior of silicate rocks containing water, it must be concluded that as these rocks attain temperatures that exceed their melting point they greatly expand even for temperatures well below the vaporization temperatures. Consequently, when material composing the cavity wall is heated by the cavity gas to a high enough temperature, it can be expected to blow off into the cavity.

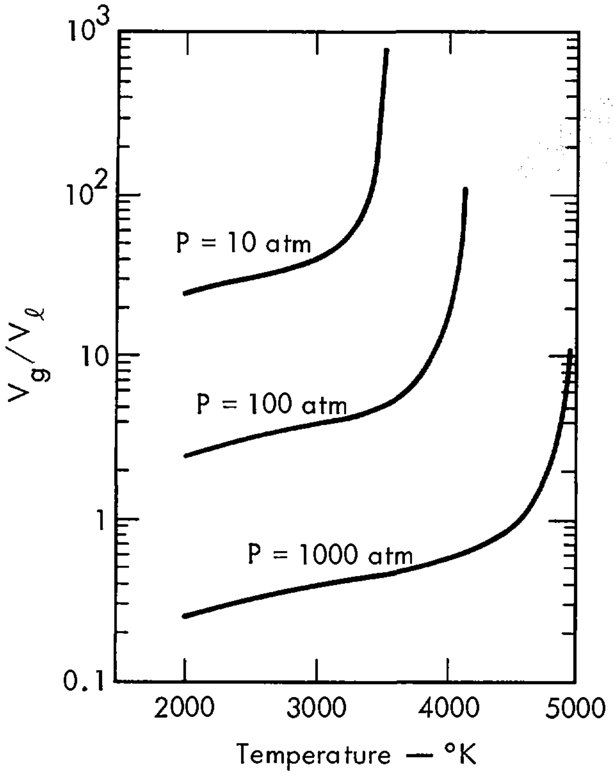

Fig. 7. Gas-to-liquid-volume ratio— equilibrium SiO_2 + 1% H_2O.

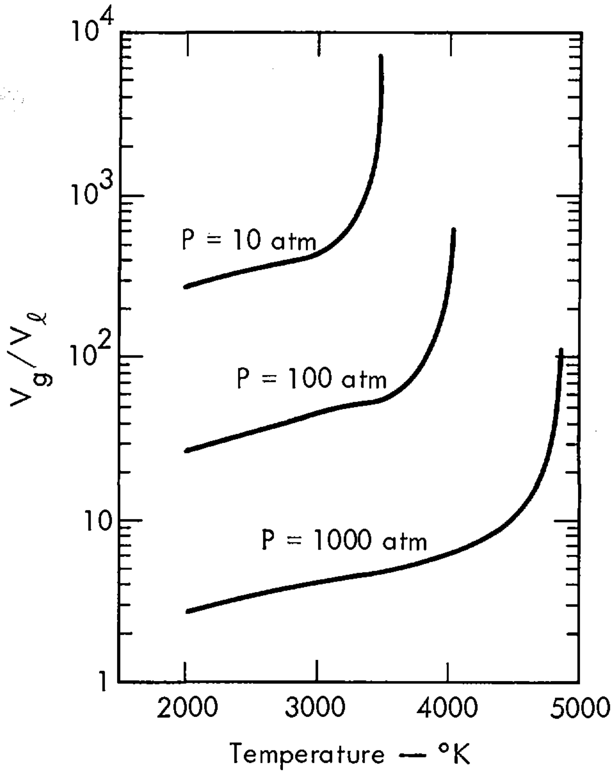

Fig. 8. Gas-to-liquid-volume ratio— equilibrium SiO_2 + 10% H_2O.

Blowoff of cavity material is possible, therefore, because of the way the shocked material unloads and because of expansion of the material when it is heated to a blowoff temperature. Blowoff is assumed to occur in the calculations that are performed in this paper.

Little is known about how blowoff might affect the cavity expansion. Agreement between calculations which assume no blowoff during formation of the cavity with experiments in contained nuclear explosions seems reasonably good. Since the time required to complete cavity growth is only a fraction of a second, it is doubtful that blowoff of wall material affects cavity formation, but the mixing of blowoff material with the cavity gas can affect the cavity pressure after cavity growth is complete, as will be discussed shortly. In cratering experiments where the time required for cavity expansion is much greater than for contained shots, the effects could be much more important, especially as they might affect cooling of the cavity gas, reducing its temperature and pressure. Reduced temperature could affect condensation of the cavity gas which might in turn affect the amount of radioactive material vented to the atmosphere. Reduced pressure could affect the acceleration of the mound and the air blast signal.

For dry rocks, or partially saturated porous rocks, blowoff may not be possible. Material might be removed from the cavity walls in other ways, however, such as flowing or dripping of the melted rock and thermal-stress-induced fractures at the melt-solid interface. Most rocks will have enough water that blowoff is possible. The dry, porous rocks where blowoff might not occur are not considered in this paper.

The analysis presented here assumes that blowoff does occur, but not until cavity growth is complete. At that time all of the rock that has been melted by the shock wave is assumed to blow into the cavity. The mass of shock-melted rock is estimated to be 350 metric tons per kiloton of yield.[6] Heat transfer between the solid blown-off wall material and the cavity gas is not considered. The water contained in the wall material is assumed to be rapidly mixed with the cavity gas. This mixing removes heat from the cavity gas, since the water will be at a lower temperature than the cavity gas. The continual addition of water also affects the pressure. Blowoff is assumed to continue as long as the cavity gas temperature is greater than the temperature at which the wall will greatly expand, the blowoff temperature. After the cavity cools below the blowoff temperature, heat transfer takes place by conduction through the cavity walls.

The time required for mixing of the water added to the cavity from blowoff of the shock-melted rock is difficult to estimate. A characteristic time for the process can, however, be obtained from the following considerations: During the time of cavity growth, the cavity gas moves a distance equal to the cavity radius. The cavity radius divided by the cavity growth time will therefore be characteristic of the velocity of the cavity gas. This velocity is about 100 m/sec. The mixing time is taken to be 10 cavity radii divided by this characteristic velocity, or

$$t_{mix} = 10r(m)/100 = r(m)/10 \text{ (sec)}. \tag{4}$$

As discussed above, the blowoff temperature, which is the temperature at which the cavity wall will greatly expand when heated, is very near the melting point of the wall material except for great pressures and small water contents. Calculations of cavity cooling are presented below for alluvium containing 10% water and granite containing 1% water. The blowoff temperature is taken to be 1900°K, except for granite for which it is 3700°K when the initial cavity pressure is 1000 bars, 3600°K when it is 700 bars, 3000°K when it is 300 bars, and 1900°K at all lower initial cavity pressures.

COOLING OF THE CAVITY GAS

Let ρ be the mass density of the cavity gas, e its specific internal energy, and V the cavity volume. The total energy in the cavity is ρeV and the rate of loss of this energy is equal to the heat loss

$$\frac{d}{dt}[\rho eV] = -A\ q, \tag{5}$$

where A is the area of the cavity wall and q is the heat flux.

The specific internal energy is a function of temperature and density, and has been calculated for the silica water system with the HUG code as previously mentioned. Thermodynamic equilibrium computations at various water concentrations were made for the mixture of species H, H_2, H_2O, O, O_2, OH, Si, Si_2, SiO, SiO_2, H^+, O^+, Si^+, and e^-. Thermochemical data for the calculation were taken from the JANEF tables.[7] The specific internal energy determined from these calculations is used in the cavity cooling computations presented here.

Because of the complexity of processes occurring at the cavity wall and the uncertainties connected with them, it is inappropriate to introduce anything but an approximate expression for the heat flux. The heat transfer process is different when the cavity gas temperature is greater than the blowoff temperature than when the cavity gas temperature is less than the blowoff temperature.

When the cavity gas temperature exceeds the blowoff temperature, heat transfer occurs with mass removal. It is the same as the process of melting with mass removal studied by Landau[8] except that the melting temperature in his work is to be replaced by the blowoff temperature. According to Landau's results, the time required to raise the wall temperature from T_a to the blowoff temperature T_b is

$$t_b = \frac{\pi}{4} k c \rho_w \left[\frac{T_b - T_a}{q}\right]^2 , \tag{6}$$

where k is the thermal conductivity of the wall, ρ_w the wall density and c its specific heat capacity. The heat flux is taken to be

$$q = \epsilon \sigma T^4 - \epsilon_w \sigma T_b^4 + h\,(T - T_b), \tag{7}$$

where T is the cavity gas temperature, σ the Stephan-Boltzmann constant, ϵ the emissivity of the cavity gas, ϵ_w the emissivity of the wall at temperature T_b, and h a convective heat-transfer coefficient. This expression for the heat flux is quite general. The first two terms are the difference in radiative flux between the wall and the gas. In the calculations, the gas is taken to be a blackbody radiator ($\epsilon = 1$) and the emissivity of the wall is taken as 0.9. This model for the radiation does not account for the details of radiation transfer processes that can occur at the wall. It does give a maximum rate of energy transfer for the radiation. The convective heat transfer coefficient h is likewise a very general way of accounting for thermal conduction through the boundary layer adjacent to the wall. Its value depends on many factors—the convective velocity, the viscosity of the cavity gas, turbulence, etc. The value of h used in the computations is 0.01 cal/deg/cm^2/sec. The heat flux expression, Eq. (7), also ignores any convective-radiative coupling that might occur.[9]

The thermal conductivity of the wall material is affected by many factors as well, such as temperature, pressure, porosity, nature and distribution of pores.[10-24] At the high temperatures of interest to cavity cooling, a value of 0.01 to 0.1 cal/cm/deg/sec appears to an appropriate upper limit.

Using these values, Eq. (7) shows the heat flux to vary between 100 and 1000 cal/cm^2/sec. Equation (6) shows the time required to reach the blowoff temperature with these heat fluxes varying from a fraction of a second to a few tens of seconds. These times are usually small compared with the time required for cooling of the cavity. Accordingly, all the heat flux given by Eq. (7) is assumed to instantaneously heat the cavity walls to the blowoff temperature. Let E_w be the energy required to heat the wall material to the blowoff temperature, ΔM_w be the mass of wall material that is heated, E_{H_2O} be the energy required to bring the water contained in the wall material (and which is assumed to mix with the cavity gas) to the temperature of the cavity gas, and ΔM_{H_2O} be the mass of water added to the cavity gas. Then

$$E_w \Delta M_w + E_{H_2O} \Delta M_{H_2O} = qA\Delta t. \tag{8}$$

The rate at which the density of the cavity gas changes due to water being added from material which is blowing off the wall is therefore

$$\frac{d\rho}{dt} = \lim_{\Delta t \to 0} \frac{\Delta M_{H_2O}}{V\Delta t} = \frac{q\frac{A}{V}}{E_{H_2O} + E_w/f}, \tag{9}$$

where $f = \Delta M_{H_2O}/\Delta M_w$ is the mass fraction of water contained in the rock.*

E_w is taken as 400 cal/g in all cases except for granite where when the initial cavity pressure is 1000 bars it is 1400 cal/g, when the pressure is 700 bars it is 1000 cal/g, and when the pressure is 300 bars it is 780 cal/g. E_{H_2O} is the difference in enthalpy between water at the blowoff temperature and at the cavity temperature.

Equations (5), (7) and (9) along with the equation-of-state computations calculated from HUG form a set of equations that can be numerically integrated from the initial conditions. This is done using the computer code KOOL, programed for that purpose.

As the temperature of the cavity gas drops, a point will be reached where the gaseous rock condenses. Thereafter the cavity gas is assumed entirely composed of steam. Actually, condensation takes place over a range of temperatures and pressures where a mixed phase exists. The extent of the mixed phase region is neglected in the present analysis. A temperature, pressure and water content dependence of the condensation point is used which s determined from the chemical equilibrium calculations.

Let E_c be the heat released per unit mass of condensing rock gas. The total heat released by condensation will be $\rho_R E_c V$ where ρ_R is the mass density of condensing material. This heat is much greater than the heat loss rate. In effect the condensation occurs in a rather well-insulated vessel. Furthermore, the condensation process is assumed to be isothermal and the heat loss rate during condensation will then be constant. With these assumptions the time required for condensation is estimated as

$$t_c = \frac{E_c \rho_R V}{qA} \tag{10}$$

where E_c is taken to be about 1900 cal/g. During this time the temperature is constant and water will continue to be added to the cavity at the rate given by Eq. (9).

Following condensation, the cavity gas will continue to cool according to Eqs. (5), (7) and (9) and the equation of state for pure water. Blowoff stops

---

[*] The analysis here neglects water which might be in solution with the melted rock.[25,26]

when the cavity gas temperature falls below the blowoff temperature. The melted rock will usually be extremely viscous at the blowoff temperature since in most cases this temperature is close to the melting temperature.[27,28] Further heat transfer must then take place by conduction and radiation through the cavity walls.

The thermal conductivity depends on many properties of the wall, including its temperature and pressure. Radiation plays an important role in the heat transfer in rocks at temperatures near the melting point.[14,15] There are so little data concerning the behavior of thermal conductivity at elevated temperatures and pressures in rock media that an analysis of heat conduction in the cavity wall which takes this behavior into account is not justified. Instead, the thermal conductivity is assumed to be constant and to have a value of 0.1 cal/cm/sec/deg.

The problem then reduces to one of heat transfer from a spherical cavity of radius r_c into the surrounding walls which have constant properties. The surface temperature of the cavity walls is taken as equal to the cavity gas temperature, and the distribution of temperature in the cavity wall at the time heat conduction begins and blowoff ends is assumed known. The solution to this problem is[29]

$$T(R,t)_w = T_a + \frac{u(R,t)}{R/L} \tag{11}$$

where $T(R,t)_w$ is the temperature in the wall at a distance R measured from the center of the cavity ($R \geq r_c$) at time t. L is a dimension characteristic of the extent of the initial temperature distribution, T_a is the ambient temperature at $R = \infty$, and the function u is given by

$$u(\bar{R},\bar{t}) = \frac{1}{2\sqrt{\pi\bar{t}}} \int_0^{\infty} \left(\bar{R} + \frac{r}{L}\right) f(\xi) \left\{ e^{-(\bar{R}-\xi)^2/4\bar{t}} - e^{-(\bar{R}+\xi)^2/4\bar{t}} \right\} d\xi$$

$$+ \frac{\bar{R}}{2\sqrt{\pi}} \int_0^{\bar{t}} \frac{r_c}{L} \phi(\tau) (\bar{t} - \tau)^{3/2} e^{-\bar{R}^2/[4(\bar{t} - \tau)]} d\tau \tag{12}$$

where

$$\bar{R} = \frac{R - r_c}{L},$$

$$\bar{t} = \frac{t - t_i}{t^*},$$

t_i is the time that heat conduction begins and blowoff ends,

$$t^* = L^2 \rho_w c/k,$$

f(R) is the initial temperature distribution,

$$\phi(t) = T(r_c, t) - T_a = T - T_a,$$

and T, as before, is the cavity gas temperature. The heat transfer rate into the cavity wall is

$$q = -k\left(\frac{\partial T_w}{\partial R}\right)_{R=r_c} = -\frac{k}{r_c}\left[\phi(t) - \left(\frac{\partial u}{\partial \bar{R}}\right)_{\bar{R}=0}\right]. \tag{13}$$

Assuming the initial temperature distribution to be given by

$$f\left(\frac{R}{L}\right) = \frac{r_c}{L}\,\frac{T_b - T_a}{\left(\frac{R + r_c}{L}\right)}\,e^{-\left(\frac{R}{L}\right)^2}, \tag{14}$$

the heat transfer rate can be shown to be

$$q = \frac{k}{r_c}\left[T - T_a + \frac{r_c}{L}\,\frac{4}{\sqrt{\pi}}\,(T_b - T_a)\,\frac{\sqrt{\bar{t}}}{1 + 4\bar{t}}\right]. \tag{15}$$

To obtain the solution for cooling of the cavity when the cavity gas temperature is less than the blowoff temperature, Eq. (15) can be used with Eq. (5) and the condition that the cavity gas density is constant at the value it had when blowoff ended.

RESULTS AND DISCUSSION

Cooling of cavities produced by various yields of nuclear explosives and initial cavity pressures, KP_0, have been calculated according to the scheme outlined above for granite with 1% water and alluvium with 10% water. Figure 9 shows the temperature decay for a 100-kt explosion at an initial pressure of 100 bars. The temperature rapidly diminishes until condensation takes place; it is constant during condensation, and has another rapid decay to the point where blowoff ends (which is indicated on the figure by the arrow labeled B). The temperature is shown for a larger time scale in Fig. 10 which clearly shows that cooling by heat conduction is a much slower process than cooling by blowoff into the cavity. The temperature history for other yields, initial pressures and materials are similar to the one shown in Figs. 9 and 10, except for differences in the time scale.

The cavity gas density is shown in Fig. 11. It increases rapidly for the first 6 sec due to the mixing of water from the shock-melted rock with the cavity gas. There is a further, but more gradual increase due to water added during blowoff of material from the cavity walls. When condensation takes place the density decreases, as shown by the dashed line. Following condensation, a slight increase in the density occurs until blowoff ends, and thereafter it is constant.

Figure 12 shows pressure histories for several different initial pressures. Condensation is indicated by a dotted line because the actual condensation path is not calculated, only the end points. The pressure monotonically

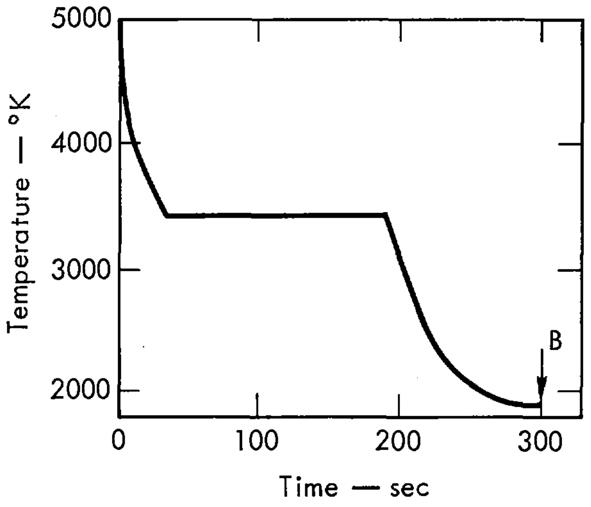

Fig. 9. Cavity temperature history—granite with 1% water. KP_0 = 100 bars; W = 100 kt.

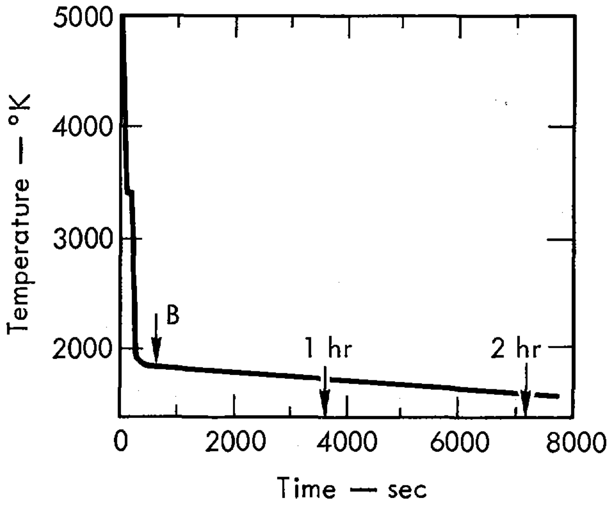

Fig. 10. Cavity temperature history—granite with 1% water. KP_0 = 100 bars; W = 100 kt.

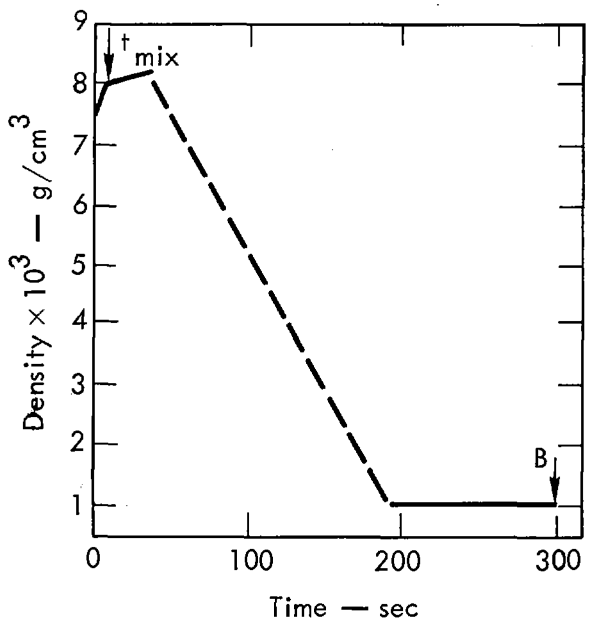

Fig. 11. Cavity gas density—granite with 1% water; KP_0 = 100 bars, W = 100 kt.

decays until blowoff ends, which is indicated by the arrow labeled B. The pressure decay thereafter is more gradual. The arrow labeled WC indicates the point at which the steam in the cavity condenses. The effect of different yields at the same initial pressure is shown in Fig. 13. Increasing the yield at the same initial pressure will increase the time for pressure decay. The same series of 1-kt explosions as shown in Fig. 12 for granite with 1% water is shown in Fig. 14 for alluvium with 10% water. The pressure histories are quite different from those shown in Fig. 12. The pressure actually increases slightly due to the large amount of water added to the cavity from the shock-melted rock and blowoff. If two explosions are detonated having the same yield and initial pressure, one in granite with 1% water and the other in alluvium with 10% water, the explosion in the wet rock will take significantly longer to decay. The pressure histories of two different yields at the same initial pressure are shown in Fig. 15. Just as was concluded for granite, increasing the yield at the same initial pressure results in a longer cooling time.

The time at which the steam in the cavity condenses is roughly the same at all initial pressures for a given material. When the steam condenses, the pressure in the cavity can drop to very small values, even produce

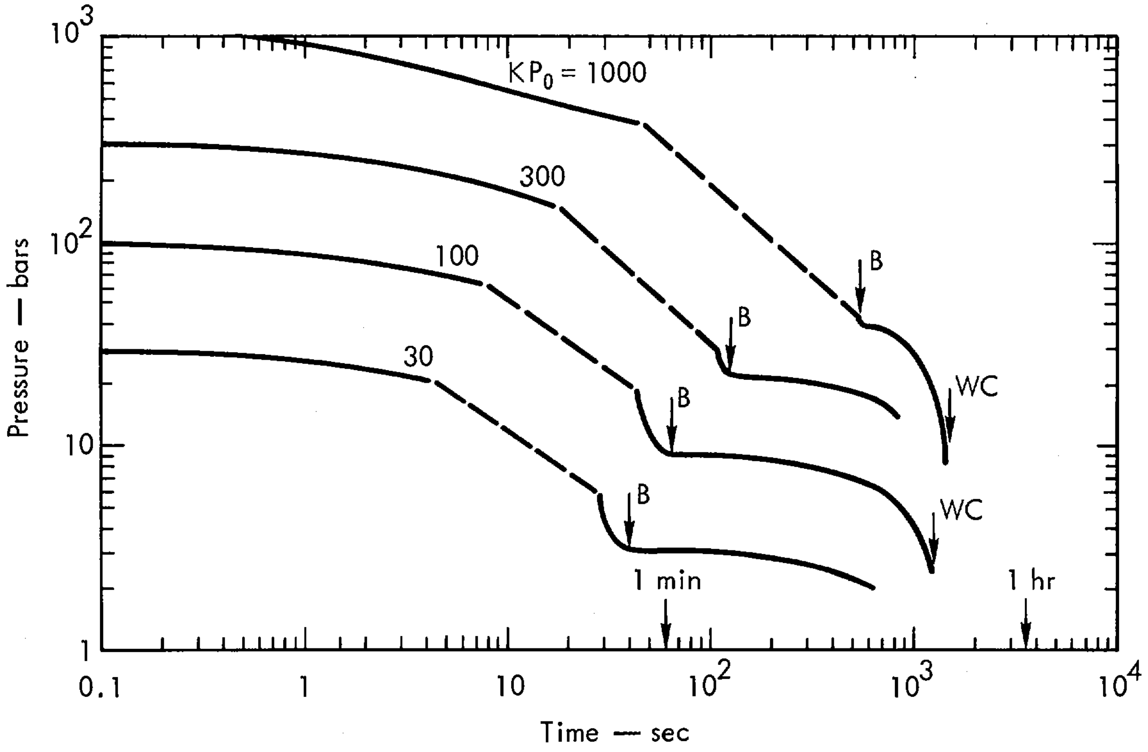

Fig. 12. Cavity pressure—granite with 1% water; W = 1 kt.

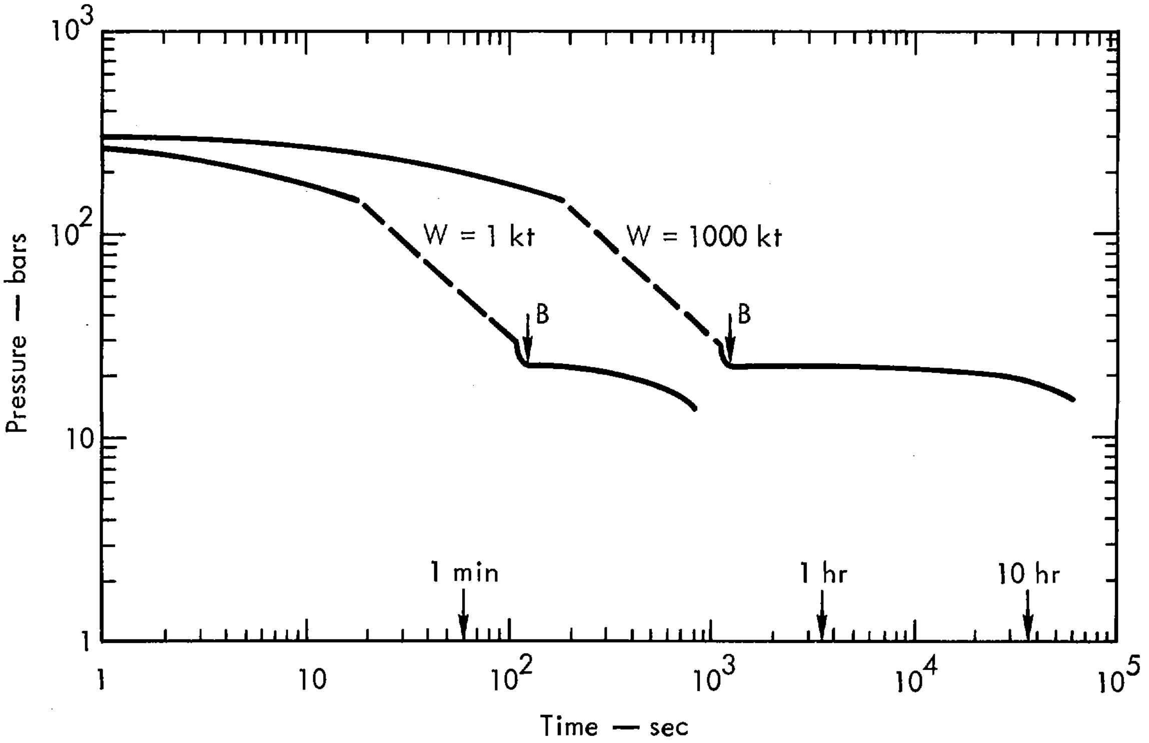

Fig. 13. Cavity pressure—granite with 1% water; KP_0 = 300 bars.

a vacuum. The full overburden pressure could therefore be applied to the standing cavity at this time and collapse, if it has not already occurred, could then take place.

Cavity collapse could occur much before this time, however. It is plausible that cavity collapse will occur for weak materials when the cavity pressure is slightly less than the overburden pressure.

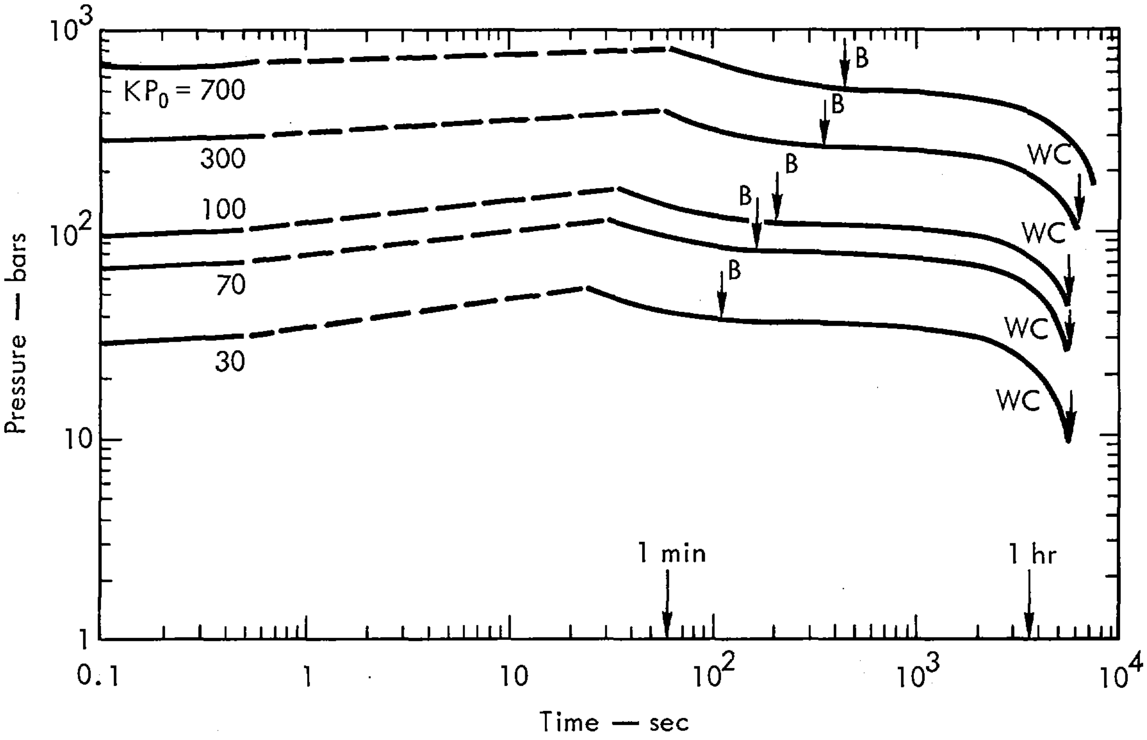

Fig. 14. Cavity pressure—alluvium plus 10% water; W = 1 kt.

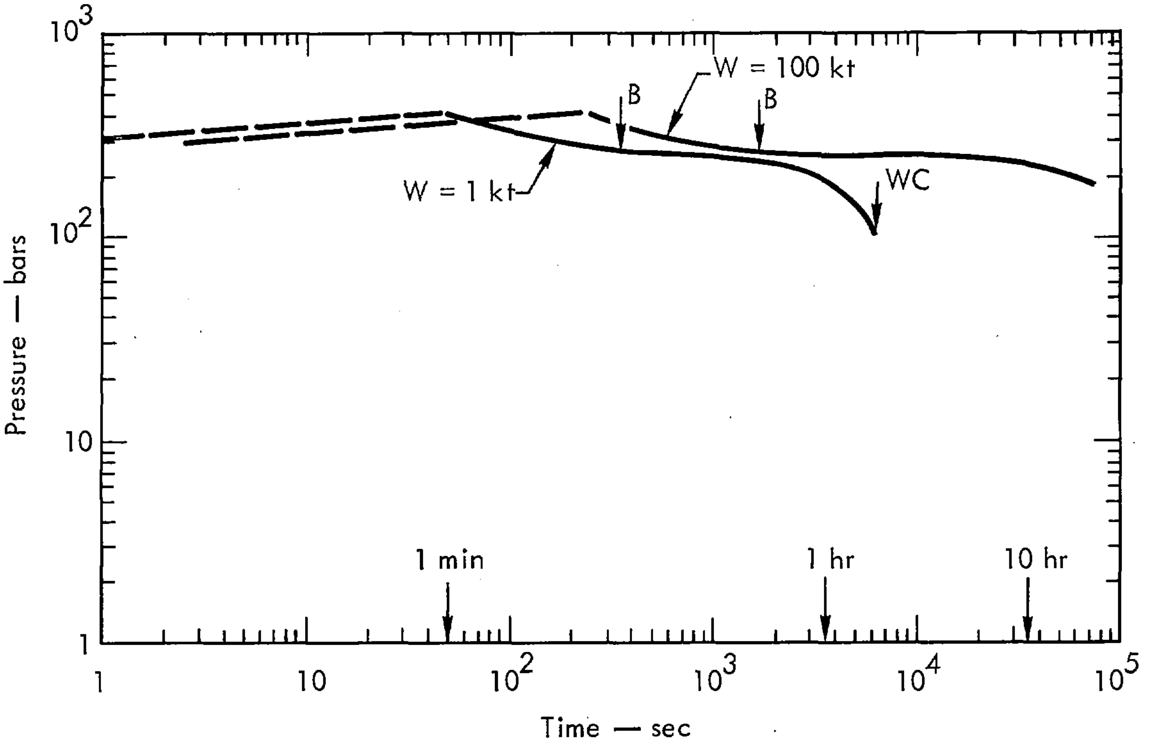

Fig. 15. Alluvium cavity pressure—10% water; KP_0 = 300 bars.

Although there have been several attempts to measure the pressure history of standing cavities, only one measurement by Olsen[30] has been reported. His measurements were from pressure transducers placed 95 and 123 meters along a pipe extending upward from a nuclear explosion. Communication between the pipe and the cavity was established at about 15 sec after detonation, as indicated by pressure transducers as well as heat and radiation sensors.

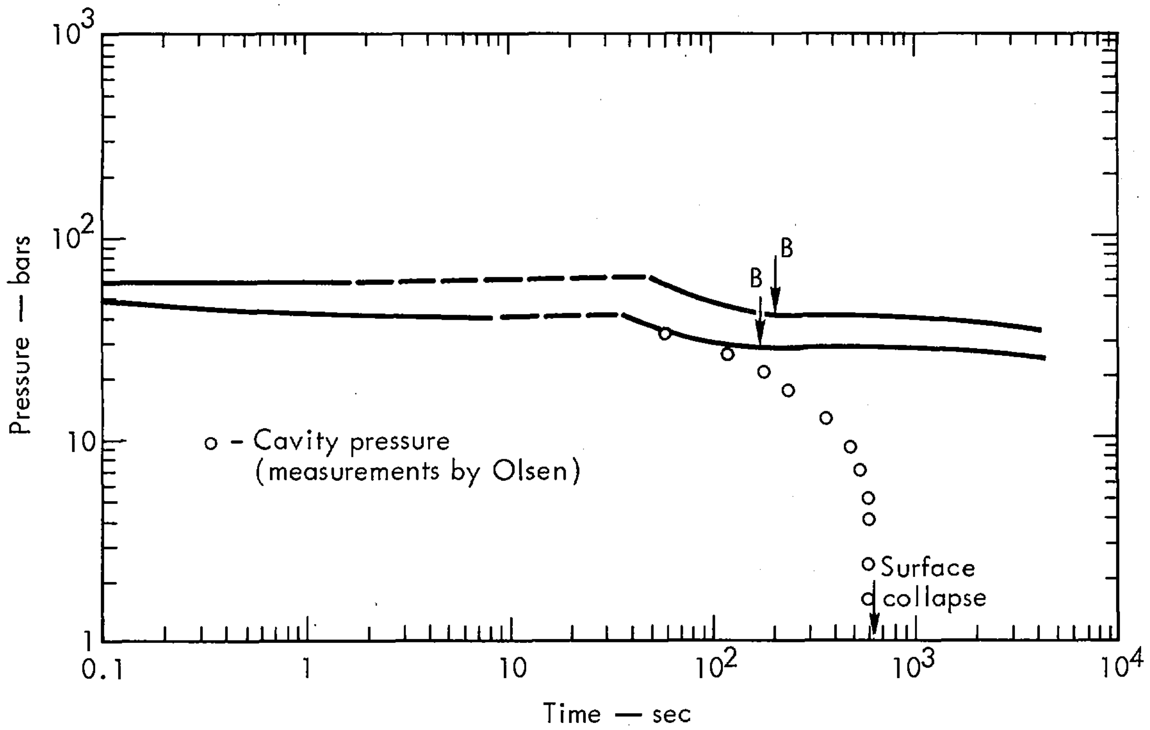

Fig. 16. Experimental measurement of cavity pressure.

Figure 16 shows the cavity pressure history predicted by the methods outlined above for the shot Olsen reported. There are uncertainties in the yield, water content, density and cavity radius for this shot, so the maximum and minimum values of these quantities have been used to predict the two curves on the figure. The cavity pressure is expected to lie somewhere between these two curves. Agreement with Olsen's data is good at first, but subsequently the differences are great.

The good initial agreement indicates that the cooling model, with mixing of water from the shock-melted rock and blowoff from the walls, does predict the correct initial pressure.

The poor agreement following blowoff could mean that the conduction cooling part of the model needs more work. However, the nature of the connection with the cavity is unclear. If the connection with the cavity was lost, the pressure decay would indicate processes occurring in this long pipe. A large pressure difference is not needed to explain the collapse at 10.2 min.

It is, however, unwise to judge the cavity cooling model or this experimental work on the basis of just one isolated measurement.

REFERENCES

1. T. R. Butkovich, "The Gas Equation of State for Natural Materials," Lawrence Radiation Laboratory, Livermore, Report UCRL-14729, 1967.

2. G. H. Higgins and T. R. Butkovich, "Effect of Water Content, Yield, Medium, and Depth of Burst on Cavity Radii," Lawrence Radiation Laboratory, Livermore, Report UCRL-50203, 1967.

3. Ref. 1, p. 17.

4. Ref. 1, p. 13.

5. P. F. Bird, R. E. Duff and G. L. Schott, "HUG, a FORTRAN-FAP Code for Computing Normal Shock and Detonation Wave Parameters in Gases," Los Alamos Scientific Laboratory, Report LA-2980, 1964.

6. T. R. Butkovich, Lawrence Radiation Laboratory, Livermore, private communication.

7. JAFAF Thermochemical Data, Dow Chemical Company Thermal Laboratory, Midland, Michigan,

8. H. G. Landau, Quart. J. Appl. Math. 8, 81 (1950).

9. E. M. Sparrow and R. D. Cess, Radiation Heat Transfer (Brooks/Cole, Belmont, California, 1967).

10. J. B. Walsh and E. R. Decker, J. Geophys. Res. 71, 3053 (1966).

11. H. Clark, "The Effects of Simple Compression and Wetting on the Thermal Conductivity of Rocks," Trans. Am. Geophys. Union, p. 543, 1941.

12. A. Sugawara and Y. Yoshizawa, Australian J. Phys. 14, 469 (1961).

13. A. D. Brailsford and K. G. Major, Brit. J. Appl. Phys. 15, 313 (1964).

14. H. Fujisawa, N. Fujii, H. Mizutani, H. Kanamori and S. Akimoto, J. Geophys. Res. 73, 4727 (1968).

15. H. Kanamori, N. Fujii and H. Mizutani, J. Geophys. Res. 73, 595 (1968).

16. W. H. Somerton and G. D. Boozer, "Thermal Characteristics of Porous Rocks at Elevated Temperatures," J. Petrol. Tech., p. 77, June 1960.

17. W. H. Somerton and G. D. Boozer, Am. Inst. Chem. Eng. J. 7, 87 (1961).

18. W. H. Somerton "Some Thermal Characteristics of Porous Rocks," J. Petrol. Tech., p. 61, May 1958.

19. A. M. Khan and I. Fatt, "A Thermoelectric Device for Measuring Thermal Conductivity of Rock," Soc. of Petrol. Eng. J., p. 113, June 1965.

20. J. M. Beck and A. E. Beck, J. Geophys. Res. 70, 5227 (1965).

21. A. Beck, J. Sci. Instr. 34, 186 (1957).

22. D. Kunii and J. M. Smith, "Thermal Conductivities of Porous Rocks Filled with a Stagnant Fluid," Soc. Petrol. Eng. J., p. 37, March 1961.

23. T. A. Edmondson, "Thermal Diffusivity of Sedimentary Rocks Subjected to Simulated Overburden Pressure," M.S. Thesis in Petroleum Engineering, University of California, No date.

24. J. D. T. Scorer, "The Relationship Between Thermal Conductivity and Other Rock Properties," M.S. Thesis in Petroleum Engineering, University of California, 1961.

25. G. C. Kennedy, G. J. Wasserburg, H. C. Heard and R. C. Newton, "The Upper Three-Phase Region in the System SiO_2 - H_2O," in Progress in Very High Pressure Research (John S. Wiley, New York, 1961).

26. C. W. Burnham and R. H. Jahns, Am. J. Sci. 260, 721 (1962).

27. R. Rossin, J. Bersan and G. Urbain, Compt. Rend. Acad. Sci. Paris 258, 562 (1964).

28. S. P. Clarke, Jr., ed., Handbook of Physical Constants, Geol. Soc. of America Inc., Boulder, Colorado, 1966.

29. H. S. Carslaw and J. C. Jaeger, Conduction of Heat in Solids (Oxford Univ. Press, 1959), p. 359.

30. C. W. Olsen, J. Geophys. Res. 72, 5037 (1967).

XA04N0764

THERMODYNAMICS OF THE SILICA-STEAM SYSTEM*

Oscar H. Krikorian
Lawrence Radiation Laboratory, University of California
Livermore, California 94550

ABSTRACT

In most nuclear cratering and cavity formation applications, the working fluid in the expanding cavity consists primarily of vaporized silica and steam. The chemical reaction products of silica and steam under these conditions are not known, although it is known that silica is very volatile in the presence of high-pressure steam under certain geologic conditions and in steam turbines. A review is made of work on the silica-steam system in an attempt to determine the vapor species that exist, and to establish the associated thermodynamic data.

The review indicates that at 600-900°K and 1-100 atm steam pressure, $Si(OH)_4$ is the most likely silicon-containing gaseous species. At 600-900°K and 100-1000 atm steam, $Si_2O(OH)_6$ is believed to predominate, whereas at 1350°K and 2000-9000 atm, a mixture of $Si(OH)_4$ and $Si_2O(OH)_6$ is consistent with the observed volatilities. In work at 1760°K in which silica was reacted either with steam at 0.5 and 1 atm, or with gaseous mixtures of H_2/H_2O and O_2/H_2O at 1 atm total pressure, only part of the volatility could be accounted for by $Si(OH)_4$. Hydrogen was found to greatly enhance the volatility of silica, and oxygen to suppress it. The species most likely to explain this behavior is believed to be SiO(OH). A number of other species may also be significant under these conditions. Thermodynamic data have been estimated for all species considered. The Si-OH bond dissociation energy is found to be ~117 kcal/mole in both $Si(OH)_4$ and $Si_2O(OH)_6$.

INTRODUCTION

Although silica is known to be a major constituent in most rocks, it may not be recognized that water is also present in high concentrations in a number of rocks that are of interest to Plowshare. For a rock that is vaporized in a nuclear explosion, the contributions of its various components to the total pressure are best indicated by expressing their compositions in mole%. Thus, the importance of water in a rock is enhanced because of its low molecular weight. According to the data of Pettijohn,[1] which has been converted to mole%, the average shale contains 54.5% SiO_2, 15.7% H_2O, and 8.5% Al_2O_3 as its main components. The average igneous rock is similar in composition to this average shale except for a lowering of the water content to about 4%. The average sandstone contains 75.7% SiO_2, 6.6% CO_2, 5.7% CaO and 5.3% H_2O. In the average sediment, the water content is about 10%. In limestones, CaO and CO_2 predominate, of course, but such a low silicate material will not be considered here.

---

*Work performed under the auspices of the U. S. Atomic Energy Commission.

Analysis of shales from the Gasbuggy[2] and Dragontrail[3] sites give average water contents of 12 mole% (3.6 wt%) and 16 mole% (5 wt%), respectively. In Sedan,[4] a cratering explosion in alluvium, the water content was of the order of 30 mole% (8.7-21.5 wt%). In the Logan, Blanca and Rainier shots in tuff,[5] the water content was ~36 mole% (~16 wt%), which makes it about equal to the silica content. For explosions fired in hard rock the water contents are very low, as would be expected from analyses on dense igneous and metamorphic rocks.[6]

These wide variations in water content among various rock types, and even within the same rock type, add to the variability of performance of nuclear cratering and underground engineering explosions. Some of the effects of steam in a nuclear cavity may be summarized as follows: (1) contributions to the equation of state of the working fluid in the expanding cavity; (2) effects on the condensation point and composition of the silica-rich matrix; (3) contributions to the residual pressure in the cavity after condensation of the silica matrix; (4) chemical reaction and equilibration with other major gaseous products in the cavity; and (5) chemical interactions leading to fractionation and distribution of radionuclides within the cavity and surrounding regions. These effects will be commented on briefly, in turn.

The regime in which steam would be expected to substantially affect the equation of state of the working fluid is that regime where the fluid has cooled sufficiently so that a plasma is no longer important, but condensation has not yet begun. Complex molecular species should be important in this region and should alter the equation of state from that expected from a simple mixture concept. The types and amounts of molecular species will be primarily dependent upon steam pressure and temperature. The condensation point of the silica-rich matrix will also be affected by the presence of molecular species. This is most aptly illustrated by the observation by Kennedy and co-workers[7] that in a steam environment at a total pressure of 9.7 kbar, the condensation point of silica is 1350°K. Their data further show that the composition of the condensed phase, as well as that of the vapor in equilibrium with it, each contain roughly equal molar amounts of SiO_2 and H_2O.

After condensation of a silica matrix, steam remains in the cavity as a residual gas until the temperature drops to some point below its critical temperature of 647°K. During this period, additional steam may enter the cavity from the surrounding rock, or steam may vent out of the cavity. Also, during this period, the steam will undergo various types of chemical reactions with its environment. For example, it may be partially reduced to H_2 by iron from the nuclear device and drill-hole casing, or it may undergo gas phase reactions with CO or CH_4. Barring venting, condensation of steam may occur either directly through formation of water, through formation of hydroxides, or at high temperatures, by solution in a silica-rich melt. The condensation of trace quantities of radionuclides will depend in part upon the partial pressures of their gaseous species and in part upon their condensation mechanisms. Steam may play a role in both of these factors. In particular, a number of fission products are known to form volatile hydroxides, e.g., CsOH, $Ba(OH)_2$, $MoO_2(OH)_2$ and $TeO(OH)_2$.[8]

In this study, a review is made of work on the volatility of silica in steam in order to establish the vapor species that are present and to derive the thermodynamic data for the species. A considerable amount of experimental information is avialable for the review because of geologic interest in the volatility of silica in steam and because of engineering interest in the carrying of silica by steam in steam boilers and turbines.

REVIEW OF LITERATURE DATA

Data on the volatility of silica in steam will be treated by methods similar to those used by Elliott,[9] in which volatilities are assumed to result from specific molecular species. Identification of the species is made by observing the variation of volatility with pressure and temperature, and by the use of thermodynamic arguments based upon bond energies and entropies of reaction.

An extensive amount of literature data exists on the volatility of silica in steam, covering steam pressures of 0.3 to 10^4 atm and temperatures of 400 to 1800°K. Only those investigations considered to be the most extensive or reliable[9-15] have been selected for this study, although the results of various workers generally show good agreement. Volatilities have been measured by determining the silica content of steam that has been equilibrated with quartz, cristobalite, silicic acid or silica glass. Equilibration has been attained either in flow experiments where steam is passed very slowly over a high surface area silica material, or in static experiments using sealed capsules containing silica and water. The volatilities are summarized in terms of a log-log plot of the effective fugacity, "f_{SiO_2}", of vapor phase silica versus the fugacity of steam along various isotherms (see Fig. 1). The effective fugacity of silica is defined by taking the volatile species to be ideal gaseous SiO_2. Fugacity coefficients for steam are obtained from a corresponding states chart given by Hougen and Watson.[16] Code letters are used on Fig. 1 to reference the literature sources. Code letters at the lower ends of the curves signify data extending up to $f_{H_2O} \approx 100$ atm, whereas code letters at the upper ends cover the higher pressure region. Individual data points are not shown in Fig. 1 because of the extensive nature of the data. Precision of the data is usually within ±10%, with the following exceptions. The data of Wendlandt and Glemser[13] below 200 atm steam pressure lie considerably below that of other workers for "f_{SiO_2}". It is possible that equilibrium was not attained in their experiments; hence their data in that region are omitted. Silicic acid and silica glass show higher volatilities in steam than does quartz.[10, 14] This difference is most pronounced at pressures exceeding ~20 atm but below the critical point of water, and amounts to factors of 2-8. In these cases the highest volatilities are used for the curves.

The structure and composition of the equilibrium condensed phase is not reliably known for most, or perhaps all, of the experimental work; nor can it be said with certainty that equilibrium was attained in all experiments. It has generally been assumed that the equilibrium phase is the bulk phase that is being reacted with steam, in spite of the fact that reversibility for the reaction has not been established. There is some information on the types of phases that are produced by the condensation process. According to Straub,[11] the deposits on steam turbine blades are a mixture of solid hydrated silica and various other forms of silica. These deposits may occur either at the low-pressure end of the high-pressure turbine or at the high-pressure end of the low-pressure unit. Elliott[9] concludes that the turbine blade deposits are an amorphous or glassy form of silica. It may be surmised that the condensed phases on turbine blades consist of the lowest hydrate of silica, $SiO_2 \cdot 1/2\ H_2O$, together with varying amounts of silica glass, depending upon turbine conditions. Typically, such deposits may form at 500-600°K at steam pressures of ~50 atm. Kennedy et al.[7] found that when silica originating from crystalline quartz was carried across a temperature gradient of a few degrees at 1350°K by steam at a pressure of several kilobars, it gave a deposit of amorphous silica.

It seems reasonable at this point to assume that $SiO_2 \cdot 1/2\ H_2O(s)$ is the equilibrium phase for work at the lowest temperatures. At higher temperatures, the apparent equilibrium phase may be silica glass or one of the

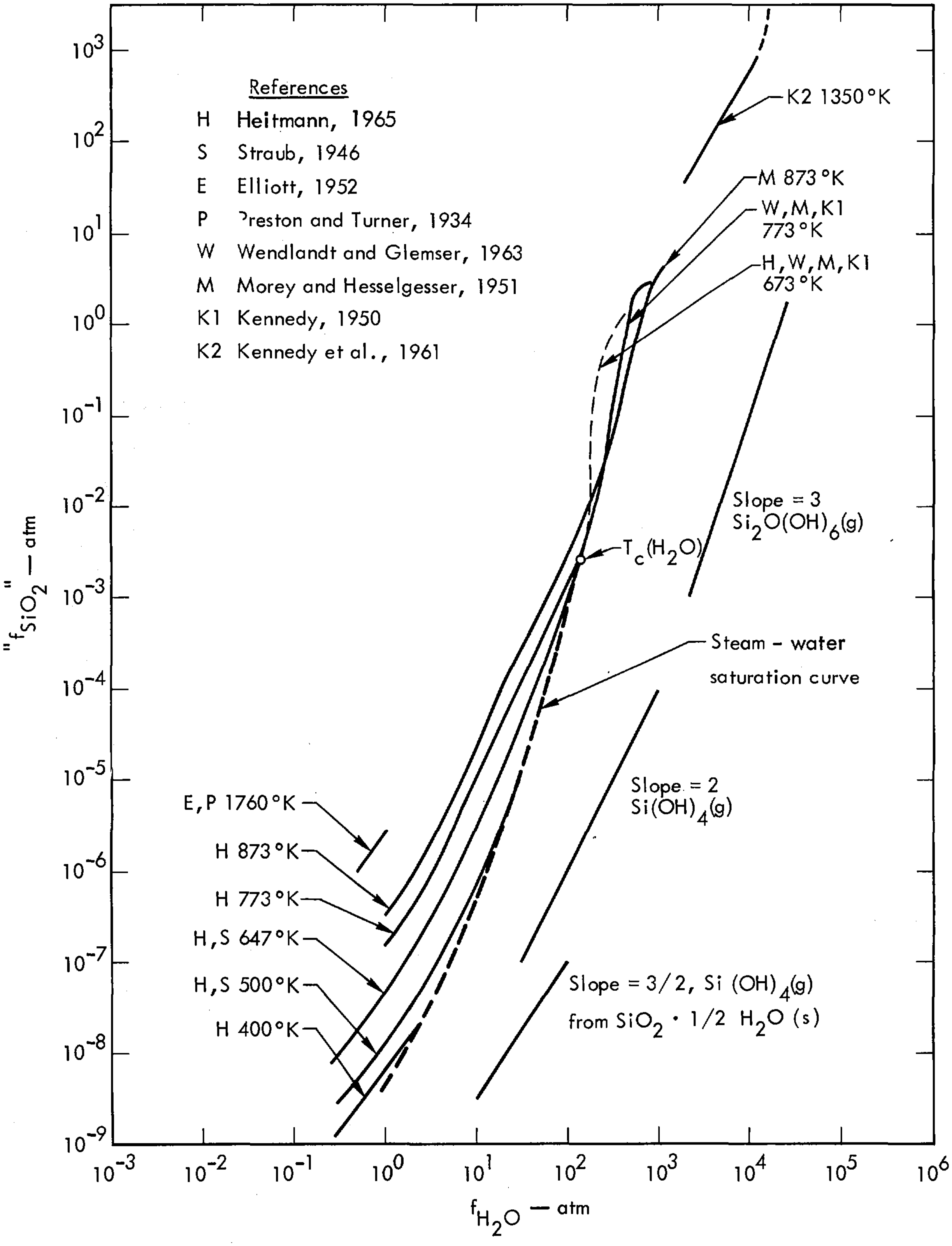

Fig. 1. Plot of apparent fugacity of silica versus fugacity of steam.

crystalline forms of silica, depending upon starting materials, degree of equilibration, temperature, etc.

For the two stoichiometries of condensed phases considered, a set of balanced volatilization reactions may be written as follows:

$$m\ SiO_2\cdot 1/2\ H_2O(s) + n\ H_2O(g) = Si_m(OH)_{2n+m}O_{1\frac{1}{2}m-n}(g) \tag{1}$$

and

$$m\ SiO_2(s,\ell) + n\ H_2O(g) = Si_m(OH)_{2n}O_{2m-n}(g). \tag{2}$$

For these reactions the assumption is made that silicon is in the +4 valence state, and does not form Si-Si or Si-H bonds. These assumptions are believed to be valid for all but the 1760°K data shown in Fig. 1. Equations (1) and (2) are applicable for regions in which bond energies predominate over entropy effects in determining the free energies of formation of vapor species and, as will be shown later in this paper, the Si-O and O-H bond strengths are found to significantly exceed those of Si-Si or Si-H. Experimental work by Kuts[17] provides supporting evidence for these conclusions. Kuts found that when mixtures of steam and gaseous combustion products (CO_2, O_2, N_2, etc.) were passed over silica at 708-913°K and total pressures of 1-15 atm, the volatility of silica was only a function of steam content. The proportion of steam to combustion products from a flame was varied from 0.2 to 0.65 without a noticeable change in the volatilization process. These experiments clearly indicate that CO_2, O_2 and N_2 are inert toward the silica-steam volatilization reaction in this temperature and pressure regime.

The equilibrium constants for reactions (1) and (2) are of the form,

$$K_{eq} = \frac{\left(f_{complex}\right)}{\left(a_{s,\ell}\right)^m \left(f_{H_2O}\right)^n},$$

which may be rewritten,

$$\ell n\ f_{complex} - m\ \ell n\ a_{s,\ell} = n\ \ell n\ f_{H_2O} + \ell n\ K_{eq}.$$

The activity of the solid or liquid condensed phase, $a_{s,\ell}$, is relatively insensitive to pressure, and $f_{complex}$ is proportional to "f_{SiO_2}", so that values of n may be inferred from the slopes of the various isotherms in Fig. 1. At temperatures of 400 to about 700°K and steam fugacities of 0.3-3 atm, n is ~3/2. Assuming that m = 1, and referring back to reaction (1), the formula of the volatile species is predicted to be $Si(OH)_4(g)$. Although the data are consistent with this formula, other more complex species such as, for example, $Si_3O_3(OH)_6(g)$ with m = 3 would also satisfy the fugacity slope criterion. It is highly unlikely, however, that such complex molecules would increase in importance with increasing temperature, although such an increase is consistent with the thermodynamic data for $Si(OH)_4(g)$ as will be shown later on in this paper.

At temperatures of 773 and 873°K with steam fugacities of 1-300 atm, n = 2 which is consistent with the reaction $SiO_2(s,\ell) + 2\ H_2O(g) = Si(OH)_4(g)$. At 500 and 647°K the fugacity curves show a marked curvature, with n increasing from about 3/2 to 3 as the fugacity of steam goes from 3 atm to the water saturation curve. The simplest molecule consistent with n = 3 is $Si_2O(OH)_6(g)$, which is a molecule that would be expected to decrease slowly in importance with increasing temperature. At yet higher fugacities of steam, the data at 773 and 873°K tend to confirm $Si_2O(OH)_6(g)$, but at 673°K an anomalously abrupt increase occurs in "f_{SiO_2}" at a steam fugacity of ~170 atm which is followed by a tailing off of the slope. This abrupt rise in slope cannot be interpreted in terms of a simple volatilization process. The closeness of the conditions to the critical point of water (T_c = 647.3°K, P_c = 218.4 atm) suggests that the anomaly may be related to the critical phenomenon. The concentration of silica (~0.1 mole%) is still sufficiently low that the critical point of the silica-saturated mixture would be expected to be below 673°K. However, T_{max} on the dew point curve may extend past 673°K, and P_{max} may exceed the critical pressure of water.[18]

The data at 1350°K correlate roughly with n = 2 over most of the fugacity range. A more rapid increase in slope begins at a steam fugacity of ~10^4 atm. At slightly higher fugacities (total pressure ≈ 9.7 kbar), a critical end point is reached in which the condensed phase can no longer be substained.[7] $Si(OH)_4$ is probably the predominant molecule at the lower fugacities, and a mixture of $Si(OH)_4$ and $Si_2O(OH)_6$ seems likely at the higher fugacities.

At 1760°K, the temperature is sufficiently high that both bond energy and entropy of reaction become important in determining the volatilization products. Under these conditions lower-valent silicon and Si-Si bonds may be contributors to new species. Elliott[9] did not take sufficient data to establish the presence of equilibrium or to give an accurate value for the slope of the fugacity curve, but he did demonstrate very effectively that oxygen suppresses the volatility reaction and hydrogen greatly enhances it. The work of Preston and Turner[12] at 1-atm steam pressure, although not very sophisticated, is in agreement with Elliott's results. The likely species at 1760°K will be discussed later on in this paper.

SOURCES OF THERMODYNAMIC DATA

Standard third-law methods[19] are used for the thermodynamic calculations. Free energy functions, $(G^\circ_T - H^\circ_0)/T$, are referred to 0°K. Thermodynamic data for the several forms of silica and available data for various known gaseous species are from the JANAF Tables.[20] Activity corrections for silica at high pressures were calculated from the thermodynamic relation, $\ell n\ a_{SiO_2} = V_{SiO_2}(P-1)/RT$.

For $SiO_2 \cdot 1/2\ H_2O(s)$, decomposition pressure data are available at 318-343°K,[21] but thermodynamic functions need to be developed to extend the data to higher temperatures. To do this, the entropy contribution of water in solid hydrates, S°_{298}, was estimated by subtracting out the entropies of oxides from the entropies of several hydrated oxides. For these hydrates,[22] $A\ell_2O_3 \cdot H_2O$ (boehmite), $A\ell_2O_3 \cdot H_2O$ (diaspore), $A\ell_2O_3 \cdot 3H_2O$, $A\ell_2Si_2O_7 \cdot 2H_2O$, $CaSO_4 \cdot 1/2\ H_2O$, $MgSO_4 \cdot H_2O$, and $Mg_3Si_2O_7 \cdot 2H_2O$, the S°_{298} contributions for water of hydration are 11.0, 4.7, 7.1, 8.1, 11.4, 8.3, and 7.1 cal/mole-°K, respectively. Similarly, for the hydrated sodium phosphates, Andon and co-workers[23] obtain S°_{298} = 7.45 cal/mole-°K for the water of hydration. A value of 8.0 cal/mole-°K is therefore chosen for the S°_{298} of water of hydration. This corresponds to an enthalpy increment, $H^\circ_{298} - H^\circ_0$, of ~1350 cal/mole, and a free energy function, $(G^\circ_T - H^\circ_0)/T$, of -3.47 cal/mole-°K at 298°K. From high-temperature enthalpy data for the hydrated minerals—perlite,[24] muscovite,[25] antigorite[26] and boehmite,[27] thermodynamic functions may be derived for water of hydration as shown in Table I. These functions may now be applied to the decomposition pressure data of Thiessen and Korner.[21] Taking the functions for $SiO_2 \cdot 1/2\ H_2O(s)$ to be those for quartz plus water of hydration gives for the reaction $SiO_2(glass) + 1/2\ H_2O(g) = SiO_2 \cdot 1/2\ H_2O(s)$, $\Delta H^\circ_0 = -7.4 \pm 0.2$ kcal/mole.

TABLE I. Thermodynamic functions for water of hydration in solid hydrates.

T (°K)	C_p (cal/mole-°K)	$H^\circ_T - H^\circ_0$ (cal/mole)	$(G^\circ_T - H^\circ_0)/T$ (cal/mole-°K)
298.15	9.7	1,350	-3.47
400	10.9	2,380	-4.82
500	12.0	3,510	-6.36
600	13.1	4,765	-7.89
700	14.2	6,140	-9.32
800	15.2	7,610	-10.60
900	16.0	9,170	-11.72
1000	16.5	10,800	-12.69

In order to establish the importance of various molecular species under a given set of conditions and to show the variation of concentration of these species with temperature, fairly good estimates of free-energy functions will be needed. Calculations have been made for a selected set of such potential species (see Table II), and although not necessarily complete, a sufficient variety has been included to show the variations in behavior with molecular complexity or type. The calculations have been made by standard methods,[19] based on the following estimates: $Si(OH)_4(g)$ is assumed to be in point group C_{2v} with oxygens located tetrahedrally around a central silicon, and having Si-O-H bond angles of 105°. Bond distances are taken to be 1.63 A for Si-O and 0.96 A for O-H bonds. Vibrational frequencies are estimated to be 3600(4), 1300(4), 900(4), 400(6), 250(1), and 200(2) cm^{-1}. For $Si_2O(OH)_6(g)$, the space group is taken as C_s. The silicons form an Si-O-Si chain having a 130° angle, and are each tetrahedrally bonded to three additional oxygens. Bond distances and the Si-O-H angles are the same as in $Si(OH)_4(g)$. The vibrational frequencies are estimated as 3600(4), 1300(8), 1000(4), 900(8), 400(7), 300(4), 200(2) and 70(1) cm^{-1}. There is in addition a three-fold internal rotation of $-Si(OH)_3$ groups for which the energy barrier is estimated to be 2000 cal/mole. For SiO(OH)(g), the O=Si-O angle is taken to be 109° and the Si-O-H angle, 105°. Bond distances are 1.54, 163 and 0.96 A for Si=O, Si-O and O-H, respectively. Vibrational frequencies are 3600, 1300, 1200, 900, 300 and 200 cm^{-1}. The multiplicity of the ground state is taken to be 2 in analogy with Si^{+3} or HC=O. For the remaining molecules, symmetry numbers are: $Si(OH)_2$ - 1, $SiO(OH)_2$ - 2, $Si_2(OH)_6$ - 6, $Si_3O_3(OH)_6$ - 6, and $Si[OSi(OH)_3]_4$ - 2. $Si_2(OH)_6$ is assumed to have an ethane-like structure; $Si_3O_3(OH)_6$, a six-membered ring; and $Si[OSi(OH)_3]_4$, is assumed to have $-OSi(OH)_3$ groups tetrahedrally bonded to a central Si. Moments of inertia for the remaining molecules are estimated by comparison with data on similar molecules. The vibration frequencies for $Si(OH)_2$ are 3600(2), 1300(2), 900(2), 400(2) and 200(1) cm^{-1}. Vibrational and internal rotation contributions

TABLE II. Estimated free-energy functions for gaseous $Si(OH)_4(g)$ species.

Species	$-\left(G^\circ_T - H^\circ_0\right)/T$ (cal/mole-°K) for various temperatures (°K)								
	298.15	400	600	800	1000	1200	1400	1600	1800
SiO(OH)	55.62	58.71	63.35	66.95	69.92	72.47	74.71	76.72	78.53
$Si(OH)_2$	54.07	56.37	62.50	66.60	70.05	73.05	75.71	78.11	80.29
$SiO(OH)_2$	57.86	61.75	67.94	72.97	77.23	80.94	84.24	87.21	89.91
$Si(OH)_4$	60.87	65.92	74.35	81.43	87.55	92.96	97.81	102.21	106.24
$Si_2(OH)_6$	68.90	76.19	88.66	99.58	109.22	117.83	125.61	132.70	139.21
$Si_2O(OH)_6$	75.99	83.70	96.94	108.58	118.87	128.08	136.40	143.99	150.97
$Si_3O_3(OH)_6$	71.59	80.12	95.24	108.49	120.21	130.71	140.22	148.92	156.94
$Si[OSi(OH)_3]_4$	97.22	112.37	139.47	164.07	186.16	206.10	224.26	240.89	256.22

to the free-energy functions of the remaining molecules are estimated by multiplying the contributions to $Si(OH)_4$ or $Si_2O(OH)_6$ by the factor $(3n_1-6)/(3n_0-6)$, where n_1 and n_0 are the number of atoms per molecule in the unknown and reference molecule, respectively, and 3n-6 represents the total number of vibrational modes in a non-linear polyatomic molecule.

RESULTS OF THERMODYNAMIC CALCULATIONS

From the thermodynamic data of the previous section, the decomposition pressures of $SiO_2 \cdot 1/2\ H_2O(s)$ may be calculated for the reaction $SiO_2 \cdot 1/2\ H_2O(s) = SiO_2(glass) + 1/2\ H_2O(g)$. It is found that at 400°K, the decomposition pressure of steam is ~1.5 atm so that the hydrate should decompose at lower pressures than this. The kinetics of decomposition, however, may be slow so that $SiO_2 \cdot 1/2\ H_2O(s)$ may be considered to be the equilibrium phase when silicic acid is used as the starting product. The decomposition pressure of $SiO_2 \cdot 1/2\ H_2O(s)$ reaches the saturation pressure of water-steam at 475°K and 16-atm steam pressure, hence silicic acid would be expected to decompose to silica glass or some other form of silica at higher temperatures. For the volatilization reaction $SiO_2 \cdot 1/2\ H_2O(s) + 3/2\ H_2O(g) = Si(OH)_4(g)$, the data at 400°K from Fig. 1 give $\Delta H^\circ_0 = 14.22$ kcal/mole, which leads to $\Delta H^\circ_{f,0} = -321.97$ kcal/mole for $Si(OH)_4(g)$.

Recognizing that silica is no longer likely to form a hydrate at temperatures of 500 and 647°K, the shallow slopes at 0.3-3 atm are no longer consistent with the assumptions of Eq. (2). Hypothesizing that equilibrium has not been attained for these temperatures and that the volatilities are limited by surface reaction kinetics, the conditions closest to equilibrium would be expected for the low-pressure end of the data, i.e., for the lowest volatilities. Reaction kinetics may have been less of a problem at 400°K since water is contained within the structure of $SiO_2 \cdot 1/2\ H_2O(s)$. For $SiO_2(glass) + 2\ H_2O(g) = Si(OH)_4(g)$, the low-pressure data give $\Delta H^\circ_{f,0} = -322.33$ and -322.53 kcal/mole for $Si(OH)_4(g)$ at 500 and 647°K, respectively. At 773 and 837°K, for f_{H_2O} of up to ~200 atm and assuming the preceding reaction, $\Delta H^\circ_{f,0} = -321.95$ and -322.54 for $Si(OH)_4(g)$ for the respective temperatures. The $\Delta H^\circ_{f,0}$ of $Si(OH)_4(g)$ appears to be well established from these calculations at -322.3 ± 0.2 kcal/mole.

In order to treat the data at 673, 773 and 873°K in the $Si_2O(OH)_6(g)$ region, corrections must be applied for the contributions of $Si(OH)_4(g)$. Also, the activity of silica must be corrected and "f_{SiO_2}" must be reduced by the factor 1/2 since there are two silicon atoms in each molecule of $Si_2O(OH)_6(g)$. Most of the data in this region are based upon quartz. To convert the data to a common basis of silica glass, factors of 2.2, 1.8, and 1.6 are applied to the "f_{SiO_2}" of the quartz data at temperatures of 673, 773 and 873°K, respectively. Furthermore, interpreting the 673°K data to be mostly in the dew-point region and to include solubility of silica in liquid water, only data near the high-pressure end will be used. From these considerations the equilibrium constants for the reaction, $2SiO_2(glass) + 3H_2O(g) = Si_2O(OH)_6(g)$, are found to be approximately 6.6×10^{-9} at 673°K, 2.3×10^{-9} at 773°K, and 8.0×10^{-10} at 873°K. The corresponding ΔH°_0 values for the reaction are -11.17, -11.70 and -11.70 kcal/mole, with -11.70 ± 0.7 kcal/mole chosen as the best value. The $\Delta H^\circ_{f,0}$ of $Si_2O(OH)_6(g)$ is calculated to be -612.1 ± 0.7 kcal/mole.

Equilibration of $Si_2O(OH)_6(g)$, as well as $Si(OH)_4(g)$, appears to be slow with silica at temperatures below ~700°K and steam pressures below ~200 atm, but above 1 atm. The apparent approach to equilibrium at 673°K and high steam pressures may be a consequence of a catalytic effect from trace amounts of liquid water containing dissolved silica. Some of the experiments of Morey and Hesselgesser[14] and Kennedy[15] were done at 573 and 633°K under steam fugacities of 128-152 atm, which exceed the water-steam saturation pressures. Their results would give "f_{SiO_2}" ≈ 0.1 atm, which would be consistent with the thermodynamic data for $Si_2O(OH)_6(g)$, if a steam-rich gas phase exists under these near-critical conditions. Heitmann's[10] work gives a solubility of silica (from silicic acid) in water of ~6.2 × 10^{-4} mole fraction near the critical point. Assuming the gas phase to have the same composition as the liquid at the critical point, a value of "f_{SiO_2}" ≈ 0.14 atm is obtained in agreement with the above conclusion.

The high-pressure results of Kennedy et al.[7] (see K2 on Fig. 1) at 1350°K cannot be used for a quantitative determination of thermodynamic data because of the lack of information on activities and fugacities. They may be used, however, for an approximate check of the derived thermodynamic data for $Si(OH)_4(g)$ and $Si_2O(OH)_6(g)$. In Table III a comparison is made of calculated ideal gas partial pressures of $Si(OH)_4(g)$ and $Si_2O(OH)_6(g)$ with observed volatilities which are expressed as apparent partial pressures of $Si(OH)_4$, i.e., "$p_{Si(OH)_4}$". At the lowest pressures, the calculated partial pressures of $Si(OH)_4(g)$ and $Si_2O(OH)_6(g)$ are significantly lower than the experimental results. This suggests a possible contribution of one or more additional species of silicon hydroxides that have not been taken into account. For example, $SiO(OH)_2(g)$ may be such a species. From 4000-7000 atm, the agreement is as good as can be expected, considering the uncertainties in the calculations. At pressures beyond 7000 atm, silicon hydroxide species make up a substantial fraction of the total gas, and fugacity corrections for all species become uncertain. The trend in volatilities is reasonable, however, considering the rapid increase in importance of $SiO(OH)_6(g)$ under these conditions.

TABLE III. A comparison of calculated partial pressures of $Si(OH)_4(g)$ and $Si_2O(OH)_6(g)$ with observed volatilities of silica in high-pressure steam at ~1350°K.[7] The observed volatilities are expressed as the apparent partial pressure of $Si(OH)_4(g)$, as indicated by "$p_{Si(OH)_4}$".

P_{Total} (atm)	"$p_{Si(OH)_4}$" (atm [obs])	a_{SiO_2} (quartz)	$p_{Si(OH)_4}$ (atm)	$p_{Si_2O(OH)_6}$ (atm)	p_{H_2O} (atm)	f_{H_2O} (atm)
1974	37	1.49	4.8	0.9	1968	2007
2961	75	1.86	15.1	6.5	2939	3286
3948	138	2.27	39	30	3879	4771
4935	237	2.83	92	134	4709	6687
5922	457	3.43	178	399	5344	8470
6908	686	4.17	276	830	5800	9514

Under the conditions of Elliott's study at ~1760°K,[9] it may be calculated that $Si(OH)_4(g)$ is an important molecular species (see Table IV), but that one or more additional species must also contribute to the volatility of silica. It may readily be shown by thermodynamic calculations that $Si_2O(OH)_6(g)$ or more complex molecules are unimportant under these conditions. The molecule SiO(g) attains its greatest importance with a partial pressure of 2.6 × 10^{-7} atm in the run at 1765°K containing 0.21-atm hydrogen. Although unimportant for its contribution to the partial pressure, SiO(g) may be an important intermediate in the kinetics of volatilization and equilibration. After correcting the observed volatility, "$p_{Si(OH)_4}$", for the known contribution of $Si(OH)_4(g)$ (see Table IV) the remaining one or more species seem to show approximately a 1/4-power dependence on oxygen pressure. The two most likely reactions that satisfy this behavior are

$$SiO_2(\text{crist.}) + 1/2\ H_2O(g) = SiO(OH)(g) + 1/4\ O_2(g),\ \text{and}$$

$$SiO_2(\text{crist.}) + 3/2\ H_2O(g) = Si(OH)_3(g) + 1/4\ O_2(g).$$

Bond energy arguments will be used to choose between the two probable species, $SiO(OH)(g)$ and $Si(OH)_3(g)$.

TABLE IV. Equilibrium partial pressures of molecular species and the enthalpy of formation of $SiO(OH)(g)$ as based on the work of Elliott[9] on reactions between silica and steam at ~1760°K.

T (°K)	p_{H_2O} (atm)	p_{O_2} (atm)	"$p_{Si(OH)_4}$" (atm, obs)	$p_{Si(OH)_4}$ (atm, calc)	$p_{SiO(OH)}$ (atm)	ΔH_0° (kcal/mole)
1775	0.90	0.10	0	1.04×10^{-6}	—	—
1763	1.00	7.04×10^{-4}	2.6×10^{-6}	1.26×10^{-6}	1.34×10^{-6}	127.60
1753	0.50[a]	4.14×10^{-4}	1.0×10^{-6}	0.31×10^{-6}	0.69×10^{-6}	128.46
1765	0.79[b]	2.03×10^{-8}	23×10^{-6}	0.79×10^{-6}	22.21×10^{-6}	126.65

[a] The flow gas consisted of a mixture of 0.5 atm steam and 0.5 atm argon.

[b] The flow gas consisted of a mixture of 0.79 atm steam and 0.21 atm hydrogen.

Assuming the residual partial pressures of silicon-containing species to be all from $Si(OH)_3(g)$ and estimating its free-energy function as -91 cal/mole-°K at 1760°K gives a $\Delta H_{f,0}^{\circ}$ of -246 kcal/mole for $Si(OH)_3(g)$. For the reaction $Si(OH)_3(g) = Si(g) + 3\ OH(g)$, ΔH_0° is then 381 kcal/mole and the average Si-OH bond energy is 127 kcal/mole. This may be compared with an average Si-OH bond energy of 116.5 kcal/mole in $Si(OH)_4(g)$ as derived from the selected value of $\Delta H_{f,0}^{\circ}$. Hildenbrand[28] has shown that in fluorides of carbon and silicon, the fluorine atoms are bonded much stronger in M^{+4} fluorides than in M^{+3} fluorides. Similar considerations should apply to hydroxides, and $Si(OH)_3(g)$ should have a lower average bond energy for Si-OH bonds than $Si(OH)_4(g)$. If this is the case, then 127 kcal/mole is too high for the Si-OH bond energy, and values lower than 116.5 kcal/mole would make $Si(OH)_3(g)$ of negligible importance in Elliott's work.

If the residual partial pressures of silicon-containing species are from $SiO(OH)(g)$, thermodynamic calculations for the volatilization reaction give the ΔH_0° values shown in Table IV. Giving the most weight to the 1765°K run, a ΔH_0° of 127 ± 1 kcal/mole is chosen for the reaction, which gives a $\Delta H_{f,0}^{\circ}$ of -118 ± 1 kcal/mole for $SiO(OH)(g)$.

In order to obtain a value for the Si-OH bond energy in SiO(OH), an estimate is needed for the Si=O bond energy. The average Si=O bond energy in $SiO_2(g)$ is 149 kcal/mole, while in $SiO(g)$ the bond energy is 190 kcal/mole. The Si=O bond energy in $SiO(OH)(g)$ should be somewhere between these values. Some comparisons with known data on carbon compounds may provide insight for a better estimate of the Si=O bond energy.

From JANAF data,[20] the following reactions may be compared:

$$HC{=}O(g) = CH(g) + O(g),\ \Delta H_0^{\circ} = 203\ \text{kcal/mole, and}$$

$$H_2C{=}O(g) = CH_2(g) + O(g),\ \Delta H_0^{\circ} = 181\ \text{kcal/mole.}$$

The difference of 22 kcal/mole in C=O bond energy in these two molecules is believed to result from a higher bond order for C=O in the HC=O molecule as a consequence of the availability of additional electrons for bonding. In the reaction

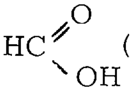

$$HC(=O)OH(g) = CH(g) + OH(g) + O(g) \text{ for which } \Delta H^\circ_0 = 302 \text{ kcal/mole,}^{29}$$

the C=O bond energy is 213 kcal/mole based upon a C-OH bond strength of 89 kcal/mole from $CH_3OH(g)$.[29] It thus appears that increases of 22-32 kcal/mole in the C=O bond energy may occur as extra bonding electrons become available or as certain structural forms provide additional bonding energy through resonance. These considerations would suggest that the Si=O bond energy in SiO(OH)(g) is probably closer to the value in SiO(g) than in $SiO_2(g)$. As additional support of this conslusion, it may be noted that the bond distances in SiO(g) and $SiO^+(g)$ are 1.509 A and 1.504 Å,[30] respectively, which suggests that since removal of an electron from SiO(g) does not affect bonding distance, bonding strength is also little affected. Similarly, adding an -OH bond to SiO(g) should have little effect on the Si=O bond strength. If a value of 180 kcal/mole is chosen for the Si=O bond energy in SiO(OH)(g), the Si-OH bond energy is 113 kcal/mole, which seems reasonable compared to 116.5 kcal/mole for $Si(OH)_4(g)$.

In order to calculate the Si-OH bond energy in $Si_2O(OH)_6(g)$, the assumption is made that the Si-O bonds in the Si-O-Si chain have the same bond energy as Si-OH bonds. On this basis, the average Si-O or Si-OH bond energy in $Si_2O(OH)_6(g)$ is calculated to be 117.5 kcal/mole, in good agreement with the value of 116.5 kcal/mole in $Si(OH)_4(g)$. The Si-O bond energy may now be compared with Si-H and Si-Si bond energies. Literature data[28] give 73.5 kcal/mole for D_0 of SiH(g) and 76 kcal/mole for the average bond energy in $SiH_4(g)$. Taking 75 kcal/mole for the Si-H bond energy gives ~51 kcal/mole for the Si-Si single bond energy from data on Si_2H_6 and Si_3H_8.[28] Thus, it is apparent that bond energies for Si-H and Si-Si are considerably weaker than for Si-O.

In conclusion, it is felt that the species SiO(OH)(g), $Si(OH)_4(g)$, and $Si_2O(OH)_6(g)$ reliably describe the existing volatility data in the silica-steam system. Bond energies derived from Si-OH bonds in these molecules appear to be in reasonable accord with expected trends. Other species undoubtedly become important at higher temperatures and other pressures. It may be possible to predict some of these species on the basis of the present observations. It is certainly desirable to acquire additional experimental data on molecular species, particularly by using high temperature mass spectrometric techniques as a means of identification.

REFERENCES

1. F. J. Pettijohn, Sedimentary Rocks (Harper and Row, Inc., Evanston, Ill., 1948).
2. J. H. Hill, Lawrence Radiation Laboratory, Livermore, private communication.
3. J. H. Hill, Lawrence Radiation Laboratory, Livermore, private communication.
4. M. D. Nordyke and M. M. Williamson, "Project Sedan," Lawrence Radiation Laboratory, Livermore, PNE 242F, Final Report, 1965.
5. G. W. Johnson, G. H. Higgins and C. E. Violet, J. Geophys. Res. 64, 1457 (1959).
6. F. J. Turner and J. Verhoogen, Igneous and Metamorphic Petrology (McGraw-Hill, New York, 1951).

7. G. C. Kennedy, G. J. Wasserburg, H. C. Heard and R. C. Newton, *Progress in Very High Pressure Research* (John Wiley and Sons, New York, 1961), p. 28.
8. D. D. Jackson, Lawrence Radiation Laboratory, Livermore, unpublished work, 1969.
9. G. R. B. Elliott, "Gaseous Hydrated Oxides, Hydroxides, and Other Hydrated Molecules," Lawrence Radiation Laboratory, Livermore, Report UCRL-1831, 1952.
10. H. G. Heitmann, Glastech. Ber. **38** (2), 41 (1965).
11. F. G. Straub, "Steam Turbine Blade Deposits," University of Illinois Bulletin 43, No. 59, 1946, Engineering Experiment Station Bulletin Series No. 364.
12. E. Preston and W. E. S. Turner, J. Soc. Glass Tech. **18**, 222 (1934).
13. H. G. Wendlandt and O. Glemser, Angew. Chem. **75**, 949 (1963).
14. G. W. Morey and J. M. Hesselgesser, Trans. Am. Soc. Mech. Eng. (ASME) **1951**, 865.
15. G. C. Kennedy, Econ. Geol. **39**, 25 (1944).
16. O. A. Hougen and K. M. Watson, *Chemical Process Principals Charts* (John Wiley and Sons, New York, 1946).
17. S. M. Kuts, Teploenergetika **14** (9), 82 (1967).
18. W. B. Kay, Accounts Chem. Res. **1** (11), 344 (1968).
19. G. N. Lewis, M. Randall, K. S. Pitzer and L. Brewer, *Thermodynamics*, 2nd ed. (McGraw-Hill, New York, 1961).
20. JANAF Thermochemical Tables, with supplements through June 30, 1969, D. R. Stull, Project Director, Dow Chemical Co., Midland, Michigan.
21. P. A. Thiessen and O. Körner, Z. anorg. Chem. **197**, 307 (1931).
22. K. K. Kelley and E. G. King, "Contributions to the Data on Theoretical Metallurgy. XIV. Entropies of the Elements and Inorganic Compounds," U. S. Bur. Mines Bull. 592, 1961.
23. R. J. L. Andon, J. F. Counsell, J. F. Martin and C. J. Mash, J. Appl. Chem. **17**, 65 (1967).
24. E. G. King, S. S. Todd, and K. K. Kelley, "Perlite: Thermal Data and Energy Required for Expansion," U. S. Bur. Mines Rept. Inv. 4394, 1948.
25. L. B. Pankratz, "High-Temperature Heat Contents and Entropies of Muscovite and Dehydrated Muscovite," U. S. Bur. Mines Rept. Inv. 6371, 1964.
26. E. G. King, R. Barany, W. W. Weller and L. B. Pankratz, "Thermodynamic Properties of Forsterite and Serpentine," U. S. Bur. Mines Rept. Inv. 6962, 1967.
27. K. K. Kelley, "Contributions to the Data on Theoretical Metallurgy. XIII. High-Temperature Heat-Content, Heat-Capacity, and Entropy Data for the Elements and Inorganic Compounds," U. S. Bur. Mines Bull. 584, 1960.
28. D. L. Hildenbrand, *Advances in High Temperature Chemistry*, Vol. I, L. Eyring, ed. (Academic Press, New York, 1967), pp. 193-217.
29. D. D. Wagman, W. H. Evans, V. B. Parker, I. Halow, S. M. Bailey, and R. H. Schumm, "Selected Values of Chemical Thermodynamic Properties," U. S. Natl. Bur. Stds. Tech. Note NBS-TR-270-3, 1968.
30. *Tables of Interatomic Distances and Configuration in Molecules and Ions*, L. E. Sutton, ed. (The Chemical Society, London, 1958).

XA04N0765

COMMENTS ON SOME OF THE PHYSICAL CHEMICAL QUESTIONS ASSOCIATED WITH THE ANALYSIS OF WATER IN EARTH MATERIALS*

Edward Catalano
Lawrence Radiation Laboratory, University of California
Livermore, California 94550

ABSTRACT

A discussion of various physical chemical questions which are associated with the quantitative analysis of water in earth materials is presented. A pseudothermodynamic approach to the binding of water in various types of earth materials is also presented. Emphasis is placed on the fact that as pore, crack, or hole sizes approach molecular dimensions, the interaction energy of water with the host material can become very large. A scale of interaction energies is suggested which would be useful for specifying operationally relevant analyses in earth materials.

INTRODUCTION

The quantitative analysis of the water content of earth materials is of great importance in various aspects of the Plowshare Program. The requirements for water analyses encompass a wide variety of problems from predictions of the strengths of earth materials to the disposition of radioactive elements in the cavities and craters created by nuclear devices. Water analyses are also useful in areas other than Plowshare where the problems are geochemical and geophysical in nature, such as predicting seismic damage in various geological regions.

A single, general method of analysis to yield pertinent information for such a wide variety of requirements does not exist, and it is doubtful that one could be found. The purpose of this report is to establish a workable set of definitions to examine the specific problem at hand and to point the way to one or more analytical methods that can yield pertinent information. The intention is to explore some of the subtleties of the questions regarding water analyses in earth materials in enough detail so that some of the commonly overlooked questions can be recognized. Finally, we shall discuss a few specific methods of analyses.

STATEMENT OF THE PROBLEM AND EXAMINATION OF DEFINITIONS

The most difficult problem we are faced with is due to a combination of incorrect preconceptions and a tendency to substitute overly simplified models for earth materials. The conventional operational mode is that of classifying water in earth materials as being either "free" or "bound" water. Presumably the word "bound" refers to some kind of binding between water molecules and the molecules (and/or ions) of the various constituents of earth materials.

---

*Work performed under the auspices of the U. S. Atomic Energy Commission.

The type of binding is usually unspecified. The term "free" water as it is commonly used seems to refer to a condensed phase of pure water.

The usual reaction to a cursory consideration of the definitions involved is to split the analysis into two parts: (a) "total" water and (b) "free" water. The definitions are now readjusted so that "free" water is condensed phase pure water (still neglecting the subtle questions).

"Total" water is then given one of a number of definitions: (1) all the water that can be driven off by heating to a given predetermined temperature (for example, with this definition, there are difficulties associated with water-producing reactions, etc.); (2) the amount obtained by counting all the hydrogen in the sample by some scheme like proton resonance, and dividing by 2 (some problem with hydrocarbons, silicates, and nonfreely rotating hydrogen); or (3) the amount obtained by any other counting technique that could give either an H count or an OH count in the sample (subject to various corrections).

Of course, the main purpose in such a separation is that by subtracting the "free" amount from the "total" amount of water, one gets back to arriving at an amount for "bound" water with an operational definition while essentially sweeping lots of problems under the carpet. Admittedly, that would be an operational definition, and it may even be valid for some specific requirement; but when dealing with earth materials, the probability of this technique being valid can be quite low.

The tendency of classifying the water as "free" or "bound" arises from the point of view of looking at the various phenomena by using pure compounds as models. Thus, we generally drive off water at ~110°C to dry samples. This procedure was assumed to drive off "free" water while "bound" water would be unaffected. Then, by heating to much higher temperatures, more water could be driven off from many compounds, such as hydrates. For example, copper sulphate can only be completely dehydrated by heating to ~1000°C. With a little reflection, one can show that such a classification is no more valid for pure substances than for mixtures such as occur in earth materials. For example, $NiSO_4 \cdot 7H_2O$ loses 1 water of hydration at ~37°C; the remaining 6 are stable to over 100°C before a step-by-step dehydration can occur.

A PSEUDOTHERMODYNAMIC APPROACH TO THE PROBLEM: THE ESTABLISHMENT OF A CLASSIFICATION SCALE

We wish to propose a more functional, and hopefully fruitful, classification for the way water is bound with other materials. The classification we propose has some thermodynamic significance and also has the advantage that we can apply some rather good models for real materials to obtain semiqualitative notions of where a given material will lie in the classification scale.

Suppose we consider the amount of energy required to overcome the interaction of the water with the rest of the material and have it end up in some standard state. Let us specify that the standard state shall be gaseous nonassociated water vapor at ambient temperatures. (By this we really mean steam behaving as an ideal gas; i.e., the partial derivative of the enthalpy with volume at constant temperature is zero.) We are concerned with earth materials which are all in a condensed state (solid, liquid, or both) and are all at ambient temperature and pressure. Then we are considering an energy which is similar (but not quite equal) to the heat of vaporization to remove the water associated with the material and bring it to the standard state mentioned above.* In the following discussions when we talk about the interaction energy of the water with the material, we really mean the amount of energy required to get the water in the standard state mentioned above.

The lowest value on such a classification scale is that for water interacting with itself. That is the case of agglomerates of water molecules in the liquid state, and the energy of interaction is about 5 kcal/mole. We shall show later that this is the lowest value on the scale. The upper end of the scale is physically equivalent to those energies which cause disproportionation of simple molecules in the region of ~100 kcal/mole. The scale is continuous. The great advantage of this proposed scale and classification is that it is independent of <u>how</u> the water is bound. Thus chemical bonding of any kind, chemisorption, physical adsorption, van der Waals bonding, hydrogen bonding, etc., are phenomena which can all be considered. We can at this point note that what is presently referred to as "free" water is water bound with interaction energies of ~5 to 20 kcal/mole. If one were to take this proposal for a scale and classification system seriously, then the term "free" should be used for interaction energies of ~5 kcal/mole. We believe that the scale itself should be the classification. So instead of saying "free" one should say "water bound with X kcal/mole." From such a scale <u>and</u> the understanding of various kinds of earth materials, it should be possible to develop functional operational analyses for water.

That the lowest energy of interaction for this scale is for the water-water interaction can be seen from the following argument. Suppose that there is, in the condensed state, an energy of interaction of water with some other substance that is less than the water-water interaction. The application of enough heat to break up the former interaction will lead to the formation of liquid-state water, and the only energy of interaction will be that of the water-water interaction. To make this particular argument clearer, let us give an invented example. Suppose there is a pure substance, "Y," which forms a series of hydrates. Furthermore, suppose that the water-splitting reaction for removal of the first water of hydration at pressure P occurs at temperatures well below ambient temperatures. The result at ambient temperatures is two phases: (1) the next lower hydrate and (2) pure water at pressure P (or a solution of "Y" in water). Therefore, the water-water interaction will be the lowest observed interaction. (In a strict thermodynamic sense, this statement is incorrect except for open systems. For closed systems some equilibrium will ensue. Thus, for instance, in a calorimetric determination (see below), it would be possible to observe interaction energies below the 5 kcal/mole.)

Let us discuss one aspect of the problem of what one might term "dispersed" water in earth materials. We shall get into this problem in some detail later, however, at this point we shall merely state some conclusions. Suppose we consider water dispersed in rock in a monomolecular (or at most a few molecular multiples) state. This means that the "pore" sizes or "hole" sizes we are considering are ~1.5 Å long. These holes are therefore much smaller than microcracks and really correspond to the size of crystal defects. For such a situation, the water is more strongly bound to the host material than it is to itself. This is so since polarizable material (host) surrounds the highly polarizable water molecules (guest) at much closer distances than that

---

*The observed heat of vaporization of water is ~10 kcal/mole. However, normal vaporization leads to associated water vapor as shown by P-V-T data (J. S. Rowlinson, Trans. Farad. Soc. <u>45</u>, 974 (1949). An average molecular weight of 32 g mole^{-1} for the vapor is <u>thus</u> quite reasonable, and rationalizes the use of the 5 kcal/mole in this discussion.

of the neighboring water molecules. This then results in a higher interaction energy between the water guest and the host earth material molecules.

We shall now discuss various materials with emphasis on earth materials in order to be able to apply such a scale. Let us first consider pure water and aqueous solutions which might be found in earth materials.

The water-water interaction in the condensed state can be considered from the viewpoint that the hydrogen bonds which bind the water molecules together are bona fide chemical bonds (that is, either electron exchange or charge transfer accounts for the bonding). Then, using these kinds of models along with observed spectroscopic properties, one can calculate an interaction energy of ~5 kcal/mole. This is the more classical viewpoint. Alternatively, one can view the interaction as that between polarizable bodies by means of electron correlation, or, in other words, van der Waals forces accounting for the intermolecular forces. When one uses the dielectric constant and average intermolecular distances in the van der Waals (London dispersion) relations, one again obtains ~5 kcal/mole for the hydrogen bond. This model, however, does not require that a bona fide chemical bond be formed. Either viewpoint leads to the same conclusion and it really is much more a matter of personal taste as to which one is used. Both are equally correct. We prefer the latter viewpoint for this discussion for two reasons. First, and most important, it is much easier to calculate the energetics involved for intermolecular forces with the London dispersion force relations (which are admittedly a bit crude) to reasonable accuracy (~10 percent) than to use the much more sophisticated chemical bond techniques to obtain answers to the same accuracy. Second, we shall be more concerned with intermolecular forces for those earth materials which are going to be most troublesome as far as water analyses are concerned.

Let us just touch on aqueous solutions. For electrolytic solutions, ions in solutions will have "atmospheres" of water dipoles associated with them. Thus some of the waters will have an interaction energy with the ions of either charge which is larger than the water-water interaction. The total interaction energy will depend principally on the charges of the ions, their sizes, and their concentration. For nonelectrolytes, the energy of interaction of the water associated with the solutes will be a function of solute size and concentration (going up with both variables). For most earth materials, the concentration of electrolytes and/or nonelectrolytes is usually low so that total water interaction energies with these materials will be small and somewhat near the low limit.

THE CASES OF INTEREST

We shall concentrate on what could probably be termed "troublesome" earth materials, rich in water and tending to be equilibrated under conditions of moderate temperature and pressure called weathering. In contrast, "fresh" igneous and metamorphic rocks contain relatively little water except in pores, cracks, and interstices. Here, the problem will be complicated only when the dimensions of the space occupied by the water becomes comparable to molecular dimensions. When the dimensions are quite large, the water-water interaction of ~5 kcal/mole will be predominant. We shall discuss the question of pores shortly. Water can be present in some of these earth materials. as strongly bound hydrates with energies of interaction of over 20 kcal/mole. In some of the metamorphic silicates and aluminates, hydroxyl groups can be found that are joined to the major structure with energies of up to 80 kcal/mole.

Salt deposits of various kinds could be somewhat complicated. In arid regions with deposits of materials containing hydroxides, carbonates, halides, and sulphate, hydrates could be obtained with a quite low interaction energy. One must be careful in selecting the analytical methods to use and the interpretation of the results. Large salt deposits of mainly NaCl are usually not troublesome, although hydrated salts can be present and the amount of water depends on the particular hydrate and its concentration in the salt deposit sample. Occluded water in salt deposits and dissolved water also can be pitfalls. Large pores or cracks of occluded water will be low on the classification scale. But, monomolecularly dispersed water is difficult to classify. (Presumably, the monomolecularly dispersed situation could arise where the salt deposits were supersaturated—in the solid state—with dissolved water.)

The really troublesome materials to analyze are the clays and zeolitic-type minerals. As is well known, there is a large number of synthetic and naturally occurring materials in these classes. Rather than using any of the classification schemes used by geologists, we shall use a scheme which comes from the study of inclusion compound chemistry.

The various types of inclusion compounds are classified according to their general crystal structure types. (This is not to be confused with structural varieties defined by either crystallographic point groups or space groups—both of which can have a large number of structure types.) To three of the four types of inclusion compounds there will correspond one or more earth materials of a clay or zeolitic variety. It is for this reason that we choose to classify the earth materials along the same scheme. Also, the behavior of synthetic clays and zeolites are such that it is clear that the chemical bonding properties of these materials are the same as those of the general class of inclusion compounds.

We will not go into great detail on inclusion compound chemistry. Several books and review articles are available for those who are interested in further pursuing this topic.[1-6] However, we will quickly cover some general aspects of the field so that analogies can be made. The manner in which crude calculations for the interaction can be made for some particular system is indicated.

Inclusion compounds are compounds that form between two or more different kinds of molecules in which the stabilization energy is not due to bona fide chemical bonding but is due mainly to van der Waals forces (or/and hydrogen bonds). By bona fide chemical bonding we mean, as stated earlier, that either electron transfer or sharing of electrons or both are involved. Also, as mentioned earlier, we choose to consider hydrogen bonding as due to van der Waals forces. The two kinds of molecular species involved are called the host and guest molecules. The four general types of inclusion compounds are illustrated in Figs. 1 through 4. Figure 5 is an illustration of a form of inclusion compound which is sometimes considered as a separate type, but which is really only an extension of the system shown in Fig. 1.

The energy stabilization for the inclusion compound can be calculated easily (not necessarily precisely) by applying the London dispersion relations to all the atoms in the system. One does this first for the complex and then for the individual host and guest molecules; the difference represents the stabilization energy. The relation is

$$E_{1,2} = k \frac{\alpha_1 \alpha_2}{r_{1,2}^6},$$

where $r_{1,2}$ is the distance between the two atomic units in question and α_1 and α_2 are the polarizabilities of the respective atomic units. One sums all pairs of atomic units for both parts of the calculation. Since bona fide chemical bonding is unaffected by the complex formation, those energetics need not be calculated. (They would be the same for the complex and the sum of the host and guest molecular terms. Thus, the chemical bonding energy is simply a constant for this case and one which need not concern us.)

Another way to do the calculation (although a little less accurate than what has been outlined above) is to calculate the stabilization energy directly. The relation has the same form, that is

$$E_{G,H} = k' \frac{\alpha_G \alpha_H}{r_{G,H}^6} .$$

However, a little care is necessary. α_G and α_H are the molecular polarizability of the guest and host molecules, respectively, $r_{G,H}$ is a mean distance. The terms over all interactions must be summed.

The main point we are trying to get across at this time is to show the origin of these stabilization energies (that they are not chemical bonds in the usual meaning) and to show the form of the interaction. Physical adsorption is due to the same type of electronic correlation phenomenon. Notice that when we make such a calculation, if we are careful about summing all pair interactions for the complex and its decomposition products, the products can be both gas-phase molecules and solids, or all gas-phase molecules. Thus, such a calculation can be made with water as the guest molecule; and, if done properly, the product of the decomposition can be gas-phase water and solid host material. Thus, we can calculate directly the interaction energy needed for the classification scale. When the energy is calculated both for the complex and the proper form of the complex decomposition products, the stabilization energy and the water-host interaction energy (which is what we use in our classification scale) are the same. When one does these calculations for the four types of inclusion compounds, the energies can range from zero to ~80 kcal/mole.

Using the same formulation that London used for arriving at the form of the interaction between molecules, attractive forces can be calculated for other interactions such as that of macromolecule and flat infinite wall, etc. These forces are completely general and are applicable to a huge number of situations. Thus, one can now see that as pore or crack sizes get down to molecular dimensions, interaction energies between water and host material can get to be large compared to the water-water interaction.

Let us return to the four types of inclusion compounds. In Fig. 1 is shown a generalized schematic of the complexes known as clathrates. Classically the clathrates consist of water molecules as host with normally gaseous molecules as guests. Probably there are no analogies of this type of inclusion compound with earth materials except for possibly the occurrence of methane hydrates in gas wells. The gas hydrate clathrates normally decompose at low pressures and moderate temperatures.

(There are two families of minerals which schematically correspond to Fig. 1. The scapolites and the noseansodalites consist of a cage-like aluminosilicate framework with a net negative charge. The guests are cations which can be associated with variable compositions of salts and/or water, CO_2, etc. The cations provide charge neutrality. The openings in the cages are rather large, i.e., of the order of 5 to 10 Å in diameter.)

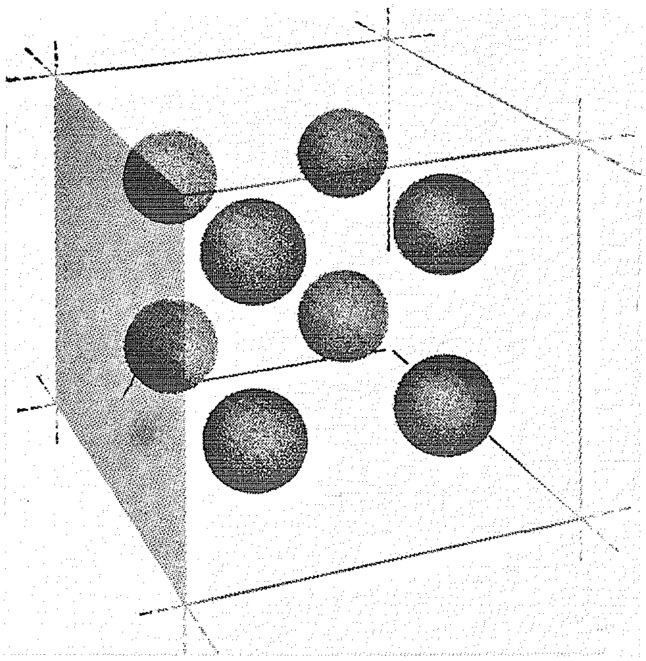

Fig. 1. Clathrates are formed when guest molecules fit into separate spherical spaces within the host material.

Figure 2 is a generalized schematic of channel-type inclusion compounds. Here the guest molecules are in long channels running through the structure. The cancrinites and fibrous clays are examples of earth materials which have structures of this type. Examples for which structural data exist

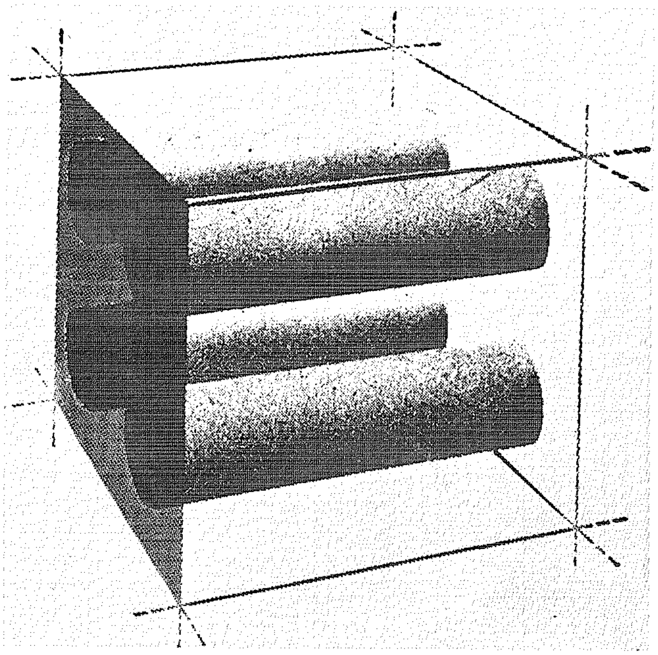

Fig. 2. Channel inclusion compounds are formed when the host material provides tubular cavities within which the guest material resides.

are cancrinite and davynite for the cancrite mineral type and attapulgite and sepiolite for the fibrous clays. In the latter two, water is the main guest molecule.

Figure 3 is a generalized schematic of the sandwich inclusion compounds. Here layers of guest and host materials alternate. An example of these kinds of complexes are the graphite intercolation compounds. Such things as bromine form stable complexes with graphite with the bromine residing in layers between the hexagonal carbon structure. There are many natural earth materials which fall into this type. For a good number of these, water is the guest. The swelling of clays with water is due to the stability of of the sandwich inclusion complex. The family of the most abundant micaceous silicates which are layer structures are muscovites, biotites, the illites, and talc. Nonsilicate micas which are layer structure are autunite, torbernite, zeunerite, trogerite, and carnotite.

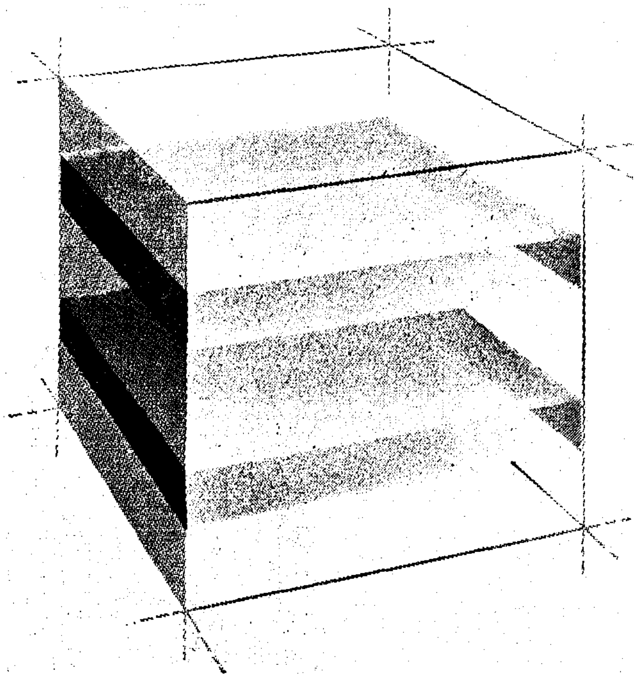

Fig. 3. Sandwich inclusion compounds consist of alternating layers of host and guest material.

One can understand, at least qualitatively, some of the physical properties of layer structure clays with water guests. For instance, besides the swelling (and also shrinking) behavior, the creep and sliding behavior of these materials are now obvious manifestations of a rather weakly bound structure. (Water molecules are the bonding links between host layers and essentially are the only slide-restraining links.) The seismic response of such materials, that of essentially liquifying under earthquake conditions, can be understood as a breaking up of the structure because a relatively small amount of energy is needed to overcome the stabilization energy. However, the range of stabilization energies can be quite large from numbers almost as low as the water-water interaction to ~80 kcal/mole for very stable structures. Also, for some of these individual layer structure clays, the water will have a range of binding energies.

With some of the layer structure clays, the water-host complex does not form because of the extra stabilization energy. Instead, the dehydrated clay structure is already a layer structure. The water can then intercolate and bind (with a range of energies) to the layer framework. The net result is the same. The water is held by van der Waals forces to the framework.

Figure 4 is a generalized schematic of zeolite inclusion compounds. This type of compound does not form from a host of some other crystal structure because of added stability of the guest molecules. Rather, the guest-free structure consists of interconnecting channels. The figure is misleading in the sense that the channels and interconnections are not really smooth. In some of the zeolites the channels are not straight but may have a number of jogs (which are periodic in the structure). Also, the interconnection space is usually considerably larger in diameter than the channel diameter. All the natural zeolites are three-dimensional networks. However, there can be large differences in the density of channels in different directions so that a nearly layer-like or nearly fibrous-like structure can be obtained.

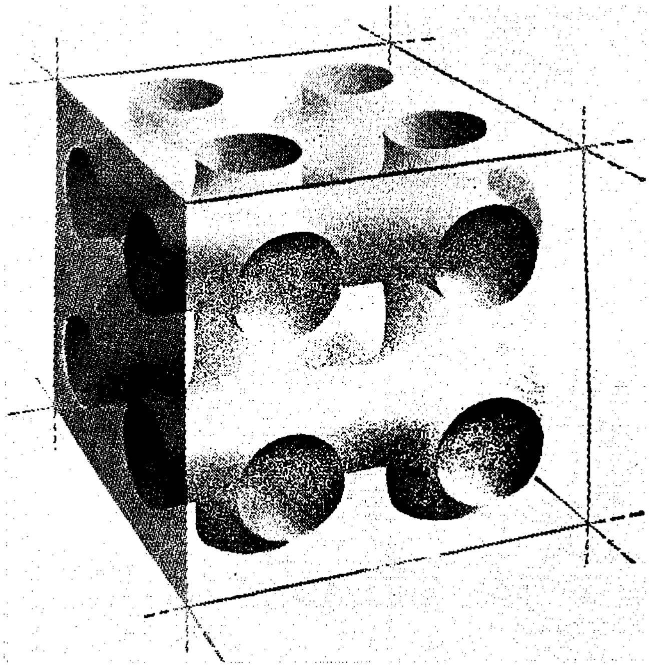

Fig. 4. Zeolites consist of interconnecting channels of host material into which guest material can be placed.

When water enters these channels, there will be a range of tightness of binding to the framework since there is a distribution of effective spaces within the channels and in the interconnecting spaces.

Thus, part of the water can be easily removed, but the removal of all of the water may be quite difficult.

The cusp-shaped guest cavities as shown in Fig. 5 have their counterparts in some silicate glasses in which the tetrahedral bond networks around the silicon ion are degraded leaving concave holes throughout the structure.

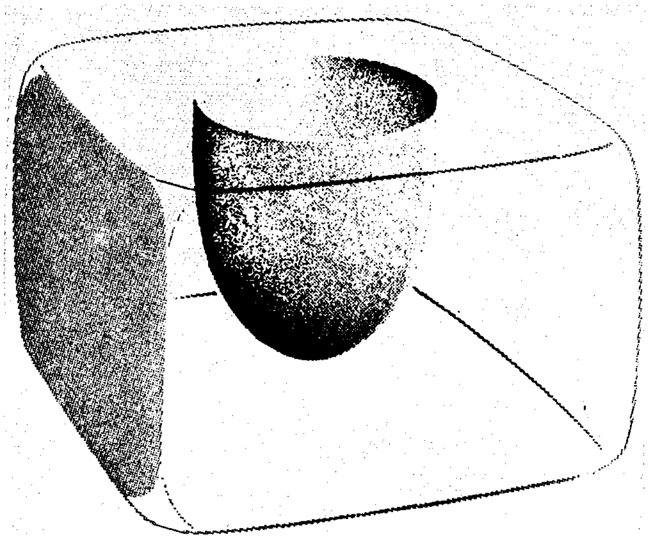

Fig. 5. Cusped inclusion compounds are formed when the host has a large concave space into which the guest can reside.

Some of these glasses also have a large concentration of hydroxyl ions. Thus water can be very tightly bound by both the silica cage and the excess hydroxyl ions.

METHODS OF ANALYSES

It now should be clear why there are no all-encompassing analytical methods available. We mentioned earlier that operationally relevant analytical techniques would have to be applied in order that the information derived would be of some value.

Such simple schemes as heating at a prescribed temperature and time, with or without evacuation, etc., could be operationally valuable techniques.

There are three techniques which may have a somewhat extensive use for determining water that is bound by just 5 to 8 kcal/mole.

The first method is by measuring the heat capacity of a large rock sample over a temperature region between -40 to +40°C. The heat of fusion of ice is 80 cal/g, so that a bump in the heat capacity curve near 0°C can give a quantitative measure of the water in such a state. This method has the advantage that it is an absolute method and is nondestructive. Its disadvantage is that data aquisition is slow and moderately difficult. (We should mention that while differential thermal analysis (DTA), thermogravimetric analysis (TGA), or differential scanning calorimetry (DSC) are all capable of giving relative quantitative analyses, they all suffer from the fact that very small amounts of sample material are involved. The problem of a representative sample for such techniques becomes insoluble. The alternative of making measurements on enough samples to obtain representative results then becomes a horrendous one.)

The other absolute method (that we know of) is to measure the isothermal compressibility of the rock specimen.[7] Water of low interaction energy has two phase transitions: one at 10 kbars and the other at 23.5 kbars. A measurement of the volume change (at the discontinuities in the PV curve) at these pressures provides two independent values for the amount of water. Thus this method has the advantage that, since there are two phase transitions, the value can be confirmed. The disadvantages are that the method is sample destructive. (The probability that there are other materials present besides water which have phase transitions at those two pressures is negligibly small.)

The third method is based on the transmission of microwaves through a sample. Water attenuates the microwave signal, although in this method spectroscopic techniques are not used. The attenuation is then a measure of the water in the sample. Surprisingly few things interfere with the measurement. However, the measurement does depend on the water molecules being in a state of free rotation. This means that some water which is more tightly bound than 5 kcal/mole but which <u>is</u> <u>free</u> to rotate along one or two of its principal axes can attenuate the signal. Thus, this measurement will show some of the water held by van der Waals forces with some moderately strong binding. This method has the disadvantage that it requires calibration, but it has the advantages of being very rapid and simple in application. It is probably an excellent tool for research on the fibrous clays, the layer clays, and the zeolites. With careful operational restrictions, it might possibly be an excellent analytical technique.

The calorimetric and compressibility method should essentially yield equivalent results on the same samples.

There are numerous other analytical techniques which can be considered for an operationally relevant analysis. What is probably most necessary at this time is some research on the more troublesome earth materials. Particularly, we suggest research on pure synthetic clays and zeolites for use as anology models of the naturally occurring minerals. There already exists rather extensive literature on some of the physical properties of the synthetic zeolites. Some of this literature is relevant to the design of useful analytical techniques. Such experiments as the addition and removal of specific amounts of water to model materials and the testing of various analytical techniques would undoubtedly be useful. Once a good understanding of these pure materials is obtained, and after an actual petrographic analysis to determine the types and relative amounts of the various troublesome materials present in the specimens, it might be possible to specify the criteria for operationally relevant analyses in an intelligent and logical fashion.

REFERENCES

1. B. Chu, Molecular Forces (Interscience, New York, 1967).
2. J. O. Hirschfelder, C. F. Curtiss, and R. B. Bird, Molecular Theory of Gases and Liquids (J. Wiley and Sons, New York, 1954). (This book contains tables of polarizabilities useful for performing the calculations indicated in the text.)
3. J. A. A. Ketelaar, Chemical Constitution (Elsevier Publishing Co., Amsterdam, 1953).
4. L. Mandelcorn, Ed., Non-Stiochiometric Compounds (Academic Press, New York, 1964).
5. J. F. Brown, Jr., Sci. Am. 207, 82 (1962).
6. D. Swern, "Inclusion Compounds," in Encyclopedia of Chemical Technology, First Supplement Volume, R. E. Kirk and D. F. Othmer, Eds. (The Interscience Encyclopedia, Inc., N. Y., 1957), pp. 429-448.
7. D. R. Stephens, private communication.

XA04N0766

UNDERGROUND NUCLEAR EXPLOSION EFFECTS IN GRANITE ROCK FRACTURING

S. DERLICH
COMMISSARIAT A L'ENERGIE ATOMIQUE (FRANCE)
Centre d'Etude de BRUYERES-LE-CHATEL

ABSTRACT

On the Saharian nuclear test site in Hoggar granite, mechanical properties of the altered zones were studied by in situ and laboratory measurements.

In situ methods of study are drillings, television, geophysical and permeability measurements.

Fracturing is one of the most important nuclear explosion effects.

Several altered zones were identified. There are : crushed zone, fractured zone and stressed zone. Collapse of crushed and fractured zone formed the chimney.

The extend of each zone can be expressed in terms of yield and of characteristic parameters.

Such results are of main interest for industrial uses of underground nuclear explosives in hard rock.

INTRODUCTION

The results of French underground nuclear tests are presented in this address. Their accuracy depends on utilised measuring methods and on chosen boundary definitions.

In order to show the value of results and to give data allowing the establishment of comparisons with underground nuclear tests in similar or different media, special interest will be given on these measuring methods and boundary definitions.

The test site was a granitic batholith in the Sahara desert near the Hoggar mountains. It has an elliptic shape 8 km along the main axis and 5. 6 km along the small one. The summit is 2 000 m. high, that is 1 000 m. above the level of Antecambrian table-land.

So, it was possible to get an overburden thickness of 1 000 m. under the highest point.

Geological and mechanical characteristics are given and will allow comparisons with other media.

This granite was studied by Lelubre (10), it is an alcaline granite with grains of regular sizes.

The mineralogical composition is shown below (in percent by weight).

Quartz	: 35
Microcline	: 37
Plagioclase	: 25
Biotite	: 2. 1
Muscovite	: 0. 6

The chemical analysis is (in percent by weight).

SiO_2	75, 8	Na_2O	3. 8
Al_2O_3	12. 5	K_2O	4. 8
Fe_2O_3	1. 3	TiO_2	0. 1
CaO	0. 6	H_2O	0. 3

Grains range from 2 to 4 millimeters large. Some feldspar crystals reach 10 millimeters (photo 1). No traces of crushing are observed but quartz commonly present ondulatory extinction and microfolds may be observed in feldspar and biotite. Inclusions of hematite exist in feldspar and quartz. Veinlets of fluorite, calcite and quartz, several millimeters thick, are sometimes visible on the drift walls (2).

Microfracture study by autoradiography method (3) (photo 2) shows numerous permeable fractures of different kinds : along the cleavage of feldspars, as separations of two contiguous quartz crystals along their common boundary. It is impossible to identify preferred orientations in microfractures.

In the rock mass, several sets of fractures are sorted into tectonic faults, or in fractures due to growth and adjustement of the granitic batholith (2). These sets cut the rock mass into strata and cubic shaped blocks, whose dimensions vary from 50 cm to several meters. These fractures are almost filled with clay, calcite or fluorite. Most of them are waterproof but some have permeability, and slight water falls may be seen in drifts.

Mechanical properties of rock were studied by in-situ seismic measurements and laboratory tests. The results are reported in the following table:

density	2. 63
Young modulus E	710, 000 to 930, 000 bars
Poisson's ratio (calculated from	

laboratory determined seismic velocities)	0. 30 to 0. 38
Uniaxial tensile strength	40 to 50 bars
Uniaxial compressive strength	2 000 b

Seismic waves velocities

compressionnal wave	: in situ measurement	5 850 m/s
	laboratory measurement	5 500 m/s
shear wave	: in situ measurement	3 230 m/s
	laboratory measurement	2 400 m/s

Porosity : 0. 3 %
Permeability : zero
Rock temperature : 30°
MOHR circles envelope (figure 1)(5)

METHODS OF STUDY

Methods for studying induced shock effects are similar to exploratory means utilized in exploratory wells or mining research : coring of interesting zones, well logging, television scanning and permeability measurements.

Two main elements had to be considered : radioactivity and high temperature in cavities. Radioactivity is concentrated in a puddle at the bottom of the cavity. It can be found in gas coming from bore holes. A high residual temperature was expected due to very low water content of the granitic rock. Several hundred degrees centigrade may be found near the shot point.

Exploratory holes were drilled from reentry drifts located at the level of zero point.

Rotary method could not be used from drillings more than 150 meters long. Turbodrilling (Dyna drill) with coring was used and permitted to reach 300 meters from the rotating head with an accuracy of 2 or 3 meters.

Two data were expected from the core examination :properties of fractured rocks and extent of damaged zones.

A shock wave has different effects depending on its amplitude. Temperature effect acts in cavity and on the walls which are melted and vaporized. After the explosion, rubble and a puddle fill up the bottom of the cavity. Farther away, mechanical effects only are involved in rock mass. Near the cavity, granite is crushed, but far away from it, material is unbroken.

Thermal and mineralogical changes are reported in another paper ; so, only mechanical properties will be studied in this report.

The geological examination of cores will permit study of fractures and then, determination of phenomenology.

Differentiation between pre and post-shot fractures : preshot fractures are always filled with mineral matter sometimes very thin. Explosion produced fractures have either fresh-looking surfaces or crushed sides. Fracture dipping is very important because it gives possibility to identify sets of parallel fractures (tectonic preshot diaclases or fractures tangential to the shock wave) or planes going through zero point (radial fractures). Core fracture examination cannot give complete spatial orientation of fractures. During the extraction phase, the core does not remain in initial position but turns with the inner core-barel around the drill hole axis.
Planes of such orientation are tangent to a core which is defined by its summit angle (figure 2). It is sometimes possible to say if fractures can or cannot be "radial". With regard to drilling length (100 to 150 m. for rotary drillings, 300 m. for turbodrillings), no attempt to get oriented core was made.

Fracture nature gives the possibility to distinguish tensile fractures from shear fractures.

Bearing of minerals, Hoggar test site granite is composed of quartz, feldspar and biotite. Crystals have quite different characteristics and their bearing may give data on developped stresses.

Preshot fracture opening

At the boundary of the fractured zone, effective stress is less than tensile strength of rock, but the remaining shock wave can open preshot fractures or diaclases. Core scanning cannot show if preshot fracture opening is due to explosion or to drilling.

Zone extents

Examination of the whole of the samples gives a possibility of defining characteristic zones. They are almost spherical around the shot point or cylindrical around vertical line through the shot point.

Microfracturing has been studied on thin sections with polarizing microscope.

So, core examination cannot give complete data on fracturing.

Orientation or direction and dipping of fracture planes are unknown.
The interior of the drillings has been studied with a television set. Axial lenses give a view along the bore-hole and a rotating mirror allows wall study. (photo 3).

Knowledge of fracture permeability around nuclear explosion is important for safe or engineering use.

FIG 1

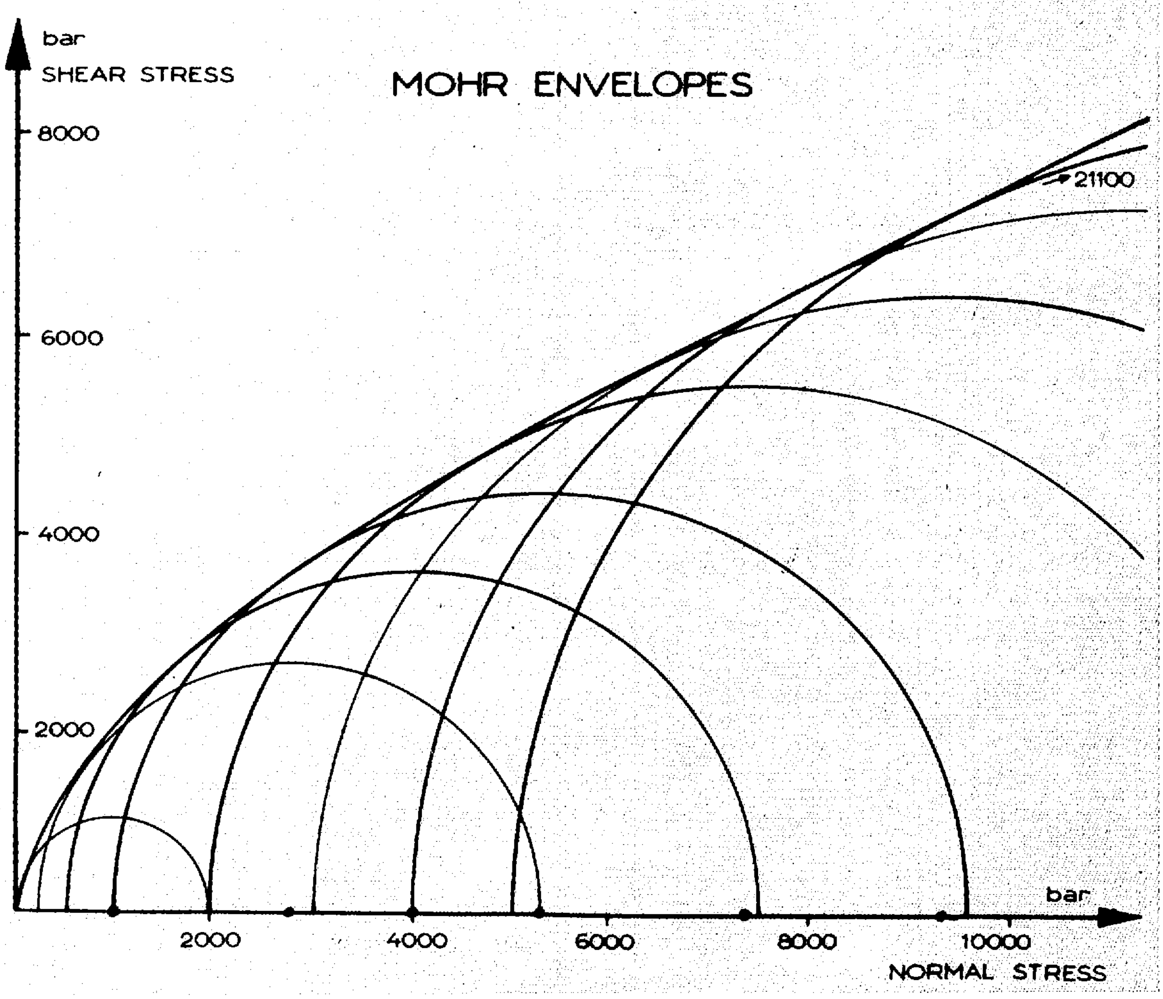

FIG. 2

THE CONE IS TANGENT TO THE FRACTURE

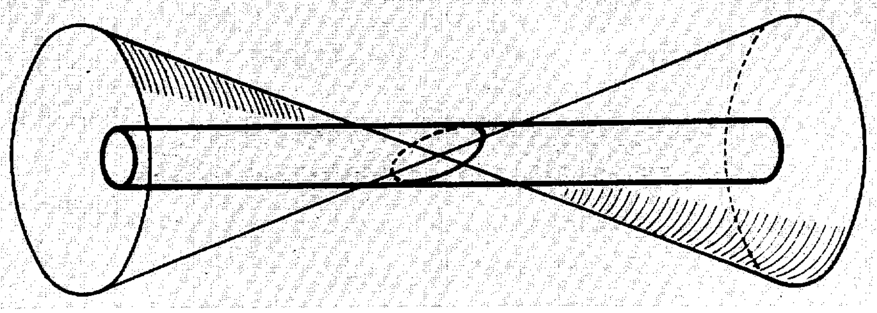

Measurements on short intervalls (5 to 10 m.) have been made in horizontal or angle holes. Water and air injection tests have been done. The main difficulties are to place inflatable packers in holes presenting sharp angles on the sides.

Study of seismic wave velocities in rock mass around the shot point, showed zones with velocities lower than preshot velocities.

A small yield chemical explosive has been fired into rock mass far from the shot point and a set of geophones were placed at the bottom of short vertical drillings on the other side of the shot point (8). Every gage gave the time of arrival which allowed calculation of velocity variations.

ALTERED ZONES

Synthesis of all results allows determination of zones with precise characteristics.

Figure 3 shows different zones whose average radii are :
$R_c = 7.3\ W^{1/3}$ R_c : cavity radius in meters
$R_b = 10\ W^{1/3}$ R_b : crushed zone radius in meters
$R_f = 26\ W^{1/3}$ R_f : fractured zone radius in meters
$R_r = 35\ W^{1/3}$ R_r : stressed zone radius in meters
W : yield in kilotons.

Crushed zone

It is encountered from 7.3 to 10 $W^{1/3}$ (scaled distance in meters when W in kilotons).

Before chimney collapse, the crushed zone was spherical around the shot point. Core samples are chalky, coherent but friable. To the naked eye, it is possible to identify quartz and feldspars. Biotites look like black spots without glitter, sometimes laminated. Under microscope, alteration seems to be less important. Granite shows its preshot features, but it is highly damaged. Close spaced (1/100 of mm) intracrystalline microfractures break grains into regular or irregular sets. Birefringence has a notable reduction and shocked quartz are darker than preshot ones when examined in polarized light. Quartz crystals are broken in square shaped polygons (photo 4) or they present branching segments like river figures in metals. Planar surface sets and lamellas developp frequently in quartz. They indicate shear stresses acting on crystallographic planes (9) (photo 5). Glass veinlets have been injected in microcracks in quartz. Kink bands develop in many biotite grains and crystals are often crumpled by other crystals. Feldspars are bended and twins are often offset in a characteristic manner (photo 6).

Mechanical properties are given below :
compressionnal wave velocity (at atmospheric pressure) - 1060 to 1400 m/s average 1350 m/s.

Porosity (laboratory measurement) : 14.4 %.

Fractured zone

It extends from 10 to 26 $W^{1/3}$. Boundary between crushed and fractured zone is not precise. Its outer limit is identified to the first postshot fractures. So, opening of diaclases is possible farther on, but the boundary is not known.

Sets of angle fractures are often observed on cores. They are preshot fractures belonging to diaclase sets mapped in drifts.

Radial and tangential fractures seem to be rare. By location, angle discing fractures cut cores. They look like shear fractures produced from tridirectional laboratory tests. May be they are shear induced fractures. Great change in degree of fracturing is marked from one point to another point ; its depends mainly on preshot fractures.

From the crushed zone boundary granite is broken more and more coarsely. There are coarse sands, then gravels, then pieces of core from 5 cm to 15 cm long.

Stressed zone

Outside the fractured zone recovered cores present typical fractures. They break into parallel discs with irregular thickness, but always normal to core axis (photo 7). This phenomenon is called core discing. It is observed in salt mines (10) and in deep mines in quarzites (11), and depends on stresses in rock around holes. It is induced by drillings, and sidewalls of boreholes present some alterations (photo 8) in almond shape.

Orientation of this "almond" figure depends on the maximum principal stress acting on the borehole.

In boreholes of the Hoggar test site, this orientation is not constant, so it may be thought that stresses have not one precise direction, but are depending on preshot fractures. This hypothesis may be confirmed by typical fracture observed on a core sample where discs were interrupted by an angle fracture showing that stresses change from one side to the other side of the fracture (figure 4).

Discs extend to a distance of 35 $W^{1/3}$, for borehole diameters from 80 to 90 cm.

Chimney

It is formed upon collapse of the cavity when the pressure of explosion produced gas is low enough. This pressure decreases quickly and the crushed zone is not able to support itself (figure 5).

Every cavity of the Hoggar test site collapsed and formed a chimney (12).

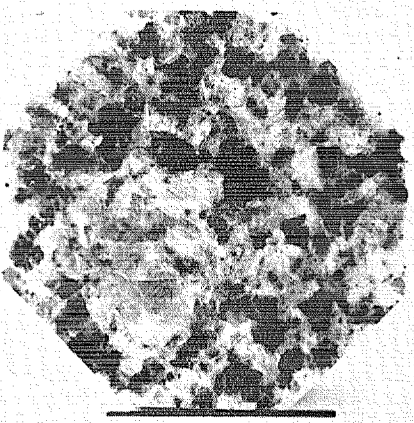

PHOTO 1

14 mm

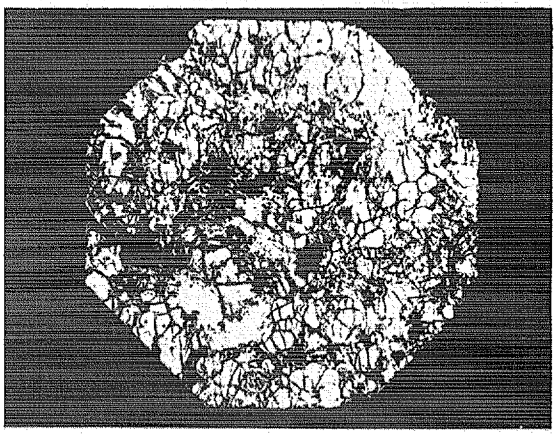

PHOTO 2

14 mm

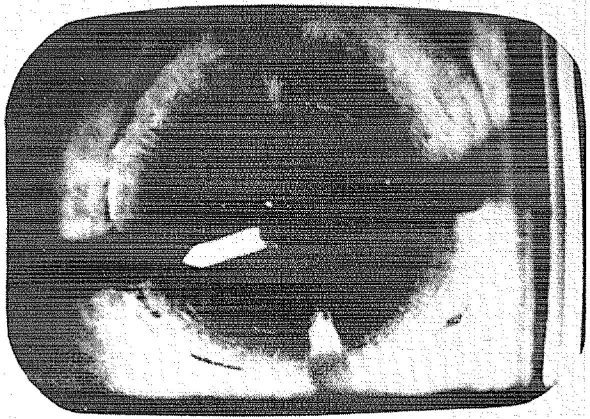

PHOTO 3

12 cm

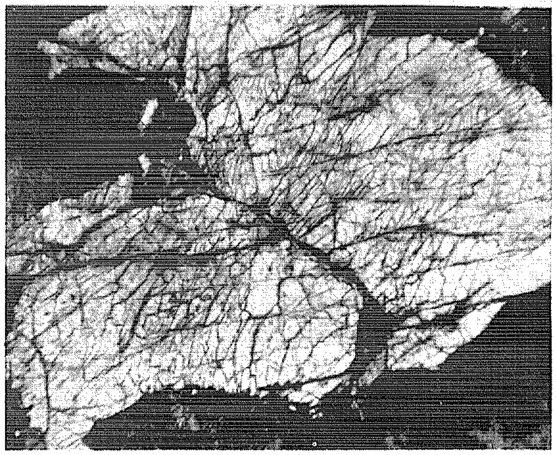

PHOTO 4

1mm

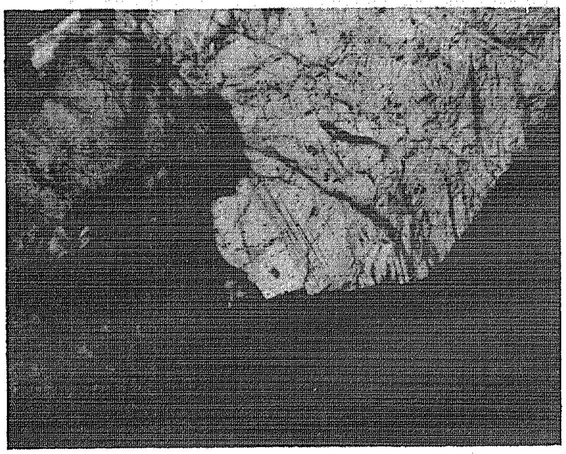

PHOTO 5

0.5 mm

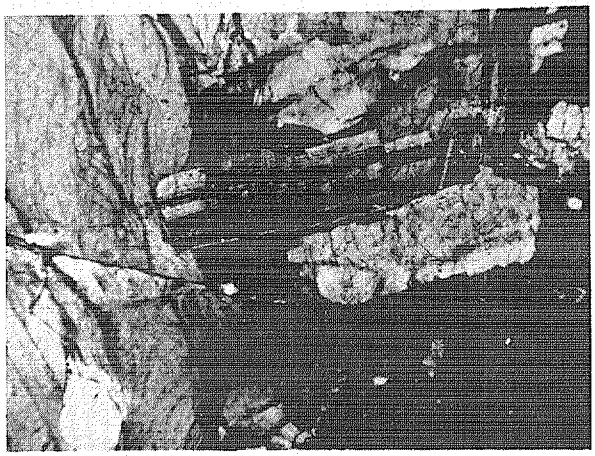

PHOTO 6

1mm

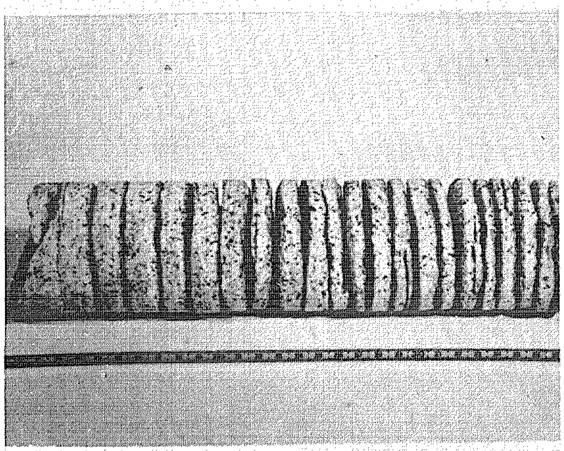

PHOTO 7

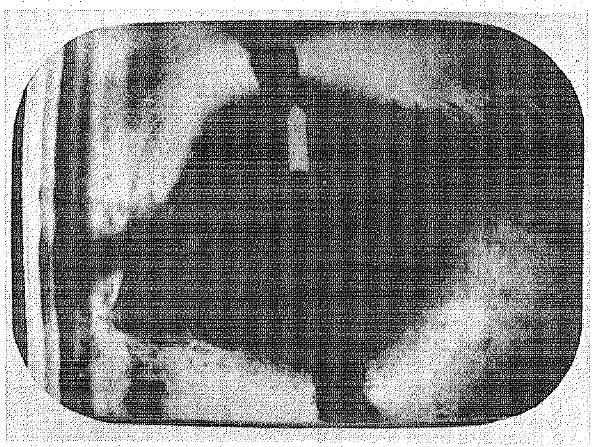

PHOTO 8

12 cm

FIGURE 3 VERTICAL CROSS SECTION THROUGH A CHIMNEY

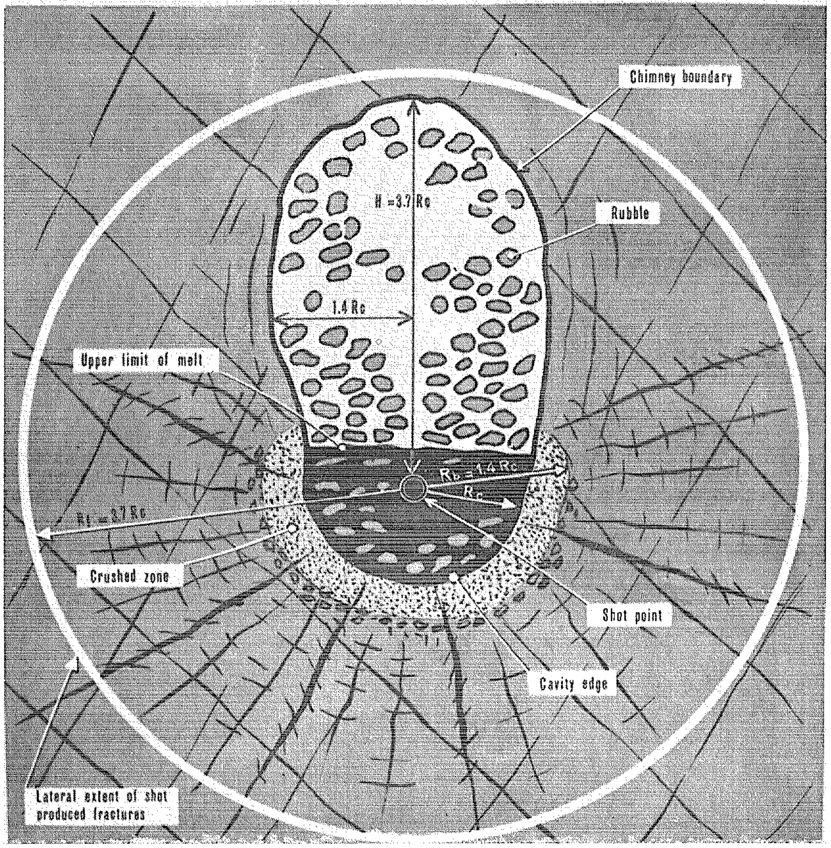

FIG. 4

ANGLE FRACTURE INTERRUPTING SEVERAL DISKS

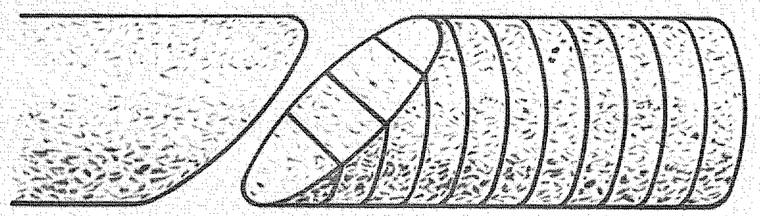

FIGURE 5

Cavity vault before the chimney formation

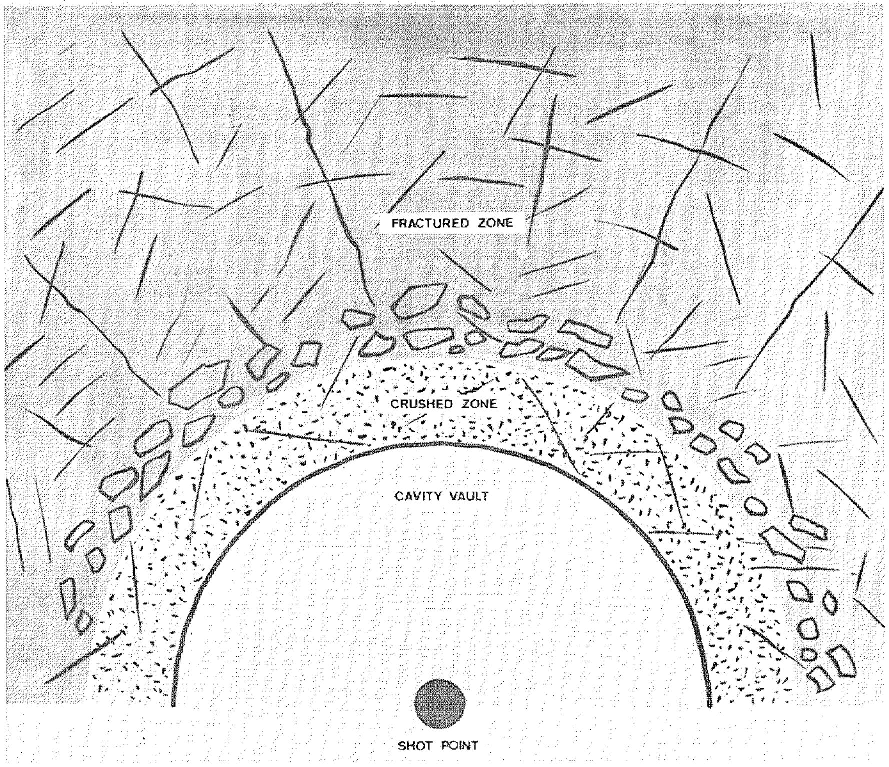

FIGURE 6

Exploratory drillings

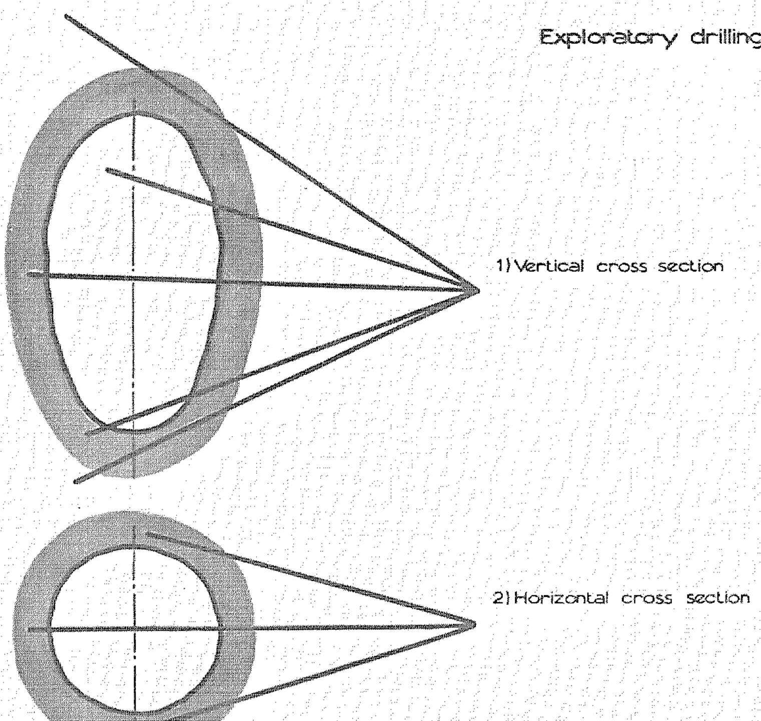

FIGURE 7

Permeability data

ZONE		CRUSHED	FRACTURED	STRESSED	UNFRACTURED	ABOVE THE CHIMNEY
Distance to shot point (meter)		10	26	35		
Permeability (milli darcy)	horizontal drill holes	2	45 to 90	30 to 40	20	
	Inclined drill holes		590	50	40	140

FIGURE 8

Seismic velocities

ZONE		CRUSHED	FRACTURED		STRESSED		UNFRACTURED	ORIGINAL VELOCITY
Distance to shot point		10	21	26	30	35	71	
Compressional wave velocity	laboratory measurement	1350	3500	4000	4240			
	in-situ measurement					5300	5600	5850

Chimneys were explored at different levels by means of angle holes (figure 6) which crossed rubble from side to side or which failed by collapse of the side-walls.

Rubble range between 4 and 10 cm.

Size of chimney is 3. 6 cavity radius height above the shot point and 1. 4 cavity radius width at level 2 cavity radius above the shot point.

Chimney existence introduces variations in rock mass :
opening of extension fractures in the surrounding rock, stress increases in the lateral walls. Permeability is also influenced by the chimney.

After displaying main geological data, mechanical and engineering results may be given.

Permeability.

For crushed zone samples (5) air permeability ranges from 6. 5 to 9. 5 md in-situ measurements (7) are given in this table (figure 7).

Seismic waves velocities (figure 8). (13)

They were measured both in-situ (8) and in the laboratory on samples.

Final results depend on media properties but also on experimental methods such as display of gages in boreholes or at the surface. Care must be taken when using them for predictions and correlations. (14)

CONCLUSION

Studies effected in boreholes drilled in altered zones around an underground nuclear explosion allowed us to get good knowledge on fracturing effects in Hoggar test site granite.

Seismic experiment results gave data on velocity variations and on porosities.

Mapping of altered zones is possible and main physical and geological data are known.

Extension of these zones is represented by an experimental law depending on the yield of the device and on characteristics of the medium.

BIBLIOGRAPHY

(1) - LELUBRE M. Recherches sur la géologie de l'Ahaggar. Bul. Ser. carte Géo. Algérie 2ème série n° 22 Alger 1952.

(2) - SANSELME H. Rapport C. E. A. (Unpublished). Le Taourirt Tan Afella et sa région. C. R. A. S. Vol. 256 - page 3160 (1963).

(3) - LEVEQUE M. et VIGNEAUX - L'autoradiographie dans l'étude de l'altération des roches. International Atomic Energy Agency - VIENNE 1967.

(4) - DUCLAUX F. (unpublished) (1962)

(5) - HABIB P. - Etude de deux granites - contrat Ecole Polytechnique.

(6) - DERLICH S., DUCLAUX F., SARCIA J.A - Etude de la cavité (1962) (unpublished).

(7) - FAURE J. - Rapport C.E.A. - Explosions nucléaires souterraines, effets sur la roche d'un massif de granite, transformations d'ordre mécanique - décembre 1968 (unpublished).

(8) - DUCLAUX F. Rapport C.E.A. - Etude seismique des zones fracturées (unpublished).

(9) - DERLICH S. - Métamorphisme de choc dans les cristaux de quartz d'un granite soumis à une explosion nucléaire souterraine.
C.R.A.S. t. 267 - pages 681-683 (1968) série D.

(10) - GIMM W.A.R., PFORR H. - Breaking behaviour of salt rock under rockburts and gas outburts. Fourth Int. Conf. on Strata Control and Rock Mechanics - New-York City. May 4-8, 1964.

(11) - LEEMAN E.R. - Nat. Mech. Eng. Res. Inst. Rock Mech. Special report : n° 29 Measurements of stress and ground movement in 35 E 12 E Stope Cinderella Section E.P.R.M. - Pretoria, March 1959.
-n° 32 Stress measurements in 64 E Stope, Driefenstein Section.
-E.A.P.M. - Pretoria C.S.I.R. Report CN301 november 1959.

(12) - DUCLAUX F. and all - Liaison entre le rayon et la durée d'existence des cavités créées par les tirs nucléaires souterrains.
C.R.A.S. tome 264 pages 496-497 (1967) série B.

(13) - FERRIEUX H - Ondes seismiques de compression liées aux explosions nucléaires souterraines (1967) (unpublished).

(14) - ALBARET A., DUCLAUX F. - Contenu spectral des mouvements seismiques dus aux explosions nucléaires souterraines - C.E.A.-R-3 767.

XA04N0767

ESTIMATING THE SIZE OF THE CAVITY AND SURROUNDING FAILED REGION FOR UNDERGROUND NUCLEAR EXPLOSIONS FROM SCALING RULES

by

Dr. Leo A. Rogers
El Paso Natural Gas Company

ABSTRACT

The fundamental physical principles involved in the formation of an underground cavity by a nuclear explosion and breakage of the rock surrounding the cavity are examined from the point of view of making preliminary estimates of their sizes where there is a limited understanding of the rock characteristics. Scaling equations for cavity formation based on adiabatic expansion are reviewed and further developed to include the strength of the material surrounding the shot point as well as the overburden above the shot point.

The region of rock breakage or permanent distortion surrounding the explosion generated cavity is estimated using both the Von Mises and Coulomb-Mohr failure criteria. It is found that the ratio of the rock failure radius to the cavity radius for these two criteria becomes independent of yield and dependent only on the failure mechanics of the rock. The analytical solutions developed for the Coulomb-Mohr and Von Mises criteria are presented in graphical form.

Introduction

Two potentially useful engineering aspects of underground nuclear explosions are (1) the creation of a large underground opening, and (2) the breakage of a large amount of rock near the explosion. Both creation of void volume and rock breakage occur together as a result of an explosion and the goal of underground nuclear explosion engineering is to adapt these two effects to useful purposes.

For preliminary technical or economic feasibility analyses of a specific application either the anticipated explosion effects or the size of explosive required to obtain the desired effects must be estimated. In early planning phases it is usually also necessary to make these estimates with a limited understanding of the rock characteristics at the site in question and with a limited understanding of how that rock will respond to an explosion. These estimates, however, need to be sufficiently accurate for the results to be close to those which will be produced by later and more thorough engineering analysis.

The most accurate predictions are made by employing computer programs that simulate explosions and the associated effects on the ground surrounding the explosion. For actual engineering design these techniques should be used. Although scaling rules are useful, they have their limitations. In reviewing and extending the use of scaling rules it is not intended to suggest that scaling should be used in place of the computer calculations. Scaling rules should be used as an aid in understanding the problem and determining the general range of effects which will be better estimated by the more sophisticated computational techniques.

Cavity Formation

When a nuclear explosive is detonated deep underground, it vaporizes a considerable amount of rock around the shot point. In a uniform (isotropic) formation the cavity and surrounding shock effects are spherically symmetrical. Within several tenths of a second after the detonation the high pressure gasses expand the cavity essentially to its final size by pushing the surrounding rock away in a radial direction. (See Figure 1). There is some

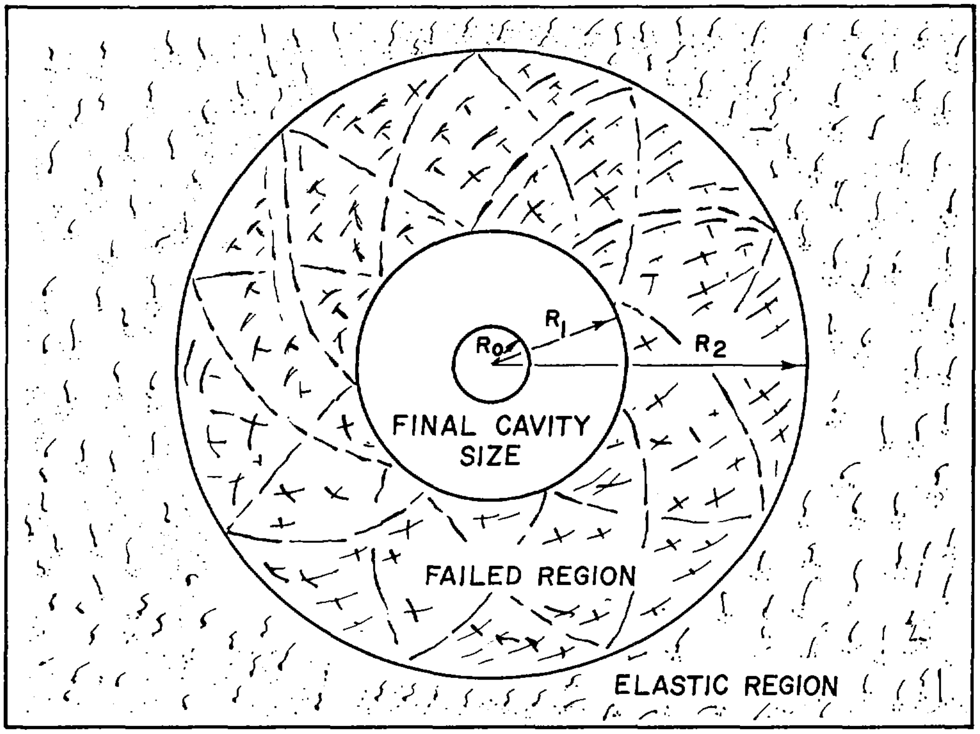

FIGURE 1. Schematic diagram of nuclear explosion cavity formation. The explosion first vaporizes the rocks surrounding the device to a radius R_o by radiation and hydrodynamic heating. This high pressure vaporized region then expands to the final cavity radius R_1. While the cavity expands R_o to R_1 the surrounding rock displaces radially and for the region between R_1 and R_2 the distortion exceeds its elastic limit and suffers permanent distortion. Beyond R_2 the ground motion is elastic only. After the explosion the melted material forms a puddle in the bottom of the cavity (not shown here).

rebound from the motion of the material and subsequent cooling of the gasses in the cavity, but these effects are not large compared to the cavity radius and a good approximation can thus be made by assuming quasistatic expansion of the cavity.

As the cavity wall expands, it suffers a large distortion which exceeds the yield point of the rock. At some point outside the cavity wall there is a boundary beyond which the material responds elastically. Between the cavity wall and this boundary the material has failed; the failure being ductile flow, brittle fracture or a complicated mode involving both ductile and brittle fracture. If the material is porous, changes in specific volume can involve compaction as well as compression.

Cavity Radius Without Rock Strength

For simplified analysis, it is normally assumed that the cavity expands adiabatically. This is considered to be a reasonable assumption since the cavity forms rapidly compared to the time involved to transfer any heat away from the cavity region by conduction. With this assumption, the two governing equations from the thermodynamics are:

$$dE = PdV \tag{1}$$

$$PV^{\gamma} = \text{Constant} \tag{2}$$

where E = Energy, P = Pressure, V = Volume and γ = adiabatic exponent.

Combining equations (1) and (2) and integrating gives the equation

$$PV = (\gamma - 1)E \tag{3}$$

Adiabatic expansion of the cavity from an initial volume V_o to a final volume V from equations (2) and (3) is then expressed by

$$V = V_o \left[\frac{(\gamma - 1)E}{PV_o}\right]^{1/\gamma} \tag{4}$$

In earlier work at Lawrence Radiation Laboratory this equation was used with the assumption that the cavity would expand until P was equal to the overburden pressure; γ was assumed to be

TABLE I

Values of C for Equation (5)
Adapted from Table 4.1 in Reference 2

	C	

Material	r = meters
	h = meters
	w = Kt
	ρ = gm/cc
		r = ft.
		h = ft.
		w = Kt
		ρ = gm/cc

Alluvium	64 - 76	285 - 335
Tuff-Alluvium	70 - 77	310 - 340
Tuff	75 - 78	330 - 345
Salt	63 - 67	280 - 295
Granite	57 - 61	250 - 270
Dolomite	51 -	225 -

TABLE II

Calculated Vaporized Region Parameters
for a 1 Kt Underground Explosion

H_V = 2.8 K cal/gm except salt = 1.185 K cal/gm
E_V = Vaporization Energy
P_V = Initial Pressure in Vaporized Radius
R_V = Radius of Vaporization

Rock	ρ_o (g/cc)	E_V (cal/gm)	P_V (K bars)	R_V m
Alluvium	1.52	3406	675	2.25
Dry Tuff	1.76	3475	865	2.16
Wet Tuff	1.97	3577	1100	2.06
Granite	2.67	4205	1800	1.83
Salt	2.24	2133	840	2.25

TABLE III

Event	Yield Kt	Depth of Burial (Meters)	Calculated Vapor Radius r_o (Meters)	Measured Cavity Radius r_1 (Meters)	Over-burden (kb)	$\frac{r_1}{r_o}$	Apparent σm (kb) from Figure 5
Hardhat	5	286	3.13	19.2	.069	6.13	.07
Shoal	13.4	367	4.35	27.1	.088	6.23	.08
Piledriver	61	463	7.20	44.5	.111	6.18	.09
Gasbuggy	26	1293	5.5	25.7	.310	4.67	.11*
Gnome	3.1	361	3.28	18.7	.088	5.70	.10
Salmon	5.3	828	3.92	16.7	.180	4.85	.14

---

* Gasbuggy had about 4% water so the SiO_2 + 1% water adiabat was shifted down slightly.

4/3; and E and V_o were both assumed linearly proportional to the total yield, W. The proportionality factors were then lumped into one empirical constant and the equation written in terms of cavity radius, r_1, which is proportional to the cube root of the volume. The resulting equation is

$$r_1 = C \frac{W^{1/3}}{(\rho h)^{1/4}} \tag{5}$$

where ρ = density, h = height, and C is the lumped constant. The values of C, found empirically from a number of nuclear explosions, are given in Table I. C is not constant for all materials. From Tables I and II it is apparent that C decreases as the material gets denser and from a general understanding of the physical properties of the materials listed in Tables I and II it is apparent that the value of C decreases as the material gets harder. Also, since equation (5) is an empirical equation with the constant selected to fit the available data, caution should be exercised in applying it much beyond the yield and depth ranges of the data used to obtain the empirical constants (Ref. 18).

By using the elastic-plastic hydrodynamic computer codes at Lawrence Radiation Laboratory, Butkovich (Ref. 3) and Higgins and Butkovich (Ref. 4) were able to determine the pressure of the initial vaporized region. Figure 2 illustrates their method and Table II gives the results of the computer calculations for 1 kt. Figure 3 shows a correlation between silicate rock density and vaporization radius and Figure 4 shows correlation between silicate rock density and pressure at vaporization. Higgins and Butkovich extended their analysis in an attempt to obtain a cavity radius scaling equation with one constant for all materials and obtained an equation involving two different γ's. An understanding of the special way they obtained the γ's is necessary to use the equation and the reader is referred to their paper (Ref. 4) for further consideration of it.

Cavity Radius Including Rock Strength

Material strength for an unspecified mode of failure (σ_m) has the same dimensions as ρgh. Therefore, in deriving a scaling law it can be included as an additive term so that the final cavity pressure, P_1, becomes

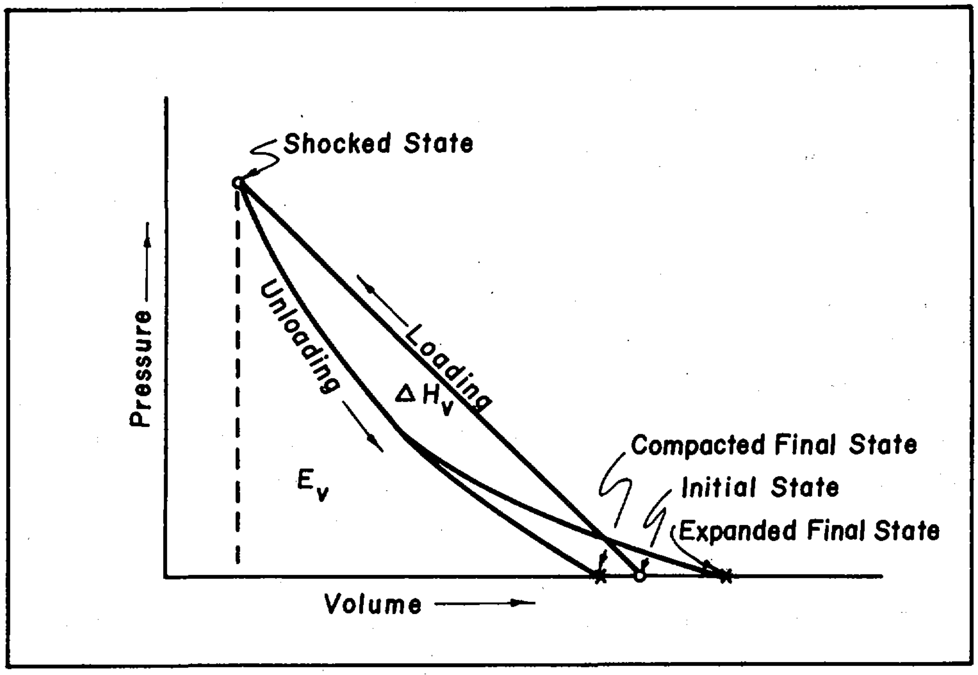

FIGURE 2. Schematic diagram illustrating hydrodynamic heating. A shock wave passing through a section of rock compresses the rock from its initial state to the shocked state by a jump process equivalent to a straight line loading path between the two states. On unloading, the path is an adiabatic curve generally lying below the loading path. When the shock wave has completely unloaded the rock may or may not return to its initial density (or specific volume). The final state may be compacted or expanded depending on the rock and the amount of distortion it experienced. The triangular area on the diagram under the loading path is proportional to the total internal energy (E_v) transmitted to the material by the shock wave. The area between the loading and unloading paths (ΔH_v) is proportional to the amount of energy left in the region of material by the passage of the shock wave. This is the hydrodynamic heating or "waste heat" that melts or vaporizes the rock near the explosion.

$$P_1 = \rho gh + \sigma_m \tag{6}$$

Adiabatic expansion from the radius of vaporization, r_o (for 1 Kt R_V in Figure 3), to final cavity radius (r_1) can be expressed as

$$\frac{r_1}{r_o} = \left[\frac{P_V}{P_1}\right]^{1/3\gamma} \tag{7}$$

where P_V is the initial pressure in the vaporized region and γ is the effective value between the vaporized and final cavity sizes to be discussed later.

For scaling purposes, the values of r_o and P_V in equation (7) for several materials can be reasonably well estimated from Table II or Figures 3 and 4. There is difficulty, however, in estimating γ because it is not constant during cavity growth. One way to estimate γ, or the entire right hand side of equation (7), is to plot the adiabatic expansion curve for the cavity gases. The expansion adiabat cannot be experimentally determined for the very high temperatures and pressures in the initial stages of expansion following a nuclear explosion, but it can be approximated by chemical thermodynamic calculations for the known chemical composition of the vaporized material. Figure 5 shows several expansion adiabatics calculated at LRL (Ref. 4). Then, once the value of P_1 is determined from equation (6), the value of V/V_o is found from Figure 5 by using the adiabat appropriate for the material in question. The ratio of cavity radii is then the cube root of V/V_o.

The apparent rock strength (σ_m) for equation (6) can be estimated by comparing the data from nuclear experiments with the appropriate adiabats. Six nuclear detonations are listed in Table III and plotted on Figure 5. The points are plotted where the pressure is ρgh for the detonation, V is the experimentally derived cavity volume, and V_o is the volume vaporized derived from R_V in Table II and the nuclear yield of the experiment. For these experiments, σ_m is taken to be the difference between the plotted point and the appropriate adiabat. This value is tabulated in the last column of Table III. Note that these strength values are low compared to reported (Ref. 15) laboratory measurements of granite, sandstone and salt.

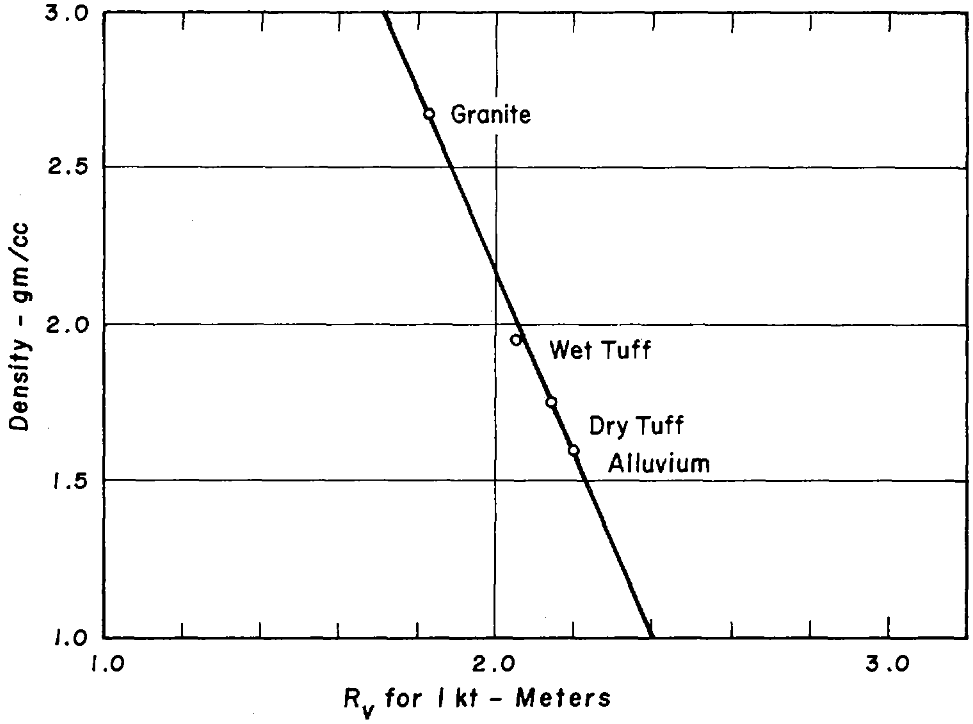

FIGURE 3. Radius of vaporization of silicate type rock for a nuclear yield of 1 kiloton. Data from Ref. 4.

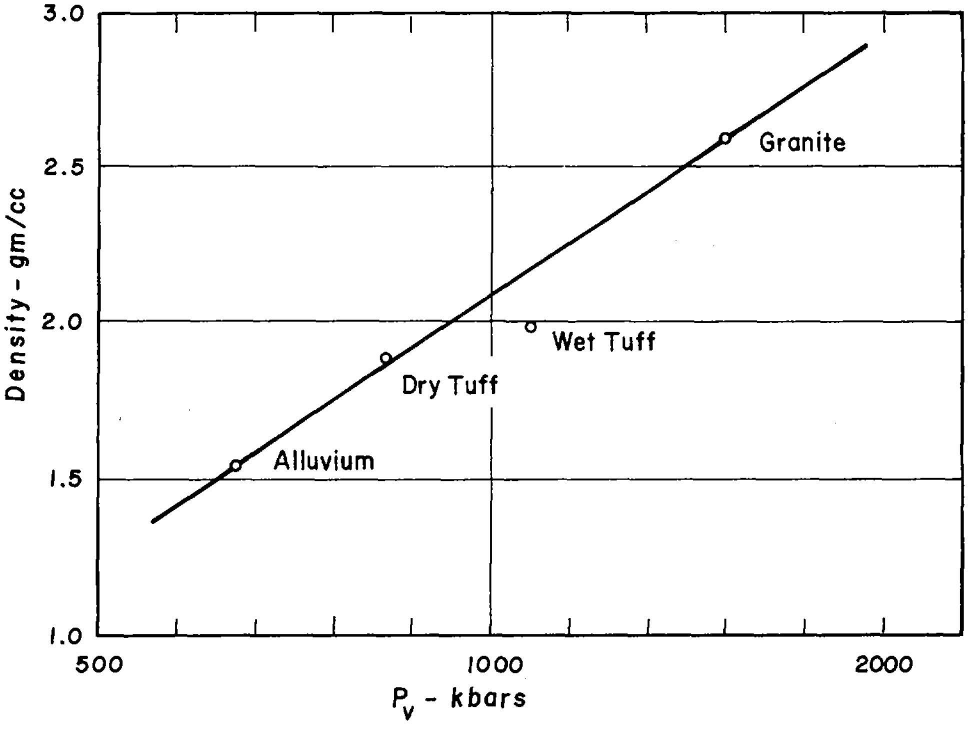

FIGURE 4. Initial pressure (P_o) within radius R_o before it expands to R_1. Data from Ref. 4.

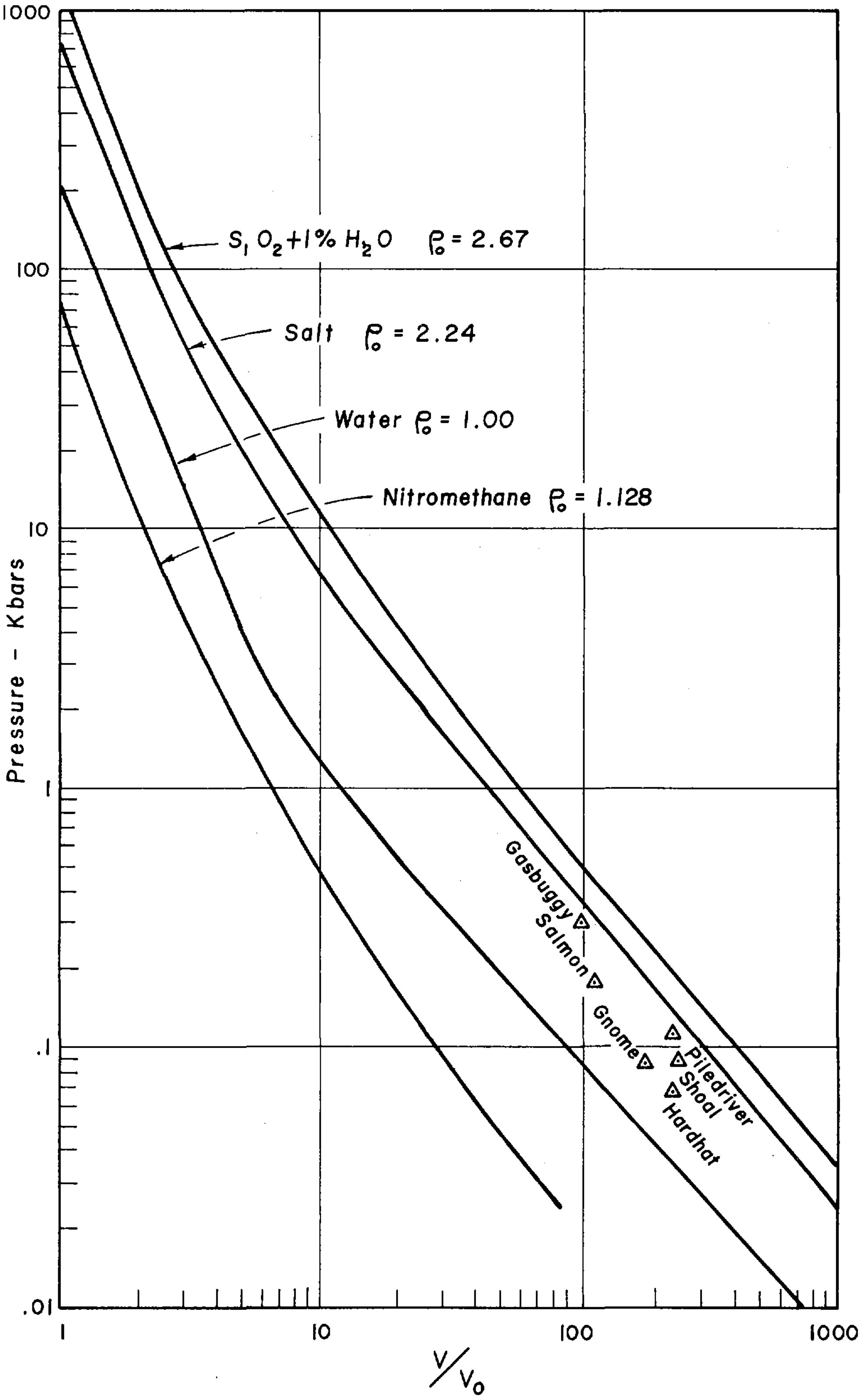

FIGURE 5. Adiabatic expansion curves from Ref. 3. The triangular data points are for the experimentally measured volumes (Table III) and the overburden pressure. The pressure difference between the data point and the appropriate expansion adiabat is interpreted as a measure of the effective material strength.

Example

Figure 6 is an example in the use of this method to make a prediction of cavity size. The hypothetical example is that of a nuclear explosion in a deep weak formation similar to salt to create a storage cavity. The steps to construct Figure 6 are as follows:

1) The radii of vaporization are calculated for several explosion yields that bracket the range of interest by multiplying the appropriate value of R_v for salt from Table II (2.25) by the cube root of each selected explosion yield to get the values for r_o.

2) The values of V_o are then calculated from r_o and used to construct the expansion adiabat for each yield by multiplying the adiabat for salt in Figure 5 by V_o. (This connects the abscissa of Figure 5 to a volume scale.) These are the solid lines in Figure 6.

3) The final cavity pressure is then related to the shot depth by equation (6). A material strength, σ_m, of 140 bars with the Von Mises yield criteria is assumed. The assumed average overburden density between the ground surface and the shot point is 2.3 gm/cc.

4) With these values of σ_m and ρ put into equation (6) and the final explosion cavity pressure, P_1, given by the vertical axis in Figure 6, a corresponding scale for shot depth, h, is calculated. This scale is inset in the upper right hand corner of the Figure. This completes the Figure, except for the dashed curves. To use the Figure, one selects a combination of depth and yield and then reads the cavity volume from the horizontal scale.

Also shown on Figure 6 (dashed lines) is the calculated cavity volume using the empirical equation (5) with $C = 280$, $\rho = 2.3$ gm/cc and h from the depth of shot scale. It is noted that at relatively shallow depth (~ 1000 ft.), both methods give about the same volume but at deeper depths the adiabats give larger volume. At 4000 feet, for example, the adiabat predicts about 60% more volume (18% larger radius). The difference between the two methods is, of course, variable depending on what values are used in equation (6).

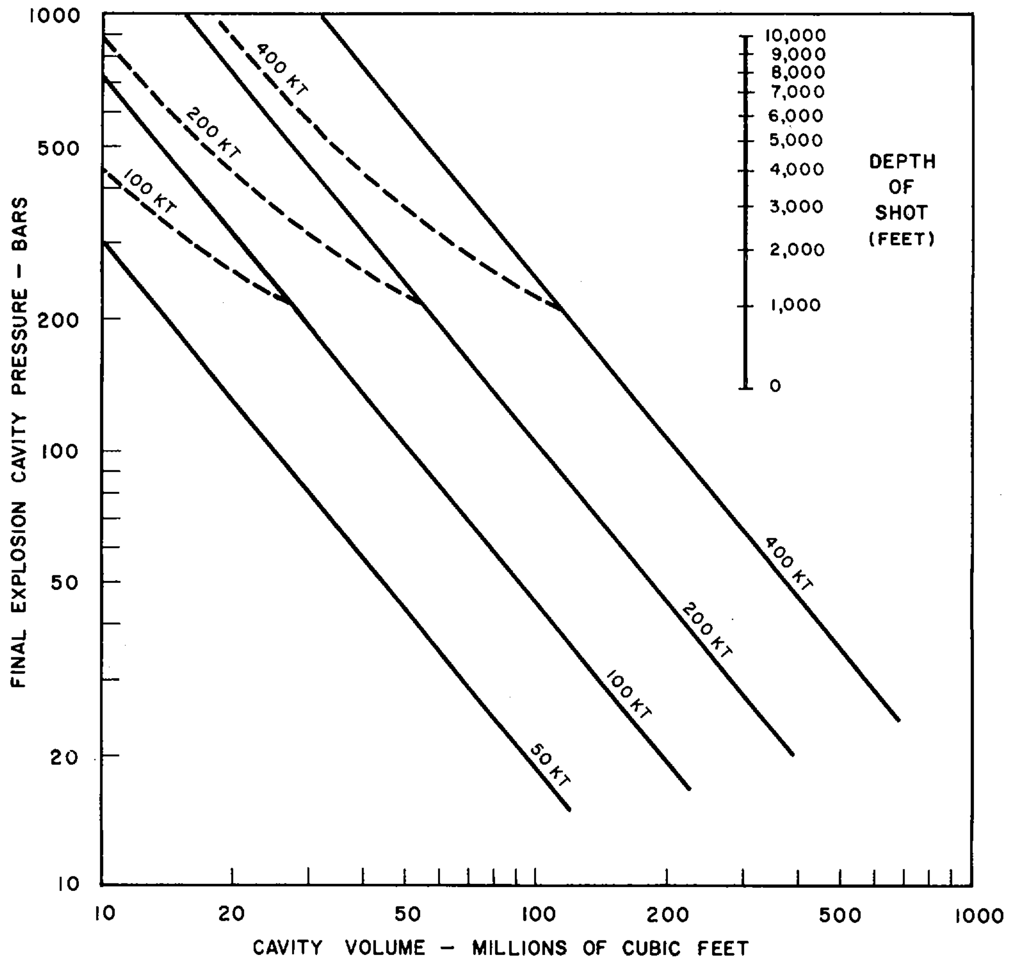

FIGURE 6. Example of the use of the expansion adiabat and material strength to predict cavity size for deeply buried nuclear explosions. In this example it is assumed that the explosion is in salt with a Von Mises yield criteria value of 140 bars and the average overburden density is 2.3 gm/cc. Equation (6) connects the final cavity pressure to the depth scale inset in the upper right hand corner of the figure. The adiabat for salt (solid lines) from Figure 5 is used with the initial cavity radius calculated from Table II and cube root scaling of radius (linear scaling of volume). The dashed lines are the predicted cavity volumes using the empirical equation (5) with C = 280, ρ = 2.3 gm/cc and h for the inset depth of shot scale.

Yield Criteria

For deeply buried nuclear explosions the overburden pressure approaches rock strengths; therefore, as the cavity expands and distorts the rock, yielding will usually be shear under compression. Under this condition, there are two prominent failure criteria that have analytical solutions that are relatively simple. One is the Von Mises criteria shown in Figure 7 and the other is the Coulomb-Mohr criteria shown in Figure 8.

The Von Mises criteria describes the condition where the material fails whenever a certain level of stress difference is reached regardless of how much overpressure the material is under. In this case the state of shear stress is described by

$$|\sigma_3 - \sigma_1| \leq Y. \qquad \text{(Ref. 5)} \qquad (8)$$

where σ_1 is maximum principal stress, σ_3 is minimum principal stress and Y is the yield stress (constant).

The Coulomb-Mohr criteria describes the material in the sense of two surfaces in contact and the amount of shear stress across the interface depends on the force pushing the surfaces together and the coefficient of friction between the surfaces. In this case the shear stress is described by

$$|\sigma_3 - \sigma_1| \leq (2\sigma_o - \sigma_1 - \sigma_3)\sin\phi \qquad \text{(Ref. 14)} \qquad (9)$$

where ϕ and σ_o are as shown in Figure 8. Each of these two criteria can be used to obtain a mathematical relationship which couples the failure radius to the final cavity radius, assuming radial motion only. For the Von Mises criteria a good description of the derivation is given in Chapter 5 of Hill's book, (Ref. 5). The resulting equation is

$$\frac{r_1^3}{r_o^3} = 1 + \frac{(1-\nu)}{(1-2\nu)} \frac{Y}{K} \frac{r_2^3}{r_o^3} - \frac{2}{3} \frac{Y}{K} \left[3 \ln \frac{r_2}{r_o} + 1 \right] \qquad (10)$$

where ν is Poisson's ratio and K is the bulk modulus.

For the Coulomb-Mohr criteria, the author made a new derivation based on a paper by Haskell (Ref. 14). The resulting equation is

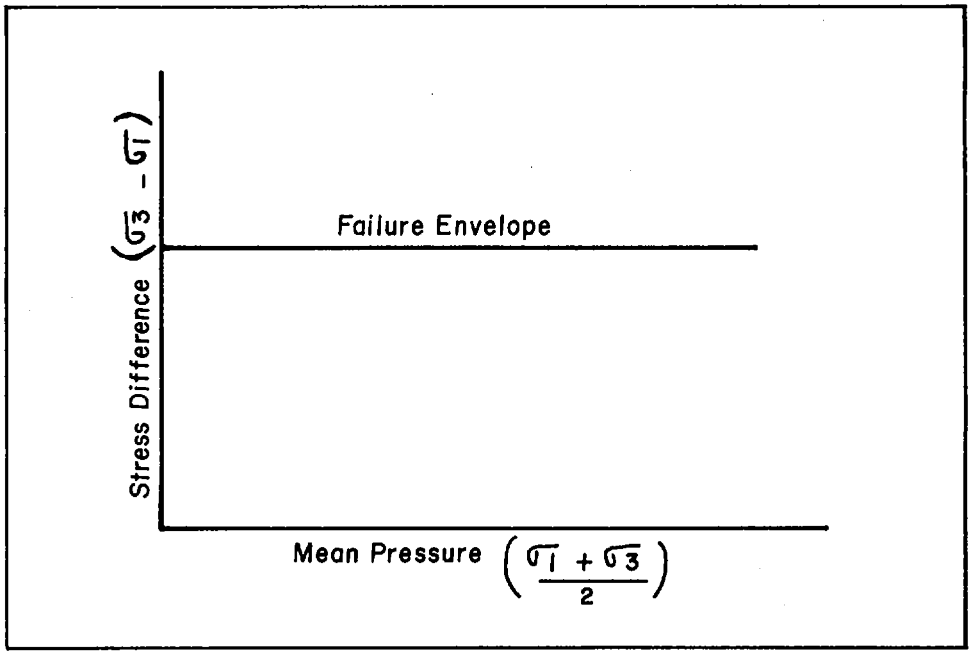
Stress Difference $(\sigma_3 - \sigma_1)$
Failure Envelope
Mean Pressure $\left(\frac{\sigma_1 + \sigma_3}{2}\right)$

FIGURE 7. Schematic diagram of Von Mises failure criteria. Failure depends only on the difference in principal stresses. Overburden or confining stress is not a factor.

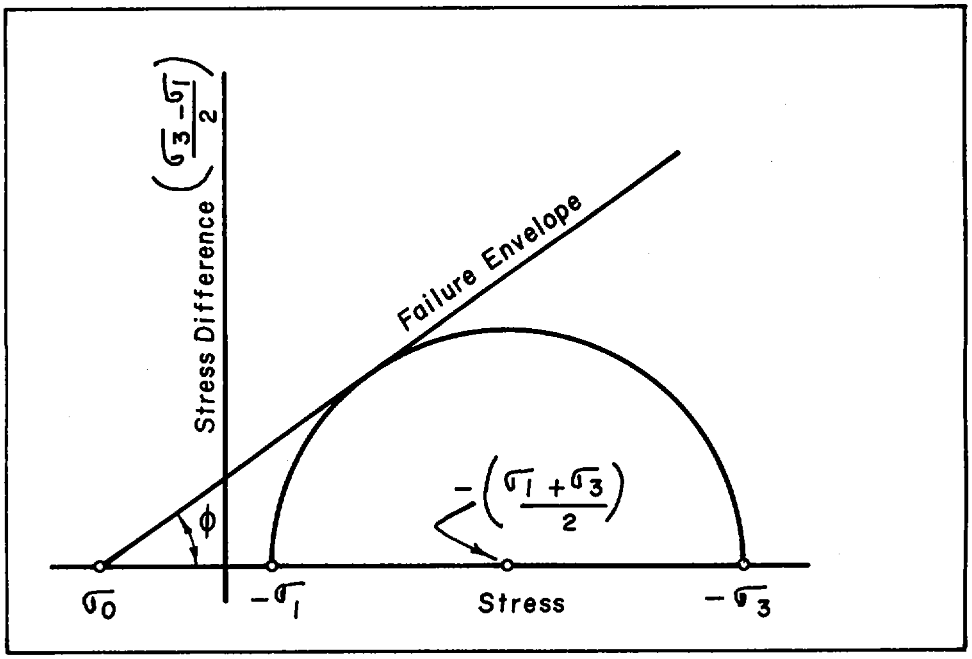
Stress Difference $\left(\frac{\sigma_3 - \sigma_1}{2}\right)$
Failure Envelope
ϕ
$-\left(\frac{\sigma_1 + \sigma_3}{2}\right)$
σ_0
$-\sigma_1$
Stress
$-\sigma_3$

FIGURE 8. Schematic diagram of the Coulomb-Mohr failure criteria. The maximum difference in principal stresses than can be maintained before failure is dependent on the mean stress which includes overburden.

$$\frac{r_o^3}{r_1^3} = \frac{(P_\infty+\sigma_*)}{K}\left[\frac{6k}{(3-k)}\,\frac{(1-\nu)}{(1-2\nu)}\,\frac{r_2^3}{r_1^3} + \frac{3(1-k)}{(3-k)}\,\frac{r_2^m}{r_1^m} - 1\right] + \frac{\rho_1}{\rho_o} \tag{11}$$

where $k = \sin\phi$, P_∞ = overburden pressure, $\sigma_* = \sigma_o - P_p \tan\phi$, P_p = pore pressure, $m = 4K/(1+\ )$, ρ_o = initial density and ρ_1 = final density. The details of the derivation and explanation of terms are given in the Appendix.

The compressional failure conditions of real, underground rock usually will not follow either one of these mathematical simplifications perfectly. A more usual situation is as shown in Figure 9. The failure envelope starts out above zero with an initial slope on the shear stress versus mean pressure plot similar to the Coulomb-Mohr conditions and at higher pressures the curve flattens out more like the Von Mises condition. Some judgement is needed, therefore, to determine which failure criteria best represents the rock in question.

If the complete failure envelope is known, then the general shape of the curve in the range areas where the mean pressure is equal to the overburden plus estimated yield strength can be used as a guide to determine which yield criteria to use. For shallow shot depths and strong rock, yielding will probably still be on the rising portion of the failure curve and be best estimated by the Coulomb-Mohr criteria. For deep shot depths and weak rock, the state of stress will probably be on the more constant part of the yield curve and will be best estimated by the Von Mises criteria. For something in between, it is, of course, possible to do both calculations and devise some method of averaging the results.

In the plots of r_2/r_o for equation (10) (Figure 10) and equation (11) (Figure 11), it is noted that r_2/r_1 approaches a constant value as r_1/r_o increases above the value of about 2. For nuclear explosions, as seen in Table III, the values of r_1/r_o are in the range where a constant value of r_2/r_1 can be expected. This condition is expressed in equations (10) and (11) by the condition that $r_o \to 0$. Equation (10) then simplifies to

$$\frac{r_1^3}{r_2^3} = \frac{(1-\nu)}{(1-2\nu)}\,\frac{Y}{K} \tag{12}$$

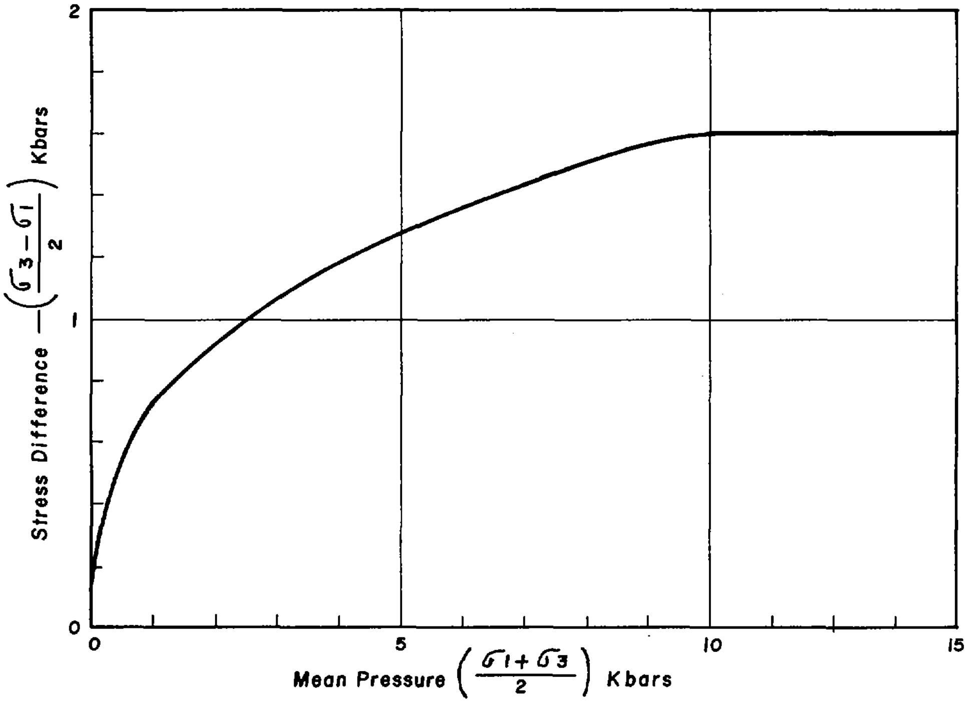

FIGURE 9. Diagram of the familiar envelope used at LRL for some of the computer calculations of explosions in shale.

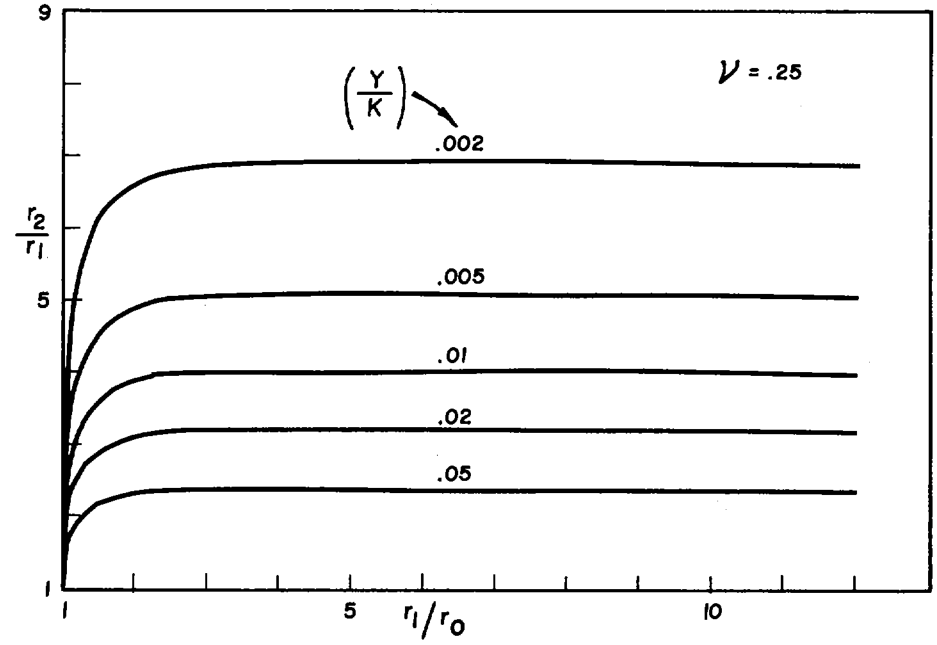

FIGURE 10. Plot relating the failure radius to the cavity radius for several different strengths of material using the Von Mises failure criteria. Dimensionless parameters are used as indicated by equation 10.

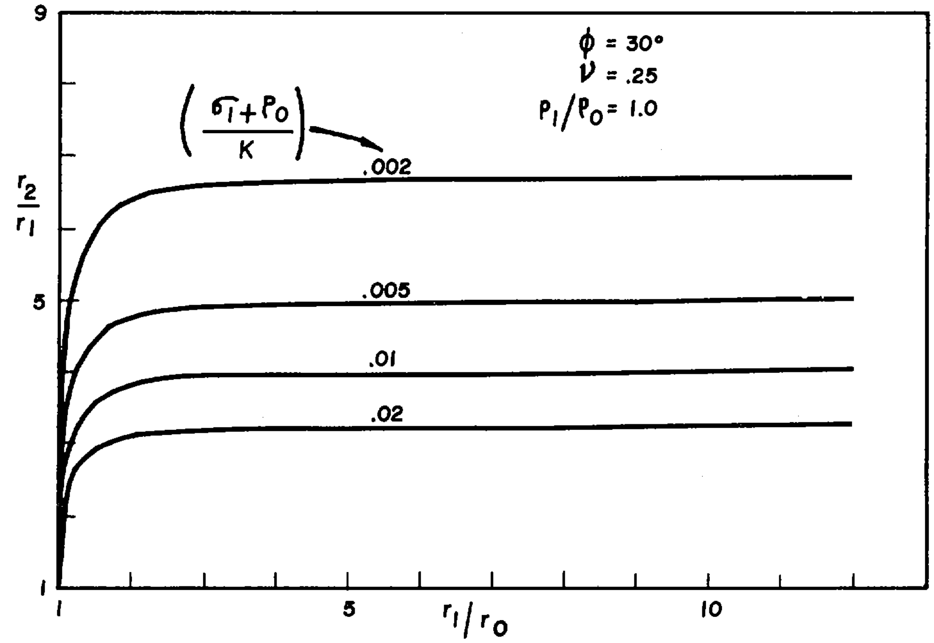

FIGURE 11. Plot of the failure radius related to the cavity radius for several Coulomb-Mohr failure criteria values. Dimensionless parameters are used in agreement with equation 11.

and equation (11) simplifies to

$$\frac{6k}{(3-k)}\frac{(1-\nu)}{(1-2\nu)}\frac{r_2^3}{r_1^3} - \frac{3(1-k)}{(3-k)}\frac{r_2^m}{r_1^m} + 1 = \frac{K}{(\sigma_*+P_\infty)}\frac{\rho_1}{\rho_o} \qquad (13)$$

From equations (12) and (13) plots of r_2/r_1 versus the yield strength relative to the bulk modules can be made. Examples of these are shown in Figures 12 and 13. The values used to plot Figures 10-13 were chosen to be in line with observed parameters of rock: yielding is in the range of .001-.01 of the bulk modulus; Poisson's ratio is in the range of .15-.35; and the Coulomb-Mohr angle of internal friction is in the range of 30°. For these particular values, if Figures 10 and 11 are compared and Figures 12 and 13 are compared, it is observed that there is very little difference in the shapes of the curves. This suggests that either yield criteria can be used if the proper yield value is used. In using the curves, however, the value of Y/K for Figure 12 may not be the same as $(\sigma_* + P_o)/K$ for Figure 13.

Example

The failure radius around the cavity in the above example for cavity size can now be estimated. In the hypothetical example shown in Figure 6 and a Von Mises yield of 140 bars, ν about .25, and K (for salt) about 290 Kbars the ratio r_2/r_1 from equation (12) is about 15. This rather large ratio is a result of the yield (140 bars) being such a small fraction (.0005) of the bulk modulus. For the Coulomb-Mohr criteria with σ_1 about 100 bars (Ref. 15), the r_2/r_1 ratio is found to be about 10 at 1000 feet and decreasing slowly with depth. This large r_2/r_1 value is not inconsistent with the results from a nuclear shot in an existing cavity. In the Sterling experiment (Ref. 16) (.36 Kt in the ~ 17 meters radius Salmon cavity), analysis of the free field motion data indicated nonelastic motion at radii ratios larger than 15. The strain for radii ratios above about 5 is so small, however, that there is negligibly small change in the physical strength or character of the salt. For significant deformation of the salt crystal matrix, the yield strength appropriate to the type of yielding needs to be used. In analysis of the deformation in the Salmon experiment salt, Braun (Ref. 17) crystallographic slip out to a radii ratio of about 7.5 which corresponds to a Von Mises yield ratio (Y/K) of

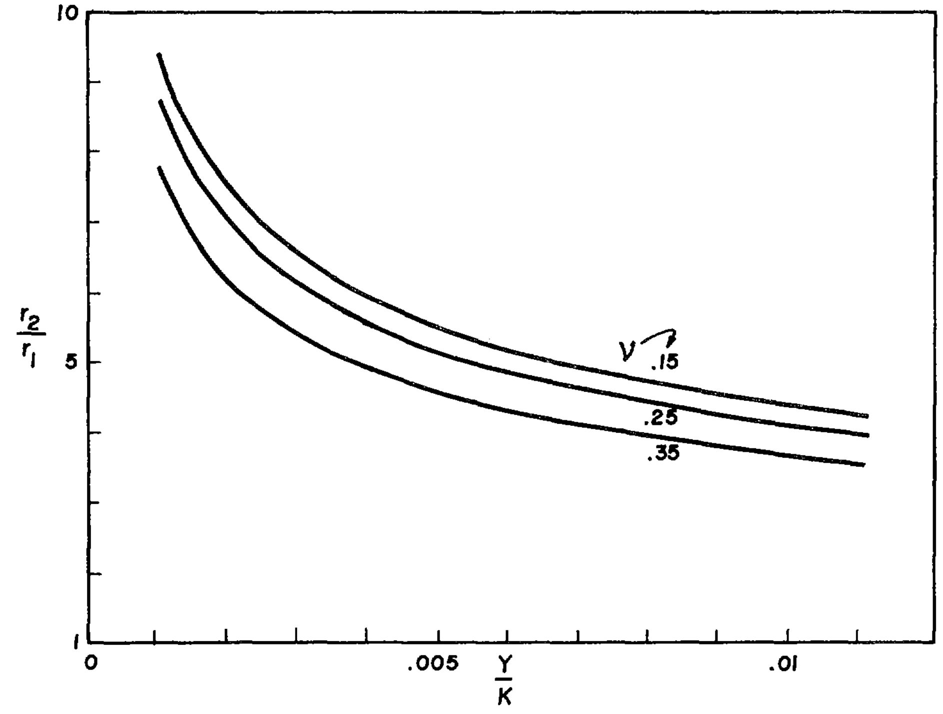

FIGURE 12. Ratio of the failure radius to the cavity radius for large cavity expansions and the Von Mises failure criteria (equation 12).

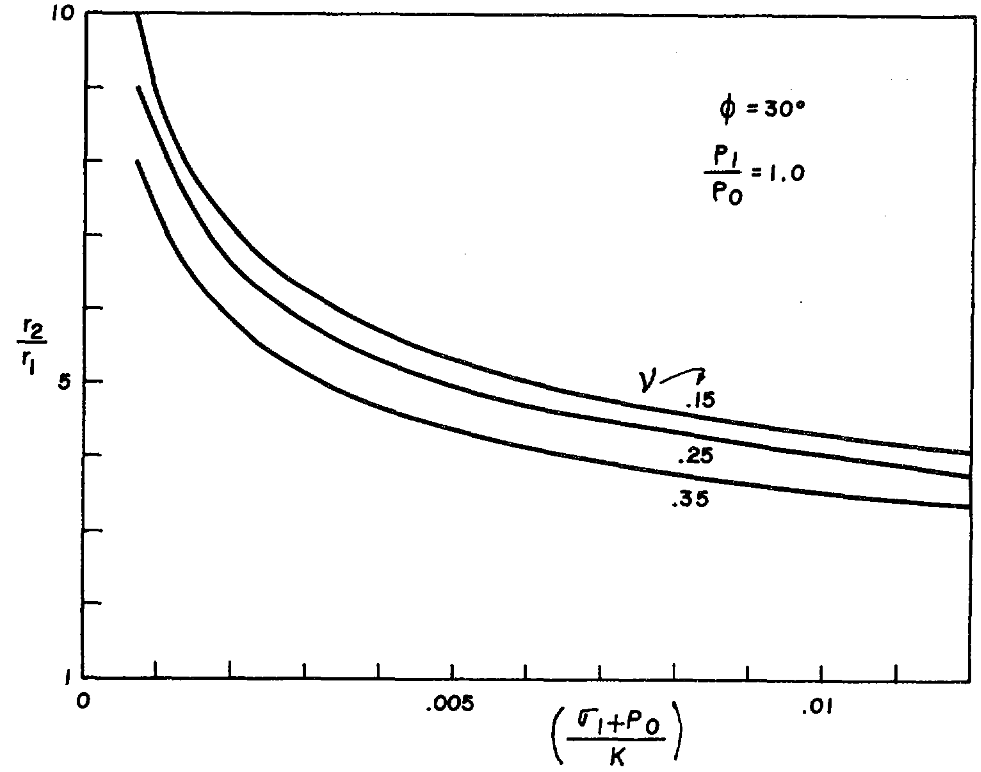

FIGURE 13. Ratio of failure radius to cavity radius for large cavity expansion and the Coulomb-Mohr failure criteria (equation 13).

about .002 or a yield strength of about 600 bars. This is consistent with the dynamic yield strength found in the computer calculation for Salmon (Ref. 10) and only a little higher than the values reported by Handin (Ref. 15) for salt.

These yield values are the point at which yielding begins, not where the material physically fails. After plastic yielding begins, there must be a certain amount of strain before there is loss of coherence. For the two nuclear shots in salt, the cavity stayed open without chimney formation, attesting to the high plasticity of salt under compression. For shots in hard rock, such as granite, shales and sandstone, however, chimneys have been found to form with the height to cavity radii ratio about 3-5. For the shale yield curve shown in Figure 8 and a bulk modulus of about 200 kb and moderate shot depths (where the confining pressure is less than 1 kb) the yield ratio Y/K is in the range of .001-.008. From Figure 12 the corresponding ratio r_2/r_1 is about 5-10, which is somewhat larger than the experimentally observed chimney height/cavity radius ratio. It is apparent that to determine how much of the yielded rock loses its coherence, an estimation needs to be made of how much strain the rock will suffer before separation and relate this to the strain distribution throughout the yielded region.

Conclusions

For preliminary engineering predictions, a graphical solution for cavity size is relatively easy to construct if the cavity gas expansion adiabat is known and the effective strength of the rock surrounding the cavity can be approximated. Several expansion adiabats have been published to date and are the ones used in the analysis given here. They do not cover all the materials compositions of interest, however, and it would be helpful if additional adiabats were calculated and made available.

A prediction of the size of the failure region around the explosion generated cavity can be made from a knowledge of the strength characteristics of the material around the cavity and the analytical solutions for the Von Mises and Coulomb-Mohr failure criteria. With the analytical solutions presented in graphical form, the ratio of failure radius to cavity radius can be easily found once the elastic properties and failure criteria of the material are estimated.

REFERENCES

1. Teller, Edward, Wilson K. Talley, Gary H. Higgins, Gerald W. Johnson, The Constructive Uses of Nuclear Explosives. New York: McGraw-Hill Book Company, 1968.

2. Boardman, Charles R., David D. Rabb, Richard D. McArthur, Characteristic Effects of Contained Nuclear Explosions for Evaluation of Mining Applications. Livermore, California: Lawrence Radiation Laboratory, September 1963.

3. Butkovich, T. R., The Gas Equation of State for Natural Materials. Livermore, California: Lawrence Radiation Laboratory, January 1967.

4. Higgins, G. H., T. R. Butkovich, Effect of Water Content, Yield, Medium, and Depth of Burst on Cavity Radii. Livermore, California: Lawrence Radiation Laboratory, February 1967.

5. Hill, R., The Mathematical Theory of Plasticity. London: Oxford University Press, 1967.

6. Boardman, Charles R., James Skrove, Changes in the Fracture Permeability of a Granitic Rock Mass Resulting from A Contained Nuclear Explosion. Livermore, California: Lawrence Radiation Laboratory, August 1965.

7. Butkovich, Theodore R., "Calculation of the Shock Wave from an Underground Nuclear Explosion in Granite," Journal of Geophysical Research, Vol. 70, No. 4, February 15, 1965, pp. 885-892.

8. Boardman, Charles R., Some Characteristics of the Hardhat Chimney and Surrounding Wall Rock. Livermore, California: Lawrence Radiation Laboratory, October 1966.

9. Boardman, Charles R., Results of an Exploration into the Top of the Piledriver Chimney. Livermore, California: Lawrence Radiation Laboratory, October 1967.

10. Rogers, Leo A., "Free-Field Motion Near a Nuclear Explosion in Salt: Project Salmon," Journal of Geophysical Research, Vol. 71, No. 14, July 15, 1966, pp. 3415-3426.

11. Braun, R. L. and J. S. Kahn, "X-Ray Diffraction Analysis of Plastic Deformation in the Salmon Event," Journal of Geophysical Research, Vol. 74, No. 8, April 15, 1969, pp. 2103-2117.

12. Wells, W. M., "Calculation of Shrinkage of the Salmon Cavity," Journal of Geophysical Research, Vol. 74, No. 10, May 15, 1969, pp. 2791-2794.

13. Handin, John, "On the Coulomb-Mohr Failure Criterion," Journal of Geophysical Research, Vol. 74, No. 22, October 15, 1969, pp. 5343-5348.

14. Haskell, Norman A., "A Static Theory of the Seismic Coupling of a Contained Underground Explosion," Journal of Geophysical Research, Vol. 66, No. 9, September 1961, pp. 2937-2944.

15. Clark, S. P., Jr., Handbook of Physical Constants. New York: The Geological Society of America, Inc., 1966.

16. Sisemore, Clyde J., Leo A. Rogers and William R. Perret, "Project Sterling: Subsurface Phenomenology Measurements Near a Decoupled Nuclear Event," Journal of Geophysical Research, Vol. 74, No. 27, December 15, 1969, pp. 6623-6637.

17. Braun, R. L., J. S. Kahn and S. Weissmann, "X-Ray Diffraction Analysis of Plastic Deformation in the Salmon Event," Journal of Geophysical Research, Vol. 74, No. 8, April 15, 1969, pp. 2103-2117.

18. Higgins, Gary H., Technical Problems and Future Underground Engineering Experiments. Lawrence Radiation Laboratory: Livermore, California, March 26, 1969. (UCRL-71439).

APPENDIX

A schematic diagram of the Coulomb-Mohr yield criteria is shown in Figure 7. With the three principal stresses $\sigma_3 \geq \sigma_2 \geq \sigma_1$ (tension is positive) the difference in stress between the maximum and minimum principal stress is given by

$$\sigma_3 - \sigma_1 \leq (2\,\sigma_o - \sigma_1 - \sigma_3)\,\sin\phi \quad \text{(Ref. 14).} \tag{1}$$

The quantity σ_o is related to the uniaxial tensile strength (σ_t) by the expression

$$\sigma_o = \frac{\sigma_t\,(1 + \sin\phi)}{2\,\sin\phi}\,. \tag{2}$$

Pressure from pore fluid (P_p) is included in the equation by subtracting $P_p \tan\phi$ from σ_o. The combined yield condition at the yield point where the equality in equation (14) holds is

$$\sigma_3 - \sigma_1 = \left[2\,(\sigma_o - P_p \tan\phi) - (\sigma_1 + \sigma_3)\right] \sin\phi \tag{3}$$

This expression is independent of strain which is not completely correct for real rocks. Flow or nonelastic strain may cause strain weakening which might be viewed as the opposite of strain hardening which occurs in most metals. This expression is thus in error to the extent of how $\sigma_3 - \sigma_1$ is related to the state of strain. But, assuming equation (3) holds for the region $r_1 < r < r_2$ then $\sigma_1 = \sigma_r$, (radial stress) and $\sigma_3 = \sigma_\theta$ (tangential stress).

For spherical symmetry the static stress equilibrium equation that must be satisfied is

$$\frac{d\sigma_r}{dr} + \frac{2}{r}\,(\sigma_r - \sigma_\theta) = 0 \tag{4}$$

Using equations (3) and (4) and performing the integration with the boundary condition

$$\sigma_r\,(r_1) = -\,P_1 \tag{5}$$

gives, for the failed region $r_1 \leq r \leq r_2$

$$\sigma_r = \sigma_* - (\sigma_* + P_1)\left[\frac{r_1}{r}\right]^m \tag{6}$$

$$\sigma_\theta = \sigma_* - \left[\frac{1-k}{1+k}\right](\sigma_* + P_1)\left[\frac{r_1}{r}\right]^m \tag{7}$$

where

$k = \sin\phi$

$\sigma_* = \sigma_o - P_p \tan\phi$ and $m = 4k/(1+k)$.

The displacement (u) in the region $r_1 < r < r_2$ is considered a function of the final coordinate

$$U(r) = r - a(r). \tag{8}$$

That is, a particle originally at radius a is displaced amount U to the radius r. The expression relating the displacement to the dilation (Δ) when $\Delta << 1$ is

$$U = r - \left(r_o^3 + r^3 - r_1^3 - 3\int_{r_1}^{r} \Delta r^2 dr\right)^{1/3} \tag{9}$$

The dilitation is comprised of elastic compression and permanent compaction. The elastic compression Δ_E is given by

$$\Delta_E = \frac{1}{3\lambda + 2\mu} \left(\sigma_r + 2\sigma_\theta + P_\infty\right) \tag{10}$$

where P_∞ is the overburden pressure. The permanent compaction ($\Delta\rho$) is given by

$$\Delta\rho = \frac{\rho_1 - \rho_o}{\rho_o} \tag{11}$$

and is assumed constant over the region $r_1 < r < r_2$. The Lame constants in equation (10) are for the failed material, which are in reality different than the original material; we will assume λ the same in both the elastic and failed regions, but that μ can change when the material fails.

Combining equations (6), (7), (9), (10) and (11) and using the approximation $(1 + x)^n = 1 + nx$ (keeping only first order term in a series expansion) for $r = r_2$, the resulting equation is

$$\begin{aligned} B = r_2^2\, U(r_2) &= \frac{r_1^3 - r_o^3}{3} \\ &+ \frac{r_1^3}{3\lambda + 2\mu} \left[(\sigma_* + P_\infty) \left\{ \left[\frac{r_2}{r_1}\right]^3 - 1 \right\} - (\sigma_* + P_1) \left\{ \left[\frac{r_2}{r_1}\right]^{3-m} - 1 \right\} \right] \\ &+ \left[\frac{\rho_1 - \rho_o}{\rho_o}\right] \left[\frac{r_2^3 - r_1^3}{3}\right] \end{aligned} \tag{12}$$

which describes the condition on the plastic side of the elastic-plastic boundary.

On the elastic side of the boundary, the stresses are given by

$$\sigma_r = - P_\infty - 4\mu B r_2^{-3} \tag{13}$$

$$\sigma_\theta = - P_\infty + 2\mu B r_2^{-3} \tag{14}$$

Continuity of displacement requires the B's in equations (12), (13) and (14) to be the same. If we presume the Lame constants to be the same for both regions there is continuity of both radial and tangential stress at r_2. Here, however, it is assumed that the shear modulus can change from the elastic value (μ_e) to the plastic value (μ_p) at the boundary. The continuity of radial stress and the discontinuity of tangential stress are found by combining equations (6), (7), (13) and (14) where μ_e replaces μ in (6) and μ_p replaces μ in equation (7).

$$(\sigma_* + P_\infty) - (\sigma_* + P_1) \left[\frac{r_1}{r_2}\right]^m = - 4\mu_e B r_2^{-3} \tag{15}$$

$$(\sigma_* + P_\infty) - \left[\frac{1 - k}{1 + k}\right] (\sigma_* + P_1) \left[\frac{r_1}{r_2}\right]^m = 2\mu_p B r_2^{-3} \tag{16}$$

Eliminating B between equations (15) and (16) gives an expression relating the cavity pressure to the overburden pressure.

$$\frac{\sigma_* + P_1}{\sigma_* + P_\infty} = \frac{(\mu_p + 2\mu_e)\ (1 + k)}{\left[\mu_p(1+k)+2\mu_e(1-k)\right]} \left[\frac{r_2}{r_1}\right]^m \tag{17}$$

Combining equations (17) and (12) to eliminate $(\sigma_* + P_1)$ gives an expression for B for the dilitation condition. Combining equations (15) and (16) to eliminate $(\sigma_* + P_1)$ gives an expression for B from the stress continuity conditions. This latter equation is

$$B = \frac{(\sigma_* + P_\infty)\ k\ r_2^3}{\left[\mu_p(1+k)+2\mu_e(1-k)\right]} . \tag{18}$$

Equating the equations for B gives the expression

$$\frac{r_1}{r_o} = \left[C_1 \left[\frac{r_2}{r_1}\right]^3 + C_2 \left[\frac{r_2}{r_1}\right]^m + C_3 \right]^{1/3} \tag{19}$$

where

$$C_1 = \frac{-3(\sigma_* + P_\infty)k}{\left[\mu p(1+k)+2\mu_e(1-k)\right]} + \frac{3(\sigma_* + P_\infty)}{(3\lambda + 2\mu_p)} \left[1 - \frac{(\mu_p + 2\mu_e)(1+k)}{\left[\mu_p(1+k)+2\mu_e(1-k)\right]} \right]$$

$$+ \left[\frac{\rho_1 - \rho_o}{\rho_o}\right]$$

$$C_2 = \frac{3(\sigma_* + P_\infty)}{(3\lambda + 2_\mu)} \quad \frac{(\mu_p + 2\mu_e)(1 + k)}{\left[\mu_p(1+k)+2\mu_e(1-k)\right]}$$

$$C_3 = 1 - \frac{3(\sigma_* + P_\infty)}{(3\lambda + 2\mu_p)} - \left[\frac{\rho_1 - \rho_o}{\rho_o}\right]$$

To determine r_2 as a function of r_1 and r_o it is necessary to assume a series of values for (r_2/r_1) that converge to the desired value for (r_1/r_o).

Equation (19) has the charaacteristic that when $r_1 >> r_o$, the ratio (r_2/r_1) approaches a constant value. Thus, for the condition $r_1 >> r_o$, a reasonable approximation for underground nuclear explosions can be made for (r_2/r_1) by equating the terms inside the bracket to zero to get

$$\left[\left[\frac{r_2}{r_1}\right]^3 + \frac{C_2}{C_1}\left[\frac{r_2}{r_1}\right]^m + \frac{C_3}{C_1} = 0\right]_{r_1 >> r_o} \qquad (20)$$

For the analysis in the body of the report, the equations were used for $\mu_E = \mu_P$ and the elastic constants given in terms of bulk modules and Poisson's ratio from the connecting identities

$$\lambda = 3\ K \frac{\nu}{1 + \nu} \qquad (21)$$

$$\mu = 3\ K \frac{1 - 2\nu}{2 + 2\nu} \qquad (22)$$

where K is the bulk modulus.

XA04N0768

SCALING CRITERIA FOR ROCK DYNAMIC EXPERIMENTS*

Barbara K. Crowley
Lawrence Radiation Laboratory, University of California
Livermore, California 94550

ABSTRACT

A set of necessary conditions for performing scaled rock dynamics experiments is derived from the conservation equations of continuum mechanics. Performing scaled experiments in two different materials is virtually impossible because of the scaling restrictions imposed by two equations of state. However, performing dynamically scaled experiments in the same material is possible if time and distance use the same scaling factor and if the effects of gravity are insignificant. When gravity becomes significant, dynamic scaling is no longer possible. To illustrate these results, example calculations of megaton and kiloton experiments are considered.

INTRODUCTION

Scaling concepts have been extensively used in the design of nuclear experiments. This use has been due to both the previous lack of theoretical models and the relatively large cost of obtaining full-scale experimental information. A variety of scaling criteria have been proposed for both underground cavity production[1,2] and cratering experiments.[1,3-9] These proposed scaling criteria have been vigorously debated and frequently confusion has existed about the importance of: (1) high explosive versus nuclear sources; (2) rock equation of state and other material properties; (3) gravity; and (4) water content of the rock.

The numerical simulation of nuclear rock dynamic experiments has recently been shown to fairly successfully predict the dimensions of cavities and craters.[10,11] The numerical codes SOC[10] and TENSOR[11] have been used for these simulations, and their accuracy presently appears to be limited only by the accuracy of the description of the rock properties.

To investigate scaling, the SOC and TENSOR equations are considered here. Using these equations, an algebraic analysis is performed to obtain a set of necessary conditions which must be satisfied for similar solutions of the equations. The necessary conditions for similar solutions are also the necessary conditions for scaled experiments. Some example SOC calculations are described here which verify the necessary conditions for similar solutions.

I. THE SOC AND TENSOR EQUATIONS

The SOC and TENSOR equations consider the same physics; their apparent differences are due to the differences in the expression of the generalized coordinate operators (divergence and gradient) in one-dimensional spherical (SOC) and two-dimensional cylindrical (TENSOR) geometries. These codes

---

*Work performed under the auspices of the U. S. Atomic Energy Commission.

start with a set of initial conditions and descriptions of the rock properties and integrate, with respect to time, the conservation equations of continuum mechanics.[12] Since SOC and TENSOR are cast in the Lagrangian form, mass is implicitly conserved. The momentum equation considers both the stress tensor, which is composed of an isotropic and a deviatoric part, and gravity. Velocities obtained from the momentum equation are integrated with respect to time to obtain displacements. From the velocities and displacement, strain rates are calculated; and stresses are obtained from Hooke's Law. The energy equation considers work done by the total stress tensor. Equations of state for the pressure as a function of the compression and/or energy of a zone may be used for each material region under consideration. For brevity, only the SOC equations are considered here.

The SOC Equations (notation in Appendix A)

Momentum: $$\frac{\partial U}{\partial t} = -\frac{1}{\rho}\left\{\frac{\partial P}{\partial R} + \frac{4}{3}\frac{\partial K}{\partial R} + \frac{4K}{R}\right\} + g$$

Displacement: $$\frac{\partial R}{\partial t} = U$$

Deviatoric Strain Rate: $$\dot{e} = \frac{1}{2}\left[\frac{U}{R} - \frac{\partial U}{\partial R}\right]$$

Hooke's Law for Deviatoric Stress Rate: $$\dot{K} = \frac{\partial K}{\partial t} = \mu\left[\frac{U}{R} - \frac{\partial U}{\partial R}\right] = 2\,\mu\,\dot{e}$$

Energy: $$\frac{\partial \epsilon}{\partial t} = \frac{4}{3}\,\frac{K\,\dot{K}}{\eta\,\mu} - \frac{P}{V^0}\,\frac{\partial V}{\partial t} = \frac{4}{3}\,\frac{K\,2\,\dot{e}}{\eta} - \frac{P}{V^0}\,\frac{\partial V}{\partial t}$$

Equation of State: $$P = a + a_1\eta + a_2\eta^2 + \ldots + b_1\epsilon + b_2\epsilon^2 + \ldots + c_1\eta\epsilon + c_2\eta^2\epsilon^2 + \ldots$$

In SOC, any function or table of pressure versus compression and/or energy may be used for the equation of state. A simple polynomial function is considered here merely for illustrative purposes.

II. DERIVATION OF THE SIMILAR CONDITIONS

To obtain the necessary conditions for similar solutions, the SOC equations are now examined. The approach used here is more laborious but more systematic than either the Vaschy-Buckingham π[13] or the dimensional analysis method,[14] to which it is equivalent.[15]

It is assumed that two experiments, denoted by a set of unprimed and primed variables respectively, can be adequately simulated by SOC and TENSOR. Dimensionless parameters which are denoted by the subscript 0 are formed for ALL of the variables as the ratio of unprimed to primed variables.

Derivatives with respect to distance and time for an arbitrary dependent variable ($\phi = \phi_0\phi'$) in the two experiments are related by:

$$\frac{\partial \phi}{\partial R} = \frac{\partial \phi}{\partial R'} \cdot \frac{\partial R'}{\partial R} = \frac{1}{R_0} \cdot \frac{\partial \phi}{\partial R'}$$

where $R_0 = R/R'$

$$\frac{\partial\phi}{\partial t} = \frac{\partial\phi}{\partial t'} \cdot \frac{\partial t'}{\partial t} = \frac{1}{t_0} \cdot \frac{\partial\phi}{\partial t'}$$

where $t_0 = t/t'$. With these relationships, an unprimed SOC momentum equation may be written in terms of a primed momentum equation:

$$\frac{\partial U'}{\partial t'} = \frac{-t_0}{U_0\rho_0} \cdot \frac{1}{\rho'}\left\{\frac{P_0}{R_0}\frac{\partial P'}{\partial R'} + \frac{K_0}{R_0}\frac{4}{3}\frac{\partial K'}{\partial R'} + \frac{K_0}{R_0}\frac{4K'}{R'}\right\} + \frac{t_0 g_0}{U_0} g'$$

If

$$\frac{t_0}{U_0\rho_0}\frac{P_0}{R_0} = 1, \quad \frac{t_0K_0}{U_0\rho_0R_0} = 1, \text{ and } \frac{t_0g_0}{U_0} = 1,$$

the primed and unprimed momentum equations are similar. The SOC momentum equation thus imposes these three conditions on the dimensionless scaling parameters for the two experiments.

Applying the same technique to the remaining SOC equations, a set of necessary conditions for similar solutions is obtained. With minor algebraic manipulations and omitting redundant conditions, the following complete set of seven necessary conditions is obtained:

(1) $\dfrac{t_0P_0}{U_0\rho_0R_0} = 1$

(2) $P_0 = K_0 = \mu_0$ All "pressure-like" variables must use the same scaling factor.

(3) $\dfrac{t_0g_0}{U_0} = 1$

(4) $\dfrac{t_0U_0}{R_0} = 1$

(5) $e_0 = \dfrac{U_0}{R_0}$

(6) $\dfrac{P_0}{\epsilon_0\eta_0} = 1$

(7) Polynomial equation of state:

$$\frac{a_0}{P_0} = 1, \quad \frac{a_{10}\eta_0}{P_0} = 1, \quad \frac{a_{20}\eta_0^2}{P_0} = 1, \quad \text{etc.}$$

$$\frac{b_{10}\epsilon_0}{P_0} = 1, \quad \frac{b_{20}\epsilon_0^2}{P_0} = 1, \quad \text{etc.}$$

$$\frac{c_{10}\eta_0\epsilon_0}{P_0} = 1, \quad \frac{c_{20}\eta_0\epsilon_0^2}{P_0} = 1, \quad \text{etc.}$$

The two-dimensional TENSOR equations introduce the following conditions: (1) the R and Z (radial and axial) distances must use the same scaling factor; (2) the radial and axial velocities must use the same scaling factor; (3) all strains scale the same; and (4) all stresses scale the same. The complete three-dimensional equations impose the condition that the same scaling factors must be used for all three dimensions.

III. SCALING EXPERIMENTS IN THE SAME SOLID MATERIAL

The necessary conditions (7) impose such stringent conditions on the ratios of equation-of-state parameters that scaling in two different solid materials is nearly impossible. However, if the two experiments are performed in the same material, a very general equation of state imposes no restrictions in addition to those imposed by an unrealistically simple equation of state. These conditions are: $\eta_0 = P_0 = \epsilon_0 = 1$.

When the same material is being considered, $\eta_0 = 1$ implies that $\rho_0 = 1$. Then, using $t_0/R_0 = 1/U_0$ from condition (4) in condition (1) gives $U_0^2 = 1$, i.e., velocities must be the same. This criterion is physically reasonable if one considers that P and ρU^2 are both energies per unit volume. The strain rate is a change in length per unit length per unit time, $e_0 = R_0/R_0 t_0 = 1/t_0$. Using $e_0 = 1/t_0$ and $\eta_0 = 1$, conditions (5) and (1) in Section II are essentially the same.

Thus, for two experiments in the same material, the seven necessary conditions found in Section II may be written as:

$$P_0 = \eta_0 = \epsilon_0 = U_0 = K_0 = \mu_0 = 1$$

$$R_0 = t_0$$

$$t_0 g_0 = 1 \quad \text{or} \quad R_0 g_0 = 1 \ .$$

The condition $R_0 = t_0$ means that time and distance must scale the same, and is sometimes referred to as dynamic scaling.

When gravity cannot be neglected, $t_0 g_0 = 1$ must be satisfied; and $g_0 = 1$ for two "earth-bound" experiments. If $g_0 = 1$, then $t_0 = 1$. With $t_0 = 1$, it is required that $R_0 = 1$. However, $R_0 = 1$ means that dimensions in the two experiments are identical; and scaled experiments are not possible when gravity is significant. This lack of dynamic similarity when gravity becomes significant was demonstrated by Galilei,[16] and is illustrated in the following sections for rock mechanics experiments.

A pertinent scaling question is whether a 1-kiloton experiment can be used to scale a 1-megaton experiment. In the next two sections, SOC calculations which simulate two sets of kiloton (primed) and megaton (unprimed) experiments are considered: (1) Normal depth of burial – working point located at 100 $(kt)^{1/3}$ meters from the surface – normal cavity formation experiments; and (2) deeply buried – working point location at 400 $(kt)^{1/3}$ meters from the surface – deep cavity formation experiments.

In these sections, it is supposed that both the kiloton and megaton experiments are conducted in tuff. An actual equation of state and the associated material parameters which were obtained for a tuff from the Nevada Test Site is used (Figs. 1a, b, and c and Table I). This tuff equation of state is more complicated than a polynomial, and depends on the variables of density, stress, and rigidity modulus. Because $\eta = K_0 = \mu_0 = 1$ are already imposed by the scaling conditions, this equation of state imposes no new scaling conditions.

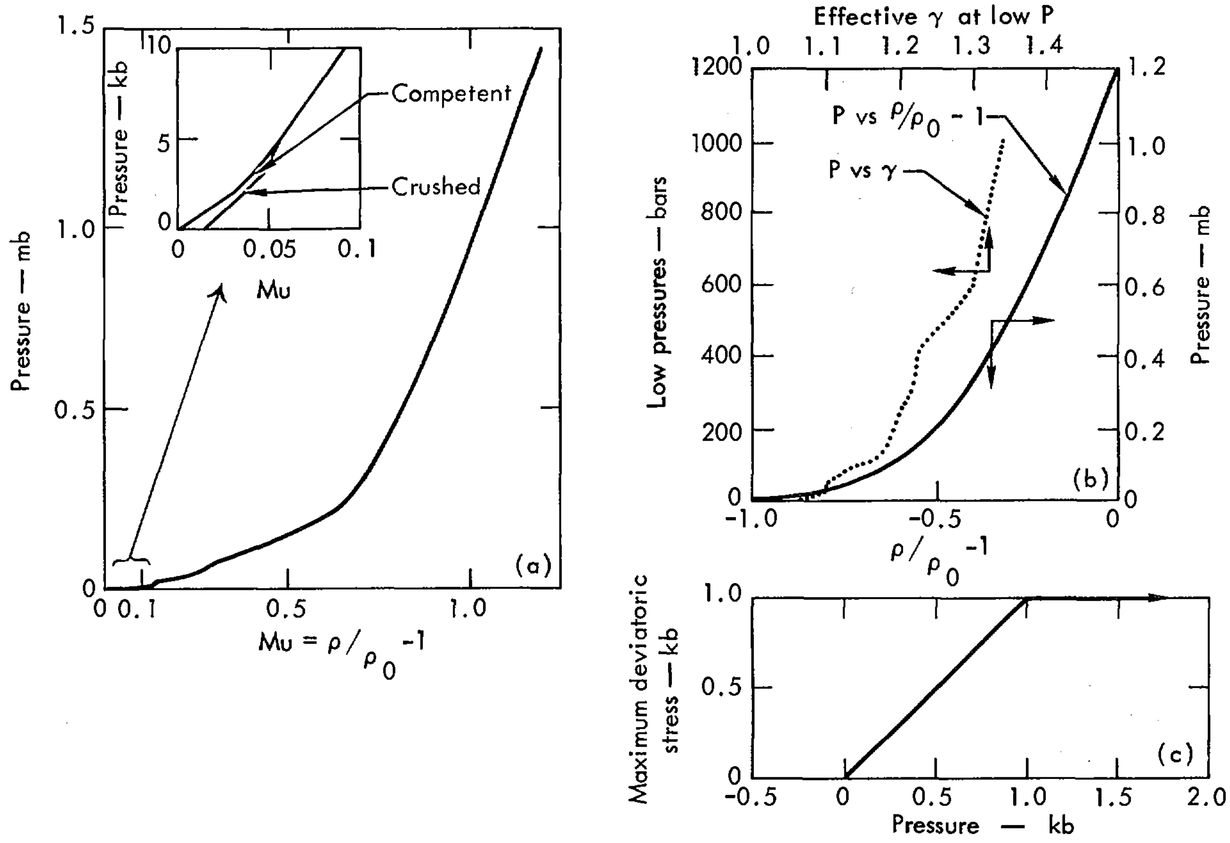

Fig. 1. (a) Pressure versus Mu = $(\rho/\rho_0) - 1$ loading curve for competent tuff equation of state. Insert shows low-pressure portion of the competent curve and the curve used for crushed material. (b) Pressure versus Mu for gas for low pressures. The effective ratio of specific heats γ has been calculated using adiabatic expansion from the P-Mu curve, and is also shown. (c) Maximum deviatoric stress versus mean stress for both consolidated and crushed material.

Table I. Equation-of-state parameters for tuff used in SOC calculations.

Initial density, $\rho_0 = 2.1$ g/cm^3

Poisson's ratio, $\sigma = 0.25$

Bulk modulus, calculated from local slope of P-Mu curve (Fig. 1a). Between 0 and 2 Kb, k = 66 Kb.

Rigidity modulus, $\mu = \frac{3}{2} k \frac{(1-2\sigma)}{1+\sigma}$

Deviatoric stress is limited by the local limiting value, K^{lim}, found in the K-P curve, Fig. 1c for both consolidated and crushed material.

For $K \geq K^{\mathrm{lim}}$ and $P < 5$ Kb, the crushed P-Mu curve in Fig. 1a is used.

Gas P-Mu is given in Fig. 1b where the effective specific heat ratio, γ, is also shown.

Elastic P-Mu curve, Fig. 1a, is used until a maximum value of Mu, (MuX), is reached and unloading starts. If MuX > 0.5, a Gruenisen type of Γ which is dependent on MuX is used to calculate the pressure during unloading. This effectively results in a series of unloading P-Mu curves which give higher pressures than the Fig. 1a curve.

The examples in the next sections show that when gravity is negligible, experiments DO dynamically scale when this general equation of state is used.

It is convenient to start rock dynamics calculations at the time when vaporization is completed. This time, which is yield-dependent, is of the order of a few tens of microseconds after nuclear time and is taken to be "zero-time" for all of both the megaton and kiloton calculations considered here. At this "zero-time," the calculations assume that the total energy yield is homogeneously contained within the vaporized region. Butkovich[17] indicates that the radius of vaporization, R_V, for 1 kt in tuff is approximately 220 cm, and that R_V scales as the cube root of the energy yield. If $R_V = R_V' (E/E')^{1/3}$ and if the energy is homogeneously distributed over R_V, then the necessary condition $\epsilon_0 = 1$ is satisfied.

Using $R_V' = 220$ cm, $E' = 1$ kt and $E = 1$ Mt, $R_V = 2200$ cm. Therefore, the distance scaling factor is $R_0 = R/R' = 10$, and the time scaling factor is $t_0 = R_0 = 10$. These initial conditions are used in the following kiloton-megaton SOC calculations that are outlined in Table II.

(When radiation is included in the SOC energy equation, it can be shown that radiation mean free paths and dimensions must use the SAME scaling factor.[18] Thus, when radiation is significant, dynamic scaling is nearly impossible. The initially vaporized, homogenous, energy source region assumed here is a useful approximation; however, it is not presently known how closely this approximates reality.)

Table II. Initial conditions for SOC calculations

Name	Total Energy (kt)	R_V (m)	R_{sur} (m)	Gravity
Section IV. Normally buried cavity production calculations:				
4-K-O	1	2.2	100	No
4-M-O	1000	22	1000	No
4-K-g	1	2.2	100	Yes
4-M-g	1000	22	1000	Yes
Section V. Deeply buried cavity production calculations:				
5-K-O	1	2.2	400	No
5-M-O	1000	22	4000	No
5-K-g	1	2.2	400	Yes
5-M-g	1000	22	4000	Yes

Between $R = 0$ and $R = R_V$, the vapor radius, the gas P-Mu curve (Fig. 1b) is used with initial energy/volume = 0.94×10^{12} mb, pressure = 1.2 mb, and density = 2.1 g/cm^3.

Between $R = R_V$ and $R = R_{sur}$, the free surface, initially competent tuff (Figs. 1a, 1c and Table II) is used with initial density - 2.1. Initial pressure is either zero or overburden pressure when gravity is considered.

IV. SCALING OF NORMAL CAVITY EXPERIMENTS

Results of the SOC calculations are considered here for experiments with depths of burial of 100 m (for 1 kt) and 1000 m (for 1 Mt) (Table II). Figures 2a, b, and c show pressure versus distance from the kiloton SOC calculation at times of 5, 15, and 33 msec, respectively. These same figures

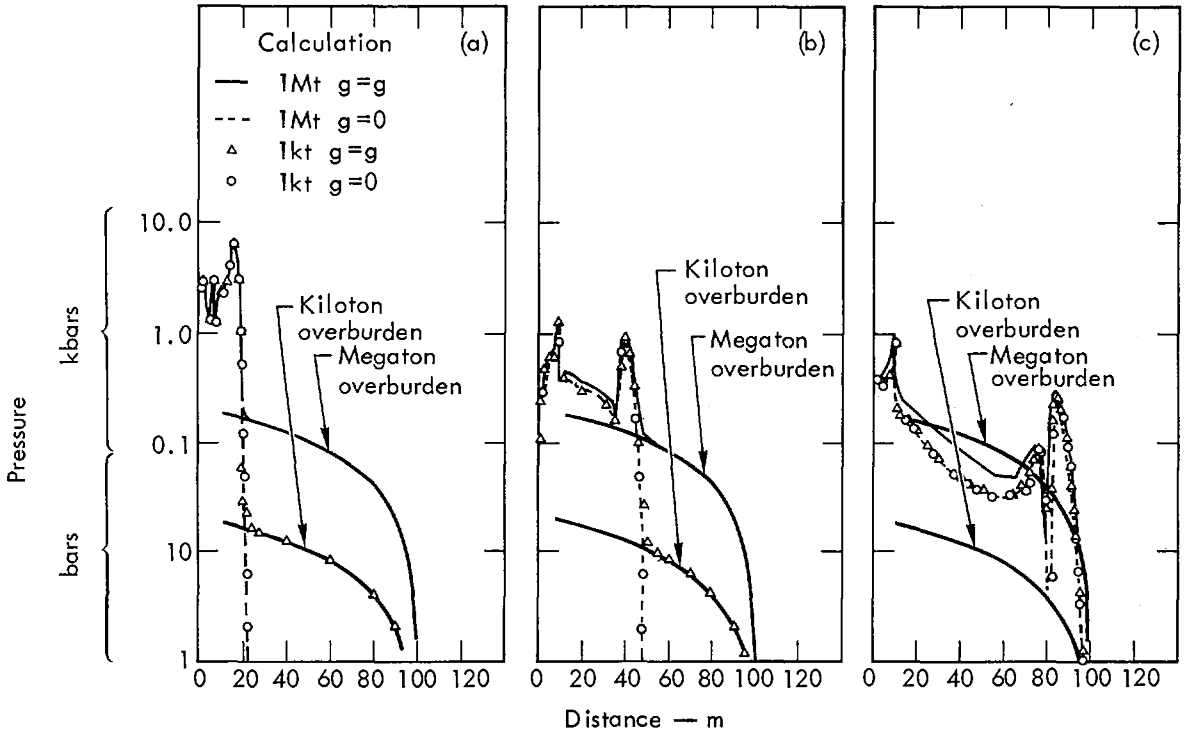

Fig. 2. Pressure versus distance for the normally buried kiloton and megaton SOC calculations respectively at: (a) 5 and 50 msec; (b) 15 and 150 msec; and (c) 33 and 330 msec.

also show the results of the megaton calculation at times (note: time scaling factor $t_0 = 10$, Section III) of 50, 150, and 330 msec, respectively. The radial distances in Figs. 2 represent 1/10 of the actual radial distance for the megaton results (distance scaling factor $R_0 = 10$, sec Section III).*

Figure 2a shows that at 5 and 50 msec the SOC results are identical, and hence the experiments scale. However, Figs. 2b and c indicate that the results diverge at later times when the shock is nearing the surface. The reason for this divergence at later times is attributed to the presence of overburden pressures which are no longer negligible in the region behind the shock in the megaton calculation. From the megaton calculation, the ratios of overburden pressure to pressure behind the shock (see Figs. 2) at 50, 150, and 330 msec is approximately 0.1, 0.5, and 1.0, respectively. The ratios of overburden pressure to pressure behind the shock from the kiloton calculation at 5, 15, and 33 msec are approximately an order of magnitude less than the above ratios. Hence, the kiloton calculation is virtually independent of gravity until the shock reaches the surface (at about 38 msec).

---

*In the following, whenever the kiloton and megaton results are shown together, this same technique of plotting at real values of time and distance for the kiloton results and at real time and distance values divided by 10 for the megaton results is used. Since $P_0 = U_0 = \rho_0 = K_0 = 1$, this plotting technique results in identical curves for the flow variables as long as the solutions are similar; that is, as long as the experiments scale.

To verify that gravity acting in the megaton calculation is what causes the loss of similarity, two additional SOC calculations which used the acceleration of gravity set to zero are also shown in Figs. 2. These no-gravity calculations continued to give identical solutions until they were terminated. Therefore, extraneous calculational errors are not causing the observed lack of similarity. In Figs. 2, the calculations without gravity are seen to agree closely with the kiloton gravity calculation.

In Figs. 3a and 3b the maximum mean pressure and maximum particle velocity, respectively, are plotted versus radial distance. It can be seen that by assuming dynamic scaling to hold, reasonable estimates can be made for maximum pressures and particle velocities in normally buried cavity experiments. The actual slopes of the scaled points depends on the equation of state of the material.

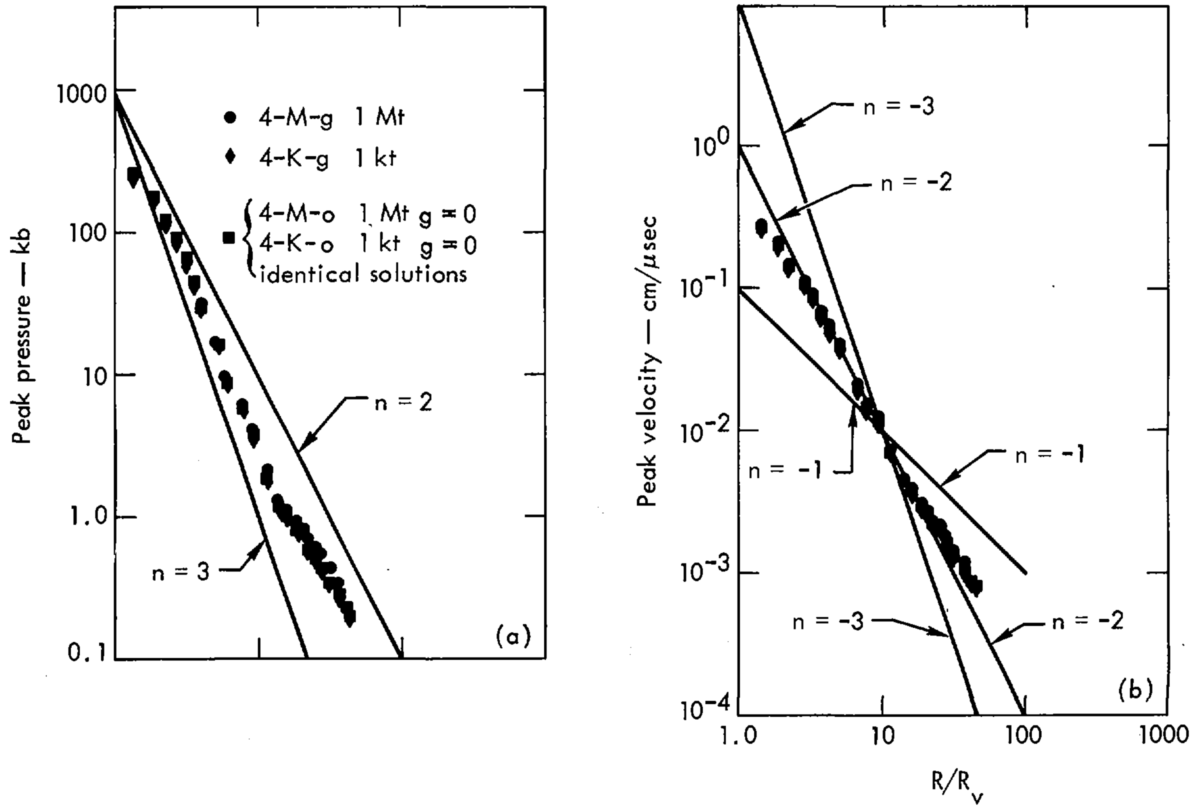

Fig. 3. (a) Maximum pressure versus distance for normally buried kiloton and megaton SOC calculations. (b) Maximum particle velocity versus distance for normally buried kiloton and megaton SOC calculations.

After the shock reaches the surface, a rarefraction wave moves back toward the cavity and relieves the pressures in the material between the cavity and the surface. This rarefraction wave travels at approximately local sound velocity in the tuff, and reaches the kiloton and megaton cavities at approximately 80 and 800 msec respectively. After the rarefraction wave releases pressures in the mound above the cavity, the cavity may continue to expand until cavity pressure is reduced to a value as low as overburden pressure. Because overburden pressure in the megaton calculation is ten times overburden in the kiloton calculation, scaling of the two calculations degenerates when the cavity pressures approach overburden pressures.

However, the late-time cavity pressure need not decrease to overburden pressure. The late-time cavity growth and pressure depends directly on the relatively little-known properties of the material which immediately surrounds the cavity at late times. At late times, deviatoric stresses can develop in the material immediately surrounding the cavity. These stresses can inhibit cavity growth, and enable the cavity to sustain pressures considerably above overburden. Such material properties as: improved equations of state (particularly for the cavity gas and the melted regions); yield strength criteria; pressure unloading of the yielded material; stress-strain relations for the yielded material; and in situ values for the elastic moduli of both the competent and the failed materials are examples of properties which become significant for determination of the final cavity size. More complete information about material properties will enable better prediction of the final cavity size.

Figures 4 and 5 show the radii and pressure of the cavities versus time from the kiloton and megaton SOC calculations with gravity. SOC is a one-dimensional calculation, and its validity for times after the shock reaches the surface is questionable. However, a one-dimensional calculation overestimates the effect of the rarefraction; and SOC indicates an earlier release of cavity pressure, a lower final cavity pressure, and a larger final cavity size

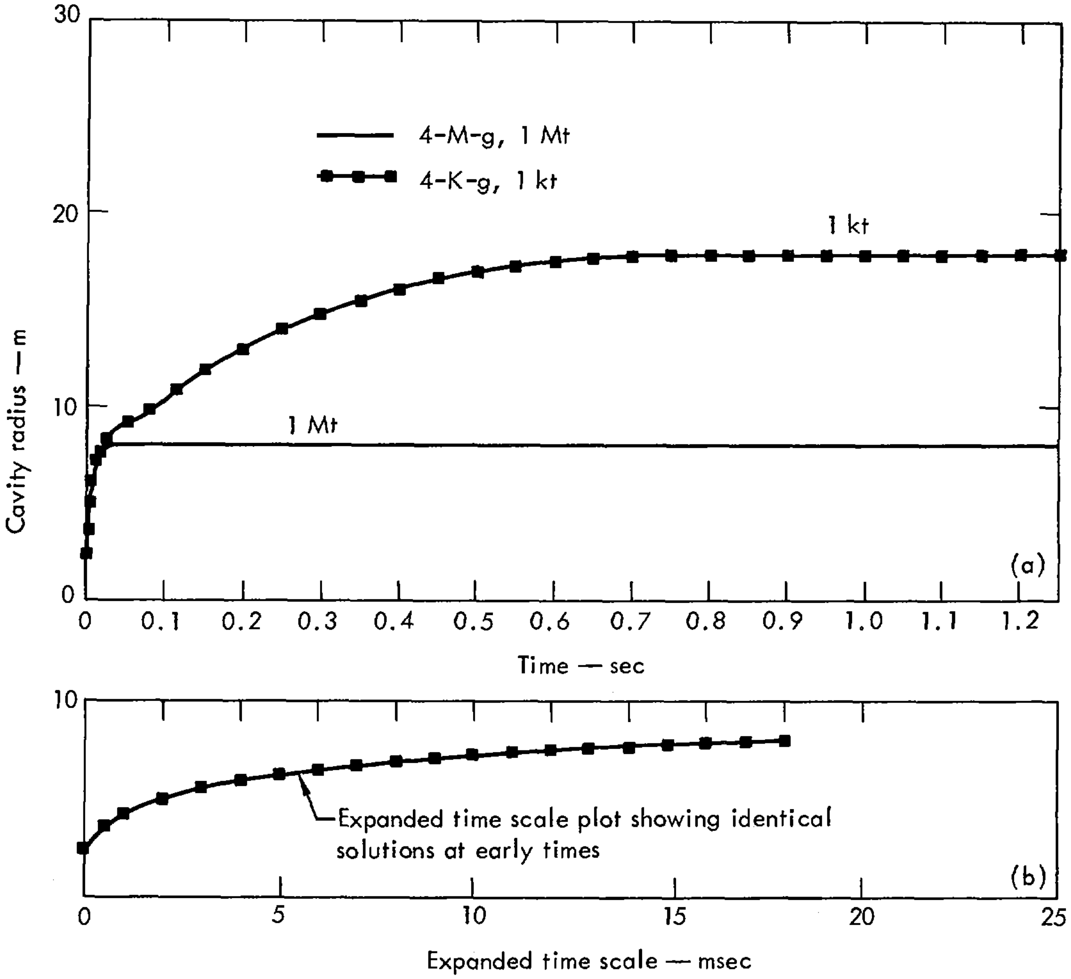

Fig. 4. (a) Cavity radius versus time for the normally buried kiloton and megaton SOC calculations with gravity. (b) Expanded time scale showing identical solutions at early times.

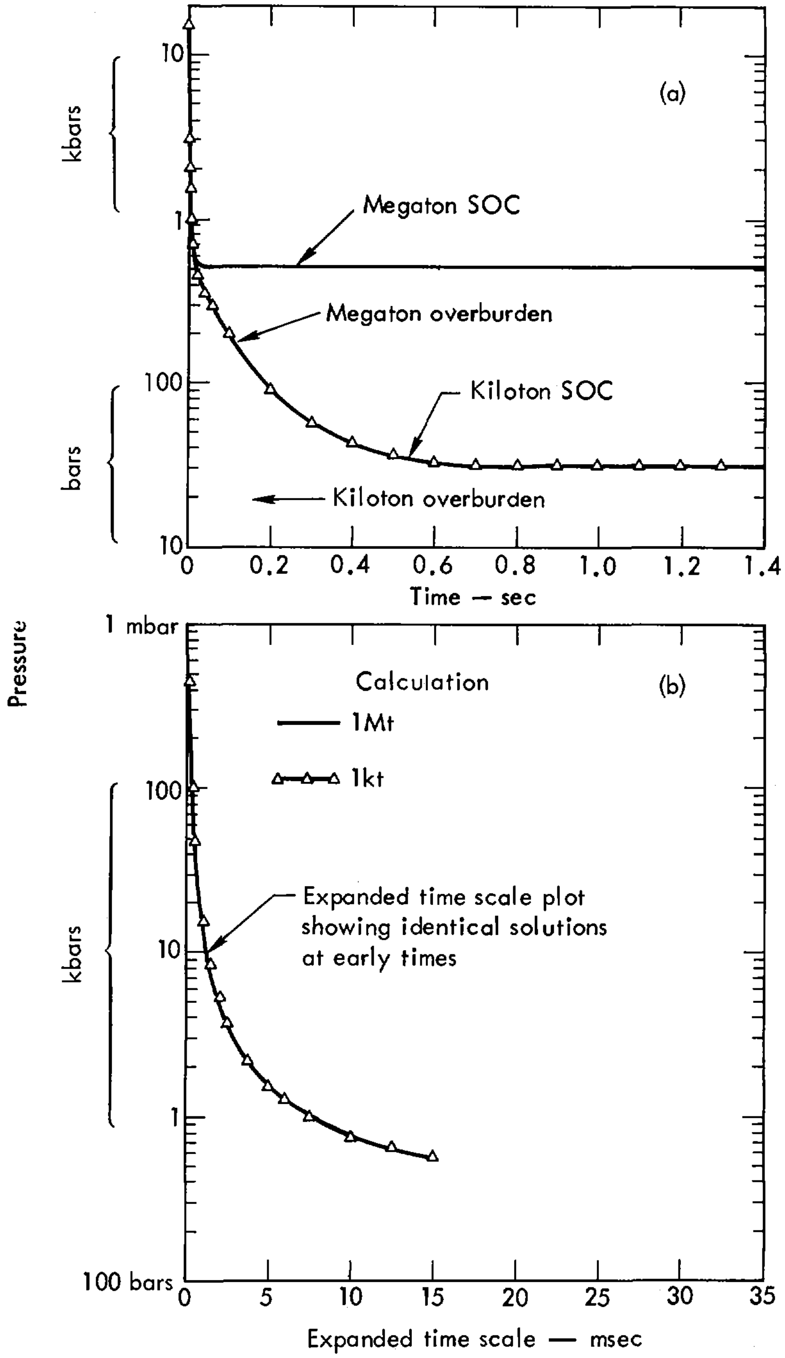

Fig. 5. (a) Cavity pressure versus time for the normally buried kiloton and megaton SOC calculations with gravity. (b) Expanded time scale showing identical solutions at early times.

than is actually expected in three dimensions. Thus, Fig. 5 indicates that the cavity pressure in the megaton cavity could remain at 2.5 times overburden pressure at late times of second.

V. SCALING OF DEEPLY BURIED CAVITY EXPERIMENTS

This section considers SOC calculations of the kiloton and the megaton experiments with depths of burial of 400 and 4000 meters respectively (Table II).

Figures 6a, b, c, and d show the pressure versus distance at times of 1, 10, 50, and 150 msec from the kiloton, and at times of 10, 100, 500, and 1500 msec from the megaton calculation. These calculations indicate the tendency for the pressure in front of the cavity and behind the shock to "seek" overburden pressures.

The results from a kiloton and a megaton SOC calculation without gravity, also shown in Figs. 6, are identical throughout.

Figures 7a and b show respectively the peak pressure and peak overpressure versus distance from the working point. These figures indicate that predictions of peak pressure, which are based on scaling, can be substantially

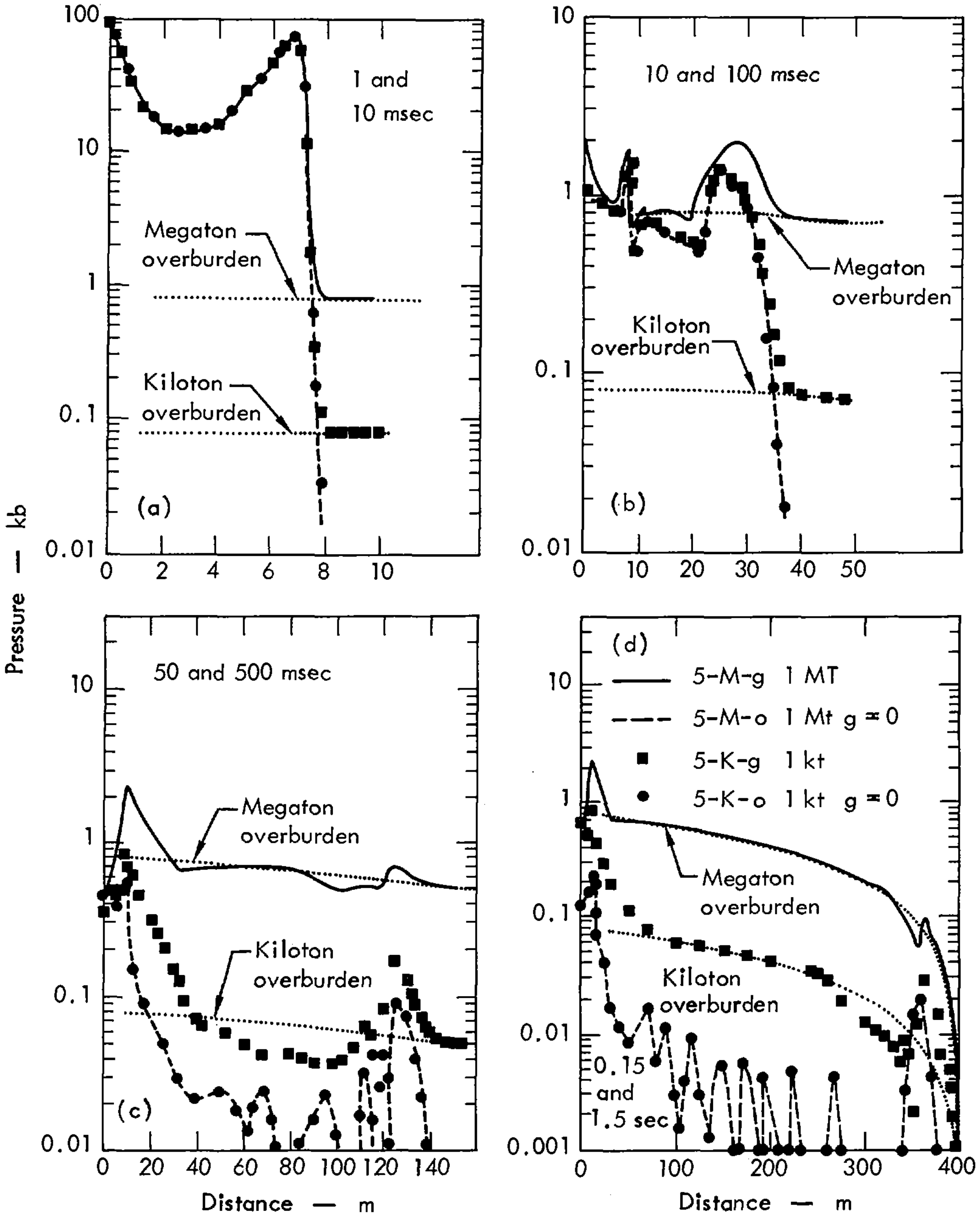

Fig. 6. Pressure versus distance for the deeply buried kiloton and megaton SOC calculations respectively at: (a) 1 and 10 msec; (b) 10 and 100 msec; (c) 50 and 500 msec; and (d) 0.15 and 1.5 sec.

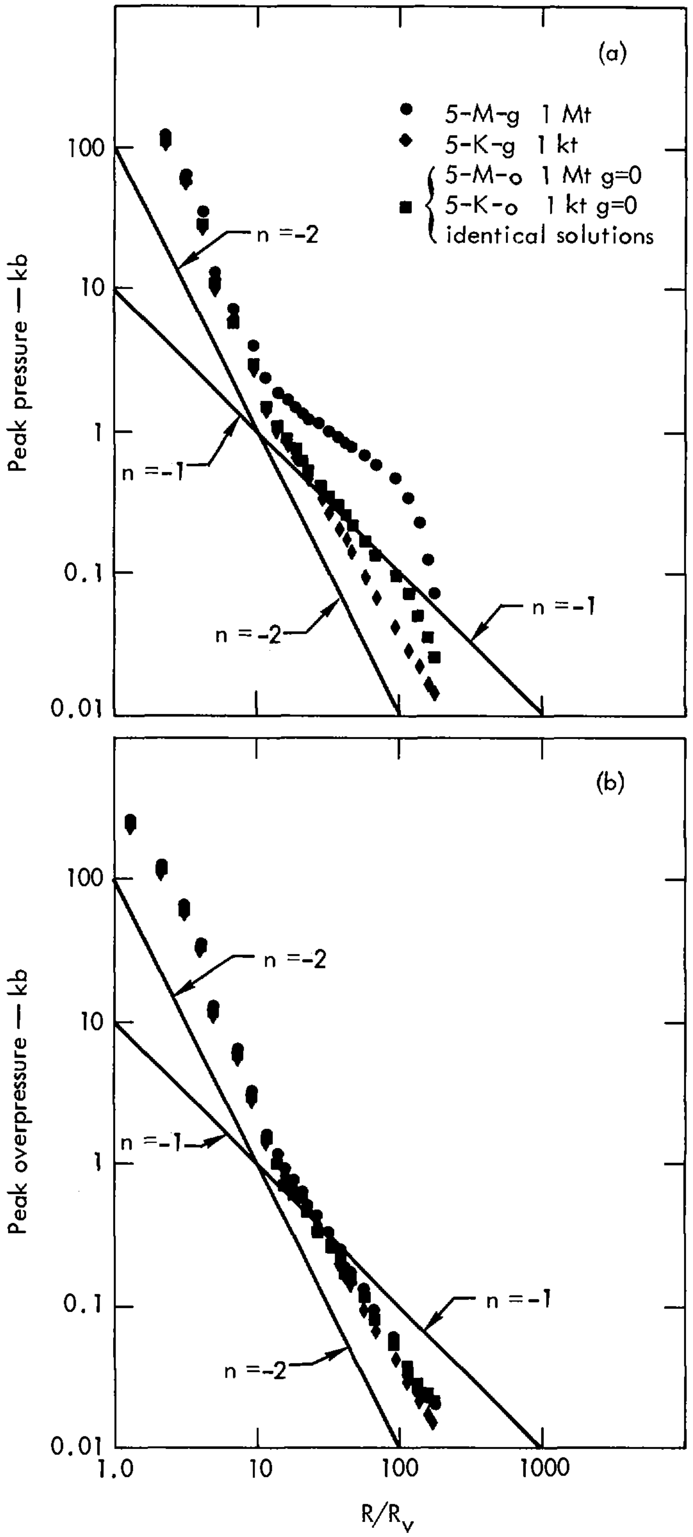

Fig. 7. (a) Maximum pressure versus distance for deeply buried kiloton and megaton SOC calculations. (b) Maximum overpressure versus distance for deeply buried kiloton and megaton SOC calculations.

in error for deeply buried experiments where overburden is large. However, the peak overpressure does scale reasonably well. Figure 8 indicates that peak velocities can also be reasonably estimated by assuming scaling.

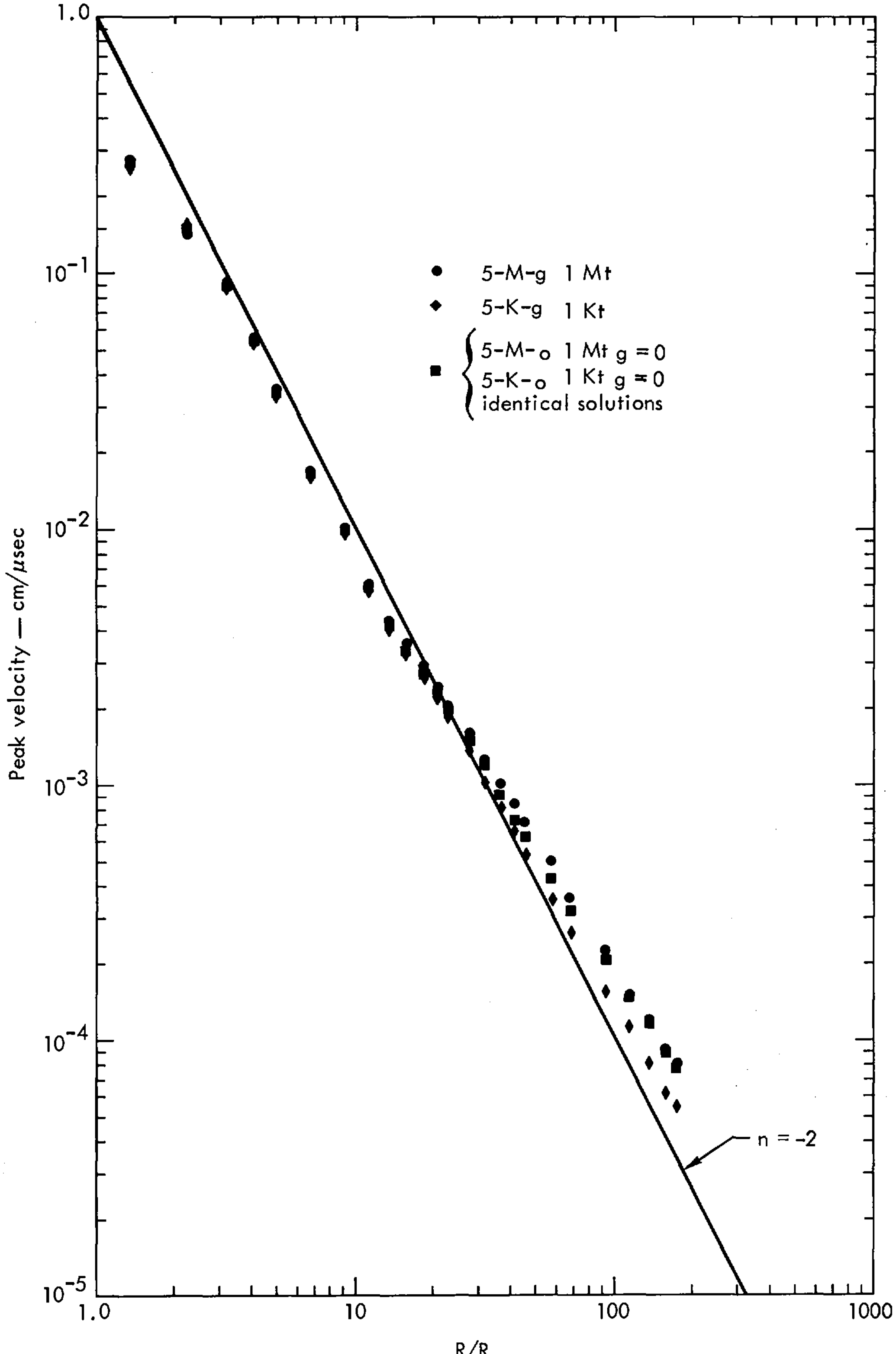

Fig. 8. Maximum particle velocity versus distance for deeply buried kiloton and megaton SOC calculations.

ACKNOWLEDGMENTS

Thanks are very gratefully tendered to: J. T. Cherry, L. S. Germain, G. H. Higgins, J. B. Knox, J. H. Nuckolls, R. F. Rohrer, and R. W. Terhune for many helpful discussions; to F. L. Peterson, E. A. Reed, and to S. L. Skoog for the calculations and plotting.

REFERENCES

1. P. Kruger, "Nuclear Civil Engineering," Dept. of Civil Engineering, Stanford Univ., Tech. Report No. 70, 1966.
2. C. R. Boardman, D. D. Rabb, R. D. McArthur, "Characteristic Effects of Contained Nuclear Explosions for Evaluation of Mining Applications," Lawrence Radiation Laboratory, Livermore, Report UCRL-7350, 1963.
3. M. D. Nordyke, "Cratering Experience with Chemical and Nuclear Explosives," Lawrence Radiation Laboratory, Livermore, Report UCRL-7793, 1964.
4. A. J. Chabai, "Crater Scaling Laws for Desert Alluvium," Sandia Laboratories, Albuquerque, New Mexico, Report SC-4391, Dec. 1959.
5. A. J. Chabai, J. Geophys. Res., 70, [No. 20], 5075 (1965).
6. L. I. Sedov, Similarity and Dimensional Methods in Mechanics, (Academic Press, New York, 1959).
7. G. I. Pokrovskii and I. S. Fedorov, Effect of Shock and Explosion on Deformable Media, (Gos. Izd., Moscow, 1957).
8. R. B. Vaile, Jr., "Crater Survey," Operation Castle Report WT-920, 1955, later partially reprinted in J. Geophys. Res. 66, 3413 (1961).
9. C. E. Violet, J. Geophys. Res. 66, 3461 (1961).
10. J. T. Cherry, Intern. J. Rock Mech. Min. Sci., 4, 1 (1967).
11. J. T. Cherry, D. B. Larson, E. G. Rapp, "Computer Calculations of the Gasbuggy Event, Lawrence Radiation Laboratory, Livermore, Report UCRL-50419, 1968.
12. J. Von Neumann and R. D. Richtmyer, J. Appl. Phys. 21, 232 (1950).
13. G. Birkhoff, Hydrodynamics: A Study in Logic, Fact and Similitude, (Princeton Univ. Press, Princeton, New Jersey, 1960).
14. L. Rosenhead, (editor), Laminar Boundary Layers, (Oxford at the Clarendon Press, 1963).
15. B. K. Crowley, "Necessary Conditions for Similar Solutions of Problems of Turbulent-Gas Dynamics," Lawrence Radiation Laboratory, Livermore, Report UCRL-50211, 1967.
16. G. Galilei, Dialogue Concerning the Two Chief World Systems-Ptolemaic and Copernican, transl. by Stillman Drake, (Univ. of Calif. Press, Berkeley, Calif., 1953).
17. T. R. Butkovich, "The Gas Equation of State for Natural Materials," Lawrence Radiation Laboratory, Livermore, Report UCRL-14729, 1967.
18. S. I. Pai, Radiation Gas Dynamics, (Springer-Verlag Inc., New York, 1966).

APPENDIX A — NOTATION

a, a_1, a_2, b_1, b_2	coefficients in equation of state
e	strain
g	acceleration of gravity
K	deviatoric stress
P	pressure
R	radial distance
t	time
v	velocity
V	volume
V^0	initial volume
ϵ	energy/initial volume
η	compression
μ	rigidity modulus
ρ	density

Generally the subscript zero (0) refers to dimensionless scaling parameters.

XA04N0853

NUCLEAR ECOLOGY

OR

CAN A LIBERAL BE A CONSERVATIONIST?

Dr. Edward Teller
University of California, Lawrence Radiation Laboratory
Livermore, California

The question of pollution is serious; we must do something and that is one of the very few things on which practically everybody in the United States, young or old, Democrat or Republican, is agreed. It is important to do something about clean air and clean water. At the same time, any good cause can be exaggerated, even conservationism can be exaggerated.

There are those who worry about a slight rise in temperature and call it thermal pollution. I, for one am for thermal pollution in the winter.

I like to think about myself as a progressive; and I like to imagine that the best possible state of the world is not the present state, not even the past state. With imagination, with work, with restraint, with proper thoughtfulness, we can make sure that the future will be better than the present and the past.

On generalities it is easy to agree. Specifics raise more problems, and so it is in the case of Nuclear Ecology. The use of nuclear energy, and particularly, the use of nuclear explosives for peaceful purposes can produce harmful effects, and of these there is one which already has received a great deal of attention and which seems to receive increasing attention at the present time—radioactive contamination.

I would like to tell you a few things about radioactive contamination and also about the question: What can Plowshare, the constructive use of nuclear explosives, do for all of us? In what manner can it make life more abundant and also, particularly, can it make our environment more clean?

Radioactive contamination is frightening; its horrors have excellent spokesmen, like Linus Pauling. It is disquieting because the danger of radiation itself is something of which our senses give no warning, and at the same time, the damage that has been discussed does exist.

Radioactivity is also frightening by association. It is connected with the atom—with nuclear explosions—and this association of ideas is, of course, closer in the case of Plowshare than in other cases. Radioactivity is, furthermore, frightening in a very practical sense because radiation can be so easily detected, not by our senses, but by our instruments. While you have seen nothing of it, felt nothing of it, somebody can come along with a Geiger counter and show you: it clicks, get scared! What can be more frightening in this day and age than a piece of apparatus that clicks in an ominous manner?

There are also reasons, clear and simple reasons, why radioactivity need not be frightening when proper care is exercised. This is so, in the first place, precisely because of these clicking pieces of apparatus. What can be easily discovered by a simple counter can be easily guarded against.

But there is more than that to it; life is full of danger. In fact, I can think of nothing as dangerous as life. And, in life, I am really scared of the microorganisms and of chemistry. I am scared of these because two microorganisms which appear similar might be very different in their effect upon us. Two similar molecules may differ so greatly in their effects that one is a useful medicine and the other is a deadly poison. At the same time the actual chemical difference consists in a rather small rearrangement of the constituent parts of the molecule. It is very difficult for chemists to predict which will act in which way, and it takes a long and arduous research enterprise to find out whether a certain kind of sugar substitute is indeed dangerous or not.

With radiation it is very different. In good approximation one can say that all radiation acts alike. If, in a certain cell a certain amount of high energy radiation is deposited, the effect is similar, whether the energy has been deposited by alpha particles, by beta particles, by gamma particles, by cosmic rays, by neutrons, or by any other hard radiation. Possible harmful effects of radiation can therefore be evaluated much more simply in a much more complete and reliable manner.

All of us, including our ancestors who lived in the trees, those who went around on four legs, those who swam in the oceans, and even those who were in the monocellular state, all of them have been exposed to some radiation. On the average, this radiation was constant ever since the human race existed on earth. The present guidelines which regulate the safety of radiation prescribe that we should add no more than one hundred percent to the natural background or more precisely to the radiation which we get anyway. This limit is to be applied separately to each tissue in the human body.

It is an interesting footnote, that people who are foolhardy enough to live in Colorado—who spend their lives closer to the sky, the source of cosmic rays and who are in greater proximity of uranium deposits—are exposed to almost as much radiation as the Atomic Energy Commission permits. Many thousands of people in Brazil and in the Kerala Province of India are exposed, and have been exposed for centuries to ten times as much as the maximum permissible dose. Maybe they suffer from it, but they are backward people and they suffer from being backward much more. Thus their additional suffering on account of radiation has not, as yet, been verified.

I am a progressive; I believe in progress. I am also a conservationist, and I believe in clean air and clean water. I also know that only in case of radioactive contamination have we demanded that the pollutant be essentially no more than the natural amount to which all of us would have been exposed in the original pristine natural state—if indeed anybody can tell me precisely what the word "natural" means. Imagine that similarly stringent conditions should be imposed on all materials which cause pollution. Automobiles would, of course, be banned. The same would hold for our power plants, except the hydroelectric plants and the nuclear plants. Our industry would be reduced to a negligible fraction of what it is today, and I am also a little uncertain what would happen to the production of iron.

All this should at least in part be considered in a serious manner. One may hope that in the foreseeable future most of the electricity will be produced by nuclear reactors. Electricity may become cheap enough to be used for space heating, thus eliminating further contamination due to burning of coal and oil. It is not impossible that electricity will play a greater role for providing motive power in the transportation of people and one might even hope that with cheap electricity aluminum that can be cheaply produced in a clean way by electrical processes will replace iron to some extent. In all of these ways contributions can be made to greater cleanliness although the transition will necessarily take a long time if it is to be executed at a reasonable cost. At the same time, it should be remembered that the needed growth of nuclear energy consumption will be accompanied by some release of radioactivity. These releases have been held to minimal values and standards similar to those prevailing at present can be enforced with proper and continuous care. Thus we can fight pollution whenever it becomes serious—provided we do not introduce unnecessarily rigid limitations on radioactive releases, but are satisfied with the standards which are based on the long experience of all human existence and on the even longer history of the living world.

The fight against pollution has entered into a particularly popular phase but thoughts on pollution are older. In 1954 Otto Frisch, one of the discoverers of fission, wrote a short parody on the safety measures connected with nuclear reactors. He pretends that in the year 4995 the uranium and thorium mines from the earth and moon mining systems near exhaustion and says:

> The recent discovery of coal (black, fossilized plant remains) in a number of places offers an interesting alternative to the production of power from fission. . . . The power potentialities depend on the fact that coal can be readily oxidized, with the production of a high temperature and an energy of about 0.0000001 megawatt day per gramme. . . .

Further on, he remarks:

> The main health hazard is attached to the gaseous waste products. They contain not only carbon monoxide and sulphur dioxide (both highly toxic) but also a number of carcinogenic compounds such as phenanthrene and others. To discharge those into the air is impossible; it would cause the tolerance level to be exceeded for several miles around the reactor.

These words sound to me a little more appropriate than some recent discussions.

But let us return to the particular role that the constructive uses of nuclear explosives can play in improving our ecology.

In order to clean up our continent, in order to keep the civilized world free of dangerous contamination, we not only should tolerate Plowshare—we need it. Plowshare can make positive contributions to cleanliness; and the words "nuclear ecology" should not mean that the use of Plowshare must be further restricted, it should mean that Plowshare must be expanded to fulfill its proper purposes. It is true that if we should not exercise careful control we would be in trouble; but no big-scale enterprise has ever been carried out with as much assurance to human health, to human life and cleanliness as the atomic energy enterprises.

Where are the positive uses? We are engaged in producing more natural gas. The amount of the natural gas in the United States which we now have available will keep us supplied at the present rate of usage for less than 15 years. Yet, natural gas is valuable, because it contains practically no sulphur and, therefore, it is one of the cleanest fuels that we can use. Los Angeles has to use it almost exclusively. New York would like to use it; but because there is not enough of it, New York must burn more sulphur-containing fuels. At the time of any extended period of atmospheric inversion in

New York (when released contaminants stay near their source of origin), statistics show that there are several hundred excess deaths in New York hospitals. I cannot say that this is proven, but according to the figures I have seen, the correlation is impressive.

There is once again as much natural gas in the United States than the amount I have already mentioned; only, this additional one hundred percent is contained inside tight rock formations from which we cannot extract the gas in an economical manner. By exploding a nuclear device a few thousand feet underground, one can loosen up the rock formations and produce the appropriate rubble chimneys. Thus we have an excellent chance to make these additional amounts of gas available.

We have actually performed an experiment in breaking up rock and stimulating gas production. The name of the experiment was "Gasbuggy" and it was performed near the "Four Corners" where the states of New Mexico, Arizona, Utah and Colorado meet. A nuclear explosive was buried 4,000 feet under the surface in a gas-bearing formation. The general arrangement and the chimney of broken rock is shown in the schematic Figure 1, together with the arrangement of several chimneys which could be utilized in a systematic exploitation of a gas-bearing tight formation.

This experiment was carried out December 10, 1967, and it was a success in that it produced more gas and gas carrying less radioactivity than we had expected. The photograph shown in Figure 2 was taken one day after the explosion. The red balloons mark the spot. It is very clear that the nuclear explosion did not cause the end of the world, not even in a strictly local sense. In the meantime an attempt is being made in Colorado for the massive exploitation of gas production by the same principle. It is too early to say whether or not this will succeed in the near future. In the long run I have little doubt of success.

Another similar example is the following: Gas is consumed in our big cities and the demand is much greater when there is a cold spell. Gas is brought in by pipelines. We need storage space for this gas, and on the eastern seaboard all the natural storage space has been exhausted. We could produce lots more storage space by nuclear explosions. Similar storage places could be used in any location where gas is brought in by ships in a refrigerated form. The storage space could be established below the sea bottom on the continental shelf and could be brought in to population centers by relatively short pipelines.

In connection with the general power economy, I should mention one more example. It is a 10-year old dream, and I hardly believed it 10 years ago. My good friend at the University of California, Los Angeles, Dr. George Kennedy, was its first apostle; my colleagues in the Livermore branch of the Lawrence Radiation Laboratory have been converted by him.

In many places there is a lot of usable heat underground; in Italy, in New Zealand, even in California, some of the accessible heat has been used as a power source. But this amounts to a dribble. Deep underground, much geothermal heat can be found. Logically enough, there seems to be a lot of it around extinct volcanoes, some of which are located all along the Pacific coast in the northwest part of the United States. A nuclear explosion could be used not so much to produce heat but to open up this geothermal reservoir. The explosion would produce a rubble cone, expose a lot of surface of the hot rock so that we can pump water down, convert it into steam and use it. All this could be done in a closed cycle, and hopefully no radioactivity need escape. We might get a source of energy as clean, as power from a waterfall.

I would like to mention just one more example connected with ecology. I have already told you that we can make holes deep underground, open spaces, or partly open spaces. These spaces can be produced cheaply in many locations and we can use them for waste disposal. We can remove dirt from the biosphere. We must dispose of the by-products which we throw away each day. The most inaccessible place, the place best isolated and yet reached when needed could be established a couple of thousand feet right under the surface of the earth. Places could be selected where no ground water would get to them, and where the dirt would never bother us again—at least not for the next few million years.

The word ecology has a somewhat flexible meaning. One might be justified in including the question of how to improve the conditions of life for people in general. There are many people in the world and there will be more; a good life for the billions is, in the end, our great problem, and water is one of the most important necessities for a good life. Plowshare can be used to divert streams to store water, even possibly to distill water underground using, again, geothermal heat. If there is a real way to make the desert bloom, I think that Plowshare is the best candidate to accomplish this goal.

It is also worthwhile to reflect on a general class of necessities of our modern civilization: raw materials. By using new methods of shattering the rocks deep underground and of employing liquid extraction methods, some important raw materials could be obtained. In the case of copper, a method utilizing weak acid solution has been worked out. In other cases it will take more research to find proper methods.

Decades ago scarcity of raw materials was considered the main reason for international conflict and eventually for war. Today this problem has been displaced in people's minds by the danger of the nuclear weapons. One should not forget, however, that nuclear explosives might be used to supply human needs and thereby decrease the reasons for international conflict.

Along similar lines, one may remember the increasing role that big oil tankers play in the cheap distribution of the necessities of modern life. Many new ships have a displacement of 300,000 tons and ships of 700,000 tons are on the drawing board. Compared to these carriers, one may consider the "Queen Mary" as an oversized canoe. These carriers

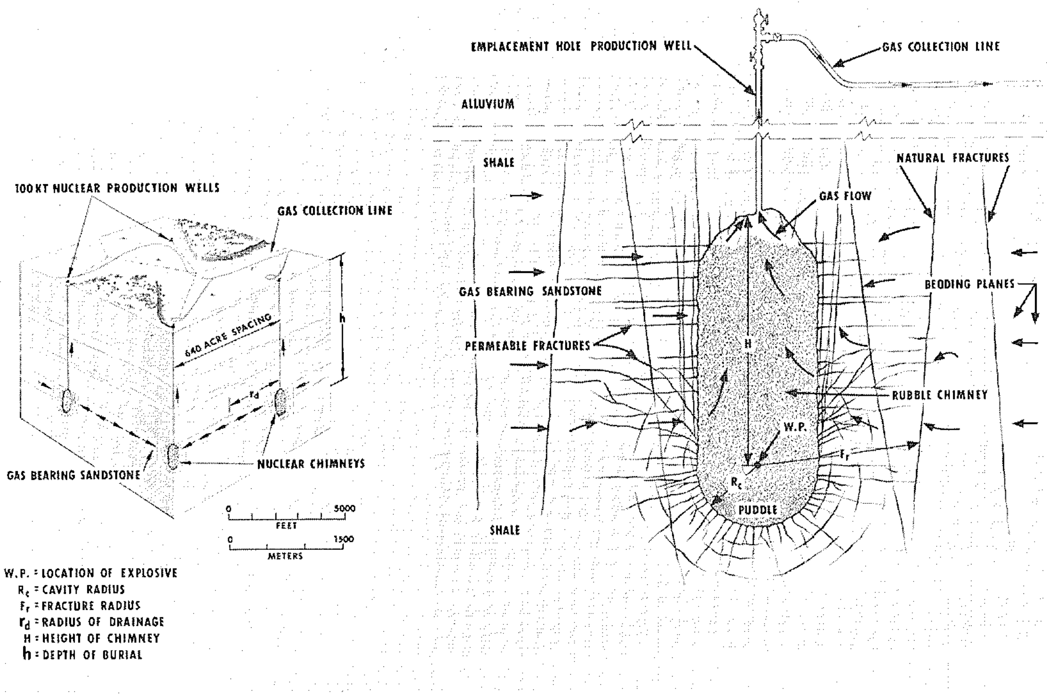

Fig. 1—Gas Reservoir Stimulation.

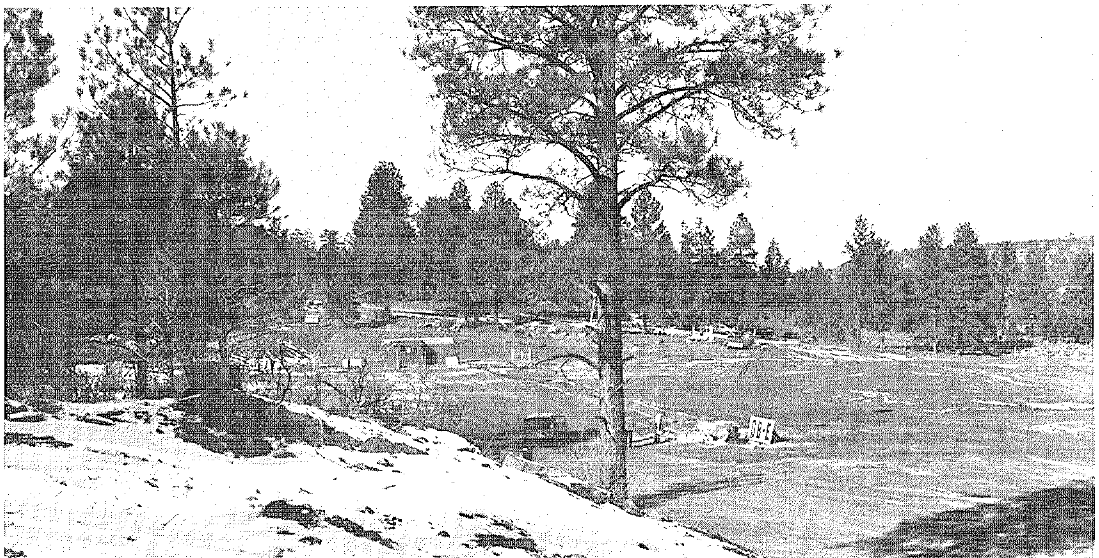

Fig. 2—Gasbuggy surface zero one day after detonation.

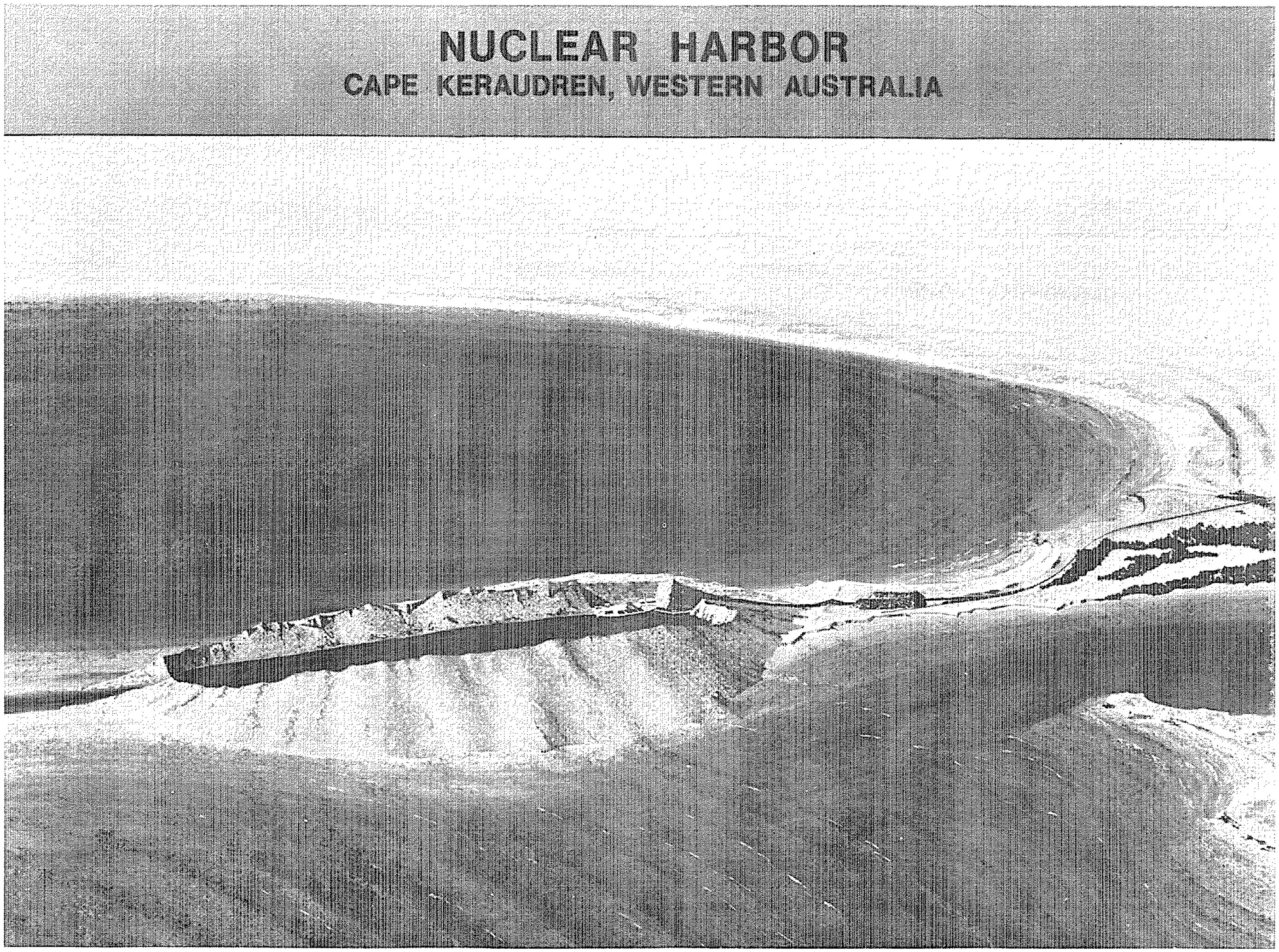

Fig. 3—The Concept of a Nuclear Harbor.

may become important not only to transport oil, but to haul iron ore from the abundant deposits of Northwest Australia to all corners of the world. The difficulty is that neither our canals nor our harbors can accommodate these new monstrous ships. Plowshare may be the best means by which to create the appropriate waterways and the necessary harbor facilities.

Figure 3 shows the concept of a nuclear harbor. By a number of simultaneous explosives placed in a row, one can produce an elongated crater whose rim would rise above the waves and would also serve as a windbreak. The entrance of this artificial crater could be adjacent to water of a depth of little more than 100 feet, thus permitting the biggest ships to enter. If a causeway to the shore is needed, as shown in the figure, it would probably be located in shallow water and might be constructed by conventional means.

Ambitious plans for canals through which big ships could pass have been discussed. One extensive discussion is centered around a new canal connecting the Atlantic and Pacific oceans. The map showing this region and the location of two promising routes is shown in Figure 4. Thus it is possible that by shipping, and indirectly, by the use of Plowshare, the economy of the world can become more united and more efficient.

I want to conclude by returning to the question of the association between Plowshare and nuclear weapons. There is no doubt that this "guilt by association" does influence, consciously or otherwise, the feelings of many people. Nuclear explosions killed people—women and children—at the end of the Second World War. They are now considered as weapons of terror; they must be banned and not be used for anything.

I want to remind you of a remarkable historic parallel, one that is known but perhaps not sufficiently recognized. I refer to a horrible, ancient weapon, a weapon more than 1,000 years old, the "Greek Fire", a mixture considered mysterious because it caught fire on contact with water; it was this "Greek Fire", an invention of the eastern Roman Empire, which turned back the first Arab invasion and which saved the eastern half of the Roman Empire and kept it safe for hundreds of years. The weapon was effective; it also was considered horrible. It was outlawed and this limitation stuck. Constantinople lost its defenses; in the end it fell.

The Greek Fire also happened to be the first really impressive use of chemical energy in human affairs, the first big step beyond the most primitive and the most important control of fire itself. I suspect that suppression of Greek Fire, the fact that Greek Fire was not only outlawed but kept secret, delayed the industrial development of the world by almost a millennium. If the discovery of the Greek Fire would have evoked more interest and less horror, more openness and less secrecy, the dark ages may have been avoided.

I think progress cannot be and will not be stopped, and I know that Plowshare will proceed. Whether it will proceed as rapidly as it should, whether it will proceed in the United States or in some other part of the world, these are most important questions of detail that we should consider with some care.

Today those conservationists who have become reactionary, who are opposed to all progress, who seem to believe that everything that is good lies in the past, may bring about another dark age. I hope that they will not succeed.

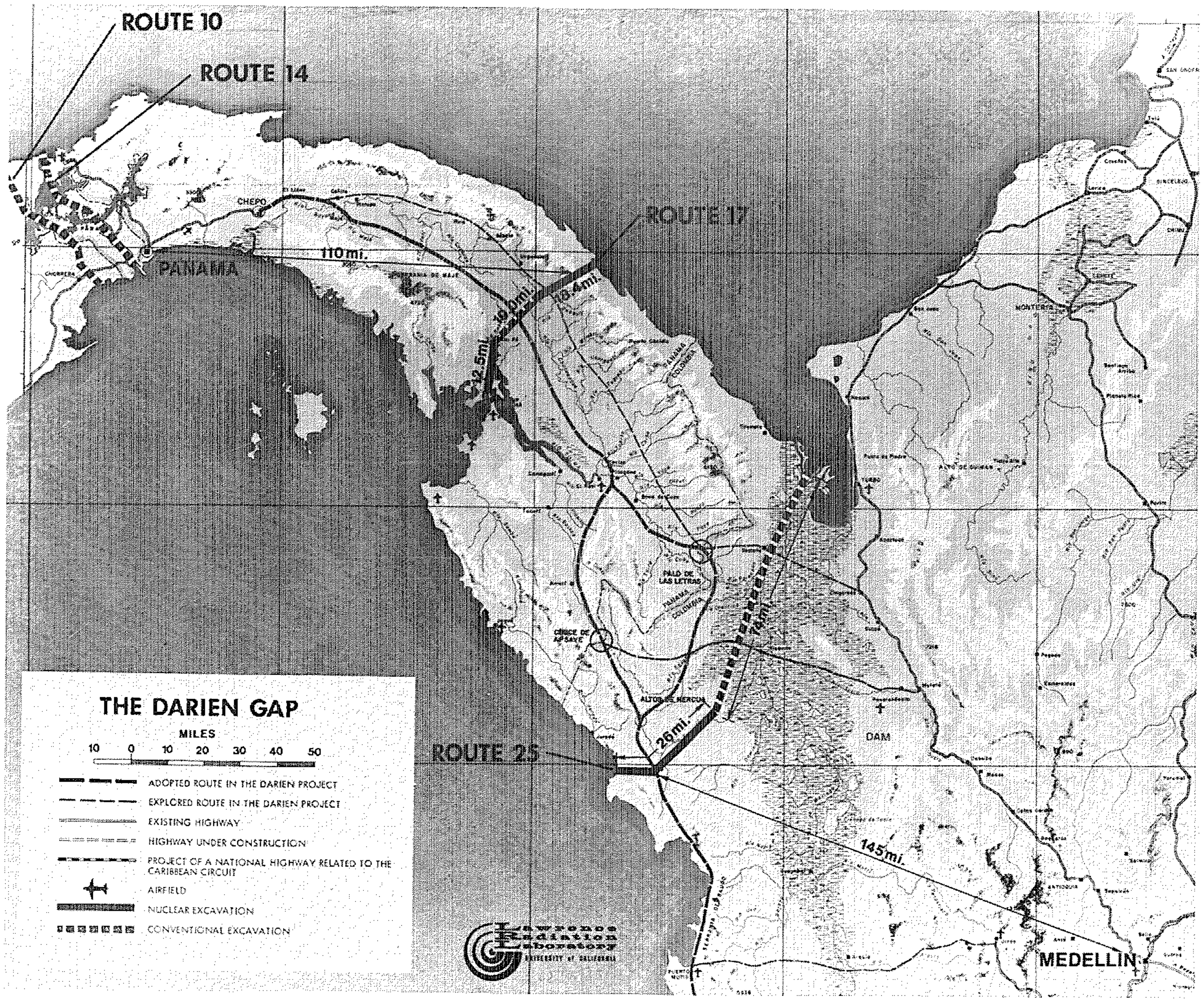

Fig. 4—Map of Central America showing the location of two promising routes using nuclear explosives.

XA04N0854

HYDROCARBON PRODUCTION WITH NUCLEAR EXPLOSIVES

by

J. Wade Watkins[1]

ABSTRACT

The tremendous energy of nuclear explosives and the small dimensions of the explosive package make an ideal combination for drill-hole explosive emplacement in deep, thick hydrocarbon deposits. Potential applications exist in fracturing low permeability natural-gas and petroleum formations for stimulating production, fracturing oil shale to permit in situ retorting, and creating storage chimneys for natural gas, liquefied petroleum gas, petroleum, petroleum products, helium, and other fluids. Calculations show, for example, that less than 100 shots per year would be needed to stabilize the natural gas reserves to production ratio. Under the Government-industry Plowshare program, two experiments, Projects Gasbuggy and Rulison, were conducted to stimulate natural gas production from low-permeability formations. Incomplete information indicates that both were technically successful.

Potential problems associated with the use of nuclear explosives for underground engineering applications are radioactive contamination, maximum yield limitations, high costs of detonating contained nuclear explosives, and adverse public opinion.

Results at Project Gasbuggy and other considerations indicated that the problem of radioactive contamination was about as predicted and not an insurmountable one. Also, it was demonstrated that shots at adequate depths could be detonated without appreciable damage to existing surface and subsurface buildings, natural features, and equipment. However, costs must be reduced and the public must be better informed before these techniques can be widely used in field operations.

On the basis of present knowledge, the potential of nuclear-explosive stimulation of hydrocarbon production appears good. Additional field experiments will be required to adequately explore that potential.

INTRODUCTION

The potential of peaceful uses of nuclear explosives is greatest in the production and storage of hydrocarbons and associated substances. Some uses of this technique are: (1) Fracturing deep, thick formations of low permeability containing natural gas and/or petroleum; (2) fracturing deep, thick oil-shale deposits to permit in situ retorting; and (3) creating storage chimneys for natural gas, liquefied petroleum gases, crude petroleum, petroleum products, helium, and other fluids.

---

[1] Director of Petroleum Research, Bureau of Mines, U.S. Department of the Interior, Washington,D.C.

The first Government-industry Plowshare experiment, Project Gasbuggy, was successful, although not all technical questions were answered by the results obtained. The explosive yield and consequent subsurface effects appear to be very close to those predicted. There was no venting of radioactivity, and surface seismic damage was negligible. The concentrations of the principal radionuclides were close to those predicted for krypton-85 and xenon-133. They were less than those predicted for tritium and iodine-131 was not detected. Presumably, 200 days after detonation, 95 percent of the tritium then in the chimney was present as tritiated water, a fortunate circumstance since in this form it is easily handled for disposal. Production from the chimney at high rates was possible for limited periods, and it was apparent that fresh gas was entering the chimney as production tests were conducted, although at a rate somewhat lower than that predicted. It was not possible, however, to assess fully the productivity of the fractured zone because efforts to drill into it did not produce satisfactory test wells.

The Rulison (Colorado) experiment, detonated September 10, 1969, went about as scheduled. However, its effect on stimulating natural gas production will not be known until production tests are conducted this spring. These and other planned experiments should further demonstrate the technical feasibility and economic practicability of this new stimulative technique.

Promising results have been obtained from experiments in retorting random-size and random-grade oil shale in special retorting vessels, and in retorting oil shale in situ at a shallow depth fractured by more conventional means. This knowledge is being used in planning a nuclear-explosive fracturing, in situ retorting experiment in oil shale--Project Bronco. However, no site has been selected, and there as yet is no Government-industry contract for a joint experiment.

Likewise, for the storage of natural gas, Project Ketch has a design concept, but no site has been selected and no contract has been negotiated. As yet, there are no known experiments designed for nuclear-chimney storage of other fluids, or for nuclear-explosive stimulation of low-permeability oil reservoirs.

ENERGY DEMANDS AND SUPPLIES

The demand for energy is growing exponentially (fig. 1). By 1980, energy consumption in this country will be about 88 quadrillion Btu's; a 64-percent increase over that actually consumed in 1965.

Petroleum and natural gas will continue to provide most of the Nation's energy needs, but there is growing concern over industry's ability to meet the tremendous future demands for those commodities. The basis for this concern lies in the relationship between reserves and production.

Between 1959 and 1968, proved reserves of crude oil remained essentially constant at 30.7 to 31.8 billion barrels, while production increased 27 percent, from 2.6 to 3.3 billion barrels per year (fig. 2). Because of constant reserves and increasing production, the reserves-production (R/P) ratio decreased consistently from 12.3 in 1959 to the uncomfortably low value of 9.2 at the end of 1968.

Proved reserves of natural gas increased nearly every year over the same 10-year period, but production increased even faster (fig. 3). Thus, the R/P situation for natural gas nearly parallels that of petroleum, decreasing from 21.1 in 1959 to 14.6 at the end of 1968. This decline is actually the extension of a consistent and broad decline that began 23 years ago at an R/P ratio of 32.5 in 1946.

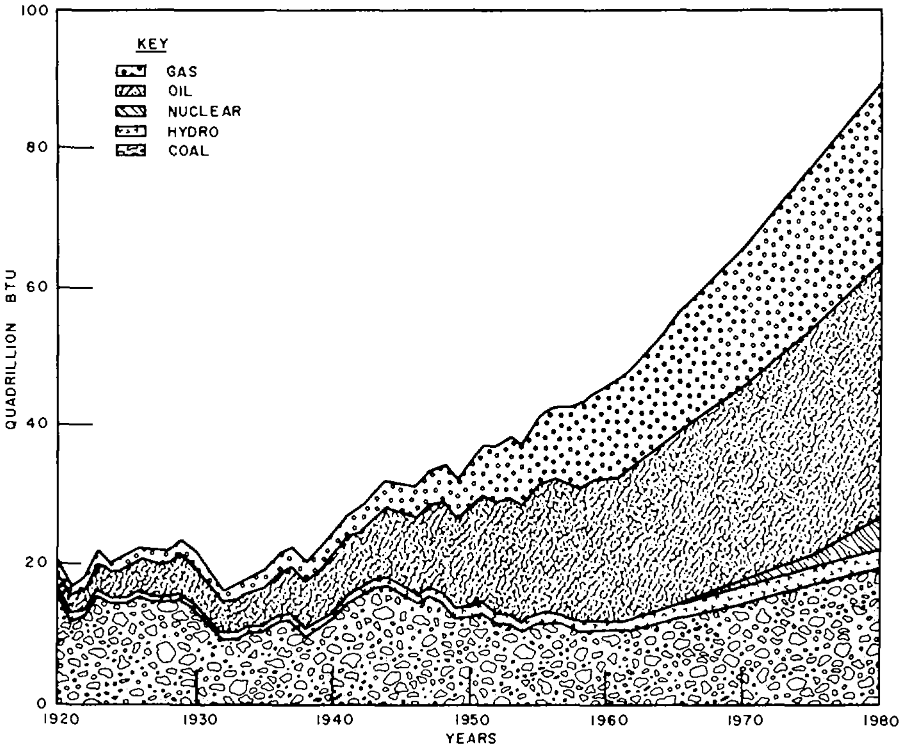

FIGURE 1.- United States Energy Consumption.

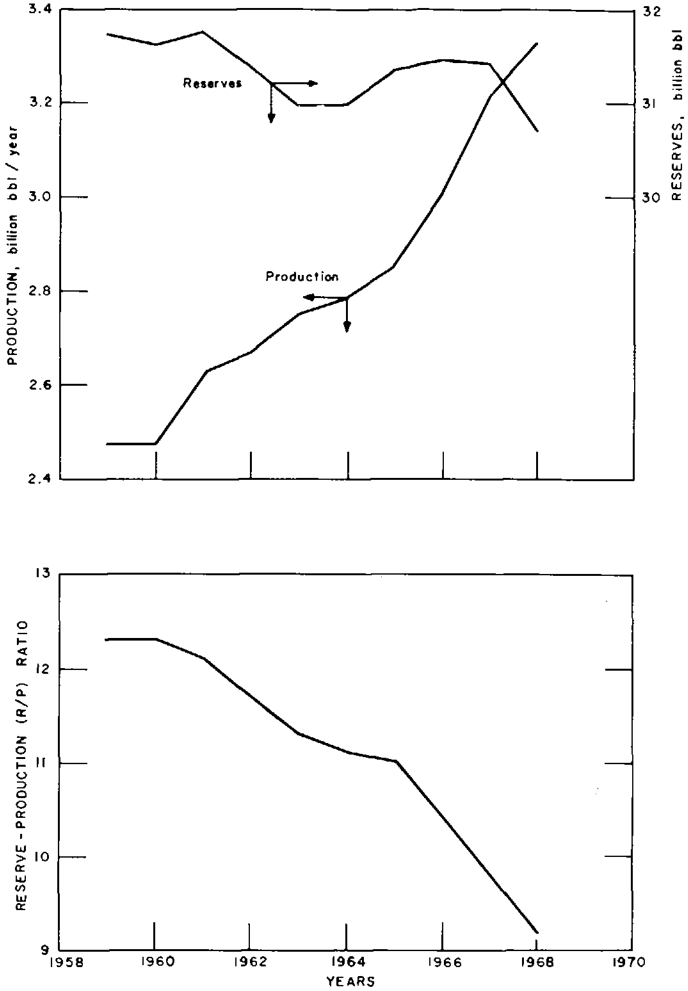

FIGURE 2.– United States Crude Oil Reserves and Production.

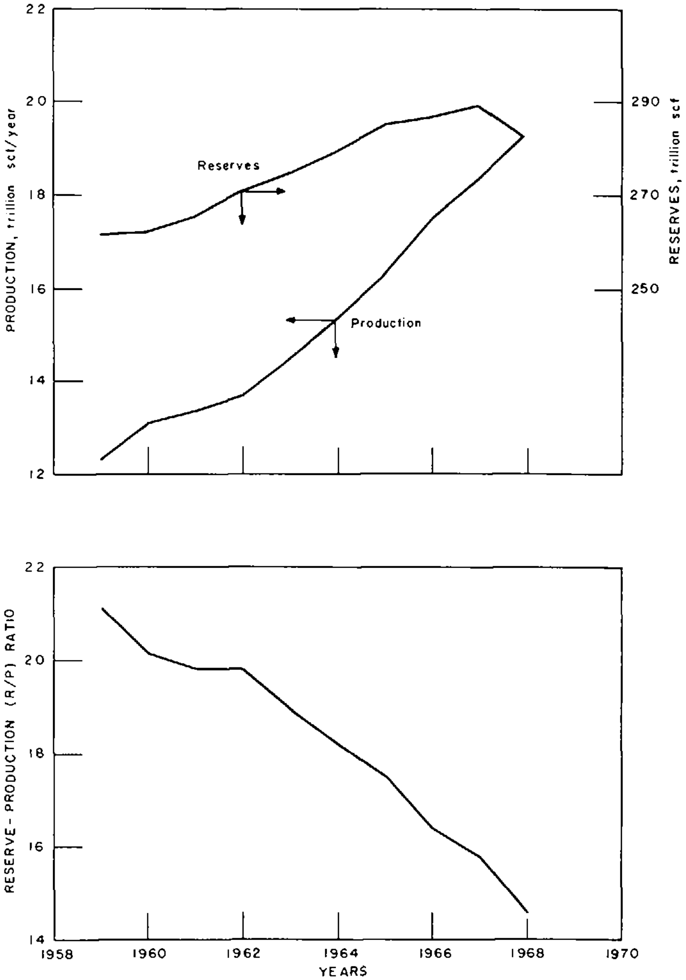

FIGURE 3.– United States Natural Gas Reserves and Production.

In the immediate future, the demand for oil and gas is expected to grow faster than reserve additions, leading to further declines in the R/P ratios. Alaskan oil will help arrest, or may temporarily reverse, the declining trend for oil, but further efforts will be required to stabilize these R/P ratio balances.

The methods by which our future supplies of petroleum and natural gas might be augmented are: (1) Increase foreign imports; (2) utilize substitute fuels; (3) find new reserves; and (4) convert resources into recoverable reserves through new technology.

Foreign imports might serve domestic needs, provided no national emergency caused imports to be cut off. However, the cost of foreign imports likely may increase as reserves decrease and foreign countries extract higher reimbursement for concessions. Practical substitutes for petroleum and natural gas are not now available economically, although technological breakthroughs in the production of gaseous and liquid fuels from oil shale and coal, favorable Government policies, or price increases for crude products could alter this situation. It is becoming increasingly difficult to find and produce new reserves of petroleum and natural gas, as evidenced by the problems and costs of offshore and Arctic North Slope exploration and production. New technology, therefore, appears to be the most immediately promising of the cited supply alternatives. The Plowshare program offers one means of exploiting deep, thick petroleum, natural-gas, and oil-shale deposits that cannot be economically developed with existing technology.

Figure 4 is a projection of the impact that nuclear-explosive fracturing may have on reversing the downward trend of the natural gas R/P ratio, provided it can be used economically. The assumptions here are: (1) Depth, 8,000 to 16,000 feet; (2) gas in place, 200 billion cubic feet per 640 acres; (3) area drained, 640 acres per shot; (4) yield, 100 kilotons per shot; and (5) recovery, 50 percent. As indicated, 10 shots per year would have comparatively little impact, whereas 100 shots per year would affect the R/P ratio appreciably. Between these extremes an optimum number of shots could be planned that would stabilize the R/P ratio at a predetermined level.

UNDEVELOPED RESOURCES

There are significant domestic deposits of petroleum and natural gas in deep, thick formations having permeabilities so low that the contained fluids can be neither practically nor economically produced by conventional well-completion and production-stimulation methods. Bureau of Mines engineers have estimated that, in Rocky Mountain basins alone, the potential reserves of natural gas producible through nuclear-explosive fracturing, if economically practicable, equal more than 300 trillion cubic feet, or more than our present proved natural-gas reserves. No estimate has been made for the petroleum resources in similar formations, but it is believed that they are significant.

Many estimates have been made of the oil potential of the Green River oil shale of Colorado, Utah, and Wyoming. Depending upon the grade and thickness of shale included in the resource estimates, the oil-equivalent estimate ranges as high as 2 trillion barrels. Obviously, all of this organic matter would not be recoverable, but a practicable, economic in situ process might be used to recover a very large portion where the deposits are both thick and deep, as in the Piceance Basin of Colorado where as much as 2,000 feet of continuous oil shale lies under up to 1,000 feet of overburden.

NUCLEAR EXPLOSIVES VERSUS CHEMICAL HIGH EXPLOSIVES

The tremendous difference in size of nuclear-explosive packages and the volume of conventional explosives required for an equivalent yield is easily illustrated (fig. 5). The nominal 40-kiloton Rulison fission explosive was encased in a canister 9 inches in diameter and 15 feet long. The underground emplacement of even 1 kiloton of pelletized TNT would require a sphere 40 feet in diameter or a room 50 by 100 by 10 feet. To emplace 40 kilotons of pelletized TNT would require a void volume of 2,000,000 cubic feet, an obviously impractical situation. Cost is another consideration in comparing nuclear explosives and conventional explosives. Projected costs for nuclear-explosive services cited by the Atomic Energy Commission range from $350,000 (10 kilotons) to $600,000 (2 megatons). The costs are projected on the assumptions of production in quantity and legislation authorizing AEC to sell nuclear-explosive services and include nuclear materials, fabrication, arming, firing, and supporting activities. As a basis of comparison, assuming the cost of pelletized TNT or other comparable chemical high explosives to be about 20 cents per pound, 10 kilotons would cost $4 million and 2 megatons would cost $800 million. In other words, chemical high explosives, based on yield only, are about 11 times more costly than nuclear explosives in a 10-kiloton range and 1,300 times more costly in the 2-megaton range.

For nuclear explosives to be used in extensive commercial applications, the highest yield devices compatible with containment and minimal seismic-shock damage must be used. Also, the present ancillary costs of contained nuclear detonations must be reduced materially.

POTENTIAL PROBLEMS

It is not a unique situation that the use of nuclear explosives presents potential problems. The same can be said for any method of rock breaking. None of the potential problems, however, is so serious that it cannot be solved.

Radioactivity

The three considerations with regard to radioactivity in using nuclear explosives are the necessity of preventing venting of radioactivity to the atmosphere, the necessity of preventing contamination of ground water, and the problems of radionuclides in the product.

Adequate data are available from more than 270 contained nuclear explosions in a number of rock media that containment may be assured, provided no fractures are present that might permit the transmission of radionuclides to the surface. Detailed geological studies can determine whether there is any likelihood of venting through fractures. Thus, the possibility of accidental venting in a properly designed experiment is essentially nil.

Similarly, detailed hydrological and geological studies, such as are made prior to all nuclear-explosive tests, yield data that may be used to so design the experiment to prevent the contamination of any ground water that may be used for any industrial purpose or that may migrate to the earth's surface.

Some radioactive contamination of produced hydrocarbons may be expected. The amount and kind of radioactive contaminants depend principally upon the kind of explosive used and the medium in which it is detonated. All-fission explosives may be preferable for natural-gas stimulation because they produce the least tritium and would minimize contamination of the gas by tritium exchange with hydrogen.

The quantity of radionuclides in the hydrocarbon fluid produced may be reduced by waiting for radioactivity decay, removal, and dilution. In natural-gas stimulation, iodine-131, for example, may be reduced to acceptable levels by waiting for the 8-day half-life radionuclide to decay. Any particulate matter or liquid may be easily separated from gases, and the unwanted substances may

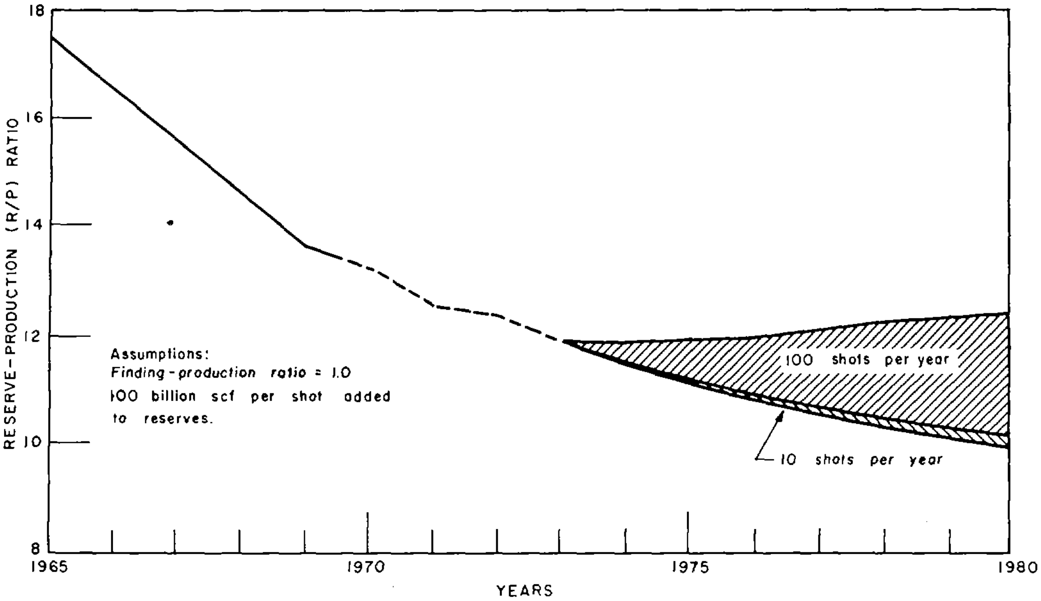

FIGURE 4.- Effect of Nuclear Explosion Stimulation on Natural Gas Reserve-Production Ratio.

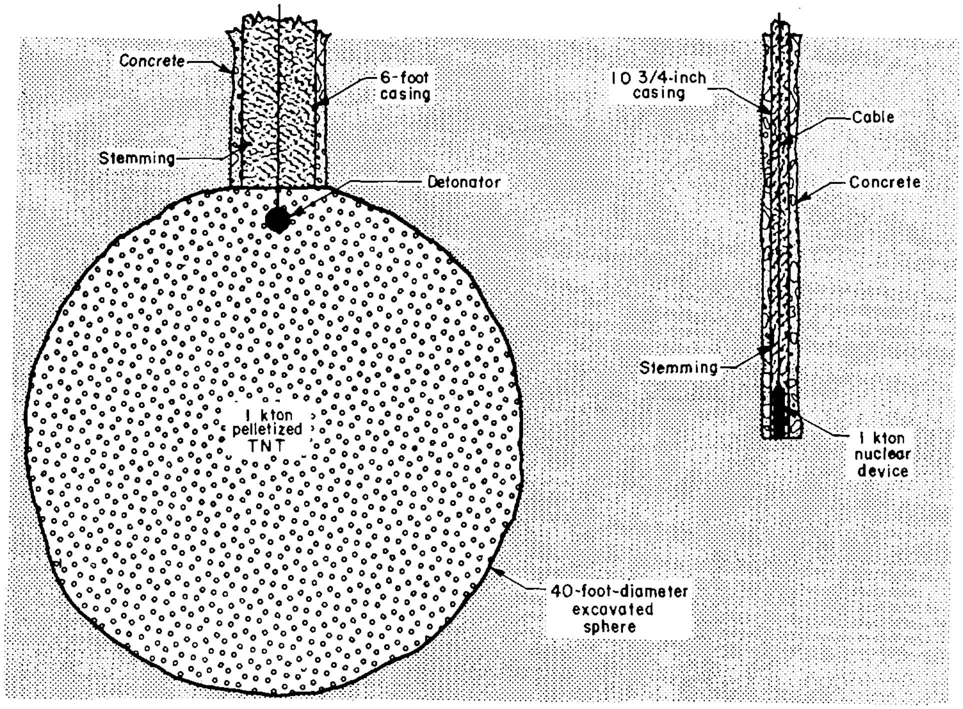

FIGURE 5.-Comparative Emplacement Techniques for Nuclear and Chemical Explosives.

be disposed of by safe and acceptable means. In the case of the Gasbuggy gas, for instance, the tritiated water, which contains most of the tritium, is easily separable from the gas. Finally, contaminated fluids may be mixed with uncontaminated fluids to reduce the specific radioactivity to acceptable levels.

The maximum permissible concentrations (MPC's) set by the International Commission on Radiation Protection, the National Committee on Radiation Protection, and the Federal Radiation Council have been accepted by AEC. However, these standards were not designed to cover the situation of tritium or krypton-85 in natural gas that is to be burned in a power-generation plant or a residence. Realistic guidelines for acceptable radionuclide levels in hydrocarbons are sorely needed and are in the process of derivation.

Seismic Shock

It has become increasingly apparent that the limiting factor in the maximum yield of contained nuclear explosives that can be permitted is not containment but the amount of surface seismic shock that can be tolerated. Fortunately, most of the known areas where nuclear explosives might be used to stimulate hydrocarbon production are relatively remote and are sparsely populated.

Costs of Using Contained Nuclear Explosives

It has been mentioned earlier that, for widespread commercial application of nuclear explosives, the present high costs of nuclear-explosive experiments will have to be reduced appreciably. A significant part of present costs results from associated scientific experiments and diagnostics and the intensive safety and environmental studies required to insure public health and safety and protect the environment and ecology. For strictly commercial applications, the costly add-on experiments would not be required and the necessity for diagnostic measurements would be greatly reduced. All of us want to protect public health and safety and preserve the environment. Therefore, safety, environmental, and ecological studies and controls still would be required. However, when such studies have been made and the results have been found acceptable for a general area, the studies should not have to be repeated in detail for each separate detonation within the area previously studied.

Public Opinion

The contrast in expressed public opinion before the Gasbuggy and the Rulison detonations was extreme. Prior to Gasbuggy, there was great interest, but essentially no local concern was expressed and there were few general adverse comments. Conversely, the Rulison experiment occasioned both local and national criticism, demonstrations, and motions for injunctions and restraining orders. In the court hearings, however, the plaintiffs established no case for opposing the experiment. It appears that much of the opposition came from those who were not fully aware of the facts pertinent to nuclear-explosive technology and phenomenology. It is obvious that improved public relations are required to better inform the general public of the real facts concerning nuclear detonations.

The point should be made that there is no method of providing the energy and minerals that the Nation requires, for either the civilian or the military economy, that does not affect the environment in some manner. This is true for the combustion of fossil fuels, nuclear-power generation, and even hydropower. Our objective, therefore, must be to assure an adequate supply of energy, at the lowest cost to the consumer, and with the <u>least</u> adverse impace on the environment and the ecology.

NATURAL GAS AND PETROLEUM PRODUCTION STIMULATION

The yield and chimney characteristics of Project Gasbuggy were very close to those predicted, as was the apparent extent of fracturing outside the nuclear chimney. Production from the chimney was materially increased, as evidenced by the fact that about 260 million cubic feet of gas has been produced in about 1 year's time from the chimney reentry well, whereas only about 80 million cubic feet of gas had been recovered over a producing life of 10 years from the nearest preshot production well, some 436 feet away from the chimney reentry well. The radioactivity was somewhat less than expected for tritium and about as expected for krypton-85; no iodine-131 was detected. Also, at this time, about 95 percent of the tritium apparently is present as tritiated water, rather than as a gas. This is fortunate, since tritiated water may be separated easily from the gas. Immediately after reentry, the hydrocarbon content of the chimney gas was about 52 percent, compared with the usual 99 percent in field wells. As a result of dilution by fresh gas from the formation, the hydrocarbon content is now about 90 percent. The radioactivity also has been reduced appreciably by dilution with uncontaminated formation gas. One of the unanswered questions in the Gasbuggy experiment is the productivity of the fractured zone. The postshot wells drilled into the fractured zone have quite low rates of production, indicating that communication between them and the chimney is probably poor.

The Rulison explosive was detonated with no venting of radioactive gases, an apparent yield close to that expected, and low surface seismic damage. The wellhead pressure on the Rulison emplacement well has been increasing since the detonation, indicating that the rock in the Mesaverde formation has been fractured appreciably around the point of detonation and that the gas is migrating upward in the casing of the well through the gravel, sand, and clay used as stemming material to the wellhead, where it is confined by a high-pressure "Christmas tree." Present plans call for reentry no sooner than 6 months after detonation.

NUCLEAR-EXPLOSIVE FRACTURING, IN SITU RETORTING OF OIL SHALE

The concept of fracturing essentially impermeable oil shale to permit retorting it in place is the most technically complex of all the proposed Plowshare hydrocarbon-production experiments. However, the advantages of a technically feasible and economically practicable in situ retorting experiment are so apparent, and the domestic oil-shale resource is so great, that testing of the concept deserves a high priority. The advantages are that: (1) Air and water pollution would be virtually eliminated; (2) disfigurement of the earth's surface would be greatly minimized; (3) a higher percentage of oil conversion and recovery may be possible than with room-and-pillar mining and aboveground retorting; (4) the cost and difficulty of disposing of spent shale would be eliminated; and (5) it may be possible to produce a higher quality oil than that produced from aboveground retorts.

Recent experiments on retorting random-size and random-grade particles of oil shale at the Bureau of Mines, Laramie Petroleum Research Center, approximating the particle-size and grade range that might be expected in a nuclear chimney, have been successful. Up to 85 percent of Fischer assay has been recovered. This, and the results of recent, shallow in situ retorting experiments, near Rock Springs, Wyo., have enhanced the potential attractiveness of in situ retorting. This is particularly true for the use of nuclear-explosive fracturing in the very deep, thick, rich oil-shale deposits that now do not appear amenable to production by present mining and retorting methods.

FLUID STORAGE

The first proposed application of nuclear explosives for creating a chimney to be used for natural-gas storage, Project Ketch, has not materialized. The principal reason for this was the opposition to the experiment voiced within Pennsylvania.

Regardless of the merits of the proposed Ketch experiment and the validity of the opinions of the opposition, the concept of using nuclear chimneys for fluid storage has many advantages. There is ample evidence that underground storage of natural gas is safer, cheaper, and much less deleterious to aesthetics and the environment than aboveground storage.

Most of the natural gas stored underground is kept in aquifers or depleted natural-gas reservoirs. Some is stored in salt formations, and there is one storage project in an abandoned coal mine. There are appreciable geographical areas of the United States, however, in which there are no suitable subsurface permeable formations with adequate caprocks, or rock salt in domes or sediments, that could be used for underground fluid storage. Underlying many of these areas, however, are massive deposits of impermeable shale or granite that could be converted for fluid storage through the use of nuclear explosives. The study made for Project Ketch indicated that nuclear-explosive creation of gas-storage chimneys can be economic. The storage of more valuable fluids, such as helium, and of strategically important fluids, such as petroleum products, should make the economics even more favorable.

CONCLUSIONS

Conclusions from the experience of Bureau of Mines personnel in Plowshare applications are:

1. There is a great potential in using nuclear explosives for converting certain domestic hydrocarbon resources to usable reserves.

2. For economic utilization of underground nuclear explosives, high-yield explosives will be required and the present cost must be reduced appreciably.

3. The use of nuclear explosives for creating fluid-storage chimneys appears attractive, especially in some geographic areas and for the more valuable and strategic fluids.

4. The limiting factor in using high-yield nuclear explosives is the maximum seismic shock that can be tolerated.

5. Radioactivity is a problem but not an insurmountable one.

6. Adverse public opinion probably is the most serious present problem, and more effective public relations are mandatory.

XA04N0855

ECONOMICS OF NUCLEAR GAS STIMULATION

G. W. Frank
Austral Oil Company Incorporated
Houston, Texas

H. F. Coffer
CER Geonuclear Corporation
Las Vegas, Nevada

G. R. Luetkehans
CER Geonuclear Corporation
Las Vegas, Nevada

ABSTRACT

Nuclear stimulation of the Mesaverde Formation in the Piceance Basin appears to be the only available method that can release the contained gas economically. In the Rulison Field alone estimates show six to eight trillion cubic feet of gas may be made available by nuclear means, and possibly one hundred trillion cubic feet could be released in the Piceance Basin.

Several problems remain to be solved before this tremendous gas reserve can be tapped. Among these are (1) rates of production following nuclear stimulation; (2) costs of nuclear stimulation; (3) radioactivity of the chimney gas; and (4) development of the ideal type of device to carry out the stimulations. Each of these problems is discussed in detail with possible solutions suggested.

First and foremost is the rate at which gas can be delivered following nuclear stimulation. Calculations have been made for expected production behavior following a 5-kiloton device and a 40-kiloton device with different permeabilities. These are shown, along with conventional production history. The calculations show that rates of production will be sufficient if costs can be controlled. Costs of nuclear stimulation must be drastically reduced for a commercial process. Project Rulison will cost approximately \$3.7 million, excluding lease costs, preliminary tests, and well costs. At such prices, nothing can possibly be commercial; however, these costs can come down in a logical step-wise fashion.

Radiation contamination of the gas remains a problem. Three possible solutions to this problem are included.

INTRODUCTION

The greatest challenge to the oil industry has always been how to make available oil and gas at an economic rate. The increasing costs of exploration have made the economic development of marginal resources not only attractive, but necessary.

Over the years, the development of stimulation methods have made it possible to produce from reservoirs which earlier would have been written off as dry holes. Among the first successful methods was the use of the chemical explosive (nitroglycerine) to break up the area immediately surrounding the well bore. Later, another method still in common use in limestone reservoirs, was acidizing to open up flow channels in the rock further out into the reservoir. These two stimulation methods have now been dwarfed by hydraulic fracturing,(1) the most commonly used technique available to the industry today. The object of fracturing is to increase the flow from the reservoir by increasing the flow capacity of the rock close to the well bore. It works extremely well in thin formations where the entry point of fracturing fluid can be controlled.

Stimulation is more difficult when thick, tight formations are the targets. This is because it is hard to force the fractures into the desired zones of the formation and connect up all of the sand lenses with the well bore. The introduction of nuclear fracturing (2), (3) should solve the thick formation stimulation problem. Massive fractures are created by the nuclear explosive which cross the sand and shale sequences of such thick, tight formations. Use of nuclear stimulation should allow economic production from zones which are non-commercial by ordinary stimulation methods.

EFFECT OF NUCLEAR EXPLOSIVES

Numerous other papers at this symposium have discussed nuclear explosions and their effects on various rock types. In review, a completely contained explosion creates a chimney and fractured rock zone much like the ones shown in Figure 1. (4), (5) The size of the chimney and fractured zone varies with the size of device or amount of energy used. Let's look briefly at how these huge rock piles can be used to increase gas production.

Under normal situations a hole is drilled into the gas formation and 5-1/2 inch or 7-inch casing is cemented in place. Gas flow is initiated into the well bore by perforating and then reducing the pressure in the well bore. As the gas moves from the higher pressure in the reservoir into the well, it flows through the area immediately surrounding the well (See Figure 2). There is a restriction to flow due to the limited area through which the fluid can pass. The rate at which the gas can be produced is a function of the permeability of the reservoir and the available flow areas.

When a nuclear device is exploded in a reservoir, it yields the configuration as shown in the bottom half of Figure 2. (6) Superimposed on the well bore is a highly fractured area surrounding a rubble of broken rock. The gas flows toward these fractures from the tighter or less permeable original reservoir. The flow rate into such a well will be a function of the size of

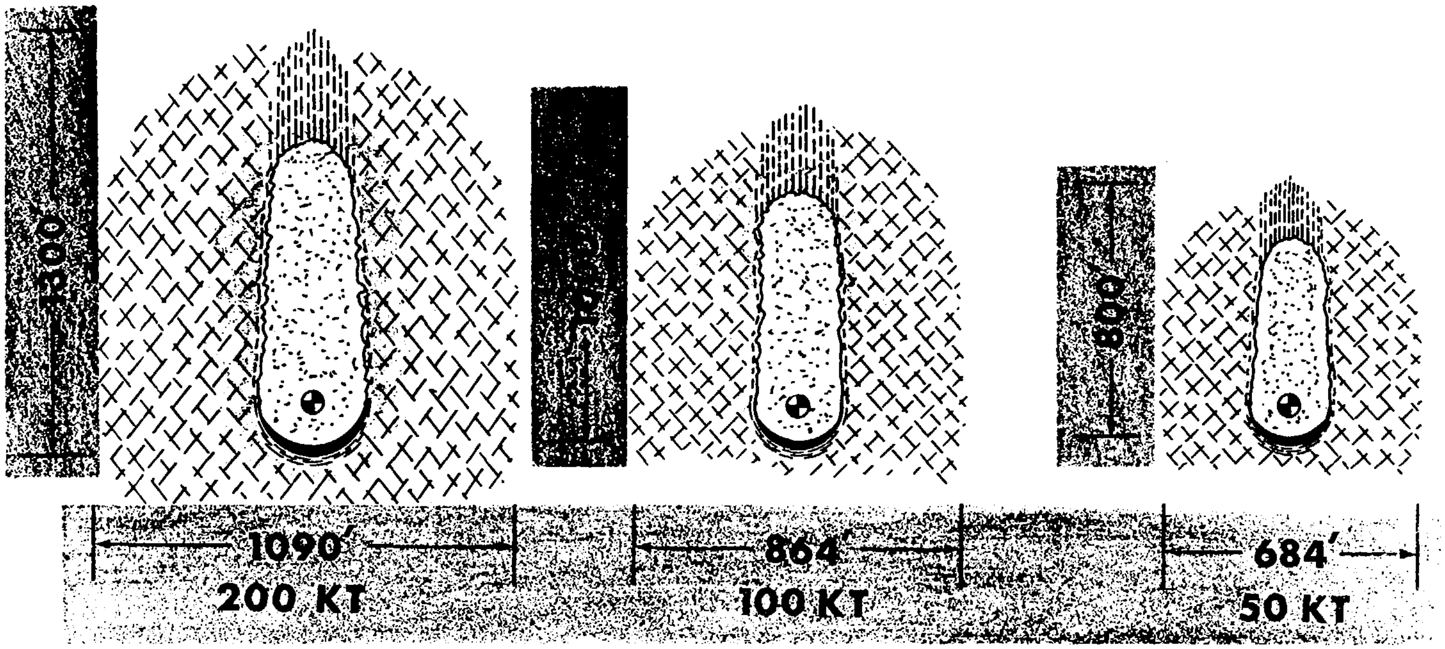

SHOT DEPTH 3000′

Fig. 1—Chimney and Broken Rock Zones Resulting From Various Size Nuclear Detonations In Oil Sands.

the broken up area and the formation permeability. In other words, the larger the area of fractures, the faster the flow rate into the new well. If the nuclear stimulated well rates are much greater than the original unfractured rates, it will be economic to use nuclear explosives and fewer wells should be required to drain the reservoir.

Two nuclear gas stimulation experiments have been carried out--Projects Gasbuggy (7) and Rulison. (8) The objective in both cases was to open up a tight formation and allow a higher rate of production. Preliminary results are in on Gasbuggy and are discussed by others at this symposium. A reentry is planned for Rulison in April of this year.

RULISON RESULTS

The paper by Reynolds et al (9) presents much of the pre-shot test data from Rulison. Using the mathematical model discussed there we have calculated a series of curves showing the effect of shot size and permeability on the predicted performance of a gas reservoir. These calculations should allow us to zero in on the economic future of nuclear stimulation and the limits of usefulness of the method.

Figure 3 gives our pre-shot predictions on recovery from the Rulison test. The measured reservoir permeability was 0.008 md. Using a 40-kiloton device, we should obtain a 7-fold increase over normal production in 20 years. Obviously, the experimental shot is not predicted to pay for itself since only 6 billion cubic feet of gas is expected in 20 years.

Using the same model, Figure 4 was made. It shows the effect of variation in permeability on recovery predicted in 20 years using a 40-kiloton device. As expected, recoveries are much higher with an increase in permeability. At very low permeability, gas recovery following nuclear stimulation will be too low to make the method economic.

Figure 5 is the same plot using a 5-kiloton device. In this kind of application it would be assumed that a sufficient number of small devices would be used in one well bore to break across the entire production interval. Thus, the results are comparable to those of Figure 4 for the 40-kiloton device. It is apparent that a 5-kiloton device needs a much higher permeability to recover a substantial amount of the gas-in-place in 20 years.

Figures 6 through 8 show the comparison of recovery from 5- and 40-kiloton devices as a function of permeability. These data show that larger size devices become more desirable as the reservoir permeability decreases. The device yield selected will be governed by the seismic effects as well as the economics of recovering the gas-in-place.

In Figure 9, we have attempted to summarize the data by plotting 20-year recoveries versus permeability as a function of shot size. It is readily seen that 20-year recoveries fall off rapidly as the permeability decreases. This means there will be a limiting permeability below which even the tremendous power of the nuclear explosion will not yield production rates that are economic.

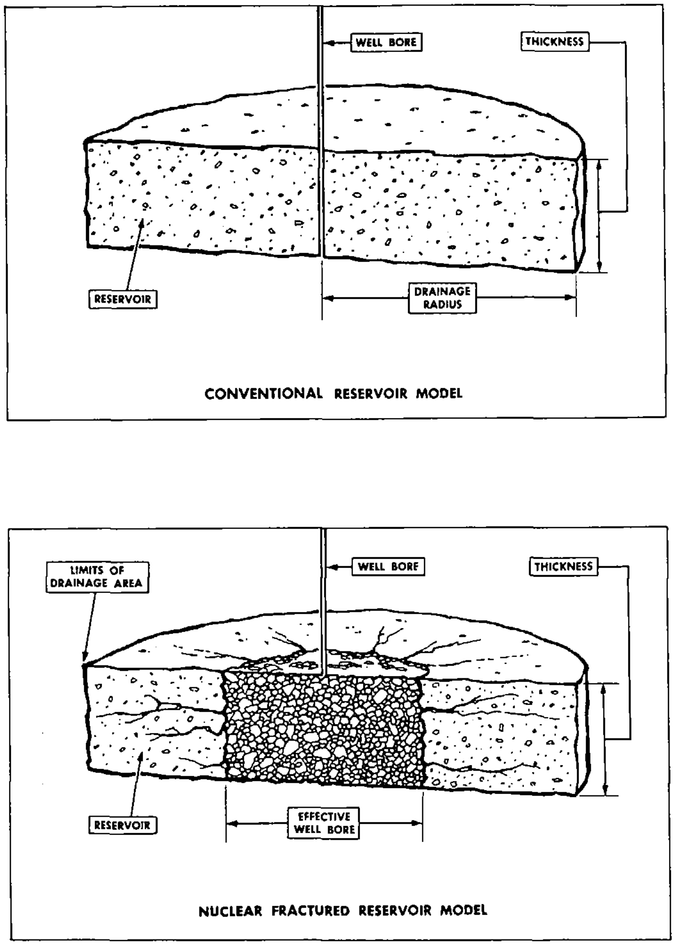

Fig. 2—Effect of Nuclear Fracturing on Well Bore.

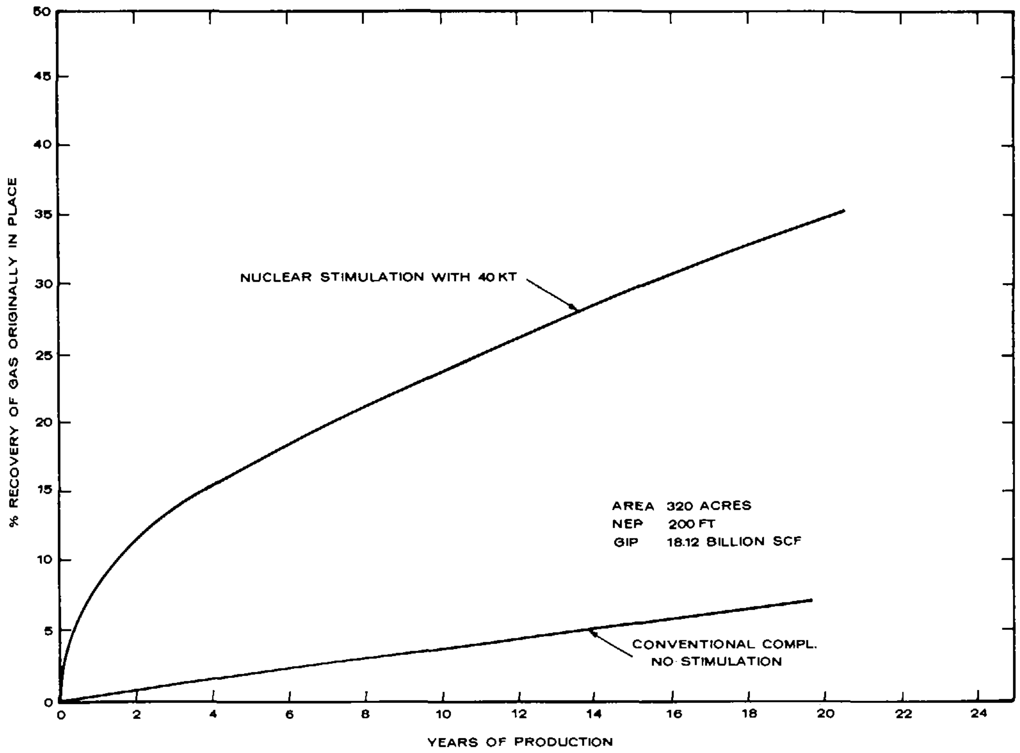

Fig. 3—Effect of Nuclear Stimulation on Gas Recovery.

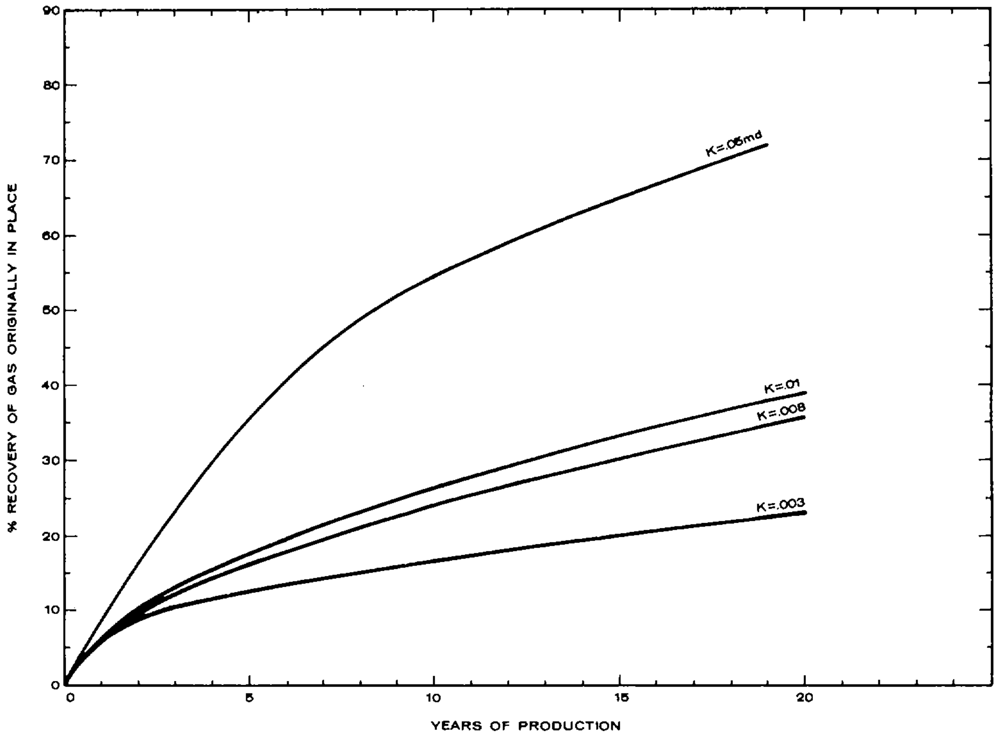

Fig. 4—Effect of Permeability on Gas Recovery After Nuclear Stimulation With a 40 kt Device and 320 Acre Spacing.

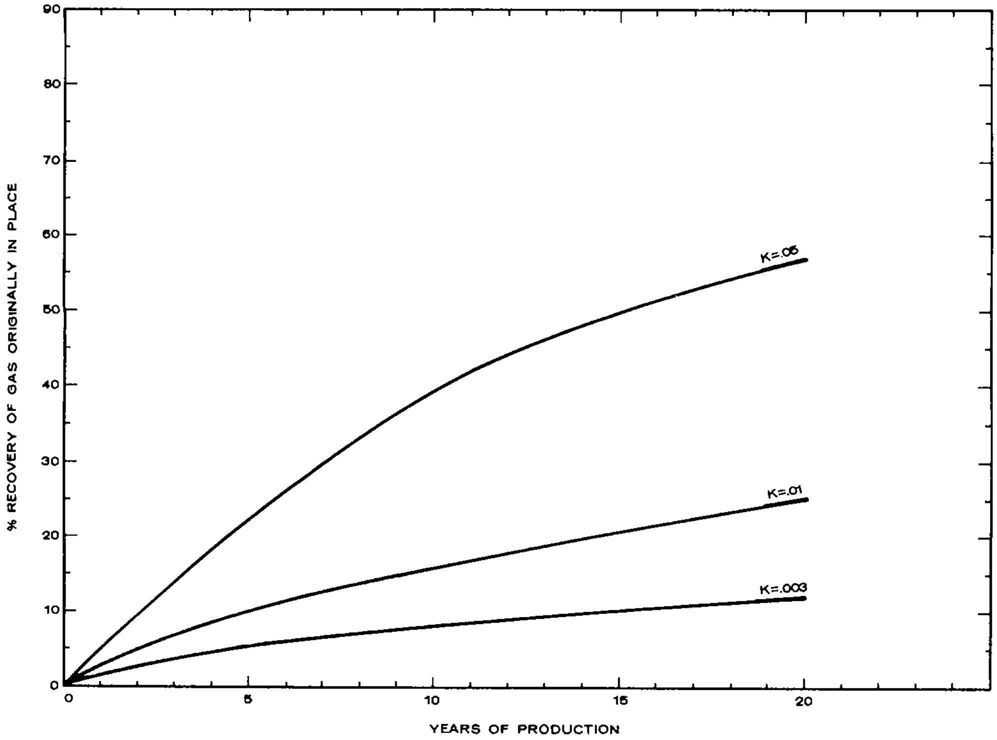

Fig. 5—Effect of Permeability on Gas Recovery After Nuclear Stimulation With a 5 kt Device and 320 Acre Spacing.

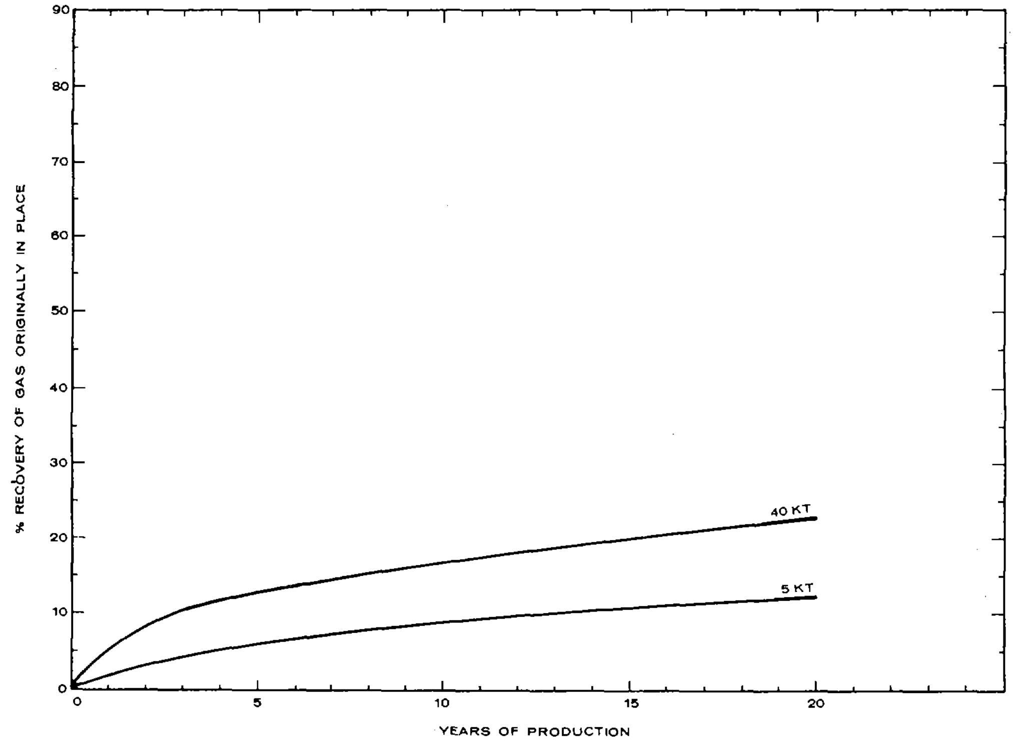

Fig. 6—Effect of Device Size on Gas Recovery in a .003 md Permeability Reservoir and 320 Acre Spacing.

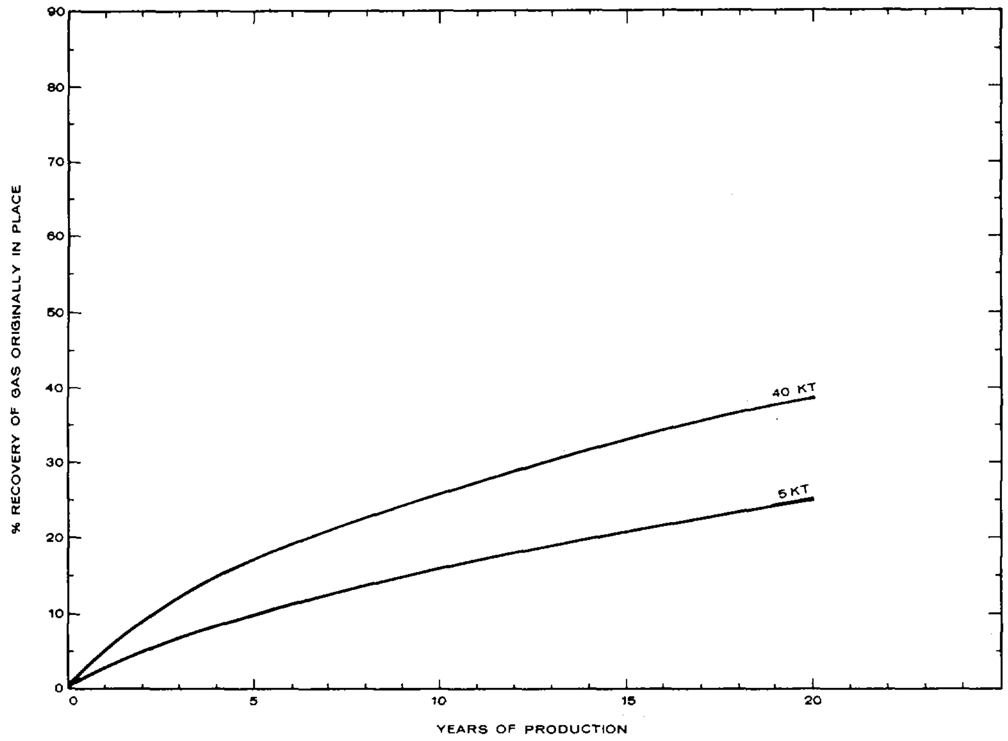

Fig. 7—Effect of Device Size on Recovery in a .01 md Permeability Reservoir and 320 Acre Spacing.

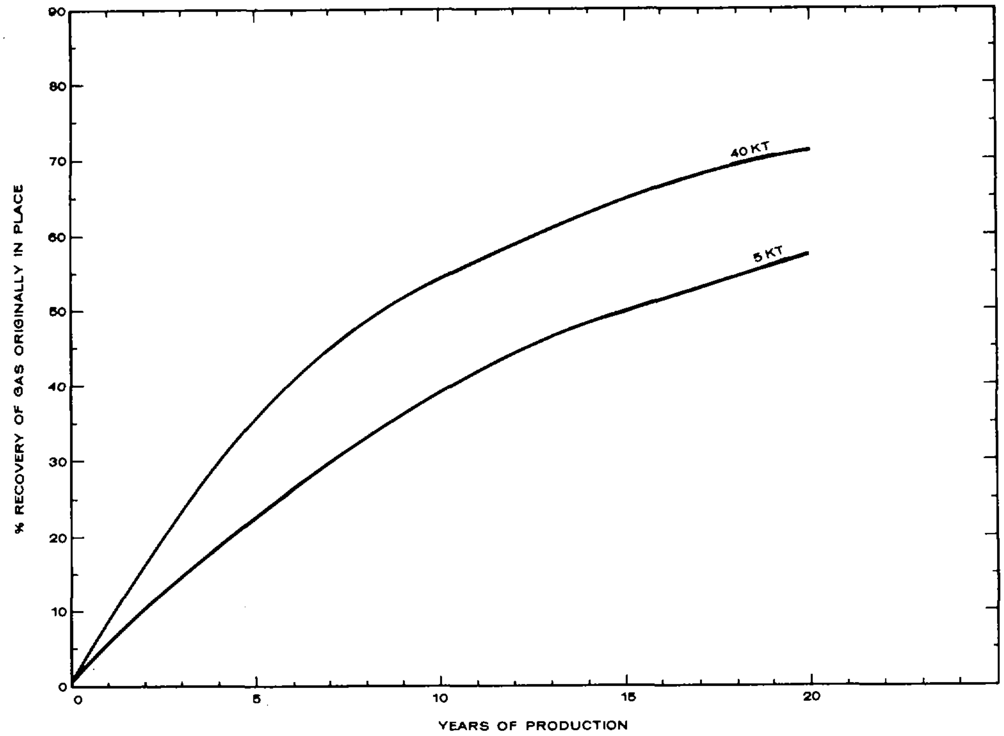

Fig. 8—Effect of Device Size on Recovery in a .05 md Permeability Reservoir and 320 Acre Spacing.

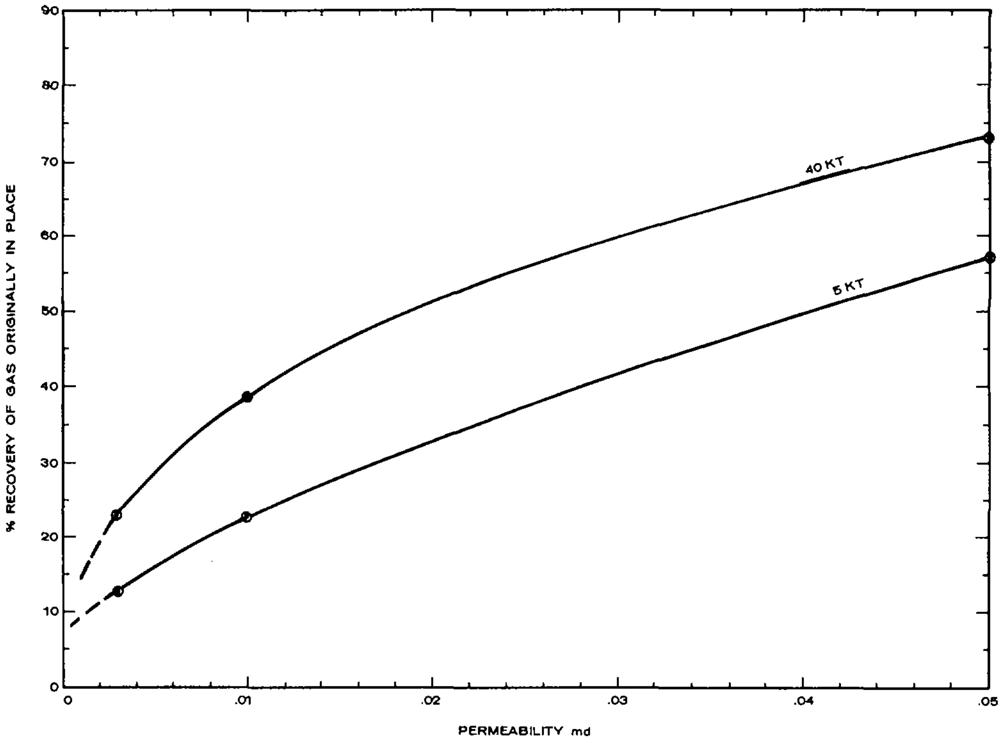

Fig. 9—Effect of Permeability on Gas Recovery in 20 Years Using 40 kt and 5 kt Devices on 320 Acre Spacing.

Comparison of the data in Figures 3 and 9 lets us draw some interesting conclusions about the type of gas reservoirs applicable to economic stimulation. With higher permeability reservoirs, we can use small devices in series and still obtain high recoveries. If the permeability is low, less than 0.01 md for example, we will be forced to use larger devices in order to obtain adequate production and recovery rates. If the permeability approaches 0.002 md, probably even large devices (100 kt or so) cannot be economically used unless we have tremendous quantities of gas-in-place.

At higher permeabilities (above 0.03 md) it may well be possible to increase the spacing to 640 acres. This would be especially attractive if larger devices (50 kt or more) could be used in the area without seismic damage.

After this analysis one is tempted to ask how good is it? Of course, it can be no better than the assumptions on which the reservoir model is constructed. First indications from Rulison are that the model may be somewhat conservative. We hope this statement is borne out by our Rulison test program since that would mean smaller devices than originally planned can be used.

Figure 10 gives the pressure buildup in the Rulison emplacement hole. By 30 days (720 hours) surface pressure was 2300 psi (approximately 2700 psi bottomhole) which is within less than 250 psi of original reservoir pressure of 2930 psi. It is interesting to speculate on what is happening and the gas flow rates across the fractured zone into the nuclear chimney.

Seismic measurements indicate that the device behaved as predicted (40 kt $^{+20}_{-4}$). Therefore, we would expect the cavity configuration to be in the range given in Table I. Gas accumulation in the chimney at the original reservoir pressure (2930 psi) might vary between 200 to 700 million standard cubic feet. We won't know which number is correct until the cavity is entered and its size determined.

Predicted chimney void space varies from 1.5 to 5 million cubic feet. This void volume comes from squeezing the rock in the vicinity of the shot and the vaporizing and resolidifying of the rock in the immediate area of the blast. If we assume the squeezing process takes place evenly on the sand grains and shale with no effect on the sand porosity, all of the void space will be newly created by the shot. (In actual fact, part of the new volume would come from squeezing the original porosity and thus all of the void space is not newly made. Since porosity is only 9.7% and sand is only about 40% of total rock, this assumption probably isn't too bad.)

If we consider the minimum fracturing case and consult Table I, we see that the total fractured zone void space (4.5 x 10^6 cubic feet) is only 3 times the chimney void space created by the device. Total gas in the fractured area should be about 900 MMSCF. If no flow occurred from the unfractured portion of the reservoir across the fractured boundary, the gas pressure in the well bore after 30 days of buildup should not be above 3/4 of the original pressure or 2200 psi. Since the observed pressure is approximately 2700 psi, the increase in pressure of 500 psi over a non-flow situation will give a measure of the gas flow rate across the fracture boundary.

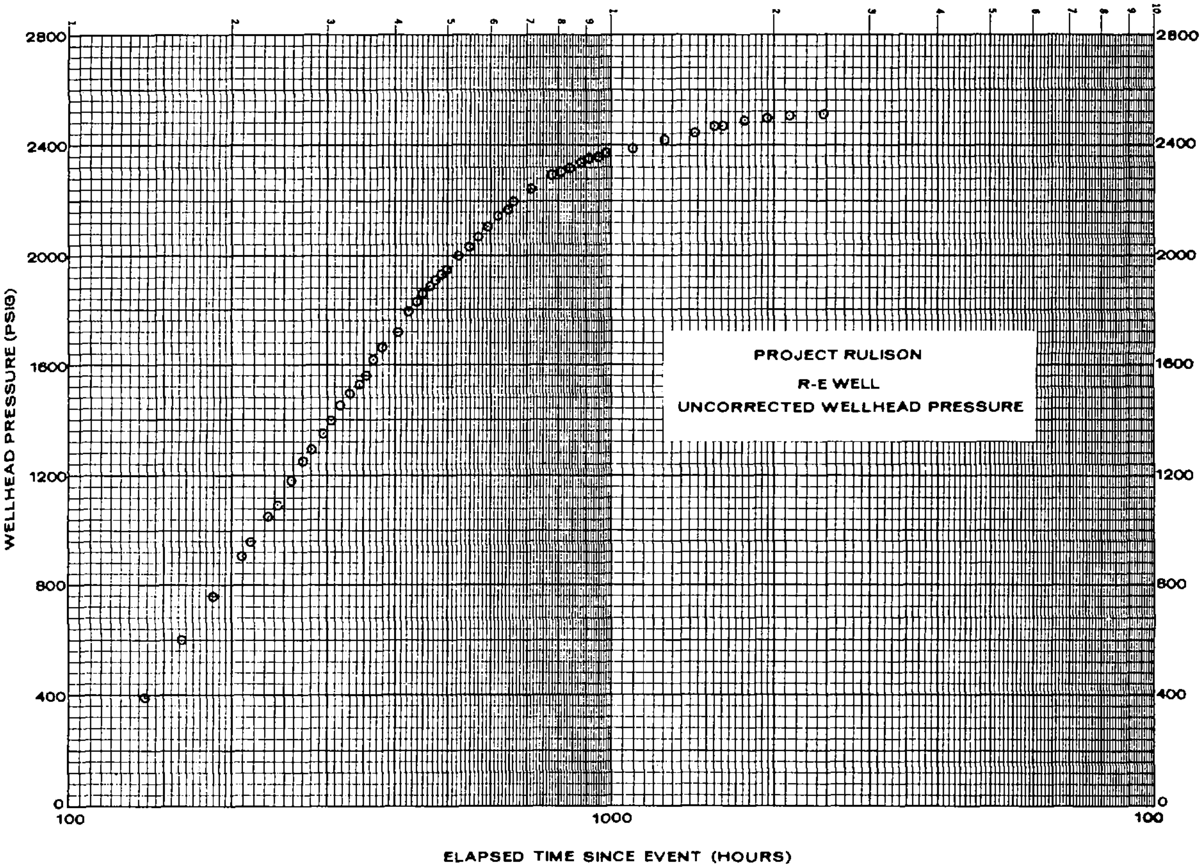

PROJECT RULISON
R-E WELL
UNCORRECTED WELLHEAD PRESSURE
WELLHEAD PRESSURE (PSIG)
ELAPSED TIME SINCE EVENT (HOURS)
2800
2400
2000
1600
1200
800
400
0
100
1000

Figure 10

TABLE I

PREDICTED CAVITY PROPERTIES FROM RULISON EXPLOSION (10)

	Maximum	Mean	Minimum	Units
Cavity Radius	108	90	72	feet
Cracking Radius	580	485	390	feet
Chimney Height	451	376	301	feet
Chimney Volume (Broken rock)	1.65×10^7	9.57×10^6	4.90×10^6	feet^3
Cavity Volume (or Chimney Void Space)	5.28×10^6	3.05×10^6	1.56×10^6	feet^3
Gas in Place @ 2930 psi 375° F (in Chimney)	721×10^6	417×10^6	214×10^6	feet^3
Fracture Zone Volume (Fractured rock)	854×10^6	----	256×10^6	feet^3
Fracture Zone Void Space	15.3×10^6	----	4.5×10^6	feet^3

$$\text{Gas Flow/30 days} = \left(\begin{matrix}\text{Fractured zone}\\ \text{void space}\end{matrix} + \begin{matrix}\text{Cavity}\\ \text{volume}\end{matrix}\right) \times \frac{\text{Observed pressure increase}}{15}$$

$$\text{Gas Flow/30 days} = (4.5\text{x}10^6 + 1.5\text{x}10^6) \times \frac{500}{15}$$

$$\text{Gas Flow/day} = 7.5 \text{ MMSCF}$$

This calculation neglects the effect of temperature which will, of course, bring the figure down slightly. It should be pointed out that this flow rate occurs with only a differential pressure of from 730 to 230 psi during the 30-day period.

The results are much higher than expected since the production across the fracture boundary is taking place at such a low differential pressure. Rates should be higher across the boundary during production where the well bore pressure will be held at a much lower value. The actual flow rates and cavity volume will be determined from re-entry and flow testing of the well.

If one uses the maximum case:

$$\text{Gas Flow/30 days} = (15.3\text{x}10^6 + 5.3\text{x}10^6)\frac{500}{15}$$

$$\text{Gas Flow/30 days} = 20.6\text{x}10^6 \times \frac{500}{15}$$

$$\text{Gas Flow/day} = 23 \text{ MMSCF}$$

Both the minimum and maximum flow rates appear quite high and probably indicate a larger fracture area to chimney volume ratio than our model. This would be highly desirable since the expected flow rates and ultimate recovery increase with fracture extent.

If the testing results on Rulison verify the preliminary data, it may be possible to develop the field commercially with smaller shots than originally predicted. This would be an exciting development since safety costs and damages would go down if the explosive yield is reduced.

FUTURE DEVELOPMENT OF NUCLEAR STIMULATION

Production data on Rulison are vital in determining how successful nuclear stimulation will be. If production rates hold up as the pressure buildup indicates, many areas of the western United States will be amenable to economic nuclear stimulation.

In our previous discussion we listed a possible cut-off point of 0.002 md as being attractive by nuclear stimulation. Of course, if the fractures are much longer than those simulated in our model, it may be possible to go to reservoirs of lower permeabilities. The slope of the curve (Figure 9) doesn't give us too much hope of ever going below 0.001 md, however. Here the production rates across the boundary between the virgin reservoir and the fractured zone wouldn't be high enough to make development economic. Of course one could still deplete the fractured area of the reservoir at a high rate, but this doesn't have enough volume (25 acres for 200 kt) in a gas reservoir to be economic. The situation might be different in an oil reservoir where conceivably one could fracture the entire reservoir economically by closely spaced nuclear shots.

Figure 11 shows a map of the areas where nuclear stimulation looks promising. In the Rulison Field alone there is an accumulation of some 8 trillion standard cubic feet. In this entire area there may be several hundred trillion standard cubic feet. The Bureau of Mines estimated 317 trillion cubic feet of gas as recoverable by nuclear means.(11)

Successful economic use of nuclear explosives may well reverse the trend to reduced reserves of natural gas. Figure 12 shows the gas production trend and the years of reserves remaining at current production rates. Gas, which is the cleanest of all fuels, is in short supply and growing more critical. Something must be done to make more gas available to the constantly increasing market.

With the target so large and the technology almost in our grasp it seems strange that so little money has been spent by the AEC on developing nuclear stimulation. Instead they keep pouring hundreds of millions of dollars yearly into development of various types of nuclear power reactors. For only a small fraction of this investment they should be able to develop the proper type of devices to make nuclear stimulation clean, economic, and readily available to utilize our already known gas reserves in tight reservoirs. We can't help but agree completely with Dr. Henry Dunlap's (12) statement that, "It would appear we're either spending too much on reactor development or too little on nuclear stimulation of gas reservoirs." Since our society is constantly clamoring for more non-polluting energy, we advocate vigorous efforts to bring the new technology of nuclear stimulation to rapid commercialization. The U. S. Government has an additional reason for developing nuclear stimulation. Over half of the acreage is Federally owned and direct royalties to the U. S. Government would be large. For example, if the Bureau of Mines figure (317 trillion SCF) is correct, royalty income to the USA could be as high as 4 billion dollars.

PROBLEMS TO SOLVE BEFORE ECONOMIC NUCLEAR STIMULATION

Costs

Foremost among the problems that must be solved is the reduction in cost. The two gas stimulation experiments performed thus far were so expensive they could not possibly be economic. Unless costs can be reduced drastically, the nuclear method can never be made economic.

The cost of a gas stimulation experiment is highly dependent upon the technical objectives and, as such, costs can vary considerably between experiments. Because of this, the Rulison costs should not be thought of as an expected norm for either further experiments or commercial projects but rather as a reference point from which sensible deviations can be made. Rulison is estimated to cost approximately $5.9 million upon completion

MAJOR BASINS OF ROCKY MOUNTAIN STATES

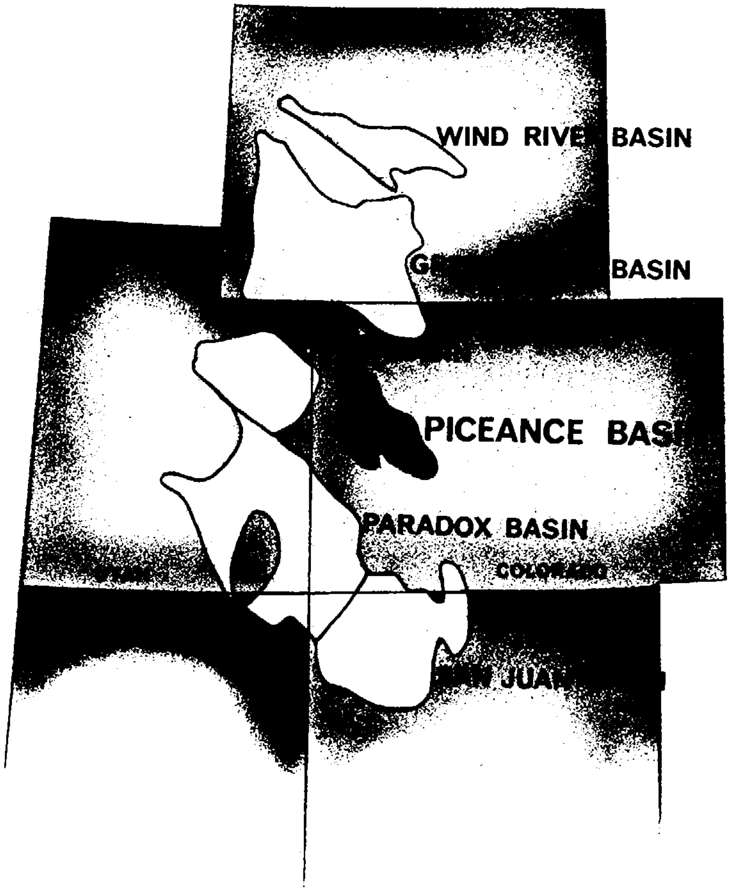

Figure 11

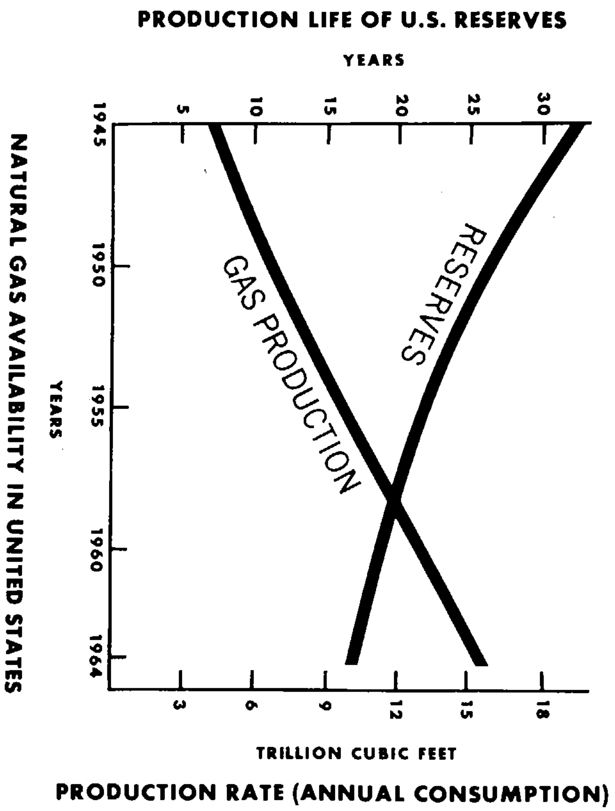

Figure 12

(See Table II); however, it is clear that on future events this could be significantly reduced. For instance, Rulison incurred costs of $271K because of a delay. One Hundred Forty-Two Thousand Dollars was incurred because of weather delays imposed by the current procedure which assumes that an accidental release of radiation will occur regardless of the depth of burial. Both of these factors should be eliminated--one by better initial planning, and the other by appropriate implementation of accidental venting safeguards. Experience gained from this event indicates that an additional million dollar-plus reduction could be achieved, even for a similar experimental event.

Table II depicts experimental cost estimates which include actual costs to date plus estimated costs to complete the experiment. The second column indicates what costs should be expected for Shot #6 in the Rulison Field. It is quite evident that significant reductions not only can be, but must be made if we are to achieve economic stimulation.

You will note that well costs are not included in the summary dealing with Shot #6. This is simply because well costs can vary significantly for different areas. For Rulison the well costs will decrease with technological development, possibly by such factors as shooting in an uncased hole, reduction in well diameter and stemming techniques allowing simplified reentry.

At first glance, a total cost of $ 700K for Shot #6, excluding well costs, might appear overly optimistic in view of the experimental costs. However, referring to the chart, Items I, II, and III , totalling almost $2. 1 million do not need to be repeated for operations in the same area. The development of the operational plan and the contract with the Government should become routine with a cost reduction of at least $130K.

Site Preparation, Maintenance, and Logistic Support could easily be reduced $95K even under experimental conditions. A reduction of $460K for explosive services remains a questionable item; however, these costs should be reduced to around $200K under the influence of the Non-Proliferation Treaty and with the development of off-the-shelf explosives.

Explosive Operation, Operational Safety, Seismic Documentation and Damage, Project Management and Public Relations are generally area-wide activities and thus the cost of performing these for five nuclear explosions on the same day would not be significantly greater than that for one. By amortizing these costs over five events, and recognizing that a good portion of these costs is due to the flaring operation, it is easy to envision another reduction of $1. 3 million.

These reductions will not just simply happen as a matter of course; active effort by both industry and Government must be made. Industry will be looking to the Government for such things as reduced device size and costs, stemming techniques (which can only be developed at the Nevada Test Site), appropriate safety criteria and encouragement. Industry is faced with developing efficient operations, technical know-how, and safety capabilities presently associated only with the Atomic Energy Commission.

TABLE II.

RULISON: EXPERIMENTAL VS. PREDICTED COST FOR SHOT #6

	Experiment $K	Shot #6 $K
Feasibility and concept	77	0
Exploratory location (drill well and test)	1089	0
Site characteristics, documentation and reporting	875	10
Develop operational plan and contract with Government	162	20
Site preparation, maintenance, and unallocated logistics	194	100
Emplacement hole	754	*
Explosive services	658	200
Explosive operations	276	140
Operational safety	656	80
Seismic documentation & damage	278	60
Post-shot drilling	230	*
Production	300	50
Project Management	299	30
Public Information	103	10
	5900	700*

* Well costs not included.

Radiation

The second major problem to tackle is radiation. Assuming the cost can be brought down to an economic level we must engineer around the contamination problem.

In gas stimulation, all of the radionuclides are initially contained. The cesium, strontium, and other insoluble silicates will be trapped at the bottom of the cavity. Such solids will not leach into aquifers since they are insoluble and further the flow is always into the nuclear-created well bore, not away from it. The remaining problem then is the radioactive gaseous byproducts.

The type and amounts of gaseous byproducts can be controlled somewhat by choice of the device and explosive environment. Here is an area where the AEC should be hard at work on device design. In the Rulison shot, a fission device was used with a boron carbide shield to cut down generated tritium by a factor of 3 or 4. Other such refinements are possible by the excellent laboratory staffs of LRL and LASL.

In general, we need to be concerned with only two gaseous radionuclides, tritium and krypton. Iodine, though produced in large quantities by a fission device has a short half-life (8 days) and can be allowed to expend itself simply by delayed reentry.

Krypton 85 is a byproduct of the fission or atom bomb. Its concentration can be reduced by using a fusion or H-bomb. However, this increases the concentration of tritium, some of which remains behind unused from a thermonuclear reaction.

The total gaseous radiation expected in Rulison is actually very small; less than 0.3g (3,000 curies) of tritium production (an isotope of hydrogen) was estimated. This would be equivalent to the amount contained in about 1 cc of pure tritiated water. The amount of krypton produced was calculated as 1,000 curies or 0.02 cubic feet of gas at standard conditions.

The problem is caused by the mixing of the radioisotopes in the gas following the detonation. These small amounts of gases are mixed in the 200-700 million standard cubic feet of methane expected in the cavity. As a further complication some of the tritium will partially exchange with hydrogen of the methane to give a small amount of tritiated methane.

Let's look a little further at the tritium problem. Since over 90% of the tritium will stay behind with bound water in the cavity, there will probably be less than 0.03g or 300 curies produced with the gas in the chimney. (For comparison, natural cosmic radiation produces about 6,000 g of tritium per year.) If we assume the gas is burned and mixes in the air above the ground within one mile of the well (a very conservative estimate), we calculate a concentration of tritium in air many times below the allowable tritium in air levels given by the standards set by the Federal Radiation Council. For the layman, if a person breathed this air for one year (which is impossible since the air would mix with other air), he would receive less total radiation than 1/30 the amount he gets from one chest x-ray--or less radiation than the amount he gets from flying from Las Vegas to New York in a jet airplane.

How serious are other gaseous radiation problems? Judging by the sound and fury of the opponents to Rulison, it must appear very dangerous. Actually, however, the total amount of krypton in the cavity at Rulison is also small compared to that encountered every day in our society. The total amount of krypton from Rulison (1, 000 curies) is produced in 2-1/2 days operation of a 1000 megawatt nuclear reactor and nuclear power is much cleaner from a radiation standpoint than coal-fired power. (13), (14)

It's obvious we have an information gap somewhere and should get busy informing the layman of the facts of radiation. Until we get the message across, we will have a public acceptance problem. Alleviating this problem is extremely important because the public should actually be demanding rapid development of nuclear gas stimulation as a way to obtain energy with minimum pollution.

But facts don't cover emotions and this radiation was created by a bomb. Thus, uncontrolled venting of the gas, though it would be safe, is probably not a good answer to the radiation problem. Further, it would be a terrific waste of energy which our economy can ill afford.

The first solution to the problem might be achieved by mixing. In other words, take the slightly contaminated chimney gas and dilute it several times with non-contaminated gas before it goes into a pipeline. This solution is technically sound but again, because of the emotional aspect, may not be feasible.

A second solution is to pipe the chimney gas out of the basin to a remote area and use it to generate electric power. All that is needed is an ample supply of cooling water and controlled burning so that radiation levels are maintained far below any possible radiation damage. This plan is under study and may well be the best answer.

A third solution is to work out a method of separating the contaminated from non-contaminated gas. This would be quite a technical undertaking since krypton has a boiling range close to that of methane. Further, any tritium which has formed tritiated methane is extremely difficult to separate from non-tritiated methane. But the separation may be possible and research should be done in this area. In other applications such as storage, removal of the radioactive gas would present much less of a problem.

SUMMARY AND CONCLUSIONS

Nuclear gas stimulation is close to economic use. Though the two gas shots Gasbuggy and Rulison have been expensive experiments, we have shown how these costs can be reduced to make nuclear stimulation attractive. Successful development of the method may radically change the gas shortage which is developing in the U. S.

Preliminary results from Rulison are encouraging. Pressure in the cavity has built up rapidly, indicating a high flow rate from the virgin reservoir rock into the fractured zone. If the build-up data is confirmed by long-term flow tests, we'll find that our original predictions were far too conservative. This would mean we can produce the stimulated gas wells at higher rates than expected or reduce the size of device needed to stimulate gas wells economically.

Several problems need further concentrated effort. Costs of the operation must be reduced drastically or it will never be economic. Such reductions can only be achieved through close cooperation between the AEC and industry.

Radiation has emerged as the major problem to be solved. Here the major answer lies in education of the population since nuclear stimulation will allow increased production of gas which is the cleanest power source available. However, other solutions such as device design changes to reduce the actual amounts of radiation, burning chimney gas for generating electricity, and methods of physically separating the krypton and tritium from methane should be studied.

REFERENCES

1. "Formation Fracturing", Tulsa, Oklahoma, Oil and Gas Journal, 1960 (73 page booklet).

2. Atkinson, C. H., and Lekas, M. A., Oil and Gas Journal, December 2, 1963, 154 - 156.

3. Coffer, H. F., Bray, B. G., Knutson, C. F., Proc. Third Plowshare Symposium, U.S. AEC TID-7695, April, 1964, 269-288.

4. Aronson, H. H., and Brundage, R. S., Nuclex 1969, Basel, Switzerland, October 6-11, 1969.

5. Boardman, C. R., Rabb, D. D. and McArthur, R. D., Lawrence Radiation Laboratory (Livermore), UCRL-7350, May 1963.

6. Coffer, H. F., Grier, H. E., and Aronson, H. H., The Canadian Mining and Metallurgical Bulletin, June, 1968.

7. "Project Gasbuggy," Joint Study, El Paso Natural Gas Company, U.S. AEC, U. S. Bureau of Mines, Lawrence Radiation Laboratory, U. S. Plowshare Program PNE-1000, May 14, 1965.

8. "Project Rulison Feasibility Study," Proposal to the U.S. AEC, Austral Oil Company Incorporated and CER Geonuclear Corporation, September 14, 1966.

9. Reynolds, M., Bray, B. G., and Mann, R. L., Paper #36, Symposium on Engineering with Nuclear Explosives, Las Vegas, Nevada, January 14 - 16, 1970.

10. "Predictions of Seismic Motion and Close-In Effects, Rulison Event", Environmental Research Corporation, NVO-1163-180, PNE-R-5.

11. "BuMines Chief Says Nuclear Blasts Offer Key to Future Supply," Oil and Gas Journal, (August 15, 1966) p. 44-46.

12. Dunlap, Henry F., "Importance of Early Development of the Nuclear Stimulation Process". Paper presented at AIF Conference in San Francisco, December, 1969.

13. Coffer, H. F. and Higgins, G. H., "Nuclear Explosives for Oil and Gas Stimulation and Shale Oil Recovery," Exploration and Economics of the Petroleum Industry, March 6 - 8, 1968.

14. Eisenbud, Petrov, Science 144, (April 17, 1964), pp. 288-9.

XA04N0856

PROJECT RULISON: A PRELIMINARY REPORT

Miles Reynolds, Jr.
Assistant Vice President
Austral Oil Company Incorporated
Houston, Texas

Bruce G. Bray
Director of Engineering
CER Geonuclear Corporation
Las Vegas, Nevada

Robert L. Mann
Senior Staff Engineer
CER Geonuclear Corporation
Las Vegas, Nevada

ABSTRACT

Project Rulison was designed to use underground nuclear technology to determine the potential of this technique for commercial development of the deep, thick, lenticular, low permeability, Mesaverde Formation of the Rulison Field in Garfield County, Colorado. Since discovery in 1952, this reservoir has been tested by nine widely-spaced conventionally completed wells. A method of stimulation, far greater in magnitude and efficiency than conventional hydraulic fracturing, is needed to recover this gas at economic rates.

A feasibility study completed in July 1966 indicated that nuclear explosives were a potentially economic method of stimulating recovery of natural gas from the reservoir. The gas-in-place, estimated to be between 90 - 125 billion cubic feet per 640 acres from earlier wells, was confirmed from information obtained on two conventional wells completed in 1966.

The Project Rulison exploratory well, R-EX, was completed in May 1968. Detailed testing of this well provided data on geology, hydrology and reservoir characteristics. The data obtained from the testing have been used to determine the flow capacity of the Mesaverde reservoir. The reservoir characteristics were then used as input data to make predictions of post-shot reservoir performance in the nuclear stimulated well, using a radial, unsteady state gas flow computer model.

A nuclear explosive with a design yield of 40 kilotons was emplaced in a 10-3/4 inch hole at a depth of 8426 feet below ground surface and detonated on September 10, 1969. A preliminary appraisal of the data taken at shot time indicate that the explosive behaved as predicted. The explosion was

completely contained underground as predicted and no major seismic damage occurred.

The post-shot drilling program, to reenter the chimney, will commence in March 1970, approximately six months after detonation. A test program will be initiated at that time to determine the degree of reservoir stimulation achieved.

INTRODUCTION

Project Rulison was detonated on September 10, 1969, in the Battlement Mesa area of Garfield County, Colorado (Figure 1). Project Rulison was the second joint Industry-Government sponsored gas stimulation experiment using a nuclear explosive, and was made possible under the provisions of the United States Atomic Energy Commission's Plowshare Program. Austral Oil Company Incorporated of Houston, Texas, was the industrial sponsor, and employed CER Geonuclear Corporation of Las Vegas, Nevada, as Program Manager. Project Rulison was designed to determine the potential of underground nuclear technology for commercial development of the Mesaverde formation of the Rulison Field (Figure 2).

Austral's interest in the use of underground nuclear engineering in the Rulison Field commenced early in 1965. Austral initially acquired approximately 20, 000 acres, and, through additional leasing and farmout agreements have increased their leasehold interests in the Rulison Field area to approximately 60, 000 acres.

In 1965-1966 Austral drilled and tested two wells in the Rulison Field for the purpose of collecting data for a feasibility study. Prior to this 7 wells had been drilled into the Mesaverde gas reservoir by other operators, the discovery well having been drilled in 1952.

The feasibility study completed in mid-1966 indicated that nuclear explosives could be applied economically as a method of stimulating the production of natural gas from the Mesaverde reservoir. The study also confirmed that the Mesaverde formation in the Rulison Field contained an estimated 90-125 billion standard cubic feet of gas-in-place per 640 acres.(1)

The development of a Technical Plan was initially undertaken in 1967 with the AEC's Lawrence Radiation Laboratory, Livermore, California. In April, 1968, however, the supporting laboratory assignment for Project Rulison was given to the Los Alamos Scientific Laboratory, Los Alamos, New Mexico. The subsequent Project Definition Plan(2) and the implementation of that plan was accomplished with the Los Alamos Scientific Laboratory, the U. S. Bureau of Mines, and the AEC Nevada Operations Office. The Project Definition Plan set forth the general Technical, Nuclear Operations, Safety Program, Administrative, Logistics and Support, and Engineering and Construction activities to accomplish the objectives of the experiment. Development of the Plan lead to contract negotiation between the government and the industrial sponsor. The contract for the conduct of Project Rulison was signed by the parties on March 27, 1969.

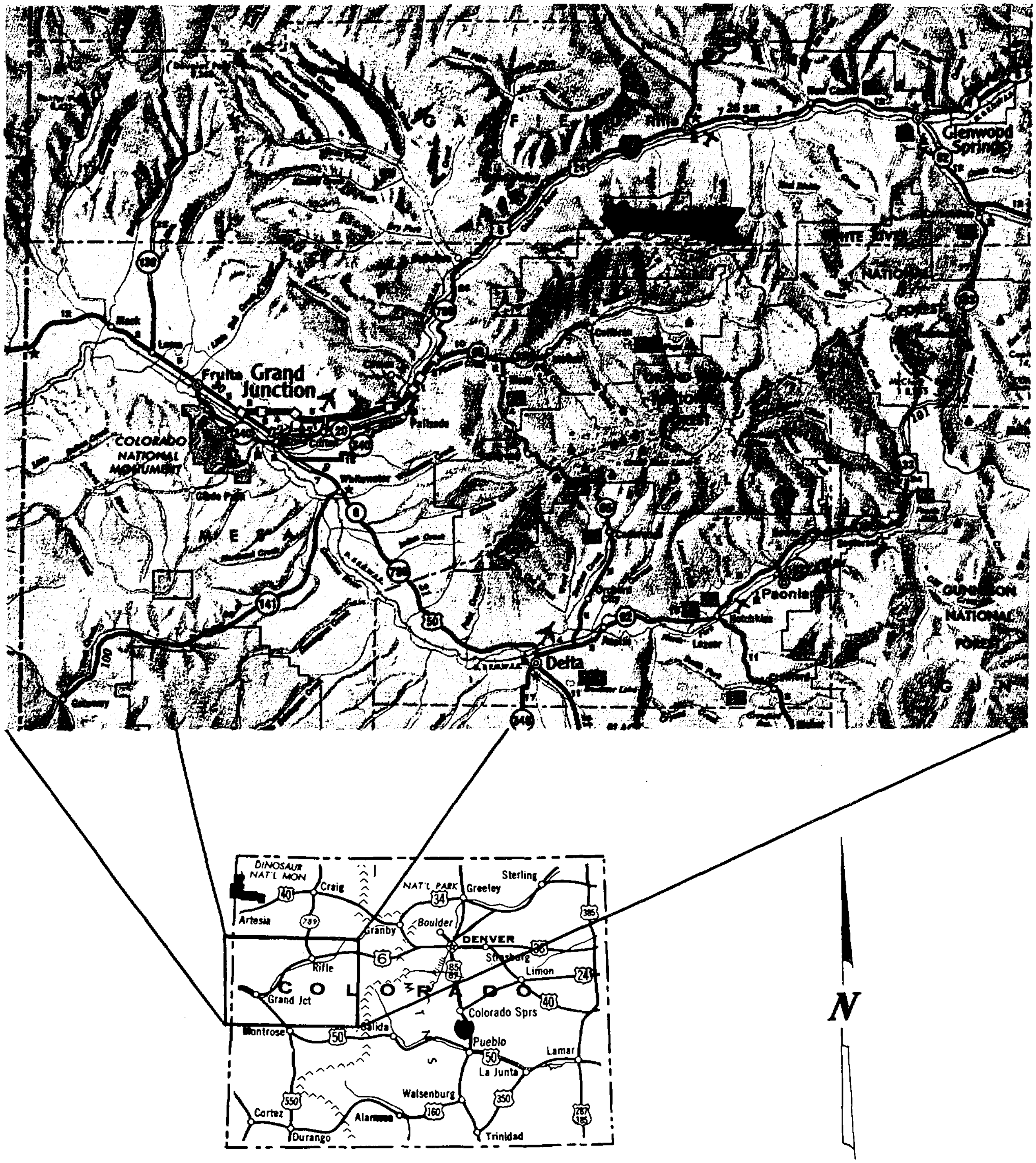

MAP OF NORTHWEST COLORADO

FIGURE 1

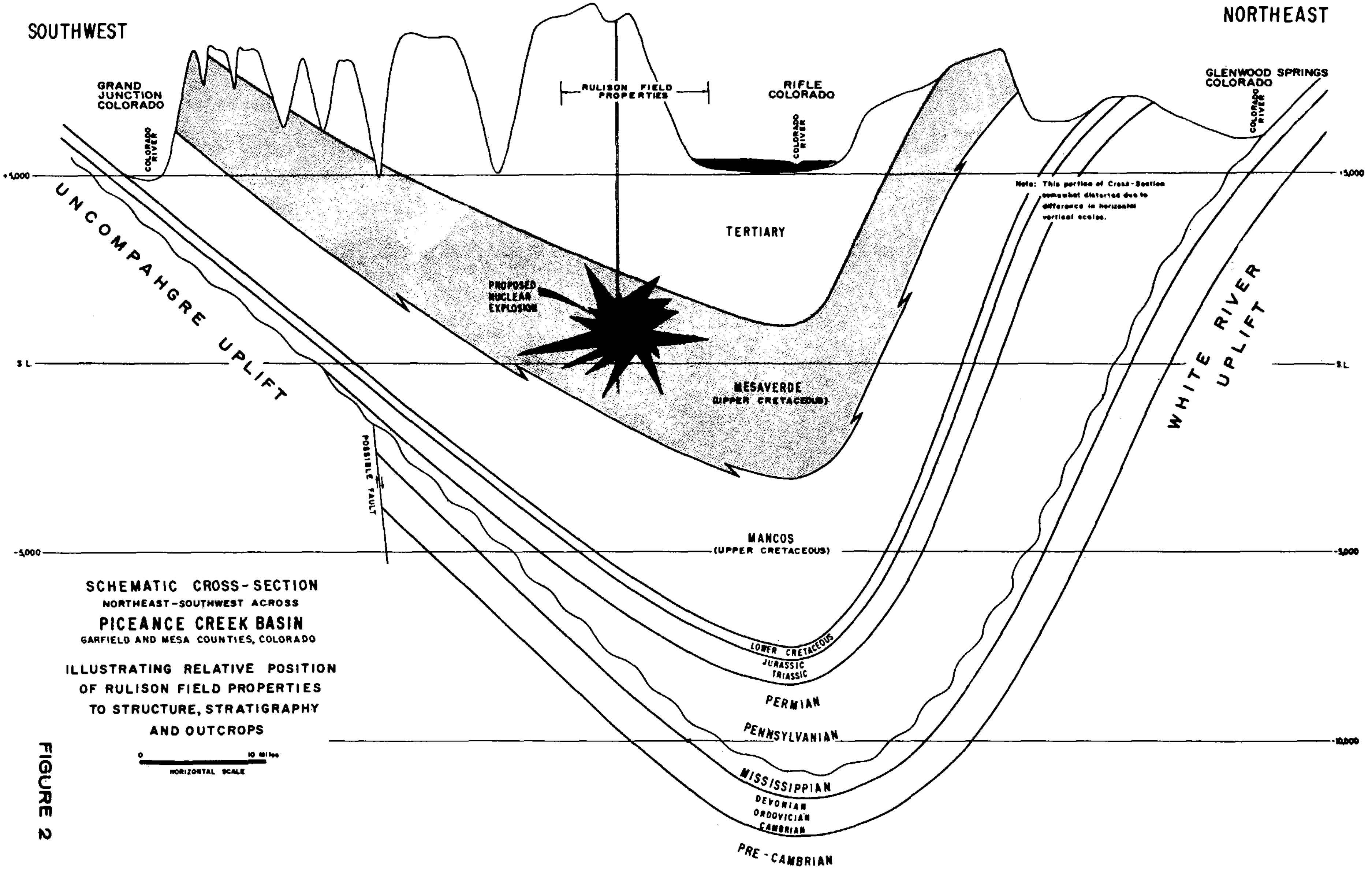

Note: This portion of Cross-Section somewhat distorted due to difference in horizontal vertical scales.

SCHEMATIC CROSS-SECTION
NORTHEAST-SOUTHWEST ACROSS
PICEANCE CREEK BASIN
GARFIELD AND MESA COUNTIES, COLORADO

ILLUSTRATING RELATIVE POSITION
OF RULISON FIELD PROPERTIES
TO STRUCTURE, STRATIGRAPHY
AND OUTCROPS

FIGURE 2

The conduct of the experiment is divided into three phases corresponding to the three major site activities:

I. Site Acceptability -- to detail and document the geologic, hydrologic, and reservoir characteristics and assure that safety criteria can be met.

II. Operational -- to perform site construction and activities associated with the nuclear portion of the project and securing the site while waiting for reentry.

III. Post-shot Investigations -- to reenter the nuclear "chimney," evaluate the stimulated reservoir production, radioactivity, ground motion and structural response characteristics and perform an economic evaluation of the project.

OBJECTIVE

The objective of Project Rulison is to determine the potential of nuclear stimulation for the commercial development of the Rulison Field. The Rulison area, with its moderately deep, thick, lenticular, low permeability sequences of the Mesaverde, Wasatch, Fort Union, Lewis and Erickson Formations, is typical of many undeveloped gas fields. The information obtained from the project would have an important bearing on the commercial possibilities of nuclear stimulation of other areas. Details of the information desired to fulfill this objective is found in the Project Definition Plan.(2)

SITE EVALUATION

Geology and Hydrology

The Rulison Field encompasses approximately 60, 000 acres. A general evaluation of the geologic, hydrologic and reservoir characteristics was made on the basis of the seven older wells completed in the gas-bearing Mesaverde formation and the drilling and testing of two additional wells. (1) The Mesaverde Formation in the Rulison Field contains an estimated 8-10 trillion standard cubic feet of gas-in-place and is not commercially productive using conventional completion techniques.

Rocks ranging in age from recent alluvial fill in the valleys to Precambrian "basement" are present in the Rulison area. The sequence of rocks present and their relation to the general stratigraphy of the Piceance Creek Basin are shown in Figure 3.

Geological background investigations of the Rulison area (3-7) show a uniformly simple structural picture. The Rulison structure is part of the Piceance Creek Basin with the field in the Southwest limb of the Basin. Upper Cretaceous beds in this area dip towards the northeast at the rate of approximately 150 feet per mile while the overlying Tertiary beds are relatively flat.

RULISON AREA STRATIGRAPHY

SYSTEM AND PERIOD			"FORMATIONS"	GENERAL LITHOLOGY	APPROX. THICKNESS
Quaternary			"Recent"	Low terrace, floodplane, and alluvial deposits	100'
			"Pleistocene"	Terrace and fan sand and gravel, pediment gravel, colluvium, mudflow, and solifluction deposits	200'
Tertiary			(?)	Basalt flows underlain by variegated claystones and gravel	1,000'
			Green River	Oil shales, marlstones, and sandstones (dark color)	2,100'
			Wasatch	Bright colored clays and shale with minor sandstone	5,000'
			Fort Union	Brown-gray shale and coal	1,000'
			Ohio Creek	Sandstone and conglomerate	50'
Cretaceous	Upper	Mesaverde	Lewis-Lance Equiv.	Shale - sandstone	2,500'
			Williams Fork	Shale	
			Isle	Shale - sandstone	
	Lower		Mancos	Gray shale	1,700'
			Naturita	Shale - sandstone	600'
			Dakota Cedar Mt.	Sandstone	200'
Jurassic			Morrison	Variegated shale and sandstone with interbedded tuff and ash	300'
Triassic			State Bridge	Red arkosic sandstone	600'
			Schoolhouse	Sandstone	60'
Permian			Minturn	Continental red beds interbedded with white Weber type sandstone	1,000'
Pennsylvania			Maroon	Buff-red sandstone	
			Eagle Valley	Evaporites (chiefly anhydrite)	2,800'
			Belden	Gray to black shale with basal conglomerate	
Cambrian through Mississippian			Madison, etc.	Limestone, dolomite and quartzite	~700'
Pre-Cambrian				"Basement" metamorphics and plutonics	

FIGURE 3

The Mesaverde Formation in the Rulison Field area was deposited in the near shore environment that included marine, floodplain and coastal swamp conditions. This depositional setting resulted in lenticular sandstones that, from available data, have limited areal extent. The lenticularity of the Mesaverde sandstone reservoirs is the cause of gas entrapment in the Rulison Field. (Figure 4)

The Rulison Surface Ground Zero is located in Section 25, Township 7, South, Range 95, West, shown in Figure 5. The site is on the upper reaches of Battlement Creek at an elevation of about 8200 feet. The site was picked on the basis of both technical and safety considerations detailed in the initial feasibility study(1) and confirmed by the data obtained from an exploratory well, R-EX drilled at the site. (2, 10)

R-EX was completed in May of 1968 to a total subsurface depth (TD) of 8516 feet. Representative intervals of the Wasatch and Ohio Creek Formations were cored and tested and all were found non-productive of water. The well was cased through the Ohio Creek Formation to a depth of 6367 feet with 7-5/8 casing. A 6-1/8 inch hole was air- and mud-drilled in the Mesaverde Formation from the intermediate casing point to the total depth (TD) of 8516 feet.

Representative cores and a comprehensive suite of logs were obtained in the Mesaverde section. A 5-1/2 inch liner was cemented through the Mesaverde section and the well was production tested.

The "bedrock" at the Project Rulison site is the lower Green River Formation. The base of the Green River occurs at a subsurface depth of approximately 1700 feet in the R-EX well. Relatively impermeable Wasatch and Fort Union shales and siltstones were encountered below the Green River in the interval from approximately 1700 feet to 6134 feet in R-EX. The Ohio Creek Formation occurs between the Fort Union and the Mesaverde, and is encountered from 6124 to 6175 feet.

The ground-water resources in the Rulison area are confined primarily to alluvium and terrace deposits. The underlying bedrock formations are generally impermeable and yield little or no water. After installation of the casing in the exploratory hole, R-EX, hydrologic drillstem and swab tests were performed by the USGS by perforating the casing and testing all zones below 6000 feet which produced any water during the drilling or in which geophysical logs suggested the possibility of water.(8) In addition wireline formation sample tests were made on 6 zones in the Wasatch from 2000 feet to 6000 feet.(2) All tests were dry. The pressures recorded during the drillstem tests of the different zones indicated negligible or no fluid entry to the hole. No fluid was recovered on any of the swab tests performed during the drillstem tests. Spectrographic, radiochemical and chemical analyses of the fluid collected from the tubing immediately above the test tool after each test indicated that the fluid was from the drilling and cementing operations rather than formation water.(8, 9)

GRAPH SHOWING RELATIVE POSITION
MESAVERDE SANDS IN PRODUCTIVE WELLS
RULISON FIELD PROPERTY
GARFIELD COUNTY, COLORADO

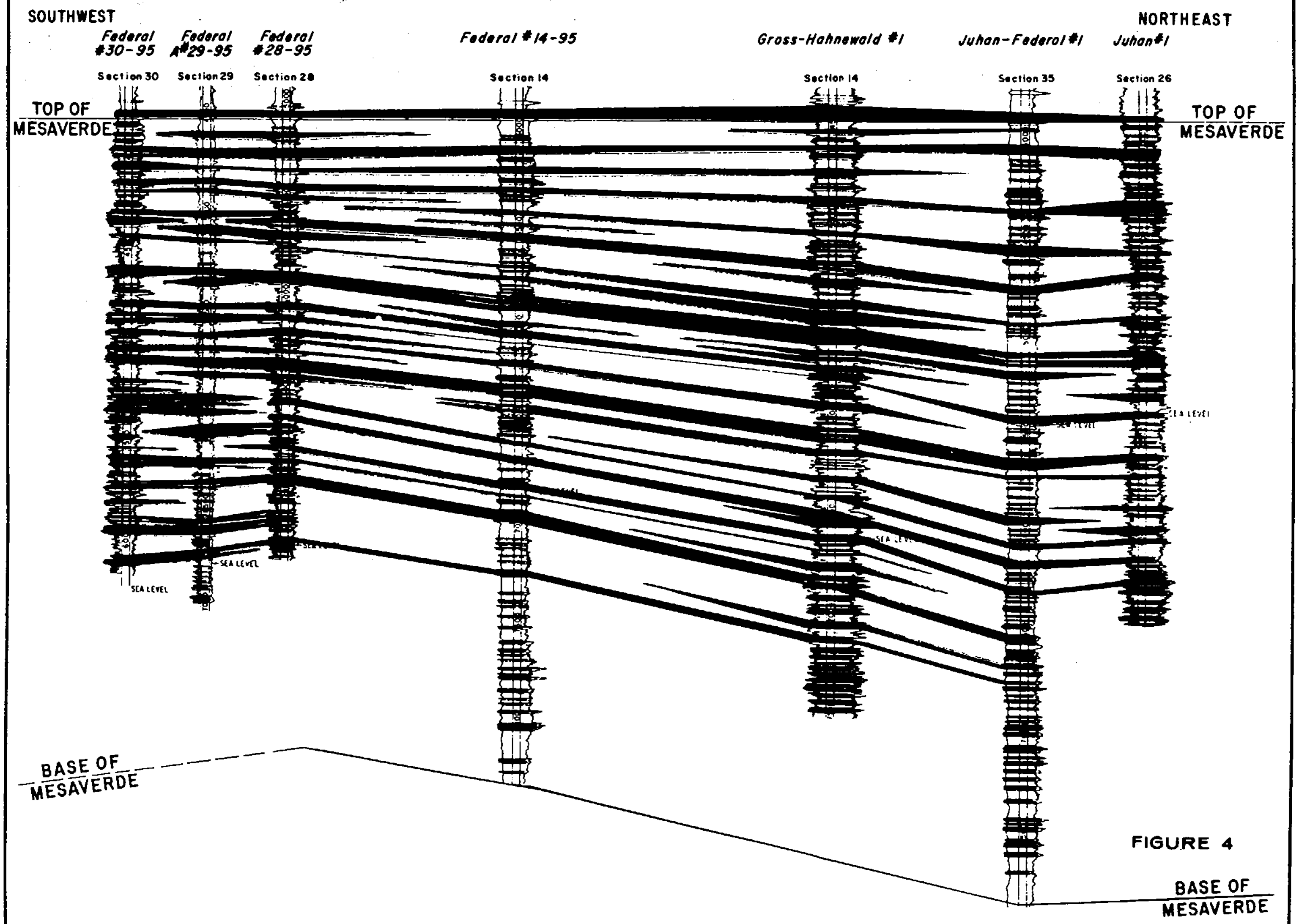

FIGURE 4

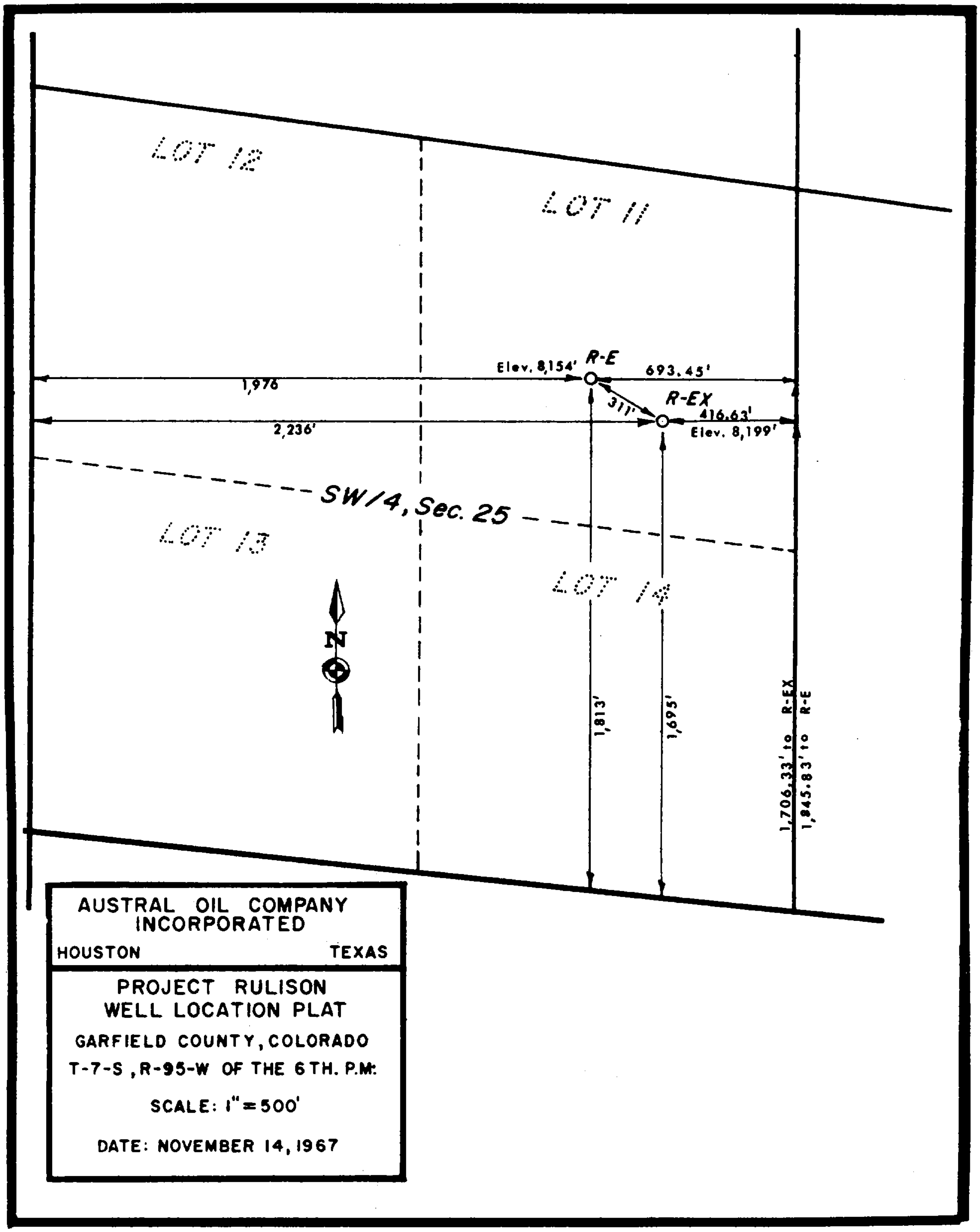

LOCATION R-E AND R-EX

FIGURE 5

Reservoir Characteristics

The average Mesaverde Formation characteristics obtained from an analysis of logs, core, and production data from existing wells in the field summarized from the Feasibility Study are given in Table I. The same average characteristics from the initial evaluation of core and log analyses from R-EX are also given in the Table for comparison.

Initial production tests in the gas bearing intervals of the R-EX well conducted immediately following completion were not representative of the reservoir due to formation damage from filtrate invasion. The well was perforated over four different intervals from 7302 to 8464 feet, each interval was flow tested, and the well shut-in for pressure buildup. The initial testing analysis indicated severe formation damage was present throughout the entire interval.

In order to determine true formation characteristics from flow and buildup tests, a typical zone (8140' - 8172') was isolated and given a small volume hydraulic fracture treatment so that the reservoir properties beyond the damaged zone could be evaluated. After completion of the fracturing treatment the well was flowed to allow it to clean up and then was shut-in for pressure buildup prior to testing

Two sets of drawdown and buildup data were obtained on the fractured interval in the R-EX well. However, only the analysis of the second set is considered reliable because rate control problems, insufficient cleanup of the well after fracturing, and mechanical problems clouded the first test results. Bottom hole pressures were obtained using surface recording downhole pressure equipment. Figure 6 is a schematic diagram of the flow rate control and measurement equipment. The complete fracture treatment and numerical reservoir well test data for both tests are given in reference 10.

The drawdown and buildup data from the second set of tests (Figures 7 and 8) are typical of what might be expected from a tight,fractured formation and have been analysed by conventional techniques .(11, 12, 13)

Since R-EX had been hydraulically fractured prior to testing, the drawdown data were plotted as the real gas potential, M(p), versus the square root of time, (Figure 9). Two straight line portions are observed, the first portion lasts until about $\sqrt{t} = 11$ or 121 hours and the second straight line segment lasting to about $\sqrt{t} = 25$ or 625 hours. These straight line segments represent the linear and transitional regions respectively(12, 13). The radial flow segment probably occurs after 625 hours but is poorly defined by the drawdown.

Figure 10 is a plot of the real gas potential M(p) versus log time. The end of the drawdown period is probably in the radial regime, but again, the slope is poorly defined as a result of, 1) fluid production at the end of the test, and 2) shutting the well in before accurate definition of the final slope was attained. However, maximum and minimum slope values for the radial flow portion of the plot were estimated in order to determine a probable

TABLE I

AVERAGE RESERVOIR PROPERTIES

Sandstone Lens Property	Feasibility Study(1)	R-EX Well(2)	
		Core	Log
Porosity, percent	9.7	8.7	7.8
Permeability, millidarcies	0.5	11	--
Saturation, percent			
Water	45	44	38-55
Gas	54	55	45-62
Oil	1	1	
Temperature at 8400 ft subsurface, °F		214	

Basis for Volumetric Calculations	Average from 9 Original Wells	R-EX Well
Net Sand, feet	500**	375*
Base Pressure, psia	15.025	15.025
Base Temperature, °F	60	60
Initial Gas Deviation Factor (Z)	0.88	.88
= SCF/ft^3	123-171	170
Gas-in-place, Billion scf/640 acres	90-125	110

*Net sand over gross interval from 7302 to 8464 feet

** Net sand over entire Mesaverde section

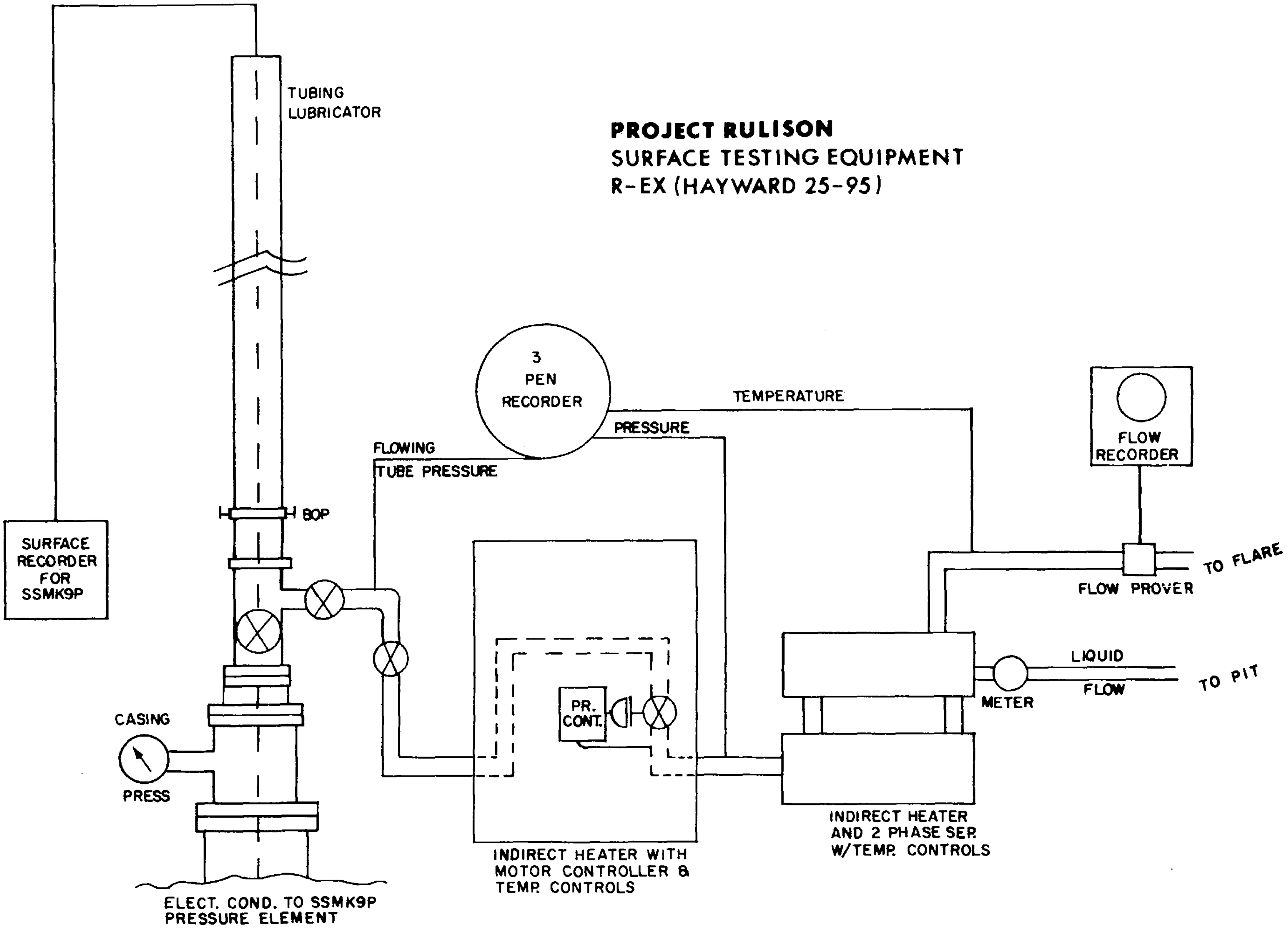
PROJECT RULISON
SURFACE TESTING EQUIPMENT
R-EX (HAYWARD 25-95)
TUBING LUBRICATOR
SURFACE RECORDER FOR SSMK9P
BOP
CASING PRESS
ELECT. COND. TO SSMK9P PRESSURE ELEMENT
FLOWING TUBE PRESSURE
3 PEN RECORDER
PRESSURE
TEMPERATURE
PR. CONT.
INDIRECT HEATER WITH MOTOR CONTROLLER & TEMP. CONTROLS
INDIRECT HEATER AND 2 PHASE SEP. W/TEMP. CONTROLS
FLOW RECORDER
FLOW PROVER
TO FLARE
METER
LIQUID FLOW
TO PIT

FIGURE 6

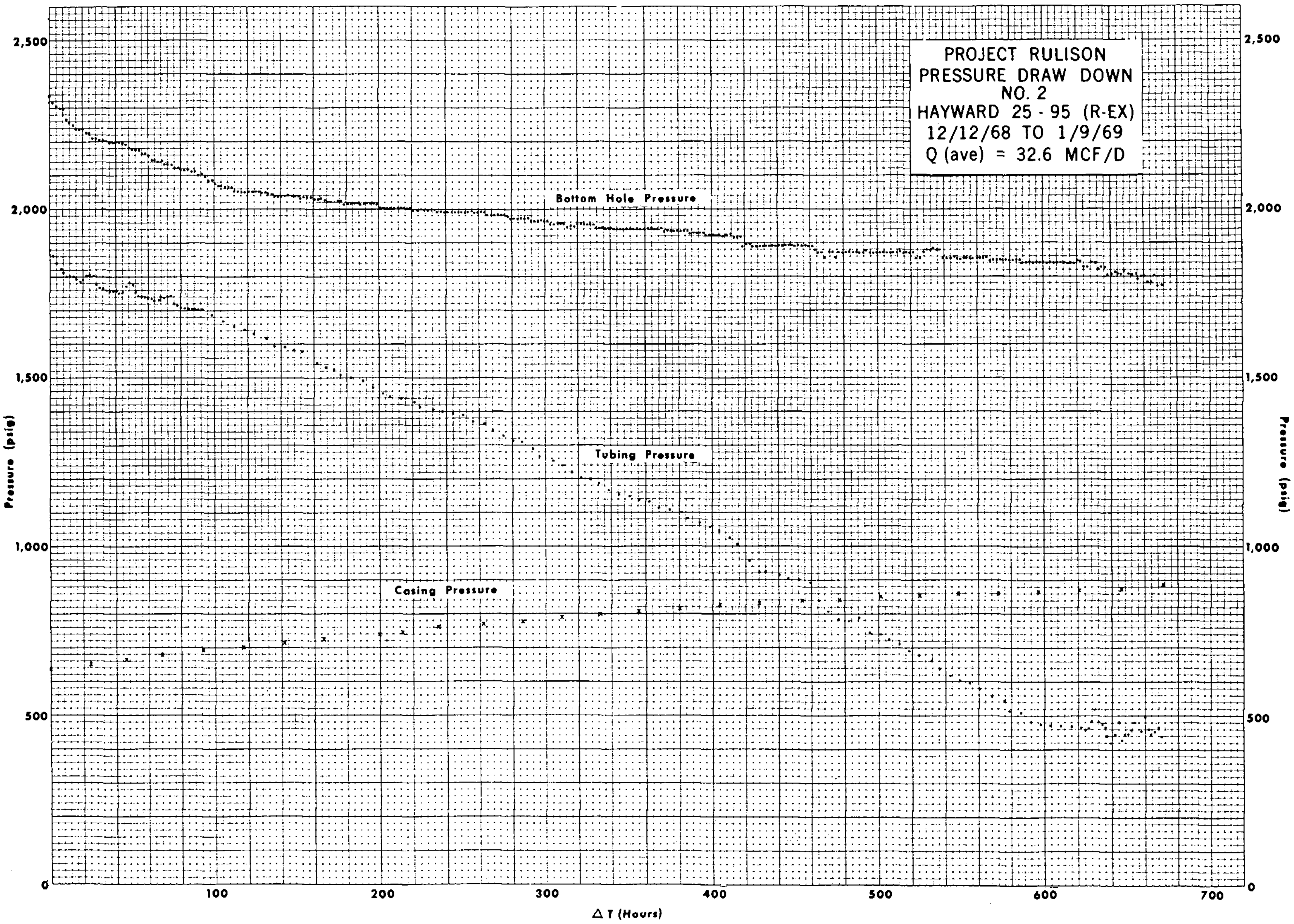
PROJECT RULISON
PRESSURE DRAW DOWN
NO. 2
HAYWARD 25 - 95 (R-EX)
12/12/68 TO 1/9/69
Q (ave) = 32.6 MCF/D
Bottom Hole Pressure
Tubing Pressure
Casing Pressure
Pressure (psig)
2,500
2,000
1,500
1,000
500
0
100
200
300
400
500
600
700
Δ T (Hours)

FIGURE 7

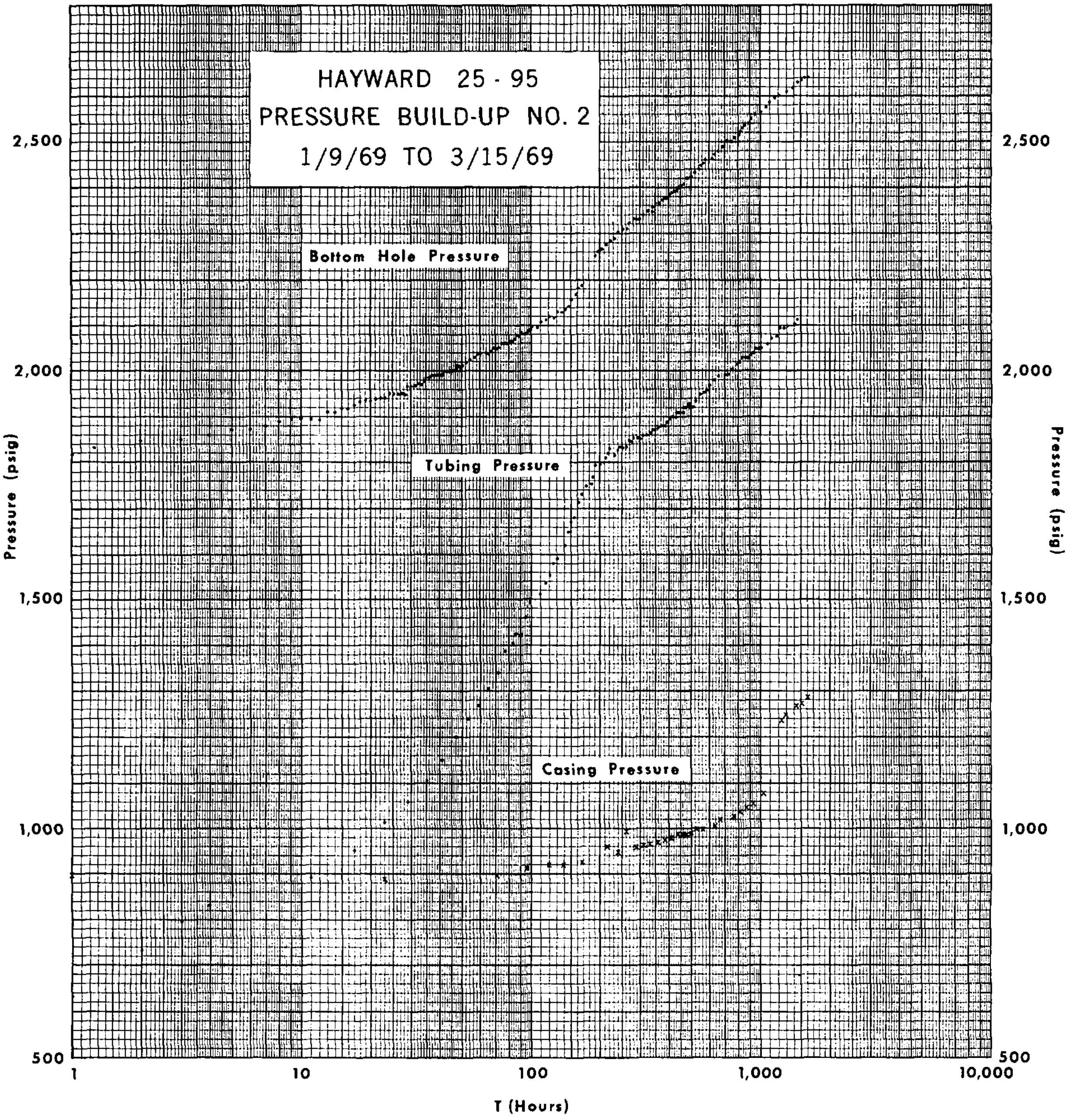
HAYWARD 25 - 95
PRESSURE BUILD-UP NO. 2
1/9/69 TO 3/15/69
Bottom Hole Pressure
Tubing Pressure
Casing Pressure
Pressure (psig)
Pressure (psig)
2,500
2,000
1,500
1,000
500
1
10
100
1,000
10,000
T (Hours)

FIGURE 8

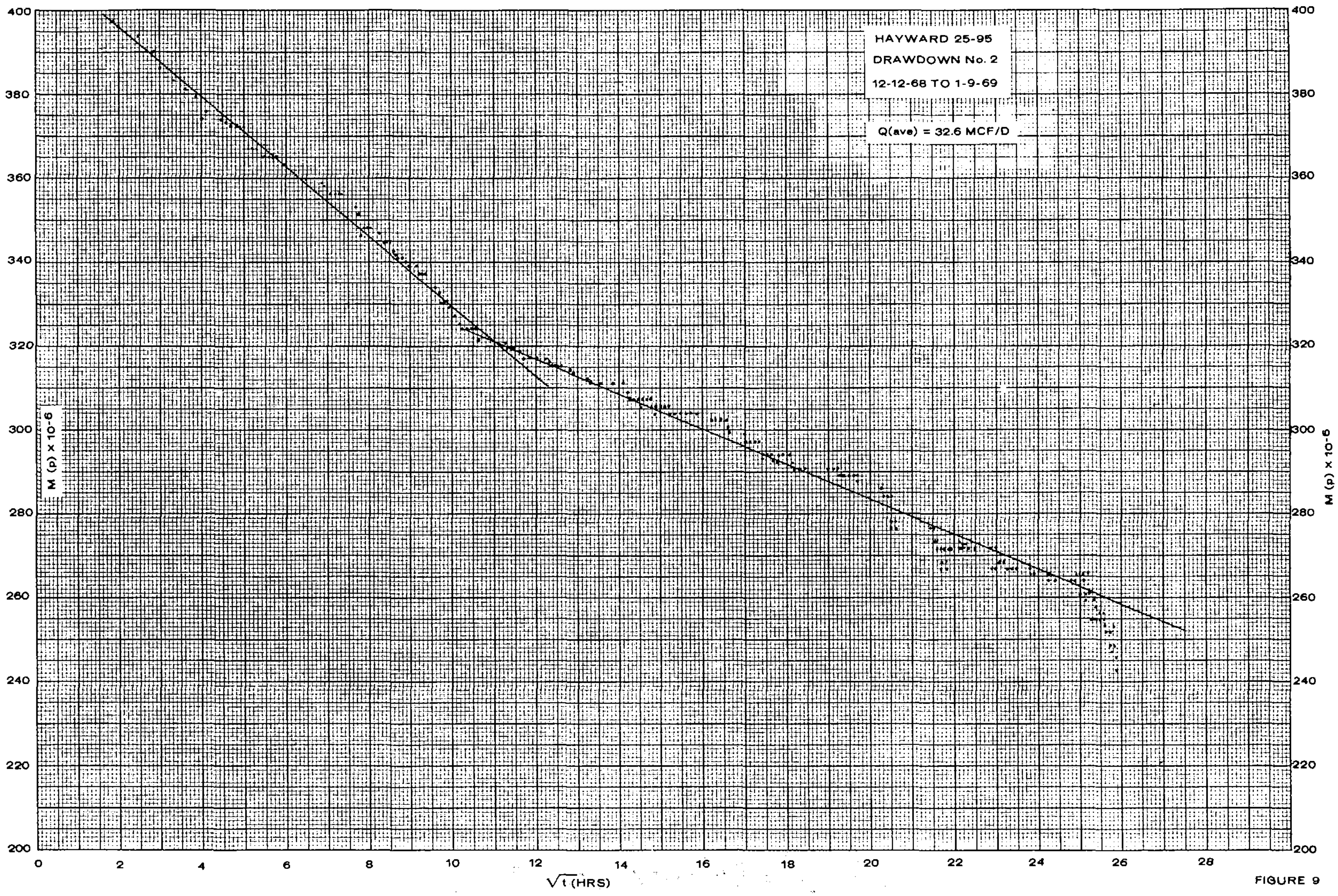
HAYWARD 25-95
DRAWDOWN No. 2
12-12-68 TO 1-9-69
Q(ave) = 32.6 MCF/D
M (p) x 10-6
M (p) x 10-6
400
380
360
340
320
300
280
260
240
220
200
0
2
4
6
8
10
12
14
16
18
20
22
24
26
28
√t (HRS)

FIGURE 9

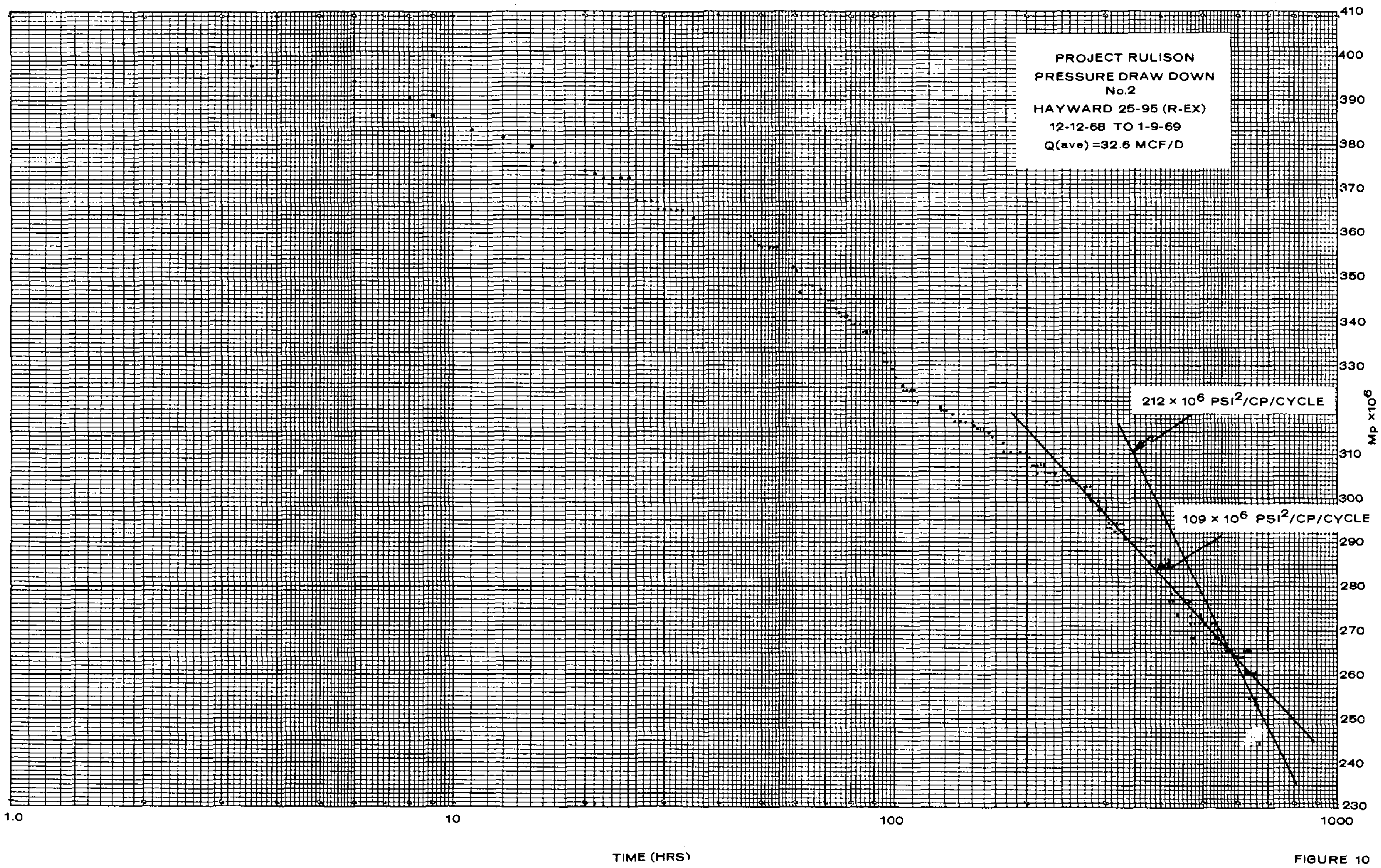
PROJECT RULISON
PRESSURE DRAW DOWN
No.2
HAYWARD 25-95 (R-EX)
12-12-68 TO 1-9-69
Q(ave) =32.6 MCF/D
212 x 10^6 PSI^2/CP/CYCLE
109 x 10^6 PSI^2/CP/CYCLE
1.0
10
100
1000
TIME (HRS)
410
400
390
380
370
360
350
340
330
310
300
290
280
270
260
250
240
230
Mp x10^6 (PSI^2/CP

FIGURE 10

range of formation capacity. The range of values calculated are:

		Maximum	Minimum
b ($psi^2/cp/cycle$)	=	-109×10^6	-212×10^6
kh (md ft)	=	.337	.173
h (ft)	=	32	32
k (md)	=	.0105	.0054

Two different techniques were used to analyse the pressure buildup data of Figure 8. The conventional Horner technique(14) using a t_o of 3735 hours in order to account for previous production history is given in Figure 11. The initial bottom hole pressure was determined to be 2940 psia, with an associated formation permeability of .0058 md.

Because a tight reservoir such as the Mesaverde has a "long memory" for earlier pressure transients, an alternative analysis technique to account for the earlier flow periods is to use the method of "superposition." Prior production history is accounted for in the "superposition" method by plotting M(p) against the term:

$$\sum_{i=1}^{n}(q_i - q_{i-1})\log(t - t_{i-1})$$

where t_i is the time at which flow rate q_i is terminated. Since the buildup was run well beyond the time expected for the transition zone, this method probably gives the most realistic results.

The flow capacity is determined from the slope of the superposition plot given in Figure 12 and calculates to be .252 md-ft from which the permeability calculates to be .008 md for the 32 foot zone. The initial reservoir pressure calculates to be 2936 psia.

A multirate, line source solution using a computer to match buildup data was used to determine the fracture radius. The best performance match was achieved with a skin of between -4 and -5 which are equivalent to effective fracture radii of 17 feet and 47 feet, respectively. An estimated fracture radius based on the treatment record has been calculated at about 43 feet, thus there appears to be reasonable agreement between the two methods.

Fairly good agreement was found between the different methods of analyzing the data. Since the final pressure buildup was run for a prolonged period of time, the results of these data analyzed using the method of superposition to account for previous production history should give the most reliable results. The values of k = .008 md and p_i = 2936 psia are considered to be the best reservoir parameters for the Project Rulison site.

NUCLEAR OPERATIONS

The major site activities during the nuclear operations phase were the drilling and preparation of the explosive emplacement well (R-E), engineering and construction activities associated with the control point, cabling, emplacing the explosive, stemming both the R-EX and R-E wells, and preparing and

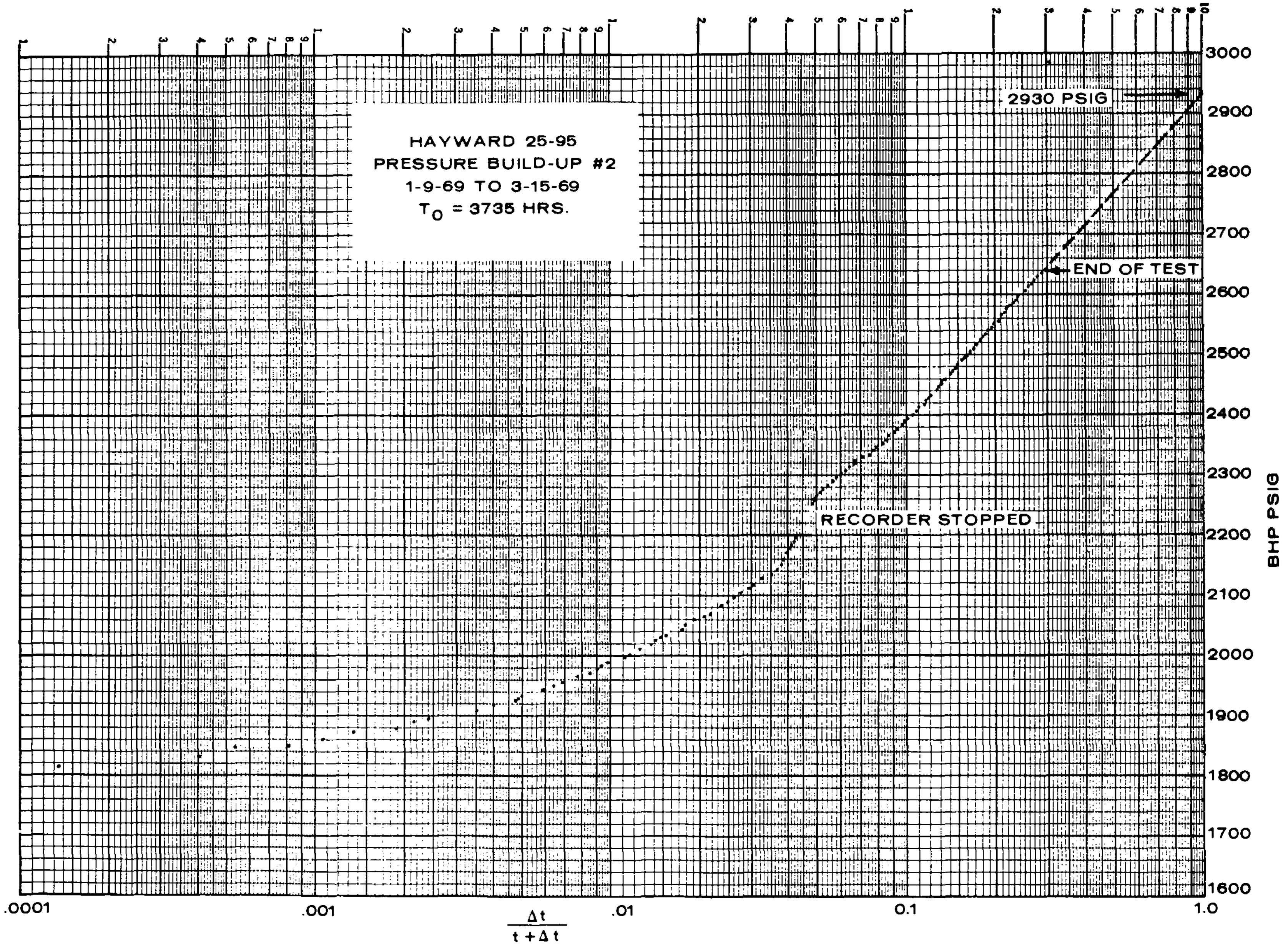
HAYWARD 25-95
PRESSURE BUILD-UP #2
1-9-69 TO 3-15-69
T_O = 3735 HRS.
2930 PSIG
END OF TEST
RECORDER STOPPED
BHP PSIG
3000
2900
2800
2700
2600
2500
2400
2300
2200
2100
2000
1900
1800
1700
1600
.0001
.001
.01
0.1
1.0
$\frac{\Delta t}{t + \Delta t}$

FIGURE 11

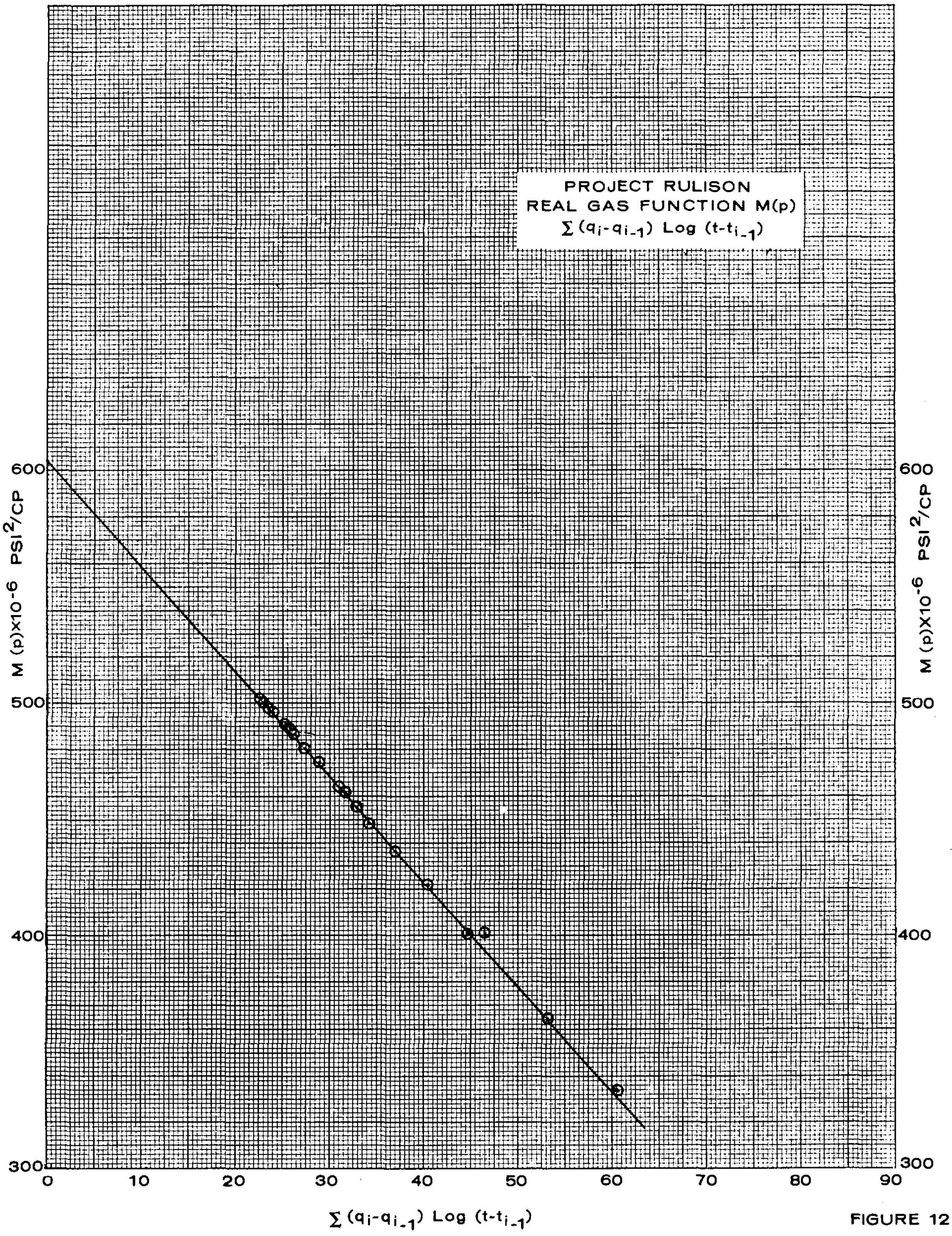
PROJECT RULISON
REAL GAS FUNCTION M(p)
$\Sigma (q_i - q_{i-1})$ Log $(t - t_{i-1})$
M (p)X10^{-6} PSI^2/CP
300
400
500
600
0
10
20
30
40
50
60
70
80
90
$\Sigma (q_i - q_{i-1})$ Log $(t - t_{i-1})$

FIGURE 12

supporting the safety programs for shot time. Since the safety programs and engineering and construction activities are well documented elsewhere(2, 9, 15), only the emplacement well drilling, completion, and stemming and the R-EX stemming are summarized here.

The emplacement hole, R-E, was drilled approximately 311 feet northwest of R-EX (see Figure 5). A 15 inch hole was drilled from under the 16 inch surface pipe set at 800 feet to a depth of 8700 feet, or approximately 270 feet below the proposed shot point. Core was cut from the 8400 to 8460 foot interval and a suite of wet hole logs was run. A string of 10-3/4 inch casing was run to TD and cemented from TD to 6240 feet and from 1000 feet to the surface. The casing was plugged from TD back to 8437 feet (GL) with cement. A boron carbide container located opposite the selected explosive depth at 8426 (GL) was run integral to the 10-3/4 inch casing.

The nuclear explosive constructed by LASL was lowered into place on a .72 inch multiconductor, armored cable, which was also used for timing and firing. The explosive canister was 9 inches in diameter, 15 feet long, and weighed approximately 1200 pounds.

Stemming of the emplacement hole (Figure 13) was accomplished by filling the bottom 2100 feet with nominal 3/8 inch pea gravel and then alternating with 10 foot layers of Bentonite mixed with fine sand and 90 foot layers of the 3/8 inch pea gravel to within 200 feet from the surface. The R-EX well was stemmed using two cement plugs with water in between, (Figure 13). Wellhead assemblies rated at 3000 psi working pressure and tested to 6000 psi were used on each well.

PRELIMINARY POST-SHOT DATA

The Project Rulison nuclear explosive was detonated at 1500 hours, zero minutes and .1 seconds, Mountain Daylight Time, at a depth of 8426 feet subsurface. Preliminary ground motion data indicate the the Rulison explosive behaved as expected with the designed yield of 40^{+20}_{-4} kilotons. The explosion was completely contained and no radioactivity above background has been detected by surveys in the area and instrumentation located at the R-E wellhead.

Geophones located near the surface ground zero showed subsurface noise from 48 seconds to about 150 seconds post-shot. The subsurface noise can be interpreted as an indication of a prompt collapse of the cavity to produce the anticipated chimney. Seismometers also show some noise above background up to 9 hours following the detonation which is consistent with cavity collapse experience.

Other preliminary data for the stations monitoring seismic activity of the shot have been compared with the pre-shot predicted peak ground motion.(9, 16) This comparison is given in Figure 14.

From the seismic monitoring data 37 sets which are of good quality and seem appropriate have been selected for comparison with predicted ground motions. For each of data points selected, the higher of the two

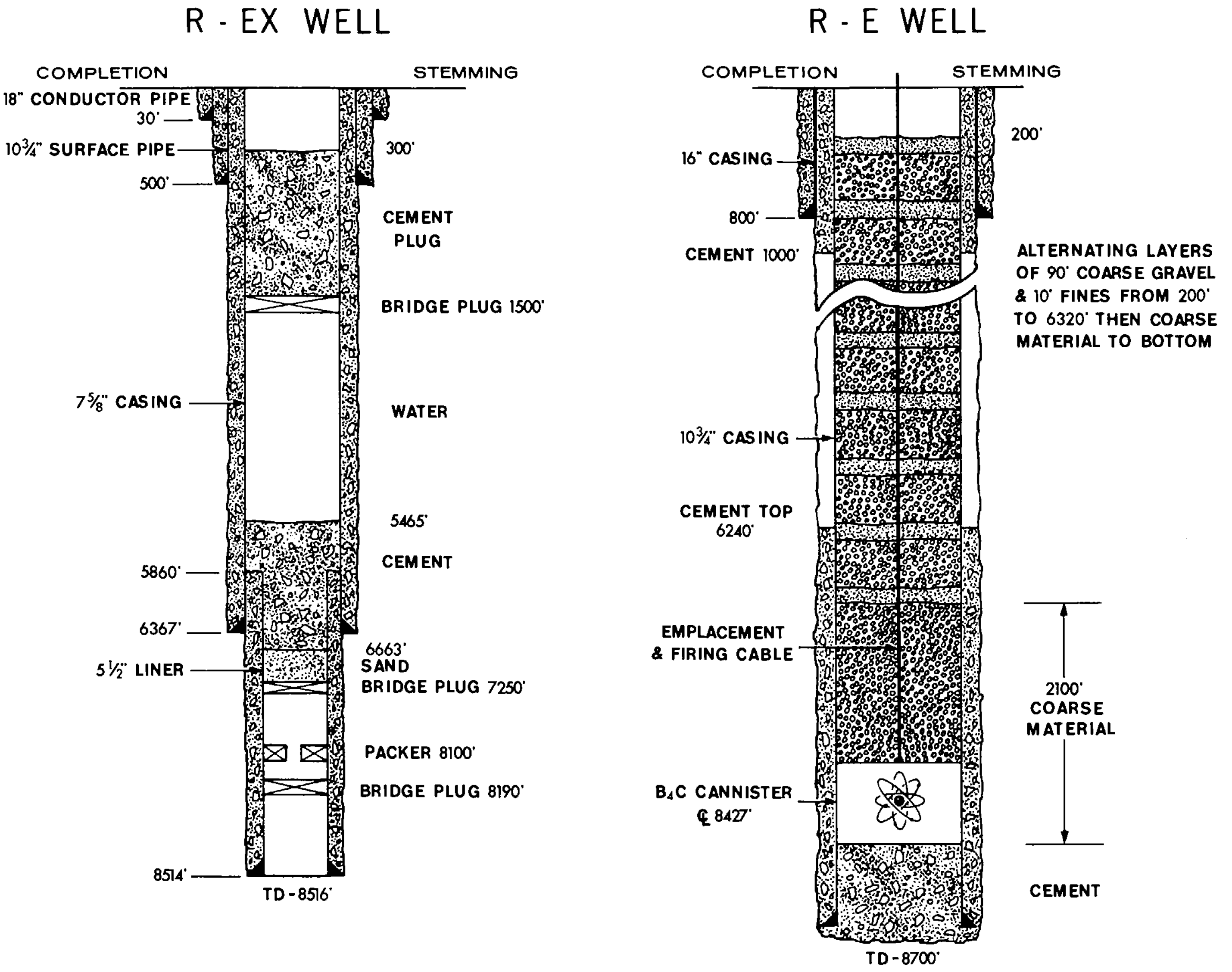

PROJECT RULISON
WELL COMPLETIONS AND STEMMING

FIGURE 13

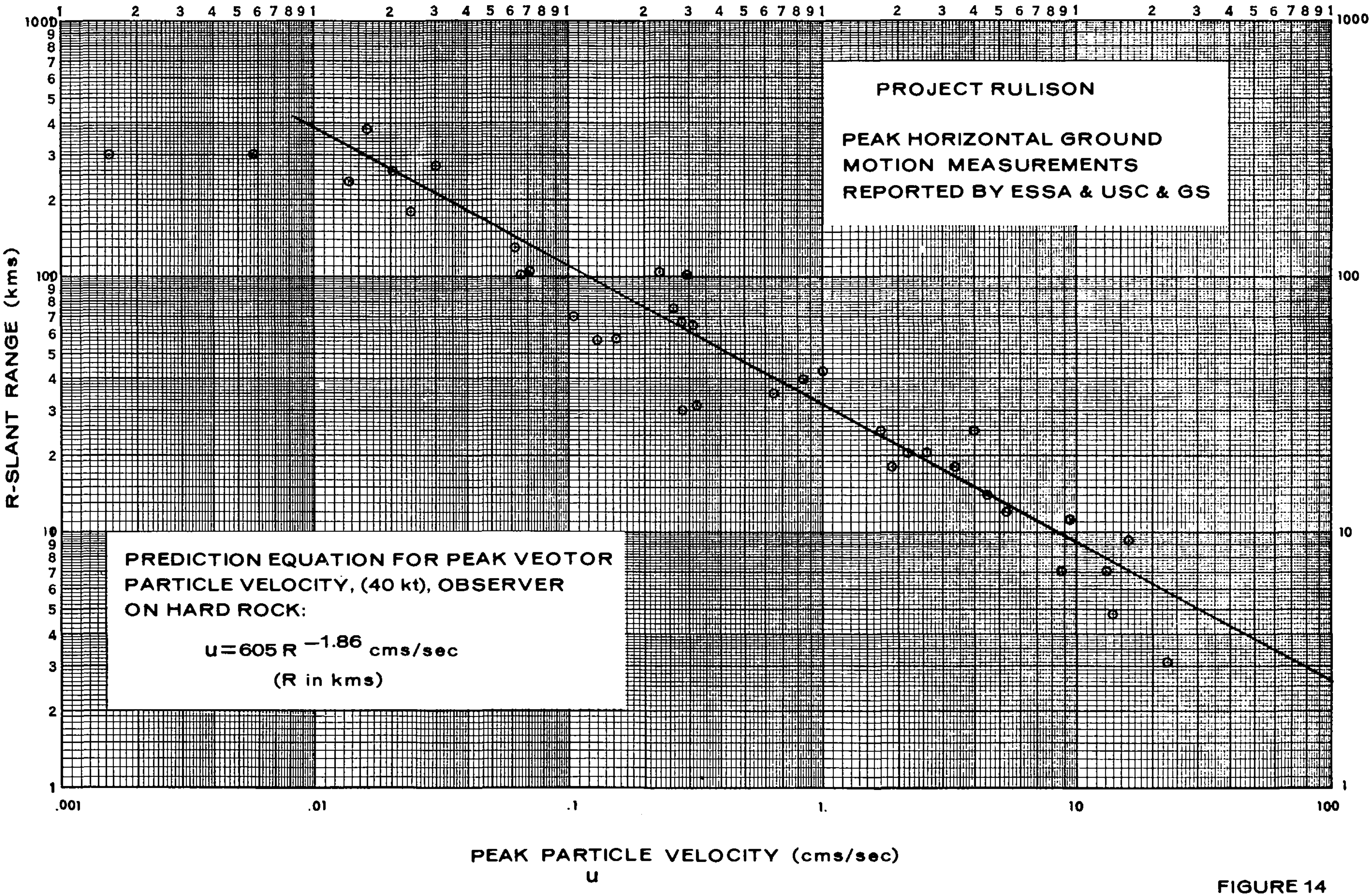
PROJECT RULISON
PEAK HORIZONTAL GROUND
MOTION MEASUREMENTS
REPORTED BY ESSA & USC & GS
PREDICTION EQUATION FOR PEAK VEOTOR
PARTICLE VELOCITY, (40 kt), OBSERVER
ON HARD ROCK:
$u = 605\,R^{-1.86}$ cms/sec
(R in kms)
R-SLANT RANGE (kms)
1000
100
10
1
.001
.01
.1
1.
10
100
PEAK PARTICLE VELOCITY (cms/sec)
u

FIGURE 14

horizontal components (those which impose the most stress on structures) has been plotted in Figure 14. The prediction equation(16) for peak vector particle velocity for the design yield of 40 kt for the case of an observer on hardrock has been plotted for comparison. The observed data points scatter generally about the prediction line except for the two or three closest to surface ground zero, where the vertical component makes an important contribution to the vector velocity.

Less than one-third of the available Rulison data has been processed. On the basis of this, the preliminary observation is made that the observed ground motions compare quite closely with predicted values. The principal exception is that the spectral composition at stations closer than about 18 kilometers is richer in high frequency components than predicted. For example, a spectral analysis of the record of a station at a range of about 7 kilometers indicates a peak period of about 0.145 seconds in lieu of the predicted peak over the range, 0.23 - 0.28 seconds. An effect of this shift in period is an increase in peak accelerations. This may be attributable to the overburied condition of Rulison with respect to Gasbuggy, from which the Rulison ground motion predictions were derived.

Until flow tests are conducted, following reentry into the explosion environment, there is no way of determining the actual chimney or fracture characteristics. All information to date indicate that the explosion behaved as predicted and should provide an environment in the range of that given in Table 2.

On September 16, 1969, after a total elapsed time of 138 hours, a wellhead pressure of 390 psig was observed at the emplacement hole wellhead. Since that time the pressure has been monitored and shows an increase to a value of 2500 psig on December 14, 1969, (Figure 15). The related bottom hole pressure calculates to be 2937 psia after accounting for the weight of the gas column.

Data presented in this section are of a preliminary nature and all data have not been received from participants in the project. Formal reports from all project participants regarding their activity will be forthcoming from time to time and will be placed in the Open File for Project Rulison.(15)

PREDICTION OF POST-SHOT WELL PERFORMANCE

Based on the pre-shot data from the R-EX well, Figures 16 and 17 are typical plots of the computer prediction runs for various well configurations. Prediction runs were made simulating four configurations as follows:

1. Nuclear stimulated well with a chimney radius of 87.2 feet, and very little associated fracturing.
2. Nuclear stimulated well with a chimney radius of 87.2 feet and fracture radius of 510 feet.
3. Conventional well - hydraulically fractured.

TABLE II

PREDICTED EXPLOSION-CREATED DIMENSIONS FOR PROJECT RULISON(9)

	Maximum	Mean	Minimum	Units
Cavity Radius	108	90	72	feet
Cracking Radius	580	485	390	feet
Chimney Height	451	376	301	feet
Cavity Volume (or Chimney Void Space)	5.28×10^6	3.05×10^6	1.56×10^6	ft^3
Chimney Volume	1.65×10^7	9.57×10^6	4.90×10^6	ft^3

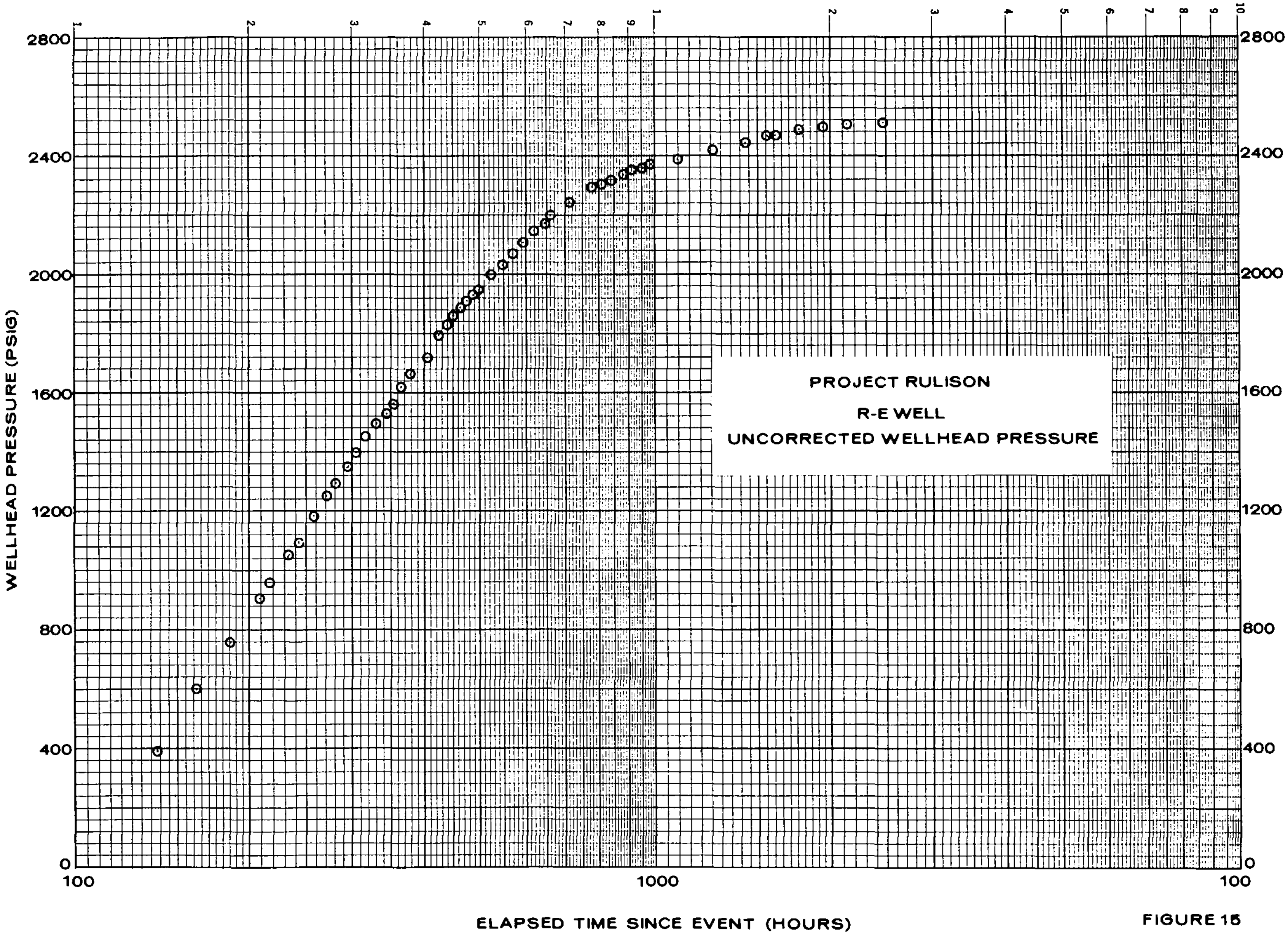
PROJECT RULISON
R-E WELL
UNCORRECTED WELLHEAD PRESSURE
WELLHEAD PRESSURE (PSIG)
ELAPSED TIME SINCE EVENT (HOURS)
0
400
800
1200
1600
2000
2400
2800
100
1000
100
1
2
3
4
5
6
7
8
9
1
2
3
4
5
6
7
8
9
10

FIGURE 15

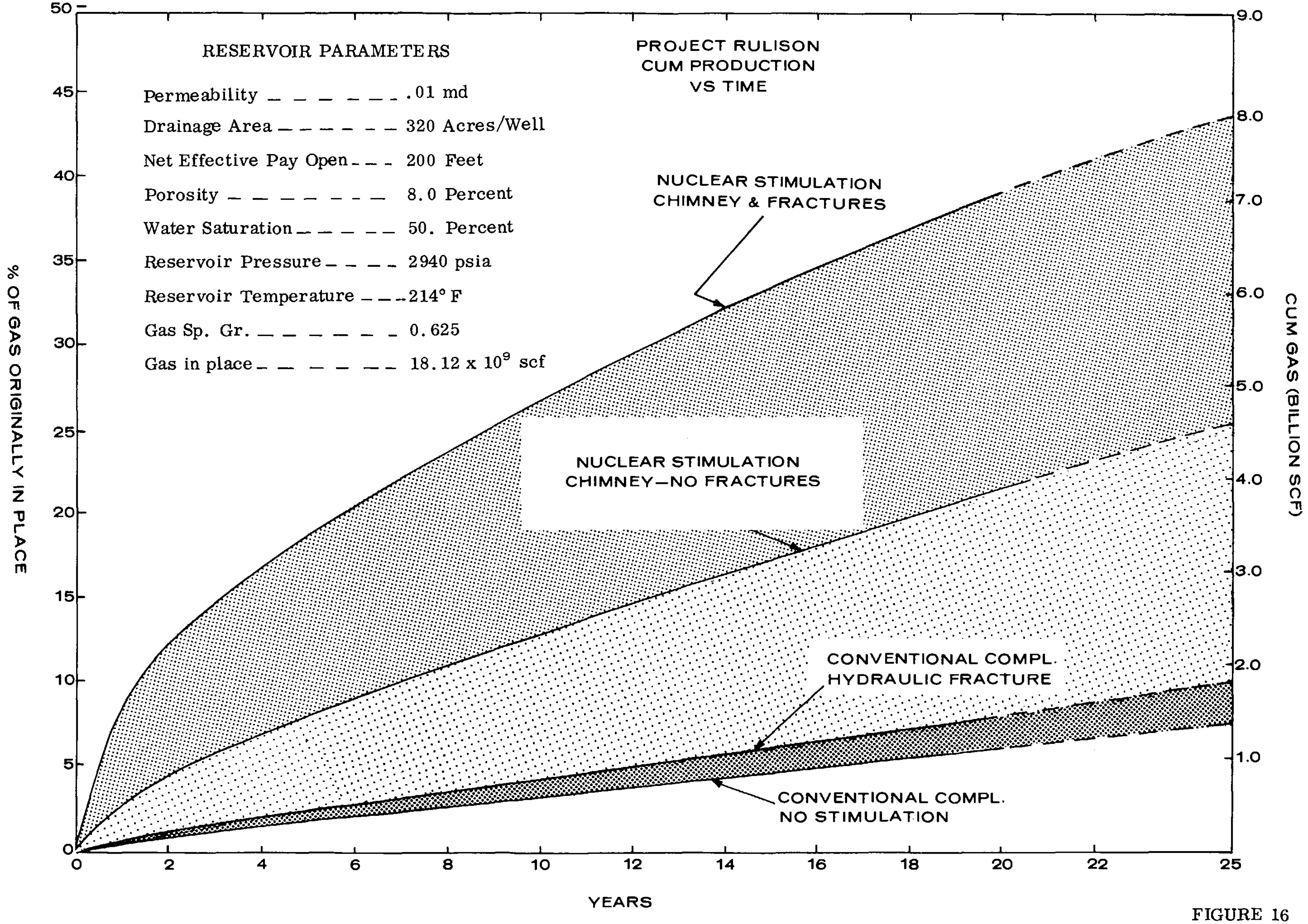
RESERVOIR PARAMETERS
Permeability - - - - - - - .01 md
Drainage Area - - - - - - - 320 Acres/Well
Net Effective Pay Open - - - 200 Feet
Porosity - - - - - - - - 8.0 Percent
Water Saturation - - - - - 50. Percent
Reservoir Pressure - - - - 2940 psia
Reservoir Temperature - - -214° F
Gas Sp. Gr. - - - - - - - 0.625
Gas in place - - - - - - 18.12 x 10^9 scf
PROJECT RULISON
CUM PRODUCTION
VS TIME
NUCLEAR STIMULATION
CHIMNEY & FRACTURES
NUCLEAR STIMULATION
CHIMNEY—NO FRACTURES
CONVENTIONAL COMPL.
HYDRAULIC FRACTURE
CONVENTIONAL COMPL.
NO STIMULATION
% OF GAS ORIGINALLY IN PLACE
0
5
10
15
20
25
30
35
40
45
50
CUM GAS (BILLION SCF)
1.0
2.0
3.0
4.0
5.0
6.0
7.0
8.0
9.0
YEARS
0
2
4
6
8
10
12
14
16
18
20
22
25

FIGURE 16

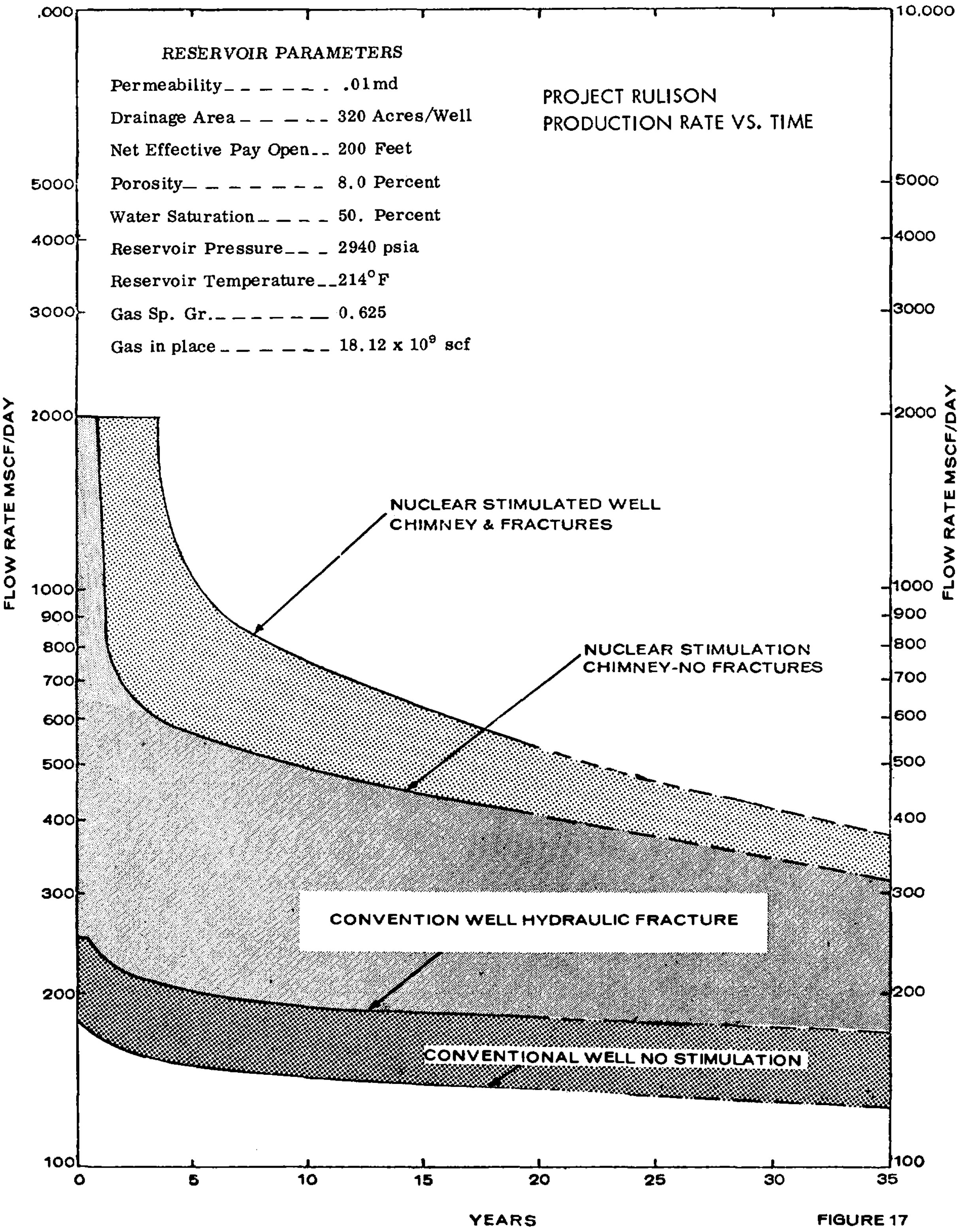
.000
10.000
RESERVOIR PARAMETERS
Permeability _ _ _ _ _ _ .01md
Drainage Area _ _ _ _ _ 320 Acres/Well
Net Effective Pay Open _ _ 200 Feet
Porosity _ _ _ _ _ _ _ 8.0 Percent
Water Saturation _ _ _ _ 50. Percent
Reservoir Pressure _ _ _ 2940 psia
Reservoir Temperature _ _ 214°F
Gas Sp. Gr. _ _ _ _ _ _ 0.625
Gas in place _ _ _ _ _ _ 18.12 x 10^9 scf
PROJECT RULISON
PRODUCTION RATE VS. TIME
5000
4000
3000
2000
1000
900
800
700
600
500
400
300
200
100
FLOW RATE MSCF/DAY
NUCLEAR STIMULATED WELL
CHIMNEY & FRACTURES
NUCLEAR STIMULATION
CHIMNEY-NO FRACTURES
CONVENTION WELL HYDRAULIC FRACTURE
CONVENTIONAL WELL NO STIMULATION
0
5
10
15
20
25
30
35
YEARS

FIGURE 17

4. Conventional well - no stimulation.

A formation permeability of .01 md was used for the probable case and a permeability of .003 md for the most conservative case. Two runs, for each of the above four configurations, were made to determine the range of probable deliverability with time. The reservoir parameters and predicted twenty-year production performance are summarized in Table III. Other input data for the model were:

Reservoir temperature	-	214°F
Reservoir pressure	-	2940 psia
Drainage area	-	320 acres/well
Net effective pay in the stimulated interval	-	200 feet
Total porosity	-	8.0%
Water saturation	-	50%
Gas-in-place	-	18.12×10^9 scf
Standard conditions	-	15.025 psia and 60°F
Specific gravity of gas	-	.625
Bottom hole pressure cut off	-	500 psia

The prediction runs are based on a 2-dimensional, unsteady state, radial flow model. The computer model combines the continuity equation and Darcy's law in a solution of the following non-linear differential equation of the form:

$$\left(\frac{2\phi\mu}{k}\right)\frac{\partial P}{\partial t} = \left(\frac{1}{r}\right)\frac{\partial}{\partial r}\left(r\frac{\partial P^2}{\partial r}\right)$$

which is further modified to account for non-darcy behavior of real gas flow. The solution of the equation is non-linear and is solved by the finite difference method using a high-speed computer. A comprehensive explanation of the model is given in References 16, 17, and 18.

The model was developed by assigning values of permeability and porosity to concentric annular cylinders. In the cases of the non-nuclear stimulated wells permeability and porosity do not change with distance from the wellbore; however, in the case of the hydraulically fractured well, the wellbore radius is increased to account for the fracture radius.

The nuclear stimulated well required several innovations to the radial model in order to simulate the nuclear environment. A permeability matrix for the nuclear stimulated wells was developed by arbitrarily assigning a large permeability value (1000 md) to the chimney and decreasing it in the individual annular cells making up the fractured area until the original reservoir permeability was obtained. A decline in permeability rather than a sudden change at the chimney interface is used in the model to eliminate mathematical convergence problems.

The additional void volume created in the reservoir by the explosion was handled in the model by assigning a total porosity in the chimney equal to the void volume over the net effective pay interval. In other words, the porosity

TABLE III

SUMMARY OF COMPUTER PREDICTION RUNS

	Nuclear Stim. Chimney & Fractures		Conventional Completion No Stimulation		Conventional Completion Hyd. Fractured		Nuclear Stim. Very Little Assoc. Fracturing	
Case	1	2	3	4	5	6	7	8
k(md)	.01	.003	.01	.003	.01	.003	.01	.003
r_w(ft)	2.0	2.0	0.4	0.4	3.0	3.0	2.0	2.0
r_{cavity}(ft)	87.2	87.2	-	-	-	-	87.2	87.2
$r_{fract.}$(ft)	510	510	-	-	-	-	139	139
	CUMULATIVE GAS PRODUCED WITH TIME MMSCF							
1 Year	1626	1457	65	21	88	31	467	298
5 Years	3426	2343	292	95	400	136	1417	686
10 Years	4940	3082	560	182	753	254	2366	1066
	PRODUCTION PERFORMANCE AT END OF 20 YEARS							
Cum Produced at 20 Years (MMSCF)	7105	4205	1081	352	1443	481	3916	1708
Percent of Gas-in-Place	39.1	23.1	5.95	1.94	7.97	2.67	21.6	9.42
Pressure at Drainage radius (Psia)	2075	2696	2814	2926	2771	2921	2466	2857
Production Rate at 20 Years (MCF/D)	532	292	136	44	176	59	404	169

matrix in the model was represented by a high value of hydrocarbon porosity out to the chimney radius and then normal reservoir hydrocarbon porosity to the drainage radius.

The results indicate that an increase in the 20 year recovery of gas from the nuclear stimulated well will be between 5 and 9 times the gas recovered using conventional stimulation techniques. A further discussion of the computer prediction runs is presented in an associated paper.(20)

The results of the actual testing of the explosion environment after reentry, the long term production characteristics, and the costs of commercial fielding of nuclear explosions will determine if use of nuclear energy can indeed be a commercial method for unlocking the tremendous reserves of gas that are needed to insure an adequate supply for the increasing energy demands of these United States.

ACKNOWLEDGMENTS

The authors express their thanks to Dr. C. F. Knutson for much of the project planning and geologic investigations; Mr. R. S. Brundage for the seismic evaluation; and Dr. H. C. Walther and Dr. O. G. Kiel for the computer program development used in the data analysis and prediction work.

This work was done in part under: "Contract No. AT-(26-1)-429 between the United States of America acting jointly through the Atomic Energy Commission and the Department of the Interior and the Austral Oil Company Incorporated, and CER Geonuclear Corporation, Program Manager.

REFERENCES

1. "Project Rulison Feasibility Study," Austral Oil Company Inc., CER Geonuclear Corp. Open File Report, PNE-R-12 (July 1966).

2. "Project Rulison Definition Plan," Austral Oil Company Inc., CER Geonuclear Corp., U. S. Atomic Energy Commission. Open File Report, PNE-R-11 (March 26, 1969)

3. M. D. Quigley, "Geologic History of the Piceance Creek - Eagle Basin," AAPG Bulletin, V. 49, No. 11 (1965) pg. 1924.

4. J. D. Haun, "Introduction to the Geology of Northwestern Colorado," RMAG Guidebook (1962) pg. 7.

5. B. F. Curtis, "The Geological Development of Northwestern Colorado," RMAG Guidebook (1962) pg. 15.

6. R. J. Weimer, "Upper Cretaceous Stratigraphy, Colorado," RMAG Guidebook (1959) pg. 9.

7. W. E. Yeend, "Quaternary Geology of the Grand and Battlement Mesa Area, Colorado," USGS Professional Paper 617 (1969).

8. P. T. Voegeli, "Geology and Hydrology of the Project Rulison Exploratory Hole, Garfield, County, Colorado," USGS Open File Report, USGS 474-16, PNE-R-2 (April 4, 1969).

9. "Effects Evaluation for Project Rulison," USAEC Open File Report, NVO-43, PNE-R-4 (June 1969).

10. "Project Rulison - Site Evaluation Pre-Shot R-EX Well Test Data," Austral Oil Company Inc., CER Geonuclear Corp., Open File Report, PNE-R-7 (Oct. 1969).

11. R. A. Wattenbarger, H. J. Ramey, Jr., "Well Test Interpretation of Fractured Gas Wells," Trans AIME 246 pgs. 625-632 (1969), Journal of Petroleum Technology (May 1969).

12. R. Al-Hussainy and H. J. Ramey, Jr., "Application of Real Gas Flow Theory to Well Testing and Deliverability Forecasting," Journal of Petroleum Technology, 637-642 (May 1966).

13. K. Millheim and L. Cichowicz, "Testing and Analyzing Low-Permeability Fractured Gas Wells," Journal of Petroleum Technology, 193-198 (February, 1968).

14. D. R. Horner, "Pressure Buildup in Wells," Proc., Third World Petroleum Congress, Sect. II, 503 (1951).

15. Project Rulison Open File System containing project data and safety contractor reports, etc., is located in Las Vegas, Nevada, Denver, Colorado, and Bartlesville, Oklahoma. Copies of all material can also be obtained from USAEC, Division of Technical Information, Oak Ridge, Tennessee.

16. B. G. Weetman, et al, "Predictions of Seismic Motion and Close-In Effects Rulison Event," Environmental Research Corporation, NVO-1163-180, PNE-R-5 (August 1969).

17. O. G. Kiel and J. M. Campbell, "Analysis of Gas Well Behavior Using a Two-Dimensional Unsteady State Model, "AIME Paper 562, April 29-30 (1963).

18. G. W. Swift and O. G. Kiel, "The Prediction of Gas Well Performance Including the Effect of Non-Darcy Flow," Journal of Petroleum Technology, 791 (July 1962).

19. O. G. Kiel, "Theoretical Investigation of Gas Well Transient Phenomena and Its Effects on Conventional Well-Test Data Interpretations," PhD Thesis, University of Oklahoma, Norman, Okla. (1963).

20. G. W. Frank, H. F. Coffer, G. R. Luetkehans, "Economics of Nuclear Gas Stimulation," Engineering with Nuclear Explosives, (Jan. 14-16, 1970), Las Vegas, Nevada.

XA04N0857

Engineering with Nuclear Explosives near Populated Areas - A Survey from the Technological and Economic Viewpoint

K. Parker
AWRE, Aldermaston, U.K.

Summary

Current experience with underground firings of nuclear explosives and of large charges of conventional explosives is largely confined to sparsely populated areas such as the Nevada and Sahara deserts and parts of Siberia. On the other hand many of the commercial applications proposed for nuclear explosives are directly relevant to industrialized areas, where consumptions of energy and natural resources are high, as are population densities. In many of these areas there is a need to increase the efficiency with which natural gas, oil and electrical power are supplied and to make safe disposal of fluid wastes; completely contained nuclear explosions could be a useful tool in achieving some or all of these aims.

Whilst radioactivity and air blast hazards are likely to rule out nuclear cratering operations near densely populated areas, the prospects for carrying out completely contained explosions are much better, providing seismic damage is kept within reasonable bounds. In large areas of Western Europe and on the eastern, southern and western seaboards of the United States this might be achieved by using nuclear explosions beneath the seabed at a reasonable distance from the nearest coastline, always provided the relevant political issues can be resolved.

Stimulation and storage of North Sea natural gas, construction of off-shore oil storage and storage of electrical energy are areas where engineering with nuclear explosives merits more detailed investigation and some of the relevant technical problems are discussed.

1. Introduction

In the past fifteen years considerable progress has been made towards demonstrating the use of nuclear explosives as a feasible, safe and economic technique in civil, mining and petroleum engineering. The United States Plowshare programme has led to an improved understanding of the effects and potentialities of nuclear explosives important in their peaceful application. The Soviet Union has also gained considerable experience in this field [1] and has indicated its willingness to provide a peaceful nuclear explosive service under article V of the Non-Proliferation Treaty [2]. Again the Russians have discussed and carried out civil engineering works involving detonation of large charges of conventional explosives [3]. Whilst both the United States and the USSR have large populations, their territories are large and their population distributions uneven so that areas can fairly easily be found in which to carry out nuclear explosive engineering experiments and projects.

Once it becomes apparent that an engineering technique is feasible, safe and economic under particular circumstances it is natural to ask what are the ultimate limits on its use. By analogy, open cast mining is a proved technique but its application in urban areas would be uneconomic,whilst methods used to demolish buildings must be varied on safety grounds according to the nature of the surroundings. Many of the possible engineering applications of nuclear explosives relate to economic activities which are concentrated in heavily-populated, industrialised areas. Oil storage is often required near major ports. Gas storage is generally most important near to consumers. For these reasons it is no academic question to examine the possibility of engineering with nuclear explosives near populated areas.

If one looks at maps showing population density such as are shown in figures 1 and 2 one readily confirms that the Nevada, Sahara and Australian deserts are low density areas as is Novaya Zemlya. On the other hand there are well-known areas of high population density such as the eastern United States seaboard, Japan, the United Kingdom and much of the coast lands bordering the North Sea and the Mediterranean Sea. These are areas of high economic activity where much of the world's consumption of energy and natural resources takes place and where any remaining minerals of commercial importance are won only with increasing difficulty. Engineering techniques involving nuclear explosives could be useful in these areas providing they are both safe and economic.

Section 2 of the paper considers possible applications of nuclear explosive engineering near populated areas from a West European viewpoint. There follows in section 3 a discussion of how the hazards of nuclear explosives might be minimized or avoided so as to make such application possible. Specific examples of possible projects are referred to in section 4 and the paper concludes in section 5 with a discussion of outstanding technical problems and possible future developments.

2. Possible Uses of Nuclear Explosives near Populated Areas

General

From a West European viewpoint the applications of nuclear explosives which first merit detailed examination appear to be those concerned with improving the economics of fuel and energy supply. The exploitation of mineral and water resources may also be assisted by the use of nuclear explosives but there are probably more problems to be overcome in these areas.

Oil Storage

Over the past fifteen years natural gas and uranium have taken their places alongside coal and oil to give a four-fuel economy in many parts of Western Europe. Following the Middle East crisis of 1956 there has been considerable diversification in the sources of imported oil but in the absence of substantial indigenous production (17.3 million tons in 1968 out of a world annual production of over 2,000 million tons) a healthy stock level is always a useful safeguard against any interruption of supplies. It has been argued [4] that commercial stock levels in European countries, typically at two or three month demand level, should be at least doubled. This implies the provision of some 80 million tons of oil storage in Western Europe. Nuclear chimneys either on land or beneath the seabed might provide a sizable fraction of any such large increase in storage capacity. But there is another reason for providing oil storage beneath the seabed. The continual increase in tanker sizes is giving rise to a need for special berthing facilities. At Bantry Bay in south-west Ireland an off-shore terminal has been provided at a cost of about $24 million [5] which provides storage for nearly a million tons of crude oil

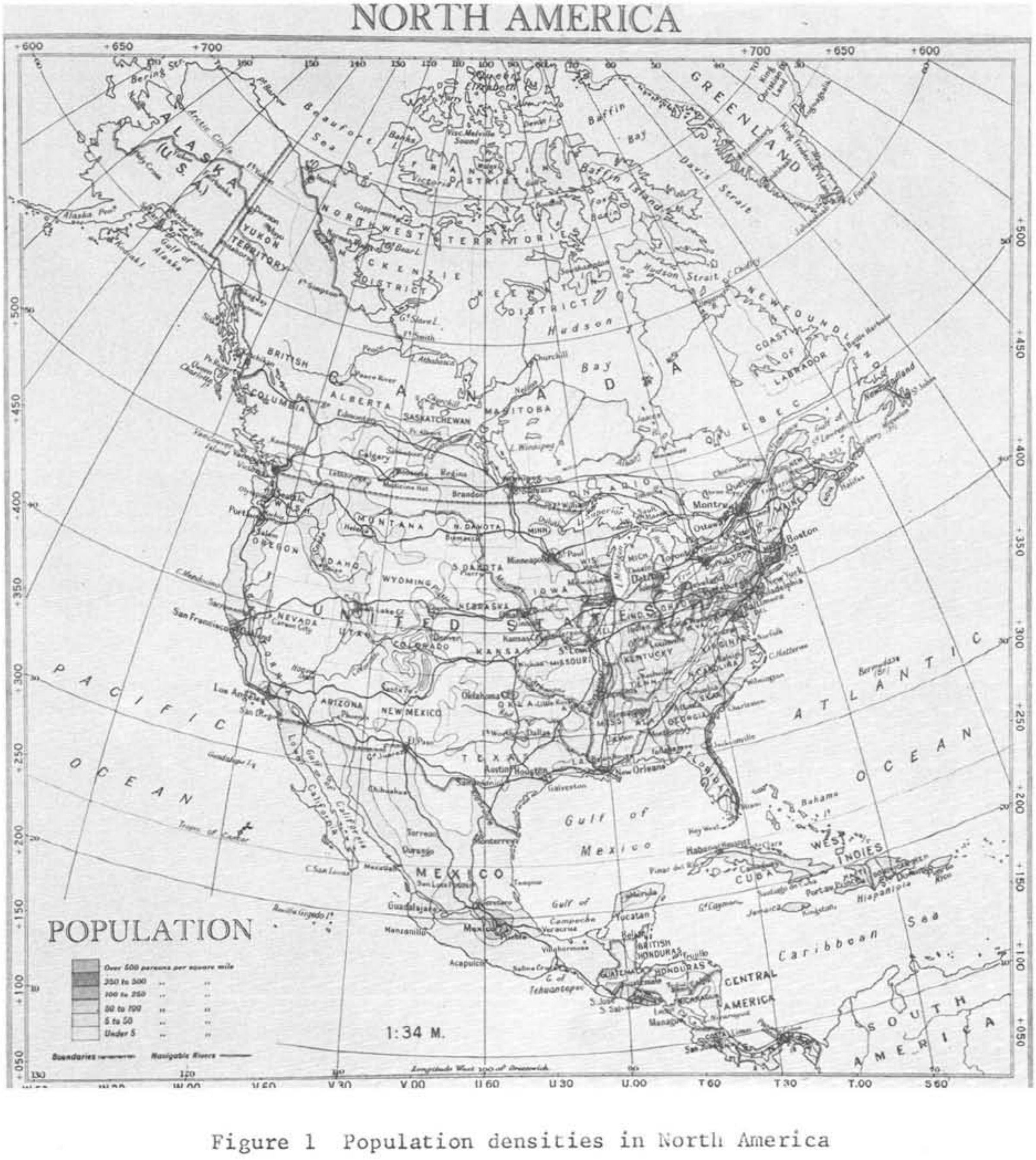

Figure 1 Population densities in North America

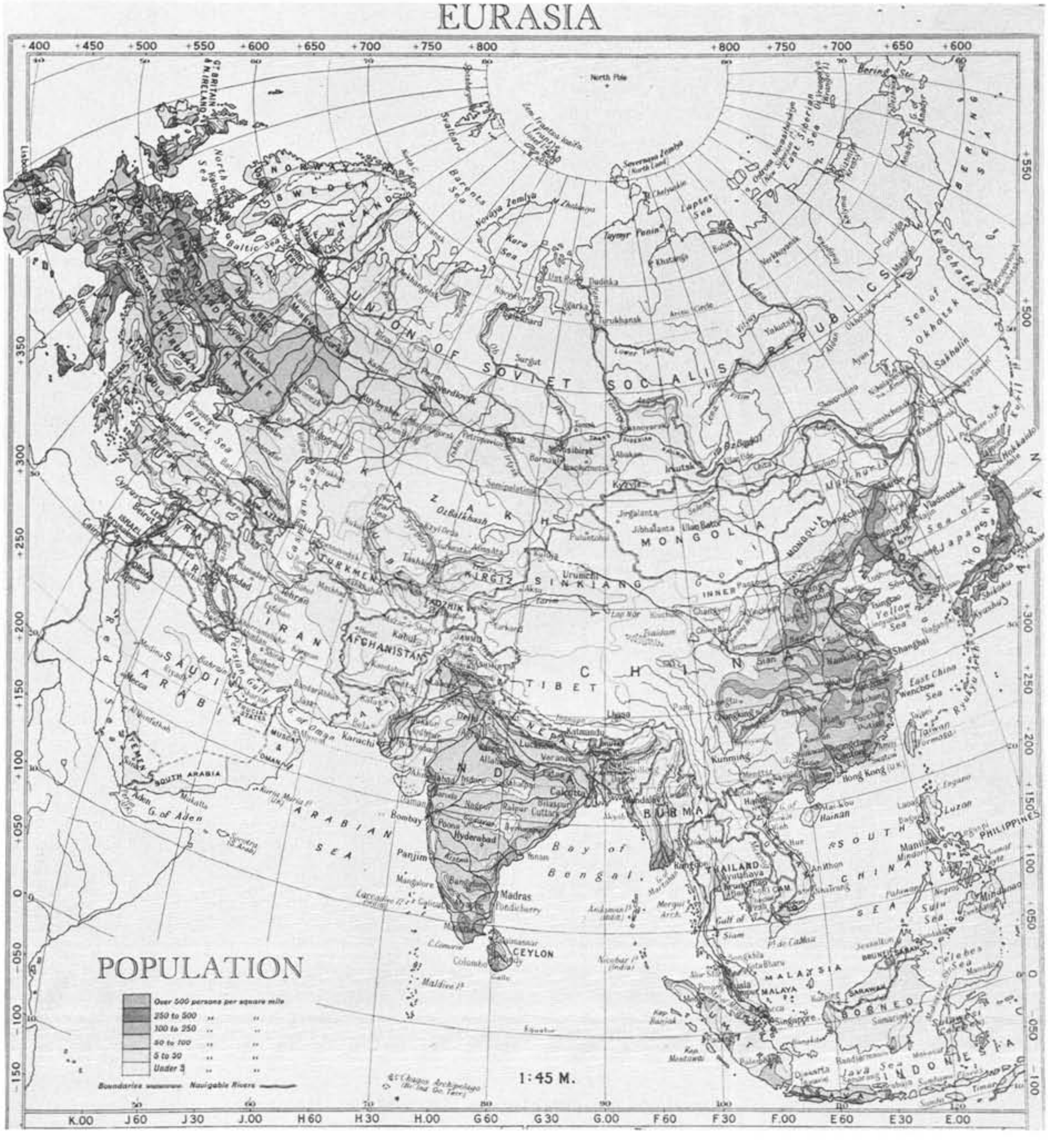

Figure 2 Population densities in Eurasia

in 12 tanks each 262 ft. in diameter by 64 ft. high [6]. This handles tankers of 300,000 dwt. and allows trans-shipment to smaller tankers for onward transport to several European refineries. At Milford Haven, an excellent natural harbour in west Wales developed primarily for tanker traffic, it has become necessary to spend about $28 million in dredging and navigational aids in order to allow regular entry by tankers of 250,000 tons [7]. Fully laden tankers with a draught of 63 ft. will then be able to enter and berth on every tide throughout the year. However if tankers of 750,000 tons or even a million tons are built then it may be necessary to cater for fully laden draughts of 95 ft. Figure 3 is a map of the European Continental shelf showing the 17 fathom (102 ft.) line. This shows that the English Channel and the southern North Sea might be excluded to such large tankers and has led the Mersey Docks and Harbour Board [8] to study the possibility of building a terminal ten miles or more off the North Wales coast. Such a project would probably cost over a hundred million dollars and, for efficient operation, it would be advantageous to provide on-the-spot flow storage for a million tons of oil or more. Other large oil terminals are planned for a position 12 miles off the coast near the French/Belgian border [9] and off Heligoland [10]. A third possible need for substantial oil storage-again beneath the seabed might arise should oil be discovered on the Continental Shelf. Although the major finds in the North Sea have been the gas fields in the United Kingdom sector, it is reported that oil has been found near the boundary of the Norwegian and United Kingdom sectors [11] although it is not yet known whether recovery would prove economic at a point 150 miles off-shore. It could be that here, and for any other fields that may be discovered, recovery will be most economically achieved by direct transfer to tankers using suitable mooring near the drilling platforms, rather than by laying seabed pipelines. In this case buffer storage could prove advantageous in maintaining steady production during periods of bad weather when tankers were prevented from loading.

Oil Stimulation

A further future use of nuclear explosives in relation to West Europe's oil supplies might be in stimulating tight fields. As long as indigenous production remains small this might be considered worthwhile under conditions where it might be uneconomic in the United States or other major producing areas, although there do not appear to be any promising areas at the moment. The current emphasis on gas rather than oil stimulation experiments in the United States appears to stem partly from concern at the declining level of natural gas reserves available by conventional techniques and partly from the existence of fewer unworked tight oil fields (the value of oil in place having justified greater use of conventional stimulation techniques).

Gas Stimulation

Turning to natural gas one immediately asks what are the prospects of employing nuclear stimulation in the North Sea fields. Certainly the North Sea explorations have revealed areas where gas occurs in tight formations and could perhaps be extracted by nuclear stimulation. But the economic situation is currently almost the opposite of that in the United States; the proved reserve to annual production ratio is rising strongly and gas is tending to displace other fuels. However, if the nuclear stimulation technique is proved in the United States, or elsewhere, it may eventually be employed on the European Continental Shelf. An application of nuclear stimulation which might be tried somewhat earlier could be the stimulation to improve the overall economics of working the proved productive fields shown in figure 3. Exploitation usually involves the drilling of twelve to fifteen production wells from a single platform [12] at a cost of 10-20 million dollars. It may be worth examining whether

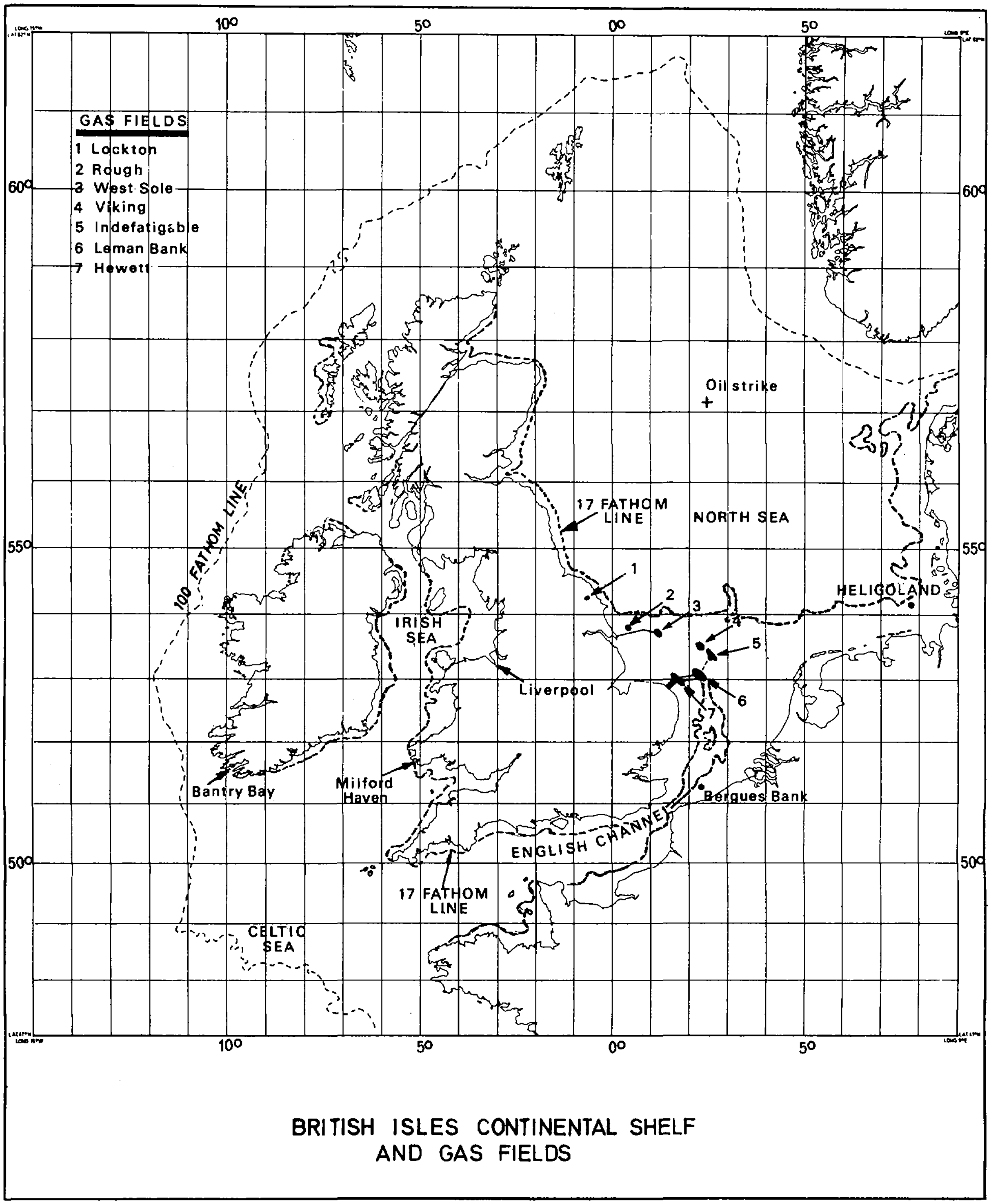

Figure 3 The European Continental Shelf

a single stimulated well can achieve the same production rate at a lower total cost. The gas from such a well could be burnt in a specially designed power station or used to provide total energy systems for large industrial concerns; in either case any radiation could be dealt with under closely controllable conditions.

Gas Storage

In the present decade a substantial high pressure gas pipeline system has developed in Western Europe and further growth can be expected. Figure 4 shows the current position. Even before the discovery of natural gas in the North Sea, the United Kingdom Gas Council had begun to develop such a pipeline grid to distribute natural gas transported in liquid form from Algeria to Canvey Island in the Thames Estuary. The system has been extended and further developments are planned (figure 5). The total mileage of high pressure transmission pipeline - about 2,500 miles should be in use by 1973 [13] - is very small compared with that in North America - about 250,000 miles - but it is still desirable on grounds of supply security and peak-shaving economics to provide storage, particularly near the extremities of the grid in South-West England, North-West England, Wales and Scotland. The eventual pipeline mileage in continental Europe is likely to be much higher. By the end of 1968 over 15,000 miles of pipeline were in use in Europe [13], mainly as a result of developing the Slochteren field in the Netherlands. The network is likely to undergo considerable extensions particularly if, as seems likely, Russian gas is piped to Austria, Italy and other West European countries, and the provision of stand-by storage will probably become increasingly necessary. Although storage in aquifers, disused coal mines and salt cavities is possible there are certainly not the same number of depleted oil and gas fields available for storage as in the United States. In any case nuclear cavity storage has the advantage of high deliverability. Liquefied natural gas may be stored to provide peak-shaving facilities. Although a competitor to nuclear cavity storage this method in itself requires sophisticated storage facilities which may in certain circumstances be provided using nuclear explosives.

Shale Oil Production

Deposits of shale oil occur in France, Germany, Italy, Scotland, Spain and Sweden. In the absence of indigenous oil supplies there are strong incentives to exploit these resources. However the economics are so unfavourable that shale oil production has been very small except during the 1939-1945 war. In many cases deposits are very thin and are unlikely to be an attractive proposition for extraction techniques involving nuclear fracturing.

Stored Energy in National Electricity Systems

The efficiency of the production and distribution of electricity in densely populated areas depends strongly on the effect of the peak load problem and electrical engineers are constantly seeking means of disposing of surplus off-peak cheap electricity in energy storage devices [14]. Probably the water pumped storage scheme is the best known but if the two storage reservoirs are both above ground then the number of topographically suitable sites may be limited. This problem could be lessened by constructing the lower reservoir below ground. An alternative storage scheme involves the compression of air into underground tunnels or cavities during off-peak periods. At peak periods this air is used to burn oil fuel in a gas turbine thus generating additional power; the net output of the turbine can be increased by a factor of about 3 with a reduction in generation costs. Without discussing the overall economics of these and other energy storage methods it can be seen that the construction of underground cavities using nuclear explosives could be helpful in exploiting the two systems mentioned, particularly by reducing construction costs.

THE MAIN NATURAL GAS PIPELINES OF WESTERN EUROPE

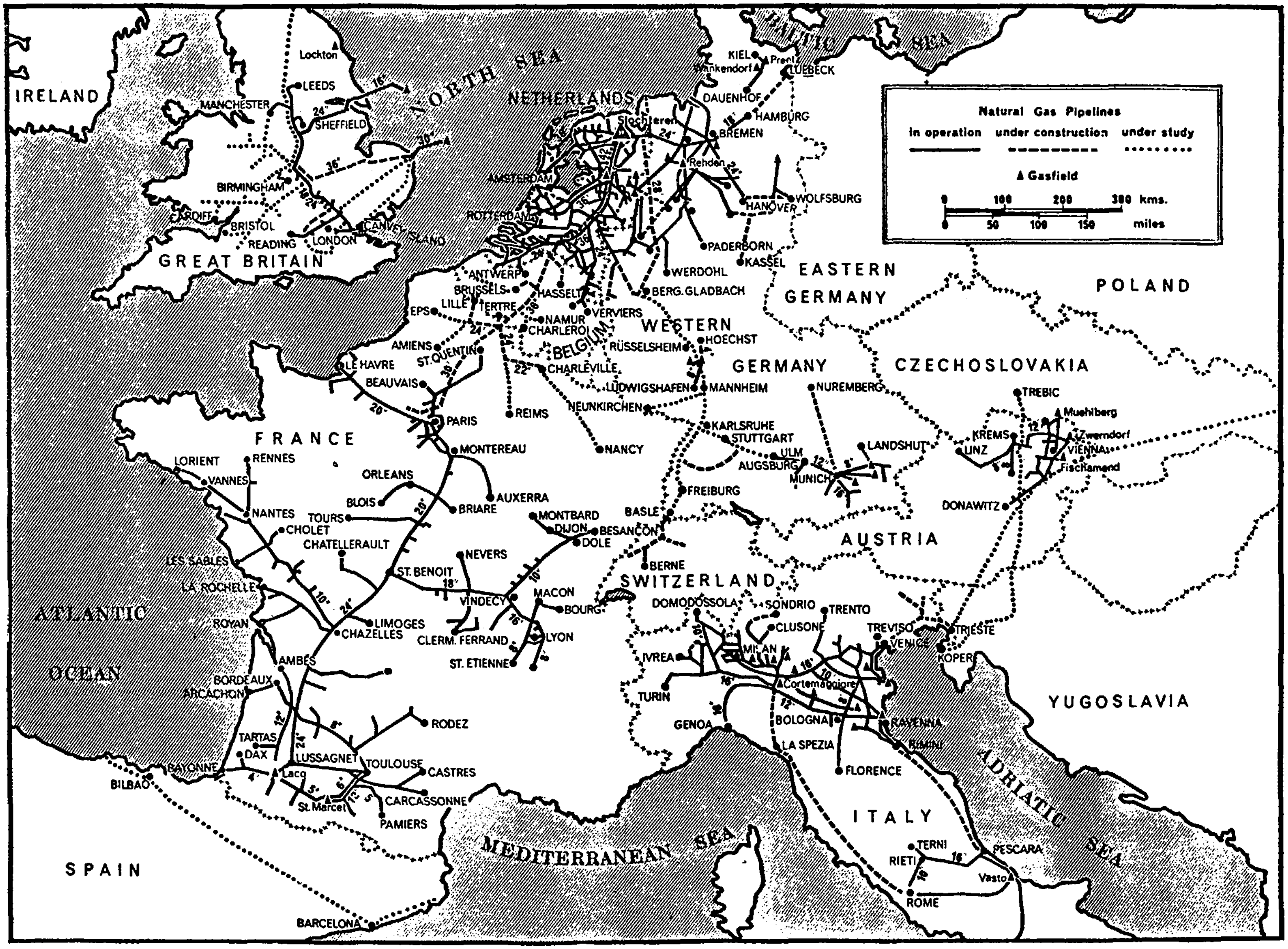

Figure 4 Gas pipelines in Western Europe

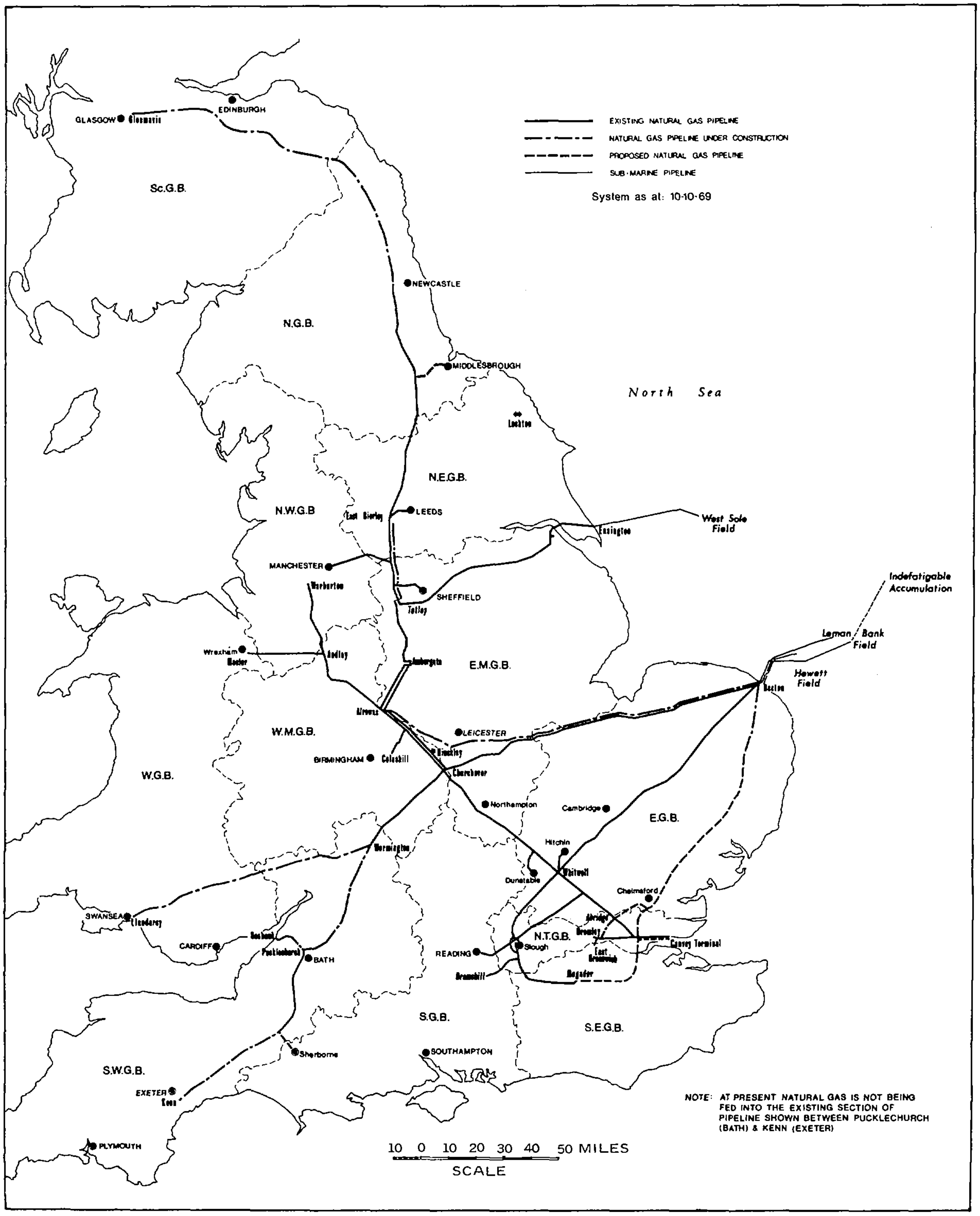

NOTE: AT PRESENT NATURAL GAS IS NOT BEING FED INTO THE EXISTING SECTION OF PIPELINE SHOWN BETWEEN PUCKLECHURCH (BATH) & KENN (EXETER)

Figure 5 The Gas Council natural gas transmission system

Waste Disposal

Again the problems of waste disposal will be greater in densely populated areas. It is to be expected that nuclear chimneys will be considered as a means of storing radioactive waste arising from nuclear power generation and as a facility in the treatment of sewage and industrial effluents.

Mineral Exploitation

For their size the British Isles were well endowed by Nature with mineral resources but, of course, the inevitable result of early industrialisation has been early exhaustion of the best deposits of many ores, particularly those containing lead, copper and tin of which the United Kingdom was once the world's leading producer. The intensive prospecting of the Continental Shelf for gas and oil raises the obvious question of whether other useful minerals can be recovered from beneath the seabed. Off the north coast of Cornwall tin lodes are known to extend under the seabed as do coal seams in Cumberland and Durham. There is already a large underwater sand and gravel industry meeting about 10% of the United Kingdom demand. The economic geology of the Continental Shelf around Britain has been reviewed by Dunham [15]. Because of the additional costs of exploration and of drilling and tunnelling beneath the seabed there will be strong economic incentives to reduce the costs of overburden removal and rock breaking and crushing and the use of nuclear explosives for this purpose is bound to receive consideration. On the other hand the use of nuclear explosives in mining on land near populated areas seem less likely. Quite apart from the inherent problems in their use, increasing objections on amenity grounds are likely to preclude large-scale mining near densely populated areas.

Figure 6 summarises the possible uses of nuclear explosives near populated areas.

3. Eliminating the Hazards of Nuclear Explosives

The principal hazards which could arise in the commercial application of nuclear explosives are airblast, radioactivity and ground motion. Leaving aside very large completely contained explosions, which will be economically unacceptable in populated areas because of seismic damage considerations, airblast would only be a problem with cratering explosions used in certain mining operations and in civil engineering projects. Similarly, it would only be in cratering explosions that radioactivity would be released into the atmosphere at the time of the explosion. None would be released in a contained explosion, providing that precautions were taken to prevent venting up the emplacement hole. On present experience, as reviewed by Rapp [16] and by Germain and Kahn [17] it appears that containment can be assured. The probability of seepage of radioactive gases to the surface following the shot is very small as is the quantity of radioactivity involved. The remaining radioactive hazards in a contained shot would be those arising in the development and use of the cavity or chimney and those arising from radionuclide migration in ground water. Seismic damage resulting from ground motion is a common hazard of all underground explosions, nuclear or conventional.

Clearly the use of cratering explosions near densely populated areas would raise very considerable problems in relation to these three main hazards. But in practice the need for such cratering explosions is likely to arise in lightly populated areas, not because the hazards are thereby lessened, although of course they are, but simply because these are the areas where harbours are needed, where overburden must be removed and new roads, railways and dams constructed in order to develop new sources of minerals and power. Most densely populated areas are already well equipped with good means of communication and most mineral resources have already been worked or are being worked by conventional methods.

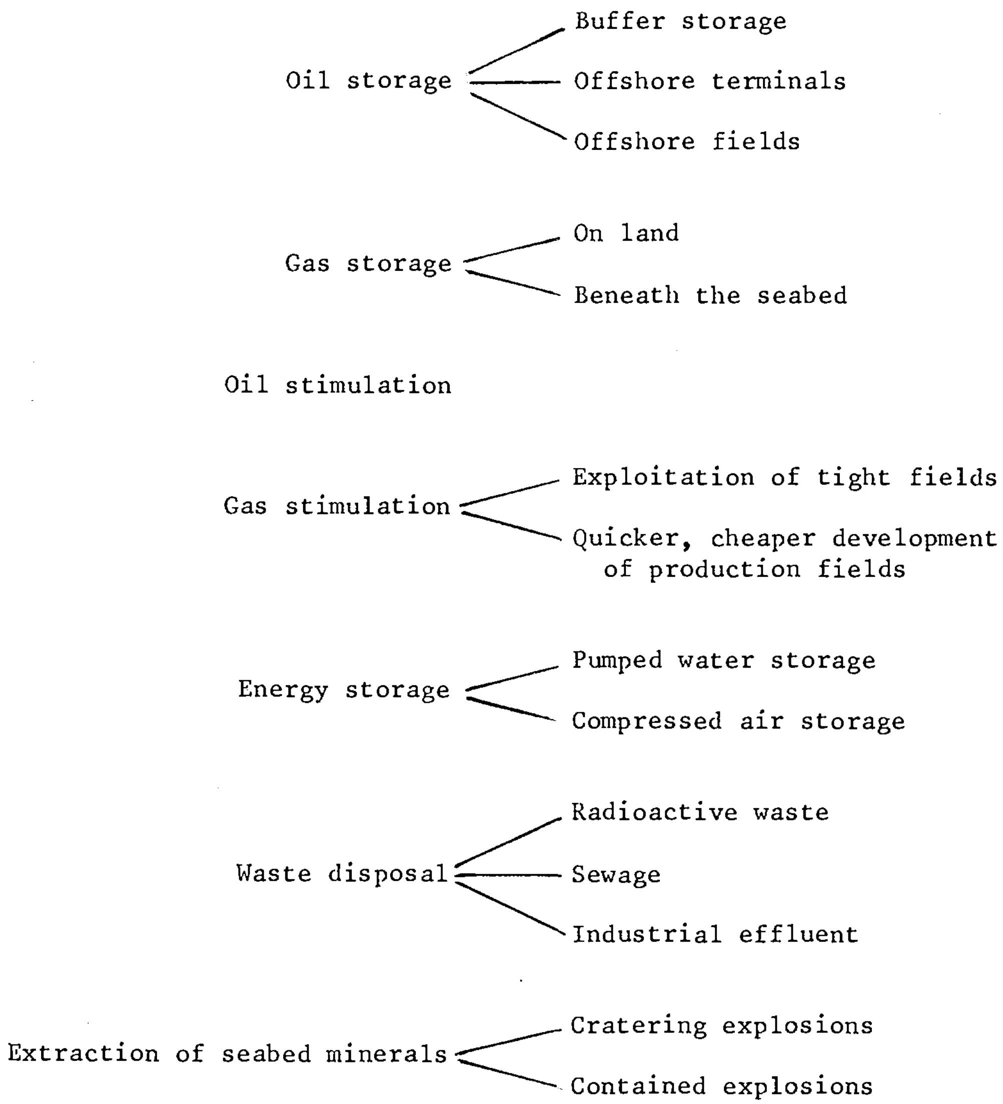

Figure 6 Possible uses of nuclear explosives near populated areas

Turning to completely contained explosions the picture is different. For a suitably designed device of up to 100 kton yield, say, suitably emplaced in a carefully chosen geological structure the potentially mobile radioactivity produced should be small. Contamination of ground water by fission products should then be negligible [18, 19] and the chimney could be purged to reduce radioactivity to an acceptable level. Tritium - from thermonuclear reactions and from neutron reactions with surrounding rock - is likely to be the most troublesome radionuclide. In gas and oil stimulation work and in the development of water resources [18] it may be necessary to use all-fission devices. This may be necessary in all contained shots if tritium proves to be troublesome to remove from storage cavities by purging or presents a contamination hazard to ground water [18, 19]. Given the demand, the economic penalty, if any, of using all-fission devices should not be large.

With the elimination of air blast and the reduction of radioactivity to acceptable levels, seismic damage caused by ground motion remains as the crucial hazard of the contained nuclear explosion. An immediate reaction is that seismic damage precludes the use of nuclear explosions near populated areas. Of course this is true as far as explosions beneath the centre of, say, London or Las Vegas are concerned but even in densely populated countries there are considerable areas of lightly populated land. About an eighth of England and Wales has a population density less than 100 per square mile which implies a building density of something like 30 per square mile; in Scotland sparsely populated areas are more common. It appears from the Rulison shot [20] that explosions of up to about 50 kton could be carried out within 5 to 7 miles of sizable centres of population without causing unacceptable seismic damage. Naturally the costs of strengthening buildings, temporarily evacuating homes and meeting justified compensation claims must be considered in the overall assessment of any scheme and may impose unacceptable economic penalties but there appear to be no insuperable short or long term safety problems associated with shots of up to 100 ktons.

The economic penalties of seismic damage may indeed be sufficient to preclude many nuclear explosive engineering projects near populated areas but often a simple remedy would be to hand - site the project beneath the sea bed at a sufficient distance from shore. As already shown the off-shore oil terminals are often a considerable distance from shore because of navigation problems. Nuclear explosions beneath the seabed at terminals sites should then pose few seismic damage problems. Tsunamis - or seismic sea waves - will need to be considered but around Western Europe at least their effects, if any, should be small compared with those from typical stormy weather [21].

A final hazard which must be mentioned is earthquakes and aftershocks related to nuclear explosions [22]. For contained explosions of up to 100 kilotons seismic tremors outside the chimney growth area are most unlikely, particularly in the many regions of low natural seismic activity such as the Eastern United States and Northern Europe.

It seems that the safety problems associated with contained nuclear explosions of up to about 100 kton yield are sufficiently limited and sufficiently well understood as to make their use in engineering works near populated areas possible. The close proximity of the sea to many densely populated areas provides the key for a successful solution to the principal problem of seismic damage, providing the overall economics of any engineering scheme are not adversely affected.

4. Nuclear Explosive Engineering in and around Western Europe

Having suggested that nuclear explosive engineering can be both useful and practicable near densely populated areas it is natural to ask what are the immediate prospects for this technology. Some of the broad possibilities in and around Western Europe are brought out in the discussion of section 2 but it seems worthwhile to consider a few aspects in more detail.

For safety reasons the cratering explosion has already been seen to be a doubtful starter near densely populated areas. An important exception is the cratering explosion on the seabed with its possible application to mineral exploitation on the Continental Shelf. Here the seismic damage and blast hazards can be overcome by going a sufficient distance from the shore but there are obvious problems concerned with sea waves, the base surge and radioactivity in seawater - problems which have been discussed very briefly by Tomblin et al of AWRE [23]. Another application of the less than fully contained under-seabed nuclear explosion might be the removal of navigation hazards but much as it may be desired to remove such notorious hazards as the Seven Stones Rocks (scene of the grounding of the Torrey Canyon) it is unlikely that such sites will be sufficiently far from land to permit the use of uncontained nuclear explosions. The main application of cratering explosions then is likely to be in exploiting the mineral resources of the Continental Shelf; they may be used as a complement or alternative to the completely contained explosion. In both cases the rate of application is likely to be governed by economics and by the speed with which other branches of underwater technology develop.

The storage of oil in nuclear excavated chimneys seems most likely to be developed first in connection with large tanker terminals. Figure 7 is an artist's impression of a possible design for the Mersey Docks and Harbour Board's Liverpool Bay oil terminal. The island, 3,800 feet long, situated 11 miles off the coast, would be capable of berthing million ton tankers 1800 feet long by 283 feet with a draught of 95 feet. Two submarine pipelines would connect the island to a point on the coast about 14 miles away from where a main pipeline would run to oil refineries in North West England. In this design the base of the island provides storage for 1¼ million tons of oil. Using nuclear explosives it would be possible to provide additional storage beneath the seabed at the island itself or - at a later date - 2 or 3 miles away, connected to the existing storage by additional pipeline. In a possible alternative scheme tankers would tie up to a single buoy mooring [24] and all the storage would be provided beneath the seabed. An important economic factor in favour of off-shore storage linked with tanker terminals is that the pipeline must be provided as part of the overall scheme. Off-shore buffer storage filled from land would be considerably more expensive.

As far as the gas industry is concerned the main North Sea fields are 15-50 miles off shore (figure 3) - sufficiently far from the shore to allow for gas stimulation shots being undertaken without risk of seismic damage to shore installations. The same is likely to hold true in the Irish and Celtic Seas where a period of intensive prospecting is now being followed by the first drilling. The storage of gas may also be feasible and economic in nuclear chimneys either beneath the seabed or on land. A study of conditions in the United Kingdom suggests that, apart from seismic damage costs, which must vary from site to site, on-land storage costs should be very much in line with those given in the feasibility report for Ketch [25].

5. The Future

At a time when Gasbuggy and Rulison are the only reported applications of nuclear explosive engineering which can be considered as being of a commercial or near-commercial nature it cannot be claimed that the application of nuclear explosives in engineering projects near to densely populated areas is imminent. Nevertheless there is sufficient evidence of potential use to justify a continuing appraisal of the possibilities as nuclear explosive engineering

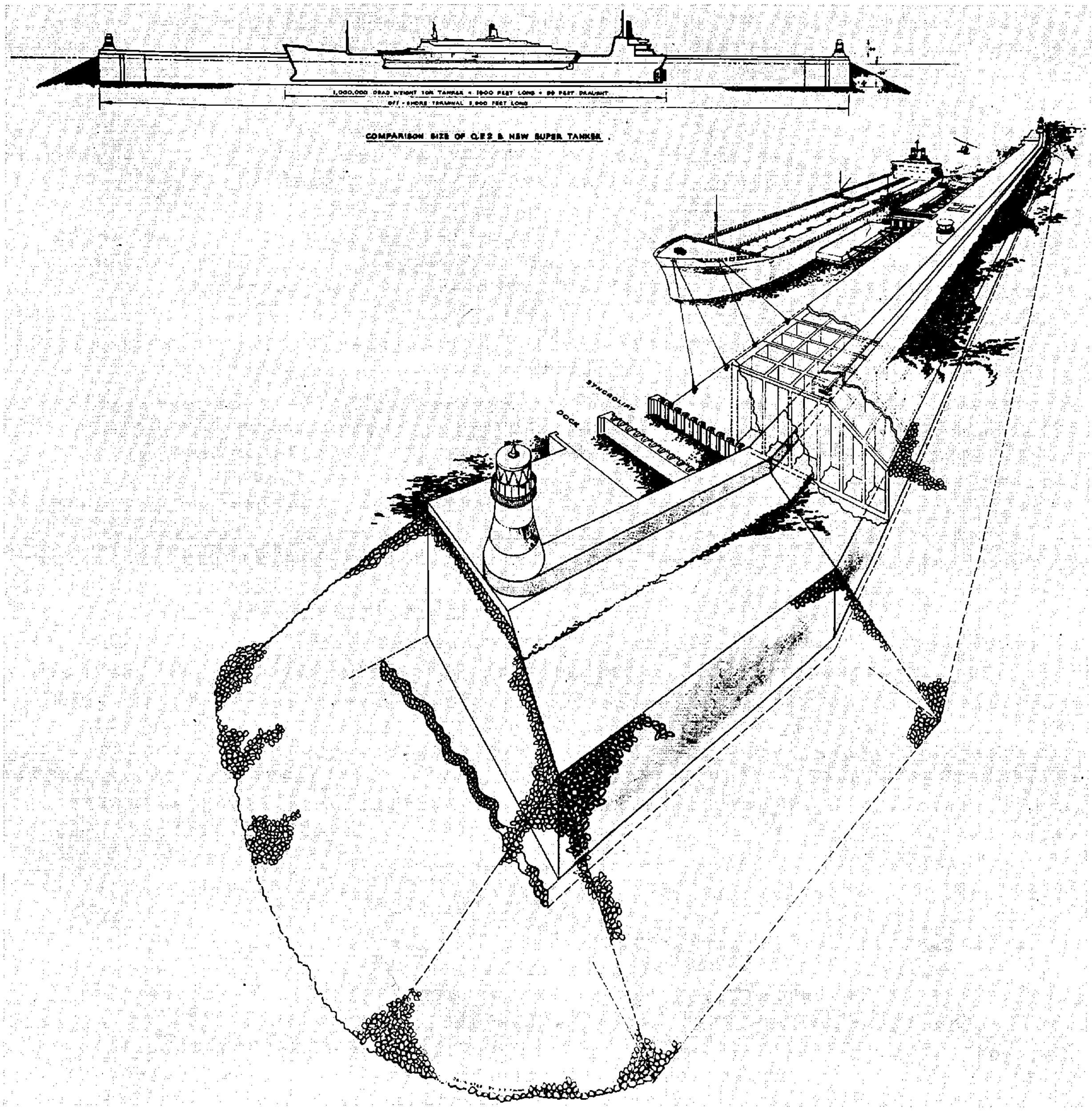
1,000,000 DEAD WEIGHT TON TANKER · 1900 FEET LONG · 90 FEET DRAUGHT
OFF-SHORE TERMINAL 3,000 FEET LONG
COMPARISON SIZE OF Q.E.2 & NEW SUPER TANKER.
SYNCROLIFT
DOCK

Figure 7 Artistic impression of a million ton tanker terminal

develops. The substantial American and Russian development programmes appear likely to answer many of the technical problems now facing us. Of primary economic importance is the seismic damage problem.

Figure 8 illustrates how seismic damage effects can vary with geology. Using the pseudo absolute acceleration (PSAA) or building response as a criterion for seismic damage one finds variations of 200-250% in response depending whether buildings are situated on hard rock (favourable) or alluvium (unfavourable). In practice a variety of site conditions will probably be found. When these variations are converted into costs of investigating claims and paying justified claims the uncertainties can be very great. In Table 1 are the results of a calculation of seismic damage costs using the procedure recommended by the United States Army Engineers' Nuclear Cratering Group [26] for a hypothetical population and building distribution in a densely populated area around a 25 kton shot. Several conclusions can be drawn from these figures:

(i) The percentage variation in damage costs may be much greater between hardrock and alluvium sites than the percentage variation in pseudo-absolute accelerations (which is a constant 220% in this example).

(ii) Although the proportion of complaints and the cost of settling claims decreases with distance the major contribution to damage costs can easily come from many small claims at large distances.

(iii) In the case of a city (population 180,000) at 30 km the total compensation becomes very difficult to estimate.

(iv) Present estimates of seismic damage costs for a shot near densely populated areas could be uncertain by a factor of 5.

It may be argued that the assumptions made in deriving Table 1 are unrealistic. Certainly the first reports of the Rulison shot suggest that the assumptions may be pessimistic. Nevertheless there remains a great deal of uncertainty about the costs of seismic damage. If nuclear explosions are to be used near to populated areas a great deal more theoretical and experimental knowledge and practical experience will have to be acquired and thoroughly analysed so that realistic costs can be incorporated in economic assessments of particular projects. No amount of sophistication in device design, drilling techniques and the like will ensure the use of nuclear explosives near populated areas unless this problem is tackled and solved. It is salutary to remember the proportion of breakdowns in nuclear power stations which arise from failure in their (possibly less well tested and proved) conventional equipment.

Because of the seismic damage problem it is hardly possible to contemplate development experiments near populated areas; the use of nuclear explosions in such regions must be limited to proved applications which can be guaranteed safe and which are virtually certain to achieve their engineering objectives. An analogy can again be drawn with nuclear power stations - siting close to centres of population becomes more acceptable as design and operating experience develop. This need not mean that development shots are limited to the United States and Russia. They could be safely carried out in many other sparsely populated locations in other parts of the world.

Similar considerations apply to peaceful applications of nuclear explosives on or beneath the seabed. Here the pace of progress is strongly dependent on the development of undersea technology although, as compared with the effects of on land explosions, there is relatively little information available on underwater cratering, the generation of water waves by explosions and the disposal of

Table 1

Illustrative Estimates of Seismic Damage Costs for a 25 kton Nuclear Explosion

Damage zone, km	Average distance from shot point, km	Population	Number of buildings	Sites on hardrock			Sites on alluvium		
				Complaint factor (CF)	Damage factor (DF)	Cost, 000 dollars	Complaint factor (CF)	Damage factor (DF)	Cost, 000 dollars
0-2	1	0	0	1.0	1.0	Nil	1.0	1.0	Nil
2-4	3	50	15	0.50	0.79	59.25	0.80	1.0	120.00
4-6	5	300	100	0.19	0.47	89.30	0.70	0.39	273.00
6-8	7	600	200	0.098	0.26	50.96	0.50	0.21	210.00
8-10	9	900	300	0.059	0.15	26.55	0.37	0.13	144.30
10-15	12.5	6,000	2,000	-	0.059	118.00	0.18	0.068	244.80
15-20	17.5	24,000	8,000	-	0.016	128.00	0.080	-	640.00
20-25	22.5	42,000	14,000	-	0.005	70.00	0.034	-	476.00
30	30	180,000	60,000	-	0.0015	36.00	0.011	-	660.00
					Total cost	578.06		Total cost	2768.1

Zone I ($\leqslant 16$ cm/sec^2) cost = Number of complaints × \$400

Zone II (16 to 100 cm/sec^2) cost = Number of complaints × \$1,000

Zone III ($\geqslant 100$ cm/sec^2) cost = Number of complaints × damage factor (DF) × \$10,000.

Number of complaints = Number of buildings × complaints factor (CF)

Number of buildings ≈ Population × $^1/_3$. Average value of a building in zone III = \$10,000.

Values of CF, DF and PSAA versus distance from figure 8.

PSAA = 2 peak ground acceleration = $1{,}000\ W^{0.7}\ R^{-2}$ cm/sec^2, W = 25 ktons, R = distance from shot point in km.

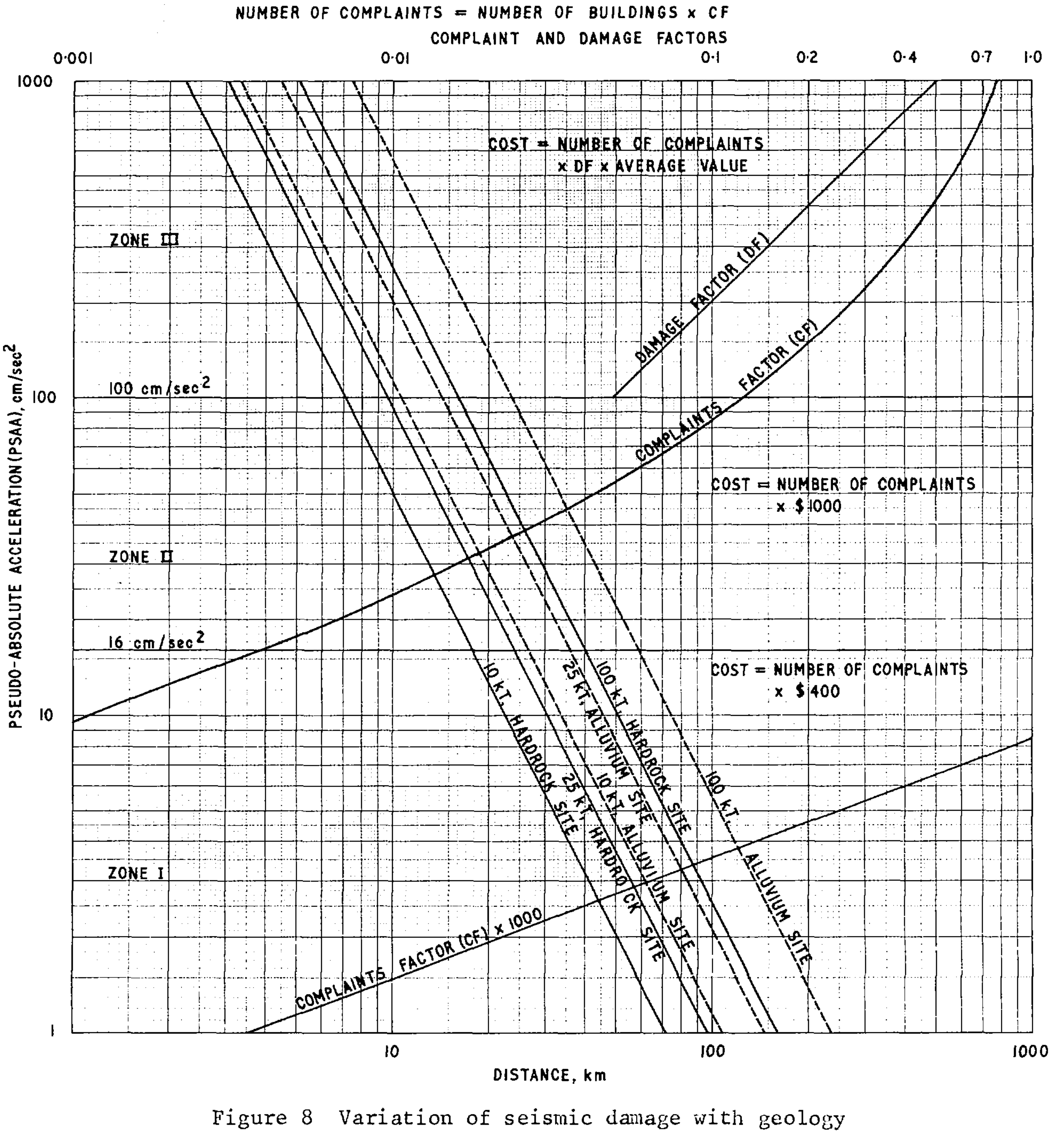

Figure 8 Variation of seismic damage with geology

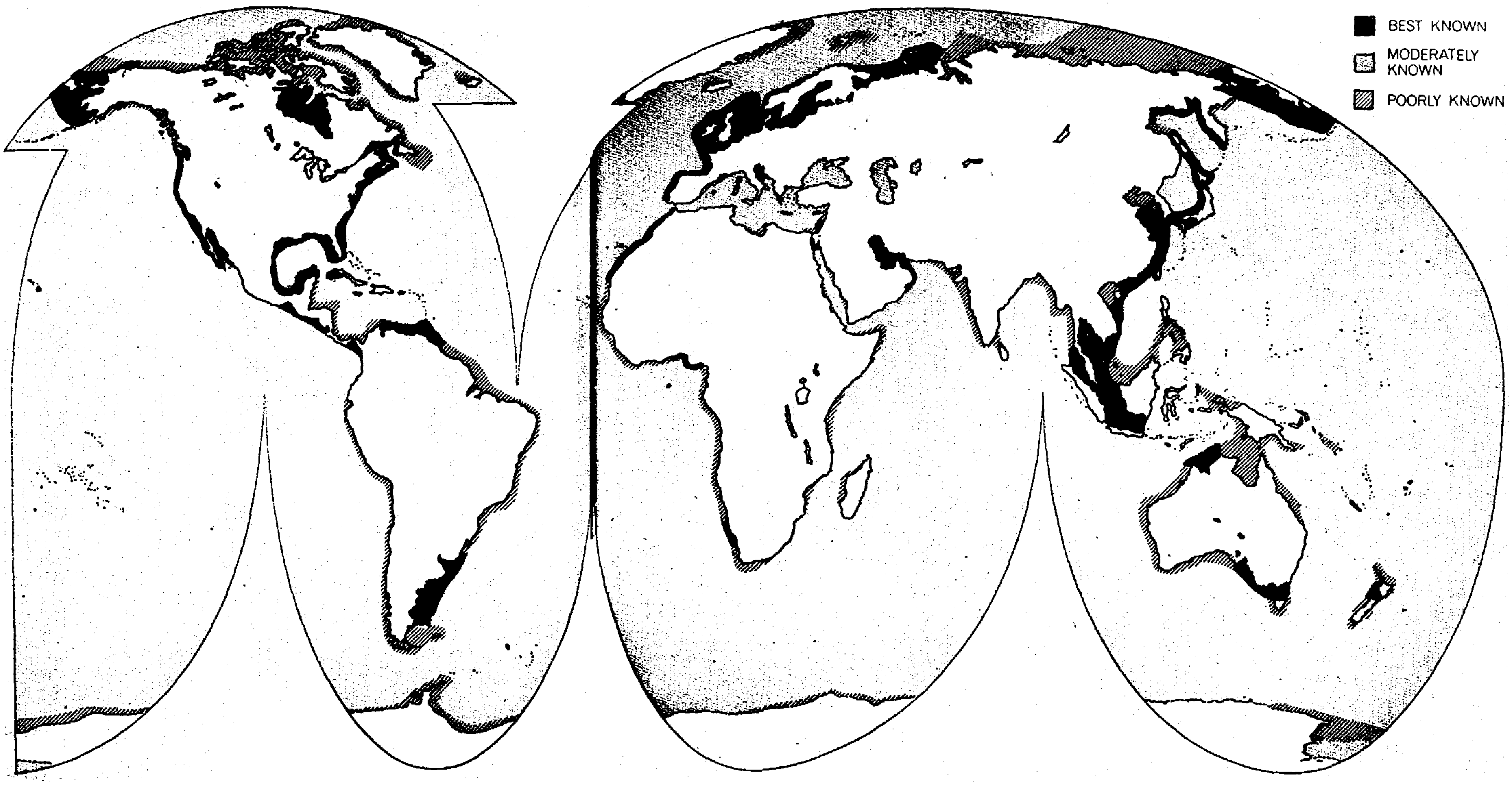

Figure 9 Continental shelves of the World.

any released radioactivity. Given the vast area of the world's continental shelves (figure 9) and their economic potential, the incentive for research in these fields is high.

To summarize, the use of nuclear explosives near populated areas may be practicable and further detailed studies of the technical problems involved are now justified. This is a necessary prelude to the assessment of the wider economic and political issues which must be undertaken before national policy decisions can be made. In the meantime it is desirable to bring to the attention of engineers both the potentialities and the limitations of the use of nuclear explosives in a variety of environments.

Acknowledgments

In preparing this paper I have consulted many individuals and organisations including my AWRE colleagues and staff of Associated Nuclear Services, the Central Electricity Generating Board, the Gas Council and the Mersey Docks and Harbour Board; but the views expressed and the conclusions reached are my own.

References

1. Article in Komsomolskaya Pravda, November 1, 1969.
2. Tape, G.F., Quoted in Nuclear Industry, 16 (4), 11 (April 1969).
3. "An explosion tames the Vakhsh", Krasnaya Zvezda, March 30, 1968.
4. "Insurance for Oil", Economist, 224, 344 (July 18, 1967).
5. "Deep water tankers in Bantry Bay", Financial Times (March 15, 1968).
6. "Gulf's Bantry terminal is now open for business", Petroleum Review, 23, 175 (June, 1969).
7. "Milford Haven will take 250,000 ton tankers", The Engineer, 227, 124 (January 24, 1969).
8. "Million ton tankers for Liverpool?", Mersey Docks and Harbour Board Press Release, (May 16, 1969).
9. "Off-shore port", New Scientist, 44, 128 (October 16, 1969).
10. Kruger, K., "Heligoland prepares for 800,000-ton super-tankers", Ocean Industry, 4 (8), 46 (August, 1969).
11. Gillen, W., "North Sea oil found by gas drilling firms", Daily Telegraph (June 21, 1969).
12. Cronen, A.D., "Well spacing in North Sea gas fields", J. Inst. Petr., 55, 141 (May 1969).
13. "Natural Gas Survey - 1968", Pipes and Pipelines International, 13 (12), 30 (December, 1968).
14. Eaves, P.S.K., "Energy storage in power systems", Elec. Rev., 185, 235 (August 15, 1969).

15. Dunham, K.C., "Economic geology of the Continental Shelf around Britain", Proc. of Conf. on Technology of the Sea and the Sea-Bed, AERE, Harwell, May 5-7, 1967, AERE-R5500 (Vol. 2) 328.

16. Rapp, E.G., "Containment of buried nuclear explosions", UCRL-50604 (October, 1968).

17. Germain, L.S., and Kahn, J.S., "Phenomenology and containment of underground nuclear explosions", UCRL-50482 (November, 1968); reproduced in NVO-40 (Revision No. 2), chapter 4 (May, 1969).

18. Piper, A.M., "Potential applications of nuclear explosives in development and management of water resources - preliminary canvass of the groundwater environment", TEI - 873 (1968).

19. Fenske, P.R., "Prediction of radionuclide migration in ground water", NVO-40 (Revision No. 2), chapter 6 (May, 1969).

20. Coffer, H.F., Private communication (October, 1969).

21. "Tsunamis and other water-wave effects",TID-24996, 14 (April 1969).

22. Weart, W., "Earthquakes and aftershocks related to nuclear detonations", NVO-40 (Revision No. 2), chapter 11 (May, 1969).

23. Tomblin, J.T. et al., "The use of nuclear explosives for seabed mining", Proc. of Conf. on Technology of the Sea and the Sea-Bed, AERE, Harwell, May 5-7, 1967, AERE-5500 (Vol. 2) 371.

24. Cameron, I., "Off shore mooring devices",Petroleum Review, 23, 169 (June 1969).

25. "Project Ketch, A feasibility study on creating natural gas storage with nuclear explosions", PNE-1200 (July, 1967).

26. Hughes, B.C., "Nuclear construction engineering technology", NCG Tech. Report No. 2 (September, 1968).

XA04N0858

NUCLEAR STIMULATION OF OIL-RESERVOIRS

F. DELORT - F. SUPIOT
Commissariat à l'Energie Atomique (France)
Centre d'Etudes de Bruyère-le-Châtel

ABSTRACT

Underground nuclear explosions in the Hoggar nuclear test site have shown that the geological effects may increase the production of oil or gas reservoirs.

By studying the permanent liquid flow-rate with approximate DUPUIT's equation, or with a computer code, it is shown that the conventional well flow-rate may be increased by a factor between 3 and 50, depending on the medium and explosion conditions.

INTRODUCTION

The rentability of an oil-field production is related with two main parameters :
- the permanent well flow-rate,
- the total amount of recovered oil.

In this report, the permanent flow is only considered and we show how to evaluate the production after a nuclear stimulation.

Two methods are described, the first one is a simple analytic calculation; the second one has a necessary computer code and it gives more information.

Both methods are applied to hypothetic nuclear stimulation explosions in various conditions.

STIMULATION FACTOR - EXPLOSION EFFECTS

1. Stimulation factor (1).

In a permanent regime, with a circum radial symmetry, the well flow-rate is given by the DUPUIT's law which is obtained from DARCY's law : $\vec{V} = - k \,\vec{\text{grad}}\, \varphi$ - ($\vec{V}$: filtration velocity, k : kinematic permeability, φ : hydraulic potential).

The DUPUIT's law is written :

$$Q = \frac{2 \pi h \bar{k} (P_a^2 - P^2)}{\mu T \, z \, \text{Log} \frac{R}{a}} \quad \text{for gas}$$

$$Q = \frac{2 \pi h \vec{k} (P_a - P_r)}{\mu B \operatorname{Log} \frac{R}{a}} \quad \text{for liquid}$$

with =

Q = well flow-rate
h = thickness of the reservoir rock
$\vec{k}$ = average reservoir permeability between the well and the radius of drainage area
P_a = pressure at well-bore
P_r = pressure at drainage radius
μ = fluid viscosity
T = gas temperature
z = gas compression factor
B = oil volumetrical factor
R = radius of drainage area
a = well-bore radius

If Q_f is the flow-rate after stimulation, and Q_i the natural flow-rate without stimulation, we propose to evaluate the stimulation factor $\lambda = \frac{Q_f}{Q_i}$ in function of the explosion conditions.

$$\lambda = \frac{\operatorname{Log} \frac{R_i}{a_i}}{\bar{k}_i \displaystyle\sum_{j=1}^{j=n} \frac{\operatorname{Log} \frac{r_j}{r_{j-1}}}{k_j}}$$

with

R_i = drainage radius
a_i = conventional well-bore radius (before stimulation)
$\bar{k}_i$ = average permeability between the well bore and the drainage radius
r_j = radius of the zone with a permeability k_j
n = number of zones of different permeabilities.

The stimulation factor depends for one part on parameters which are not directly in relation with the explosion conditions (drainage radius, well-bore radius) and for the other part, on parameters which are modified by the explosion (created chimney, permeability, etc ...).

We briefly recall hereafter the nuclear explosion phenomenology and particularly the effects which are interesting for the stimulation. We also show by using the experimental results collected on Hoggar Test Site and those published in the foreign literature, how we have evaluated the different parameters necessary for the calculations.

2. Underground nuclear explosion effects (2).

In the first microseconds after the zero time almost instantaneously an enormous amount of energy ($4.18\ 10^{19}$ ergs by kt) is released in a very small volume (less than one cubic meter). A strong shock wave appears in the medium which propagates and produces important medium transformations.

We can successively distinguish :

- a vaporised rock zone (a few meters large) and farther, a melted rock zone.
- A fractured zone in which we can distinguish, a crushed rock zone which looks like sand and gravel becoming more and more rough when the distance to the shot point increases. This zone stretches to about a few tens of meters. This distance is related with the energy released and with the medium.
  At distance, the rock shows a fractured system of decreasing intensity.
- An elastic zone where the medium is in a permanent state of stress.
- A seismic zone in which there is no permanent deformation.

After the shock wave passed through, the gas of vaporised rocks expands and pushes away the initial chamber wall until the pressure inside the cavity is equal to the lithostatic one at the level of the explosion point.

This expansion stays during about some hundreds of milliseconds, and the cavity radius may be calculated with a good precision by using the experimental formula : (3).

$$R_c = \frac{52\ W^{1/3}}{(\rho\ g\ H + C_s)^{1/3\ \gamma}}$$

with :

R_c cavity radius (meters)
W explosion yield (kt)
ρ density
H depth of burst
C_s structural coefficient of the medium
γ adiabatic expansion coefficient of the gas created by the vaporised medium.

It must be noticed the influence of the oil-content in the medium, which acts upon the cavity radius by means of the gas expansion coefficient.

Table 1 shows the influence of the oil content on the cavity radius.

TABLE 1 : Influence of oil content on the cavity radius.

Rate of oil (in weight)	Cavity radius (W = 125 kt)	Cavity radius (W = 1 Mt)
5 %	42 m	85 m
10 %	45 m	90 m
20 %	50 m	100 m

The structural coefficients calculated by means of experimental results of different media (4) are reported on table 2.

/TABLE 2/: Structural coefficients for different media.

Medium	Structural coefficient : C_s in bars
Tuff	$0 < C_s < 15$
Alluvium	$5 < C_s < 40$
Salt	$20 < C_s < 35$
Granite (Hoggar Test Site)	$120 < C_s < 320$
Dolomite	About 100

For deep enough explosions there is no crater, and after a few minutes to a few hours, the fractured rocks above the cavity fall down.

The formation of a chimney (5) is stopped by an equilibrium of the new vault in the undisturbed rock, or by complete filling with rubble. Generally 50 to 60 % of the rubble has dimensions less than 20 centimeters. We can consider that the permeability of the chimney is infinite.

Experimentally, we established that the chimney has an ellipsoïdal shape.

Its height, H_c, is expressed in cavity radius unit, R_c.

$$H_c = k\,R_c$$

Table 3 gives some experimental results for k in different media.

/TABLE 3/

Medium	k
Salt	1
Dolomite	3.2
Granite	3.6 to 6
Sandstone	4
Tuff	3.8 to 6.8

Table 3 shows that, for the same medium, the height of chimney may be different.

These differences are partially in connection with :

- the initial fracturation state of the medium
- the medium stratigraphy
- the vault effect for large yields.

Figure 1 describes the zones created by a contained underground nuclear explosion.

The scheme was established after the study of the Hoggar experimental underground nuclear tests, and various results from foreign countries.

The dimensions of the zones and their permeability are those observed on the Hoggar Test Site (figure 1).

The particular fractured shapes around the chimney are present in most of the media. This zone is produced by the chimney formation.

The vaporised and melted zones are created by the waste heat left by the shock wave.

In a hard rock (granitic rock) it is calculated that within 3 meters, for 1 kt yield, 70 % of energy is lost in the medium by the shock wave. On the whole, 90 % of the yield is put in the medium by the shock wave into heat, inside a few meters radius zone. (8).

A thermal gradient is created after the cavity and chimney formations. (9). Its evolution is related with the thermal conductibility of the rock in the different zones around the cavity. The results of the Hoggar Test Site are in agreement with those observed in other Test Sites.

The oil contained in a reservoir may support cracking reactions, but the temperature gradient at the vicinity of the chimney, in the crushed rock, may favourably influence the flow at the beginning of production.

ANALYTICAL CALCULATION OF THE STIMULATION FACTOR (10)

In order to calculate easily the average permeability, $\bar{k}_1$, in the stimulation factor, we must consider that the oil-field, after the explosion, has the same characteristics all along a cylinder, with vertical axis passing through the zero point.

We have calculated the stimulation factor variations in relation with the explosion yield on the pattern drawn on figure 2 which is the figure 1 scheme.

We have studied the influence of the following parameters :

- Radius of drainage area of the stimulated well (figure 3)
- Permeability of the various zones (figure 4)
- Depth of burst (figure 4)
- Characteristics of the medium (water content, oil content, density, etc . . .) (figure 5)
- Reclosed fractures (figure 4)

Effects of successive explosions.

Figure 3 shows a very important increase of the factor λ , for yield greater than 100 or 200 kt in the case of a radius of drainage area equals 400 m, because the selected drainage area is supposed to be entirely fractured. For small radius (400 m), the stimulation factor is twice the corresponding ones for usual drainage radius, and there is no large difference for 800, 1200, and 1600 meters drainage radius stimulation factor.

With a hypothetical but probable effect of reduction of permeability due to fracture closing under the lithostatic pressure, figure 4 shows that the stimulation factor may not be too much affected by the depth of burst.

Figure 5 reports that for media of low permeability ($k \leq 5$ md), the effect of nuclear stimulation is almost constant. The stimulation factor is maximum for these small permeabilities and the nuclear stimulation

FIGURE 1

Altered zones after a nuclear explosion in a granite. Type rock

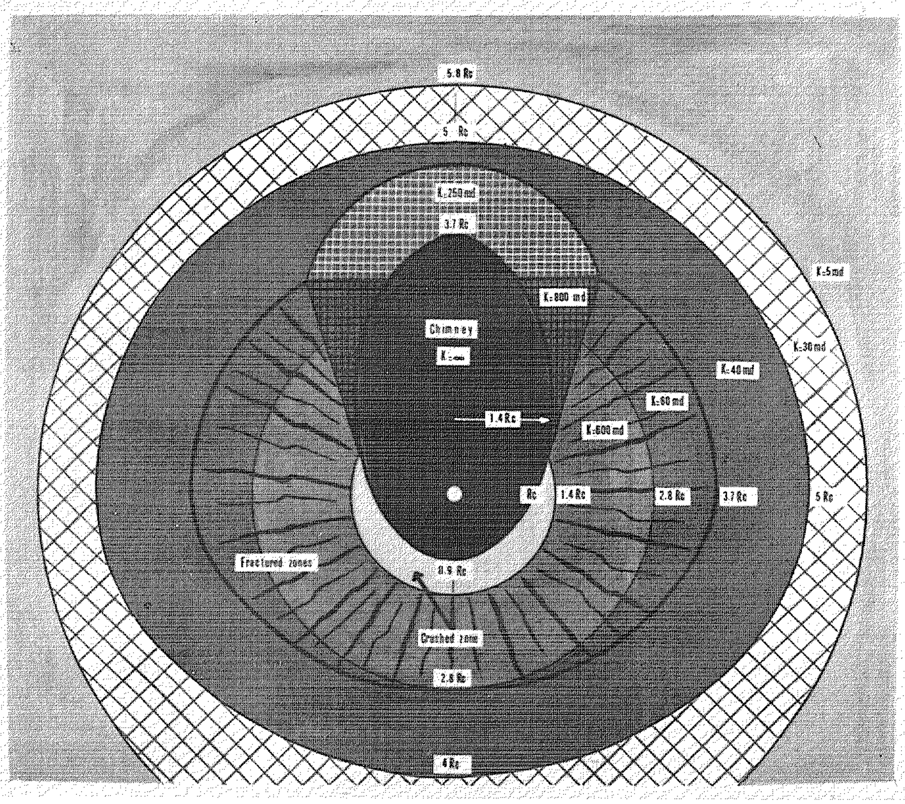

FIG. 2

Schematic representation of

the permeability changed zones

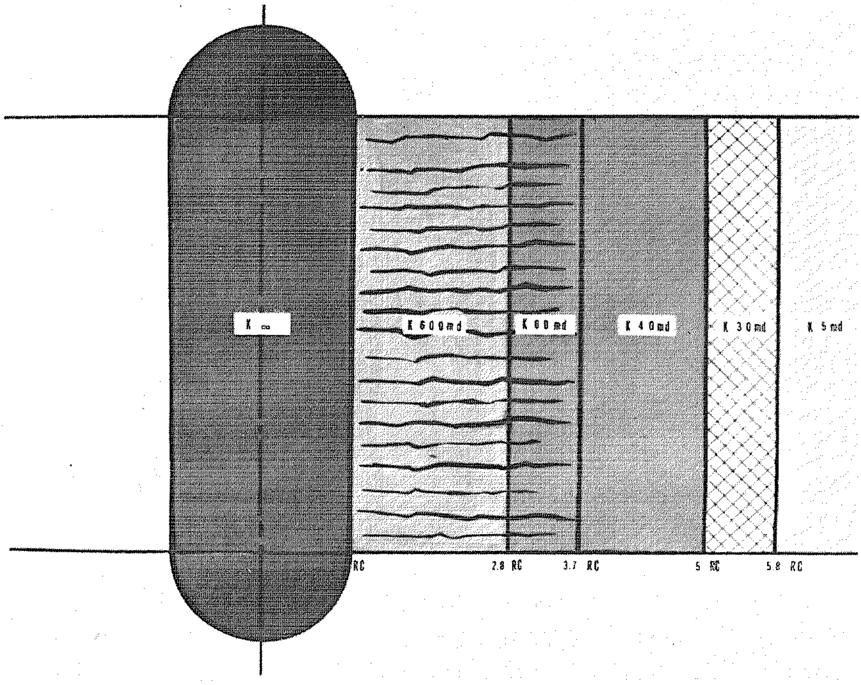

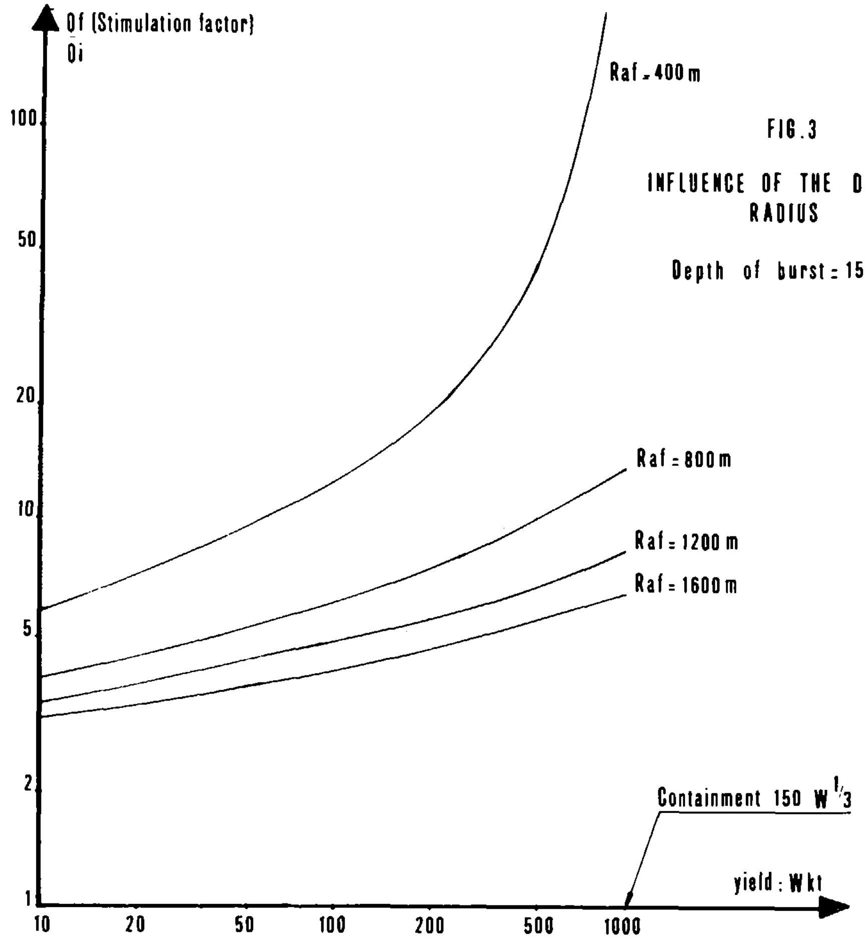

FIG.3

INFLUENCE OF THE DRAINAGE RADIUS

Depth of burst: 1500m

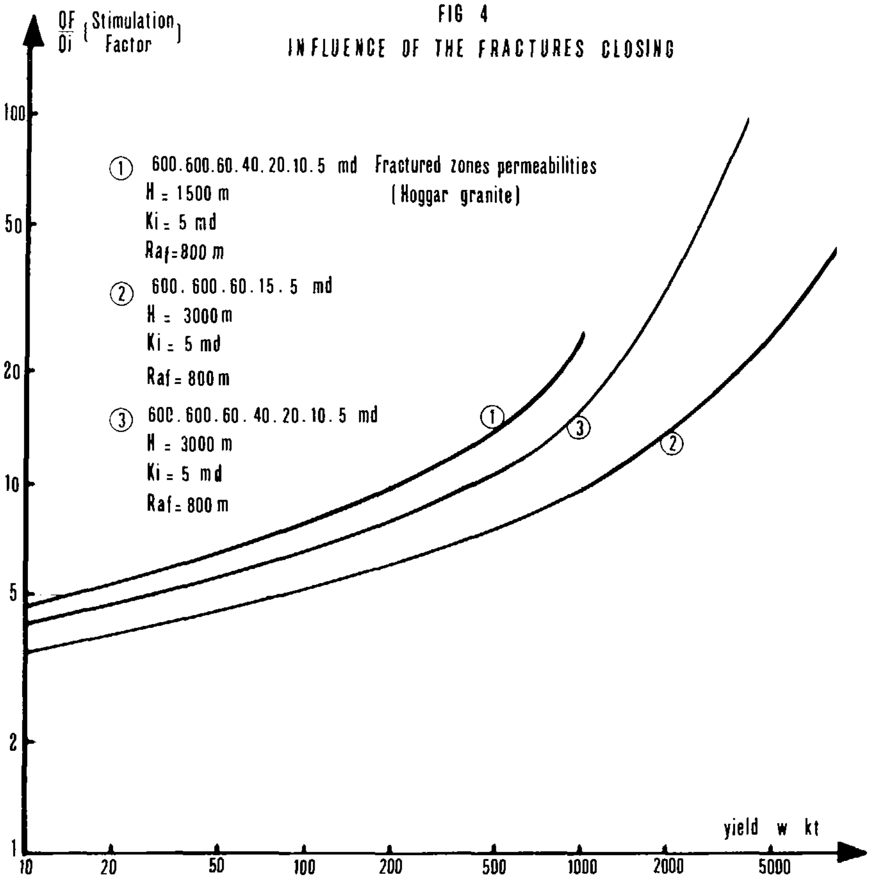

FIG 4

INFLUENCE OF THE FRACTURES CLOSING

interest appears clearly. The explosion yield does not change the stimulation factor when initial permeability is high.

We see that this analytical calculation gives interesting results on the stimulation factor variations in function of some important parameters.

In the case of a prospective study, a common problem is that of reduction of the number of wells by the nuclear stimulation of the oil-field.

We shall investigate this problem by use of the analytical method (10).

When the reservoirs are deep, the drilling conditions are difficult, and of course, the expenses grow up.

In these conditions, the nuclear stimulation may be interesting.

Suppose that the cost of the nuclear stimulation is known, and equals to the price of x conventional wells.

The nuclear stimulation is interesting when :

Nuclear stimulated production > production of x conventional wells

This is written : $Q_f > x\ Q_i$

The x conventional wells draining the same surface as one nuclear well give us :

$$R_2 = R_1 \sqrt{x},$$

with R_1 and R_2, respectively drainage radii of the conventional well and of the nuclear well.

A slightly different formula has been used, taking into account that the circular draining areas are tangent.

We have calculated the nuclear stimulated well flow rate in taking drainage radii equal to conventional well drainage radii.

Calculations have been made when the following stimulation conditions are so chosen:

- Depth of burst : 1 500 m
- Radius of drainage area : 1 000 m.

In these conditions, if

$$W > 60 \text{ kt then } Q_{\text{nuclear}} > Q_{4 \text{ conventional wells}}$$

When the conventional drainage radius is 300 m, and if

$$W > 80 \text{ kt then } Q_{\text{nuclear}} > Q_{5 \text{ conventional wells}}$$

$$W > 3 \text{ Mt then } Q_{\text{nuclear}} > Q_{12 \text{ conventional wells}}$$

This method has a limited application because it allows us only to consider a simplified model (cylindrical zones on the whole height of the bed).

For an optimisation study, it is often necessary to consider a more accurate model.

We now show a calculation method which allows us to consider more realistic geometrical shapes for chimney and fractured zones.

NUMERICAL METHOD OF FLOW STIMULATION (11)

We consider only permanent flow, but a similar method may be used for a transient flow calculation.

The question is to solve, by use of a computer, the equations of flow for uncompressible fluid.

- Continuity equation :

$$\operatorname{div}(\vec{V}) = 0$$

- DARCY's law :

$$\vec{V} = k\ \overrightarrow{\text{grad}}\ \varphi$$

These two equations lead to $\Delta\varphi = 0$

(LAPLACE's equation).

In these conditions :

$\vec{V}$ = fluid parcel velocity vector

k = kinematic permeability
φ = hydraulic potential.

The LAPLACE's equation $\Delta\varphi = 0$ is solved by taking into account the boundary and continuity conditions.

The boundary conditions are :

- Dirichlet = φ = constant(filtration surface, at the drainage radius)
- Neuman $\frac{\partial\varphi}{\partial n} = 0$ (impervious surface, top and bottom of the reservoir).

The continuity condition is related to the flow conservation through two different permeability zones.

For the computer calculations, LAPLACE's equation and the limit conditions are discretised and a Gauss-Seidel method is used.

The explosion effects zones are netted and, at each knot, the potential is calculated.

The values of the potential, φ, give the flow characteristics at each point, especially the flow rate which is written :

$$dq = 2\pi k r \frac{\partial\varphi}{\partial t} dl$$

Choice of the grid

All the dimensions of the chimney and fractured zones are expressed in the cavity radius unit, as shown.

We have chosen a square cell whose side length, L, is equal to a fraction of the cavity radius, chosen in function of the calculation needs and in the following numerical results, $\frac{L}{R_c}$ is constant and equals $\frac{1}{3}$.

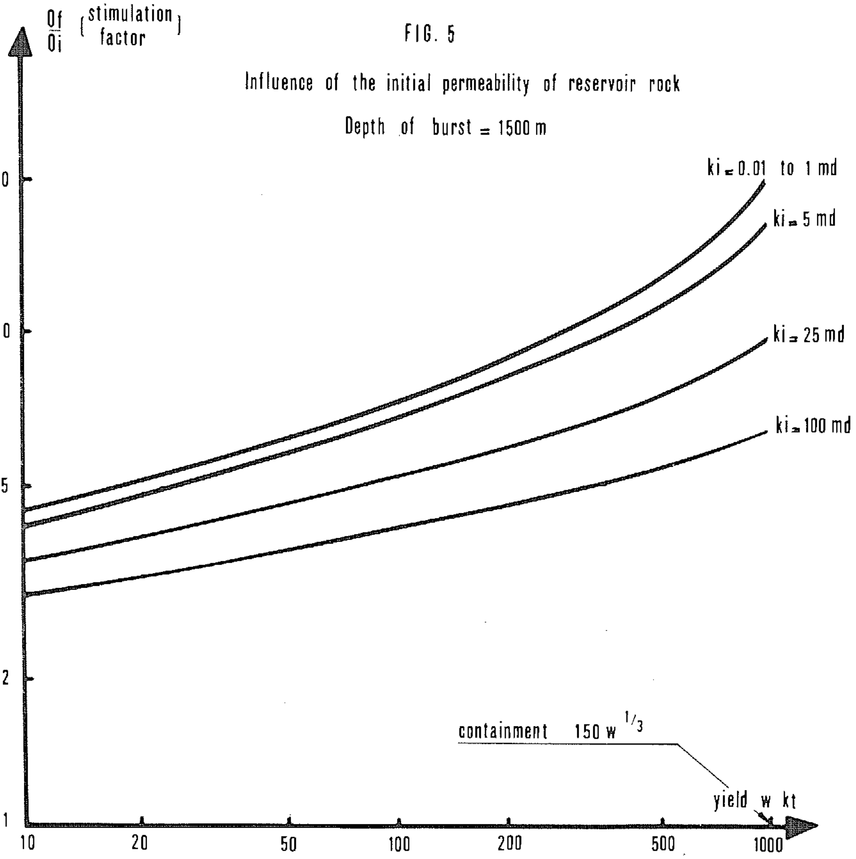

FIG. 5

Influence of the initial permeability of reservoir rock

Depth of burst = 1500 m

FIG 6

Flow in unaffected medium with a chimney

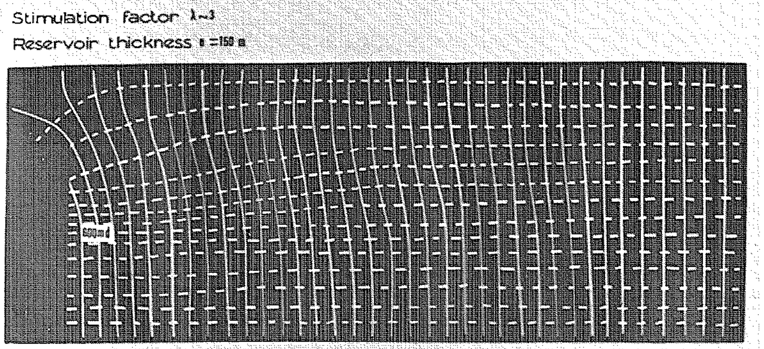

FIG 7

Flow in hardly fractured zones

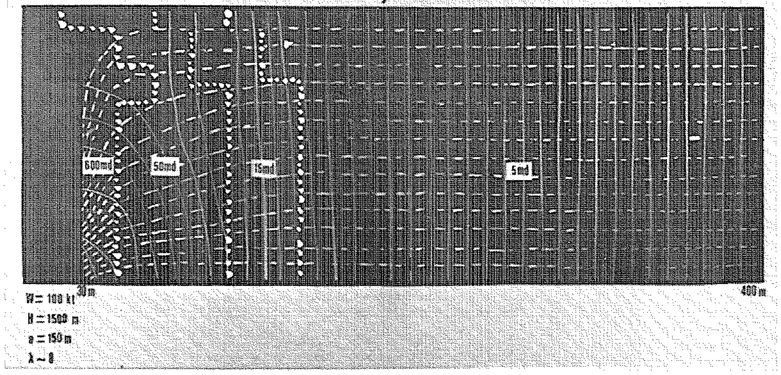

FIG 8

Flow in highly fractured zones

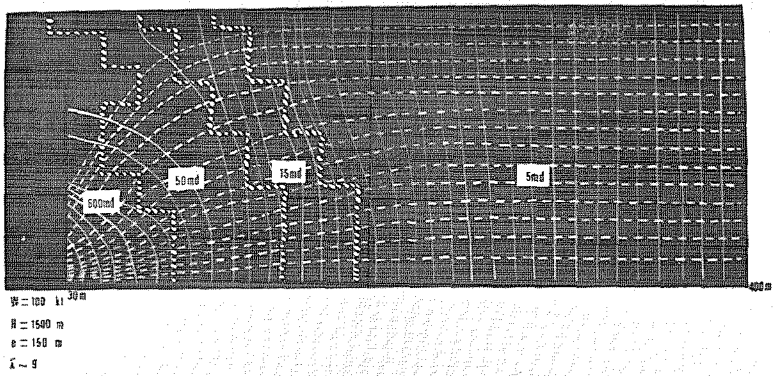

FIG 9

Flow in highly fractured zones (no effect above chimney)

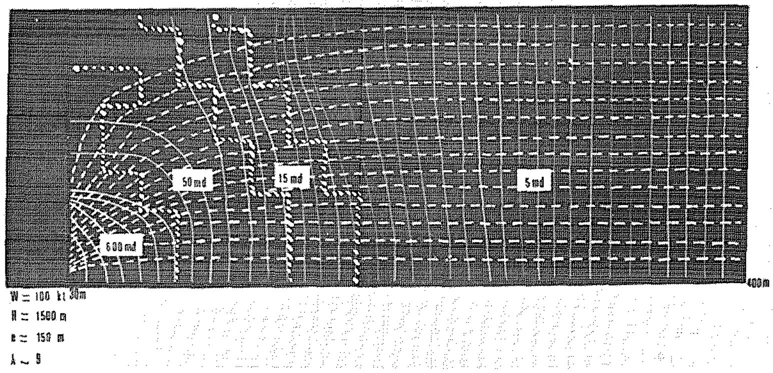

FIG 10

Flow within a chimney fully contained in the reservoir

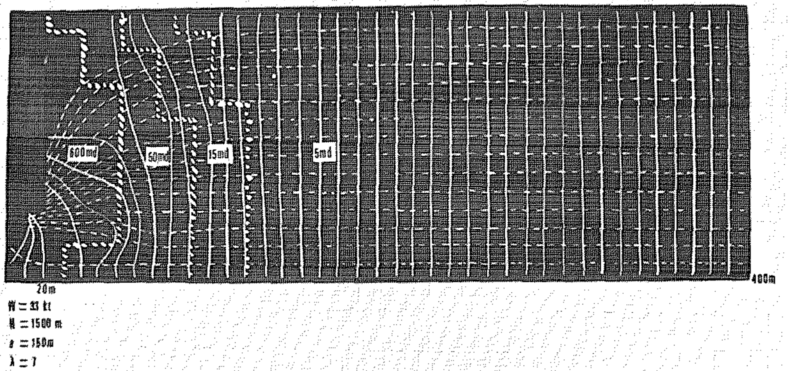

FIG 11

Flow for high-yield explosion

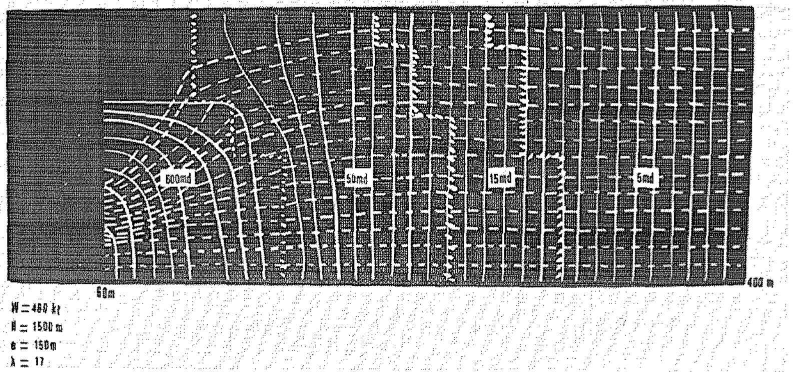

In that case, the calculation gives almost the same stimulation factor as by the analytical method. However, it may be noticed that, with these calculations, we can see the influence on the flow of the shape and characteristics of zones.

We use this possibility in the study on the flow by using the parameters,
- height of the chimney
- position of the shot point.

Both studied cases are shown in figures 6 to 11.

Generally flow lines are concentrated at the bottom of the chimney. It seems interesting to make explosions deeper than the reservoir, and to use medium heterogeneities.

Figures 7., 8. 9 show that fracture permeability can modify the flow, but less the stimulation efficiency.

The influence of the yield appears figures 10. 11 which are of interest for operational safety and production considerations.

CONCLUSION

The study of mechanical effects of underground nuclear explosion and particularly those of the explosions at the Hoggar Test Site, shows that the medium transformations due to nuclear explosions are favourable for oil-field stimulation.

The chimney and fractured zones dimensions, and permeabilities after the explosion are very much greater than those observed after any conventional stimulation.

Nuclear stimulation can multiply flow rate by 10, 50 or even more than 100 with large yields (some hundreds or thousands of kt). This cannot be reached by conventional means.

For great depth of explosion (deeper than 2 000 m) the fractures created by shock wave may be closed by the lithostatic pressure. In the case of about 10 kt, the production may be decreased by 10 per cent.

If the nuclear stimulation objective is to decrease the number of wells on the field, the calculations show that for yield equal or greater than 100 kt, one nuclear well may be equivalent to 4 or 5 conventional wells with a 2 000 meters spacing in a low permeability rock.

BIBLIOGRAPHY

(1) - I. F. P. Cours de Production - A. HOUPEURT - Editions TECHNIP Paris 1959.

(2) - Phénoménologie générale des explosions nucléaires souterraines. S. DERLICH - F. SUPIOT - Rapport CEA-R 3750 1969.

(3) - Explosions nucléaires souterraines - Etude des rayons de cavité. L. MICHAUD - Rapport CEA-R 3594 1968.

(4) - Effects of water content, yield medium and depth of burst on cavity radii - G. HIGGINS - T.R. BUTKOVICH - UCRL 50 203 - 1967.

(5) - Explosions nucléaires souterraines. Etude de la cheminée. S. DERLICH - Rapport CEA-R 3851 - 1969.

(6) - Explosions nucléaires souterraines. Etude des zones fracturées. S. DERLICH - Rapport CEA-R 3941 1969.

(7) - Essais de représentation schématique des effets géologiques d'explosions nucléaires souterraines. Y. ROLLIN - F. ROSE - Rapport CEA en cours de diffusion - 1969.

(8) - Calcul de l'onde de choc en zone proche d'une explosion nucléaire souterraine. Méthode CADES - F. SUPIOT - J. BRUGIES - Rapport CEA-R 3736 1969.

(9) - Distribution de la température après une explosion nucléaire souterraine dans un terrain granitique. PH. LAVOLLEE - Rapport CEA-R - en cours de diffusion - 1969.

(10) - Productivité des gisements d'hydrocarbures stimulés avec des explosions nucléaires. F. DELORT - F. SUPIOT - Rapport CEA-R 3968 - 1970.

(11) - Stimulation numérique d'écoulement permanent de fluides dans les zones d'effets d'explosions nucléaires souterraines. F. ROLLIN - Y. ROSE - Rapport CEA en cours de diffusion - 1970.

XA04N0859

GASBUGGY IN PERSPECTIVE*

Alfred Holzer
Lawrence Radiation Laboratory, University of California
Livermore, California 94550

ABSTRACT

The Gasbuggy experiment set out to answer a number of questions: To what degree could a low-permeability, gas-bearing formation be stimulated? What were the mechanisms responsible for stimulation of gas? What were the problems of product contamination and potential ground shock damage? After two years of postshot work, some of these questions are being answered; more precisely, pressures, temperatures and concentrations of radioactive and non-radioactive constituents of the gas are being established. However, analyzing these quantities and their dependence on variables such as flow rates in terms of a self-consistent model of all the detonation phenomena has been a difficult and slow process. The validity of such a model must be tested by data from other detonations with geologies, reservoir properties and, perhaps, explosive yields different than those of Gasbuggy. The gas stimulation projects now being planned must be capable of furnishing some of these data before they can be called experiments in the fullest sense.

INTRODUCTION

The purpose of this paper is to examine some of the key results of two years of postshot investigation at the Gasbuggy site and to reach some tentative conclusions about the meaning of these results. We will summarize in rather concise form what we set out to find in Gasbuggy, what we did in fact learn, what questions can be raised about what we have (and have not) learned, and what the key issues are that we need to know and learn from future gas stimulation experiments before the method of underground nuclear explosions can be used in gas recovery applications. In addition, results from the various technical areas of investigation - geophysical, reservoir test, gas analysis - will be examined in order that tentative conclusions about the relative success or failure of Gasbuggy may be reached.

The considerations and background which led to the design of the Gasbuggy experiment have been reported in a number of places.[1, 2, 3, 4] The basic relationships governing phenomena of underground nuclear explosions have also been reported numerous times.[5, 6] Of more direct importance are some measurements that were concerned with one of the basic quantities of relevance in gas

---

* Work performed under the auspices of the U. S. Atomic Energy Commission.

stimulation, namely, the increase in permeability around a chimney produced by an underground explosion.[7] This work consisted of in-situ permeability measurements in the region outside the chimney produced by the Hardhat experiment, a 5-kiloton explosion in granite. These measurements indicated an increase of about 2 to 3 orders of magnitude above the preshot permeability in a region 100 to 200 feet from the shot point. In addition, the absolute permeabilities found were between a tenth and one darcy as far as 200 feet from the shot point. Figure 1 summarizes these measurements.

To anticipate some of the items later in this paper, no such dramatic increase or large absolute permeabilities have been observed in the region around Gasbuggy. To anticipate even further, understanding the quantitative difference between the Hardhat and the Gasbuggy results is one of the questions that needs to be answered for the future.

PRESHOT BASELINES

Descriptions of the Gasbuggy preshot program have been reported previously.[2, 22] They are not repeated here. A summary of some of the key findings is given in Table I. Purposes of the preshot program with respect to the over-all technical objectives of Gasbuggy were primarily:

1) To establish preshot baselines of quantities such as the number and locations of fractures and gas entries, the permeability and porosity in the water as well as gas-bearing formations, the lateral variability of the geology, and the preshot ability to produce gas.

2) To use all available information to make realistic predictions of the final cavity size, chimney height, and fracture extent. (A similar effort was undertaken to predict the quantities of radioactive constituents in the postshot gas.)

3) To utilize the results to prepare for and to design the most meaningful postshot program possible.

POSTSHOT RESULTS

Postshot information from Gasbuggy has been derived primarily as the result of activity in four areas: First, from the prompt measurements on fracture formation, cavity collapse and ground motion;[8, 9] second, from the drilling and geophysical investigations in postshot holes;[10] third, from the analysis of a number of gas withdrawal tests [11, 12]; and, fourth, from the analysis from both chemical and radiochemical species of samples of gas withdrawn throughout the postshot period.[13, 14] My purpose is to concentrate on what I consider to be the main results which emphasize our state of knowledge as well as our state of ignorance about Gasbuggy.

I. YIELD

Gasbuggy employed a thermonuclear explosive whose nominal yield was expected to be 26 kilotons. Recently, information from all postshot measurements has been analyzed to refine this number; as a result, the energy release has now been determined to be 29 ± 3 kilotons.

II. MECHANICAL EFFECTS

Most of the information on the postshot effects and their comparison with preshot quantities has been by way of drill holes. In addition to the emplacement hole GB-E, three holes were drilled preshot: GB-1 and GB-2, for the

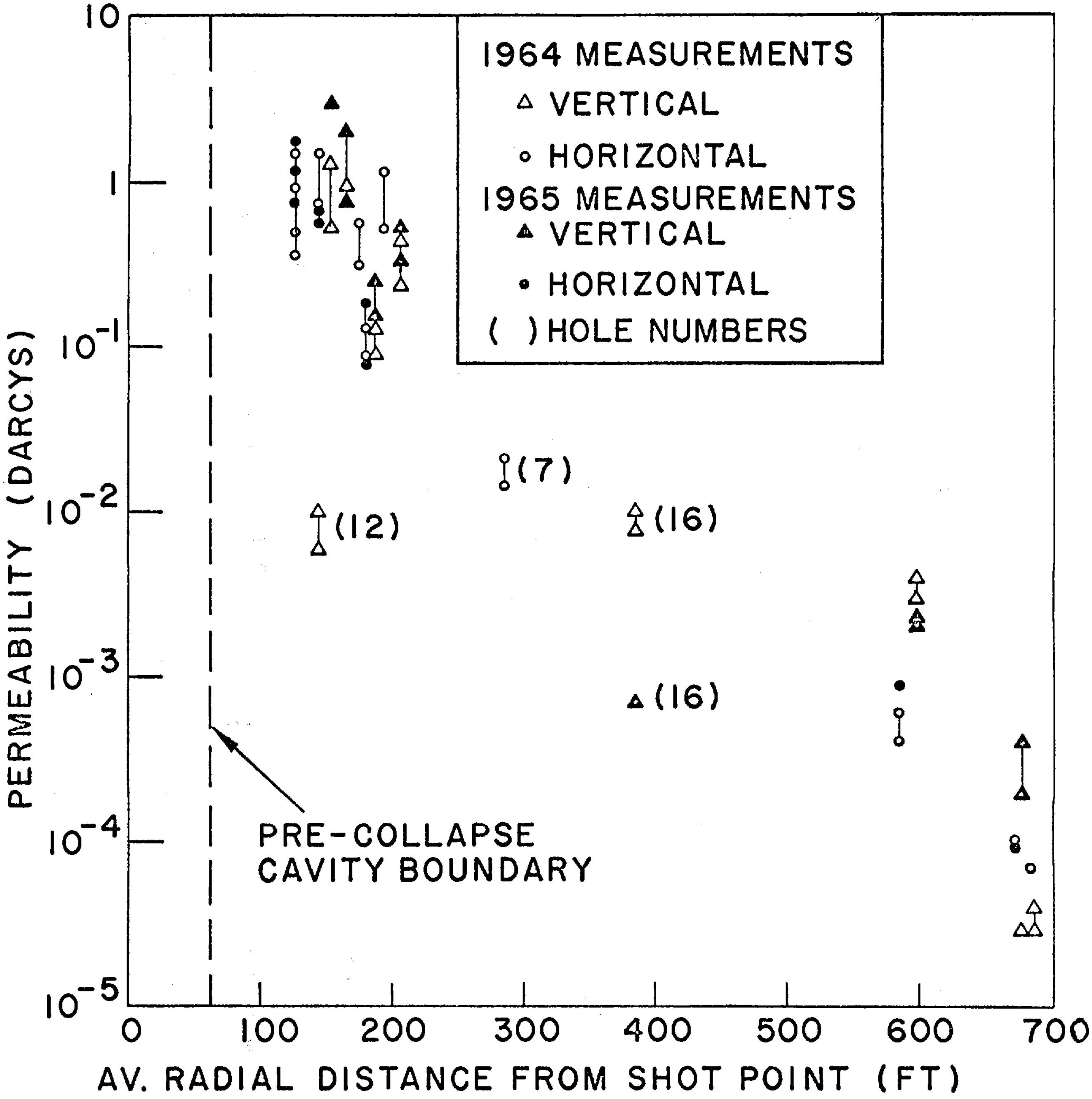

Fig. 1

In-situ permeability measurements in granite following the Hardhat detonation. A number of drill holes were packed off, pressurized with air, and permeabilities calculated from the relation between pressure and volume of air flow.

TABLE I

STUDY AREA	DATA	REFERENCES
Stratigraphy	Tertiaries 0 - 3464'	2, 3, 22
	Ojo Alamo Sandstone (Aquifer) 3464'-3637'	
	Kirtland Fruitland Shales & Coals 3637'-3900'	
	Pictured Cliffs Sandstone (Reservoir 3900'-4186'	
	Lewis Shale - 4186'	
Reservoir Properties	Gas in place:	
	5.8 x 10^9 ft^3/160 acres	2, 3, 11
	4.7 x 10^9 ft^3/160 acres in sands with <60% water saturation	
	Porosity:	
	11.8%, less than 60% liquid saturation	
	8% more than 60% liquid saturation	
	Gas Saturation:	
	42% average	
	Core permeability:	
	.14 md, less than 60% saturation	
	.02 md, more than 60% saturation	
	In-situ permeability:	
	.01 - .02 md.	
	Net producing interval:	
	153 ft.	
	Pressure:	
	1050 psia	
	Temperature:	
	55^{o}C	
Location of Gas Entries	GB-1: about 50% between 4000' and 4030' and 50% between 3840' and 3900'	3
	GB-2: most at about 3920'	
Flow tests	GB-1: 35 x 10^3 ft/day after a series of flow tests and pressure build-ups	3, 11
	GB-2: 4.5-5.5 x 10^3 ft/day initial open flow	
Production History in Gasbuggy Area	Closest conventional well at 435' from GB-E produced 81 x 10^6 ft^3 in 10 years. Total production of all five wells closer than one mile is 312 x 10^6 ft^3 in 8 - 11 years	3, 11

TABLE I - Continued

STUDY AREA	DATA	REFERENCES
Hydrology	Ojo Alamo permeability 1.05 md; static water level 945 ft below ground surface	22
Elastic	Pictured Cliffs Sandstone: ρ = 2.4-2.5, V_l = 10,000-13,000 ft/sec[3] V_s = 7100-8100 ft/sec Lewis Shale: ρ = 2.6, V_L = 12,000-14,000 ft/sec V_s = 8000-9300 ft/sec Fruitland Coal: ρ = 1.7, V_0 8800 ft/sec, V_s = 5500 ft/sec	3
	NOTE: ρ = density, gm/cm^3, V_L = compressional vel. V_s = shear vel.	3, 19
Gas Composition	Methane 85, Ethane 7.4, Propene 4.0, Heavy Hydrocarbons 2.4, CO_2 .3, N_2 .6 (all in mole %)	

purpose of deriving geologic and hydrologic information, reservoir properties, and core samples; and GB-D, for purposes of measurement primarily of interest to the subject of seismic wave generation. Postshot, the emplacement hole was reentered (GB-ER); GB-2 was also reentered and sidetracked (GB-2RS). A conventional well (29-4#10) which had been drilled in 1957 was also reentered, and a new hole (GB-3) was recently completed. The location of these holes and their relation to the Gasbuggy chimney are shown in Figs. 2 and 3.

A. VOID VOLUME

One of the items of primary interest is the size of the final cavity created by the explosion prior to its collapse in the chimney formation process. The radius of this cavity depends on yield, material properties and depth of burial. Initial cavity volume is, upon chimney formation, distributed as intersticial volume within the chimney. As a first approximation, one can assume that the radius of the cavity is equal to the chimney radius although there are indications that sometimes the chimney may have a larger radius than that of the cavity.[15] No direct measure exists of the radius of either the Gasbuggy cavity or the chimney, in that there has been no measurement by a slant or whipstock drill hole intersecting the lateral boundary of the chimney or cavity. While such a measurement was included in the initial plans for the Gasbuggy experiment, money limitations forced its elimination. The Gasbuggy cavity size therefore has been calculated by determining the void volume in the Gasbuggy chimney.

One method to measure this quantity uses data from gas withdrawal tests where the ideal gas equation of state (together with a compressibility factor of .94) is used to derive a volume commensurate with the observed drop in pressure for a given amount of gas withdrawn. Methods which use the totality of the flow data in a non-steady state calculation either yield a void volume directly, or one can be derived. A method independent of drawdown data uses the observed initial concentrations of a gaseous radioisotope [13] such as krypton 85 and calculates a void volume based on the known amount of total krypton deposited within the cavity by the detonation. This last method may be more accurate than those based on flow measurements since the latter must correct for gas flowing into the chimney from the surrounding formation during the period of the test.

As shown in Table IIa, the uncorrected void volumes based on gas withdrawal tests result in volumes of about three million cubic feet. If it is assumed that the influx of formation gas into the chimney for any two adjacent tests is equal, the influx term can be eliminated from two simultaneous equations and a void volume of 2.6 million ft^3 results. One of the non-steady state calculations gives 2.8 million ft^3, while another one gives values between 2.5 and 2.8 million ft^3, depending on the values of the average chimney temperature and gas compressibility chosen. The volume based on krypton concentrations is somewhat lower, namely 2.35 million ft^3. Table IIb shows these corrected values.

The void volume measurements include not only the volume of the initial cavity, but also the volume due to fractures in the rock immediately surrounding and connected with the chimney as well as some fraction of the porosity in the rock which has filled the chimney by collapsing from above the cavity. By assuming that all the gas-filled porosity of the rock (about 5%) residing within the chimney is in communication with the interstitial void space, the cavity radii shown in Table IIc are obtained. Also included in Table IIc is the value obtained from permanent displacement measured at a distance of about 1500 feet from the detonation center [9].

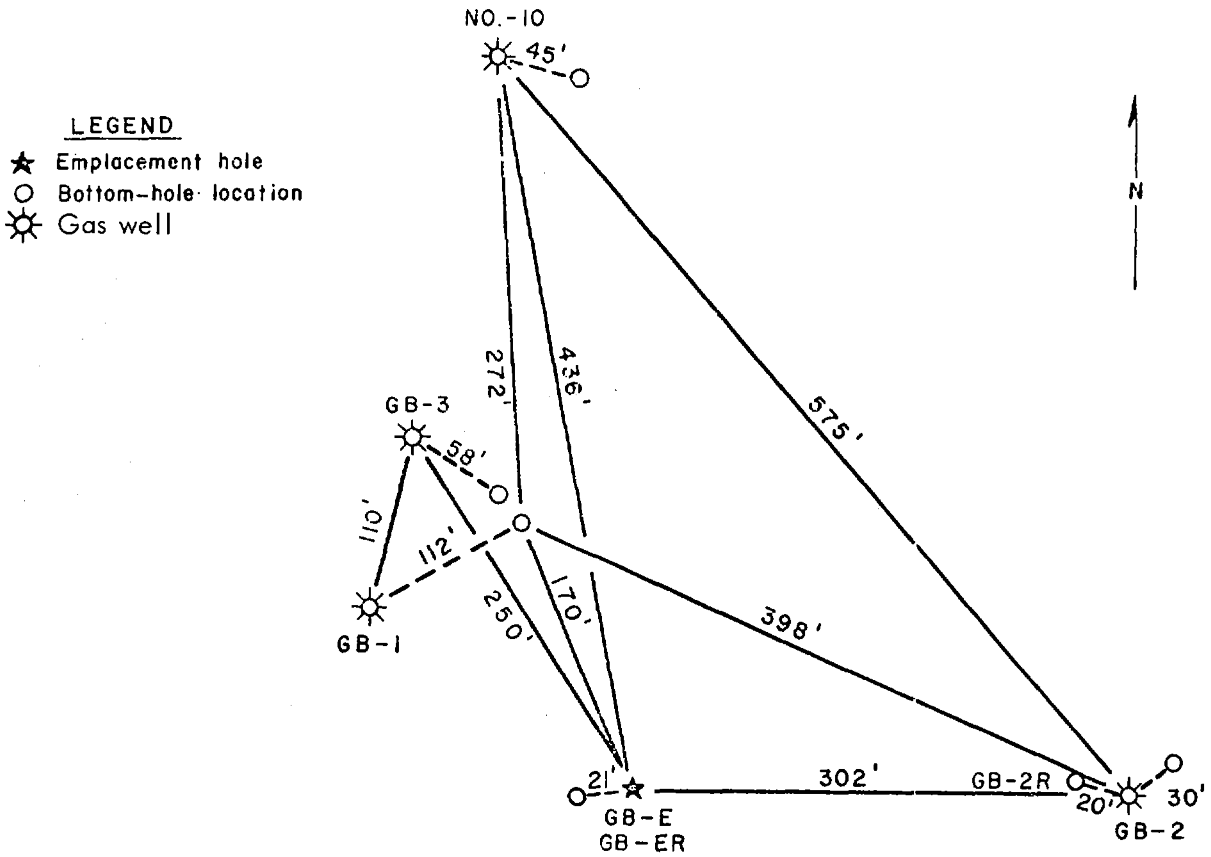

Fig. 2

Locations of holes drilled for Gasbuggy, GB-1 and GB-2 were drilled pre-shot, as was the conventional well No. -10 and the emplacement hole GB-E. Post-shot, three of these were reentered (GB-ER, GB-2R, and No. 10) and one new hole (GB-3) was drilled.

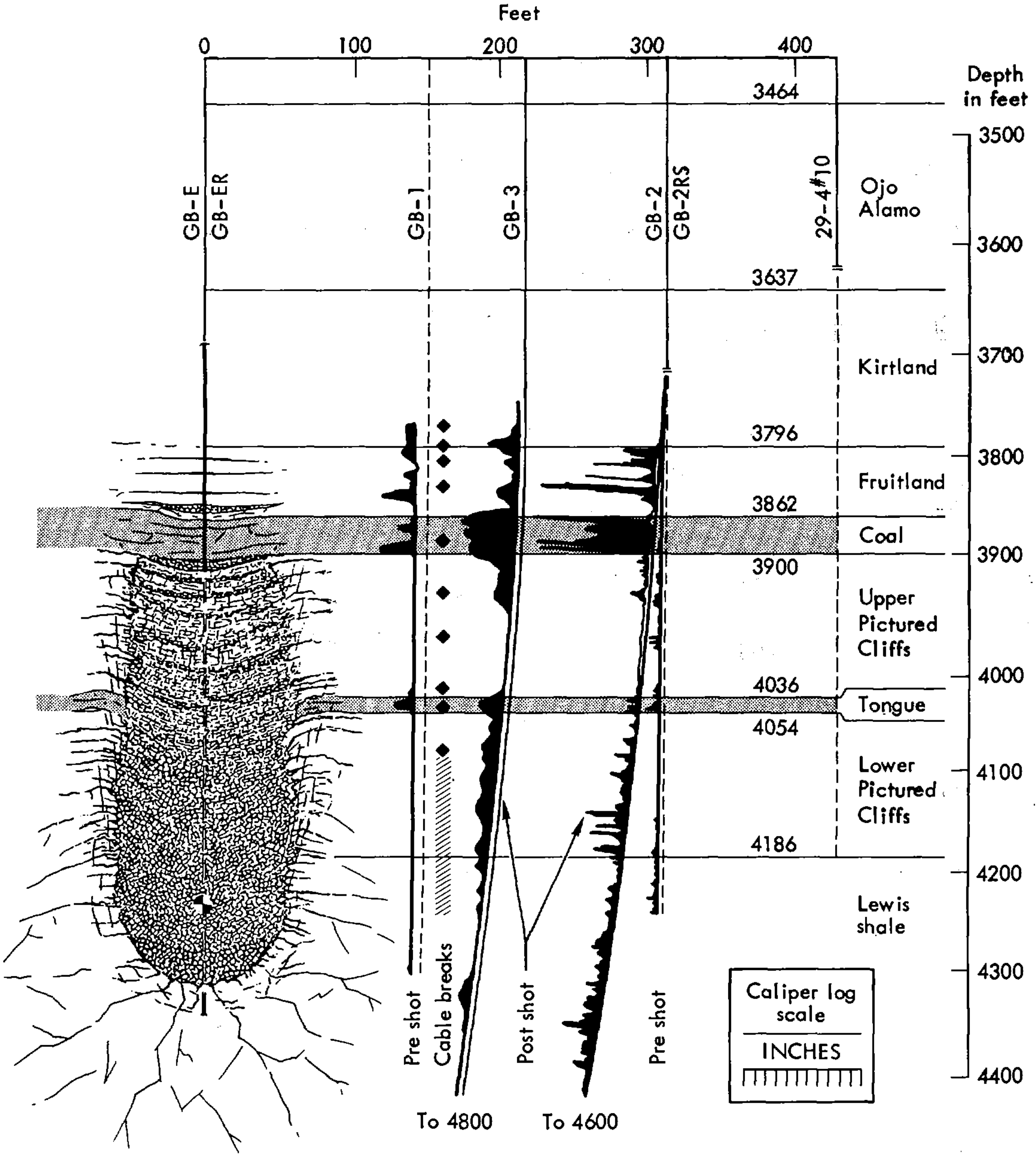

Fig. 3

Schematic cross-section through Gasbuggy. The scale of this figure is approximate only. The results of pre-shot and post-shot caliper logs, giving an indication of the fractured nature of the formation, are shown.

TABLE IIa

CALCULATED VOID VOLUMES - UNCORRECTED

HIGH-VOLUME FLOW TEST DATA AND VOID VOLUMES UNCORRECTED FOR INFLUX

TEST DATES	BOTTOM HOLE PRESSURES (PSI) INITIAL	FINAL	TEMP°K	AMOUNT OF GAS PRODUCED, $10^6 ft^3$	UNCORRECTED VOID VOLUME $10^6 ft^3$
12/7/68-12/10/68	854	763	375	13.7	2.9
12/10/68-12/12/68	763	706	388	9.17	3.1
1/11/69-1/14/69	687	601	385	12.9	2.9
1/14/69-1/17/69	601	536	388	10.1	3.0
10/31/69-11/11/69	221	134	373	12.8	2.8

Z = .94 in all cases

TABLE IIb

VOID VOLUME COMPARISONS

High-Flow Tests 12/68 - 1/69, Corrected for Influx	2.6×10^6 ft^3
High-Flow Test 10/31/69 - 11/7/69, Corrected for Influx	2.3×10^6 ft^3
Non-Steady State Calculations	$2.5 - 2.8 \times 10^6$ ft^3
Initial Kr-85 concentration (2.8×10^{-6} Ci/ft^3) and total Kr source (350 ± 20 Ci)	$2.35 \pm .14 \times 10^6$ ft^3

TABLE IIc

CAVITY RADIUS

From Dec. 1968 - Jan. 1969 flow tests, corrected for porosity	83 ft
From Nov. 1969 flow tests, corrected for porosity	82 ft
From krypton concentrations, corrected for porosity	80 ± 2 ft
From permanent displacement measured 1500 ft from detonation porosity	88 ± 4 ft

By assuming that the observed permanent displacements are caused solely by the expanding cavity and neglecting any compaction of the material, a cavity radius somewhat larger than that obtained by the other methods is calculated.

B. CHIMNEY HEIGHT

A chimney height of 333 feet above the original detonation level was identified during the reentry of the Gasbuggy emplacement hole. A void was encountered at a depth of 3907 feet below the surface. This void extended to 3916 feet and carried both pressure and gaseous radioactivities. No drilling below 3916 feet was possible. An earlier void encountered at a depth of 3856 feet, while probably connected to the chimney, did not show sufficient activity or gas pressure to be identified as the chimney top.

C. FRACTURE RADIUS

The distance that fractures radiate from the shot point formation is an important quantity closely related to the chimney height. The relationship of fracture distance to yield, material properties and depth of burial is of major importance in future gas stimulation experiments and ultimately, applications. Preshot predictions anticipated fracture extent to about 400 feet in the Pictured Cliffs sandstone and to about 500 feet in the shale. The prompt measurement of fracture propagation in GB-1 [8] established that fractures are created concurrently with the outgoing shock wave which is consistent with the predictive model. The postshot investigations in GB-2RS and more recently in GB-3 show that fracture extent is consistent with the predictions and establishes that fractures extend about as far below the shot point as they do above the shot horizon [10].

The influence of geologic weaknesses and discontinuities on the fracture extent appears to be stronger than was initially anticipated. This seems to be true both relatively close to the shot point and at distances of several hundred feet. Thus, both the caliper log and core from the GB-3 hole shows extensive fracturing and weak hole conditions in the lower part of the Pictured Cliffs sandstone as compared to the upper part. The two are separated by a twenty-foot section of coal and shale, materials that are considerably weaker than the sandstone on either side. Of equal interest and perhaps more long range in importance, are the effects at relatively large distances. These are summarized in Table III, indicating shifts and offsets along geologic bedding plains or weaknesses at a considerably larger distance from the shot point than would calculations based on a simple matrix failure model; offset and casing breaks have been observed as far as 760 feet away from the shot point. In addition, permanent displacements of about one inch have been measured as far away as 1500 feet. [9].

D. HYDROLOGIC EFFECTS

Water level measurements made in holes 29-4 #10, GB-2R, and GB-3, leave no doubt that water from the Ojo Alamo aquifer is flowing into the Gasbuggy chimney. Figure 4 shows how the decrease of the static water level in 29-4 #10 correlates with the high volume withdrawal tests. Figure 5 compares the water levels as they existed in September, 1969 as compared with their preshot values. Together with this decrease in water level an increase in the permeability of the Ojo Alamo aquifer may have occurred.

Preliminary interpretation of hydrologic tests in GB-3 indicate permeabilities of about 4 millidarcy [16] compared with preshot values of about 1 millidarcy. If this finding is borne out by a more complete analysis, it is a surprising result.

TABLE III

SUBSURFACE EFFECTS OBSERVED ALONG GEOLOGIC WEAKNESSES

HOLE	NATURE OF OBSERVATION	DEPTH IN HOLE (ft)	DISTANCE FROM EXPLOSION CENTER (ft)
GB-ER	Casing break	3790	450
GB-1	Fracture cable broken	3780	480
GB-2RS	Casing offset	3700	620
	Gas entry	4600	460
29-4 #10	Casing offset	3612	760
GB-3	Fractured core	3662	615
	Gas entry	4800	590

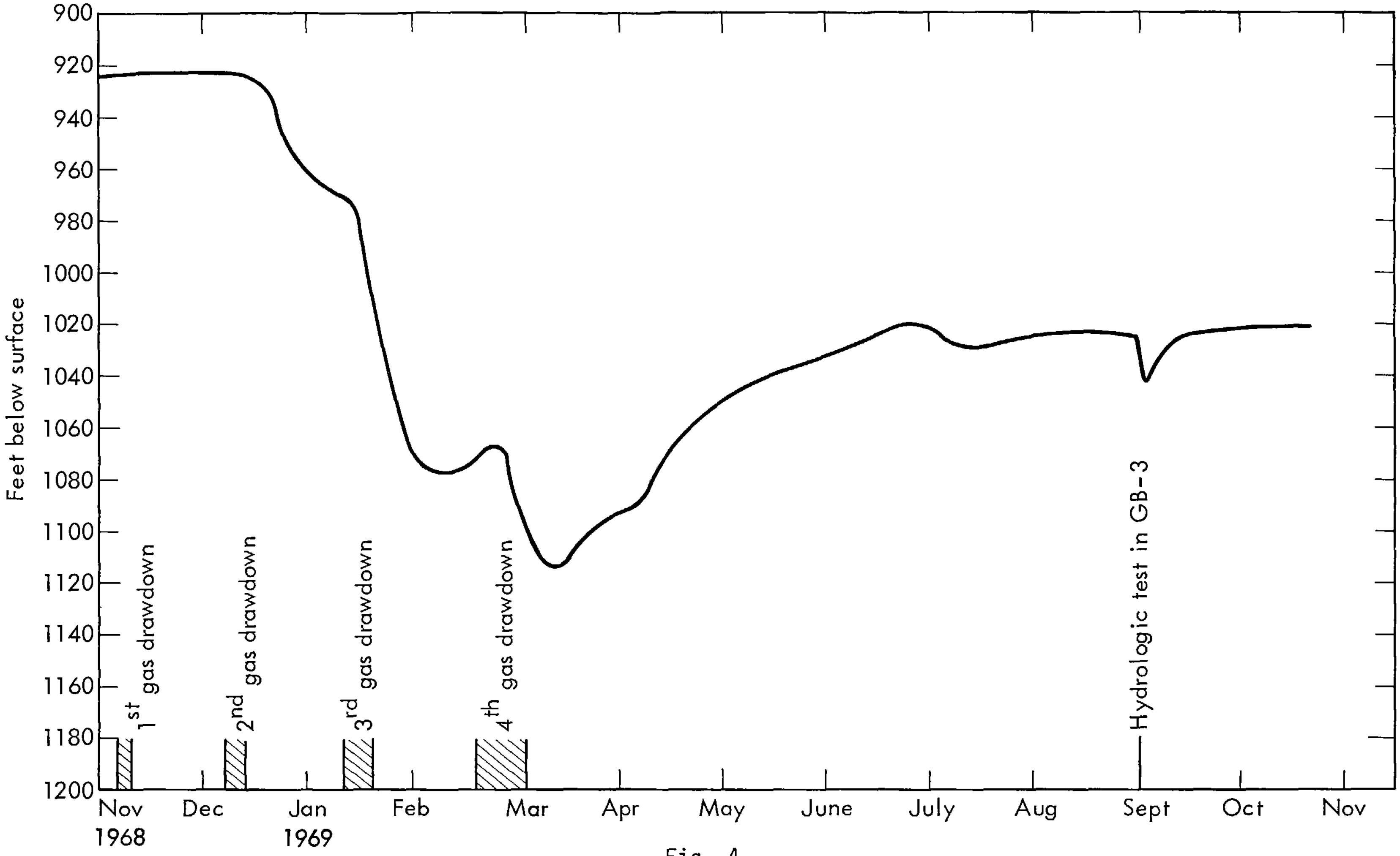

Fig. 4

This figure shows how the water level in well 29-4 #10 has changed as a result of the gas flow withdrawals from the chimney. Gas volume flow during the four drawdown tests was about 10, 23, 28, and 30 million cubic feet of gas respectively. Smaller rates of gas flow were maintained through most of the interval shown (see Figs. 6 and 7).

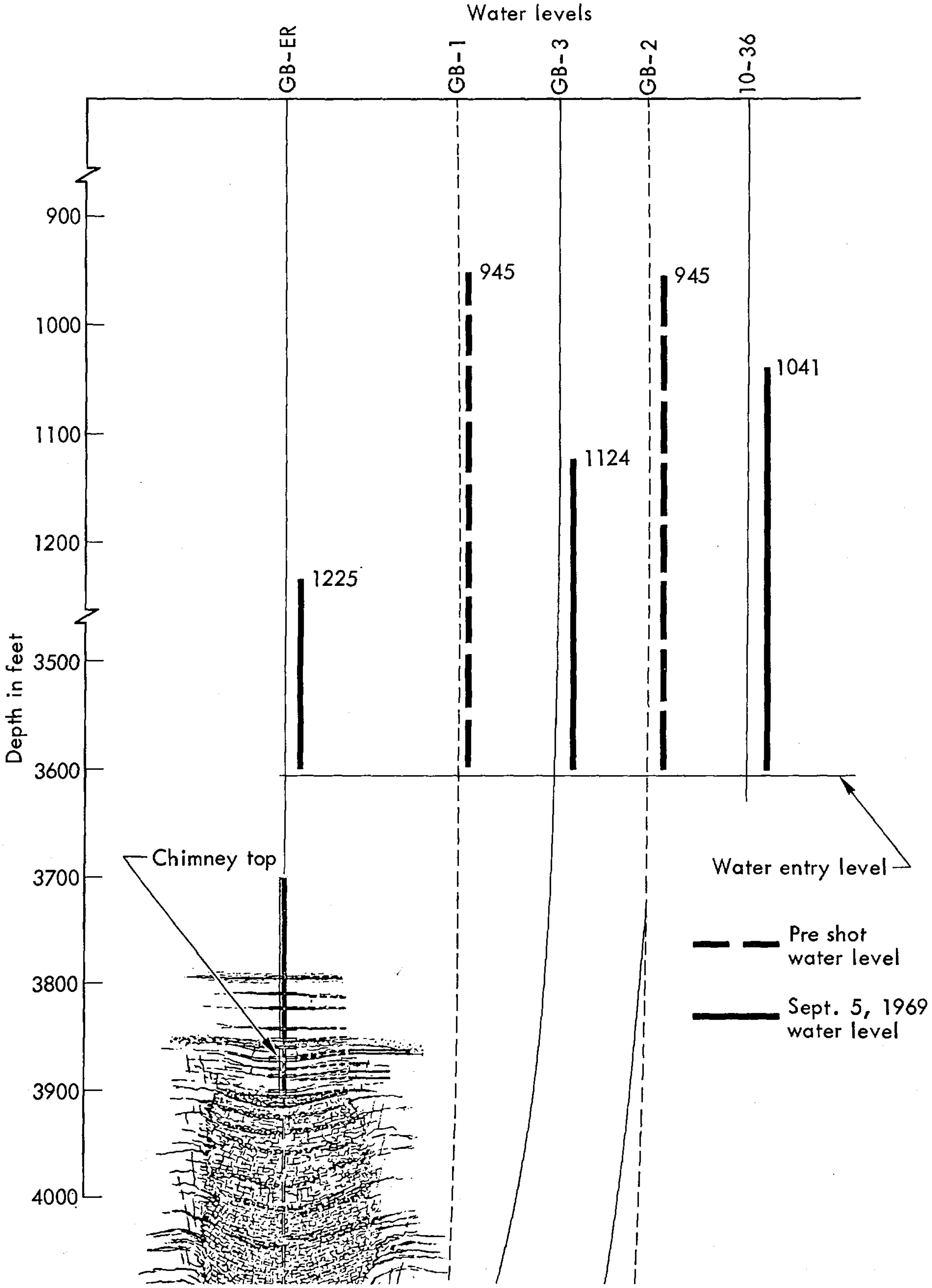

Fig. 5

An example of the water levels in September, 1969, as measured in the post-shot holes as compared with pre-shot data. The lower ends of the bars terminate in the Ojo Alamo aquifer, whose characteristics are depicted here.

At the present time, neither the path of water entry into the chimney nor the amount that has flowed in has been determined. The most likely path, in my opinion, appears to be through the port in the casing of the emplacement hole where water problems were encountered preshot and water entries during the GB-ER reentry were observed [25].

Waste water samples gathered in connection with the flow tests have shown a steadily decreasing concentration of tritium indicating that a dilution effect is taking place. Unfortunately, no quantitative estimate of the water influx is possible from these numbers. It should be noted, however, that the void volume measurements performed at the beginning of November, 1969 indicate that perhaps 1×10^5 to 3×10^5 ft^3 of water are now in the Gasbuggy chimney.

III. GAS FLOW AND RESERVOIR EVALUATION

As in the summary of the shock wave effects on the mechanical properties of the reservoir, the changes in the gas flow and reservoir properties can best be described in terms of several subcategories. One of these compares flow rates and productivities with those observed in the preshot wells and with the experience based on the conventional wells in the area. The gas flow data also provides a mechanism for evaluating the changes in permeability brought about by the detonation. In both of these areas, the unique character of the nuclearly stimulated reservoir makes itself felt through the large well storage effect that it exhibits.

A. FLOW TEST COMPARISONS

The gas flow tests on the postshot Gasbuggy reservoir have been analyzed by Atkinson, Ward and Lemon [12]. Figures 6 and 7 in their report summarize the flow rates, pressures and temperatures obtained during these tests. Figure 8 depicts the cumulative gas production as a function of time, and also shows the total volumes of gas produced by the five conventional wells nearest to Gasbuggy. Table IV compares some of these data with those from the preshot wells and the conventional wells. Compared with the five nearest wells, the Gasbuggy well either has or is expected to exceed the capability of the non-nuclear stimulated wells by factors of 5 to 8 [12]. Somewhat different numbers are obtained when all the wells in the area are included.

B. PERMEABILITY THICKNESS

Comparison of preshot and postshot production volumes is not possible in areas where there is essentially no history of commercial production and where the absolute rather than the relative numbers are of importance. For the purpose of assessing the stimulation one might obtain in different reservoirs, under different conditions, a comparison and study of the permeabilities postshot as compared to those observed preshot is of great importance. The fracture-controlled nature of the preshot Gasbuggy reservoir [11] and the very low permeabilities have made it difficult to arrive at an initial permeability thickness. The preshot flow tests yield numbers between 1.7 and 3 millidarcy feet [3]. The long-term flow test, commencing in March, 1969, established a rate of about 170,000 ft^3 per day and a bottom hole pressure of 260 psi, permitting the application of the steady state, one dimensional flow equation to determine permeability thickness. Using the associated stable pressures in GB-3 and GB-2RS, this procedure can be applied to cylindrical shells surrounding the chimney defined by the distances of these holes from the chimney. This procedure gives a permeability thickness of 14 millidarcy feet in a region between the chimney edge at 80 feet and the GB-3 hole at about

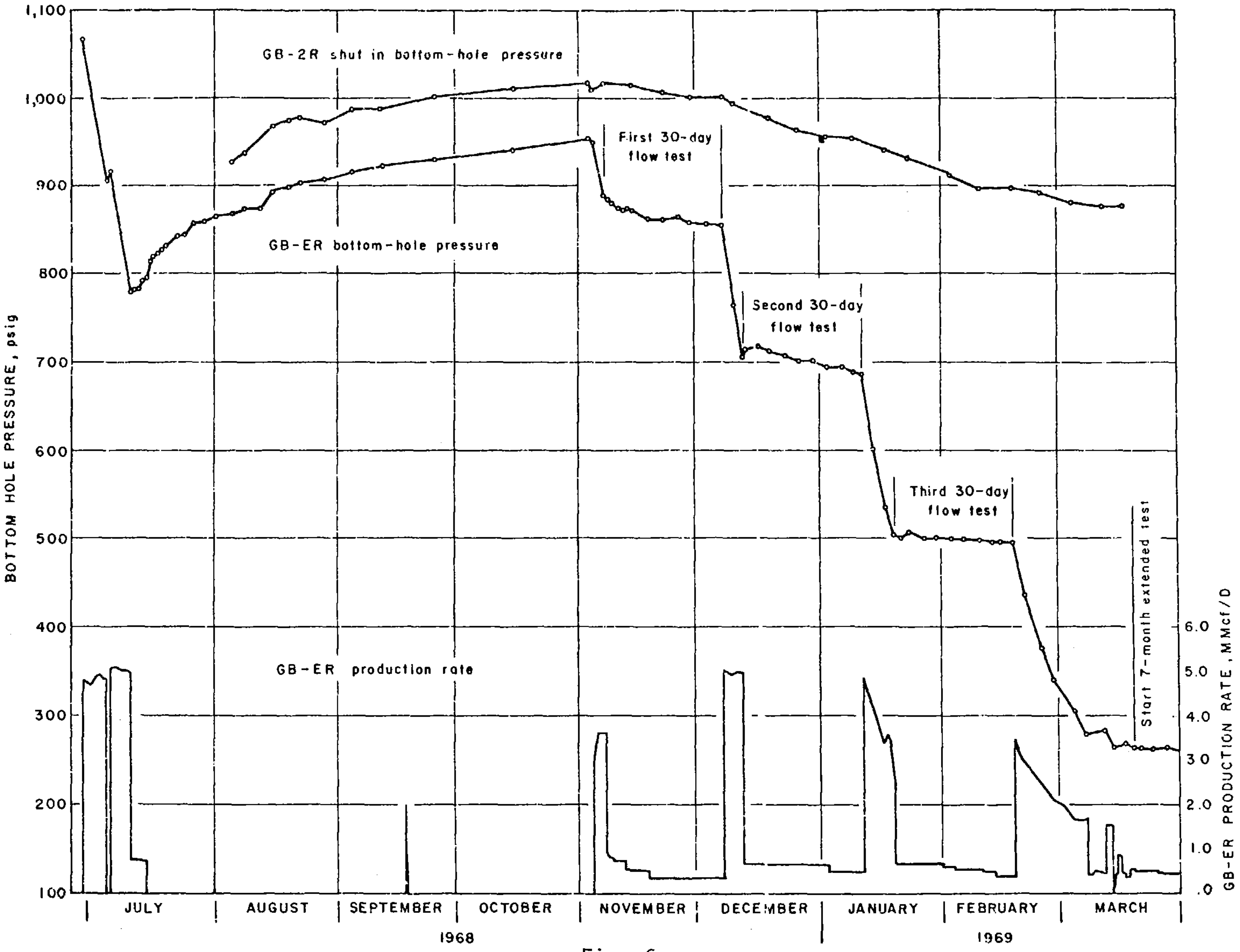

Fig. 6

Flow rates and pressures, June 1968 - March 1969; courtesy C. Atkinson, D. Ward, and R. Lemon (Ref. 12).

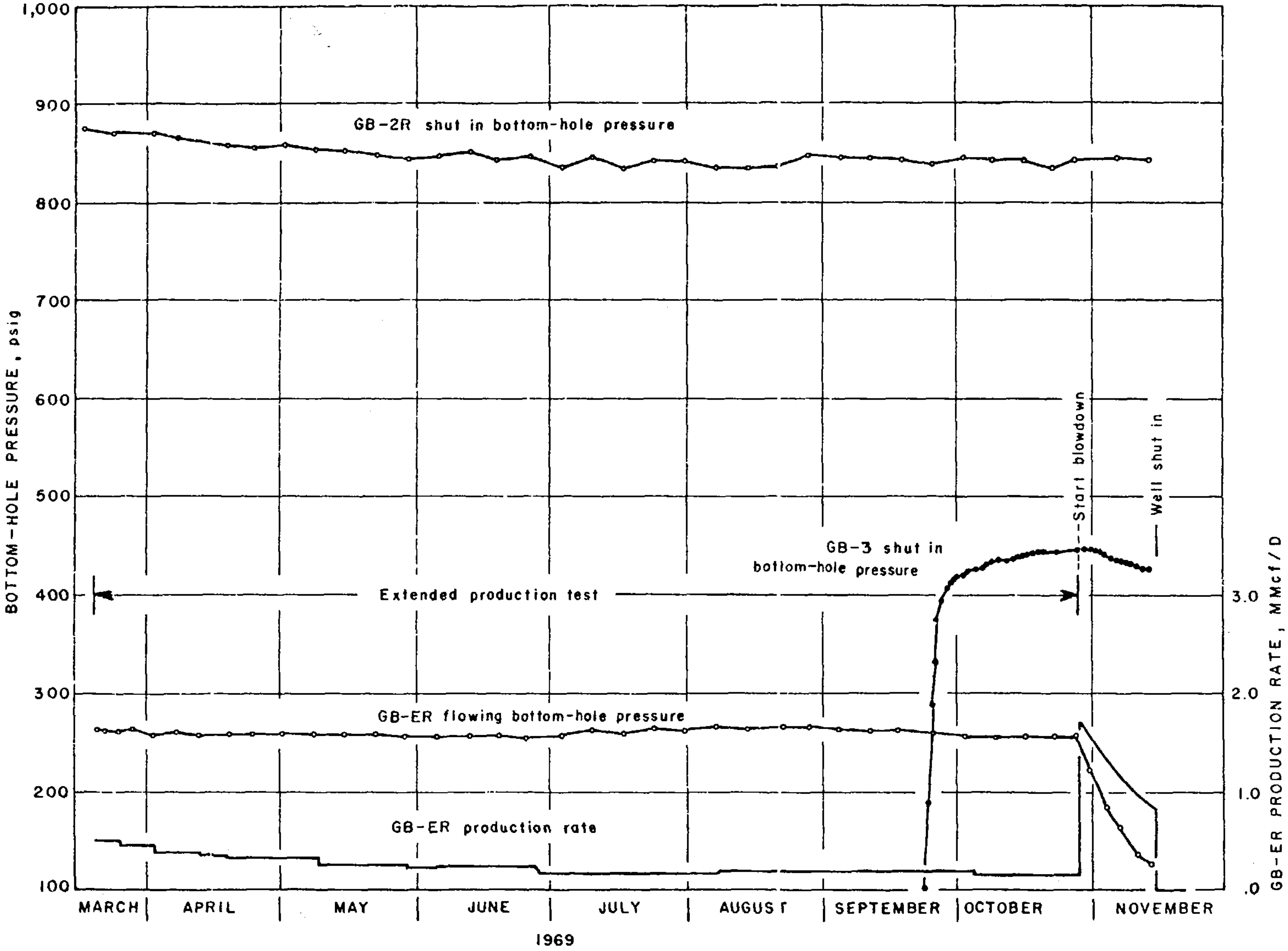

Fig. 7

Flow rates and pressures, March 1969 - November 1969. Courtesy C. Atkinson, D. Ward, and R. Lemon (Ref. 12).

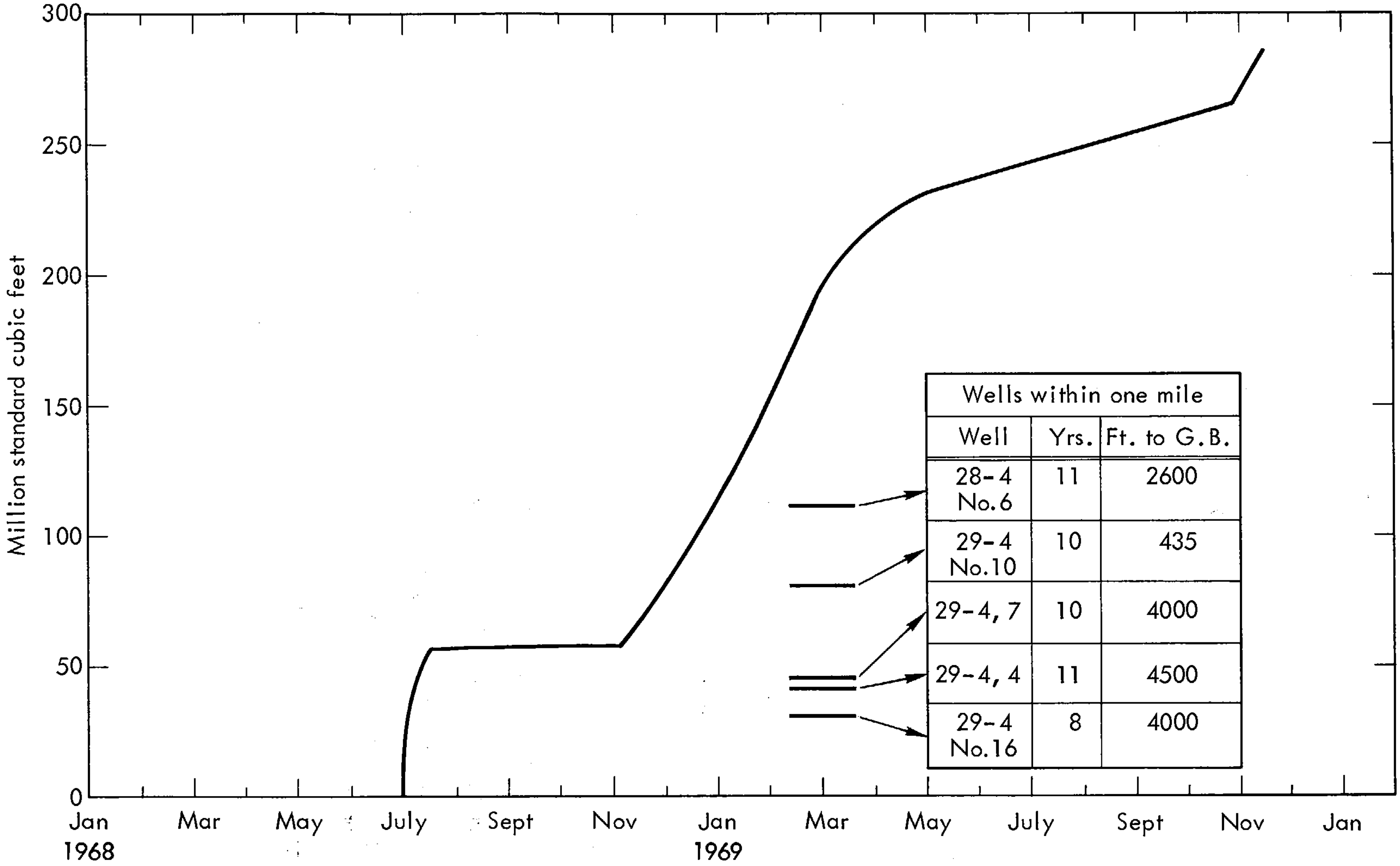

Wells within one mile		
Well	Yrs.	Ft. to G.B.
28-4 No.6	11	2600
29-4 No.10	10	435
29-4, 7	10	4000
29-4, 4	11	4500
29-4 No.16	8	4000

Fig. 8

Cumulative gas production from Gasbuggy. Total production from the five nearest conventional wells is shown on the same scale.

TABLE IV

	DISTANCE TO GB-ER (ft)	PRODUCTION		GAS RECOVERY
		Daily Ave. (a) 10^3 ft^3/day	Est. in 20 yrs (b) 10^6 ft^3	Est. in 20 years (% of Gas in 160 acres) (c)
GB-ER	----	135(e)	900	19
29-4 #10	435	22	170	3.5
Average of Five nearest Wells	<4500	18	112	2.5
Average of all wells in field	<6800	61	342	7.2
Best in field	6800	159	900	19 (d)
Worst in field	4500	10.5	65	1.4

(a) Based on all production since well was drilled until 1966.

(b) Assuming production in 1966 can be maintained for remainder of the time.

(c) Assuming the same amount of gas in place as at the Gasbuggy site.

(d) Since this well is completed in a fracture system, this is probably not a valid number.

(e) Calculated against 500 psi line pressure.

200 feet, and 1.2 millidarcy feet between the GB-3 hole and the GB-2RS hole at 300 feet. If one assumes that the reservoir beyond 400 feet is essentially undisturbed at the original formation pressure of 1050 psi, one obtains an overall permeability thickness of about 4 millidarcy feet for the region between this point and the chimney.

Sherwood [17] has matched the pressure buildup data between the time of detonation and the first substantial gas withdrawal in June of 1968 with computer calculations based on a simplified reservoir model. This calculation yields a permeability thickness of about 9 millidarcy feet. When the calculation is extended to later times to include pressures through the long-term tests, the agreement between calculations and data, using 9 millidarcy feet, becomes progressively worse. The later portions are more closely in agreement with calculations which assume a permeability thickness of between 3 and 4 millidarcy feet. Such a shift is not inconsistent with the concept that most of the early gas influx is through region of relatively high permeability, while, later, the lower permeability regions are more important.

This conclusion was also reached by Rogers [18] who developed a non-steady state calculation for combining various reservoir geometry and permeability variations. For instance, a close-in region, where flow is spherical, can be followed by one in which flow has cylindrical symmetry. Up to now, the best agreement with observations is obtained from a cylindrical model consisting of three shells each with a different permeability. Here too the calculations agree reasonably well with early data but not with later data. Part of this disagreement may be due to the assumption of a .05 millidarcy permeability for radii greater than 250 ft. This permeability is clearly too high. Table V summarizes the permeability thicknesses determined by these various methods.

Despite the low permeabilities in the reservoir beyond the chimney edge, most of the 275 million ft^3 of gas that has been withdrawn from the chimney and the adjacent region has been replaced by influx from the reservoir. Of the 323 million ft^3 of gas in place preshot within a 400-foot radius cylinder, about 250 million ft^3 were in place within that same region near the end of the seven months long-term test in October, 1969. These values, separated into the regions defined by the postshot holes, are listed in Table VI. They were obtained by multiplying the amount of gas per unit area initially in place by the ratio of the October, 1969 pressures to the preshot reservoir pressure --- assuming a linear pressure dependence on radius between the chimney edge, GB-3 and GB-2RS.

IV. GASEOUS RADIOACTIVITIES AND CHEMICAL COMPOSITION

The concentrations of the radioactive as well as of the chemical constituents of the Gasbuggy chimney gas have been reported periodically since the start of postshot activities [13, 14, 19]. To date, about 89 samples have been analyzed at the Lawrence Radiation Laboratory alone, and more have been analyzed by the El Paso Natural Gas Company and others.

As expected, krypton-85 and tritium (distributed between hydrogen and the various hydrocarbons) are responsible for essentially all of the radioactivities in the gas. The only other activities which have been observed in the gas are xenon-133, argon-37, argon-39, and carbon-14. Xenon-133, with a 5.27 day half life, was only detected in the early reentry operations. Argon-37, with a half-life of 35 days, has also effectively decayed. Concentrations of the long-lived isotopes argon-39 and carbon-14 in the early samples were about 3 x 10^{-3} and 3 x 10^{-2} microcuries per cubic foot respectively. About 350 ± 20 curies of krypton-85 and about 4.5 x 10^4 curies of tritium were initially deposited in the chimney as a result of the Gasbuggy explosion.

TABLE V

CALCULATION & MODEL	PERMEABILITY THICKNESS (Millidarcy-feet)		ASSUMPTIONS, REFERENCES	
Radial flow steady-state analytic solution	14	(80' < r < 210')	$kh = \frac{q\,(\mu ZT)\,\frac{r_f}{r_s}}{.705\text{x}10^{-6}(P_f^2-P_s^2)}$	
	1.2	(210'< r < 300')	q = 170 MCFD	Z = .94
	4	(80' < r < 400')	μ = .011	T = 616°R
			P(80')= 260	P(210')=430
			P(300')=845	P(400')=1050
Non-steady state computer calculation in cylindrical symmetry	22	(85' < r < 150') (a)		
	15	(150'< r < 250')	Reference 18	
	7	(> 250') (a)		
Non-steady state computer calculations	9	(for data to 11/4/68)	Reference 17	
	3-4	(for later data)	Reference 27	

(a) These numbers are from a preliminary calculation which L. Rogers kindly showed the author; the final report may cite somewhat different values.

TABLE VI

GAS IN PLACE, OCTOBER 31, 1969

REGION	AMOUNT (Million cubic feet)
Chimney	31
Between 80' and 200'	23
Between 200' and 300'	65
Between 300' and 400'	130
TOTAL	249
Preshot to 400'	323
TOTAL GAS WITHDRAWN	275

Concentrations in samples taken immediately after the chimney reentry show concentrations of about 3 microcuries of krypton-85 per cubic foot of gas and about 20 microcuries of tritium per cubic foot of gas. Of this latter amount, about 13 microcuries per cubic foot were in the form of tritiated methane (CH_3T). The rest were distributed among the higher hydrocarbon factions as well as tritiated hydrogen (HT). With 125 x 10^6 ft^3 of gas in the chimney, the total amount of tritium in the gas phase was 2500 curies, or about 5% of total amount.

A. KRYPTON AND TRITIUM VARIATION WITH GAS PRODUCTION

Figure 9 shows the decrease in the krypton and tritium concentrations during the period following the initial chimney reentry. This figure also shows the total gas produced during the same period. As new gas from the formation has flowed into the chimney to replace the gas withdrawn, the concentrations in the samples taken in the gas stream have decreased by a factor of between 15 and 20 over the period of analysis shown. During this time about 275 million ft^3 of gas have been withdrawn. The detailed variations of these curves depend, in a marked way, on the rate of gas withdrawal. Changing the flow rate from 5 million ft^3/day to 0.75 million ft^3/day during the initial withdrawal tests in July, 1968, resulted in a very rapid reduction in both krypton and tritium concentrations. Following the resumption of flow tests, after a three and a half month shut-in period, initial concentrations were higher than those found when the July tests were terminated. Only after the beginning of the long-term test in March, 1969, do the concentrations show a monotonic decrease.

Only a small fraction of the amounts in the initial postshot gas are still in the chimney; most have been removed by the gas flow tests. This is made clear by Fig. 10 which shows the total amount of krypton-85 withdrawn from the chimney. Using the pressures, temperatures and concentrations measured at the end of October, 1969, it is computed that approximately 7 curies of krypton-85 remain in the chimney. Similar calculations can be made for tritium. Of the 2500 curies initially present in the gas phase, about 40 curies remain in the chimney.

During a high-flow withdrawal test during the first two weeks of November, 1969, the chimney pressure dropped from about 260 psi to approximately 125 psi. Thus, when the chimney was closed on the 14th of November, about three and a half curies of krypton-85 and 20 curies of tritium should have remainded in the gas within the chimney. The well is now closed, and new gas will continue to flow into the chimney until its pressure again equals the formation pressure. During this process, a further drastic dilution of the activities will take place. Assuming that the chimney at the end of influx will again contain about 125 million ft^3 of gas, krypton concentrations should be about 0.03 microcuries per cubic foot, and tritium concentrations approximately 0.15 microcuries per cubic foot.

B. RAPID ACTIVITY REMOVAL

As part of the design of the Gasbuggy experiment, calculations [20] indicated that a continuous and rapid withdrawal of gas could, after flowing about 2.5 chimney volumes, result in a decrease of radioactivities at a rate significantly in excess of what one would expect if the activities were distributed at all times uniformly throughout the chimney volume. Figure 11 shows the decrease of krypton-85 concentrations as a function of the number of initial chimney volumes withdrawn. The solid line of this graph represents

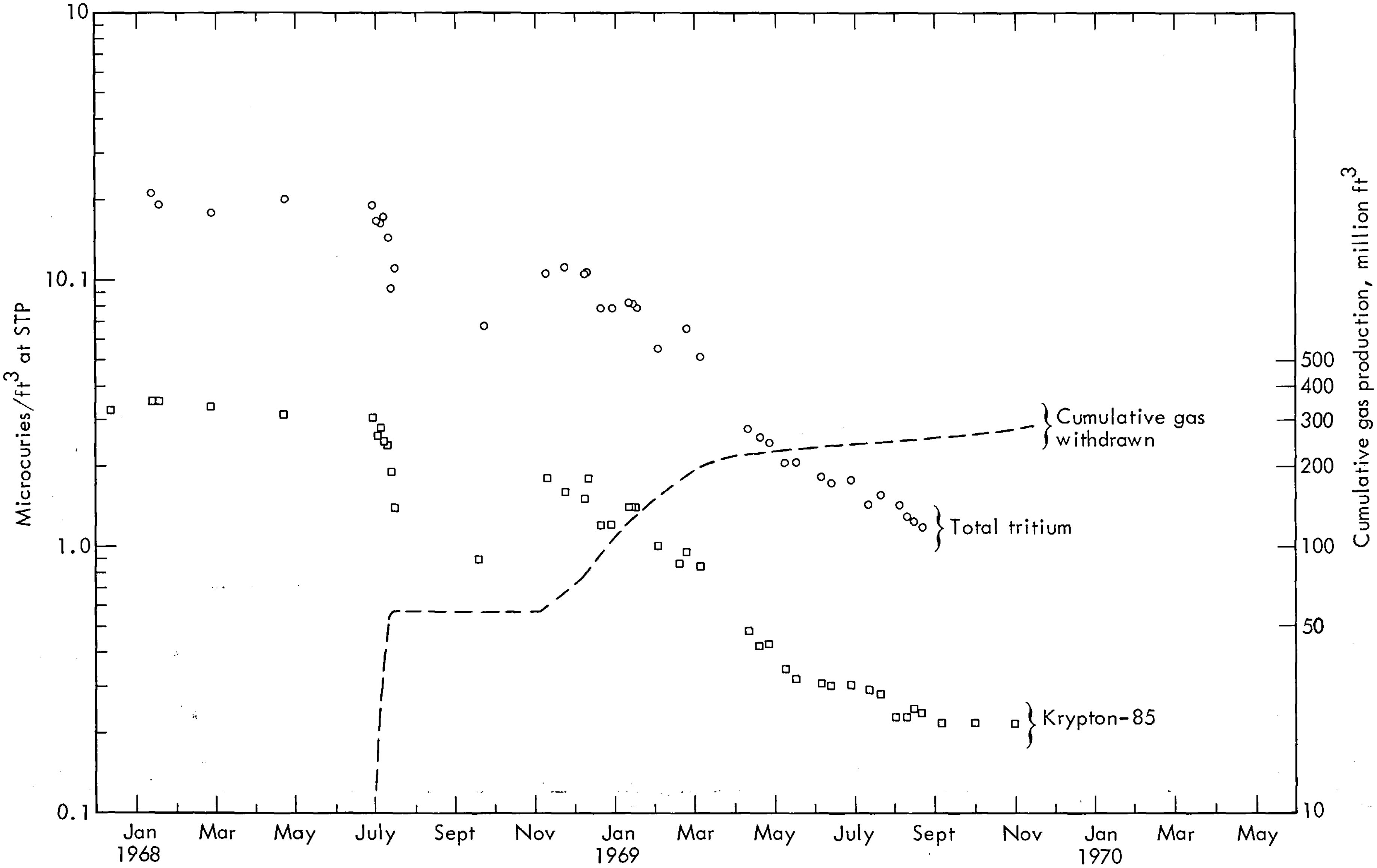

Fig. 9
Decrease in the krypton and tritium concentrations in the gas sampled at the well head since the chimney gas was initially sampled. Most of the analyses were performed by C. Smith (Ref. 13).

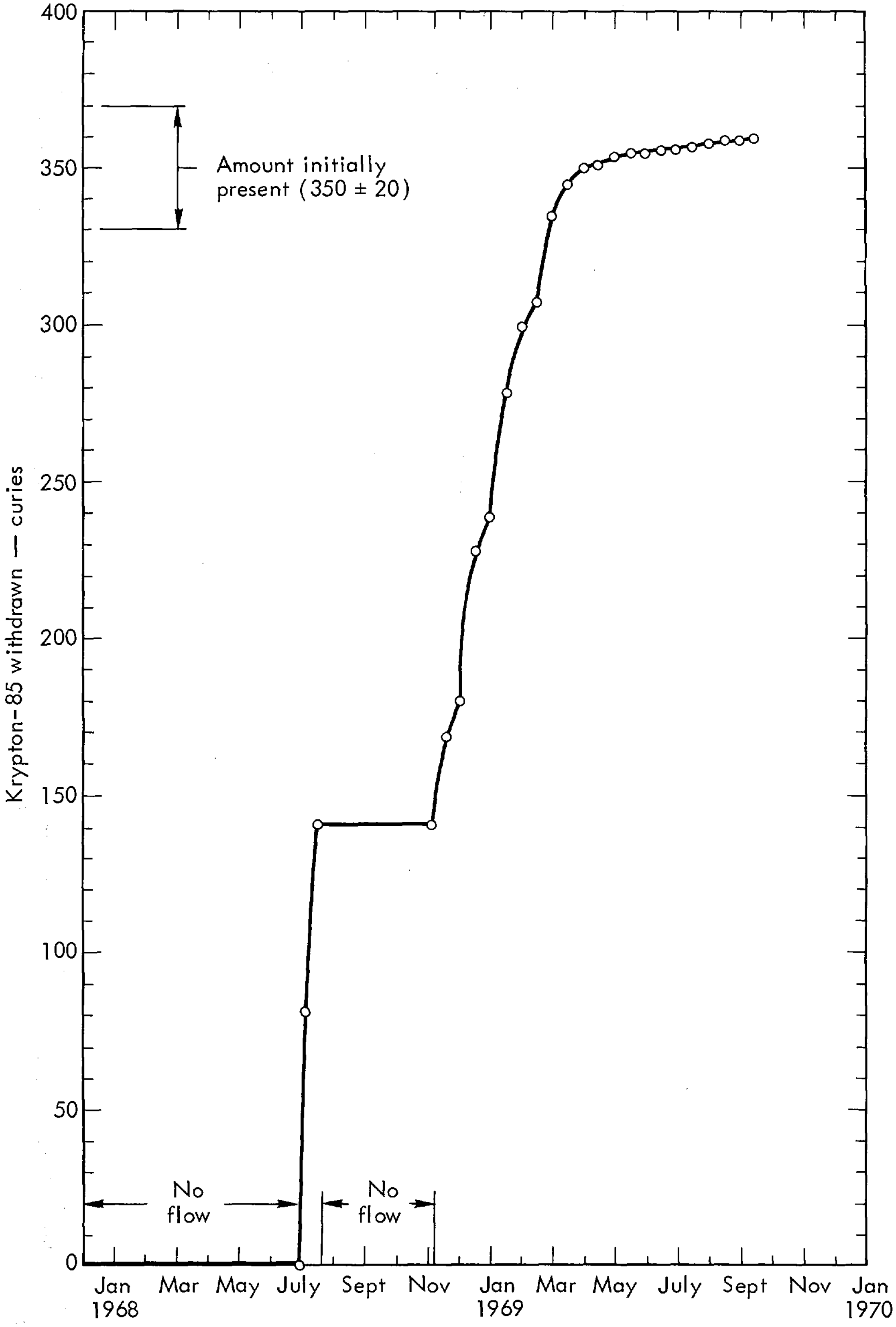

Fig. 10

By taking the sums of the concentration - flow rate products, the cumulated amount of a radioactive species withdrawn is calculated. Shown is the result of this procedure for krypton.

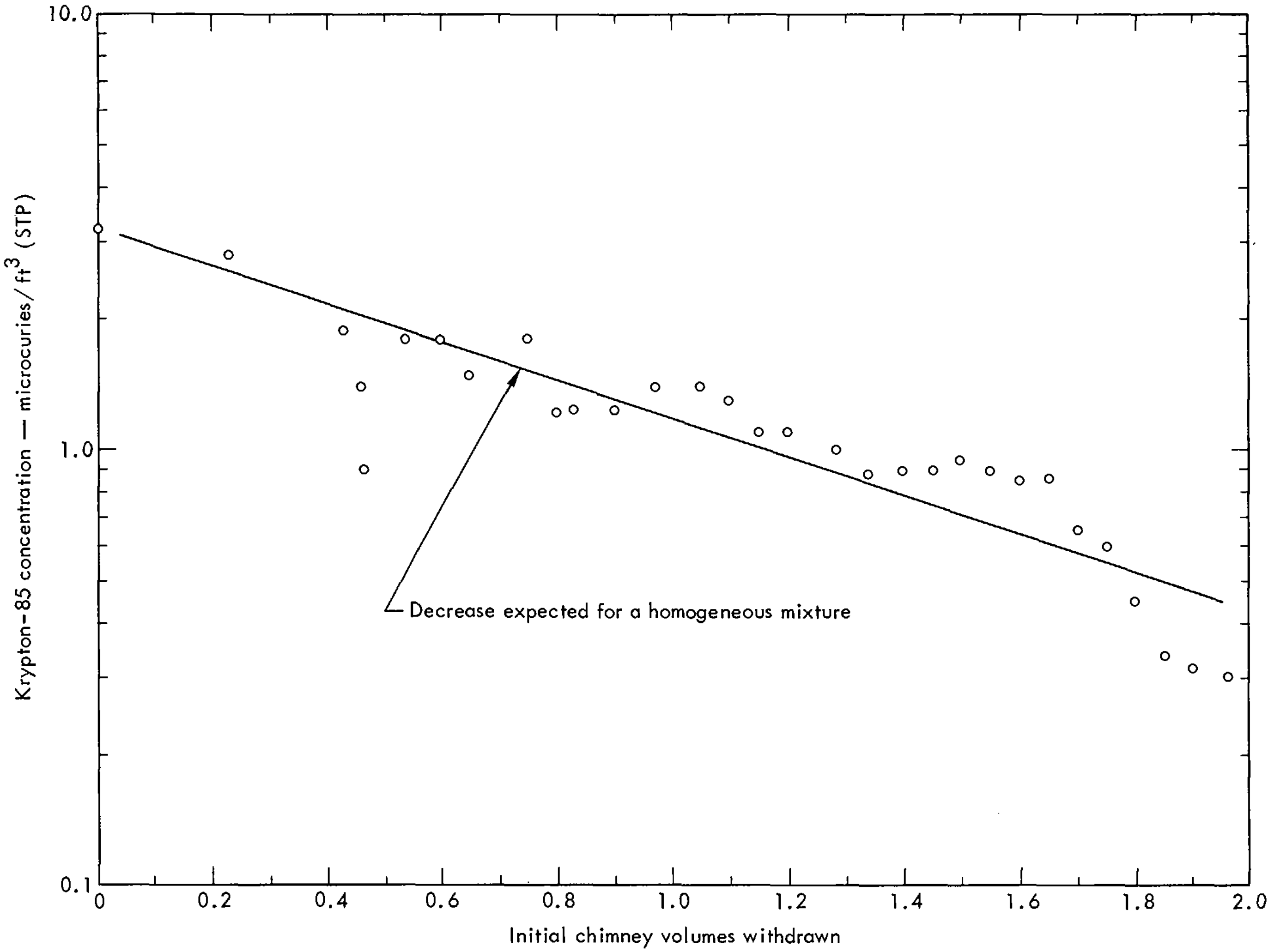

Fig. 11

Assuming the krypton is at all times perfectly mixed with the gas in the chimney. the relation between concentrations and chimney volumes withdrawn shown by the solid line is obtained. This is compared with the actual data.

the exponential decrease expected on the basis of uniform mixing. Since the flushing model only shows significant departures from the uniform mixing line after about two chimney volumes have been withdrawn, the data so far neither confirm nor deny this hypothesis.

C. CHEMICAL COMPOSITIONS

Analysis of samples obtained in January, 1968 showed significantly higher percentages of CO_2, CO and hydrogen than did the preshot gas. The methane and higher hydrocarbon content of the gas was correspondingly reduced. In particular, the 35% CO_2 concentration was unexpectedly high.

Quantitative calculations to explain these amounts have been undertaken by Taylor, Lee and Hill [21]. Using the chemical and mineralogical compositions of the rock in the vicinity of the shot point together with the thermodynamics of the reactions involved, Taylor et al conclude that CO_2 was most likely generated by the decomposition of dolomite.

Two processes may have contributed to the amount of hydrogen observed: 1) the reaction of free carbon in the shale with water to form H_2 and CO_2; and, 2) the oxidation of iron in the casing and the explosive container by water vapor in the hot cavity environment immediately following the detonation. The subsequent reaction of hydrogen with CO_2 to produce methane and water, postulated by Smith [19], is assumed responsible for the later reduction in the hydrogen concentration.

In the course of gas withdrawal tests, the hydrocarbon concentrations have increased while CO, CO_2 and hydrogen concentrations have decreased. Table VII compares concentrations observed near the end of the test period with those observed in January, 1968 and the preshot values. During this time the CO_2 concentration decreased from about 36% to approximately 8%. This decrease, however, was not as rapid as the corresponding decrease in the radioactive constituents. Smith has plotted CH_3T/CO_2 and krypton-85/CO_2 ratios as a function of time. His data are reproduced in Figs. 12 and 13 and show a definite relative increase in CO_2 concentrations following the December, 1968 period. This effect may be related to the start of high volume production testing in November, 1970 and the decrease in chimney pressure which accompanied it. Such a decrease would permit CO_2 initially dissolved in the water to be evolved and mixed in with the chimney gas.

CONCLUSIONS AND SUMMARY

The relative success or failure of Gasbuggy can be viewed from a number of aspects. The aspect emphasized in this paper relates to the success of Gasbuggy as a scientific experiment. There are, of course, many other facets to Gasbuggy, which, in the material presented up to now, may be conspicuous by their absence. Among these, the potential for structural damage from ground motion has received considerable attention. While peak accelerations were higher than were predicted based on the Nevada Test Site experience, [23] essentially no manmade structures were damaged. A total of three complaints of structural damage was received, and only one shows some indication that the Gasbuggy detonation may have been responsible for part of the damage observed. [24]

A second area which has received a large amount of attention concerns the radiological health aspects connected with the reentry of the chimney and the flaring of the gas. The drilling to the chimney containing radioactive gas at pressure took place without any difficulties or incident [25, 26]. None of the personnel involved in this operation were exposed to any radiological hazard.

TABLE VII

GAS COMPOSITIONS - MOL %

	PRESHOT	JAN. 1968	OCT. 1969
Methane (CH_4)	85.4	37	75
Ethane (C_2H_6)	7.4	3.6	8
Propane (C_3H_8)	4.0	1.2	4.5
Hydrogen (H_2)	----	17	2
Carbon dioxide (CO_2)	.3	36	2
Carbon monoxide (CO)	----	4.0	<1

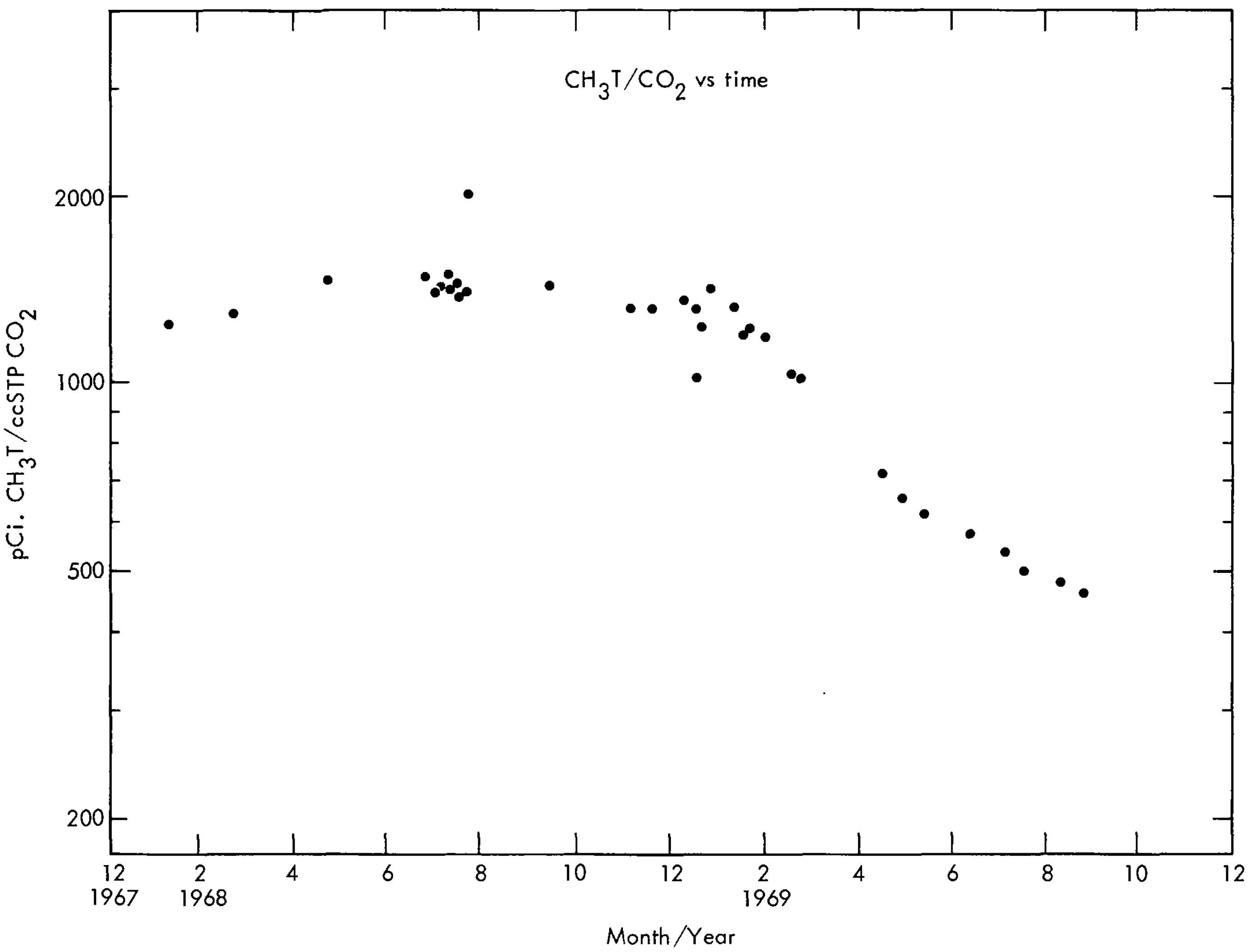

Fig. 12

CH_3T/CO_2 variation with time. Courtesy C. F. Smith (Ref. 14).

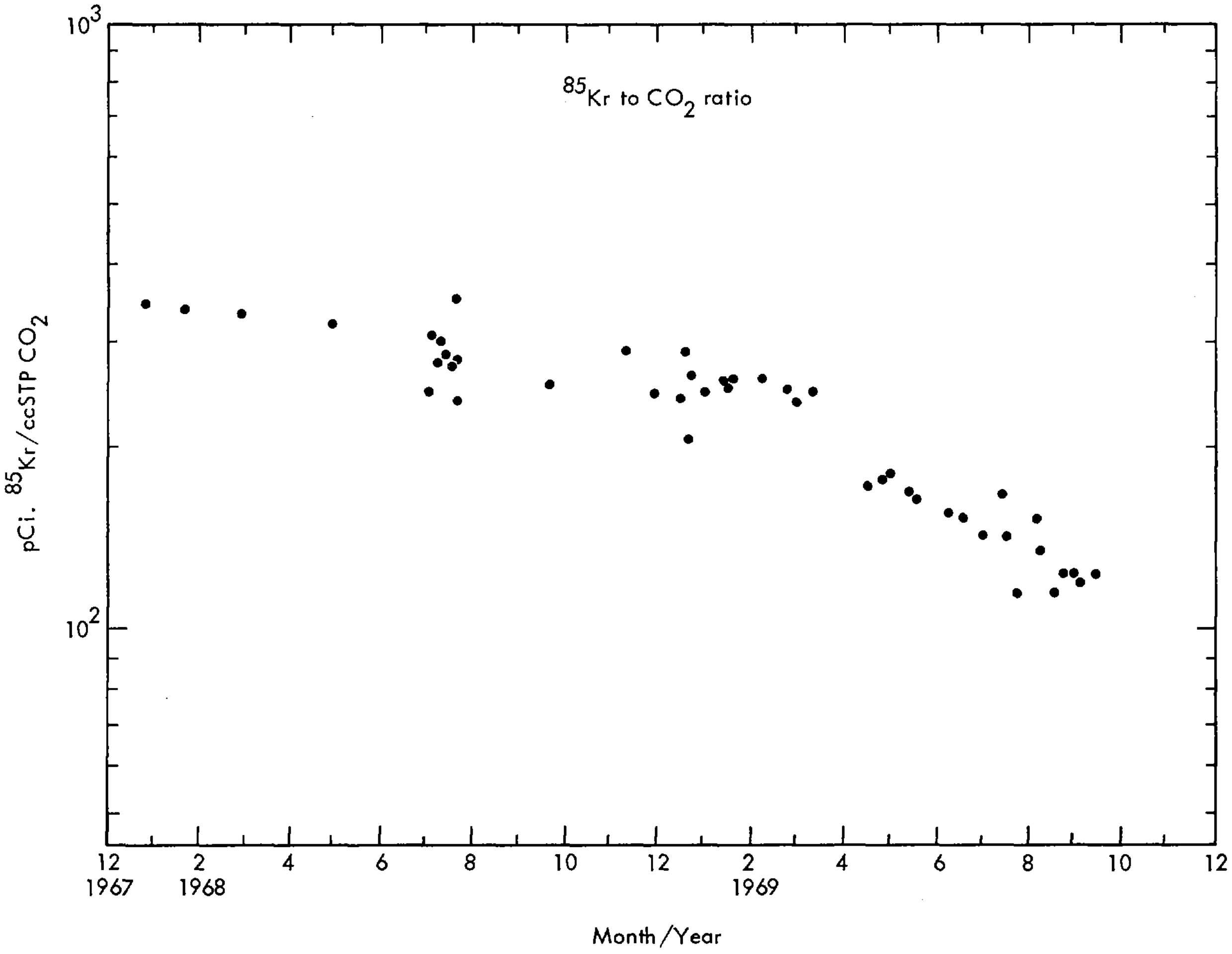

Fig. 13

Kr^{85}/CO$_2$ variation with time. This and the previous figure indicate the presence of a process which transfers CO$_2$ into the gas. Courtesy C. F. Smith (Ref. 14).

During the flow tests, the tritium and krypton-85 concentrations in the gas were continuously monitored and recorded. No problem was encountered with the well head assembly, the measuring apparatus or the flare system. Tritiated water produced together with the gas during the June - July, 1968 flow tests was sealed in containers and stored. Water produced during subsequent tests was first stored in a large tank and later re-injected into the flare. Again, no problems were encountered with this procedure nor was there any hazards to any of the personnel involved.

Nothing has been said so far about the economic aspects of Gasbuggy. Gasbuggy could never be economic from the standpoint of the value of gas produced, nor was it ever meant to be economic. At a well head price of 20¢ per thousand cubic feet, the total value of gas in the 160 acres at the Gasbuggy site is approximately $1 million. This of course assumes complete recovery of the gas in place. Up to now the stimulated area of Gasbuggy has been approximately 10 acres and the value of the gas produced about $50,000.

The value of Gasbuggy lies, of course, in its yield of technical information. What is the impact of this information and what results can be drawn at this time from the technical data?

First of all, Gasbuggy has shown that a nuclear explosive can be safely detonated and fully contained in a high pressure gas bearing formation, and that subsequent reentry can be safely handled. The predictions concerning cavity size, chimney height and fracture radii appear to have been quite accurate although a direct confirmation of chimney or cavity radii by drill hole penetration is lacking. It has been established that fractures radiate spherically from the shotpoint and penetrate perhaps as far below the shotpoint as they do above. This will have an important bearing on the design of future experiments where a detonation can be placed in the center of the gas bearing formation with high expectations that the thickness of reservoir stimulated below the shot level may be comparable to that stimulated above the shot level.

For very thick reservoirs the use of two or more explosives in a single emplacement hole appears to be extremely desirable. The spacing of such multiple explosives will be strongly influenced by considerations of fracture extent below the shotpoint.

The offsets along geologic weaknesses at relatively large distances from the shotpoint may be important in future experiments. For example, in very thick reservoirs consisting of alternate lenses of sandstone and shale, explosion effects may be found at considerably larger distances than might be predicted from the strength of the rocks alone. A better understanding of the effects of such weaknesses and discontinuities is clearly needed. The surprisingly large influence which the weak rocks of the Fruitland tongue formation seemed to have had in increasing the fracture density in the lower part of the Pictured Cliffs as compared with that in the upper part underlines this need for understanding.

One of the disappointments of Gasbuggy was that no postshot permeabilities in the 100 to 1000 millidarcy region (similar to those found in the Hardhat measurements) were observed. The Gasbuggy measurements indicate that the permeability in the region within one cavity radius of the Gasbuggy chimney may have increased by a factor of up to 100 over the preshot permeabilities; in Hardhat such increases were observed out to four or five cavity radii. These results have also served to focus attention on the method of permeability measurements on the preshot rock.

Irrespective of the size of the chimney and the premeability of the close-in region, gas eventually must flow into the chimney through and from the original reservoir. The permeabilities of partially saturated sandstone at overburden pressures corresponding to a few thousand feet is apparently considerably less than that measured on core under ambient laboratory conditions. Techniques of measuring permeabilities on samples under pressure need to be refined and extended.

The volumes and flow rates of Gasbuggy are certainly encouraging when compared to the nearest conventional wells existing in the area. However, care should be taken in using the ratio of these various quantities as indications of a figure of merit of Gasbuggy over a conventional well. Such ratios may have been quite different had Gasbuggy been shot in a somewhat different location. It is rather interesting to note that the flow rate factors of 5 to 8 in Gasbuggy production, as compared to well 29-4 #10, are in agreement with the logarhithm of the ratio of the two well bore radii, neglecting any affect due to the hydrofracking of the conventional well. This implies that the ratios observed may be explained by a simple well bore effect.

The postshot geologic investigations at Gasbuggy have also emphasized the importance of understanding the hydrologic regime. The apparent increase in permeability of the aquifer is certainly surprising. Its explanation might invoke a hydrofracking mechanism induced by increase in pore pressure due to the passage of the stress wave. The actual amount of water flowing into the Gasbuggy chimney is not known. Comparisons of void volumes determined by the latest high volume flow tests and those found earlier indicate that perhaps 10% or some 200,000 ft^3 of chimney volume has been filled with water. The actual path of influx is not known, although it is most likely confined to the immediate area of the emplacement hole. If water flows through cracks in the formation rather than by way of the emplacement hole, the permeability of the formation could be greatly effected. It is not likely, however, that this will ever be resolved for Gasbuggy.

A large portion of the technical information came through the analysis of samples for their chemical and radiochemical constituents. The fact that only some 5% of the tritium produced was detected in the gas phase six months after the detonation is certainly a gratifying result. However, no direct proof of the assumption that the remaining tritium is retained in the water exists. No valid water samples have yet been obtained as the highest tritium concentrations observed were about 1.5 microcuries per milliliter (such a concentration corresponds to an amount of water equal to between one and two chimney volumes). Since the partition of tritium between gas and liquid follows the ratio of hydrogen these phases, it is reasonable to assume that most of the tritium is in the water; a rough calculation shows that the Lewis shale contains about 30 times more hydrogen in water than in hydrocarbons. This same formation, however, contained free carbon which was available to react with steam to form hydrogen; thus a portion of the tritium could form tritiated hydrogen gas. The very rapid decrease in the amount of hydrogen (and hence tritium) concentrations observed indicate a rapid exchange with water in the chimney rubble, but some of the tritiated hydrogen will react with carbondioxide to form methane and water. Taylor [21] has treated this subject quantitatively. His calculations suggest that detonating Gasbuggy in the Lewis shale may not have resulted in significantly less radioactivity in the gas than would have been the case for a shotpoint in the sandstone. Both formations contain about the same amount of water; since the shale contains about five times the amount of free carbon than the sandstone, more tritiated hydrogen gas was produced. The shale contains much less methane and dolomite than the sandstone, resulting in smaller amounts of tritiated methane, and carbon dioxide. Results from future experiments are needed to confirm the correctness of the basic assumption and of the calculational model.

Up to now, no exchange of tritium between the water and the gas phases has been observed. This is supported by Fig. 14 which indicates a constant tritiated methane to krypton-85 ratio. If tritium exchange between H_2O and CH_4 were to occur, this ratio would show larger values at later times. It will be interesting to see whether it remains constant with time. It is plausible that decomposition of dolomite is responsible for the generation of CO_2.

Analysis of gas from future experiments are required to put this hypothesis on a firmer basis and to indicate steps that might be taken to prevent the generation of relatively large amounts of CO_2.

It is my opinion that Gasbuggy as an experiment was eminently successful. This does not negate the often-repeated statement that a number of experiments are needed to evaluate all aspects of stimulating a gas reservoir by means of nuclear detonations. Gasbuggy has provided a great deal of data which have led to many conclusions and interpretations. Other experiments are needed to verify or modify these conclusions, and, undoubtedly, new facts and facets will be uncovered that were not detected in Gasbuggy.

ACKNOWLEDGEMENTS

The help and cooperation of all participants in the Gasbuggy project is gratefully acknowledged. In particular, I wish to thank H. L. Kendrick of the El Paso Natural Gas Company's Farmington Office for his conscientious compilation and dissemination of pressure and flow data; C. H. Atkinson of the U. S. Bureau of Mines, and R. F. Lemon of EPNG for many helpful discussions throughout the course of Gasbuggy, and for the opportunity to read and cite material from the paper they are presenting at this symposium; and to L. Rogers of EPNG for discussing his gas flow calculations with me. Among my colleagues at the Lawrence Radiation Laboratory, continuing discussions with C. F. Smith, A. Sherwood, and J. Korver have been invaluable.

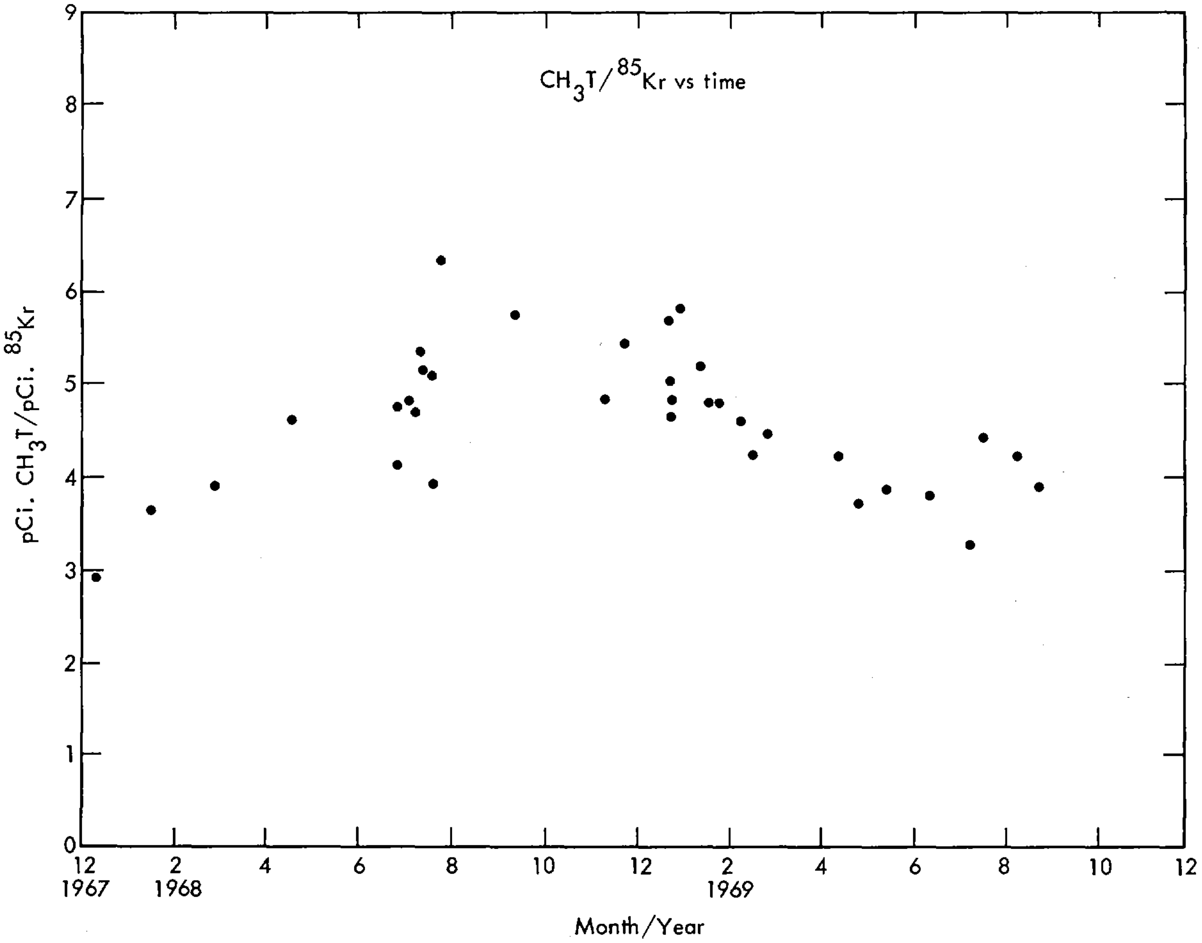

Fig. 14

CH_3T/Kr^{85} variation with time. The fact that this relation is essentially constant with time is taken to mean that no tritium is moving from the liquid to the gas phase. Courtesy C. F. Smith (Ref. 14).

REFERENCE LIST

1. Project Gasbuggy Feasibility Study, PNE-G-1, May 1965.
2. Preshot Symposium on the Gasbuggy Experiment, Farmington, NM, Sept. 1967.
3. F. Holzer, Gasbuggy Preshot Summary Report, UCRL-50345 (PNE-G-2), Nov. 1967.
4. C. F. Smith, Pre-Operational Report, Geo Quality Analysis and Evaluation Program, UCID-15136, March 1967.
5. G. H. Higgins and T. R. Butkovich, Effect of Water Content, Yield, Medium, and Depth of Burst on Cavity Radii, UCRL-50203, Feb. 1967.
6. Rapp, E. G., Containment of Buried Nuclear Explosions, UCRL-50604, Oct. 1968.
7. C. R. Boardman and J. Skrove, Distributions in Fracture Permeability of a Granite Rock Mass Resulting from a Contained Nuclear Explosion, UCRL-14292, Rev. II, Feb. 1966.
8. F. Holzer, Gasbuggy Preliminary Postshot Summary Report, UCRL-50386 (PNE-1003) January 1968.
9. W. R. Perret, Gasbuggy Seismic Source and Surface Motion, PNE-1002, (to be published).
10. D. E. Rawson, J. A. Korver, R. L. Pritchard, W. Martin, Postshot Geologic Investigations, UCRL-71354 (PNE-G-11), Sept. 1968.
11. D. C. Ward and R. F. Lemon, Status of Reservoir Evaluations, PNE-G-13, Sept. 1968.
12. C. H. Atkinson, P. C. Ward, R. F. Lemon, Gasbuggy Reservoir Evaluation - 1969 Report, (Presented at this Symposium).
13. C. F. Smith, Tabulation of Radiochemical and Chemical Analytical Results, UCRL-50635 (PNE-G-44), April 1969.
14. C. F. Smith, Gas Quality and Evaluation Program for Project Gasbuggy (presented at this Symposium).
15. T. S. Sterrett, Post-Piledriver Evaluation Program - Drilling, UCRL-50765 (in preparation).
16. J. A. Korver, Private Communication.
17. A. E. Sherwood, Transient Flow in a Gas Reservoir Stimulated by a Nuclear Explosion: Project Gasbuggy, UCRL-71868 (July 1969).
18. L. Rogers, Determining the Explosion Effects on the Gasbuggy Reservoir from Computer Simulation of the Post-shot Gas Production History (presented at this Symposium).
19. C. F. Smith and F. F. Momyer, Gas Quality Investigation Program Status Report for Project Gasbuggy, UCRL-71514 (Sept. 1968).

REFERENCE LIST - Continued

20. G. H. Higgins, D. D. Rabb, and H. C. Rodean, Theoretical and Experimental Studies Relating to the Purging of Radioactivity from a Gas Well Stimulated by a Nuclear Explosion, UCRL-50519 (December 1968).

21. R. W. Taylor, E. L. Lee and J. H. Hill, Interpreting the Chemical Results of the Gasbuggy Experiment (presented at this Symposium).

22. D. E. Rawson and J. A. Korver, Acceptability of the Gasbuggy Site, UCID-15132, April 1967.

23. R. W. Klepinger, Analysis of Ground Motion and Containment Data, Gasbuggy Event, AEC Report NVO-1163-158, Sept. 1968, Project Gasbuggy.

24. J. A. Blume, Final Report on Structural Response, PNE-1012, Nov. 1969.

25. J. A. Korver and D. E. Rawson, Gasbuggy Post-shot Investigations in GB-ER, UCRL-50425, April 1968.

26. K. R. Kase, N. A. Greenhouse, W. J. Silver and G. R. Sorenson, Project Gasbuggy Operational Experiences, UCRL-71356, January 1969.

27. A. E. Sherwood, Private Communication.

XA04N0860

Determining the Explosion Effects on the Gasbuggy Reservoir from Computer Simulation of the Postshot Gas Production History

Dr. Leo A. Rogers

El Paso Natural Gas Company

ABSTRACT

Analysis of the gas production data from Gasbuggy to deduce reservoir properties outside the chimney is complicated by the large gas storage volume in the chimney because the gas flow from the surrounding reservoir into the chimney cannot be directly measured. This problem was overcome by developing a chimney volume factor F (M^2CF/PSI) based upon analysis of rapid drawdowns during the production tests. The chimney volume factor was in turn used to construct the time history of the required influx of gas into the chimney from the surrounding reservoir. The most probable value of F to describe the chimney is found to be 0.150 M^2CF/PSI.

Postulated models of the reservoir properties outside the chimney are examined by calculating the pressure distribution and flow of gas through the reservoir with the experimentally observed chimney pressure history applied to the cavity wall. The calculated influx from the reservoir into the chimney is then compared to the required influx and the calculated pressure at a radius of 300 feet is compared to the observed pressures in a shut-in satellite well (GB-2RS) which intersects the gas-bearing formation 300 feet from the center of the chimney. A description of the mathematics in the computer program used to perform the calculations is given.

Gas flow for a radial model wherein permeability and porosity are uniform through the gas producing sand outside the chimney was calculated for several values of permeability. These calculations indicated that for the first drawdown test (July 1968) the permeability-producing height product (kh) was in the region of 15 to 30 millidarcy-feet (md-ft) and that after several months of testing, the effective kh had dropped to less than 8 md-ft.

Calculations wherein (1) the permeability decreases from the chimney out to the "fracture" radius, and (2) an increased production height is used near the chimney, match the data better than the simple radial model. Reasonable fits to the data for the first 150-200 days of testing have been obtained with permeability which decreases through the fracture region with a 1/r or e^{fr} dependence. For these fits the kh has been in the range of 3-7.5

md-ft., near and beyond the fracture radius.

After 150-200 days, the calculations presented in this paper give too much gas influx into the chimney and a rate of decrease in pressure at the range of GB-2RS which is too rapid. It is therefore apparent that smaller values of kh must be considered in the outer portion of the fractured region and beyond. Future calculations will further refine these models as required to match the influx to the chimney and the pressure observed in GB-2RS during the long term production and buildup tests which followed the time period considered in this paper. A match to pressure observed in the recently completed GB-3 well will also be required for the long term buildup test.

INTRODUCTION

This report assumes that the reader is generally familiar with the Gasbuggy* experiment. It has been extensively reported (Refs. 1-12) and the reports and experimental data are also available at Open File repositories maintained by the government. More than a year's production testing has taken place to develop data for evaluation of the effect of the detonation upon gas production.

At the time the Project Gasbuggy feasibility study was completed (1965), the limited information on permeability around nuclear explosion generated cavities suggested that a network of open fractures extending several hundreds of feet from the shot point would be created in the rock by the explosion. This concept was coupled to the assumption that the effective well bore radius for gas production would then be equal to this fractured region. Predictions of the stimulation effects were then made based upon the information available at that time.

After the shot (December 10, 1967), the rate of initial pressure buildup in the chimney and the low gas production observed upon reentering the GB-2 well in June 1968 raised serious questions regarding the earlier assumption of a very large permeability increase in the fractured region (Refs. 5, 6, 7).

The primary information for this analysis consists of (1) the gas production and bottom-hole pressures for the chimney (GB-E) and (2) the bottom hole shut-in pressure for a satellite well (GB-2RS) about 300 feet from the emplacement shot hole. This data was developed from a series of draw-down and buildup tests which began June 28, 1968 and are still in progress at the time of this report (January 1970). The portion of the data used in this report is shown in Figure 1. The draw-down and buildup test program was designed to allow calculation of the chimney void volume with rapid blowdowns and calculations of well performance characteristics based upon analyses of constant back pressure data at several pressures.

The analysis technique used in this study centers on the amount of gas that flows into the chimney from the surrounding reservoir. The experimental data (bottom hole pressures and the amount of gas produced from the chimney) are first used to determine the required gas influx into the chimney. Computer calculations using various descriptions of the reservoir around the chimney are then made and the computed influx compared to that required by the experimental data. There is no unique set of reservoir parameters of permeability, height, and porosity distribution that match the data; therefore, the main point of the study is to hypothesize reservoir models which are plausible and then use computer simulation to calculate the gas production for the hypothesized model. The postshot permeability and producing height of the reservoir surrounding the chimney is then inferred

---

* Project Gasbuggy is a joint effort under the U.S. Atomic Energy Commission's Plowshare Program by El Paso Natural Gas Company, the Bureau of Mines of the U. S. Department of Interior and the Atomic Energy Commission with technical assistance provided by Lawrence Radiation Laboratory, Livermore, California.

from the parameters in those calculations which reasonably match the experimentally required influx and satellite hole pressure.

GAS INFLUX TO THE CHIMNEY

The first deduction made from the experimental data presented in Figure 1 is a determination of how much gas must flow into the chimney from the surrounding reservoir during the production testing period. This is accomplished by the following expression for volume balance of gas in and out of the chimney:

$$Q_I = Q_P - (P_o - P)F \tag{1}$$

where Q_I is the cumulative influx of gas from the surrounding rock from the beginning of testing to the time of interest (SCF)*, Q_P is the quantity of gas produced from the chimney since the begining of testing to the time of interest (SCF), P_o is the initial pressure in the chimney (PSI), P is the pressure at the time of interest (PSI), and F is a chimney volume factor in units of cubic feet of gas per psi pressure change in the chimney (SCF/PSI). F also includes the gas compressibility factor which for this analysis is assumed to be unity. Using experimental measurements for Q_P, P_o and P throughout the test period, curves of Q_I for given values of F can be calculated from equation (1).

Figure 2 shows a family of curves of the required influx (Q_I) from the surrounding reservoir into the chimney for several different chimney volume factors. The value of F is estimated from the rapid blowdown data by dividing the net amount of gas removed from the chimney by the associated pressure drop in the chimney where the net amount of gas removed is the amount of gas produced minus the amount of influx during the blowdown period. The gas produced is accurately measured, but the influx must be estimated from the initial shut-in pressure rise following blowdown, flow for constant back pressure immediately before or after blowdown, or the computer simulation results. The most accurate values of F are derived from the rapid blowdowns where the influx into the chimney is small compared to the production from the chimney during the blowdown period. F is thus determined from equation (1) using only small portions of the test period (the rapid drawdowns) and then applied back into equation (1) for the entire test period.

In calculating F from the several draw-down tests shown in Figure 1, its value varies from about .12 M^2CF/PSI to about .16 M^2CF/PSI depending upon the influx estimated for each drawdown test. The best estimate of F is about .15 M^2CF/PSI.

The value of F is tied to the volume of the void space in the chimney by the gas equation of state and pressure. The initial pressure multiplied by F is the amount of gas in the chimney at the beginning of testing. If this volume is corrected for

---

* SCF = Standard cubic feet of gas
MCF = 1,000 cubic feet
M^2CF = 1,000,000 cubic feet

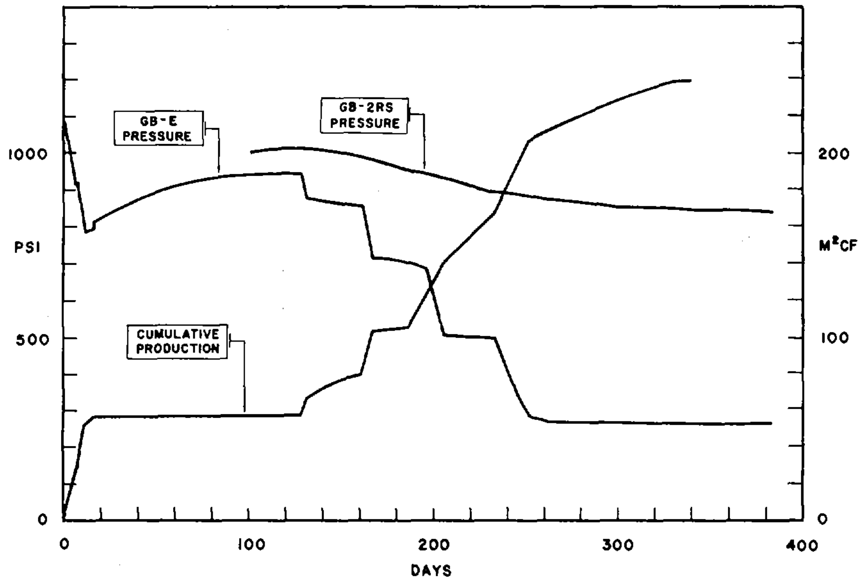

FIGURE 1

Gasbuggy production test data. Chimney pressure is that measured at approximately 3790 feet in GB-ER. Satellite hole pressure is that measured at approximately 4235 feet in GB-2RS. The cumulative production is the cubic feet at 14.7 psia and 60°F.

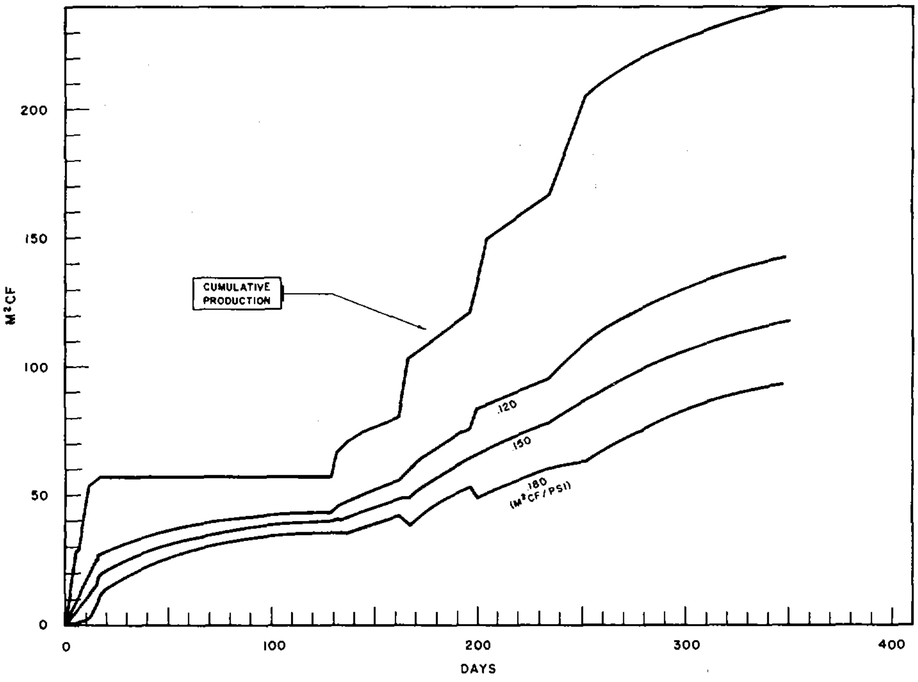

FIGURE 2

Family of curves for the required influx of gas from the surrounding reservoir into the Gasbuggy chimney for three different chimney volumes factors. For a constant chimney volume the required influx curve defines the quantity of gas that must influx from the surrounding reservoir in order to obtain the experimental pressure and cumulative production from the Gasbuggy chimney, Equation (1).

the downhole conditions of pressure, temperature and compressibility factor, it will be equal to the chimney void volume. Using the preshot prediction of about 2 M^2CF void space, the calculated F is .135 M^2CF/PSI which is in agreement with the value deduced from draw-down tests. It is not necessary, however, to know the chimney void volume for the analysis presented in this paper.

Since the F = .15 M^2CF/PSI curve may not be exactly correct, the curves for F = .12 M^2CF/PSI and F = .18 M^2CF/PSI were included in Figure 2 to indicate how the curve changes as F deviates from .15 M^2CF/PSI. The object of the calculations is thus to match the <u>shape</u> of the required influx curve <u>near</u> the value of F = .15 M^2CF/PSI, <u>not</u> to exactly match the .15 M^2CF/PSI curve. If the chimney void volume, temperature, and gas composition remain constant, then the F will be constant throughout the test period and the required influx curve will lie on the family of curves near the .15 M^2CF/PSI curve. If, on the other hand, there were some shrinkage of the chimney, or influx of water with time, then the required influx curve should start near the F = .15 M^2CF/PSI curve but later shift towards the F = .120 curve. Analysis of the blowdown data does not reveal the need for such a model.

An upper bound on the value of F can be derived from the shapes of the influx curves in Figure 2. Where there is a sudden increase of production from the chimney there should be a corresponding increased flow of gas into the chimney from the surrounding reservoir. This is seen in the .120 M^2CF/PSI and .15 M^2CF/PSI curves in Figure 2; but the .180 M^2CF/PSI curve shows the physically impossible situation of flow decrease, or even reverse flow, for the rapid production from the reservoir. F must, therefore, be less than .180 M^2CF/PSI.

The computations to follow assume the chimney wall is a boundary whose pressure history is the observed GB-ER bottom hole pressure and that the initial pressure is 1067 psi in the entire reservoir outside the chimney. The study consists of examining various assumed permeability distributions outside the chimney. The test of each assumed permeability distribution is based upon comparisons of: (1) the calculated gas inflow to the chimney (Q_I) to that given in Figure 2 for F in the range of 0.120 M^2CF/D to 0.150 M^2CF/PSI; and, (2) the calculated pressure history 300 feet from the chimney with the observed pressure history of GB-2RS. Some of the models assume an increase in producing height as a result of shale fracturing by the explosion.

It is recognized that no unique solution in terms of a permeability distribution is possible. The approach therefore has been to start with a very simple model and add complexities as required to obtain a fit with the experimental data.

MODEL STUDIES

A description of the mathematics in the computer program used for the analyses to follow is given in the Appendix. The computer program calculates the flow through a three-dimensional matrix with a specified description of initial pressure, permeability, porosity, temperature, gas equation-of-state and the geometry of the producing section. This computational technique allows more flexibility in studying the problem than can be obtained from a best fit analysis to a cylindrical-radial flow model. In maintaining such flexibility, however, one gives up the convenience of the computer doing the iteration to get the best fit to the permeability or other parameters.

1) Cylindrical-radial; constant permeability

A cylindrical-radial flow model (Figure 3) was first considered with the nuclear chimney wall treated as the well bore and the permeability assumed constant in the sand portion of reservoir outside the chimney. The computation results for an assumed net pay sand thickness of 150 feet and for three different permeabilities are shown in Figures 4-5.

Examination of Figure 4 reveals that the calculated influx for k = 0.1 and 0.2 reasonably match the required influx from the first two draw-down tests (first 16 days). After this period, however, the calculated influx deviates above the required influx. For this early time the effective kh of the reservoir near the chimney is therefore in the range of 15-30 md-ft. If, on the other hand, the producing height were assumed to be about the same as the chimney height or total gas-bearing section (300 ft.), then the permeability would have been in the range of 0.05 - 0.1 md. During the first buildup test (16-130 days), the curve for k = 0.05 has about the right slope, but is displaced somewhat below the required influx curve. This suggests that at some distance from the chimney, the permeability drops to a value of less than 0.05 md. and kh is less than 8 md-ft.

Figure 5 reveals that for later times (greater than 100 days) the calculated GB-2RS pressure reasonably matches the pressure history in the satellite hole for k = 0.1 or 0.2 md. Since the calculation for k = 0.05 md. lies well above the observed GB-2RS data, the reduction of permeability to this value apparently occurs at about the GB-2RS distance of 300 feet from the chimney. The pressure in GB-2RS earlier than 100 days is omitted from the comparison since GB-2RS was subjected to a series of flow tests and did not adequately represent the reservoir pressure until after it had been shut in for several weeks.

An analytical solution for the effective kh for this model can be made using the radial flow equation and the buildup data following the first rapid drawdown. The equation (Ref. 8) for deducing kh from the buildup data is

$$kh = 1637 \frac{Q\mu TZ}{m} \qquad (2)$$

where Q is the flow (MCF/D) before shut-in, μ is the viscosity of the gas (.012 centipoise), T is temperature (about 600°R), Z is gas compressibility and m is the slope on the buildup curve (Figure 6) (psi^2/cycle versus reduced time, $t/t + \theta$, where θ = flow time before shut-in). Figure 6 shows the curve for the July 16, 1968 through November 4, 1968 buildup (16-130 days). The data does not result in a good straight line as the reduced time approached 1.0, but for the line shown, the slope is approximately 1.3 million psi^2/cycle. In using equation (2), it must be remembered that the equation is derived on the basis of negligible well

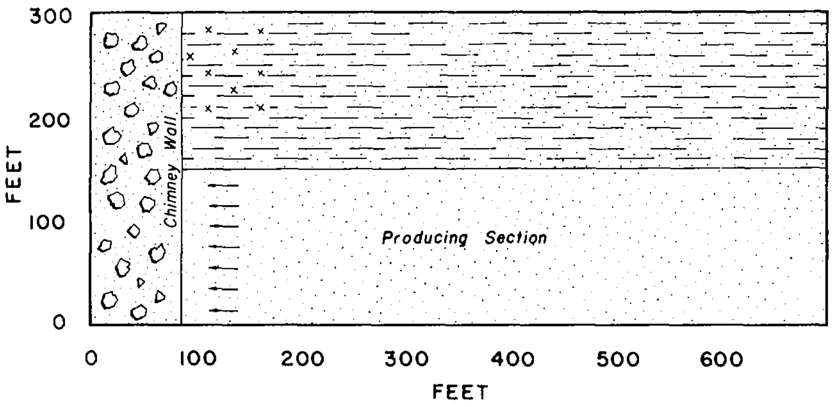

FIGURE 3

Schematic drawing of the cylindrical-radial flow model for the Gasbuggy chimney and surrounding reservoir. The entire producing section is approximately 300 feet thick with alternating layers of producing sands and barren rocks. However, for the computation, it was assumed that the net producing sands could be combined into a single layer approximately 150 feet thick.

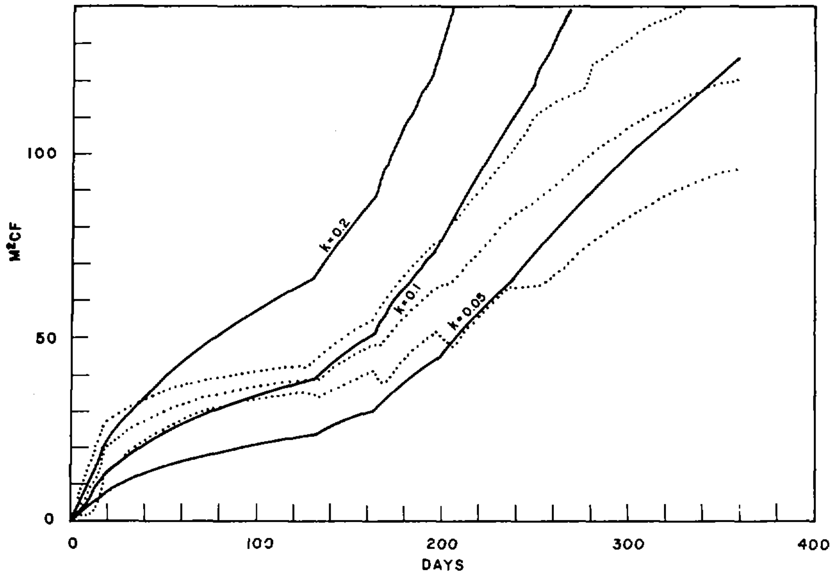

FIGURE 4

Calculated influx (solid lines) compared to the required influx (dotted lines) for the simple radial flow model where permeabilities are 0.5, .1, 12 millidarcys. Other parameters in the calculation are: porosity, 5%; chimney wall radius, 85 feet; gas viscosity, .0125 centipoise; chimney gas, 23.63 cubic feet = 1 weight pound; and the deviator to account for temperature and gas compressibility corrections (see Appendix) = 1.14.

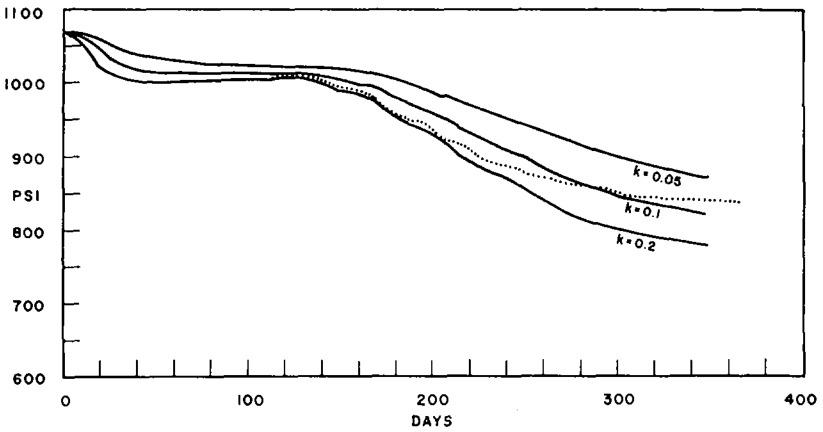

FIGURE 5

Calculated pressures (solid lines) at the satellite hole for the simple radial model compared to the experimental pressure (dotted line). Same calculation as shown in Figure 4.

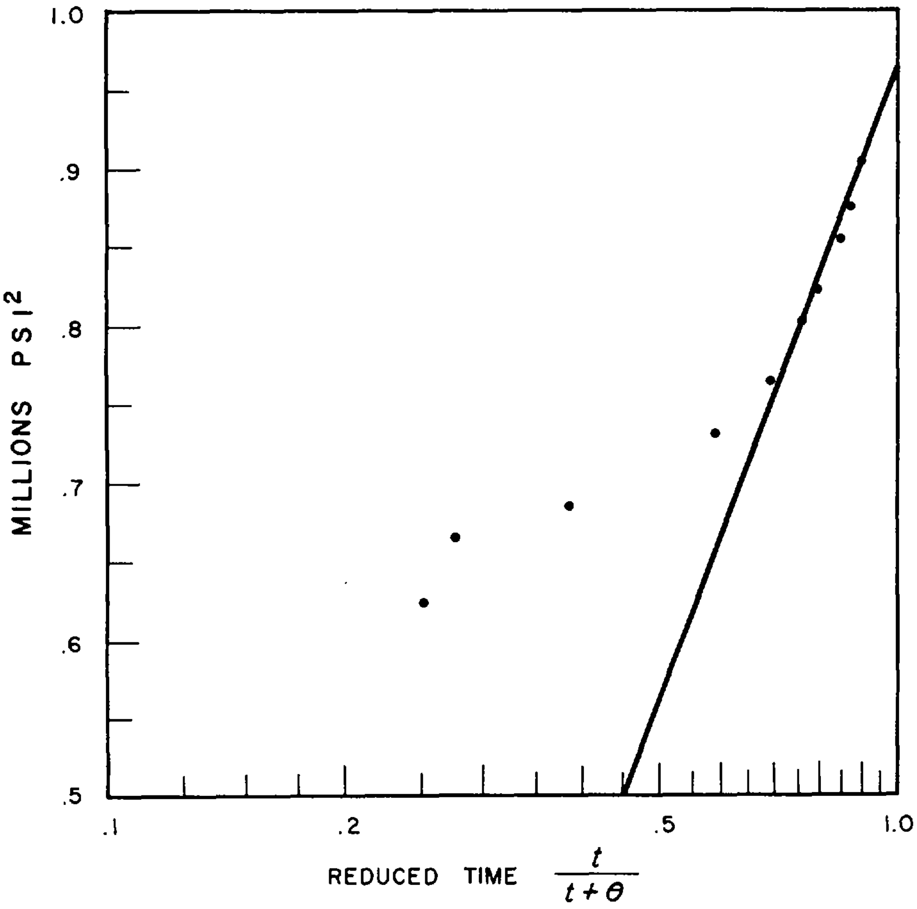

FIGURE 6

Plot of July - November 1968 pressure buildup data for the Gasbuggy chimney. Flow period prior to shut-in is twelve days and the initial shut-in pressure 780 psi.

bore volume. Q is really Q_I, the influx from the reservoir into the well bore. If the flow from the required influx curves of about 0.9 M^2CF/D before shut-in is substituted into equation (2), then the resulting kh is about 8 md-ft. which is consistent with the k = 0.05 developed above.

2) Cylindrical-radial; permeability change at discreet radii

The first complication added to the simple radial model was that of allowing the permeability to have discreet changes at certain radii. Figure 7 shows the calculated influx and GB-2RS pressure for the case where the permeability from the cavity radius to approximately two cavity radii has a constant value of 0.15 millidarcys; from two cavity radii to approximately three cavity radii the permeability is 0.1 millidarcys and beyond three cavity radii the permeability is 0.05 millidarcys. For these conditions the required influx to the chimney is reasonably matched for the first 120 days and the observed GB-2RS pressure is matched for the full 210 days of the calculation. For times longer than 120 days, the calculated influx into the chimney is too high, indicating that the assumed permeability for the far out region, which controls the late time flow, is too high. However, a better match to the data is achieved when using this three-ring model than when the simple radial model is used.

3) Fractured shale and permeability changes at discreet radii

Figure 8 shows a model where the fracture radius is considered spherical around the shot point so that near the chimney wall gas will flow through all of the fractured rock--including the non-gas-bearing shales. Beyond the fracture region, however, the gas flow is only through the net gas-producing sand. Figure 9 shows the results of a calculation with a combined case of a variable k with distance from the center of the chimney and spherical symmetry of fracturing. Again, there is a reasonable match between the calculation and the data for approximately the first 120-150 days. But beyond that, the calculated influx is still too high, indicating that the far out permeabilities used in the calculation were too high.

4) Permeability a smooth function of radius in the "fractured region"

It is apparent that the experimental data is best fit where the permeability decreases with distance away from the chimney wall. The nature of this variability is not known, but there are several rather simple mathematical functions that can be used as first approximations. One such function is for the condition where, from the chimney wall out to some specified radius, flow is described by the linear flow equations rather than the cylindrical-radial flow equations. In order for cylindrical symmetry to describe flow in a linear manner (pseudolinear), it is necessary for the effective permeability to change as a function of radius by the relation

$$\begin{aligned} k &= k_o \frac{R_m}{r} \quad ; \quad r < R_m \\ k &= k_o \quad ; \quad r > R_m \end{aligned} \tag{3}$$

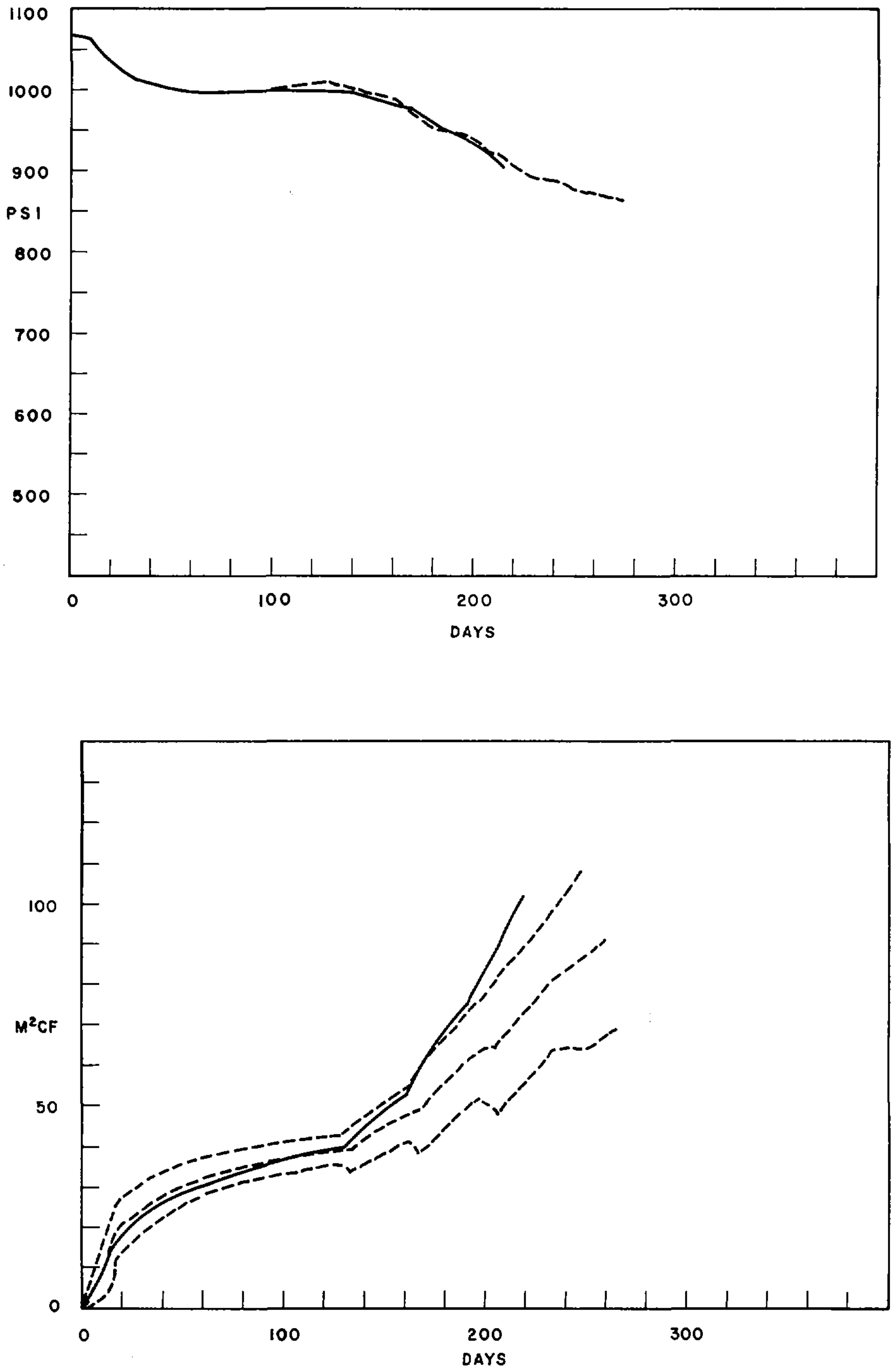

FIGURES 7

Calculated influx and satellite hole pressures for a three-ring radial model. Permeabilities vary as follows: for r = 85' to 150', k = 0.15 md; for r = 150' to 250', k = 0.10 md; and for r greater than 250', k = .05 md. Other parameters are the same as given in Figure 4. Dashed line in upper plot is observed GB-2RS pressure. Dashed lines in lower plot are required influx curves from Figure 2.

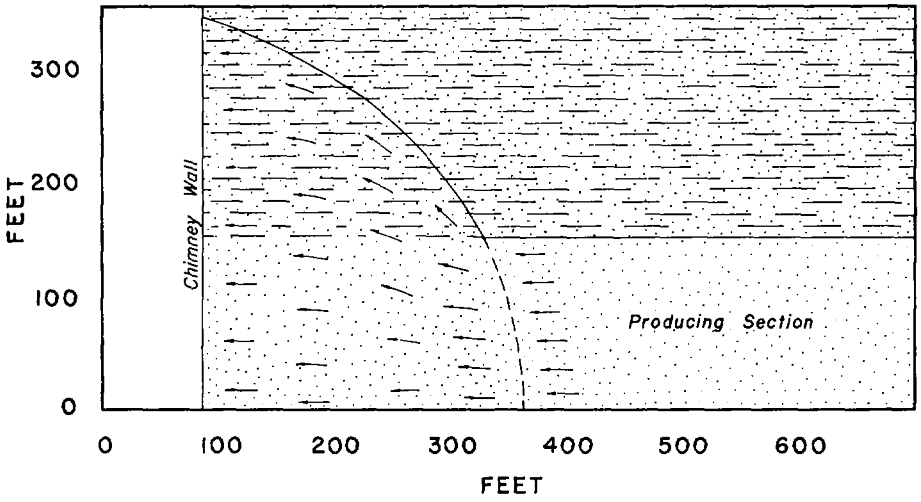

FIGURE 8

A computational model using spherical symmetry for the flow region around the shot point. In the calculations a series of concentric cylindrical shells was used with varying values of height to model the spherical section. The fractured shale and the producing section assumed to a porosity of five percent.

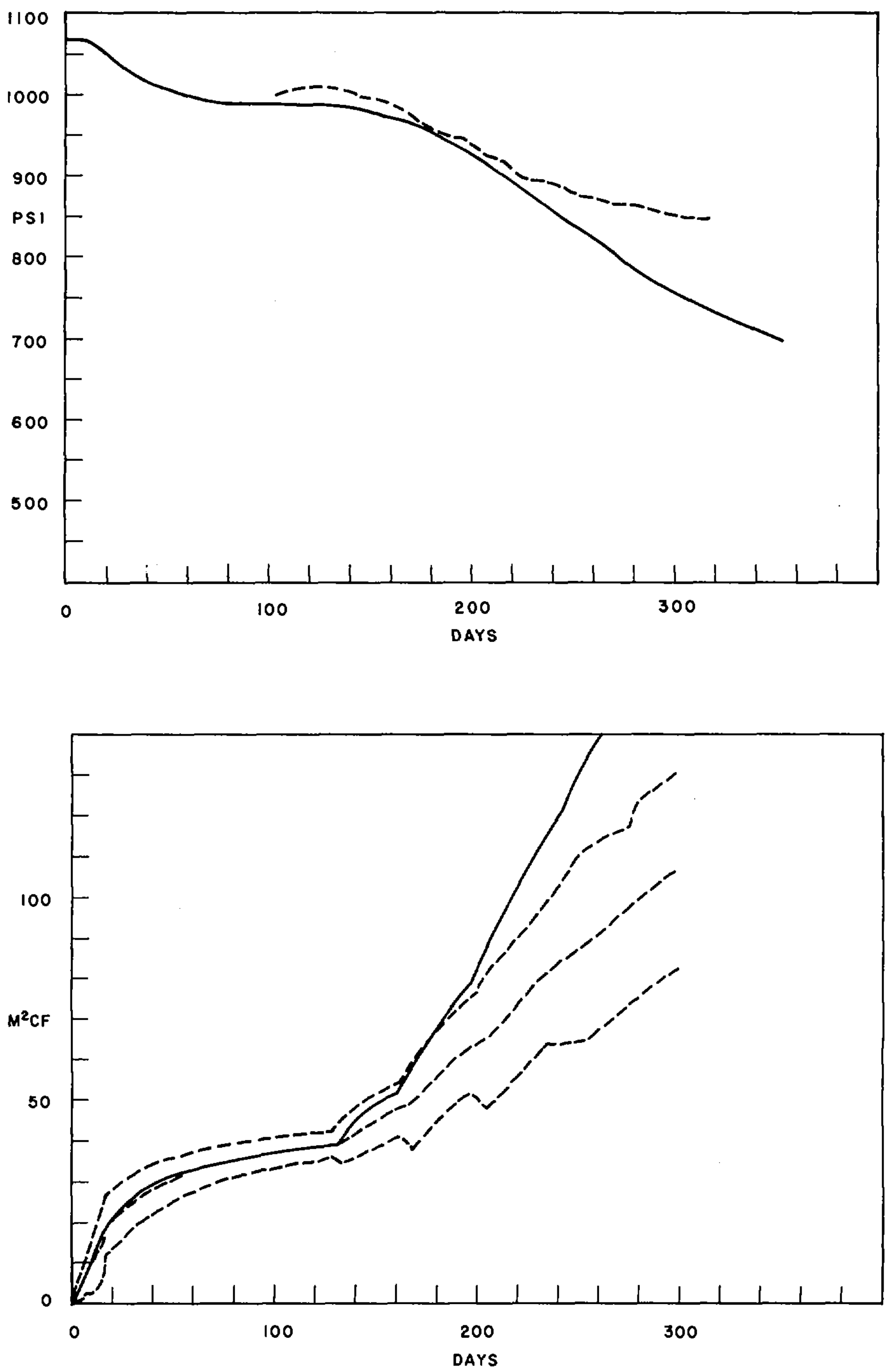

FIGURES 9

Calculated influx of satellite hole pressures for the three-ring permeability case combined with the spherical model in Figure 11. Permeabilities are: for r = 85' to 150', k = 0.6 md; for r = 150' to 250', k = 0.5 md; for r = 250' to 340', k = .04 md; and for r greater than 340', k = .02 md. Dashed line in upper figure is GB-2RS pressure from Figure 1. Dashed lines in the lower figure are the required influx curves from Figure 2.

(R_m is the radius at which $k = k_o$, the unstimulated permeability). Figure 10 shows two examples. Figure 11 shows the calculated results for these two examples. The calculated influx into the cavity for the first 40 to 60 days is very similar for these two models, but both give values which fall below the influx required by F = 0.150 M^2CF/PSI during that time period. After the initial shut-in at 16 days, the slope of the influx curve for the k = 0.05 model is too great. For the k = 0.02 model, the slope of the influx curve after initial shut-in appears reasonable until the blowdown starting at 162 days. The slope then becomes too great. The calculated GB-2RS pressure is in moderately good agreement with the data for the first 220 days. However, after that time the calculated rate of pressure decrease is too large. These observations demonstrate that the k = 0.02 md. model comes closer to describing the true postshot permeability distribution than the k = 0.05 md. model.

Further insight into possible refinement of the models is gained by comparing the k = 0.02 calculation of Figure 11 with Figure 9. Both calculations assume increased height of the permeable region due to fractured shale, as indicated in Figure 8, and a porosity of five percent in the fractured shale. In addition, both calculations have similar values of about 20 md-ft. for kh near the chimney wall. The difference in these calculations is a factor of about two in the permeability, through the range of two to four chimney radii. Comparison of the calculated influxes and calculated pressures at the range of GB-2RS reveals the high sensitivity of this analysis to permeability in the fracture region.

In Figure 10 the functional relationship between k and radius is a gentle curve. Another mathematical representation that has a similar trend is a straight line on a semi-log plot where permeability is given by

$$\begin{aligned} k &= k_o e^{fr} \quad ; \quad r < R_m \\ k &= k_o \quad ; \quad r > R_m \end{aligned} \qquad (4)$$

where f is the slope of the line. Computer calculations (not shown here) using equation (4) to approximate the curves in Figure 10 show results similar to the pseudolinear flow shown in Figure 11.

5) Permeability less than preshot near limit of "fractured region"

A flow or permeability model of the region surrounding the chimney can also be developed based on the observation that the overburden above the chimney must be supported by the rock around the chimney. It can then be argued that the rock above the chimney develops a supporting arch (as it settles after the shot). The resultant arch would form a compression ring around the chimney which could conceivably lower the permeability throughout the rock which supports the arch. If this occurred, the long term production would be highly controlled by the decreased permeability in this compression ring.

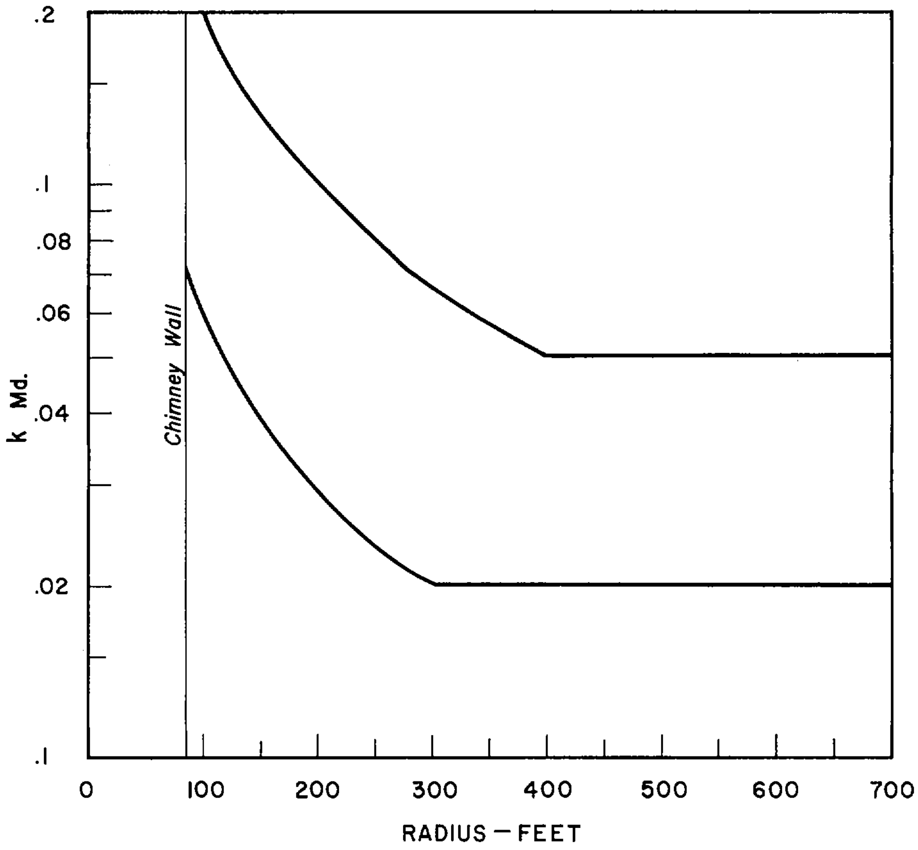

FIGURE 10

Plot showing how permeability must vary between the chimney wall and the radii 400' (upper curve) and 300' (lower curve) to simulate linear flow (pseudolinear flow) in equation (3).

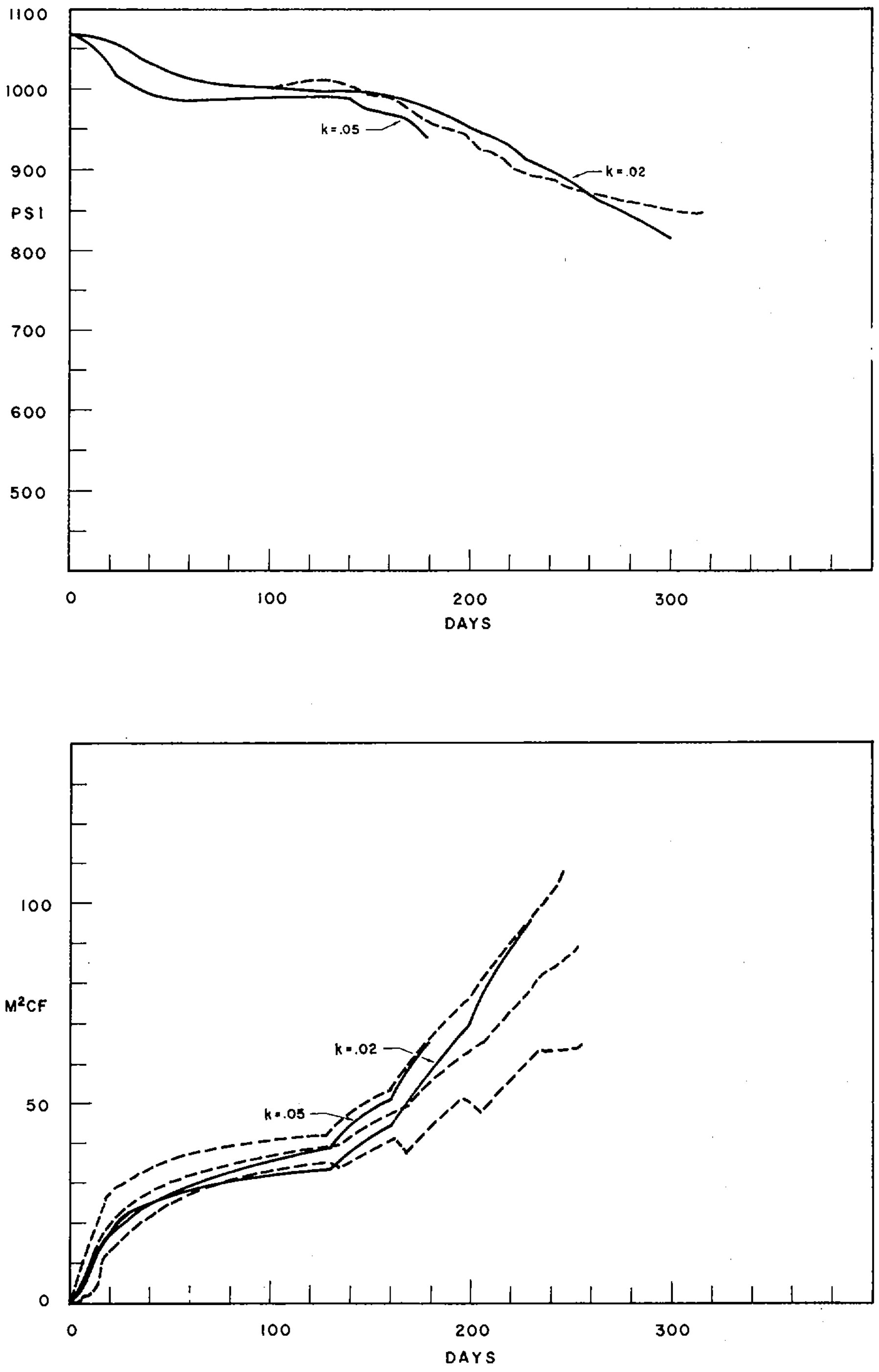

FIGURES 11

The curve labeled "k = .02" uses the permeability distribution shown in Figure 10 with that value beyond 300 feet and the model shown in Figure 11. The curve labeled "k = .05' uses the permeability distribution shown in Figure 10 which has that value beyond 400 feet and the model shown in Figure 4. The dashed line in the upper figure is the GB-2RS pressure from Figure 1. The dashed lines in the lower figure are the required influx curves from Figure 2.

Several calculations were made with different porosities, flow geometries and permeability distributions (not shown here), but they were not definitive with respect to this concept. Future comparisons with production data extending over a time period of about two years are expected to provide a stringent test of this hypothesis.

6) Future work

A long term (7 mos.) flow at constant downhole pressure was ended October 28, 1969 (487 days after start of production testing). Then a rapid blowdown from 255 psi to 125 psi was accomplished in 17 days following which the well was shut in for a long term buildup test. During September and October 1969, another postshot well (GB-3) was drilled which intersected the gas-bearing section about 200 feet from the center of the chimney. This well was extensively cored and logged and then shut in to obtain reservoir pressure. Additional calculations are needed to analyze these recent data in terms of possible gas flow or explosion effects models. It is expected that future efforts will result in refinement of the description of permeability in the vicinity of the Gasbuggy chimney developed in this paper.

CONCLUSIONS

This paper has shown that a computational model to match the data from the first 150-200 days of Gasbuggy production testing must be one in which the permeability-producing height product decreases with radius from the chimney. Further, computations to date suggest that models where both the permeability and the producing height decrease with radius will give the best fit to the data.

It is apparent that for Gasbuggy there is only moderate increase of the permeability through the fracture region and little, if any, increased effective permeability of the reservoir at or beyond the fracture radius. Comparison of computations for a simple radial model wherein permeability does not change with position in the producing formation outside the chimney reveals that: (1) for early time gas production, the kh is in the range of 15-30 md-ft., and (2) for late time gas production the kh decreases to less than 8 md-ft. Reasonable fits to the data for the first 150-200 days of testing have been obtained with permeabilities that decreased through the fracture region with a 1/r or e^{fr} dependence. For these fits, the permeability-producing height product has been in the range of 15 to 40 md-ft. at the chimney boundary and decreasing to the range of 3 to 7.5 md-ft. near and beyond the fracture radius.

After 150-200 days, the calculations presented in this paper give too much gas influx into the chimney and a rate of decrease in pressure at the range of GB-2RS which is too rapid. It is therefore apparent that smaller values of kh must be considered in the outer portion of the fractured region and beyond. Future calculations will further refine these models as required to match the influx to the chimney and the pressure observed in GB-2RS during the long term production and buildup tests which followed the time period considered in this paper. A match to pressure observed in the recently completed GB-3 well will also be required during the long term buildup test.

ACKNOWLEDGEMENT

The work which made this analysis possible is the result of outstanding individual efforts on the part of many people in El Paso Natural Gas Company, the Atomic Energy Commission, Lawrence Radiation Laboratory, and the Department of Interior. Special mention is in order for Richard F. Lemon, Charles H. Atkinson and Don C. Ward for their ingenuity in defining a meaningful well test program which was consistent with the conflicting requirements to study flushing radioactivity from the chimney; H. L. Kendrick and his associates who braved the elements to collect the test data and promptly distributed it to project participants; Nancy E. McIntyre for her efforts in computer programming and in running the problems, as well as Philip L. Randolph for his suggestions during the work and for critical review of the manuscript.

REFERENCES

1. El Paso Natural Gas Company, Project Gasbuggy Feasibility Study. El Paso: El Paso Natural Gas Company, May 14, 1965, Abstract, p. 6 and p. 17, (PNE-G-1).
2. Ward, D. C., R. F. Lemon and C. H. Atkinson, Project Gasbuggy--Results of 1969 Production Tests. American Nuclear Society Symposium on Engineering with Nuclear Explosives, Las Vegas, Nevada, January 14-16, 1970.
3. Cherry, J. T., D. B. Larson, E. G. Rapp, Computer Calculations of the Gasbuggy Event. Livermore, California: Lawrence Radiation Laboratory, May 10, 1968, (UCRL-50419, PNE-G-6).
4. Holzer, Fred, Gasbuggy Preshot Summary Report. Livermore, California: Lawrence Radiation Laboratory, November, 1967, (PNE-G-2, PNE 1001).
5. Rawson, D. E. and J. A. Korver, Gasbuggy Postshot Geologic Investigations. Livermore, California: Lawrence Radiation Laboratory, November, 1968, (UCRL-71354, PNE-G-11).
6. Cutler, W. G. and H. L. Kendrick, Drilling and Testing Operations for Project Gasbuggy. El Paso: El Paso Natural Gas Company, October 2, 1968, PNE-G-9, Society of Petroleum Engineers, Houston, Texas, September 24, 1968.
7. Ward, D. C. and R. F. Lemon, Status of Reservoir Evaluation Project Gasbuggy. El Paso: El Paso Natural Gas Company, September 29, 1968, PNE-G-13, Society of Petroleum Engineers, Houston, Texas, September 29, 1968.
8. Katz, Donald L., et al., Handbook of Natural Gas Engineering. New York: McGraw-Hill Book Company, 1959.
9. Eilerts, C. Kenneth, Eudora F. Sumner, Transient Flow Characteristics of Low-Permeability Gas Reservoirs and Improvement of Deliverability by Nuclear Explosion. Dallas: Society of Petroleum Engineers of AIME, October, 1967.
10. Holzer, Fred, Preliminary Postshot Summary Report. Livermore, California: Lawrence Radiation Laboratory, January, 1968, (PNE 1003, PNE-G-3).
11. Power, D. V. and C. R. Bowman, An Evaluation of the Water Production from the Gasbuggy Reentry Well. American Nuclear Society Symposium on Engineering with Nuclear Explosives, Las Vegas, Nevada, January 14-16, 1970.
12. Test data and completed reports designated by PNE-G numbers are placed on Open File at the U. S. Bureau of Mines, Bartlesville Petroleum Research Center, Bartlesville, Oklahoma; U. S. Bureau of Mines, Office of Mineral Resources Evaluation, Denver, Colorado; and the University of Nevada, Las Vegas, Nevada.

APPENDIX

A Computer Method for Approximating Three Dimensional Darcy Gas Flow

Introduction

To avoid the complications from numerically solving the second order time dependent flow equation in three dimensions, a technique was devised which does a time averaging of steady state integrated solutions for relatively small interconnected volume elements. Arbitrary boundary conditions of flow or pressure as functions of time are easily specified. The result is a versatile, simple, reasonably accurate computational method for low velocity gas flow through a permeable matrix.

Basic Equations

The volume flow ($\vec{q}$) through an element of matrix is given by

$\vec{q} = -K \nabla P$ (Equation of Motion) (A1)

where K is the volume conductivity and ∇P is the pressure gradient. For Darcy flow, $K = kA/\mu$ where k = permeability, A = area and μ = viscosity.

The description of the gas is given by the expression

$P = \rho \xi$ (Equation of State) (A2)

obtained from the gas equation of state[8] PV = ZnRT where

$\rho = \frac{n}{V}$ = Gas density (weight pounds/volume)

ξ = zRT = Combined proportionality factor (PSI-CF/wt pounds)

P = Pressure (PSI)

V = Volume (CF)

Z = Gas compressibility factor (dimension less function of P or ρ)

R = Gas constant (PSI-CF/^{o}R - wt pounds)

n = Mass of gas (wt pounds)

T = Temperature (^{o}R).

The value of ξ is specified in the program as a function of gas density and volume element position to account for the variability of Z and T.

Equation (A1) multiplied by density gives the mass flow equation

$\vec{m} = - \rho K \nabla P$ (A3)

substituting for ρ from equation (A2) and integrating gives

$$m_{\alpha\beta} = C_{\alpha\beta} \left(P_e^2 - P_d^2\right) \quad \text{(Steady State Mass Flow)} \qquad \text{(A4)}$$

where $C_{\alpha\beta}$ is the partial flow constant between connected volume elements with pressures P_e and P_d. In this notation the subscript α is the symmetry (1 = linear, 2 = cylindrical, 3 = spherical) and the subscript β is the axis in the α symmetry. The equation for $C_{\alpha\beta}$ in cartesian, cylindrical and spherical coordinates are listed below. In these equations the mass flow rate is from the center of one volume element to the center of the other volume element through the common interface. The underlined subscripts in the denominators indicate the mid-point of the volume element. The permeabilities k_β indicate the permeability in the direction of the β axis.

Cartesian
Coordinates

$$C_{11} = - \frac{(y_2 - y_1)\ (z_2 - z_1) k_x}{2\xi\ \mu\ (x_{\underline{2}} - x_{\underline{1}})}$$

$$C_{12} = - \frac{(x_2 - x_1)\ (z_2 - z_1) k_y}{2\xi\ \mu\ (y_{\underline{2}} - y_{\underline{1}})}$$

$$C_{13} = - \frac{(x_2 - x_1)\ (y_2 - y_1) k_z}{2\xi\ \mu\ (z_{\underline{2}} - z_{\underline{1}})}$$

Cylindrical
Coordinates

$$C_{21} = - \frac{(\phi_2 - \phi_1)\ (z_2 - z_1) k_r}{2\xi\ \mu \ell n \left[\frac{r_2}{r_1}\right]}$$

$$C_{22} = - \frac{(z_2 - z_1)\ \ell n \frac{(r_2)}{(r_1)} k_\phi}{2\xi\ \mu\ (\phi_{\underline{2}} - \phi_{\underline{1}})}$$

$$C_{23} = - \frac{(\phi_2 - \phi_1)(r_2^2 - r_1^2) k_z}{4\xi\ \mu\ (z_{\underline{2}} - z_{\underline{1}})}$$

Spherical Coordinates

$$C_{31} = -\frac{(\theta_2 - \theta_1)(\phi_2 - \phi_1)k_r}{2\xi\ \mu\ (\frac{1}{r_1} - \frac{1}{r_2})}$$

$$C_{32} = -\frac{(\phi_2 - \phi_1)(r_2 - r_1)k_\theta}{2\xi\ \mu \ln \left| \frac{\text{Csc}\ \theta_2 - \text{Cot}\ \theta_2}{\text{Csc}\ \theta_1 - \text{Cot}\ \theta_1} \right|}$$

$$C_{33} = -\frac{(r_2 - r_1) \left| \frac{\text{Csc}\ \theta_2 - \text{Cot}\ \theta_2}{\text{Csc}\ \theta_1 - \text{Cot}\ \theta_1} \right| k\phi}{2\xi\ \mu\ (\phi_2 - \phi_1)}$$

Equation (A4) is applied with the condition that the amount of gas leaving one volume element is the same as enters an adjoining element through a common interface.

$$(\dot{m}_{\alpha\beta})_e - (\dot{m}_{\alpha\beta})_d = 0 \quad \text{(Continuity Equation)} \qquad \text{(A5)}$$

Time Average of Flow

Transient flow is approximated by a time derivitive of the steady state mass flow equation (A4) allowing P_e to change at a different rate than P_d. For every connection of volume elements d and e the mass flow through the common interface $\alpha\beta$ is given by

$$\frac{d\dot{m}_{\alpha\beta}}{dt} = 2C_{\alpha\beta} \left| P_e \frac{dP_e}{dt} - P_d \frac{dP_d}{dt} \right| \qquad \text{(A6)}$$

Using finite differences to approximate the differentials, the average flow between connected volume elements over a time increment is approximated by

$$\dot{m}^{n+1/2}_{\alpha\beta} = 1/2 \left[\dot{m}^{n}_{\alpha\beta} + \dot{m}^{n+1}_{\alpha\beta} \right] = \dot{m}^{n}_{\alpha\beta} + \frac{\Delta t}{2} \frac{d\dot{m}_{\alpha\beta}}{dt} \qquad \text{(A7)}$$

where superscripts refer to time -- n = t, n + 1 = t + Δt, n + 1/2 = t + 1/2 Δt. Equations (A6) and (A7) combine to give

$$\dot{\bar{m}}_{\alpha\beta} = C_{\alpha\beta} (P^n_e P^{n+1}_e - P^n_d P^{n+1}_d) \text{ (Averaged Mass Flow)} \qquad \text{(A8)}$$

This is the fundamental equation to be solved by the computer. A word description of the process is as follows:

Between volume element d at pressure P_d^n and adjacent volume element e at pressure P_e^n let steady state flow occur according to equation (A4). During time Δt an amount Δm of gas will leave one cell and enter the connected cell. The gas density in the cells at the end of the time increment has changed and the pressure associated with the new density can be found from equation (A2). These new pressures, P_d^{n+1} and P_e^{n+1}, are those which would occur if steady state flow occurred over the entire time step. Since the steady state mass flows are different at the beginning and end of a time increment, equation (A8) is an average of the mass flow between the beginning and ending of the time increment Δt which centers the mass flow at time

$$t + 1/2\ \Delta t.$$

In practice a volume element will usually be connected to several adjacent volume elements so that the gas density in a cell at the end of a time increment is the net volume after summing up all the flows to the connected volume elements.

Determining the Time Increment

The time increment needs to be small enough so the finite differences are adequate representations of the differentials and the computation is stable. This is done by specifying the condition that the net mass change in any cell during a time increment will be small compared to the total mass in the cell. With this fractional mass change (f) specified, the time step is the minimum Δt for all the cells in the matrix from the equation

$$\Delta t = \text{Minimum}\ (f) \left| \frac{m_j}{\dot{m}_j} \right| \qquad \text{(A9)}$$

where the subscript j refers to an arbitrary volume element. The value of f for a reasonable approximation and a stable calculation depends on the relative sizes of the volume elements and mismatches of material properties for adjacent volume elements. The time increment also needs to be small enough to insure that the direction of flow from equation (A8) will be the same as that required by equation (A4). This requires a lower limit cutoff below which the value zero is used for equations (A4) and (A8) to avoid difficulty from machine round-off and computation noise.

Boundary Conditions

Boundaries are handled as special volume elements. The conductivity links connect to them, but the pressure or flow through them are specified by equations or tabular input of pressure or flow as a function of time. The specification of pressure at a boundary is straightforward. The specification of flow at a boundary, however, requires an additional calculation to determine the boundary pressure which gives the desired flow. There may be more than one volume element connected to a boundary so that the total mass flow across a boundary is given by

$$\dot{M} = \Sigma\, \dot{m}_j = \Sigma\, {}_j C_{jb} \left(P_j^n\, P_j^{n+1} - P_b^n\, P_b^{n+1}\right) \qquad \text{(A10)}$$

where the subscript b refers to the boundary connected to volume element j. Further, at any instant of time, the pressure at the boundary is taken to be the same for all the volume elements connected to the boundary. In equation (A10), P_b^n and P_b^{n+1} are the same for all terms in the sum for each time step. The value of P_b^{n+1} is thus found by solving equation (A10). Having thus determined the boundary pressures required to get the specified $\dot{m}$, the boundary can be considered as a special cell and the flow calculated by equation (A8). Mass flow then is converted to volume of flow by dividing by the density of the gas.

The Computer Program

The most complicated part of the computer program is the input routine that calculates the volume elements and the interconnecting network constants. The material description is input by volume element and the conductivity links are between the midpoints of connected volume element. The permeability along the conductivity link is a weighted average of the permeability for the two connected volume elements. The computer output prints for selected times n + 1/2 the pressures in the volume elements according to $P_j = \sqrt{P_j^n\, P_j^{n+1}}$. The computer program was checked by running problems that had analytical solutions. The results were in close enough agreement to verify that the program was operating correctly. The accuracy, however, depends on size of the volume element, the magnitude of property changes between adjacent volume elements and the size of the time step.

XA04N0861

GASBUGGY RESERVOIR EVALUATION - 1969 REPORT

C. H. Atkinson and Don C. Ward (Bureau of Mines,
U.S. Department of the Interior) and R. F. Lemon
(El Paso Natural Gas Company)

ABSTRACT

The December 10, 1967, Project Gasbuggy nuclear detonation followed the drilling and testing of two exploratory wells which confirmed reservoir characteristics and suitability of the site. Reentry and gas production testing of the explosive emplacement hole indicated a collapse chimney about 150 feet in diameter extending from the 4,240-foot detonation depth to about 3,900 feet, the top of the 300-foot-thick Pictured Cliffs gas sand. Production tests of the chimney well in the summer of 1968 and during the last 12 months have resulted in a cumulative production of 213 million cubic feet of hydrocarbons, and gas recovery in 20 years is estimated to be 900 million cubic feet, which would be an increase by a factor of at least 5 over estimated recovery from conventional field wells in this low permeability area. At the end of production tests the flow rate was 160,000 cubic feet per day, which is 6 to 7 times that of an average field well in the area. Data from reentry of a preshot test well and a new postshot well at distances from the detonation of 300 and 250 feet, respectively, indicate low productivity and consequently low permeability in any fractures at these locations.

INTRODUCTION

The nominal 26-kiloton nuclear explosive for Project Gasbuggy was detonated December 10, 1967. Project Gasbuggy, a nuclear fracturing experiment conducted jointly by the U. S. Atomic Energy Commission, El Paso Natural Gas Co., and the U.S. Department of the Interior's Bureau of Mines, was designed to test the effectiveness of nuclear explosives to fracture and thus increase the productivity of low-permeability natural gas reservoirs (1-2).[1]

The Bureau of Mines and El Paso Natural Gas Co. designed and executed the reservoir evaluation program for the experiment. This report is part of a continuing effort to keep industry informed of its progress and results. Test data and completed reports are placed on open file at the U.S. Bureau of Mines' Bartlesville Petroleum Research Center, Bartlesville, Okla; the U.S. Bureau of Mines' Office of Mineral Resource Evaluation, Denver, Colo.; and the University of Nevada, Las Vegas, Nev.

BACKGROUND

To supplement reservoir and production data available from the eight original field wells in the Gasbuggy test area (Fig. 1), two preshot test wells,

---

[1] Underlined numbers in parentheses refer to items in the list of references at the end of this report.

GB-1 and GB-2, were drilled in 1967. These wells were completed naturally, rather than being artificially fractured which is the customary practice in the San Juan basin. The Pictured Cliffs sandstone formation was cored using natural gas as the drilling medium in both wells. Induction, gamma ray, density, flowing temperature, and flowmeter logs were run in the gas-filled holes. Production tests were run on GB-1. The very low productivity precluded obtaining meaningful production tests on GB-2 so they were not attempted. Laboratory analyses were obtained on produced fluids. Fig.2 shows locations of preshot test wells and postshot well GB-3, and their relation to field well No. 10 and the emplacement hole, GB-E. Preshot test data and evaluations have been reported previously (3-4), and core analysis data and preshot reservoir characteristics are summarized in table I.

The detonation occurred at a 4,240-foot depth, 40 feet below the base of the 300-foot-thick Pictured Cliffs formation. Seismic results indicated that the explosive performed satisfactorily.

POSTSHOT PRODUCTION TESTS

After the explosive emplacement hole, GB-E, was reentered and completed as gas well GB-ER, brief production tests were run before the well was shut in January 17, 1968, for pressure buildup. Bottomhole pressure (BHP) was measured at 3,790 feet, 126 feet above the top of the Pictured Cliffs formation; BHP increased gradually from about 950 to 1,067 pounds per square inch gauge (psig) when production was resumed June 28, 1968. This BHP was 84 psi higher than that measured preshot in test well GB-1 and approximately 160 psi lower than pressures measured initially in nearby field wells 13 years ago.

A 15-day production test begun June 28 consisted of flowing GB-ER at 5 million cubic feet per day (5 MMcf/D, where M = 1,000) for 6 days, during which time BHP dropped to 906 psig at 248°F bottomhole temperature (BHT); then the well was shut in for 24 hours. During this shut-in period, the BHP rose to 917 psig and BHT declined to 174°F. Production testing was resumed for 5 days at 5 MMcf/D, resulting in 780 psig BHP and 247°F BHT. The production rate was lowered to 750 Mcf/D, and at the end of 4 days the BHP had increased 16 psi. The well was then shut in and remained so until testing was resumed November 4, 1968, except for one brief production period for collecting gas samples. Fig. 3 shows BHP and production rate versus time.

A series of three 30-day production tests on GB-ER, each at successively lower (and constant) chimney pressure, followed by a 7-month production period at a still lower pressure, was begun November 4, 1968. Having built up to 950 psig BHP at that time, GB-ER was blown down to 884 psig BHP, and based on past performance, an 850-Mcf/D rate was set. It was necessary to lower the producing rate three times in attempting to maintain constant BHP, and the final rate was 350 Mcf/D. Following the first 30-day period, the BHP was lowered from 854 to 706 psig by producing 5 MMcf/D for 5 days, then the rate was set at 600 Mcf/D. The rate was lowered to 500 Mcf/D toward the end of the 30-day period; however, the pressure continued to decline, and final BHP was 687 psig. The BHP was then reduced to 506 psig by producing at about 4 MMcf/D for 7 days. The initial 650-Mcf/D rate for the last 30-day test had to be decreased four times to 400 Mcf/D, with the final pressure being 496 psig.

For the 7-month test, which was begun March 19, 1969, blowdown to 264 psig BHP was accomplished, and a 500-Mcf/D rate was selected to maintain constant pressure. The rate was gradually decreased to 160 Mcf/D by June 26, 1969. An increasing pressure then dictated raising the production rate to 175 Mcf/D on August 3, 1969. This rate was maintained until October 4, 1969, when the rate was decreased to 160 Mcf/D. Further rate adjustments were unnecessary.

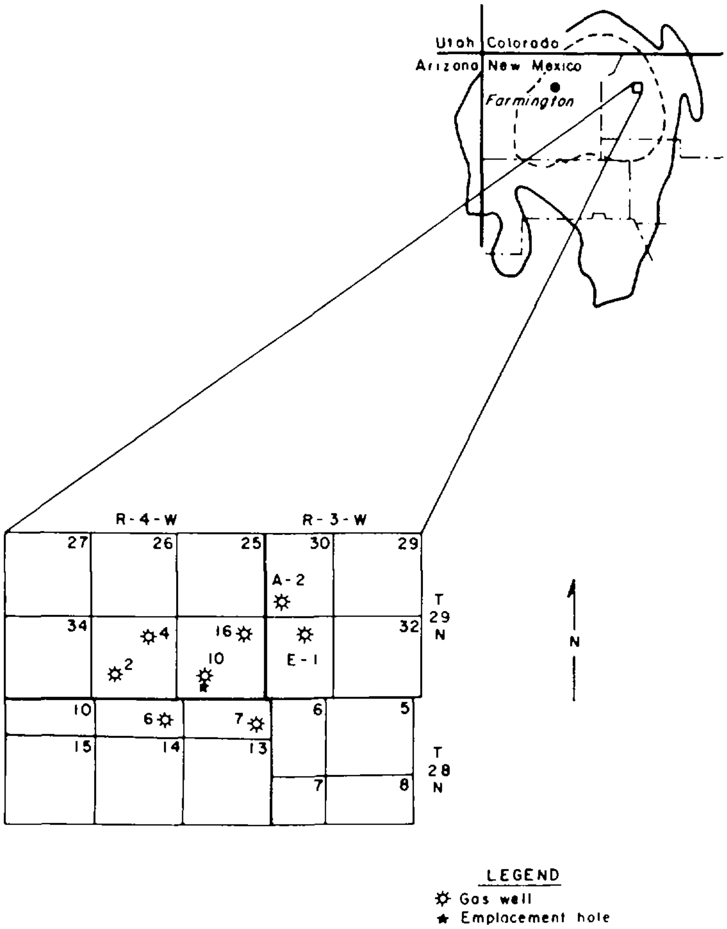

FIGURE 1.-Gasbuggy Test Area.

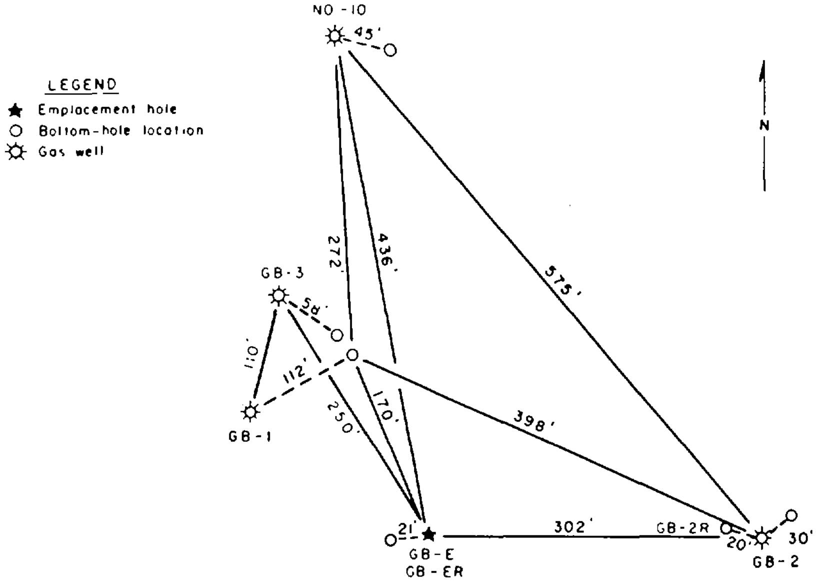

FIGURE 2.-Plat of Wells, Gasbuggy Test Site.

TABLE I--AVERAGE RESERVOIR PROPERTIES AT GASBUGGY SITE

	Gas-saturated sand with 60% or less water saturation			Total gas-saturated sand		
	Preshot		Postshot	Preshot		Postshot
	GB-1	GB-2	GB-3	GB-1	GB-2	GB-3
Porosity, percent	11.2	12.4	10.6	9.6	10.6	9.1
Gas saturation, percent	52.0	52.7	55.5	42.5	41.8	41.4
Permeability, millidarcys	0.14	0.19	0.15	0.10	0.15	0.10
Thickness, feet	156	149	143	254	255	255
Temperature, °F	130	130	--	130	130	--
Pressure, psia	1,050	--	--	1,050	--	--
Gas-in-place, MMcf/160 acres	4,512	4,912	4,192	5,504	6,064	5,152

Gas volumes expressed at 15.025 psia and 60°F.

A final pressure drawdown for this test series was begun October 28, 1969, and was terminated November 14 with 125 psig BHP. GB-ER is shut in for a long-term pressure-buildup test. Fig. 4 shows data for this test series.

REVIEW OF WORK ON OTHER WELLS

Preshot test well GB-2 was reentered in June 1968. A 6-1/4-inch hole was gas-drilled to 4,600 feet after sidetracking out of a window milled in 7-inch casing at 3,691 feet. Sidetracking was necessary because casing damage at 3,812 feet prevented further progress. Logs were run and the well, GB-2R, was completed with production tubing landed in the uncased hole at 4,224 feet. The open hole apparently collapsed around the bottom of the tubing and sealed it off sufficiently to prevent use of the well for production tests. Production tests that were made during drilling of the sidetracked hole and a flowmeter survey that was run after reaching total depth indicated that productivity had been improved by the detonation; however, very little connection with the chimney was evidenced. BHP of GB-2R versus time is shown in figs. 3 and 4. More detail on reentry of GB-2 is given in ref. 4.

Well No. 10, located 436 feet northwest of GB-ER, was reentered in October 1968. Stemming material was cleaned out of the 5-1/2-inch casing to a 3,612-foot depth (about 300 feet above the top of the Pictured Cliffs gas sand), where damaged casing prevented further penetration. The well then was completed in the Ojo Alamo sand as an aquifer monitor well.

Well GB-3 was drilled in August and September 1969 during GB-ER production testing to investigate changes in the Ojo Alamo and Pictured Cliffs formations and in the underlying shale to a 4,800-foot depth. An extensive coring program together with logs and natural-flow gauges was successful in defining reservoir characteristics, which were similar to preshot conditions in nearby well GB-1 (see Fig. 2 for well locations) except that GB-3 core showed more fractures and was generally more fragmented on removal from the core barrel. Average values of the gas reservoir properties found in GB-3 are listed in table I.

Gas production was first encountered during coring at a 3,871-foot depth immediately above the Pictured Cliffs sand, and the production reached a maximum rate of 54 Mcf/D at a 4,058-foot depth, about the middle of the Pictured Cliffs. The production rate was less than expected and showed a lack of open fracture communication with the chimney, as had GB-2R. After completion, the BHP in GB-3 built up in approximately 1 month to 445 psig, while chimney pressure remained at 256 psig. During the final blowdown of GB-ER to 125 psig BHP, GB-3 BHP declined to 426 psig. No experiment-related radioactivity was detected in GB-3 cores or produced fluids. The well is being used to monitor reservoir pressure.

EVALUATION

In analyzing the behavior of the chimney well, the open-flow potentials (theoretical producing rate at zero psig backpressure) that were indicated from backpressure curves, constructed from data obtained near the end of each constant BHP test, were examined. The open-flow potentials are as follows:

		Approx. open-flow potential, Mcf/D
July 1968:	Short-term test	2,800
Dec. 1968:	End of first 30-day test	930
Jan. 1969:	End of second 30-day test	840
Feb. 1969:	End of third 30-day test	500
July - October 1969:	Last half of 7-month test	170

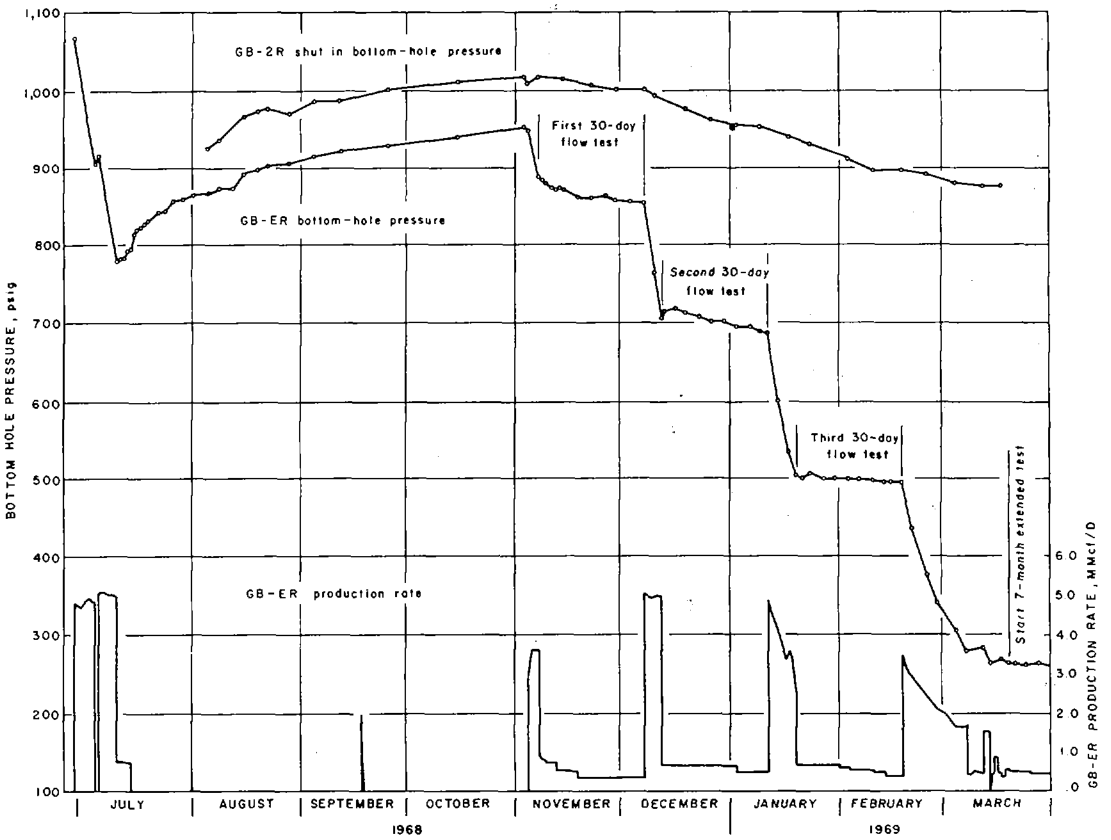

FIGURE 3.- Project Gasbuggy Production Performance, June 1968-March 1969.

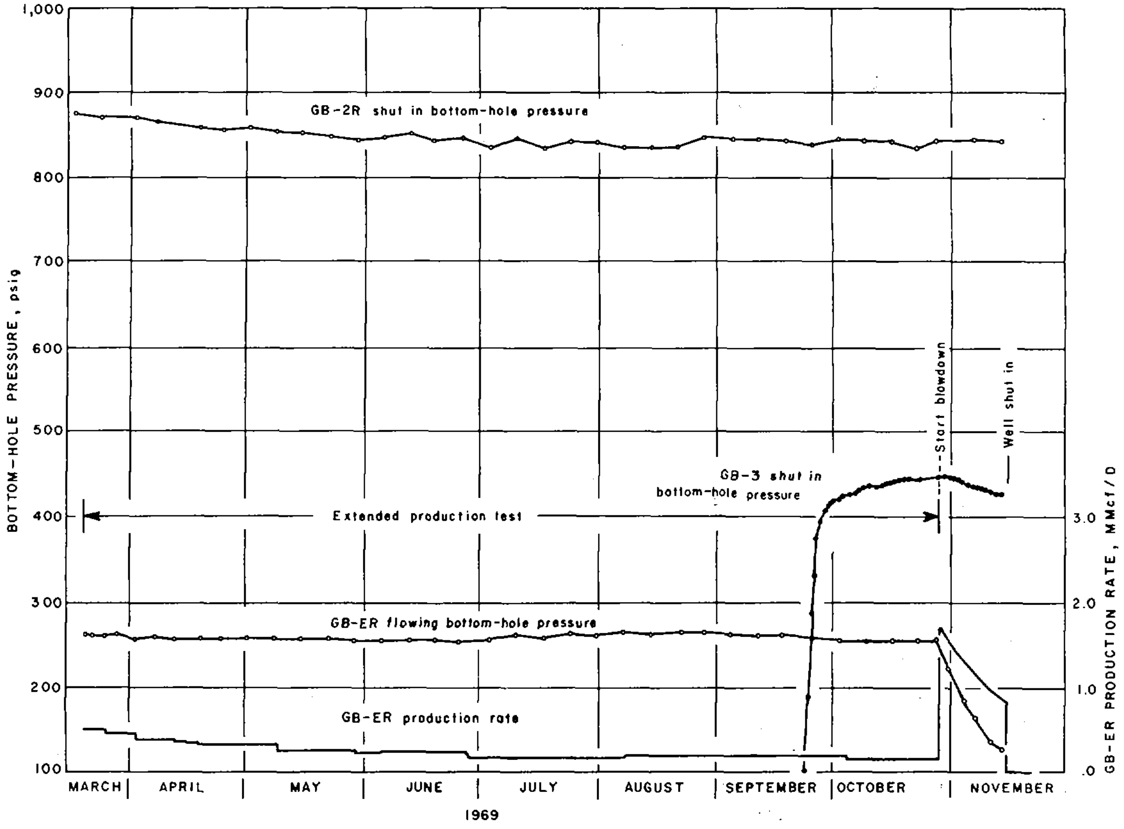

FIGURE 4.- Project Gasbuggy Production Performance, March-November 1969.

The marked decline in open-flow potential makes it clear that short test periods in the early life of a well in this type of reservoir do not reflect true long-term productivity. During the 7-month test, the BHP and production rate were stabilized; consequently production-rate data from that test were considered to be adequate for comparison with preshot productivity data from field wells, which have been producing for about 10 years. Table II gives production history of the original field wells. The GB-ER 160-Mcf/D production rate was obtained with a 232-psig surface backpressure. At a 500-psig surface pressure, which corresponds to the field gas-gathering line pressure, GB-ER should produce 135 Mcf/D. After the initial flush production period, the five field wells nearest the test site produced at an average rate of 11 to 30 Mcf/D. Well No. 10, only 436 feet from GB-ER, produced an average of 22 Mcf/D. Therefore, the Gasbuggy postshot well produces at 6 to 7 times the rate of the average of these five field wells, which were hydraulically fractured when completed. Three field wells, Nos. 2, A-2, and E-1, were not included in the comparison because they are farther from GB-ER; also, natural fracture systems encountered in these three wells gave them much higher productivity than is believed representative of the test area.

In comparing postshot productivity with that of the preshot test wells, the 30-day production tests of GB-1 (4) provided the most reliable data of all the preshot tests. Although 30 days is not enough time to obtain a stabilized producing rate, the 125-Mcf/D open-flow potential for GB-1 indicated at the end of the 30-day test should be comparable with that of GB-ER after producing for an equal time under similar conditions. As previously stated, the open-flow potential of GB-ER after the first 30-day test was 930 Mcf/D, a 7.4-fold increase.

GB-ER has produced approximately 284 MMcf of gas (213 MMcf of hydrocarbons) and, based on preliminary estimates of projected performance, should produce 900 MMcf in 20 years, which would amount to about 19 percent of the gas originally in place under 160 acres (a normal producing unit area for the field). With Well No. 10 having produced 81 MMcf in 10 years, total recovery in 20 years for a well at that location (No. 10 is no longer completed in the Pictured Cliffs sand) can be estimated with fair confidence. The 20-year production for Well No. 10 is estimated at 170 MMcf maximum, which is slightly more than twice the 10-year volume; an anticipated gathering-line pressure reduction would increase producing rates. Therefore, GB-ER is expected to produce at least 5 times the estimated production from a conventionally completed well in the area.

Pressure behavior during blowdown periods of the recent tests confirms the previously determined 2.6-million-cu.-ft. void volume. This volume is equivalent to the void volume of a resultant chimney from a nuclear-created cavity with an 80- to 85-foot radius, depending on volume in fractures emanating from the chimney. As mentioned previously, drillback data from GB-2 and GB-3, both within 300 feet of GB-E, show little increase in productivity and indicate a smaller radius of effective fracturing than was anticipated.

Initially 52 percent of the chimney gas was hydrocarbons, instead of the usual 99 percent in gas from field wells. This decrease resulted from dilution by CO_2 and H_2, which were byproducts of the detonation. As expected, fresh gas entering the chimney has increased the hydrocarbon content by flushing CO_2 and H_2 from the chimney. On November 14, 1969, when GB-ER was shut in, the hydrocarbon content of the produced gas had increased to 88 percent, while radioactivity in the gas had decreased by over a factor of 10 as a result of this chimney flushing. Gas composition was determined during production tests, and table III shows representative analyses at various times.

TABLE II--CHOZA MESA PICTURED CLIFFS FIELD PRODUCTION HISTORY

Well	28-4 No. 6	28-4 No. 7	29-4 No. 2	29-4 No. 4	29-4 No. 10	29-4 No. 16	Indian A-2	Indian E-1
Location, Section-Township-Range	11-28-4	12-28-4	35-29-4	35-29-4	36-29-4	36-29-4	30-29-3	31-29-3
Initial potential, Mcf/D	3,182	1,058	6,928	801	1,348	635	5,709	20,200
Open-flow potential, Mcf/D	---	---	---	---	1,403	647	7,984	---
Annual production, MMcf:								
1955	1.7	4.3	---	---	---	---	---	138.8
1956	11.0	---	144.6	9.2	---	---	---	37.2
1957	---	---	89.3	4.1	2.3	---	---	---
1958	18.6	6.1	84.2	2.6	12.5	---	131.7	63.4
1959	12.1	5.0	60.2	6.0	9.0	5.7	108.9	23.8
1960	12.4	4.3	42.7	4.5	8.2	3.9	68.6	23.3
1961	11.9	4.8	44.9	4.4	8.5	4.3	53.8	8.7
1962	10.3	3.1	39.5	2.9	9.3	3.1	47.7	10.5
1963	10.6	3.9	39.0	2.2	7.5	3.6	32.7	11.7
1964	10.0	4.1	24.2	2.4	6.6	4.2	17.1	5.7
1965	8.1	4.8	33.0	1.7	8.6	3.7	26.3	8.8
1966	5.8	4.1	30.1	2.3	8.4	2.9	34.6	6.7
Cumulative production, 1-1-67, MMcf	112.5	44.5	631.7	42.3	80.9	31.4	521.4	338.6
1966 New Mexico State test, Mcf/D	20	14	112	8	22	4	1/219	27

1/ 1965 test.

TABLE III--GAS COMPOSITION (Mol. Percent) GB-ER

Component	Preshot	Short-term production test, June 1968	Blowdown prior to first 30-day prod. test, Nov. 1968	Blowdown prior to extended prod. test, Feb. 1969	Blowdown at end of extended prod. test, Nov. 1969
Carbon dioxide	0.29	35.60	24.27	16.37	8.89
Hydrogen	--	12.03	10.11	6.38	2.35
Hydrogen sulfide	--	0.11	0.02	0.04	0.02
Nitrogen	0.59	0.51	0.80	0.65	0.54
Methane	85.36	45.45	56.35	65.66	73.24
Ethane	7.40	4.83	5.30	6.03	7.20
Propane	4.00	0.95	1.93	2.86	4.41
I-Butane	0.75	0.19	0.39	0.58	0.86
N-Butane	0.94	0.16	0.41	0.69	1.18
I-Pentane	0.29	0.05	0.12	0.22	0.39
N-Pentane	0.20	0.03	0.08	0.16	0.29
Hexane	0.18	0.09	0.22	0.36	0.63
Heating value (Btu/cu. ft.)	1178	588	790	938	1112
Specific gravity	0.673	0.890	0.808	0.776	0.768

REFERENCES

1. El Paso Natural Gas Co., Atomic Energy Commission, U.S. Bureau of Mines, Lawrence Radiation Laboratory: "Project Gasbuggy (Feasibility Study Report)," PNE 1000 - Clearinghouse for Federal Scientific and Technical Information, National Bureau of Standards, U.S. Department of Commerce, Springfield, Virginia.

2. Ward, Don C., Atkinson, Charles H., and Watkins, J. Wade: "Project Gasbuggy -- A Nuclear Fracturing Experiment," J. Petrol. Technol. (February 1967) 139-145.

3. Atkinson, C. H., and Ward, Don C.: "Project Gasbuggy--Status Report," J. Petrol. Technol. (October 1967) 1319-1324.

4. Ward, Don C., and Lemon, R. F.: "Status of Reservoir Evaluation, Project Gasbuggy," presented at the Annual SPE Fall Meeting, Houston (September 29, 1968). To be available from the Clearinghouse for Federal Scientific and Technical Information, Springfield, Va. (PNE-G-13).

XA04N0862

AN EVALUATION OF WATER PRODUCTION FROM THE GASBUGGY REENTRY WELL

Dean V. Power
Charles R. Bowman

El Paso Natural Gas Company

ABSTRACT

During the gas production testing of the Gasbuggy chimney, water production rates increased from an initial 4 to 5 barrels per 10^6 standard cubic feet of gas to 40 to 50 barrels per 10^6 standard cubic feet of gas. This unexpected occurrence hampered operations and increased waste disposal costs. A model is developed which calculates the amount of water produced from condensation of water vapor through the cooling and expansion of the gas in the production tubing. Results from this model are compared with the observed water production from November of 1968 through May of 1969. This comparison shows that up to seven times more water is being produced at high gas flow rates than can be explained by condensed vapor, indicating that water is being introduced into the production tubing in particulate or liquid form. A correlation of excess water with the pressure, temperature and gas flow velocity parameters is performed to determine the relationship between this excess water and these parameters. It is found that the excess produced water varied linearly with downhole pressure when a threshold gas flow velocity was exceeded. The relationship is expressed by the equation H_2O (in barrels per day) = 126.5 - 0.1473 BHP (in pounds per square inch). The threshold gas velocity for excess water production was found to be about 6 feet per second in the 7" casing or 40 feet per second in the 2 7/8" tubing.

An examination of the radioactivity of the gas and water produced from GB-E indicates that the tritiated water vapor in the chimney and tubing has been diluted by extraneous water. The tritium in the gas decreased as expected from about 10.9 µCi/SCF in November 1968 to 6.2 µCi/SCF in late February 1969. During this same period, the tritium in the water decreased from about 1.2 µCi/ml to 0.12 µCi/ml.

Examination of water chemistry, preshot and during the production testing, indicates that at early times when there was no excess water, the produced water was distilled. At times of high water production, the trace chemical constituents are characteristic of undistilled water from the Ojo Alamo Formation (SO_4 concentrations of about 3000-5000 ppm).

It is concluded that a decrease in the bottom hole pressure of GB-E resulted in Ojo Alamo water entering GB-E and either being produced or flowing down GB-E into the chimney. The water entry rate follows Darcy's Law in that it is proportional to the pressure gradient between the hydrostatic head and the chimney pressure. It is postulated that the water is flowing directly from the Ojo Alamo into GB-E and then flowing downward through the stemming material until it enters the inner casing through a break at 3796 feet, just 3 feet below the bottom of the production tubing.

A calculation of the water volume which could enter the chimney in this manner is less than could be detected by chimney volume measurement techniques presently available.

Hydrologic data shows that the hydrostatic level fluctuation of the Ojo Alamo correlates with chimney pressure and a sink is indicated at or near GB-ER.

Preliminary analyses from data obtained during the test period of October and November 1969 indicate that the leak in GB-ER has been sealed, water production during this period corresponds to the calculated vapor model, water levels have risen to near normal in the Ojo Alamo and tritium levels in produced water have increased to 0.5 μCi/ml.

INTRODUCTION

Gasbuggy was a 26-kiloton nuclear explosion which was detonated underground at a depth of 4240 feet. The event occurred on December 10, 1967 at a site 55 air miles east of Farmington, New Mexico. The purpose of the explosion was to create a chimney of broken rock and induce fractures in the rock beyond the chimney boundary in order to increase the rate of gas production in a gas-bearing formation just above the detonation point.

It was anticipated that the gas produced from this chimney would contain water vapor and perhaps condensed water. The source of this water was expected to be the bound and the free water which existed preshot in the rock which was vaporized, melted, broken and fractured by the explosion.

Initially, the amount of water produced from the chimney through the reentry well was minor. During the November 1968 "blowdown," about 4 to 5 barrels of water per million standard cubic feet of gas was produced. As the program progressed, the water production rate increased. During the blowdown period in February and March of 1969 this rate of water production reached 40 to 50 barrels per million standard cubic feet of gas. Since this water contained tritium, it required special handling which in turn increased safety program and waste disposal costs.

Initially, (during the summer tests in 1968) the tritiated water was put into barrels and shipped to the Nevada Test Site for disposal. A vaporizing unit was fielded prior to November 1968 which could disperse the water vapor safely to the atmosphere.

The increase in water production rate was unexpected and a program was initiated to determine the source of the water and its relationship to the Gasbuggy chimney. A first step in understanding the situation was to develop an appropriate model which could calculate, reasonably well, the amount of water which should be produced under the observed conditions. In this we were fortunate in that the Production Department of El Paso Natural Gas Company had kept very good records of temperatures, pressures, flow rates and liquids production.

MODEL OF WATER PRODUCTION

A schematic diagram of the chimney and reentry well (GB-ER) is shown in Figure 1. Bottom-hole temperature and pressure measurements were made by lowering an instrument package on a wire line through the 2 7/8" tubing to four feet below the packer which was set at 3786 feet. (Measurements at lower levels were not made even though the hole was open to a depth of 3916' because of the fear of not being able to retract the instrument package back into the 2 7/8" tubing.)

The model incorporates the assumption that sufficient water is present in the chimney to maintain a 100% humidity condition in the gas delivered from within the chimney to the bottom of the 2 7/8" tubing. This assumption results in a model which produces the greatest amount of water possible by condensation of vapor within the production tubing. Gas is transported from the cavity through a 7" OD casing to the lower end of a 2 7/8" OD tubing at the observed temperatures and pressures. The volume of gas and total water vapor entering the 2 7/8" OD tubing and the gas velocities in both the 7" casing and 2 7/8" tubing can be calculated as follows:

Gas volume transported per unit time (cubic feet per second) at bottom-hole conditions:

$$V_B = \frac{QT_B P_O}{T_O P_B} Z_B \frac{1}{8.64 \times 10^4}$$

where Q = Flow rate in standard cubic feet/day

T_B = Measured bottom hole temperature (^oR)

T_O = Standard temperature (520^oR)

P_B = Bottom-hole partial gas pressure (psi)

Z_B = Gas compressibility (Ref. 1)

P_O = Standard pressure (14.7 psi)

It should be noted that P_B is a partial gas pressure and not the measured total pressure. The total pressure is the sum of the partial gas pressure and the vapor pressure of water at the bottom-hole temperature.

The average gas velocity in a given diameter conduit is then given by

$$v = V_B/A$$

where A = inside cross section area of the pipe.

The amount of water vapor, W_B entering the 2 7/8" tubing is given by

$$W_B = \int V_B \rho_B \, dt = V_B \rho_B t$$

where t = time in seconds, and
where ρ_B = density of water vapor at a given temperature.

Identical calculations can be made to calculate volume (V_T), velocity (v_T), and water vapor by weight (W_T), at observed tophole conditions. If W_B is greater than W_T, the excess vapor will condense out of the vapor phase into a liquid. If the gas velocity is sufficiently great, this water, in the form of droplets, will be carried up the tubing and collected in the baffle separator at the surface.

The critical gas velocity for a given droplet of water to be carried up the pipe can be determined by using Stokes' Law. Stokes' Law calculates the terminal velocity of a sphere moving in a gravitational field through a viscous media. The equation is

$$v_s = \frac{2 g r^2 (\rho_1 - \rho_2)}{9\eta}$$

where g = 980 cm/sec^2
r = radius of sphere
ρ_1 = density of sphere (gm/cm^3)
ρ_2 = density of viscous media (gm/cm^3)
η = viscosity of viscous media (poises)

Stokes' velocity (v_s) is the relative velocity between the sphere and the viscous media. If the gas or viscous media is moving upward, the absolute velocity of the sphere will be the difference of the two velocities ($v - v_s$). Thus, if the terminal velocity of a sphere of water is greater than the upward gas velocity, the water will fall back into the chimney. If the terminal velocity is less than the gas velocity, the water will be carried up the tubing and into the separator. Figure 2 shows a plot of terminal velocity versus droplet size. (Actually, η is dependent upon both temperature and pressure of the viscous media. For the range involved, however, the effect is small and has been neglected here.)

In actual practice small droplets spend enough time in the pipe to coalesce into bigger drops with resultant higher terminal velocities. As a result, there is a tendency for all or most of the condensed water to return downward to the chimney at low upward gas velocities. As the gas velocity is increased, water droplets and surface film collect in increasing amounts in the tubing causing an effective reduction in tubing diameter and a further increase in gas velocity. As gas velocities approach some critical value, the condensed water is produced to the surface, sometimes as

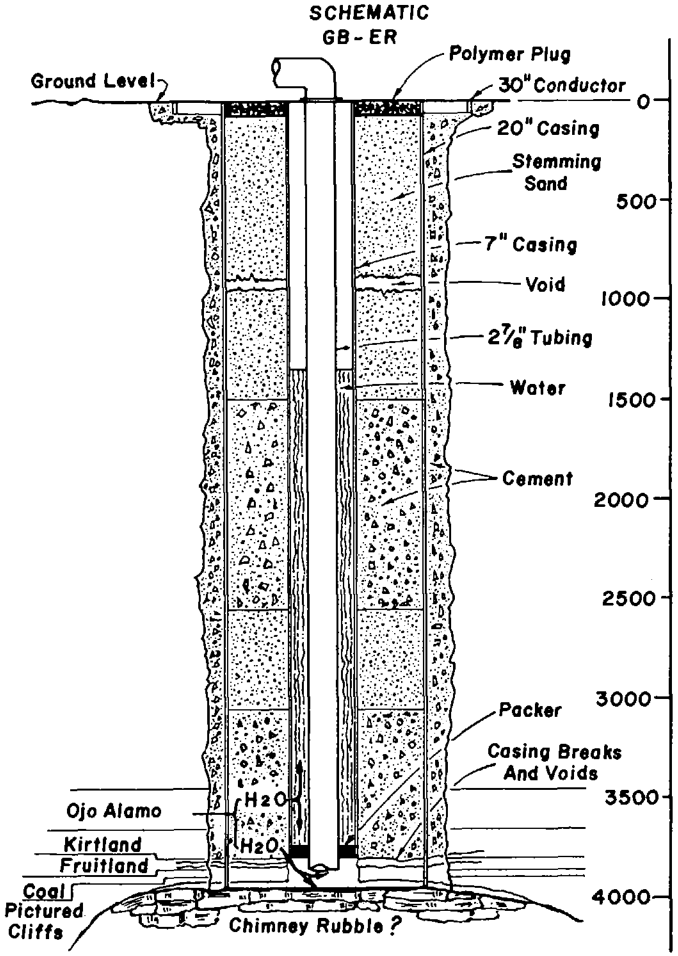

FIGURE 1. Schematic drawing of the Gasbuggy reentry well showing its relationship to the chimney region and geologic formations.

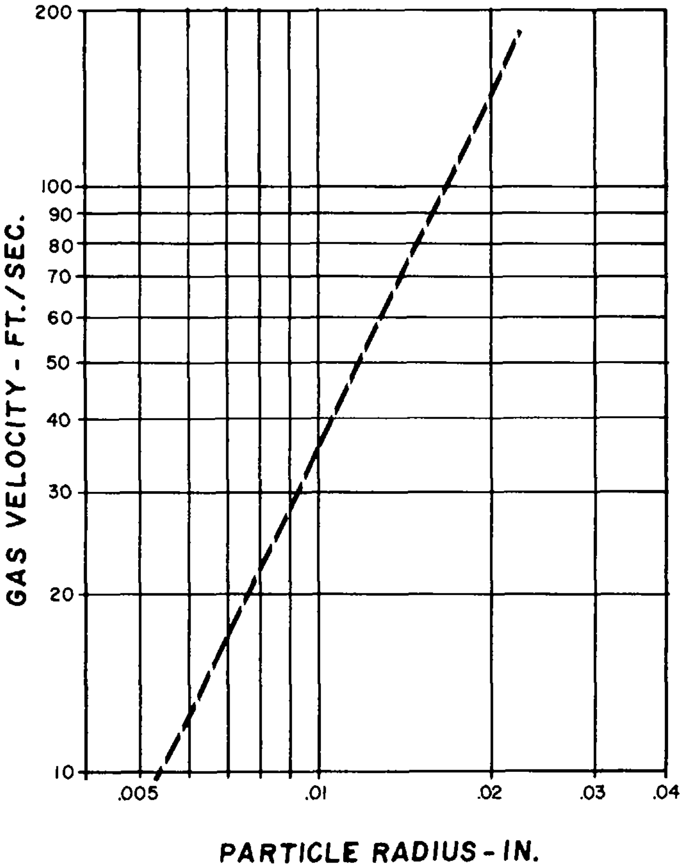

FIGURE 2. A plot of terminal velocity in methane for spherical water droplets as a function of droplet radius according to Stokes' Law.

intermittent slugs. At greater than critical velocities the water is produced at a more uniform rate.

The critical velocity used in the model was set at zero to simplify the calculations. The model, therefore, calculates the maximum water possible from condensed vapor sources and should give high values at low gas production rates. The total water is given by the equation

$$W_P = W_B - W_T$$

where W_P is the difference between the water vapor in the gas at the bottom and the top of the tubing.

COMPARISON OF MODEL WITH EXPERIMENTAL RESULTS

The period for this comparison extends from November 5, 1968 through May 7, 1969. This includes four rapid drawdowns, three thirty-day constant bottom-hole pressure runs and one long-term constant pressure run. (Some preliminary data from a rapid drawdown in October - November of 1969 are discussed briefly in a later section. However, it was too late to include this data in the main analysis.) This test program results in data points which form clusters at the high and low gas velocities. It is unfortunate that there is a paucity of data for intermediate flow rates.

Figure 3 shows the gas flow rate and cumulative gas production for this period. Figure 4 shows the top and bottom-hole temperatures and the corresponding partial gas pressures are shown in Figure 5. These quantities along with Z, T_0 and P_0 were used to calculate the water production which is compared to the measured water production in Figure 6.

It can be seen from Figure 6 that the model matches the data well at early times and at later times during periods of low flow rates. During periods of low flow rates the model predicts some water production whereas none was experienced. This is a result of using a zero value for Stokes' critical velocity in the model, as noted earlier.

It is obvious that during the last two high flow periods, considerably more water was produced than would be expected from the model. During these periods it is calculated that over 90% of the total water entering into the bottom of the tubing in vapor form condenses ($W_P \geq 0.9\ W_B$). Since the observed produced water is from three to over seven times the calculated water vapor during these periods, it must be concluded that quantities of additional water are entering the 2 7/8" tubing in droplet or liquid form.

In an effort to explain and locate this source of additional water, several correlations were performed.

EXCESS WATER CORRELATED WITH GAS PARAMETERS

Gas velocities in the well were calculated for several points

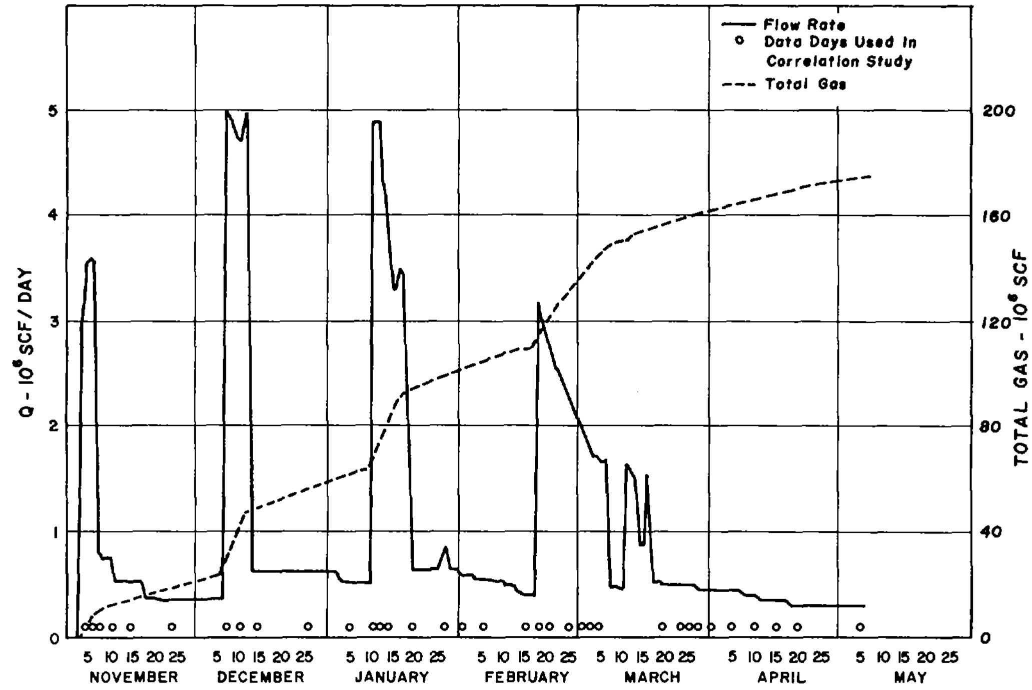

FIGURE 3. Gas production history and cumulative total gas for the Gasbuggy reentry well. The circles indicate those days which were used to perform the correlation study.

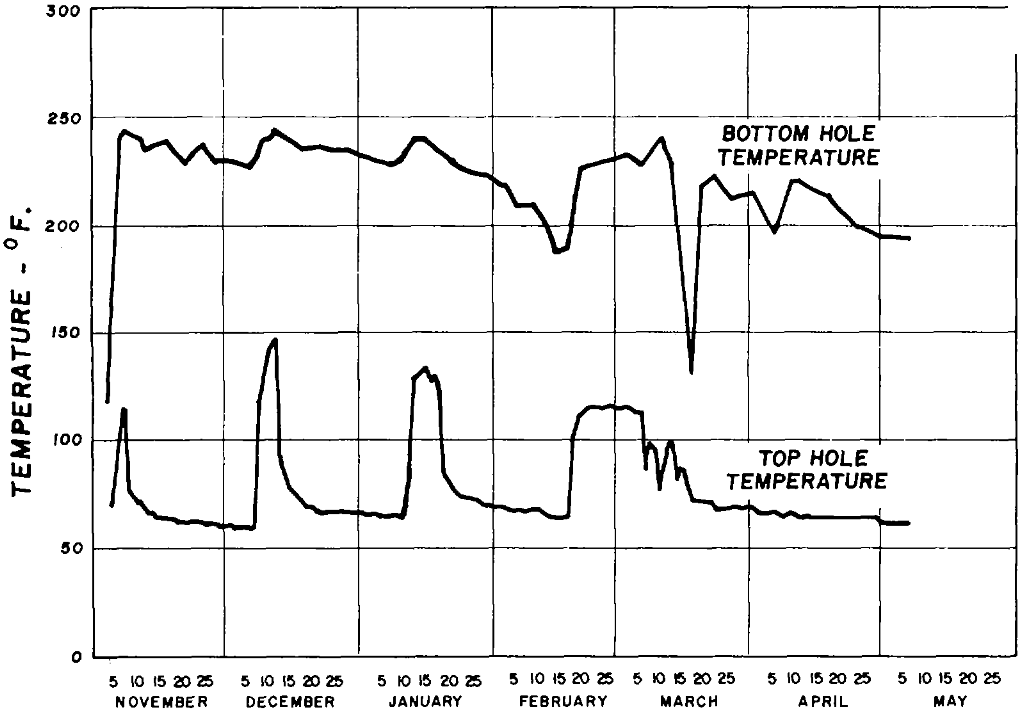

FIGURE 4. Temperature history in GB-ER at 2 points: top hole (surface) and bottom hole (in the 2 7/8" tubing at a depth of 3790 feet).

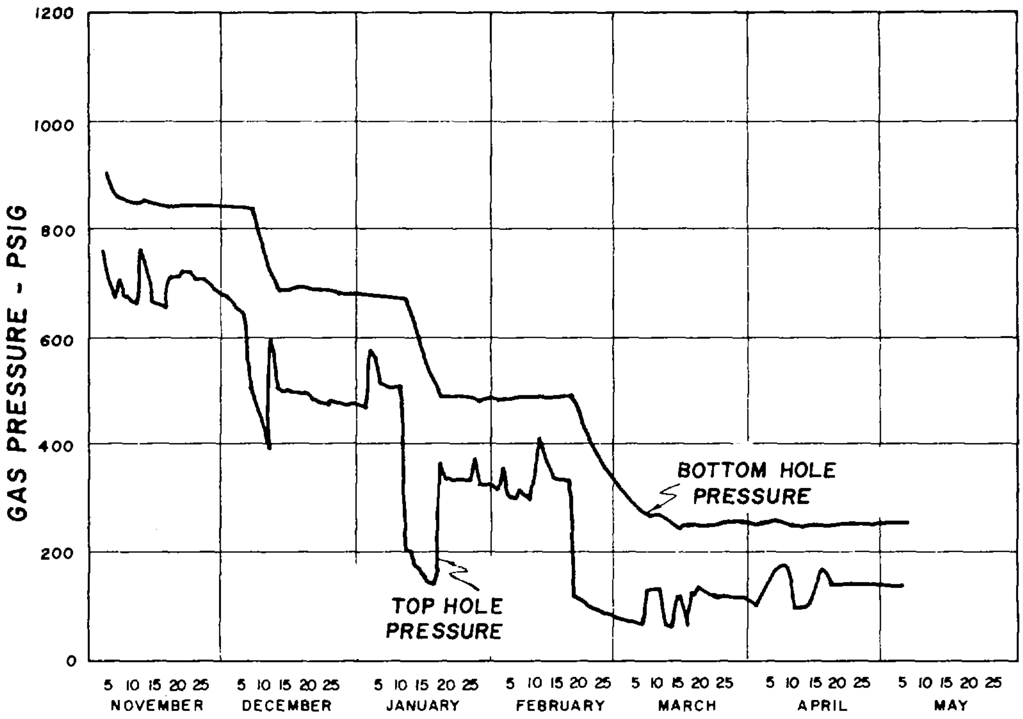

FIGURE 5. Gas partical pressure history for GB-ER at two points: top hole (surface) and bottom hole (in the 2 7/8" tubing at a depth of 3790 feet).

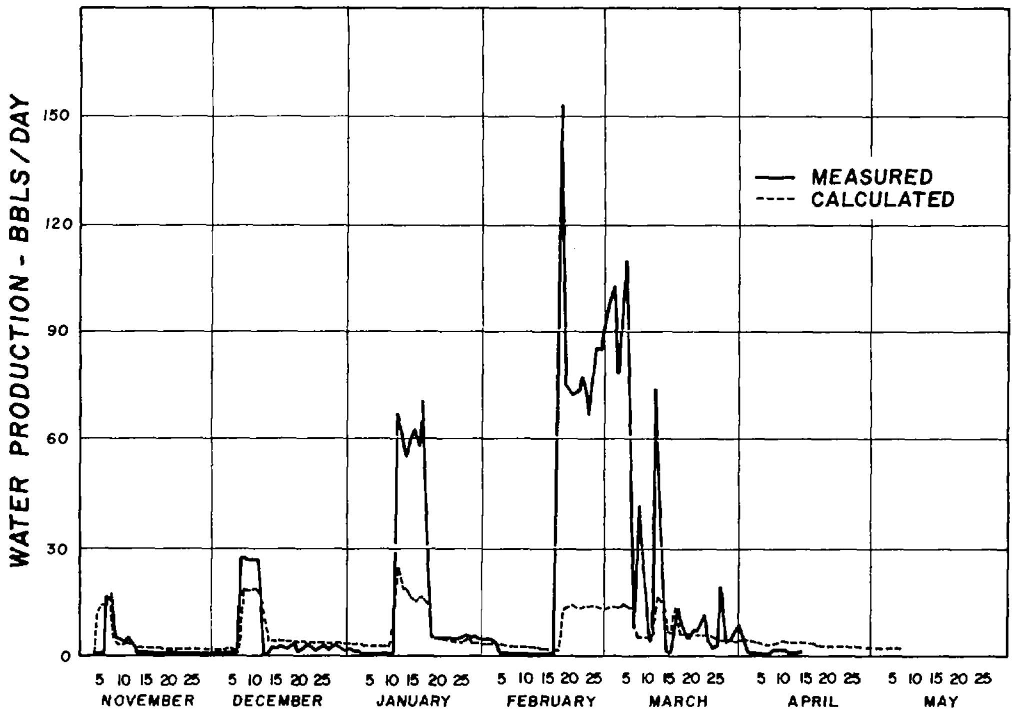

FIGURE 6. Observed and calculated water production for GB-ER.

in the tubing and casing. The values calculated for the top and bottom of the 2 7/8" OD tubing are shown in Figure 7. (Velocities calculated for the 7" casing are not shown.) The model does not allow for frictional forces or a closure of the tubing due to the condensed liquid film adhering to the inner walls; hence, these calculated average velocities should not be greater than the actual gas velocities in the well bore. In fact, they are probably considerably less.

In order to do a correlation on the available data, it was necessary to select time intervals of one day. This interval was necessary because water production records were kept only on a daily basis. Data points were selected such that each drawdown and long-term test was represented by at least two and no more than five data points except for the period of April to May. An attempt was made to limit data points to days when no changes in conditions or flow rates occurred. The data points selected for the correlation studies consisted of the 35 points shown as dots in Figure 3. The correlation study was performed using the graphical regression analysis described by Ezekiel (Ref. 3).

Since the water produced from GB-ER is apparently only partly due to water vapor in the gas, the first step in determining the other source or sources of water is to calculate the excess water. This residual or excess water can be easily obtained from Figure 6 since it is simply the difference between the calculated and the measured water. This method results in a negative excess water for some days as a result of the zero critical velocity in the model, which has already been discussed. This is not a serious problem since these negative values are never very large.

The residual or excess water is then correlated with the various parameters of temperature, pressure and velocity. In Figure 8, residual water is plotted as a function of the velocity at the lower end of the 2 7/8" OD tubing. This Figure indicates that there is a probable cut-off at about 40 ft/sec below which the gas has insufficient velocity to carry the excess water up the 2 7/8" tubing.

A good linear correlation was found between excess water and total bottom-hole pressure. This is shown in Figure 9. The concept of a critical velocity is very apparent in Figure 9 where the data points fall into two distinct groups, those which cluster about the abscissa and those which cluster about the line,

$$H_2O_{Res} = 126.5 - 0.1473\ BHP_{Total}.$$

This linear relationship between excess water and pressure strongly suggests Darcy flow where the volumetric flow across a given surface is proportional to the pressure difference. If we were to assume the excess water were coming from a source of constant hydrostatic head, the available excess water would be proportional to bottom-hole pressure. This can be seen by the following form of Darcy's Law:

$$Q = \frac{k}{\eta} \nabla P = \frac{k}{\eta} (P_H - BHP)$$

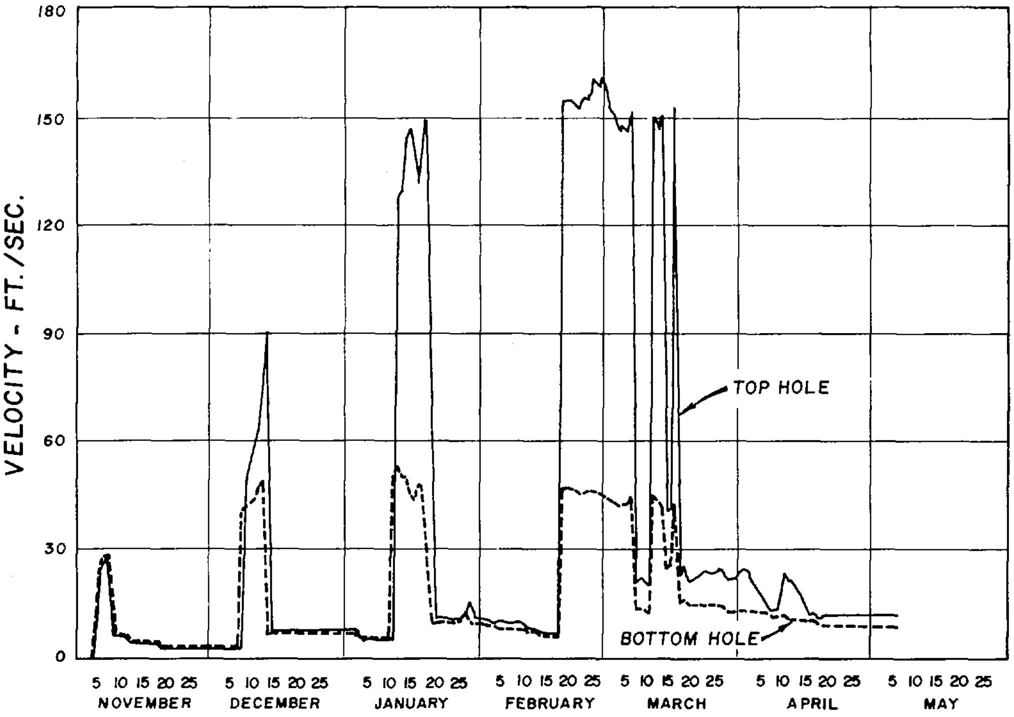

FIGURE 7. Calculated average gas velocities at two points in the 2 7/8" tubing in GB-ER: Top hole (surface) and bottom hole (at a depth of 3790 feet).

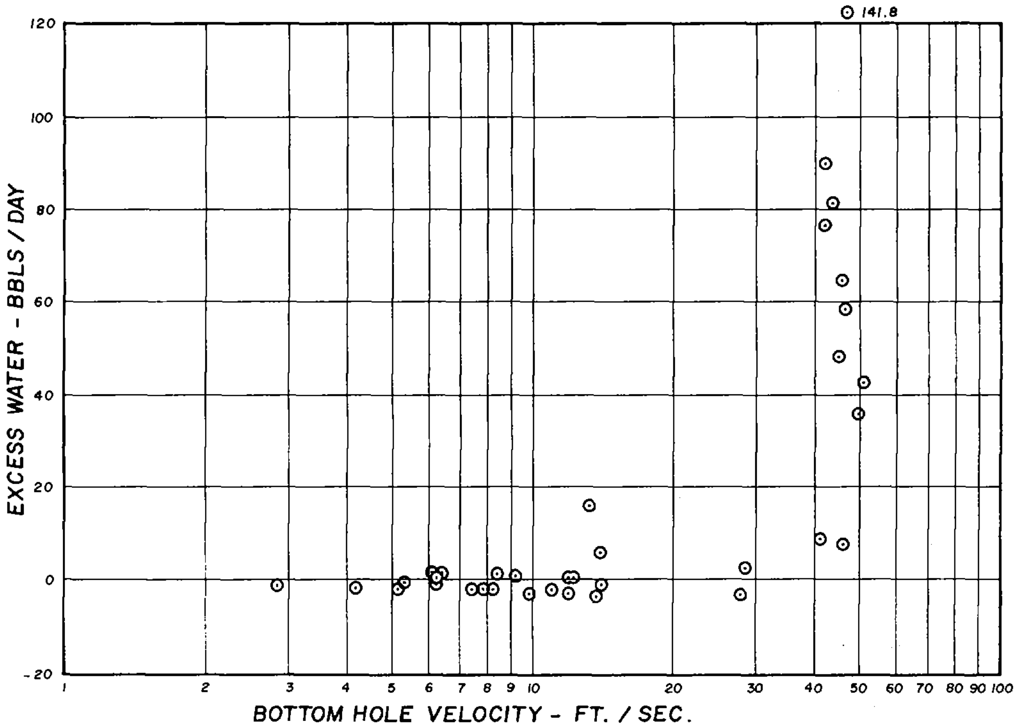

FIGURE 8. Correlation of excess water from GB-ER with bottom hole gas velocity. It appears that little or no excess water is produced below a velocity of 40'/sec.

If k (permeability), η (viscosity) and P_H (hydrostatic head) are constant, then

$$Q = A - B\ (BHP)$$

where A and B are constants.

The residual or excess water is also shown as a function of top-hole pressure in Figure 10. Clearly this does not result in a linear relationship. Similar plots using the pressure at various depths within the well bore would yield a family of curves ranging between those shown in Figures 9 and 10. Because of the excellent correlation between the data and a linear relationship to bottom-hole pressure, it is most likely that the excess water is entering the well bore near the bottom of the 2 7/8" tubing. This is consistent with what was found during drill-back through the 7" OD casing when it was noted that the cement in the emplacement hole was wet below a depth of 3029 feet and casing breaks were detected at 3796 feet and lower in the 7" casing (Ref. 4).

The most probable source of water is the aquifer in the Ojo Alamo Formation. However, since production is through the 2 7/8" tubing and a packer is set at 3786 feet, the water would have to be entering the gas stream either through the joints in the 2 7/8" tubing or through the bottom opening of the tubing which extends through the packer to 3793 feet. The measurements which put the bottom of the tubing at 3793 feet and the casing break at 3796 feet are close enough (considering the degree of accuracy involved) to suggest that the excess water is probably entering at this point.

Borehole photographs of the well bore (Ref. 4, Figure 5) indicate that just after drill back, considerable water was present in droplets and adhering to the side of the 7" casing in a uniform manner at a depth of 3828 feet. It is possible that water is being sprayed through the casing break and into the 7" casing just below the packer where it is either caught directly into the gas stream entering the 2 7/8" tubing or it is collecting on the surface of the 2 7/8" tubing and running down to the lip where it is then drawn into the production tubing.

Assuming that all hole surveys are accurate to within one foot, it appears most reasonable that water is entering the 7" casing just below the 2 7/8" tubing in such a manner that at that point the water is in the form of a fine mist. If this mist were close enough to the bottom of the tubing, the critical Stokes' velocity that would apply would be the 40 ft/sec threshold value from Figure 8. This would mean that all or most of the droplets must be less than .01" in radius. If we use the velocity in the 7" casing (6 ft/sec), we must conclude that the droplets are less than .004" in radius. The conclusion that six feet per second is the critical velocity is supported by the fact that when the gas velocity in the 2 7/8" tubing drops to less than ten feet per second, no water is produced at all and even condensed water vapor returns to the chimney.

If we assume that water is seeping into GB-ER and is either being produced or, at low flow rates, is entering the chimney, we can use Figures 5 and 9 to calculate the total influx of water into GB-ER. This is shown in Figure 11. Between November 4, 1968 and October 25, 1969, about 25,000 barrels of water are estimated to

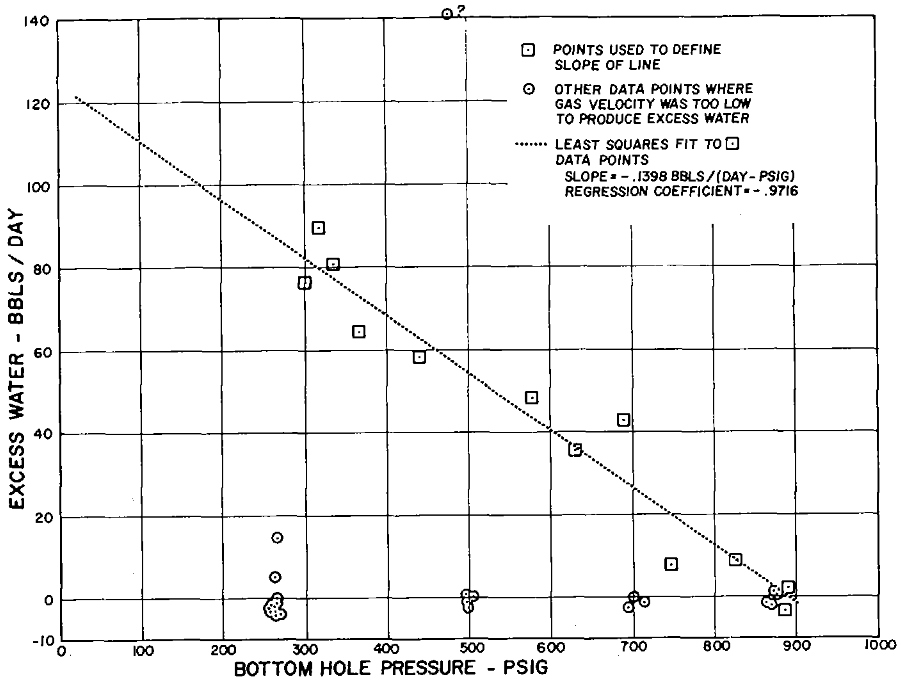

FIGURE 9. Correlation of excess water produced from GB-ER with chimney (bottom hole) gas partial pressure. The squares are data points for which gas velocities exceeded 40'/sec with the 3 following exceptions: The two squares at the extreme right are at velocities of about 28'/sec and are the only points which exist between 15'/sec and 40'/sec (the exclusion of these points does not change the slope of the line) and datum point marked by a (?) at the top center of the Figure. The validity of this point is questionable since it occurs at the start of a "blowdown" and may reflect some peculiarity in the data collection and analysis.

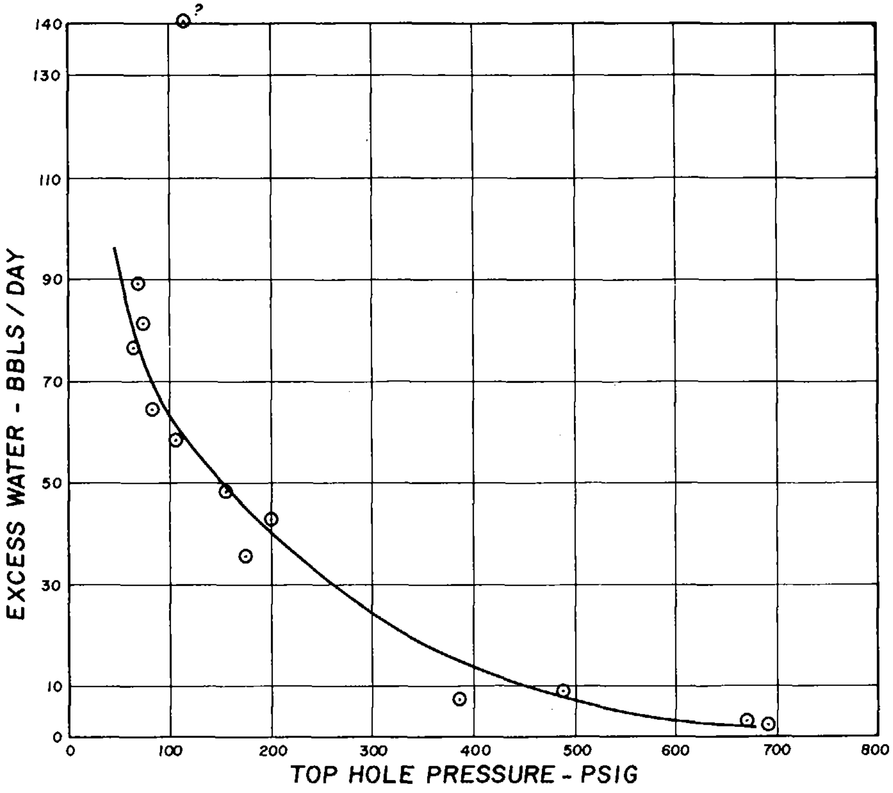

FIGURE 10. Correlation of excess water production with top-hole pressure. The only points shown are those for which gas velocity exceeded 15'/sec. The relationship is nonlinear and hence it is doubtful that a positive correlation can be deduced.

have entered GB-ER. After subtracting the water which was produced at the surface, we find that about 125,000 cubic feet of water has entered the chimney. This volume change is just at the level of detectibility using the present volumetric measurement methods available to us. No volume change greater than this limit of accuracy has been observed and it can be concluded that no more than about 125,000 cubic feet of water has entered the chimney during this time. Thus, it is unlikely that water is entering the chimney through any other path.

WATER RADIOACTIVITY

Radioactivity in the produced water further indicates a dilution of the chimney water. Liquid samples containing water from the cavity gas have been extracted by dehydration and particulate removal at the wellhead complex. These samples have been analyzed for both chemical composition and tritium radioactivity (HTO) since the inception of the first flow tests in late June 1968. Figure 12 presents the radioactivity concentration in the produced water. Liquid scintillation measurements were made by LRL (Ref. 5) and Eberline Instruments (Ref. 6). The concentration of early tritium radioactivity appears relatively constant slightly above 1.0 µCi/ml through December 1968. During the drawdown for the second thirty-day test in mid-January 1969, a sharp decline in the water radioactivity occurred. From February 1969 until October 1969 the concentrations remained consistently below about .2 µCi/ml, declining gradually to a level of about .05 µCi/ml. This sudden and large change in radioactivity at all flow rates seems to indicate a dilution in either or both the chimney vapor and produced water.

A very interesting sidelight is the fact that it is difficult to account for the total tritium. If one were to assume uniform mixing in the cavity water, then the initial radioactivity concentration of about 1.2 µCi/ml combined with the assumption that about 90% of the initial four gms. of tritium went into the water (only about 10% can be accounted for in the gas) would require that the chimney contain something like 800,000 cubic feet of water. This is roughly one-third of the calculated void volume of the Gasbuggy cavity! In order to get a concentration of < .1 µCi/ml, many times the cavity void volume of water would be required.

Two questions are emphasized by the foregoing considerations:

1) What happened to the tritium?

2) Why the order of magnitude decrease in water radioactivity during January of 1969?

It is possible (a) a considerable fraction of the tritium was trapped at early time in the melt; (b) a considerable fraction of tritium exists in a form which is bound chemically with rocks in the cavity; or (c) an isolated tritium-rich water pool exists somewhere in the cavity. It may be possible for tritium in these forms to exchange with circulating gas or free liquids containing hydrogen. No indication that such an exchange establishes a base level tritium concentration for the gas has been observed to date.

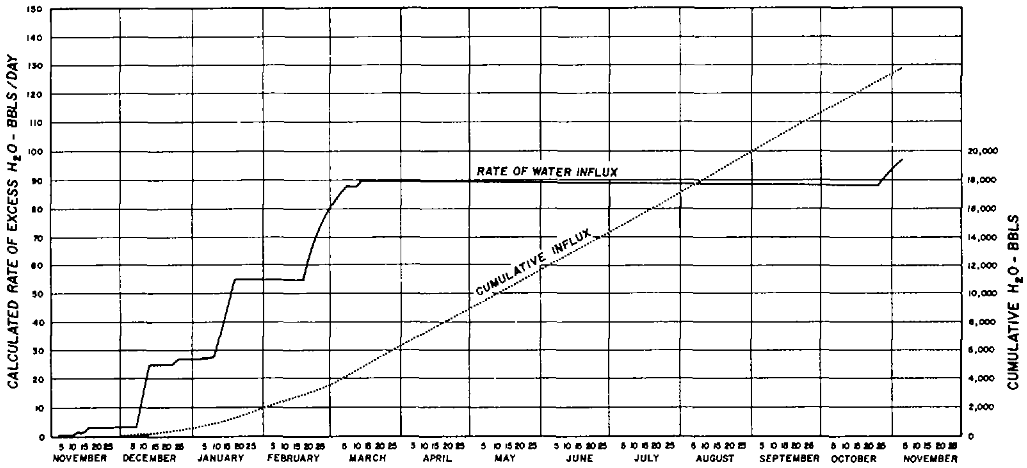

FIGURE 11. Rate of water influx into GB-ER with the chimney and cumulative water history. Net influx would be the amount shown less the excess water produced from GB-ER.

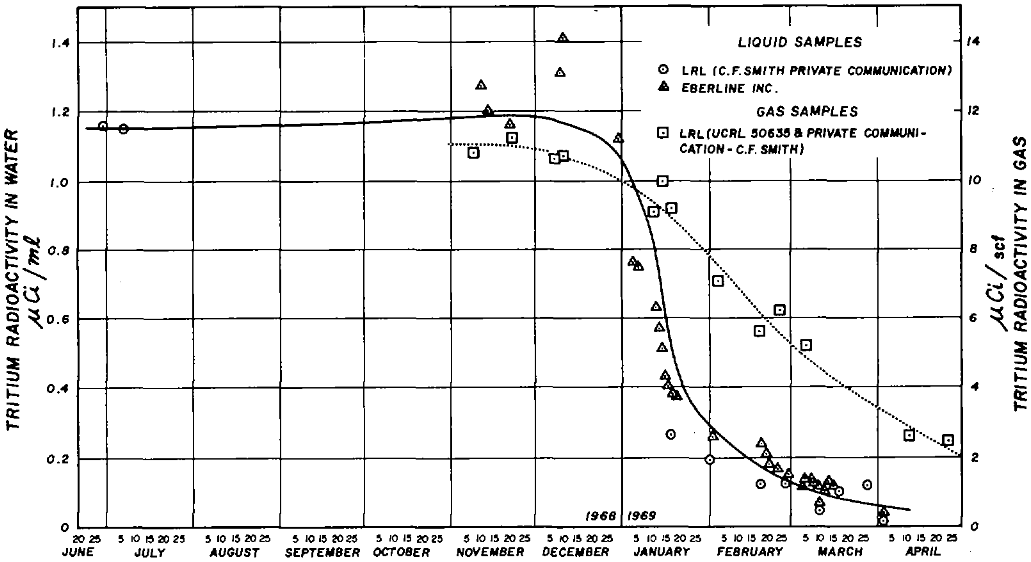

FIGURE 12. Tritium radioactivity in water and gas produced from GB-ER.

The decrease in radioactive concentration since January could have resulted from dilution by water from outside the cavity environment. Two possible sources of water suggest themselves:

1) water from Ojo Alamo, and

2) water from Pictured Cliffs.

CHEMICAL COMPOSITION

The top of the Gasbuggy chimney occurs at 3906 feet. This is very near to the boundary between the Pictured Cliffs sandstone and the Fruitland coal. The Ojo Alamo sandstone aquifer occurs some 200-250 feet above the top of the chimney. Chemical composition analyses of water samples taken from the Ojo Alamo Formation and the Pictured Cliffs Formation are depicted in Table I. This table shows the characterization of water by formation association in a rather straightforward way by sulfate or chloride content. One can characterize Pictured Cliffs water as having high chloride content and relatively low sulfate content, contrasted with the Ojo Alamo water which has high sulfate and relatively low chloride.

Table I

Water Chemical Composition

Location	Sample	Date	Cl ppm.	SO_4 ppm.
Ojo Alamo Formation				
3450'	GB	Nov. 2, 1967	140	3580
3539	GB	Nov. 2, 1967	120	3700
3650'	GB	Nov. 2, 1967	130	3340
3636'	GB-1	Mar. 1, 1967	170	5470
3696	GB-1	Mar. 1, 1967	170	5470
3505'	GB-ER	Jan. 12, 1968	280	4330
Pictured Cliffs Formation				
3920	GB-2	May 1, 1967	5320	480
Indian E-1	Well	May 5, 1967	3700	0
Feasel #2	Well	Feb. 8, 1968	12,100	0

With the exception of the reentry sample from GB-ER and Feasel #2, all samples shown in Table I were taken preshot from their respective formations. Feasel #2 is the only well listed which is not in the immediate area of the GB-E well; i.e., within a three-mile radius. It does not appear that water chemical composition changes will occur in samples taken from the same formation at this distance (three miles) in the absence of a geologic anomaly.

Table II shows the results of chemical analyses on water produced from GB-ER. Analyses of the data in Table II strongly indicate the presence of Ojo Alamo water in the produced gas postshot. Samples taken on November 7, 1968 and between December 14, 1968 and December 30, 1968 are strongly indicative of distilled water. During the high flow rate periods and continuously after

January 11, 1969, the water produced from GB-ER shows chemical composition very similar to the Ojo Alamo water. The concentration of ions during these periods is so high as to indicate this water has not passed through the vapor state since it left the aquifer. At no time has water been detected postshot in the produced water which has characteristic Pictured Cliffs chemical composition. This, of course, does not preclude the possibility that Pictured Cliffs water is entering the chimney at lower depths where gas velocities are insufficient to carry the liquids into the production tubing.

Table II

Date	Cl ppm	SO_4 ppm
11/ 7/68	20	82
11/10	190	1620
11/12	140	2095
11/14	185	2135
11/16	170	2180
11/18	144	2220
11/20	135	2160
11/24	310	550
11/26	200	2160
11/29	135	2180
12/ 1	140	2200
12/ 3	80	2240
12/ 7	32	158
12/ 8	28	267
12/10	8	178
12/11	40	257
12/12	40	247
12/14	16	0
12/16	20	0
12/18	4	59
12/20	16	0
12/22	20	0
12/24	20	0
12/26	48	0
12/28	20	0
12/30	6	0
1 /11/69	148	2372
1 /12	168	2866
1 /13	140	3222
1 /14	184	3360
1 /15	208	3560
1 /16	212	3140
1/17/69	216	3500
1/23	10	583
1/25	14	208
1/29	16	208
2/18	160	2945
2/19	220	3200
2/20	240	4033
2/21	220	3993
2/22	240	3934
2/24	280	3380
2/25	248	3875
2/26	232	3855
2/27	252	3555
2/28	248	3695
3/ 1	248	3890
3/ 2	256	3500
3/ 3	264	3830
3/ 4	264	4360
3/ 5	276	4690
3/ 6	285	4690
3/ 7	268	4550
3/ 8	275	4740
3/10	264	4600
3/12	84	3260
3/13	264	4640
3/15	285	4520
3/17	255	4395
3/19	285	3980
3/21	48	1150
3/24	225	3090
3/27	28	820
4/ 2	320	3260
4/24	225	3090

HYDROSTATIC LEVEL OBSERVATIONS

If water from the Ojo Alamo Formation were entering GB-ER, the hydrostatic level in this aquifer should reflect this by showing an appropriate fluctuation. Good level measurements were obtained during the entire program in the nearby well designated as San Juan 29-4 Unit Well #10, which is about 420 feet from GB-ER. In addition, several observations were made in the 7" casing in

GB-ER beginning in March of 1969 and a single data point was taken in GB-3 in September 1969 (Ref. 7). GB-3 is located about 200 feet from GB-ER at the Ojo Alamo Formation depth of 3550 feet.

Figure 13 shows the hydrostatic level history in all three locations. The level in 29-4 #10 well shows a distinct response to the decreases in chimney pressure and suggests a "sink" somewhere in the vicinity. It was not until March of 1969 that a measurement was accomplished in the GB-ER annulus which verified the existence of a sink. The observation in GB-3 appears to indicate (when combined with other observations) that GB-ER is at or near the center of the sink.

LATER RESULTS

On October 28, 1969 a drawdown was started to lower the chimney pressure to about 125 psig. This was completed on November 14, 1969 and GB-ER was then shut in for pressure buildup studies. Because of the time limitation in getting this paper to the publisher, it was impossible to include data from this late period in the graphs and figures. However, we can report the following preliminary results.

1) Chimney volume measurements during the October 28 to November 14 period show no decrease in chimney volume greater than the uncertainty in the calculations (10^5 cubic feet).

2) Water production during this period corresponds to that which would result from condensed vapor alone; i.e., no excess water was observed. This in spite of the fact that calculated gas velocities were greater than critical.

3) Tritium in water increased from 0.1 μCi/ml to roughly 0.5 μCi/ml during the first few days of production and remained at that level for the rest of the period. (Ref. 8)

4) During this seventeen-day period, the water level in 29-4 #10 rose from 1021' to 976'. Correspondingly, the water level in GB-ER was at 1225' on October 28 and rose to about 1010' or 1020'.

All of this indicates that the leak has been sealed during this last test period. An examination of the history of 29-4 #10 shows that a partial sealing of the leak may have occurred in mid-April 1969.

CONCLUSIONS

The production of water during the period of November 1968 to May of 1969 from GB-ER exceeded that which could be expected from condensed vapor entrained in the gas flow. Radioactivity levels of the produced water indicated a high dilution from an extraneous source. Chemical analyses of this water and hydrostatic level observations support the proposition that the source of the

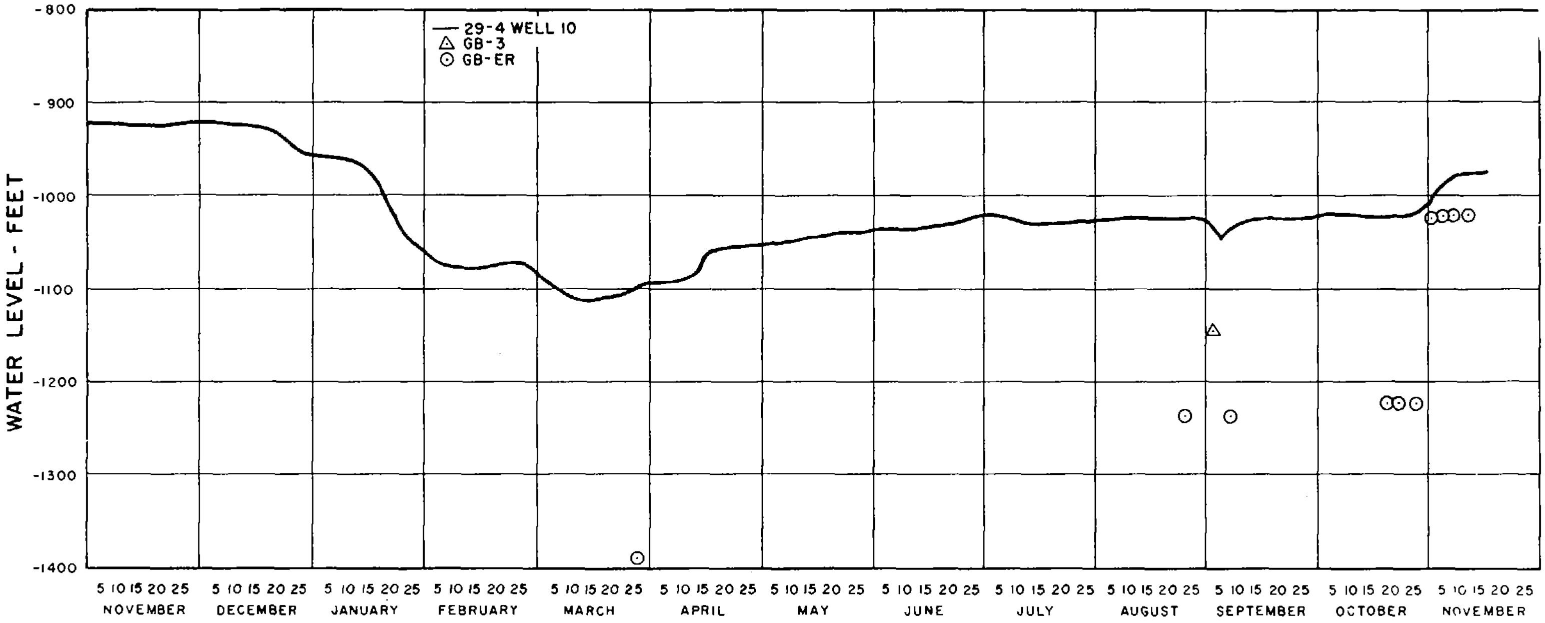

FIGURE 13. Ojo Alamo Formation hydrostatic level histories at and near GB-ER.

extraneous water is the Ojo Alamo Aquifer. The hydrostatic level and chimney volume measurements support the thesis that the "sink" is at or near GB-ER. In view of the difficulties encountered during cementing operations on the lower portion of GB-E, it is not surprising that there was a leak into the chimney area through the stemming materials in this hole. It now appears that the leak has been plugged by some obscure process although the permanency of this plug is not assured.

It is important to realize that the device explosion did not alter the region such that the chimney region was flooded by massive quantities of water from the overlying aquifer and the leak in GB-ER should be regarded as an exception due to the difficulties which were encountered in cementing the emplacement hole at the depth of the Ojo Alamo Formation

ACKNOWLEDGEMENT

Project Gasbuggy is a joint effort under the U. S. Atomic Energy Commission's Plowshare Program by El Paso Natural Gas Company, the Bureau of Mines of the U. S. Department of the Interior, and the Atomic Energy Commission with technical assistance provided by Lawrence Radiation Laboratory, Livermore, California.

The authors gratefully acknowledge the invaluable assistance rendered by the personnel of El Paso Natural Gas Company's Production Department, Farmington Region, in gathering and processing the majority of the data upon which this work is based. Particularly noteworthy were the efforts of H. L. Kendrick, H. E. McAnally, R. E. Stauffer, and F. W. Sattler.

REFERENCES

1. Stone and Webster Engineering Corporation, "Report on Gas Storage at the Point of Use." American Gas Association, Inc.; Revised, 1965.
2. Chemical Rubber Publishing Company, Handbook of Chemistry and Physics, 37th Edition, pp. 2260-2271. Cleveland, Ohio.
3. Ezekiel, Mordecai, Methods of Correlation Analysis, Chapter 15 and Appendix 1. New York: John Wiley & Sons; 1956.
4. Korver, J. A. and D. E. Rawson, Gasbuggy Postshot Investigation in GB-ER, UCRL-50425. Livermore, California: Lawrence Radiation Laboratory; April 19, 1968.
5. Personal Communication, Charles Smith, Lawrence Radiation Laboratory, Livermore, California.
6. To be published.
7. Personal Communication, John Korver, Lawrence Radiation Laboratory, Livermore, California.
8. Personal Communication, Richard Powell, Eberline Instrument Corporation, Santa Fe, New Mexico.

PROJECT RULISON

Film Presentation

R. H. Campbell
Los Alamos Scientific Laboratory

XA04N0863

Studies of Radioactivity from Nuclear Explosions for Peaceful Purposes

R. A. Siddons

(AWRE, Aldermaston, UK)

Summary

Estimates are made of the extent and duration of hazards from radioactivity to the general public due to fallout from a cratering explosion. The nuclear explosive is assumed to be "clean" in the sense that only a small fraction of the yield is derived from fission. Hypothetical examples take an explosive of total yield 100 kT, of which 10 kT, 1 kT and zero - the ultimate in cleanliness - are derived from fission. The maximum permitted level to the public is taken as 0.5 rem in a period of one year.

Sources of activity considered are fission products, residual thermonuclear material (tritium), neutron induced activity in the device materials and neutron induced activity in the surrounding rock. Estimates of the production are made, and are associated with a distribution function derived from the Sedan fallout measurements.

The hazards from radioactivity associated with the creation of a storage reservoir for natural gas have also been considered. In this case the main problem is contamination of the product by tritium left in the chimney. The possibility of flushing out this tritium with water is discussed.

I. INTRODUCTION

Two possible applications of nuclear explosives for peaceful purposes, posing different problems in regard to radioactivity, have been considered in Parts II and III of this paper. They are a cratering shot of yield 100 kT which might be used, for example, to create a water reservoir or part of a harbour, and a deeply buried contained shot of yield 25 kT which could be used to create storage for natural gas or oil.

These studies are entirely theoretical. They depend heavily on published data obtained from US Plowshare Program reports.

II. CRATERING EXPLOSION

1. Model

A 100 kT explosion at optimum depth for cratering is considered. Project Sedan {1} of July 1962 is a practical example, in which a 100 kT device was emplaced at 635 ft depth in alluvium and produced a crater of radius 608 ft and maximum depth 323 ft. The crater volume was about 6.6 million cubic yards corresponding to the removal of about 8.4 million tons of material. The radioactive fallout pattern of Sedan is well documented and it is used here to define a typical distribution function in a way which will be described later on.

There are important differences between the hazards from dynamic effects and radioactivity. Dynamic effects - air blast and ground shock (or seismic disturbance) - are effectively instantaneous and may cause damage to property. On the other hand, radioactivity can persist for a long time and may put the public health at risk. But, whereas dynamic effects are a direct consequence of the force of the explosion, and cannot be greatly changed for a given yield, radioactivity is really incidental to the purpose of the explosion and can be reduced by technological skill.

The obvious method of reducing the radioactivity produced by a nuclear explosion is to reduce the fission yield. Sedan, for example, produced less than 30% of its yield from fission. To explore this aspect we shall consider three hypothetical examples each of 100 kT total yield but including 10 kT, 1 kT and zero fission yield.

Most of the yield in "clean" devices must be obtained from fusion, a typical reaction being that between tritium and deuterium

$$T + D = {}^{4}He + n + 17.6 \text{ MeV}$$

The reacting particles must have high energies if the reaction is to proceed with sufficient speed. The neutrons produced (1.45×10^{24} per kT of fusion yield) are ultimately captured by nuclei in the environment, either in the device itself or surrounding rock. They might be used to manufacture the tritium from ^{6}Li, viz,

$${}^{6}Li + n = {}^{4}He + T + 4.7 \text{ MeV}$$

so creating a reaction cycle. The function of the fission trigger is to create the conditions needed to start the cycle.

A basic model explosive could therefore comprise a fission trigger, a mass of ^{6}LiD, and a container of heavy material to restrain the expansion of the reacting material. Lead would be a suitable container material as its neutron activation cross section are small and the radioactive products decay quite quickly. A possible alternative is tungsten.

2.- Amounts of Activity Produced

Four different sources of activity produced in the explosion are considered. These are fission products, residual materials from the nuclear explosive, neutron induced activity in inert device materials and neutron induced activity in the surrounding rock.

2.1 Fission Products

The activity produced is directly proportional to the fission yield. Beta and gamma energy emission rates from the fission products are well known as a function of time after fission {2} and the data for 1 kT of fission products are shown in Figures 1 and 2. A general measure of the relative fallout level is the energy emission from 1 hour to infinite time, assuming a continuous exposure beginning at 1 hour. Variations in the commencement of exposure will be considered later. The actual fallout source is found by

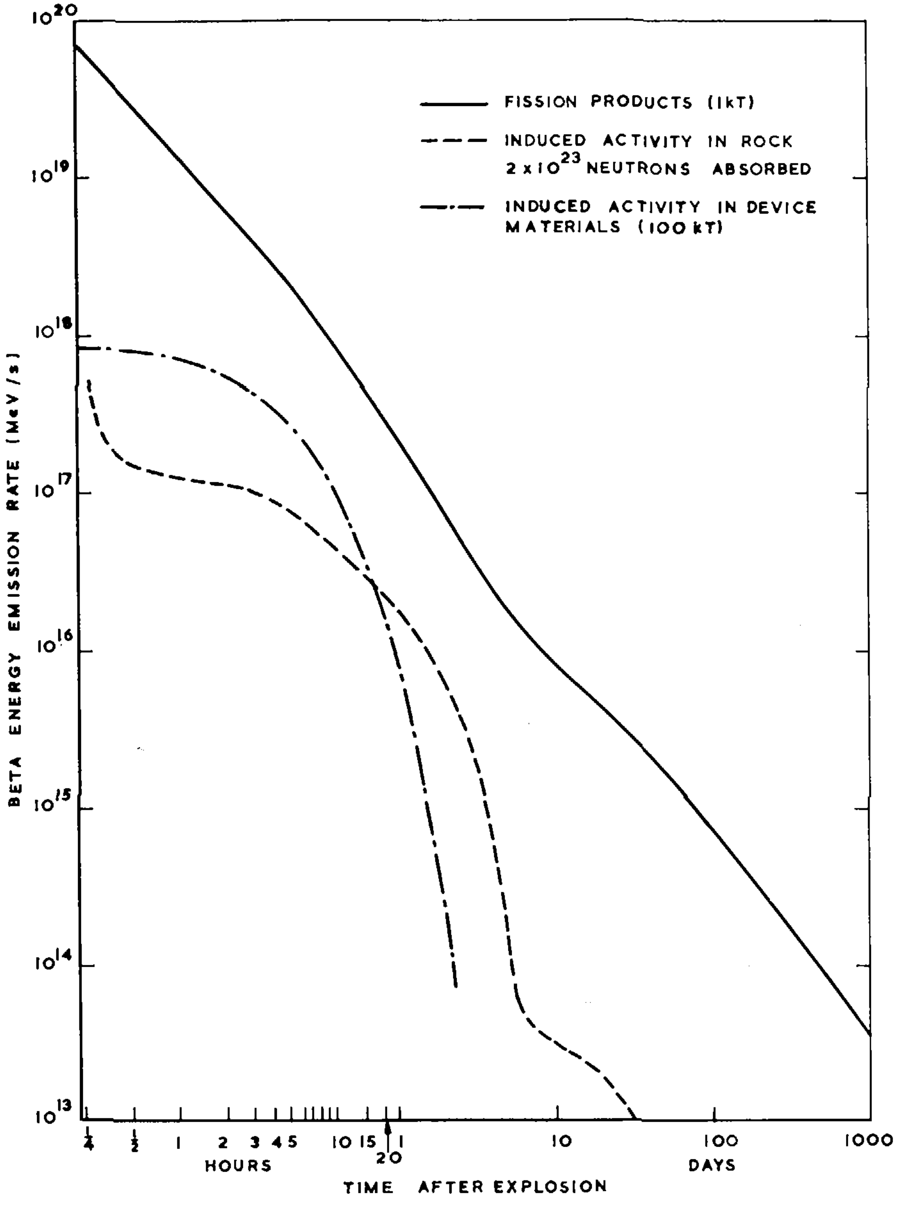

FIGURE I. BETA ENERGY EMISSION RATES

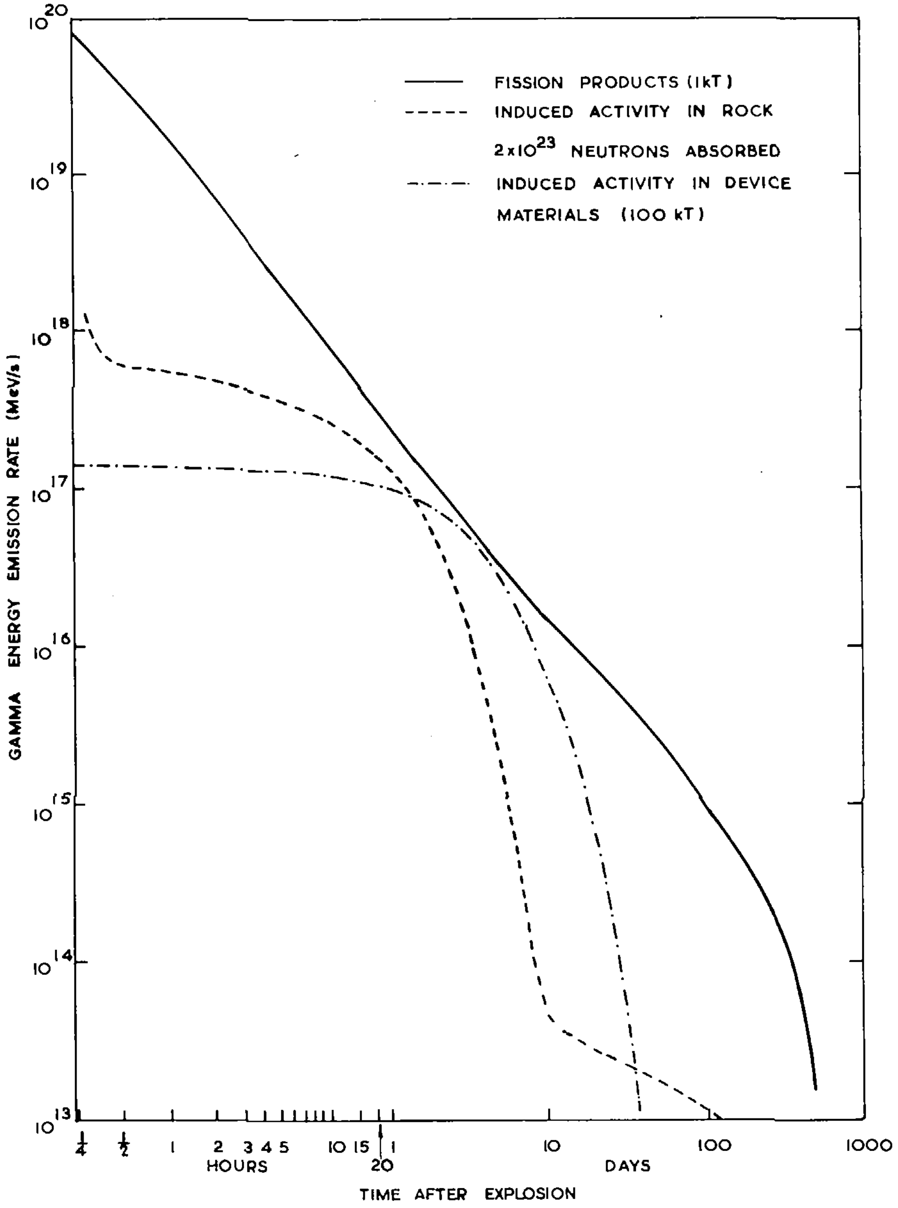

FIGURE 2. GAMMA ENERGY EMISSION RATES

multiplying by the distribution function (see section 3). Integration of the emission rates over time gives

β-energy emission from 1 hr to infinite time = 1.8×10^{23} MeV/kT

γ-energy emission from 1 hr to infinite time = 1.8×10^{23} MeV/kT*

2.2 Residual material from the explosive

The residual activity of concern is tritium. As tritium decays by the emission of weak β particles it is mainly an internal hazard to the body and, as such, its quantity is most usefully expressed in curies. The amount remaining after an explosion producing 100 kT fusion yield may range from 7×10^5 to 5×10^6 Ci {3}. For definiteness, we assume an amount of 2×10^6 Ci, and therefore subsequent estimates of tritium levels will be uncertain by a factor of at least 3. The assumed amount of residual tritium corresponds to 200 g, compared with about 700 g which react in producing 100 kT fusion yield.

2.3 Neutron induced activity in the device

The materials of which the device is made are exposed to a high fast neutron flux and, in general, both stable and active nuclides will be produced. Activity produced by neutron capture in the fissile and thermonuclear materials is insignificant compared with that of fission products and tritium already considered. The container, however, deserves separate consideration. If it is lead the principal products of neutron capture reactions are stable isotopes and the active nuclides ^{203}Pb and ^{209}Pb both of which have short lives. In Sedan tungsten was present, but this gives rise to a substantially greater hazard over an extended period of time than lead.

Our estimates of the radiation from the activity induced in lead in a 100 kT explosive are

β-energy emission from 1 hr to infinite time = 1.15×10^{22} MeV

γ-energy emission from 1 hr to infinite time = 3.8×10^{22} MeV

By comparison with the energy emission from fission products (1.8×10^{23} MeV/kT) these amounts are small if the fission yield is 1 kT or more. But there would be a significant contribution to the gamma emission if the fission yield is less than 1 kT in a total yield of 100 kT, which is likely to become dominant if the total yield were increased without increasing the initiating fission yield. Our calculations indicate that a ten fold increase in total yield would result in about 7 times more induced activity.

The energy emission rates for a 100 kT device encased with pure lead are shown in Figures 1 and 2. Activation calculations show that the small amounts of certain impurities present in commercially pure lead, namely, Sb, Fe, Ni and Zn, make an insignificant contribution over the period shown.

2.4 Neutron induced activity in rock

Neutrons escaping from the device will be captured in the surrounding medium. Typical rock consists mainly of SiO_2, but also contains appreciable amounts of Na, Al, Mg, K, Ca and Fe, and small amounts of many other elements. Neutron capture in most elements produces some radioactive nuclides. A detailed study of the products with half lives greater than 24 hours has been made for a typical granite by Ng {4}. The compositions of several other types

---

* The equality of these results is coincidental

of rock are also listed, so that one can estimate the probable variation of any specified product from one type of rock to another. Generally, the most important products are formed in maximum or near-maximum amounts in the granite to which the study applies. We have extended this work to include some products with shorter half lives, which are important in the initial fallout.

The number of neutrons entering the rock can be reduced by encasing the device in a neutron shield which consists, essentially, of a moderator, hydrogen, and an efficient, non-activating, slow neutron absorber, boron. In principle, a shield of sufficient thickness could reduce the neutron induced activity in the rock to any desired level, but in practice the cost of excavating space sets a limit. It can reasonably be assumed that the required thickness will be decided by the magnitude of the activity induced in the rock relative to that from the other sources.

A calculation in which a 100 kT device was shielded with water containing 5% by weight of boron in solution gave about 2×10^{23} neutrons entering the rock. It showed that 95% of these neutrons were captured within the first 100 cm of rock, which was taken to be dry, 35% of the captures occurring at high neutron energy (above $2\frac{1}{2}$ MeV) and 65% after slowing to low energies. Table I shows the percentages of neutrons captured by the principal absorbing elements in granite. Fast captures have been calculated explicitly only for those elements against which a figure is shown in the table.

Table I. Fate of the neutrons in granite

Element	Per cent by weight	Number atoms per g	Per cent of neutrons captured	
			Fast	Slow
Li	0.007	6.1×10^{18}		3.80
B	0.0015	8.4×10^{17}		5.55
O	48.66	1.83×10^{22}	22.0	
Na	2.77	7.26×10^{20}		3.35
Mg	0.56	1.39×10^{20}	0.08	0.08
Al	7.70	1.72×10^{21}	1.3	3.65
Si	32.30	6.93×10^{21}	10.7	9.76
Cl	0.024	4.1×10^{18}		1.21
K	3.34	5.14×10^{20}		9.36
Ca	1.58	2.37×10^{20}	0.05	0.92
Ti	0.23	2.89×10^{19}		1.48
Mn	0.06	6.6×10^{18}		0.77
Fe	2.70	2.91×10^{20}	0.08	6.71
Sm	0.0006	2.4×10^{16}		1.18
Eu	0.00017	6.8×10^{15}		0.26
Gd	0.001	3.8×10^{16}		15.52
Others	0.066		0.8	1.40

It is noteworthy that small fractions of powerful absorbers such as Gd and B account for a significant number of neutrons. Changes in the amounts present may be represented by a change in the total absorption coefficient. The change in production of a radioactive nuclide of interest can therefore be estimated by scaling by the ratio of the amounts of its parent present and the inverse ratio of the total absorption coefficients for the two rocks.

These calculations are for dry rock with zero hydrogen content. Hydrogen is a useful, non-activating, slow neutron absorber, however, accounting for about 10% of the slow captures in rocks containing 5% by weight of water. The presence of hydrogen also increases the moderating properties of the rock, and increases the fraction of slow captures at the expense of fast captures. At 5% water content these factors balance approximately and the activation by slow neutrons is scarcely changed.

Table II shows the principal products which contribute to the beta and gamma energy emission integrated from 1 hour to infinite time. Clearly, ^{24}Na is the dominant nuclide for both radiations. Examining the 11 analyses quoted by Ng {4} the maximum sodium content is 2.84% and, taking account of the effect of fast captures in Mg and Al, the maximum ^{24}Na production could be about 15% greater than Table II shows. Similarly, worst case estimates of ^{31}Si and ^{42}K are 15% and 30% greater respectively than in Table II.

The major activities decay quite rapidly and after a few days become insignificant compared with more slowly decaying nuclides. The results of Ng's work have been used to find the beta and gamma energy emission rates at these later times, scaling the slow neutron captures to 1.3×10^{23} (65% of 2×10^{23} neutrons entering). Results are shown in Figures 1 and 2. Although Ng calculates the fast captures on the assumption that the neutrons entering are all at 14 MeV, we do not think neglect of moderation in the device and shield makes much difference. The production of ^{54}Mn from ^{54}Fe (n,p) was found to be only 17% less with a degraded spectrum than Ng obtains for the same flux of 14 MeV neutrons.

It is clear that, with appropriate shielding, the energy emission from the induced activity in the rock from 1 hour onwards is of the same order of magnitude as that from induced activity in lead in the device. After about 10 days, however, the gamma energy emission rate from the induced activity in rock decays rather slowly indicating a possible long term residual hazard from the fallout, but this is always considerably less than the energy emission rate from even 1 kT of fission products.

3. Distribution of activity in the fallout

In this study a fallout distribution based on data obtained from the Sedan experiment is assumed. In order to apply these data to the model explosions (0, 1 and 10 kT of fission products and set amounts of induced activities) values are needed for the amounts of activity produced by the Sedan device. In particular, we need to estimate its fission yield, the precise value of which has not been disclosed. We know that "less than 30 per cent of the energy came from fission", but for our purpose an upper limit is not good enough because scaling to a different fission yield leads to an underestimate of the levels. Some additional data reported by Nordyke and Williamson {1} can be used to make a better estimate for the present purpose.

First, they give the fallout pattern in terms of the gamma dose-rate at 24 hours after the explosion constructed from a radiation survey between 20 and 28 hours. Radiochemistry results show that about 42 per cent of these dose-rates are due to fission product activity, 55 per cent to ^{187}W and 3 per cent to ^{24}Na and other induced activities. Secondly, they integrate over the area of the fallout pattern and find that the dose from 1 hour to infinite time is equivalent to a total deposition of 2.0 kT of fission product activity, and we assume that this evaluation includes a terrain shielding factor. We also assume that a component due to ^{187}W is included, and by consideration of the decay rates of fission products and ^{187}W, we deduce that the actual amount of fission product activity deposited is equivalent to 1.4 kT of fission. Thirdly, the most probable value of the fraction of activity produced which is deposited in the fallout is 10 per cent, with a possible spread between 6 and 17 per cent {5}. Taking 10 per cent venting gives us an estimate of 14 kT for the fission yield of Sedan. It is assumed that there is no significant fractionation, and this is supported by radiochemical analysis of the local fallout {6} but is not true of long range fallout in which high enrichment of volatile chain products has been observed in activity brought down by rain{7}.

Table II. Induced activities in acid rocks –

β and γ energy emission from 1 hour to infinite time for 2 × 10^{23} neutrons entering the rock

Radio-nuclide	Half life	Parent element and weight %	Abundance of parent nuclide	Fraction of neutrons captured	Average energy per disintegration (MeV)		Energy emission from 1 hour to infinite time (10^{22} MeV)	
					β	γ	β	γ
^{24}Na	15.0 h	Na 2.77	1	0.0335	0.465	4.122	0.289	2.64
		Al 7.70	1	0.0047			0.042	0.37
		Mg 0.56	0.786	0.0006			0.005	0.05
^{31}Si	2.62 h	Si 32.30	0.0305	0.00205	0.49	∿ 0	0.016	0
^{32}P	14.3 d	P 0.07	1	0.00024	0.57	∿ 0	0.003	0
		S 0.04	0.95	0.00023			0.003	0
^{42}K	12.52 h	K 3.34	0.069	0.00344	1.09	0.275	0.072	0.02
^{56}Mn	2.58 h	Mn 0.06	1	0.0077	0.62	1.81	0.073	0.21
		Fe 2.70	0.917	0.0007			0.007	0.02
^{152}Eu	13 y	Eu 1.7 × 10^{-4}	0.478	0.0020	0.10	1.05	0.004	0.04
TOTAL							0.523	3.35

This estimate allows us to set up a reference pattern, Figures 3 and 4, which shows the gamma dose-rate contours at 24 hours due to fission products alone when a 100 kT explosion including 1 kT fission yield occurs under Sedan conditions. The observed dose-rates are multiplied by the factor 0.42/14 = 0.03. Figure 5 shows the corresponding dose-rate as a function of range along the "hot line" of the pattern.

4. Dose limits

Before conclusions can be drawn about the areas and duration of hazards to members of the public from given amounts and distribution of activity some limiting levels must be specified. It would be inappropriate to discuss this problem at length here, so we shall simply take the figures given by the ICRP{8} for small populations, which we interpret as limits suitable for planning purposes, but which may not necessarily be accepted in the authorization of a specific project.

These dose limits are one tenth of the recommended annual maximum permissible dose for occupational workers, with the single exception that for irradiation of the thyroid of children the limit is one twentieth of the occupational maximum permissible dose. We therefore adopt the dose limits given in Table III.

Table III. Dose limits for members of the public

Organ	Annual dose limit (rems)
Gonads, red bone marrow	0.5
Whole body in uniform irradiation	0.5
Skin, bone	3.0
Thyroid (children under 16)	1.5
Hands, forearms, feet, ankles	7.5
All other organs	1.5

These limits are regarded as allowable in addition to the dose received from natural background radiation and by the patient in the course of medical procedures. They do not allow for possible genetic risks because the exposure of large numbers of people is not envisaged and the dose rate to the critical organ is expected to decay within a relatively short time. Genetic hazards require the gonad dose to be less than 5 rems in 30 years.

5. External hazards

The primary external hazard is from radioactive fallout. To assess the extent of the hazard the gamma dose-rate contours shown in Figures 3 and 4 must be related to the dose limits for whole body irradiation. For the present purpose it is sufficiently accurate to assume that the gamma dose-rate is proportional to the energy emission rate, and then the data of Figure 2 for fission products lead to the result that an integrated dose of D mR from 1 hour to infinite time corresponds to a dose-rate of 4.6×10^{-3} D mR/hr at 24 hours. If gamma rays from the fission products were the only hazard we should take D = 500 mR. Then, if the fission yield is 1 kT, the approximate boundary of the region within which the dose limit is exceeded would be shown by the 2.3 mR/hr contour of Figure 3. The connection is not quite exact because the integrated dose depends on the time of arrival of the fallout, which is not necessarily 1 hour and is not the same everywhere on the contour.

This simple calculation can readily be extended to take account of beta radiation from the fission products and radiation from induced activities. It is assumed that all types of activity are distributed in the local fallout in

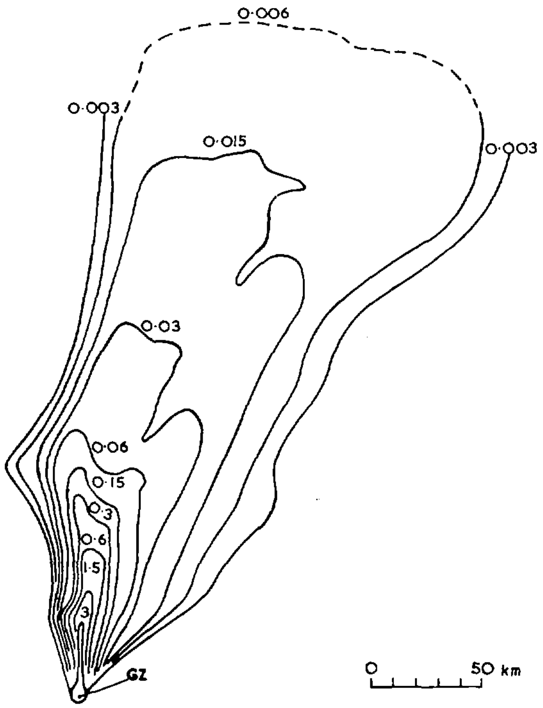

GAMMA DOSE-RATES IN mR/HR AT H+24 HOURS

FIGURE 3. MEDIUM RANGE FALLOUT PATTERN FOR FISSION PRODUCTS FROM 100 kT CRATERING EXPLOSION WITH 1 kT FISSION. SCALED FROM SEDAN PATTERN.

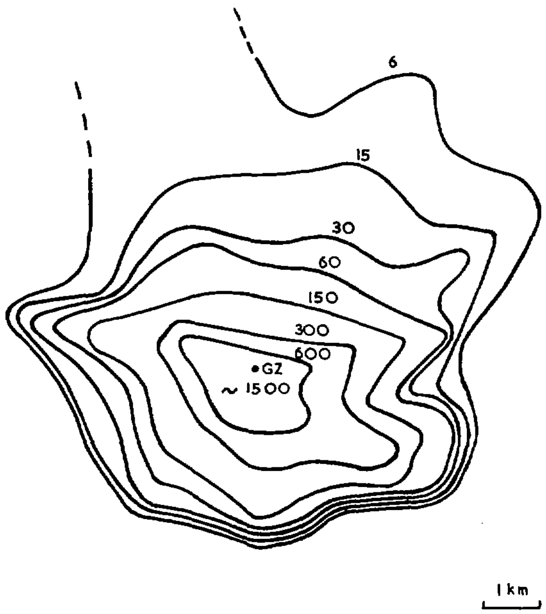

GAMMA DOSE RATES IN mR/HR AT H 24+HOURS

FIGURE 4. SHORT RANGE FALLOUT PATTERN FOR FISSION PRODUCTS FROM 100 kT CRATERING EXPLOSION WITH 1 kT FISSION. SCALED FROM SEDAN PATTERN.

the same way as the fission product gamma activity. The most susceptible organs, the gonads and red bone marrow, are protected against beta particles from an external source by the body tissue itself. The critical organ is the skin for which the annual dose limit is 3 rems. Introducing additive dose terms for the induced activities there are two criteria, both of which should be satisfied, to determine the region where the dose does not exceed either 500 mR to the whole body from gamma rays or 3000 mrem to the skin from beta and gamma rays, viz.,

$$D_{\gamma F}(t) + D_{\gamma d}(t) + D_{\gamma r}(t) < 500 \text{ mR} \qquad \ldots (1)$$

$$\text{and } D_{\gamma F}(t) + D_{\gamma d}(t) + D_{\gamma r}(t) + D_{\beta F}(t) + D_{\beta d}(t) + D_{\beta r}(t) < 3000 \text{ mrem} \qquad \ldots (2)$$

where $D(t)$ represents the dose in mrem from time t to infinite time to a man standing on a uniformly contaminated plane, and the subscripts β, γ, F, d, r identify, respectively, beta and gamma contributions, and the sources fission products, induced activity in the device and induced activity in the rock.

It is convenient to divide both criteria by $D_{\gamma F}(1)$ the gamma dose from $t = 1$ hour to infinite time from fission products. Then, if $\beta(t)$ and $\gamma(t)$ with appropriate subscripts represent the ratios of each partial dose to $D_{\gamma F}(1)$, the criteria (1) and (2) may be rearranged as

$$D_{\gamma F}(1) < \frac{500}{\gamma_F(t) + \gamma_d(t) + \gamma_r(t)} \qquad \ldots (3)$$

$$\text{and } D_{\gamma F}(1) < \frac{3000}{\gamma_F(t) + \gamma_d(t) + \gamma_r(t) + \beta_F(t) + \beta_d(t) + \beta_r(t)} \qquad \ldots (4)$$

These expressions define limiting values of $D_{\gamma F}(1)$, and allow the appropriate contour on Figures 3 and 4 to be found by using

$$\text{Dose rate at 24 hours} = 4.6 \times 10^{-3} D_{\gamma F}(1) \text{ mR/hr} \qquad \ldots (5)$$

These criteria apply to an explosive with 1 kT fission yield. An example with W_F kT fission yield, and no other change, can be handled by introducing a factor W_F multiplying $\gamma_F(t)$ and $\beta_F(t)$ in (3) and (4).

The dose ratios for gamma ray sources may be obtained from the data of Figure 2 by integration over time. The dose ratios for beta particle sources require some further calculation because of the small range of betas compared with gammas. The area of the contaminated plane which can contribute is smaller, but, on the other hand, the energy deposition density at the body surface is larger. We do not feel that the determinations of beta to gamma dose ratios known to us are entirely satisfactory, but we shall use here a value of 12:1 calculated by Dale {9} for the ratio of the doses delivered over the interval 1 hour to 1 year to a lightly clothed man standing on a plane contaminated with fission products. This value appears to agree reasonably well with data obtained by Dunning {10} over the first few days following fallout deposition if one allows for the change in relative energy emission rates over Dunning's period of observation.

Table IV gives values of the dose ratios required to evaluate (3) and (4). It will be apparent that the dose to the skin (beta + gamma) is limiting. However, the conditions which lead to this conclusion are rather artificial as it has been assumed that exposure to both the beta and gamma field is continuous. Any light building or vehicle will give good protection against the beta particles, but possibly not against gamma rays, so that one can reasonably assume that actual beta doses are substantially overestimated by

Table IV. For this reason we shall use the gamma dose criterion (3) subsequently in this paper, but the beta dose should be taken into account if totally unprotected people might be exposed.

The accuracy of the values in Table IV may decrease for exposure beginning a long time after deposition because no account has been taken of weathering or redistribution in wind blown dust.

Table IV. Ratios of doses to fission product gamma dose from 1 hour to infinite time

Exposure begins at time t	Fission Products		Induced activity in device		Induced activity in rock		Total	Total
	$\beta_F(t)$	$\gamma_F(t)$	$\beta_d(t)$	$\gamma_d(t)$	$\beta_r(t)$	$\gamma_r(t)$	$\beta + \gamma$	γ
¼ hr	16.7	1.47	0.89	0.21	0.39	0.20	19.98	1.88
½ hr	14.3	1.22	0.85	0.21	0.38	0.19	17.2	1.62
1 hr	12.0	1.00	0.77	0.21	0.36	0.19	14.5	1.40
2 hr	9.89	0.81	0.62	0.21	0.33	0.18	12.0	1.20
3 hr	8.66	0.72	0.50	0.21	0.31	0.17	10.6	1.10
6 hr	6.98	0.59	0.27	0.20	0.25	0.14	8.43	0.93
1 d	4.38	0.39	0.006	0.16	0.10	0.068	5.10	0.62
10 d	2.24	0.20	-	0.009	0.010	0.006	2.47	0.22
100 d	1.07	0.041	-	-	0.005	0.005	1.12	0.046
1 yr	0.35	0.007	-	-	0.004	0.004	0.37	0.011

Applying the ratios of Table IV and the equations (3) and (5) one can see the contraction of the limiting contour with increasing delay before reentry. For the example with 1 kT fission yield Figure 6 shows typical limiting contours and Table V shows maximum downwind extent. After about 10 days only the area of short range fallout extending to a radius of some 5 km around ground zero needs to be restricted.

Introducing the fission yield factor into (3) similar results can be found for different amounts of fission. Figure 7 compares limiting contours for 10 kt, 1 kT and zero fission yields for exposure beginning at 1 hour.

Table V. Maximum extent of limiting dose contours for exposure beginning at different times - 1 kT fission

Exposure begins at time	Equivalent 24 hr dose rate (mR/hr)	Maximum range (km)
1 hr	1.64	45
3 hr	2.1	40
6 hr	2.5	37
1 d	3.7	28
10 d	10.5	< 10
100 d	50	5

From the results obtained in this section it is clear that a substantial reduction in the area enclosed by the limiting contour for the external gamma dose from the fallout is to be expected if the fission yield is reduced from

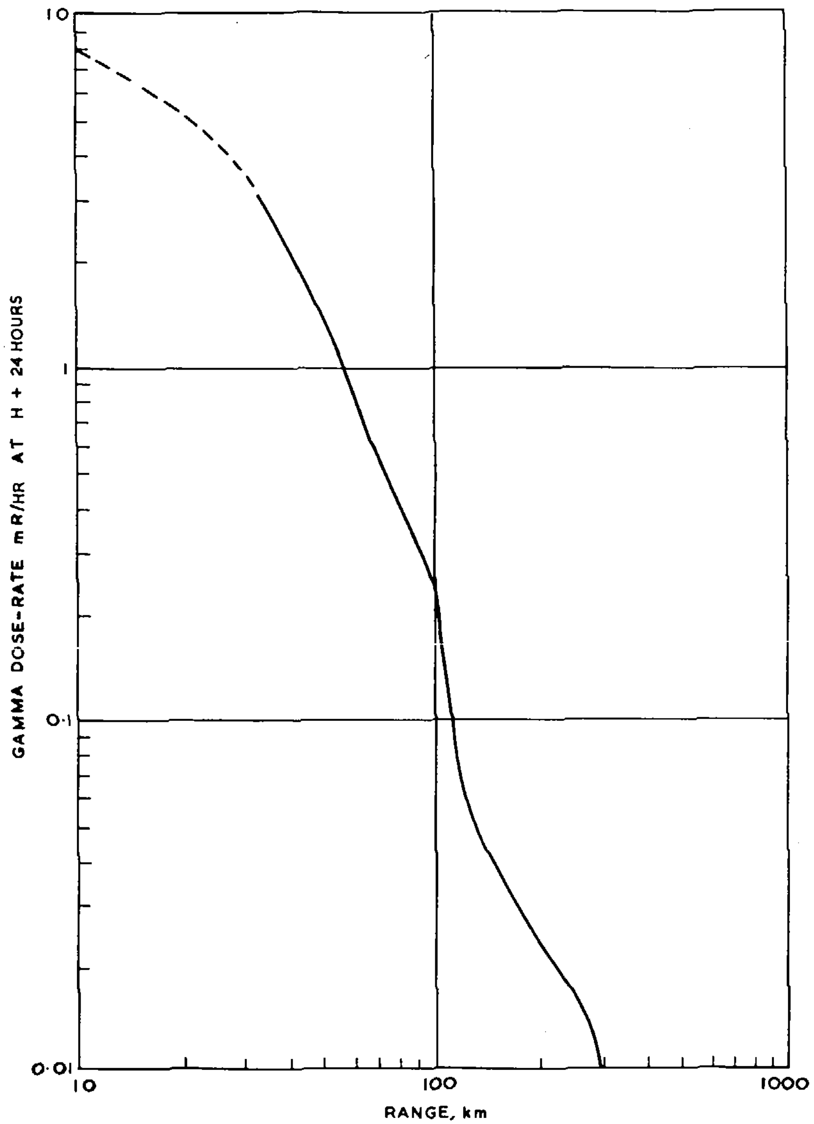

FIGURE 5. GAMMA DOSE RATE FROM FISSION PRODUCTS ALONG HOT LINE OF ILLUSTRATIVE FALL OUT PATTERN

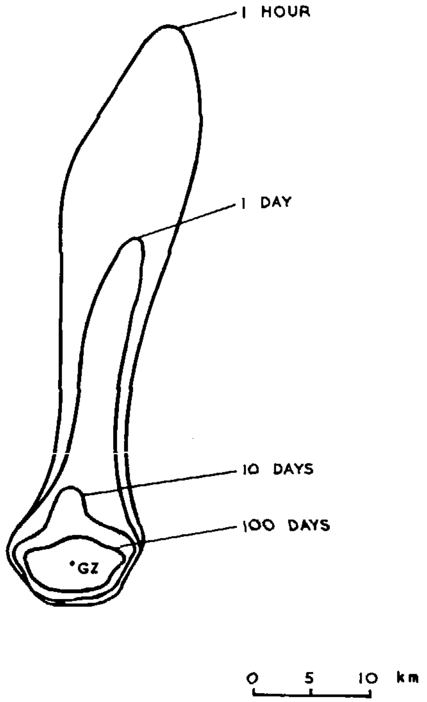

FIGURE 6. 0·5 R DOSE CONTOURS FOR EXPOSURE BEGINNING AT DIFFERENT TIMES 100 kT CRATERING EXPLOSION WITH 1 kT FISSION

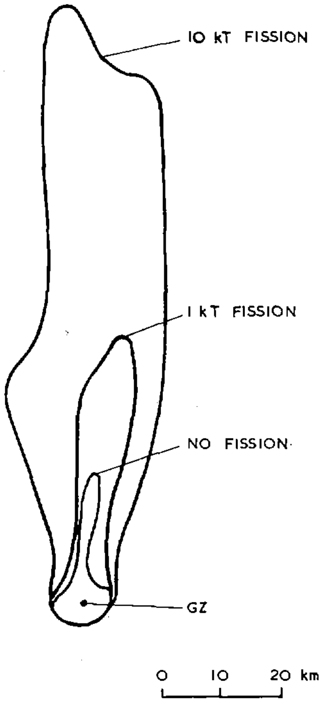

FIGURE 7. 0·5R DOSE CONTOURS FOR 100kT CRATERING SHOTS WITH DIFFERENT FISSION YIELDS

10 kT to 1 kT in a 100 kT explosive. Some further reduction could be achieved by reducing the fission yield below 1 kT, but at about the 0.2 kT level the inevitable induced activities are roughly equal to the fission product contribution. In these examples the neutron shielding has been held constant, the amount being chosen so that the gamma emission from induced activity in the rock is of the same order as that from induced activity in the device. Obviously, if the fission yield is several kT the neutron shielding requirement could be relaxed without undue penalty.

The external dose received from exposure to the drifting cloud has also been considered. Sedan data {11} were scaled to the 1 kT fission example and show that the dose received at a given distance may be of order 15% of the dose to infinite time from the fallout. For example, at 66 km range the cloud dose would be about 20 mR, delivered between 2½ and 4 hours after explosion, whereas the dose from fallout is about 150 mR. The cloud dose is regarded as an insignificant extra hazard, bearing in mind the low accuracy of all these calculations.

6. Internal Hazards

Internal hazards may arise from the entry of radioactivity into the body from the environment. Possible routes are inhalation, consumption of contaminated food or water and injection into the bloodstream through injuries. Because the source is within the body short range radiations, such as α and soft β particles, as well as γ rays are important.

The ICRP {8} recommends limiting doses for the various body organs, and gives the equilibrium fractions of practically all nuclides of interest present in the organs under conditions of steady intake and elimination. These factors are used to establish maximum permissible concentrations (MPC) of each nuclide in air and water for occupational workers. To set concentration limits for members of the general public we reduce the occupational MPC by a factor 10 for all nuclides except iodine, for which the factor is 20. In our problem, however, intake (in terms of curies of activity) is sometimes decreasing with time and to allow for this it is assumed that the annual dose limit may be received within a shorter time interval if this increases the concentration limit. Then the steady intake concentration limit for a given nuclide may be increased by the factor 365 λ_r, where λ_r is the physical decay constant in units $(\text{days})^{-1}$, provided this factor is greater than unity. No account has been taken of any difference in the distribution within the body between steady and transient cases.

Some problems in which internal hazards might be important have been studied and are briefly discussed below. To assess the relative importance of internal hazards a comparison is made with the local external hazard (where one exists). It is necessary to express the activity distribution in curie units. To convert the data of Figures 3 and 4 the gamma dose-rate 1 metre above a uniform ground distribution of 1 mCi/m^2 of fission products at 1 hour is taken to be 10 mR/hr {12} assuming a terrain shielding factor 0.7. At 24 hours this dose-rate has fallen to 0.16 mR/hr. Thus the 1 mR/hr level on Figures 3 and 4 corresponds to about 6 mCi/m^2 of 1 hour fission products.

6.1 Short term hazards

Short term hazards arise from the intake of fairly rapidly decaying nuclides at early times. Inhalation of activity from the initial cloud and of volatile elements, iodine in particular, evaporating from the fallout is considered.

To deal with inhalation of the cloud debris let the concentation of a nuclide X_j in the cloud at the time it reaches the individual be C_j µCi/cm³ and q_j µCi be the limiting amount of X_j that may be inhaled during a single exposure. Then the intake may be expressed in terms of the concentration limit by

$$I_j = \frac{B \int C_j dt}{q_j} \qquad \text{... (6)}$$

where B cm³/s is the breathing rate, and the integral is taken over the time of passage of the cloud in seconds. We take B = 350 cm³/s, the value appropriate to the working part of the day. $\int C_j dt$ can be estimated by making use of the external dose measurement for the passage of the cloud and q_j can be calculated from ICRP formulae and data {8}. For total fission products q is evaluated by assuming a $t^{-1.2}$ decay law instead of a specific decay constant λ, and in this case q depends on the time of inhalation.

Table VI summarises the results for inhalation at 66 km range for the example with 1 kT fission.

Table VI. Inhalation hazards from debris cloud at 66 km range

Nuclide	Total activity at 3 hours µCi	q_j µCi	Critical Organ	I_j (concentration limits)
Fission Products	1.2×10^{14}	300	GI (LLI)	0.21
^{203}Pb	1.2×10^{13}	1000	Kidney	0.006
^{209}Pb	5.0×10^{13}	2200	GI (LLI)	0.012
^{24}Na	2.0×10^{12}	180	GI (LLI)	0.006
^{56}Mn	1.4×10^{12}	540	GI (LLI)	0.0014
^{131}I	1.0×10^{11}	0.6	Thyroid	0.088
^{133}I	1.3×10^{12}	4.2	Thyroid	0.17
^{135}I	5×10^{12}	12	Thyroid	0.22

These results relate to members of the public, and where the thyroid is the critical organ they relate to children below the age of 16. The thyroid receives 0.46 of the dose limit and the gastro-intestinal tract 0.23 of the dose limit, but this is at a range rather greater than the limiting range for the external dose limit from initial fallout. Closer in the intake will be larger, so the problem of inhalation of cloud debris appears quite serious, although it can be avoided by temporary evacuation.

Data from Sedan {4} indicate that 2.8% of the expected ^{131}I deposition in the fallout evaporates daily between days 3 and 10. The continuous source from a place where the level of fission product activity at 1 hour was σ(r) mCi/m² is therefore at most

$$S(r) = \frac{0.028 \times 1.5 \times 10^5}{8.64 \times 10^4 \times 4 \times 10^8} \sigma(r) \text{ mCi/m}^2\text{s} \qquad \text{... (7)}$$

where 1.5×10^5 Ci is the maximum quantity of ^{131}I produced and 4×10^8 Ci is the total activity of 1 kT of fission products at 1 hour.

Consider a surface wind blowing along the hot line of the fallout pattern carrying the vapour to a person at 50 km range. Sutton {13} gives the concentration at distance x metres from a cross-wind line source of material (gas, smoke or evaporating liquid) as

$$\text{Concentration} = 0.035\ S\ dx \left(\frac{x}{100}\right)^{-0.9}\ \text{mCi/m}^3 \qquad \ldots (8)$$

Substituting for S, putting x = 50000 - r and integrating along the hot line of the fallout pattern, using the fact that 1 mR/hr observed gamma dose rate at 24 hours corresponds to 6 mCi/m^2 of 1 hour fission products, leads to a maximum concentration of 3×10^{-4} $\mu\text{Ci/m}^3$. With breathing rate 20 m^3/day, and allowing for decay of the ^{131}I, the intake by a person continuously exposed is at most 0.07 µCi, which is a factor 8 lower than the limiting intake for a child under 16 (Table VI). The intakes of ^{133}I and ^{135}I are about 0.1 µCi each, but the limits are also higher. Most (∿ 80%) of the intake comes from activity carried from the ground zero circle. Variable winds will therefore result in an actual intake over several days which is less than the amount calculated, and inhalation of iodine vapour is expected to be a minor hazard.

Another example in which a person at the limit of the ground zero circle, 5 km range, inhales vapour from an air current across the crater zone resulted in an intake 6 times the value calculated above. This is close to the limit for uncontrolled persons, but such persons are not likely to be so near in the relevant time period.

6.3 Long term hazards from inhalation

A hazard will exist if resuspended contaminated dust is inhaled. It is a difficult one to evaluate with reasonable accuracy because of the uncertainties in the concentration in the air of active particles of sizes which will be retained in the lung, and in the level of surface contamination over long periods of time. Particles of interest are those less than 10 microns diameter at unit density, for sand the corresponding diameter is 6 µ. When such small particles become airborne they will be carried some distance by the wind before being deposited again, and so over long period they will become widely dispersed.

Stewart{14} has discussed in detail the estimation of airborne concentrations above contaminated surfaces, describing both experimental and theoretical studies. He expresses the relationship in terms of a resuspension factor K, defined as

$$K(\text{m}^{-1}) = \frac{\text{Airborne concentration (units m}^{-3})}{\text{Surface contamination level (units m}^{-2})}$$

The value of K depends on a number of parameters, some of which are difficult to quantify. The important ones seem to be violence of disturbance of the surface, roughness, moisture content, particle size, wind speed, height above the surface and effects of weathering. Insufficient data exist for a complete understanding of the variation of K with these parameters, but Stewart recommends values outdoors of 10^{-6} m^{-1} under quiescent conditions and 10^{-5} m^{-1} under conditions of moderate activity. These are certainly upper limits; some of the experiments result in factors a few orders of magnitude lower, particularly when the particles are small. In the experiments in which values of order 10^{-5} m^{-1} were found only about 10% of the activity was carried on small particles in the hazardous size range. Furthermore, Stewart shows by eddy diffusion theory that small particle contamination can persist for times of order one year only if K is less than 10^{-6} m^{-1} (except under a continuous inversion in the atmosphere). Therefore, we believe it is safe to adopt a value of $K = 10^{-6}$ m^{-1} as an upper limit, which may, in some circumstances, be a substantial overestimate.

The inhalation hazard from resuspension of deposited fission products and induced activity is estimated,assuming continuous exposure for at least one year. The amount of each nuclide present is expressed in terms of the limiting air concentration using ICRP data {8}, allowing for decay of nuclides with moderately short half lives and reducing the limits by an extra factor 3 because intake of a mixture of radionuclides should be assumed to affect the whole body rather than a specific critical organ. Inhalation of fission products is more important than inhalation of induced activities, the hazard being due principally to ^{90}Sr and ^{144}Ce. In terms of the fission product activity present at 1 hour the limiting air concentration is 10^{-3} mCi/m^3 when exposure begins at 10 days after the explosion, rising to 2×10^{-3} mCi/m^3 and 3×10^{-3} mCi/m^3 for exposures beginning at 100 days and 1 year respectively.

Taking the resuspension factor $K = 10^{-6}$ m^{-1}, the limiting surface deposition of fission products is therefore at least 10^3 mCi/m^2 at 1 hour. This level of fallout corresponds to a gamma dose-rate of 170 mR/hr at 24 hours, which occurs only within the ground zero circle even for the example with 10 kT fission yield (Figure 4). Similar calculations for the other examples show that the inhalation hazard exceeds its limit only within an area where uncontrolled access must in any case be prevented because of the external gamma dose, for reentry times up to at least one year.

6.4 Long term hazards from ingestion

Ingestion of activity might occur through drinking water or consuming food from a contaminated area. Contamination of the ground water supply is considered. An assessment requires a determination of the probable concentrations of radionuclides in the water at the explosion site. For a few nuclides these concentrations are high by comparison with the limiting concentrations in drinking water, so the transport of activity from the site to the source of the drinking water supply is important. Flow rates can vary enormously, but in general ground water moves slowly, taking years rather than days to move a distance of one mile. In these circumstances, short-lived nuclides decay to insignificance within short distances. The biologically significant long-lived nuclides are tritium, the fission products ^{90}Sr and ^{137}Cs and the neutron activation product ^{60}Co.

Contamination of ground water by undergound nuclear explosions has been discussed in detail by Piper and Stead {15}. To calculate the initial concentration of activity for a cratering explosion they consider the volatile nuclides to be dispersed in four equal parts: (a) to the atmosphere, (b) in ejecta surrounding the crater, (c) uniformly through the fall-back material within the crater, and (d) uniformly through the lower hemisphere of the shock zone. The shock zone is the region within which propagation of the pressure pulse is supersonic in the medium. It extends to about twice the initial cavity radius, and within it the rock is deformed beyond its elastic limit and is well broken up. In post-shot drilling to contained explosions activity has been found within this region, but little has been found beyond it even though fractures have occurred.

The activity which gets into ground water is that within regions (c) and (d). The mass of rock in each of these regions is about 7×10^{12} g for a 100 kT explosion and it is assumed here that the mass of contained water is 5% of the rock mass, 3.5×10^{11} g in each region.

Tritium is likely to be chemically combined in the water and move with it. 2×10^6 Ci are assumed to be left after the explosion, so the initial concentration in the water is about 1.5 μCi/cm^3. The concentration limit in drinking water is 3×10^{-3} μCi/cm^3 for the general public {8} so the level is 500 times the limit.

The other nuclides mentioned above will be preferentially held in the solid debris rather than the water, the distribution coefficient depending on the characteristics of the nuclide-rock-water system. Using the same values as Piper and Stead the ^{90}Sr concentration is about 40 times the concentration limit in the 1 kT fission example, but ^{137}Cs and ^{60}Co are not important.

Tritium is therefore the principal hazard in ground water, unless the fission yield is 10 kT or more in a 100 kT shot. The level is likely to be so high that it is vital to determine the motion of water at the explosion site whenever there is any chance of it reaching supplies used for human or agricultural consumption. Reported flow rates are generally a few feet per day or less, so one would expect any hazard to be limited to within about 20 km of the explosion because sufficient radioactive decay would occur by the time the tritiated water had travelled this distance. However, the time involved is of order 100 years. Dilution of the tritium as it moves has been neglected.

7. Conclusions

Calculations on a hypothetical model of a 100 kT explosive with low fission yield indicate the value of a fission yield of 1 kT or less. Reduction below 1 kT fission gives a diminishing return, and at the 0.2 kT level the induced activity in the device structure (lead) contributes as much to the fallout dose as the fission products. Neutron shielding between the device and the surrounding rock is necessary.

Taking the Sedan fallout distribution pattern as an illustrative example, the external gamma dose limit, assumed to be 0.5 R, extends to 45 km when the fission yield is 1 kT. After 10 days resettlement beyond 10 km from ground zero may be possible, but continuous residence close to the crater may not be permissible for at least one year.

In general, the external gamma dose from fallout will be the controlling hazard, but in special cases the beta dose should be taken into account.

Possible internal hazards could arise from inhalation of iodine in the airborne cloud and drinking water contaminated with the tritium. The first is transient and can be avoided by temporary evacuation of people along the cloud track. Evacuation may be necessary beyond the limiting range for the external fallout dose, but in practice a safety factor is likely to be applied to fallout predictions in any case. The level of tritium in water at the explosion site is certain to exceed the limiting level in drinking water. Whether or not this is hazardous depends on the flow of this water towards sources of water supply. If the flow is slow, of order a few feet per day, the risk is likely to be confined to any sources within 20 km of the explosion site. However, it will not immediately be apparent that a source is at risk.

III. CONTAINED EXPLOSIONS FOR STORAGE

1. The Problem

One possible application of contained nuclear explosions is gas storage in the chimney. In this application there will be no uncontrolled release of radioactivity in the environment, provided proper precautions are taken to prevent venting up the emplacement hole and to avoid contamination of aquifers. The principal problem is contamination of the product by tritium and ^{85}Kr.

As an example consider a 25 kT explosive at a depth of 2000 feet. The cavity volume, the available storage volume, is then of order 10^5 m^3. The explosive yield in this case would come mainly from fission, but if a thermonuclear device is used there would be some residual tritium and we shall assume here that 4 g(4×10^4 Ci) remain as in the Gasbuggy shot. {16}

Apart from tritium, noble gas activities and potentially volatile products such as iodine must be considered. The most important of these in the long term is ^{85}Kr, a fission product with half life 10.6 years. Gasbuggy produced 350 Ci of ^{85}Kr. Other noble gas activities are produced initially in far greater amounts, but decay fairly quickly. For example ^{133}Xe, a fission product with half life 5.3 days, has an initial activity of 10^7 Ci from 25 kT fission, but after 80 days its activity falls below that of ^{85}Kr. There may also be substantial production of ^{37}Ar, half life 35 days, in the surrounding rock by the ^{40}Ca (n, α) ^{37}Ar reaction. The concentration in early Gasbuggy samples was about 40 times greater than that of ^{85}Kr {17} but the maximum permissible concentration in air is 300 times that of ^{85}Kr {8}. The concentration of 8-day ^{131}I observed in the Gasbuggy samples was very low {17}. These considerations suggest that tritium and ^{85}Kr are the only gaseous nuclides of concern provided a few months elapse before operations begin on the chimney.

The chimney could be filled with gas at a pressure of about 80 atmospheres. Assuming all the tritium is dispersed uniformly in the gas, its concentration when released at atmospheric pressure is 5×10^{-3} Ci/m^3. There will be dilution when the gas is used, but the concentration limit for uncontrolled release is only 2×10^{-7} Ci/m^3 {8}, so the tritium concentration in the gas appears to be too high to permit domestic consumption.

Some form of purging is therefore necessary. It is considered that gaseous purging may be unsatisfactory, because the passage of many void volumes will be needed to flush out the contaminants to the degree required {18}. Gaseous purging would be more attractive if one could be sure that the tritium was present only in the form of water vapour, for the stored gas would be dried when it is drawn off and 97% of the water vapour removed. But it is thought that significant exchange of tritium between water vapour and stored gas will take place during the residence time in storage, typically of order one year, and this exchange will be promoted by the radiation field existing in the chimney.

For these reasons flushing the chimney with water has been considered. This is particularly attractive if the storage is offshore below the sea bed or near the shore on land. Filling the cavity with sea water will drive out whatever gas is initially contained, including ^{85}Kr and some tritium. The water itself will become contaminated with tritium, ^{90}Sr and ^{137}Cs, but it is not likely to leach out refractory nuclides held in the solidified residue at the chimney base. After the cavity is emptied a large area of wet rock surface and saturated water vapour will be left, and will, of course, be contaminated. If necessary, the cycle could be repeated. The radiological consequences of these operations are briefly discussed below.

2. Venting of cavity gas

Release of cavity gas to the atmosphere should be at a controlled rate such that the concentration at some reasonable distance downwind of the point of release is below the limit for uncontrolled exposure. Suppose the desired concentrations 2×10^{-7} Ci/m^3 of tritium and 3×10^{-7} Ci/m^3 of ^{85}Kr {8} are to be achieved at 1 km range. Sutton {13} gives the peak concentration at x metres downwind of a continuous point source emitting S units/sec as

$$2 \times 10^{-3} \left(\frac{x}{100}\right)^{-1.76} \quad S \text{ units/m}^3$$

when the wind speed at 2m height is 5 m/s. Hence, we find $S_{\max} = 6 \times 10^{-3}$ Ci/s for tritium, $S_{\max} = 9 \times 10^{-3}$ Ci/s for ^{85}Kr. If we assume, pessimistically, that <u>all</u> the tritium is present in the gas phase, its concentration in the cavity gas is 0.4 Ci/m^3, so the venting rate could be 1.5 × 10^{-2} m^3 of cavity gas per second. At this rate, complete venting would take about 2000 hours. However, it is more likely that most of tritium will be present in the liquid phase. Gasbuggy samples suggest that about 30% of the tritium was present as HT and CH_3T as early times (23 hours), but the HT decreased rapidly so that by 38 days only about 6% of the tritium was present in gaseous species, mostly as CH_3T. The concentration of tritium is still several times that of ^{85}Kr, however. These data suggest that the gas release time could probably be reduced to 600 hours, and possibly to about 120 hours, without exceeding continuous exposure limits at 1 km range. But it should be borne in mind that the rock composition may affect the exchange rate between hydrogen and water, for example, equilibrium may be established more quickly in carbonate than in silicate formations.

3. Discharge of water from chimney

The water filling the chimney will become contaminated by T, ^{90}Sr and ^{137}Cs, the last two fission products having gaseous precursors and therefore being dispersed through the rubble. The tritium concentration is at most 0.4 Ci/m^3 which is 130 times the concentration limit in drinking water. The ^{90}Sr and ^{137}Cs, however, will not all be in solution. In ground water contamination studies {15} it was found that these nuclides are held preferentially in the rock, and the greatest fraction in the water was

$$\frac{1}{10} \times \frac{\text{volume of water}}{\text{mass of rock}}$$

for dolomite. This fraction can be much less for other rock types. Taking the chimney height to be 4 times the cavity radius and the rock density as 2 g cm^{-3}, the fraction is 1/60. The total amount of each nuclide in the water in our example is then 75 Ci. For ^{90}Sr, the concentration corresponds to 7500 times the concentration limit.

Howells {19} gives guidance on the rate at which this contaminated water could safely be discharged into the sea. He was concerned with discharge from the Windscale reactor site in Cumberland, UK, of beta active effluent at concentrations of 10^{-2} - 10^{-1} Ci/m^3 of which a few per cent is ^{90}Sr, that is, a concentration of ^{90}Sr of the same order of magnitude as ours. Maximum discharge rates for ^{90}Sr when the limiting criteria are uptake by fish and uptake by edible seaweed are 10^5 and 1.2 × 10^4 Ci/month respectively. On this basis 75 Ci of ^{90}Sr could be discharged within one day.

4. Residual contamination in the chimney

After pumping out the water, saturated vapour filling the void volume and a film of water on the rock surfaces will remain. Assuming a chimney temperature of 35°C saturated air contains 40 g/m^3 water. Thus the tritium concentration in the vapour is 1.6 × 10^{-5} Ci/m^3 or 80 times the limit for direct inhalation. This level might be acceptable for gas storage under pressure because the dilution factors mentioned previously would apply. But exchange reactions may increase the tritium concentration above that due to water vapour alone, so an estimate of the total amount of tritium left in the chimney is necessary.

The amount of water left in the chimney depends on the surface areas of the broken rock and the average film thickness both of which are difficult to evaluate. Rodean {20} gives a value for the specific surface (surface : volume ratio) of 5.78 ft^{-1} determined from Hardhat photographs. This leads to a total surface area of about 6 × 10^6 m^2 in our example. From surface tension data the maximum droplet thickness is estimated to be 0.05 cm, so assuming a film of this thickness the total liquid volume is of order 3×10^3 m^3, i.e. 0.03 of the void volume. Probably this is an overestimate unless the rock is porous (unlikely in a storage application) or a pool is left at the chimney base.

This rough estimate of the tritium left after one flushing is 3% of the initial amount. Thus two cycles might be expected to reduce the tritium by a factor of 1000, and if it is assumed that the tritium then remaining is transferred by exchange reactions to stored gas at 80 atmospheres, the concentration in the gas at atmospheric pressure is 5×10^{-6} Ci/m^3, or 25 times the limit for uncontrolled release. Further dilution when the gas is used may be expected to reduce this concentration below the limit for uncontrolled release.

5. Conclusions

This preliminary survey has not revealed any serious health hazards underlying the proposal to flush out storage cavities with sea water. Venting of the gaseous activity initially present, ^{85}Kr and tritiated gas, could take 25 days, possibly less, if an area 1 km in radius was controlled. Disposal at sea of the water, with principal contaminant ^{90}Sr, should be permissible within one day.

The major uncertainty is the fraction of tritium remaining after flushing which is estimated to be 3%. Experimental determination of this fraction is desirable, but for the present this study suggests that two or three flushing cycles will be enough to reduce the tritium concentration in burnt gas below the limit for uncontrolled release. Complete exchange of tritium into the stored gas has been assumed.

As tritium is a greater problem than ^{85}Kr in this application the use of an all fission explosive might be considered. Even then tritium will be produced from lithium in the rock, but the production can be reduced by neutron shielding. The shielded Rulison shot is expected to yield an initial concentration of tritium in the cavity gas which is one tenth that of Gasbuggy {21}.

Acknowledgement

I am indebted to several colleagues at AWRE, in particular Dr. R. Lapage, Dr. K. Parker and Mr. G. C. Scorgie, for their help in preparing this paper.

References

1. M. D. Nordyke and M. M. Williamson, "The Sedan event", PNE-242 F, August 6, 1965.

2. H. Goldstein, "Fundamental aspects of reactor shielding", Pergamon, 1959.

3. E. Teller, W. K. Talley, G. H. Higgins and G. W. Johnson "The constructive uses of nuclear explosives", McGraw-Hill, 1968.

4. Y. C. Ng, "Neutron activation of the terrestrial environment as a result of underground nuclear explosions", UCRL-14249, June 22, 1965.

5. M. M. Williamson "Fallout calculation and measurement", Engineering with Nuclear Explosives, University of California, Livermore, TID 7695, April 1964.

6. W. B. Lane, "Some Radiochemical and physical measurements of debris from an underground nuclear detonation, Project Sedan", PNE - 229F, June 1963.

7. S. Koyama, T. Sotobayashi and T. Suzuki, "Highly fractionated nuclear debris resulting from the venting of a Soviet underground nuclear test", Nature 209, 239, Jan. 15, 1966.

8. International Commission on Radiological Protection, Publication No. 2, 1959 (also Health Physics 3, 1).

9. G. C. Dale, unpublished.

10. G. M. Dunning, "External β-doses from radioactive fallout", Health Physics 1, 379, 1959.

11. US Weather Bureau, "Weather and surface radiation prediction activities", PNE-201 F, May 15, 1963.

12. D. A. Holme and K. Stewart, "The gamma dose-rate above an infinite plane source", AWRE Report E-6/63, May 1963.

13. O. G.Sutton, "Atmospheric turbulence", Methuen, 2nd Ed. 1955.

14. K. Stewart, "The resuspension of particulate matter from surfaces", ORNL Symposium on "Surface Contamination", June 1964.

15. A. M. Piper and F. W. Stead, "Potential applications of nuclear explosives in development and management of water resources - Principles". TEI - 857, March 1965.

16. F. Holzer, "Gasbuggy Experiment", PNE - G - 43 (UCRL 71624) March 10, 1969.

17. C. F. Smith, "Project Gasbuggy. Gas quality analysis and evaluation program. Tabulation of radiochemical and chemical analytical results." UCRL-50635, April 22, 1969.

18. J. J. Cohen, "Purging of nuclear chimneys", UCID 15259, 1967.

19. H. Howells, "Discharges of low activity radioactive effluent from the Windscale works into the Irish Sea", Paper SM 72/50 of IAEA Symposium on "Disposal of radioactive wastes into seas, oceans and surface waters", Vienna 1966.

20. H. C. Rodean, "The particle statistics of rubble produced by underground nuclear explosions", Geophysics 30, 616, August 1965.

21. "Project Rulison", World Oil 169 (Issue 4) 67, September 1969.

XA04N0864

GAS QUALITY ANALYSIS AND EVALUATION PROGRAM FOR PROJECT GASBUGGY*

C. F. Smith

Lawrence Radiation Laboratory, University of California
Livermore, California 94550

ABSTRACT

Experimental results of the gas quality analysis program for Project Gasbuggy through August 1969 are presented graphically, addressing the questions raised by the preshot program goals. The chemical composition and the concentrations of tritium, krypton-85, carbon-14 and argon-37, 39 are presented as a function of time and gas production from the nuclear chimney. Chemically, the presence of CO_2, CO and H_2 served to dilute the formation gas and caused reactions which significantly altered the gas composition at early times. The radionuclide content of the chimney gas at reentry was some 800 pCi/cm^3 of which about 80% was CH_3T. Lesser quantities of tritium were observed as HT, C_2H_5T and C_3H_7T. The other major contaminant was Kr^{85} which was present at about one-fifth the level of CH_3T. Small quantities of carbon-14 and argon-39 were also identified. The only other radionuclides identified in the gas were relatively short-lived rare gases.

During the production testing, about two and one-half chimney volumes of gas at formation pressure were removed. This removal, accompanied by dilution, has reduced the radionuclide concentrations to about 7% of their levels at reentry. The production characteristics of the Gasbuggy environment prevented an adequate test of the effectiveness of chimney flushing. However, the rapid drawdown concept is supported by the available data as an effective means of reducing contaminant levels. The changes in composition during production or testing are seen to be consistent with a model involving a non-uniform gas influx rate and flow distribution over the chimney region. Mixing times are estimated to be on the order of a few days, so that increasing concentrations following a sudden gas influx can be explained.

I. INTRODUCTION

Since inception, plans for Project Gasbuggy have included a program of one sort or another for analysis of the gas in the postshot nuclear chimney. The first formalization of this program was made by the Gasbuggy Feasibility Study[1] issued by El Paso Natural Gas Company in May of 1965. Among the experimental objectives listed in that study were the measurement of (1) the "extent of radioactive contamination of the produced gas," and (2) "extent of mixing of formation gas with contaminated chimney gas, and investigation of production techniques for controlling the degree of mixing." More recently, these objectives have been re-stated as a need "to determine the gas quality

---

[*] Work performed under the auspices of the U. S. Atomic Energy Commission.

with regard to contamination by radioactivity and to evaluate various techniques suggested for reducing this contamination."[2,3]

In this paper, the accumulated data of the last two years will be discussed in relation to these specific program objectives. Interpretation and evaluation of the Gasbuggy results in more general terms, related to the expanded goals of the Gas Quality program, are discussed in subsequent papers.[4,5]

II. EXPERIMENTAL PROCEDURES

The physical operations involved in the procurement of data are sampling, chemical analysis, radiochemical analysis, and monitoring. Each operation depends to some extent upon the others, and each must be optimized to ensure reliable experimental results. Conversely, appreciation of the significance of these results is dependent upon an appreciation of these operations and their associated limitations and uncertainties. No useful purpose is served here by a detailed discussion of these procedures; they are so discussed elsewhere.[6,7] I shall, however, attempt to summarize some of the significant aspects which are necessary to the discussions which follow. An overview of the gas production and our analytical results is shown in Fig. 1.

Sampling

Because of the potential problems associated with early release of chimney gas, initial samples of the gas were obtained using a downhole sampling system. These problems did not materialize, and surface snap sampling, following sufficient production to flush the production tubing, was attempted shortly after chimney reentry was completed in January 1968. No significant differences in quality of samples obtained by these two methods were seen; therefore, all samples obtained since that time have been taken by the surface snap method.

Eighteen samples were obtained prior to the start of the first production test in June 1968, constituting four independent sets of replicate samples. During short-term production testing, we have attempted to define each test period with at least three samples (start, middle, and end). Bi-weekly samples were taken during the long-term production test beginning in February of 1969. Analyses of these selected samples were used to anchor the day-by-day trends observed by the monitoring system.

The data included in this paper have been obtained through analysis of 57 of the 75 samples obtained for LRL through August 1969.[8] Eighteen samples have been preserved for historical record.

Chemical Analysis

The chemical composition of Gasbuggy samples was determined by mass spectrometry, as was the purity of the separated components. Because of the implementation of routine snap sampling, a small quantity of air is collected along with the chimney gas. The quantity of air is estimated from the oxygen concentration, and is subtracted to obtain a true sample volume. Chemical compositions reported are normalized to 100% exclusive of air. Routinely, this correction is of the order of 1% or less, but occasional samples contained considerably more air. In the extreme, the first four samples obtained from the sealed annulus atop the emplacement well at 1 day following detonation were about 80% air.

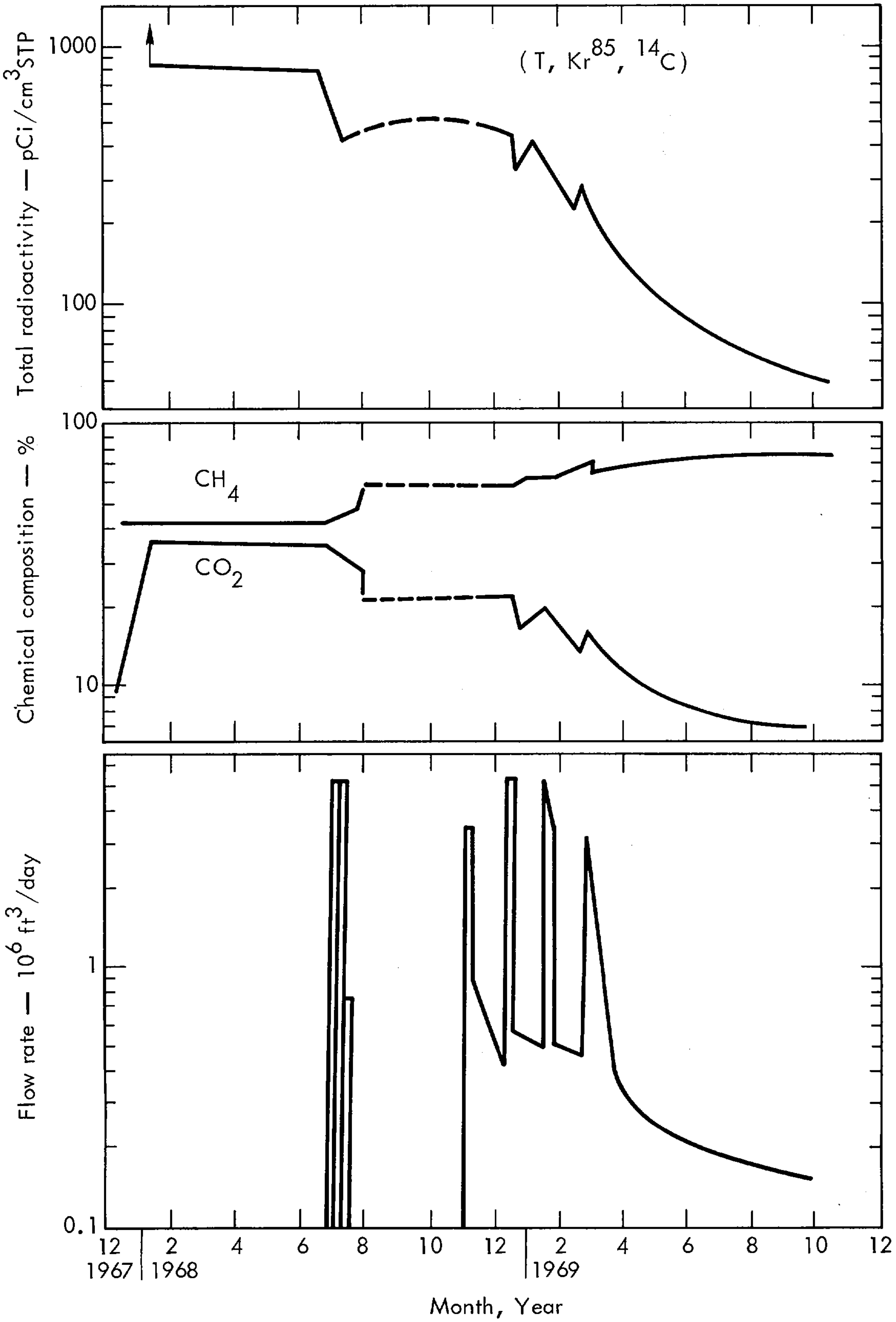

Fig. 1. Project Gasbuggy Gas Quality analysis results.

Radiochemical Analysis

Radiochemical analysis of a Gasbuggy sample begins with separation and purification of the desired components by elution chromatography. The purified fractions are then placed in appropriate counters for radio assay. Krypton-85 is determined in quadruplicate by thin-window beta proportional counting. Compounds containing tritium and C^{14} are determined by internal proportional counting of duplicate or quadruplicate fractions.

For intercomparison of the radionuclide concentrations, all data have been corrected for decay to the time of detonation.

Monitoring

The Stallkat system for monitoring the concentration of Kr^{85} and tritium in the gas flowing from the Gasbuggy nuclear chimney has been in operation since the onset of production testing in June 1968. The instrument was conceived, and has been most valuable, for continuous monitoring in connection with the on-site safety program. Reports of the Eberline Instrument Corporation should be consulted in this regard.[9] The principal value of the Stallkat system to the Gas Quality Analysis program has been to delineate trends in the concentrations of Kr^{85} on a day-to-day basis. The ability to normalize these trends to our laboratory results has been a significant factor in reducing the number of analyses required for adequate documentation and investigation of phenomenology.

III. LIMITATIONS AND UNCERTAINTIES OF THE ANALYTICAL RESULTS

The absolute uncertainty associated with determination of chemical composition by mass spectrometry is related to the actual concentration, but for those species of interest here can be assumed to be on the order of ±5% or less. Precision of the radiochemical determinations is measured by replicate analyses, the uncertainty being generally on the order of a few percent. The absolute uncertainty of these measurements is not known, but is probably less than ±10% for the species listed.

The data summary graphs which are to be presented here are based upon information published in tabular form for the open file system of Project Gasbuggy.[8] This tabulation includes actual values for the precision of radiochemical determinations for each sample. Error bars have, in general, been omitted from the graphical presentation because they typically fall within the plotted point symbols. Where such bars do appear, they represent the spread observed in results obtained from analyses of two or more presumably similar samples, and do not reflect the precision of a determination for an individual sample or component.

Potentially, large uncertainties may be present due to the very nature of the experiment. Among these are the single sampling point at the top of the nuclear chimney, non-ideal gas influx and mixing, and an extremely complex environment in which to study chemical and radiochemical reactions. It is extremely difficult to separate those phenomena associated with peculiarities of the Gasbuggy environment from observations characteristic of gas stimulation by nuclear means in the general case. The need for further detailed experimentation, both in the laboratory and in the field, is particularly evident in this area.

IV. RESULTS AND DISCUSSION

For the present discussion, results from Project Gasbuggy may be grouped according to major gas production periods. The initial 200-day shut-in period has provided significant chemical and radiochemical data. A high flow-rate test followed shut-in, and is a partial test of the concept of chimney flushing. Two periods of production testing, the first composed of three test segments and the second a long-term production test, are useful in defining the relationship between flow rate and concentration of chimney gas components.

Chimney Shut-In Period (12/10/67 to 6/28/68)

During the first 200 days following detonation, the Gasbuggy chimney served as a great reaction vessel in which essentially all important chemical and radiochemical reactions observed to-date took place. Considerable interest has, therefore, been accorded to the information gained from this period.[4,5,6]

There are only five sets of samples taken during this period, including that obtained at 1 day via the cable leak, and the initial (after 5 million ft^3 of gas had been produced) sample of the June/July production test. Although the method of obtaining the 1-day sample was far from ideal and considerable uncertainty regarding its true worth persists, we feel that it merits consideration relative to establishment of trends in the chimney gas composition prior to the reentry samples (at 34 days). However, a detailed description of the actual changes in composition is not known. Arbitrary dashed lines are used to connect points, without intent to define the true rate of composition change.

Chemical composition of the chimney gas during this period is presented in Fig. 2. Immediately apparent is the fact that the most significant changes in composition occurred during the first month. The lack of reliable experimental data during this period may preclude an unambiguous interpretation of these results. Quite evident, however, is the early, rapid conversion of CO to CO_2, probably by a reaction with steam. This reaction appears to have reached equilibrium prior to the 1-month datum point. The observed decrease in H_2 concentration is slight, possibly due to a combination of its production in the aforementioned reaction and its reduction through various methane-producing reactions involving CO and CO_2. Methane and ethane as components of both the chimney gas and the formation gas are less easily interpretable. The illustrated trend probably is misleading, and methane was essentially constant. Within the uncertainties involved with the exceptionally large air correction for these early samples, it is quite possible to assume that the observed behavior of both methane and ethane can be accounted for by influx of natural gas from the formation as a result of cooling of the chimney.

Following chimney reentry, only H_2 and CO exhibit significant changes in abundance. The decreases observed are consistent with the assumption that they react to produce methane and CO_2 at a relatively slow rate.[5] Additional formation gas influx is expected as chimney cooling occurs, and indeed must be assumed to explain the extent of the increase in the percentages of CH_4 and C_2H_6. The observed decrease in C_3H_8 is probably due to fractionation of the sample in transit through the production tubing.

The concentrations of Kr^{85}, and of tritium in various chemical forms are presented in Fig. 3. Again, the most significant changes are observed during the first month. The most dramatic of which is exhibited by HT which decreases by a factor of about 20. This tritium is partially incorporated in methane and ethane, but is primarily removed from the gas presumably by incorporation in water, via exchange reactions.[4] Most probably these reactions have reached equilibrium prior to chimney reentry. The concentration of C_3H_7T is essentially constant, although the data are influenced by the same fractionation effects noted previously.

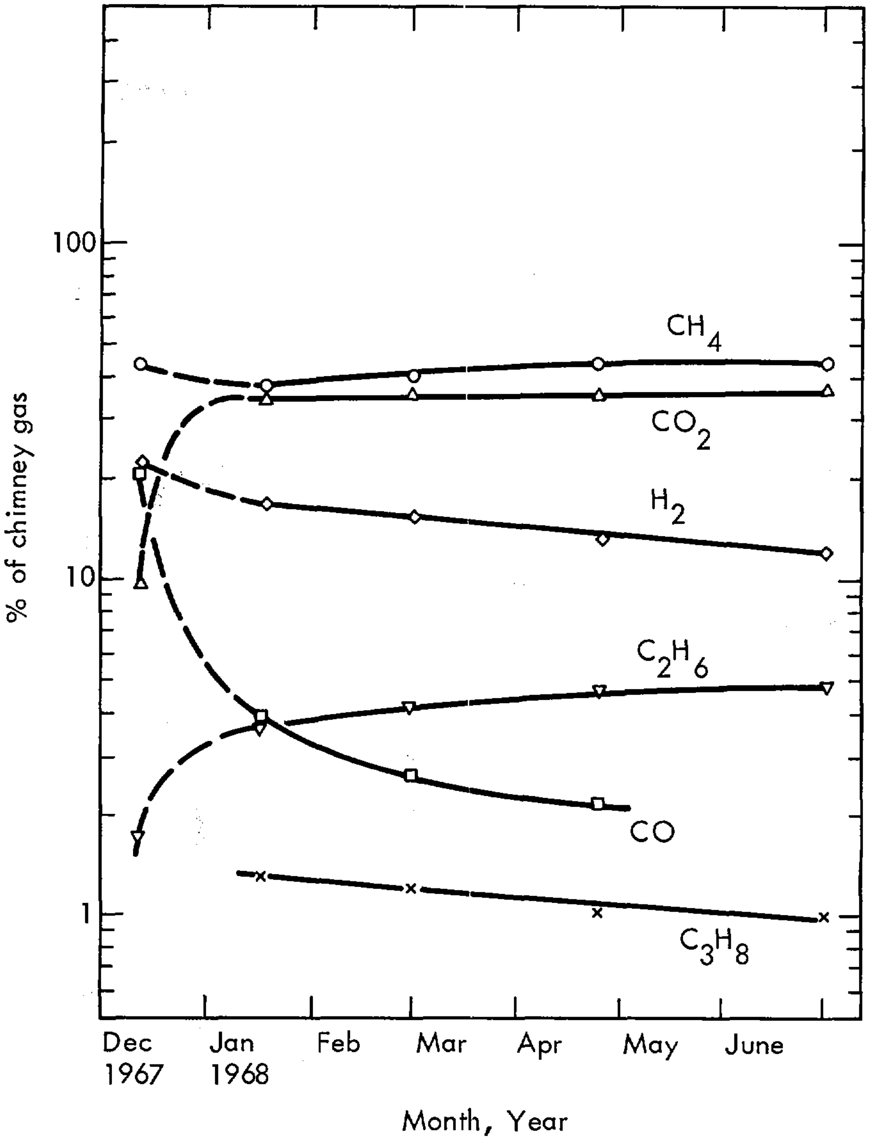

Fig. 2. Initial shut-in period, chemical composition.

The total tritium content of the gas decreased during the first month from about 30% to about 5% of the expected total of 4 g of this isotope. Presumably, the remaining 95% is in the form of water. The principal contaminant of the gas after the first month is seen to be CH_3T.

The near constancy, within experimental uncertainty, of the Kr^{85} concentration over the entire shut-in period implies mixing with a constant volume of gas and rapid pressurization of the chimney. Essentially all the mass-85 fission yield is Kr^{85} by 10 minutes following the detonation. Although entrapment of the gas in solidified melt could occur, the measured total Kr^{85}, using a known amount of Xe^{127} tracer added to the device preshot, was 350 ± 20 Ci, which corresponds to the preshot estimate. The actual volume of gas with which the Xe^{127} must have mixed to give the observed concentrations was $3.0 \pm 0.2 \times 10^9$ liters at standard temperature and pressure ($1.06 \pm 0.05 \times 10^8$ ft^3 STP). This quantity of gas would be contained in a void

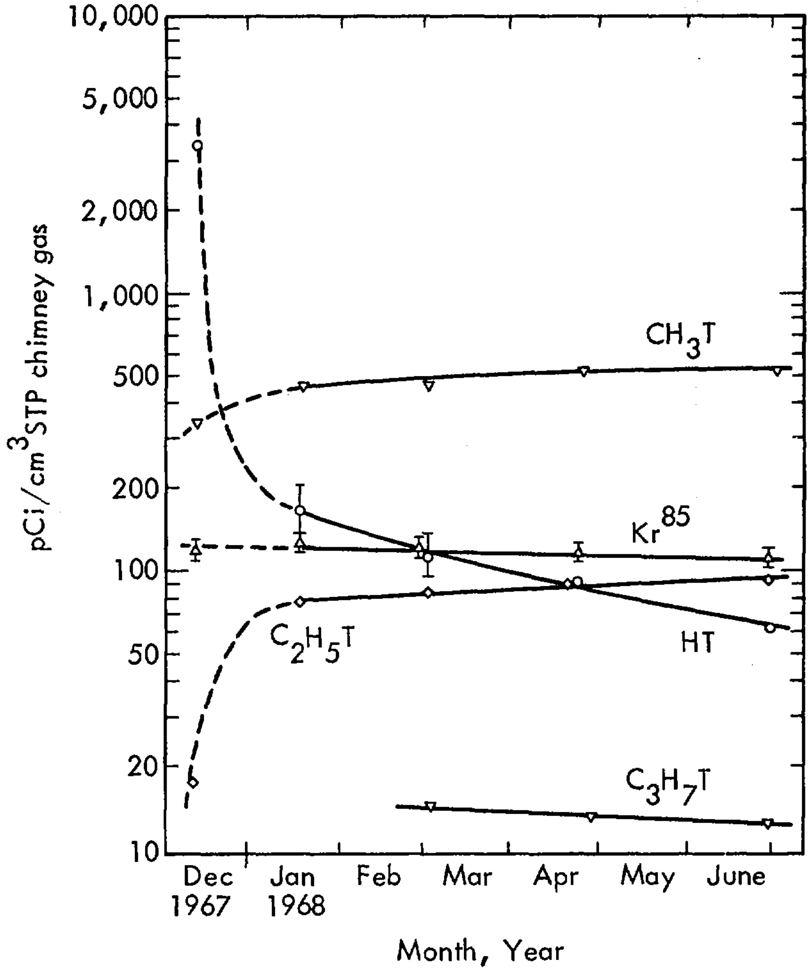

Fig. 3. Initial shut-in period, radionuclide concentrations.

of 5.8 ± 0.3 × 10^7 liters (2.0 ± 0.1 × 10^6 ft^3) at 150°F and 950 psig (the observed condition on Jan. 23, 1968). Such a void was estimated preshot, and is in reasonable agreement with volumes derived during chimney drawdowns.

Experimental concentrations of C^{14} in the principal carbon-containing gases are presented in Fig. 4. Clearly apparent is the decreasing $C^{14}O$ and correspondingly increasing $C^{14}H_4$. These data support the observation that methane is being produced. Total C^{14} in the gas is essentially constant at about 2.5 pCi/cm^3, implying a total C^{14} content in the gas of about 7.5 Ci. No indication of the actual total C^{14} produced is available, since some unknown fraction of this isotope may exist in one or more non-gaseous forms in the nuclear chimney.

Other radionuclides have been identified in the chimney gas during this period. During the first few months, appreciable quantities of short-lived

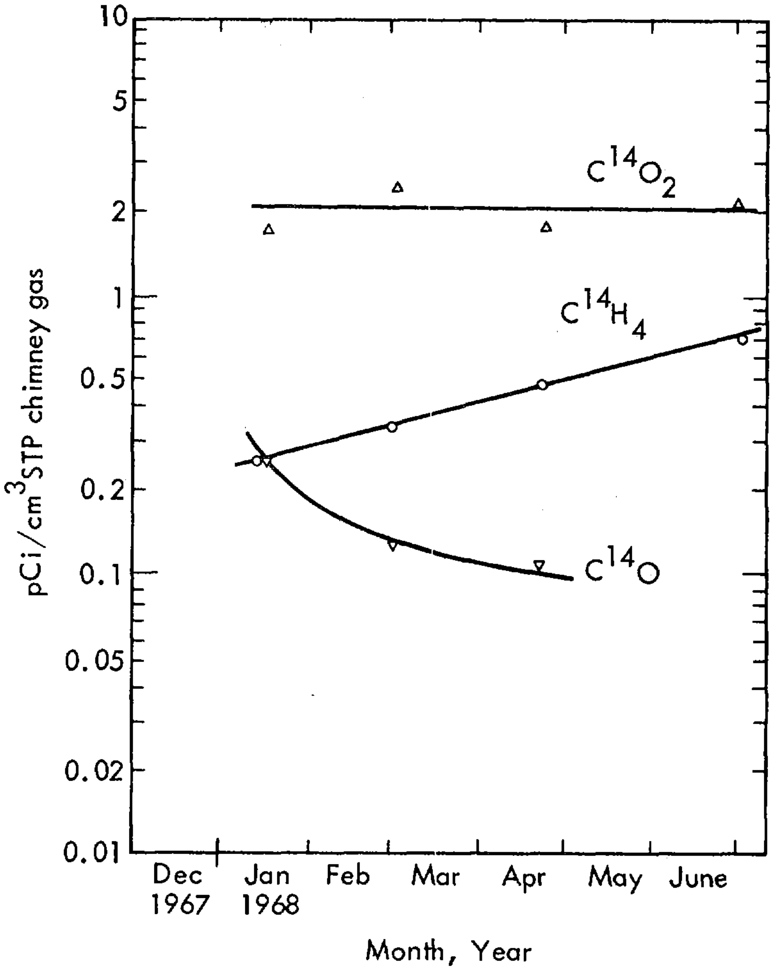

Fig. 4. Initial shut-in period, radionuclide concentrations.

fission product gases and activation products, principally Ar^{37} and Ar^{39}, were present. By the end of the 6-mo period, essentially all of the fission product gases except Kr^{85} had decayed. Concentrations of Ar^{37} were comparable to those of Kr^{85}, while the Ar^{39} was some 1000 times less abundant. Aside from Rn^{222}, which is normally present in natural gas, no other radionuclides have been detected. A search for the possible presence of non-gaseous isotopes was made during this period by gamma spectroscopy.[10] No such species was identified, and maximum possible concentrations based upon detection limits were established. These range from 0.04 pCi/cm^3 for I^{131} to about 10^{-5} pCi/cm^3 for Cs^{137}. More recently, a beta-count survey of filters taken during a rapid drawndown in November 1969 was made. Total beta activity on these particulate samples is estimated to be less than or equal to 10^{-7} pCi/cm^3 of gas passing the filter.

In summary, the principal radioactive contaminants of the Gasbuggy chimney gas at about 6 mo following the detonation are T, Kr^{85}, Ar^{37} and C^{14}. The relative abundances are listed in Table I.

Table I. Relative contribution to total gaseous radioactivity at 6 mo.

Tritium (principally CH_3T)	78%
Kr^{85}	12.5%
Ar^{37}	9.2%
C^{14} (principally $C^{14}O_2$)	0.25%
Other	0.05%

High Flow Rate Production Tests (6/28/68 to 7/14/68)

At the end of the shut-in period, the chimney gas was flared at the rate of 5 million ft^3 per day for 6 days, shut-in for 2 days, then produced for 5 more days. The flow rate was then dropped to 3/4 million ft^3 per day for 4 days, at which time the well was closed off. The observed changes in chemical composition during this period are shown in Fig. 5. At the high flow rate, the produced gas is

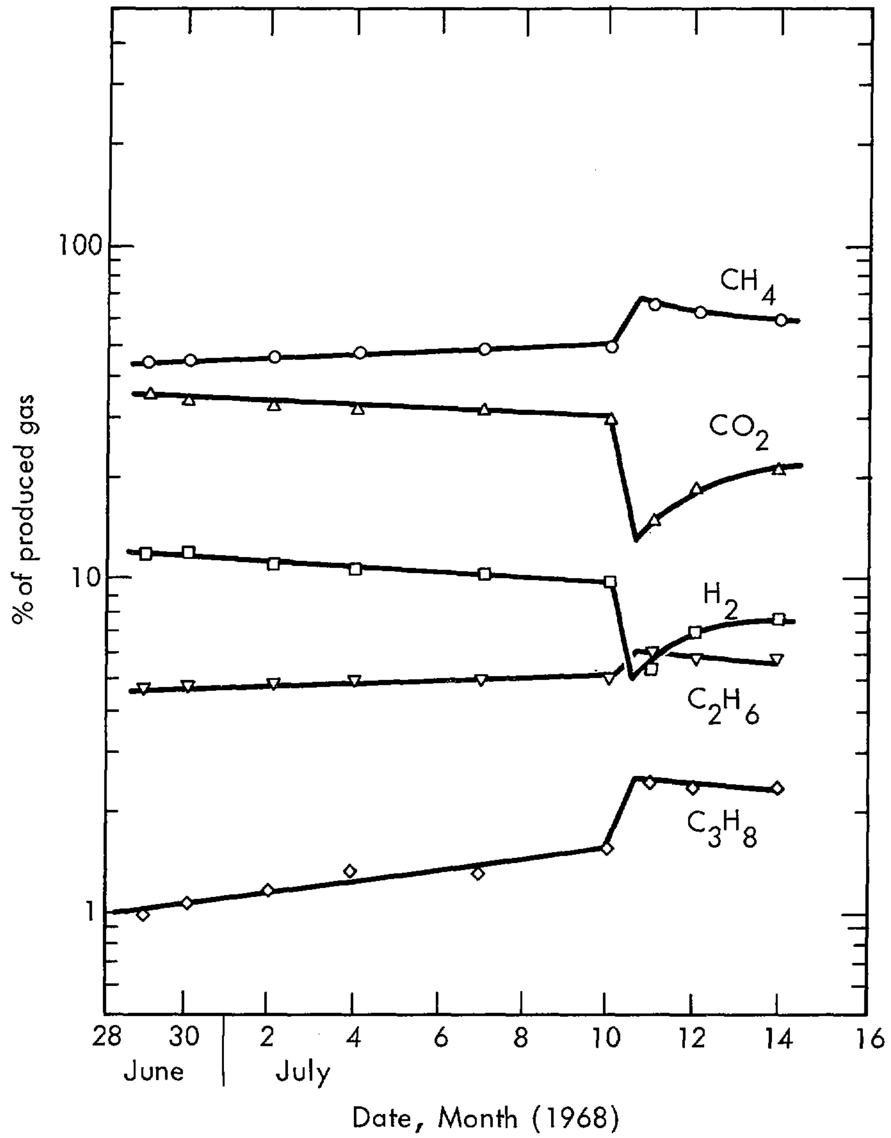

Fig. 5. High rate production test, chemical composition.

drawn principally from the chimney. Only 17% of the gas removed actually came from the formation. A significant dilution in the produced gas was observed when the flow rate was cut back on July 10. The concentrations of the various species after the 4-day lower flow period are about what would be expected by applying a dilution correction, based upon top hole pressure measurements, to the final high flow rate composition. We are forced to conclude that when the flow was reduced, the dilution was greater than could be explained by simple formation gas influx and rapid mixing. The observed behavior can be explained by a significant influx of gas into the top of the chimney at about the time the flow was reduced, causing the large dilution observed. Over the 4-day period the components of the chimney become essentially mixed, resulting in an apparent increase in concentration of CO_2 and H_2. These conclusions are supported by gas analysis data from subsequent production tests. The increased productivity of the upper portions of the Pictured Cliffs as related to deeper sections is made plausible by comparison of pre- and postshot caliper logs[11] and by production results[12] of satellite wells.

Concentration of radionuclides during this period are presented in Fig. 6. Lines of similar shape are drawn through data for each component. These are based upon the trends observed in CO_2 and H_2 in the preceeding figure. No difference in shape is warranted by the fit of these lines to the data, indicating absence of the effects of chemical reactions.

Inferences drawn from these data with regard to the effectiveness of chimney flushing suffer two main drawbacks. In the first place, the duration of the high-rate tests were not sufficient to demonstrate the effects of formation gas influx at relatively low chimney pressures. Although 40% of a chimney volume of gas was produced, more than 80% of this was initially within the chimney. The degree and rate of mixing of formation gas with chimney gas under high production rate conditions thus remains undefined.

The second drawback is due to the geology of the Gasbuggy site. Production of gas occurs principally via fractures, with the matrix permeability being quite low. Postshot investigations[11] have deduced a sketch of the chimney which reveals sagging geologic bedding planes rather than a void in the upper portion of the chimney. Since the reentry well penetrates only the uppermost layers of these planes, horizontal communication with formation gas through fractures is probable. Furthermore, access of chimney gas to this region may be impeded (permeability within the chimney is finite). We may, therefore, be observing a mixture of gases in a flow situation which is related to the true chimney gas composition via the relative values of horizontal and vertical permeabilities. In other words, at a given influx rate, the gas observed during high flow rate tests may contain a higher proportion of the true chimney gas than that observed during low production rates. Presumably, mixing occurs under static conditions so that the concentrations following shut-in are essentially uniform throughout the chimney.

Having stated these caveats, and with the limited data available, it is imprudent to speculate upon the extent to which the Gasbuggy chimney could have been decontaminated by a long-term, high-rate production experiment. However, decontamination by rapidly removing a contaminated chimney volume or two of gas appears to be effective, so long as production well in excess of gas influx is possible. The process is useful only when gas in this quantity can economically be flared, produced to controlled usage or produced to storage.

Constant Bottom Hole Pressure Production Tests — (11/7/68 to 2/18/69)

Between July 14 and November 11, 1968 the Gasbuggy chimney remained shut-in. A series of three production tests followed in which an attempt to maintain a constant bottom hole pressure by varying flow rate was

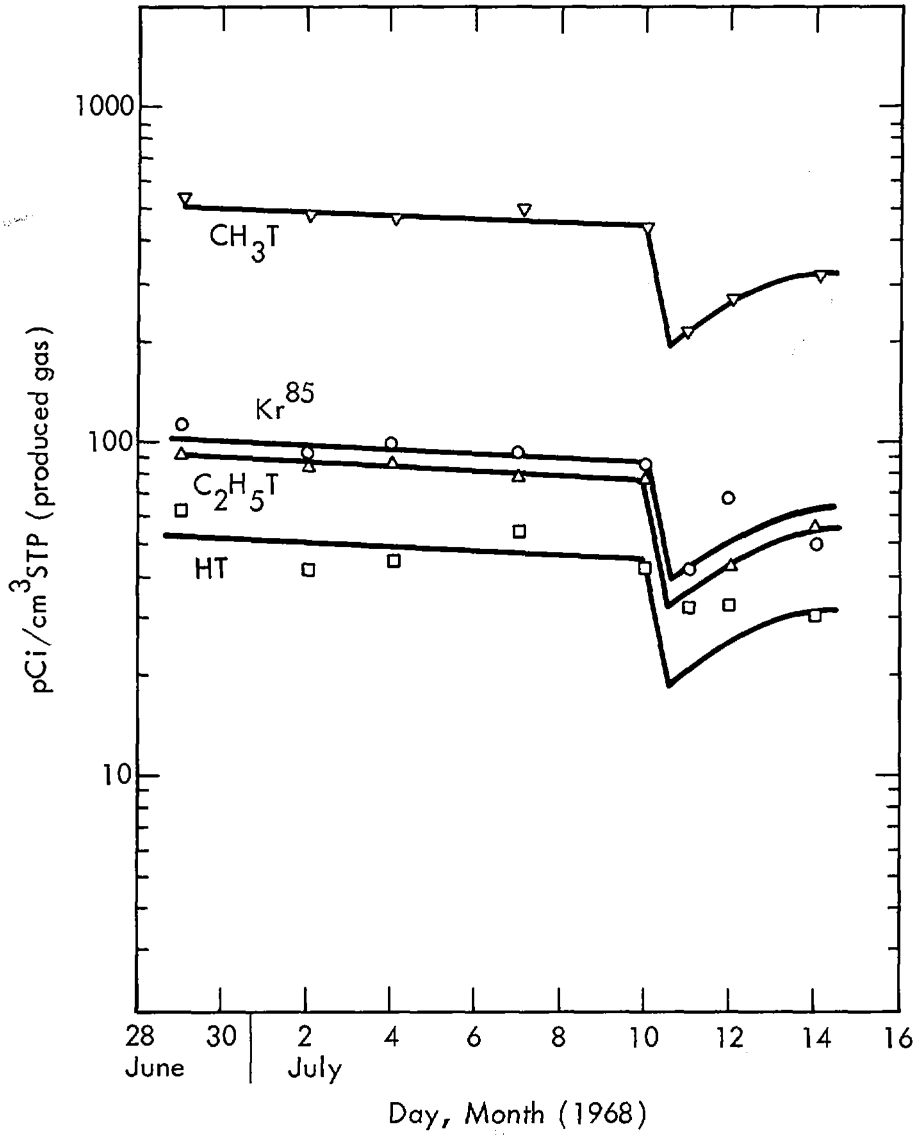

Fig. 6. High rate production test, radionuclide concentrations.

made. Each test was preceded by a rapid drawdown to adjust the initial pressure. Presented in Fig. 7 are fractional abundances of the principal components of formation gas. Aside from the dilution which occurred following the second rapid drawdown, no distinct trends are obvious. These species are, however, quite insensitive as indicators of dilution since their concentrations in the chimney are approaching those in the formation.

Much more sensitive are the components of chimney gas alone, CO_2 and H_2, as illustrated in Fig. 8. The complex behavior of these concentrations is plausibly explained by the following chain of events: During the initial test period only a slight admixture of formation gas occurred, and essentially only chimney gas was being produced. Little mixing and dilution of the chimney gas took place, as evinced by the apparent return of the concentrations to their initial levels during the rapid drawdown in December. The pressure drop resulting from this drawdown induced a rapid influx of formation gas and produced

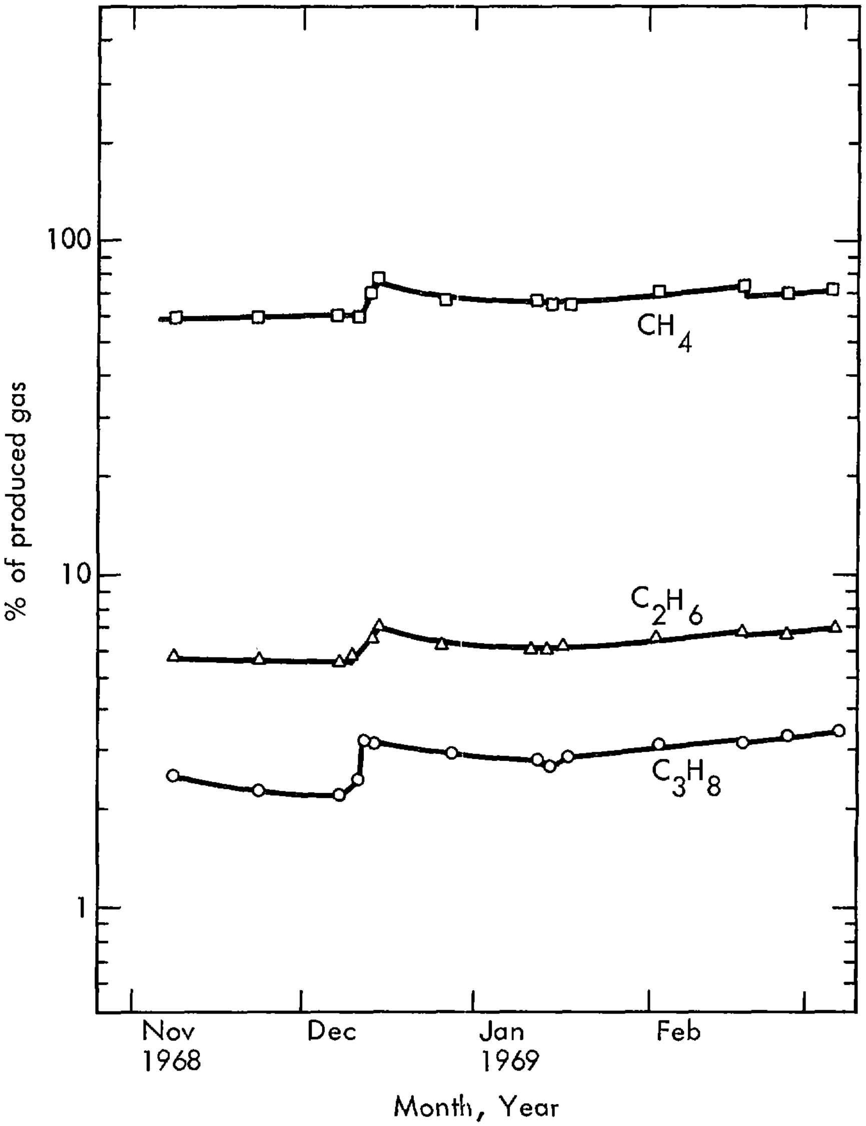

Fig. 7. Constant bottom hole pressure production tests, chemical composition.

the initial large dilution observed. Gradual mixing of this diluent with the chimney contents produced the observed increase in concentrations during the second test period. These observations are analogous to those made previously from the June/July production test data. The rapid drawdown of January 1969 was apparently not followed by a rapid gas influx from the formation. Nevertheless, the decreased pressure stimulated the flow of diluent gases through the third month of production, and concentrations of these species in the produced gas continued to decrease. Illustrated at the end of February is the effect of the high production rate which began a long-term drawdown of the Gasbuggy chimney. Again the lack of efficient mixing is demonstrated by increasing concentrations. This is due to inclusion of relatively more chimney gas in the produced mixture as a result of the high withdrawal rate.

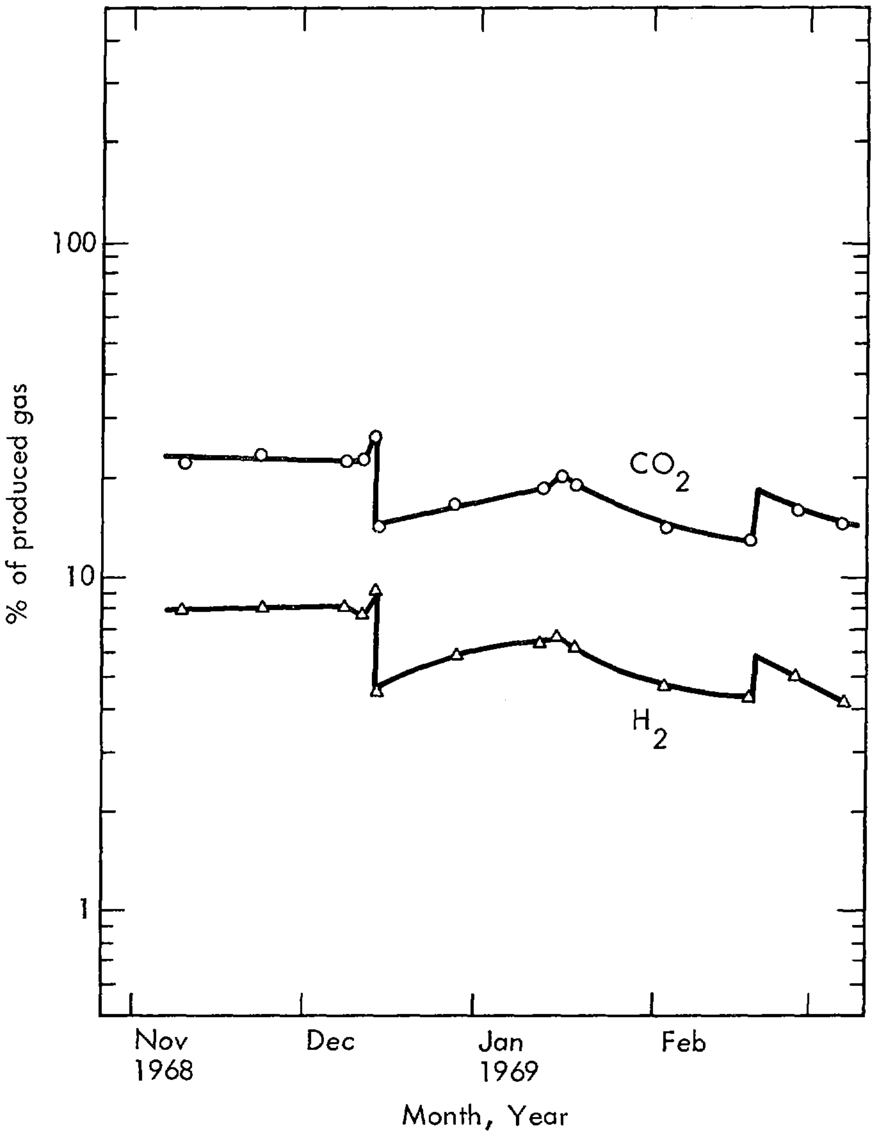

Fig. 8. Constant bottom hole pressure production tests, chemical composition.

Radionuclide concentrations through these tests are plotted in Fig. 9. As expected, the changes observed in these concentrations generally parallel those observed for CO_2 and H_2. Although some differences appear they are not described by a consistent trend, and are therefore probably not related to chemical reactions in the gas. We conclude that no significant effect other than dilution is detectable, within experimental uncertainty, during this period.

Long Term Production Test (2/18/69 to 10/28/69)

An 8-mo production test was begun in February 1969 at a flow rate of 3.5 million ft^3 per day. This production more or less gradually decreased until June where it was essentially stabilized at about 160,000 ft^3 per day. The percentage composition of components of the chimney gas through August

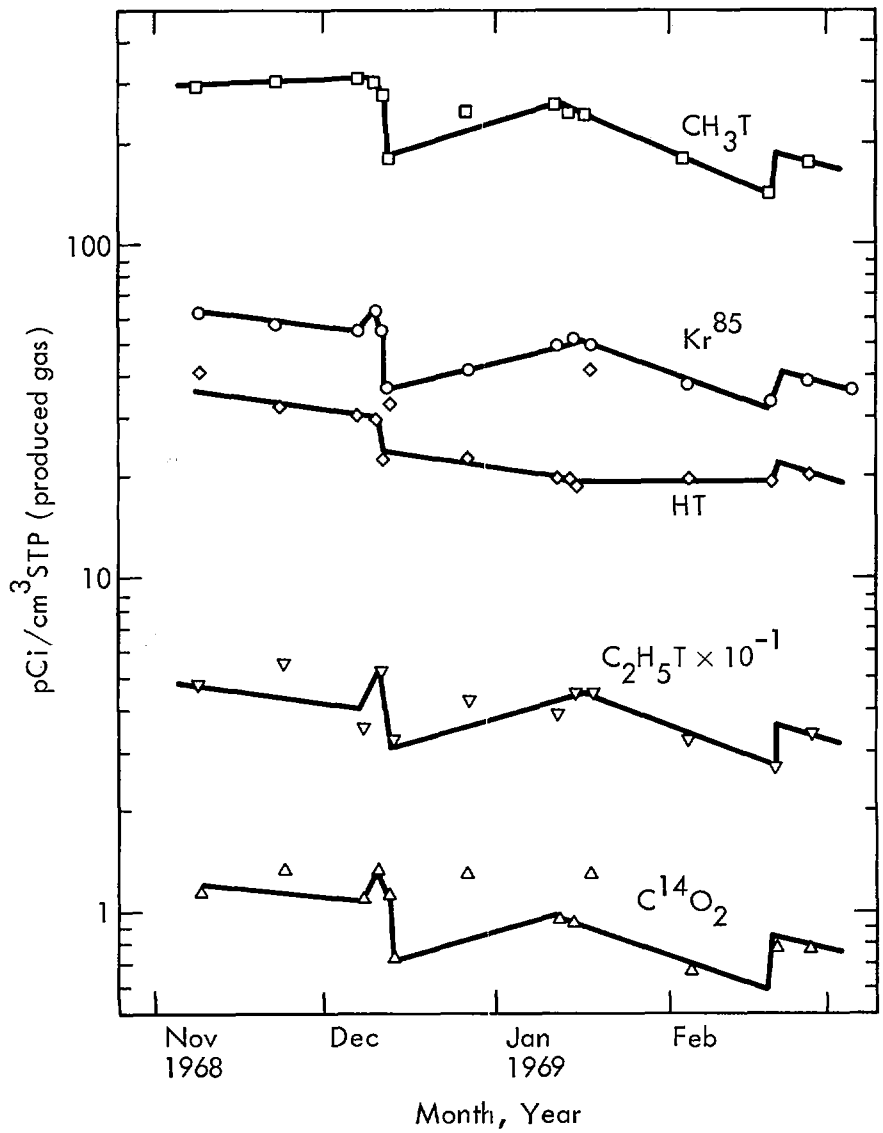

Fig. 9. Constant bottom hole pressure production tests, radionuclide concentrations.

is shown in Fig. 10. Effects of dilution are demonstrated by the gradually decreasing concentrations of CO_2 and H_2. Formation gas influx was decreasing throughout this period, as evidenced by the necessity to adjust flow rates downward to maintain a reasonably constant down-hole pressure. Concentrations of CO_2 and H_2 are seen to reflect this decreasing availability of diluent gas from the formation. Note, for future reference, that the overall decline in concentrations of CO_2 and H_2 amounts to a dilution of a little more than a factor of two, and that they appear to be changing relatively little during the final few months. The components of the formation gas exhibit increasing concentrations, as expected.

Concentration changes of the radioactive chimney gases are shown in Fig. 11 for this production period. The similarity of the rates of decrease of these concentrations is indicative of the effects of dilution with formation gas.

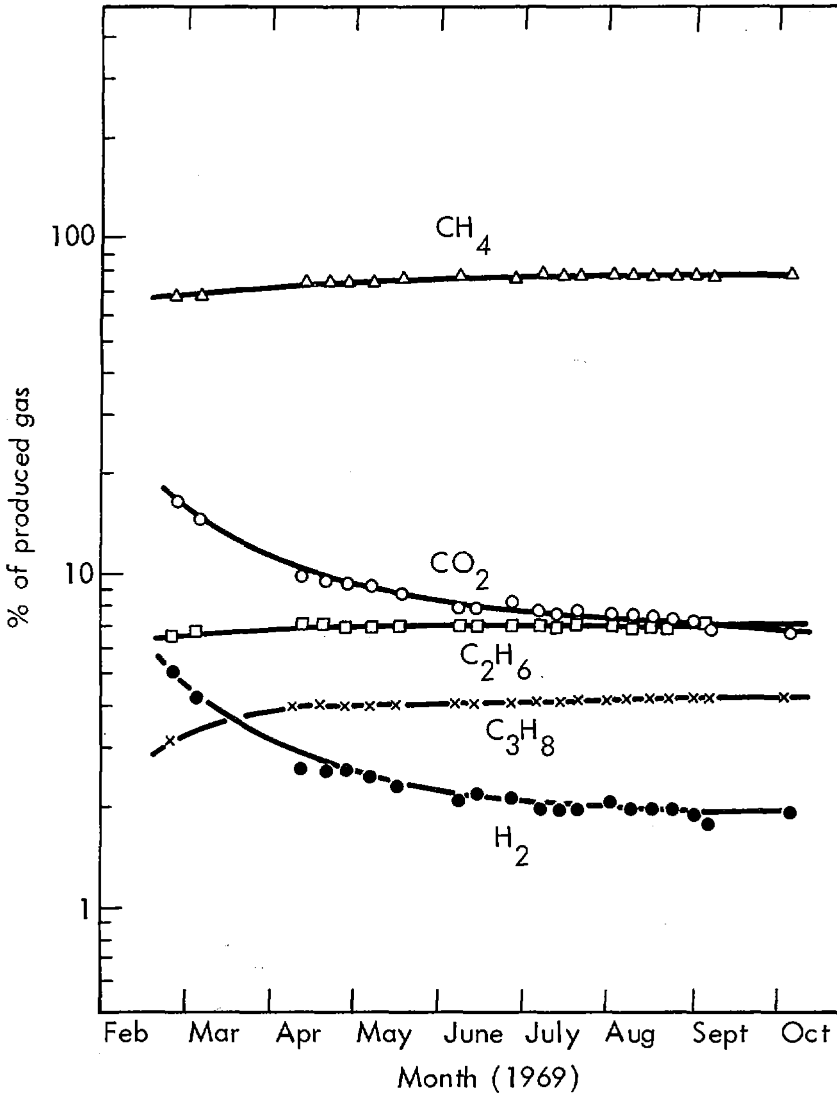

Fig. 10. Long-term production test, chemical composition.

Comparison of the shape of these curves with that shown for CO_2 and H_2 in Fig. 10 presents an interesting anomaly. Relative changes for the radioactive components amount to more than a factor of four due principally to a greater rate of decrease during the final months. To illustrate, the ratio of Kr^{85} to H_2 and to CO_2 is plotted in Fig. 12 over the entire Gasbuggy postshot period. Although the deviation is most marked toward the end of the extended production period, the trend is observed throughout. Evidently, the concentrations of CO_2 and H_2 are decreasing less rapidly than the concentration of Kr^{85} during production. This trend implies a source of CO_2 and H_2 which is not initially mixed with the Kr^{85} in the chimney gas. Such a source for CO_2 may be gas dissolved in the water within the chimney. H_2 is much less soluble and the soda water concept cannot explain its similarity to the CO_2. A possible source for additional H_2 could be diffusion into the formation at early times and subsequent diffusion back to the chimney when the pressure was significantly

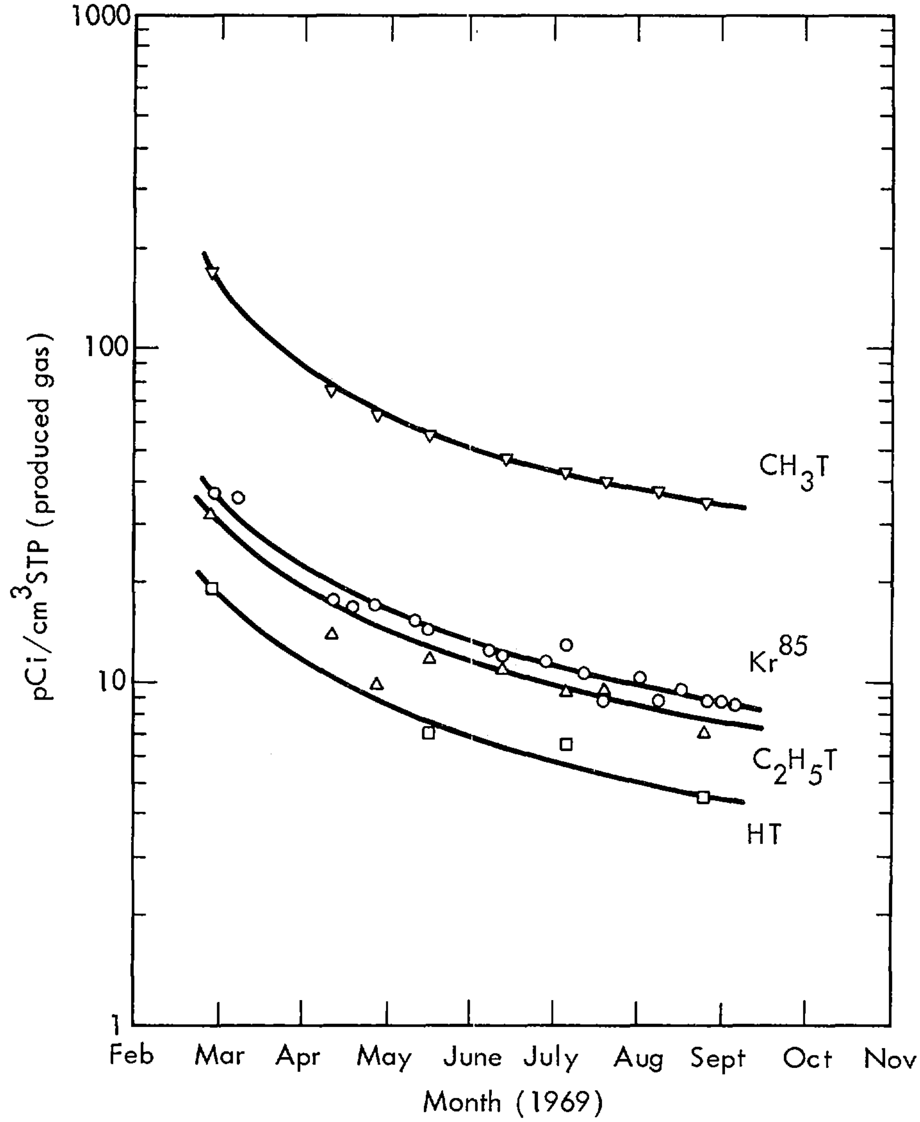

Fig. 11. Long-term production test, radionuclide concentrations.

lowered by production. All radionuclide concentrations including the Kr^{85} have been corrected for radioactive decay to the time of detonation.

V. SUMMARY

Drawing from the data presented here, it is possible to address the questions raised by the principle goals of the Gas Quality Program. The gas quality, both with regard to chemical composition and radionuclide concentrations, has been well defined. Chemically, the presence of CO_2, CO and H_2 served to dilute the formation gas and participated in reactions which significantly altered the gas composition at early times. The radionuclide content of the chimney gas at reentry was some 800 pCi/cm^3 of which about 80% was CH_3T. Lesser quantities of tritium were observed as HT, C_2H_5T and C_3H_8T.

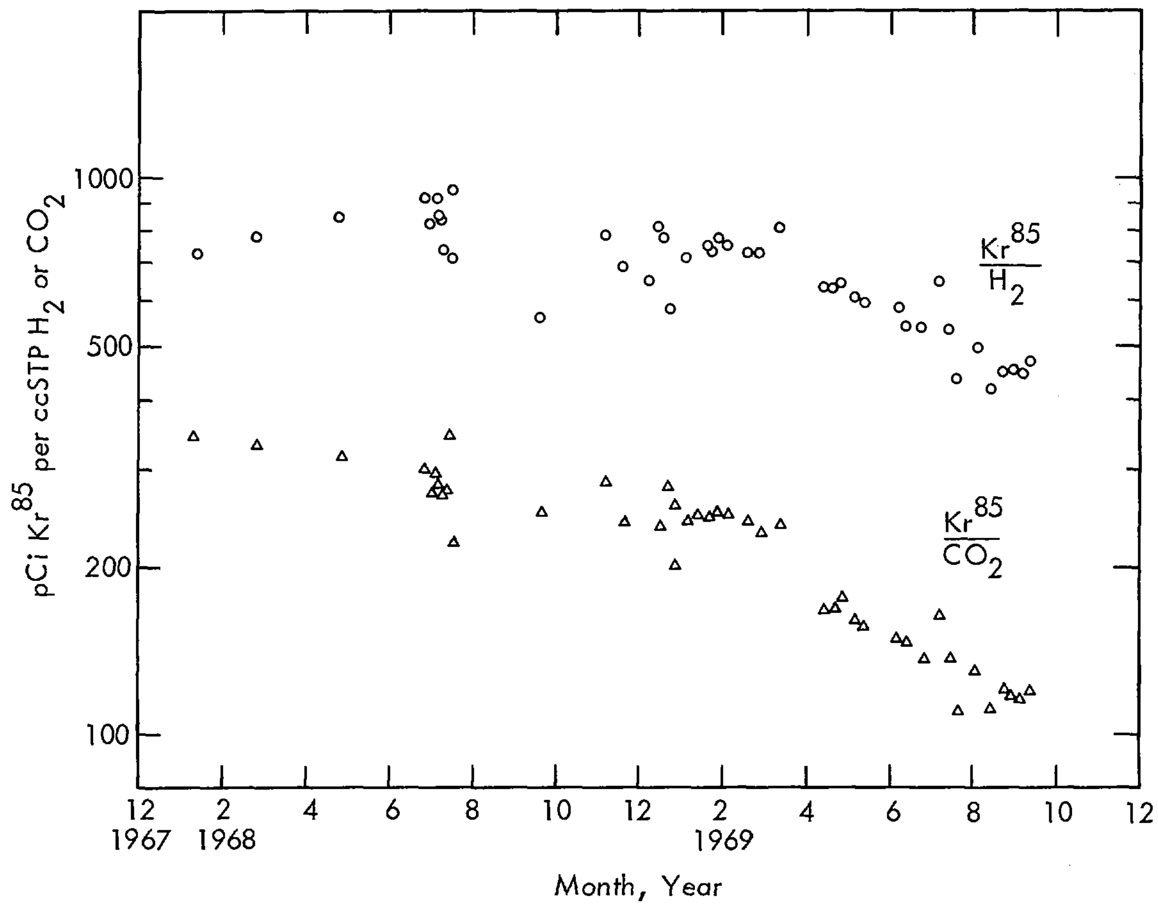

Fig. 12. Ratios of Kr^{85} to H_2 and CO_2.

The other major contaminant was Kr^{85} which was present at about one-fifth the level of CH_3T. Small quantities of C^{14} and Ar^{39} were also identified. The only other radionuclides identified in the gas were relatively short-lived rare gases.

During the production testing, about two and one-half chimney volumes of gas at formation pressure were removed. This removal, accompanied by dilution, has reduced the radionuclide concentrations to about 7% of their levels at reentry. The production characteristics of the Gasbuggy environment prevented an adequate test of the effectiveness of chimney flushing. However, the rapid drawdown concept is supported by the available data as an effective means of reducing contaminant levels. The changes in composition during production testing are seen to be consistent with a model involving a non-uniform gas influx rate and flow distribution over the chimney region.

Mixing times are estimated to be on the order of a few days, so that increasing concentrations following a sudden gas influx can be explained.

Much of the information gathered from this work, especially the gas production effects, may be unique to the Gasbuggy environment. Considerably more information must be available from experiments, both laboratory and in the field, before these data can be generalized to the benefit of nuclear stimulation. The great volume of data which have been summarized here have not yet been fully evaluated and correlated with information gained in other Gasbuggy programs. The interpretative efforts of the Gas Quality program are, therefore, continuing in an attempt to gain a better understanding of the phenomena involved.

ACKNOWLEDGMENTS

The Gas Quality Analysis and Evaluation Program for Project Gasbuggy has drawn upon the talents of a large number of people to produce the results tabulated here. In particular, the efforts of the following groups and individuals deserve recognition:

Mass spectrometry for both chemical analysis of samples and chemical purity of separated fractions was performed by Richard W. Crawford and the Analytical Chemistry Section of the LRL General Chemistry Division.

Sample procurement was a combined effort of many LRL Chemical Engineering, LRL Hazard Control, and Eberline Instrument Corporation personnel.

Radiochemistry was performed by the Gas Analysis Group of the LRL Radiochemistry Division under the immediate supervision of Dr. Floyd F. Momyer.

In addition, the continued interest of the project participants, El Paso Natural Gas, U.S. Bureau of Mines, and the Atomic Energy Commission, as well as valuable discussions with their representatives and with colleagues at LRL has been of great help to the continuing effort to obtain and evaluate these results.

REFERENCES

1. "Project Gasbuggy," El Paso Natural Gas Co., El Paso, Texas, May 14, 1965.

2. "Project Gasbuggy Technical Directors Concept," Anon. SDK 65-1, July 30, 1965.

3. "Test Group Directors Operational Plan—Project Gasbuggy," Anon. SDK 66-41, December 1, 1966.

4. R. W. Raylor, E. L. Lee and J. H. Hill, "Chemical Effects of Nuclear Explosions in Hydrocarbon and Carbonate Bearing Rocks," Proc. 4th Plowshare Symp., Engineering with Nuclear Explosives, Jan. 14-16, 1970, to be published.

5. C. F. Smith, "The Behavior of Radionuclides in Nuclear Gas Stimulation Applications," Proc. 4th Plowshare Symp, Engineering with Nuclear Explosives, Jan. 14-16, 1970, to be published.

6. C. F. Smith and F. F. Momyer, "Studies of Chemical and Radiochemical Composition of Natural Gas from the Cavity Produced by the Project Gasbuggy Nuclear Shot," Radiochem. Data and Reports 10, 281 (1969).

7. F. F. Momyer, "Radiochemistry of the Rare Gases," NAS-NS 3025, Oct. 1960.

8. C. F. Smith, "Project Gasbuggy Gas Quality Analysis and Evaluation Program, Tabulation of Radiochemical and Chemical Analytical Results," UCRL-50635, April 1969 and UCRL-50635 Rev. I, to be published.

9. J. R. Curtis, S. S. Fox, E. L. Geiger and J. G. Phillips, "Project Gasbuggy On Site Radiological Safety and Medical Support Services," Eberline Instrument Corporation, 1968.

10. C. F. Smith, "Non-Gaseous Radioisotopes — Project Gasbuggy Chimney Gas," UCRL-50634, April 7, 1969.

11. D. E. Rawson, J. A. Korver, R. L. Pritchard and W. Martin, "Postshot Geologic Investigations — Project Gasbuggy," SDK-68-31.

12. F. Holzer, "Gasbuggy Preshot Summary Report," UCRL-50345, November 1967.

XA04N0865

INTERPRETING THE CHEMICAL RESULTS OF THE GASBUGGY EXPERIMENT*

R. W. Taylor, E. L. Lee and J. H. Hill
Lawrence Radiation Laboratory, University of California
Livermore, California 94550

ABSTRACT

Nuclear explosions in carbonate-bearing rocks release large amounts of CO_2. In some cases, for example, when the explosion is contained and dolomite is the principal carbonate mineral, sufficient CO_2 may be generated to drive the formation gas away from the chimney. Rocks which contain free carbon, such as the shales of the recent Gasbuggy and proposed Bronco and Dragon Trail experiments, will liberate CO and H_2 in amounts predicted from the yield of the explosive and the C, CO_2 and H_2O concentration in the rock. In general, the greater the amount of free carbon in a rock, the more H_2 will be produced and the higher will be the fraction of tritium in the gas phase.

SUMMARY AND CONCLUSIONS

It is possible to foretell the composition of the gas in the chimney as a function of time as well as the distribution of tritium among water, hydrogen, and methane when nuclear explosives are contained within hydrocarbon and carbonate-bearing rocks.

The estimates are based on the chemical results of the Gasbuggy experiment—interpreted in a manner which is both consistent with chemical thermodynamics and the little we know about the amounts of rock heated to various temperatures by nuclear explosives.

Data needed to make these predictions are the concentrations, at shot point, of CO_2, H_2, hydrocarbon, and free carbon. The specific carbonate minerals present must also be identified. In addition, the composition and pressure of gas in the formation surrounding shot point must be known.

We are uncomfortable with some of the guesses we have had to make in order to make these predictions. The careful study of further nuclear explosions in hydrocarbon-bearing rock will replace some of the guesses with fact. Other guesses need to be investigated by laboratory experiment. For example, we need to know the rate of decomposition of carbonate minerals in the temperature range 500° K to 1200° K, and the importance of cracks and grain size of the decomposition. We should also measure the temperature below which reactions become very slow for mixtures of H_2O, CO_2, CO, H_2, CH_4 and C.

INTRODUCTION

Tritium will be in the gas and oil produced from wells stimulated by nuclear explosives; the amount is critical to the success of the technique. We also need to know what gases to expect and how the gas composition, pressure, and tritium concentration will change with time in forthcoming experiments such as Rulison, Dragon Trail, and Bronco.

---

*Work done under the auspices of the U. S. Atomic Energy Commission.

These primary questions are very difficult to answer. The answers depend upon many factors we have considered, and probably others we have yet to discover. There is often rather scant information on factors that we do consider. Certainly, the amounts of gases released from rocks by heating depends upon the temperature, the amount of rock heated, the length of time it is heated, the particle size of the fractured rock, as well as the chemical composition and mineralogy of the rock. In addition, the gas pressure due both to the lithostatic pressure and the so-called "formation pressure" play a role, for the higher the pressure, the hotter the gas-containing minerals (carbonates, for example) must be heated to liberate gas.

We have made substantial steps toward the prediction of post-shot gas chemistry through the study of thermal and chemical effects of nuclear explosions during the past ten years. Nevertheless, it was not possible to predict the composition or tritium distribution in the gas in the Gasbuggy chimney. The goal of this study is to understand the chemical results of the Gasbuggy experiment and to use this understanding to predict the chemical effects of other nuclear explosives in other hydrocarbon-bearing rock.

GASBUGGY, A SECOND LOOK

Problems

Our lack of understanding of the chemical and thermal effects of underground nuclear explosions was illustrated in a striking manner when we compared our prediction of post-shot gas composition with the actual composition of the gas found on drilling into the Gasbuggy chimney.

Our prediction of the amount of CO_2 generated by the Gasbuggy explosion was based on experience with many nuclear explosions in silicate rock where 500 to 700 tons of rock were melted per kt (10^{12} cal) of energy released. The melting range of silicate rock is about the same as the temperature range where carbonates decompose; so we concluded that the amount of CO_2 to be expected in the chimney would be equal to the amount of CO_2 released from the melted rock. The CO_2 concentration in the rock was 4.7 wt%, measured by the amount of CO_2 evolved by acid from samples taken from a drill hole called GB-1, located 188 ft northwest of the shot point.[1] The expected amount of CO_2 was calculated as follows:

$$(26\ \text{kt}) \left(\frac{700 \times 10^6\ \text{g rock}}{\text{kt}}\right) \left(\frac{4.7\ \text{g } CO_2}{100\ \text{g rock}}\right)$$
$$\times \left(\frac{1\ \text{mole } CO_2}{44\ \text{g}}\right) = 19 \times 10^6\ \text{moles } CO_2$$

The observed composition of gas in the Gasbuggy chimney 36 days after the explosion is given in Table 1. These data indicate the production of twice as much CO_2 as we predicted. In addition, we did not anticipate the 16.8% H_2 and 3.9% CO which were found.[2] Thus, it was clear that we needed a better understanding of the chemical effects of the Gasbuggy experiment.

The specific objective of this part of this report is to show how the gas found upon entering the Gasbuggy chimney could have been generated by the thermal decomposition of the Lewis shale—in a way which is consistent with both the fundamentals of chemistry and our limited knowledge of the thermal history of underground nuclear explosions. Mechanisms to explain the high concentration of CO_2, the large and time-dependent concentration of H_2, CO, and CH_4, and the tritium distribution will be considered in that order.

Table 1. Observed composition of gas in Gasbuggy chimney at 36 days.

	Mole %$^{(a)}$ (observed)	Moles × $10^{-6(b)}$ (calculated)
(1) CH_4	36.9	43.5
(2) CO_2	35.8	42.2
(3) H_2	16.8	19.8
(4) CO	3.9	4.6
(5) C_2H_6	3.6	4.2
(6) C_3H_8	1.3	1.5
(7) C_4H_x	1.1	1.3
(8) N_2	0.5	0.6
	99.9	~118

[a] See Ref. 2.

[b] Based on a gas volume of 5.9 × 10^{10} cm^3 at 338.5°K (65.5°C) and 64.6 atm (950 psi).

Source and Evolution of CO_2

Could it be that the carbonate concentration at shot point was twice what we thought? It has been mentioned that CO_2 analyses were made at shot depth, 4240 ft, in a hole called GB-1. Unfortunately, samples of the Lewis shale at shot depth in the emplacement hole were not taken although at one time "side wall" samples were planned.[3] Once we realized the importance of knowing the carbonate concentration at shot point, we made measurements of the CO_2 concentration in cores taken from GB-2 (300 ft east of the emplacement hole GB-E). In Fig. 1 the amount of CO_2 evolved by acid from samples from GB-1 and GB-2 is plotted as a function of depth. The variation among samples from GB-1 is larger than the variation among samples from GB-2, possibly because larger amounts of samples were taken in GB-2. The average of fourteen samples from GB-1 is 4.68 wt% CO_2, about the same as the CO_2 concentration of a composite sample from GB-1 (4.64%) and about the same as the average of the seven samples from GB-2, which is 4.5%.[1]

From these analyses we conclude that it is not likely that the Lewis shale at shot point contained twice as much carbonate as the average of GB-1 and GB-2. However, the possibility cannot be disregarded entirely.

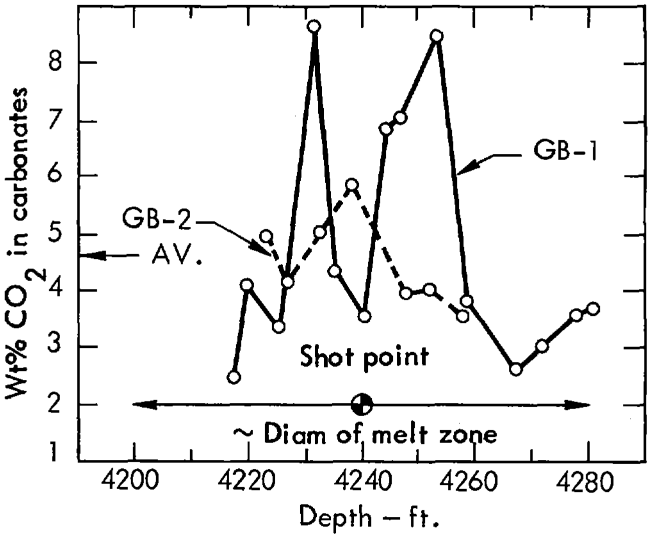

Fig. 1. CO_2 in carbonate as a function of depth.

This conclusion leads us to consider other possible explanations of the high CO_2 concentration in the post-shot gas. Were there carbonate minerals present which decompose at lower temperatures than the melting range of the principal silicate minerals? Did much more Lewis shale than expected get heated to high temperatures?

When viewed through a microscope the Lewis shale is made up of very small quartz and other mineral grains cemented together with carbonate. The carbonate is either dolomite [$CaMg(CO_3)_2$] or calcite ($CaCO_3$), or a mixture of the two; but the analysis is difficult on such a fine-grained rock.[4, 5] X-ray diffraction analysis suggests that dolomite is the dominant carbonate at shot depth in GB-1.

It is important to find out the ratio of dolomite to calcite because the temperature where dolomite begins to decompose at a given pressure is about 400° K lower than the decomposition temperature of calcite (see Fig. 2).

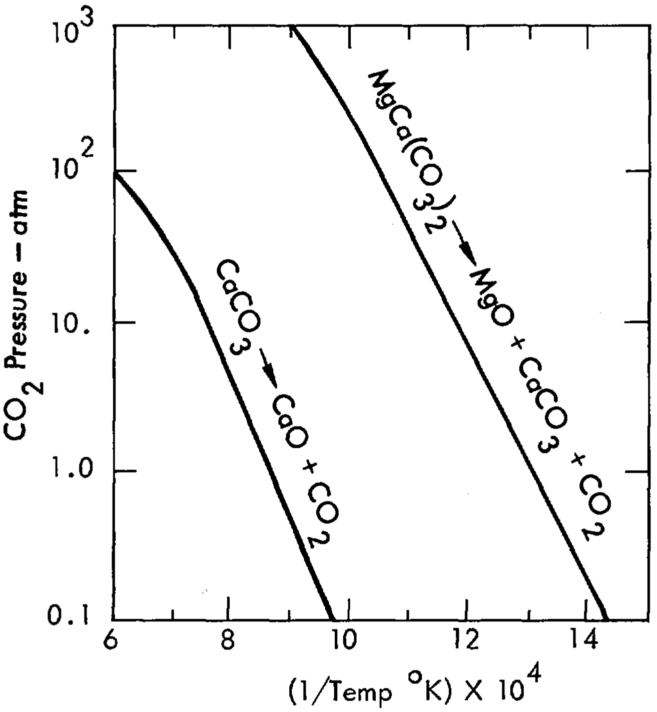

Fig. 2. Vapor pressure of calcite and dolomite as a function of temperature.

Thermogravimetric analysis of samples of Lewis shale clearly show three distinct temperature zones where most of the weight was lost. These were at 100° C, 500° C, and 820° C[6] when the pressure was 1 atm. These temperatures corresponded to the vaporization of water, decomposition of dolomite, and the decomposition of calcite, respectively. Judging by the amount of weight lost at about 500° C, the carbonate mineral in the Lewis shale is mostly dolomite.

The total amount of weight lost by samples from GB-1 and GB-2 when they were heated to 1000° C in air was very nearly equal to the sum of the acid-soluble carbonate and water. The carbonate minerals in the Lewis shale are those which decompose below 1000° C.

Limits for the calcite/dolomite ratio can be calculated from the quantitative chemical analysis of a composite sample of the Lewis shale. Carbon dioxide made up, on the average, 4.64% of the sample; MgO, 2.46%; and CaO, 4.26%. This corresponds to a mole ratio of $CO_2 = 1$, $MgO = 0.579$, and $CaO = 0.720$. Accordingly, all the CO_2 may be contained in the mineral dolomite leaving a little CaO and MgO in non-carbonate phases.

Assuming dolomite is the principal carbonate mineral, we now will calculate the amount of shale which must have been heated to release the observed 42.2×10^6 moles of CO_2 (see Table 1).

From the melted shale, release of 13.6×10^6 moles of CO_2 can be expected. (The amount of shale melted per kt of explosive yield is taken to be 500 metric tons, on the basis of the exploration of sites of other nuclear explosives.) This leaves 28.6×10^6 moles of CO_2 to be explained. Figure 2 reveals the low-temperature decomposition of dolomite that takes place at decreasing temperatures as the partial pressure of CO_2 decreases. It takes place at 770° K at a CO_2 pressure of one atmosphere, and the decomposition temperature increases about 100° K for each 10-fold increase in CO_2 pressure. Thus it seems reasonable that a considerable amount of CO_2 could have been derived from this source.

Another source of CO_2 will be discussed in the next section and in Appendix A. This is the generation of CO_2 and H_2 by the oxidation of carbon by steam. About 7.7×10^6 moles of CO_2 were probably generated in this way, leaving about 20.9×10^6 moles of CO_2 to be derived from the low-temperature decomposition of dolomite. This corresponds to about 1500 tons of shale per kt heated above about 850° K but below 1600° K.

Genesis of H_2 and CO

The Gasbuggy chimney at about 36 days appears to have contained 19.8×10^6 moles of H_2, and 4.6×10^6 moles of CO.[2] Neither of these gases were found in wells in the area before the explosion, and neither of them are normal components of rocks. Shales, particularly black shales, are known to contain high molecular weight hydrocarbons and, in some cases, graphite. We knew that if the Lewis shale contained graphite or hydrocarbons, CO and H_2 could be formed by high-temperature reactions among graphite, H_2O, and CO_2.

Thus we carefully studied the chemical composition of the Lewis shale and found that the total amount of carbon in the rock was in excess of the carbon as carbonate. This was expected, but it was also expected that this excess carbon was in the rock as high-molecular weight hydrocarbons "C_nH_{2n}." However, essentially all the hydrogen in each shale sample was found in water; none as hydrocarbons. The average amount of "free" carbon in GB-1 was about 0.5 wt% as shown in Table 2.

Table 2. Free carbon in Lewis shale (GB-1).

Sample No.	Sample depth (ft)	Moles per 100 g of sample			Wt% free C
		C in carbonate	Total C	Free C	
L-14	4280.3 - 4280.8	0.0845 ± 0.004[a]	0.1322 ± 0.007[a]	0.048 ± 0.01[a]	0.58 ± 0.1[a]
L-15	4278.0 - 4278.4	0.0818	0.1389	0.057	0.69
L-17	4272.1 - 4272.4	.0684	.1281	.060	.72
L-19	4266.1 - 4266.6	.0604	.1264	.066	.79
L-22	4258.4 - 4258.8	.870	.1373	.050	.60
L-24	4252.6 - 4253.8	.194	.1980	.004	.05
L-26	4246.7 - 4247.3	.160	.1347	.000	.00
L-28	4243.8 - 4244.6	.158	.2055	.047	.57
L-29	4240.1 - 4240.7	.081	.1206	.040	.48
L-31	4234.7 - 4235.3	.0986	.1331	.034	.41
L-32	4231.8 - 4232.3	.196	.1996	.004	.04
L-35	4224.9 - 4225.2	.075	.1489	.074	.89
L-37	4219.8 - 4220.3	.0929	.1256	.033	.39
L-38	4217.6 - 4218.1	0.0509	0.09733	0.046	0.56
				Average	0.48 ± 0.07[b]

[a] From an analytical error of ±5% of the concentration of the total carbon as well as the carbon as carbonate. This error applies to all 14 analyses.

[b] Mean error.

Although the free carbon in the Lewis shale is not volatile, there is little doubt that it is oxidized by steam and CO_2 at high temperatures. The most important reactions among C, CO_2 and H_2O are presented in Table 3 where the free energy changes for these reactions are plotted as a function of temperature.

It is essential that these fundamental reactions are understood before attempting to interpret the composition of the Gasbuggy gas. They provide the theoretical background for the prediction of the results of future experiments of this kind.

Table 3. Outline of thermochemistry of the system H_2O - CO_2 - C - H.

Part 1: Principal reactions

(1) $C + H_2O \rightarrow CO + H_2$
(2) $C + CO_2 \rightarrow 2\ CO$
(3) $C + H_2O \rightarrow 1/2\ CH_4 + 1/2\ CO_2$
(4) $CO + H_2O \rightarrow CO_2 + H_2$
(5) $4\ H_2 + CO_2 \rightarrow CH_4 + 2\ H_2O$
(6) $CO + 3\ H_2 \rightarrow CH_4 + H_2O$
(7) $CO + H_2 \rightarrow 1/2\ CH_4 + 1/2\ CO_2$

Part 2: Free energy of formation (ΔG), kcal/mole gas[a]

Gas	298°K	500°K	1000°K	1500°K	2000°K
H_2O	-54.63	-52.36	-46.03	-39.26	-32.31
CO_2	-94.26	-94.39	-94.61	-94.71	-94.72
CO	-32.81	-37.18	-47.94	-58.37	-68.51
CH_4	-12.145	- 7.845	+ 4.625	+17.86	+31.19

Part 3: Free energy change for reactions 1-7, kcal/mole carbon

(1)	+21.82	+15.18	- 1.91	-19.00	-36.20
(2)	+28.64	+20.03	- 1.27	-22.03	-42.30
(3)	+ 1.43	+ 1.20	+ 1.14	+ 0.83	+ 0.54
(4)	- 6.82	- 4.85	- 0.65	+ 2.92	+ 6.10
(5)	-27.14	-18.17	+ 7.17	+34.05	+61.29
(6)	-33.96	-23.02	+ 6.50	+36.97	+67.39
(7)	-20.39	-13.93	+ 2.95	+19.95	+36.74

---

[a] Data for H_2O, CO_2, and CO from J. Coughlin, Bull. 542, USBM, 1954. Data for CH_4 from JANAF Tables, Dow Chemical Co., Midland, Michigan, 1964.

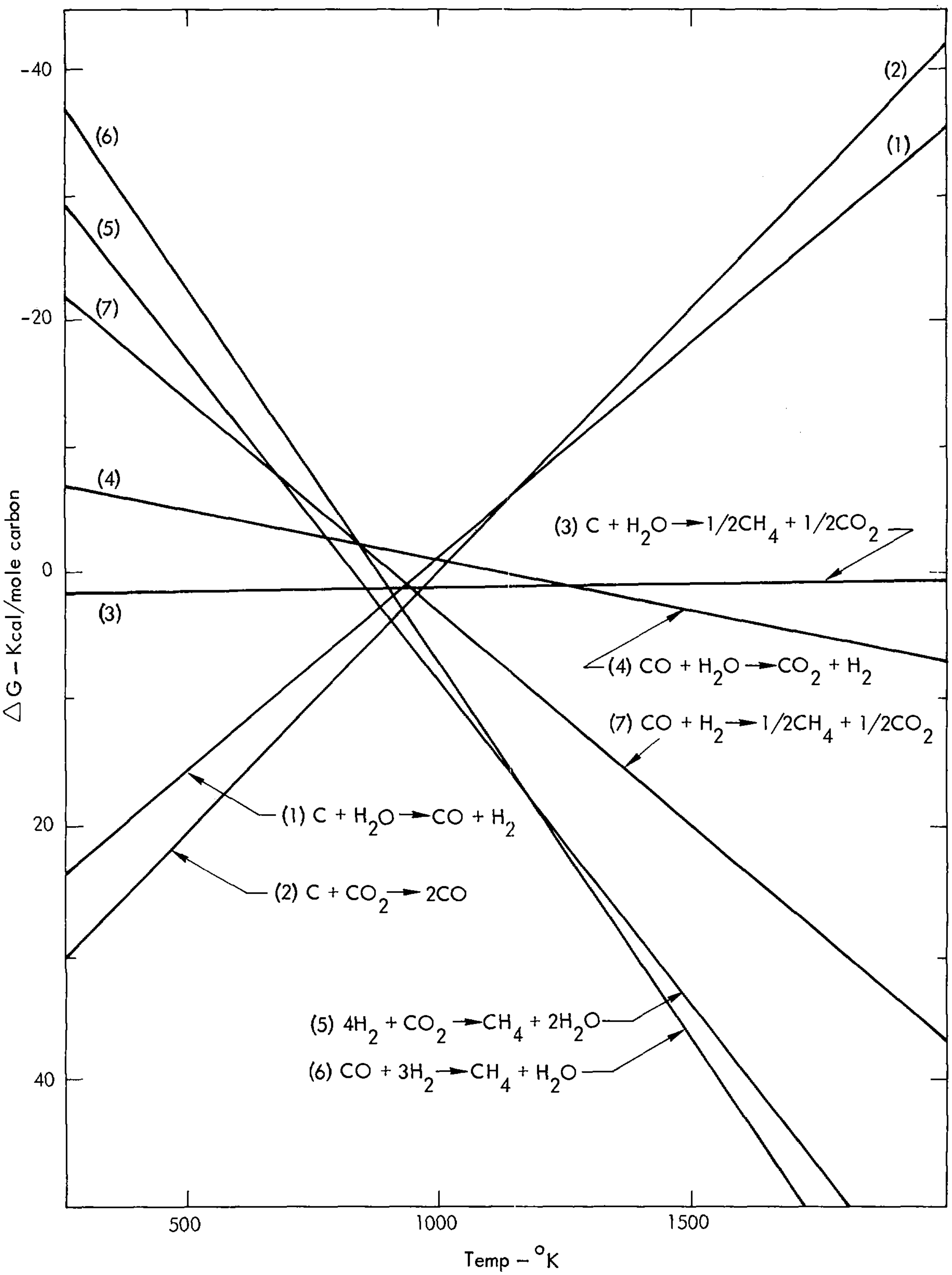

Fig. 3. Free energy changes as a function of temperature for principal reactions among C, CO, CO_2, H_2, and H_2O.

It is noteworthy that a gas rich in H_2O and CO_2 reacts with carbon to produce CO and H_2 at temperatures above 1000° K, and that carbon monoxide reacts with H_2O to make H_2 at temperatures between about 800° K and 1000° K. Hydrogen, in turn, reacts with CO_2 to make CH_4 at temperatures below 800° K. This is shown in Fig. 3. The more negative the free energy (Δ G) for a reaction, the more that reaction is favored. Thus reactions (1) and (2) of Table 3 are the main reactions above 1000° K. They both produce CO. Reaction (4), producing H_2, predominates from 1000° K to about 800° K. Methane forming reactions (5), (6) and (7), predominate below 800° K, but the rate at which CH_4 forms at temperatures as low as 800° K is very slow.

Other reactions are possible, and many other molecular species will be present in minor amounts. To know the concentration of each species as a function of temperature at a fixed chimney volume, computerized calculations have been made in which C_2H_6, C_3H_8, etc., were considered as possible gases. A typical plot is shown in Fig. 4. This particular calculation is based on a fixed C/H/O ratio, one resulting when all the C, H_2O, and CO_2 in 700 tons of shale/kt were equilibrated in a volume of 5.9×10^{10} cm^3, starting at a pressure of 200 atm at 2000° K. Notice that the sequence of reaction products with decreasing temperature is CO, H_2, and CH_4 at low temperatures. This sequence is in agreement with the brief thermodynamic treatment outlined in Table 3 and Fig. 3. Ethane, C_2H_6, forms in minor concentrations. This same sequence is observed for a wide range of starting compositions and pressure as will be shown in the discussion of the Dragon Trail experiment to follow in the second part of this report.

Thus we hypothesize that the H_2 and CO found in the Gasbuggy chimney came from the oxidation of free C by H_2O and CO_2. Judging by the amount of H_2 and CO found, about 12.2×10^6 moles or about 146 tons of free C was burned. The details of this estimate are given in Appendix A.

Because Lewis shale contains about 0.5 wt% free carbon, the total mass of shale which was heated hot enough to burn the free carbon appears to be about 1100 tons per kt of explosive yield. This is not an unreasonable amount considering that 1000 tons of salt per

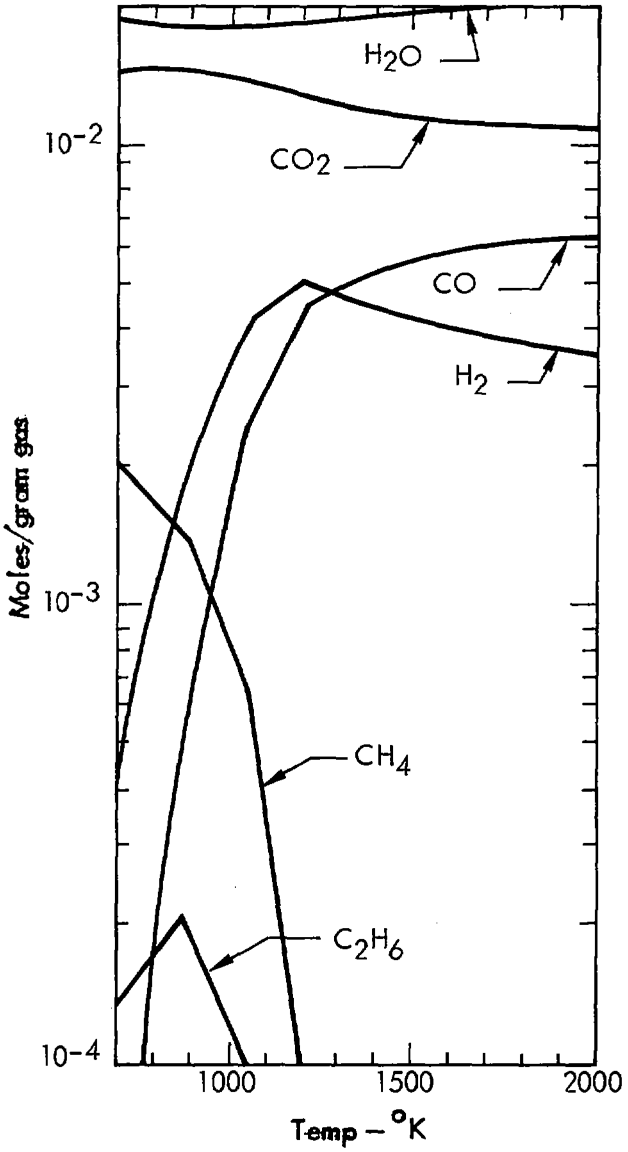

Fig. 4. Concentrations of molecular species as a function of temperature.

kt were heated to 1000° K and melted as a result of the nuclear explosion (called Salmon) in salt.[7] Furthermore, reduction of CO_2 and H_2 by C is expected to take place rapidly at temperatures above 1000° K, but probably not at temperatures far below 1000° K.

As a summary of the previous deductions, we tentatively conclude:

1. About 1100 tons of shale per kt are heated hot enough so that the free C in it reacts with CO_2 and H_2O.
2. About 500 tons of shale per kt are heated above 1600° K, hot enough to melt and release all of its CO_2.
3. About 1500 tons of shale per kt are heated above 800° K, but less than 1600° K, which is hot enough to release CO_2 from the low temperature decomposition of dolomite.
4. All the water from at least 2000 tons of shale per kt is released.

In the above estimation of the amount of free carbon burned, we have assumed that no CH_4 forms. Yet below about 800° K the formation of methane by reactions (5), (6) and (7) is predicted by theory if equilibrium is maintained. The formation of CH_4 should cause both H_2 and CO to almost disappear by the time the temperature falls to 700° K. Yet the gas withdrawn from the chimney at 36 days contained 16.8% H_2 and 3.9% CO, even though the temperature was less than 400° K.[2] If both CO and H_2 persist, the formation of CH_4 must have been very slow. The H_2/CO ratio increased from 1 to 6 during the first 100 days, and then remained almost constant. A H_2/CO ratio of 6 corresponds to the ratio expected under equilibrium conditions at 800 ± 50° K. Thus we conclude that reactions essentially ceased below about 800° K. A laboratory confirmation of this quench temperature should be made, for no truly applicable experiments have been done.

Experience with the composition of gases from the detonation of high explosives in a calorimeter suggest an equilibrium is frozen at temperatures of about 1200° K.[8] Gases are cooled very rapidly under the conditions existing in a bomb calorimeter. A vast amount of data on the temperatures to which H, CO and CH_4 must be heated in oxygen and air in order to initiate oxidation has recently been reviewed.[9] Although it is not correct to assume that the temperature to which $CH_4 \pm O_2$, for example, must be heated to initiate oxidation corresponds to the temperature below which CH_4 will no longer form by reaction between H_2 and CO, it is a valuable supplemental sort of information. Reaction between H_2 and CO probably becomes slow below 800° K and very slow below 700° K, but so many factors are important in addition to temperature that it is almost meaningless to generalize.

Influx of CH_4 Upon Steam Condensation

Up to this point attention has been directed to an explanation of the CO_2, H_2 and CO found in the Gasbuggy chimney. In this section we show how the amount of CH_4 found can be used to deduce something about the late-time chimney history. Methane in the Lewis shale before the explosion floods the chimney only when the gas pressure in the chimney falls below formation pressure. A striking decrease in pressure is expected when the steam condenses.

It is not possible to be sure of the total amount of steam that may have been in the chimney. The Lewis shale heated hot enough to lose any CO_2 (2000 tons per kt) lost almost all of its H_2O. The minimum amount of steam was thus 10^8 moles based on an average water content of 3.6 wt %. It is assumed that no chemical reaction takes place below about 800°K. It is also assumed that except for CH_4, the molecular composition of chimney gas at 36 days was approximately the same as the composition at the time steam started condensing. The amounts of the various molecules before condensation were:

CO_2	4.2×10^7 moles
CO	0.5×10^7 moles
H_2	2.0×10^7 moles
H_2O (min) ~	10.0×10^7 moles
Total	16.7×10^7 moles

At a chimney of 5.9×10^{10} cm^3 and an average temperature of 900° K, the total pressure (P_T) was at least 208 atm. The partial pressures of the various components are shown in Fig. 5. With decreasing temperature the

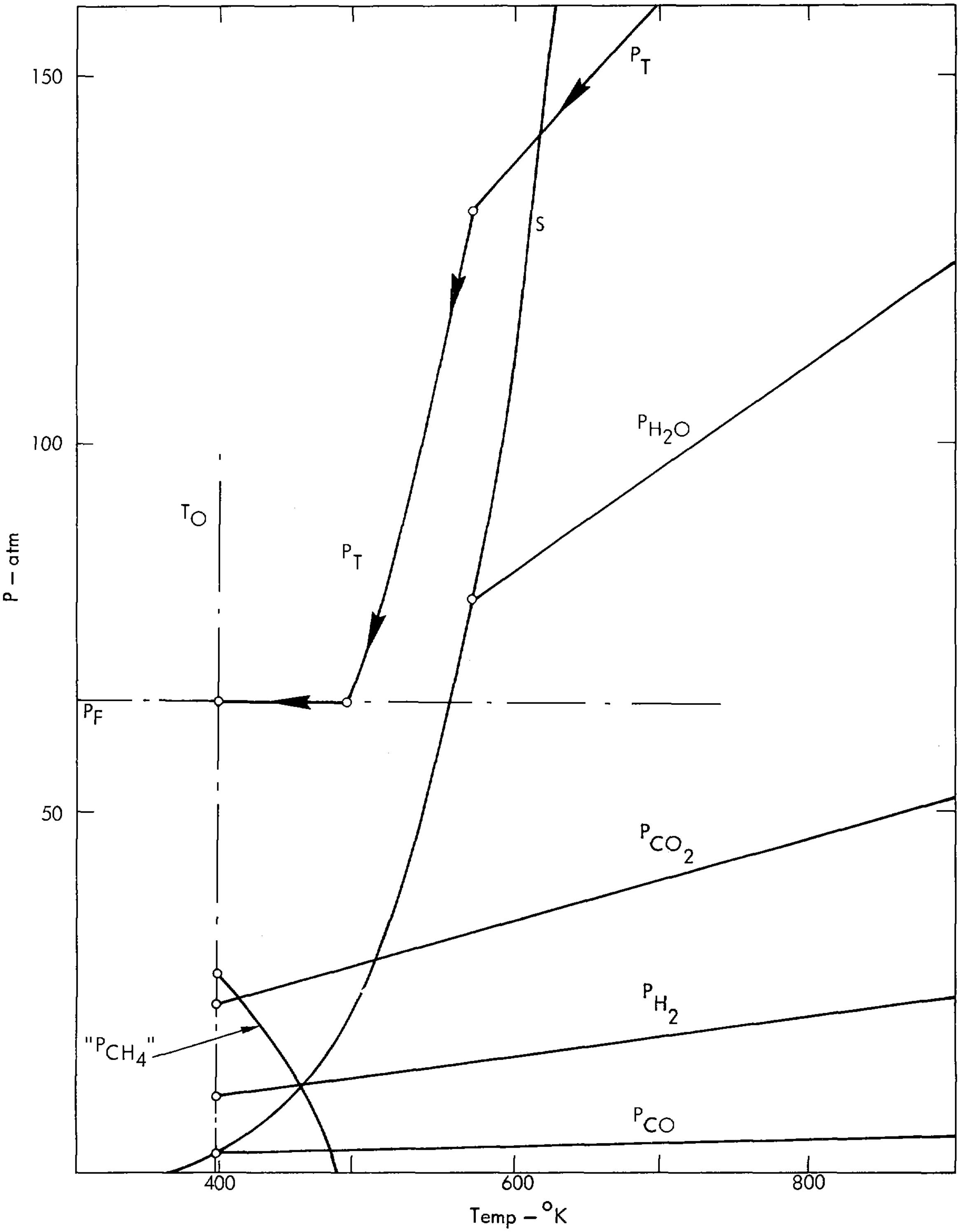

Fig. 5. Partial pressure of gases in the chimney as a function of temperature showing the condensation of steam.

total pressure fell according to the line P_T, and the partial pressures of the various gases also fell as shown. When the temperature fell to 570° K, the chimney gas became saturated with water and condensation started. This is shown in Fig. 5 by the intersection of line P_{H_2O} with curve (S) representing the vapor pressure of liquid water. With further cooling, the partial pressure of water followed down the saturation curve, resulting in a rapid decrease in the total pressure until the temperature reached the observed chimney temperature, T_0, about 400° K.

Notice that at about 500° K, and independent of the amount of steam assumed in the system at the start, the total pressure fell to the formation pressure, P_F. Below this temperature it became possible for formation gas to enter the chimney. The gas in nearby rock was made up of about 85% CH_4, 7.4% C_2H_6, 4% C_3H_8, and other heavier hydrocarbons.[10] In Fig. 5 the partial pressure of formation gases as a function of temperature is given by a single "CH_4" which, of course, represents the sum of several partial pressures.

Preshot gas from the area had a CH_4/C_2H_6 ratio of 11.5. The post-shot chimney gas at 36 days had a CH_4/C_2H_6 ratio of 10.2. As discussed earlier, we are inclined to believe that most of the CH_4 and C_2H_6 in the chimney came from "formation gas" outside the chimney rather than by chemical reactions within the chimney.

Tritium Distribution

The measurements of Smith and Momyer[2] of the distribution of tritium among H_2, CH_4, and C_2H_6 as a function of time contribute a great deal to our understanding of post-shot chemical changes. The CO- and H_2-rich gas sample collected the first day after detonation suggested that a chimney full of such gas would contain about 30% of the tritium as HT and about 3% of the total tritium as CH_3T. The remaining 67% is assumed to be in water as HTO. According to the model presented here, the H_2O/H_2 ratio in the initial chimney gas is about 5. That is, as much as 20% of the tritium could be in the non-condensible gas and about 80% in liquid H_2O. With time, the availability of substantially more water with which the tritium can exchange is expected. With time, in fact, the fraction of the total tritium in CH_4 and H_2 decreased to 5% and the remaining 95% is presumed to be in liquid water.

PREDICTION OF THE COMPOSITION OF GAS AND THE TRITIUM DISTRIBUTION IN FUTURE GAS-STIMULATION EXPERIMENTS

Introduction

The study of the Gasbuggy experiment in the first part of this report pointed out the relation among the chemical and mineralogical composition of rock at shot point and the composition and tritium distribution in post-shot gas. This part of the report is to show how these relations may be used to predict chemical results of nuclear explosions in hydrocarbon-bearing rock of a different composition.

Although we believe our interpretation of the observed chemical results is correct in principle, we must emphasize that many of the arguments used to make the detailed predictions to follow are neither positive nor conclusive. We hope that this attempt at prediction will arouse sufficient interest so that a strong effort will be made to test the assumptions.

Parameters for the Dragon Trail Experiment[11]

At the present time, two proposals for nuclear explosions in hydrocarbon-bearing rock have been studied in sufficient detail to make predictions of the chemical effects. These experiments are Dragon Trail and Bronco. Because the Dragon Trail rock is similar to the Gasbuggy rock, this experi-

Table 4. Carbonate mineralogy from chemical analysis.

	Moles per 100 g of rock									Wt% of rock			
				I[b] (all Mg in carbonate)			II[b] (all Ca in carbonate)			Assumption I		Assumption II	
Sample No.	Ca	Mg	CO_2[a]	$MgCO_3$	$CaCO_3$	Ca (non-carbonate)	$MgCO_3$	$CaCO_3$	Mg (non-carbonate)	$MgCa(CO_3)_2$	$CaCO_3$	$MgCa(CO_3)_2$	$CaCO_3$
201	0.108	0.0728	0.1561	0.0728	0.0833	0.02	0.0480	0.108	0.03	13.4	1.0	8.8	6.0
202	.1033	.0724	.1479	.0724	.0755	.03	.0446	.103	.03	13.3	0.2	8.2	5.9
203	.1569	.0695	.2095	.0695	.1400	.02	.0529	.157	.02	12.8	7.0	9.7	10.4
204	.1202	.0666	.1552	.0666	.0886	0.03	.0350	.120	0.03	12.3	2.2	6.4	8.5
205	.2797	.1234	.4090	.1234	.2797	None	.1234	.280	None	22.8	15.6	22.7	16.6
206	.1139	.06911	.1727	.06911	.1036	0.01	.0588	.114	0.01	12.7	3.4	10.8	5.5
207	.1070	.0609	.1386	.0609	.0777	0.03	.0316	.107	0.03	11.2	1.7	5.8	7.5
208	0.0891	0.05841	0.1234	0.05841	0.0650	0.02	0.0343	0.089	0.02	10.8	0.6	6.3	5.5
		Av	0.1890						Av	13.7	4.0	9.8	8.2
	Av wt% CO_2		8.3 ± 1.4[c]					Wt% total carbonates		17.7		18.0	

[a] Acid soluble carbonate. Analytical accuracy ±5% of the concentration.

[b] Assumption "I" may be preferred on the basis that Ca silicates are more stable than Mg silicates. On the other hand, $CaCO_3$ is considerably more stable than $MgCO_3$, the basis of Assumption II.

[c] Mean error.

ment is used as an example. A similar treatment for the Bronco experiment can be made if there is sufficient interest.

Although the explosive yield for Dragon Trail has not been set, it will probably be in the range 18 ± 6 kt. The depth of burial will be about 2800 ft (853m). Shot point will probably be in the "B layer" of the Mancos shale, the density of which is about 2.4 g/cm^3. Thus the lithostatic pressure at shot point is about 200 atm. The cavity volume, at a yield of 18 kt and this confining pressure, is expected to be 5.9×10^{10} cm^3, scaled from Gasbuggy. The pressure of the natural gas in the area is 32 atm.[*]

A complete quantitative chemical analysis of eight samples of Mancos-B shale has been published.[12] The results of these analyses, pertinent to the carbonate mineralogy, are abstracted in Table 4. Notice that the average amount of CO_2 in carbonates is 8.3 wt%. It appears that the carbonate minerals are similar to, but more abundant than, the carbonate in the Lewis shale (the Gasbuggy rock).

The pressure of free carbon is of special interest because it may generate CO and H_2. The average amount of free C is about 1.1 wt% as shown in Table 5. The average amount of water in the shale is about 5.1 wt%.[12]

Table 5. Amount of free carbon.

Sample No.	Moles/100 g rock			Wt% C
	Total C	CO_2	Noncarbonate C	
201	0.2356	0.1561	0.0795	0.95 ± 0.2[a]
202	.2447	.1479	.0968	1.2
203	.2881	.2095	.0786	0.94
204	.2614	.1552	.1062	2.4
205	.4863	.4090	.0773	0.2
206	.2873	.1727	.1146	1.4
207	.2065	.1386	.067	0.8
208	0.2231	0.1234	0.0997	1.2
			Av wt% free C	1.1 ± 0.2[b]

[a] Analytical errors.

[b] Mean error.

Molecular Species and Bulk Composition of Chimney Gas

From the chemical composition of the Dragon Trail site, and from what we have learned from Gasbuggy, we conclude that the 18-kt Dragon Trail

---

[*] Natural gas produced in the area is made up of 88% CH_4, 5.7% C_2H_6, 2.5% C_3H_8, approximately 1% heavier hydrocarbons, 2.2% N_2, and 0.25% CO_2.

explosive will release the following amounts of C, CO_2, and H_2O from the Mancos shale:

$$\text{C:}\quad 18 \times 1.1\% \times 1100 = 218 \text{ tons} = 18 \times 10^6 \text{ moles}$$

$$CO_2\text{:}\quad 18 \left(8.3\% \times 500 + \frac{8.3\%}{2} \times 1500\right) = 1867 \text{ tons} = 42 \times 10^6 \text{ moles}$$

$$H_2O\text{:}\quad 18 \times 5.1\% \times 2000 = 1836 \text{ tons} = {\sim}102 \times 10^6 \text{ moles}$$

$$\text{Total} \qquad 162 \times 10^6 \text{ moles}$$

No doubt more than this amount of H_2O will be involved because the vapor pressure of H_2O in this shale is higher than the vapor pressure of CO_2 at a given temperature.

A pressure of ~180 atm is generated when this amount of gas is in the Dragon Trail chimney at 800° K. This pressure is taken as a starting point for a computer calculation of the temperature dependence of molecular equilibria shown in Fig. 6. Notice that these results are in agreement with the trends outlined in the first part of this report; i. e., CO becomes important at high temperatures and H_2 is the principal reaction product around 1000° K. Below about 850° K, CH_4 becomes increasingly stable relative to H_2 and CO, and graphite (Cg) forms at temperatures below about 400° K according to theory. The rate at which CH_4 or Cg forms is very slow, an important point which was discussed in detail in the first part of this report.

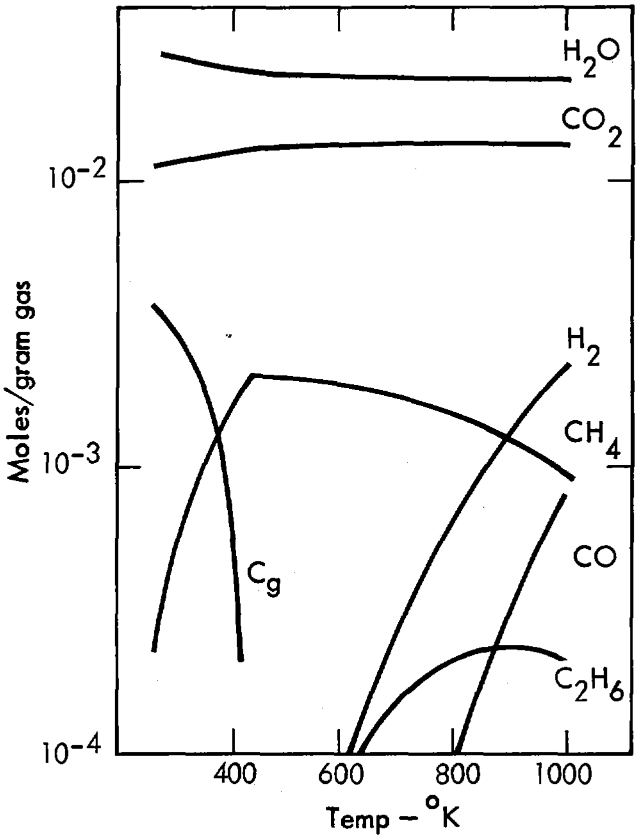

Fig. 6. Calculated distribution of molecular species for a fixed C/H/O ratio as a function of temperature, valid at temperatures between 700 - 1000° K.

From the H_2/CO ratio of 5 in the chimney gas at Gasbuggy, we assume that homogeneous equilibria "freeze out" or quench at about 850 ± 50°K. The H_2/CO ratio at 850°K in the Dragon Trail chimney is also expected to be about 5 according to Fig. 6. The amount of the various molecular species can be approximated from these assumptions. The net reaction for the oxidation of free carbon is:

$$C + 2H_2O \rightarrow CO_2 + 2H_2$$

The number of moles of H_2 produced is 36×10^6, twice the number of moles of C burned. In order that $H_2/CO = 5$, we can formulate:

$$H_2 + CO_2 \rightarrow H_2O + CO$$

(In reality the CO is formed before the H_2 by direct reaction of C with CO_2 and H_2O.) By this reaction, one mole of CO is produced per mole of H_2 used. When the number of moles of CO formed is 6.0×10^6, the number of moles of H_2 remaining is 30.0×10^6 and the condition $H_2/CO = 5$ is met. Also, considering the CO_2 made and the H_2O lost by the above idealized reactions, the final composition is:

$H_2 = 30 \times 10^6$ moles (18.5%)

$CO_2 = 54 \times 10^6$ moles (33.3%)

$H_2O = 72 \times 10^6$ moles (44.5%)

$CO = 6 \times 10^6$ moles (3.7%)

Total 162×10^6 moles 100%

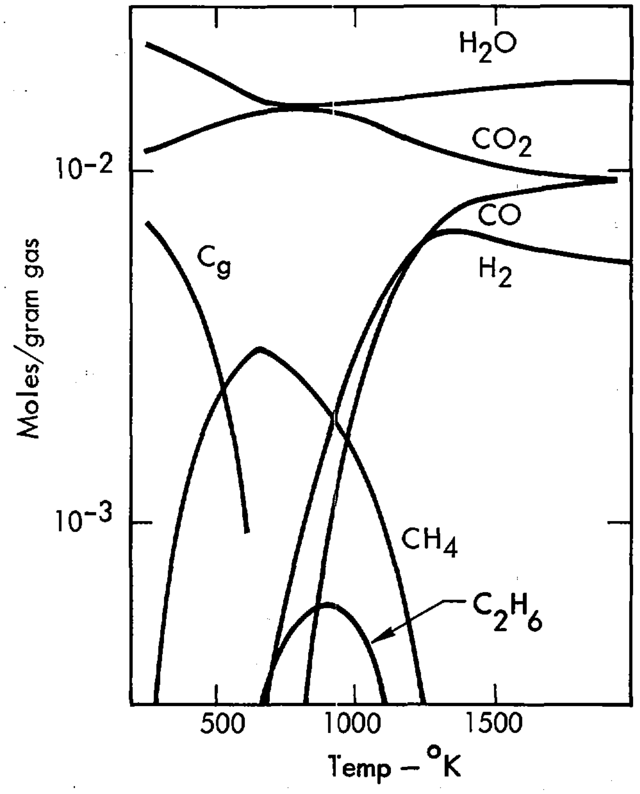

Fig. 7. Molecular species distribution calculated from assumptions valid for temperatures of about 1200 ± 200° K.

Before we conclude with a discussion of the condensation of steam and tritium distribution, we must point out that the assumptions used to make the above estimate of gas composition at a "freeze out" temperature of 850° K does not apply at high temperatures. In order to estimate the gas composition at ~1200° K, for example, it would be more realistic to assume that:

1. All the H_2O and C are released from 1000 tons of shale per kt.
2. All the CO_2 is released from ~500 tons of shale per kt.
3. Half the CO_2 is released from an additional 500 tons of shale per kt.

The calculated distribution of molecular species for such a C/H/O ratio as a function of temperature is shown in Fig. 7.

Likewise, to better estimate the gas composition and distribution of molecular species at 1600 ± 400° K, we should consider only the gases evolved from the ~500 tons of shale melted per kt. This was done by machine calculation and the results are shown in Fig. 8. Although this calculation describes equilibria at temperatures down to 550° K, the assumptions used to make the calculation are realistic, at most, over the temperature range 1600 ± 400° K.

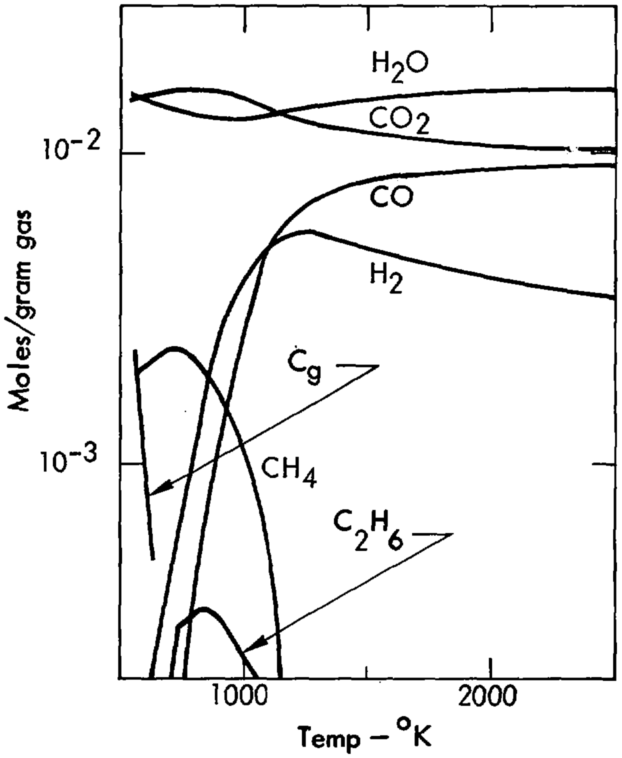

Fig. 8. Distribution of molecular species at temperatures in the range 1600 ± 400° K.

Figure 9 is a composite of Figs. 6, 7 and 8. It represents our best guess of the distribution of molecular species as a function of temperature if no quenching takes place.

Condensation of Steam

Figure 10 represents an idealized picture of condensation in the Dragon Trail chimney. The so-called "late time" or low temperature pressure history is given by the line of total pressure (P_T). At 550° K the chimney gas becomes saturated with water, condensation ensues, and the total pressure

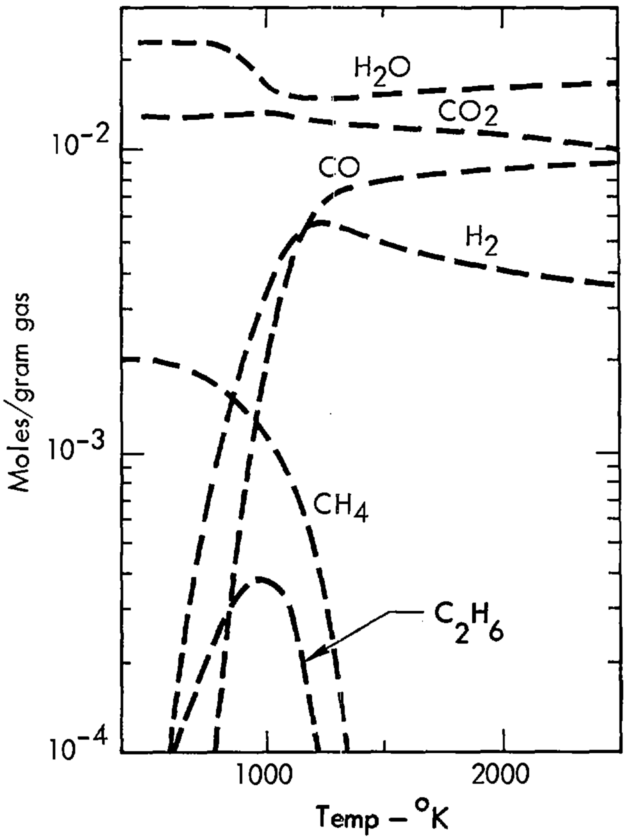

Fig. 9. Composite of Figs. 6, 7 and 8.

falls rapidly. The total pressure expected during the first few months is 50 atm, compared to a formation pressure (P_F) of 32 atm. This leads to the conclusion that <u>no methane will be found in the chimney when it is first opened.</u> The rate at which the cavity pressure approaches formation pressure depends upon the permeability of the surrounding rocks. The final gas composition following condensation will be the same as that calculated in the last section except that almost all the steam is gone, as follows:

H_2 ~	30×10^6 moles	(33%)
CO_2 ~	54×10^6 moles	(60%)
CO ~	6×10^6 moles	(7%)
Total	90×10^6 moles	100%

It is interesting to compute the distance that CH_4 is driven away from the chimney by the high-pressure chimney gas. If the void volume in the shale is about 10%,[11] CO_2, H_2 and CO displaces CH_4 an <u>average</u> distance of ~50 m (160 ft) from the chimney. This outflow of gas may be detected by the presence of tritium (as HT).

The temperature expected (T_E) upon re-entry, a few months after detonation, is ~400° K based on experience following Gasbuggy.

Tritium Distribution

At temperatures above about 900° K, where chemical reactions among gases in the chimney are expected to approach equilibrium, isotopic exchange

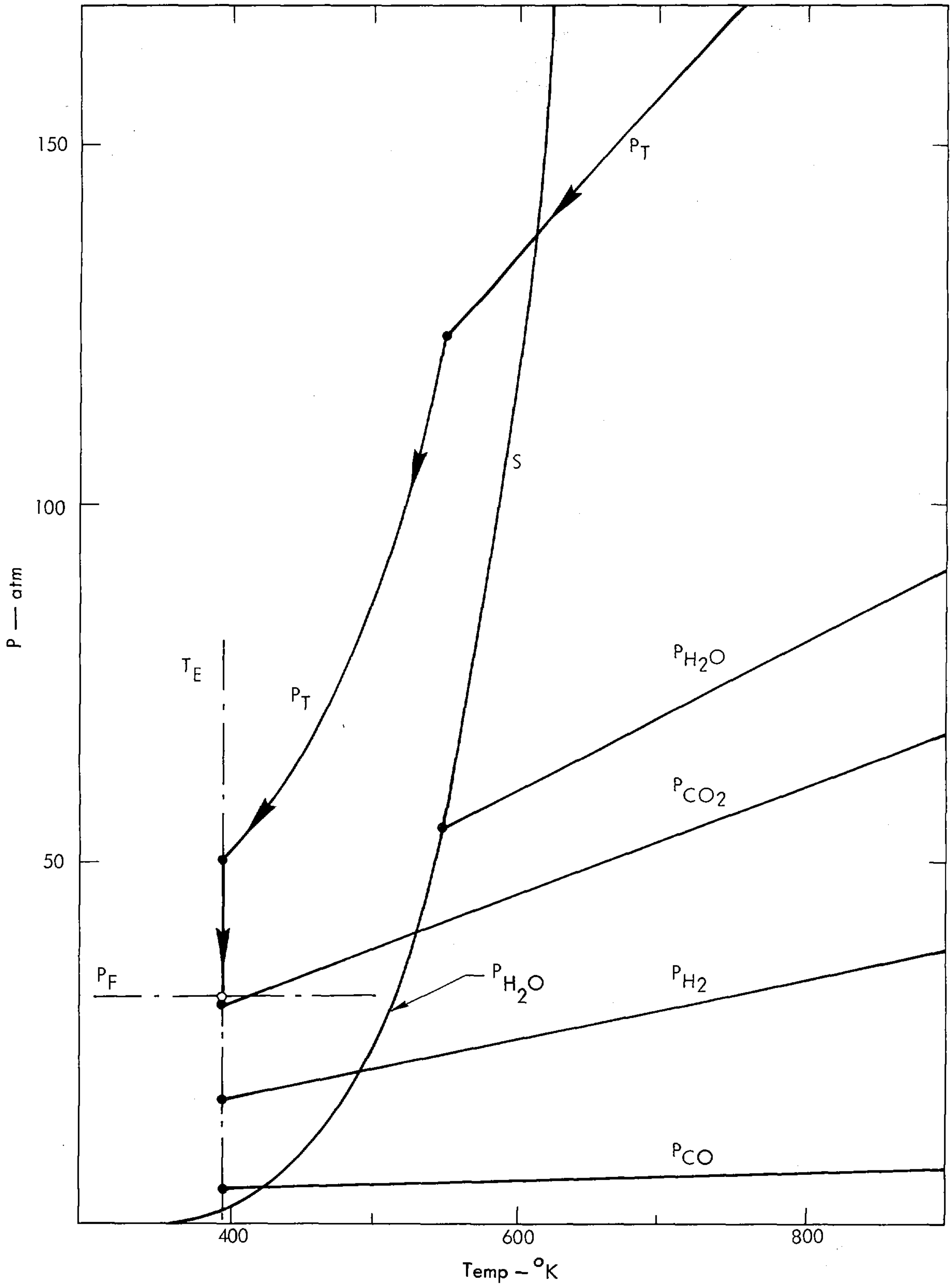

Fig. 10. Condensation in the Dragon Trail chimney.

is also expected to be rapid, and tritium (T) will be distributed in an equal atom fraction among all hydrogen-containing molecules. (That is, the T/H ratio in hydrogen will be the same as in steam.) The ratio of H_2O/H_2 at 900° C is expected to be at least $72 \times 10^6 / 30 \times 10^6 = 2.4$. This is a minimum because it is based on the amount of steam liberated from about 3.6×10^4 tons of rock (2000 tons/kt). This is the mass of rock expected to be heated hot enough to lose some CO_2 from dolomite, considerably hotter than necessary to liberate steam.

The total amount of tritium expected is 4.3 ± 4 g (1.4 moles). The total number of moles of H at ~900° K is expected to be 2.0×10^8, 0.6×10^8 in H_2, and 1.4×10^8 in H_2O. Thus the net T/H ratio is expected to be $1.4/2.0 \times 10^8 = 7 \times 10^{-9}$.

The distribution of tritium between H_2O and H_2 is 30% in H_2 and 70% in H_2O. Upon the condensation of water about 1 mole of T is removed from the gas phase, leaving 0.4 moles of T as HT. The total amount of non-condensible gas in the chimney is expected to be 90×10^6 moles.

The tritium concentration at about 30 days is thus expected to be $\sim 4 \times 10^{-9}$ moles T/mole of chimney gas.

In terms of volume at N T P, this corresponds to 1.7×10^{-10} moles of T/liter or 6×10^{-12} moles T/ft^3, resulting in a measurement of about 5 μCi/liter of chimney gas. This is a maximum. Exchange with additional water may reduce the concentration by a factor of 5. Because CH_4 is kept out of the chimney until production starts, the tritium exchange reaction.

$$THO_{(1)} + CH_{4(g)} = CH_3T_{(g)} + H_2O_{(1)}$$

is not expected to take place to the extent observed in Gasbuggy.

APPENDIX A

Estimation of the Amount of Free Carbon Burned to Produce the Observed Amounts of H_2 and CO

The principal CO-forming reactions are:

$$1.9X(C + H_2O = CO + H_2) \qquad (1)$$

$$X(C + CO_2 = 2CO) \qquad (2)$$

These reactions are about equally probable at temperatures between 1000° K and 1500° K (Fig. 3). The relative importance of these reactions can be estimated by the relative amounts of H_2O and CO_2 in the Lewis shale. The H_2O/CO_2 ratio is 1.9, so if the amount of C required by reaction (2) is X, the amount required by reaction (1) is 1.9X, and the total amount of carbon burned (C) is 2.9X.

The principal H_2-producing reaction is:

$$Y(CO + H_2O = CO_2 + H_2) \qquad (3)$$

Let:
A = amount of CO found in chimney (4.6×10^6 moles)
B = amount of H_2 found in chimney (19.8×10^6 moles)
C = total amount of free carbon burned to make A and B

Then:

$$\begin{array}{rcl} A &=& 3.9X - Y \\ B &=& 1.9X + Y \\ \hline A + B &=& 5.8X \end{array}$$

$$X = \frac{A + B}{5.8} = 4.2 \times 10^6$$

and

$$C = 2.9X = \frac{A + B}{2} = \underline{\underline{12.2 \times 10^6}} \text{ moles of free carbon burned}$$

Also consider the formation and loss of CO_2 by reactions due to the presence of free carbon.

a. CO_2 generation

$$Y(CO + H_2O = CO_2 + H_2)$$

$$Y = B - 1.9X = 19.8 \times 10^6 - 7.9 \times 10^6 = 11.9 \times 10^6 \text{ moles}$$

b. CO_2 consumption

$$X(C + CO_2 = 2CO)$$

$$X = 4.2 \times 10^6 \text{ moles}$$

Net amount of CO_2 generated by the oxidation of C is $(11.9 - 4.2)\ 10^6 = \underline{\underline{7.7 \times 10^6}}$ moles.

REFERENCES

1. J. Hill, *Chemical Analysis for the Gasbuggy Event*, GCTN-266 (1968).
2. C. Smith and F. Momyer, *Gas Quality Investigation Program Status Report for Project Gasbuggy*, Lawrence Radiation Laboratory, Livermore, Rept. UCRL-71314 (1968). Also F. Momyer, *Preliminary Radiochemical Results on Gas from Gasbuggy Experiment*, Memorandum (1968).
3. G. Higgins, *Critique of the Gasbuggy Technical Program*, Memorandum UOPK-6801 (1968) (Appendix A, GB-E).
4. L. Ramspott, *Gasbuggy Petrography*, Memorandum UOPK 68-25 (1968).
5. L. D. Ramspott and R. L. Braun, *Gasbuggy Petrography*, UOPK 68-68 (1968).
6. D. Seaton, High Explosive Group, Chemistry Department, Lawrence Radiation Laboratory, Livermore.
7. D. E. Rawson, R. W. Taylor, and D. L. Springer, *Review of the Salmon Experiment A Nuclear Explosion in Salt*, Naturwiss. 20, 525 (1967).
8. D. L. Ornellas, J. H. Carpenter, and S. R. Gunn, *A Detonation Calorimeter with Pentaerythriton Tetranitrate (PETN)*, Lawrence Radiation Laboratory, Livermore, Rept. UCRL-12421 (1966).
9. W. Jost, Editor, *Low Temperature Oxidation*, Gordon and Breach, New York (1965).
10. F. Holzer, Editor, *Gasbuggy Preshot Summary Report*, U. S. Atomic Energy Commission, Rept. PNE-1001 (1967).
11. Data from T. Sterrett and D. Rawson, personal communications, October 30, 1968, and January 15, 1969; and H. Tewes and D. Rawson, *Radiological Safety Program for Project Dragon Trail*, UOPKG 68-19, July 8, 1968. J. Korver and D. Rawson, *Gasbuggy Postshot Investigation in GB-ER*, Lawrence Radiation Laboratory, Livermore, Rept. UCRL-50425 (1968).
12. J. Hill, *Chemical Analysis of Shale Samples from the Dragon Trail Event*, UOCC-68-4 (1968); also, *Total Hydrogen Analysis for Samples from the Dragon Trail Event*, Memorandum (1968).

XA04N0866

ADDITIONAL COMMENTS ON THE CHEMICAL RESULTS OF THE GASBUGGY EXPERIMENT*

Russell E. Duff
Applied Nuclear Company
La Jolla, California

The sequence of events which influences the chemical composition of the gas found in the Gasbuggy chimney proposed by Taylor in the previous paper is a valuable contribution to the understanding of the phenomenology involved, but it does not lead to results in quantitative agreement with observations. This fact is illustrated in the first two columns of the following table which compare the observed concentrations of several prominent species with the corresponding values determined from equilibrium calculations as suggested by Taylor.

COMPONENT	PERCENTAGE CONCENTRATION		
	Experiment (36 day)	Taylor Theory	This work
CO_2	35.8	30.8	37.3
CO	3.9	0.3	4.0
H_2	16.8	2.4	17.8
CH_4	36.9	66.5	40.9

The agreement between the theoretical and experimental values was not considered satisfactory, and an alternate model was sought. The hint for the construction of this alternate description came from the evidence of chemical reaction many days and months after the explosion. The concentrations of CO and H_2 changed during the first shut-in period, and significant distributions of T and C^{14} developed in CH_4 and C_2H_6 after the influx of formation gas. Therefore, a set of chemical and physical conditions was determined under which significant reaction could occur at relatively late time leading to better agreement with observations.

It was postulated that the CO_2, H_2O and C contained in 1550 tons of formation/KT of yield came to equilibrium at 800°K in the observed cavity volume of 5.9×10^{10} cc (15.1 cc/g). The concentrations were assumed not to change as the temperature dropped to lower values. When the H_2O condensed and the pressure fell

---

*The El Paso Natural Gas Company supported this investigation.

below the formation pressure, hydrocarbons entered the chimney from the formation so as to maintain formation pressure in the void space. The original cavity gas and the inflowing hydrocarbons were assumed to react heterogeneously on hot rock surfaces which, by chance, were not covered with condensed water. The reflux process, through which energy is distributed throughout the chimney by evaporation and condensation of water, was assumed to provide a 0.32 mole fraction of water vapor to the reacting system at the hot surfaces near the bottom of the chimney.

The last column of the above table lists the equilibrium composition calculated on this basis at a temperature of $900^{\circ}K$ and a pressure of 69 atm. The agreement between the theoretical and the observed values is excellent. During the shut-in period the hot rock surfaces cooled, and the observed composition shifted as predicted by this model for approximately a $40^{\circ}K$ temperature decrease.

In one respect this model fails. In equilibrium one would expect very little C_2H_6, but the observed concentration was close to that characterizing formation gas. No satisfactory explanation for this discrepancy has been developed.

The sensitivity of this result to variations in the relative amounts of material considered in the initial reaction phase has not yet been adequately investigated, nor has the use of gases from 1550 tons/KT of initial material and 32% H_2O vapor from refluxing been justified. Nevertheless, it appears this model is quite capable of explaining the observed chemical composition and its change in time within experimental error.

It should be noted that the possible effects of gas nonideality on the reaction system have been investigated and found to be relatively unimportant.

If subsequent investigation shows this model to be correct, the contamination of product gas by radioactive species may be dramatically reduced if appropriate formation can be chosen for the shot point. The criteria are:

1. The formation must be free of graphite or solid carbon.
2. The carbonate concentration must be sufficiently high that the CO_2 partial pressure exceeds formation pressure after the water condenses.

If the first condition is satisfied, no hydrogen gas will be produced in the initial phases of the reaction, and all of the tritium will exist in the form of water. This water will then condense. Much of it will hydrate the calcium and magnesium oxides remaining after carbonate decomposition and will be permanently removed from the reaction system. If the second condition is satisfied, little methane will be present to react with $C^{14}O_2$ and HTO while the hot rock cools below reaction temperature.

A paper describing this work in more detail is in preparation. It is expected to be submitted for publication in the near future.

This work could not have been done without the continuing assistance and advice of Dr. Lewis Schalit, Dr. Albert Petschek and Mr. Webb Simmons. Special thanks are also extended to Professor Simon Bauer, Cornell University, to Professor George Kennedy, UCLA, and to Professor Jacob Bigeleisen, Rochester University, for their help in several aspects of this investigation.

XA04N0867

BEHAVIOR OF RADIONUCLIDES IN NUCLEAR GAS STIMULATION APPLICATIONS*

C. F. Smith, Jr.
Lawrence Radiation Laboratory, University of California
Livermore, California 94550

ABSTRACT

The Gasbuggy experiment has presented a unique opportunity to investigate the behavior of radionuclides over an extended period of time in a somewhat unusual environment. In addition to the obvious practical utility of this investigation for Plowshare applications, the information gained has value of a purely scientific nature. Both aspects of the Gas Quality program for Gasbuggy are discussed in this presentation. The study of Gasbuggy results is divided into two distinct periods, according to the field operations. During the initial six months following detonation, the chimney reentry well was shut-in, and the nuclear chimney served as a chemical and radiochemical reaction vessel. A detailed examination of the concentrations and specific activities of tritium and C^{14} is presented as a function of the changing chemical composition of the chimney gas and as a function of time. The effects of radiochemical exchange reactions, together with the tritium isotope effect, are demonstrated. Following this shut-in period, a series of production and flushing tests was conducted. During these experiments, the chimney gas composition was seen to change about as would be expected due to dilution of the chimney gas with formation gas. An examination of radionuclide concentrations and specific activities during the production tests demonstrated the relative unimportance of isotopic exchange and chemical reactions during this period, as compared to the early shut-in periods. Within the limitations of the Gasbuggy experience a generalized model of the behavior of tritium and C^{14} can be deduced. The discussion involves estimation of initial distribution of activities, the effects of chemical reactions and isotopic exchange on this distribution, and the importance of the environment in determining the level of radioactivity contamination to be expected.

I. INTRODUCTION

Prior to the Gasbuggy experiment, very little was known about the long-term behavior of volatile radionuclides in an underground environment. The few events for which experimental data were obtained were sampled over only a short time span, usually within a few days of the detonation. Furthermore, no previous nuclear detonation had occurred in as strong a reducing medium as that surrounding the Gasbuggy explosive. These facts complicated efforts to predict the postshot chemistry and distribution of radionuclides within the chimney. Because of the uncertainties involved, the preshot predictions did not attempt to treat changes in composition of the chimney gas following the quenching effect of the collapse. Conservative estimates for the expected tritium distribution were made, assuming chemical reactions ceased when collapse of the chimney occurred. One such estimate predicted about 70% of

---

*Work performed under the auspices of the U.S. Atomic Energy Commission.

the available tritium would be HT, with about 0.2% as CH_3T.[1] When reentry of the Gasbuggy chimney was made 34 days after the detonation, only about 5% of the tritium was gaseous, and most of this was tritiated methane. For lack of a more objective method, most predictions assumed the volatile fission products and activation products were distributed uniformly through the gas. Obviously, this worst possible case was unrealistic for many of these nuclides.

The lack of an adequate capability was clearly a major problem in the development of Plowshare Applications. Project Gasbuggy, then, was viewed as an undeniable opportunity to study the behavior of significant radionuclides in an experimental situation over an extended period of time. Although it was recognized that several such experiments would be required before an adequate predictive model could be developed, the observations made in the Gasbuggy program were expected to be valuable in defining important problems, and would contribute significantly to our understanding of the phenomenology involved.

Discussions of the experimental data of the Gasbuggy Gas Quality Program[2] and its interpretation from a chemical standpoint[3] have been presented. With this background, it is possible to examine the radiochemical results in some detail. The results of this examination can then be generalized, and their applicability for use as a predictive tool can be examined.

II. RADIOCHEMISTRY OF PROJECT GASBUGGY

For the purposes of this discussion, let us define four classes of radioactive species which may be important to nuclear gas stimulation applications. In the order of discussion these are: (1) The rare gases; (2) the chemically reactive species which form gaseous compounds; (3) the species which could conceivably form gaseous compounds; and (4) everything else.

A. Rare-Gas Radioactivities

Aside from several short-lived krypton and xenon isotopes, the only important rare-gas radionuclides identified in the Gasbuggy chimney were Kr^{85}, Ar^{37}, and Ar^{39}. Radon, a naturally occurring component of natural gas, was also detected in low concentration.

The preshot estimate for the total Kr^{85}, based upon expected device performance, was about 350 Ci. So that the total of this and other gaseous species could be measured, a known amount of Xe^{127} tracer was added to the device prior to detonation. For Kr^{85}, the measured total is 350 ± 20 Ci.

The observed presence of 100% of the Kr^{85} in the gas deserves comment. The best estimate of the time of chimney collapse for the Gasbuggy event is "within the first 30 seconds" after detonation.[4] At this time the mass-85 fission yield chain existed primarily as Br^{85} and its precursors, the materials which would ultimately decay to produce Kr^{85}. The observation that the Kr^{85} from this decay did in fact enter the gas phase implies little or no entrapment of its precursors in the solidified melt. Since iodine should behave chemically like bromine, we should expect that at least the direct fission yield of the iodine isotope would also have escaped entrapment, and might be a potential health hazard during early production of chimney gas.

Neutrons escaping the device at the time of detonation interact with components of the medium to produce activation products. Two of these products are isotopes of argon, and are therefore mixed with the chimney gases. About 13 kCi of Ar^{37} were present at zero time in the Gasbuggy chimney gas. Most of this is formed by Ca^{40} (n, α) Ar^{37}. Because of its half-life, the concentrations found several months following the detonation were comparable to those of Kr^{85}. Only about 250 mCi of Ar^{39}, produced principally by $K^{39}(n,p)Ar^{39}$, were observed in the gas.

B. Chemically Reactive Nuclides Forming Gaseous Compounds

Considering the time scale of the Gasbuggy experiment, the only isotopes expected to form gaseous compounds and to be present in significant quantities in the postshot chimney gas are tritium and carbon-14. Tritium is present in the debris of a nuclear explosion as a by-product of the fusion reaction and as an activation product of the lithium in the rock through the $Li^6(n,\alpha)T$ reaction. About 4 g of tritium were expected to reside in the postshot nuclear chimney. Carbon-14 is produced by the $N^{14}(n,p)C^{14}$ reaction. A total of about 7.5 Ci of this isotope was found in the gas. This is considered a lower limit for the total C^{14} in the chimney, since some unknown fraction of this isotope may be present in a non-gaseous form.

The behavior of tritium and carbon-14 during the initial shut-in period can be described by the basic chemistry of the carbon, hydrogen, and oxygen system comprising the chimney gas. Indeed, the observed changes in the distribution of these species has been of significant value in defining those chemical reactions of importance. Once these reactions are defined, however, the role is reversed, and the chemistry becomes useful in defining the importance of radiochemically measurable effects such as isotope exchange and isotope effect. During the later stages of the Gasbuggy experiment, no important chemical effects have been identified. The observed behavior of chimney gas components following the initial shut-in is essentially that expected from dilution with formation gas. That this is also basically true with regard to exchange reactions involving tritium or carbon-14 remains to be demonstrated.

Chimney shut-in period. The experimental concentrations of tritium in various chemical forms during the initial shut-in period are presented in Fig. 1.

The significant features from a radiochemical standpoint are the reduction of tritium as hydrogen gas during the first month, and a gradual decrease thereafter. Initial concentrations of CH_3T and C_2H_5T are lower than those observed at reentry, and a noticeable increase is seen to occur during the period. The apparent decrease in C_3H_7T is not considered significant. Total tritium content of the gas is essentially constant after the first month through the onset of production.

Figure 2 shows concentrations of carbon-14 over the same period. Although the $C^{14}O_2$ shows considerable bounce, it is most probably constant. Within analytical uncertainty, the increase observed in $C^{14}H_4$ is balanced by the decreasing $C^{14}O$. After the first month and prior to production, the C^{14} in the gas is essentially constant.

It is instructive, when the radiochemistry of these species is considered, to examine the ratio of a radioactive isotope of a given element to the total amount of the element in its various chemical compounds. This ratio, referred to as the specific activity, is conveniently expressed in units of picocuries of tritium or carbon-14 per standard cubic centimeter of the chemical compound of interest. Defined in this way, the specific activities presented here are related to the more conventional definition (based upon atom ratios) according to the number of hydrogen or carbon atoms per molecule of the gas. Thus, for example, at an equal tritium-to-hydrogen-atom ratio, the specific activities defined here for methane will be twice those for hydrogen and two-thirds those for ethane. Specific activities are useful for observing the behavior of an isotope, as opposed to the chemical interactions of its compounds.

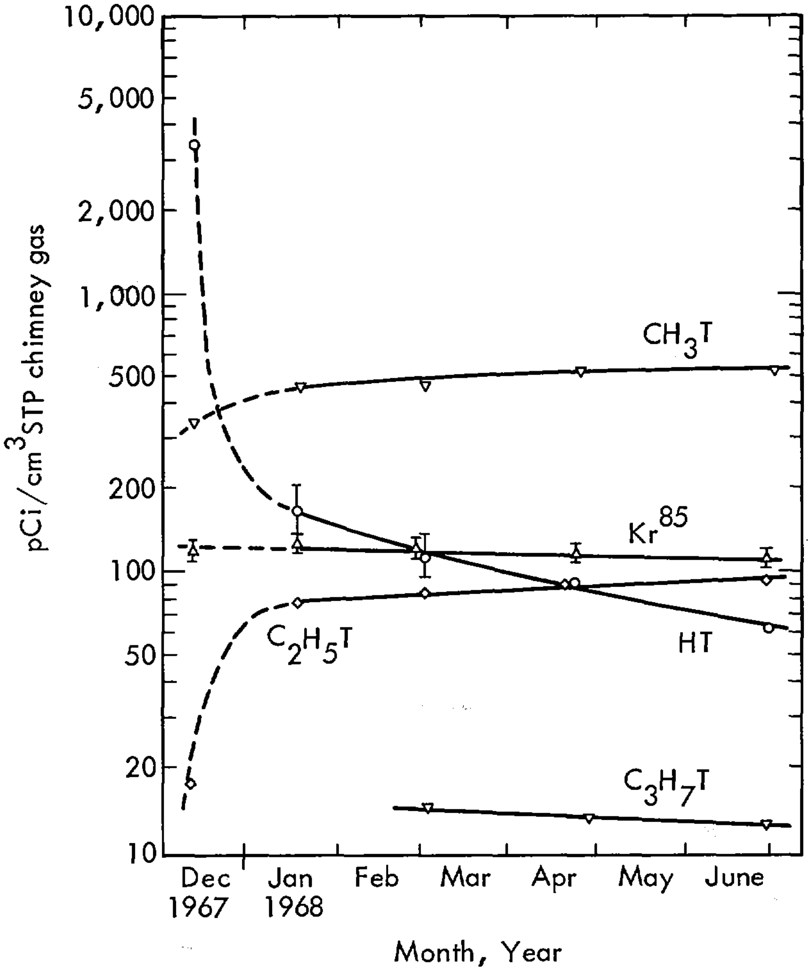

Fig. 1. Initial shut-in period—radionuclide concentrations.

Specific activities for the seven principle chemical species observed during the shut-in period are presented in Fig. 3. Two distinct behavior patterns are seen. During the first month major changes have occurred, while only the tritium content of hydrogen and carbon-14 content of methane are obviously changing in the following five months. Interpretation of these curves, therefore, requires separate treatment of early and late time.

We assume that an equal tritium-to-hydrogen ratio is established within the initial postshot cavity in all hydrogen-containing species, and that chimney collapse introduces large quantities of uncontaminated water. In addition, condensation of steam resulting from the cooling effect of collapse significantly lowers the pressure in the void space and allows influx of formation gas. Adopting this model, our preshot estimates of 70% of the T as HT and 0.2% of the T as CH_3T and using the chemical composition determined in the cable leak samples, we would expect specific activities prior to any chemical reaction or radionuclide exchange of about 4×10^4 pCi of T per cm^3 of H_2 and about 60 pCi of T per cm^3 of CH_4. About one-third this amount of tritium was observed as HT, and more than ten times the amount predicted was CH_3T. The quantity of methane present in the cavity at collapse time is quite sensitive to temperature. The disparity observed can be easily explained by the selection of a gas equilibrium temperature of the order of 1000°C. Because of the possibility of reaction in the gas prior to transit up the cable and exchange in the cable, the HT specific activity must be considered a lower limit. The factor of three can therefore be easily rationalized, if not completely explained.

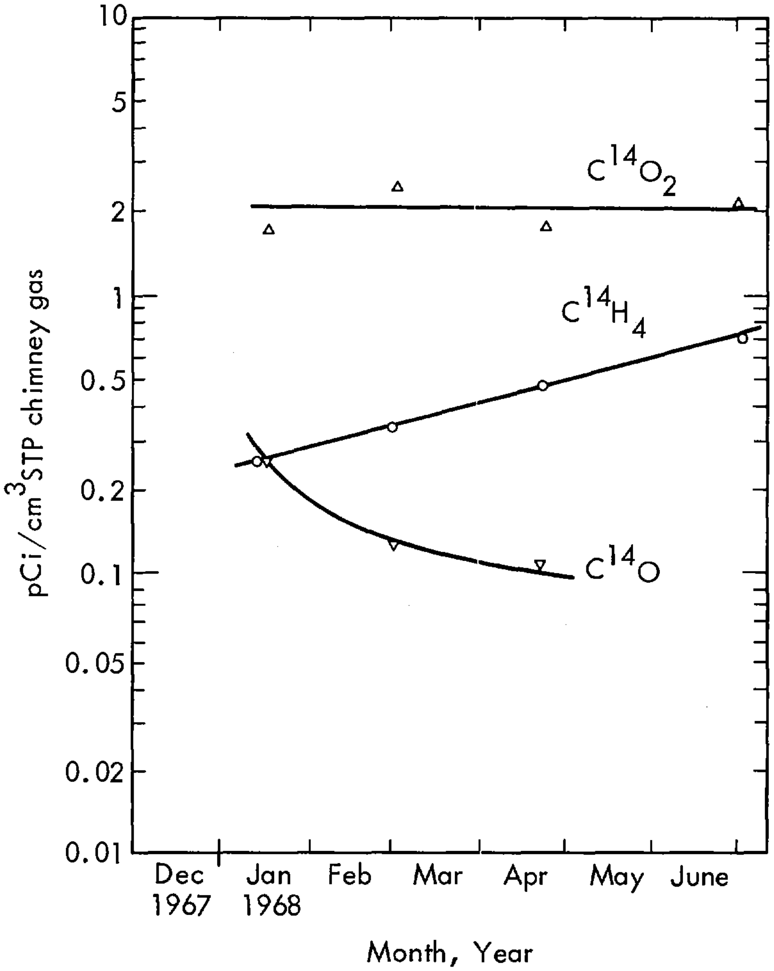

Fig. 2. Initial shut-in period—radionuclide concentrations.

The decrease observed in the hydrogen specific activity is dramatic in the first month. The tritium content of this gas at one month is about 1/15 that observed earlier. Although increases are observed in CH_4 and C_2H_6, these account only for about 10% of the observed decrease. The other 90%, about 1g of tritium, is presumed to have been taken up in water, by participation in an exchange reaction. The simplest form of the hydrogen-water exchange may be written:

$$HT + H_2O \rightleftharpoons H_2 + HTO \qquad (1)$$

This reaction may be catalyzed by the chimney rock, and could be responsible in part for the observation, particularly at these early times when chimney temperatures are relatively high. At lower temperatures, tritium exchange may be facilitated by the presence of equilibrium reactions. The simplest such process is the water gas reaction:

$$H_2 + CO_2 \rightleftharpoons H_2O + CO \qquad (2)$$

The presence of large amounts of these reactants in the chimney suggests the importance of this equilibrium. In addition, the chemistry of this period is largely a conversion of CO to CO_2,[3] presumably by virtue of reaction (2) attaining equilibrium. At these early times we expect that if reaction (1) is not at equilibrium, reaction (2) will provide a relatively rapid path for tritium exchange. However, the rapid drop in HT is not seen later in the shut-in period. We conclude that exchange equilibrium was probably attained within the first month.

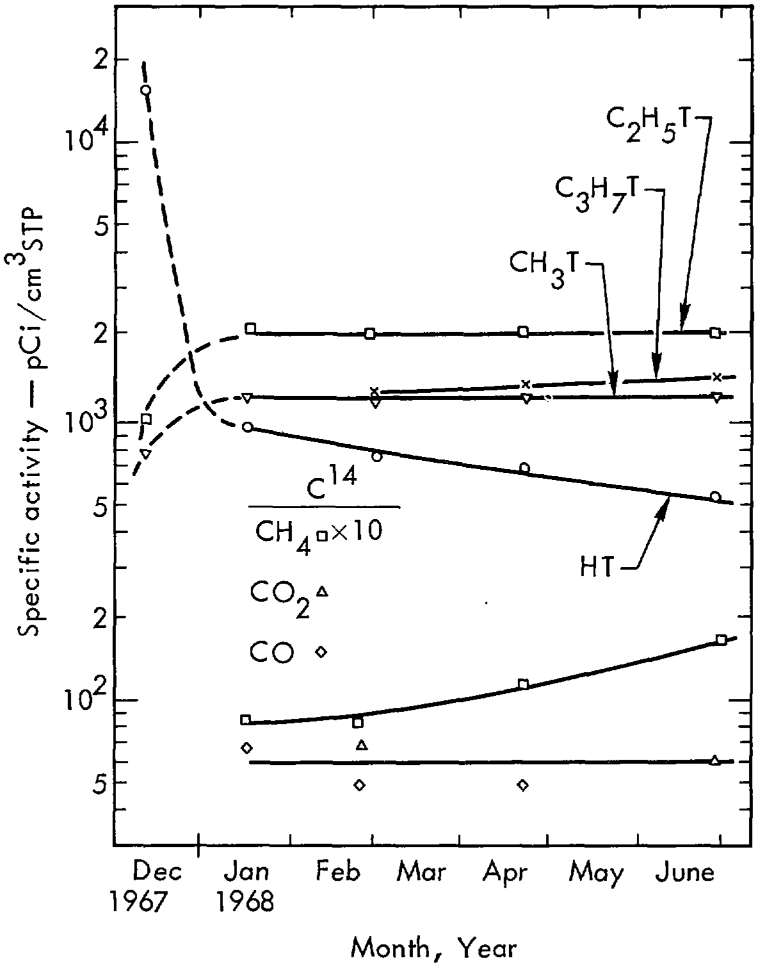

Fig. 3. Chimney shut-in period specific activity.

If hydrogen and tritium were chemically identical, reaction (1) would reach equilibrium when an equal partition of the available tritium between water and hydrogen had occurred. Only at high temperatures is this an adequate approximation. This difference in chemical behavior is termed an isotope effect. As the equilibrium temperature is lowered, reaction (1) shifts to increase tritium in water relative to hydrogen. At 100°C, the maximum gas temperature observed during production tests,[*] the ratio of the specific activities of water to hydrogen is about 4. If 95% of 4g of tritium is HTO in exchange equilibrium with the hydrogen observed upon chimney reentry, then 8000 tons of water is implied. This volume of water is about 13% of the chimney volume obtained from the Xe^{127} measurements.

During the first month, the specific tritium content of the hydrocarbon gases is seen to almost double. Such an increase, most probably, does not represent an exchange equilibrium with hydrogen. For example, the ratio of the specific activities of methane to that of hydrogen at 100° is expected to be

---

[*] The observed temperature at chimney reentry was about 65°C. This is considered a lower limit as temperatures of 100°C were observed a year later during the constant bottom hole pressure production tests. Probably, the boiling point of water at chimney pressure (~230°C) is an upper limit.

about 7 at equilibrium. The ratio of specific activities of ethane to methane is assumed to be 3/2, and this is observed. If, as we have presumed, the HT content of the gas represents an equilibrium with water at about 100°C, then the observed HT/CH_3T ratio indicates no equilibrium of tritiated methane with either HT or water. The incorporation of tritium in methane and ethane, then, must have been by reactions which became seriously retarded as the chimney cooled.

The latter five months of the shut-in period exhibit changes in only the HT/H_2 and $^{14}CH_4/CH_4$ ratios. No significant variation is observed in other measured specific activities. However, significant increases in the tritium content of both methane and ethane were observed. Chemically, the concentration of CO_2 was about constant, while that of hydrogen decreased. Concentrations of components of formation gas also increased. No detectable quantity of CO was found in the June sample (or in subsequent samples).

Disappearance of CO implies that the water-gas reaction [reaction (2)] has shifted equilibrium to favor CO_2 and H_2. Such a shift is expected below about 800°C, so that the persistence of appreciable quantities of CO for several months suggests a relatively slow reaction rate. The consumption of CO is presumed due principally to the water-gas reaction. The direct conversion of CO to methane according to

$$CO + 3H_2 \rightleftharpoons CH_4 + H_2O \qquad (3)$$

is also possible. However, utilization of all the hydrogen which disapppeared from the gas to convert CO by this process would still leave a net CO concentration of 2.3%.

Another methane-forming reaction, considered somewhat more likely, involves CO_2 according to

$$CO_2 + 4H_2 \rightleftharpoons CH_4 + 2H_2O \qquad (4)$$

Note that the net effect of reactions (1) and (4) is given by reaction (3). However, by treating (1) and (4) separately we do not require the stoichiometry of (3), and can for example, consume CO without making methane.

By analogy with the preceding, it is assumed that the principle ethane-forming reaction is:

$$CH_4 + CO_2 + 3H_2 \rightleftharpoons C_2H_6 + 2H_2O \qquad (5)$$

Other possible reactions contribute to some extent to the observed composition changes. The available information is neither precise enough nor extensive enough to allow evaluation of their effects. The simple model, which is used here, based upon reactions (1), (4), and (5) can therefore be expected to describe general trends but may be found wanting with regard to detailed evaluation.

A material balance, involving the total available hydrogen and the observed increases in methane and ethane, can be used to estimate the amount of CO_2 converted by reactions (4) and (5).* An approximation of the specific activity of the hydrogen available for use in these reactions is obtained by averaging the observed final specific activity and the total HT per cm^3 of H_2 available if all the hydrogen produced by reaction (1) were added to the existing

---

*1.7% CO_2 converted to CH_4 by reaction (4); 0.57% CO_2 converted to C_2H_6 by reaction (5).

HT in the chimney gas.* This calculation assumes that chimney water is in exchange equilibrium with the HT at 30 days.†

From these approximations it is possible to calculate a net increase in tritiated methane of 85 pCi/cm^3 cavity gas as compared to an observed 86.3. This assumes an exchange equilibrium at 100°C with hydrogen ($K_{eq} \approx 7$). Exchange, with isotope effect, is required to effect a change in the observed hydrogen specific activity as shown in Fig. 3.†† This treatment gives a net production of tritiated ethane of about twice the observed 13.6 pCi/cm^3 cavity gas. The tritium used in forming CH_3T, C_2H_5T and HTO in the model is about 90% of the available total. The calculated residual HT is a factor of two lower than the observed 62.8 pCi of HT per cm^3 of cavity gas. The changes in specific activity of methane and CO_2 to be expected from the model are only a few percent and would not be detected within experimental error. The predicted increase of C^{14} in the methane is about a factor of 6 lower than the 0.4 pCi/cm^3 chimney gas which was observed. Carbon dioxide, the other chemical species which might aid the interpretation, should show a net increase of about 1.6%. This is close to experimental uncertainty (0.4% increase was observed), and CO_2 may also have been absorbed by water.

Because we are dealing with experimental measurements possessing uncertainties of the same order of magnitude as many of the effects which we wish to interpret, the model appears reasonable. Clearly, it is only of use in describing general trends and not for detailed evaluation. The lack of samples during the first month when major composition changes were occurring is quite unfortunate. There is no doubt that an understanding of the radiochemistry of this early period would be a significant advantage in evaluating the causes of the relatively minor changes observed later. Without this, the establishment of a completely satisfactory model for Gasbuggy becomes doubtful.

High flow-rate production test. Specific activities for the tritiated species during the high flow rate production test are shown in Fig. 4. No changes other than dilution are observed. The significance of this test from the standpoint of radiochemical observation is slight, because of its short duration. The dilution did, however, reduce the possibility of carbon monoxide being observed or of being a significant contributor to long-term reactions within the chimney.

Constant bottom-hole pressure production tests. No change is observed in the specific activities of the tritiated species during the four-month shut-in between July and November 1968, when this series of tests began. The tritium specific activities for these tests are shown in Fig. 5. Again, no change other than dilution is detectable.

These curves clearly illustrate the significant influx of unmixed formation gas during the second rapid drawdown in December and the subsequent mixing of this diluent. No such influx was observed when the flow was increased in January, but a gradually increasing admixture of formation gas was observed during the third test. The start of the long-term drawdown is indicated by the dotted lines, the increased specific activities being indicative of the lack of efficient mixing.

---

*An average of about 10^3 pCi of HT per cm^3 of H_2.

†The specific activity of water is assumed to be 4 times the observed HT specific activity of 10^3 pCi of HT per cm^3 of H_2. Note that an additional source of HT other than hydrogen is required by stoichiometry to obtain the observed constant gaseous tritium concentration.

††Exchange with additional water does not provide sufficient HT to obtain the observed increase in CH3T and C_2H_5T.

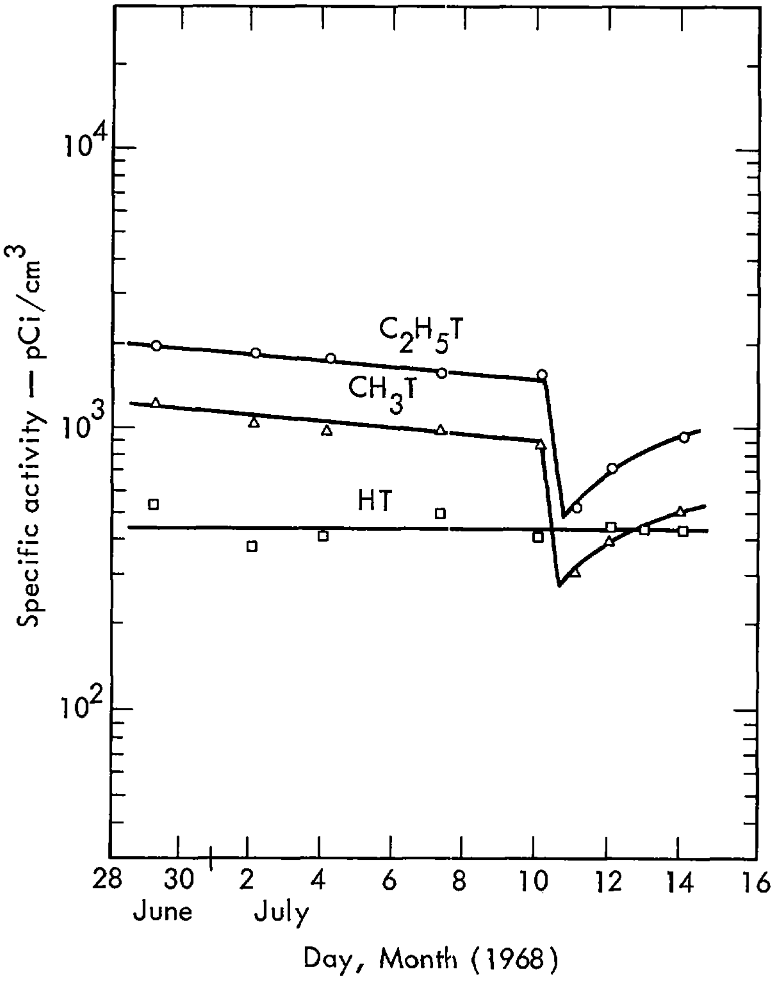

Fig. 4. High-rate production test specific activity.

Long-term production test. During the long-term production test, the specific activities of the principal reactive gases changed as shown in Fig. 6. The decrease observed in the tritium content of methane and ethane is explained by dilution with formation gas. The apparent decrease in the specific activity of hydrogen is evidence for dilution with relatively uncontaminated hydrogen. Such a source of hydrogen has been alluded to previously but has not satisfactorily been explained.* The essential constancy of the $C^{14}O_2$ specific activity at about the same level as seen during the initial shut-in period implies that the CO_2 dissolved in water was in equilibrium with the CO_2 in the chimney gas.

Throughout our investigation, we have noted a seemingly random bounce in the tritiated hydrogen and $C^{14}O_2$ results. Since the variations are well outside experimental uncertainties, a suggested rationalization of this bounce is the occurrence of exchange reactions at the top of the chimney with water or carbonates, respectively. These localized effects have, presumably, little effect on the radiochemistry of the chimney gases, but seriously complicate interpretation of the data.

The behavior of tritiated methane relative to Kr^{85} is shown in Fig. 7 for the entire postshot period of project Gasbuggy. Aside from the previously described increase in CH_3T during the first six months, we do not wish to

---

*Both CO_2 and H_2 were seen to decrease in concentration less rapidly than Kr^{85}.[3]

identify a trend. A long-term upward slope of these data would imply an exchange of tritium from water to methane. Within experimental uncertainty no such up-slope is observed.

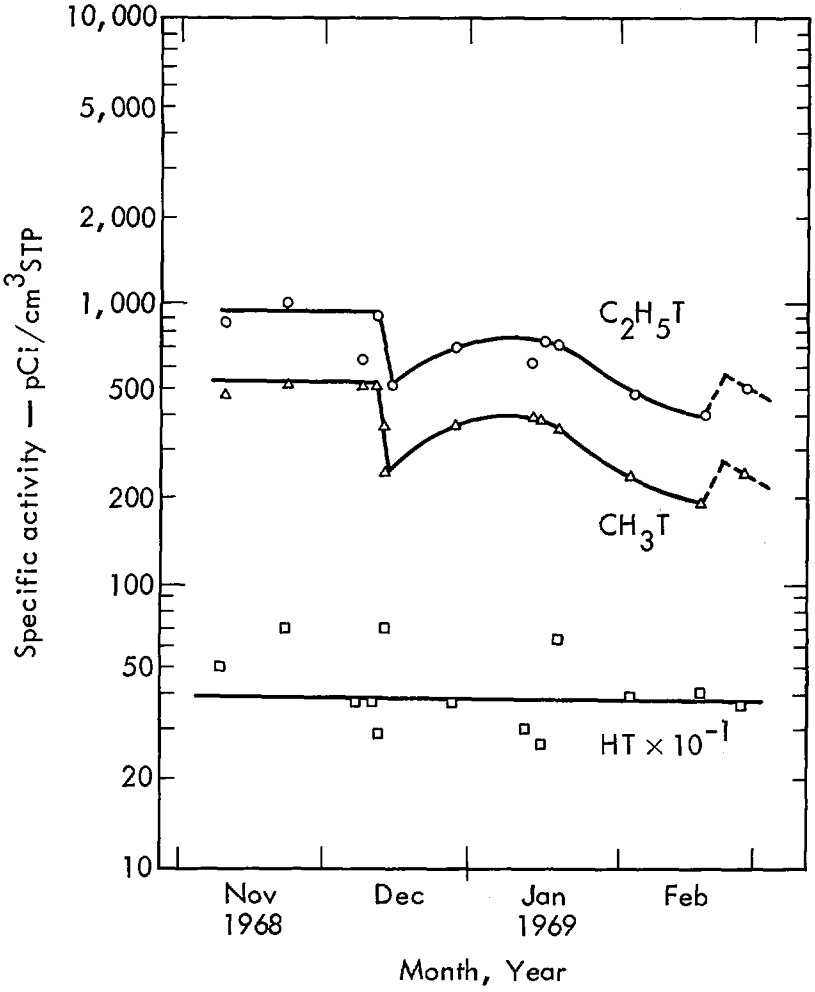

Fig. 5. Constant bottom hole pressure production tests specific activity.

C. Chemically Reactive Species Which Might Form Gaseous Compounds

Because of the complicated chemical environment which is the Gasbuggy chimney, it was recognized that volatile organic compounds of such elements as antimony, tellurium, tin, ruthenium and iodine could possibly be formed. Although these species were not expected to pose a problem, they could be present in the produced gas. Several attempts to locate the gamma radiations characteristic of these isotopes, both in the laboratory and in the field, produced negative results.[5] Based upon calculated detection limits for laboratory surveys of downhole sample bottles and charcoal filters, a series of experimental upper limits for the concentration of these species was established. These ranged from 0.04 pCi/cm^3 STP chimney gas for I^{131} to 10^{-4} pCi/cm^3 chimney gas for the ruthenium isotopes. The only detection limits calculated which were higher than 0.04 pCi/cm^3 were for short-lived $Sb^{125,127}$. In view of the reductions to be expected from decay and dilution, these limits were considered sufficient to allay fears that these nuclides might present a safety problem during the Gasbuggy production testing.

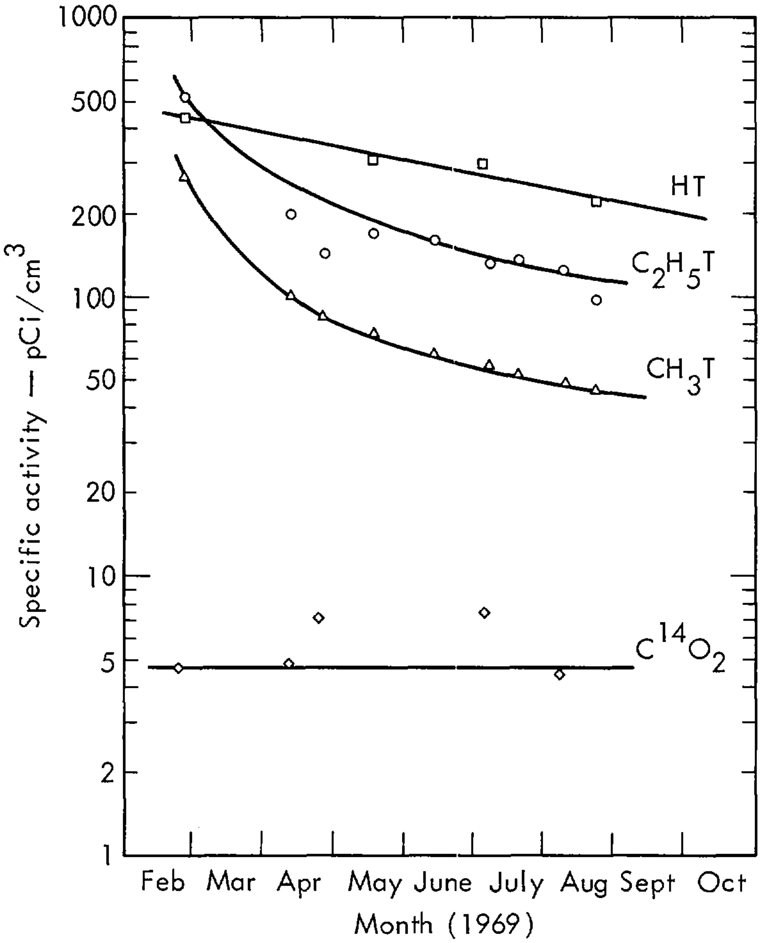

Fig. 6. Long-term production test specific activity.

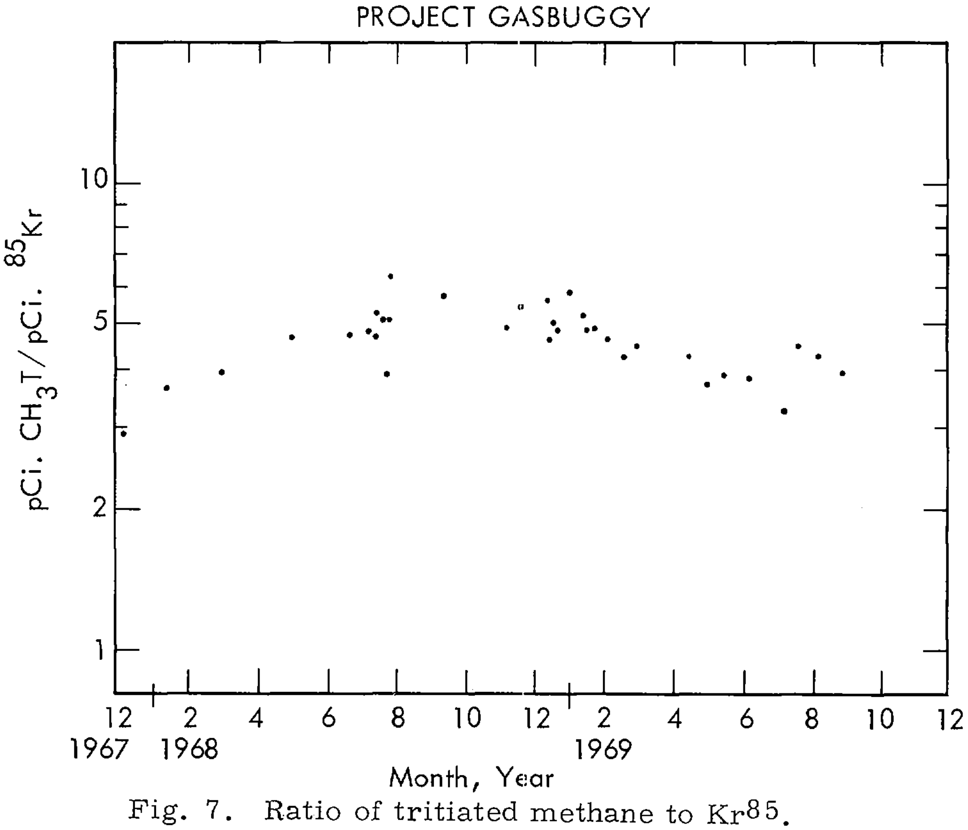

Fig. 7. Ratio of tritiated methane to Kr^{85}.

D. Other Radionuclides

Although very improbable, there exists a possibility that particulate matter carrying some radioactive material could be carried to the surface by the flowing gas stream. Conceivably, any radionuclide produced could be present, but the most likely class of materials which might appear would be those fission products distributed throughout the chimney region. This class, the so-called volatiles, is composed of isotopes produced by decay of short-lived fission product gases, and is typified by the biologically important nuclides Sr^{90} and Cs^{137}. To investigate the possibility, a known volume of gas was passed through filters during a high-rate production test. These filters were scanned for both gamma and beta radiation. No identification of the presence of these radionuclides has been made. Maximum concentrations deduced from the results indicate less than 4×10^{-8} pCi/cm^3 gamma (assuming Cs^{137}) and less than 2×10^{-7} pCi/cm^3 beta (assuming Sr^{90}). We conclude that the only significant radionuclides produced with the gas are tritium, C^{14}, and the rare-gas fission and activation products.

III. GENERALIZATION OF THE GASBUGGY EXPERIENCE

Within the limitations of our understanding of the important chemical and radiochemical phenomena of Project Gasbuggy, a generalized model can be developed. The applicability of this model has yet to be independently tested, and most probably will require modification as a result of future events. The attainment of a true predictive capability will require development of a detailed model and will depend upon the results of many field and laboratory experiments. A summary of the preceding discussions with regard to their general applicability can be offered as a guide to the behavior of radionuclides in gas stimulation applications.

The rare-gas fission and activation products are expected to mix with the chimney gases. Experience suggests no evidence for precursor entrapment, implying that the total amount of these isotopes produced by the detonation is present in the gas. A late times the only such isotope likely to be a major contributor to the contamination of chimney gases is Kr^{85}.

Small quantities of I^{131} and other fission products could be present in the chimney gas or on particulate matter carried by the gas. No such radionuclides were detected in the Gasbuggy experiment, but the degree of uniqueness of this result is unknown. Considerably more experience is necessary before this potential safety hazard can be dismissed, or generalized.

The behavior of tritium and C^{14} may be described according to the principal chemistry of three indistinct temperature regions. At high temperatures, the isotope effect is not important, and chemical reactions are rapid. Thus, initially these radionuclides are distributed according to chemical equilibrium considerations. During cooling, the isotope effect gains in importance while chemical reactions proceed to new equilibrium positions. Carbon monoxide is converted to carbon dioxide, hydrocarbon gases are produced and exchange equilibrium is established between water and hydrogen. As an equilibrium temperature is reached, reaction rates are significantly retarded, although the nature of the processes involved remains unchanged. The observations made from the Gasbuggy data are consistent with this scheme. Although the relative importance of the several reactions involved will change from experiment to experiment there is no reason to assume that a different chemistry will apply to the generalized case.

IV. CONCLUSION

A partial interpretation of the composition and contaminant levels of the Gasbuggy chimney gas has been presented. It is, unfortunately, more of a rationalization of the experimental data than a comparison of an independent chemical and radiochemical model to a set of observations. In view of our limited prior experience, this is not surprising. Nevertheless, a general model has been generated which may describe the major trends in the chimney gas of future experiments.

The lack of early samples precludes comparison with a detailed model, and the relatively minor changes which occurred subsequently do not generally permit an unambiguous interpretation. Other possible explanations of the data may, in the long run, prove more factual. Further, Gasbuggy is in many undefined ways unique. Simple scaling of these results to another experiment may be dangerous. This caution is especially applicable to minor components, and in particular to considerations of non-gaseous radionuclide concentrations.

A detailed predictive model has not resulted from interpretation of the Gasbuggy results. In fact, more questions were raised by this experiment than were answered in this regard. Reliable kinetic and equilibrium data are unavailable for the chemical and exchange reactions of importance over the extreme temperature range required. A strong need exists for extensive laboratory investigation. The importance of carefully executed field experiments designed to further the understanding of chemical and radiochemical phenomena cannot be overstated.

ACKNOWLEDGMENTS

The data gathered by the Gas Quality Analysis and Evaluation Program for Project Gasbuggy and presented here is the result of the combined efforts of many individuals. Of special significance were valued discussions regarding interpretation of these data with colleagues at LRL. Deserving special mention in this regard are Dr. F. F. Momyer and Dr. R. W. Taylor. In addition, the continued interest and cooperation of the project participants was significant in advancing the gas quality program, and contributed greatly to its success.

REFERENCES

1. F. Holzer, "Gasbuggy Preshot Summary Report," UCRL-50345, Lawrence Radiation Laboratory, Livermore,
2. R. W. Taylor, E. L. Lee, and J. H. Hill, "Chemical Effects of Nuclear Explosions in Hydrocarbon and Carbonate Bearing Rock," in Proc. Fourth Plowshare Symp., Engineering with Nuclear Explosives, January 14-16, 1970, Las Vegas, Nevada.
3. C. F. Smith, "Gas Quality Analysis and Evaluation Program for Project Gasbuggy," Proc. Fourth Plowshare Symp., Engineering with Nuclear Explosives, January 14-16, 1970, Las Vegas, Nevada.
4. F. Holzer, "Gasbuggy Preliminary Postshot Summary Report," UCRL-50386, Lawrence Radiation Laboratory, Livermore,
5. C. F. Smith, "Non-Gaseous Radioisotopes—Project Gasbuggy Chimney Gas," UCRL-50634, Lawrence Radiation Laboratory, Livermore,

XA04N0868

A PRELIMINARY ASSESSMENT OF THE RADIOLOGICAL IMPLICATIONS OF COMMERCIAL UTILIZATION OF NATURAL GAS FROM A NUCLEARLY STIMULATED WELL[a]

D. G. Jacobs and E. G. Struxness

Health Physics Division
Oak Ridge National Laboratory
Oak Ridge, Tennessee

and

C. R. Bowman
El Paso Natural Gas Company
El Paso, Texas

Abstract

Widespread utilization of nuclear explosives, in conjunction with the natural gas industry, can result in radiation exposure of sizable population groups. It is prudent to make realistic assessments of such potential radiation exposures before they occur and, unless the expected exposures are clearly insignificant, to consider these exposures in evaluating the net benefit of this particular use of nuclear energy. All pertinent facts relating to such assessments should be made public and presented in such a way that those who are to assume the risks, if any, can make a reasonable judgment as to whether the risks are acceptable.

Radioactivity in natural gas from the Gasbuggy cavity has been analyzed prior to and during flaring operations. None of this gas has entered the collection and distribution system, but a theoretical analysis has been made of the hypothetical impact on members of the public that would have occurred if the gas had been introduced into the commercial stream. Dose equivalents have been estimated for both workers and consumers. In this analysis, Gasbuggy gas has been traced through a real gas-collection system and processing plant, as represented by the present situation existing in the San Juan Production Division, El Paso Natural Gas Company. In addition, a number of considerations are presented which would apply to radiation exposure in metropolitan areas.

Results of this analysis for the Gasbuggy well indicate hypothetical dose equivalents to various population groups to be well within the annual dose limits suggested by the International Commission on Radiological Protection. Projection to a steady-state situation involving extensive natural gas production from many producing wells also resulted in hypothetical dose equivalents within the annual dose limits.

---

[a] Research sponsored by the U. S. Atomic Energy Commission under contract with the Union Carbide Corporation.

Simple extrapolation of the results from this analysis to potential exposures resulting from nuclear stimulation of other gas reservoirs cannot be made on a direct basis, but this method of evaluation should point to the potential exposure situations of greatest concern in any exploitation of this technique.

Introduction

If the peaceful utilization of nuclear explosives becomes widespread, radiation exposures to rather sizable population groups will be unavoidable. It is prudent to make realistic assessments of such potential radiation exposures before they occur and, unless the expected exposures are clearly insignificant, to consider these exposures in evaluating the net benefit of this particular use of nuclear energy. All pertinent facts relating to such assessments should be made public and presented in such a way that those who are to assume the risks, if any, can make a reasonable judgment as to whether the risks are acceptable.

This paper reflects the progress to date of a theoretical study directed to considerations of potential radiation impact on consumer population groups from commercial application of nuclear explosives in the natural gas industry. Potential exposure pathways are evaluated in light of the technology related to production, processing, transmission, and distribution of natural gas.

Federal and state regulatory agencies must become involved in any considerations leading to the actual marketing of natural gas or its by-products which may contain radioactivity resulting from nuclear stimulation of gas reservoirs. These considerations will constitute a "risk versus benefit" judgment.[1,2,3] It must be recognized that the focal point of such a decision will be the potential radiation exposure of a very large number of people and the potential biological risk involved. We hope that studies such as ours will provide the type of realistic information that will allow a reasonable decision to be made. Responsible representatives of federal, state, and local government must make continued efforts to effectively evaluate the potential benefits to be derived against the potential biological risks that may be incurred, but the ultimate decision will lie with the potential consumers.

Recommended Standards for Radiation Exposure

The International Commission on Radiological Protection (ICRP), the National Committee on Radiation Protection and Measurement (NCRP), the Federal Radiation Council (FRC), and other recognized authorities have standards and interpretations that can be applied to Plowshare situations. The basic recommendations are given in terms of maximum permissible radiation doses (MPD's) to organs of the body and maximum permissible body burdens (MPBB's) that will deliver these doses. It is from these basic standards that working limits are derived in the form of maximum permissible intakes (MPI's) and maximum permissible concentrations (MPC's). The ICRP and NCRP recommendations are effectively equivalent.[4,5] These recommendations have been largely adopted by the FRC, reformulated as Radiation Protection Guides,[6] and issued as guidance to federal agencies, such as the Atomic Energy Commission (USAEC) and the Public Health Service (USPHS). The MPD's recommended by the ICRP and NCRP were intended primarily for the protection of occupational workers; that is, individuals directly engaged in radiation work. These workers, by definition, are typical adult males and females in the United States or Europe that are expected to work with radiation and/or radioactive materials and be potentially exposed thereby for a period of 50 years. These basic limits are intended for planning the design and operation of radiation sources subject to close control and for exposure situations that can be carefully monitored.

Radiation exposure situations involving the public differ from occupational exposure situations in a number of ways. First, they may be less subject to control than radiation sources used in the nuclear industry. Second, they may involve contamination of the environment, the assessment of which must be done through procedures of environmental sampling and statistical calculations far more complex than those used in monitoring occupational workers. Third, they involve other considerations because of inhomogeneities in the exposed population groups (for example, age distribution, dietary habits, sources of food and water, etc.).

Concept of Critical Nuclides, Pathways, and Population Groups

When radionuclides are introduced into the environment, there may be numerous and complex pathways through which the nuclides may move and ultimately cause radiation exposure to man. Although it is prudent to consider all of the likely pathways of exposure, experience has shown that certain nuclides and certain pathways are much more important than others. These nuclides and pathways have been designated "critical" by the ICRP, although we would be more inclined to consider them as being "important" rather than "critical." After preliminary study indicates which are the important nuclides and pathways, it is recommended that the major effort be devoted to assessing the radiation exposures resulting from these nuclides and pathways. This does not necessarily mean that other nuclides and pathways can be neglected, only that the major effort should be directed at those that could potentially result in the greatest radiation exposures.

Unlike the group of radiation workers, which constitutes a reasonably homogeneous group of adults, the general public is composed of groups which vary widely in their characteristics, such as habits, location, age, etc. Because of this, certain groups within the population will receive a higher radiation exposure than other groups or individuals in the population. Such groups are termed "critical population groups" by the ICRP[7] and require separate consideration. Of special concern is the possible radiation exposure to children, and it is recommended that specific data for children be used in cases where the radiation dose to children may be higher than that to other members of an exposed group.

The critical group represents a small, rather homogeneous group receiving, or potentially receiving, the highest dose in a given situation. When the critical group has been identified, a representative sample from the group should be considered for more detailed assessment of actual or potential radiation exposure. In assessing such a sample, the ICRP's annual dose limits for members of the public should be applied.[8] In some cases, when the potential dose to the population will undoubtedly be very small, it may not be necessary to clearly identify the critical group. In this situation it may suffice to postulate a hypothetical group of extreme characteristics that would obtain an upper limit to the dose that any real critical group could possibly receive.

Radioactivity in Gasbuggy Products

The Project Gasbuggy device was detonated on December 10, 1967. Postshot gas samples have been periodically withdrawn from the Gasbuggy cavity and have been analyzed by Lawrence Radiation Laboratory.[9,10,11] It is of interest to note that no ^{131}I was found in the gas and that gamma scans have indicated no gamma emitters other than ^{85}Kr to be present. Tests for the presence of particulates in the gas stream have indicated that nongaseous fission products are absent.[10] Recent particulate tests on the gas stream have lowered the minimum detection threshold for ^{90}Sr by four orders of magnitude from the previously reported value.[12] Traces of ^{37}A (35-day half-life), ^{131}Xe (8-day half-life), and low concentrations of ^{14}C (5700-year half-life) were the only radionuclides reported to be found in the gas besides tritium and ^{85}Kr. The ^{14}C exists primarily as CO_2 in the cavity gas, although it also exists in the form of CH_4 and CO.

A small amount of gas was removed from the cavity and flared in early 1968, but the major program of production testing and flaring began in late June 1968. Samples at the beginning of production testing showed approximately 707 pCi/cm^3 of tritium and 112 pCi/cm^3 of ^{85}Kr. The concentrations of tritium and ^{85}Kr in the products removed from the Gasbuggy cavity have been decreasing with time. When the concentrations are plotted as a function of the cumulative volume of gas removed from the cavity (Fig. 1), the drop in concentration follows the curve anticipated for the case in which gas removed from the cavity is replenished by uncontaminated gas from the formation with mixing occurring in the cavity. The equation for the straight lines in Fig. 1 is:

$$C_p = C_o e^{-P/V_o} \tag{1}$$

where

C_o is the concentration of the radionuclide in the cavity gas at one atmosphere of pressure at the time production starts, corrected for radioactive decay to the date of the detonation (pCi/cm^3),

P is the cumulative production of gas from the cavity in millions of cubic feet (M^{2}cf),

V_o is the initial volume of gas at one atmosphere of pressure in the cavity (M^{2}cf), and

C_p is the concentration of the radionuclide in the gas at the wellhead at one atmosphere of pressure after a cumulative production of P. (C_p is in units of pCi/cm^3, corrected for radioactive decay to the date of the detonation.)

The initial volume of gas in the cavity was assumed to be 128 M^{2}cf, corrected to normal conditions of one atmosphere of pressure and 65°F. It should be recognized that a close fit of the data to the assumed exponentially declining curve would be obtained only if the influx of gas into the cavity from the formation occurs as rapidly as removal of gas at the wellhead. This is not always the case since the bottom-hole pressure decreases during periods of rapid gas withdrawal and changes in flow rate are evidenced by departures from the curve.

Based on radiochemical analyses and flow-rate data,[11] it is estimated that 1860 curies of tritium and 290 curies of ^{85}Kr were produced through February 3, 1969, in the first 161 M^{2}cf of gas. Estimates of the total quantity of tritium and ^{85}Kr that will be produced during the lifetime of the well are approximately 2500 and 350 curies, respectively, from Eq. (1). The krypton value agrees closely with the predicted quantity that was estimated to have been produced.[9] The projected value for tritium assumes that no appreciable

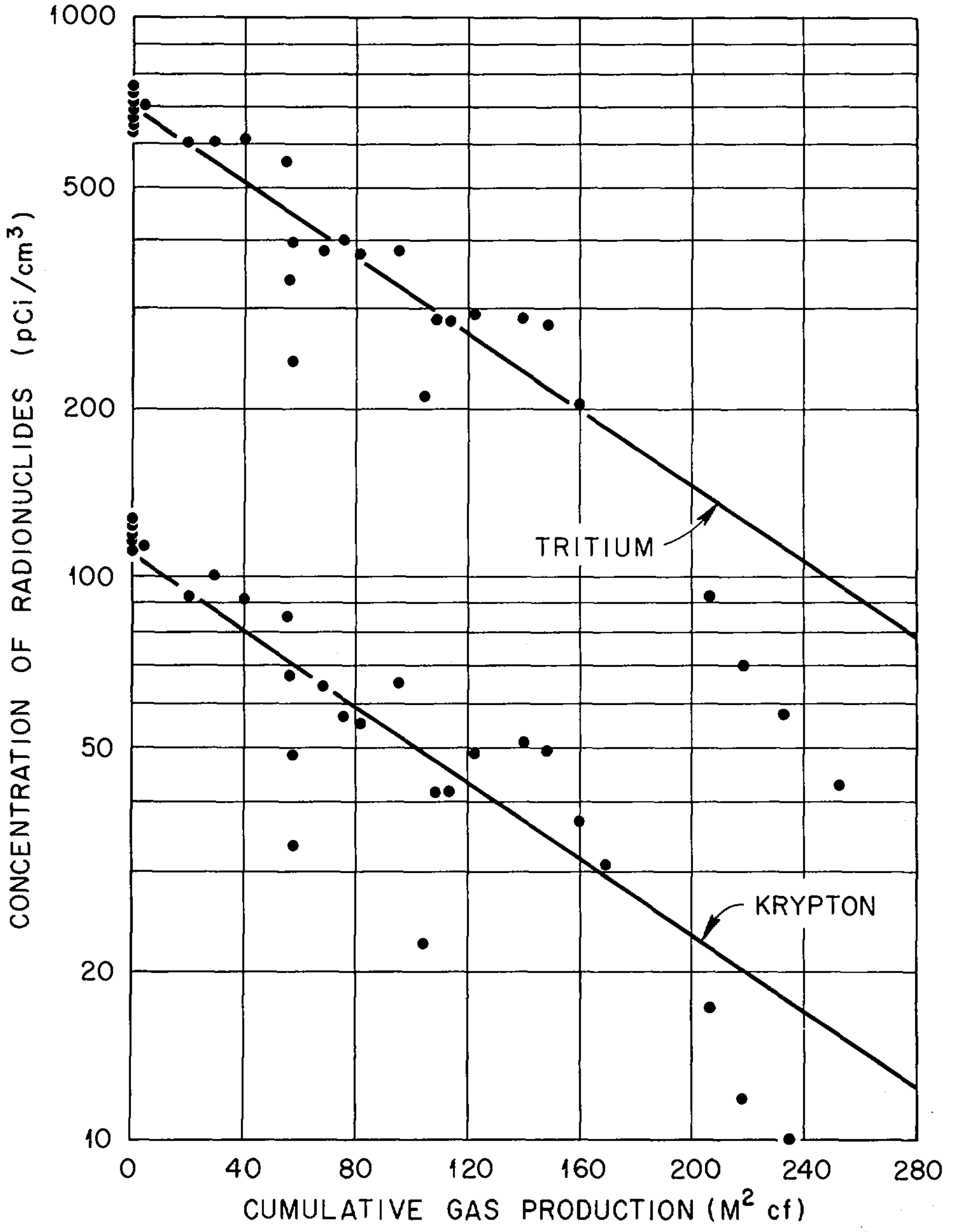

Concentrations of Tritium and Krypton-85 in Gasbuggy Gas as a Function of the Total Volume of Gas Produced (the Straight Line Represents the Predicted Concentrations Based on Complete Mixing of 128 M^2 cf of Gas in the Chimney).

Fig. 1. Concentrations of Tritium and Krypton-85 in Gasbuggy Gas as a Function of the Total Volume of Gas Produced.

exchange of tritium from water to methane will occur, since approximately 40,000 curies of tritium were estimated to be present initially.

Samples of liquid hydrocarbons taken from the Gasbuggy well on February 25, 1969, were fractionated by distillation. Total tritium and chromatographic analyses on these fractions were performed by the Analytical Chemistry Division of the Oak Ridge National Laboratory. Except for the low boiling fraction (97 to 219°F), there was very good correlation between the measured activity levels (about 0.14 μCi/ml) and the activity levels for the mixtures of hydrocarbons in the various fractions predicted assuming a constant tritium to hydrogen ratio. It appears reasonable to assume that tritium is uniformly distributed over all the hydrocarbons in relation to their hydrogen content, although there is a suggestion from this, and other available data, that the tritium concentration of propane through heptane is somewhat lower than one would estimate on the basis of a constant tritium ratio for all hydrogen-containing species.

Collection and Processing of Natural Gas

The gas-collection system in the San Juan Basin is internally quite complex, but only two principal outlets exist through Blanco plant or Ignacio plant (Fig. 2). Discussion of this collection and processing system is useful in developing an understanding of potential exposure pathways that would result from real disposition of natural gas and by-products from a nuclearly stimulated well. In this hypothetical situation the gas from the Gasbuggy well would enter a trunk line heading toward either the Blanco or Ignacio processing plants. As the gas moves along the system, it is mixed with uncontaminated gas being produced from other wells in the basin.

A landowner under lease agreement with El Paso Natural Gas Company may request installation of a "farm tap" on a gas wellhead near his house so that he can obtain gas for domestic use directly from the well. These farm taps are isolated from the collection system by means of a one-way valve which prevents backflow of gas from the collection system. Several farm taps exist in the San Juan Basin. The potential dilution of gas introduced into the system from the Gasbuggy well would be least at these farm taps if the one-way valve should fail. The location of farm taps lying closest to the main collection trunks are shown in Fig. 2.

Ordinarily, gas wells produce liquid hydrocarbons and water as well as gaseous products. Some of these liquids, called "drip liquids," condense at the wellhead and are collected in tanks for sale to local refineries in the Farmington-Aztec-Bloomfield area where they are fractionated and further refined. Most of the water is removed from these drip liquids at the wellhead, generally by adsorption into glycol, and disposed by evaporation.

During transmission of the gas, further condensation of water vapor and higher hydrocarbons also occurs. The quantity varies seasonally due to temperature changes. These liquids tend to accumulate at low spots in the gathering lines and must be removed periodically so that they do not impede the flow of gas. Removal is accomplished by sending rubber balls (pigs) through the lines to facilitate removal of the liquids at pigging stations along the lines. These pigged liquids are stored in tanks and sold to the local refineries.

At the processing plants the gas stream is further dehydrated and liquid hydrocarbons (propane and higher) are removed from the product gas. Liquid hydrocarbons from Blanco plant are piped to Wingate plant near Gallup, New Mexico, where they are fractionated and distributed by rail and truck. At

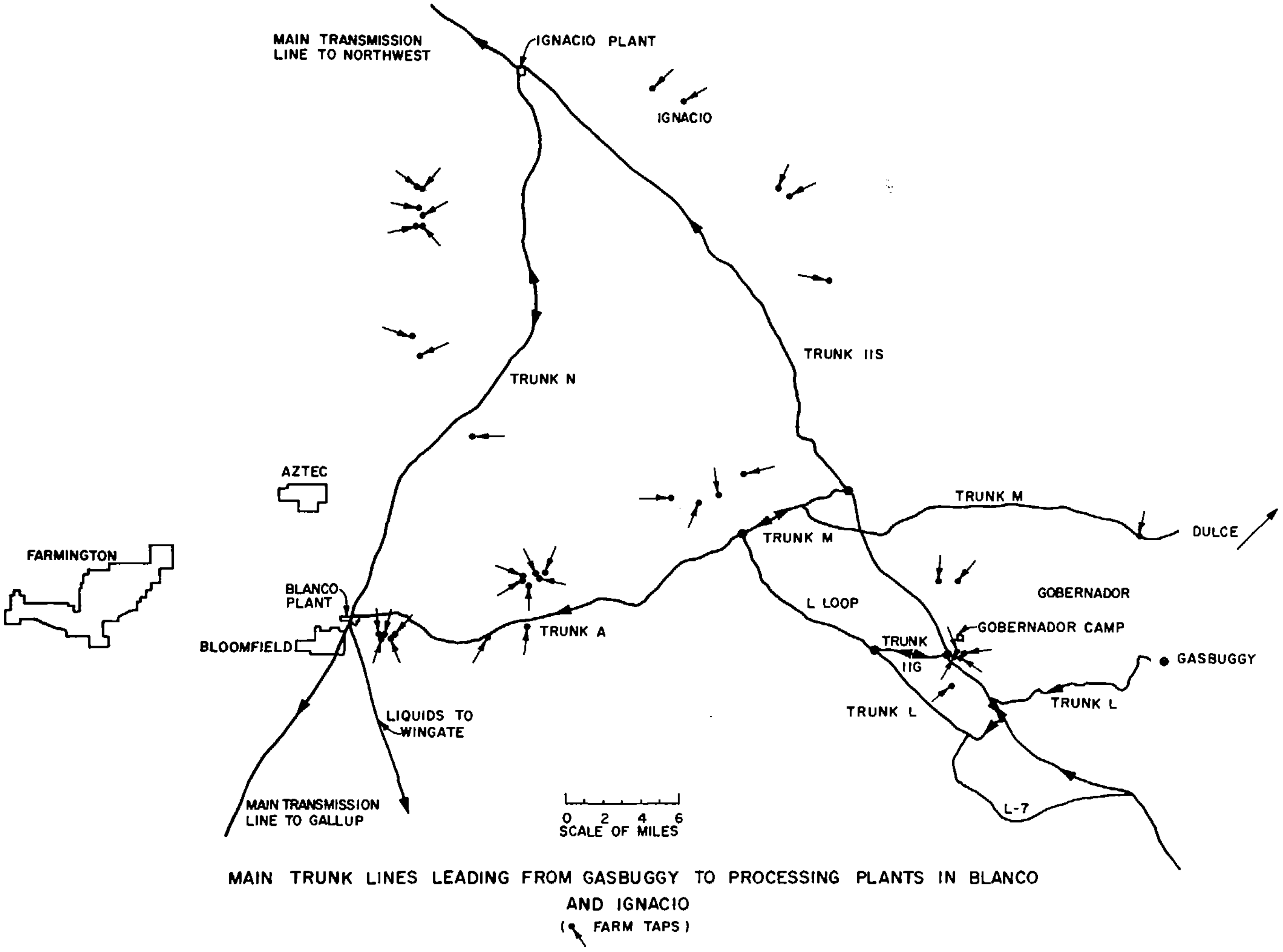

Fig. 2. Main Trunk Lines Leading from Gasbuggy to Processing Plants in Blanco and Ignacio.

Ignacio plant some butane and propane is separated and may be marketed locally. Mercaptan is added to the product gas (primarily methane), and it enters pipelines leading to California to the southwest from the Blanco plant or to the Pacific Northwest from the Ignacio plant. Fuel for the operation of compressors, electric power plants, and dehydrators is removed from the product stream and is combusted at the plant site. Wet fuel (containing hydrocarbons above propane) is used for the operation of gasoline absorbers. Excess wet fuel and residue from the absorption plant which cannot be economically recovered is flared in a surface pit.

The Approach to Assessment

In order to facilitate the assessment of the radiological impact from the commercial use of gas from nuclearly stimulated well, the study is divided into three phases. Phase I is a consideration of the potential population and employee exposures within the San Juan Basin from the hypothetical utilization of gas from the Gasbuggy well. It seems likely that in this region the possible dilution of the radioactivity from this single source would be the lowest and the potential exposures, the highest.

In Phase II the considerations are extended to include the hypothetical utilization of natural gas and other contaminated by-products from the Gasbuggy well by population groups outside the San Juan Basin. In this phase we take into account the dilution of gas from the San Juan Basin with gas produced in other fields, such as the Permian Basin.

The final extension of the problem, Phase III, will consider the potential nuclear stimulation of an entire reservoir in which temporal sequencing of detonations combined with decreasing concentrations of radioactivity in the individual wells would lead to a steady-state condition in which the concentration of radioactivity in consumed gas would remain relatively constant. Before we begin this phase of the study, we hope to have more representative information available on the likely radionuclide content of cavity gas from wells stimulated using nuclear explosives and emplacement configurations designed to produce lower quantities of residual tritium in the gas.

This paper reflects our progress to date, but it should be emphasized that our analysis is not yet complete. We anticipate making similar assessments for product disposition from Rulison before beginning Phase III.

In assessing each of these phases, we attempt to make conservative, but realistic, assumptions regarding the disposition and use of natural gas and its by-products. Using such information, the more important exposure pathways are delineated. Potential radiation exposure situations and estimates of the associated dose equivalents using existing computer programs are made. These programs include the flexibility to consider external beta and gamma radiation from submersion and from contaminated surfaces, as well as internal exposures following ingestion, skin absorption, and inhalation. Furthermore, information is built into the computer programs to allow consideration of age-dependent factors in the dose rate that would be obtained from tritium.

Hypothetical Population Exposures

Tritium and ^{85}Kr are the radionuclides of major concern in the gas removed from the Gasbuggy cavity. Although there is some ^{14}C present in the gas, it exists primarily as CO_2. The CO_2 would have to be removed before the gas could be marketed, and this would result in a reduction of the ^{14}C content in product gas by about a factor 3 to 5. Krypton is not retained to any significant extent by the body, and the primary mode of exposure is from submersion in contaminated air.[4] In the case of tritium, retention by the body is about two orders of magnitude greater for the oxide than for the gas. Human exposure to methane would be quite limited, and it is presumed that tritiated methane would behave much like tritiated hydrogen gas and would not be retained to any significant extent by body water. Thus, the most significant radiation exposures from use of natural gas from nuclearly stimulated wells are likely to occur after combustion of gas to form carbon dioxide and water vapor. This mode of exposure is especially important since more than 98% of the total production of natural gas and its associated liquid hydrocarbons is consumed as fuel. Tritiated water vapor enters the body from the air in approximately equal amounts by inhalation and absorption through the skin.[4]

Numerous exposure pathways can be postulated. The most direct modes of exposure are submersion, inhalation, and absorption through the skin. Only these modes of exposure have been considered in this preliminary analysis, though we are awaiting with interest the experimental results being obtained by the U. S. Public Health Service so that we can consider intake by ingestion of food and water that have been exposed to the combustion products in homes where natural gas is used as a source of fuel.[14]

Drip liquids from the San Juan Basin are sold to local refineries where they end up primarily as fuels. Any drip liquids collected from the Gasbuggy well would be diluted with uncontaminated liquid hydrocarbons from other gas wells in the basin, and the tritium concentration of combustion products from these fuels would be the same as from combustion of natural gas having the same tritium to hydrogen ratio. Thus, if the production of liquid hydrocarbons is assumed to be uniform throughout the basin, though this is known not to be completely true, the liquid fuels produced from the drip liquids would give rise to the same concentration of tritium in their combustion products as would the natural gas processed through the Blanco or Ignacio plants. However, the primary use of liquid fuels is for internal combustion engines, and the combustion products are ordinarily discharged directly into the atmosphere rather than being vented into a closed space, such as a house.

There are a number of factors which affect the concentration of radionuclides available for the exposure of domestic consumers. These factors include:

1. Concentration of radionuclide at the wellhead.
2. Production rate.
3. Pipeline dilution.
4. Quantity of gas consumed.
5. Fraction of combustion products vented inside the home.
6. Home dilution.
7. Home occupancy.

Home Heating and Other Domestic Uses[15]

Open flame burning of natural gas in a dwelling results in the production of heat, carbon dioxide, and moisture within a confined space. Nonventilated heating is not representative; however, it represents a "worst" case for this preliminary assessment. In warm weather ventilation will be at a maximum to remove undesirable heat and dilution of combustion products from nonheating appliances would be at a maximum. In the winter the opposite occurs and minimum dilution of these combustion products and those from heating would be achieved. Hence, use of natural gas from a nuclearly stimulated well would probably give rise to maximum radiation exposures during the heating season.

A consistent approach to the problem is to consider heat requirements as the independent variable and gas usage dependent on the heat required to maintain a normal inside temperature (70°F). Exchange of outside air with that inside the dwelling unit must also be evaluated so that we may determine the average dilution of combustion products within the living space. Several types of dwellings have been considered, and the estimated dilution factors during one 80-degree day of nonvented heating are shown, along with the characteristics of the dwellings, in Table 1. All of the tritium is assumed to be present as HTO following combustion of the gas.

Dilution factors during periods when heating is required are based on heat conduction through typical construction materials and infiltration of air into dwelling units around doors and windows. Heat requirements are based on the thermal input required to warm infiltrating air and to balance conductive losses. The quality of construction is reflected in the rate of heat loss from the dwelling. As an example, a dilution factor of 190 is obtained during heating at an inside-outside temperature differential of 80°F for a 1000 ft^2 house of normal construction. During periods when the heating requirements are lower, gas consumption is also lower and the effective dilution factor is greater. Heat losses are related to the surface area exposed to the outside air; therefore, larger dwellings require less heat per unit volume to maintain a given temperature and the dilution factor increases with an increasing size of house.

When heating is not required, residential gas consumption is restricted to ranges, water heaters, refrigerators, clothes dryers, and other nonheating appliances. A study of nonheating gas usage in Indiana indicates an average total consumption of about 150 ft^3/day for this combination of appliances.[16] This can be compared to 12.5 ft^3 of gas required per degree day of heating for a normally constructed house with 1000 ft^2 of floor area. This consumption of natural gas does not vary widely with season, and it is much more difficult to establish dilution factors of the combustion products within the dwelling. To be conservative, we can assume that the infiltration rate of air remains constant throughout the year. This would then give a dilution factor of 1270 for the combustion products of the gas under nonheating conditions for the Type B residence.

In addition to these considerations, appropriate corrections in the calculated dose equivalents for exposure situations from domestic consumption of gas should be made for the fraction of combustion products vented outside the home and home occupancy.

Potential Radiation Exposure from Domestic Use at Farm Taps

As mentioned previously, several farm taps exist in the San Juan Basin and those lying closest to the main transmission lines are shown in Fig. 2. Potential dilution of Gasbuggy gas introduced into the collection system would be minimal in laterals and trunks near the well. The nearest farm tap is located near a point in the collection system having an average daily gas flow over 50 M^2cf. Failure of the one-way isolation valve could result in potential domestic consumption of gas having the highest concentration of radioactivity. Dose equivalents have been estimated for the occupants of the hypothetical normal house of 1000 sq ft of floor area (Type B) for average

Table 1. Dilution Factors for Typical Dwellings During Heating at an Inside-Outside Temperature Differential of 80°F

Identity	Description	Dilution Factor
Residence A	10-ft x 10-ft x 8-ft shack; walls made of 1-in. wood; one door; two windows, 3 ft x 4 ft.	110
Residence B	Normally constructed dwelling unit of 1000 sq ft of floor area; 4 in. of rock wool insulation; doors and windows constituting 15% of the outside surface; windows curtained.	190
Residence C	Same as Residence B but with 3000 sq ft of floor area.	215
Residence D	Extremely well -designed and well-built house with storm doors and windows; 1000 sq ft of floor area.	335

nonheating usage and for heating corresponding to about 6000-degree days per year.[17] Measured values for the production of gas and for the concentration of tritium, ^{85}Kr, and ^{14}C during production testing of the Gasbuggy well were used (Fig. 1). The values listed in Table 2 are potential annual dose equivalents for an occupant of such a house, assuming continuous occupancy. The dose from all forms of ^{14}C is shown in the table. Although CO_2 would undoubtedly be removed from the gas to render the gas of sufficient quality for commercial uses, such removal would probably occur at the processing plants.

Exposures from Releases of Activity at Processing Plants

As mentioned previously, gas produced in the vicinity of the Gasbuggy well in the San Juan Division of El Paso Natural Gas Company is processed at either Blanco plant or Ignacio plant. Since Blanco plant has the larger capacity, our initial consideration is limited to that plant. Nearly 95% of the input gas stream leaves the plant as dry product gas. Approximately 2.4% of the material is used or released at the plant site, and about 2.6% of the input stream is separated as liquid hydrocarbons which are pumped to Wingate plant for further distribution. The average input of gas to Blanco plant is about 576 M^{2}cf/day. About 4.3 M^{2}cf/day is used as fuel for compressors; approximately 5.2 M^{2}cf/day is used as fuel for boilers and as other fuel; and roughly 1.3 M^{2}cf/day of nonmarketable material is flared in an open pit. In each of these cases, combustion products are released to the environment. In addition to these releases, about 0.2 M^{2}cf/day is released in desiccant dehydration and 0.01 M^{2}cf/day in glycol dehydration.

The various releases from the plant are not uniform in composition. Thus the hypothetical amount of tritium released is not directly proportional to the amount of gas released. The hypothetical quantities of tritiated hydrocarbons entering the plant were estimated on the basis of the chemical and radiochemical quality of Gasbuggy gas during production testing. The various tritiated hydrocarbons were assumed to be diluted with equivalent species from other wells. Krypton was assumed to follow the gaseous releases, but not to go into the liquids pumped to the Wingate plant. With these assumptions, the estimated dispositions of tritium and krypton are indicated in Table 3.

The probable behavior of these releases to the environment was estimated by W. M. Culkowski and G. A. Briggs of the Air Resources Atmospheric Turbulence and Diffusion Laboratory, Environmental Science Services Administration, Oak Ridge, Tennessee.[18] Their estimates were based on the assumption that wind data from Farmington, New Mexico, is representative of the plant site.

Releases from the Flare Pit.-- Winds blow toward the residential area of the Blanco camp about 12% of the time. During the time when wind speeds in this direction exceed 10 miles per hour, the plume from the flare pit would not rise but would travel along the ground. Wind vectors meeting both these direction and speed conditions occur about 5% of the time. When wind speeds are lower than 10 miles per hour, the heat of the plume would permit a sufficient rise to carry it above the plant and residential areas.

Using these conditions, Culkowski and Briggs[18] suggest that typical annual average dilution of the combustion products for both the residential and plant areas would be about 5×10^5 ft^3/sec. During the hypothetical production of the first 161 M^{2}cf of Gasbuggy gas, the average ground level atmospheric concentrations would be about 1.3×10^{-11} μCi/cm^3 for ^{3}H and 2×10^{-12} μCi/cm^3 for ^{85}Kr.[19] The dose equivalents from 168 hr per week exposure to these concentrations would be primarily due to tritium and would amount to about 0.025 mrem to the total body for an annual exposure.

Table 2. Annual Dose Equivalents from the Hypothetical Use of Gas from the Gasbuggy Well at a Point in the San Juan Basin Where the Average Daily Flow in the Pipeline is 50 M^2cf

Production Year	Annual Hypothetical Dose Equivalents (mrem)		
	^{3}H (Total Body)	^{85}Kr (Skin Dose from Submersion)	^{14}C (Total Body)
1968	4.1	0.25	0.04
1969	2.8	0.17	0.08
1970[a]	0.29	0.017	0.01
1971[a]	0.24	0.014	0.01
1972[a]	0.20	0.012	0.01

[a] Projected on the basis of 0.2 M^2cf/day gas production with a decreasing concentration of tritium and krypton-85. The concentration of carbon-14 has remained relatively constant during the first 161 M^2cf of gas production.

Table 3. Disposition of Tritium and Krypton During the Hypothetical Processing of Gasbuggy Gas at the Blanco Plant During the First 160 M^2cf Production

Disposition	Estimated Hypothetical Quantity of Activity Released (curies)	
	^{3}H	^{85}Kr
Flare pit	6	1
Boiler fuel	20	2.5
Compressor fuel	13	2
Dehydration	1	0.1
Liquid product (to Wingate)	90	---
Dry gas product	1720	290
Not accounted for	10	2

Releases from Compressor and Boiler Fuel Use.-- The exhaust stacks of the compressor facilities and the boiler plant are low, allowing a great deal of the effluent to reach the ground within the first few hundred meters. Downwash from the exhausts of the compressor facilities begins at wind speeds of 3 to 6 mph, and at about 10 to 15 mph these exhausts are not effective in dispersing the combustion product effluents. Boiler plant stacks might become ineffective at wind speeds higher than about 25 mph.

Culkowski and Briggs[18] estimate the average dilution factor for all emissions from the plant, except for the flare pit, to be about 10^6 ft^3/sec. In the plant area the concentrations would be higher, especially near the compressor facilities. In this area the annual average concentration of the combustion products may be as high as $x = Q(3 \times 10^{-5})$ parts/ft^3 where Q is the total emission of each of the compressor facilities.

For the residential area the average ground level atmospheric concentration of tritium and ^{85}Kr from emissions other than the flare pit is estimated to be 5×10^{-11} μCi/cm^3 and 7×10^{-12} μCi/cm^3, respectively. The dose equivalents to the whole body from an annual exposure to these air concentrations would be about 0.09 mrem.

Near the compressor facilities the average concentrations of ^{3}H and ^{85}Kr are estimated to be about 2×10^{-10} μCi/cm^3 and 3×10^{-11} μCi/cm^3, respectively, during the production of the hypothetical 161 M^{2}cf of Gasbuggy gas. Dose equivalents to the whole body from an annual exposure at these concentrations for 40 hr per week would be about 0.14 mrem.

Considering the sum of these hypothetical exposures, the dose equivalents to the whole body for a nonworking resident of the Blanco camp is estimated to be a maximum of 0.12 mrem during the first year of production testing; and, for a Blanco plant employee residing at the camp, the maximum is estimated to be 0.23 mrem. An additional 0.5 mrem would potentially have been received during this period if we assume normal gas consumption for appliances and home heating by nonvented heaters for 6000-degree days of heating in a normally constructed house. Hypothetical exposures in subsequent years would be considerably lower, because the concentrations of radioactivity in the gas being removed from the Gasbuggy well are more than an order of magnitude lower than the original levels.

Hypothetical Population Exposures in Metropolitan Areas

Gas leaving the San Juan Basin is mixed with gas from other basins during its transmission to eventual consumer areas. While an analysis of a specific area using real input data has not been made, we have made some preliminary estimates of exposure situations that might be encountered in a metropolitan area.

Natural gas is used in metropolitan areas for operation of steam plants to generate electricity and for a wide variety of industrial and commercial applications, as well as for domestic consumption. Releases of combustion products from steam plants are through tall stacks, and they represent elevated point sources, while the releases from most of the industrial and domestic uses can be considered to be spread uniformly over a sizable area of ground surface.

S. R. Hanna and F. A. Gifford of the Air Resources Atmospheric Turbulence and Diffusion Laboratory, ESSA, are in the process of developing models to describe the dispersion of pollutants from ground level area sources in metropolitan areas.[19] Data is introduced into their computer program in a grid format. This program can be used to describe the ground level atmospheric concentration of any type of pollutant, including radioactivity, for a ground level area source. Some of their preliminary trials indicate that the ground level air concentration of a pollutant will be on the order of 10^{-5} ppm for the daily generation of a unit concentration of the pollutant per square mile. In considering the total atmospheric concentration of radioactivity over metropolitan areas from the hypothetical use of natural gas from nuclear stimulated wells, the concentrations estimated for the ground level area sources need to be added to the concentrations estimated for releases from elevated point sources, which can be estimated using local meteorological conditions with available mathematical models. In addition to these potential contributions to the radiation exposure from general atmospheric levels of radioactivity in a metropolitan area, it will also be necessary to consider the potential contributions from radiation exposure inside dwellings from domestic consumption of gas.

We can describe a hypothetical exposure situation based on these types of releases. Table 4 shows dose equivalents calculated for a hypothetical situation for the center of a metropolitan area where the average daily use of gas is 2 M^2cf/day per square mile, where heating for 1700-degree days for a 1000-sq-ft house is accomplished with nonvented heaters, and where nonvented appliances are assumed to be used. In most localities, the use of gas would be lower than the rate we have assumed, as would the resultant atmospheric concentration.

There is a lower limit to the average annual tritium concentration due to tritium from natural sources and weapons testing. If we assume that air is 1% water vapor by volume (8 ml of liquid water per cubic meter of air) and that the tritium ratio of atmospheric water vapor is 100, the lower limit of tritium concentration in air is about 2.6 pCi/m^3, which would give rise to an annual whole body dose of 0.0048 mrem.

The estimated radiation exposure from domestic consumption could be largely eliminated by using proper venting. The radiation exposure from nonheating use of natural gas would be about the same, regardless of geographic location, but the exposure from heating would be directly related to the degree days of heating required. In the United States the number of degree days ranges from less than 100 for Key West, Florida, to 10,000 in some areas of the Rocky Mountains. The population is distributed rather normally with respect to the required degree days of heating with average requirements of about 5100 ± 1600.

Looking ahead to the possible wide-scale application of nuclear devices for stimulation of natural gas reservoirs, we anticipate that a steady-state concentration of radioactivity in the gaseous products would result from dilution of gas from newly stimulated wells with gas from other basins or from stimulated wells in which the radioactivity had been depleted. Although one cannot predict, at this time, what this steady-state concentration would be, if the original concentrations of tritium in the Gasbuggy well were representative and each well could produce 1 M^2cf/day for 25 years, the steady-state concentration of tritium would be about 0.3 μCi/ft^3 or 10 pCi/cm^3. These levels of tritium are not representative of those expected in future applications of nuclear stimulation where explosive design and emplacement techniques will be used to reduce the quantity of residual tritium. We are looking forward to the analysis of gas samples from the Rulison cavity. In order for nuclear stimulation of gas reservoirs to be economically attractive, the rate of production associated with each detonation will need to be on the order of 5 to 10 M^2cf/day.[20] Furthermore, it is unlikely that all future supplies of natural gas will be produced from nuclearly stimulated wells; so there would be further dilution afforded by mixing of the contaminated gas with uncontaminated gas from other basins. Each of these factors would contribute to lowering the steady-state concentration of tritium at the point of natural gas consumption.

Table 4. Annual Potential Dose Equivalents from Hypothetical Exposure of Populations in Metropolitan Areas

	Maximum Potential Dose from Tritium (mrem/year)		
	From Atmospheric Exposure for Ground Level Release of 2 M^2cf/mi^2-day	From Domestic Consumption in Type B Residence	
Tritium Concentration in Gas at the Point of Use (pCi/cm^3)		Heating for 1700-degree days[a]	Nonheating[b]
10 (~ 0.3 μCi/ft^3)	0.38	5.8	15
5	0.19	2.9	7.4
2	0.08	1.2	2.9
1	0.042	0.58	1.5
0.5	0.024	0.29	0.74
0.2	0.012	0.12	0.29
0.1	0.0086	0.06	0.15
0.05	0.0067	0.03	0.07
0.0	0.0048[c]	0.00	0.00

[a] Assumes no venting and gas consumption of 12.5 ft^3/degree-day of heating.

[b] Assumes no venting and 150 ft^3/day gas consumption.

[c] Whole body dose from tritium due to its presence from natural sources and from fallout from weapons testing.

In considering the dose values presented in Table 4, we must remember that, although these hypothetical radiation exposures would give rise to potential doses of less than 170 mrem per year, the use of natural gas from nuclearly stimulated wells represents only one potential source of exposure. Also, in this preliminary analysis, only direct modes of exposure through inhalation, submersion, and absorption through the skin have been considered. The recommendations of the ICRP and other authorities specifically require that radiation exposures from all sources, other than natural background, be considered in any radiological safety evaluation.[4-6] Furthermore, these potential exposures could involve many millions of people; so extreme caution should be used in establishing "permissible" concentrations of man-made radioactivity in natural gas that would be considered acceptable for industrial and domestic consumption.

Summary and Conclusions

Preliminary estimates have been made of the potential radiation exposures that might result from the domestic and commercial utilization of natural gas from a nuclearly stimulated well. Although none of the gas from the Gasbuggy well has been introduced into the gathering and distribution system of the El Paso Natural Gas Company, the analysis was based on historical data from production testing of the well. Such an analysis is useful since it makes possible the consideration of a real system with regard to collection, processing, and distribution.

The hypothetical dose equivalents to various population groups were well within the annual dose limits prescribed by the ICRP and other authorities when the single well was considered.[4-6] Projection to a steady-state situation also yielded dose equivalents that are within these limits, even though we have considered the very conservative condition of domestic consumption with no provision for venting of combustion products. In spite of the fact that the prescribed limits seem attainable, because of anticipated improvements in device, design, and emplacement techniques, we feel that extreme caution should be used in establishing "permissible" concentrations of man-made radioactivity in natural gas for industrial and domestic consumption. We base our caution on the fact that nuclear stimulation of natural gas reservoirs represents only one of many potential sources of radiation exposure and that an extremely large population is involved. We subscribe to the philosophy that any amount of radiation exposure involves some risk and that every practicable effort should be made to keep the dose levels to members of the public as low as possible.

Acknowledgment

The authors would like to acknowledge considerable assistance provided by Mr. C. D. Catt, Mr. L. M. Parrish, Jr., and Dr. P. L. Randolph of El Paso Natural Gas Company; Dr. F. A. Gifford, Dr. W. M. Culkowski, Dr. S. R. Hanna, and Mr. G. A. Briggs of the Air Resources Atmospheric Turbulence and Diffusion Laboratory, ESSA; and Dr. M. J. Kelly, Dr. P. S. Rohwer, and Dr. A. S. Meyer of the Oak Ridge National Laboratory.

References

1. P. C. Tompkins, "The Philosophy Behind Federal Radiation Council Guides," pp. 498-507 in Proceedings for the Symposium on Public Health Aspects of Peaceful Uses of Nuclear Explosives, Las Vegas, Nevada, April 7-11, 1969, Southwest Radiological Health Laboratory, U. S. Department of Health, Education, and Welfare Report SWRHL-82 (1969).

2. L. R. Rogers, "Development of Regulatory Criteria Applicable to Control of Radiation Exposure to the Population from Products Containing Radioactive Material," pp. 529-542 in Proceedings for the Symposium on Public Health Aspects of Peaceful Uses of Nuclear Explosives, Las Vegas, Nevada, April 7-11, 1969, Southwest Radiological Health Laboratory, U. S. Department of Health, Education, and Welfare Report SWRHL-82 (1969).

3. H. M. Parker, "Plowshare Radiation Protection Guidance," pp. 543-549 in Proceedings for the Symposium on Public Health Aspects of Peaceful Uses of Nuclear Explosives, Las Vegas, Nevada, April 7-11, 1969, Southwest Radiological Health Laboratory, U. S. Department of Health, Education, and Welfare Report SWRHL-82 (1969).

4. International Commission on Radiological Protection, Recommendations of the International Commission on Radiological Protection (Report of Committee 2), ICRP Publication 2, Pergamon Press, London (1959).

5. National Committee on Radiation Protection, Maximum Permissible Body Burdens and Maximum Permissible Concentrations of Radionuclides in Air and Water for Occupational Exposure, National Bureau of Standards Handbook 69 (June 5, 1959).

6. Federal Radiation Council, Background Material for the Development of Radiation Protection Standards, Federal Radiation Council Report No. 5 (July 1964).

7. International Commission on Radiological Protection, Principles of Environmental Monitoring Related to the Handling of Radioactive Materials (Report of Committee 4), ICRP Publication 7, Pergamon Press, London (1966).

8. International Commission on Radiological Protection, Recommendations of the International Commission on Radiological Protection (adopted September 17, 1965), ICRP Publication 9, Pergamon Press, London (1966).

9. C. F. Smith, Jr., and F. F. Momyer, Gas Quality Investigation Program Status Report for Project Gasbuggy, UCRL-7314, Revision 1 (September 18, 1968).

10. C. F. Smith, Jr., Nongaseous Radioisotopes--Project Gasbuggy Chimney Gas, UCRL-50634 (April 7, 1969).

11. C. F. Smith, Jr., Project Gasbuggy Gas Quality Analysis and Evaluation Program Tabulation of Radiochemical and Chemical Analytical Results, UCRL-50635 (April 22, 1969). Revision 1 (November 17, 1969).

12. C. F. Smith, Jr., private communication with C. R. Bowman, December 1969.

13. D. G. Jacobs, P. S. Rohwer, and K. E. Cowser, Third Quarterly Progress Report on the Theoretical Safety Evaluation of Consumer Products from Project Gasbuggy, ORNL-TM-2657 (July 1969).

14. D. N. McNelis, "Exposure-Dose Research for Radionuclides in Natural Gas," pp. 585-594 in Proceedings for the Symposium on Public Health Aspects of Peaceful Uses of Nuclear Explosives, Las Vegas, Nevada, April 7-11, 1969, Southwest Radiological Health Laboratory, U. S. Department of Health, Education, and Welfare Report SWRHL-82 (1969).

15. M. J. Kelly, P. S. Rohwer, D. G. Jacobs, and C. R. Bowman, Second Quarterly Progress Report on the Theoretical Evaluation of Consumer Products from Project Gasbuggy, ORNL-TM-2513 (March 1969).

16. C. G. Segeler (ed.), Gas Engineers Handbook, the Industrial Press, 93 Worth Street, New York, 1966, Section 23, pp. 51-58.

17. C. G. Segeler (ed.), Gas Engineers Handbook, the Industrial Press, 93 Worth Street, New York, 1966, Section 12, pp. 97-109.

18. Letter from W. M. Culkowski, Air Resources Atmospheric Turbulence and Diffusion Laboratory, Environmental Science Services Administration, Oak Ridge, Tennessee, to D. G. Jacobs, Oak Ridge National Laboratory, June 24, 1969.

19. S. R. Hanna and F. A. Gifford, Air Resources Atmospheric Turbulence and Diffusion Laboratory, Environmental Science Services Administration, Oak Ridge, Tennessee, private communication with D. G. Jacobs, October 1969.

20. "Project Rulison: More Hope of Success," Chem. and Eng. News 47(42), 10-11 (October 6, 1969).

XA04N0869

STUDY OF CHEMICAL REACTIONS IN THE NUCLEAR UNDERGROUND EXPLOSION - INCIDENCE ON RADIOACTIVITY

Jean Maurice PICQ
Commissariat à l'Energie Atomique (France)
Centre d'Etudes de Bruyères-le-Chatel

We have been working in order to find out and state the theoretical or semi-empirical laws governing the reaction of radioactivity in contained nuclear explosion. To do so, we are studying the chemical reactions during the different stages of the cavity and chimney formation, as well as thermal transfers. At the same time, we are carrying an experimental study on melted rock and gas samples taken from the French underground explosions. The results of which can be found in this paper are derived from our present experiments at the plant (have been obtained from partial studies).

During the French underground explosions, we took gaseous samples. The gas analysis, without taking water vapour into consideration, showed that those samples were composed of hydrogen, carbon dioxide, carbon monoxide with small quantities of hydrocarbones (chiefly methane - about one per cent). The total amount of gas being quite large and proportional to the burst power, we came to the conclusion that those gases were produced by rock reactions (that rock was granite). We considered the following reagents because they were found in sufficient quantities to alter the balance between the different components : ferrous ions contained in mica, biotite, carbon dioxide from carbonates and water, either free or in a component state, contained in the rock. A comparison between theoretical and experimental results led us to notice among other things (fig. 1).

- temperature : the temperature of rock re-solidificating
- pressure : a pressure nearing lithostatic pressure

Since the components of the environment, water not included, is quite homogeneous, the gas volume produced by "1 kiloton" is quite constant. On the other hand, the relative proportion of the gases undergoes a few changes, particularly the ratio CO/CO_2 which normally depends on the quantity of water contained in the environment. This statement is verified by the calculation of thermodynamic equilibriums (figure 2).

In order to work out this calculation of simultaneous chemical equilibrium we have first selected five reactions. Our method of reasoning is as follows : we work by loop, studying each reaction in turn. After a certain number of loops, we reach a stable equilibrium. We felt

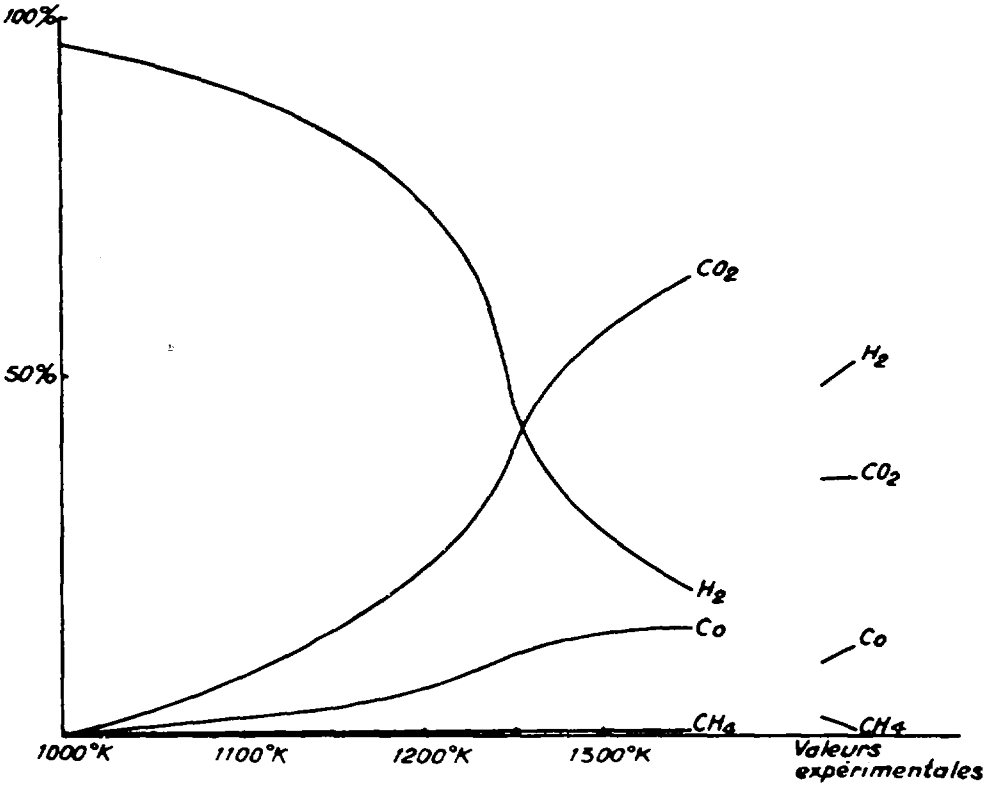

. — Variation des concentrations des principaux gaz (100 atm, gaz secs)'

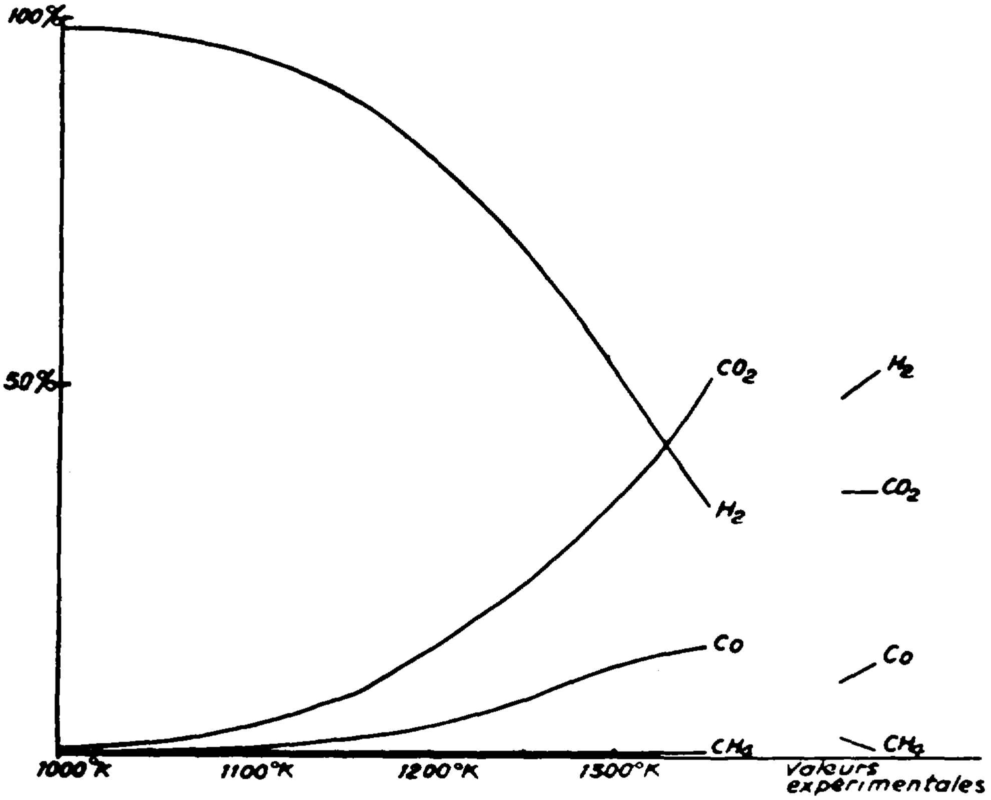

— Variation des concentrations des principaux gaz (200 atm, gaz secs).

Fig. 1 — Variations of the relative proportion gases with variations of temperature and pressure.

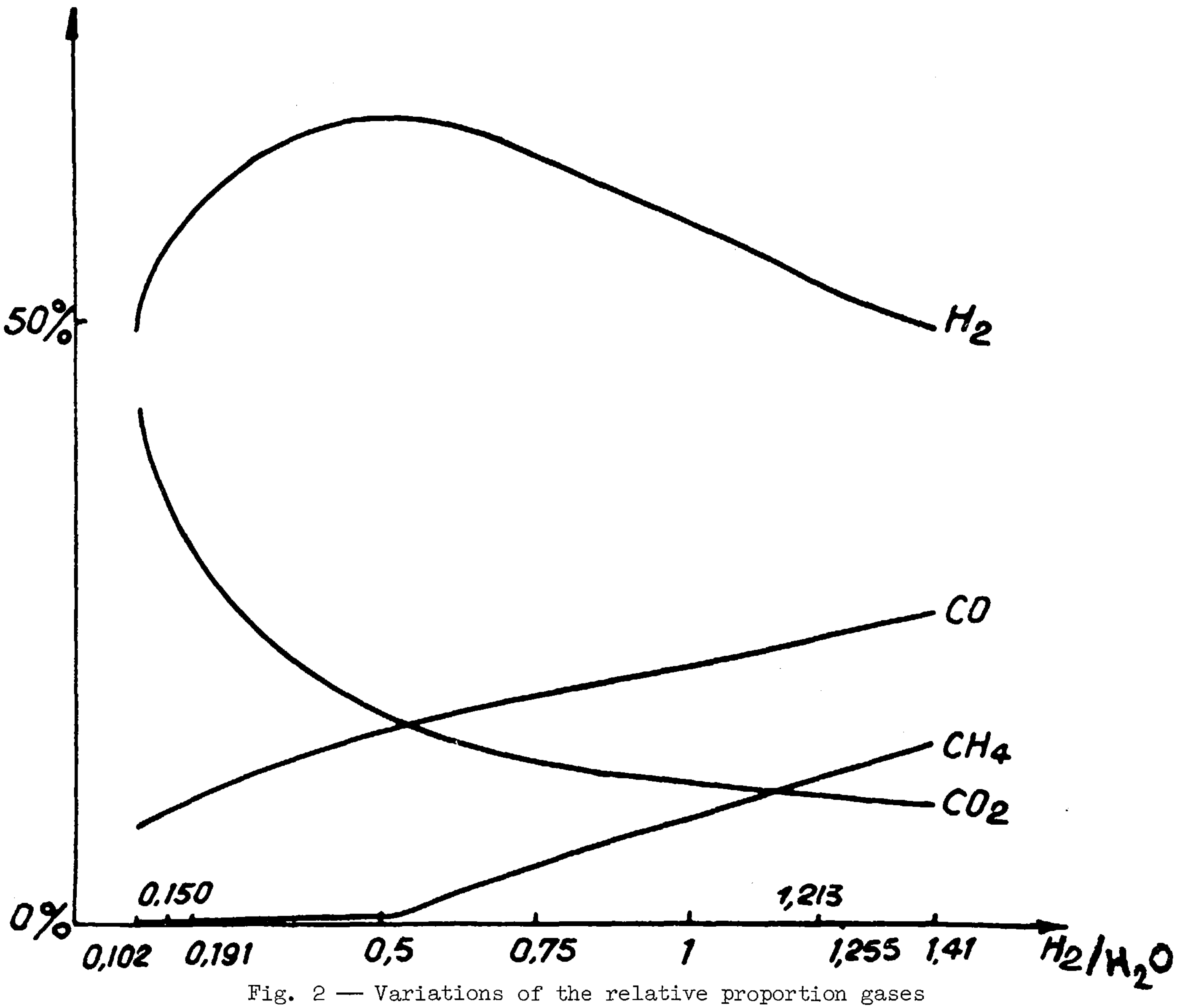

Fig. 2 — Variations of the relative proportion gases with quantity of water contained.

sufficiently satisfied with the results to set a programme in which we take all macroconstituants.

The programme is used for temperature as high as 6000°K. We cannot go beyond that temperature for lack of thermodynamic data. It enables us to study the chemical behaviour of refractory elements. Macroconstituents govern the reactional medium and microconstituents (chiefly radioactive elements) react in that medium.

Another part in our theoretical study is the incidence of chemical reactions inside a chimney on radioactivity. We noticed two main points : long term thermical evolution and chemical reactions in a hydrocarbon environment.

To study thermical evolution, we took the case of granite, where thermical conduction phenomena are preponderant.

In that study, we take as zero time the collapse of the chimney and as source part of a sphere whose radius, for granite, is roughly given by the formula $R = 10\ W^{1/3}$ for a 500 to 1000 m deep explosion. This source has an even temperature : about 900 to 1000°K corresponding to the calorific energy stored up by the rock : calorific energy is about 85 per cent of total energy.

The temperature determined by calculation is in agreement with the measurements taken on the 178th and 221st days after the explosion. These comparisons were made with horizontal drill, the only one we had for the considered explosion. To measure the temperature along a vertical drill, we must consider thermical transfers by convection due to condensable components : water, hydrocarbons... (not very important in the particular case of granite, containing little water)(figure 3).

The chemical reactions in the chimney were studied limitating the temperature range to oil shale decomposition. These cracking reactions as well as the exchange reactions determine the fixation of radioactivity in oil.

To study the rock reactions at high temperature, we have conceived a simulation apparatus based on inductive plasma. In an inductor surrounding the sample the generator produces a current as high as 10 000 V with a 3 to 9 megahertz frequency. The energy stored in the sample is about 10 kJ for a plasma lasting one second. The temperature in the center of the plasma is supposed to be more than 15 000°K. This plasma is made in a hole drilled in a sample of the rock to study. That rock, overheated, is partially vaporized and melted, and it releases gases which are cryogenically trapped out at the end of the heating cycle. Then these gases are analysed either in gaseous phase chromatography or with mass spectrometer (fig. 4 and 5).

We find some difficulties to know the temperature and pressure undergone by the samples to be analysed. The tests were made on different sorts of granite, then on marble chosen because, when heated, it

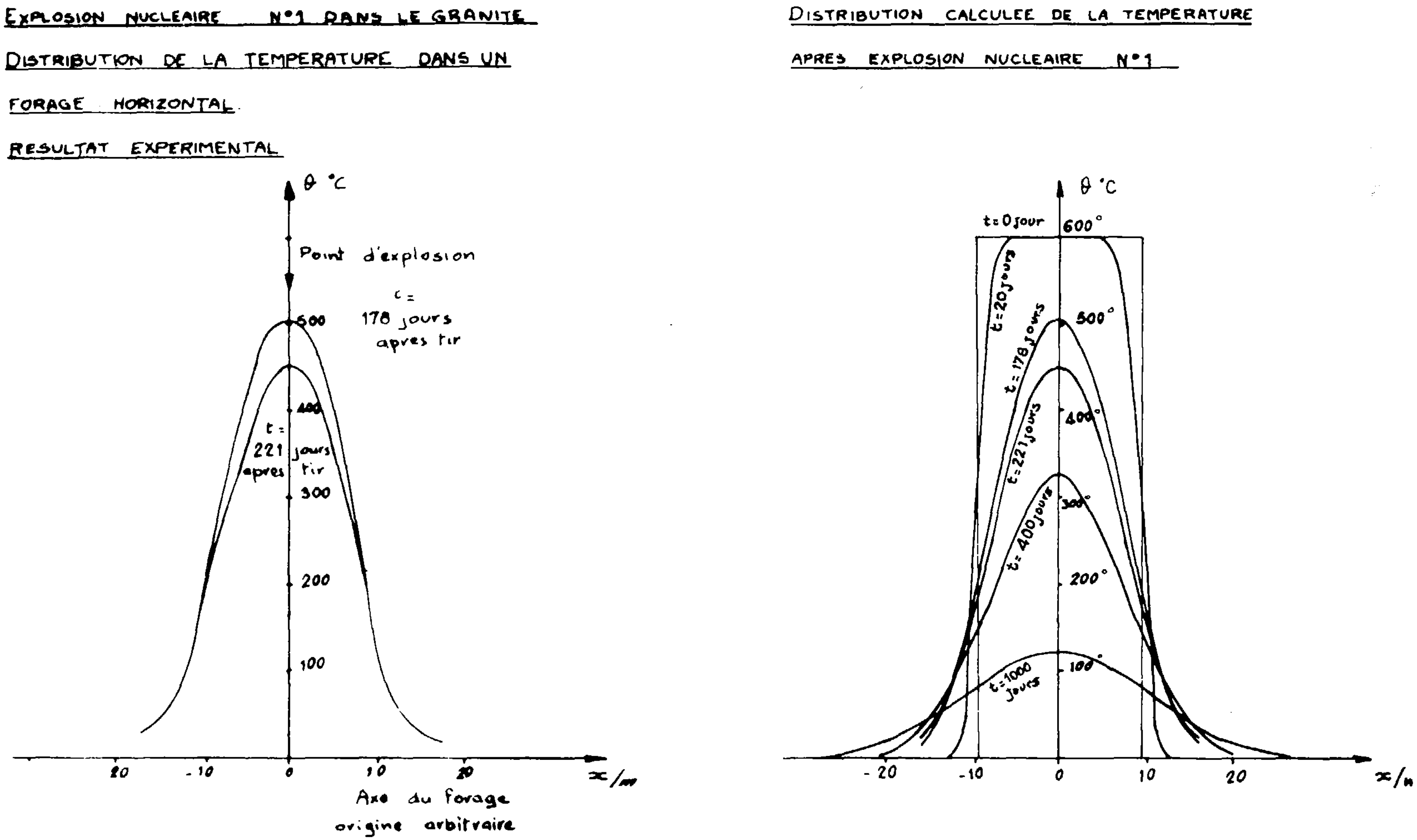

EXPLOSION NUCLEAIRE N°1 DANS LE GRANITE

DISTRIBUTION DE LA TEMPERATURE DANS UN FORAGE HORIZONTAL.

RESULTAT EXPERIMENTAL

DISTRIBUTION CALCULEE DE LA TEMPERATURE APRES EXPLOSION NUCLEAIRE N°1

Fig. 3 — Temperatures by calculation and by measurement.

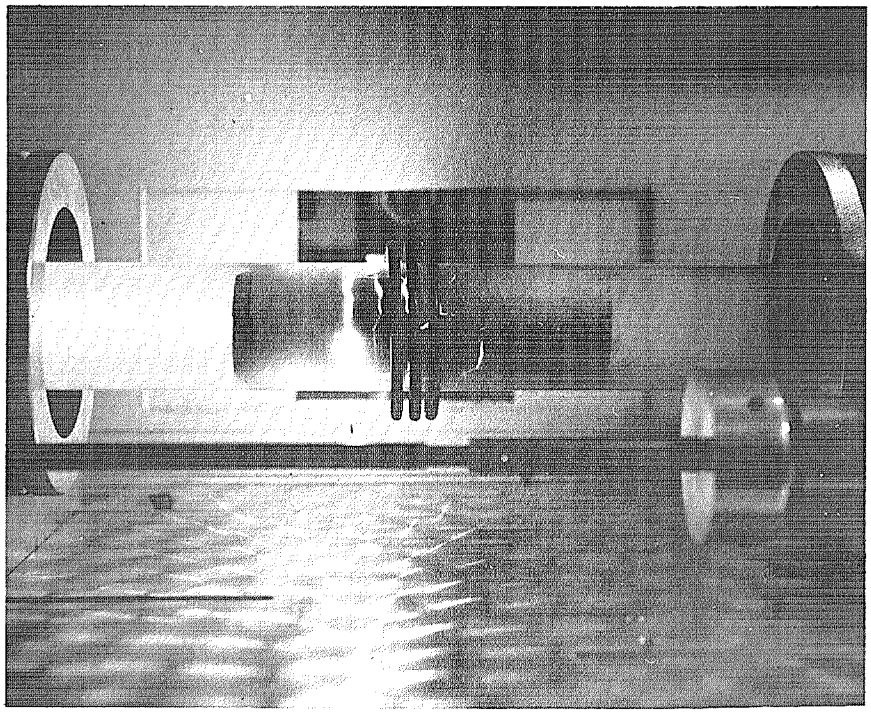

Fig. 4 Simulation apparatus.

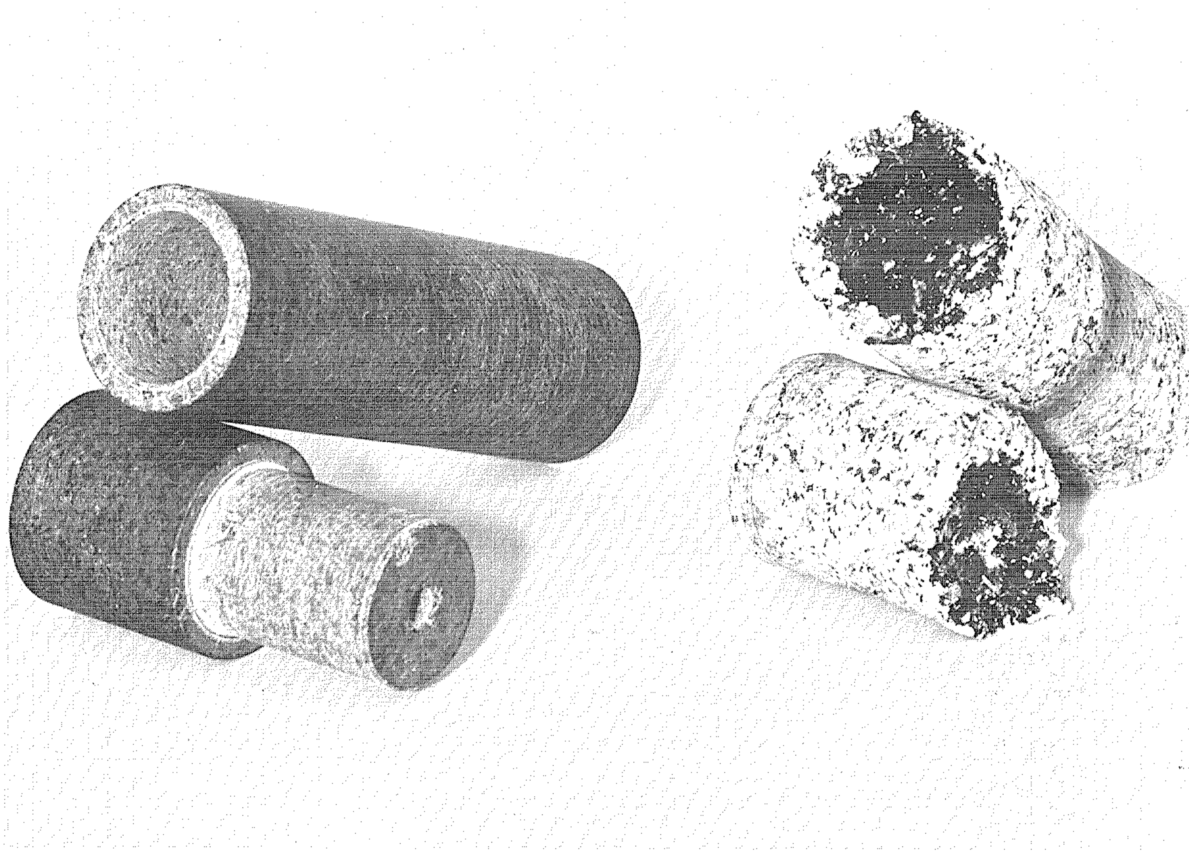

Fig. 5 Samples before and after plasmas heating.

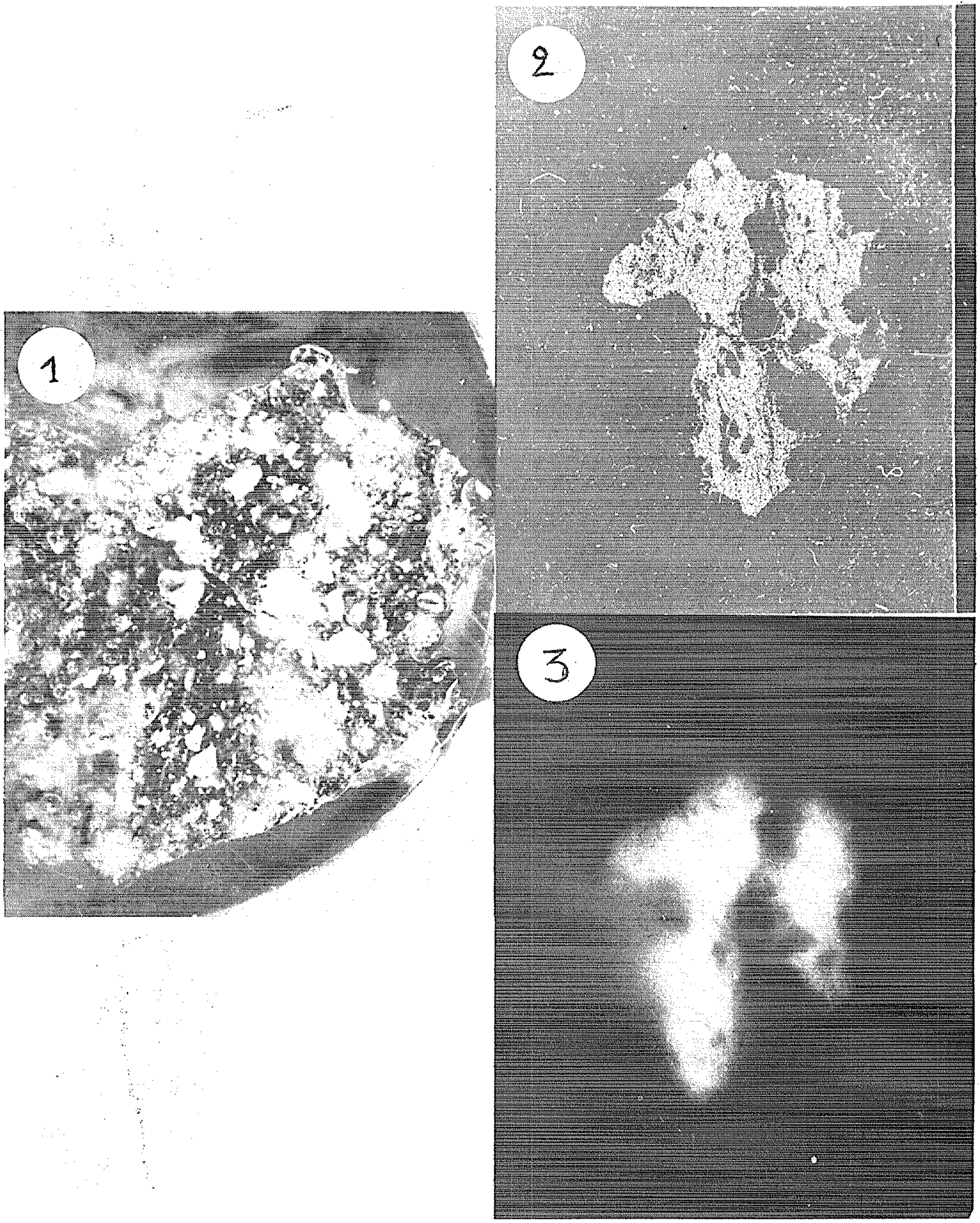

Fig. 6

1 - Photo of the sample
2 - α autoradiography
3 - β-γ autoradiography

Melted rock included no radioactivity

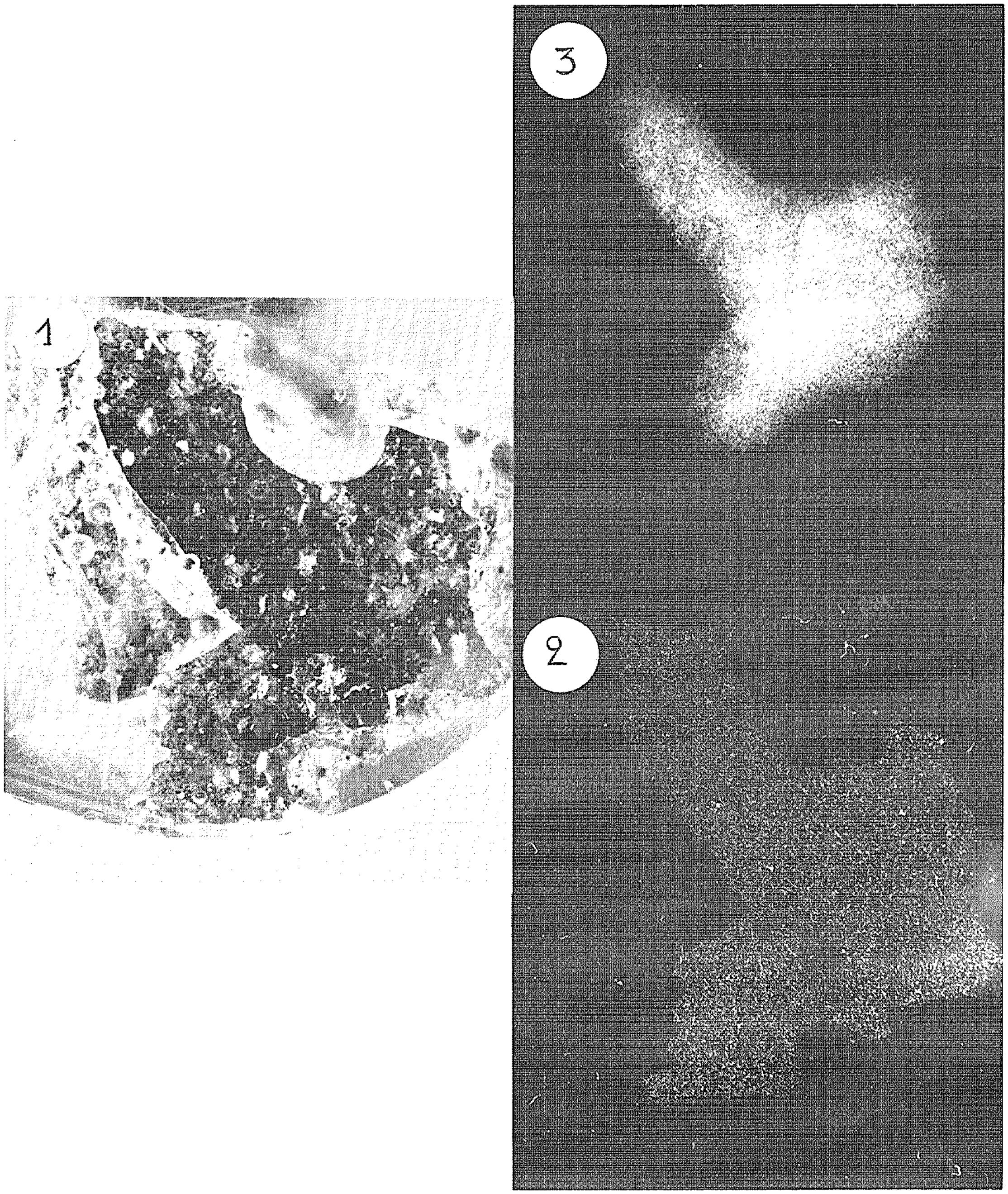

Fig. 7

1 - Photo of the sample
2 - α autoradiography
3 - β-γ autoradiography

Differences between β and γ radioactivity releases large quantities of gas. The melting of the lime resulting from the decomposition of marble showed that the temperature had been raised up to 3000°K, or more. As from granite samples, we obtained green melted rocks with lots of bubbles, quite like the samples taken out from nuclear burst.

We took a certain number of β - γ as well as α autoradiography snaps of the piece of melted rock from a nuclear explosion. We compared them with each other and them with a snap of the sample.

We noticed :

- some parts of the melted rock included no radioactivity.
- In the radioactive parts, α activity was quite homogeneous, while β - γ was not.
- The strongest β - γ activity parts corresponded to the parts of the melted rock scattered with bubbles. From the fact that the bubble lining is more radioactive than the melted product rock, we suppose that the elements concentrated in bubble linings are isotopes with gaseous antecedents having periods compatible with their inclusion as bubbles in the melted rocks, and we hope to obtain more concrete results soon (figures 6 and 7).

We also studied dissolved or occluded gases in the same melted rock. Occluded gases represent only a small part of the gases contained in the rock.

But, on the other hand, large quantities of active gases, particularly tritium, seem to be contained in those melted rocks. We think it may be interesting, particularly in case of an industrial application, and we mean to pursue these studies with other kinds of rocks.